HAI2025

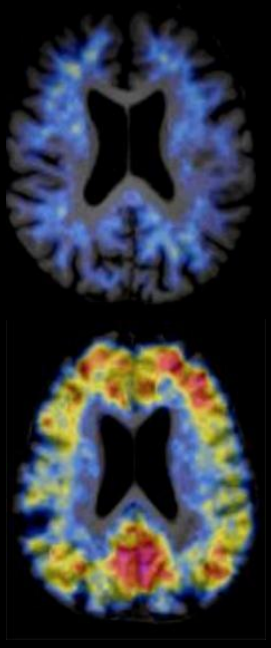


TABLE OF CONTENTS

TABLE OF CONTENTS **2**
WELCOME! **16**
SUPPORTERS **17**
HAI COMMITTEES **18**
POSTER INDEX *(by board number)* **19**
POSTER INDEX *(by presenter's last name)* **34**
HAI 2025 PROGRAM *(short)* **43**
HAI 2025 PROGRAM *(detail)* **50**
HAI 2025 ABSTRACTS **67**
Wednesday, January 15, 2025 - 08:55 am - 10:35 am .. 67
Podium Session 67
SESSION I: Harmonization **67**
Bettcher, Brecca **68**
Longitudinal amyloid burden with combined [11C]PiB and [18F]NAV4694 PET Scans 68
Zhang, Jiaxiuxiu **70**
Exploring Centiloids robustness: Impact of sample size and image resolution on Centiloid conversion accuracy 70
Blazhenets, Ganna **73**
Every Centiloid, from everywhere, all at once 73
Povala, Guilherme **77**
The Uniτ Ecosystem for tau-PET harmonization and visualization 77
Tissot, Cécile **81**
Comparative sensitivity analysis of tau-PET tracers in Alzheimer's disease 81
Wednesday, January 15, 2025 - 10:35 am - 10:40 am ... 83
Podium Session 83
Blitz Session 1A: Short Poster Presentations **83**
Mormino, Elizabeth **84**
Pathological and clinical trajectories of preclinical Alzheimer's disease patients with divergent cortical tau patterns 84
Rahmouni, Nesrine **88**
Association between early and late tau aggregation across tau imaging agents: The HEAD Study 88
Qiu, Ting **91**
Unraveling the impact of amyloid-β and tau pathology on brain structure and cognitive function during preclinical and prodromal Alzheimer's disease 91
Wednesday, January 15, 2025 - 10:40 am - 11:35 am ... 95
Poster Session 1A **95**
Dubbelman, Mark **101**
1 Decline in everyday functioning over time relates to amyloid and tau in cognitively unimpaired older adults 101
Capotosti, Francesca **103**
2 From the clinical utility of a-synuclein PET imaging in Multiple System Atrophy to the possible diagnosis of Parkinson's disease 103
Qiu, Ting **104**
3 Unraveling the impact of amyloid-β and tau pathology on brain structure and cognitive function during preclinical and prodromal Alzheimer's disease 104
Villemagne, Victor **108**
4 Astrogliosis, a potential non-Aβ pathway to tau 108
Grube, Jill **111**
5 APOE ε4 carriers exhibit attenuated habituation in pupil size and practice effects on a repeated auditory oddball task 111

Fu, Jessie Fang-Lu 115

6 Baseline tau burden and performance on a digital clock drawing test uniquely contributes to predicting future tau accumulation in preclinical AD..... 115

Bischof, Gerard 119

7 Molecular correlates of apraxia in Alzheimer's disease: A PET imaging study 119

Ekuta, Victor 120

8 Understanding the impact of race on white matter hyperintensities in Alzheimer's disease: Findings from the ADNI Study 120

Corriveau-Lecavalier, Nick 121

9 Characterization of a limbic-predominant amnestic neurodegenerative syndrome..... 121

Bilgel, Murat 123

10 Positron emission tomography analysis with the dynamicpet Python package.... 123

Colón-Badillo, Vanessa 126

11 Targeted plasma eQTL and pQTL to identify potential novel biomarker for Alzheimer's disease in African Americans 126

Mormino, Elizabeth 127

12 Pathological and clinical trajectories of preclinical Alzheimer's disease patients with divergent cortical tau patterns..... 127

Geremia, Danielle 130

13 Evaluation of a label-free X-ray based method for estimating amyloid load in the human brain..... 130

Duggan, Michael 132

14 Proteomic analyses of A-T-N reveal plasma mediators of neurodegeneration and dementia risk 132

Cassa Macedo, Arthur 136

15 The spatial spread of tauopathy precedes the increase in tau-PET load in Alzheimer's disease 136

Unschuld, Paul 140

16 Distinct patterns of Iron distribution in the entorhinal cortex-hippocampus system for characterization of mild cognitive impairment..... 140

Ziontz, Jacob 141

17 Pathological asymmetry in early onset AD reflects heterogenous disease trajectories 141

Abu Raya, Maison 145

18 Characterizing amyloid-positive with low Tau (A+T-) profiles and their association with cognitive trajectories in the Longitudinal Early-Onset Alzheimer's Disease Study (LEADS): A multi-method approach..... 145

Dong, Yiwen 148

19 The association between amyloid and physical activity in a racially diverse cohort of older adults 148

Buckley, Rachel 150

20 Whole blood gene expression is associated with plasma p-tau217 levels via amyloid-PET and sex..... 150

Gogola, Alexandra 153

21 Plasma Aβ as predictor of Aβ accumulation in non-demented participants..... 153

Cody, Karly 156

22 The relative prevalence of tau severity stages is related to amyloid burden, clinical diagnosis and age 156

Bellaver, Bruna 160

23 Head-to-head trajectories of tau PET and plasma p-tau217 as a function of Aβ160

Lawn, Timothy 163

24 Functional submodules in the human locus coeruleus are differentially susceptible to tau pathology..... 163

Gills, Joshua..... 167

25 Sex-specific associations of BMI, amyloid, and regional tau deposition in community-dwelling cognitively normal older adults..... 167

Gnörich, Johannes..... 168

26 Assessment of ATN with a single dynamic [18]F-PI-2620 recording..... 168

Grothe, Michel..... 169

27 Tau-PET detects advanced primary age-related tauopathy mimicking early-stage AD..... 169

Callow, Daniel..... 170

28 Amyloid status moderates associations between hippocampal microstructure, PET tau burden, and memory in dementia-free older adults..... 170

DelBene, Alexander..... 171

29 Performance of an MR-independent analysis pipeline for quantification of tau abnormality using [18F]flortaucipir PET .171

Gallego-Rudolf, Jonathan..... 173

30 Functional and structural connectivity patterns predict longitudinal tau spreading in asymptomatic individuals expressing Aβ pathology..... 173

Gatchel, Jennifer..... 176

31 Plasma phospho-tau 217, neurofilament-light, and glial fibrillary acidic protein are differentially associated with longitudinal neuropsychiatric symptoms across the early cognitive spectrum..... 176

Gatto, Rodolfo..... 180

32 An assessment of the utility of flortaucipir PET to detect four-repeat tau pathology in a globular glia tauopathy case-series..... 180

Clarke, Mica..... 182

33 Molecular imaging of neurodegeneration – mitochondria, associated proteins and synapses (MIND-MAPS) in frontotemporal dementia..... 182

Engels-Domínguez, Nina..... 184

34 Evaluating tVNS effects on cognitive outcomes and modulating factors in asymptomatic older adults: study design of the WALLe Trial..... 184

Dhaynaut, Maeva..... 188

35 Cerebral perfusion indices from early-phase [18F]-MK6240 dynamic Tau PET imaging in brain regions associated with Alzheimer's disease progression in an aging population. 188

Baillet, Marion..... 189

36 Transcutaneous auricular vagus nerve stimulation improves learning and sleep-wake quality in older APOE-ε4 carriers.. 189

Brown, Christopher..... 192

37 Biological-clinical mismatch reflects co-pathology and vulnerability to neurodegeneration..... 192

Del Carmen Montenegro, Grace..... 196

38 Validation of PET spatial extent as sensitive amyloid biomarker in early stages of amyloidosis..... 196

Frontzkowski, Lukas..... 199

39 Developing a novel reference region for PI-2620-PET imaging to facilitate assessment of 4-repeat tauopathies 199

Arnold, Steven..... 201

40 P-TAU217, GFAP, and NFL plasma biomarker associations with demographic, medical and neurocognitive features from middle-aged through older adulthood... 201

Bourgeat, Pierrick..... 202

41 DeepSUVR: Using temporal constraints to improve tau quantification 202

Aumont, Etienne 206

42 Increasing the granularity of tau-PET Braak staging using medial temporal lobe segmentations to detect early memory impairment 206

Povala, Guilherme 208

43 The universal tau PET scale (Uniτ) for Flortaucipir, MK6240, PI2620 and RO948 harmonization..... 208

Garrone, Aurélie 212

44 Assessing the relationship between neuropsychiatric symptoms, amyloid and tau pathology, and white matter hyperintensity volume across sexes in preclinical Alzheimer's disease 212

Diez, Ibai 215

45 Unveiling the heterogeneity of tau spreading in aging and Alzheimer's disease using polygenic combinations: Towards personalized models 215

Guzmán, Diana S 218

46 Regional amyloid and tau: Exploring regional sex-based differences in a middle-aged community-based cohort . 218

Amaral, Livia 220

47 Comparison of topographical patterns of abnormalities of the tau PET tracers [18F]Flortaucipir, [18F]MK6240, [18F]PI2620, and [18F]RO948..... 220

Felix, Cynthia 224

48 Subtle cognitive deficits detected through routine in-office tests are associated with global Aβ and temporal tau in cognitively unimpaired individuals.... 224

Banks, Sarah 228

49 Estradiol-dependent associations between sleep complaints and tau deposition in women at elevated AD risk 228

Ghatamaneni, Sujala 230

50 Impact of age and sex on extra-cerebral off-target binding in tau PET scans (18F-FTP) 230

Adams, Jenna 233

51 Metabolic inefficiency is associated with regional vulnerability to tau deposition 233

Garcia Condado, Jorge 235

52 Relationship between Polygenetic Risk Score of BrainAge and plasma biomarkers in the A4/Elearn Study 235

Dodge, Hiroko 236

53 Combined impact of plasma phospho-tau 217 and NfL on longitudinal domain-specific cognitive decline 236

Bezgin, Gleb 240

54 Comparison of distribution volume and standardized uptake value ratio for a MAO-B tracer in mild cognitive impairment .. 240

Rahmouni, Nesrine 242

55 Association between early and late tau aggregation across tau imaging agents: The HEAD Study..... 242

Fajardo-Valdez, Alfonso 245

56 The impact of spatial smoothing on the accuracy of Centiloid thresholds 245

Betthauser, Tobey 248

57 Longitudinal amyloid PET trajectories in the HABS-HD cohort..... 248

Patsyuk, Yuliya 251

58 Lower microstructural integrity of the locus coeruleus to entorhinal cortex pathway is related to elevated astrocyte reactivity and tau burden in cognitively unimpaired individuals: a 7T dMRI study 251

Wednesday, January 15, 2025 - 11:35 am - 01:00 pm . 254

Podium Session 254
SESSION II: Spatial Patterns 254
Farrell, Michelle 255
The interaction of initial medial temporal lobe tauopathy and amyloid-beta spatial extent in driving caTAUstrophe 255
Adams, Jenna 258
Mapping spatial white matter integrity linked to tau accumulation: Insights from tractometry with multi-shell diffusion imaging 258
Fonseca, Corrina 259
Spatial patterns of voxel-wise tau accumulation across the Alzheimer's disease spectrum 259
Rahmouni, Nesrine 263
PET astroglia and microglia follow tau propagation patterns in Alzheimer's disease 263
Wednesday, January 15, 2025 - 02:00 pm - 02:30 pm 266
Kolb, Hartmuth 266
Keynote: From click chemistry to precision neuroscience 266
Wednesday, January 15, 2025 - 02:45 pm - 04:25 pm 267
Podium Session 267
SESSION III: Neuropath I 267
Chao, Yishu 268
Correlation between in vivo 18F-flortaucipir PET and whole brain postmortem histological tau signals in Alzheimer's disease 268
Moloney, Christina 271
Tau-PET, structural MRI, and cognitive measures are differentially correlated with tangle and neuritic pathology across the neurofibrillary tangle lifespan 271
Ikonomovic, Milos 273
Binding of [3H]MK-6240 to different tau lesions: a brain autopsy study 273
Grothe, Michel 274
Plasma extracellular vesicle TDP-43 and hippocampal volume as complementary biomarkers for LATE-NC and hippocampal sclerosis: a pathologic validation study 274
Capotosti, Francesca 275
Discovery and preclinical development of [18F]ACI-19626, a first-in-class TDP-43 PET tracer 275
Wednesday, January 15, 2025 - 04:25 pm - 04:30 pm 276
Podium Session 276
Blitz Session 1B: Short Poster Presentations 276
Ziontz, Jacob 277
Pathological asymmetry in early onset AD reflects heterogenous disease trajectories 277
Lawn, Timothy 280
Functional submodules in the human locus coeruleus are differentially susceptible to tau pathology 280
Povala, Guilherme 284
The universal tau PET scale (Uniτ) for Flortaucipir, MK6240, PI2620 and RO948 harmonization 284
Thursday, January 16, 2025 - 08:45 am - 10:00 am ... 288
Podium Session 288
ISTAART Collaborations: Addressing Accessibility and Acceptability of Neuroimaging in Diverse Populations 288
Thursday, January 16, 2025 - 10:00 am - 10:05 am 289
Podium Session 289
Blitz Session 2A: Short Poster Presentations 289
Liu, Peiwei 290
The role of cohort heterogeneity in predicting AD/ADRD cognitive decline . 290
Li, Annie 291
Sex moderates the association between regional tau and longitudinal cognitive decline in A4 and LEARN studies 291
Ioannou, Konstantinos 294

Low tau in Aβ-positive cognitively impaired individuals: Alzheimer's disease or something more? 294

Thursday, January 16, 2025 - 10:05 am - 11:00 am 298

P2A: Poster Session 2A 298

Jones, David 304

59 Interpretable prediction of amyloid PET positivity using non-negative matrix factorization 304

Kuchenbecker, Lindsey 306

60 Data-driven biomarker discovery nominates novel diagnostic plasma biomarkers and provides insights into Alzheimer's disease pathophysiology in an African American cohort 306

Lussier, Firoza 307

62 Longitudinal multicenter head-to-head harmonization of tau PET tracers: an overview of the HEAD study cohort 307

Javanray, Mohammadali 311

63 Higher time varying brain functional connectivity is associated with slower tau accumulation at the preclinical stage of Alzheimer's disease 311

Kang, Min Su 315

64 Graph convolutional networks to predict cognitive decline at the individual level in Alzheimer's disease 315

Ioannou, Konstantinos 317

65 Low tau in Aβ-positive cognitively impaired individuals: Alzheimer's disease or something more? 317

Petersen, Kellen 321

66 A plasma clock for Alzheimer disease based on %p-tau217 321

He, Hengda 324

67 Network-based amyloid-β pathology predicts subsequent cognitive decline in cognitively normal older adults 324

Mooney, Katelyn 328

68 Associations between APOE-TOMM40 '523 haplotype variants and limbic system white matter microstructure in Black and White individuals 328

Laymon, Charles 331

69 Multi element MRI template method for analysis of Down syndrome PET 331

Klinger, Hannah 333

70 Whole-blood gene expression associations with Aβ-PET accumulation and cognitive decline 333

Bilgel, Murat 336

71 Longitudinal change in five dominant dimensions of brain aging in relation to brain amyloid status and Alzheimer's-related plasma biomarkers 336

Mundada, Nidhi 339

72 Enrichment of patients with concomitant LATE on the Alzheimer's disease continuum using hippocampal volume 339

Lopresti, Brian 343

73 AT(N) staging of Alzheimer's disease: Comparison of visual interpretation and automated quantification pipelines 343

Heuer, Lauren 345

74 MK-6240 off-target binding patterns in relation to microglia density, measured through TSPO PET 345

Mroué, Rayan 347

75 Association between medication use and [18F]MK6240 and [18F]Flortaucipir uptake across the Alzheimer's disease spectrum 347

Koops, Elouise 350

76 Lower LC-EC tract integrity is associated with entorhinal tau in autosomal-dominant Alzheimer's disease 350

McVea, Andrew 353

77 APOE4 associated with higher off-target meninges signal with [F-18]MK6240 PET 353

Minhas, Davneet..... 356

78 An accurate and automated technique for removing spill-over contamination and off-target retention from a cerebellar reference region for tau PET..... 356

Schwarz, Christopher 360

79 Updated public CenTauR pipelines to measure CenTauR, CenTauRZ, and SUVR tau PET units 360

Moon, Hasom..... 361

80 Predicting regional Alzheimer's disease pathology with plasma p-tau217 in preclinical AD..... 361

Pascual, Belen 364

81 TSPO-PET before and after low-dose interleukin-2 in patients with mild to moderate Alzheimer's disease 364

Hanseeuw, Bernard 365

82 In low neocortical tau individuals, high amygdala tau predicts faster cognitive decline 365

Katsumi, Yuta..... 368

83 EOAD-signature atrophy predicts progression to dementia in patients with early-onset MCI due to Alzheimer's disease 368

McLachlan, Max 369

84 FDG reference region selection using PiB amyloid status-guided iterative normalization in a Down syndrome cohort 369

Kunach, Peter 372

85 Microscopic visualization of fluorescent MK-6240..... 372

Leuzy, Antoine 373

86 Conversion of Tau PET SUVR data to CenTauR units using the Joint Propagation Model 373

Liu, Peiwei..... 376

87 The role of cohort heterogeneity in predicting AD/ADRD cognitive decline ..376

Khurelbaatar, Bayarjargal 377

88 Differential tau accumulation in early-onset and late-onset Alzheimer's disease: Insights from [18F]-Florzolotau PET 377

Silva-Rodríguez, Jesús..... 379

89 Heterogeneity of FDG-PET patterns among tau-negative amnestic patients 379

Huang, Shao-Yi 381

90 Predicting amyloid positivity and tau burden in dementia using a combination of different biomarkers 381

Kulagowska, Laura..... 383

91 Evaluation of [^{3}H]SynVesT - 1 binding in post-mortem brain tissue from control and Alzheimer's Disease as a biomarker of synaptic loss.....383

Johns, Emily.....384

92 Exploring the predictive power of graph-theoretic metrics for tau pathology in cognitively unimpaired older adults.. 384

Gallego-Rudolf, Jonathan..... 385

93 Tracking biomarkers accuracy for predicting progression to mild cognitive impairment.....385

Rani, Nisha 389

94 Tau burden across Braak stages is associated with regionally specific amyloid accumulation: insights from the BIOCARD cohort 389

Singh-Reilly, Neha..... 390

95 Relationship between neuroinflammatory ER176-PET and functional connectivity in Progressive Apraxia of Speech..... 390

Li, Annie 392

96 Sex moderates the association between regional tau and longitudinal cognitive decline in A4 and LEARN studies 392

Lutz, Olivia 395

97 Evaluation of the Uni-tau and CenTauR frameworks in new datasets for tau PET harmonization in Alzheimer's disease... 395

Moret, Sophia 399

98 Hemispheric lateralization of tau-related network dysfunction and its association with neuropsychiatric symptoms in preclinical Alzheimer's disease 399

Olafson, Emily 401

99 Characterization and correction of extracerebral [18F]MK-6240 tau PET off-target signal in Alzheimer's disease 401

Lim, Seokbeen 404

100 Investigation of optimal intensity threshold for tau-PET overlap index 404

Bourgeat, Pierrick..... 406

101 DeepSUVR: Towards redefining the Centiloid masks using a data-driven approach 406

Provenzano, Frank 410

102 Mechanical stress of the entorhinal cortex: A potential driver of tau pathology? 410

Lyu, Xueying..... 412

103 Amyloid-Tau to neurodegeneration mismatch from inter-modality image translation using deep learning..... 412

Millar, Peter 415

104 Tau PET subgroups differ in network patterns of functional connectivity and amyloid PET 415

Hall, Brandon..... 419

105 Cortical freewater increases with tau tangle aggregation..... 419

Ottoy, Julie 422

106 Distinct spatiotemporal patterns of vascular disease in Alzheimer's disease subtypes 422

Houlihan, Hannah 424

107 Annual percent change of microglia density in relation to tau accumulation in older adults 424

Palmgren, Kailee 426

108 Physical frailty as a risk factor for increased tau accumulation and cognitive decline in cognitively unimpaired older adults 426

Jacobson, David 430

109 Assessing neuroinflammation in Alzheimer's disease: A TSPO-PET study using ER176 and its correlation with amyloid and tau pathology..... 430

Chen, Charles 432

110 Two distinct sources of 18F-MK-6240 off-target signal identified by individualized head modeling and PET kinetics 432

Lao, Patrick..... 435

112 TSPO PET mediates tau-associated neurodegeneration in limbic and temporal regions across clinical variants of Alzheimer's disease 435

Bluma, Marina 437

114 Tracking plasma biomarker abnormalities with amyloid time accumulation.....437

Honer, Michael 440

115 Advancing antibody-based pretargeted PET imaging of protein aggregates in the brain 440

Kraft, Jessica 441

116 Longitudinal change in mnemonic discrimination and influence of Aβ burden 441

Thursday, January 16, 2025 - 11:00 am - 12:40 pm 442

Podium Session 442

SESSION IV: Neuropath II 442

Lemoine, Laetitia 443

Understanding the mechanisms of synaptic vesicle glycoprotein 2A change in Alzheimer's disease 443

Vrillon, Agathe 444

Association of [18F]Flortaucipir-PET and plasma p-tau217 with tau neuropathology in AD and other neurodegenerative disorders 444

Maboudian, Samira 448

Tau-related cortical thinning is concentrated in sulcal depths 448

Betthauser, Tobey 452

Comparison of [3H]MK-6240 and [3H]AV-1451 binding in relation to brain concentrations of p-tau: A postmortem biochemistry study 452

Saturnino Guarino, Dinahlee 453

In vitro binding of the tau PET tracer [3H]JSS20-183A and its comparison with PI-2620, T807 and PM-PBB3 in human postmortem brain tissue 453

Thursday, January 16, 2025 - 01:40 pm - 02:10 pm 454

Grinberg, Lea 454

Keynote: From neuropathology to biomarkers: Novel strategies for detecting and monitoring Early Alzheimer's disease in vivo 454

Thursday, January 16, 2025 - 02:25 pm - 03:50 pm 455

Podium Session 455

SESSION V: Clinically Relevant Applications 455

Boon, Baayla 456

Neuropathologic and ARIA-related findings in aducanumab-treated Alzheimer's disease: a postmortem analysis of superficial cortical Aβ clearance 456

Schwarz, Adam 459

Robustness of the centiloid scale across research and commercial software using [18F]flutemetamol PET images 459

Tonietto, Matteo 462

Impact of ARIA on cerebral volume changes with Gantenerumab 462

Shirzadi, Zahra 465

Independent effects of baseline white matter hyperintensity and APOE ε4 on future ARIA-H emergence in A4 trial 465

Thursday, January 16, 2025 - 03:50 pm - 03:55 pm 469

Podium Session 469

Blitz Session 2B: Short Poster Presentations 469

Hall, Brandon 470

Cortical freewater increases with tau tangle aggregation 470

Chen, Charles 473

Two distinct sources of 18F-MK-6240 off-target signal identified by individualized head modeling and PET kinetics 473

Bluma, Marina 476

Tracking plasma biomarker abnormalities with amyloid time accumulation 476

Thursday, January 16, 2025 - 04:50 pm - 06:15 pm 479

Podium Session 479

SESSION VI: Heterogeneity 479

Schultz, Stephanie 480

Improving history-based prediction of biomarker and clinical progression of autosomal dominant Alzheimer's disease using mutation-level analysis of Aβ production 480

Chiotis, Konstantinos 484

Tau PET load in early- and late-onset Alzheimer's disease: A cross-sectional and

longitudinal comparison of the LEADS and ADNI cohorts 484

Otero Svaldi, Diana..... 488

Regional tau quantification methodologies in early symptomatic participants with presence of tau pathology 488

Franzmeier, Nicolai 492

Alpha Synuclein co-pathology accelerates amyloid associated tau accumulation in Alzheimer's disease..... 492

Friday, January 17, 2025 - 09:00 am - 10:40 am 495

Podium Session 495

SESSION VII: Factors which Influence ATN 495

Cohen, Ann..... 496

Evaluating the ATN framework in a racially and ethnically diverse cohort: Preliminary analysis from the Health Aging Brain Study- Health Disparities Study 496

Molina-Henry, Doris 499

Racial and ethnicity differences in plasma biomarker eligibility prior to amyloid PET imaging in the AHEAD 3-45 Study 499

Heston, Margo..... 501

Examining neighborhood disadvantage as a factor explaining amyloid onset age ...501

Reese, Alexandria..... 505

Intersections of sex and neighborhood disadvantage on Alzheimer's disease pathology..... 505

Coughlan, Gillian 508

Sex moderates relationships between P-Tau217 and longitudinal tau-PET: A multi-cohort study 508

Friday, January 17, 2025 - 10:40 am - 10:45 am 511

Podium Session 511

Blitz Session 3A: Short Poster Presentations 511

Yakoub, Yara 512

Head-to-head comparison of longitudinal plasma assays in relation to longitudinal amyloid pathology in Alzheimer's disease 512

Soleimani-Meigooni, David 516

Calibration of multi-site raters for prospective visual read of amyloid PET scans acquired across the ADRC Consortium for Clarity in ADRD Research Through Imaging (CLARiTI)..... 516

Yang, Hyun-Sik..... 519

Plasma phosphorylated tau 217 and longitudinal trajectories of Aβ, tau, and cognition in cognitively unimpaired older adults 519

Friday, January 17, 2025 - 10:45 am - 11:40 am..... 523

P3A: Poster Session 3A 523

Vrillon, Agathe 529

117 Concordance between visual and quantitative amyloid PET and CSF biomarkers in the ADNI-DOD cohort..... 529

Soleimani-Meigooni, David 533

118 Calibration of multi-site raters for prospective visual read of amyloid PET scans acquired across the ADRC Consortium for Clarity in ADRD Research Through Imaging (CLARiTI).....533

Pezzoli, Stefania 536

119 Evaluating the effect of APOE genotype in real-world clinical settings: results from the IDEAS-ANGI study.....536

Xiao, Yu 539

120 Brain connectivity drives tau distribution while regional vulnerability drives tau load in Alzheimer's disease ...539

Ramirez Tirado, Laura Alejandra 543

121 Synergistic effects of peripheral inflammation and neuroinflammation on amyloid, vascular, and neurodegeneration markers across the Alzheimer's disease spectrum..... 543

Tonietto, Matteo..... 547

122 Impact of amyloid removal on cerebral volume changes with Gantenerumab ... 547

Schweitzer, Noah 550

123 Astrocyte reactivity explains tau-related effects on hippocampal dysfunction and longitudinal atrophy in preclinical Alzheimer's disease 550

Yang, Hyun-Sik 553

124 Plasma phosphorylated tau 217 and longitudinal trajectories of Aβ, tau, and cognition in cognitively unimpaired older adults 553

Rissman, Robert 557

125 Detection of TDP-43 from plasma-derived astrocyte extracellular vesicles for identification of LATE 557

Winer, Joseph 558

126 Short sleep duration is associated with higher subsequent plasma p-tau217 in aging 558

Sai, Isha 560

127 Impacts of testing language and rates of amyloid positivity among underrepresented groups in the A4 Study 560

Wiklund, Emma E 563

128 Lower locus coeruleus metabolism is associated with greater year-to-year intraindividual cognitive variability in older individuals with elevated levels of Alzheimer's disease pathology 563

Silva-Rodríguez, Jesús 566

129 Long-term cognitive and biomarker trajectories of cognitively unimpaired individuals with elevated plasma ptau-217 566

Schwarz, Christopher 567

130 A large public release of PIB PET and MRI from the Mayo Clinic Study of Aging567

Ruppert, Emma 569

131 Harmonizing visual readings of Flortaucipir and MK-6240 using head-to-head data 569

Wu, Chao-Yi 573

132 Twin-mapping techniques in clinical trials: a proof-of-concept application to the Internet-Based Conversational Engagement Clinical Trial (I-CONECT)...573

Cody, Karly 574

133 Effects of amyloid and tau status on multiplex plasma CNS and inflammatory proteins in a normal aging cohort 574

Gogola, Alexandra 577

134 Tau imaging thresholds within NIA-AA multilevel tau staging as predictors of tau accumulation and cognitive decline in non-demented individuals.....577

Smith, Anna 581

135 Multi-morbidity and Alzheimer's disease pathology across the lifespan in adults with Down syndrome..... 581

Schwartz, Daniel 583

136 Cortical atrophy is correlated with the discrepancy between neuroradiological assessment and binary quantitation of florbetapir PET in nondemented older adults 583

Silva Oliveira Junior, Markley 586

137 Vascular pathology influences the association of tau-PET with neurodegeneration and cognition in Aβ-negative individuals 586

Van Egroo, Maxime 590

138 Concomitant neurodegeneration of the lateral hypothalamus and locus coeruleus is associated with early Alzheimer's disease-related pathophysiological and cognitive processes..... 590

Roemer-Cassiano, Sebastian Niclas . 594

139 Amyloid-associated hyperconnectivity drives tau spreading across connected brain regions in Alzheimer's disease..... 594

Saha, Pampa 598

140 Association of plasma GFAP with tau PET in cognitively unimpaired Aβ-negative subjects..... 598

McLachlan, Max 601

141 The striatum is an early, accurate indicator of [C-11]PiB amyloid burden for the Down syndrome population.....601

Tissot, Cécile 604

142 Best practices for tau-PET tracer harmonization in Alzheimer's research . 604

Tennant, Victoria 605

143 Relationship between metabolic syndrome biomarkers and regional tau accumulation in cognitively unimpaired older adults..... 605

Groh, Jenna..... 609

144 Association of a unique pattern of white matter T2 FLAIR hyperintensities with plasma and tau PET biomarkers in former American football players 609

Singh-Reilly, Neha..... 613

145 Relationship between flortaucipir-PET and quantitative susceptibility mapping in atypical Alzheimer's disease 613

Gatto, Rodolfo..... 615

146 Neuropathological evaluation of the off-target binding of flortaucipir in FTLD subcortical regions: interconnecting tau aggregates with iron deposition and neuroinflammation 615

Townsend, Diana..... 617

147 Patterns of cognitive decline in individuals with elevated p-tau217 and low levels (<20 Centiloids) of neocortical Aβ-PET signal..... 617

Pascual, Belen 620

148 Anatomic specificity of inflammation TSPO PET biomarkers in dementia 620

Yakoub, Yara 621

149 Head-to-head comparison of longitudinal plasma assays in relation to longitudinal amyloid pathology in Alzheimer's disease 621

Soares, Carolina..... 625

150 Characterization of PART using MK-6240, Flortaucipir, and plasma p-tau217625

Rani, Nisha 629

151 Longitudinal rate of change in CSF biomarkers is associated with subsequent Tau PET burden in Braak stages I and II: Findings from the BIOCARD study..... 629

Cassa Macedo, Arthur..... 630

152 Head-to-head comparison of four tau-PET tracers for in vivo Braak staging: the HEAD Study 630

Villemagne, Victor 633

153 Astrogliosis in the early-stages of Alzheimer's disease 633

Bourgeat, Pierrick..... 636

154 Identifying an optimal aβ cutoff point for progression from mild cognitive impairment to Alzheimer's disease: comparing cognitive performance and aβ pet insights 636

Yau, Wai-Ying Wendy 638

155 Amyloid modifies the association between late-life BMI and longitudinal cognition in cognitively unimpaired individuals 638

Thompson, Jackson 642

156 Amyloid spatial extent captures early tau burden and cognitive deficits, measured by PACC and digital clock drawing test, in preclinical Alzheimer's disease..... 642

Tiss, Amal 646

157 Findings from dynamic [18F]-MK6240 PET imaging after motion and partial volume corrections 646

Rocha, Andreia 650

158 Harmonization of MK6240 and Flortaucipir Braak Staging..... 650

Scop Medeiros, Marina..... 653

159 Comparison of MK-6240 PET and Flortaucipir tau PET imaging for the biological staging of Alzheimer's disease 653

Slade, Elliott..... 657

160 Impact of early-stage amyloidosis on tau accumulation throughout the medial temporal lobe and neocortex 657

Sheng, Jintao..... 661

161 Associations between age-related tau deposition and neural selectivity in cognitively unimpaired older adults 661

Saukkonen, Daniel 664

162 Posterior white matter hyperintensity is related to the emergence of lobar cerebral microbleeds in ADNI 664

Povala, Guilherme 668

163 Defining the grey zone thresholds for tau PET positivity using the Uniτ scale . 668

Thibault, Emma..... 670

164 Neocortical amyloid spatial extent predicts cognitive decline over time in memory and executive function domains 670

Trudel, Lydia 673

165 Patterns of tau-PET accumulation and clinical progression according to biological AD stages 673

Razlighi, Qolamreza.....677

166 The Tau Progression Index (TPI): an individualized, clinically applicable, multimodally-derived score to predict AD progression 677

Wilson, Rachael..... 679

167 Dried plasma spot optimization for the NULISAseq CNS panel.....679

Chan, Tevy 682

168 Clinical validation of the Lumipulse G1200 automated immunoassay for the measurement of Alzheimer's disease plasma biomarkers 682

Galbraith, Jordan 685

169 Sex differences in synaptic loss in early Alzheimer's disease 685

An, Gordon Zhaoqi 686

170 Assessing the generalizability of AD subtypes across diverse cohorts: HABS-HD and ADNI 686

Heinrich, Lukas 688

171 Locus coeruleus - medial temporal lobe functional connectivity confers protection against amyloid-related cognitive decline in the context of high cognitive reserve 688

Rodrigues, Matheus 692

172 Effect of AD risk factors on tau-PET tracer uptake and its association with amyloid-β pathology 692

Phillips, Jeffrey..... 695

173 PI-2620 uptake in the medial temporal lobes discriminates Alzheimer's disease from normal cognition and non-Alzheimer's dementias 695

Robinson, Talia..... 696

174 Characterizing associations with Aβ burden in non-Hispanic Black participants across US POINTER and A4/LEARN cohorts 696

Friday, January 17, 2025 - 12:40 pm - 01:10 pm 699

O'Bryant, Sid 699

Keynote: Alzheimer's disease biomarkers among diverse populations – Data from the HABS-HD Study 699

Friday, January 17, 2025 - 01:25 pm - 02:50 pm 700
Podium Session 700
SESSION VIII: Plasma Biomarkers: New Methods 700
Salvadó, Gemma 701
Plasma tau biomarkers and staging of Alzheimer's disease 701
Malpetti, Maura 704
Novel blood-based proteomic signatures across neurodegenerative diseases 704
Kac, Przemyslaw 707
Association of CSF P-tau and MTBR-Tau biomarkers with amyloid and tau PET .. 707
Hanseeuw, Bernard 709
VeraBIND Tau test, a novel plasma assay for active tau pathology, identifies individuals with positive F18MK6240 tau-PET signal regardless of amyloid status 709
Friday, January 17, 2025 - 02:50 pm - 02:55 pm 712
Podium Session 712
Blitz Session 3B: Short Poster Presentations 712
Heinrich, Lukas 713
Locus coeruleus - medial temporal lobe functional connectivity confers protection against amyloid-related cognitive decline in the context of high cognitive reserve 713
Groh, Jenna 717
Association of a unique pattern of white matter T2 FLAIR hyperintensities with plasma and tau PET biomarkers in former American football players 717
Friday, January 17, 2025 - 03:50 pm - 05:15 pm 721
Podium Session 721
SESSION IX: Plasma Biomarkers: Application 721
Feizpour, Azadeh 722
Positive plasma Aβ42/40 despite negative Amyloid PET: A harbinger of progression to amyloid PET positivity? 722
Ferreira, Pamela 723
Head-to-head association of plasma p-tau217 with MK6240, Flortaucipir, PI2620, and RO948 Tau PET Tracers 723
Cogswell, Petrice 726
Modeling the temporal progression of plasma and PET AD biomarkers with cognition 726
Zammit, Matt 730
Comparison of amyloid PET, tau PET, and pTau217 biomarker progression between Down syndrome and neurotypical adults with sporadic Alzheimer's disease 730

WELCOME!

Dear Attendees,

On behalf of the HAI2025 Executive Committee, it is my distinct pleasure to welcome you to the vibrant and sunny shores of San Juan, Puerto Rico! After many wonderful years in Miami, we decided it was time to pack our scientific curiosity (and sunscreen) and set sail for new horizons. Puerto Rico's rich culture, historic charm, and warm hospitality promise to add a unique flair to this year's conference—and perhaps inspire a few research breakthroughs along the way.

This year's program is nothing short of remarkable, with **174 posters** and **41 podium presentations** carefully selected from a pool of **221 outstanding submissions**. These numbers aren't just metrics; they're a testament to the brilliance and dedication of our community. From innovative imaging techniques to the relentless pursuit of understanding dementia, you've once again shown that the frontiers of science are never static.

We owe a debt of gratitude to our sponsors, whose support has been instrumental in making HAI2025 possible. A heartfelt *igracias!* to our sponsors for believing in the transformative power of this community.

Special thanks go to the Program Committee members, Theme Co-Chairs, Award Judges and Executive Committee whose expertise and countless hours of work have shaped an exceptional program. Their dedication ensures these three days will be a rich tapestry of **scientific discovery, networking, and mentorship opportunities.**

As we gather here in Puerto Rico, let us celebrate not just the knowledge we'll share but the connections we'll forge. This conference is more than an event; it's a community—a dynamic, collaborative force driving progress in our field.

So, let's dive into the science, soak in the inspiration, and perhaps take a moment to appreciate the beauty of our surroundings. After all, innovation flourishes when fueled by curiosity, collaboration—and just a little Caribbean breeze.

Welcome to HAI2025. Let's make it unforgettable.

With best regards,



Keith Johnson, MD

DIAMOND ELITE

PALLADIUM

GOLD

SILVER/ SCHOLARSHIP

SILVER

BRONZE

ALZHEIMER'S® ASSOCIATION

LANTHEUS™

Lilly

Eisai

ENIGMA BIOMEDICAL GROUP

Biogen

Bristol Myers Squibb™

RAINWATER Charitable Foundation

perceptive

Life HEALTH CARE Molecular Imaging

Johnson&Johnson

XingImaging
Radiopharmaceutical Production and PET Acquisition

abbvie

ALAMAR BIOSCIENCES

C2N DIAGNOSTICS

FUJIREBIO

GE HealthCare

Quanterix
Discovery Fueled by Ultra-Sensitivity

sanofi

HAI COMMITTEES

HAI 2025 EXECUTIVE COMMITTEE

Keith Johnson, MD, *Massachusetts General Hospital*
Maria Carrillo, PhD, *Alzheimer's Association*
Teresa Gomez-Isla, MD, PhD, *Massachusetts General Hospital*
Thomas Karikari, PhD, *University of Gothenburg*
Beth Mormino, PhD, *Stanford University*
Julie Price, PhD, *Massachusetts General Hospital*

HAI 2025 THEME CO-CHAIRS

Suzanne Baker, PhD, *Lawrence Berkeley National Laboratory*
Tobey Betthauser, PhD, *University of Wisconsin*
Anne Cohen, PhD, *University of Pittsburgh*
Brad Christian, PhD, *University of Wisconsin*
Teresa Gomez-Isla, MD, *Massachusetts General Hospital*
Ansel Hillmer, PhD, *Yale University School of Medicine*
Milos Ikonomovic, MD, *University of Pittsburgh*
Heidi Jacobs, PhD, *Massachusetts General Hospital*
Thomas Karikari, PhD, *University of Pittsburgh*
Susan Landau, PhD, *University of California, Berkeley*
Laetitia Lemoine, PhD, *Perceptive*
Beth Mormino, PhD, *Stanford University*
Melissa Murray, PhD, *Mayo Clinic*
Julie Price, PhD, *Harvard Medical School*
Gil Rabinovici, MD, *University of California, San Francisco*
Pedro Rosa-Neto, PhD, *McGill University*
Suzanne Schindler, MD, PhD, *Washington University in St Louis*
Henrik Zetterberg, MD, *University of Gothenburg*

HAI 2025 YOUNG INVESTIGATOR AWARD JUDGES

Hartmuth Kolb, PhD, *Enigma Biomedical Group*
Dawn Matthews, PhD, *ADM Diagnostics*
Michael Pontecorvo, PhD, *Avid Radiopharmaceuticals*
Sandra Sanabria, PhD, *Genentech*

HAI 2025 PROGRAM COMMITTEE

Suzanne Baker, PhD, *Lawrence Berkeley National Laboratory*
Tobey Betthauser, PhD, *University of Wisconsin*
Marianne Chapleau, PhD, *Life Molecular Imaging*
Brad Christian, PhD, *University of Wisconsin*
Anne Cohen, PhD, *University of Pittsburgh*
Teresa Gomez-Isla, MD, *Massachusetts General Hospital*
Ansel Hillmer, PhD, *University of Michigan*
Kenji Ishii, MD, *Tokyo Metropolitan Inst. of Gerontology*
Milos Ikonomovic, MD, *University of Pittsburgh*
Clifford R. Jack, MD, *Mayo Clinic*
Heidi Jacobs, PhD, *Massachusetts General Hospital*
Renaud La Joie, PhD, *University of California, San Francisco*
Susan Landau, PhD, *University of California, Berkeley*
Laetitia Lemoine, PhD, *Perceptive*
Beth Mormino, PhD, *Stanford University*
Melissa Murray, PhD, *Mayo Clinic*
Agneta Nordberg, MD, PhD, *Karolinska Institute*
Rik Ossenkoppele, PhD, *VU University Medical Center*
Julie Ottoy, PhD, *University of Toronto*
Julie Price, PhD, *Harvard Medical School*
Gil Rabinovici, MD, *University of California, San Francisco*
Susan Resnick, PhD, *National Institute on Aging*
Dorene Rentz, PsyD, *Brigham and Women's Hospital*
Pedro Rosa-Neto, MD, PhD, *McGill University*
Stephen Salloway, MD, *Brown University*
Sandra Sanabria, PhD, *Genentech*
Suzanne Schindler, MD, PhD, *Washington University in St Louis*
Christopher Schwarz, PhD, *Mayo Clinic*
Reisa Sperling, MD, *Brigham and Women's Hospital*
Rik Vandenberghe, MD, PhD, *KU Leuven*
Victor Villemagne, MD, *University of Pittsburgh*
Sylvia Villeneuve, PhD, *McGill University*
Christina Young, PhD, *Stanford University*
Henrik Zetterberg, MD, *University of Gothenburg*

POSTER INDEX *(by board number)*

Board #	Poster Title	Authors	Presenter
DAY 1			
01	Decline in everyday functioning over time relates to amyloid and tau in cognitively unimpaired older adults	Dubbelman | Liu | Donohue | Langford | Raman | Rentz | Amariglio | Sperling | Aisen | Marshall	**Dubbelman, Mark**
02	From the clinical utility of a-synuclein PET imaging in Multiple System Atrophy to the possible diagnosis of Parkinson's disease	Vokali | Molette | Rodriguez | Changizi2 | Kuzkina | Ravache | Dimitrakopoulos | Delgado | Kocher | Pittet | Vallet | Hliva | Pfeifer | Kosco-Vilbois | Derouazi | Khurana | Capotosti	**Capotosti, Francesca**
03	Unraveling the impact of amyloid-β and tau pathology on brain structure and cognitive function during preclinical and prodromal Alzheimer's disease	Qiu | Liu | Gallego-Rudolf | Edde | Caron | Zhang | Soucy | Spreng | Descoteaux | Villeneuve	**Qiu, Ting**
04	Astrogliosis, a potential non-Aβ pathway to tau	Villemagne | Cohen | Lopresti | Saeed | Tudorascu | Gogola | Matan | Reese | Snitz | Ikonomovic | Reis | Launer | Lopez	**Villemagne, Victor**
05	APOE ε4 carriers exhibit attenuated habituation in pupil size and practice effects on a repeated auditory oddball task	Grube | Rodríguez Alonso | Engels-Domínguez | Jacobs | Riphagen	**Grube, Jill**
06	Baseline tau burden and performance on a digital clock drawing test uniquely contributes to predicting future tau accumulation in preclinical AD	Fu | Robinson | Farrell | Jutten | Thibault | Rodriguez Alonso | Thompson | Lois | Tiss | Gong | Chen | Penney | Davis | Sperling | Johnson | Rentz | Price	**Fu, Jessie Fang-Lu**
07	Molecular correlates of apraxia in Alzheimer's disease: A PET imaging study	Bischof | Jaeger | Giehl | jessen | Onur | O'Bryant | Kara | Weiss | Drzezga	**Bischof, Gerard**
08	Understanding the impact of race on white matter hyperintensities in Alzheimer's disease: Findings from the ADNI Study	Ekuta | Ahn | Tripodis | Hamilton	**Ekuta, Victor**
09	Characterization of a limbic-predominant amnestic neurodegenerative syndrome	Corriveau-Lecavalier | Waniger | Stricker | Machulda | Fields | Botha | Graff-Radford | Ramanan | McCarter | Nguyen | Reichard | Boeve | Knopman | Lowe | Dickson | Murray | Graff-Radford | Petersen | Jack | Jones	**Corriveau-Lecavalier, Nick**
10	Positron emission tomography analysis with the dynamicpet Python package	Bilgel | Amer | Bae | Bouhrara | Gong | Guo | Uriarte-Lopez | Singh | Matheson | Nørgaard	**Bilgel, Murat**
11	Targeted plasma eQTL and pQTL to identify potential novel biomarker for Alzheimer's disease in African Americans	Colón-Badillo | Reddy | Jin | Lincoln | Ho | Crook | Wang | Malphrus | Nguyen | Marrero-Polanco | Tamvaka | Lucas | Graff-Radford | Ertekin-Taner | Carrasquillo	**Colón-Badillo, Vanessa**

Board #	Poster Title	Authors	Presenter
12	Pathological and clinical trajectories of preclinical Alzheimer's disease patients with divergent cortical tau patterns	Young | Carlson | Cody | Winer | Schultz | Mormino	**Mormino, Elizabeth**
13	Evaluation of a label-free X-ray based method for estimating amyloid load in the human brain	Geremia | Amer | Dahal | Badano	**Geremia, Danielle**
14	Proteomic analyses of A-T-N reveal plasma mediators of neurodegeneration and dementia risk	Duggan | Bilgel | Chen | Moghekar | Davatzikos | Coresh | Resnick | Walker	**Duggan, Michael**
15	The spatial spread of tauopathy precedes the increase in tau-PET load in Alzheimer's disease	Cassa Macedo | Therriault | Rahmouni | Tissot | Aumont | Wang | Servaes | Trudel | Hall | Hosseini | Fernandez-Arias | Bezgin | Chan | Zheng | Ferrari-Souza | Ferreira | Bellaver | Lussier | Pascoal | Rosa-Neto	**Cassa Macedo, Arthur**
16	Distinct patterns of Iron distribution in the entorhinal cortex-hippocampus system for characterization of mild cognitive impairment	Kagerer | Vionnet | van Bergen | Meyer | Gietl | Prüssmann | Hock | Unschuld	**Unschuld, Paul**
17	Pathological asymmetry in early onset AD reflects heterogenous disease trajectories	Ziontz | Maiti | Zhang | Chiotis | Blazhenets | Rocha | Shankar | Amuiri | Schonhaut | Hammers | Eloyan | Koeppe | Carrillo | Dickerson | Apostolova | Rabinovici | La Joie	**Ziontz, Jacob**
18	Characterizing amyloid-positive with low Tau (A+T-) profiles and their association with cognitive trajectories in the Longitudinal Early-Onset Alzheimer's Disease Study (LEADS): A multi-method approach	Abu Raya | Soleimani-Meigooni | Schonhaut | Blazhenets | Chiotis | Lagarde | Vrillon | Maiti | Windon | Zeltzer | Zhang | Yballa | Shankar | Amuiri | Rocha | Hammers | Eloyan | Carrillo | Koeppe | Dickerson | Apostolova | Rabinovici | La Joie	**Abu Raya, Maison**
19	The association between amyloid and physical activity in a racially diverse cohort of older adults	Dong | Wu | Minhas | Laymon | Villemagne | Lopez | Snitz | Gogniat | Glynn | Tudorascu | Cohen	**Dong, Yiwen**
20	Whole blood gene expression is associated with plasma p-tau217 levels via amyloid-PET and sex	Buckley | Janve | Seto | Klinger | Brown | Birkenbihl | Coughlan | Townsend | Properzi | Zyski | Wang | Clifton | Hanseeuw | Chhatwal | Yang | Rissman | Aisen | Cuppels | Donohue | Raman | Johnson | Sperling | Dumitrescu | Hohman	**Buckley, Rachel**
21	Plasma Aβ as predictor of Aβ accumulation in non-demented participants	Gogola | Cohen | Lopresti | Snitz | Ikonomovic | Tudorascu | Minhas | Kofler | Matan | Aizentein | Lopez | Karikari | Villemagne	**Gogola, Alexandra**
22	The relative prevalence of tau severity stages is related to amyloid burden, clinical diagnosis and age	Cody | Sokolowski | Carlson | Medina | Winer | Young | Younes | Durant | Dumitrescu | Archer | Tosun-Turgut | Johnson | Harrison | Hohman | Mormino	**Cody, Karly**
23	Head-to-head trajectories of tau PET and plasma p-tau217 as a function of Aβ	Bellaver | Povala | L. Ferreira | Bauer-Negrini | Lussier | Amaral | Soares | Rocha | Masdeu | Tudorascu | Soleimani-Meigooni	**Bellaver, Bruna**

Board #	Poster Title	Authors	Presenter
		| Fortea | Lowe | Oh | Pascual | A. Gordon | Rosa-Neto | Baker | A. Pascoal	
24	Functional submodules in the human locus coeruleus are differentially susceptible to tau pathology	Lawn | Prokopiou | Van Egroo | Ashton | Janelidze | Blennow | Hansson | Zetterberg | Jacobs	**Lawn, Timothy**
25	Sex-specific associations of BMI, amyloid, and regional tau deposition in community-dwelling cognitively normal older adults	Gills | Cesar | Dominguez | Sogade | Browne | Weisgerber | McBride | Valkanova | Mbah | Figueredo | Jean-Louis | Masurkar | Osorio | Bubu	**Gills, Joshua**
26	Assessment of ATN with a single dynamic [18]F-PI-2620 recording	Gnörich | Kusche-Palenga | Kling | Zatcepin | Dehsarvi | Bronte | Zaganjori | Frontzkowski | Roemer | Groß | Schöberl | Scheifele | Bauer | Bernhardt | Jäck | van Eimeren | Drzezga | Perneczky | Bürger | Levin | Bartenstein | Sabri | Barthel | Rullmann | Stöcklein | Höglinger | Franzmeier | Brendel	**Gnörich, Johannes**
27	Tau-PET detects advanced primary age-related tauopathy mimicking early-stage AD	Grothe | Moscoso | Labrador-Espinosa | Silva-Rodríguez | Heeman | Costoya-Sánchez | Camacho | van Essen | Mainta | Perissinotti | Rodríguez-Fonseca | Ribaldi | Devous, Sr. | Pontecorvo | Frisoni | Garibotto | Schöll	**Grothe, Michel**
28	Amyloid status moderates associations between hippocampal microstructure, PET tau burden, and memory in dementia-free older adults	Callow | Rani | Alm | Pettigrew | Soldan | Miller | Albert | Bakker	**Callow, Daniel**
29	Performance of an MR-independent analysis pipeline for quantification of tau abnormality using [18F]flortaucipir PET	DelBene | Gogola | Reese | Matan | Chiang | Snitz | Cohen | Lopez | Villemagne | Lopresti	**DelBene, Alexander**
30	Functional and structural connectivity patterns predict longitudinal tau spreading in asymptomatic individuals expressing Aβ pathology	Gallego-Rudolf | Qiu | Javanray | Wiesman | St-Onge | Fajardo-Valdez | Baillet | Villeneuve	**Gallego-Rudolf, Jonathan**
31	Plasma phospho-tau 217, neurofilament-light, and glial fibrillary acidic protein are differentially associated with longitudinal neuropsychiatric symptoms across the early cognitive spectrum	Gatchel | Yu | Palmer | Wu | Beltran | Munro | Webb | Blacker | Arnold | Marshall | Dodge	**Gatchel, Jennifer**
32	An assessment of the utility of flortaucipir PET to detect four-repeat tau pathology in a globular glia tauopathy case-series	Gatto | Youssef | Ghatamaneni | Uruk | Min | Fu | Reichard | Lowe | Dickson | Whitwell | Josephs	**Gatto, Rodolfo**
33	Molecular imaging of neurodegeneration – mitochondria, associated proteins and synapses (MIND-MAPS) in frontotemporal dementia	Clarke | Whittington | Passchier | Lewis | Passamonti | Chen | Salinas | Tsukada | Cash | Rabiner | Rohrer	**Clarke, Mica**
34	Evaluating tVNS effects on cognitive outcomes and modulating factors in asymptomatic older adults: study design of the WALLe Trial	Engels-Domínguez | Grube | Fenlon | Wiklund | Heinrich | Baillet | van Egroo | Papp | Riphagen | Garcia | Sclocco | Johnson | Napadow | Jacobs	**Engels-Domínguez, Nina**

Board #	Poster Title	Authors	Presenter
35	Cerebral perfusion indices from early-phase [18F]-MK6240 dynamic Tau PET imaging in brain regions associated with Alzheimer's disease progression in an aging population.	Dhaynaut | Lois | Tiss | Thibault | Fanglu Fu | Ouyang | Johnson | El Fakhri | Normandin | Guehl	**Dhaynaut, Maeva**
36	Transcutaneous auricular vagus nerve stimulation improves learning and sleep-wake quality in older APOE-ε4 carriers	Baillet | Van Egroo | Engels-Domínguez | Grube | Fenlon | Wiklund | Heinrich | Riphagen | Papp | Garcia | Sclocco | Napadow | Jacobs	**Baillet, Marion**
37	Biological-clinical mismatch reflects co-pathology and vulnerability to neurodegeneration	Brown | Das | Xie | Nasrallah | Detre | Yushkevich | McMillan | Wolk	**Brown, Christopher**
38	Validation of PET spatial extent as sensitive amyloid biomarker in early stages of amyloidosis	Del Carmen Montenegro | Thibault | Fanglu Fu | Price | Hanseeuw | Jacobs | Sperling | Johnson | Farrell	**Del Carmen Montenegro, Grace**
39	P-TAU217, GFAP, and NFL plasma biomarker associations with demographic, medical and neurocognitive features from middle-aged through older adulthood	Arnold | Kivisakk | Fatima | Gentsch | Cruchaga | Wu | Dodge | Ances | Salat	**Arnold, Steven**
40	DeepSUVR: Using temporal constraints to improve tau quantification	Bourgeat | Fripp | Gillman | Feizpour | Schwarz | Jack | Lowe | Weiner | Masters | Villemagne | Rowe | Dore	**Bourgeat, Pierrick**
41	Developing a novel reference region for PI-2620-PET imaging to facilitate assessment of 4-repeat tauopathies	Frontzkowski	**Frontzkowski, Lukas**
42	Increasing the granularity of tau-PET Braak staging using medial temporal lobe segmentations to detect early memory impairment	Aumont | Hall | Trudel | Chan | Hosseini | Macedo | Fernandez Arias | Rahmouni | Therriault | Servaes | Bezgin | Stevenson | Rosa-Neto	**Aumont, Etienne**
43	The universal tau PET scale (Uniτ) for Flortaucipir, MK6240, PI2620 and RO948 harmonization	Povala | Bauer-Negrini | Bellaver | Z. Lussier | Amaral | Lukasewicz Ferreira | L. Tudorascu | Finn | Masdeu | Soleimani-Meigooni | Fortea | Lowe | Oh | Pascual | A. Gordon | Rosa-Neto | Baker | A. Pascoal	**Povala, Guilherme**
44	Assessing the relationship between neuropsychiatric symptoms, amyloid and tau pathology, and white matter hyperintensity volume across sexes in preclinical Alzheimer's disease	Garrone | Yakoub | Fajardo-Valdez | Qiu | Ourry | Villeneuve	**Garrone, Aurélie**
45	Unveiling the heterogeneity of tau spreading in aging and Alzheimer's disease using polygenic combinations: Towards personalized models	Diez | Lois | Garcia Condado | Farrell | Thibault | Jacobs | Buckley | Hanseeuw | Properzi | Yang | Sperling | Cortes | Quiroz | Sepulcre | Johnson | Gomez-Isla	**Diez, Ibai**
46	Regional amyloid and tau: Exploring regional sex-based differences in a middle-aged community-based cohort	Guzmán | Aziz | Smith | Houlihan | Sanchez | Luchsinger | Lao	**Guzmán, Diana S**
47	Comparison of topographical patterns of abnormalities of the tau PET tracers [18F]Flortaucipir, [18F]MK6240, [18F]PI2620, and [18F]RO948	Amaral | Povala | Bauer-Negrini | Ruppert | Bellaver | Lussier | L. Ferreira | Masdeu | Tudorascu | Soleimani-Meigooni | Fortea |	**Amaral, Livia**

Board #	Poster Title	Authors	Presenter
		Lowe | Oh | Pascual | Gordon | Rosa-Neto | Baker | Pascoal	
48	Subtle cognitive deficits detected through routine in-office tests are associated with global Aβ and temporal tau in cognitively unimpaired individuals	Felix | Rebok | Kollasserry | Snitz | Ferreira | Tudorascu | Povala | Saha | Amaral | Lussier | Masdeu | Soleimani-Meigooni | Fortea | Lowe | Oh | Gordon | Rosa-Nato | Baker | Nasreddine | Pascoal	**Felix, Cynthia**
49	Estradiol-dependent associations between sleep complaints and tau deposition in women at elevated AD risk	Lui | Wang | Deyong | Malhotra | Sundermann | Banks	**Banks, Sarah**
50	Impact of age and sex on extra-cerebral off-target binding in tau PET scans (18F-FTP)	Ghatamaneni | Kim | Nycklemoe | Lundt | Schwarz | Kandimalla | Jacobson | Albertson | Jack | Gunter | Peterson | kung | sharma | seokbeen | Lowe | Min	**Ghatamaneni, Sujala**
51	Metabolic inefficiency is associated with regional vulnerability to tau deposition	Adams | Parker | Zhao | Yassa	**Adams, Jenna**
52	Relationship between Polygenetic Risk Score of BrainAge and plasma biomarkers in the A4/Elearn Study	Garcia Condado | Birkenbihl | Cortes | Buckley | Diez	**Garcia Condado, Jorge**
53	Combined impact of plasma phospho-tau 217 and NfL on longitudinal domain-specific cognitive decline	Dodge | Wu | Chen | Gatchel | Das | Kivisäkk | Arnold	**Dodge, Hiroko**
54	Comparison of distribution volume and standardized uptake value ratio for a MAO-B tracer in mild cognitive impairment	Bezgin | Rahmouni | Harada | Okamura | Benedet | Ashton | Zetterberg | Blennow | Rosa-Neto	**Bezgin, Gleb**
55	Association between early and late tau aggregation across tau imaging agents: The HEAD Study	Rahmouni | Tissot | Therriault | Hosseini | Macedo | Servaes | Lussier | Trudel | Hall | Fernandez-Arias | Wang | Stevenson | Gauthier | Baker | Pascoal | Rosa-Neto	**Rahmouni, Nesrine**
56	The impact of spatial smoothing on the accuracy of Centiloid thresholds	Fajardo-Valdez | Qiu | Gallego-Rudolf | Javanray | Villeneuve	**Fajardo-Valdez, Alfonso**
57	Longitudinal amyloid PET trajectories in the HABS-HD cohort	Betthauser | Morse | Heston | Langhough | Carey | Wisch | Ances | Cohen | Toga | Braskie | Zuelsdorff | O'Bryant | Meeker	**Betthauser, Tobey**
58	Lower microstructural integrity of the locus coeruleus to entorhinal cortex pathway is related to elevated astrocyte reactivity and tau burden in cognitively unimpaired individuals: a 7T dMRI study	Patsyuk | Van Egroo | Beckers | Ashton | Janelidze | Blennow | Hansson | Zetterberg | Poser | Jacobs	**Patsyuk, Yuliya**
DAY 2			
59	Interpretable prediction of amyloid PET positivity using non-negative matrix factorization	Zhang | Barnard | Gogineni | Corriveau-Lecavalier | Botha | Burkett | Johnson | Lowe | McCarter | Ramanan | Graff-Radford | Knopman | Petersen | Jones	**Jones, David**
60	Data-driven biomarker discovery nominates novel diagnostic plasma biomarkers and provides insights into	Kuchenbecker | Thompson | Hurst | Opdenbosch | Heckman | Reddy | Nguyen | Casellas | Sotelo | Redy | Lucas | Day |	**Kuchenbecker, Lindsey**

Board #	Poster Title	Authors	Presenter
	Alzheimer's disease pathophysiology in an African American cohort	Willis | Graff-Radford | Ertekin-Taner | Kalari | Carrasquillo	
62	Longitudinal multicenter head-to-head harmonization of tau PET tracers: an overview of the HEAD study cohort	Lussier | Povala | Bauer-Negrini | Silva do Amaral | Lukasewicz Ferreira | Bellaver | Masdeu | Tudorascu | Soleimani-Meigooni | Fortea | Lowe | Oh | Pascual | Gordon | Rosa-Neto | Baker | Pascoal	**Lussier, Firoza**
63	Higher time varying brain functional connectivity is associated with slower tau accumulation at the preclinical stage of Alzheimer's disease	Javanray | St-Onge | Bellec | Misic | Soucy | Villenueve	**Javanray, Mohammadali**
64	Graph convolutional networks to predict cognitive decline at the individual level in Alzheimer's disease	Kang | Heaton | Nyman | Biparva | McSweeney | Ottoy | Masellis | Shirzadi | Johnson | Sperling | Schultz | Jasmeer | Swardfager | Lipsman | Black | Rabin | Goubran	**Kang, Min Su**
65	Low tau in Aβ-positive cognitively impaired individuals: Alzheimer's disease or something more?	Ioannou | Abdullaieva | J. Perrin | Bluma | Poulakis | Leuzy | Religa | Rodriguez-Vieitez | Chiotis	**Ioannou, Konstantinos**
66	A plasma clock for Alzheimer disease based on %p-tau217	Petersen | Milà-Alomà | Tosun | Li | Shaw | Dage | Zetterberg | Saef | Holtzman | Morris | Xiong | Bateman | Bannon | Potter | Schindler	**Petersen, Kellen**
67	Network-based amyloid-β pathology predicts subsequent cognitive decline in cognitively normal older adults	He | Razlighi | Gazes | Habeck | Stern	**He, Hengda**
68	Associations between APOE-TOMM40 '523 haplotype variants and limbic system white matter microstructure in Black and White individuals	Mooney | Archer | Sathe | Hohman | Kadiri | Lamar | Arfanakis | Yu | Barnes | Deters	**Mooney, Katelyn**
69	Multi element MRI template method for analysis of Down syndrome PET	Laymon | Minhas | Heffley | Gilmore | Kondaveeti | Gogola | Royse | Joshi | Lopresti | Luo | Davuluri | Matan | Tudorascu | Christian | Zaman | Beau | Cohen | Handen	**Laymon, Charles**
70	Whole-blood gene expression associations with Aβ-PET accumulation and cognitive decline	Klinger | Janve | Seto | Brown | Birkenbihl | Coughlan | Townsend | Zyski | Wang | Amariglio | Papp | Rentz | Yang | Chhatwal | Clifton | Donohue | Raman | Rissman | Aisen | Johnson | Sperling | Dumitrescu | Hohman | Buckley	**Klinger, Hannah**
71	Longitudinal change in five dominant dimensions of brain aging in relation to brain amyloid status and Alzheimer's-related plasma biomarkers	Bilgel | Shah | Cooper | An | Walker | Moghekar | Yang | Erus | Davatzikos | Resnick	**Bilgel, Murat**
72	Enrichment of patients with concomitant LATE on the Alzheimer's disease continuum using hippocampal volume	Mundada | Lyu | Sadeghpour | Brown | McCrew | Xie | Yushkevich | Das | Wolk	**Mundada, Nidhi**

Board #	Poster Title	Authors	Presenter
73	AT(N) staging of Alzheimer's disease: Comparison of visual interpretation and automated quantification pipelines	Lopresti | Cohen | DelBene | Reese | Matan | Gogola | Chiang | Snitz | Royse | Lopez | Villemagne	**Lopresti, Brian**
74	MK-6240 off-target binding patterns in relation to microglia density, measured through TSPO PET	Heuer | Johnson | Smith | Guzman | Houlihan | Okafor | Sanchez | Talmasov | Dass | Chikwem | Provenzano | Kreisl | Noble | Small | Lao	**Heuer, Lauren**
75	Association between medication use and [18F]MK6240 and [18F]Flortaucipir uptake across the Alzheimer's disease spectrum	Mroué | Lukasewicz Ferreira | Povala | Bellaver | Bauer-Negrini | Lussier | Amaral | Scop Medeiros | Ruppert | Silva da Rocha | Scarpatto Rodrigues | Silva Oliveira | Soares Katz | Teixeira Leffa | Saha | Felix | Masdeu | Soleimani-Meigooni | Fortea | Lowe | Oh | Pascual | Gordon | Rosa-Neto | Baker | Pascoal	**Mroué, Rayan**
76	Lower LC-EC tract integrity is associated with entorhinal tau in autosomal-dominant Alzheimer's disease	Koops | Giudicessi | Bonillas-Felix | Medrano | Martinez | Gonzalez | Alvarez | Aguillon | Quiroz | Jacobs	**Koops, Elouise**
77	APOE4 associated with higher off-target meninges signal with [F-18]MK6240 PET	McVea | DiFilippo | McLachlan | Bettcher | Tudorascu | Johnson | Zammit | Betthauser | Christian	**McVea, Andrew**
78	An accurate and automated technique for removing spill-over contamination and off-target retention from a cerebellar reference region for tau PET	Minhas | DelBene | Gogola | Reese | Luo | Laymon | Lopresti | Dore | Pascoal | Baker | Tudorascu | Villemagne	**Minhas, Davneet**
79	Updated public CenTauR pipelines to measure CenTauR, CenTauRZ, and SUVR tau PET units	Schwarz | Leuzy | Doré | Villemagne | Xiao | Pappas | Przybelski | Prakaashana | Senjem | Lowe | Gunter | Kantarci | Vemuri | Graff-Radford | Petersen | Knopman | Jack	**Schwarz, Christopher**
80	Predicting regional Alzheimer's disease pathology with plasma p-tau217 in preclinical AD	Moon | Chen	**Moon, Hasom**
81	TSPO-PET before and after low-dose interleukin-2 in patients with mild to moderate Alzheimer's disease	Pascual | Faridar | Finn | Gamez | Appel | Masdeu	**Pascual, Belen**
82	In low neocortical tau individuals, high amygdala tau predicts faster cognitive decline	Hanseeuw | Thibault | Farell | Buckley | Properzi | Gatchel | Amariglio | Marshall | Beiser | Seshadri | De Carli | Sperling | Jacobs | Johnson	**Hanseeuw, Bernard**
83	EOAD-signature atrophy predicts progression to dementia in patients with early-onset MCI due to Alzheimer's disease	Paranhos | Katsumi | Brickhouse | Eckbo | Zaitsev | Du | Eloyan | Nudelman | Foroud | Dage | Carrillo | Rabinovici | Apostolova | Dickerson | Touroutoglou | Consortium	**Katsumi, Yuta**
84	FDG reference region selection using PiB amyloid status-guided iterative normalization in a Down syndrome cohort	McLachlan | Keator | Price | Tudorascu | Laymon | Cohen | Lao | Handen | Fryer | Ances | Zaman | Head | Mapstone | Bettcher | Guerrero Gonzalez | LeMerise | McVea | DiFillipo | Zammit | Hartley | Christian	**McLachlan, Max**

Board #	Poster Title	Authors	Presenter
85	Microscopic visualization of fluorescent MK-6240	Kunach | S. Smith | I. Antczak | Gupta | Monistrol | Tripathi | Jalapati | Guiot | Stoddard | H. Shahmoradian | K. Shoichet | Vaquer-Alicea | Rosa-Neto | M. Ready | I. Diamond	**Kunach, Peter**
86	Conversion of Tau PET SUVR data to CenTauR units using the Joint Propagation Model	Leuzy | Raket | Villemagne | Klein | Tonietto | Olafson | Baker | Saad | Bullich | Lopresti | Sanabria Bohorquez | Lutz | Boada | Betthauser | Charil | Collins | Collins | Gunn | Higuchi | Hostetler | Hutchison | Iaccarino | Insel | Irizarry | Jack Jr | Jagust | Johnson | Johnson | Karten | Marquié | Mathotaarachchi | Mintun | Ossenkoppele | Pappas | Petersen | Rabinovici | Rosa-Neto | Schwarz | Smith | Stephens | Whittington | Carrillo | Pontecorvo | Haeberlein | Dunn | Kolb | Stephenson | Rowe | Hansson | Doré	**Leuzy, Antoine**
87	The role of cohort heterogeneity in predicting AD/ADRD cognitive decline	Liu | Taggett | Harrison | Snyder | DeCarli | Vemuri | Harvey | Jagust | Baker | Landau	**Liu, Peiwei**
88	Differential tau accumulation in early-onset and late-onset Alzheimer's disease: Insights from [18F]-Florzolotau PET	Khurelbaatar | Huang | Lin | Huang | Hsu | Huang | Wu | Huang | Chang | Hsiao	**Khurelbaatar, Bayarjargal**
89	Heterogeneity of FDG-PET patterns among tau-negative amnestic patients	Silva-Rodríguez | Moscoso | Labrador-Espinosa | Sánchez-Juan | Scholl | Grothe	**Silva-Rodríguez, Jesús**
90	Predicting amyloid positivity and tau burden in dementia using a combination of different biomarkers	Huang | Lin | Huang | Huang | Wu | Chang | Hsiao	**Huang, Shao-Yi**
91	Evaluation of [^{3}H]SynVesT - 1 binding in post-mortem brain tissue from control and Alzheimer's disease as a biomarker of synaptic loss	Kulagowska | Lemoine | King | Gladstein | Bevis | Bonsall | Finnema | Spires-Jones | Wells | SV2A project team	**Kulagowska, Laura**
92	Exploring the predictive power of graph-theoretic metrics for tau pathology in cognitively unimpaired older adults	Johns | Vin | Abuwarda | Fredericks	**Johns, Emily**
93	Tracking biomarkers accuracy for predicting progression to mild cognitive impairment	Gallego-Rudolf | Wiesman | Baillet | Villeneuve	**Gallego-Rudolf, Jonathan**
94	Tau burden across Braak stages is associated with regionally specific amyloid accumulation: insights from the BIOCARD cohort	Rani | Alm | Callow | Pettigrew | Soldan | Miller | Albert | Bakker	**Rani, Nisha**
95	Relationship between neuroinflammatory ER176-PET and functional connectivity in Progressive Apraxia of Speech	Singh-Reilly | Sintini | Satoh | Duffy | Utianski | Clark | Stephens | Lowe | Josephs | Whitwell	**Singh-Reilly, Neha**
96	Sex moderates the association between regional tau and longitudinal cognitive decline in A4 and LEARN studies	Li | Klinger | Seto | Birkenbihl | Farrell | Thibault | Rissman | Properzi | Schultz | Townsend | Yang | Johnson | Reman |	**Li, Annie**

Board #	Poster Title	Authors	Presenter
		Langford | Donohue | Sperling | Buckley | Coughlan	
97	Evaluation of the Uni-tau and CenTauR frameworks in new datasets for tau PET harmonization in Alzheimer's disease	Lutz | Olafson | Tonietto | Klein | Pascoal | Negrini | Povala | Leuzy | Raket | Doren | Sanabria Bohorquez | Teng	**Lutz, Olivia**
98	Hemispheric lateralization of tau-related network dysfunction and its association with neuropsychiatric symptoms in preclinical Alzheimer's disease	Moret | Vin | Fredericks	**Moret, Sophia**
99	Characterization and correction of extracerebral [18F]MK-6240 tau PET off-target signal in Alzheimer's disease	Olafson | Tonietto | Doren | Sanabria Bohórquez	**Olafson, Emily**
100	Investigation of optimal intensity threshold for tau-PET overlap index	Lim | Lee | Min | Moloney | Mester | Ghatamaneni | Senjem | Nguyen | Graff-Radford | Schwarz | Gunter | Kantarci | Boeve | Vemuri | Jones | Jack | Petersen | Murray | Lowe	**Lim, Seokbeen**
101	DeepSUVR: Towards redefining the Centiloid masks using a data-driven approach	Bourgeat | Fripp | Lebrat | Gillman | Cox | Goyal | Tosun-Turgut | LaMontagne | Benzinger | Weiner | Morris | Villemagne | Masters | Rowe | Dore	**Bourgeat, Pierrick**
102	Mechanical stress of the entorhinal cortex: A potential driver of tau pathology?	Zhang | Crary | Provenzano	**Provenzano, Frank**
103	Amyloid-Tau to neurodegeneration mismatch from inter-modality image translation using deep learning	Lyu | Yushkevich | Dong | Khandelwal | Brown | Duong | Li | Xie | Wisse | Das | Wolk	**Lyu, Xueying**
104	Tau PET subgroups differ in network patterns of functional connectivity and amyloid PET	Millar | Doering | Adeyemo | McKay | Metcalf | Roman | Canfield | Jindal | Flores | Strain | Wisch | Hassenstab | Schindler | Morris | Gordon | Ances | Benzinger	**Millar, Peter**
105	Cortical freewater increases with tau tangle aggregation	Hall | Aumont | Rahmouni | Therriault | Hosseini | Trudel | Fernandez-Arias | Macedo | Servaes | Bezgin | Wang | Zheng | Stevenson | Sanjeewa | Benedet | Triana-Baltzer | Kolb | Ashton | Zetterberg | Blennow | Pascoal | Klostranec | Rosa-Neto	**Hall, Brandon**
106	Distinct spatiotemporal patterns of vascular disease in Alzheimer's disease subtypes	Ottoy | Yin | Kang | Gibson | Clappison | Yang | Carver | Rahmouni | Stevenson | Servaes | Therriault | Pascoal | Soucy | Gauthier | Black | Rosa-Neto | Goubran	**Ottoy, Julie**
107	Annual percent change of microglia density in relation to tau accumulation in older adults	Houlihan | Johnson | Smith | Guzman | Okafor | Heuer | Sanchez | Talmasov | Chikwem | Dass | Noble | Kreisl | Small | Lao	**Houlihan, Hannah**
108	Physical frailty as a risk factor for increased tau accumulation and cognitive decline in cognitively unimpaired older adults	Palmgren | Matos | Kirn | Robinson | Pintucci | Properzi | Schultz | Amariglio | Rentz | Johnson | Sperling | Chhatwal | Yau	**Palmgren, Kailee**

Board #	Poster Title	Authors	Presenter
109	Assessing neuroinflammation in Alzheimer's disease: A TSPO-PET study using ER176 and its correlation with amyloid and tau pathology	Kandimalla | Jacobson | Lim | Lee | Min | Botha | Graff-Radford | Jones | Vemuri | Kantarci | Knopmam | Jack | Petersen | Lowe	**Jacobson, David**
110	Two distinct sources of 18F-MK-6240 off-target signal identified by individualized head modeling and PET kinetics	Chen | Fu | Puonti | Thibault | Johnson | Price	**Chen, Charles**
112	TSPO PET mediates tau-associated neurodegeneration in limbic and temporal regions across clinical variants of Alzheimer's disease	Lao | Johnson | Smith | Guzman | Houlihan | Okafor | Heuer | Sanchez | Talmasov | Chikwem | Dass | Noble | Kreisl | Small	**Lao, Patrick**
114	Tracking plasma biomarker abnormalities with amyloid time accumulation	Bluma | Chiotis | Bucci | Savitcheva | Matton | Kivipelto | Jeromin | De Santis | Di Molfetta | Ashton | Blennow | Zetterberg | Nordberg	**Bluma, Marina**
115	Advancing antibody-based pretargeted PET imaging of protein aggregates in the brain	Gustavsson | Honer | Hvass | Shalgunov | Clausen | Stotz | Wünsche | Lopes van den Broek | Knudsen | Aldana | Niewoehner | Gobbi | Kustermann | Battisti | Kjær | Herth	**Honer, Michael**
116	Longitudinal change in mnemonic discrimination and influence of Aβ burden	Kraft | Nair | Gonen | Skotnicki | Rodrigue | Kennedy	**Kraft, Jessica**
DAY 3			
117	Concordance between visual and quantitative amyloid PET and CSF biomarkers in the ADNI-DOD cohort	Vrillon | Blazhenets | Lagarde | Chiotis | Abu Raya | Soleimani-Meigooni | Rabinovici | Weiner | Silbert | Hantke | Schwartz | Livny Ezer | Lesman Segev | Yaffe | Shaw | Landau | La Joie | Gardner	**Vrillon, Agathe**
118	Calibration of multi-site raters for prospective visual read of amyloid PET scans acquired across the ADRC Consortium for Clarity in ADRD Research Through Imaging (CLARiTI)	Soleimani-Meigooni | Blazhenets | La Joie | Lin | Soppe | Johnson | Koran | McConathy | Nasrallah | Tanner | Villemagne | Windon | Zeineh | Mormino | Johnson | Rabinovici	**Soleimani-Meigooni, David**
119	Evaluating the effect of APOE genotype in real-world clinical settings: results from the IDEAS-ANGI study	Pezzoli | Jonson | Blazhenets | Schonhaut | Perez | Oddi | Castruita | Casaletto | Hanna | March | Gatsonis | Carrillo | Foroud | La Joie | Yokoyama | Rabinovici	**Pezzoli, Stefania**
120	Brain connectivity drives tau distribution while regional vulnerability drives tau load in Alzheimer's disease	Xiao | Bazinet | Strandberg | Hansen | Shafiei | Spotorno | Behjat | Stomrud | Smith | Palmqvist | Mattsson-Carlgren | Dagher | Misic | Hansson | Vogel	**Xiao, Yu**
121	Synergistic effects of peripheral inflammation and neuroinflammation on amyloid, vascular, and neurodegeneration markers across the Alzheimer's disease spectrum	Ramirez Tirado | Cohen | Shaaban | Matan | Lopresti | Ikonomovic | Karikari | Villemagne | Lopez	**Ramirez Tirado, Laura Alejandra**
122	Impact of amyloid removal on cerebral volume changes with Gantenerumab	Tonietto | Silvestri | Belder | Barkhof | Fox | Smith | Klein	**Tonietto, Matteo**

Board #	Poster Title	Authors	Presenter
123	Astrocyte reactivity explains tau-related effects on hippocampal dysfunction and longitudinal atrophy in preclinical Alzheimer's disease	Schweitzer | Iordanova | Chen | Jin | Thurston | Lopresti | Snitz | Tudorascu | Cohen | Kamboh | Halligan-Eddy | Karikari | Villemagne | Aizenstein | Wu	**Schweitzer, Noah**
124	Plasma phosphorylated tau 217 and longitudinal trajectories of Aβ, tau, and cognition in cognitively unimpaired older adults	Yang | Anzai | Yau | Román Viera | Maa | Kirn | Properzi | Schultz | Farrell | Jacobs | Buckley | Papp | Marshall | Amariglio | Rentz | Braunstein | Johnson | Sperling | Chhatwal	**Yang, Hyun-Sik**
125	Detection of TDP-43 from plasma-derived astrocyte extracellular vesicles for identification of LATE	Rissman	**Rissman, Robert**
126	Short sleep duration is associated with higher subsequent plasma p-tau217 in aging	Winer | Cody | Young | Mormino	**Winer, Joseph**
127	Impacts of testing language and rates of amyloid positivity among underrepresented groups in the A4 Study	Sai | D. Grill | C. Mormino | B Young	**Sai, Isha**
128	Lower locus coeruleus metabolism is associated with greater year-to-year intraindividual cognitive variability in older individuals with elevated levels of Alzheimer's disease pathology	Wiklund | Van Egroo | Koops | Hanseeuw | Papp | Rentz | Sperling | Johnson | Jacobs	**Wiklund, Emma**
129	Long-term cognitive and biomarker trajectories of cognitively unimpaired individuals with elevated plasma ptau-217	Silva-Rodríguez | Zhang | Valeriano-Lorenzo | López-González | Wagner-Reguero | del Ser | Grothe | Sánchez-Juan	**Silva-Rodríguez, Jesús**
130	A large public release of PIB PET and MRI from the Mayo Clinic Study of Aging	Schwarz | Kremers | Prakaashana | Przybelski | Christenson | Williams | Gunter | Senjem | Arani | Reid | Machulda | Fields | Lowe | Kantarci | Graff-Radford | Vemuri | Petersen | Knopman | Jack	**Schwarz, Christopher**
131	Harmonizing visual readings of Flortaucipir and MK-6240 using head-to-head data	Ruppert | Medeiros | Rocha | Soares | Amaral | Povala | Bauer-Negrini | L. Ferreira | Lussier | Oliveira Jr. | Scarpatto Rodrigues | Mroue | Zalzale | Leffa | Saha | Bellaver | L. Tudorascu | Soleimani-Meigooni | Fortea | Lowe | Oh | Pascual | A. Gordon | Rosa-Neto | Baker | A. Pascoal	**Ruppert, Emma**
132	Twin-mapping techniques in clinical trials: a proof-of-concept application to the Internet-Based Conversational Engagement Clinical Trial (I-CONECT)	Wu | Chen | Arnold | Dodge	**Wu, Chao-Yi**
133	Effects of amyloid and tau status on multiplex plasma CNS and inflammatory proteins in a normal aging cohort	Trelle | Cody | Nguyen | Winer | Weiss | Romero | Sai | Wilson | Wagner | Maecker | Mormino	**Cody, Karly**
134	Tau imaging thresholds within NIA-AA multilevel tau staging as predictors of tau accumulation and cognitive decline in non-demented individuals	Gogola | Cohen | Snitz | Minhas | Tudorascu | Ikonomovic | Shaaban | Dore | Matan | DelBene | Bourgeat | Leuzy | Aizenstein | Lopez | Lopresti | Villemagne	**Gogola, Alexandra**

Board #	Poster Title	Authors	Presenter
135	Multi-morbidity and Alzheimer's disease pathology across the lifespan in adults with Down syndrome	Smith | Edwards | Flores Aguilar | Alshikho | Tudorascu | Rosas | Yassa | Hartley | Handen | Christian | Gutierrez | Wilcock | Head | Brickman | Lao	**Smith, Anna**
136	Cortical atrophy is correlated with the discrepancy between neuroradiological assessment and binary quantitation of florbetapir PET in nondemented older adults	Schwartz | Villamizar Alvarado | Szidonya | Choudhary | Marcoe | Mar | Gillan | Hendricks | Kaye | Silbert	**Schwartz, Daniel**
137	Vascular pathology influences the association of tau-PET with neurodegeneration and cognition in Aβ-negative individuals	Silva Oliveira Junior | Bellaver | C.L. Ferreira | Povala | Bauer-Negrini | Lussier | do Amaral | Rodrigues | da Rocha | Saha | Ruppert | Soares | Leffa | Felix | Mroue | Tudorascu | Zalzale | Pascual | Gordon | Lowe | Oh | Soleimani-Meigooni | Fortea | Rosa-Neto | Baker | Pascoal	**Silva Oliveira Junior, Markley**
138	Concomitant neurodegeneration of the lateral hypothalamus and locus coeruleus is associated with early Alzheimer's disease-related pathophysiological and cognitive processes	Van Egroo | Baillet | Becker | Price | Properzi | Papp | Rentz | Sperling | Johnson | Jacobs	**Van Egroo, Maxime**
139	Amyloid-associated hyperconnectivity drives tau spreading across connected brain regions in Alzheimer's disease	Roemer-Cassiano | Wagner | Evangelista | Dehsarvi | Steward | Dewenter | Biel | Zhu | Malpetti | Höglinger | Brendel | Jäkel | Scholl | Franzmeier	**Roemer-Cassiano, Sebastian Niclas**
140	Association of plasma GFAP with tau PET in cognitively unimpaired Aβ-negative subjects	Saha | Bellaver | Povala | Ferreira | Bauer-Negrini | Silva | Lussier | Rodrigues | Oliveira | Rocha | Felix | Ruppert | Medeiros | Katz | Masdeu | Tudorascu | Soleimani-Meigooni | Fortea | Lowe | Oh | Pascual | Gordon | Rosa-Neto | Baker | Pascoal	**Saha, Pampa**
141	The striatum is an early, accurate indicator of [C-11]PiB amyloid burden for the Down syndrome population	McLachlan | Price | Tudorascu | Laymon | Lao | Handen | Fryer | Ances | Johnson | Betthauser | Zaman | Head | Mapstone | Bettcher | LeMerise | McVea | DiFillipo | Zammit | Hartley | Christian	**McLachlan, Max**
142	Best practices for tau-PET tracer harmonization in Alzheimer's research	Tissot | Tsai | Giorgio | Blazhenets | Harrison | Olafson | Sanabria | Leuzy | Doré | Jagust | Rosa-Neto | Pascoal | Baker	**Tissot, Cécile**
143	Relationship between metabolic syndrome biomarkers and regional tau accumulation in cognitively unimpaired older adults	Tennant | Luu | Hand | Lee | Toga | O'Bryant | Yaffe | Braskie	**Tennant, Victoria**
144	Association of a unique pattern of white matter T2 FLAIR hyperintensities with plasma and tau PET biomarkers in former American football players	Groh | Farris | Brickman | Alshikho | Miner | Tripodis | Cui | Adler | Balcer | Bernick | Cantu | Coleman | Dodick | Ashton | Zetterberg | Blennow | Peskind | McKee | Mez | Bouix | Cummings | Reiman | Stern | Shenton | Alosco	**Groh, Jenna**

Board #	Poster Title	Authors	Presenter
145	Relationship between flortaucipir-PET and quantitative susceptibility mapping in atypical Alzheimer's disease	Singh-Reilly | Satoh | Graff-Radford | Machulda | Lowe | Josephs | Whitwell	**Singh-Reilly, Neha**
146	Neuropathological evaluation of the off-target binding of flortaucipir in FTLD subcortical regions: interconnecting tau aggregates with iron deposition and neuroinflammation	Gatto | Youssef | Uruk | Fu | Reichard | Lowe | Whitwell | Josephs	**Gatto, Rodolfo**
147	Patterns of cognitive decline in individuals with elevated p-tau217 and low levels (<20 Centiloids) of neocortical Aβ-PET signal	Townsend | Properzi | Klinger | Schultz | Coughlan | Yau | Birkenbihl | Seto | Hanseeuw | Jacobs | Farrell | Yang | Papp | Rentz | Johnson | Sperling | Chhatwal | Amariglio | Buckley	**Townsend, Diana**
148	Anatomic specificity of inflammation TSPO PET biomarkers in dementia	Finn | Faridar | Toledo | Nakawah | Roman | Masdeu | Pascual	**Pascual, Belen**
149	Head-to-head comparison of longitudinal plasma assays in relation to longitudinal amyloid pathology in Alzheimer's disease	Yakoub | Qiu | Villeneuve | Pichet Binette | ADNI Foundation for the National Institutes of Health (FNIH) Biomarkers Consortium	**Yakoub, Yara**
150	Characterization of PART using MK-6240, Flortaucipir, and plasma p-tau217	Soares | L. Ferreira | Ruppert | S. Medeiros | Rocha | Bellaver | Povala | Bauer-Negrini | Amaral | Bloomquist | Lussier | Masdeu | L. Tudorascu | Soleimani-Meigooni | Fortea | Lowe | Oh | Pascual | A. Gordon | Rosa-Neto | Baker | A. Pascoal	**Soares, Carolina**
151	Longitudinal rate of change in CSF biomarkers is associated with subsequent Tau PET burden in Braak stages I and II: Findings from the BIOCARD study	Rani | Moghekar | Callow | Alm | Pettigrew | Soldan | Miller | Wang | Albert | Bakker	**Rani, Nisha**
152	Head-to-head comparison of four tau-PET tracers for in vivo Braak staging: the HEAD Study	Cassa Macedo | Rahmouni | Tissot | Therriault | Servaes | Wang | Trudel | Aumont | Hall | Chan | Zheng | Lussier | Ferreira | Bellaver | Povala | Pascual | Gordon | Lowe | Oh | Soleimani-Meigooni | Baker | Pascoal | Rosa-Neto	**Cassa Macedo, Arthur**
153	Astrogliosis in the early-stages of Alzheimer's disease	Dore | Bourgeat | Harada | Furumoto | Mulligan | Xia | Paranawithana | Laws | Feizpour | Bozinovski | Huang | Lopresti | Ikonomovic | Fripp | Okamura | Rowe | Villemagne	**Villemagne, Victor**
154	Identifying an optimal aβ cutoff point for progression from mild cognitive impairment to Alzheimer's disease: comparing cognitive performance and aβ pet insights	Shishegar | Bourgeat | Dore | Laws | Porter | Weiner | Masters | Maruff | Sohrabi | Fripp | Villemagne | Rowe	**Bourgeat, Pierrick**
155	Amyloid modifies the association between late-life BMI and longitudinal cognition in cognitively unimpaired individuals	Yau | Raman | Wang | Aggarwal | Brickman | Chhatwal | Cogswell | Graff-Radford | Pillai | Rafii | Aisen | Sperling | A4 and Learn Study Teams	**Yau, Wai-Ying Wendy**

Board #	Poster Title	Authors	Presenter
156	Amyloid spatial extent captures early tau burden and cognitive deficits, measured by PACC and digital clock drawing test, in preclinical Alzheimer's disease	Thompson | Fu | Farrell | Thibault | Slade | Del Carmen Montenegro | Robinson | Jutten | Davis | Penney | Rodriguez Alonso | Sperling | Rentz | Price | Johnson	**Thompson, Jackson**
157	Findings from dynamic [18F]-MK6240 PET imaging after motion and partial volume corrections	Tiss | Gong | Lois | Dhaynaut | Guehl | El Fakhri | Johnson | Ouyang	**Tiss, Amal**
158	Harmonization of MK6240 and Flortaucipir Braak Staging	Rocha | Bellaver | Ruppert | L. Ferreira | Soares | Medeiros | Povala | Amaral | Bauer-Negrini | Lussier | Scarpatto Rodrigues | Oliveira Jr. | Saha | Bloomquist | Masdeu | L. Tudorascu | Soleimani-Meigooni | Fortea | Lowe | Oh | Pascual | A. Gordon | Rosa-Neto | Baker | A. Pascoal	**Rocha, Andreia**
159	Comparison of MK-6240 PET and Flortaucipir tau PET imaging for the biological staging of Alzheimer's disease	Scop Medeiros | L. Ferreira | Bellaver | Ruppert | Zalzale | Soares | Povala | Bauer-Negrini | Rocha | S. Rodrigues | Oliveira | Mroue | Saha | Amaral | Lussier | Bloomquist | L. Tudorascu | Masdeu | Soleimani-Meigooni | Fortea | Lowe | Oh | Pascual | A. Gordon | Rosa-Neto | P. Schilling | Baker | A. Pascoal	**Scop Medeiros, Marina**
160	Impact of early-stage amyloidosis on tau accumulation throughout the medial temporal lobe and neocortex	Slade | Thibault | Thompson | Fu | Becker | Price | Tiss | Gong | Sperling | Johnson | Farrell	**Slade, Elliott**
161	Associations between age-related tau deposition and neural selectivity in cognitively unimpaired older adults	Sheng | Trelle | Young | Romero | Park | Sai | Vossler | Wagner | Mormino	**Sheng, Jintao**
162	Posterior white matter hyperintensity is related to the emergence of lobar cerebral microbleeds in ADNI	Saukkonen | Yang | Loghmani | Schultz | Greenberg | Sperling | Chhatwal | Shirzadi	**Saukkonen, Daniel**
163	Defining the grey zone thresholds for tau PET positivity using the Uniτ scale	Povala | Bellaver | Bauer-Negrini | Ruppert | Medeiros | Amaral | Lussier | Lukasewicz | Soares | Tudorascu | Masdeu | Pascual | Gordon | Lowe | Oh | Soleimani-Meigooni | Rosa-Neto | Baker | A. Pascoal	**Povala, Guilherme**
164	Neocortical amyloid spatial extent predicts cognitive decline over time in memory and executive function domains	Thibault | Fu | Thompson | Slade | Jacobs | Price | Rentz | Sperling | Johnson | Farrell	**Thibault, Emma**
165	Patterns of tau-PET accumulation and clinical progression according to biological AD stages	Trudel | Therriault | Rahmouni | Cassa Macedo | Servaes | Aumont | Hosseini | Fernandez-Arias | Zheng | Wang | Chan | Hall | Stevenson | Hopewell | Hung-Hsin Hsiao | Gauthier | Vitali | Pascoal | Rosa-Neto	**Trudel, Lydia**
166	The Tau Progression Index (TPI): an individualized, clinically applicable, multimodally-derived score to predict AD progression	Chiang | Butler | Ghaderi Yazdi | Ozoria | Chernek | Calimag | Blum | Pahlajani | Foldi | Khalafi | Devanand | He | Hojjati | Gholipour Picha | Habeck | Stern | Razlighi	**Razlighi, Qolamreza**

Board #	Poster Title	Authors	Presenter
167	Dried plasma spot optimization for the NULISAseq CNS panel	Wilson | Rea Reyes | Fredricks | team | Rusch | VandenLangenberg | Jensen | Marshall | Keske | Weninger | Jeffers | Huber | Johnson | Zetterberg	**Wilson, Rachael**
168	Clinical validation of the Lumipulse G1200 automated immunoassay for the measurement of Alzheimer's disease plasma biomarkers	Chan | Rahmouni | Zheng | Congalves | Macedo | Aumont | Therriault | Hall | Wang | Trudel | Servaes | Fernandez-Arias | Hopewell | Zetterberg | Pascoal | Benedet | Rosa-Neto	**Chan, Tevy**
169	Sex differences in synaptic loss in early Alzheimer's disease	Galbraith | Abuwarda | O'Dell | Mecca | van Dyck | Fredericks	**Galbraith, Jordan**
170	Assessing the generalizability of AD subtypes across diverse cohorts: HABS-HD and ADNI	An | Gordon | Sotiras | Millar | O'Bryant | Ances | Meeker	**An, Gordon Zhaoqi**
171	Locus coeruleus - medial temporal lobe functional connectivity confers protection against amyloid-related cognitive decline in the context of high cognitive reserve	Heinrich | Prokopiou | Wiklund | Papp | Rentz | Sperling | Johnson | Jacobs	**Heinrich, Lukas**
172	Effect of AD risk factors on tau-PET tracer uptake and its association with amyloid-β pathology	Rodrigues | Bellaver | Povala | Bauer-Negrini | Lussier | Lulasewicz Ferreira | Silva Oliveira Junior | Rocha | Saha | Rupert | Scop Medeiros | Masdeu | Tudorascu | Soleimani-Meigooni | Fortea | Lowe | Oh | Pascual | Gordon | Rosa-Neto | Baker | Pascoal	**Rodrigues, Matheus**
173	PI-2620 uptake in the medial temporal lobes discriminates Alzheimer's disease from normal cognition and non-Alzheimer's dementias	Phillips | Temirova | Kamel | Hareras | Ibe | Hlava | Xie | Cousins | Shaw | Das | Maneval | Manning | Brown | Lopez | Keegan | Stephens | McMillan | Irwin | Li | Nasrallah | Wolk	**Phillips, Jeffrey**
174	Characterizing associations with Aβ burden in non-Hispanic Black participants across US POINTER and A4/LEARN cohorts	Robinson | Papp | Harrison | Baker | Snyder | Sperling | Amariglio | Landau | STUDYTEAM | Study Group	**Robinson, Talia**

POSTER INDEX *(by presenter's last name)*

Presenter	Day	Board #	Poster Title
Abu Raya, Maison	**Wednesday**	**18**	Characterizing amyloid-positive with low Tau (A+T-) profiles and their association with cognitive trajectories in the Longitudinal Early-Onset Alzheimer's Disease Study (LEADS): A multi-method approach
Adams, Jenna	**Wednesday**	**51**	Metabolic inefficiency is associated with regional vulnerability to tau deposition
Amaral, Livia	**Wednesday**	**47**	Comparison of topographical patterns of abnormalities of the tau PET tracers [18F]Flortaucipir, [18F]MK6240, [18F]PI2620, and [18F]RO948
An, Gordon Zhaoqi	**Friday**	**170**	Assessing the generalizability of AD subtypes across diverse cohorts: HABS-HD and ADNI
Arnold, Steven	**Wednesday**	**39**	P-TAU217, GFAP, and NFL plasma biomarker associations with demographic, medical and neurocognitive features from middle-aged through older adulthood
Aumont, Etienne	**Wednesday**	**42**	Increasing the granularity of tau-PET Braak staging using medial temporal lobe segmentations to detect early memory impairment
Baillet, Marion	**Wednesday**	**36**	Transcutaneous auricular vagus nerve stimulation improves learning and sleep-wake quality in older APOE-ε4 carriers
Banks, Sarah	**Wednesday**	**49**	Estradiol-dependent associations between sleep complaints and tau deposition in women at elevated AD risk
Bellaver, Bruna	**Wednesday**	**23**	Head-to-head trajectories of tau PET and plasma p-tau217 as a function of Aβ
Betthauser, Tobey	**Wednesday**	**57**	Longitudinal amyloid PET trajectories in the HABS-HD cohort
Bezgin, Gleb	**Wednesday**	**54**	Comparison of distribution volume and standardized uptake value ratio for a MAO-B tracer in mild cognitive impairment
Bilgel, Murat	**Wednesday**	**10**	Positron emission tomography analysis with the dynamicpet Python package
Bilgel, Murat	**Thursday**	**71**	Longitudinal change in five dominant dimensions of brain aging in relation to brain amyloid status and Alzheimer's-related plasma biomarkers
Bischof, Gerard	**Wednesday**	**07**	Molecular correlates of apraxia in Alzheimer's disease: A PET imaging study
Bluma, Marina	**Thursday**	**114**	Tracking plasma biomarker abnormalities with amyloid time accumulation
Bourgeat, Pierrick	**Wednesday**	**40**	DeepSUVR: Using temporal constraints to improve tau quantification
Bourgeat, Pierrick	**Thursday**	**101**	DeepSUVR: Towards redefining the Centiloid masks using a data-driven approach
Bourgeat, Pierrick	**Friday**	**154**	Identifying an optimal aβ cutoff point for progression from mild cognitive impairment to Alzheimer's disease: comparing cognitive performance and aβ pet insights
Brown, Christopher	**Wednesday**	**37**	Biological-clinical mismatch reflects co-pathology and vulnerability to neurodegeneration
Buckley, Rachel	**Wednesday**	**20**	Whole blood gene expression is associated with plasma p-tau217 levels via amyloid-PET and sex

Presenter	Day	Board #	Poster Title
Callow, Daniel	**Wednesday**	**28**	Amyloid status moderates associations between hippocampal microstructure, PET tau burden, and memory in dementia-free older adults
Capotosti, Francesca	**Wednesday**	**02**	From the clinical utility of a-synuclein PET imaging in Multiple System Atrophy to the possible diagnosis of Parkinson's disease
Cassa Macedo, Arthur	**Wednesday**	**15**	The spatial spread of tauopathy precedes the increase in tau-PET load in Alzheimer's disease
Cassa Macedo, Arthur	**Friday**	**152**	Head-to-head comparison of four tau-PET tracers for in vivo Braak staging: the HEAD Study
Chan, Tevy	**Friday**	**168**	Clinical validation of the Lumipulse G1200 automated immunoassay for the measurement of Alzheimer's disease plasma biomarkers
Chen, Charles	**Thursday**	**110**	Two distinct sources of 18F-MK-6240 off-target signal identified by individualized head modeling and PET kinetics
Clarke, Mica	**Wednesday**	**33**	Molecular imaging of neurodegeneration – mitochondria, associated proteins and synapses (MIND-MAPS) in frontotemporal dementia
Cody, Karly	**Wednesday**	**22**	The relative prevalence of tau severity stages is related to amyloid burden, clinical diagnosis and age
Cody, Karly	**Friday**	**133**	Effects of amyloid and tau status on multiplex plasma CNS and inflammatory proteins in a normal aging cohort
Colón-Badillo, Vanessa	**Wednesday**	**11**	Targeted plasma eQTL and pQTL to identify potential novel biomarker for Alzheimer's disease in African Americans
Corriveau-Lecavalier, Nick	**Wednesday**	**09**	Characterization of a limbic-predominant amnestic neurodegenerative syndrome
Del Carmen Montenegro, Grace	**Wednesday**	**38**	Validation of PET spatial extent as sensitive amyloid biomarker in early stages of amyloidosis
DelBene, Alexander	**Wednesday**	**29**	Performance of an MR-independent analysis pipeline for quantification of tau abnormality using [18F]flortaucipir PET
Dhaynaut, Maeva	**Wednesday**	**35**	Cerebral perfusion indices from early-phase [18F]-MK6240 dynamic Tau PET imaging in brain regions associated with Alzheimer's disease progression in an aging population.
Diez, Ibai	**Wednesday**	**45**	Unveiling the heterogeneity of tau spreading in aging and Alzheimer's disease using polygenic combinations: Towards personalized models
Dodge, Hiroko	**Wednesday**	**53**	Combined impact of plasma phospho-tau 217 and NfL on longitudinal domain-specific cognitive decline
Dong, Yiwen	**Wednesday**	**19**	The association between amyloid and physical activity in a racially diverse cohort of older adults
Dubbelman, Mark	**Wednesday**	**01**	Decline in everyday functioning over time relates to amyloid and tau in cognitively unimpaired older adults
Duggan, Michael	**Wednesday**	**14**	Proteomic analyses of A-T-N reveal plasma mediators of neurodegeneration and dementia risk
Ekuta, Victor	**Wednesday**	**08**	Understanding the impact of race on white matter hyperintensities in Alzheimer's disease: Findings from the ADNI Study
Engels-Domínguez, Nina	**Wednesday**	**34**	Evaluating tVNS effects on cognitive outcomes and modulating factors in asymptomatic older adults: study design of the WALLe Trial

Presenter	Day	Board #	Poster Title
Fajardo-Valdez, Alfonso	**Wednesday**	**56**	The impact of spatial smoothing on the accuracy of Centiloid thresholds
Felix, Cynthia	**Wednesday**	**48**	Subtle cognitive deficits detected through routine in-office tests are associated with global Aβ and temporal tau in cognitively unimpaired individuals
Frontzkowski, Lukas	**Wednesday**	**41**	Developing a novel reference region for PI-2620-PET imaging to facilitate assessment of 4-repeat tauopathies
Fu, Jessie Fang-Lu	**Wednesday**	**06**	Baseline tau burden and performance on a digital clock drawing test uniquely contributes to predicting future tau accumulation in preclinical AD
Galbraith, Jordan	**Friday**	**169**	Sex differences in synaptic loss in early Alzheimer's disease
Gallego-Rudolf, Jonathan	**Wednesday**	**30**	Functional and structural connectivity patterns predict longitudinal tau spreading in asymptomatic individuals expressing Aβ pathology
Gallego-Rudolf, Jonathan	**Thursday**	**93**	Tracking biomarkers accuracy for predicting progression to mild cognitive impairment
Garcia Condado, Jorge	**Wednesday**	**52**	Relationship between Polygenetic Risk Score of BrainAge and plasma biomarkers in the A4/Elearn Study
Garrone, Aurélie	**Wednesday**	**44**	Assessing the relationship between neuropsychiatric symptoms, amyloid and tau pathology, and white matter hyperintensity volume across sexes in preclinical Alzheimer's disease
Gatchel, Jennifer	**Wednesday**	**31**	Plasma phospho-tau 217, neurofilament-light, and glial fibrillary acidic protein are differentially associated with longitudinal neuropsychiatric symptoms across the early cognitive spectrum
Gatto, Rodolfo	**Wednesday**	**32**	An assessment of the utility of flortaucipir PET to detect four-repeat tau pathology in a globular glia tauopathy case-series
Gatto, Rodolfo	**Friday**	**146**	Neuropathological evaluation of the off-target binding of flortaucipir in FTLD subcortical regions: interconnecting tau aggregates with iron deposition and neuroinflammation
Geremia, Danielle	**Wednesday**	**13**	Evaluation of a label-free X-ray based method for estimating amyloid load in the human brain
Ghatamaneni, Sujala	**Wednesday**	**50**	Impact of age and sex on extra-cerebral off-target binding in tau PET scans (18F-FTP)
Gills, Joshua	**Wednesday**	**25**	Sex-specific associations of BMI, amyloid, and regional tau deposition in community-dwelling cognitively normal older adults
Gnörich, Johannes	**Wednesday**	**26**	Assessment of ATN with a single dynamic [18]F-PI-2620 recording
Gogola, Alexandra	**Wednesday**	**21**	Plasma Aβ as predictor of Aβ accumulation in non-demented participants
Gogola, Alexandra	**Friday**	**134**	Tau imaging thresholds within NIA-AA multilevel tau staging as predictors of tau accumulation and cognitive decline in non-demented individuals
Groh, Jenna	**Friday**	**144**	Association of a unique pattern of white matter T2 FLAIR hyperintensities with plasma and tau PET biomarkers in former American football players

Presenter	Day	Board #	Poster Title
Grothe, Michel	**Wednesday**	**27**	Tau-PET detects advanced primary age-related tauopathy mimicking early-stage AD
Grube, Jill	**Wednesday**	**05**	APOE ε4 carriers exhibit attenuated habituation in pupil size and practice effects on a repeated auditory oddball task
Guzmán, Diana S	**Wednesday**	**46**	Regional amyloid and tau: Exploring regional sex-based differences in a middle-aged community-based cohort
Hall, Brandon	**Thursday**	**105**	Cortical freewater increases with tau tangle aggregation
Hanseeuw, Bernard	**Thursday**	**82**	In low neocortical tau individuals, high amygdala tau predicts faster cognitive decline
He, Hengda	**Thursday**	**67**	Network-based amyloid-β pathology predicts subsequent cognitive decline in cognitively normal older adults
Heinrich, Lukas	**Friday**	**171**	Locus coeruleus - medial temporal lobe functional connectivity confers protection against amyloid-related cognitive decline in the context of high cognitive reserve
Heuer, Lauren	**Thursday**	**74**	MK-6240 off-target binding patterns in relation to microglia density, measured through TSPO PET
Honer, Michael	**Thursday**	**115**	Advancing antibody-based pretargeted PET imaging of protein aggregates in the brain
Houlihan, Hannah	**Thursday**	**107**	Annual percent change of microglia density in relation to tau accumulation in older adults
Huang, Shao-Yi	**Thursday**	**90**	Predicting amyloid positivity and tau burden in dementia using a combination of different biomarkers
Ioannou, Konstantinos	**Thursday**	**65**	Low tau in Aβ-positive cognitively impaired individuals: Alzheimer's disease or something more?
Jacobson, David	**Thursday**	**109**	Assessing neuroinflammation in Alzheimer's disease: A TSPO-PET study using ER176 and its correlation with amyloid and tau pathology
Javanray, Mohammadali	**Thursday**	**63**	Higher time varying brain functional connectivity is associated with slower tau accumulation at the preclinical stage of Alzheimer's disease
Johns, Emily	**Thursday**	**92**	Exploring the predictive power of graph-theoretic metrics for tau pathology in cognitively unimpaired older adults
Jones, David	**Thursday**	**59**	Interpretable prediction of amyloid PET positivity using non-negative matrix factorization
Kang, Min Su	**Thursday**	**64**	Graph convolutional networks to predict cognitive decline at the individual level in Alzheimer's disease
Katsumi, Yuta	**Thursday**	**83**	EOAD-signature atrophy predicts progression to dementia in patients with early-onset MCI due to Alzheimer's disease
Khurelbaatar, Bayarjargal	**Thursday**	**88**	Differential tau accumulation in early-onset and late-onset Alzheimer's disease: Insights from [18F]-Florzolotau PET
Klinger, Hannah	**Thursday**	**70**	Whole-blood gene expression associations with Aβ-PET accumulation and cognitive decline
Koops, Elouise	**Thursday**	**76**	Lower LC-EC tract integrity is associated with entorhinal tau in autosomal-dominant Alzheimer's disease
Kraft, Jessica	**Thursday**	**116**	Longitudinal change in mnemonic discrimination and influence of Aβ burden
Kuchenbecker, Lindsey	**Thursday**	**60**	Data-driven biomarker discovery nominates novel diagnostic plasma biomarkers and provides insights into

Presenter	Day	Board #	Poster Title
			Alzheimer's disease pathophysiology in an African American cohort
Kulagowska, Laura	**Thursday**	**91**	Evaluation of [^{3}H]SynVesT - 1 binding in post-mortem brain tissue from control and Alzheimer's disease as a biomarker of synaptic loss
Kunach, Peter	**Thursday**	**85**	Microscopic visualization of fluorescent MK-6240
Lao, Patrick	**Thursday**	**112**	TSPO PET mediates tau-associated neurodegeneration in limbic and temporal regions across clinical variants of Alzheimer's disease
Lawn, Timothy	**Wednesday**	**24**	Functional submodules in the human locus coeruleus are differentially susceptible to tau pathology
Laymon, Charles	**Thursday**	**69**	Multi element MRI template method for analysis of Down syndrome PET
Leuzy, Antoine	**Thursday**	**86**	Conversion of Tau PET SUVR data to CenTauR units using the Joint Propagation Model
Li, Annie	**Thursday**	**96**	Sex moderates the association between regional tau and longitudinal cognitive decline in A4 and LEARN studies
Lim, Seokbeen	**Thursday**	**100**	Investigation of optimal intensity threshold for tau-PET overlap index
Liu, Peiwei	**Thursday**	**87**	The role of cohort heterogeneity in predicting AD/ADRD cognitive decline
Lopresti, Brian	**Thursday**	**73**	AT(N) staging of Alzheimer's disease: Comparison of visual interpretation and automated quantification pipelines
Lussier, Firoza	**Thursday**	**62**	Longitudinal multicenter head-to-head harmonization of tau PET tracers: an overview of the HEAD study cohort
Lutz, Olivia	**Thursday**	**97**	Evaluation of the Uni-tau and CenTauR frameworks in new datasets for tau PET harmonization in Alzheimer's disease
Lyu, Xueying	**Thursday**	**103**	Amyloid-Tau to neurodegeneration mismatch from inter-modality image translation using deep learning
McLachlan, Max	**Thursday**	**84**	FDG reference region selection using PiB amyloid status-guided iterative normalization in a Down syndrome cohort
McLachlan, Max	**Friday**	**141**	The striatum is an early, accurate indicator of [C-11]PiB amyloid burden for the Down syndrome population
McVea, Andrew	**Thursday**	**77**	APOE4 associated with higher off-target meninges signal with [F-18]MK6240 PET
Millar, Peter	**Thursday**	**104**	Tau PET subgroups differ in network patterns of functional connectivity and amyloid PET
Minhas, Davneet	**Thursday**	**78**	An accurate and automated technique for removing spill-over contamination and off-target retention from a cerebellar reference region for tau PET
Moon, Hasom	**Thursday**	**80**	Predicting regional Alzheimer's disease pathology with plasma p-tau217 in preclinical AD
Mooney, Katelyn	**Thursday**	**68**	Associations between APOE-TOMM40 '523 haplotype variants and limbic system white matter microstructure in Black and White individuals
Moret, Sophia	**Thursday**	**98**	Hemispheric lateralization of tau-related network dysfunction and its association with neuropsychiatric symptoms in preclinical Alzheimer's disease

Presenter	Day	Board #	Poster Title
Mormino, Elizabeth	**Wednesday**	**12**	Pathological and clinical trajectories of preclinical Alzheimer's disease patients with divergent cortical tau patterns
Mroué, Rayan	**Thursday**	**75**	Association between medication use and [18F]MK6240 and [18F]Flortaucipir uptake across the Alzheimer's disease spectrum
Mundada, Nidhi	**Thursday**	**72**	Enrichment of patients with concomitant LATE on the Alzheimer's disease continuum using hippocampal volume
Olafson, Emily	**Thursday**	**99**	Characterization and correction of extracerebral [18F]MK-6240 tau PET off-target signal in Alzheimer's disease
Ottoy, Julie	**Thursday**	**106**	Distinct spatiotemporal patterns of vascular disease in Alzheimer's disease subtypes
Palmgren, Kailee	**Thursday**	**108**	Physical frailty as a risk factor for increased tau accumulation and cognitive decline in cognitively unimpaired older adults
Pascual, Belen	**Thursday**	**81**	TSPO-PET before and after low-dose interleukin-2 in patients with mild to moderate Alzheimer's disease
Pascual, Belen	**Friday**	**148**	Anatomic specificity of inflammation TSPO PET biomarkers in dementia
Patsyuk, Yuliya	**Wednesday**	**58**	Lower microstructural integrity of the locus coeruleus to entorhinal cortex pathway is related to elevated astrocyte reactivity and tau burden in cognitively unimpaired individuals: a 7T dMRI study
Petersen, Kellen	**Thursday**	**66**	A plasma clock for Alzheimer disease based on %p-tau217
Pezzoli, Stefania	**Friday**	**119**	Evaluating the effect of APOE genotype in real-world clinical settings: results from the IDEAS-ANGI study
Phillips, Jeffrey	**Friday**	**173**	PI-2620 uptake in the medial temporal lobes discriminates Alzheimer's disease from normal cognition and non-Alzheimer's dementias
Povala, Guilherme	**Wednesday**	**43**	The universal tau PET scale (Uniτ) for Flortaucipir, MK6240, PI2620 and RO948 harmonization
Povala, Guilherme	**Friday**	**163**	Defining the grey zone thresholds for tau PET positivity using the Uniτ scale
Provenzano, Frank	**Thursday**	**102**	Mechanical stress of the entorhinal cortex: A potential driver of tau pathology?
Qiu, Ting	**Wednesday**	**03**	Unraveling the impact of amyloid-β and tau pathology on brain structure and cognitive function during preclinical and prodromal Alzheimer's disease
Rahmouni, Nesrine	**Wednesday**	**55**	Association between early and late tau aggregation across tau imaging agents: The HEAD Study
Ramirez Tirado, Laura Alejandra	**Friday**	**121**	Synergistic effects of peripheral inflammation and neuroinflammation on amyloid, vascular, and neurodegeneration markers across the Alzheimer's disease spectrum
Rani, Nisha	**Thursday**	**94**	Tau burden across Braak stages is associated with regionally specific amyloid accumulation: insights from the BIOCARD cohort

Presenter	Day	Board #	Poster Title
Rani, Nisha	**Friday**	**151**	Longitudinal rate of change in CSF biomarkers is associated with subsequent Tau PET burden in Braak stages I and II: Findings from the BIOCARD study
Razlighi, Qolamreza	**Friday**	**166**	The Tau Progression Index (TPI): an individualized, clinically applicable, multimodally-derived score to predict AD progression
Rissman, Robert	**Friday**	**125**	Detection of TDP-43 from plasma-derived astrocyte extracellular vesicles for identification of LATE
Robinson, Talia	**Friday**	**174**	Characterizing associations with Aβ burden in non-Hispanic Black participants across US POINTER and A4/LEARN cohorts
Rocha, Andreia	**Friday**	**158**	Harmonization of MK6240 and Flortaucipir Braak Staging
Rodrigues, Matheus	**Friday**	**172**	Effect of AD risk factors on tau-PET tracer uptake and its association with amyloid-β pathology
Roemer-Cassiano, Sebastian Niclas	**Friday**	**139**	Amyloid-associated hyperconnectivity drives tau spreading across connected brain regions in Alzheimer's disease
Ruppert, Emma	**Friday**	**131**	Harmonizing visual readings of Flortaucipir and MK-6240 using head-to-head data
Saha, Pampa	**Friday**	**140**	Association of plasma GFAP with tau PET in cognitively unimpaired Aβ-negative subjects
Sai, Isha	**Friday**	**127**	Impacts of testing language and rates of amyloid positivity among underrepresented groups in the A4 Study
Saukkonen, Daniel	**Friday**	**162**	Posterior white matter hyperintensity is related to the emergence of lobar cerebral microbleeds in ADNI
Schwartz, Daniel	**Friday**	**136**	Cortical atrophy is correlated with the discrepancy between neuroradiological assessment and binary quantitation of florbetapir PET in nondemented older adults
Schwarz, Christopher	**Thursday**	**79**	Updated public CenTauR pipelines to measure CenTauR, CenTauRZ, and SUVR tau PET units
Schwarz, Christopher	**Friday**	**130**	A large public release of PIB PET and MRI from the Mayo Clinic Study of Aging
Schweitzer, Noah	**Friday**	**123**	Astrocyte reactivity explains tau-related effects on hippocampal dysfunction and longitudinal atrophy in preclinical Alzheimer's disease
Scop Medeiros, Marina	**Friday**	**159**	Comparison of MK-6240 PET and Flortaucipir tau PET imaging for the biological staging of Alzheimer's disease
Sheng, Jintao	**Friday**	**161**	Associations between age-related tau deposition and neural selectivity in cognitively unimpaired older adults
Silva Oliveira Junior, Markley	**Friday**	**137**	Vascular pathology influences the association of tau-PET with neurodegeneration and cognition in Aβ-negative individuals
Silva-Rodríguez, Jesús	**Thursday**	**89**	Heterogeneity of FDG-PET patterns among tau-negative amnestic patients
Silva-Rodríguez, Jesús	**Friday**	**129**	Long-term cognitive and biomarker trajectories of cognitively unimpaired individuals with elevated plasma ptau-217
Singh-Reilly, Neha	**Thursday**	**95**	Relationship between neuroinflammatory ER176-PET and functional connectivity in Progressive Apraxia of Speech

Presenter	Day	Board #	Poster Title
Singh-Reilly, Neha	**Friday**	**145**	Relationship between flortaucipir-PET and quantitative susceptibility mapping in atypical Alzheimer's disease
Slade, Elliott	**Friday**	**160**	Impact of early-stage amyloidosis on tau accumulation throughout the medial temporal lobe and neocortex
Smith, Anna	**Friday**	**135**	Multi-morbidity and Alzheimer's disease pathology across the lifespan in adults with Down syndrome
Soares, Carolina	**Friday**	**150**	Characterization of PART using MK-6240, Flortaucipir, and plasma p-tau217
Soleimani-Meigooni, David	**Friday**	**118**	Calibration of multi-site raters for prospective visual read of amyloid PET scans acquired across the ADRC Consortium for Clarity in ADRD Research Through Imaging (CLARiTI)
Tennant, Victoria	**Friday**	**143**	Relationship between metabolic syndrome biomarkers and regional tau accumulation in cognitively unimpaired older adults
Thibault, Emma	**Friday**	**164**	Neocortical amyloid spatial extent predicts cognitive decline over time in memory and executive function domains
Thompson, Jackson	**Friday**	**156**	Amyloid spatial extent captures early tau burden and cognitive deficits, measured by PACC and digital clock drawing test, in preclinical Alzheimer's disease
Tiss, Amal	**Friday**	**157**	Findings from dynamic [18F]-MK6240 PET imaging after motion and partial volume corrections
Tissot, Cécile	**Friday**	**142**	Best practices for tau-PET tracer harmonization in Alzheimer's research
Tonietto, Matteo	**Friday**	**122**	Impact of amyloid removal on cerebral volume changes with Gantenerumab
Townsend, Diana	**Friday**	**147**	Patterns of cognitive decline in individuals with elevated p-tau217 and low levels (<20 Centiloids) of neocortical Aβ-PET signal
Trudel, Lydia	**Friday**	**165**	Patterns of tau-PET accumulation and clinical progression according to biological AD stages
Unschuld, Paul	**Wednesday**	**16**	Distinct patterns of Iron distribution in the entorhinal cortex-hippocampus system for characterization of mild cognitive impairment
Van Egroo, Maxime	**Friday**	**138**	Concomitant neurodegeneration of the lateral hypothalamus and locus coeruleus is associated with early Alzheimer's disease-related pathophysiological and cognitive processes
Villemagne, Victor	**Wednesday**	**04**	Astrogliosis, a potential non-Aβ pathway to tau
Villemagne, Victor	**Friday**	**153**	Astrogliosis in the early-stages of Alzheimer's disease
Vrillon, Agathe	**Friday**	**117**	Concordance between visual and quantitative amyloid PET and CSF biomarkers in the ADNI-DOD cohort
Wiklund, Emma	**Friday**	**128**	Lower locus coeruleus metabolism is associated with greater year-to-year intraindividual cognitive variability in older individuals with elevated levels of Alzheimer's disease pathology

Presenter	Day	Board #	Poster Title
Wilson, Rachael	**Friday**	**167**	Dried plasma spot optimization for the NULISAseq CNS panel
Winer, Joseph	**Friday**	**126**	Short sleep duration is associated with higher subsequent plasma p-tau217 in aging
Wu, Chao-Yi	**Friday**	**132**	Twin-mapping techniques in clinical trials: a proof-of-concept application to the Internet-Based Conversational Engagement Clinical Trial (I-CONECT)
Xiao, Yu	**Friday**	**120**	Brain connectivity drives tau distribution while regional vulnerability drives tau load in Alzheimer's disease
Yakoub, Yara	**Friday**	**149**	Head-to-head comparison of longitudinal plasma assays in relation to longitudinal amyloid pathology in Alzheimer's disease
Yang, Hyun-Sik	**Friday**	**124**	Plasma phosphorylated tau 217 and longitudinal trajectories of Aβ, tau, and cognition in cognitively unimpaired older adults
Yau, Wai-Ying Wendy	**Friday**	**155**	Amyloid modifies the association between late-life BMI and longitudinal cognition in cognitively unimpaired individuals
Ziontz, Jacob	**Wednesday**	**17**	Pathological asymmetry in early onset AD reflects heterogenous disease trajectories

HAI 2025 PROGRAM *(short)*

Wednesday, January 15, 2025		
08:00 am - 08:30 am	Check-in and Breakfast	
08:30 am - 08:45 am	Welcome Notes	**Keith Johnson**, Massachusetts General Hospital
08:45 am - 08:55 am	Alzheimer's Association Note	**Maria Carrillo**, Alzheimer's Association
08:55 am - 10:35 am	**SESSION I Harmonization**	**Suzanne Baker,** Lawrence Berkeley National Laboratory **Bradley Christian,** University of Wisconsin School of Medicine and Public Health
08:55 am - 09:00 am	Session Overview	**Chairs**
09:00 am	Longitudinal amyloid burden with combined [11C]PiB and [18F]NAV4694 PET Scans	**Brecca Bettcher**, University of Wisconsin-Madison School of Medicine and Public Health and Waisman Center, Madison, WI, US
09:15 am	Exploring Centiloids robustness: Impact of sample size and image resolution on Centiloid conversion accuracy	**Jiaxiuxiu Zhang**, Memory and Aging Center, Department of Neurology, University of California, San Francisco, San Francisco, CA, US
09:30 am	Every Centiloid, from everywhere, all at once	**Ganna Blazhenets**, Memory and Aging Center, Department of Neurology, University of California, San Francisco, San Francisco, CA, US
09:45 am	The Uniτ Ecosystem for tau-PET harmonization and visualization	**Guilherme Povala**, University of Pittsburgh, Department of Psychiatry, Pittsburgh, PA, US
10:00 am	Comparative sensitivity analysis of tau-PET tracers in Alzheimer's disease	**Cécile Tissot**, Lawrence Berkeley National Laboratory, Berkeley, CA, US
10:15 am - 10:35 am	Discussion	
10:35 am - 10:40 am	**Blitz Session 1A Short Poster Presentations**	
10:35 am	Introduction	
10:37 am	Pathological and clinical trajectories of preclinical Alzheimer's disease patients with divergent cortical tau patterns	**Elizabeth Mormino**, Department of Neurology and Neurological Sciences, Stanford University School of Medicine, Stanford, CA, US
10:38 am	Association between early and late tau aggregation across tau imaging agents: The HEAD Study	**Nesrine Rahmouni**, McGill University, Montreal, QC, CA
10:39 am	Unraveling the impact of amyloid-β and tau pathology on brain structure and cognitive function during preclinical and prodromal Alzheimer's disease	**Ting Qiu**, Douglas Mental Health University Institute, McGill University, Montreal, QC, CA
10:40 am - 11:35 am	**Poster Session 1A** *(repeating in the afternoon as 1B)* **- Boards 1-58**	
11:35 am - 01:00 pm	**SESSION II Spatial Patterns**	**Ansel Hillmer,** University of Michigan, Ann Arbor, MI, USA **Pedro Rosa-Neto,** McGill University, Montreal, QC, Canada
11:35 am - 11:40 am	Session Overview	**Chairs**
11:40 am	The interaction of initial medial temporal lobe tauopathy and amyloid-beta spatial extent in driving caTAUstrophe	**Michelle Farrell**, Massachusetts General Hospital, Boston, MA, US

11:55 am	Mapping spatial white matter integrity linked to tau accumulation: Insights from tractometry with multi-shell diffusion imaging	**Jenna Adams**, University of California Irvine, Irvine, CA, US
12:10 am	Spatial patterns of voxel-wise tau accumulation across the Alzheimer's disease spectrum	**Corrina Fonseca**, Department of Neuroscience, University of California Berkeley, Berkeley, CA, US
12:25 am	PET astroglia and microglia follow tau propagation patterns in Alzheimer's disease	**Nesrine Rahmouni**, McGill University, Montreal, QC, CA
12:40 pm - 01:00 pm	Discussion	
01:00 pm - 02:00 pm	Lunch break	
02:00 pm - 02:30 pm	**KEYNOTE: From click chemistry to precision neuroscience**	**Hartmuth Kolb,** Enigma Biomedical Group
02:30 pm - 02:45 pm	Keynote Discussion	
02:45 pm - 04:25 pm	**SESSION III Neuropath I**	**Tobey Betthauser,** University of Wisconsin School of Medicine and Public Health, Madison, WI, USA **Teresa Gomez-Isla,** Massachusetts General Hospital, Boston, MA, USA
02:45 pm - 02:50 pm	Session Overview	**Chairs**
2:50 pm	Correlation between in vivo 18F-flortaucipir PET and whole brain postmortem histological tau signals in Alzheimer's disease	**Yishu Chao**, University of California Berkeley, Berkeley, CA, US
3:05 pm	Tau-PET, structural MRI, and cognitive measures are differentially correlated with tangle and neuritic pathology across the neurofibrillary tangle lifespan	**Christina Moloney**, Department of Neuroscience, Mayo Clinic, Jacksonville, FL, US
3:20 pm	Binding of [3H]MK-6240 to different tau lesions: a brain autopsy study	**Milos Ikonomovic**, University of Pittsburgh School of Medicine, Department of Psychiatry, Pittsburgh, PA, US
3:35 pm	Plasma extracellular vesicle TDP-43 and hippocampal volume as complementary biomarkers for LATE-NC and hippocampal sclerosis: a pathologic validation study	**Michel Grothe**, Reina Sofia Alzheimer Center, CIEN Foundation, ISCIII, Madrid, ES
3:50 pm	Discovery and preclinical development of [18F]ACI-19626, a first-in-class TDP-43 PET tracer	**Francesca Capotosti**, AC Immune SA, EPFL Innovation Park, Building B, Lausanne, CH
04:05 pm - 04:25 pm	Discussion	
04:25 pm - 04:30 pm	**Blitz Session 1B Short Poster Presentations**	
04:25 pm	Introduction	
04:27 pm	Pathological asymmetry in early onset AD reflects heterogenous disease trajectories	**Jacob Ziontz**, Memory and Aging Center, Department of Neurology, University of California San Francisco, San Francisco, CA, US
04:28 pm	Functional submodules in the human locus coeruleus are differentially susceptible to tau pathology	**Timothy Lawn**, Athinoula A. Martinos Center for Biomedical Imaging, Department of Radiology, Massachusetts General Hospital and Harvard Medical School, 02129, Boston, MA, USA, Boston, MA, US

04:29 pm	The universal tau PET scale (Uniτ) for Flortaucipir, MK6240, PI2620 and RO948 harmonization	**Guilherme Povala**, University of Pittsburgh, Department of Psychiatry, Pittsburgh, PA, US
04:30 pm - 05:25 pm	**Poster Session 1B**	
05:25 pm - 07:30 pm	**Networking Reception**	

Thursday, January 16, 2025

08:15 am - 08:45 am	Mentoring Session	
08:45 am - 10:00 am	**ISTAART Collaborations Addressing Accessibility and Acceptability of Neuroimaging in Diverse Populations**	**Shana Stites,** University of Pennsylvania, Philadelphia, PA, USA **Tobey Betthauser,** University of Wisconsin, Madison, WI, USA
08:45 am	Introduction	**Reisa Sperling,** Brigham and Women's Hospital/HMS, Boston, MA, USA
08:50 am	Background and collaboration	**Tobey Betthauser,** University of Wisconsin, Madison, WI, USA
08:55 am	A-Frame: Actionable framework for accessibility, acceptability, and alliance in aging studies using imaging	**Shana Stites,** University of Pennsylvania, Philadelphia, PA, USA
09:05 am	Community-engaged research for increasing representation in brain aging studies – the HABS-HD approach and lessons learned	**Sid O'Bryant,** University of North Texas Health Science Center, Fort Worth, TX, USA
09:15 am	Neuroimaging of older Latino adults in Boston: Linking established and new cohorts	**Yakeel Quiroz,** Massachusetts General Hospital, Boston, MA, USA
09:25 am – 09:55 am	Discussion	
09:55 am - 10:00 am	Concluding remarks and resources	
10:00 am - 10:05 am	**Blitz Session 2A Short Poster Presentations**	
10:00 am	Introduction	
10:02 am	The role of cohort heterogeneity in predicting AD/ADRD cognitive decline	**Peiwei Liu**, Department of Neuroscience, University of California, Berkeley, Berkeley, CA, US
10:03 am	Sex moderates the association between regional tau and longitudinal cognitive decline in A4 and LEARN studies	**Annie Li**, Department of Neurology, Massachusetts General Hospital, Harvard Medical School, Boston, MA, US
10:04 am	Low tau in Aβ-positive cognitively impaired individuals: Alzheimer's disease or something more?	**Konstantinos Ioannou**, Karolinska Institutet, Stockholm, SE
10:05 am - 11:00 am	**Poster Session 2A** *(repeating in the afternoon as 2B)* - **Boards 59-116**	
11:00 am - 12:40 pm	**SESSION IV Neuropath II**	**Keith Johnson,** Massachusetts General Hospital, Boston, MA, USA **Christina Moloney,** Mayo Clinic, Jacksonville, FL, USA
11:00 am - 11:05 am	Session Overview	**Chairs**
11:05 am	Understanding the mechanisms of synaptic vesicle glycoprotein 2A change in Alzheimer's disease	**Laetitia Lemoine**, Perceptive, London, GB
11:20 am	Association of [18F]Flortaucipir-PET and plasma p-tau217 with tau neuropathology in AD and other neurodegenerative disorders	**Agathe Vrillon**, University of California San Francisco, San Francisco, CA, US

11:35 am	Tau-related cortical thinning is concentrated in sulcal depths	**Samira Maboudian**, Department of Neuroscience, University of California, Berkeley, Berkeley, CA, US
11:50 am	Comparison of [3H]MK-6240 and [3H]AV-1451 binding in relation to brain concentrations of p-tau: A postmortem biochemistry study	**Tobey Betthauser**, University of Wisconsin-Madison, School of Medicine and Public Health, Department of Medicine, Madison, WI, US
12:05 am	In vitro binding of the tau PET tracer [3H]JSS20-183A and its comparison with PI-2620, T807 and PM-PBB3 in human postmortem brain tissue	**Dinahlee Saturnino Guarino**, Department of Radiology, University of Pennsylvania, Philadelphia, PA, US
12:20 pm - 12:40 pm	Discussion	
12:40 pm - 01:40 pm	Lunch break	
01:40 pm - 02:10 pm	**KEYNOTE: From neuropathology to biomarkers: Novel strategies for detecting and monitoring Early Alzheimer's disease in vivo**	**Lea Grinberg**, University of California, San Francisco, San Francisco, CA, USA
02:10 pm - 02:25 pm	Keynote Discussion	
02:25 pm - 03:50 pm	**SESSION V Clinically Relevant Applications**	**Renaud La Joie,** University of California, San Francisco, San Francisco, CA, USA **Reisa Sperling,** Brigham and Women's Hospital/HMS, Boston, MA, USA
02:25 pm - 02:30 pm	Session Overview	**Chairs**
2:30 pm	Neuropathologic and ARIA-related findings in aducanumab-treated Alzheimer's disease: a postmortem analysis of superficial cortical Aβ clearance	**Baayla Boon**, Department of Neuroscience, Mayo Clinic, Jacksonville, FL, US
2:45 pm	Robustness of the centiloid scale across research and commercial software using [18F]flutemetamol PET images	**Adam Schwarz**, GE HealthCare, Chalfont St. Giles, GB
3:00 pm	Impact of ARIA on cerebral volume changes with Gantenerumab	**Matteo Tonietto**, Research and Early Development (pRED), Hoffmann-La Roche, Basel, CH
3:15 pm	Independent effects of baseline white matter hyperintensity and APOE ε4 on future ARIA-H emergence in A4 trial	**Zahra Shirzadi**, Department of Neurology, Massachusetts General Hospital, Brigham and Women's Hospital, Harvard Medical School, Boston, MA, US
03:30 pm - 03:50 pm	Discussion	
03:50 pm - 03:55 pm	**Blitz Session 2B Short Poster Presentations**	
3:50 pm	Introduction	
3:52 pm	Cortical freewater increases with tau tangle aggregation	**Brandon Hall**, McGill University, Montreal, QC, CA
3:53 pm	Two distinct sources of 18F-MK-6240 off-target signal identified by individualized head modeling and PET kinetics	**Charles Chen**, Athinoula A. Martinos Center for Biomedical Imaging, Massachusetts General Hospital, Charlestown, MA, US
3:54 pm	Tracking plasma biomarker abnormalities with amyloid time accumulation	**Marina Bluma**, Karolinska Institutet, Department of Neurobiology, Care Sciences and Society,

		Division of Clinical Geriatrics, Center of Alzheimer Research, Stockholm, SE
03:55 pm - 04:50 pm	**Poster Session 2B**	
04:50 pm - 06:15 pm	**SESSION VI Heterogeneity**	**Sylvia Villeneuve,** McGill University, Montreal, QC, Canada **David Wolk,** Penn Memory Center, Philadelphia, PA, USA
04:50 pm - 04:55 pm	Session Overview	**Chairs**
4:55 pm	Improving history-based prediction of biomarker and clinical progression of autosomal dominant Alzheimer's disease using mutation-level analysis of Aβ production	**Stephanie Schultz**, Harvard Medical School, Cambridge, MA, US
5:10 pm	Tau PET load in early- and late-onset Alzheimer's disease: A cross-sectional and longitudinal comparison of the LEADS and ADNI cohorts	**Konstantinos Chiotis**, University of California San Francisco, San Francisco, CA, US
5:25 pm	Regional tau quantification methodologies in early symptomatic participants with presence of tau pathology	**Diana Otero Svaldi**, Eli Lilly and Company, Indianapolis, IN, US
5:40 pm	Alpha Synuclein co-pathology accelerates amyloid associated tau accumulation in Alzheimer's disease	**Nicolai Franzmeier**, Institute for Stroke and Dementia Research (ISD), LMU University Hospital, Munich, DE
05:55 pm - 06:15 pm	Discussion	

Friday, January 17, 2025

08:15 am - 08:45 am	Mentoring Session and Breakfast	
09:00 am - 10:40 am	**SESSION VII Factors which Influence ATN**	**Heidi Jacobs,** Massachusetts General Hospital, Boston, MA, USA **Suzanne Schindler,** Washington University School of Medicine in St Louis, St Louis, MO, USA
09:00 am - 09:05 am	Session Overview	**Chairs**
09:05 am	Evaluating the ATN framework in a racially and ethnically diverse cohort: Preliminary analysis from the Health Aging Brain Study- Health Disparities Study	**Ann Cohen**, University of Pittsburgh School of Medicine, Department of Psychiatry, Pittsburgh, PA, US
09:20 am	Racial and ethnicity differences in plasma biomarker eligibility prior to amyloid PET imaging in the AHEAD 3-45 Study	**Doris Molina-Henry**, Alzheimer's Therapeutic Research Institute, University of Southern California, San Diego, CA, US
09:35 am	Examining neighborhood disadvantage as a factor explaining amyloid onset age	**Margo Heston**, Wisconsin Alzheimer's Disease Research Center, University of Wisconsin School of Medicine and Public Health, Madison, WI, US
09:50 am	Intersections of sex and neighborhood disadvantage on Alzheimer's disease pathology	**Alexandria Reese**, Department of Epidemiology, University of Pittsburgh, Pittsburgh, PA, US
10:05 am	Sex moderates relationships between P-Tau217 and longitudinal tau-PET: A multi-cohort study	**Gillian Coughlan**, Department of Neurology, Massachusetts General Hospital, Harvard Medical School, Boston, MA, US
10:20 am - 10:40 am	Discussion	

10:40 am - 10:45 am	**Blitz Session 3A Short Poster Presentations**	
10:40 am	Introduction	
10:42 am	Head-to-head comparison of longitudinal plasma assays in relation to longitudinal amyloid pathology in Alzheimer's disease	**Yara Yakoub**, Douglas Mental Health University Institute, Montréal, QC, CA
10:43 am	Calibration of multi-site raters for prospective visual read of amyloid PET scans acquired across the ADRC Consortium for Clarity in ADRD Research Through Imaging (CLARiTI)	**David Soleimani-Meigooni**, Department of Neurology, Memory and Aging Center, Weill Institute for Neurosciences, University of California, San Francisco, CA, US
10:44 am	Plasma phosphorylated tau 217 and longitudinal trajectories of Aβ, tau, and cognition in cognitively unimpaired older adults	**Hyun-Sik Yang**, Brigham and Women's Hospital, Boston, MA, US
10:45 am - 11:40 am	**P3A Poster Session 3A** *(repeating in the afternoon as 3B)* - **Boards 117-174**	
11:40 am - 12:40 pm	Lunch break	
12:40 pm - 01:10 pm	**KEYNOTE: Alzheimer's disease biomarkers among diverse populations – Data from the HABS-HD Study**	**Sid O'Bryant,** The University of North Texas HSC at Fort Worth
01:10 pm - 01:25 pm	Keynote Discussion	
01:25 pm - 02:50 pm	**SESSION VIII Plasma Biomarkers: New Methods**	**Bruna Bellaver,** University of Pittsburgh, Pittsburgh, PA, USA **Robert Rissman,** Keck School of Medicine, USC, San Diego, CA, USA
01:25 pm - 01:30 pm	Session Overview	**Chairs**
01:30 pm	Plasma tau biomarkers and staging of Alzheimer's disease	**Gemma Salvadó**, Lund University, Lund, SE
01:45 pm	Novel blood-based proteomic signatures across neurodegenerative diseases	**Maura Malpetti**, University of Cambridge, Cambridge, GB
02:00 pm	Association of CSF P-tau and MTBR-Tau biomarkers with amyloid and tau PET	**Przemyslaw Kac**, Institute of Neuroscience and Physiology, Department of Psychiatry and Neurochemistry, The Sahlgrenska Academy at University of Gothenburg, Mölndal, SE
02:15 pm	VeraBIND Tau test, a novel plasma assay for active tau pathology, identifies individuals with positive F18MK6240 tau-PET signal regardless of amyloid status	**Bernard Hanseeuw**, Cliniques Universitaires Saint-Luc, Brussels, BE
02:30 pm - 02:50 pm	Discussion	
02:50 pm - 02:55 pm	**Blitz Session 3B Short Poster Presentations**	
02:50 pm	Introduction	
02:52 pm	Locus coeruleus - medial temporal lobe functional connectivity confers protection against amyloid-related cognitive decline in the context of high cognitive reserve	**Lukas Heinrich**, Department of Radiology, Massachusetts General Hospital / Harvard Medical SChool, Boston, MA, US
02:53 pm	Association of a unique pattern of white matter T2 FLAIR hyperintensities with plasma	**Jenna Groh**, Boston University Chobanian & Avedisian School of Medicine, Boston, MA, US

	and tau PET biomarkers in former American football players	
02:55 pm - 03:50 pm	**Poster Session 3B**	
03:50 pm - 05:15 pm	**SESSION IX Plasma Biomarkers: Application**	**Jasmeer Chhatwal,** Massachusetts General Hospital, Boston, MA, USA **Thomas Karikari,** University of Pittsburgh, Pittsburgh, PA, USA
03:50 pm - 03:55 pm	Session Overview	**Chairs**
03:55 pm	Positive plasma Aβ42/40 despite negative Amyloid PET: A harbinger of progression to amyloid PET positivity?	**Azadeh Feizpour**, Florey Institute of Neuroscience and Mental Health, Melbourne, AU
04:10 pm	Head-to-head association of plasma p-tau217 with MK6240, Flortaucipir, PI2620, and RO948 Tau PET Tracers	**Pamela Ferreira**, University of Pittsburgh, Department of Psychiatry, Pittsburgh, PA, US
04:25 pm	Modeling the temporal progression of plasma and PET AD biomarkers with cognition	**Petrice Cogswell**, Mayo Clinic, Rochester, MN, US
04:40 pm	Comparison of amyloid PET, tau PET, and pTau217 biomarker progression between Down syndrome and neurotypical adults with sporadic Alzheimer's disease	**Matt Zammit**, University of Wisconsin, Madison, WI, US
04:55 pm - 05:15 pm	Discussion	
05:15 pm - 05:30 pm	**Awards Ceremony**	

HAI 2025 PROGRAM *(detail)*

Wednesday, January 15, 2025		
08:00 am - 08:30 am	Check-in and Breakfast	
08:30 am - 08:45 am	Welcome Notes	**Keith Johnson**, Massachusetts General Hospital
08:45 am - 08:55 am	Alzheimer's Association Note	**Maria Carrillo**, Alzheimer's Association
08:55 am - 10:35 am	**SESSION I Harmonization**	**Suzanne Baker,** Lawrence Berkeley National Laboratory, Berkeley, CA, USA **Bradley Christian,** University of Wisconsin School of Medicine and Public Health, Madison, WI, USA
08:55 am - 09:00 am	Session Overview	**Chairs**
09:00 am	Longitudinal amyloid burden with combined [11C]PiB and [18F]NAV4694 PET Scans	**Brecca Bettcher**, University of Wisconsin-Madison School of Medicine and Public Health and Waisman Center, Madison, WI, US
09:15 am	Exploring Centiloids robustness: Impact of sample size and image resolution on Centiloid conversion accuracy	**Jiaxiuxiu Zhang**, Memory and Aging Center, Department of Neurology, University of California, San Francisco, San Francisco, CA, US
09:30 am	Every Centiloid, from everywhere, all at once	**Ganna Blazhenets**, Memory and Aging Center, Department of Neurology, University of California, San Francisco, San Francisco, CA, US
09:45 am	The Uniτ Ecosystem for tau-PET harmonization and visualization	**Guilherme Povala**, University of Pittsburgh, Department of Psychiatry, Pittsburgh, PA, US
10:00 am	Comparative sensitivity analysis of tau-PET tracers in Alzheimer's disease	**Cécile Tissot**, Lawrence Berkeley National Laboratory, Berkeley, CA, US
10:15 am - 10:35 am	Discussion	
10:35 am - 10:40 am	**Blitz Session 1A Short Poster Presentations**	
10:35 am	Introduction	
10:37 am	Pathological and clinical trajectories of preclinical Alzheimer's disease patients with divergent cortical tau patterns	**Elizabeth Mormino**, Department of Neurology and Neurological Sciences, Stanford University School of Medicine, Stanford, CA, US
10:38 am	Association between early and late tau aggregation across tau imaging agents: The HEAD Study	**Nesrine Rahmouni**, McGill University, Montreal, QC, CA
10:39 am	Unraveling the impact of amyloid-β and tau pathology on brain structure and cognitive function during preclinical and prodromal Alzheimer's disease	**Ting Qiu**, Douglas Mental Health University Institute, McGill University, Montreal, QC, CA
10:40 am - 11:35 am	**Poster Session 1A** *(repeating in the afternoon as 1B)* **- (posters 1-58)**	
	Decline in everyday functioning over time relates to amyloid and tau in cognitively unimpaired older adults	**Mark Dubbelman**, Center for Alzheimer Research and Treatment, Department of Neurology, Brigham and Women's Hospital, Harvard Medical School, Boston, MA, US

	From the clinical utility of a-synuclein PET imaging in Multiple System Atrophy to the possible diagnosis of Parkinson's disease	**Francesca Capotosti**, AC Immune SA, EPFL Innovation Park, Building B, Lausanne, CH
	Unraveling the impact of amyloid-β and tau pathology on brain structure and cognitive function during preclinical and prodromal Alzheimer's disease	**Ting Qiu**, Douglas Mental Health University Institute, McGill University, Montreal, QC, CA
	Astrogliosis, a potential non-Aβ pathway to tau	**Victor L Villemagne**, Department of Psychiatry, University of Pittsburgh, Pittsburgh, PA, US
	APOE ε4 carriers exhibit attenuated habituation in pupil size and practice effects on a repeated auditory oddball task	**Victor L Villemagne**, Department of Psychiatry, University of Pittsburgh, Pittsburgh, PA, US
	Baseline tau burden and performance on a digital clock drawing test uniquely contributes to predicting future tau accumulation in preclinical AD	**Jessie Fang-Lu Fu**, Athinoula A. Martinos Center for Biomedical Imaging, Boston, MA, US
	Molecular correlates of apraxia in Alzheimer's disease: A PET imaging study	**Gerard Bischof**, University of Cologne, University Hospital of Cologne, Department of Nuclear Medicine, Multimodal Neuroimaging Group, Cologne, Germany, Cologne, DE
	Understanding the impact of race on white matter hyperintensities in Alzheimer's disease: Findings from the ADNI Study	**Victor Ekuta**, Morehouse School of Medicine, Atlanta, GA, US
	Characterization of a limbic-predominant amnestic neurodegenerative syndrome	**Nick Corriveau-Lecavalier**, Department of Psychiatry and Psychology, Mayo Clinic, Rochester, MN, US
	Positron emission tomography analysis with the dynamicpet Python package	**Murat Bilgel**, Laboratory of Behavioral Neuroscience, National Institute on Aging, Baltimore, MD, US
	Targeted plasma eQTL and pQTL to identify potential novel biomarker for Alzheimer's disease in African Americans	**Murat Bilgel**, Laboratory of Behavioral Neuroscience, National Institute on Aging, Baltimore, MD, US
	Pathological and clinical trajectories of preclinical Alzheimer's disease patients with divergent cortical tau patterns	**Elizabeth Mormino**, Department of Neurology and Neurological Sciences, Stanford University School of Medicine, Stanford, CA, US
	Evaluation of a label-free X-ray based method for estimating amyloid load in the human brain	**Danielle Geremia**, Division of Imaging, Diagnostics, and Software Reliability, Office of Science and Engineering Laboratories, Center for Devices and Radiological Health, Food and Drug Administration, Silver Spring, MD, US
	Proteomic analyses of A-T-N reveal plasma mediators of neurodegeneration and dementia risk	**Michael Duggan**, Laboratory of Behavioral Neuroscience, National Institute on Aging, National Institutes of Health, Baltimore, MD, US
	The spatial spread of tauopathy precedes the increase in tau-PET load in Alzheimer's disease	**Arthur Cassa Macedo**, Department of Neurology and Neurosurgery, McGill University, Montreal, QC, CA
	Distinct patterns of Iron distribution in the entorhinal cortex-hippocampus system for characterization of mild cognitive impairment	**Paul Unschuld**, Institute for Regenerative Medicine (IREM), University of Zurich, Zurich, CH
	Pathological asymmetry in early onset AD reflects heterogenous disease trajectories	**Jacob Ziontz**, Memory and Aging Center, Department of Neurology, University of California San Francisco, San Francisco, CA, US
	Characterizing amyloid-positive with low Tau (A+T-) profiles and their association with cognitive trajectories in the Longitudinal Early-	**Maison Abu Raya**, Memory and Aging Center, Department of Neurology, Weill Institute for Neurosciences, University of California, San

	Onset Alzheimer's Disease Study (LEADS): A multi-method approach	Francisco, San Francisco, San Francisco, CA, US
	The association between amyloid and physical activity in a racially diverse cohort of older adults	**Yiwen Dong**, Department of Biostatistics and Health Data Science, School of Public Health, Pittsburgh, PA, US
	Whole blood gene expression is associated with plasma p-tau217 levels via amyloid-PET and sex	**Yiwen Dong**, Department of Biostatistics and Health Data Science, School of Public Health, Pittsburgh, PA, US
	Plasma Aβ as predictor of Aβ accumulation in non-demented participants	**Alexandra Gogola**, Department of Radiology, University of Pittsburgh School of Medicine, Pittsburgh, PA, US
	The relative prevalence of tau severity stages is related to amyloid burden, clinical diagnosis and age	**Karly Cody**, Department of Neurology and Neurological Sciences, Stanford University, Stanford, CA, US
	Head-to-head trajectories of tau PET and plasma p-tau217 as a function of Aβ	**Bruna Bellaver**, University of Pittsburgh, Department of Psychiatry, PA, United States of America, Pittsburgh, PA, US
	Functional submodules in the human locus coeruleus are differentially susceptible to tau pathology	**Timothy Lawn**, Athinoula A. Martinos Center for Biomedical Imaging, Department of Radiology, Massachusetts General Hospital and Harvard Medical School, 02129, Boston, MA, USA, Boston, MA, US
	Sex-specific associations of BMI, amyloid, and regional tau deposition in community-dwelling cognitively normal older adults	**Joshua Gills**, New York University Grossman School of Medicine, New York City, NY, US
	Assessment of ATN with a single dynamic [18]F-PI-2620 recording	**Johannes Gnörich**, Department of Nuclear Medicine, University Hospital, LMU Munich, Munich, DE
	Tau-PET detects advanced primary age-related tauopathy mimicking early-stage AD	**Michel Grothe**, Reina Sofia Alzheimer Center, CIEN Foundation, ISCIII, Madrid, ES
	Amyloid status moderates associations between hippocampal microstructure, PET tau burden, and memory in dementia-free older adults	**Daniel Callow**, Johns Hopkins School of Medicine Department of Psychiatry and Behavioral Sciences, Baltimore, MD, US
	Performance of an MR-independent analysis pipeline for quantification of tau abnormality using [18F]flortaucipir PET	**Alexander DelBene**, Department of Radiology, University of Pittsburgh School of Medicine, Pittsburgh, PA, US
	Functional and structural connectivity patterns predict longitudinal tau spreading in asymptomatic individuals expressing Aβ pathology	**Jonathan Gallego-Rudolf**, Douglas Research Centre, Montreal, QC, CA
	Plasma phospho-tau 217, neurofilament-light, and glial fibrillary acidic protein are differentially associated with longitudinal neuropsychiatric symptoms across the early cognitive spectrum	**Jennifer Gatchel**, Massachusetts General Hospital, Department of Psychiatry, Boston, MA, US
	An assessment of the utility of flortaucipir PET to detect four-repeat tau pathology in a globular glia tauopathy case-series	**Rodolfo Gatto**, Department of Neurology, Mayo Clinic, Rochester, MN, US
	Molecular imaging of neurodegeneration – mitochondria, associated proteins and synapses (MIND-MAPS) in frontotemporal dementia	**Mica Clarke**, Perceptive, London, GB
	Evaluating tVNS effects on cognitive outcomes and modulating factors in asymptomatic older adults: study design of the WALLe Trial	**Nina Engels-Domínguez**, The Athinoula A. Martinos Center for Biomedical Imaging, Department of Radiology, Massachusetts General Hospital, Harvard Medical School, Boston, MA, US
	Cerebral perfusion indices from early-phase [18F]-MK6240 dynamic Tau PET imaging in brain regions associated with Alzheimer's disease progression in an aging population.	**Maeva Dhaynaut**, Yale PET Center, Department of Radiology & Biomedical Imaging, Yale University School of Medicine, New Haven, CT, US

Transcutaneous auricular vagus nerve stimulation improves learning and sleep-wake quality in older APOE-ε4 carriers	**Marion Baillet**, Athinoula A. Martinos Center for Biomedical Imaging, Department of Radiology, Massachusetts General Hospital, Boston, MA, US
Biological-clinical mismatch reflects co-pathology and vulnerability to neurodegeneration	**Christopher Brown**, Department of Neurology, University of Pennyslvania, Philadelphia, PA, US
Validation of PET spatial extent as sensitive amyloid biomarker in early stages of amyloidosis	**Grace Del Carmen Montenegro**, Department of Radiology, Massachusetts General Hospital, Harvard Medical School, Boston, MA, US
Developing a novel reference region for PI-2620-PET imaging to facilitate assessment of 4-repeat tauopathies	**Lukas Frontzkowski**, Institute for Stroke and Dementia Research (ISD), Munich, DE
P-TAU217, GFAP, and NFL plasma biomarker associations with demographic, medical and neurocognitive features from middle-aged through older adulthood	**Steven Arnold**, Massachusetts General Hospital, Harvard Medical School, Boston, MA, US
DeepSUVR: Using temporal constraints to improve tau quantification	**Pierrick Bourgeat**, CSIRO Health and Biosecurity, Brisbane, AU
Increasing the granularity of tau-PET Braak staging using medial temporal lobe segmentations to detect early memory impairment	**Etienne Aumont**, McGill University Research Centre for Studies in Aging, Montréal, QC, CA
The universal tau PET scale (Uniτ) for Flortaucipir, MK6240, PI2620 and RO948 harmonization	**Guilherme Povala**, University of Pittsburgh, Department of Psychiatry, Pittsburgh, PA, US
Assessing the relationship between neuropsychiatric symptoms, amyloid and tau pathology, and white matter hyperintensity volume across sexes in preclinical Alzheimer's disease	**Aurélie Garrone**, Douglas Mental Health University Institute, Montreal, QC, CA
Unveiling the heterogeneity of tau spreading in aging and Alzheimer's disease using polygenic combinations: Towards personalized models	**Ibai Diez**, Gordon Center for Medical Imaging, Department of Radiology, Massachusetts General Hospital, Harvard Medical School, Boston, MA, USA, Boston, MA, US
Regional amyloid and tau: Exploring regional sex-based differences in a middle-aged community-based cohort	**Diana S Guzmán**, Columbia University Medical Center, New York, NY, US
Comparison of topographical patterns of abnormalities of the tau PET tracers [18F]Flortaucipir, [18F]MK6240, [18F]PI2620, and [18F]RO948	**Livia Amaral**, University of Pittsburgh, Department of Psychiatry, Pittsburgh, PA, US
Subtle cognitive deficits detected through routine in-office tests are associated with global Aβ and temporal tau in cognitively unimpaired individuals	**Cynthia Felix**, Department of Psychiatry, University of Pittsburgh, Pittsburgh, PA, US
Estradiol-dependent associations between sleep complaints and tau deposition in women at elevated AD risk	**Sarah Banks**, SDSU/UC San Diego Joint Doctoral Program in Clinical Psychology, San Diego, CA, US
Impact of age and sex on extra-cerebral off-target binding in tau PET scans (18F-FTP)	**Sujala Ghatamaneni**, Department of Radiology, Mayo Clinic, Rochester, MN, US
Metabolic inefficiency is associated with regional vulnerability to tau deposition	**Jenna Adams**, University of California, Irvine, Irvine, CA, US
Relationship between Polygenetic Risk Score of BrainAge and plasma biomarkers in the A4/Elearn Study	**Jorge Garcia Condado**, Computational Neuroimaging Lab, Biobizkaia Health Research Institute, Barakaldo, ES
Combined impact of plasma phospho-tau 217 and NfL on longitudinal domain-specific cognitive decline	**Hiroko Dodge**, Harvard Medical School, Boston, MA, US

	Comparison of distribution volume and standardized uptake value ratio for a MAO-B tracer in mild cognitive impairment	**Gleb Bezgin**, McGill University, Montreal, QC, CA
	Association between early and late tau aggregation across tau imaging agents: The HEAD Study	**Nesrine Rahmouni**, McGill University, Montreal, QC, CA
	The impact of spatial smoothing on the accuracy of Centiloid thresholds	**Alfonso Fajardo-Valdez**, Douglas Mental Health University Institute, Montreal, Quebec, Canada, Montreal, QC, CA
	Longitudinal amyloid PET trajectories in the HABS-HD cohort	**Tobey Betthauser**, University of Wisconsin-Madison, School of Medicine and Public Health, Department of Medicine, Madison, WI, US
	Lower microstructural integrity of the locus coeruleus to entorhinal cortex pathway is related to elevated astrocyte reactivity and tau burden in cognitively unimpaired individuals: a 7T dMRI study	**Yuliya Patsyuk**, Faculty of Health, Medicine and Life Sciences, Mental Health and Neuroscience Research Institute, Alzheimer Centre Limburg, Maastricht University, Maastricht, NL
11:35 am - 01:00 pm	**SESSION II Spatial Patterns**	**Ansel Hillmer,** University of Michigan **,** Ann Arbor, MI, USA **Pedro Rosa-Neto,** McGill University, Montreal, QC, Canada
11:35 am - 11:40 am	Session Overview	**Chairs**
11:40 am	The interaction of initial medial temporal lobe tauopathy and amyloid-beta spatial extent in driving caTAUstrophe	**Michelle Farrell**, Massachusetts General Hospital, Boston, MA, US
11:55 am	Mapping spatial white matter integrity linked to tau accumulation: Insights from tractometry with multi-shell diffusion imaging	**Dana Parker**, University of California Irvine, Irvine, CA, US
12:10 am	Spatial patterns of voxel-wise tau accumulation across the Alzheimer's disease spectrum	**Corrina Fonseca**, Department of Neuroscience, University of California Berkeley, Berkeley, CA, US
12:25 am	PET astroglia and microglia follow tau propagation patterns in Alzheimer's disease	**Nesrine Rahmouni**, McGill University, Montreal, QC, CA
12:40 pm - 01:00 pm	Discussion	
01:00 pm - 02:00 pm	Lunch break	
02:00 pm - 02:30 pm	**KEYNOTE: From click chemistry to precision neuroscience**	**Hartmuth Kolb,** Enigma Biomedical Group
02:30 pm - 02:45 pm	Keynote Discussion	
02:45 pm - 04:25 pm	**SESSION III Neuropath I**	**Tobey Betthauser,** University of Wisconsin School of Medicine and Public Health, Madison, WI, USA **Teresa Gomez-Isla,** Massachusetts General Hospital, Boston, MA, USA
02:45 pm - 02:50 pm	Session Overview	**Chairs**
2:50 pm	Correlation between in vivo 18F-flortaucipir PET and whole brain postmortem histological tau signals in Alzheimer's disease	**Yishu Chao**, University of California Berkeley, Berkeley, CA, US
3:05 pm	Tau-PET, structural MRI, and cognitive measures are differentially correlated with tangle and	**Christina Moloney**, Department of Neuroscience, Mayo Clinic, Jacksonville, FL, US

	neuritic pathology across the neurofibrillary tangle lifespan	
3:20 pm	Binding of [3H]MK-6240 to different tau lesions: a brain autopsy study	**Milos Ikonomovic**, University of Pittsburgh School of Medicine, Department of Psychiatry, Pittsburgh, PA, US
3:35 pm	Plasma extracellular vesicle TDP-43 and hippocampal volume as complementary biomarkers for LATE-NC and hippocampal sclerosis: a pathologic validation study	**Michel Grothe**, Reina Sofia Alzheimer Center, CIEN Foundation, ISCIII, Madrid, ES
3:50 pm	Discovery and preclinical development of [18F]ACI-19626, a first-in-class TDP-43 PET tracer	**Francesca Capotosti**, AC Immune SA, EPFL Innovation Park, Building B, Lausanne, CH
04:05 pm - 04:25 pm	Discussion	
04:25 pm - 04:30 pm	**Blitz Session 1B Short Poster Presentations**	
04:25 pm	Introduction	
04:27 pm	Pathological asymmetry in early onset AD reflects heterogenous disease trajectories	**Jacob Ziontz**, Memory and Aging Center, Department of Neurology, University of California San Francisco, San Francisco, CA, US
04:28 pm	Functional submodules in the human locus coeruleus are differentially susceptible to tau pathology	**Timothy Lawn**, Athinoula A. Martinos Center for Biomedical Imaging, Department of Radiology, Massachusetts General Hospital and Harvard Medical School, 02129, Boston, MA, USA, Boston, MA, US
04:29 pm	The universal tau PET scale (Uniτ) for Flortaucipir, MK6240, PI2620 and RO948 harmonization	**Guilherme Povala**, University of Pittsburgh, Department of Psychiatry, Pittsburgh, PA, US
04:30 pm - 05:25 pm	**Poster Session 1B**	
05:25 pm - 07:30 pm	**Networking Reception**	

Thursday, January 16, 2025

08:15 am - 08:45 am	Mentoring Session/Breakfast	
08:45 am - 10:00 am	**ISTAART Collaborations Addressing Accessibility and Acceptability of Neuroimaging in Diverse Populations**	**Shana Stites,** University of Pennsylvania, Philadelphia, PA, USA **Tobey Betthauser,** University of Wisconsin, Madison, WI, USA
08:45 am	Introduction	**Reisa Sperling,** Brigham and Women's Hospital/HMS, Boston, MA, USA
08:50 am	Background and collaboration	**Tobey Betthauser,** University of Wisconsin, Madison, WI, USA
08:55 am	A-Frame: Actionable framework for accessibility, acceptability, and alliance in aging studies using imaging	**Shana Stites,** University of Pennsylvania, Philadelphia, PA, USA
09:05 am	Community-engaged research for increasing representation in brain aging studies – the HABS-HD approach and lessons learned	**Sid O'Bryant,** University of North Texas Health Science Center, Fort Worth, TX, USA

09:15 am	Neuroimaging of older Latino adults in Boston: Linking established and new cohorts	**Yakeel Quiroz,** Massachusetts General Hospital, Boston, MA, USA
09:25 am – 09:55 am	Discussion	
09:55 am - 10:00 am	Concluding remarks and resources	
10:00 am - 10:05 am	**Blitz Session 2A Short Poster Presentations**	
10:00 am	Introduction	
10:02 am	The role of cohort heterogeneity in predicting AD/ADRD cognitive decline	**Peiwei Liu**, Department of Neuroscience, University of California, Berkeley, Berkeley, CA, US
10:03 am	Sex moderates the association between regional tau and longitudinal cognitive decline in A4 and LEARN studies	**Annie Li**, Department of Neurology, Massachusetts General Hospital, Harvard Medical School, Boston, MA, US
10:04 am	Low tau in Aβ-positive cognitively impaired individuals: Alzheimer's disease or something more?	**Konstantinos Ioannou**, Karolinska Institutet, Stockholm, SE
10:00 am	Introduction	
10:05 am - 11:00 am	**Poster Session 2A** *(repeating in the afternoon as 2B)* - **Boards 59-116**	
	Interpretable prediction of amyloid PET positivity using non-negative matrix factorization	**David Jones**, Department of Neurology, Mayo Clinic, ROCHESTER, MN, US
	Data-driven biomarker discovery nominates novel diagnostic plasma biomarkers and provides insights into Alzheimer's disease pathophysiology in an African American cohort	**Lindsey Kuchenbecker**, Department of Neuroscience, Mayo Clinic, Jacksonville, FL, USA, Jacksonville, FL, US
	Longitudinal multicenter head-to-head harmonization of tau PET tracers: an overview of the HEAD study cohort	**Firoza Lussier**, University of Pittsburgh, Pittsburgh, PA, US
	Higher time varying brain functional connectivity is associated with slower tau accumulation at the preclinical stage of Alzheimer's disease	**Mohammadali Javanray**, McGill University, Montreal, QC, CA
	Graph convolutional networks to predict cognitive decline at the individual level in Alzheimer's disease	**Min Su Kang**, Artificial Intelligence and Computational Neurosciences lab, Sunnybrook Research Institute, University of Toronto, Toronto, ON, CA
	Low tau in Aβ-positive cognitively impaired individuals: Alzheimer's disease or something more?	**Konstantinos Ioannou**, Karolinska Institutet, Stockholm, SE
	A plasma clock for Alzheimer disease based on %p-tau217	**Kellen K. Petersen**, Department of Neurology, Washington University in St. Louis, St. Louis, MO, US
	Network-based amyloid-β pathology predicts subsequent cognitive decline in cognitively normal older adults	**Hengda He**, Cognitive Neuroscience Division, Department of Neurology, Columbia University, Vagelos College of Physicians and Surgeons, New York, NY, US
	Associations between APOE-TOMM40 '523 haplotype variants and limbic system white matter microstructure in Black and White individuals	**Katelyn Mooney**, University of California Los Angeles, Neuroscience Interdepartmental Program (NSIDP), David Geffen School of Medicine, Los Angeles, CA, USA., Los Angeles, CA, US

Multi element MRI template method for analysis of Down syndrome PET	**Charles Laymon**, University of Pittsburgh, Pittsburgh, PA, US
Whole-blood gene expression associations with Aβ-PET accumulation and cognitive decline	**Hannah Klinger**, Massachusetts General Hospital/Harvard Medical School, Boston, MA, US
Longitudinal change in five dominant dimensions of brain aging in relation to brain amyloid status and Alzheimer's-related plasma biomarkers	**Murat Bilgel**, Laboratory of Behavioral Neuroscience, National Institute on Aging, Baltimore, MD, US
Enrichment of patients with concomitant LATE on the Alzheimer's disease continuum using hippocampal volume	**Nidhi Mundada**, University of Pennsylvania, Philadelphia, PA, US
AT(N) staging of Alzheimer's disease: Comparison of visual interpretation and automated quantification pipelines	**Brian Lopresti**, Department of Radiology, University of Pittsburgh School of Medicine, Pittsburgh, PA, US
MK-6240 off-target binding patterns in relation to microglia density, measured through TSPO PET	**Lauren Heuer**, Columbia University Medical Center, New York, NY, US
Association between medication use and [18F]MK6240 and [18F]Flortaucipir uptake across the Alzheimer's disease spectrum	**Rayan Mroué**, University of Pittsburgh, Department of Psychiatry, Pittsburgh, PA, US
Lower LC-EC tract integrity is associated with entorhinal tau in autosomal-dominant Alzheimer's disease	**Elouise Koops**, Martinos Center for Biomedical Imaging, Department of Radiology, Massachusetts General Hospital, Harvard Medical School, Boston, MA, US
APOE4 associated with higher off-target meninges signal with [F-18]MK6240 PET	**Andrew McVea**, University of Wisconsin - Madison, Madison, WI, US
An accurate and automated technique for removing spill-over contamination and off-target retention from a cerebellar reference region for tau PET	**Davneet Minhas**, University of Pittsburgh, Pittsburgh, PA, US
Updated public CenTauR pipelines to measure CenTauR, CenTauRZ, and SUVR tau PET units	**Christopher Schwarz**, Mayo Clinic, Rochester, MN, US
Predicting regional Alzheimer's disease pathology with plasma p-tau217 in preclinical AD	**Hasom Moon**, Stony Brook University, Stony Brook, NY, US
TSPO-PET before and after low-dose interleukin-2 in patients with mild to moderate Alzheimer's disease	**Belen Pascual**, Houston Methodist Stanley H. Appel Department of Neurology, Houston Methodist Research Institute, Weill Cornell Medicine, Houston, TX, US
In low neocortical tau individuals, high amygdala tau predicts faster cognitive decline	**Bernard Hanseeuw**, Mass General Brigham, Boston, MA, US
EOAD-signature atrophy predicts progression to dementia in patients with early-onset MCI due to Alzheimer's disease	**Yuta Katsumi**, Department of Biostatistics, Center for Statistical Sciences, Brown University, Providence, RI, US
FDG reference region selection using PiB amyloid status-guided iterative normalization in a Down syndrome cohort	**Max McLachlan**, University of Wisconsin - Madison, Madison, WI, US
Microscopic visualization of fluorescent MK-6240	**Peter Kunach**, Center for Alzheimer's and Neurodegenerative Diseases, Peter O'Donnell Jr. Brain Institute, Dallas, TX, US
Conversion of Tau PET SUVR data to CenTauR units using the Joint Propagation Model	**Antoine Leuzy**, Clinical Memory Research Unit, Department of Clinical Sciences, Lund University, Lund, SE
The role of cohort heterogeneity in predicting AD/ADRD cognitive decline	**Peiwei Liu**, Department of Neuroscience, University of California, Berkeley, Berkeley, CA, US
Differential tau accumulation in early-onset and late-onset Alzheimer's disease: Insights from [18F]-Florzolotau PET	**Bayarjargal Khurelbaatar**, Department of Medical Imaging and Radiological Sciences,

		Chang Gung University, Taoyuan, Taiwan, ROC., Taoyuan, TW
	Heterogeneity of FDG-PET patterns among tau-negative amnestic patients	**Jesús Silva-Rodríguez**, Reina Sofia Alzheimer Centre, CIEN Foundation, ISCIII, Madrid, ES
	Predicting amyloid positivity and tau burden in dementia using a combination of different biomarkers	**Shao-Yi Huang**, Department of Medical Imaging and Radiological Sciences, Chang Gung University, Taoyuan, TW
	Evaluation of [^{3}H]SynVesT - 1 binding in post-mortem brain tissue from control and Alzheimer's disease as a biomarker of synaptic loss	**Laura Kulagowska**, Perceptive, London, GB
	Exploring the predictive power of graph-theoretic metrics for tau pathology in cognitively unimpaired older adults	**Emily Johns**, Department of Neurology, Yale University School of Medicine, New Haven, CT, US
	Tracking biomarkers accuracy for predicting progression to mild cognitive impairment	**Jonathan Gallego-Rudolf**, Douglas Research Centre, Montreal, QC, CA
	Tau burden across Braak stages is associated with regionally specific amyloid accumulation: insights from the BIOCARD cohort	**Nisha Rani**, Department of Psychiatry and Behavioral Sciences, Johns Hopkins University School of Medicine, Baltimore, MD, US
	Relationship between neuroinflammatory ER176-PET and functional connectivity in Progressive Apraxia of Speech	**Neha Singh-Reilly**, Department of Neurology, Mayo Clinic, Rochester, MN, US
	Sex moderates the association between regional tau and longitudinal cognitive decline in A4 and LEARN studies	**Annie Li**, Department of Neurology, Massachusetts General Hospital, Harvard Medical School, Boston, MA, US
	Evaluation of the Uni-tau and CenTauR frameworks in new datasets for tau PET harmonization in Alzheimer's disease	**Olivia Lutz**, Research and Early Development (gRED), Genentech, Inc, South San Francisco, CA, US
	Hemispheric lateralization of tau-related network dysfunction and its association with neuropsychiatric symptoms in preclinical Alzheimer's disease	**Sophia Moret**, Yale University, New Haven, CT, US
	Characterization and correction of extracerebral [18F]MK-6240 tau PET off-target signal in Alzheimer's disease	**Emily Olafson**, Research and Early Development (gRED), Genentech, Inc., South San Francisco, CA, US
	Investigation of optimal intensity threshold for tau-PET overlap index	**Seokbeen Lim**, Department of Radiology, Mayo Clinic, Rochester, MN, US
	DeepSUVR: Towards redefining the Centiloid masks using a data-driven approach	**Pierrick Bourgeat**, CSIRO Health and Biosecurity, Brisbane, AU
	Mechanical stress of the entorhinal cortex: A potential driver of tau pathology?	**Frank Provenzano**, Columbia University, New York, NY, US
	Amyloid-Tau to neurodegeneration mismatch from inter-modality image translation using deep learning	**Xueying Lyu**, University of Pennsylvania, Philadelphia, PA, US
	Tau PET subgroups differ in network patterns of functional connectivity and amyloid PET	**Peter Millar**, Washington University in St. Louis, St. Louis, MO, US
	Cortical freewater increases with tau tangle aggregation	**Brandon Hall**, McGill University, Montreal, QC, CA
	Distinct spatiotemporal patterns of vascular disease in Alzheimer's disease subtypes	**Julie Ottoy**, Hurvitz Brain Sciences Program, Sunnybrook Research Institute, University of Toronto, Toronto, ON, CA
	Annual percent change of microglia density in relation to tau accumulation in older adults	**Hannah Houlihan**, Columbia University Medical Center, New York, NY, US
	Physical frailty as a risk factor for increased tau accumulation and cognitive decline in cognitively unimpaired older adults	**Kailee Palmgren**, Department of Neurology, Massachusetts General Hospital, Boston, MA, US
	Assessing neuroinflammation in Alzheimer's disease: A TSPO-PET study using ER176 and its correlation with amyloid and tau pathology	**David Jacobson**, Department of Neurology, Mayo Clinic, Rochester, MN, US

	Two distinct sources of 18F-MK-6240 off-target signal identified by individualized head modeling and PET kinetics	**Charles Chen**, Athinoula A. Martinos Center for Biomedical Imaging, Massachusetts General Hospital, Charlestown, MA, US
	TSPO PET mediates tau-associated neurodegeneration in limbic and temporal regions across clinical variants of Alzheimer's disease	**Patrick Lao**, Columbia University Medical Center, New York, NY, US
	Tracking plasma biomarker abnormalities with amyloid time accumulation	**Marina Bluma**, Karolinska Institutet, Department of Neurobiology, Care Sciences and Society, Division of Clinical Geriatrics, Center of Alzheimer Research, Stockholm, SE
	Advancing antibody-based pretargeted PET imaging of protein aggregates in the brain	**Michael Honer**, Cluster for Molecular Imaging, Department of Biomedical Sciences, University of Copenhagen, Copenhagen, DK
	Longitudinal change in mnemonic discrimination and influence of Aβ burden	**Jessica Kraft**, Center for Vital Longevity, University of Texas at Dallas, Dallas, TX, US
11:00 am - 12:40 pm	**SESSION IV Neuropath II**	**Keith Johnson,** Massachusetts General Hospital, Boston, MA, USA **Christina Moloney,** Mayo Clinic, Jacksonville, FL, USA
11:00 am - 11:05 am	Session Overview	**Chairs**
11:05 am	Understanding the mechanisms of synaptic vesicle glycoprotein 2A change in Alzheimer's disease	**Laetitia Lemoine**, Perceptive, London, GB
11:20 am	Association of [18F]Flortaucipir-PET and plasma p-tau217 with tau neuropathology in AD and other neurodegenerative disorders	**Agathe Vrillon**, University of California San Francisco, San Francisco, CA, US
11:35 am	Tau-related cortical thinning is concentrated in sulcal depths	**Samira Maboudian**, Department of Neuroscience, University of California, Berkeley, Berkeley, CA, US
11:50 am	Comparison of [3H]MK-6240 and [3H]AV-1451 binding in relation to brain concentrations of p-tau: A postmortem biochemistry study	**Tobey Betthauser**, University of Wisconsin-Madison, School of Medicine and Public Health, Department of Medicine, Madison, WI, US
12:05 am	In vitro binding of the tau PET tracer [3H]JSS20-183A and its comparison with PI-2620, T807 and PM-PBB3 in human postmortem brain tissue	**Dinahlee Saturnino Guarino**, Department of Radiology, University of Pennsylvania, Philadelphia, PA, US
12:20 pm - 12:40 pm	Discussion	
12:40 pm - 01:40 pm	Lunch break	
01:40 pm - 02:10 pm	**KEYNOTE: From neuropathology to biomarkers: Novel strategies for detecting and monitoring Early Alzheimer's disease in vivo**	**Lea Grinberg**, University of California, San Francisco, San Francisco, CA, USA
02:10 pm - 02:25 pm	Keynote Discussion	
02:25 pm - 03:50 pm	**SESSION V Clinically Relevant Applications**	**Renaud La Joie,** University of California, San Francisco. San Francisco, CA, USA **Reisa Sperling,** Brigham and Women's Hospital**,** Boston, MA, USA
02:25 pm - 02:30 pm	Session Overview	**Chairs**
2:30 pm	Neuropathologic and ARIA-related findings in aducanumab-treated Alzheimer's disease: a	**Baayla Boon**, Department of Neuroscience, Mayo Clinic, Jacksonville, FL, US

	postmortem analysis of superficial cortical Aβ clearance	
2:45 pm	Robustness of the centiloid scale across research and commercial software using [18F]flutemetamol PET images	**Adam Schwarz**, GE HealthCare, Chalfont St. Giles, GB
3:00 pm	Impact of ARIA on cerebral volume changes with Gantenerumab	**Matteo Tonietto**, Research and Early Development (pRED), Hoffmann-La Roche, Basel, CH
3:15 pm	Independent effects of baseline white matter hyperintensity and APOE ε4 on future ARIA-H emergence in A4 trial	**Zahra Shirzadi**, Department of Neurology, Massachusetts General Hospital, Brigham and Women's Hospital, Harvard Medical School, Boston, MA, US
03:30 pm - 03:50 pm	Discussion	
03:50 pm - 03:55 pm	**Blitz Session 2B Short Poster Presentations**	
3:50 pm	Introduction	
3:52 pm	Cortical freewater increases with tau tangle aggregation	**Brandon Hall**, McGill University, Montreal, QC, CA
3:53 pm	Two distinct sources of 18F-MK-6240 off-target signal identified by individualized head modeling and PET kinetics	**Charles Chen**, Athinoula A. Martinos Center for Biomedical Imaging, Massachusetts General Hospital, Charlestown, MA, US
3:54 pm	Tracking plasma biomarker abnormalities with amyloid time accumulation	**Marina Bluma**, Karolinska Institutet, Department of Neurobiology, Care Sciences and Society, Division of Clinical Geriatrics, Center of Alzheimer Research, Stockholm, SE
03:55 pm - 04:50 pm	Poster Session 2B	
04:50 pm - 06:15 pm	**SESSION VI Heterogeneity**	**Sylvia Villeneuve,** McGill University, Montreal, QC, Canada **David Wolk,** Penn Memory Center, Philadelphia, PA, USA
04:50 pm - 04:55 pm	Session Overview	**Chairs**
4:55 pm	Improving history-based prediction of biomarker and clinical progression of autosomal dominant Alzheimer's disease using mutation-level analysis of Aβ production	**Stephanie Schultz**, Harvard Medical School, Cambridge, MA, US
5:10 pm	Tau PET load in early- and late-onset Alzheimer's disease: A cross-sectional and longitudinal comparison of the LEADS and ADNI cohorts	**Konstantinos Chiotis**, University of California San Francisco, San Francisco, CA, US
5:25 pm	Regional tau quantification methodologies in early symptomatic participants with presence of tau pathology	**Diana Otero Svaldi**, Eli Lilly and Company, Indianapolis, IN, US
5:40 pm	Alpha Synuclein co-pathology accelerates amyloid associated tau accumulation in Alzheimer's disease	**Nicolai Franzmeier**, Institute for Stroke and Dementia Research (ISD), LMU University Hospital, Munich, DE
05:55 pm - 06:15 pm	Discussion	

Friday, January 17, 2025

08:15 am - 08:45 am	Mentoring Session and Breakfast	
09:00 am - 10:40 am	**SESSION VII Factors which Influence ATN**	**Heidi Jacobs,** Massachusetts General Hospital, Boston, MA, USA **Suzanne Schindler,** Washington University School of Medicine in St Louis, St Louis, MO, USA
09:00 am - 09:05 am	Session Overview	**Chairs**
09:05 am	Evaluating the ATN framework in a racially and ethnically diverse cohort: Preliminary analysis from the Health Aging Brain Study- Health Disparities Study	**Ann Cohen**, University of Pittsburgh School of Medicine, Department of Psychiatry, Pittsburgh, PA, US
09:20 am	Racial and ethnicity differences in plasma biomarker eligibility prior to amyloid PET imaging in the AHEAD 3-45 Study	**Doris Molina-Henry**, Alzheimer's Therapeutic Research Institute, University of Southern California, San Diego, CA, US
09:35 am	Examining neighborhood disadvantage as a factor explaining amyloid onset age	**Margo Heston**, Wisconsin Alzheimer's Disease Research Center, University of Wisconsin School of Medicine and Public Health, Madison, WI, US
09:50 am	Intersections of sex and neighborhood disadvantage on Alzheimer's disease pathology	**Alexandria Reese**, Department of Epidemiology, University of Pittsburgh, Pittsburgh, PA, US
10:05 am	Sex moderates relationships between P-Tau217 and longitudinal tau-PET: A multi-cohort study	**Gillian Coughlan**, Department of Neurology, Massachusetts General Hospital, Harvard Medical School, Boston, MA, US
10:20 am - 10:40 am	Discussion	
10:40 am - 10:45 am	**Blitz Session 3A Short Poster Presentations**	
10:40 am	Introduction	
10:42 am	Head-to-head comparison of longitudinal plasma assays in relation to longitudinal amyloid pathology in Alzheimer's disease	**Yara Yakoub**, Douglas Mental Health University Institute, Montréal, QC, CA
10:43 am	Calibration of multi-site raters for prospective visual read of amyloid PET scans acquired across the ADRC Consortium for Clarity in ADRD Research Through Imaging (CLARiTI)	**David Soleimani-Meigooni**, Department of Neurology, Memory and Aging Center, Weill Institute for Neurosciences, University of California, San Francisco, CA, US
10:44 am	Plasma phosphorylated tau 217 and longitudinal trajectories of Aβ, tau, and cognition in cognitively unimpaired older adults	**Hyun-Sik Yang**, Brigham and Women's Hospital, Boston, MA, US
10:45 am - 11:40 am	**Poster Session 3A** *(repeating in the afternoon as 3B)* **- (posters 117-174)**	
	Concordance between visual and quantitative amyloid PET and CSF biomarkers in the ADNI-DOD cohort	**Agathe Vrillon**, University of California San Francisco, San Francisco, CA, US
	Calibration of multi-site raters for prospective visual read of amyloid PET scans acquired across the ADRC Consortium for Clarity in ADRD Research Through Imaging (CLARiTI)	**David Soleimani-Meigooni**, Department of Neurology, Memory and Aging Center, Weill Institute for Neurosciences, University of California, San Francisco, CA, US
	Evaluating the effect of APOE genotype in real-world clinical settings: results from the IDEAS-ANGI study	**Stefania Pezzoli**, Memory and Aging Center, Department of Neurology, University of California, San Francisco, San Francisco, CA, US
	Brain connectivity drives tau distribution while regional vulnerability drives tau load in Alzheimer's disease	**Yu Xiao**, Department of Clinical Sciences Malmö, SciLifeLab, Lund University, Lund, SE

	Synergistic effects of peripheral inflammation and neuroinflammation on amyloid, vascular, and neurodegeneration markers across the Alzheimer's disease spectrum	**Laura Alejandra Ramirez Tirado**, Department of Epidemiology, University of Pittsburgh, Pittsburgh, PA, US
	Impact of amyloid removal on cerebral volume changes with Gantenerumab	**Matteo Tonietto**, Research and Early Development (pRED), Hoffmann-La Roche, Basel, CH
	Astrocyte reactivity explains tau-related effects on hippocampal dysfunction and longitudinal atrophy in preclinical Alzheimer's disease	**Noah Schweitzer**, Department of Bioengineering, University of Pittsburgh, Pittsburgh, PA, US
	Plasma phosphorylated tau 217 and longitudinal trajectories of Aβ, tau, and cognition in cognitively unimpaired older adults	**Hyun-Sik Yang**, Brigham and Women's Hospital, Boston, MA, US
	Detection of TDP-43 from plasma-derived astrocyte extracellular vesicles for identification of LATE	**Robert Rissman**, University of Southern California, Neuroscience Translational Research Division, Alzheimer's Therapeutic Research Institute, SAN DIEGO, CA, US
	Short sleep duration is associated with higher subsequent plasma p-tau217 in aging	**Joseph Winer**, Department of Neurology and Neurological Sciences, Stanford University, Stanford, CA, US
	Impacts of testing language and rates of amyloid positivity among underrepresented groups in the A4 Study	**Isha Sai**, Department of Neurology and Neurological Sciences, Stanford University, Stanford, CA, US
	Lower locus coeruleus metabolism is associated with greater year-to-year intraindividual cognitive variability in older individuals with elevated levels of Alzheimer's disease pathology	**Emma E Wiklund**, The Athinoula A. Martinos Center for Biomedical Imaging, Department of Radiology, Massachusetts General Hospital, Harvard Medical School, Boston, MA, US
	Long-term cognitive and biomarker trajectories of cognitively unimpaired individuals with elevated plasma ptau-217	**Jesús Silva-Rodríguez**, Reina Sofia Alzheimer Centre, CIEN Foundation, ISCIII, Madrid, ES
	A large public release of PIB PET and MRI from the Mayo Clinic Study of Aging	**Christopher Schwarz**, Mayo Clinic, Rochester, MN, US
	Harmonizing visual readings of Flortaucipir and MK-6240 using head-to-head data	**Emma Ruppert**, University of Pittsburgh, Department of Psychiatry, Pittsburgh, PA, US
	Twin-mapping techniques in clinical trials: a proof-of-concept application to the Internet-Based Conversational Engagement Clinical Trial (I-CONECT)	**Chao-Yi Wu**, Neurology, Massachusetts General Hospital (MGH), Harvard Medical School, Charlestown, MA, US
	Effects of amyloid and tau status on multiplex plasma CNS and inflammatory proteins in a normal aging cohort	**Karly Cody**, Department of Neurology and Neurological Sciences, Stanford University, Stanford, CA, US
	Tau imaging thresholds within NIA-AA multilevel tau staging as predictors of tau accumulation and cognitive decline in non-demented individuals	**Alexandra Gogola**, Department of Radiology, University of Pittsburgh School of Medicine, Pittsburgh, PA, US
	Multi-morbidity and Alzheimer's disease pathology across the lifespan in adults with Down syndrome	**Anna Smith**, Columbia University Medical Center, New York, NY, US
	Cortical atrophy is correlated with the discrepancy between neuroradiological assessment and binary quantitation of florbetapir PET in nondemented older adults	**Daniel Schwartz**, OHSU Neurology, Portland, OR, US
	Vascular pathology influences the association of tau-PET with neurodegeneration and cognition in Aβ-negative individuals	**Markley Silva Oliveira Junior**, University of Pittsburgh, Department of Psychiatry, Pittsburgh, PA, US
	Concomitant neurodegeneration of the lateral hypothalamus and locus coeruleus is associated with early Alzheimer's disease-related pathophysiological and cognitive processes	**Maxime Van Egroo**, Faculty of Health, Medicine and Life Sciences, Mental Health and Neuroscience Research Institute, Alzheimer

		Center Limburg, Maastricht University, Maastricht, NL
	Amyloid-associated hyperconnectivity drives tau spreading across connected brain regions in Alzheimer's disease	**Sebastian Niclas Roemer-Cassiano**, Department of Neurology, University Hospital, LMU Munich, Germany, Munich, DE
	Association of plasma GFAP with tau PET in cognitively unimpaired Aβ-negative subjects	**Pampa Saha**, University of Pittsburgh, Department of Psychiatry, Pittsburgh, PA, US
	The striatum is an early, accurate indicator of [C-11]PiB amyloid burden for the Down syndrome population	**Max McLachlan**, University of Wisconsin - Madison, Madison, WI, US
	Best practices for tau-PET tracer harmonization in Alzheimer's research	**Cécile Tissot**, Lawrence Berkeley National Laboratory, Berkeley, CA, US
	Relationship between metabolic syndrome biomarkers and regional tau accumulation in cognitively unimpaired older adults	**Victoria R. Tennant**, Mark and Mary Stevens Neuroimaging and Informatics Institute, Keck School of Medicine, Los Angeles, CA, US
	Association of a unique pattern of white matter T2 FLAIR hyperintensities with plasma and tau PET biomarkers in former American football players	**Jenna Groh**, Boston University Chobanian & Avedisian School of Medicine, Boston, MA, US
	Relationship between flortaucipir-PET and quantitative susceptibility mapping in atypical Alzheimer's disease	**Neha Singh-Reilly**, Department of Neurology, Mayo Clinic, Rochester, MN, US
	Neuropathological evaluation of the off-target binding of flortaucipir in FTLD subcortical regions: interconnecting tau aggregates with iron deposition and neuroinflammation	**Rodolfo Gatto**, Department of Neurology, Mayo Clinic, Rochester, MN, US
	Patterns of cognitive decline in individuals with elevated p-tau217 and low levels (<20 Centiloids) of neocortical Aβ-PET signal	**Diana Townsend**, Department of Neurology, Massachusetts General Hospital, Boston, MA, US
	Anatomic specificity of inflammation TSPO PET biomarkers in dementia	**Belen Pascual**, Houston Methodist Research Institute, Weill Cornell Medicine, Houston, TX, US
	Head-to-head comparison of longitudinal plasma assays in relation to longitudinal amyloid pathology in Alzheimer's disease	**Yara Yakoub**, Douglas Mental Health University Institute, Montréal, QC, CA
	Characterization of PART using MK-6240, Flortaucipir, and plasma p-tau217	**Carolina Soares**, University of Pittsburgh, Department of Psychiatry, Pittsburgh, PA, US
	Longitudinal rate of change in CSF biomarkers is associated with subsequent Tau PET burden in Braak stages I and II: Findings from the BIOCARD study	**Nisha Rani**, Department of Psychiatry and Behavioral Sciences, Johns Hopkins University School of Medicine, Baltimore, MD, US
	Head-to-head comparison of four tau-PET tracers for in vivo Braak staging: the HEAD Study	**Arthur Cassa Macedo**, Department of Neurology and Neurosurgery, McGill University, Montreal, QC, CA
	Astrogliosis in the early-stages of Alzheimer's disease	**Victor Villemagne**, The Australian e-Health Research Centre, The Commonwealth Scientific and Industrial Research Organisation (CSIRO), Melbourne, AU
	Identifying an optimal aβ cutoff point for progression from mild cognitive impairment to Alzheimer's disease: comparing cognitive performance and aβ pet insights	**Pierrick Bourgeat**, School of Psychological Sciences and Turner Institute for Brain and Mental Health, Monash University, Melbourne, Australia, Melbourne, AU
	Amyloid modifies the association between late-life BMI and longitudinal cognition in cognitively unimpaired individuals	**Wai-Ying Wendy Yau**, Massachusetts General Hospital, Boston, MA, US
	Amyloid spatial extent captures early tau burden and cognitive deficits, measured by PACC and digital clock drawing test, in preclinical Alzheimer's disease	**Jackson Thompson**, Massachusetts General Hospital, Harvard Medical School, Boston, MA, US

	Findings from dynamic [18F]-MK6240 PET imaging after motion and partial volume corrections	**Amal Tiss**, Department of Radiology, Massachusetts General Hospital and Harvard Medical School, Boston, MA, US
	Harmonization of MK6240 and Flortaucipir Braak Staging	**Andreia Rocha**, University of Pittsburgh, Department of Psychiatry, Pittsburgh, PA, US
	Comparison of MK-6240 PET and Flortaucipir tau PET imaging for the biological staging of Alzheimer's disease	**Marina Scop Medeiros**, University of Pittsburgh, Pittsburgh, PA, US
	Impact of early-stage amyloidosis on tau accumulation throughout the medial temporal lobe and neocortex	**Elliott Slade**, Athinoula A. Martinos Center for Biomedical Imaging, Charlestown, MA, US
	Associations between age-related tau deposition and neural selectivity in cognitively unimpaired older adults	**Jintao Sheng**, Stanford University, Stanford, CA, US
	Posterior white matter hyperintensity is related to the emergence of lobar cerebral microbleeds in ADNI	**Daniel Saukkonen**, Department of Neurology, Brigham and Women's Hospital, Harvard Medical School, Boston, MA, US
	Defining the grey zone thresholds for tau PET positivity using the Uniτ scale	**Guilherme Povala**, University of Pittsburgh, Department of Psychiatry, Pittsburgh, PA, US
	Neocortical amyloid spatial extent predicts cognitive decline over time in memory and executive function domains	**Emma Thibault**, Massachusetts General Hospital, Boston, MA, US
	Patterns of tau-PET accumulation and clinical progression according to biological AD stages	**Lydia Trudel**, Translational Neuroimaging Laboratory, McGill University, Montreal, QC, CA
	The Tau Progression Index (TPI): an individualized, clinically applicable, multimodally-derived score to predict AD progression	**Qolamreza Razlighi**, Weill Cornell Medicine, New York, NY, US
	Dried plasma spot optimization for the NULISAseq CNS panel	**Rachael Wilson**, Wisconsin Alzheimer's Disease Research Center, School of Medicine and Public Health, University of Wisconsin - Madison, Madison, WI, US
	Clinical validation of the Lumipulse G1200 automated immunoassay for the measurement of Alzheimer's disease plasma biomarkers	**Tevy Chan**, Translational Neuroimaging Laboratory, The McGill University Research Centre for Studies in Aging, Montréal, QC, Canada, Montreal, QC, CA
	Sex differences in synaptic loss in early Alzheimer's disease	**Jordan Galbraith**, Department of Neurology, Yale School of Medicine, New Haven, CT, US
	Assessing the generalizability of AD subtypes across diverse cohorts: HABS-HD and ADNI	**Gordon Zhaoqi An**, Devision of Computational and Data Sciences at Washington University in St. Louis, St. Louis, MO, US
	Locus coeruleus - medial temporal lobe functional connectivity confers protection against amyloid-related cognitive decline in the context of high cognitive reserve	**Lukas Heinrich**, Department of Radiology, Massachusetts General Hospital / Harvard Medical SChool, Boston, MA, US
	Effect of AD risk factors on tau-PET tracer uptake and its association with amyloid-β pathology	**Matheus Rodrigues**, University of Pittsburgh, Department of Psychiatry, Pittsburgh, PA, US
	PI-2620 uptake in the medial temporal lobes discriminates Alzheimer's disease from normal cognition and non-Alzheimer's dementias	**Jeffrey Phillips**, University of Pennsylvania, Philadelphia, PA, US
	Characterizing associations with Aβ burden in non-Hispanic Black participants across US POINTER and A4/LEARN cohorts	**Talia Robinson**, Brigham and Women's Hospital, Boston, MA, US
11:40 am - 12:40 pm	Lunch break	

12:40 pm - 01:10 pm	**KEYNOTE: Alzheimer's disease biomarkers among diverse populations – Data from the HABS-HD Study**	**Sid O'Bryant,** The University of North Texas HSC at Fort Worth, TX, USA
01:10 pm - 01:25 pm	Keynote Discussion	
01:25 pm - 02:50 pm	**SESSION VIII Plasma Biomarkers: New Methods**	**Bruna Bellaver,** University of Pittsburgh, Pittsburgh, PA, USA **Robert Rissman,** Keck School of Medicine of USC, San Diego, CA, USA
01:25 pm - 01:30 pm	Session Overview	**Chairs**
01:30 pm	Plasma tau biomarkers and staging of Alzheimer's disease	**Gemma Salvadó**, Lund University, Lund, SE
01:45 pm	Novel blood-based proteomic signatures across neurodegenerative diseases	**Maura Malpetti**, University of Cambridge, Cambridge, GB
02:00 pm	Association of CSF P-tau and MTBR-Tau biomarkers with amyloid and tau PET	**Przemyslaw Kac**, Institute of Neuroscience and Physiology, Department of Psychiatry and Neurochemistry, The Sahlgrenska Academy at University of Gothenburg, Mölndal, SE
02:15 pm	VeraBIND Tau test, a novel plasma assay for active tau pathology, identifies individuals with positive F18MK6240 tau-PET signal regardless of amyloid status	**Bernard Hanseeuw**, Cliniques Universitaires Saint-Luc, Brussels, BE
02:30 pm - 02:50 pm	Discussion	
02:50 pm - 02:55 pm	**Blitz Session 3B Short Poster Presentations**	
02:50 pm	Introduction	
02:52 pm	Locus coeruleus - medial temporal lobe functional connectivity confers protection against amyloid-related cognitive decline in the context of high cognitive reserve	**Lukas Heinrich**, Department of Radiology, Massachusetts General Hospital / Harvard Medical SChool, Boston, MA, US
02:53 pm	Association of a unique pattern of white matter T2 FLAIR hyperintensities with plasma and tau PET biomarkers in former American football players	**Jenna Groh**, Boston University Chobanian & Avedisian School of Medicine, Boston, MA, US
02:55 pm - 03:50 pm	**Poster Session 3B**	
03:50 pm - 05:15 pm	**SESSION IX Plasma Biomarkers: Application**	**Jasmeer Chhatwal,** Massachusetts General Hospital, Boston, MA, USA **Thomas Karikari,** University of Pittsburgh, Pittsburgh, PA, USA
03:50 pm - 03:55 pm	Session Overview	**Chairs**
03:55 pm	Positive plasma Aβ42/40 despite negative Amyloid PET: A harbinger of progression to amyloid PET positivity?	**Azadeh Feizpour**, Florey Institute of Neuroscience and Mental Health, Melbourne, AU
04:10 pm	Head-to-head association of plasma p-tau217 with MK6240, Flortaucipir, PI2620, and RO948 Tau PET Tracers	**Pamela Ferreira**, University of Pittsburgh, Department of Psychiatry, Pittsburgh, PA, US

04:25 pm	Modeling the temporal progression of plasma and PET AD biomarkers with cognition	**Petrice Cogswell**, Mayo Clinic, Rochester, MN, US
04:40 pm	Comparison of amyloid PET, tau PET, and pTau217 biomarker progression between Down syndrome and neurotypical adults with sporadic Alzheimer's disease	**Matt Zammit**, University of Wisconsin, Madison, WI, US
04:55 pm - 05:15 pm	Discussion	
05:15 pm - 05:25 pm	**Awards Ceremony**	**HAI Executive Committee**
5:25 pm – 5:30 pm	**Concluding Remarks**	**Keith Johnson,** Massachusetts General Hospital, Boston, MA, USA

HAI 2025 ABSTRACTS

Wednesday, January 15, 2025 - 08:55 am - 10:35 am

Podium Session

SESSION I: Harmonization

CHAIRS: Suzanne Baker, Bradley Christian

Wednesday, January 15, 2025		
08:55 am – 10:35 am	**SESSION I** Harmonization	**Suzanne Baker,** Lawrence Berkeley National Laboratory **Bradley Christian,** University of Wisconsin School of Medicine and Public Health
08:55 am - 09:00 am	Session Overview	**Chairs**
09:00 am	Longitudinal amyloid burden with combined [11C]PiB and [18F]NAV4694 PET Scans	**Brecca Bettcher**, University of Wisconsin-Madison School of Medicine and Public Health and Waisman Center, Madison, WI, US
09:15 am	Exploring Centiloids robustness: Impact of sample size and image resolution on Centiloid conversion accuracy	**Jiaxiuxiu Zhang**, Memory and Aging Center, Department of Neurology, University of California, San Francisco, San Francisco, CA, US
09:30 am	Every Centiloid, from everywhere, all at once	**Ganna Blazhenets**, Memory and Aging Center, Department of Neurology, University of California, San Francisco, San Francisco, CA, US
09:45 am	The Uniτ Ecosystem for tau-PET harmonization and visualization	**Guilherme Povala**, University of Pittsburgh, Department of Psychiatry, Pittsburgh, PA, US
10:00 am	Comparative sensitivity analysis of tau-PET tracers in Alzheimer's disease	**Cécile Tissot**, Lawrence Berkeley National Laboratory, Berkeley, CA, US
10:15 am - 10:35 am	Discussion	

Longitudinal amyloid burden with combined [11C]PiB and [18F]NAV4694 PET Scans

Brecca Bettcher[1], Max McLachlan[1], Matthew Zammit[1], Andrew McVea[1], Alexandra DiFilippo[1], Dhanabalan Murali[1], Ali Pirasteh[1], Tobey Betthauser[1], Sterling Johnson[1], Bradley Christian[1]

[1]*University of Wisconsin-Madison School of Medicine and Public Health and Waisman Center, Madison, WI, US*

Background: Amyloid tracer [18F]NAV4694 is a desirable alternative to [11C]PiB, possessing similar imaging characteristics and favorable distribution logistics. While Centiloids have proven reliable in cross-sectional studies, this work examines the accuracy of amyloid measures when transitioning from [11C]PiB to [18F]NAV4694 in longitudinal studies.

Methods: 24 Participants with ≥1 [11C]PiB scans, followed by a [18F]NAV4694 scan, were examined from ongoing AD studies at the University of Wisconsin (Table 1). PET images were realigned, summed 50-70min, coregistered to associated T1 weighted MRIs, normalized to MNI space, and smoothed by 6mm. Cortical SUVR and Centiloids (CL) were calculated using a whole cerebellum reference region. Rate of amyloid accumulation (CL/year) in NAV amyloid positive individuals was compared to published values. Longitudinal analyses were performed for participants with at least two PiB scans, allowing for direct comparison of PiB1-to-PiB2 changes and PiB2-to-NAV changes. An amyloid negative subset was defined as participants with > 1 PiB scan and who remained firmly amyloid negative (CL < 15) across all observations.

Results: Within participant PiB and NAV images were virtually indistinguishable by visual inspection (Figure 1b). The average rate of amyloid accumulation in amyloid positive participants is 5.3± 2.3 CL/year, consistent with published amyloid accumulation rate of ~4-5 CL/year in the neurotypical population (Yi Su et al, 2018). In the amyloid negative subset, rate of amyloid accumulation (CL/year) in PiB1-to-PiB2 vs PiB2-to-NAV demonstrated no significant difference ($p = 0.27$) (Figure 2). In all participants with > 1 PiB scan, differences in PiB2-to-NAV white matter signal exhibited higher variability than PiB1-to-PiB2 ($p = 0.0003$) but were not significantly different in mean ($p = 0.15$).

Conclusion: This study has investigated a direct longitudinal within participant comparison of PiB-to-PiB vs PiB-to-NAV amyloid accumulation. [18F]NAV4694 demonstrated both consistency in trending amyloid accumulation and constancy in sustained amyloid negative participants compared to [11C]PiB.

Participants (n)		**24**
Age, years (At last observation)		72 ± 7
Total [^{18}F]NAV4694 Scans		**24**
	A+	6
	A-	18
Total [^{11}C]PiB Scans		**66**
	Participants with 1 PiB Scan	6
	Participants with 2 PiB Scan	4
	Participants with 3 PiB Scan	4
	Participants with 4 PiB Scan	10
Duration Between Scans in Years		
	PiB-NAV (n = 24)	3.1 ± 1.7
	PiB-PiB (n = 18)	2.9 ± 0.7

Table 1: Participant Demographics. Participants were recruited from WRAP, PREDICT, and ADRC studies. Note that PiB-NAV refers to participants' most recent PiB scan and NAV scan. PiB-PiB refers to participants' two most recent PiB scans, if acquired.

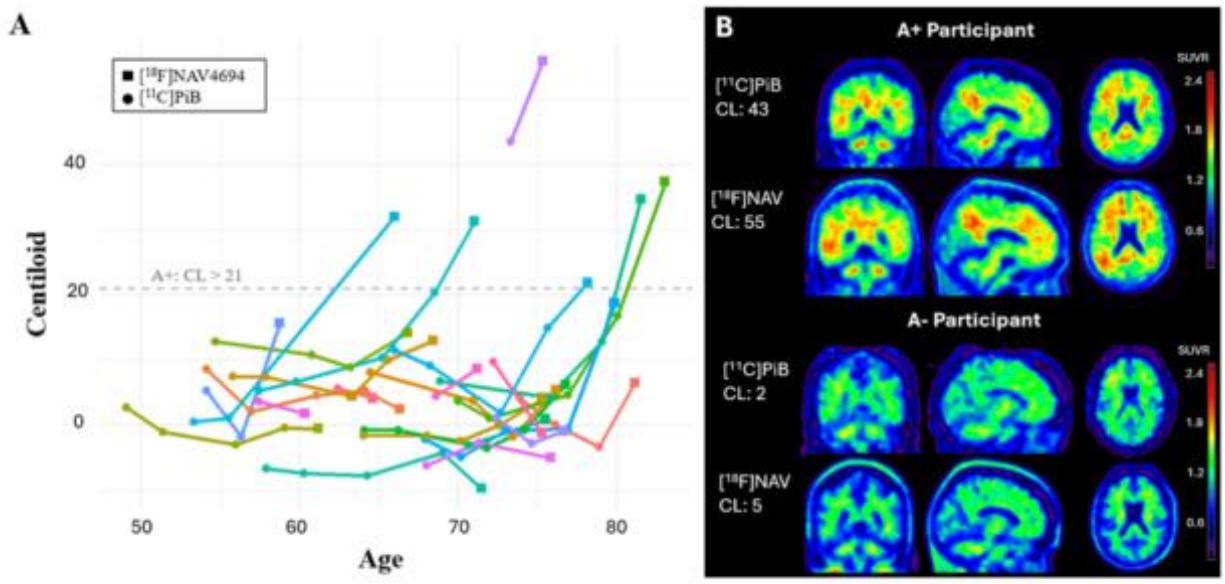


Figure 1: Spaghetti plot of CL values including 24 participants and 90 total scans (A). Amyloid burden indicated by [18F]NAV4694 was consistent with the disease timeline as projected by previous [11C]PiB scans. Representative [11C]PiB and [18F]NAV4694 scans in amyloid positive and amyloid negative participants (B). Duration between scans was 5 years and 3 years for the amyloid positive participant and negative participant respectively.

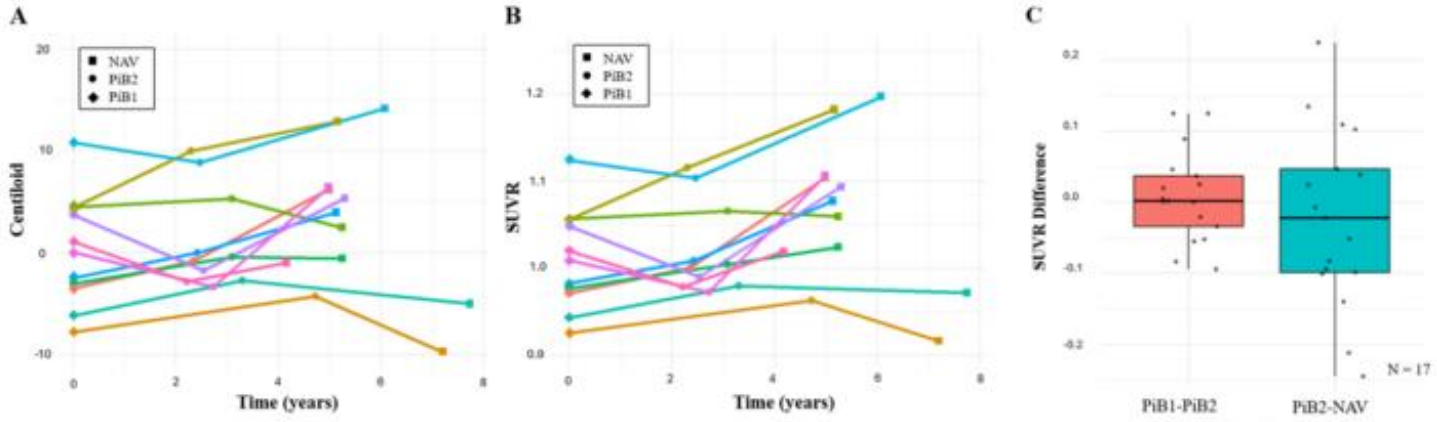


Figure 2: Amyloid trajectories of 11 amyloid negative participants expressed in CL and SUVR (A, B). Difference in PiB1-to-PiB2 CL values (expressed as PiB1 CL – PiB 2 CL) exhibited no significant difference from PiB2-to-NAV. Difference in PiB1-to-PiB2 vs PiB2-to-NAV SUVR values exhibited a slight difference in mean ($p = 0.035$). SUVR difference in white matter from PiB1-to-PiB2 vs PiB2-to-NAV scans (C).

Keywords: Amyloid, [11C]PiB, [18F]NAV4694

Exploring Centiloids robustness: Impact of sample size and image resolution on Centiloid conversion accuracy

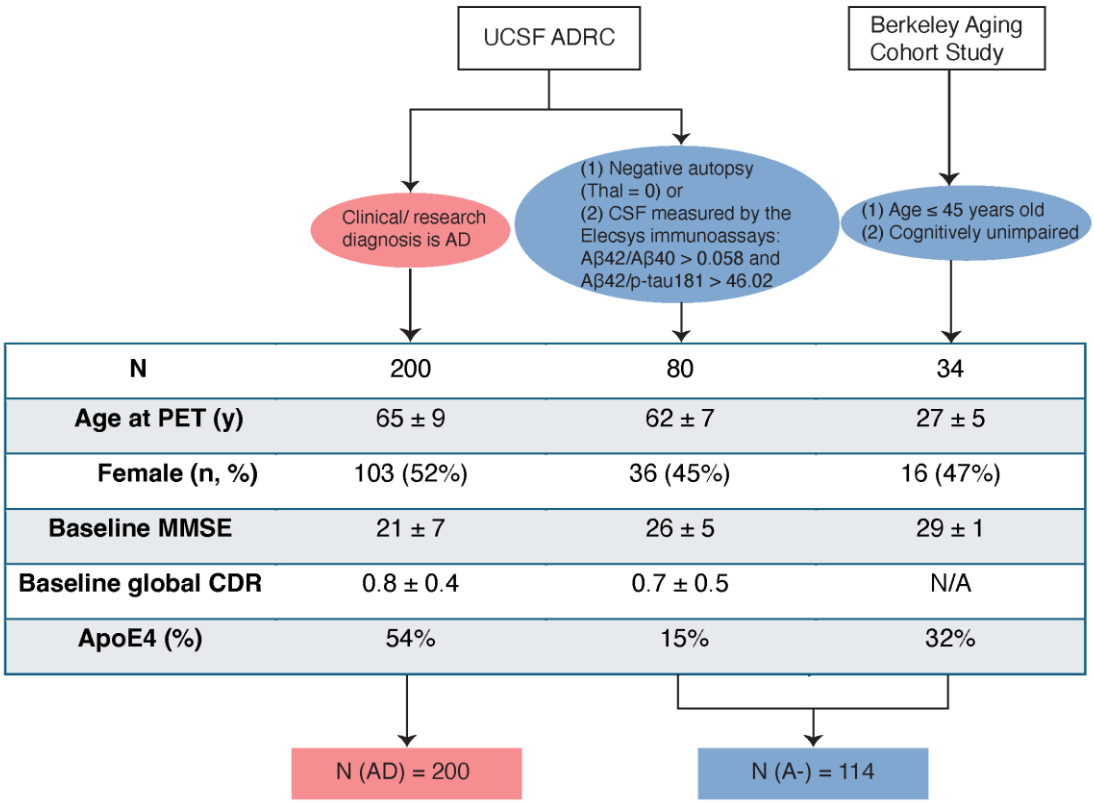
Jiaxiuxiu Zhang[1], Daniel Schonhaut[1], Jhony Mejia Perez[1], Ganna Blazhenets[1], Zoe Lin[1], William Jagust[2], Theresa Harrison[2], Lea Grinberg[1], Salvatore Spina[1], William Seeley[1], Gil Rabinovici[1], Renaud La Joie[1]

[1]*Memory and Aging Center, Department of Neurology, University of California, San Francisco, San Francisco, CA, US*
[2]*Neuroscience Department, University of California, Berkeley, Berkeley, CA, US*

Background: As Centiloids are increasingly used in trials and clinical settings to guide patient diagnosis and management, better characterization of noise sources is essential. We examined two potential factors driving measurement error: 1) variability in the SUVR-to-CL conversion equation related to random sampling of the calibration dataset and 2) PET resolution.

Methods: We analyzed [^{11}C]PIB scans in 200 participants with a clinical diagnosis of AD and 114 amyloid-negative participants (based on negative CSF, neuropathological assessment, or being a healthy control <45yo, **Table-1**). Scans were processed using the standard Centiloid method (template space, whole cerebellum reference) and a non-standard pipeline (native space, cerebellar cortex reference). We split data into training and test datasets (n=157 each). The training dataset was used to generate a standard conversion equation. In the test dataset, equations were generated from bootstrapped subsamples of n=10-to-50 amyloid-negative and n=15-to-100 AD participants **Figure-1A**). Conversion equations from both datasets were compared using root-mean-squared errors. Additionally, all images were downgraded from 7mm-FWHM to 8mm and 10mm resolution, and Centiloids were calculated using a standard conversion equation (**Figure-2A**).

Table 1. Cohort description and demographics.



N	200	80	34
Age at PET (y)	65 ± 9	62 ± 7	27 ± 5
Female (n, %)	103 (52%)	36 (45%)	16 (47%)
Baseline MMSE	21 ± 7	26 ± 5	29 ± 1
Baseline global CDR	0.8 ± 0.4	0.7 ± 0.5	N/A
ApoE4 (%)	54%	15%	32%

Results. In the smallest required sample (10 amyloid-negative, 15 AD), conversion error reached 1.7 CL at CL=25 and 3.4CL at CL=100. Error was halved when including 50 amyloid-negative and 100 AD participants (**Figure-1B**). Lower image resolution, while using the same SUVR-to-CL conversion equation, was associated with a systematic underestimation of Centiloids in highly positive scans: a scan with 100CL estimated from the 7 mm-FWHM resolution scans would be quantified as 94CL and 85CL when downgraded to 8mm and 10mm FWHM, respectively (**Figure-2B**).

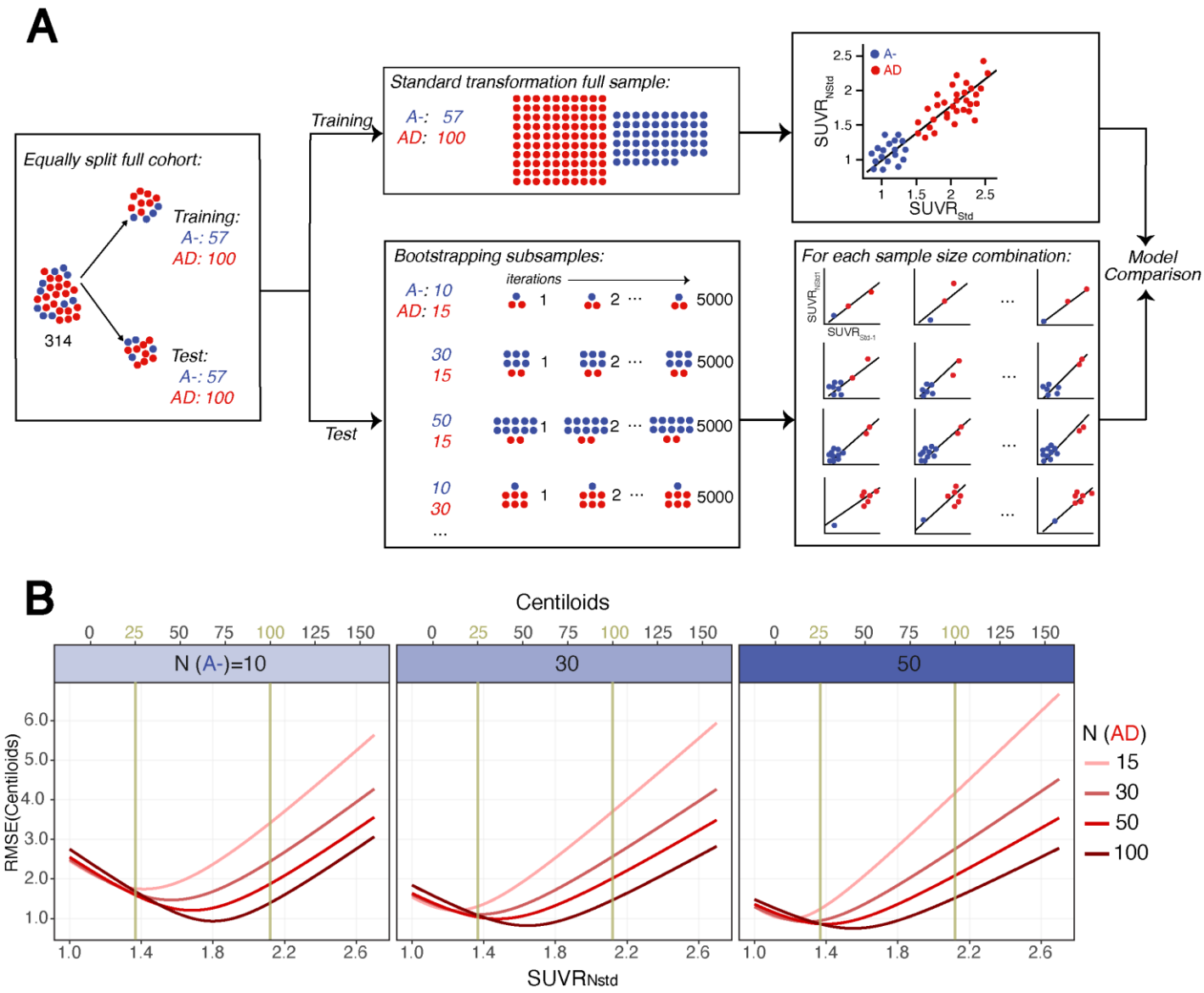


Figure 1. **Root mean squared errors (RMSE) between Centiloids estimated from standard transformation and from bootstrapping method. (A)** Flowchart showing standard transformation using training dataset and bootstrapping using test dataset. **(B)** RMSE, measured in the unit of Centiloids, show the difference between Centiloids obtained using the target conversion equation from the training dataset, versus bootstrapped conversion equation in each of the 12 subsample groups using test dataset. The green line shows the RMSE near thresholds of 25 and 100 Centiloids calculated by standard transformation. $SUVR_{std}$: SUVR calculated using the standard transformation (template space, whole cerebellum reference) proposed by Klunk et al.(2015). $SUVR_{Nstd}$: SUVR calculated using a non-standard pipeline (native space, cerebellar cortex reference).

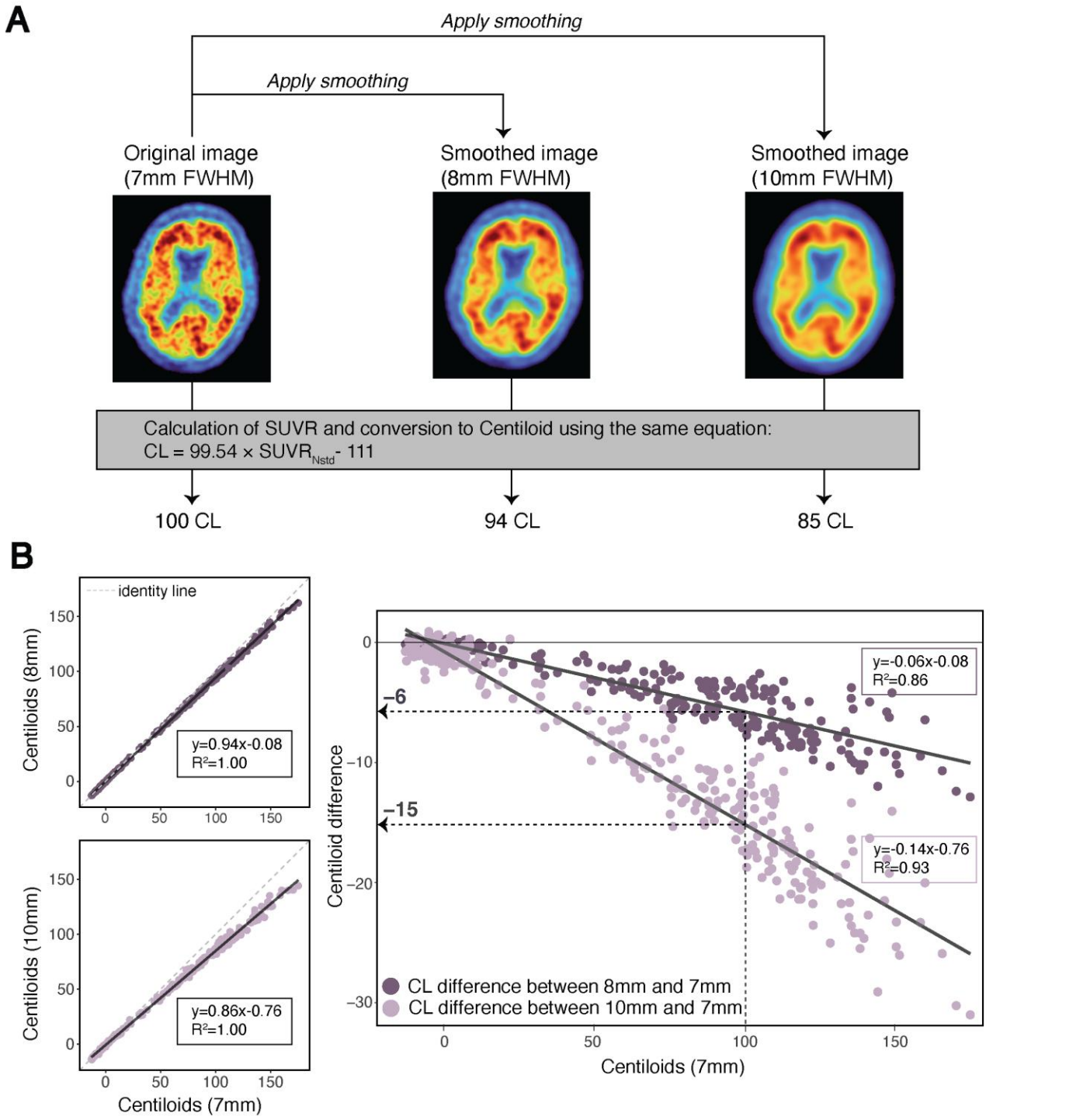


Figure 2. (A) Flowchart illustrating the smoothing analysis. **(B)** Scatterplots illustrating the association between Centiloids at the original 7mm FWHM resolution and Centiloids when scans were smoothed to 8mm and 10mm FWHM. Additionally, a scatterplot showing the Centiloid values deriving from the original data relative to the differences between the Centiloids calculated from the original and smoothed data to 8mm, and 10mm FWHM.

Conclusion: Amyloid-PET harmonization efforts could be improved by using larger than the minimally required validation datasets, especially by including a greater number of AD patients. Image resolution significantly impacts Centiloids in amyloid-positive scans and should be considered when interpreting data from different scanners.

Keywords: Centiloid, PIB, Amyloid PET, Tracer quantification, Resolution

Every Centiloid, from everywhere, all at once

Ganna Blazhenets[1], David Soleimani-Meigooni[1], Heather Snyder[2], Ioannis Pappas[3], Cally Xiao[3], Arthur W. Toga[3], Christina B. Young[4], Reisa A. Sperling[5], Susan M. Landau[6], Michael Weiner[1], Raquel C. Gardner[7], William J. Jagust[6], Pierrick Bourgeat[8], Christopher C. Rowe[8], Colin L. Masters[8], Gill Farrar[9], Mahnaz Shekari[10], Lyduine E. Collij[11,12], Ruben Smith[11], Oskar Hansson[11], Gaël Chételat[13], Victor L. Villemagne[14], Brian Lopresti[14], Yishu Chao[6], Theresa M. Harrison[6], Sid E. O'Bryant[15], Meredith N. Braskie[16], Andrew March[17], Robert A. Koeppe[18], Maria C. Carrillo[2], Bradford C. Dickerson[5], Liana G. Apostolova[19], Christopher G. Schwarz[20], Prashanthi Vemuri[20], Val J. Lowe[20], Elizabeth C. Mormino[4], Gil D. Rabinovici[1], Renaud La Joie[1]

[1]*Memory and Aging Center, Department of Neurology, University of California, San Francisco, San Francisco, CA, US*
[2]*Alzheimer's Association, Chicago, IL, US*
[3]*Laboratory of Neuro Imaging, USC Stevens Neuroimaging and Informatics Institute, Keck School of Medicine of USC, University of Southern California, Los Angeles, CA, US*
[4]*Department of Neurology and Neurological Sciences, Stanford University School of Medicine, Stanford, CA, US*
[5]*Department of Neurology, Massachusetts General Hospital, Harvard Medical School, Boston, MA, US*
[6]*Helen Wills Neuroscience Institute, University of California, Berkeley, Berkeley, CA, US*
[7]*Joseph Sagol Neuroscience Center, Sheba Medical Center, Ramat Gan, IL*
[8]*Florey Institute of Neurosciences and Mental Health, University of Melbourne, Melbourne, AU*
[9]*GE Healthcare Life Sciences, Amersham, GB*
[10]*Barcelonaβeta Brain Research Center (BBRC), Pasqual Maragall Foundation, Barcelona, ES*
[11]*Clinical Memory Research Unit, Department of Clinical Sciences Malmö, Faculty of Medicine, Lund University, Lund, SE*
[12]*Department of Radiology and Nuclear Medicine, Amsterdam UMC, location VUmc, Amsterdam, NL*
[13]*Normandie Université, Université de Caen, Institut National de la Santé et de la Recherche Médicale, Unité 1237, Groupement d'Intérêt Public Cyceron, Caen, FR*
[14]*Department of Psychiatry, University of Pittsburgh School of Medicine, Pittsburgh, PA, US*
[15]*Institute for Translational Research, University of North Texas Health Science Center, Fort Worth, TX, US*
[16]*Mark and Mary Stevens Neuroimaging and Informatics Institute, University of Southern California, Los Angeles, CA, US*
[17]*American College of Radiology, Philadelphia, PA, US*
[18]*University of Michigan, Ann Arbor, MI, US*
[19]*Indiana University School of Medicine, Indianapolis, IN, US*
[20]*Department of Radiology, Mayo Clinic, Rochester, MN, US*

Background: Ten years after the original publication, the Centiloid framework is now broadly used to harmonize amyloid-PET quantification, facilitate data sharing, and allow direct comparison across cohorts. We evaluated the global implementation of Centiloids by comparing their distribution and corresponding positivity thresholds across cohorts.

Methods: We gathered data from publicly available cohorts and reached out to investigators across the world to collect cross-sectional Centiloids, demographic, clinical, and visual read data. Gaussian mixture models (GMM) were fitted to Centiloid values for each cohort and cutoffs were calculated as mean + 2SD of the first Gaussian. When visual reads were available, we determined Centiloid cutoffs that maximized i) correspondence with visual read (Cohen's kappa) and ii) sensitivity and specificity in ROC analysis (Youden's index). Data was combined across cohorts using meta-analyses.

Results: As of October 2024, we included 17 cohorts (n=30,409 participants) with heterogeneous pipelines, radiotracers, and clinical and demographic characteristics (Table 1). In all cohorts, a two-Gaussian model best fitted the distribution according to the integrated completed likelihood criteria. While the low Gaussian peaks were near zero with mild variability across studies, the second peaks were more heterogeneous, with higher values in cohorts that were more cognitively impaired (Figure-1A-B). The meta-analysis indicated a GMM-based cutoff of 20 CL (Figure-1C) with no significant difference in cutoff by pipeline or center ($p>0.1$). When stratified by tracer (Figure-1D), the meta-analysis showed significant ($p<0.001$) threshold variability across tracers: lowest with Flutemetamol (13) and NAV (14) and highest with Florbetapir (28). Centiloid cutoffs based on visual reads tended to be slightly higher than those based on GMM and were consistent across the two statistical approaches (~26CL, Figure-2).

Conclusion: Centiloids enable a direct comparison of amyloid-PET results in otherwise different studies. Despite variability across cohorts and analysis methods, cutoffs align well with thresholds from the existing literature.

Table 1. Summary metrics across cohorts.

Cohort	Country	Center	Pipeline			N	Avg. age	Visual read	CU[§]	Tracer				
			PET-only	Template ROI	Freesurfer ROI					FBB	FBP	FLUTE	PIB	NAV
A4	USA	M		✓		4491	71	100%	100%	-	4491	-	-	-
ADNI	USA	M			✓	1,729	72	27%*	41%	368	1361	-	-	-
ADNI DoD	USA	M	✓	✓		274	70	100%	84%	-	274	-	-	-
Age-Well	France	S		✓		134	69	-	100%	-	134	-	-	-
AIBL	Australia	M	✓	✓		2281	72	-	60%	50	561	255	516	899
AMYPAD	Europe	M		✓		1548	68	100%	81%	584	-	964	-	-
BioFINDER-2	Sweden	M			✓	1396	67	82%	67%	-	-	1396	-	-
GEMS	USA	M			✓	189	86	-	78%	-	-	-	189	-
HABS	USA	S			✓	288	74	-	97%	-	-	-	288	-
HABS-HD	USA	S			✓	2366	62	-	69%[$]	2366	-	-	-	
IDEAS	USA	M	✓	✓		10,350	76	100%	0%	3032	6690	628	-	-
IMAP	France	S		✓		270	60	-	64%	-	270	-	-	-
LEADS	USA	M			✓	605	59	84%*	16%	605	-	-	-	-
MCSA	USA	S		✓		2,027	69	-	88%	-	-	-	2027	-
NACC-SCAN	USA	M	✓	✓		1198	71	-	59%	378	106	-	639	75
Pittsburg ADRC	USA	S			✓	138	71	-	30%	-	-	-	138	-
UCSF ADRC	USA	S			✓	1,125	66	81%	30%	92	438	-	595	-

Pipeline: MRI-based or PET-only spatial normalization of PET data; quantification based on ROI in template space or in native space (Freesurfer). Center: Study design (M – multiple centers, S – single center). Row colors group cohorts based on the processing pipeline. *Visual read was only performed in patients with MCI/Dementia. CU, cognitively unimpaired. [§]Based on the provided clinical diagnosis or CDR with the 0.5 cutoff. [$]Cognitive status is available in less than half of the cohort. FBB, [^{18}F]Florbetaben; FBP, [^{18}F]Florbetapir; FLUTE, [^{18}F]Flutemetamol; PIB, [^{11}C]Pittsburg compound B; NAV, [^{18}F]Flutafuranol.

Note: Data from multiple cohorts, including but not limited to BACS, Insight46, GHABS, PREVENT-AD, MEMENTO, POINTER, Yonsei University (Republic of Korea), Wisconsin ADRC, WRAP, 1FL ADRC, Washington University ADRC, and Université Catholique de Louvain are in the data transfer process and will be included later.

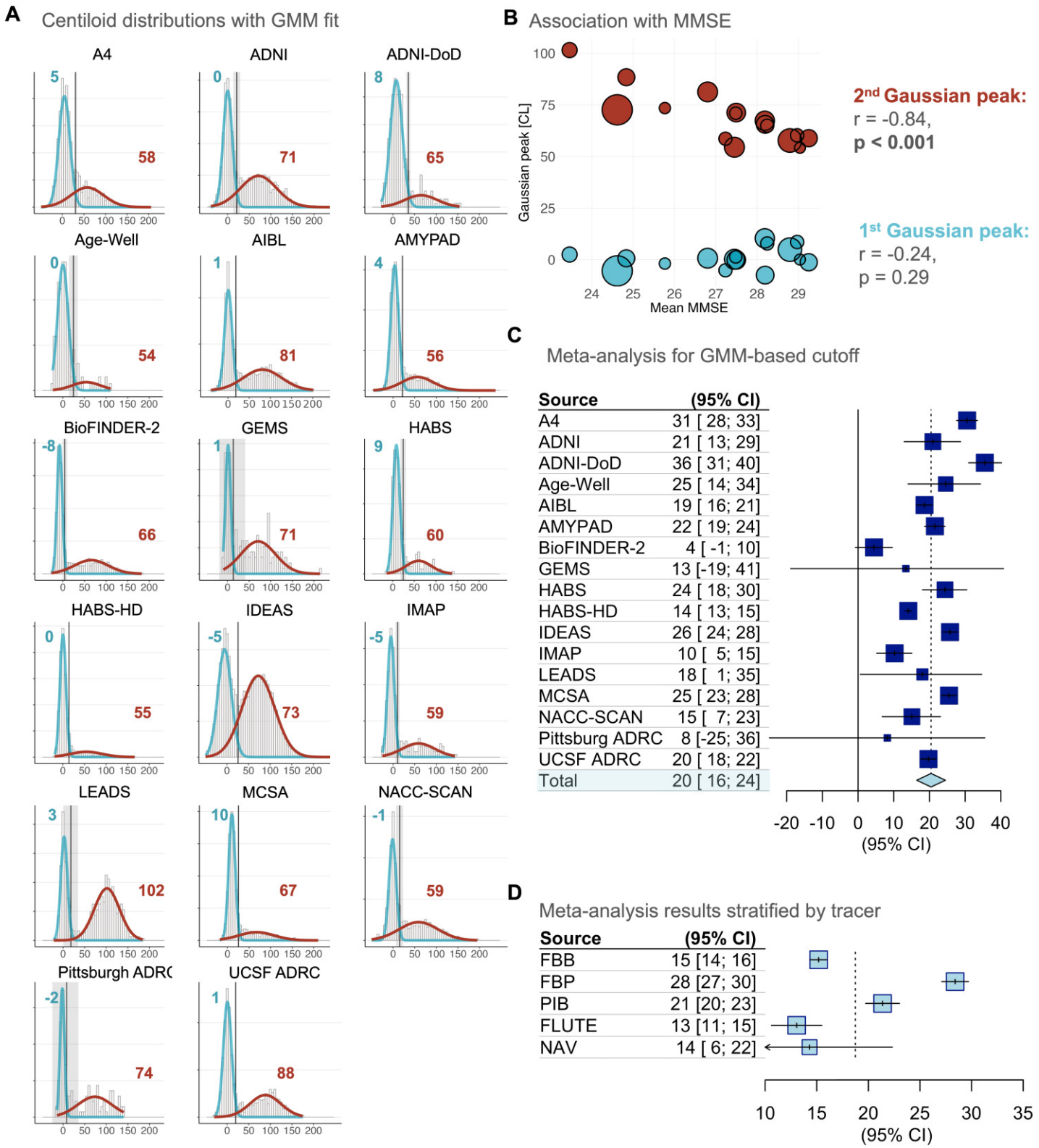


Figure-1. Centiloid distribution and derived metrics. (A) Gaussian mixture models fit for the Centiloid distribution in each cohort. Values correspond to the peak of each Gaussian. (B) Association between peaks of each Gaussian fit and mean MMSE in each cohort. The size of the bubble is proportional to the cohort size. (C) Results of the random-effect meta-analysis comparing the GMM-based cutoffs among cohorts. Total cutoff refers to the analysis combining all available cohorts and tracers. (D) GMM-based cutoffs analyzed by splitting data by tracers. Subcohorts with less than 100 participants were not included in this sub-analysis. For meta-analyses, squares reflect the study weight and whiskers are 95% confidence intervals for the estimates.

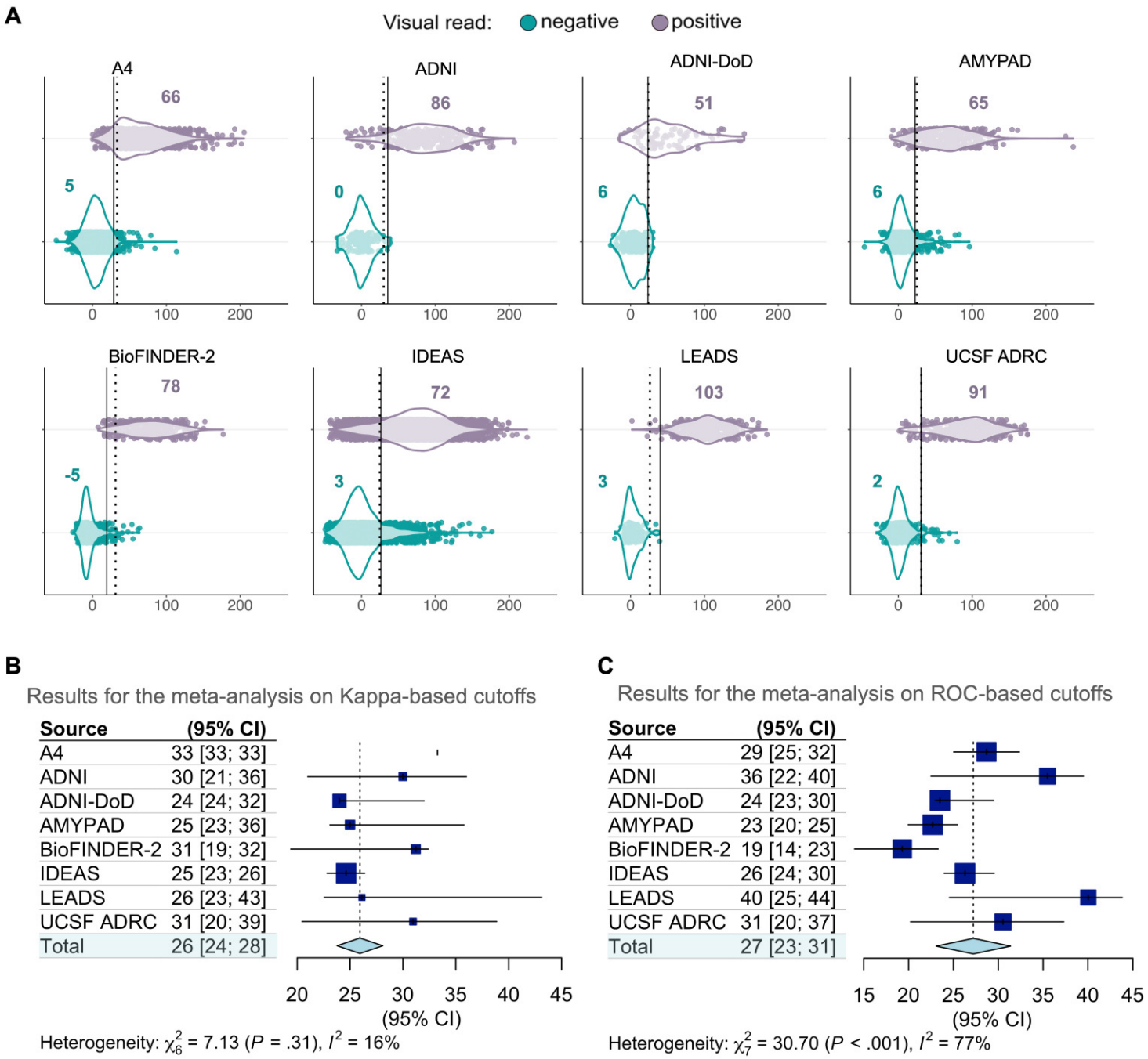


Figure 2. Distribution of Centiloid values by visual reads. (A) Violin plots for each cohort with values representing the mean Centiloids in each group. Vertical lines correspond to Centiloid cutoffs that maximized correspondence with visual read (Cohen's kappa, dashed) and sensitivity and specificity in ROC analysis (Youden's index, solid). Results of the random-effect meta-analysis comparing kappa-based (B) and ROC-based (C) positivity cutoffs among studies.

Keywords: Centiloid, cutoff, reproducibility, amyloid-PET, multi-center

The Uniτ Ecosystem for tau-PET harmonization and visualization

Guilherme Bauer-Negrini[1], Guilherme Povala[1], Bruna Bellaver[1], Pamela Lukasewicz Ferreira[1], Firoza Z. Lussier[1], Livia Amaral[1], Dana L. Tudorascu[1], Joseph Masdeu[2], David Soleimani-Meigooni[3], Juan Fortea[4], Val Lowe[5], Hwamee Oh[6], Belen Pascual[2], Brian A. Gordon[7], Pedro Rosa-Neto[8], Suzanne Baker[9], Tharick A. Pascoal[1]

[1]*University of Pittsburgh, Department of Psychiatry, Pittsburgh, PA, US*
[2]*Houston Methodist Research Institute, Department of Neurology, Houston, TX, US*
[3]*University of California San Francisco, Memory and Aging Center, San Francisco, CA, US*
[4]*Hospital de la Santa Creu i Sant Pau, Sant Pau Memory Unit, Department of Neurology, Barcelona, ES*
[5]*Mayo Clinic, Department of Radiology, Rochester, MN, US*
[6]*Brown University, Department of Psychiatry and Human Behavior, Providence, RI, US*
[7]*Washington University in St. Louis, Department of Radiology, Saint Louis, MO, US*
[8]*Translational Neuroimaging Laboratory, McGill University Research Centre for Studies in Aging, Douglas Research Institute, Montréal, QC, CA*
[9]*Lawrence Berkeley National Laboratory, Berkeley, CA, US*

Background: HEAD is a longitudinal, multi-site, non-randomized study aiming to harmonize different tau-PET tracers onto a common scale. To achieve this, the Uniτ scale is being developed using data from 620 participants scanned head-to-head with Flortaucipir and MK-6240, with a subset (n=175) also scanned with PI-2620 and RO-948. However, access to the Uniτ scale has been limited to the study community and collaborators. To address this limitation, we have developed the Uniτ Ecosystem—a set of tools to increase Uniτ functionality.

Methods: The Uniτ Ecosystem tools were developed for multiple operating systems (macOS/Windows/Ubuntu) (Fig.1) and currently include 1) a calculator app for rapid and convenient harmonization. 2) An online region-of-interest harmonization module to harmonize multiple SUVRs from spreadsheets. 3) A 3D harmonization module for voxel-wise harmonization. 4) A 3D visual reading package (under development). Researchers can use their own datasets or test harmonization models using data from a training set of participants. The tools include a feedback box that allows users to provide input to Uniτ developers, facilitating continuous scale improvement.

Results: The calculator app enables users to harmonize single SUVR values effortlessly. The online ROI harmonization module extends the calculator's capabilities by allowing users to harmonize SUVRs uploaded from spreadsheets and offers interactive visualizations such as scatter plots and histograms for tau positivity thresholds (Fig.2). The desktop application for 3D tau-PET harmonization leverages the functionalities of the previous modules to harmonize entire 3D images, eliminating the need for predefined ROIs. Additionally, this module provides visualization tools for the parametric Uniτ images and visual reading ratings (Fig.3). No module retains any type of data from users.

Conclusions: The Uniτ Ecosystem represents a major convenience in tau-PET use, providing researchers with a user-friendly platform to harmonize and visualize tau-PET data. Researchers can request free access to the Ecosystem at www.unitau.app.

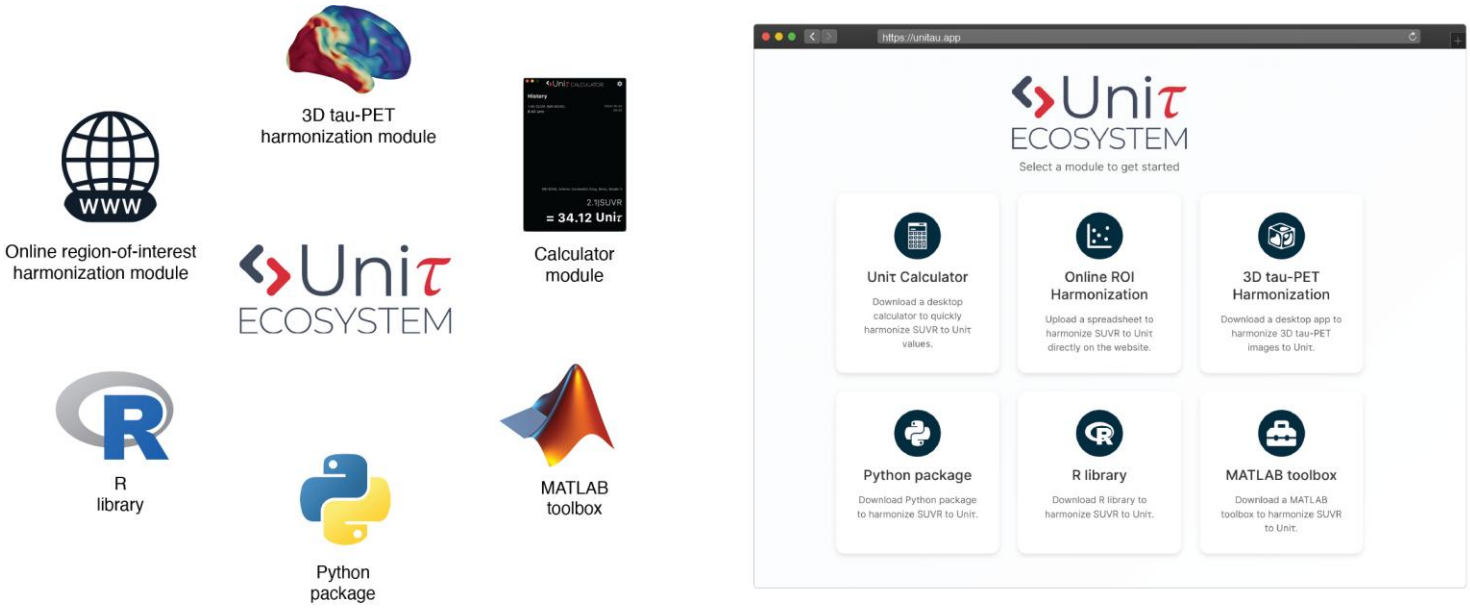


Figure 1 – The Unit Ecosystem. The Unit Ecosystem offers a suite of tools designed for users to harmonize tau-PET data based on their specific requirements. The available modules include: a calculator for quick SUVR harmonization, a region-of-interest (ROI) harmonization module for batch processing of tabular SUVR data, a 3D tau-PET harmonization module for voxel-wise analysis of entire PET images, and integration packages compatible with popular programming languages such as R, Python, and MATLAB.

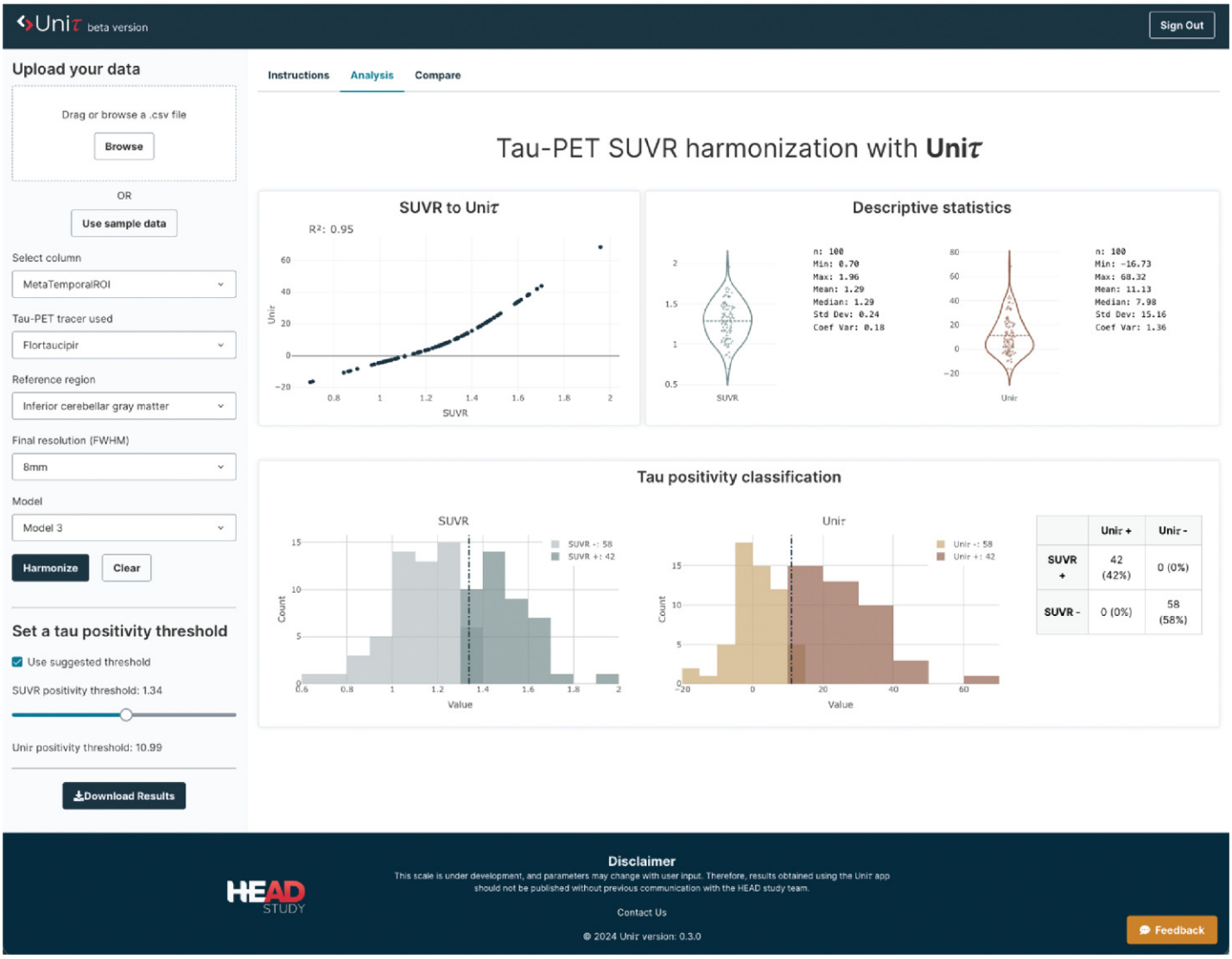


Figure 2 – The online ROI harmonization module in detail. The online ROI harmonization tool features a collection of visualization tools where users can see the resulting Unitau harmonization while testing different parameters. Users can customize the analysis parameters, including three different harmonization models, two reference regions (inferior and crus cerebellar gray matter), and three final image resolutions (6/8/10 mm full width at half maximum).

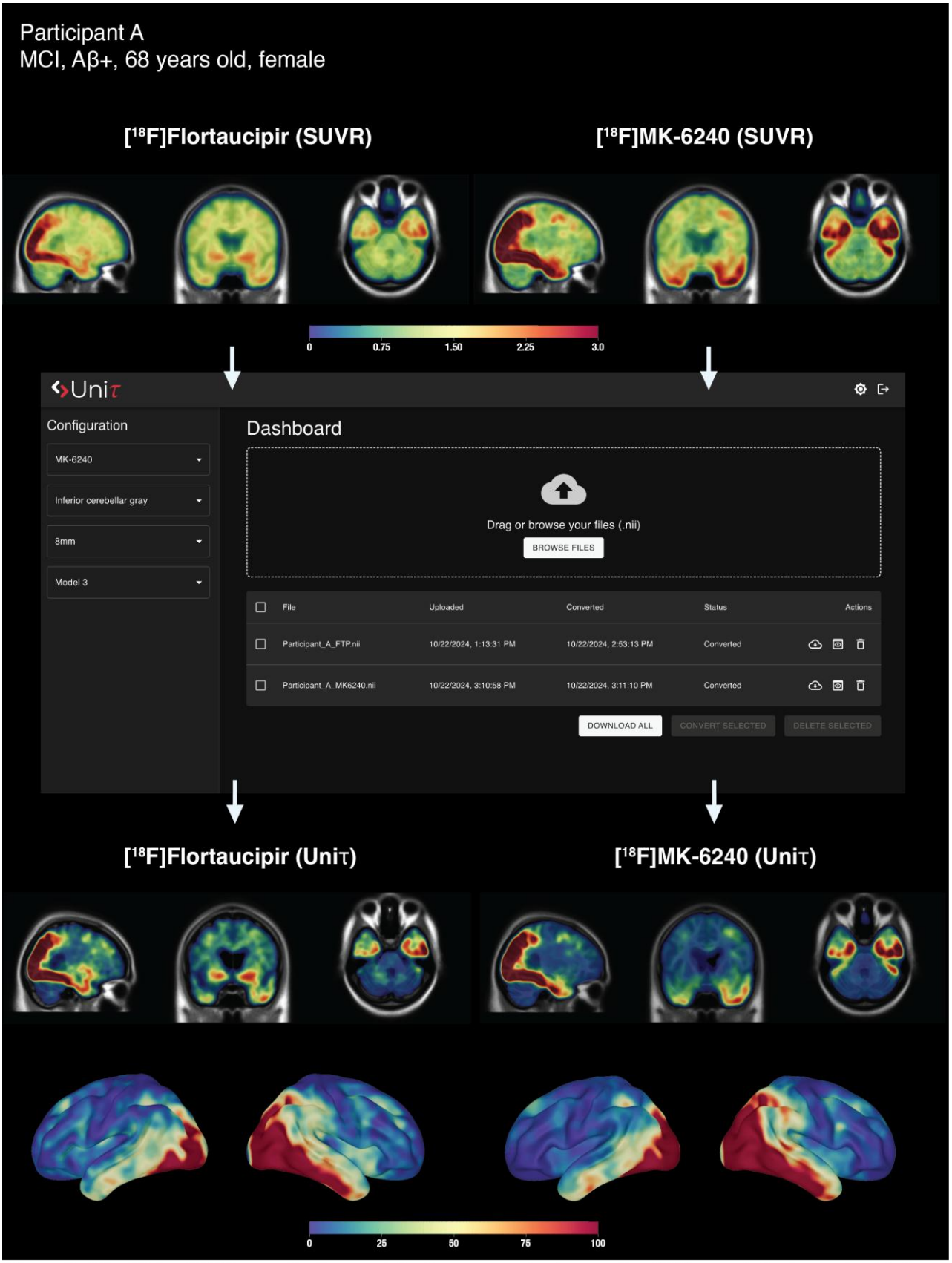


Figure 3 – The 3D tau-PET harmonization module. Users can upload several tau-PET scans to be harmonized to the Unitau scale. The example illustrates the harmonization from SUVR to Unitau of [18F]Flortaucipir and [18F]MK-6240 scans from the same study participant. The resulting Unitau parametric images can be visualized using the in-built 2D and 3D brain image viewers.

Keywords: tau,PET,harmonization,Unitau,HEAD

Comparative sensitivity analysis of tau-PET tracers in Alzheimer's disease

Cécile Tissot[1], Nesrine Rahmouni[2], Hsin-Yeh Tsai[1], Joseph Therriault[2], Stijn Servaes[2], Firoza Z. Lussier[3], Stefania Pezzoli[4], Jacob Ziontz', Brian Gordon, Belen Pascual, Val Lowe, David Soleimani-Meigooni, Hwamee Oh, William Klunk, Pedro Rosa-Neto, William Jagust, Tharick Pascoal, Suzanne Baker

[1]*Lawrence Berkeley National Laboratory, Berkeley, CA, US*
[2]*McGill University, Montreal, QC, CA*
[3]*University of Pittsburgh, Pittsburgh, PA, US*
[4]*University of California, Berkeley, Berkeley, CA, US*
[5]*Washington University in Saint Louis, Saint Louis, MO, US*
[6]*Houston Methodist, Houston, TX, US*
[7]*Mayo Clinic, Rochester, MN, US*
[8]*University of California, San Francisco, San Francisco, CA, US*
[9]*Brown University, Providence, RI, US*

Background: Tau-PET tracers are essential for visualizing pathology in Alzheimer's (AD). High sensitivity is crucial for early detection and monitoring tau deposition. This study compares the noise to dynamic range ratio (NRR) of [^{18}F]FTP, [^{18}F]MK6240, [^{18}F]PI2620, and [^{18}F]RO948.

Methods: 328 individuals from the HEAD study (178 cognitively unimpaired elderly (CUE) and 150 cognitively impaired) underwent [^{18}F]FTP and [^{18}F]MK6240 tau-PET scans; 71 additionally received [^{18}F]PI2620 and [^{18}F]RO948.

Noise was calculated as the standard deviation (SD) of CUE Aβ- participants aged ≤65 ($SD_{CUEAβ-≤65}$). The dynamic range was calculated as the SD across all subjects (SD_{range}). The lower the NRR (=$SD_{CUEAβ-≤65}/SD_{range}$) the more sensitive the tracer. Analyses were performed at both region-of-interest and voxel-wise levels.

Results: In the whole cohort, [^{18}F]MK6240 demonstrated lower NRR than [^{18}F]FTP in all on-target brain regions (Figure1A). $CUE_{Aβ-≤65}$ may exhibit real tau-PET retention in Braak I, limiting conclusions there. Within the four-tracers subset, [^{18}F]PI2620 showed the highest NRR in Braak II, followed by [^{18}F]RO948, [^{18}F]FTP and [^{18}F]MK6240. In the metatemporal-ROI, Braak III and IV, [^{18}F]RO948 had the highest value, followed by [^{18}F]PI2620, [^{18}F]FTP and [^{18}F]MK6240. For Braak V and VI, [^{18}F]RO948 again exhibited the highest values, followed by [^{18}F]FTP, [^{18}F]PI2620 and [^{18}F]MK6240 (Figure1B). Voxel-wise analyses presented a similar pattern: [^{18}F]MK6240 showed low NRR values, [^{18}F]PI2620 and [^{18}F]FTP were comparable, and [^{18}F]RO948 exhibited the highest (Figure2). The lower [^{18}F]MK6240 NRR result from large SD_{range}, while [^{18}F]FTP's are due to smaller $SD_{CUEAβ-≤65}$. In contrast, high [^{18}F]PI2620 and [^{18}F]RO948 values are driven by larger $SD_{CUEAβ-≤65}$.

Discussion: Our findings highlight significant variability in tau-PET tracers. [^{18}F]MK6240 consistently demonstrated lower NRR, implying better sensitivity across all regions; [^{18}F]FTP outperforms [^{18}F]RO948 and [^{18}F]PI2620 in metatemporal-ROI and Braak III-IV. [^{18}F]RO948 (excluding hippocampus) consistently exhibited worse sensitivity. These results provide insights into the differential tracer sensitivity, helping guide their optimal use in detecting and tracking tau.

Figure1: Noise to range ratio at the region-of-interest level

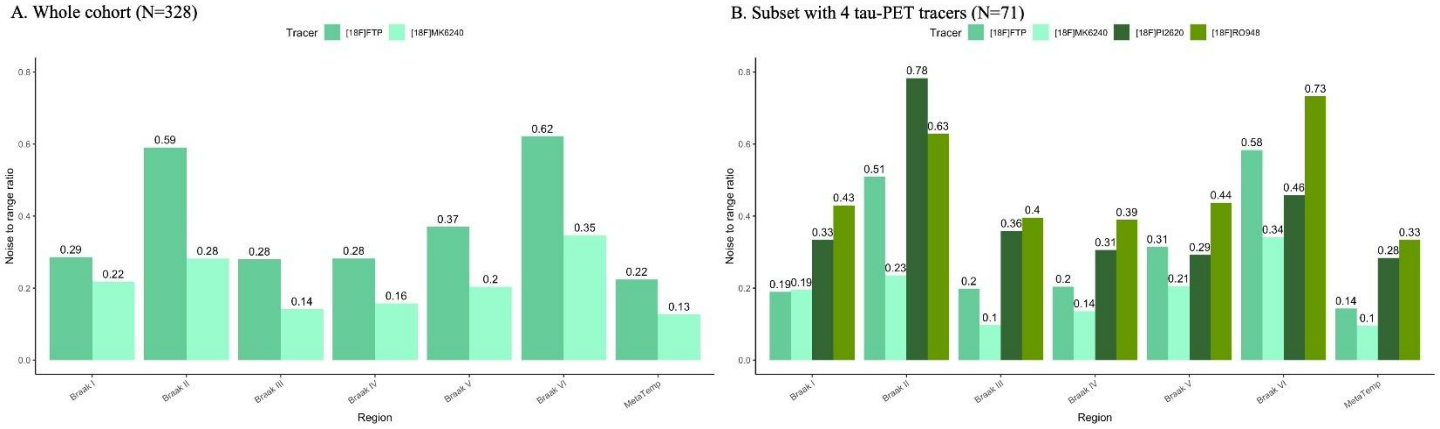
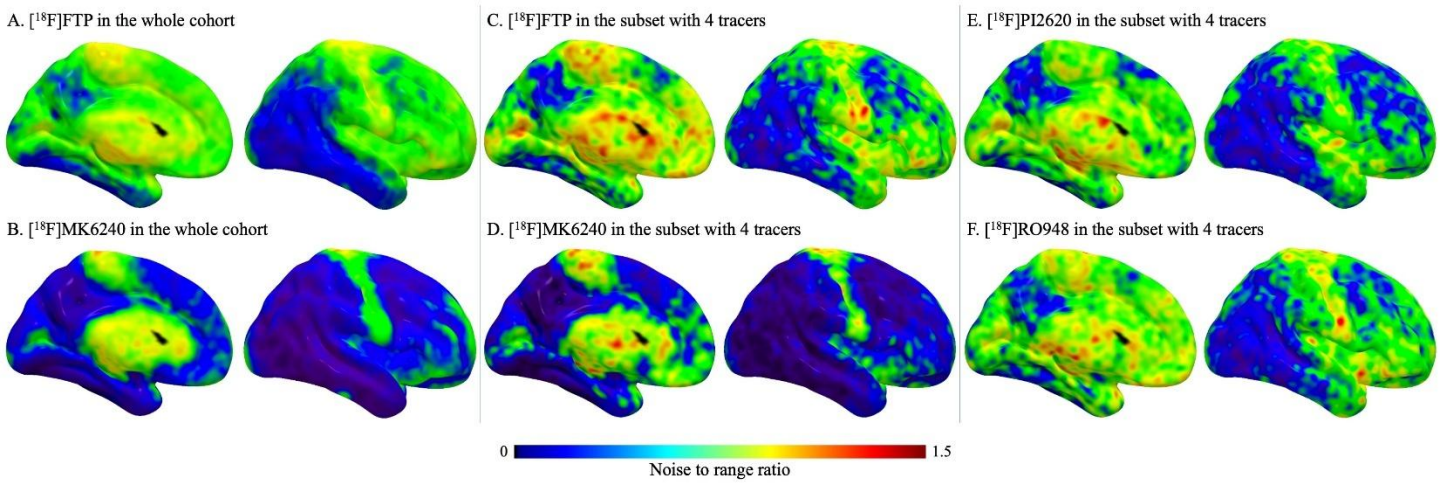


Figure2: Noise to range ratio at the voxel-wise level



Keywords: Tau, noise, sensitivity, Alzheimer's disease, head-to-head

Wednesday, January 15, 2025 - 10:35 am - 10:40 am

Podium Session

Blitz Session 1A: Short Poster Presentations

CHAIRS:

Wednesday, January 15, 2025		
10:35 am - 10:40 am	**Blitz Session 1A**	
10: 35 am – 10:37 am	Introduction	
10:37 am	Pathological and clinical trajectories of preclinical Alzheimer's disease patients with divergent cortical tau patterns	**Elizabeth Mormino**, Stanford University School of Medicine, Stanford, CA, US
10:38 am	Association between early and late tau aggregation across tau imaging agents: The HEAD Study	**Nesrine Rahmouni**, McGill University, Montreal, QC, CA
10:39 am	Unraveling the impact of amyloid-β and tau pathology on brain structure and cognitive function during preclinical and prodromal Alzheimer's disease	**Ting Qiu**, Douglas Mental Health University Institute, McGill University, Montreal, QC, CA

Pathological and clinical trajectories of preclinical Alzheimer's disease patients with divergent cortical tau patterns

Christina Young[1], Mackenzie Carlson[1], Karly Cody[1], Joseph Winer[1], Aaron Schultz[2], Elizabeth Mormino[1]

[1]*Department of Neurology and Neurological Sciences, Stanford University School of Medicine, Stanford, CA, US*
[2]*Department of Neurology, Massachusetts General Hospital, Boston, MA, US*

Background: We previously demonstrated that approximately 9% of cognitively unimpaired (CU) older adults with elevated β-amyloid (A+) exhibit more than expected cortical than medial temporal lobe (MTL) tau and/or having high cortical tau asymmetry (A+$T_{Cortical}$+).

Objective: To characterize longitudinal tau patterns and clinical trajectories of A+$T_{Cortical}$+ and determine whether trajectories differ from those with elevated medial temporal lobe tau (A+T_{MTL}+).

Methods: 18F-flortaucipir tau PET and clinical data spanning up to 8 years [mean (SD) = 4.68 (1.59) years] were examined in 393 CU participants enrolled in A4/LEARN (**Table 1**). Participants were determined to be in A-T_{MTL}- (n=47), A-T_{MTL}+ (n=1), A+T_{MTL}- (n=211), A+T_{MTL}+ (n=100), and A+$T_{Cortical}$+ (n=34) groups based on baseline amyloid and tau PET scans. We examined change in tau PET SUVR and asymmetry, as well as clinical trajectories were compared across groups using linear mixed effects models.

Results: A+$T_{Cortical}$+ participants accumulated tau in cortical regions that already showed relatively high SUVRs at baseline. Participants with asymmetrical tau at baseline accumulated tau in the corresponding region in the opposite hemisphere in addition to new regions in the original hemisphere (**Figure 1, 2A**). MTL SUVRs increased at comparable rates for the A+$T_{Cortical}$+ group compared to other A+ groups, but SUVRs in all cortical regions increased significantly faster in the A+$T_{Cortical}$+ group (**Figure 2B, 2C**). The A+$T_{Cortical}$+ group showed faster cognitive and functional decline (**Figure 2D, 2E**). Results were consistent when further accounting for baseline global tau and baseline amyloid, further indicating that findings were not driven by overall high levels of baseline pathology.

Conclusion: A+ CU with divergent cortical tau patterns are an especially high-risk subgroup. These participants continue to accumulate cortical tau at a faster rate than other preclinical AD subgroups and are at increased risk for faster cognitive and functional decline.

Table 1. Demographic characteristics of A4/LEARN participants with longitudinal tau PET data.

	CU A-T(MTL)- (N=47)	CU A-T(MTL)+ (N=1)	CU A+T(MTL)- (N=211)	CU A+T(MTL)+ (N=100)	CU A+T(Cortical)+ (N=34)	Overall (N=393)
Age at Baseline						
Mean (SD)	69.5 (4.46)	72.6 (NA)	71.6 (4.75)	73.1 (4.65)	71.2 (4.44)	71.7 (4.76)
Median [Min, Max]	68.0 [65.1, 84.5]	72.6 [72.6, 72.6]	71.3 [65.0, 85.3]	72.5 [65.0, 85.5]	70.0 [65.1, 82.3]	71.2 [65.0, 85.5]
Sex						
Male	19 (40.4%)	1 (100%)	96 (45.5%)	44 (44.0%)	10 (29.4%)	170 (43.3%)
Female	28 (59.6%)	0 (0%)	115 (54.5%)	56 (56.0%)	24 (70.6%)	223 (56.7%)
Education						
Mean (SD)	16.4 (2.53)	19.0 (NA)	16.2 (3.03)	16.1 (2.44)	16.5 (2.55)	16.2 (2.79)
Median [Min, Max]	16.0 [12.0, 20.0]	19.0 [19.0, 19.0]	16.0 [9.00, 30.0]	16.0 [11.0, 22.0]	16.5 [12.0, 21.0]	16.0 [9.00, 30.0]
Race						
White	44 (93.6%)	1 (100%)	192 (91.0%)	90 (90.0%)	34 (100%)	361 (91.9%)
Asian	1 (2.1%)	0 (0%)	13 (6.2%)	5 (5.0%)	0 (0%)	19 (4.8%)
Black	1 (2.1%)	0 (0%)	4 (1.9%)	3 (3.0%)	0 (0%)	8 (2.0%)
Unknown	0 (0%)	0 (0%)	0 (0%)	0 (0%)	0 (0%)	0 (0%)
American Indian/Alaskan	1 (2.1%)	0 (0%)	0 (0%)	0 (0%)	0 (0%)	1 (0.3%)
Pacific Islander	0 (0%)	0 (0%)	0 (0%)	0 (0%)	0 (0%)	0 (0%)
More than 1 Race	0 (0%)	0 (0%)	2 (0.9%)	2 (2.0%)	0 (0%)	4 (1.0%)
APOE						
E2/E3	3 (6.4%)	0 (0%)	14 (6.6%)	2 (2.0%)	1 (2.9%)	20 (5.1%)
E2/E4	1 (2.1%)	0 (0%)	8 (3.8%)	2 (2.0%)	1 (2.9%)	12 (3.1%)
E3/E3	32 (68.1%)	0 (0%)	90 (42.7%)	29 (29.0%)	8 (23.5%)	159 (40.5%)
E3/E4	11 (23.4%)	1 (100%)	85 (40.3%)	59 (59.0%)	18 (52.9%)	174 (44.3%)
E2/E2	0 (0%)	0 (0%)	1 (0.5%)	0 (0%)	0 (0%)	1 (0.3%)
E4/E4	0 (0%)	0 (0%)	12 (5.7%)	6 (6.0%)	5 (14.7%)	23 (5.9%)
Missing	0 (0%)	0 (0%)	1 (0.5%)	2 (2.0%)	1 (2.9%)	4 (1.0%)
Baseline Amyloid SUVR						
Mean (SD)	0.996 (0.0631)	1.03 (NA)	1.27 (0.143)	1.35 (0.180)	1.45 (0.221)	1.28 (0.193)
Median [Min, Max]	1.00 [0.860, 1.11]	1.03 [1.03, 1.03]	1.25 [0.970, 1.68]	1.34 [1.00, 2.02]	1.41 [0.970, 1.98]	1.26 [0.860, 2.02]
Baseline Global Tau SUVR						
Mean (SD)	0.895 (0.0486)	0.805 (NA)	0.939 (0.0754)	0.954 (0.0904)	1.18 (0.247)	0.958 (0.124)
Median [Min, Max]	0.901 [0.783, 0.993]	0.805 [0.805, 0.805]	0.928 [0.746, 1.37]	0.950 [0.805, 1.26]	1.08 [0.929, 2.12]	0.932 [0.746, 2.12]
Number of Tau PET Scans						
2	8 (17.0%)	1 (100%)	30 (14.2%)	15 (15.0%)	2 (5.9%)	56 (14.2%)
3	17 (36.2%)	0 (0%)	37 (17.5%)	25 (25.0%)	13 (38.2%)	92 (23.4%)
4	22 (46.8%)	0 (0%)	69 (32.7%)	32 (32.0%)	12 (35.3%)	135 (34.4%)
5	0 (0%)	0 (0%)	75 (35.5%)	28 (28.0%)	7 (20.6%)	110 (28.0%)
Years between First and Last Tau PET Scan						
Mean (SD)	4.08 (1.52)	1.38 (NA)	4.81 (1.61)	4.67 (1.59)	4.79 (1.37)	4.68 (1.59)
Median [Min, Max]	4.82 [1.35, 6.76]	1.38 [1.38, 1.38]	5.07 [1.61, 6.80]	4.90 [1.60, 8.04]	4.96 [1.71, 7.02]	4.99 [1.35, 8.04]
Treatment						
Placebo	0 (0%)	0 (0%)	97 (46.0%)	55 (55.0%)	18 (52.9%)	170 (43.3%)
Solanezumab	0 (0%)	0 (0%)	114 (54.0%)	45 (45.0%)	16 (47.1%)	175 (44.5%)
NA	47 (100%)	1 (100%)	0 (0%)	0 (0%)	0 (0%)	48 (12.2%)

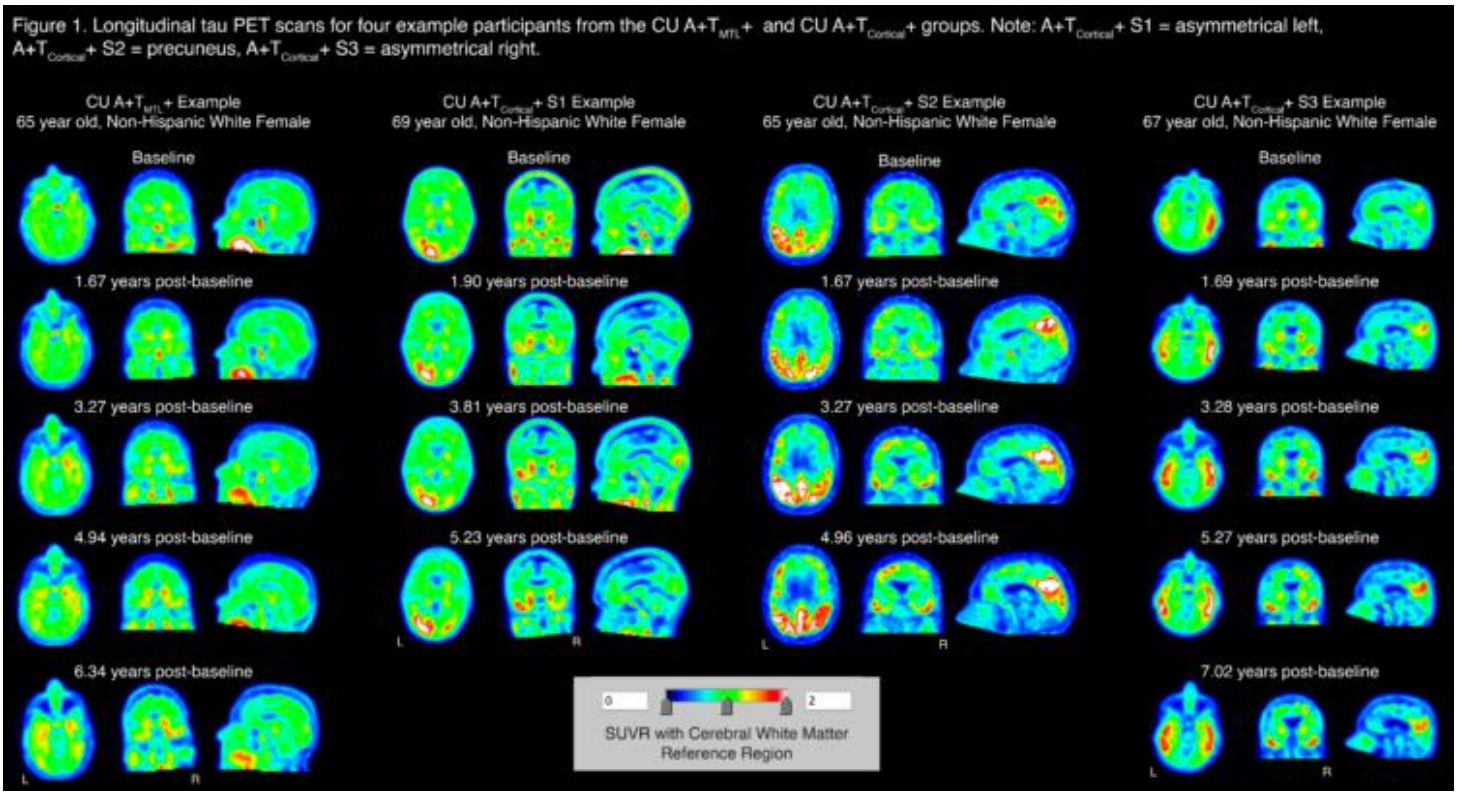
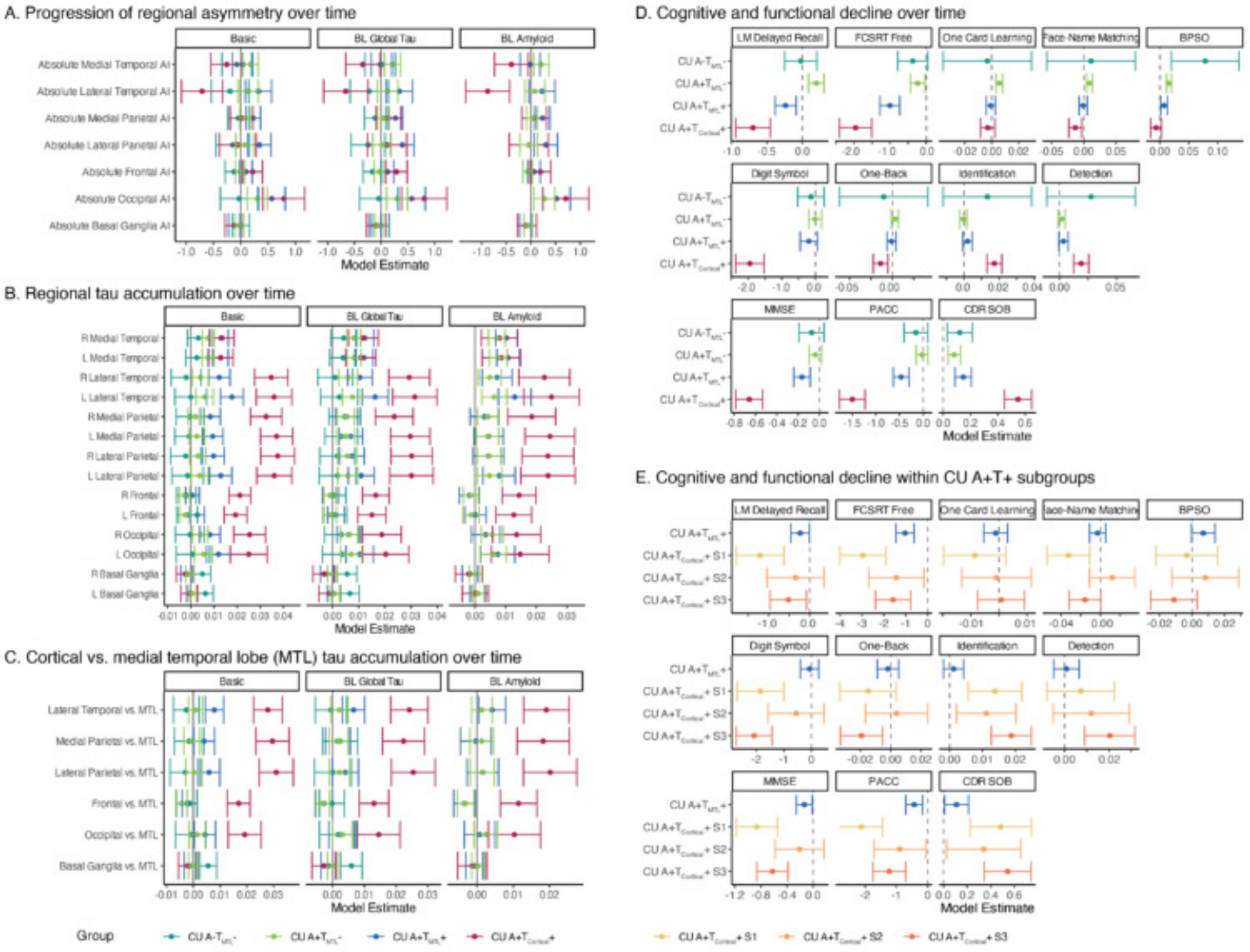

Figure 1. Longitudinal tau PET scans for four example participants from the CU A+T$_{MTL}$+ and CU A+T$_{Cortical}$+ groups. Note: A+T$_{Cortical}$+ S1 = asymmetrical left, A+T$_{Cortical}$+ S2 = precuneus, A+T$_{Cortical}$+ S3 = asymmetrical right.
CU A+T$_{MTL}$+ Example
65 year old, Non-Hispanic White Female
CU A+T$_{Cortical}$+ S1 Example
69 year old, Non-Hispanic White Female
CU A+T$_{Cortical}$+ S2 Example
65 year old, Non-Hispanic White Female
CU A+T$_{Cortical}$+ S3 Example
67 year old, Non-Hispanic White Female
Baseline
1.67 years post-baseline
3.27 years post-baseline
4.94 years post-baseline
6.34 years post-baseline
Baseline
1.90 years post-baseline
3.81 years post-baseline
5.23 years post-baseline
Baseline
1.67 years post-baseline
3.27 years post-baseline
4.96 years post-baseline
Baseline
1.69 years post-baseline
3.28 years post-baseline
5.27 years post-baseline
7.02 years post-baseline
0
2
SUVR with Cerebral White Matter Reference Region
L
R

Figure 2. Linear mixed model outputs predicting longitudinal change in (A) absolute values of regional asymmetry indices, (B) regional tau burden, (C) cortical vs. medial temporal lobe (MTL) residuals, and (D, E) cognition and functioning. In A, B, and C, the Basic Model included random intercepts and slopes as well as fixed effects of Age*Time, Sex*Time, and Group*Time in all participants except the one A-T_{MTL}+ participant; the BL Tau Model included Baseline Global Tau*Time in addition to all effects in the Basic Model in all participants except the one A-T_{MTL}+ participant; and the BL Amyloid Model included Baseline Amyloid Burden*Time in addition to all effects in the BL Tau Model in A+ participants only. In D, models included random intercepts and slopes as well as Age*Time, Sex*Time, Education*Time, Baseline Amyloid Burden*Time, and Group*Time in all participants except the one A-T_{MTL}+ participant. In E, models included all effects that were included in D but probed for differences between A+$T_{Cortical}$+ subgroups and the A+T_{MTL}+ group. Note: A+$T_{Cortical}$+ S1 = asymmetrical left, A+$T_{Cortical}$+ S2 = precuneus, A+$T_{Cortical}$+ S3 = asymmetrical right.



Keywords: tau PET, longitudinal, preclinical Alzheimer's disease, cortical tau, subtypes

Association between early and late tau aggregation across tau imaging agents: The HEAD Study

Nesrine Rahmouni[1], Cécile Tissot[2], Joseph Therriault[1], Ali Hosseini[1], Arthur Macedo[1], Stijn Servaes[1], Firoza Lussier[3], Lydia Trudel[1], Brandon Hall[1], Jaime Fernandez-Arias[1], Yi-Ting Wang[1], Jenna Stevenson[1], Serge Gauthier[1], Suzanne Baker[2], Tharick Pascoal[3], Pedro Rosa-Neto[1]

[1]*McGill University, Montreal, QC, CA*
[2]*Lawrence Berkeley National Laboratory, Berkeley, CA, US*
[3]*University of Pittsburgh, Pittsburgh, PE, US*

Background The association between medial temporal and neocortical SUVR depends on availability of cortical tau. However, tracer differences in affinity and off-target binding might interfere in these associations. Here, we examined the association between medial temporal and neocortical SUVR using voxel-based approach.

Methods: We included 68 individuals (46 Cognitively Unimpaired and 22 Cognitively Impaired) from the HEAD Study recruited at McGill University. All individuals were assessed for amyloid-β (Aβ) deposition using [^{18}F]AZD4694-PET and four tau-PET ligands ([^{18}F][^{18}F]MK6240, [^{18}F]Flortaucipir, [^{18}F]RO948 and [^{18}F]PI-2620). Correlation maps evaluated the relationship between PET tracers' uptake in the entorhinal cortex (EC), in the inferior temporal gyrus and in the posterior cingulate and their association with the tracer's uptake in later Braak regions. Correlations coefficients were compared across Braak Stages.

Results: Positive associations were observed between tau-PET SUVR in the EC (Figure1). [^{18}F]MK6240 EC was correlated with tracer uptake in the whole cortex. [^{18}F] Flortaucipir was associated with tracer uptake in similar regions, albeit showing a lower t-value. [^{18}F]PI2620 EC uptake correlated with binding in regions Braak II-V. Finally, [^{18}F]RO948 was associated with uptake. Across Braak regions, entorhinal seed covariance maps are restricted to early Braak regions in Aβ- individuals, while encompassing neocortical regions in Aβ+ individuals (Figure 2). Finally, seeds outside the MTL reflected advanced tau covariance patterns in Aβ+ individuals, with [^{18}F]MK6240 showing stronger correlation patterns in all Braak regions, followed by [^{18}F] Flortaucipir, [^{18}F]RO948 and [^{18}F]PI2620 (Figure 3).

Conclusion: [^{18}F]MK6240 showed higher and more widespread correlations between early and late tau pathology, potentially due to this tracer's higher affinity for tau tangles. Results were concordant at the voxel and region-on-interested levels. [^{18}F] Flortaucipir, [^{18}F]RO948 and [^{18}F]PI-2620 showed similar results, in lower magnitude.

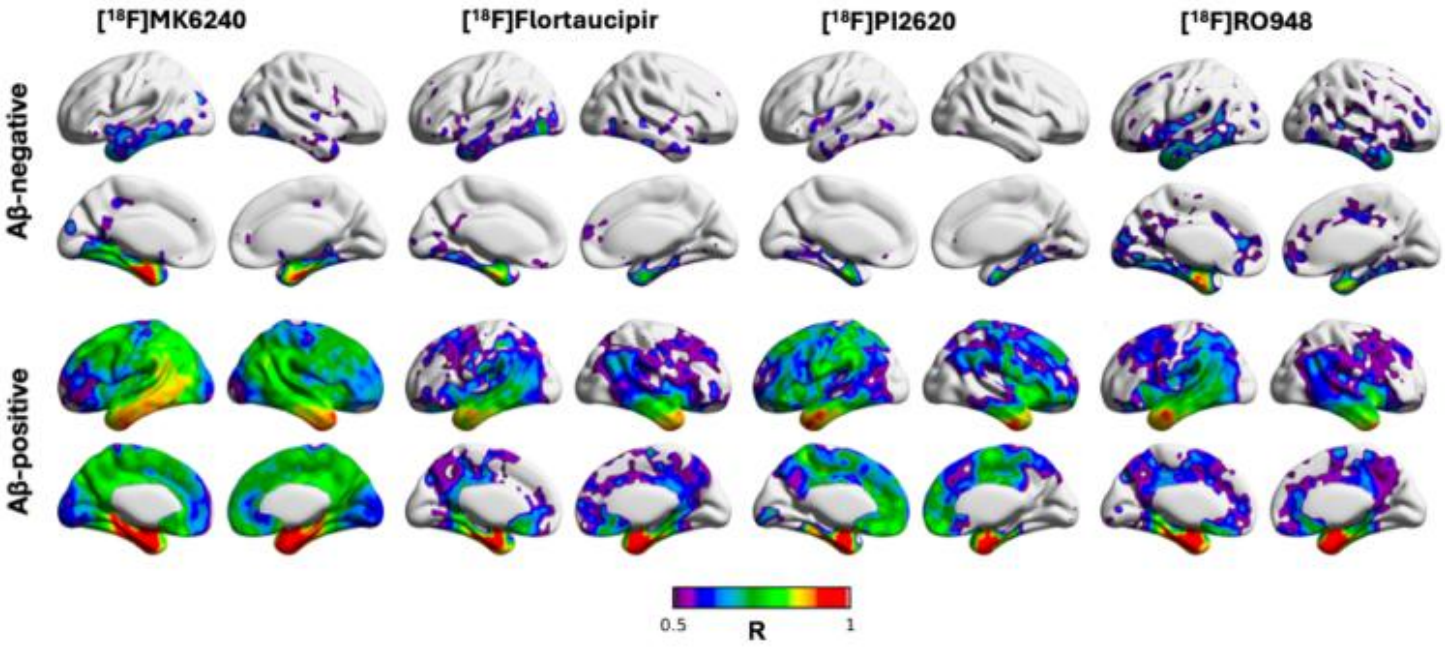


Figure 1: Patterns of Entorhinal cortex-Neocortical tau covariance.

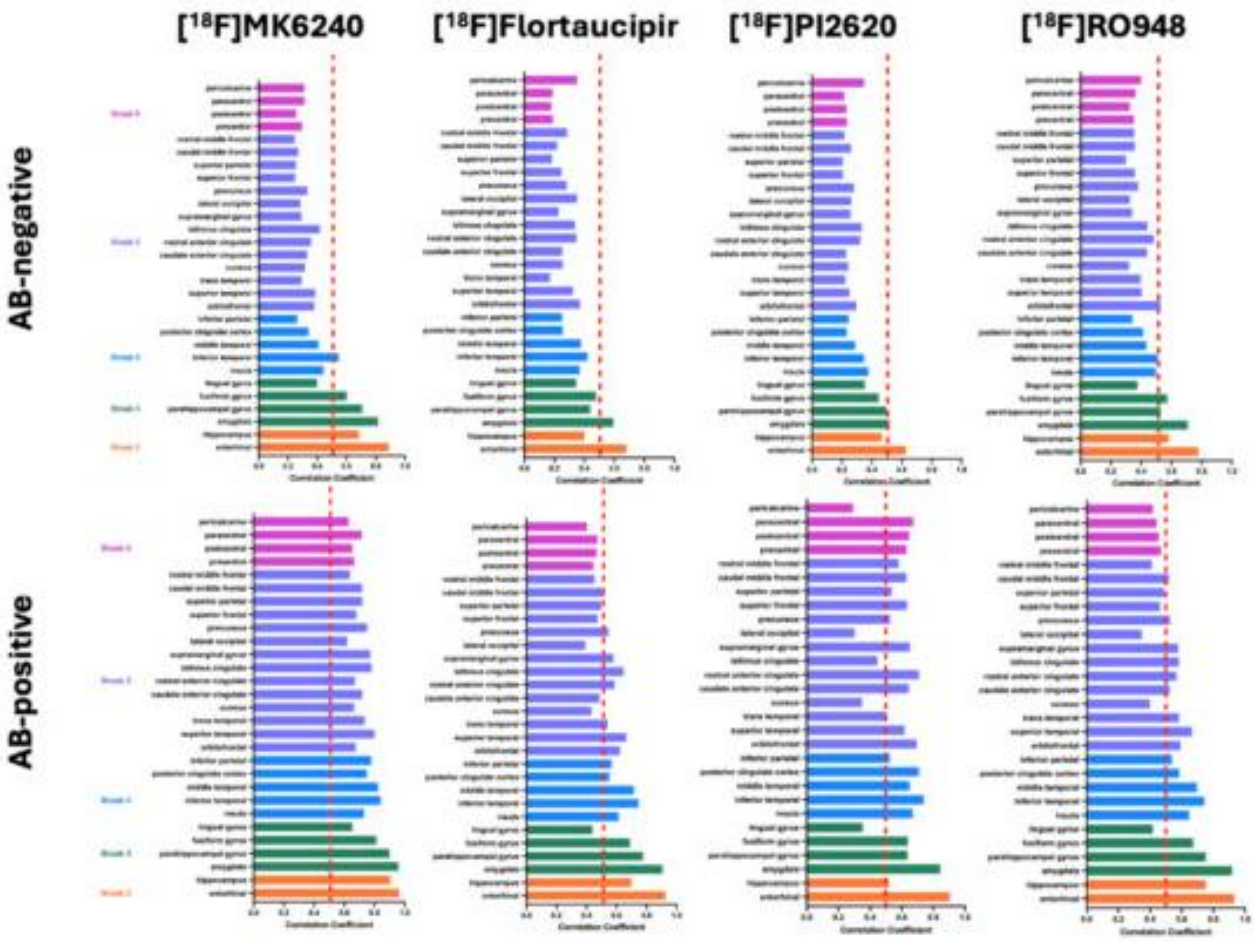


Figure 2: Entorhinal seed covariance maps across Braak Stages

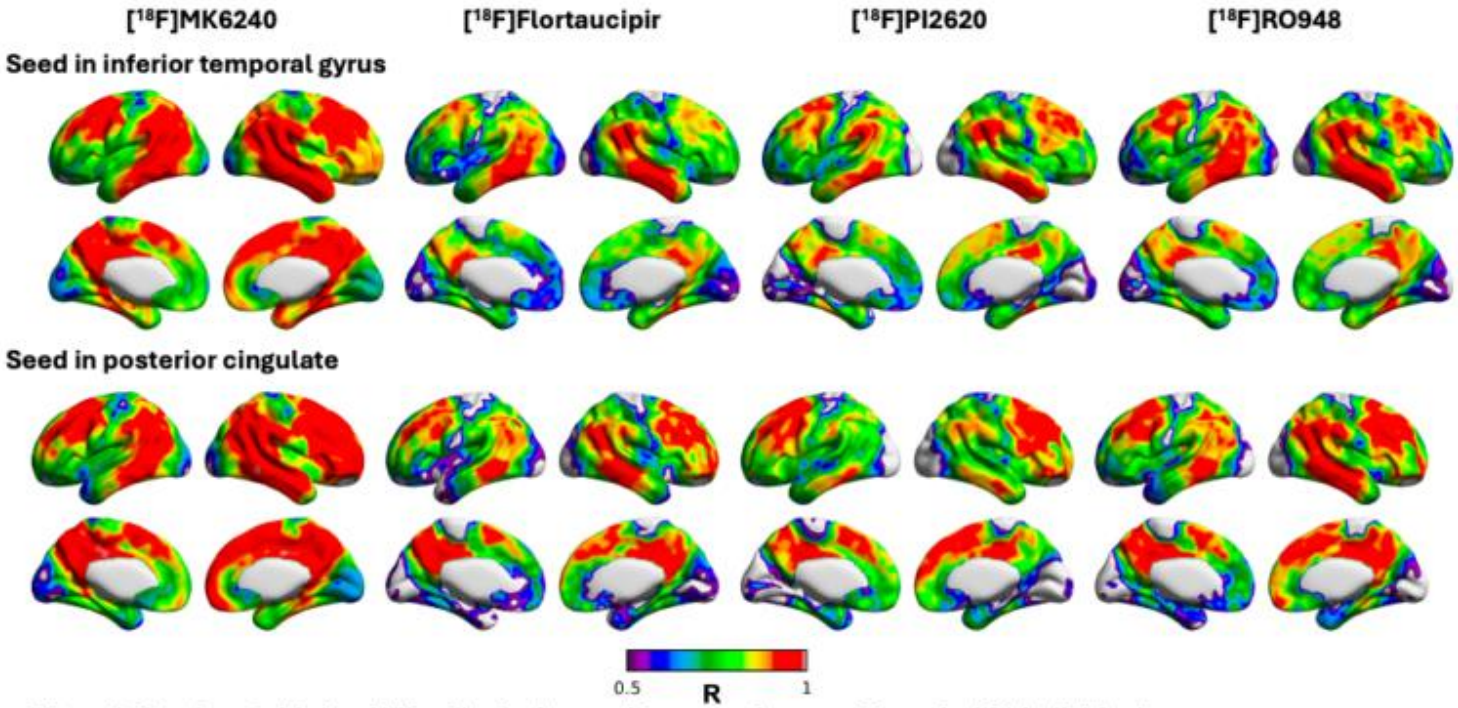


Figure 3: Seeds outside the MTL reflect advanced tau covariance patterns in Aβ+ individuals

Keywords: Tau, PET Imaging, Biomarkers, Head-to-head

Unraveling the impact of amyloid-β and tau pathology on brain structure and cognitive function during preclinical and prodromal Alzheimer's disease

Ting Qiu[1], Zhen-Qi Liu[3], Jonathan Gallego-Rudolf[1,3], Manon Edde[4], Alex Valcourt Caron[4], Yuanchao Zhang[5,6], Jean-Paul Soucy[3], R. Nathan Spreng[1,2,3], Maxime Descoteaux[4], Sylvia Villeneuve[1,2]

[1]*Douglas Mental Health University Institute, McGill University, Montreal, QC, CA*
[2]*Department of Psychiatry, McGill University, Montreal, QC, CA*
[3]*Montreal Neurological Institute, Montreal, QC, CA*
[4]*Sherbrooke Connectivity Imaging Laboratory (SCIL), Université de Sherbrooke, Sherbrooke, QC, CA*
[5]*The Clinical Hospital of Chengdu Brain Science Institute, MOE Key Lab for Neuroinformation, University of Electronic Science and Technology of China, Chengdu, CN*
[6]*School of Life Science and Technology, University of Electronic Science and Technology of China, Chengdu, CN*

Alzheimer's disease (AD) is characterized by the pathological accumulation of amyloid-beta (Aβ) and tau proteins, which progressively compromise brain function and structure, eventually leading to cognitive decline. We investigated the cross-sectional and longitudinal relationship between Aβ and tau deposition and structural properties, specifically cortical thickness, cortical free-water-corrected mean diffusivity (MD_T), and hippocampal volume (HV), during the preclinical and prodromal stages of AD. We also examined which pathological and/or structural properties are more strongly associated with memory deficits.

We first conducted partial least square analyses (PLS) to identify the pathological-structural associations between AD pathology and structural properties across three groups: cognitively unimpaired Aβ negative (CU Aβ–), cognitively unimpaired Aβ positive (CU Aβ+), and mild cognitive impairment Aβ positive (MCI Aβ+). In the CU Aβ– group, increased Aβ was associated with greater cortical thickness, larger HV, and lower MD_T. In the CU Aβ+ and MCI Aβ+ groups, elevated Aβ and tau were associated with reduced cortical thickness and increased MD_T (**Figure 1**). Similar associations were found between AD pathology and grey matter changes over time in PLS-derived key brain regions (**Figure 2A**). Combining all individuals, we observed inverse U-shaped associations between Aβ and both cortical thickness and HV, and a U-shaped association between Aβ and MD_T (**Figure 2B**). Longitudinal analyses also revealed inverse U-shaped associations between Aβ and cortical thickness/HV slopes, and a U-shaped relationship between Aβ and MD_T slope (**Figure 2C**). Lastly, we found that all pathological and structural biomarker tested were independently associated with memory in Aβ+ individuals, but only tau remained significant when including all brain markers in the same model (**Figure 3**).

This study demonstrates a biphasic trajectory of structural changes in response to Aβ pathology and emphasizes the central role of tau in neurodegeneration leading to clinical onset.

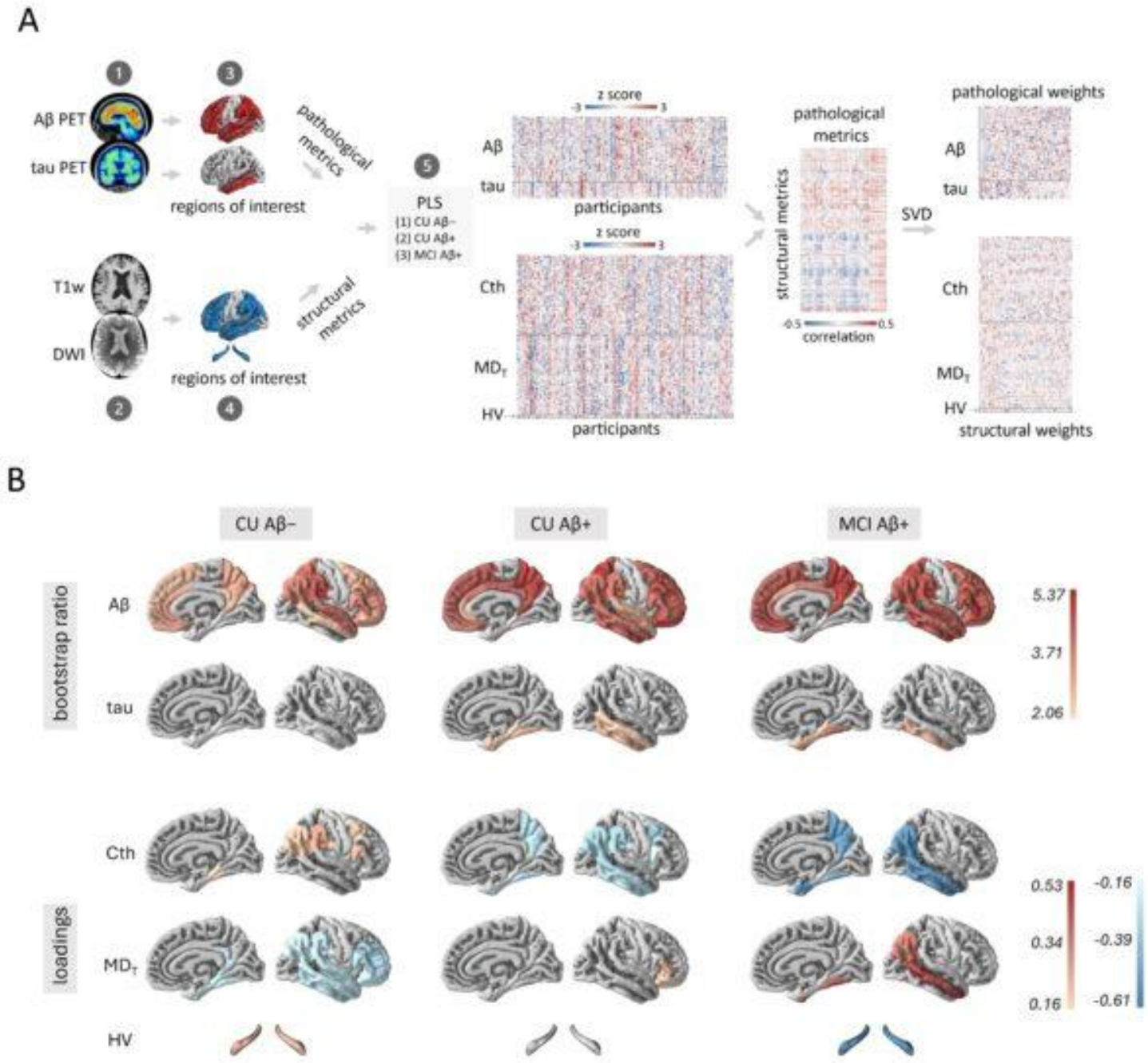


Figure 1. PLS analyses reveal covarying patterns of AD pathology and brain structure. (A). Three separate PLS analyses were defined to examine the multivariate patterns of maximum covariance between Aβ/tau deposition and cortical thickness/MD_T/HV for each group (CU Aβ−, CU Aβ+ and MCI Aβ+). **(B)**. Bootstrap ratio and loadings, reflecting the contribution of each cortical region to the association patterns between Aβ/tau and cortical thickness/MD_T/HV, are represented in the brain plots. Bootstrap ratio values > 1.96, and loadings where the 95% confidence interval did not include 0 were considered as reliably contributing to the multivariate relationship between AD pathology and structural properties. Bootstrap ratio and loadings with the same sign covary positively, while those with a different sign covary negatively. CU: cognitively unimpaired; MCI: mild cognitive impairment; Cth: cortical thickness; MD_T: free-water-corrected mean diffusivity; HV: hippocampal volume; SVD: singular value decomposition.

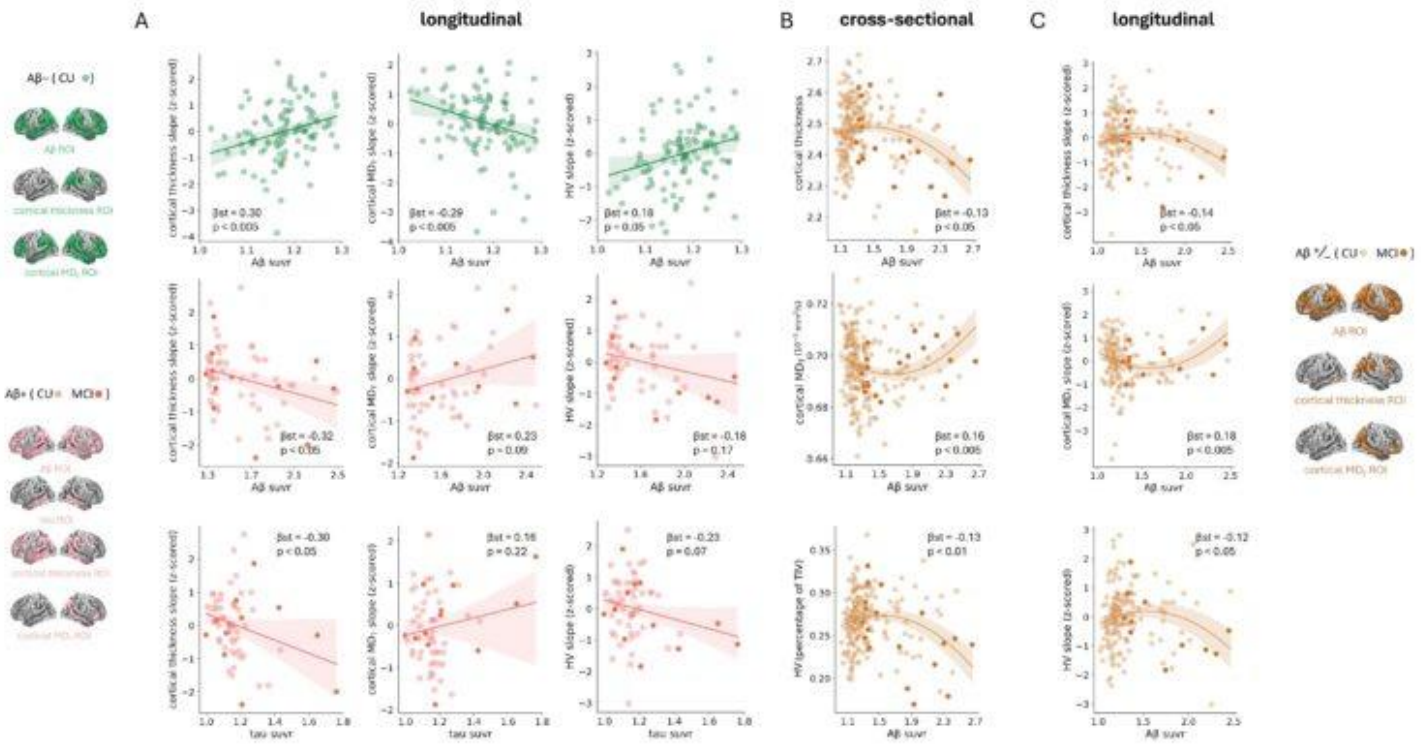


Figure 2. Univariate associations between AD pathology, structural measures, and their change in the PLS analyses derived regions. (A) Associations between Aβ and longitudinal changes in structural measures (cortical thickness, MD_T, and HV slopes) for the CU Aβ− group and Aβ+ (CU Aβ+ and MCI Aβ+). **(B)** Associations between pathological markers (Aβ and tau) and structural measures (cortical thickness, MD_T, and HV) for the entire cohort. **(C)** Associations between Aβ and longitudinal changes in structural measures (cortical thickness, MD_T, and HV slopes) for all participants. Each measure was averaged within the corresponding maps identified by PLS analyses (shown as the brain plots). In scatter plots for the Aβ+ group (combining CU Aβ+ and MCI Aβ+) and the whole cohort, darker dots indicate the MCI participants. Age, sex, APOE ε4 status were considered as covariates when performing statistical models. MD_T: free-water-corrected mean diffusivity; βst: standardized estimate β; PLS: partial least square.

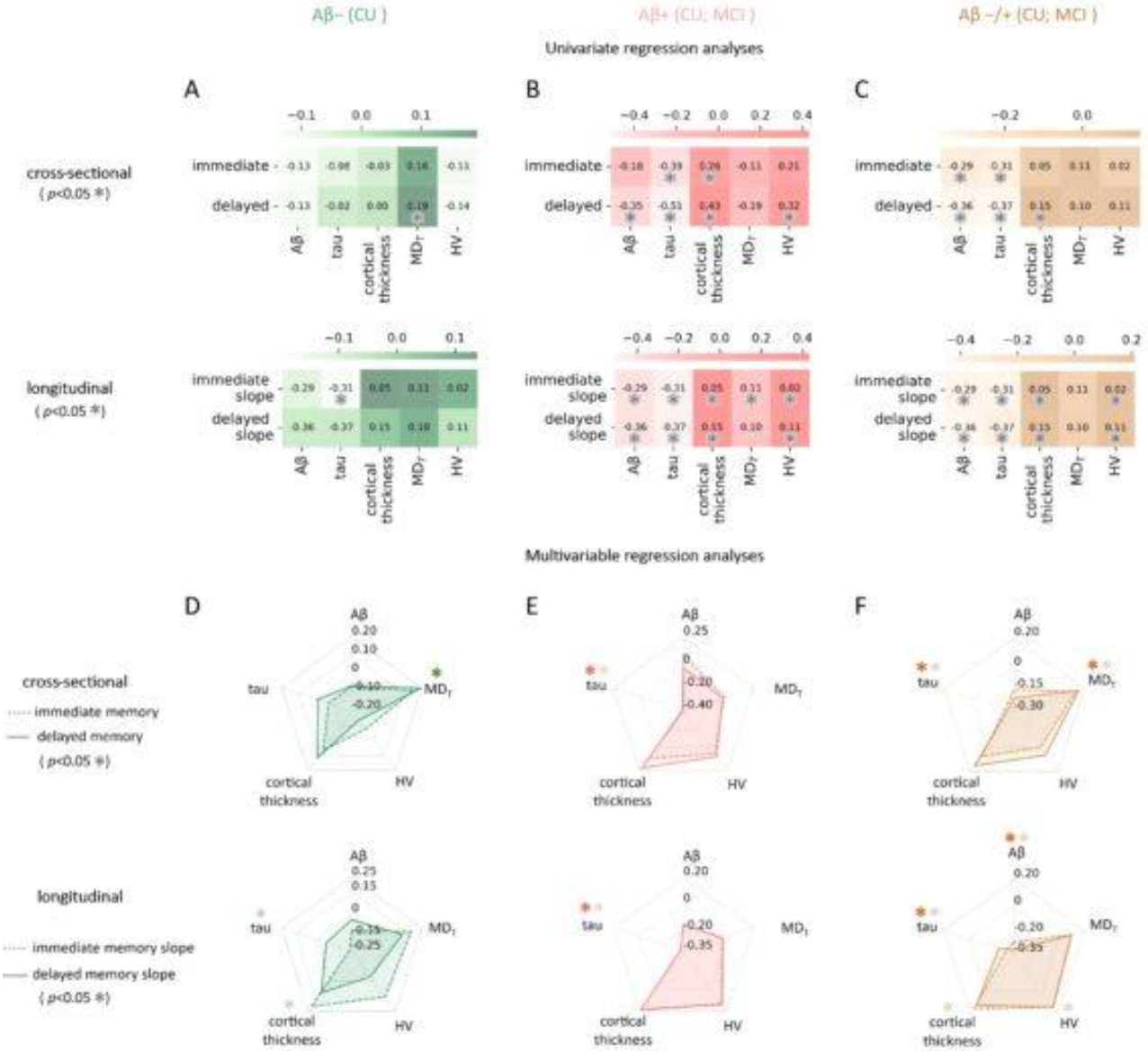


Figure 3. Univariate and multivariate regression analyses between pathological/structural measures and memory/memory change. Pathological and structural measures were averaged across significant regions identified in Fig 1B for each specific group. The univariate regression analyses, showing associations between brain biomarkers and memory performance, are displayed in **(A)**, **(B)**, and **(C)**, while multivariate regression analyses, illustrating associations between brain biomarkers and longitudinal changes in memory, are shown in **(D)**, **(E)**, and **(F)**. Specifically, **(A)** and **(D)** display the results for the CU Aβ− group; **(B)** and **(E)** present the results for the Aβ+ group (combined CU Aβ+ and MCI Aβ+); **(C)** and **(F)** display the results for the whole cohort. The heatmaps and spider plots depict the standardized beta coefficients (βst) for each predictor within the regression models. Significance is indicated by an asterisk (*), with $p < 0.05$. In panels **(D)**, **(E)**, and **(F)**, lighter asterisks indicate significant associations with immediate memory or its changes, while darker asterisks denote significance for delayed memory or its changes. Age, sex, APOE ε4 status were considered as covariates when performing statistical models. MD_T: free-water-corrected mean diffusivity; HV: hippocampal volume; βst: standardized estimate β.

Keywords: Aβ/tau, cortical thickness, cortical mean diffusivity, hippocampal volume

Wednesday, January 15, 2025 - 10:40 am - 11:35 am

Poster Session 1A

Wednesday, January 15, 2025			
10:40 am – 11:35 am	**Poster Session 1A** *(repeating in the afternoon as 1B)*		
Board 01	Decline in everyday functioning over time relates to amyloid and tau in cognitively unimpaired older adults	Dubbelman | Liu | Donohue | Langford | Raman | Rentz | Amariglio | Sperling | Aisen | Marshall	**Mark Dubbelman**, Center for Alzheimer Research and Treatment, Department of Neurology, Brigham and Women's Hospital, Harvard Medical School, Boston, MA, US
Board 02	From the clinical utility of a-synuclein PET imaging in Multiple System Atrophy to the possible diagnosis of Parkinson's disease	Vokali | Molette | Rodriguez | Changizi2 | Kuzkina | Ravache | Dimitrakopoulos | Delgado | Kocher | Pittet | Vallet | Hliva | Pfeifer | Kosco-Vilbois | Derouazi | Khurana | Capotosti	**Francesca Capotosti**, AC Immune SA, Lausanne, CH
Board 03	Unraveling the impact of amyloid-β and tau pathology on brain structure and cognitive function during preclinical and prodromal Alzheimer's disease	Qiu | Liu | Gallego-Rudolf | Edde | Caron | Zhang | Soucy | Spreng | Descoteaux | Villeneuve	**Ting Qiu**, Douglas Mental Health University Institute, McGill University, Montreal, QC, CA
Board 04	Astrogliosis, a potential non-Aβ pathway to tau	Villemagne | Cohen | Lopresti | Saeed | Tudorascu | Gogola | Matan | Reese | Snitz | Ikonomovic | Reis | Launer | Lopez	**Victor Villemagne**, Department of Psychiatry, University of Pittsburgh, Pittsburgh, PA, US
Board 05	APOE ε4 carriers exhibit attenuated habituation in pupil size and practice effects on a repeated auditory oddball task	Grube | Rodríguez Alonso | Engels-Domínguez | Jacobs | Riphagen	**Victor Villemagne**, Department of Psychiatry, University of Pittsburgh, Pittsburgh, PA, US
Board 06	Baseline tau burden and performance on a digital clock drawing test uniquely contributes to predicting future tau accumulation in preclinical AD	Fu | Robinson | Farrell | Jutten | Thibault | Rodriguez Alonso | Thompson | Lois | Tiss | Gong | Chen | Penney | Davis | Sperling | Johnson | Rentz | Price	**Jessie Fang-Lu Fu**, Athinoula A. Martinos Center for Biomedical Imaging, Boston, MA, US
Board 07	Molecular correlates of apraxia in Alzheimer's disease: A PET imaging study	Bischof | Jaeger | Giehl | jessen | Onur | O'Bryant | Kara | Weiss | Drzezga	**Gerard Bischof**, University of Cologne, University Hospital of Cologne, Department of Nuclear Medicine, Multimodal Neuroimaging Group, Cologne, Germany, Cologne, DE
Board 08	Understanding the impact of race on white matter hyperintensities in Alzheimer's disease: Findings from the ADNI Study	Ekuta | Ahn | Tripodis | Hamilton	**Victor Ekuta**, Morehouse School of Medicine, Atlanta, GA, US
Board 09	Characterization of a limbic-predominant amnestic neurodegenerative syndrome	Corriveau-Lecavalier | Waniger | Stricker | Machulda | Fields | Botha | Graff-Radford | Ramanan | McCarter | Nguyen | Reichard | Boeve | Knopman | Lowe | Dickson | Murray | Graff-Radford | Petersen | Jack | Jones	**Nick Corriveau-Lecavalier**, Department of Psychiatry and Psychology, Mayo Clinic, Rochester, MN, US

Board 10	Positron emission tomography analysis with the dynamicpet Python package	Bilgel | Amer | Bae | Bouhrara | Gong | Guo | Uriarte-Lopez | Singh | Matheson | Nørgaard	**Murat Bilgel**, Laboratory of Behavioral Neuroscience, National Institute on Aging, Baltimore, MD, US
Board 11	Targeted plasma eQTL and pQTL to identify potential novel biomarker for Alzheimer's disease in African Americans	Colón-Badillo | Reddy | Jin | Lincoln | Ho | Crook | Wang | Malphrus | Nguyen | Marrero-Polanco | Tamvaka | Lucas | Graff-Radford | Ertekin-Taner | Carrasquillo	**Murat Bilgel**, Laboratory of Behavioral Neuroscience, National Institute on Aging, Baltimore, MD, US
Board 12	Pathological and clinical trajectories of preclinical Alzheimer's disease patients with divergent cortical tau patterns	Young | Carlson | Cody | Winer | Schultz | Mormino	**Elizabeth Mormino**, Department of Neurology and Neurological Sciences, Stanford University School of Medicine, Stanford, CA, US
Board 13	Evaluation of a label-free X-ray based method for estimating amyloid load in the human brain	Geremia | Amer | Dahal | Badano	**Danielle Geremia**, Division of Imaging, Diagnostics, and Software Reliability, Office of Science and Engineering Laboratories, Center for Devices and Radiological Health, Food and Drug Administration, Silver Spring, MD, US
Board 14	Proteomic analyses of A-T-N reveal plasma mediators of neurodegeneration and dementia risk	Duggan | Bilgel | Chen | Moghekar | Davatzikos | Coresh | Resnick | Walker	**Michael Duggan**, Laboratory of Behavioral Neuroscience, National Institute on Aging, National Institutes of Health, Baltimore, MD, US
Board 15	The spatial spread of tauopathy precedes the increase in tau-PET load in Alzheimer's disease	Cassa Macedo | Therriault | Rahmouni | Tissot | Aumont | Wang | Servaes | Trudel | Hall | Hosseini | Fernandez-Arias | Bezgin | Chan | Zheng | Ferrari-Souza | Ferreira | Bellaver | Lussier | Pascoal | Rosa-Neto	**Arthur Cassa Macedo**, Department of Neurology and Neurosurgery, McGill University, Montreal, QC, CA
Board 16	Distinct patterns of Iron distribution in the entorhinal cortex-hippocampus system for characterization of mild cognitive impairment	Kagerer | Vionnet | van Bergen | Meyer | Gietl | Prüssmann | Hock | Unschuld	**Paul G. Unschuld**, Institute for Regenerative Medicine (IREM), University of Zurich, Zurich, CH
Board 17	Pathological asymmetry in early onset AD reflects heterogenous disease trajectories	Ziontz | Maiti | Zhang | Chiotis | Blazhenets | Rocha | Shankar | Amuiri | Schonhaut | Hammers | Eloyan | Koeppe | Carrillo | Dickerson | Apostolova | Rabinovici | La Joie	**Jacob Ziontz**, Memory and Aging Center, Department of Neurology, University of California San Francisco, San Francisco, CA, US
Board 18	Characterizing amyloid-positive with low Tau (A+T-) profiles and their association with cognitive trajectories in the Longitudinal Early-Onset Alzheimer's Disease Study (LEADS): A multi-method approach	Abu Raya | Soleimani-Meigooni | Schonhaut | Blazhenets | Chiotis | Lagarde | Vrillon | Maiti | Windon | Zeltzer | Zhang | Yballa | Shankar | Amuiri | Rocha | Hammers | Eloyan | Carrillo | Koeppe | Dickerson | Apostolova | Rabinovici | La Joie	**Maison Abu Raya**, Memory and Aging Center, Department of Neurology, Weill Institute for Neurosciences, University of California, San Francisco, San Francisco, San Francisco, CA, US
Board 19	The association between amyloid and physical activity in a racially diverse cohort of older adults	Dong | Wu | Minhas | Laymon | Villemagne | Lopez | Snitz | Gogniat | Glynn | Tudorascu | Cohen	**Yiwen Dong**, Department of Biostatistics and Health Data Science, School of Public Health, Pittsburgh, PA, US

Board 20	Whole blood gene expression is associated with plasma p-tau217 levels via amyloid-PET and sex	Buckley | Janve | Seto | Klinger | Brown | Birkenbihl | Coughlan | Townsend | Properzi | Zyski | Wang | Clifton | Hanseeuw | Chhatwal | Yang | Rissman | Aisen | Cuppels | Donohue | Raman | Johnson | Sperling | Dumitrescu | Hohman	**Yiwen Dong**, Department of Biostatistics and Health Data Science, School of Public Health, Pittsburgh, PA, US
Board 21	Plasma Aβ as predictor of Aβ accumulation in non-demented participants	Gogola | Cohen | Lopresti | Snitz | Ikonomovic | Tudorascu | Minhas | Kofler | Matan | Aizentein | Lopez | Karikari | Villemagne	**Alexandra Gogola**, Department of Radiology, University of Pittsburgh School of Medicine, Pittsburgh, PA, US
Board 22	The relative prevalence of tau severity stages is related to amyloid burden, clinical diagnosis and age	Cody | Sokolowski | Carlson | Medina | Winer | Young | Younes | Durant | Dumitrescu | Archer | Tosun-Turgut | Johnson | Harrison | Hohman | Mormino	**Karly Cody**, Department of Neurology and Neurological Sciences, Stanford University, Stanford, CA, US
Board 23	Head-to-head trajectories of tau PET and plasma p-tau217 as a function of Aβ	Bellaver | Povala | L. Ferreira | Bauer-Negrini | Lussier | Amaral | Soares | Rocha | Masdeu | Tudorascu | Soleimani-Meigooni | Fortea | Lowe | Oh | Pascual | A. Gordon | Rosa-Neto | Baker | A. Pascoal	**Bruna Bellaver**, University of Pittsburgh, Department of Psychiatry, PA, United States of America, Pittsburgh, PA, US
Board 24	Functional submodules in the human locus coeruleus are differentially susceptible to tau pathology	Lawn | Prokopiou | Van Egroo | Ashton | Janelidze | Blennow | Hansson | Zetterberg | Jacobs	**Timothy Lawn**, Athinoula A. Martinos Center for Biomedical Imaging, Department of Radiology, Massachusetts General Hospital and Harvard Medical School, 02129, Boston, MA, USA, Boston, MA, US
Board 25	Sex-specific associations of BMI, amyloid, and regional tau deposition in community-dwelling cognitively normal older adults	Gills | Cesar | Dominguez | Sogade | Browne | Weisgerber | McBride | Valkanova | Mbah | Figueredo | Jean-Louis | Masurkar | Osorio | Bubu	**Joshua Gills**, New York University Grossman School of Medicine, New York City, NY, US
Board 26	Assessment of ATN with a single dynamic [18]F-PI-2620 recording	Gnörich | Kusche-Palenga | Kling | Zatcepin | Dehsarvi | Bronte | Zaganjori | Frontzkowski | Roemer | Groß | Schöberl | Scheifele | Bauer | Bernhardt | Jäck | van Eimeren | Drzezga | Perneczky | Bürger | Levin | Bartenstein | Sabri | Barthel | Rullmann | Stöcklein | Höglinger | Franzmeier | Brendel	**Johannes Gnörich**, Department of Nuclear Medicine, University Hospital, LMU Munich, Munich, DE
Board 27	Tau-PET detects advanced primary age-related tauopathy mimicking early-stage AD	Grothe | Moscoso | Labrador-Espinosa | Silva-Rodríguez | Heeman | Costoya-Sánchez | Camacho | van Essen | Mainta | Perissinotti | Rodríguez-Fonseca | Ribaldi | Devous, Sr. | Pontecorvo | Frisoni | Garibotto | Schöll	**Michel Grothe**, Reina Sofia Alzheimer Center, CIEN Foundation, ISCIII, Madrid, ES
Board 28	Amyloid status moderates associations between hippocampal microstructure, PET tau burden, and memory in dementia-free older adults	Callow | Rani | Alm | Pettigrew | Soldan | Miller | Albert | Bakker	**Daniel Callow**, Johns Hopkins School of Medicine Department of Psychiatry and Behavioral Sciences, Baltimore, MD, US
Board 29	Performance of an MR-independent analysis pipeline for quantification	DelBene | Gogola | Reese | Matan | Chiang | Snitz | Cohen | Lopez | Villemagne | Lopresti	**Alexander DelBene**, Department of Radiology, University of

	of tau abnormality using [18F]flortaucipir PET		Pittsburgh School of Medicine, Pittsburgh, PA, US
Board 30	Functional and structural connectivity patterns predict longitudinal tau spreading in asymptomatic individuals expressing Aβ pathology	Gallego-Rudolf | Qiu | Javanray | Wiesman | St-Onge | Fajardo-Valdez | Baillet | Villeneuve	**Jonathan Gallego-Rudolf**, Douglas Research Centre, Montreal, QC, CA
Board 31	Plasma phospho-tau 217, neurofilament-light, and glial fibrillary acidic protein are differentially associated with longitudinal neuropsychiatric symptoms across the early cognitive spectrum	Gatchel | Yu | Palmer | Wu | Beltran | Munro | Webb | Blacker | Arnold | Marshall | Dodge	**Jennifer Gatchel**, Massachusetts General Hospital, Department of Psychiatry, Boston, MA, US
Board 32	An assessment of the utility of flortaucipir PET to detect four-repeat tau pathology in a globular glia tauopathy case-series	Gatto | Youssef | Ghatamaneni | Uruk | Min | Fu | Reichard | Lowe | Dickson | Whitwell | Josephs	**Rodolfo Gatto**, Department of Neurology, Mayo Clinic, Rochester, MN, US
Board 33	Molecular imaging of neurodegeneration – mitochondria, associated proteins and synapses (MIND-MAPS) in frontotemporal dementia	Clarke | Whittington | Passchier | Lewis | Passamonti | Chen | Salinas | Tsukada | Cash | Rabiner | Rohrer	**Mica Clarke**, Perceptive, London, GB
Board 34	Evaluating tVNS effects on cognitive outcomes and modulating factors in asymptomatic older adults: study design of the WALLe Trial	Engels-Domínguez | Grube | Fenlon | Wiklund | Heinrich | Baillet | van Egroo | Papp | Riphagen | Garcia | Sclocco | Johnson | Napadow | Jacobs	**Nina Engels-Domínguez**, The Athinoula A. Martinos Center for Biomedical Imaging, Department of Radiology, Massachusetts General Hospital, Harvard Medical School, Boston, MA, US
Board 35	Cerebral perfusion indices from early-phase [18F]-MK6240 dynamic Tau PET imaging in brain regions associated with Alzheimer's disease progression in an aging population.	Dhaynaut | Lois | Tiss | Thibault | Fanglu Fu | Ouyang | Johnson | El Fakhri | Normandin | Guehl	**Maeva Dhaynaut**, Yale PET Center, Department of Radiology & Biomedical Imaging, Yale University School of Medicine, New Haven, CT, US
Board 36	Transcutaneous auricular vagus nerve stimulation improves learning and sleep-wake quality in older APOE-ε4 carriers	Baillet | Van Egroo | Engels-Domínguez | Grube | Fenlon | Wiklund | Heinrich | Riphagen | Papp | Garcia | Sclocco | Napadow | Jacobs	**Marion Baillet**, Athinoula A. Martinos Center for Biomedical Imaging, Department of Radiology, Massachusetts General Hospital, Boston, MA, US
Board 37	Biological-clinical mismatch reflects co-pathology and vulnerability to neurodegeneration	Brown | Das | Xie | Nasrallah | Detre | Yushkevich | McMillan | Wolk	**Christopher Brown**, Department of Neurology, University of Pennyslvania, Philadelphia, PA, US
Board 38	Validation of PET spatial extent as sensitive amyloid biomarker in early stages of amyloidosis	Del Carmen Montenegro | Thibault | Fanglu Fu | Price | Hanseeuw | Jacobs | Sperling | Johnson | Farrell	**Grace Del Carmen Montenegro**, Department of Radiology, Massachusetts General Hospital, Harvard Medical School, Boston, MA, US
Board 41	Developing a novel reference region for PI-2620-PET imaging to facilitate assessment of 4-repeat tauopathies	Frontzkowski	**Lukas Frontzkowski**, Institute for Stroke and Dementia Research (ISD), Munich, DE
Board 39	P-TAU217, GFAP, and NFL plasma biomarker associations with demographic, medical and neurocognitive features from middle-aged through older adulthood	Arnold | Kivisakk | Fatima | Gentsch | Cruchaga | Wu | Dodge | Ances | Salat	**Steven Arnold**, Massachusetts General Hospital, Harvard Medical School, Boston, MA, US

Board 40	DeepSUVR: Using temporal constraints to improve tau quantification	Bourgeat | Fripp | Gillman | Feizpour | Schwarz | Jack | Lowe | Weiner | Masters | Villemagne | Rowe | Dore	**Pierrick Bourgeat**, CSIRO Health and Biosecurity, Brisbane, AU
Board 42	Increasing the granularity of tau-PET Braak staging using medial temporal lobe segmentations to detect early memory impairment	Aumont | Hall | Trudel | Chan | Hosseini | Macedo | Fernandez Arias | Rahmouni | Therriault | Servaes | Bezgin | Stevenson | Rosa-Neto	**Etienne Aumont**, McGill University Research Centre for Studies in Aging, Montréal, QC, CA
Board 43	The universal tau PET scale (Uniτ) for Flortaucipir, MK6240, PI2620 and RO948 harmonization	Povala | Bauer-Negrini | Bellaver | Z. Lussier | Amaral | Lukasewicz Ferreira | L. Tudorascu | Finn | Masdeu | Soleimani-Meigooni | Fortea | Lowe | Oh | Pascual | A. Gordon | Rosa-Neto | Baker | A. Pascoal	**Guilherme Povala**, University of Pittsburgh, Department of Psychiatry, Pittsburgh, PA, US
Board 44	Assessing the relationship between neuropsychiatric symptoms, amyloid and tau pathology, and white matter hyperintensity volume across sexes in preclinical Alzheimer's disease	Garrone | Yakoub | Fajardo-Valdez | Qiu | Ourry | Villeneuve	**Aurélie Garrone**, Douglas Mental Health University Institute, Montreal, QC, CA
Board 45	Unveiling the heterogeneity of tau spreading in aging and Alzheimer's disease using polygenic combinations: Towards personalized models	Diez | Lois | Garcia Condado | Farrell | Thibault | Jacobs | Buckley | Hanseeuw | Properzi | Yang | Sperling | Cortes | Quiroz | Sepulcre | Johnson | Gomez-Isla	**Ibai Diez**, Gordon Center for Medical Imaging, Department of Radiology, Massachusetts General Hospital, Harvard Medical School, Boston, MA, USA, Boston, MA, US
Board 46	Regional amyloid and tau: Exploring regional sex-based differences in a middle-aged community-based cohort	Guzmán | Aziz | Smith | Houlihan | Sanchez | Luchsinger | Lao	**Diana S Guzmán**, Columbia University Medical Center, New York, NY, US
Board 47	Comparison of topographical patterns of abnormalities of the tau PET tracers [18F]Flortaucipir, [18F]MK6240, [18F]PI2620, and [18F]RO948	Amaral | Povala | Bauer-Negrini | Ruppert | Bellaver | Lussier | L. Ferreira | Masdeu | Tudorascu | Soleimani-Meigooni | Fortea | Lowe | Oh | Pascual | Gordon | Rosa-Neto | Baker | Pascoal	**Livia Amaral**, University of Pittsburgh, Department of Psychiatry, Pittsburgh, PA, US
Board 48	Subtle cognitive deficits detected through routine in-office tests are associated with global Aβ and temporal tau in cognitively unimpaired individuals	Felix | Rebok | Kollasserry | Snitz | Ferreira | Tudorascu | Povala | Saha | Amaral | Lussier | Masdeu | Soleimani-Meigooni | Fortea | Lowe | Oh | Gordon | Rosa-Nato | Baker | Nasreddine | Pascoal	**Cynthia Felix**, Department of Psychiatry, University of Pittsburgh, Pittsburgh, PA, US
Board 49	Estradiol-dependent associations between sleep complaints and tau deposition in women at elevated AD risk	Lui | Wang | Deyong | Malhotra | Sundermann | Banks	**Sarah Banks**, SDSU/UC San Diego Joint Doctoral Program in Clinical Psychology, San Diego, CA, US
Board 50	Impact of age and sex on extra-cerebral off-target binding in tau PET scans (18F-FTP)	Ghatamaneni | Kim | Nycklemoe | Lundt | Schwarz | Kandimalla | Jacobson | Albertson | Jack | Gunter | Peterson | kung | sharma | seokbeen | Lowe | Min	**Sujala Ghatamaneni**, Department of Radiology, Mayo Clinic, Rochester, MN, US
Board 51	Metabolic inefficiency is associated with regional vulnerability to tau deposition	Adams | Parker | Zhao | Yassa	**Jenna Adams**, University of California, Irvine, Irvine, CA, US
Board 52	Relationship between Polygenetic Risk Score of BrainAge and plasma biomarkers in the A4/Elearn Study	Garcia Condado | Birkenbihl | Cortes | Buckley | Diez	**Jorge Garcia Condado**, Computational Neuroimaging

			Lab, Biobizkaia Health Research Institute, Barakaldo, ES
Board 53	Combined impact of plasma phospho-tau 217 and NfL on longitudinal domain-specific cognitive decline	Dodge | Wu | Chen | Gatchel | Das | Kivisäkk | Arnold	**Hiroko Dodge**, Harvard Medical School, Boston, MA, US
Board 54	Comparison of distribution volume and standardized uptake value ratio for a MAO-B tracer in mild cognitive impairment	Bezgin | Rahmouni | Harada | Okamura | Benedet | Ashton | Zetterberg | Blennow | Rosa-Neto	**Gleb Bezgin**, McGill University, Montreal, QC, CA
Board 55	Association between early and late tau aggregation across tau imaging agents: The HEAD Study	Rahmouni | Tissot | Therriault | Hosseini | Macedo | Servaes | Lussier | Trudel | Hall | Fernandez-Arias | Wang | Stevenson | Gauthier | Baker | Pascoal | Rosa-Neto	**Nesrine Rahmouni**, McGill University, Montreal, QC, CA
Board 56	The impact of spatial smoothing on the accuracy of Centiloid thresholds	Fajardo-Valdez | Qiu | Gallego-Rudolf | Javanray | Villeneuve	**Alfonso Fajardo-Valdez**, Douglas Mental Health University Institute, Montreal, Quebec, Canada, Montreal, QC, CA
Board 57	Longitudinal amyloid PET trajectories in the HABS-HD cohort	Betthauser | Morse | Heston | Langhough | Carey | Wisch | Ances | Cohen | Toga | Braskie | Zuelsdorff | O'Bryant | Meeker	**Tobey Betthauser**, University of Wisconsin-Madison, School of Medicine and Public Health, Department of Medicine, Madison, WI, US
Board 58	Lower microstructural integrity of the locus coeruleus to entorhinal cortex pathway is related to elevated astrocyte reactivity and tau burden in cognitively unimpaired individuals: a 7T dMRI study	Patsyuk | Van Egroo | Beckers | Ashton | Janelidze | Blennow | Hansson | Zetterberg | Poser | Jacobs	**Yuliya Patsyuk**, Faculty of Health, Medicine and Life Sciences, Mental Health and Neuroscience Research Institute, Alzheimer Centre Limburg, Maastricht University, Maastricht, NL

1 Decline in everyday functioning over time relates to amyloid and tau in cognitively unimpaired older adults

Mark Dubbelman[1,2], Andy Liu[3], Michael Donohue[3], Oliver Langford[3], Rema Raman[3], Dorene Rentz[1,2], Rebecca Amariglio[1,2], Reisa Sperling[1,2], Paul Aisen[3], Gad Marshall[1,2]

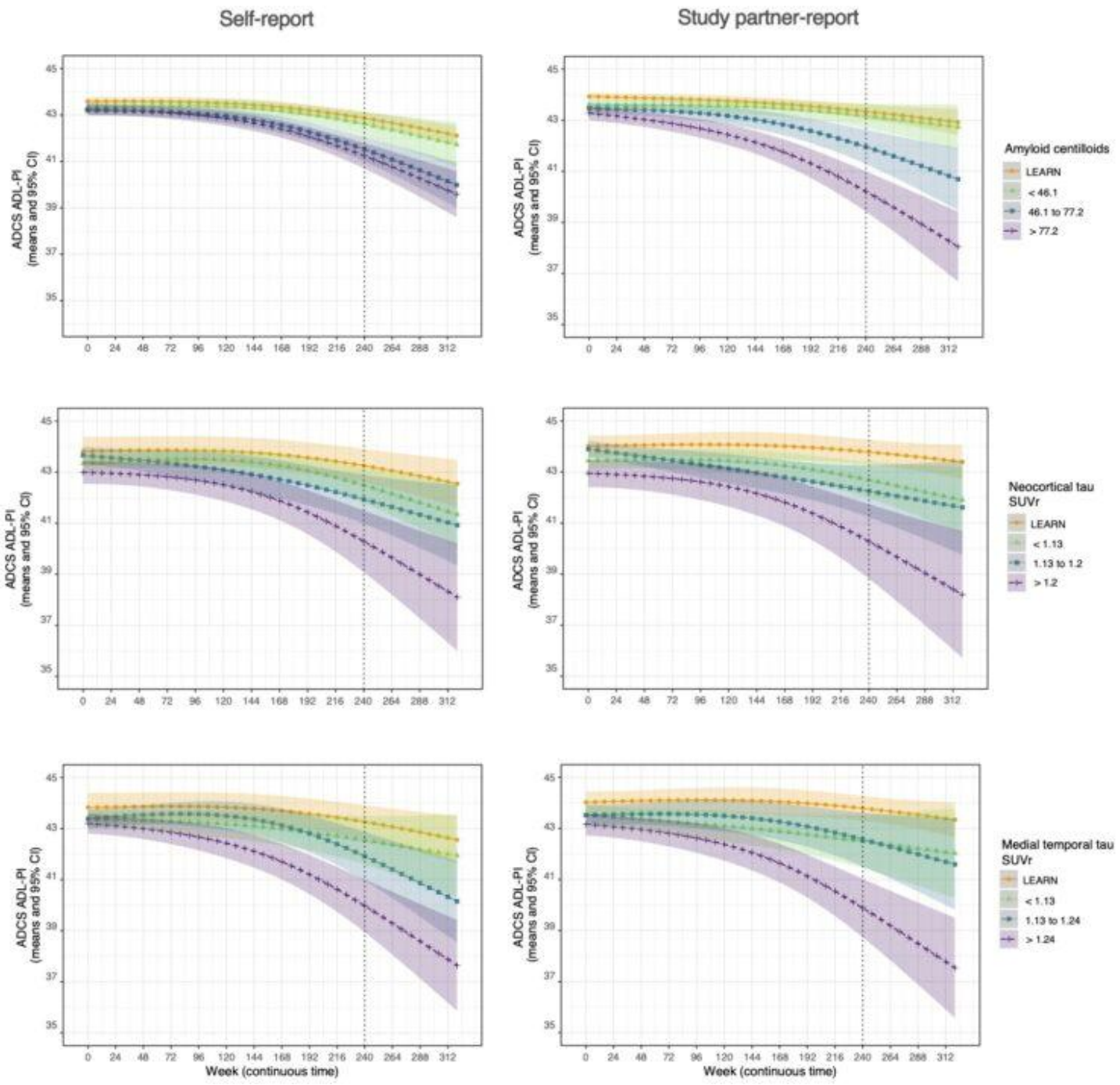
[1]*Center for Alzheimer Research and Treatment, Department of Neurology, Brigham and Women's Hospital, Harvard Medical School, Boston, MA, US*
[2]*Department of Neurology, Massachusetts General Hospital, Harvard Medical School, Boston, MA, US*
[3]*Alzheimer Therapeutic Research Institute, Keck School of Medicine, University of Southern California, San Diego, CA, US*

Introduction: Everyday functioning declines gradually over time in Alzheimer's disease, with the earliest changes occurring at the preclinical stage. We aimed to investigate how changes in everyday functioning relate to amyloid and tau in a large sample of cognitively unimpaired older adults who participated in the A4 and LEARN clinical trials.

Methods: We included 1,707 participants (71.5±4.7 years, 60% female, mean education 16 years) from the A4 Study (n=1,147, 67%) in which participants had elevated cortical amyloid at baseline and the LEARN Study (n=560, 33%) in which participants had low amyloid at baseline. All underwent amyloid positron emission tomography (PET) scans, and a subset of n=434 underwent tau PET scans. Participants and their study partners completed the Alzheimer's Disease Cooperative Study Activities of Daily Living Prevention Instrument (ADCS ADL-PI) multiple times over a six-year follow-up period. Using generalized least squares models, we analyzed how changes in everyday functioning related to a cortical aggregate of amyloid and neocortical and mediotemporal aggregates of tau. We also correlated changes in amyloid and tau PET and changes in everyday functioning.

Results: In the whole sample, everyday functioning declined marginally over time. Among individuals with elevated amyloid, those with the highest levels of neocortical and mediotemporal tau at baseline showed the largest decline in everyday functioning, as reported by the participants and their study partners (see Figure). Increases in neocortical and mediotemporal tau correlated moderately (correlation coefficient ranging from -0.2 to -0.5) with a decline in everyday functioning over time.

Conclusion: In this study, higher tau levels were associated with the fastest decline in everyday functioning in the presence of elevated amyloid, and those accumulating more tau showed a faster decline in daily functioning. This demonstrates the utility of including sensitive measures of everyday functioning in clinical trials at the stage of preclinical Alzheimer's disease.



Keywords: instrumental activities of daily living, amyloid, tau, function

2 From the clinical utility of a-synuclein PET imaging in Multiple System Atrophy to the possible diagnosis of Parkinson's disease

Efthymia Vokali[1], Jerome Molette[1], Diego Rodriguez[2], Barbara K. Changizi2[2], Anastasia Kuzkina[2], Myriam Ravache[1], Yannis Dimitrakopoulos[1], Christophe Delgado[1], Jacqueline Kocher[1], Laure Pittet[1], Coralie Vallet[1], Valerie Hliva[1], Andrea Pfeifer[1], Marie Kosco-Vilbois[1], Madiha Derouazi[1], Vikram Khurana[2], Francesca Capotosti[1]

[1]*AC Immune SA, EPFL Innovation Park, Building B, Lausanne, CH*
[2]*Division of Movement Disorders and Ann Romney Center for Neurologic Diseases, Department of Neurology, Brigham and Women's Hospital and Harvard Medical School, Boston, MA, US*

Parkinson's disease (PD) and other synucleinopathies, such as Multiple System Atrophy (MSA), involve a progressive accumulation of a-synuclein (a-syn) inclusions which correlate with clinical manifestations and disease progression. Imaging a-syn pathology using PET would transform diagnosis, patient recruitment and monitoring of therapeutic efficacy in clinical trials targeting a-syn. Here, we report new clnical data with [18F]ACI-12589 PET together with a skin-biopsy based seed amplification assay (SAA) in MSA.

Eight subjects who met the diagnostic criteria for probable MSA (MSA-P = 5, MSA-C = 3) were enrolled. Subjects underwent scans 60–90 min after injection. PET images were motion-corrected and co-registered to MRI images. Three 5-mm skin biopsies were obtained in all subjects. The SAA reaction buffer included 1 mg/mL recombinant α-syn, 10 µM thioflavin T (ThT), and 2µl of 0.5% skin biopsy lysate. Four replicates per sample were incubated at 37°C for 48 hours. Samples were positive if ≥75% of the replicates crossed the predefined fluorescence threshold.

[18F]ACI-12589 exhibited uptake in the cerebellum all tested MSA-C cases and had a positive SAA signal in 2 out 3 tested cases. Among the five tested probable MSA-P cases, two had a clear uptake in the basal ganglia by PET and a clear MSA pattern on SAA; one showed a positive MSA signal only by SAA, while the two remaining cases did not show retention by PET and either a PD pattern in SAA or a consistently negative SAA. Upon clinical re-evaluation, the diagnosis of those two cases was changed.

While the a-syn [18F]ACI-12589 PET tracer is sufficient for the diagnosis of MSA-C, the combination of both spatial (PET) and conformational (SAA) a-syn biomarkers could improve the error-prone clinical differential diagnosis of MSA-P. [18F]ACI-12589 PET tracer alone or in combination with other biomarkers promise to open up new precision-medicine approaches for this devastating disease.

Keywords: a-synuclein, new tracers, biomarkers

3 Unraveling the impact of amyloid-β and tau pathology on brain structure and cognitive function during preclinical and prodromal Alzheimer's disease

Ting Qiu[1], Zhen-Qi Liu[3], Jonathan Gallego-Rudolf[1,3], Manon Edde[4], Alex Valcourt Caron[4], Yuanchao Zhang[5,6], Jean-Paul Soucy[3], R. Nathan Spreng[1,2,3], Maxime Descoteaux[4], Sylvia Villeneuve[1,2]

[1]*Douglas Mental Health University Institute, McGill University, Montreal, QC, CA*
[2]*Department of Psychiatry, McGill University, Montreal, QC, CA*
[3]*Montreal Neurological Institute, Montreal, QC, CA*
[4]*Sherbrooke Connectivity Imaging Laboratory (SCIL), Université de Sherbrooke, Sherbrooke, QC, CA*
[5]*The Clinical Hospital of Chengdu Brain Science Institute, MOE Key Lab for Neuroinformation, University of Electronic Science and Technology of China, Chengdu, CN*
[6]*School of Life Science and Technology, University of Electronic Science and Technology of China, Chengdu, CN*

Alzheimer's disease (AD) is characterized by the pathological accumulation of amyloid-beta (Aβ) and tau proteins, which progressively compromise brain function and structure, eventually leading to cognitive decline. We investigated the cross-sectional and longitudinal relationship between Aβ and tau deposition and structural properties, specifically cortical thickness, cortical free-water-corrected mean diffusivity (MD_T), and hippocampal volume (HV), during the preclinical and prodromal stages of AD. We also examined which pathological and/or structural properties are more strongly associated with memory deficits.

We first conducted partial least square analyses (PLS) to identify the pathological-structural associations between AD pathology and structural properties across three groups: cognitively unimpaired Aβ negative (CU Aβ–), cognitively unimpaired Aβ positive (CU Aβ+), and mild cognitive impairment Aβ positive (MCI Aβ+). In the CU Aβ– group, increased Aβ was associated with greater cortical thickness, larger HV, and lower MD_T. In the CU Aβ+ and MCI Aβ+ groups, elevated Aβ and tau were associated with reduced cortical thickness and increased MD_T (**Figure 1**). Similar associations were found between AD pathology and grey matter changes over time in PLS-derived key brain regions (**Figure 2A**). Combining all individuals, we observed inverse U-shaped associations between Aβ and both cortical thickness and HV, and a U-shaped association between Aβ and MD_T (**Figure 2B**). Longitudinal analyses also revealed inverse U-shaped associations between Aβ and cortical thickness/HV slopes, and a U-shaped relationship between Aβ and MD_T slope (**Figure 2C**). Lastly, we found that all pathological and structural biomarker tested were independently associated with memory in Aβ+ individuals, but only tau remained significant when including all brain markers in the same model (**Figure 3**).

This study demonstrates a biphasic trajectory of structural changes in response to Aβ pathology and emphasizes the central role of tau in neurodegeneration leading to clinical onset.

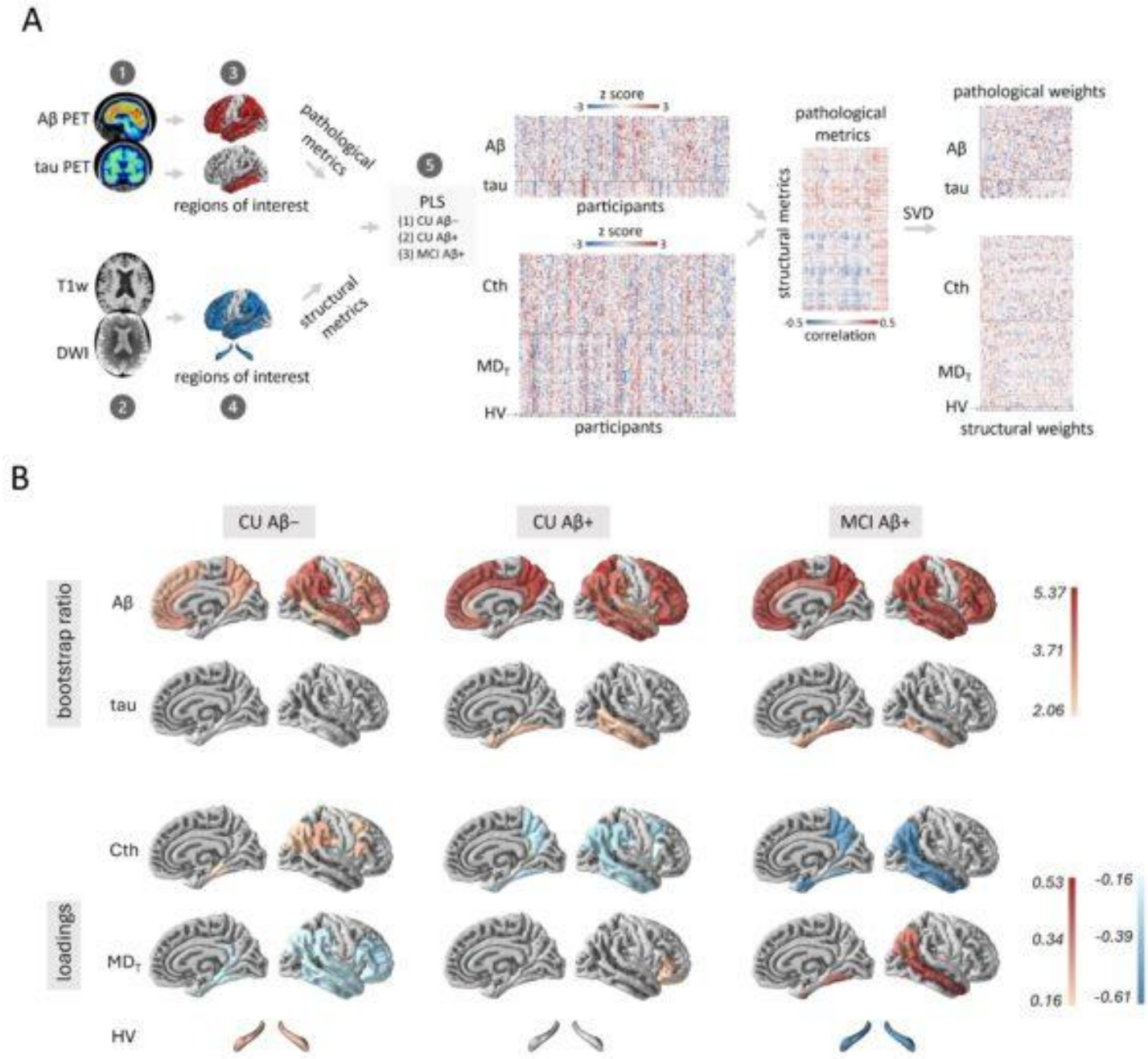


Figure 1. PLS analyses reveal covarying patterns of AD pathology and brain structure. (A). Three separate PLS analyses were defined to examine the multivariate patterns of maximum covariance between Aβ/tau deposition and cortical thickness/MD_T/HV for each group (CU Aβ−, CU Aβ+ and MCI Aβ+). **(B)**. Bootstrap ratio and loadings, reflecting the contribution of each cortical region to the association patterns between Aβ/tau and cortical thickness/MD_T/HV, are represented in the brain plots. Bootstrap ratio values > 1.96, and loadings where the 95% confidence interval did not include 0 were considered as reliably contributing to the multivariate relationship between AD pathology and structural properties. Bootstrap ratio and loadings with the same sign covary positively, while those with a different sign covary negatively. CU: cognitively unimpaired; MCI: mild cognitive impairment; Cth: cortical thickness; MD_T: free-water-corrected mean diffusivity; HV: hippocampal volume; SVD: singular value decomposition.

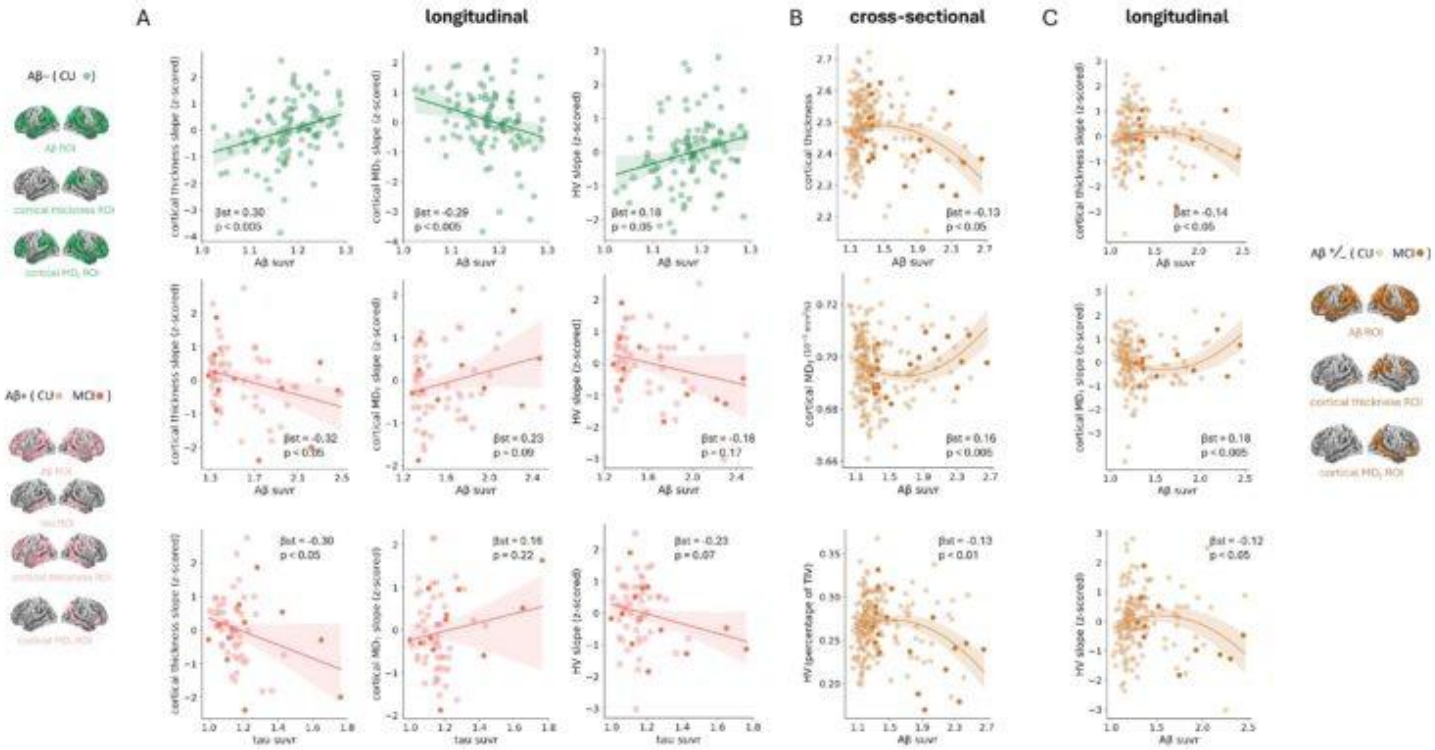


Figure 2. Univariate associations between AD pathology, structural measures, and their change in the PLS analyses derived regions. (A) Associations between Aβ and longitudinal changes in structural measures (cortical thickness, MD_T, and HV slopes) for the CU Aβ− group and Aβ+ (CU Aβ+ and MCI Aβ+). **(B)** Associations between pathological markers (Aβ and tau) and structural measures (cortical thickness, MD_T, and HV) for the entire cohort. **(C)** Associations between Aβ and longitudinal changes in structural measures (cortical thickness, MD_T, and HV slopes) for all participants. Each measure was averaged within the corresponding maps identified by PLS analyses (shown as the brain plots). In scatter plots for the Aβ+ group (combining CU Aβ+ and MCI Aβ+) and the whole cohort, darker dots indicate the MCI participants. Age, sex, APOE ε4 status were considered as covariates when performing statistical models. MD_T: free-water-corrected mean diffusivity; βst: standardized estimate β; PLS: partial least square.

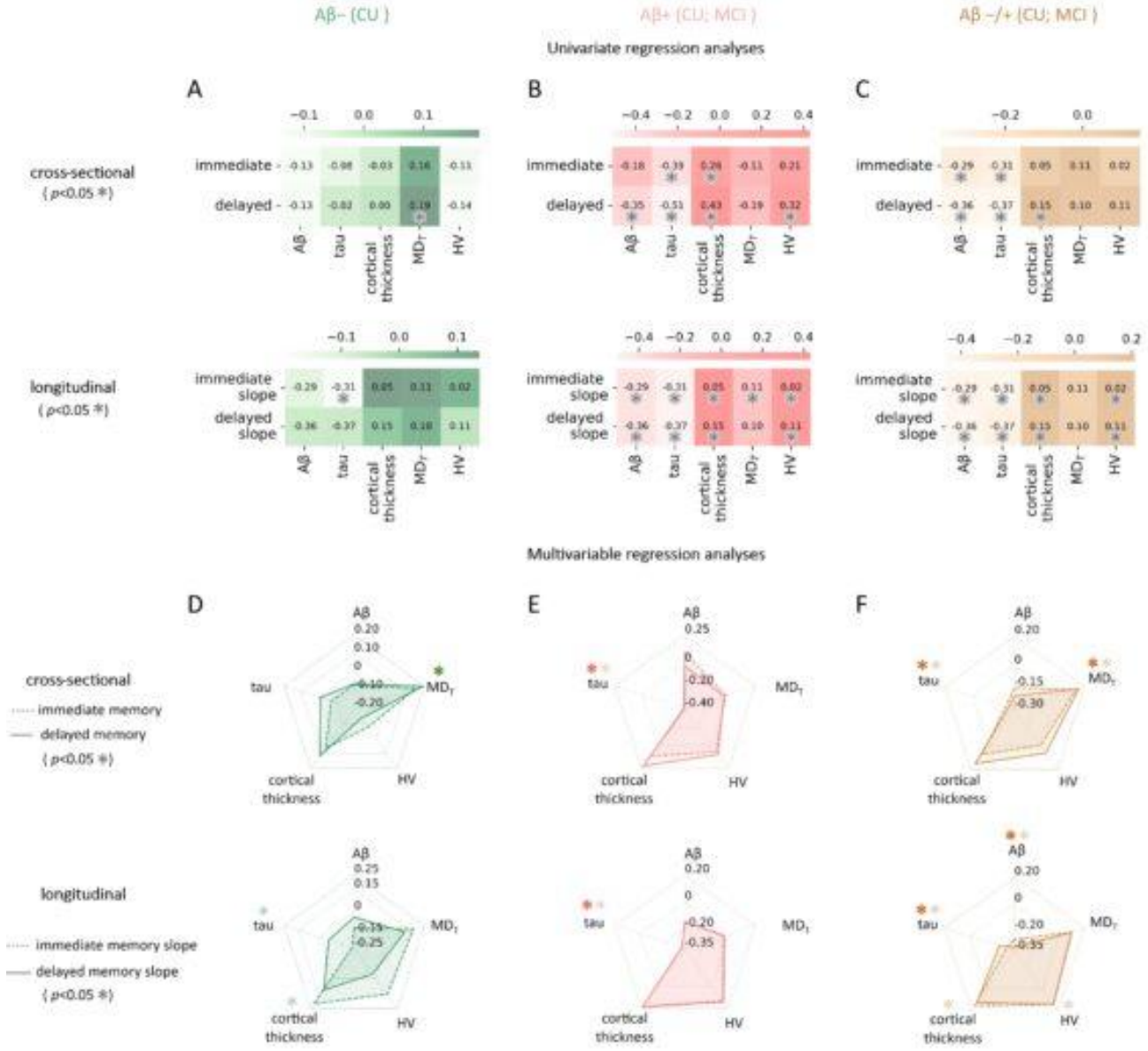


Figure 3. Univariate and multivariate regression analyses between pathological/structural measures and memory/memory change. Pathological and structural measures were averaged across significant regions identified in Fig 1B for each specific group. The univariate regression analyses, showing associations between brain biomarkers and memory performance, are displayed in **(A)**, **(B)**, and **(C)**, while multivariate regression analyses, illustrating associations between brain biomarkers and longitudinal changes in memory, are shown in **(D)**, **(E)**, and **(F)**. Specifically, **(A)** and **(D)** display the results for the CU Aβ− group; **(B)** and **(E)** present the results for the Aβ+ group (combined CU Aβ+ and MCI Aβ+); **(C)** and **(F)** display the results for the whole cohort. The heatmaps and spider plots depict the standardized beta coefficients (βst) for each predictor within the regression models. Significance is indicated by an asterisk (*), with $p < 0.05$. In panels **(D)**, **(E)**, and **(F)**, lighter asterisks indicate significant associations with immediate memory or its changes, while darker asterisks denote significance for delayed memory or its changes. Age, sex, APOE ε4 status were considered as covariates when performing statistical models. MD_T: free-water-corrected mean diffusivity; HV: hippocampal volume; βst: standardized estimate β.

Keywords: Aβ/tau, cortical thickness, cortical mean diffusivity, hippocampal volume

4 Astrogliosis, a potential non-Aβ pathway to tau

Victor L Villemagne[1], Ann D Cohen[1], Brian J Lopresti[2], Anum Saeed[4], Dana Tudorascu[1], Alexandra Gogola[2], Cristy Matan[2], Alexandria Reese[2], Beth E Snitz[3], Milos D Ikonomovic[3], Steven E Reis[4], Lenore Launer[5], Oscar L Lopez[3]

[1]*Department of Psychiatry, University of Pittsburgh, Pittsburgh, PA, US*
[2]*Department of Radiology, University of Pittsburgh, Pittsburgh, PA, US*
[3]*Department of Neurology, University of Pittsburgh, Pittsburgh, PA, US*
[4]*Heart and Vascular Institute, School of Medicine, University of Pittsburgh, Pittsburgh, PA, US*
[5]*Laboratory of Epidemiology & Population Sciences, National Institute of Aging, Bethesda, MD, US*

Background: In Alzheimer's disease (AD), widespread cortical Aβ deposition usually precedes PET-detectable cortical tau. A few PET imaging studies reported high cortical tau (T+) in ~2-15% of cases with low Aβ (A-) PET, but some of these individuals were deemed "false-negatives" when fluid biomarkers (plasma/CSF) ascertained the presence of amyloidosis.

Methods: Thirty-seven participants (27 cognitively unimpaired -CU- and 10 Mild Cognitive Impaired -MCI-; age 76.1±4.1 and 80.2±5.6 yo, respectively) enrolled in HeartSCORE Neuroimaging (a longitudinal study examining the effects of cardiovascular risk factors (CVRF) on AD pathology). CVRF were determined at baseline, 19±1 years before participants underwent detailed clinical/cognitive evaluations, 3T-MRI and PET for Aβ (^{11}C-PiB), tau (^{18}F-FTP) and astrogliosis (^{18}F-SMBT-1). Assessments were adjusted for age, sex, and Aβ burden.

Results: Seven of 22 (32%) A- CU and 4 of 7 (57%) A- MCI, were deemed T+ in the Meta-temporal region (Figure 1). Aβ burden in A-/T+ participants was low (1.14±0.03 and 1.19±1.1 SUVR for CU and MCI, respectively) and confirmed by plasma p-tau217 and/or $Aβ_{42/40}$ ratio. A-/T+ participants also presented significantly higher lateral temporal ^{18}F-SMBT-1 retention (p=0.016) (Figure 2), while no significant differences were found in CVRF or brain volumetrics across the A/T groups. There were significant correlations between ^{18}F-FTP and ^{18}F-SMBT-1 in lateral temporal (β=0.45; p=0.01), ventrolateral prefrontal (β=0.41; p=0.019), supramarginal (β=0.39; p=0.027), and lateral occipital (β=0.36; p=0.038) cortices (Figure 3). Most high cortical T+ cases (81%) were <10% above threshold, a potential explanation for the minimal impairment in this group (MMSE 29.4±0.4 and 28±2.6, for CU and MCI, respectively) at the time of assessment, with cognition mainly affected by two factors: cortical atrophy (β=0.44; p=0.009), and cortical tau (β=0.37; p=0.041). There were no significant effects of age, CVRF, Aβ, or astrogliosis on cognition.

Conclusion: In this cohort, ^{18}F-SMBT-1 astrogliosis was associated with an early, non-canonical/Aβ-independent tau deposition.

Figure 2. Temporal ^{18}F-SMBT-1 retention (SUVR) by A/T status

There was a significant higher ^{18}F-SMBT-1 retention (p=0.016) in the lateral temporal cortex in the A-T+ subgroup. This finding suggests a potential non-Aβ pathway to tau aggregation (*Chetelat, Nat Rev Neurol, 2013*) in this cohort.

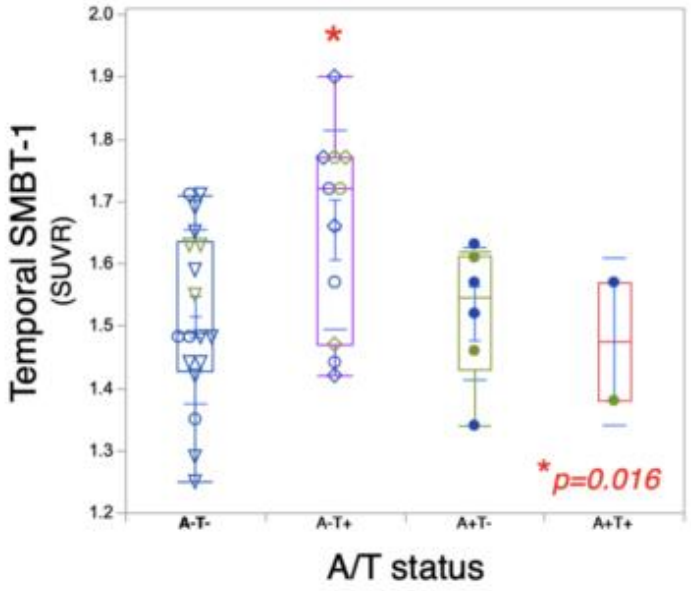
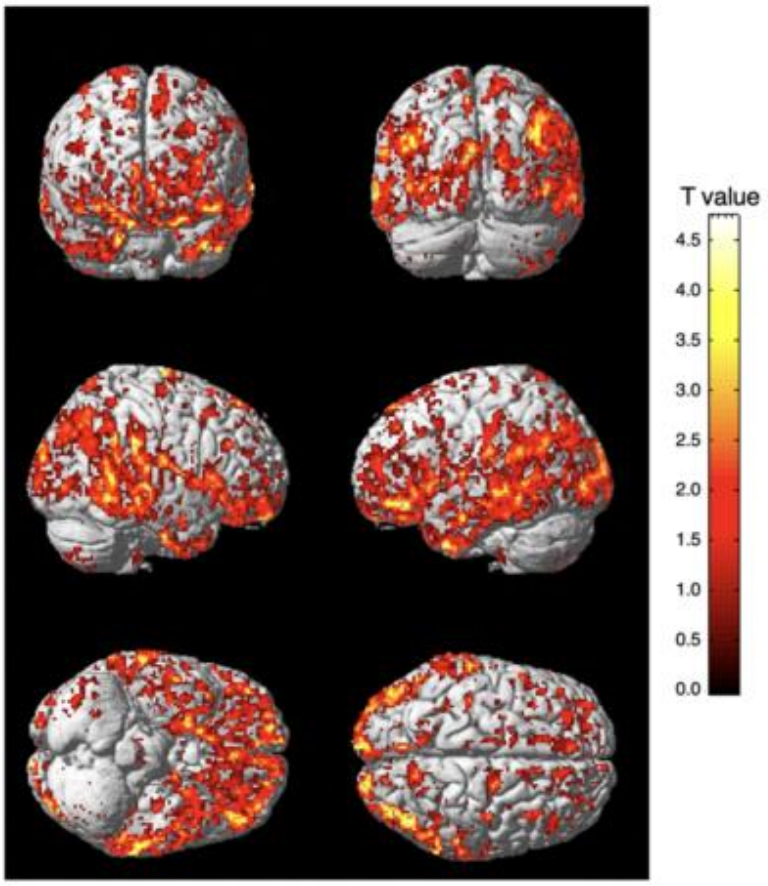


Figure 3. Regional associations between ^{18}F-SMBT-1 and ^{18}F-FTP retention. Voxelwise linear regression analyses, adjusted for age, sex and Aβ burden, showed significant regional associations ($p<0.05$) between ^{18}F-SMBT-1 and ^{18}F-FTP retention in the lateral temporal, ventrolateral prefrontal, supramarginal and lateral occipital cortices.



Keywords: Amyloid, tau, astrogliosis, cardiovascular risk factors

5 APOE ε4 carriers exhibit attenuated habituation in pupil size and practice effects on a repeated auditory oddball task

Jill A.E. Grube[1,2], Marina Rodríguez Alonso[3], Nina Engels-Domínguez[1,2,4], Heidi I.L. Jacobs[1,2,4], Joost M. Riphagen[1,2]

[1]*The Athinoula A. Martinos Center for Biomedical Imaging, Department of Radiology, Massachusetts General Hospital, Boston, MA, US*
[2]*Harvard Medical School, Boston, MA, US*
[3]*Baylor College of Medicine, Houston, TX, US*
[4]*Faculty of Health, Medicine and Life Sciences, School for Mental Health and Neuroscience, Alzheimer Centre Limburg, Maastricht University, Maastricht, NL*

Introduction: The locus coeruleus (LC), an area of early Alzheimer's disease (AD) pathology, plays a key role in regulating arousal and attention. We have previously shown that lower LC integrity is associated with attenuated practice effects in learning. Pupillometry has emerged as a reliable method for assessing LC function. Here, we compared *APOE* ε4 and non-ε4 carriers on changes in pupil dilation and reaction time during repeated exposure to an oddball task.

Methods: Older participants from the WALLe study (n=19, mean age: 67y (sd=4.70), 53% female, 32% *APOE* ε4-carrier) performed an auditory oddball task on day 1-5-10 of a two-week period (Fig. 1). Pupillometry data was simultaneously recorded with a EyeLink-1000. Habituation in pupillometry was defined as a decrease in peak height of pupil size and a faster time-to-peak pupil dilation after the target tone across visits. Practice effects in behavior was defined as faster reaction time across 3 timepoints. Linear mixed models tested pupil dilation peak height (DPH), time to peak pupil dilation (TTP), or reaction time over time (age and sex as covariates) within ε4 or non-ε4 carriers.

Results: Non-ε4 carriers showed a decrease in pupil DPH between Visit 1-5 (p=0.06) and Visit 1-10 (p=0.05), while ε4 carriers only exhibited a decreased pupil DPH between Visit 1-10 (p=0.05) (Fig. 2a). ε4 carriers showed no significant change in TTP, while non-ε4 carriers showed a decrease of their TTP between Visit 1-5 (p=0.01) and between Visit 1-10 (p=0.02; Fig. 2b). ε4-carriers showed no significant change in reaction times, while non-ε4 carriers displayed faster reaction times between Visit 1-5 (p=0.05; Fig. 3).

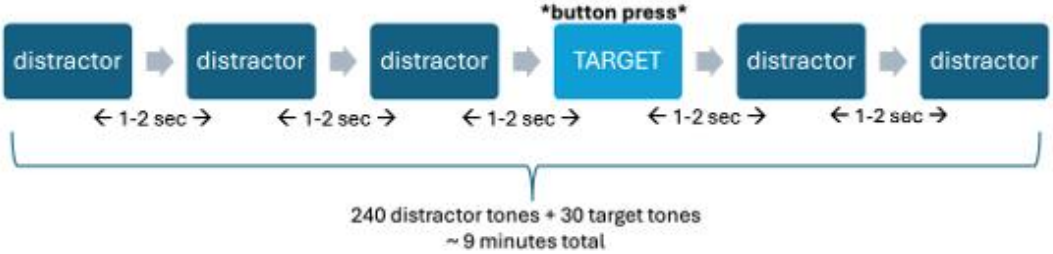
Conclusion: Individuals with the *APOE* ε4 allele exhibit decreased practice effects in performance and habituation in pupillometry during an oddball task. These findings can be important for early detection of cognitive decline in individuals at genetic risk for AD.

Figure 1:

1a. Visit breakdown



1b. Oddball paradigm



1c. Diagram of pupil measurement after target tone presentation

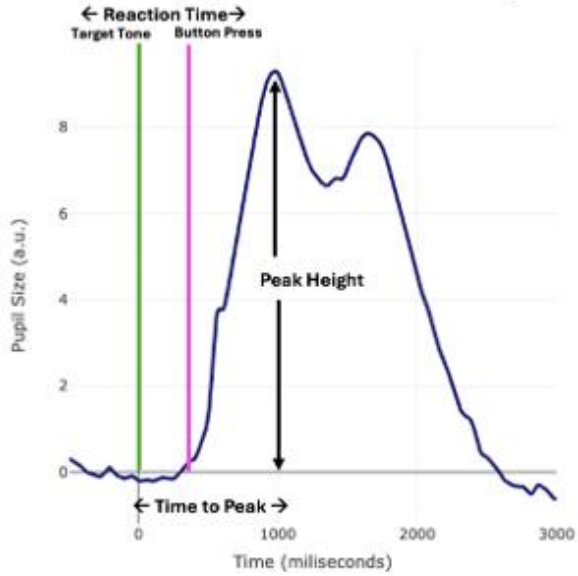
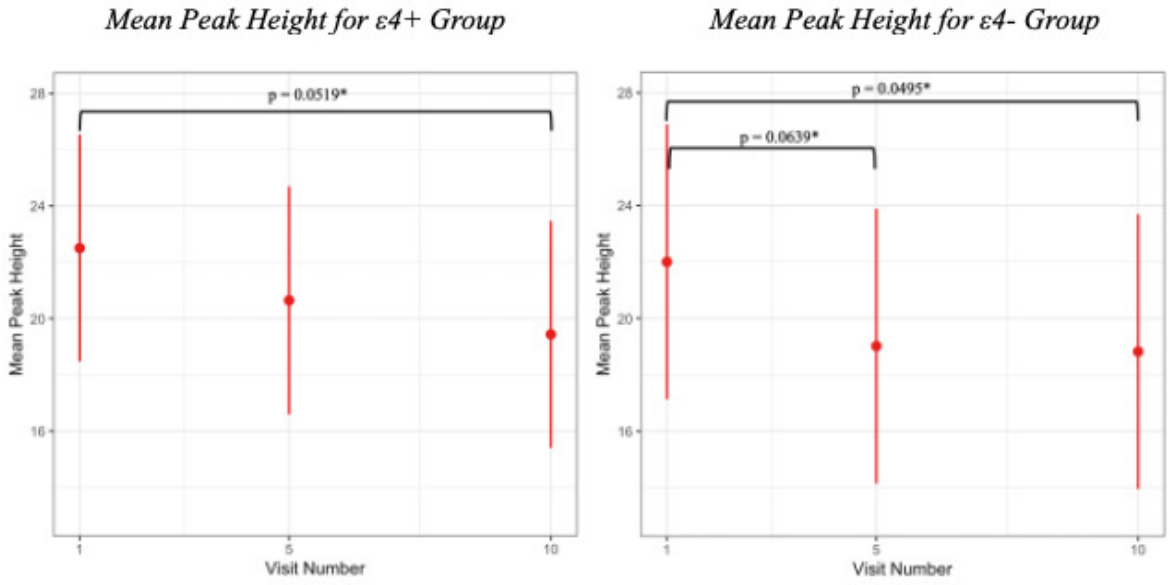


Figure 1. a: *The WALLe Study visit breakdown during the 2-week period.* b: *The auditory oddball task paradigm.* c: *A representative diagram illustrating the pupil measurement after target tone presentation, peak height, time-to-peak, and reaction time of an example participant during Visit 1.*

Figure 2:

2a. Mean peak height of pupil dilation after target tone across 3 visits



2b. Mean time to peak pupil dilation after target tone across 3 visits

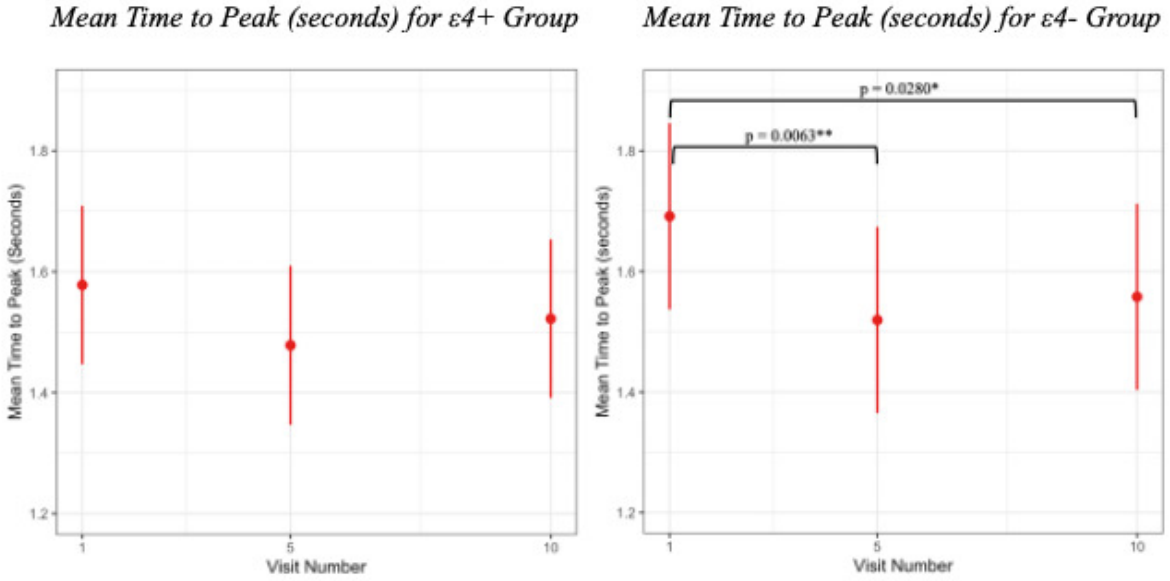


Figure 2. a: *The mean height of peak pupil dilation after target tone presentation across 3 timepoints for ε4 carriers (ε4+ group) and for non-e4 carriers (ε4- group).* b: *The time to peak pupil dilation after target tone presentation across 3 timepoints for ε4+ group and for ε4- group.*

Figure 3.

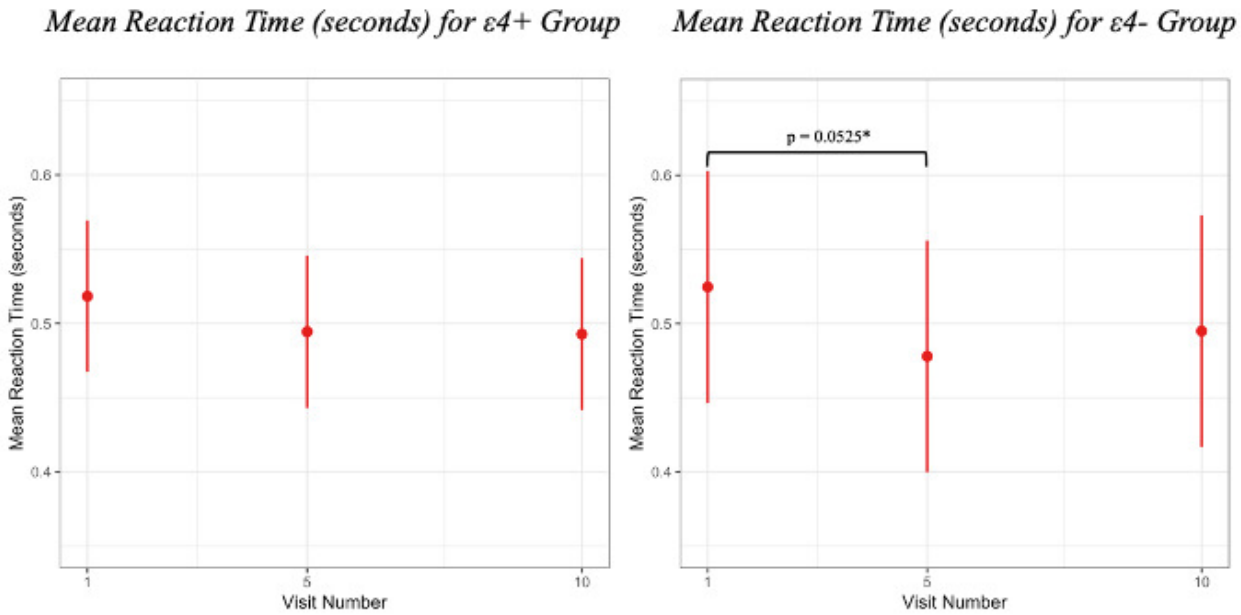


Figure 3. *The reaction time of participants' response after target tone presentation across 3 timepoints for ε4+ group and for ε4- group.*

Keywords: locus coeruleus, APOE, pupillometry, practice effects, habituation

6 Baseline tau burden and performance on a digital clock drawing test uniquely contributes to predicting future tau accumulation in preclinical AD

Jessie Fang-Lu Fu[1,2], Talia Robinson[2], Michelle Farrell[2], Roos Jutten[2], Emma Thibault[2], Marina Rodriguez Alonso[2], Jackson Thompson[2], Cristina Lois[2], Amal Tiss[2], Kuang Gong[2,3], Charles Chen[1,2], Dana Penney[4], Randall Davis[5], Reisa Sperling[2], Keith Johnson[2], Dorene Rentz[2], Julie Price[1,2]

[1]*Athinoula A. Martinos Center for Biomedical Imaging, Boston, MA, US*
[2]*Massachusetts General Hospital, Harvard Medical School, Boston, MA, US*
[3]*University of Florida, Gainesville, FL, US*
[4]*Lahey Hospital and Medical Center, Burlington, MA, US*
[5]*Massachusetts Institute of Technology, Cambridge, MA, US*

Background: Longitudinal [^{18}F]MK-6240 PET tracks tau accumulation across the AD continuum and evaluates anti-tau therapeutics. Identifying individuals likely to exhibit greater tau accumulation could improve screening efficiency. Current screening relies on Ab and tau PET and cognitive assessments (e.g., Preclinical Alzheimer's Cognitive Composite, PACC-5). We previously demonstrated association between higher baseline Ab and tau burden and worse baseline performance and accelerated decline on a 2-minute digital clock-drawing test (DCTclock™) in cognitively normal (CN) individuals. This study evaluates the extent to which baseline Ab and tau burden and DCTclock performance impact rates of subsequent tau accumulation.

Methods: Seventy-four CN individuals underwent DCTclock and PACC-5 cognitive assessments, baseline [^{11}C]PiB PET, and longitudinal [^{18}F]MK-6240 PET up to three years (**Table.1**). Global Ab and tau burden were estimated in neocortical aggregate and early-tau regions (rhinal, entorhinal, amygdala, inferior temporal cortex), respectively. Kernel-based within-reconstruction partial-volume-correction was applied to tau PET data. Linear mixed-effect models examined the impact of baseline Ab and DCTclock performance on subsequent tau accumulation, corrected for age, sex and education, with and without controlling for baseline tau burden.

Results: Higher baseline entorhinal and rhinal tau was significantly associated with higher Ab burden (β: 0.90-0.94, $p<0.001$) and lower PACC-5 scores (β: -0.10, $p<0.05$), but not DCTclock. Tau accumulation was greatest in rhinal and entorhinal (**Fig.1**). Higher baseline Ab burden and worse DCTclock, but not PACC-5, independently contributed to greater tau accumulation (**Fig.2A**). Baseline tau burden showed stronger association with subsequent tau accumulation than baseline Ab (**Fig.2B**), and moderated the association between baseline DCTclock (not PACC-5) and subsequent tau accumulation (**Fig.2C**).

Conclusion: Baseline [^{18}F]MK-6240 tau more strongly associated with subsequent tau accumulation than global Ab burden. DCTclock may offer unique predictive value for subsequent tau accumulation in addition to baseline tau burden, potentially enhancing early tau tracking and therapeutic response detection in preclinical AD.

Table 1. Demographics and imaging measures in 74 cognitively normal older adults.

	PiB+	PiB-
N	23	51
Age (years)	74.11 (7.93)	64.57 (10.2)
Sex	8 M / 15 F	26 M / 25 F
Education (years)	18.14 (2.47)	16.84 (2.27)
Cognitive Assessments		
PACC-5	-0.38 (0.72)	-0.15 (0.97)
Digital clock-drawing test (DCTclock)	66.92 (26.91)	78.16 (23.35)
PiB PET DVR		
PiB FLR	1.53 (0.19)	1.05 (0.04)
MK6240 PET SUVR (90-110 min)		
Rhinal	1.43 (0.54)	0.93 (0.27)
Entorhinal	1.41 (0.47)	0.94 (0.30)
Amygdala	0.95 (0.36)	0.60 (0.19)
Inferior Temporal	1.24 (0.46)	1.01 (0.13)
Precentral (late-tau, control region)	0.80 (0.11)	0.82 (0.13)
MK6240 PET SUVR (90-110 min) with Kernel PVC		
Rhinal	1.47 (0.58)	1.01 (0.26)
Entorhinal	1.46 (0.49)	0.99 (0.3)
Amygdala	0.96 (0.36)	0.61 (0.23)
Inferior Temporal	1.24 (0.46)	1.03 (0.14)
Precentral (late-tau, control region)	0.79 (0.10)	0.78 (0.13)
MK6240 PET time points		
Baseline	23	51
6-month follow-up	16	30
1-year follow-up	13	23
> 2-year follow-up	17	29

- Continuous values are expressed as mean (standard deviation).
- SUVR and DVR were estimated using cerebellar gray reference regions.
- PiB status was determined using PiB DVR threshold of 1.18.
- The rhinal cortex was defined using MRI between peri-allocortex and neocortex that corresponds to the transentorhinal cortex. The anterior and posterior bounds were the anterior collateral sulcus and the caudal end of the amygdala (posterior bound of FreeSurfer entorhinal cortex) [Sanchez, 2022, Sci Transl Med].
- **Abbreviations:** PACC5 = Preclinical Alzheimer's Cognitive Composite 5; DCT = digital clock drawing test summary scores (ranged between 0 to 100); PiB = [11C]Pittsburgh Compound B PET; FLR = Frontal, Lateral Temporal, and Retrosplenial cortical composite ; MK6240 = [18F]MK-6240 PET; SUVR = standardized uptake value ratio; DVR = distribution volume ratio (Logan); PVC = partial volume corrected using kernel method [Gong, 2018, IEEE Trans Med Imaging].

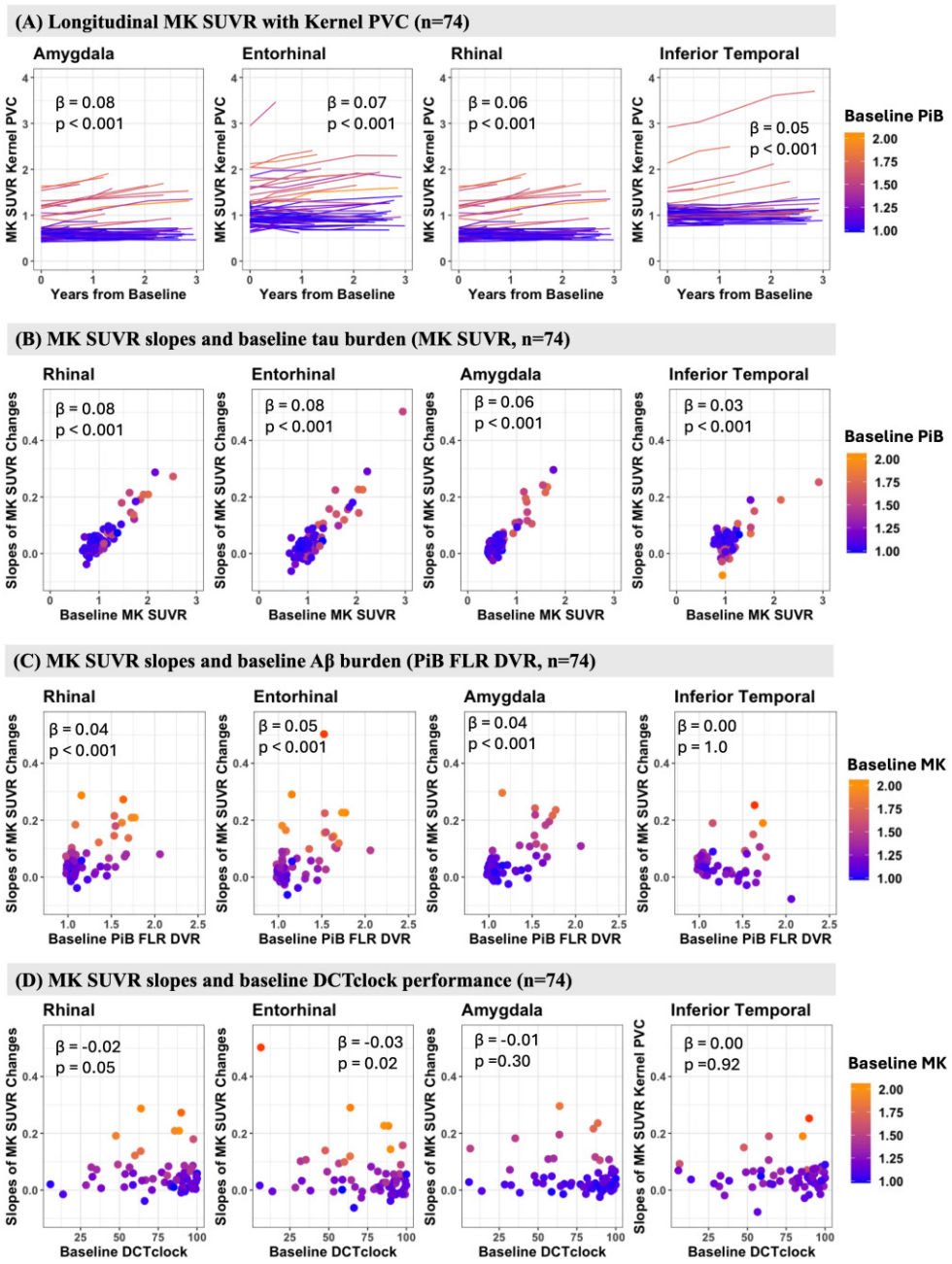


Figure 1. (A) Longitudinal MK SUVR and the association between slopes of MK SUVR changes (estimated using linear mixed-effect models) and (B) baseline tau burden, (C) baseline Aβ burden, and (D) baseline DCTclock performance in CN individuals. Significant increases in MK SUVR values were observed in all evaluated early-tau target regions, with the highest increases observed in the rhinal cortex, followed by the entorhinal cortex and amygdala, then the inferior temporal cortex. Higher baseline tau burden was significantly associated with greater tau accumulation (slopes of MK SUVR changes) in all early tau regions. Higher baseline global Aβ burden was significantly associated with greater tau accumulation in the rhinal, entorhinal and amygdala. Worse baseline DCTclock performance was significantly associated with greater tau accumulation in the entorhinal and rhinal.

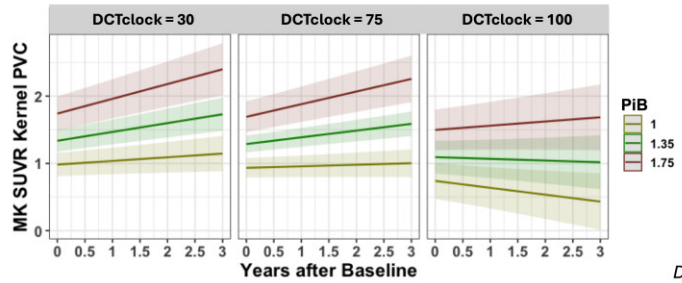
*Please note these associations did not take into account the interactions between tau and Aβ burden, between tau and DCTclock and between Aβ and DCTclock. Model results, including these interactions, are presented in Fig.2.

*Linear mixed effect model: longitudinal tau ~ β*time + age + education + sex, random = ~ 1+time|subject*
Linear mixed effect model regression coefficients and p-value for the Time term are displayed on each graph. The individualized slopes were calculated as: fixed effect of time (overall population slope) + random effect for each subject (intercept and slope for time).

Abbreviations: MK = [^{18}F]MK-6240; SUVR = standardized uptake value ratios, 90-110 min post-injection, using cerebellar gray reference region; PVC = partial volume correction using kernel method; CN = cognitively normal; PiB = [^{11}C]Pittsburgh Compound B; DVR = distribution volume ratios, Logan, using cerebellar gray reference region.

(A) Impact of baseline Aβ burden and baseline DCTclock performance on tau accumulation rates (n=74)

*longitudinal tau ~ β_1*time*Aβ + β_2*time*DCTclock + β_3*time*DCTclock*Aβ, random = ~ 1+time|subject*



Time x Aβ:
β_1 = 0.06, p < 0.001

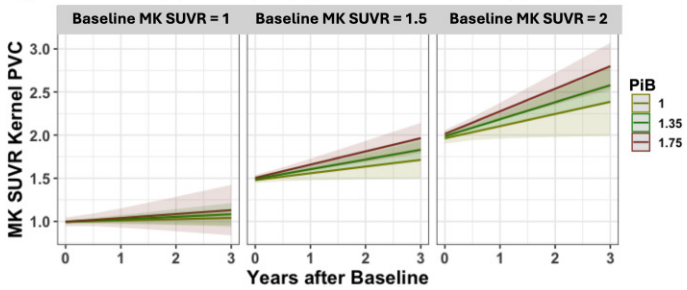
Time x DCTclock:
β_2 = -0.04, p = 0.004

Time x Aβ x DCTclock:
β_3: N.S.

DCTclock scores: 0 (worst) – 100 (best)

(B) Impact of baseline Aβ and baseline tau burden on tau accumulation rates (n=74)

*longitudinal tau ~ β_1*time*Aβ + β_2*time*baseline tau + β_3*time*Aβ*baseline tau, random = ~ 1+time|subject*



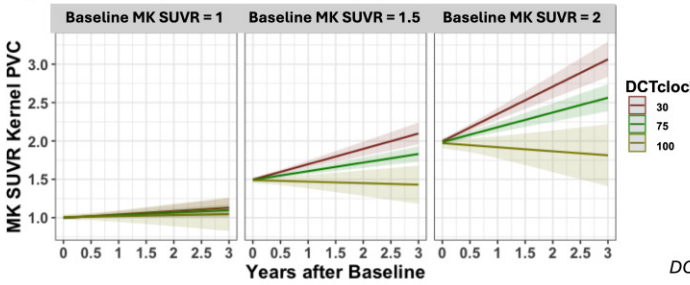
Time x Aβ:
β_1: N.S.

Time x baseline tau:
β_2 = 0.06, p < 0.001

Time x Aβ x baseline tau:
β_3: N.S.

(C) Impact of baseline DCTclock performance and baseline tau burden on tau accumulation rates (n=74)

*longitudinal tau ~ β_1*time*DCTclock + β_2*time*baseline tau + β_3*time*DCTclock*baseline tau, random = ~ 1+time|subject*



Time x DCTclock:
β_1: N.S.

Time x baseline tau:
β_2 = 0.08, p < 0.001

Time x DCTclock x baseline tau:
β_3 = -0.04, p < 0.001

DCTclock scores: 0 (worst) – 100 (best)

Figure 2. Impact of (A) baseline Aβ burden and DCTclock, (B) baseline Aβ and tau burden, and (C) baseline DCTclock and tau burden on future tau accumulation rates in the entorhinal cortex, estimated by linear mixed effect models. (A) Higher baseline Aβ burden and worse baseline DCTclock performance (lower DCTclock scores) independently contributed to greater tau accumulation in the entorhinal and rhinal cortex (not shown) over three years, without correcting for baseline tau burden. **(B)** Taking baseline tau burden into account, baseline Aβ burden no longer contributed to tau accumulation rates. **(C)** On the other hand, baseline tau burden moderated the associations between baseline DCTclock performance and tau accumulation rates, suggesting worse DCTclock performance contributed to greater tau accumulation rates in individuals with high baseline tau burden.

‡ The three colored lines displayed the marginal effects of linear mixed effect models for illustrative individuals. The shaded area represents the 95% confidence interval.
‡ Sample size for each illustrated group with similar ranges of baseline Aβ and tau burden and DCTclock performance:
baseline Aβ burden: PiB < 1.1: n=47; 1.1<PiB<1.6: n=17; PiB>1.6: n=10
baseline tau burden: MK < 1.1: n=46; 1.1<MK<1.6: n=18; MK>1.5: n=10
baseline DCTclock performance: DCT < 50: n=10; 50<DCT<85: n=32; DCT>90: n=24

Abbreviations: MK = [^{18}F]MK-6240; SUVR = standardized uptake value ratios; PVC = partial volume correction; CN = cognitively normal; PiB = [^{11}C]Pittsburgh Compound B; DCTclock = digital clock drawing test.

Keywords: Positron emission tomography, tau, digital clock drawing test, longitudinal analysis, Alzheimer's disease

7 Molecular correlates of apraxia in Alzheimer's disease: A PET imaging study

Gerard Bischof[1,2], Elena Jaeger[1,2], Kathrin Giehl[1,2], Frank jessen[3,4], Oezguer Onur[5,6], Sid O'Bryant[7,8], Esra Kara[3], Peter Weiss[6], Alexander Drzezga[1,2]

[1]*University of Cologne, University Hospital of Cologne, Department of Nuclear Medicine, Multimodal Neuroimaging Group, Cologne, Germany, Cologne, DE*
[2]*Research Center Juelich, Institute for Neuroscience and Medicine II, Molecular Organization of the Brain, Juelich, Germany, Juelich, DE*
[3]*University of Cologne, University Hospital of Cologne, Department of Psychiatry, Cologne, Germany, Cologne, DE*
[4]*German Center for Neurodegenerative Diseases, Bonn/Cologne, Germany, Cologne, DE*
[5]*University of Cologne, University Hospital of Cologne, Department of Neurology, Cologne, Germany, Cologne, DE*
[6]*Research Center Juelich, Institute for Neuroscience and Medicine III, Cognitive Neuroscience, Juelich, Germany, Juelich, DE*
[7]*Institute for Translational Research University of North Texas Health Science Center Fort Worth Texas USA., Fort Worth, TX, US*
[8]*Department of Family Medicine, Texas College of Osteopathic Medicine, University of North Texas Health Science Center, Fort Worth, Texas USA, Fort Worth, TX, US*

Apraxia is a prominent symptom of Alzheimer's disease (AD), yet the mechanisms driving this behavioral trait remain poorly understood. In this study, we aimed to systematically investigate apraxia profiles in AD patients and explore potential links to tau pathology using the second-generation tau PET tracer [18F]PI-2620. We hypothesized that distinct patterns of tau deposition in the brain might underlie the apraxic deficits observed in AD.

We recruited a cohort of 32 patients with confirmed AD and a control group of 41 cognitively unimpaired individuals (CU1). Apraxia was assessed in all participants using the Dementia Apraxia Screening Test (DATE) and the Cologne Apraxia Screening (KAS). AD patients also underwent PET imaging with [18F]PI-2620 to map tau pathology. To further examine the relationship between apraxia and tau deposition, we compared the PET data from AD patients with a separate group of 54 amyloid-negative, cognitively unimpaired individuals (CU2). Z-score deviation maps were generated, and voxel-based multiple regression analysis was performed.

Our findings revealed significant clusters of tau accumulation in regions associated with apraxia, including the angular gyrus, as well as temporal, parietal, and lateral occipital cortical areas. These areas correlated strongly with apraxia severity and were consistent across both apraxia assessment tools. In contrast, no significant correlations were found between tau uptake in primary motor or subcortical brain regions and apraxia.

These results suggest that tau deposition in specific cortical regions may lead to localized neuronal dysfunction, which in turn results in apraxic impairments in a dose-dependent manner. This study offers new insights into the relationship between tau pathology and the manifestation of apraxia in AD, advancing our understanding of the neural mechanisms underlying this complex symptom.

Keywords: Apraxia, 18F-PI2620, Alzheimer's Disease, Tau

8 Understanding the impact of race on white matter hyperintensities in Alzheimer's disease: Findings from the ADNI Study

Victor Ekuta[1], Jordan Ahn[2], Yorghos Tripodis[2], Roy Hamilton[3]

[1]*Morehouse School of Medicine, Atlanta, GA, US*
[2]*Boston University School of Public Health, Boston, MA, US*
[3]*Perelman School of Medicine at the University of Pennsylvania, Philadelphia, PA, US*

Background: White matter hyperintensities (WMH) are markers of small vessel disease associated with cognitive decline and Alzheimer's disease (AD). African Americans (AAs) are disproportionately affected by cerebrovascular risk factors, but their representation in WMH research remains limited.

Objective: This study examined the relationship between race, cognitive status, and WMH burden among African American (AA) and non-Hispanic White (NHW) participants, aiming to identify potential racial differences in WMH burden.

Methods: Data from the Alzheimer's Disease Neuroimaging Initiative (ADNI) were analyzed, including 1,649 participants: 682 cognitively normal (CN), 584 with mild cognitive impairment (MCI), and 383 with AD. Of these, 124 participants (7.5%) were African American: CN (70, 10.26%), MCI (39, 6.68%), and AD (15, 3.92%). Linear mixed effects models were employed to assess the influence of race, cognitive status, and demographic factors on total WMH burden.

Results: Preliminary analyses revealed that factors such as time since MRI, age, intracranial volume, and MRI acquisition type significantly predicted total WMH across cognitive states. Time since the first MRI scan, age, and intracranial volume were positively correlated with increased total WMH volume, with the strongest associations seen in the dementia subgroup. MRI acquisition type (FLAIR) was negatively associated with WMH, suggesting that newer MRI techniques are more sensitive in detecting WMH. Higher education levels were associated with decreased WMH burden, indicating a potential protective effect. However, after controlling for other factors, race did not independently predict WMH burden.

Conclusion: These findings suggest that while race was not an independent predictor of WMH burden, other demographic and clinical factors such as age, education, and MRI methods significantly influenced WMH volumes. Further research is needed to explore protective factors against WMH accumulation, particularly in racially diverse populations.

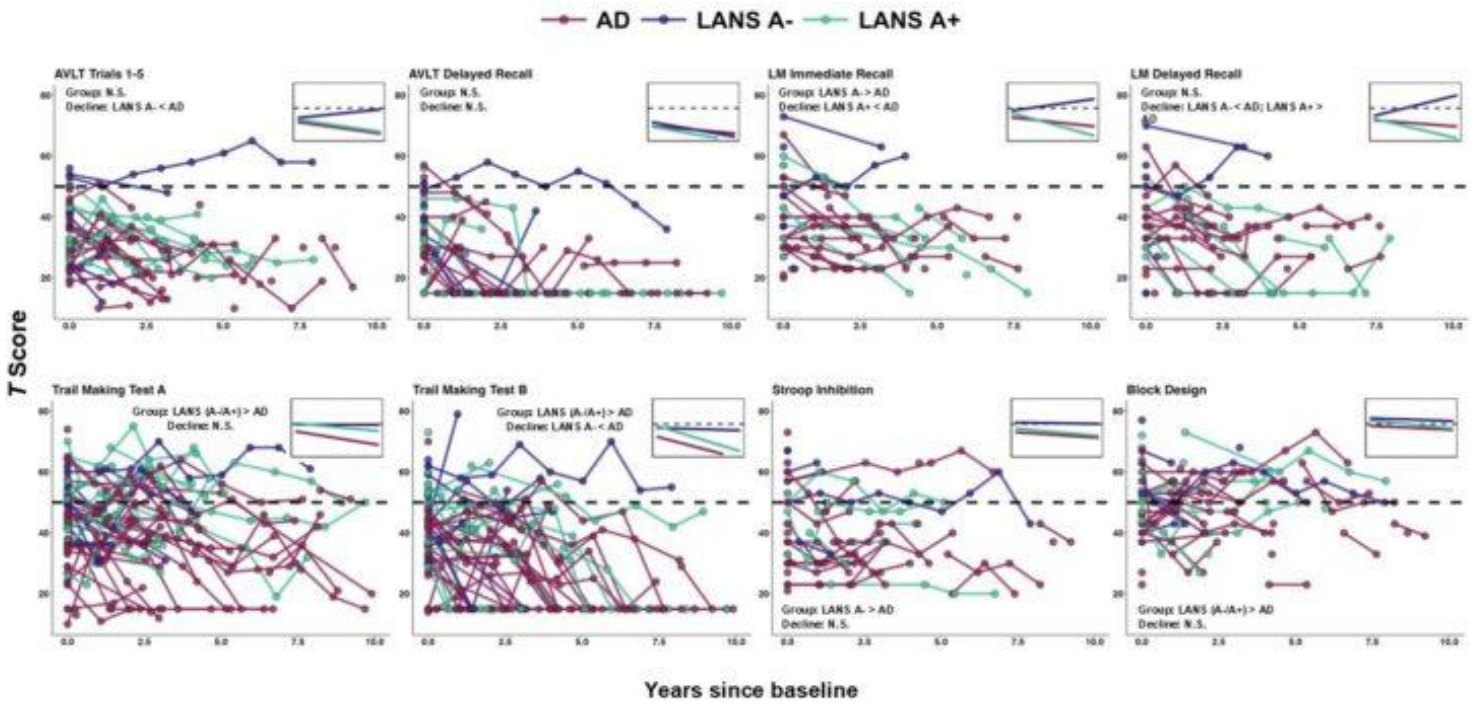
Keywords: White matter hyperintensities, race, Alzheimer's disease, cognitive status, cerebrovascular risk factors

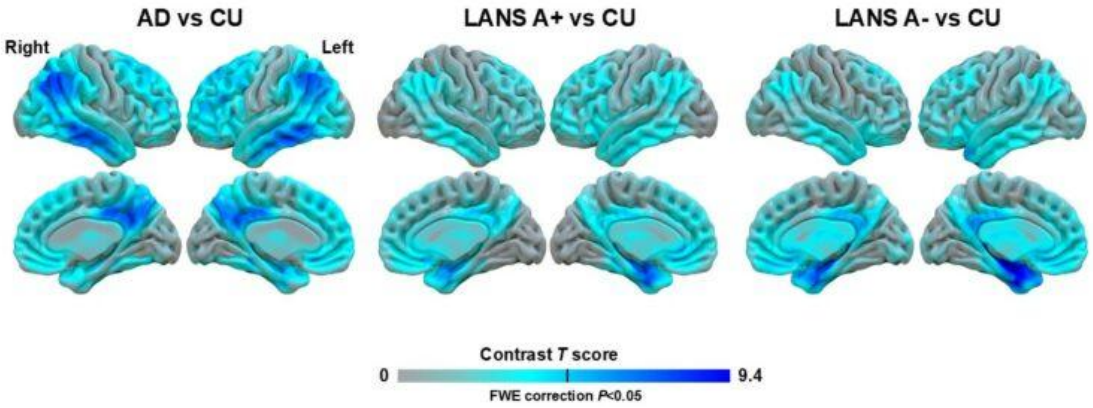
9 Characterization of a limbic-predominant amnestic neurodegenerative syndrome

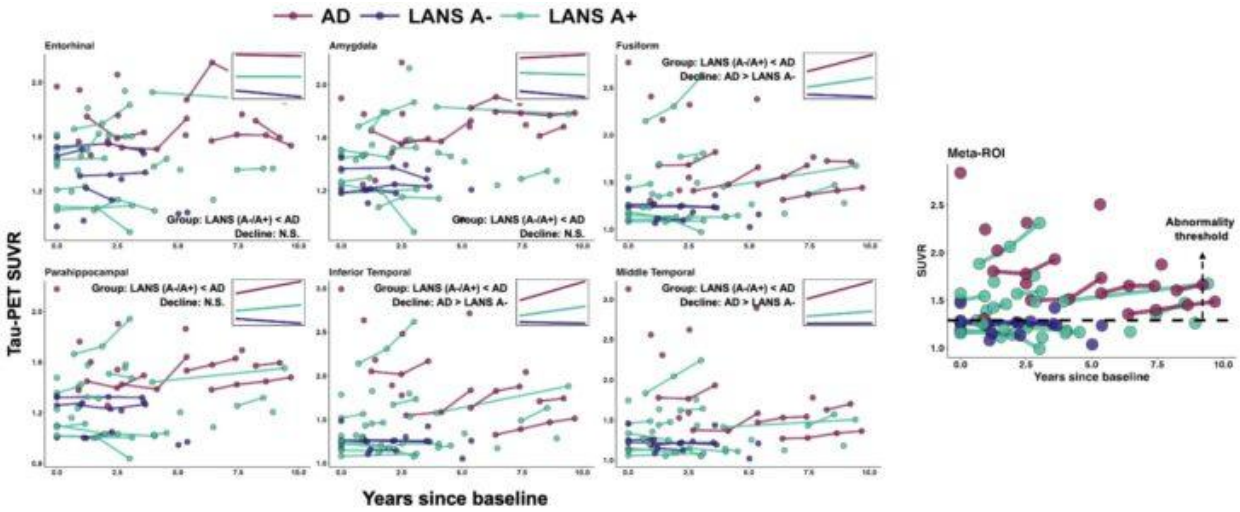
Nick Corriveau-Lecavalier[1,2], Anne Waniger[1], Nikki Stricker[1], Mary Machulda[1], Julie Fields[1], Hugo Botha[2], Jonathan Graff-Radford[2], Vijay Ramanan[2], Stuart McCarter[2], Aivi Nguyen[3], R. Ross Reichard[3], Bradley Boeve[2], David Knopman[2], Val Lowe[4], Dennis Dickson[5], Melissa Murray[5], Neill Graff-Radford[6], Ronald Petersen[2], Clifford Jack[4], David Jones[2]

[1]*Department of Psychiatry and Psychology, Mayo Clinic, Rochester, MN, US*
[2]*Department of Neurology, Mayo Clinic, Rochester, MN, US*
[3]*Department of Laboratory Medicine and Pathology, Mayo Clinic, Rochester, MN, US*
[4]*Department of Radiology, Mayo Clinic, Rochester, MN, US*
[5]*Department of Neuroscience, Mayo Clinic, Jacksonville, FL, US*
[6]*Department of Neurology, Mayo Clinic, Jacksonville, FL, US*

We recently proposed criteria for a limbic-predominant amnestic neurodegenerative syndrome (LANS). LANS presents at old age with a mild, memory-dominant course, and localizes to the limbic system. A detailed characterization of LANS is needed to guide clinical care and research efforts. Additionally, it remains unclear whether individuals with LANS and positive Alzheimer's disease (AD) biomarkers experience worse outcomes. We compared longitudinal neuropsychological and multimodal imaging (FDG-PET, tau-PET) data between individuals with LANS (n = 56; amyloid-positive n = 33, amyloid-negative n = 17) and cases of autopsy-proven AD neuropathologic change (ADNC) without limbic-predominant age-related TDP-43 encephalopathy (LATE) that had an antemortem history of Alzheimer's-type dementia (referred to as AD; n = 42). Measures of immediate recall were less impaired in LANS compared to AD, while delayed recall was equally impaired in both. Dichotomizing LANS according to amyloid status revealed a steeper decline in story memory in amyloid-positive LANS than AD. Executive functions and visuospatial processing were less impaired in LANS compared to AD, regardless of amyloid status (Fig.1). LANS individuals were selectively impaired on a measure of salient semantic knowledge, which included questions about World War II and 9/11/2001 (administered at baseline only). FDG-PET revealed greater medial temporal lobe hypometabolism and less neocortical hypometabolism in LANS compared to AD, irrespective of amyloid status (Fig.2). Tau-PET findings showed higher regional uptake in AD compared to LANS, regardless of amyloid status, although tau-PET positivity was heterogeneously distributed within amyloid-positive LANS (Fig.3). LANS is characterized by memory deficits and loss of knowledge about salient events, with these impairments associated with limbic degeneration. Amyloid status was associated with a steeper decline of story memory in LANS compared to AD, although non-memory domains remained relatively spared, regardless of amyloid status. This emphasizes the role of a functional anatomic classification to predict outcomes in degenerative syndromes.







Keywords: Limbic-predominant amnestic neurodegenerative syndrome, Alzheimer's disease, Neuropsychology, Neuroimaging, Neurology

10 Positron emission tomography analysis with the dynamicpet Python package

Murat Bilgel[1], Sabri Amer[2], Jonghyun Bae[3], Mustapha Bouhrara[3], Zhaoyuan Gong[3], Alex Guo[3], Johnny Uriarte-Lopez[2], Kavita Singh[1], Granville J. Matheson[4,5,6,7], Martin Nørgaard[8,9]

[1]*Laboratory of Behavioral Neuroscience, National Institute on Aging, Baltimore, MD, US*
[2]*Center for Alzheimer's and Related Dementias, National Institute on Aging, Bethesda, MD, US*
[3]*Magnetic Resonance Physics of Aging and Dementia, Laboratory of Clinical Investigation, National Institute on Aging, Baltimore, MD, US*
[4]*Department of Biostatistics, Columbia University Mailman School of Public Health, New York, NY, US*
[5]*Department of Psychiatry, Columbia University, New York, NY, US*
[6]*Molecular Imaging and Neuropathology Division, New York State Psychiatric Institute, New York, NY, US*
[7]*Department of Clinical Neuroscience, Center for Psychiatry Research, Karolinska Institutet and Stockholm County Council, Stockholm, SE*
[8]*Department of Computer Science, University of Copenhagen, Copenhagen, DK*
[9]*Molecular Imaging Branch, National Institute of Mental Health, Bethesda, MD, US*

The Positron Emission Tomography-Brain Imaging Data Structure (PET-BIDS) (Nørgaard et al. 2022) provides a standardized file naming and directory organization structure for PET datasets, facilitating scientific reproducibility and data sharing. It is being extended via the BIDS Extension Proposal 23: PET Preprocessing Derivatives to establish conventions for image analysis outputs. There is a need for user-friendly PET analysis tools that can integrate with PET-BIDS datasets. We present *dynamicpet*, a free and open-source Python package that provides functions for 4-D PET analysis, including extraction of regional time activity curves (TACs), denoising, kinetic modeling, and concatenation of interrupted acquisitions.

We demonstrate the functionality of *dynamicpet* on a ^{11}C-Pittsburgh compound B (PiB) amyloid PET scan acquired over 70 mins from the Baltimore Longitudinal Study of Aging. Figure 1 illustrates the Python API for loading in a 4-D image and calculating its frame duration-weighted temporal mean. The two denoising algorithms provided in *dynamicpet*, HYPR-LR (Christian et al. 2010) and NESMA (Bouhrara et al. 2018), are illustrated in Figure 2. *dynamicpet* implements several reference region-based models for estimating biological parameters of interest: standardized uptake value ratio (SUVR), the Logan reference tissue model (LRTM) (Logan et al. 1996), and several simplified reference tissue model (SRTM) variants (Figure 3). *dynamicpet* also includes utility functions such as concatenating interrupted acquisitions by accounting for decay correction differences. Code is available at https://github.com/bilgelm/dynamicpet.

dynamicpet adds to the growing list of PET analysis software developed to work with PET-BIDS data, such as *PET2BIDS* (Galassi et al. 2024), *petdeface* (https://github.com/openneuropet/petdeface), *kinfitr* (Matheson 2019), *bloodstream* (https://github.com/mathesong/bloodstream), and *petprep* (https://github.com/mnoergaard/petprep_hmc). Its simple framework facilitates the implementation of additional kinetic models. Future work will expand the collection of kinetic models and implement quality control checks for the inputs and outputs of kinetic models.

```python
from dynamicpet.petbids import petbidsimage

pet = petbidsimage.load(pet_fname)

pet_mean_over_time = pet.dynamic_mean(weight_by='frame_duration')
```

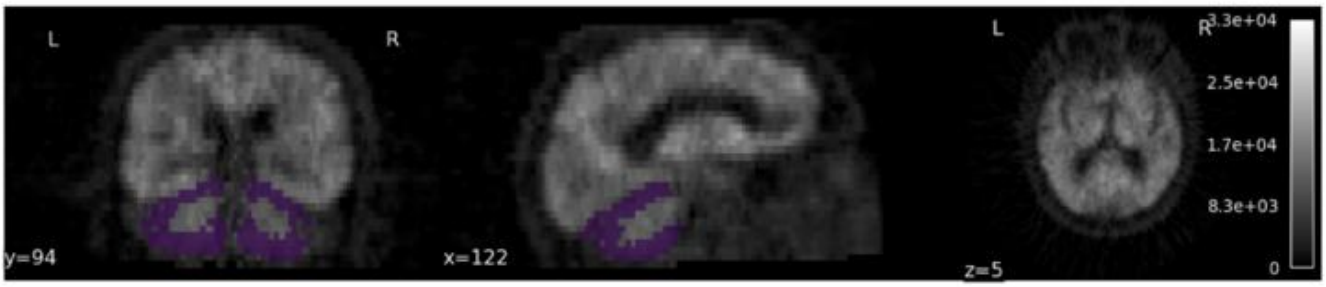


Figure 1: Mean PET with cerebellar gray matter mask overlay in purple.

```python
from dynamicpet.denoise.hypr import hypr_lr
from dynamicpet.denoise.nesma import nesma_semiadaptive as nesma

pet_hypr = hypr_lr(pet, fwhm=5)
pet_nesma, _ = nesma(pet, mask=brainmask, window_half_size=(5, 5, 5), thresh=0.2)

reftac_vx = pet.timeseries_in_mask(mask=refreg.get_fdata())

reftac = pet.mean_timeseries_in_mask(mask=refreg.get_fdata())
```

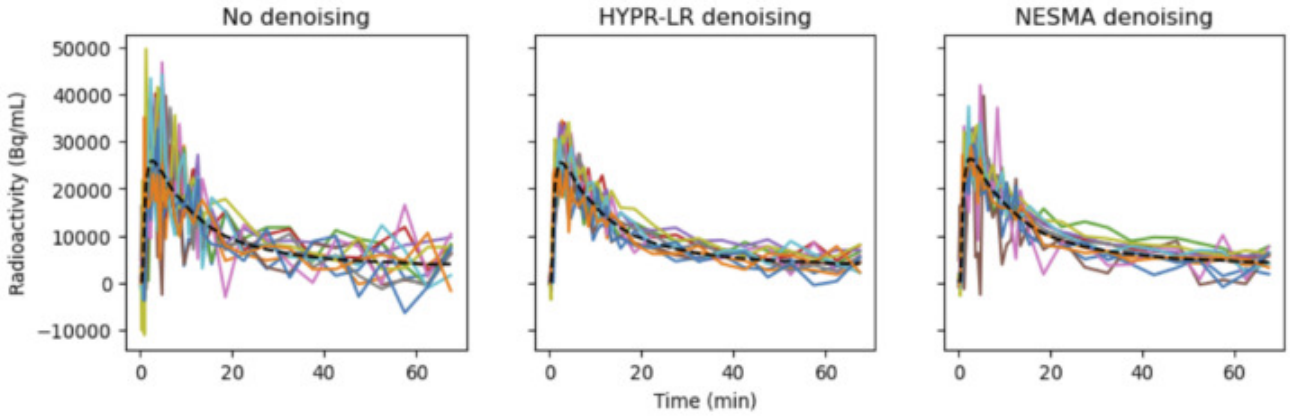


Figure 2: Time activity curves (TACs) for randomly sampled voxels in the cerebellar gray matter, calculated in the absence of denoising (left), after denoising with highly constrained backprojection method constraining the backprojections to local regions of interest (HYPR-LR) (center), and nonlocal estimation of multispectral magnitudes (NESMA) (right). Mean TAC within cerebellar gray matter is indicated by the black dashed curve.

```python
from dynamicpet.kineticmodel.srtm import SRTMZhou2003

srtm_calculator = SRTMZhou2003(reftac, pet)
srtm_calculator.fit(fwhm=5)
dvr_srtm = srtm_calculator.get_parameter('DVR')
r1_lrsc_srtm = srtm_calculator.get_parameter('R1LRSC')
```

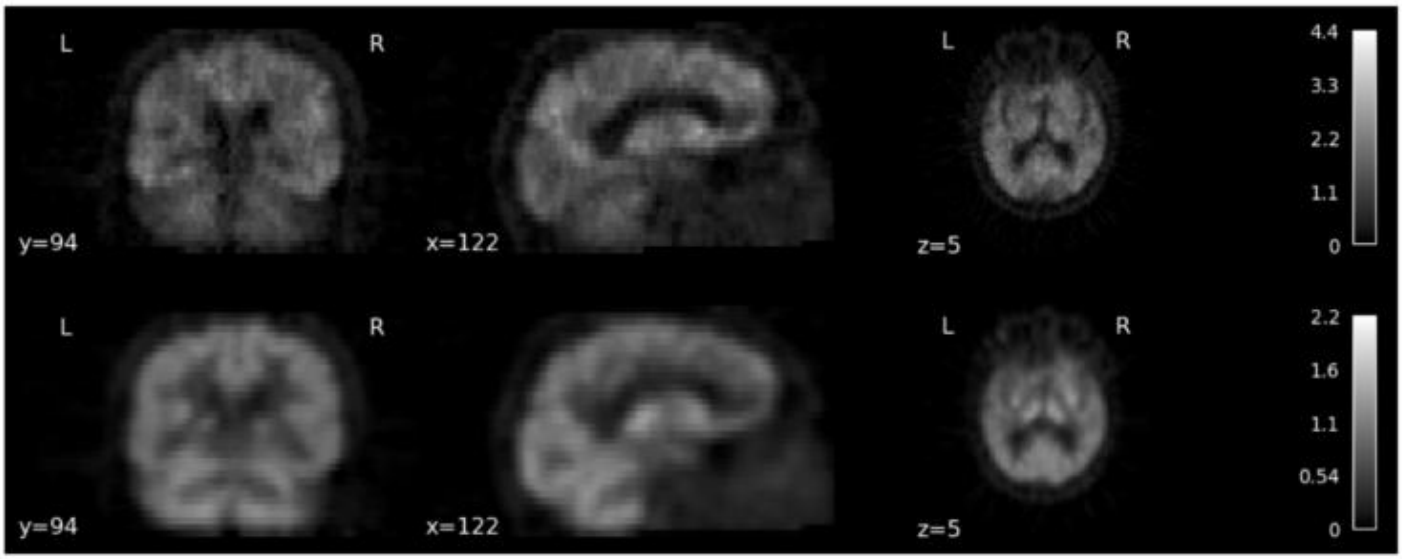


Figure 3: DVR (top) and R_1 (bottom) images calculated using SRTM-LRSC (Zhou et al. 2003).

Keywords: Python, denoising, kinetic modeling, BIDS

11 Targeted plasma eQTL and pQTL to identify potential novel biomarker for Alzheimer's disease in African Americans

Vanessa M. Colón-Badillo[1], Joseph S. Reddy[2], Jiangli Jin[1], Sarah J. Lincoln[1], Charlotte C. G. Ho[1], Julia E. Crook[2], Xue Wang[2], Kimberly G. Malphrus[1], Thuy Nguyen[1], Jean Marrero-Polanco[1], Nikoleta Tamvaka[1], John A. Lucas[3], Neill R. Graff-Radford[3], Nilüfer Ertekin-Taner[1,3], Minerva M. Carrasquillo[1]

[1]*Mayo Clinic, Department of Neuroscience, Jacksonville, FL, US*
[2]*Mayo Clinic, Department of Quantitative Health Sciences, Jacksonville, FL, US*
[3]*Mayo Clinic, Department of Neurology, Jacksonville, FL, US*

Given the overlap of symptoms between Alzheimer's disease (AD) and other dementias, it is essential to develop widely accessible biomarkers that will ensure an accurate diagnosis to enable its proper treatment. African Americans (AA) are 2x more likely to develop AD than non-Hispanic whites, and yet they remain underrepresented in AD research. The few studies conducted in AA suggest that there are different factors that influence AD in this population; therefore, it is possible that different biomarkers and/or therapies may be needed to effectively treat AD in AA. In this study, we aimed to determine if genetic variants that show association in AA with AD-risk, plasma transcript and/or protein levels, may serve as accurate and accessible AD biomarkers.

In 189 clinically-diagnosed AA AD cases and 183 AA cognitively unimpaired (CU) controls, we performed targeted DNA sequencing of 10 AD-associated loci. Genetic variants were tested for association with plasma transcripts and total tau protein levels previously measured in this cohort using a nanoString custom panel and Simoa assays, respectively. In receiver operating characteristic (ROC) analyses, the most significant e/pQTLs were added sequentially to a base model that included only age and sex to identify e/pQTL that improved the accuracy to correctly classify AD cases vs. CU.

Of the 5,112 variants identified in the targeted sequencing, 70 were nominally associated with plasma transcript/protein levels and with AD-risk. ROC analysis of age, sex, e/pQTL in *APOE*, *SORL1*, *TLR4*, *EPHA1*, *ABCA7*, *CLU*, and *CR1*, and plasma levels of *APP*, *ABCA7*, *AKAP9*, *CD14*, *CLU*, *and APOE*-ε4 dosage achieved 88.2% area under the curve to discriminate AD vs. CU, a 30.4% improvement over a model that only included age and sex.

Plasma transcript levels and e/pQTLs are promising diagnostic biomarkers for AD that may improve accessibility and reduce costs for a more accurate diagnosis of AD.

Keywords: blood biomarkers, eQTL, pQTL, African Americans, Alzheimer's disease

12 Pathological and clinical trajectories of preclinical Alzheimer's disease patients with divergent cortical tau patterns

Christina Young[1], Mackenzie Carlson[1], Karly Cody[1], Joseph Winer[1], Aaron Schultz[2], Elizabeth Mormino[1]

[1]*Department of Neurology and Neurological Sciences, Stanford University School of Medicine, Stanford, CA, US*
[2]*Department of Neurology, Massachusetts General Hospital, Boston, MA, US*

Background: We previously demonstrated that approximately 9% of cognitively unimpaired (CU) older adults with elevated β-amyloid (A+) exhibit more than expected cortical than medial temporal lobe (MTL) tau and/or having high cortical tau asymmetry (A+$T_{Cortical}$+).

Objective: To characterize longitudinal tau patterns and clinical trajectories of A+$T_{Cortical}$+ and determine whether trajectories differ from those with elevated medial temporal lobe tau (A+T_{MTL}+).

Methods: 18F-flortaucipir tau PET and clinical data spanning up to 8 years [mean (SD) = 4.68 (1.59) years] were examined in 393 CU participants enrolled in A4/LEARN (**Table 1**). Participants were determined to be in A-T_{MTL}- (n=47), A-T_{MTL}+ (n=1), A+T_{MTL}- (n=211), A+T_{MTL}+ (n=100), and A+$T_{Cortical}$+ (n=34) groups based on baseline amyloid and tau PET scans. We examined change in tau PET SUVR and asymmetry, as well as clinical trajectories were compared across groups using linear mixed effects models.

Results: A+$T_{Cortical}$+ participants accumulated tau in cortical regions that already showed relatively high SUVRs at baseline. Participants with asymmetrical tau at baseline accumulated tau in the corresponding region in the opposite hemisphere in addition to new regions in the original hemisphere (**Figure 1, 2A**). MTL SUVRs increased at comparable rates for the A+$T_{Cortical}$+ group compared to other A+ groups, but SUVRs in all cortical regions increased significantly faster in the A+$T_{Cortical}$+ group (**Figure 2B, 2C**). The A+$T_{Cortical}$+ group showed faster cognitive and functional decline (**Figure 2D, 2E**). Results were consistent when further accounting for baseline global tau and baseline amyloid, further indicating that findings were not driven by overall high levels of baseline pathology.

Conclusion: A+ CU with divergent cortical tau patterns are an especially high-risk subgroup. These participants continue to accumulate cortical tau at a faster rate than other preclinical AD subgroups and are at increased risk for faster cognitive and functional decline.

Table 1. Demographic characteristics of A4/LEARN participants with longitudinal tau PET data.

	CU A-T(MTL)- (N=47)	CU A-T(MTL)+ (N=1)	CU A+T(MTL)- (N=211)	CU A+T(MTL)+ (N=100)	CU A+T(Cortical)+ (N=34)	Overall (N=393)
Age at Baseline						
Mean (SD)	69.5 (4.46)	72.6 (NA)	71.6 (4.75)	73.1 (4.65)	71.2 (4.44)	71.7 (4.76)
Median [Min, Max]	68.0 [65.1, 84.5]	72.6 [72.6, 72.6]	71.3 [65.0, 85.3]	72.5 [65.0, 85.5]	70.0 [65.1, 82.3]	71.2 [65.0, 85.5]
Sex						
Male	19 (40.4%)	1 (100%)	96 (45.5%)	44 (44.0%)	10 (29.4%)	170 (43.3%)
Female	28 (59.6%)	0 (0%)	115 (54.5%)	56 (56.0%)	24 (70.6%)	223 (56.7%)
Education						
Mean (SD)	16.4 (2.53)	19.0 (NA)	16.2 (3.03)	16.1 (2.44)	16.5 (2.55)	16.2 (2.79)
Median [Min, Max]	16.0 [12.0, 20.0]	19.0 [19.0, 19.0]	16.0 [9.00, 30.0]	16.0 [11.0, 22.0]	16.5 [12.0, 21.0]	16.0 [9.00, 30.0]
Race						
White	44 (93.6%)	1 (100%)	192 (91.0%)	90 (90.0%)	34 (100%)	361 (91.9%)
Asian	1 (2.1%)	0 (0%)	13 (6.2%)	5 (5.0%)	0 (0%)	19 (4.8%)
Black	1 (2.1%)	0 (0%)	4 (1.9%)	3 (3.0%)	0 (0%)	8 (2.0%)
Unknown	0 (0%)	0 (0%)	0 (0%)	0 (0%)	0 (0%)	0 (0%)
American Indian/Alaskan	1 (2.1%)	0 (0%)	0 (0%)	0 (0%)	0 (0%)	1 (0.3%)
Pacific Islander	0 (0%)	0 (0%)	0 (0%)	0 (0%)	0 (0%)	0 (0%)
More than 1 Race	0 (0%)	0 (0%)	2 (0.9%)	2 (2.0%)	0 (0%)	4 (1.0%)
APOE						
E2/E3	3 (6.4%)	0 (0%)	14 (6.6%)	2 (2.0%)	1 (2.9%)	20 (5.1%)
E2/E4	1 (2.1%)	0 (0%)	8 (3.8%)	2 (2.0%)	1 (2.9%)	12 (3.1%)
E3/E3	32 (68.1%)	0 (0%)	90 (42.7%)	29 (29.0%)	8 (23.5%)	159 (40.5%)
E3/E4	11 (23.4%)	1 (100%)	85 (40.3%)	59 (59.0%)	18 (52.9%)	174 (44.3%)
E2/E2	0 (0%)	0 (0%)	1 (0.5%)	0 (0%)	0 (0%)	1 (0.3%)
E4/E4	0 (0%)	0 (0%)	12 (5.7%)	6 (6.0%)	5 (14.7%)	23 (5.9%)
Missing	0 (0%)	0 (0%)	1 (0.5%)	2 (2.0%)	1 (2.9%)	4 (1.0%)
Baseline Amyloid SUVR						
Mean (SD)	0.996 (0.0631)	1.03 (NA)	1.27 (0.143)	1.35 (0.180)	1.45 (0.221)	1.28 (0.193)
Median [Min, Max]	1.00 [0.860, 1.11]	1.03 [1.03, 1.03]	1.25 [0.970, 1.68]	1.34 [1.00, 2.02]	1.41 [0.970, 1.98]	1.26 [0.860, 2.02]
Baseline Global Tau SUVR						
Mean (SD)	0.895 (0.0486)	0.805 (NA)	0.939 (0.0754)	0.954 (0.0904)	1.18 (0.247)	0.958 (0.124)
Median [Min, Max]	0.901 [0.783, 0.993]	0.805 [0.805, 0.805]	0.928 [0.746, 1.37]	0.950 [0.805, 1.26]	1.08 [0.929, 2.12]	0.932 [0.746, 2.12]
Number of Tau PET Scans						
2	8 (17.0%)	1 (100%)	30 (14.2%)	15 (15.0%)	2 (5.9%)	56 (14.2%)
3	17 (36.2%)	0 (0%)	37 (17.5%)	25 (25.0%)	13 (38.2%)	92 (23.4%)
4	22 (46.8%)	0 (0%)	69 (32.7%)	32 (32.0%)	12 (35.3%)	135 (34.4%)
5	0 (0%)	0 (0%)	75 (35.5%)	28 (28.0%)	7 (20.6%)	110 (28.0%)
Years between First and Last Tau PET Scan						
Mean (SD)	4.08 (1.52)	1.38 (NA)	4.81 (1.61)	4.67 (1.59)	4.79 (1.37)	4.68 (1.59)
Median [Min, Max]	4.82 [1.35, 6.76]	1.38 [1.38, 1.38]	5.07 [1.61, 6.80]	4.90 [1.60, 8.04]	4.96 [1.71, 7.02]	4.99 [1.35, 8.04]
Treatment						
Placebo	0 (0%)	0 (0%)	97 (46.0%)	55 (55.0%)	18 (52.9%)	170 (43.3%)
Solanezumab	0 (0%)	0 (0%)	114 (54.0%)	45 (45.0%)	16 (47.1%)	175 (44.5%)
NA	47 (100%)	1 (100%)	0 (0%)	0 (0%)	0 (0%)	48 (12.2%)

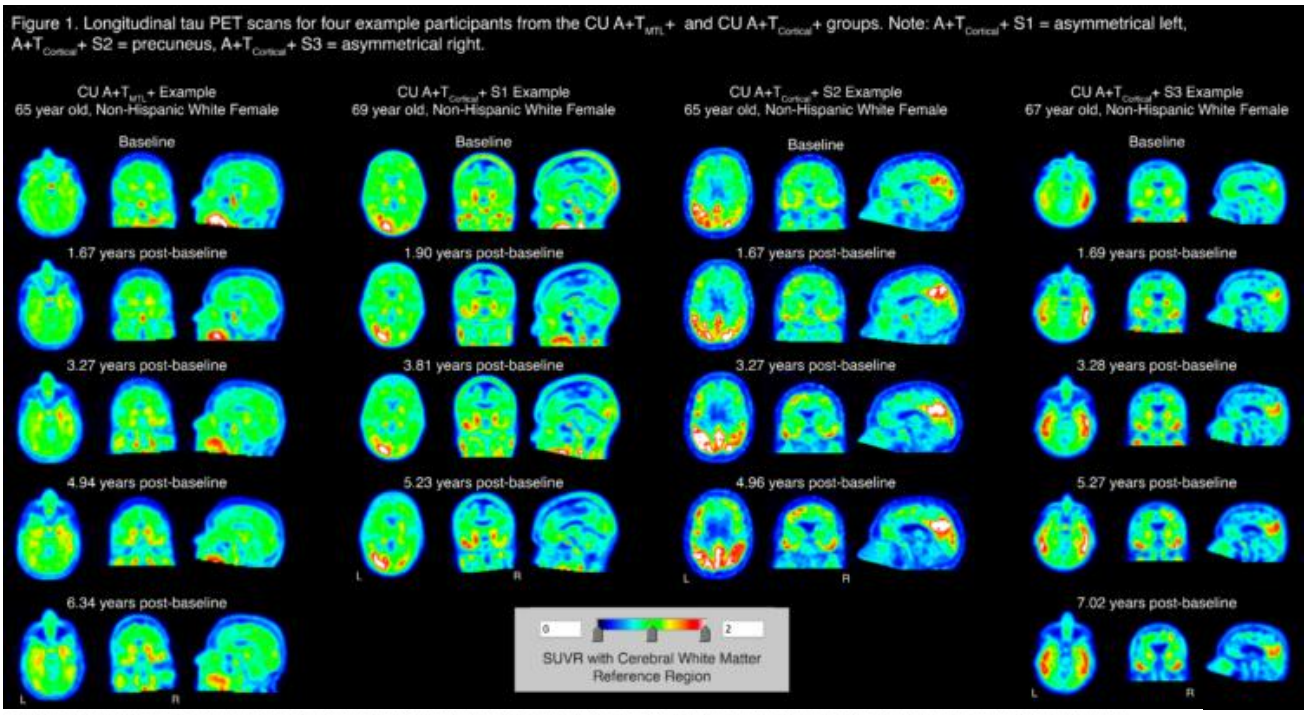


Figure 1. Longitudinal tau PET scans for four example participants from the CU A+T$_{MTL}$+ and CU A+T$_{Cortical}$+ groups. Note: A+T$_{Cortical}$+ S1 = asymmetrical left, A+T$_{Cortical}$+ S2 = precuneus, A+T$_{Cortical}$+ S3 = asymmetrical right.

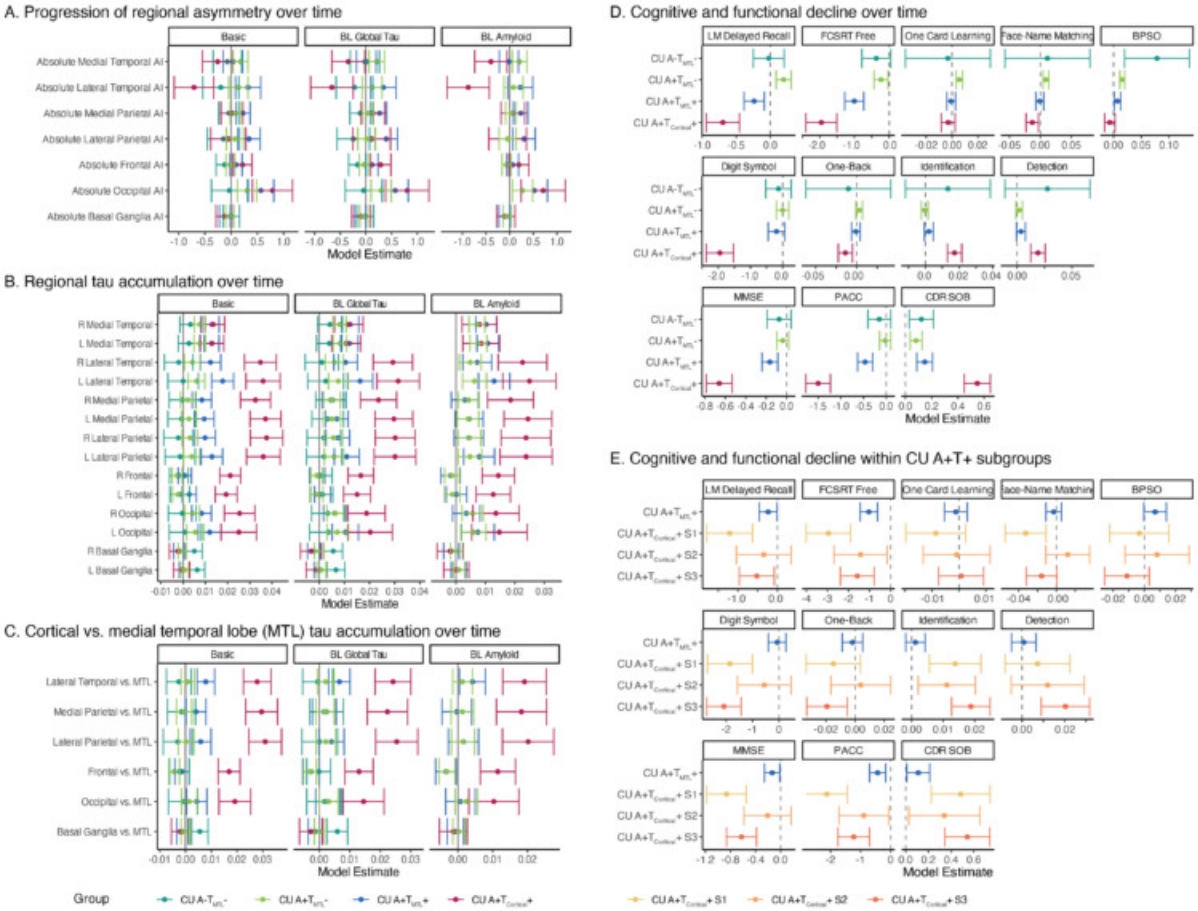


Figure 2. Linear mixed model outputs predicting longitudinal change in (A) absolute values of regional asymmetry indices, (B) regional tau burden, (C) cortical vs. medial temporal lobe (MTL) residuals, and (D, E) cognition and functioning. In A, B, and C, the Basic Model included random intercepts and slopes as well as fixed effects of Age*Time, Sex*Time, and Group*Time in all participants except the one A-T$_{MTL}$+ participant; the BL Tau Model included Baseline Global Tau*Time in addition to all effects in the Basic Model in all participants except the one A-T$_{MTL}$+ participant; and the BL Amyloid Model included Baseline Amyloid Burden*Time in addition to all effects in the BL Tau Model in A+ participants only. In D, models included random intercepts and slopes as well as Age*Time, Sex*Time, Education*Time, Baseline Amyloid Burden*Time, and Group*Time in all participants except the one A-T$_{MTL}$+ participant. In E, models included all effects that were included in D but probed for differences between A+T$_{Cortical}$+ subgroups and the A+T$_{MTL}$+ group. Note: A+T$_{Cortical}$+ S1 = asymmetrical left, A+T$_{Cortical}$+ S2 = precuneus, A+T$_{Cortical}$+ S3 = asymmetrical right.

Keywords: tau PET, longitudinal, preclinical Alzheimer's disease, cortical tau, subtypes

13 Evaluation of a label-free X-ray based method for estimating amyloid load in the human brain

Danielle Geremia[1], Sabri Amer[1], Eshan Dahal[1], Aldo Badano[1]

[1]*Division of Imaging, Diagnostics, and Software Reliability, Office of Science and Engineering Laboratories, Center for Devices and Radiological Health, Food and Drug Administration, Silver Spring, MD, US*

Introduction: Amyloid accumulation in the brain hallmarks several neurodegenerative diseases, including Alzheimer's disease (AD). Despite this, quantifying amyloid plaque levels remains limited to methods requiring tracers or amyloid-specific labeling. Spectral small-angle X-Ray scattering (sSAXS) is a label-free technique for estimating amyloid load using X-rays. Here we report on the sSAXS setup and evaluate its amyloid load estimation performance in postmortem human brains.

Methods: Paraffin-embedded brain slabs approximately 11 mm thick from AD and amyotrophic lateral sclerosis (ALS) patients were studied with our sSAXS setup (**Figures 1a** and **1b**). A polychromatic pencil beam (2.5 mm diameter) collimated using two pinholes (P1 and P2) was generated using an 80-kVp tube voltage and 2-mA current. A 2D spectroscopic detector (PCD) recorded scattered photons for 300 s per ROI. For histology, 10-µm brain slices were stained with an 6E10 antibody to detect amyloid plaques. We correlated histological and sSAXS amyloid load estimations to evaluate the performance of our method.

Results: X-ray scattering signals from grey matter regions (GM1 and GM2) in the AD brain were consistently high, regardless of how background scattering from the brain was subtracted, to recover signal from amyloid plaques (**Figure 1c**). This is consistent with histology images showing a high number of amyloid plaques in the grey matter of the AD brain in comparison to the ALS brain (**Figure 2a**). A strong correlation was found between area under the peak (AUP) values, representing X-ray based amyloid load and the amyloid load estimated from histology (ground truth), as shown in **Figures 2b** and **2c**.

Conclusion: We showed the first results demonstrating label-free estimation of amyloid load using X-rays in a 1 cm thick human brain with AD. Additional ROIs and samples are being studied to provide more data points for evaluating the correlation with histology.

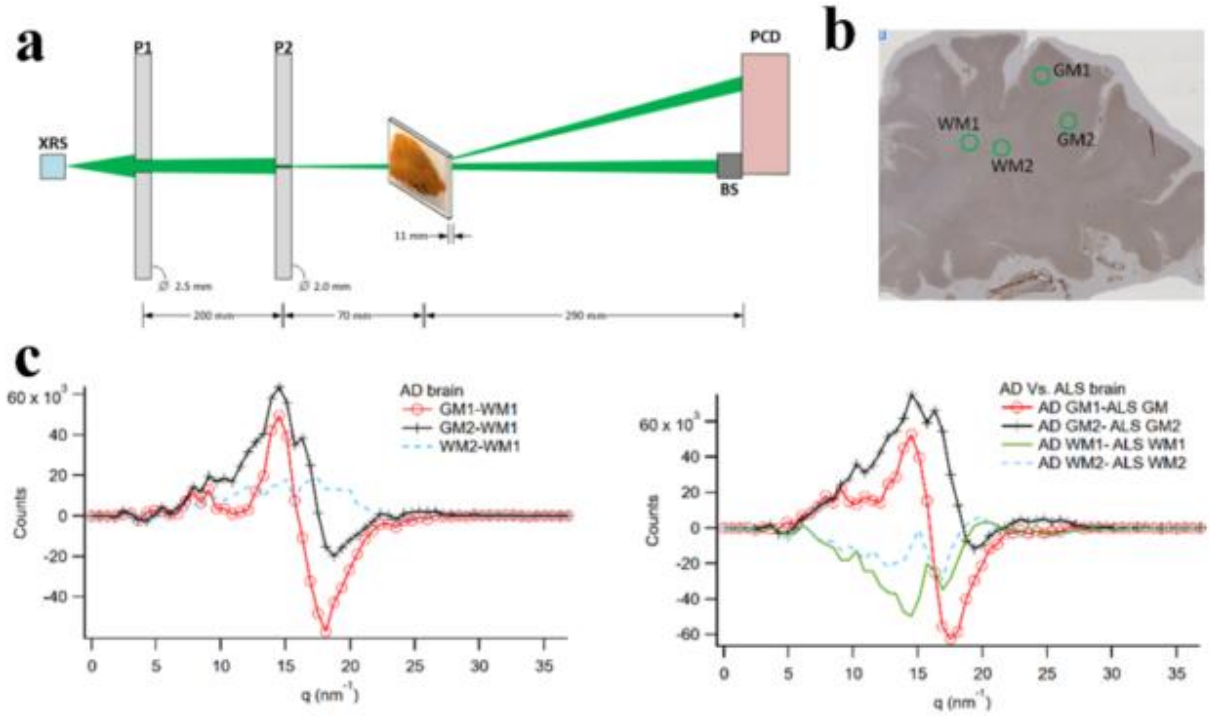


Figure 1. X-ray based method for amyloid load estimation. (**a**) Schematic of sSAXS setup, where a collimated polychromatic X-ray beam irradiates a paraffin-embedded brain slab in the ROIs to collect scattering data. (**b**) Four studied ROIs. (**c**) Corresponding scattering counts as a function of momentum transfer q of AD brain after background subtraction using its white matter (left) or the control ALS brain (right) with no amyloid plaques.

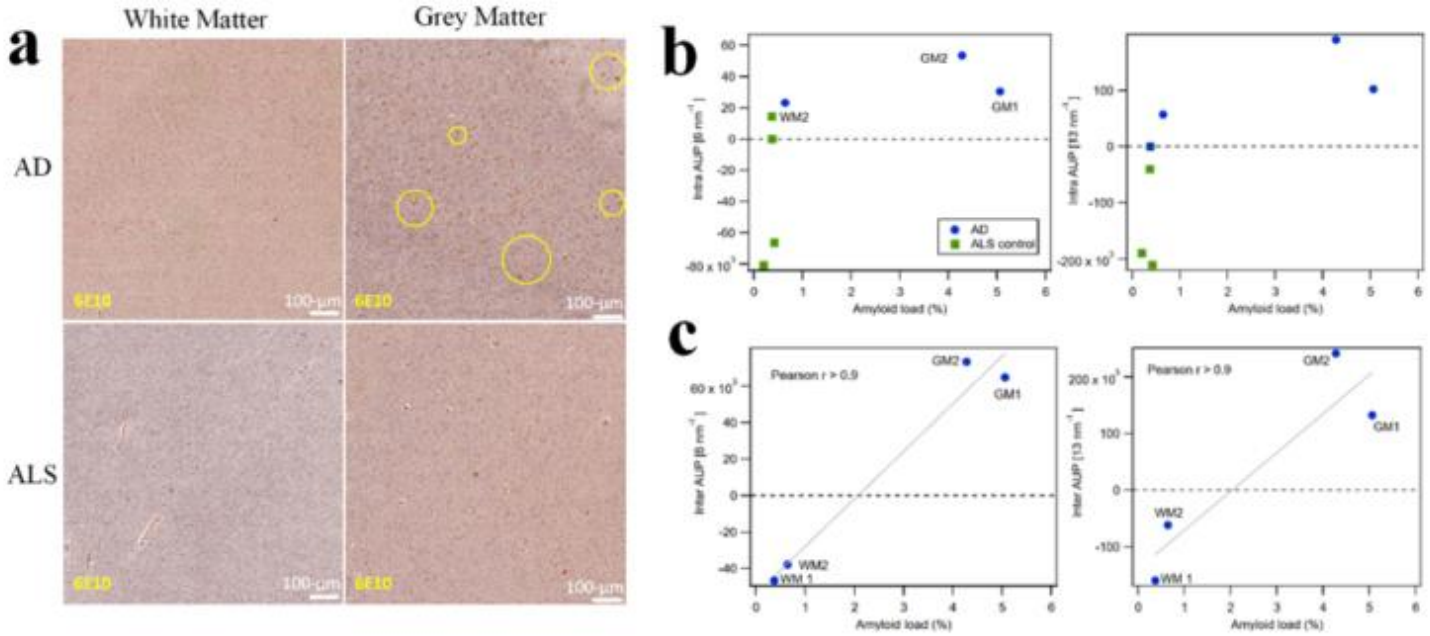


Figure 2. Correlation of sSAXS and histological amyloid load estimations. (**a**) Representative histology images of grey and white matter to detect amyloid plaques with 6E10 anti-bodies in AD and ALS brain slices. Some amyloid plaques are circled in yellow. Intra AUP values (**b**) represent X-ray based amyloid load using white matter from the same brain as a background, while inter AUP values (**c**) represent amyloid load relative to the control ALS sample with no amyloid plaques. Amyloid load (%) on x-axis are derived from histology images as the ground truth for comparison.

Keywords: amyloid, biomarkers, Alzheimer's disease

14 Proteomic analyses of A-T-N reveal plasma mediators of neurodegeneration and dementia risk

Michael Duggan[1], Murat Bilgel[1], Jingsha Chen[2], Abhay Moghekar[3], Christos Davatzikos[4], Josef Coresh[5,6], Susan Resnick[1], Keenan Walker[1]

[1]*Laboratory of Behavioral Neuroscience, National Institute on Aging, National Institutes of Health, Baltimore, MD, US*
[2]*Department of Epidemiology, Johns Hopkins University Bloomberg School of Public Health, Baltimore, MD, US*
[3]*Department of Neurology, Johns Hopkins University School of Medicine, Baltimore, MD, US*
[4]*Artificial Intelligence in Biomedical Imaging Laboratory, Perelman School of Medicine, University of Pennsylvania, Philadelphia, PA, US*
[5]*Department of Medicine, NYU Grossman School of Medicine, New York, NY, US*
[6]*Department of Population Health, NYU Grossman School of Medicine, New York, NY, US*

Identifying the molecular conduits that link amyloid (A), tau (T), and neurodegeneration (N) with distinct biological processes and downstream outcomes may illuminate important drivers of AD, while also unlocking cost-effective biomarkers to detect vulnerable populations, estimate disease risk, or track treatment response. Using 7,268 plasma proteins measured in the Baltimore Longitudinal Study of Aging (BLSA; **Figure 1**; n=681) along with an A, T, and N classification scheme that accurately predicted cognitive decline (**Figure 2A**), we found 1309, 592, and 254 proteins uniquely associated with A^+, T^+, and N^+, respectively ($p<0.05$; **Figure 2B**). These proteomic signatures were largely distinct, contained proteins previously implicated in AD, and displayed a variety of enriched biological mechanisms, including neurovascular coupling (A) and metabolic signaling (T, N; **Figure 2C-D**). We also detected an upregulated latent cluster of axonal-related proteins in A^+ and T^+ participants (**Figure 2E**). Five proteins positively associated with A^+, T^+, and N^+ (ADIPOQ, IGFBP2, EFNB1, PAPPA, HAVCR2; **Figure 2F**) showed variable correlations with intrathecal measurements of the same protein in a Johns Hopkins Neurology cohort (**Figure 3A**). After examining their associations with prevalent cognitive impairment and structural neuroimaging in the BLSA (**Figure 3B-C**), CSF biomarkers in the Emory AD Research Center (**Figure 3D**), and long-term dementia risk in the Atherosclerosis Risk in Communities study (**Figure 3E-F**), we revealed the tissue- and cell-specific expression patterns of these unique proteins, as well as their validated protein-protein interaction networks (**Figure 3G**). The top candidate protein, insulin-like growth factor binding protein 2 (IGFBP2), was associated with higher odds of dementia, greater brain volume atrophy, higher abundance of CSF biomarkers, and increased risk of both 20-year (mid-life) and 7-year (late-life) dementia risk. Our findings reveal plasma proteo-biological profiles of A, T, and N, and implicate IGFBP2 as a particularly important molecular correlate of AD pathophysiology.

Figure1.

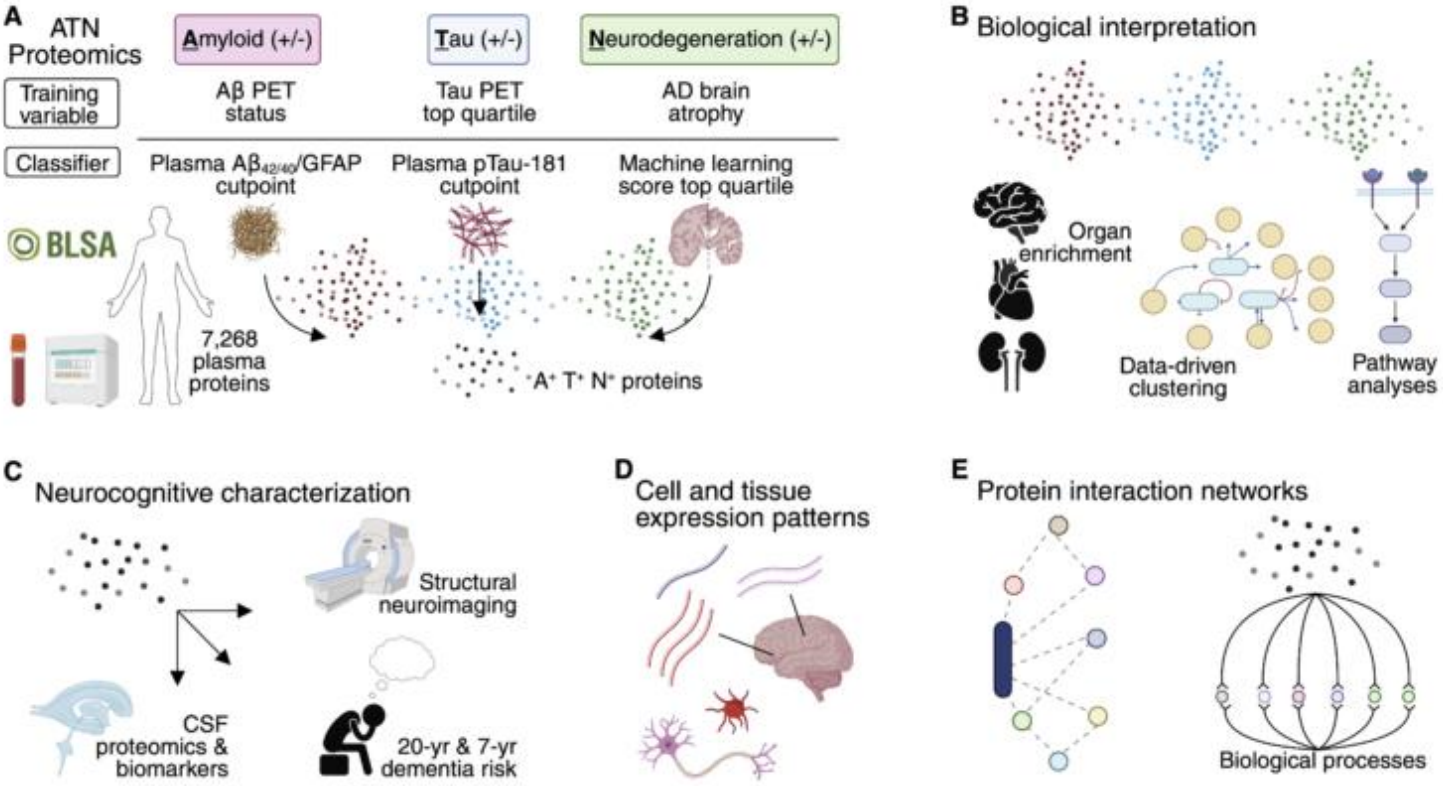

A
ATN Proteomics
Amyloid (+/-)
Tau (+/-)
Neurodegeneration (+/-)
Training variable
Aβ PET status
Tau PET top quartile
AD brain atrophy
Classifier
Plasma Aβ42/40/GFAP cutpoint
Plasma pTau-181 cutpoint
Machine learning score top quartile
BLSA
7,268 plasma proteins
A+ T+ N+ proteins
B
Biological interpretation
Organ enrichment
Data-driven clustering
Pathway analyses
C
Neurocognitive characterization
Structural neuroimaging
CSF proteomics & biomarkers
20-yr & 7-yr dementia risk
D
Cell and tissue expression patterns
E
Protein interaction networks
Biological processes

Figure2.

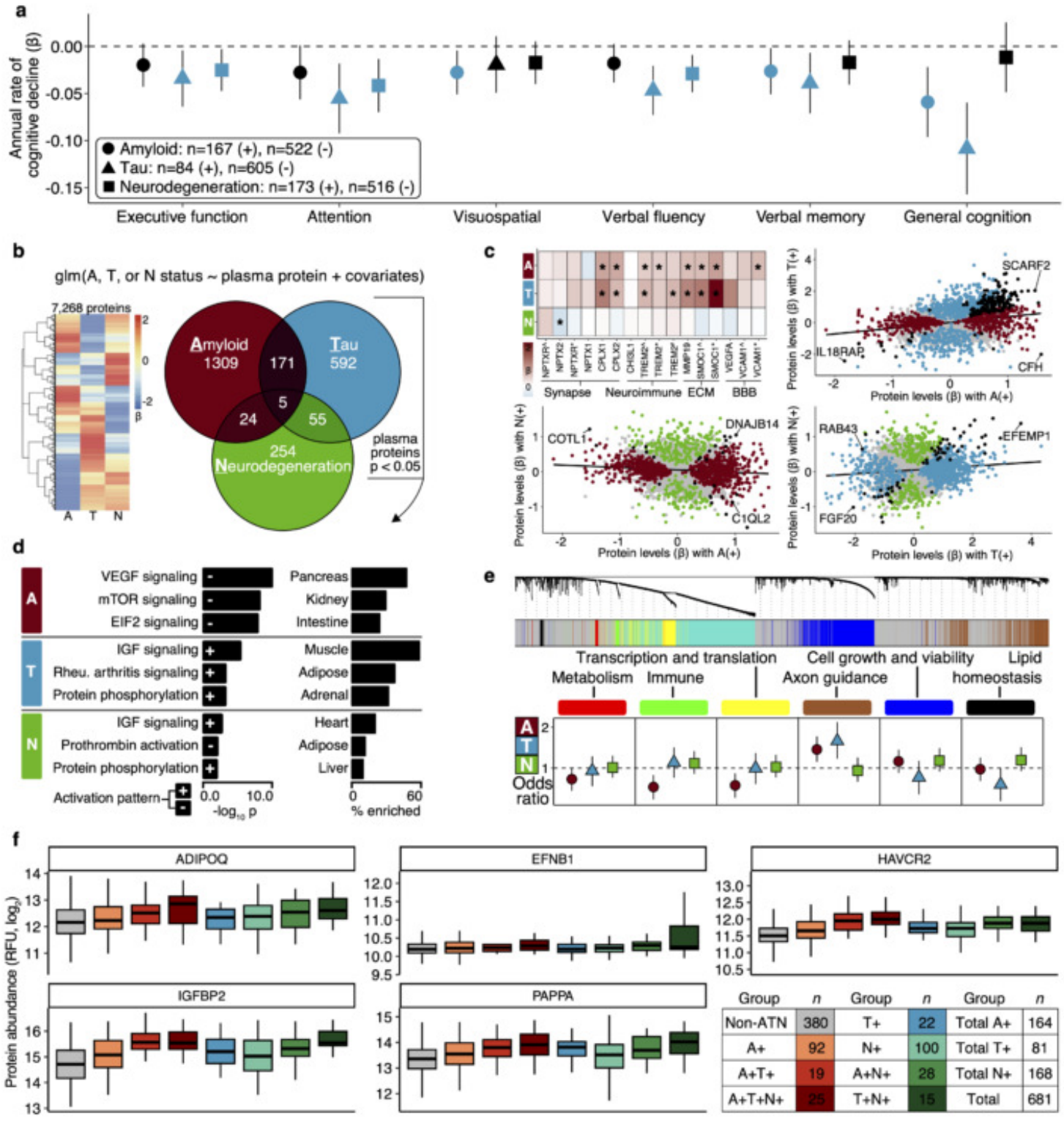
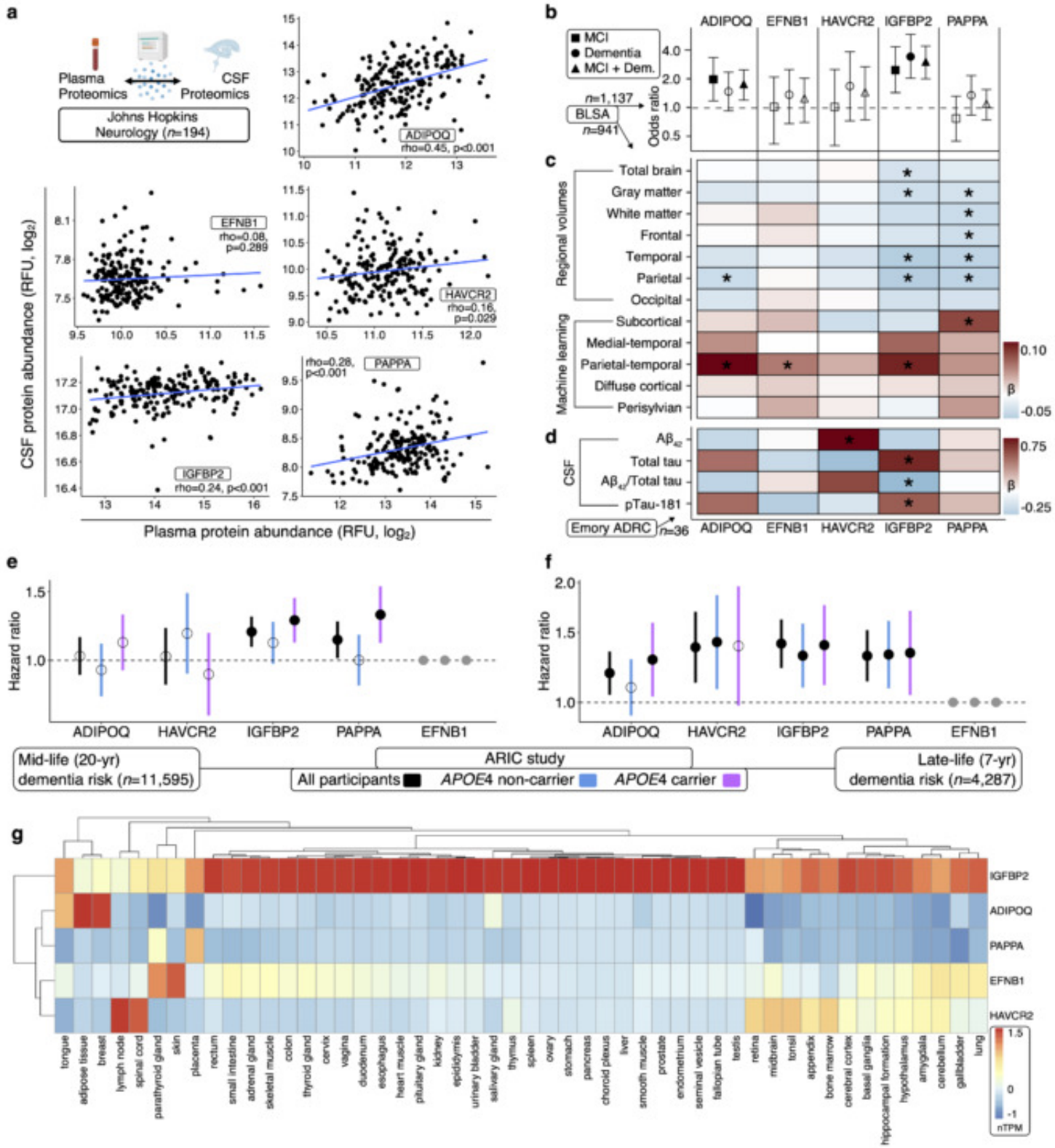

a
Annual rate of cognitive decline (β)
0.00
-0.05
-0.10
-0.15
Amyloid: n=167 (+), n=522 (-)
Tau: n=84 (+), n=605 (-)
Neurodegeneration: n=173 (+), n=516 (-)
Executive function
Attention
Visuospatial
Verbal fluency
Verbal memory
General cognition
b
glm(A, T, or N status ~ plasma protein + covariates)
7,268 proteins
A T N
β
Amyloid 1309
Tau 592
171
5
24
55
254 Neurodegeneration
plasma proteins p < 0.05
c
Synapse
Neuroimmune
ECM
BBB
SCARF2
IL18RAP
CFH
COTL1
DNAJB14
C1QL2
RAB43
EFEMP1
FGF20
Protein levels (β) with A(+)
Protein levels (β) with T(+)
Protein levels (β) with N(+)
d
VEGF signaling
mTOR signaling
EIF2 signaling
IGF signaling
Rheu. arthritis signaling
Protein phosphorylation
IGF signaling
Prothrombin activation
Protein phosphorylation
Activation pattern
-log10 p
Pancreas
Kidney
Intestine
Muscle
Adipose
Adrenal
Heart
Adipose
Liver
% enriched
e
Transcription and translation
Cell growth and viability
Lipid homeostasis
Metabolism
Immune
Axon guidance
Odds ratio
f
ADIPOQ
EFNB1
HAVCR2
IGFBP2
PAPPA
Protein abundance (RFU, log2)
Group n Group n Group n
Non-ATN 380 T+ 22 Total A+ 164
A+ 92 N+ 100 Total T+ 81
A+T+ 19 A+N+ 28 Total N+ 168
A+T+N+ 25 T+N+ 15 Total 681

Figure3.



Keywords: proteomics, amyloid, tau, neurodegeneration

15 The spatial spread of tauopathy precedes the increase in tau-PET load in Alzheimer's disease

Arthur Cassa Macedo[1], Joseph Therriault[1], Nesrine Rahmouni[1], Cecile Tissot[3], Etienne Aumont[1], Yi-Ting Wang[1], Stijn Servaes[1], Lydia Trudel[1], Brandon Hall[1], Seyyed Ali Hosseini[1], Jaime Fernandez-Arias[1], Gleb Bezgin[1], Tevy Chan[1], Yansheng Zheng[1], João Pedro Ferrari-Souza[2], Pamela CL Ferreira[2], Bruna Bellaver[2], Firoza Z Lussier[2], Tharick A Pascoal[2], Pedro Rosa-Neto[1]

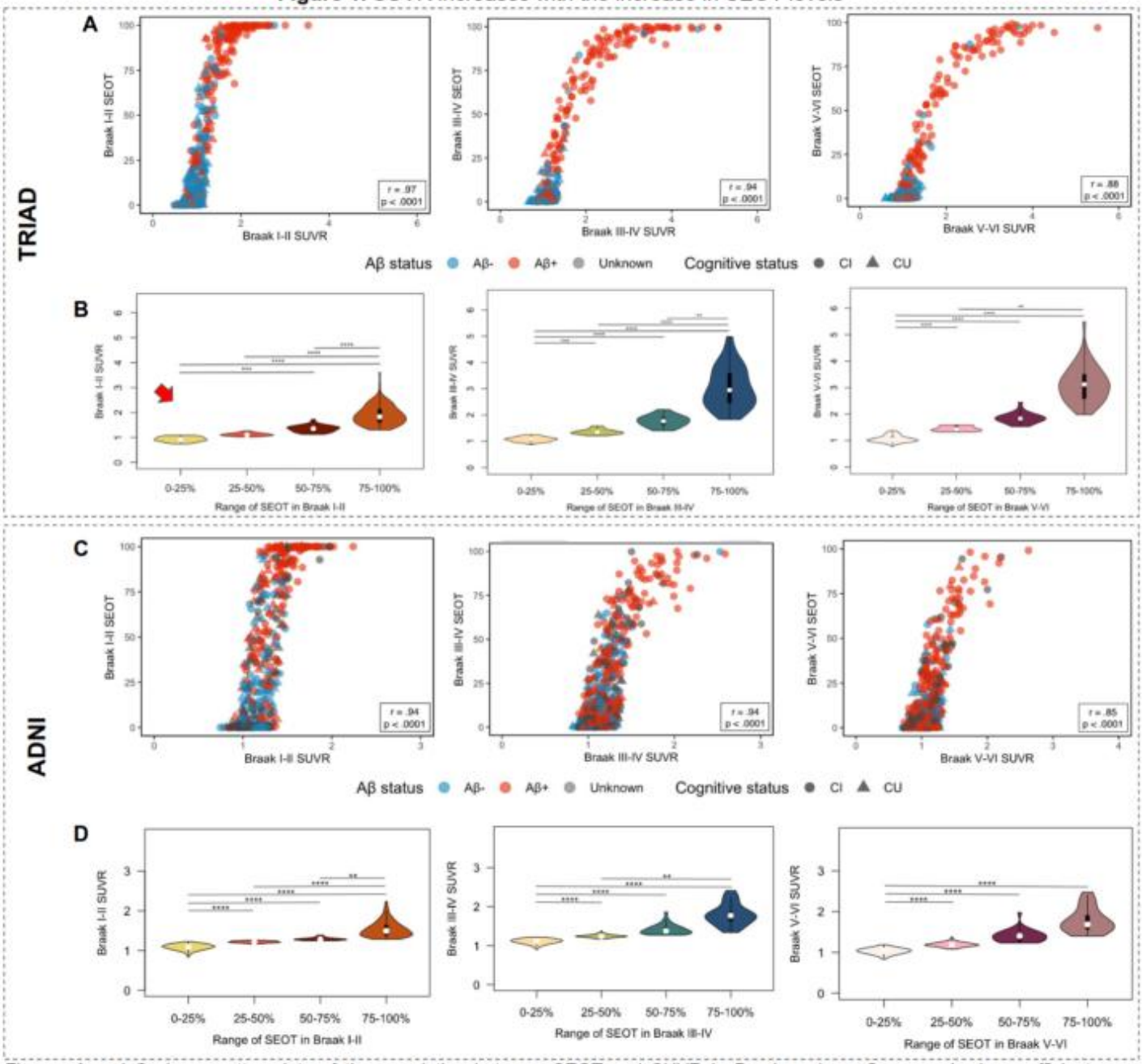
[1]*Department of Neurology and Neurosurgery, McGill University, Montreal, QC, CA*
[2]*Department of Psychiatry, University of Pittsburgh, Pittsburgh, PA, US*
[3]*Lawrence Berkeley National Laboratory, Berkeley, CA, US*

Background: Spatial extent of tauopathy (SEOT) is a promising outcome measure for trials as it correlates better with cognition in Alzheimer's disease (AD) than SUVR. We aimed to track SEOT and SUVR changes in AD-related areas to understand their temporal relationship.

Methods: We studied 606 cognitively unimpaired and 569 cognitively impaired individuals from two cohorts (TRIAD and ADNI) using [18F]MK6240 or [18F]AV1451 tau-PET. We derived SUVR as a proxy of tau load, while SEOT (i.e. proportion of abnormal voxels relative to a reference group) measured spatial spread of tauopathy. 277 participants returned for 2-year follow-up visits. At baseline, we calculated Spearman's correlations between SUVR and SEOT in Braak regions. Moreover, amyloid-positive participants were grouped by SEOT range (0-25%, 25-50%, 50-75%, 75-100%) to compare their SEOT and SUVR in the subsequent Braak region. Longitudinally, we tracked changes in SEOT and SUVR by grouping participants based on their baseline SEOT level (SEOT-HIGH [≥75%] versus SEOT-LOW [<75%]).

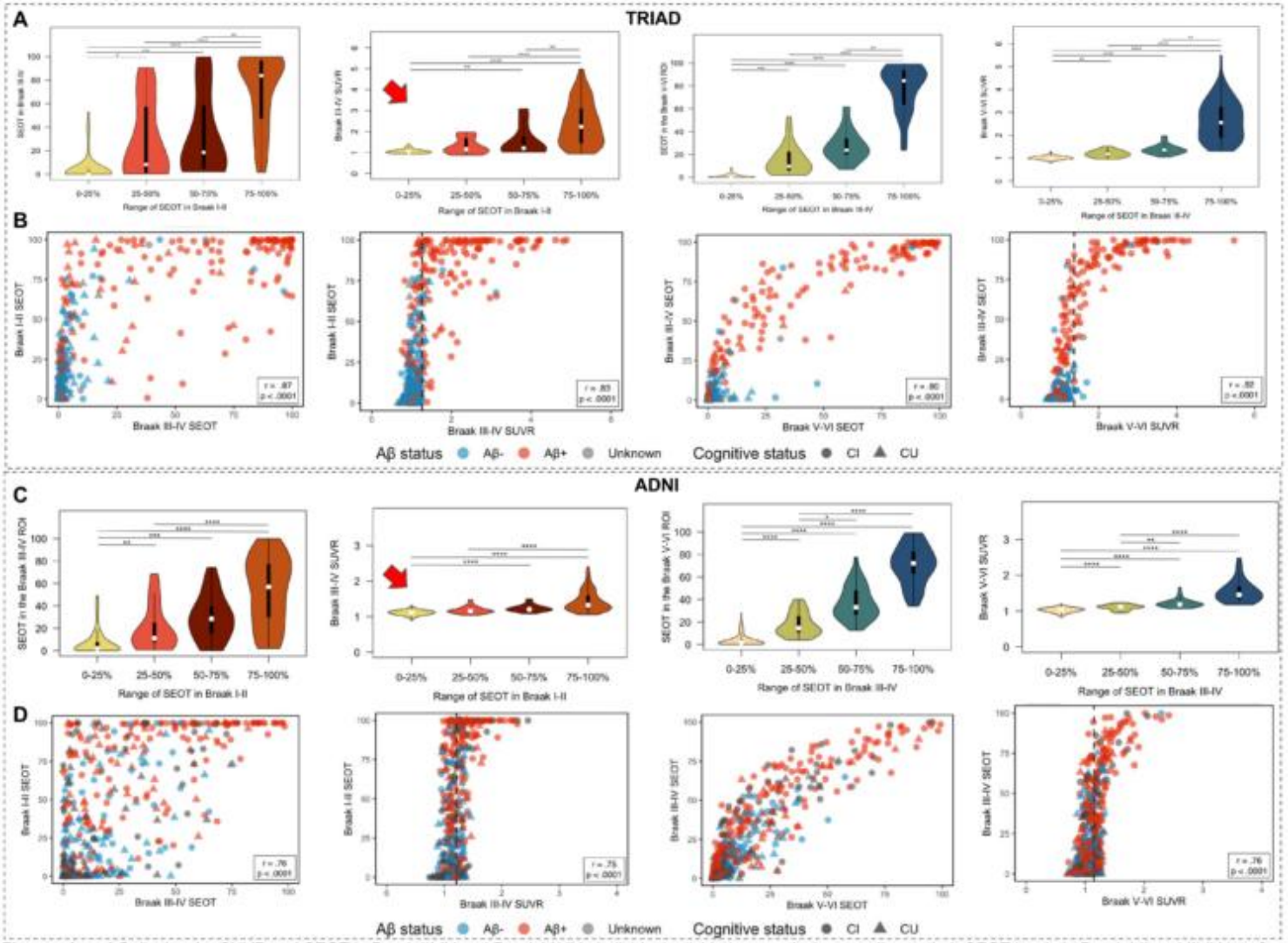
Results: Cross-sectionally, SUVR was associated with SEOT and was higher at increased SEOT levels (Fig.1). Participants with higher SEOT levels in a Braak region also had higher SEOT and SUVR in the subsequent Braak region, with SEOT differences noticeable even among participants at lower SEOT levels (Fig.2). Longitudinally, SEOT-LOW participants exhibited SEOT increases within the same and in subsequent Braak regions; SUVR increases happened only at the same and preceding regions (Fig.3). In TRIAD, SEOT-HIGH participants showed increase in SUVR at the same and subsequent Braak regions. Braak I-II SUVR but not SEOT increased in TRIAD participants with high Braak I-II SEOT.

Figure 1. SUVR increases with the increase in SEOT levels



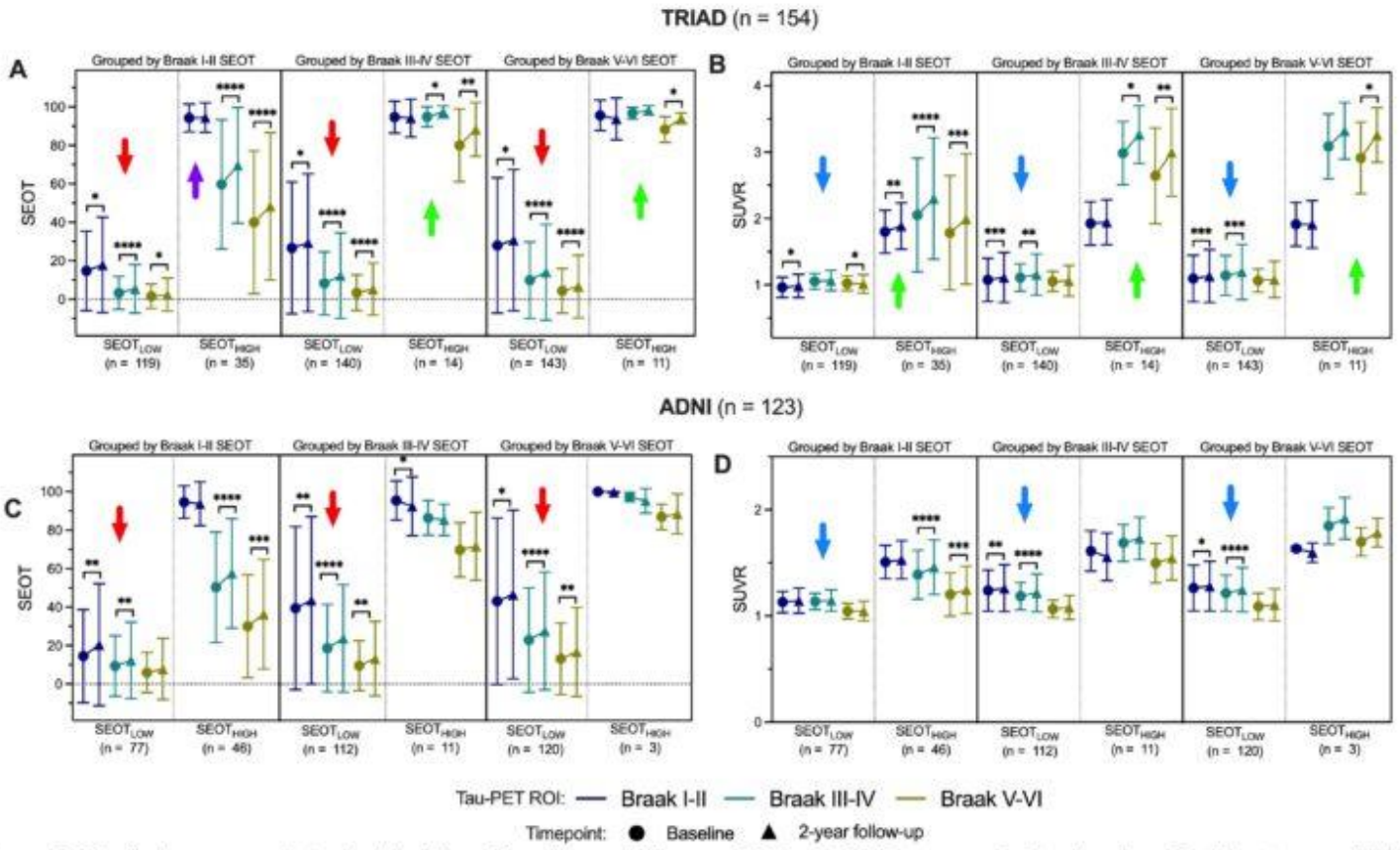
Figures A and C show scatter plots of the correlation between SEOT and SUVR in Braak regions. Spearman's rho coefficients are displayed. Notably, SEOT levels approach a plateau near 100%, where SUVR values become markedly higher. Figures B and D display the median and distribution of SUVR in Braak regions across groups with progressive levels of SEOT in that same Braak region. Pairwise comparisons were performed with the Dunn's *post hoc* test. In TRIAD, no statistical difference between the Braak $I\text{-}II_{0\text{-}25\%}$ and $I\text{-}II_{25\text{-}50\%}$ SEOT groups for Braak I-II SUVR (red arrow). *p<.05, **p<.01, ***p<.001, and ****p<.0001.

Figure 2. SUVR and SEOT in the next Braak region increase with SEOT levels in the preceding Braak region



Figures A and C display the SUVR and SEOT in Braak III-IV and Braak V-VI in individuals divided respectively according to their SEOT levels in Braak I-II and III-IV into four groups: 0-25%, 25-50%, 50-75%, and 75-100%. Pairwise comparisons were performed with the Dunn's *post hoc* test. Significant differences between the Braak I-II$_{0\text{-}25\%}$ and I-II$_{25\text{-}50\%}$ were seen for Braak III-IV SEOT but not for III-IV SUVR (red arrows). Of note, SEOT presented greater effect sizes to differentiate between earlier SEOT groups. **Figures B and D** show Spearman's correlations between SEOT in a given Braak region and SEOT and SUVR in the subsequent Braak region. *p<.05, **p<.01, ***p<.001, and ****p<.0001.

Figure 3. SEOT increase precedes the raise in SUVR in Alzheimer's disease-related areas



Figures 3 A-D display mean and standard deviation of baseline and follow-up SEOT and SUVR measures in Braak regions. Participants were divided based on their baseline SEOT levels: low (SEOT <75%) or high (SEOT ≥ 75%). Independent groups were created according to baseline SEOT levels in Braak I-II, III-IV, and V-VI regions. Participants at $SEOT_{LOW}$ groups increased SEOT at the same and subsequent Braak regions (red arrows). When SUVR increased in $SEOT_{LOW}$ groups, this only happened at the same and preceding Braak regions for which the participants had low SEOT (blue arrows). In TRIAD $SEOT_{HIGH}$ participants, SUVR and SEOT increase happened at the same and subsequent Braak region (green arrows), except in Braak I-II $SEOT_{LOW}$ participants (purple arrow), in which the average SEOT was nearly 100%. Statistical comparisons between baseline and follow-up measures were performed with the Wilcoxon signed rank test. * p<.05; ** p<.01; *** p<.001; **** p<.0001

Conclusions: Our findings suggest two distinct phases of tau accumulation: an initial phase best captured by SEOT, followed by a later phase predominantly reflected by SUVR. SEOT may refine AD staging and help choose appropriate surrogate measures in trials, particularly for early clinical populations.

Keywords: positron emission tomography; Alzheimer disease; neurofibrillary tangles; Braak staging

16 Distinct patterns of Iron distribution in the entorhinal cortex-hippocampus system for characterization of mild cognitive impairment

Sonja M. Kagerer[1,2,4], Laetitia Vionnet[5], Jiri M. G. van Bergen[1], Rafael Meyer[1,2], Anton Gietl[1,2], Klaas Prüssmann[5], Christoph Hock[1], Paul G. Unschuld[3,4]

[1]*Institute for Regenerative Medicine (IREM), University of Zurich, Zurich, CH*
[2]*Department of Geriatric Psychiatry, Psychiatric University Hospital Zurich, Zurich, CH*
[3]*Geriatric Psychiatry Service, University Hospitals of Geneva (HUG), Geneva, CH*
[4]*Department of Psychiatry, University of Geneva (UniGE), Geneva, CH*
[5]*Institute for Biomedical Engineering, University of Zurich and ETH Zurich, Zurich, CH*

Introduction: The entorhinal cortex-hippocampus system plays a central role in memory processing and is affected early in aging related neurodegenerative brain disorders such as Alzheimer's disease (AD). Cognitive dysfunction in AD is a result of progressive neuropathological alterations which include non-specific co-pathologies such as accumulation of non-heme iron in vulnerable brain regions. The current study used an experimental high-resolution 7 Tesla magnetic resonance imaging (MRI) setup to characterize iron distribution in hippocampal subfields and entorhinal cortex (EC).

Methods: 40 old-aged participants with full neuropsychological work-up (mean age [SD] 69.2 [7.42] years; 12 MCI, 28 cognitively healthy controls (HC)) underwent 7 Tesla MRI using turbo spin echo scanning for structural imaging and quantitative susceptibility mapping (QSM) for non-heme iron content. Image quality of high resolution ultra-high field MRI data was assured by real-time field control. Gray matter segmentation was performed with FreeSurfer Version 6.0 software. Intraclass correlation coefficients (ICCs) were calculated to characterize consistency of regional hippocampal subfield and EC susceptibility measures.

Results: ICCs for the mean regional susceptibilities were 0.61 for all subjects (n=40), 0.58 for the HC group (n=28), and 0.69 for the MCI group (n=12). Two-sample Kolmogorov-Smirnov test showed a significant difference of the ICCs between the HC and MCI group ($k=0.625$, $p \leq 0.05$).

Discussion: Our data suggest distinctive patterns of non-heme brain iron distribution in the EC-hippocampus system that characterize MCI. Future studies are needed to confirm whether altered brain iron distribution may serve as potential biomarker of non-specific AD co-pathology.

Keywords: Hippocampus, entorhinbal cortex, QSM, iron, MRI

17 Pathological asymmetry in early onset AD reflects heterogenous disease trajectories

Jacob Ziontz[1], Piyush Maiti[1], Jiaxiuxiu Zhang[1], Konstantinos Chiotis[1], Ganna Blazhenets[1], Salma Rocha[1], Ranjani Shankar[1], Alinda Amuiri[1], Daniel Schonhaut[1], Dustin Hammers[2], Ani Eloyan[3], Robert Koeppe[4], Maria Carrillo[5], Bradford Dickerson[6], Liana Apostolova[7], Gil Rabinovici[1], Renaud La Joie[1]

[1]*Memory and Aging Center, Department of Neurology, University of California San Francisco, San Francisco, CA, US*
[2]*Department of Neurology, Indiana University School of Medicine, Indianapolis, IN, US*
[3]*Department of Biostatistics, Brown University School of Public Health, Providence, RI, US*
[4]*Department of Radiology, University of Michigan, Ann Arbor, MI, US*
[5]*Medical & Scientific Relations Division, Alzheimer's Association, Chicago, IL, US*
[6]*Department of Neurology, Massachusetts General Hospital and Harvard Medical School, Boston, MA, US*
[7]*Department of Radiology, Mayo Clinic, Rochester, MN, US*

Background: Asymmetrical AD pathology has been observed in atypical variants and even cognitively unimpaired (CU) individuals, but how asymmetry presents and changes over time in early-onset AD (EOAD) is unknown.

Methods: We included 373 amyloid-PET-positive patients under 65 years with MCI or mild dementia and 92 CU individuals (10 amyloid-PET-positive, 82 amyloid-PET-negative) from the Longitudinal Early Onset AD study (LEADS). Patient clinical phenotypes were amnestic or nonamnestic EOAD, primary progressive aphasia (PPA), or posterior cortical atrophy. Participants had florbetaben and flortaucipir PET, MRI, and neuropsychological testing at baseline; 206 individuals had 1-3 follow-up imaging visits. We used Freesurfer7.1 segmentation to compute a global asymmetry index for the three imaging modalities reflecting left/right hemisphere signal difference relative to overall cortical signal. We defined symmetrical, left-, and right-lateralized groups using a threshold of +/-2SD from the CU amyloid-PET-negative mean for each modality.

Results: Asymmetry was observed across modalities, most prevalent in flortaucipir followed by cortical volume and florbetaben. Both left and right asymmetry was evident in all clinical phenotypes, though PPA individuals were systematically left-lateralized. Lateralization and degree of asymmetry between modalities were correlated within individuals, particularly between flortaucipir and atrophy (Figure 1). Adjusting for age, sex, education, and overall cortical signal, individuals with lateralized flortaucipir and atrophy performed worse than those with symmetrical signal across domains (Figure 2). Notably, left-lateralized individuals performed worst in verbal fluency while right-lateralized individuals performed worst in visuospatial processing (all $p < 0.001$). Longitudinally, flortaucipir asymmetry decreased over time while volumetric asymmetry increased. Flortaucipir decline was particularly driven by individuals with greater cortical signal abnormality at baseline (Figure 3).

Conclusion: Asymmetry and resulting cognitive impairment are common across clinical phenotypes in EOAD, reflecting intermediate levels of biomarker abnormality. Asymmetry thus varies with disease progression in amyloid, tau, and finally atrophy, declining longitudinally as pathology accumulates contralaterally.

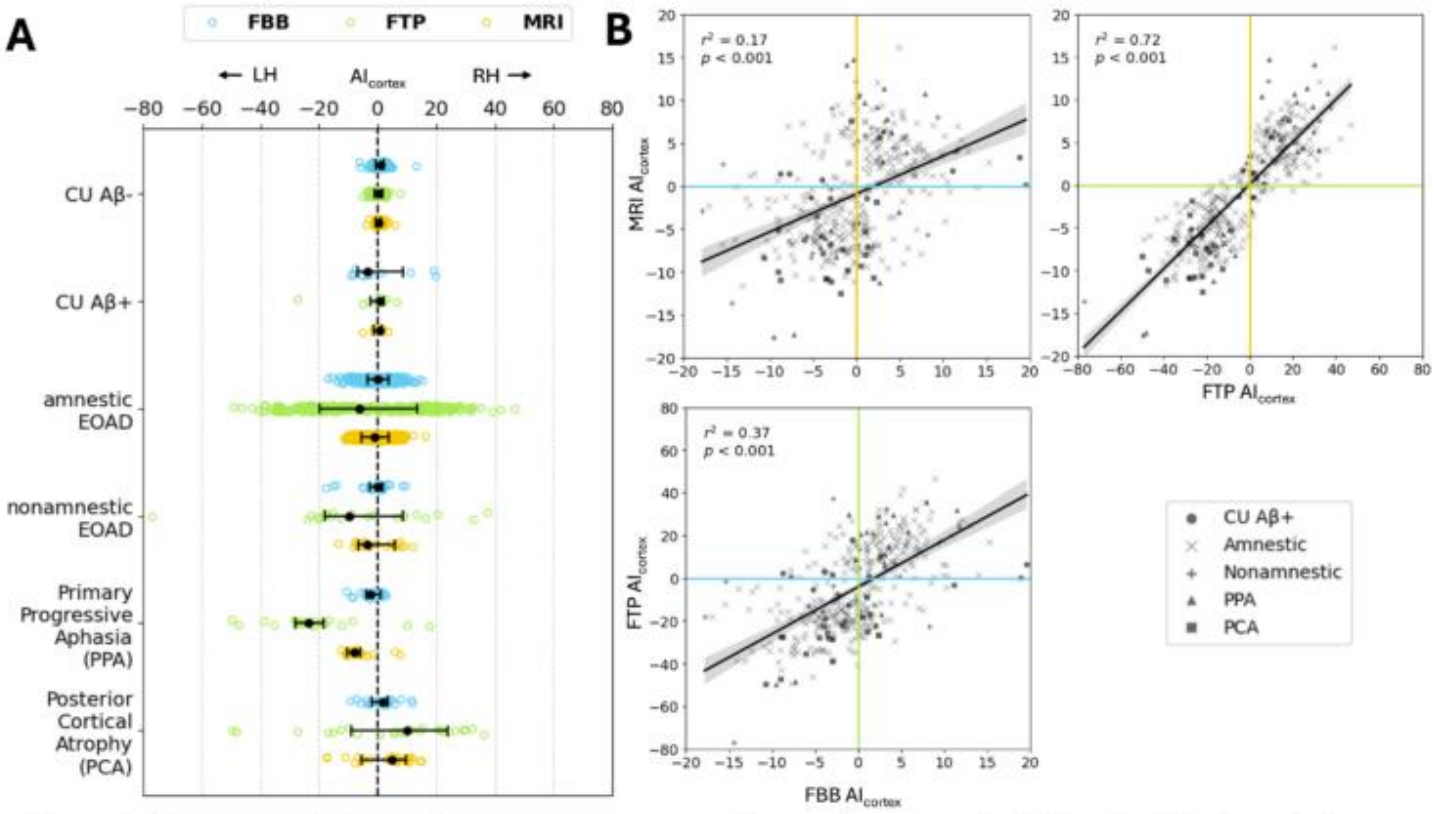


Figure 1. Aβ, tau, and volumetric asymmetry across diagnostic groups in EOAD. (A) Global cortical asymmetry index (AI_{cortex}) for florbetaben (FBB), flortaucipir (FTP), and brain volume (MRI) across diagnostic groups. Negative AI values indicate left-lateralized asymmetry, while positive values indicate right-lateralized asymmetry. Group medians with interquartile range are shown with black dots and confidence bands. **(B)** AI_{cortex} correlations between FBB and MRI *(top left)*, FTP and MRI *(top right)*, and FBB and FTP *(bottom left)*.

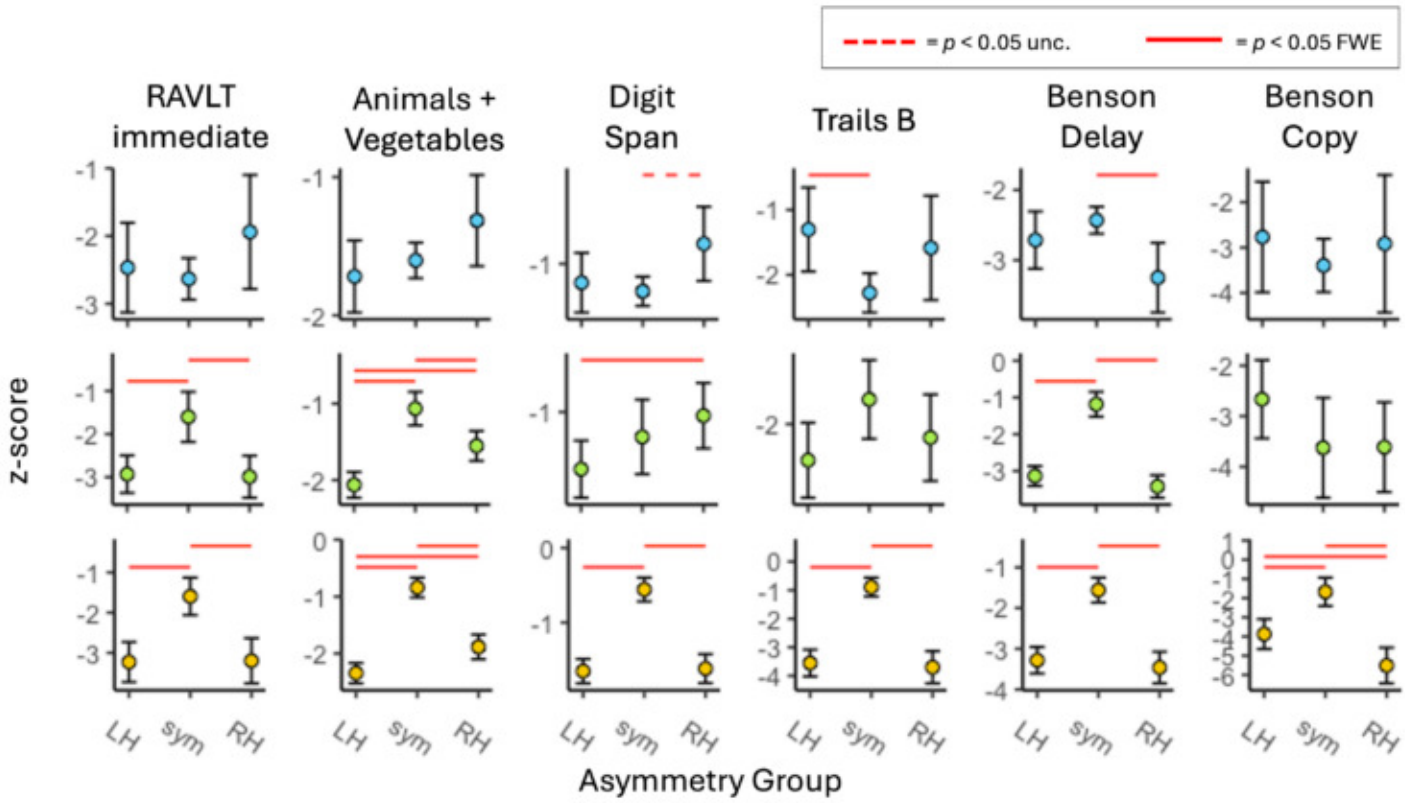


Figure 2. Association between asymmetry and cognitive performance across domains. Group differences between left-lateralized (LH), symmetrical (sym), and right-lateralized (RH) cognitive performance across cognitive tests for florbetaben (*blue*), flortaucipir (*green*), and cortical volume (*yellow*). Z-scores computed with mean and SD of the CU amyloid-PET-negative group. Colored dots visualize estimated marginal means adjusted for age, sex, education, and overall cortical signal. Groups defined using +/-2SD of mean asymmetry in the CU amyloid-PET-negative group.

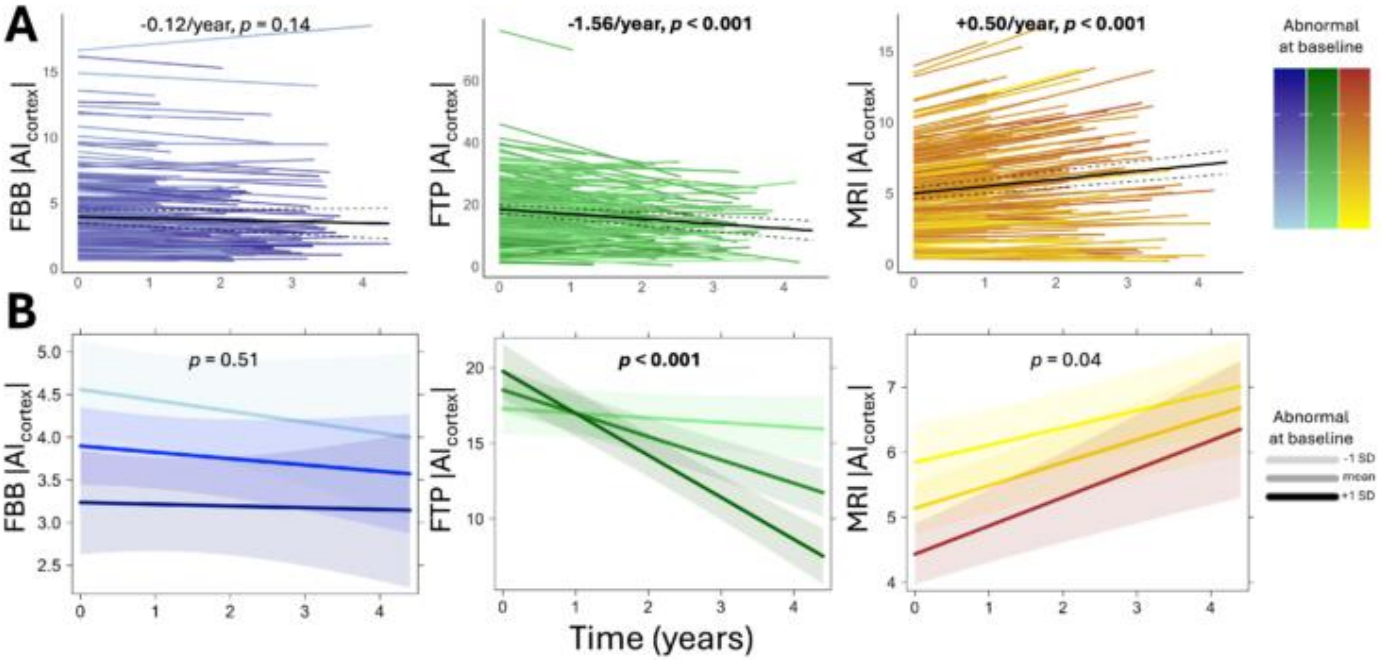


Figure 3. Longitudinal association between absolute cortical asymmetry and baseline abnormality. Y-axis values reflect absolute value of asymmetry index ($|AI_{cortex}|$) to examine asymmetry regardless of left/right lateralization. **(A)** Individualized absolute asymmetry slopes for florbetaben signal *(*FBB, *left)*, flortaucipir signal (FTP, *middle)*, and brain volume (MRI, *right*) from linear mixed effects with random effects of intercept and slope, with intensity colored by abnormality of overall cortical signal at baseline. Black lines and confidence intervals represent the group-level model effect. **(B)** Interaction between baseline cortical signal and change in absolute asymmetry over time. Lines visualize modeled effect at 3 different levels of baseline abnormality (-1SD, mean, +1SD).

Keywords: Early-onset, asymmetry, tau, amyloid, cognition

18 Characterizing amyloid-positive with low Tau (A+T-) profiles and their association with cognitive trajectories in the Longitudinal Early-Onset Alzheimer's Disease Study (LEADS): A multi-method approach

Maison Abu Raya[1,2], David Soleimani-Meigooni[1], Daniel R. Schonhaut[1], Ganna Blazhenets[1], Konstantinos Chiotis[1], Julien Lagarde[8], Agathe Vrillon[1,2], Piyush Maiti[1], Charles Windon[1,2], Ehud Zeltzer[1], Jiaxiuxiu Zhang[1], Claire Yballa[1], Ranjani Shankar[1], Alinda Amuiri[1], Salma Rocha[1], Dustin B. Hammers[6], Ani Eloyan[4], Maria C. Carrillo[3], Robert Koeppe[5], Bradford C. Dickerson[7], Liana G. Apostolova[6], Gil D. Rabinovici[1], Renaud La Joie[1,2]

[1]*Memory and Aging Center, Department of Neurology, Weill Institute for Neurosciences, University of California, San Francisco, San Francisco, San Francisco, CA, US*
[2]*Global Brain Health Institute- University of California San Francisco, San Francisco, CA, US*
[3]*Medical & Scientific Relations Division, Alzheimer's Association, Chicago, IL, US*
[4]*Department of Biostatistics, Brown University School of Public Health, Providence, RI, US*
[5]*Department of Radiology, University of Michigan, Ann Arbor, MI, US*
[6]*Department of Neurology, Indiana University School of Medicine, Indianapolis, IN, US*
[7]*Department of Neurology, Massachusetts General Hospital and Harvard Medical School, Boston, MA, US*
[8]*Hôpital Ste Anne – GHU Paris Psychiatrie & Neurosciences – Paris, Paris, FR*

Introduction: The interpretation of an A+T- PET profile in clinically impaired individuals can make it difficult to identify underlying etiology and predict future outcomes. We aimed to assess the frequency of A+T- profiles within a cohort of patients diagnosed with early-onset Alzheimer's disease (EOAD) and describe their clinical and imaging characteristics.

Methods: We analyzed 582 LEADS participants with baseline [^{18}F]florbetaben and [^{18}F]flortaucipir PET: 490 cognitively impaired (CI, i.e., clinical diagnosis of MCI or dementia) and 92 cognitively unimpaired (CU) participants. Amyloid positivity (A+) was defined using a 25-CL threshold. Tau-PET status was based on visual read following FDA-approved guidelines or SUVR extractions from various ROIs (in native space using Freesurfer or in template space with CenTauR procedures). Regional flortaucipir-SUVR thresholds were calculated using various statistical methods (Table 1).

Results: Among 372 A+ CI participants, rates of T- were minimal (4%-7%), regardless of the tau-PET approach (Table1). Subsequent analyses focused on comparing A+T+ and A+T- groups, defined using the two methods that provided the most divergent T- rates, which were visual reads (4%) or global cortical SUVR thresholds calculated using a Gaussian Mixture Model-based approach (7%). Regardless of the tau status definitions, the A+T- group exhibited milder clinical impairment than the A+T+ group despite being older and having a higher frequency of APOE-e4, hypercholesterolemia, and smoking (Table 2). The A+T- group had lower amyloid burden and larger hippocampal volumes than A+T+ patients but similar white matter hypointensity burden. Regardless of Tau status, all groups ($A+T_{\text{Visual Read/Global}}+/-$) showed an increase in CDR-SB over time, but clinical progression was more rapid in the A+T+ groups (Figure 1).

Conclusion: In amyloid-positive patients with EOAD, tau-PET results were predominantly positive regardless of tau-status definitions (93-96%). Some of the rare A+T- individuals may be in early disease stages, with tau pathology below PET detection levels.

Table 1. Number (proportion) of Tau-PET negative cases among A+ cognitively-impaired participants (n=372) based on different processing approaches and statistical methods.

Processing approach / Region of interest (ROI)	Statistical approach used to establish Tau-PET positivity threshold					
Native space extraction with Freesurfer ROIs	**95th percentile of Aβ- cognitively normal controls (n=85)**		**Gaussian Mixture Model on all dataset (N=582). Threshold based on mean +2SD of low gaussian**		**ROC analysis: Optimal Youden Index between Aβ- controls (n=85) and Aβ+ clinically-impaired (n=372)**	
	ROI SUVr threshold	**A+T-, N(%)**	**ROI SUVr threshold**	**A+T-, N(%)**	**ROI SUVr threshold**	**A+T-, N(%)**
Entorhinal cortex	1.26	17 (5%)	1.29	17 (5%)	1.27	17 (5%)
Temporal Meta-ROI	1.25	13 (4%)	1.31	21 (6%)	1.27	17 (5%)
Whole cortex	1.16	20 (5%)	1.21	27 (7%)	1.20	25 (7%)
Warping PET to template and extraction of CenTauR ROIs	**CenTauR z-score < 1.5**		**CenTauR z-score < 2**			
	ROI SUVr Threshold	**A+T-, N(%)**	**ROI SUVr Threshold**	**A+T-, N(%)**		
Mesial temporal	1.31	15 (4%)	1.35	21 (6%)		
Meta Temporal	1.30	15 (4%)	1.34	23 (6%)		
Universal	1.27	17 (5%)	1.31	23 (6%)		
Visual read	**FDA-approved method A+T-, N(%)**					
	15 (4%)					

Number (proportion) of cases classified as Tau-PET negative in the group of A+ cognitively impaired participants (n=372) based on different approaches: For Freesurfer ROIs derived from native space extraction, we employed three statistical methods to determine the Tau positivity threshold for each ROI. For CENTAUR-extracted ROIs, we applied two established CenTauR Z-scores: 1.5 (mean + 1.5 SDs of the CU group mean), CenTauR$_z$ 2.0 (mean + 2 SDs of the CU group mean) (Villemagne, 2023; Gogola, 2023). Flortaucipir_PET visual read was based on FDA approved guidelines, which defines negative visual read based on the absence of increased uptake, or increased uptake isolated to medial temporal, anterolateral temporal and/or frontal regions.

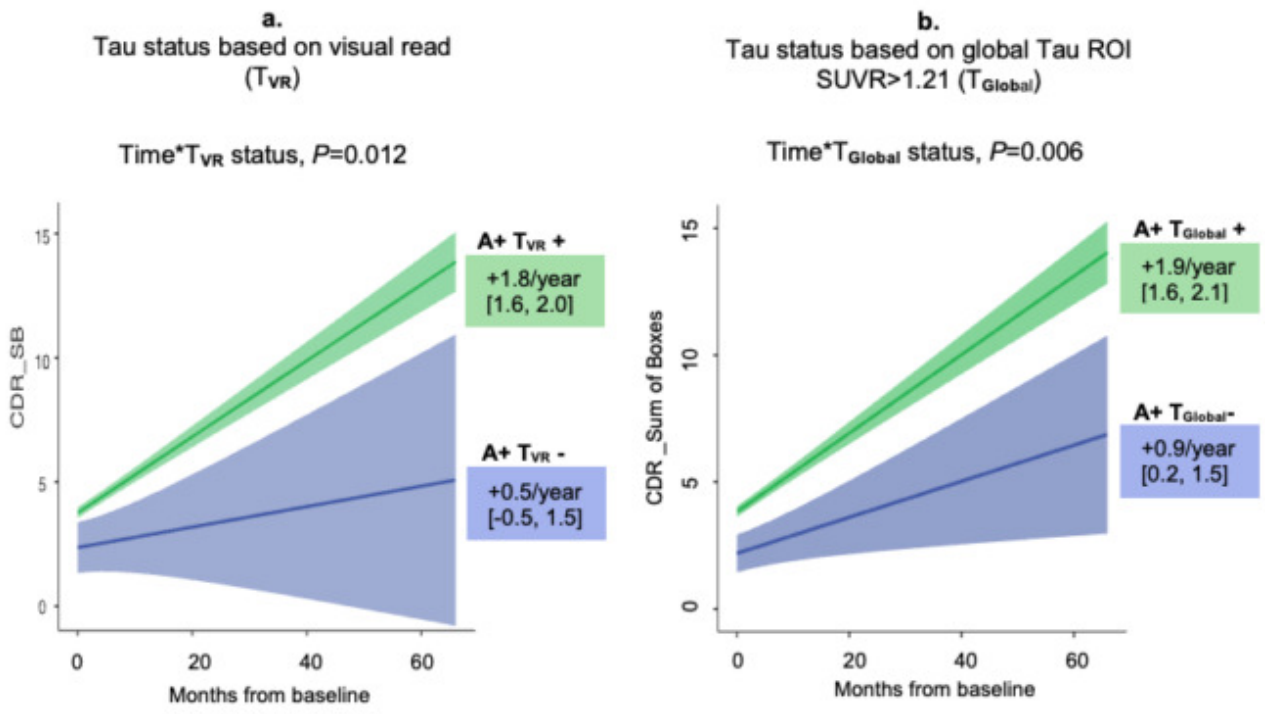
Table 2. Comparisons between cognitively-impaired A+T- and A+T+ groups.

Tau status defined:	*Based on visual read (VR) following FDA-approved guidelines*			*Based on Freesurfer-defined global cortical SUVr with GMM threshold*		
Characteristic	**A+T$_{VR}$ - 15 (4%)**	**A+T$_{VR}$ + 353 (96%)**	***P***	**A+T$_{Global}$ - 27 (7%)**	**A+T$_{Global}$ + 345 (93%)**	***P***
Age	64 (62,64)	59 (56,62)	**<.001**	64 (60, 64)	59 (56,62)	**<.001**
Sex (Female)	5 (33%)	198 (56%)	0.11	13 (48%)	190 (55%)	0.55
Education years	16 (14,18)	16 (14,18)	0.78	16 (14,16)	16 (14,18)	0.40
CDR- Sum of Boxes	2 (1.5,3)	4 (2.5,5)	**<.001**	2 (1.5,2.75)	4 (2.5,5.)	**<.001**
CDR-Global			**0.012**			**<.001**
≤0.5	14 (93%)	213 (61%)		25 (93%)	203 (59%)	
≥1.0	1 (7%)	137 (39%)		2 (7%)	139 (41%)	
Mini Mental State Examination (MMSE)	28(25, 29)	22 (18, 25)	**<.001**	27 (24, 29)	22 (18, 25)	**<.001**
Risk factors						
APOE-e4 (carriers)	12 (80%)	191 (54%)	**0.028**	22 (85%)	184 (55%)	**0.003**
Diabetes, past or current	2 (14%)	26 (8%)	0.31	3 (12%)	25 (8%)	0.45
Hypertension, past or current	4 (29%)	82 (25%)	0.75	7 (27%)	79 (24%)	0.81
Hypercholesterolemia, past or current	9 (64%)	93 (28%)	**0.006**	13 (50%)	90 (28%)	**0.024**
Tobacco use, past or current	7 (50%)	75 (23%)	**0.048**	15 (58%)	68 (21%)	**<.001**
Traumatic Brain Injury	3 (21%)	49 (15%)	0.45	6 (23%)	46 (14%)	0.25
Depression, past or current	6 (46%)	111 (34%)	0.38	15 (60%)	103 (32%)	**0.007**
Imaging measures						
Amyloid burden (Centiloids)	62 (55,68)	104 (87,122)	**<.001**	63 (52, 76)	104 (89,122)	**<.001**
*Standardized hippocampal volumes	5.22 (4.77,5.77)	4.64 (4.27, 5.03)	**0.001**	5.02 (4.61, 5.53)	4.63 (4.27, 5.02)	**0.001**
**Standardized WMH volumes	1.14 (0.71, 2.24)	1.08 (0.73,1.74)	0.53	0.73 (0.61, 1.51)	1.10 (0.78, 1.77)	0.11

Tau status was defined based on visual reads (left) or a Freesurfer-defined Global cortical ROI with a Gaussian Mixture Model-based threshold (right). Continuous variables are presented as median (Q1, Q3) and were compared using the non-parametric Kruskal-Wallis test. Categorical variables, presented as n(%), were compared using the Fisher's Exact test.
*Standardized hippocampal (HC) volumes =(HC vol./TIV) *1000,
**Standardized white matter hypointensity (WMH) volumes =(WMH vol./TIV) *1000

Figure 1. Longitudinal progression of cognitive decline in A+T+ vs A+T- groups.

CDR-SB~ Age+ Sex+ Time*Tau status+ (Time| Participant ID) + (1|Participant ID)



Linear mixed-effects models (including random slopes and intercepts) were used to assess the longitudinal progression of clinical decline, as measured by CDR-SB scores, in relation to Tau status using **(a)** Visual Reads and **(b)** Global Tau ROI. Regression lines with confidence intervals and rate of progression per year indicate the trajectory of cognitive decline for each group.

Keywords: Early-onset Alzheimer's Disease (EOAD), Amyloid-Positive with Low Tau (A+T-)

19 The association between amyloid and physical activity in a racially diverse cohort of older adults

Yiwen Dong[1], Qiong Wu[1], Davneet Minhas[2], Charles M. Laymon[2,3], Victor Villemagne[4], Oscar Lopez[5], Beth Snitz[5], Marissa A. Gogniat[5], Nancy W. Glynn[6], Dana Larisa Tudorascu[1,4], Ann D. Cohen[4]

[1]*Department of Biostatistics and Health Data Science, School of Public Health, Pittsburgh, PA, US*
[2]*Department of Radiology, School of Medicine, Pittsburgh, PA, US*
[3]*Department of Bioengineering, Swanson School of Engineering, Pittsburgh, PA, US*
[4]*Department of Psychiatry, School of Medicine, Pittsburgh, PA, US*
[5]*Department of Neurology, School of Medicine, Pittsburgh, PA, US*
[6]*Department of Epidemiology, School of Public Health, Pittsburgh, PA, US*

Introduction: Physical activity (PA) is proposed to be an effect modifier of Alzheimer's disease (AD) risk, however, it remains unclear if this modification is a result of a direct impact on AD pathophysiology or through indirect mechanisms, like increased cognitive reserve or reduced cardiometabolic risk. In this study of racially diverse older adults, we explored the association of PA and amyloid deposition measured by [11C] Pittsburgh Compound B-PET (PiB).

Methods: 128 participants (mean age 65.3 years, 68.0% female, 47.7% African American) received PiB imaging on 2 different scanners (Siemens HR+/Biograph mCT). PA data were collected via wrist-worn Actiwatch and processed using ActiLife. The association between PiB FreeSurfer-derived SUVRs and PA outcomes was assessed by Spearman's correlation, with 95% confidence intervals using bootstrapping. Results were compared before and after harmonization using ComBat to account for scanner differences. The associations between Aβ deposition in various brain regions and PA were further explored using generalized linear models (GLMs) including an interaction term with race, adjusting for age, sex, ApoE4, and education.

Results: In this study, the average global SUVR was 1.2. PA, measured using maximum steps count per minute (mean 99.2), was significantly associated with a decreased Aβ deposition and was consistent before and after harmonization (Table 1). GLMs estimates revealed that one-unit increase in maximum steps (100 steps/minute) was associated with 13%, 14%, 15%, and 18% lower Aβ deposition in the lateral temporal, parietal, posterior cingulate, and precuneus regions, respectively ($p < 0.05$ for all models).

Conclusion: The study demonstrates that higher maximum step count is associated with lower amyloid deposition in a racially diverse cohort. Further, there were no differences observed before and after scanner harmonization in results and effect sizes. Future work will explore additional PA variables, such as different PA intensity levels, to determine their effect on AD pathology.

Table 1: Association Between Step Max Count per Minute and Aβ Deposition in Various Brain Regions Before and After Harmonization

	Spearman Correlation (95% Confidence interval)	
Brain Region	Before Harmonization	After Harmonization
Global	-0.21 (-0.40, -0.04)	-0.21 (-0.38, -0.02)
Superior Frontal	-0.20 (-0.38, -0.02)	-0.19 (-0.37, -0.02)
Insula	-0.24 (-0.41, -0.07)	-0.24 (-0.40, -0.05)
Lateral Temporal	-0.20 (-0.37, -0.04)	-0.21 (-0.38, -0.03)
Parietal	-0.22 (-0.39, -0.05)	-0.22 (-0.39, -0.03)
Posterior Cingulate	-0.24 (-0.42, -0.05)	-0.24 (-0.41, -0.05)
Precuneus	-0.25 (-0.42, -0.07)	-0.25 (-0.42, -0.06)

Keywords: Physical Activity, Amyloid PiB, Harmonization

20 Whole blood gene expression is associated with plasma p-tau217 levels via amyloid-PET and sex

Rachel F Buckley[1], Vaibhav A Janve[2], Mabel Seto[4], Hannah M Klinger[1], Jane A Brown[1], Colin Birkenbihl[1], Gillian Coughlan[1], Diana L Townsend[1], Michael J Properzi[1], Jane Zyski[2], Ting-Chen Wang[2], Michelle Clifton[2], Bernard J Hanseeuw[1], Jasmeer Chhatwal[1], Hyun-Sik Yang[4], Robert A Rissman[3], Paul Aisen[3], Madison Cuppels[1], Michael Donohue[3], Rema Raman[3], Keith A Johnson[1], Reisa A Sperling[4], Logan Dumitrescu[2], Timothy J Hohman[2]

[1]*Massachusetts General Hospital, Boston, MA, US*
[2]*Vanderbilt Univeristy Medical Center, Nashville, TN, US*
[3]*University of Southern California, Los Angeles, CA, US*
[4]*Brigham and Women's Hospital, Boston, MA, US*

Objective: Higher levels of plasma p-tau$_{217}$ are associated with Aβ-PET burden and impending cognitive decline in older adults, supporting it as an early marker of AD. Identifying genes in whole blood that are associated with p-tau$_{217}$ can elucidate biological pathways implicated in these earliest disease processes.

Method: We leveraged Aβ-PET (^{18}F-Florbetapir), plasma p-tau$_{217}$(mass spectrometry, C_2N Diagnostics), and whole blood gene expression data including the autosome and X chromosomes (20,621 genes) from 724 participants (72.2years (±4.6); 63% Female; 35% *APOEε4*; 26% Aβ+) from the A4 clinical trial at baseline (placebo[31%], treatment[30%]) and the LEARN [39%] observational study. We ran a series of linear regressions predicting p-tau$_{217}$ (pg/mL) from gene expression alone, adjusting for age, BMI and cohort. Then interacted with *APOEε4*, sex, and Aβ$_{continuous}$. All analyses were FDR corrected.

Results: No genes were directly associated with p-tau$_{217}$ levels. One novel transcript was moderated by *APOEε4* to predict p-tau$_{217}$, while 1,535 genes were moderated by Aβ (8% were X-linked), and 777 genes by Aβ*sex (4% X-linked; see Fig.1). In gene*Aβ models, 62% of significant genes were found to be protective (i.e., lower p-tau$_{217}$ at higher Aβ burden). One example, RMND1 (b=-1.04(0.2), p_{FDR}=0.0001), is involved in mitochondrial translation (Fig.2A). From gene*Aβ*sex models, higher AMIGO2 expression, a novel membrane anchor of PDK1 that controls cell survival and promotes neuronal survival, was positively associated with p-tau$_{217}$ levels in women with higher Aβ (b=0.49(0.1), p_{FDR}=0.0005), but negatively in men (b=-0.44(0.1),p_{FDR}=0.003; Fig.2B). Other notable pathways implicated in our analyses were post-transcriptional modification, coordination of DNA damage, and regulation of brain homeostasis.

Conclusion: Whole-blood transcriptomic associations with p-tau$_{217}$ in clinically normal older adults are largely moderated by Aβ-PET burden and sex in these analyses. Both protective and risk genes were identified throughout the transcriptome, including the X chromosome, highlighting novel gene candidates for further replication and validation.

Table 1. Demographic characteristics

Table 1: Participant Demographics				
Characteristic	**Overall** N = 724[1]	**A4 Placebo** N = 228[1]	**A4 Treated** N = 217[1]	**LEARN** N = 279[1]
Baseline Age	72.15 (4.64)	72.26 (5.16)	72.23 (4.48)	72.00 (4.32)
Sex				
Female	457 (63%)	154 (68%)	130 (60%)	173 (62%)
Male	267 (37%)	74 (32%)	87 (40%)	106 (38%)
Years of Education	16.53 (2.60)	16.36 (2.74)	16.72 (2.66)	16.53 (2.42)
APOEε4 Status				
ε4-	398 (55%)	100 (44%)	87 (40%)	211 (76%)
ε4+	325 (45%)	128 (56%)	130 (60%)	67 (24%)
Baseline Global Amyloid Burden	1.20 (0.21)	1.31 (0.16)	1.34 (0.17)	1.00 (0.07)
Baseline p-tau$_{217}$	0.24 (0.15)	0.28 (0.15)	0.28 (0.18)	0.16 (0.06)

[1]Mean (SD); n (%)

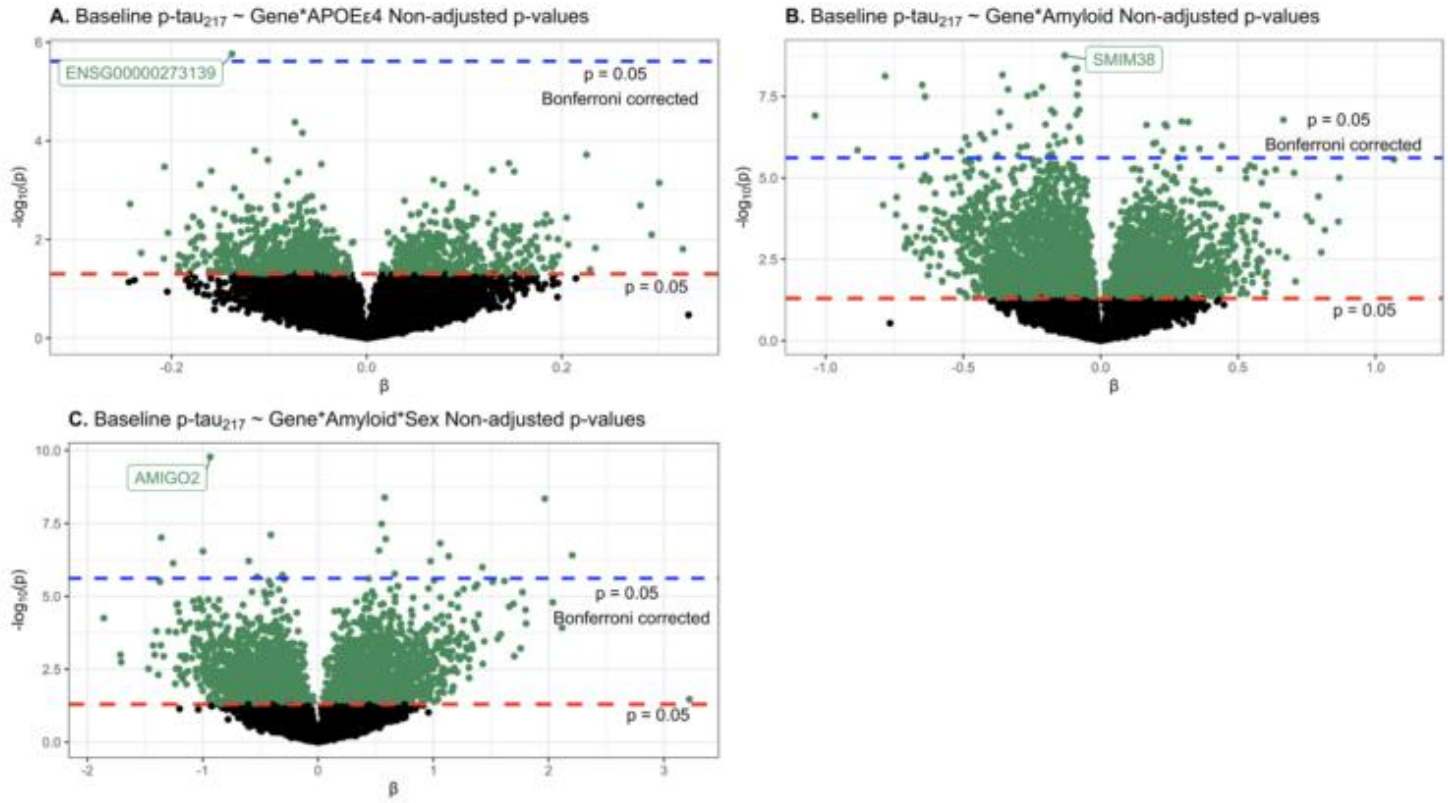


Figure 1. Volcano plots showing the strength and direction of effects of (A) gene*_APOE_ε4, (B) gene*Aβ, and (C) gene*Aβ*sex associations with cross-sectional p-tau$_{217}$. The blue dashed line indicates a multiple comparison corrected threshold, and the red line indicates an uncorrected significance threshold. Strongest hits are tagged with their gene name or Ensembl gene ID (if no gene name exists).

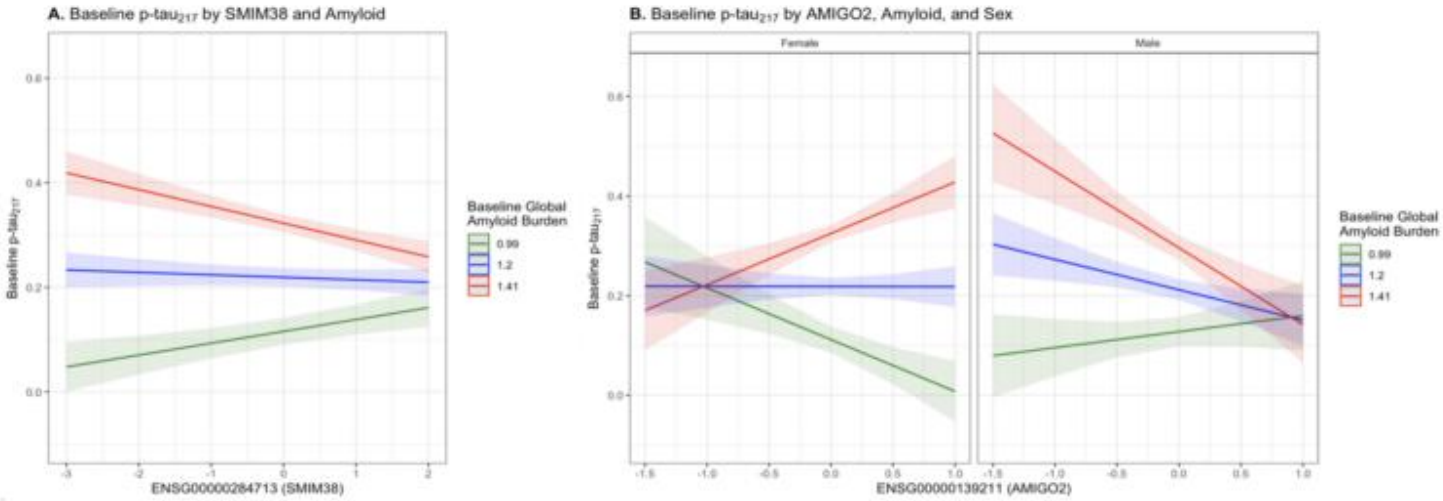


Figure 2. Model estimates predicting p-tau$_{217}$ levels from (A) an RMND1*Aβ interaction and (B) an AMIGO2*Aβ*Sex interaction after adjusting for age, BMI and cohort.

Keywords: plasma, gene expression, amyloid-PET, sex

21 Plasma Aβ as predictor of Aβ accumulation in non-demented participants

Alexandra Gogola[1], Ann Cohen[2], Brian Lopresti[1], Beth Snitz[3], Milos Ikonomovic[4,5], Dana Tudorascu[2], Davneet Minhas[1], Julia Kofler[5], Cristy Matan[1], Howard Aizentein[2], Oscar Lopez[3], Thomas Karikari[2], Victor Villemagne[2]

[1]*Department of Radiology, University of Pittsburgh School of Medicine, Pittsburgh, PA, US*
[2]*Department of Psychiatry, University of Pittsburgh, Pittsburgh, PA, US*
[3]*Department of Neurology, University of Pittsburgh, Pittsburgh, PA, US*
[4]*Geriatric Research Education and Clinical Center, VA Pittsburgh Healthcare System, Pittsburgh, PA, US*
[5]*Department of Pathology, University of Pittsburgh, Pittsburgh, PA, US*

Background: Given the increasing use of plasma biomarkers for Alzheimer's disease (AD) studies, it is necessary to better understand the associations of plasma and PET biomarkers of β-amyloid (Aβ) in relation to Aβ accumulation and conversion from PET A- to A+.

Methods: We evaluated 58 non-demented participants (31 cognitively unimpaired (CU), 27 MCI) from ADNI who had plasma Aβ42 and Aβ40 outcomes and longitudinal Centiloid values. All participants were PET A- at baseline. Participants were split into infra- and suprathreshold groups with a cutoff of 20 CL. Plasma Aβ42/40 values, analyzed through the C_2N mass spectrometry-based assay, were split based on a value of 0.13. Kaplan-Meyer survival and Cox proportional models, accounting for baseline Centiloids, sex, age, and APOE*4 status, evaluated the association of plasma Aβ42/40 status with risk of conversion to PET A+. Linear regression models, adjusting for the same covariates, assessed the association of plasma Aβ42/40 and Centiloid values with Aβ accumulation (CL/yr).

Results: Kaplan-Meyer survival analysis results showed that plasma Aβ status distinctly differentiates PET A- trajectories, predicting conversion to A+ in ~6 years. Cox proportional models found that while categorical plasma Aβ42/40 was not significantly associated with conversion to A+ (p=0.111), it had the largest hazard ratio within the model (8.69). Linear regression models of the continuous measures revealed that plasma Aβ42/40 was significantly associated (all non-demented: b=-142.29, p=0.002; CU-only: b=-162.85, p=0.008) with Aβ accumulation.

Conclusions: The models suggest that plasma Ab in PET A- participants predicts Aβ accumulation, and eventual conversion from A- to A+. This follows the notion that soluble Aβ, measured in plasma or CSF, becomes abnormal before insoluble Aβ measured with PET does. Therefore, plasma Aβ-positive, Aβ-PET negative identify individuals at the very early stages of Aβ accumulation, at risk of progression, and likely to benefit the most from anti-Aβ therapy.

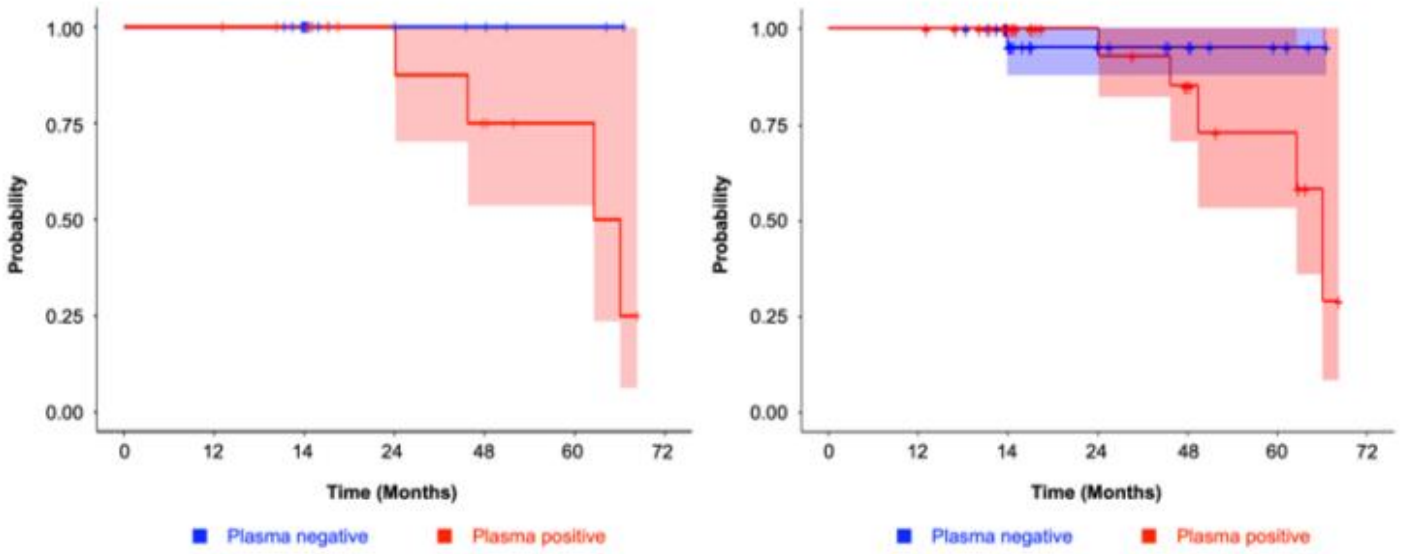


Figure 1. Kaplan-Meyer survival curves for PET A- subjects' risk of converting to A+, split into plasma A+/- groups. CU-only are on the left, all non-demented are on the right.

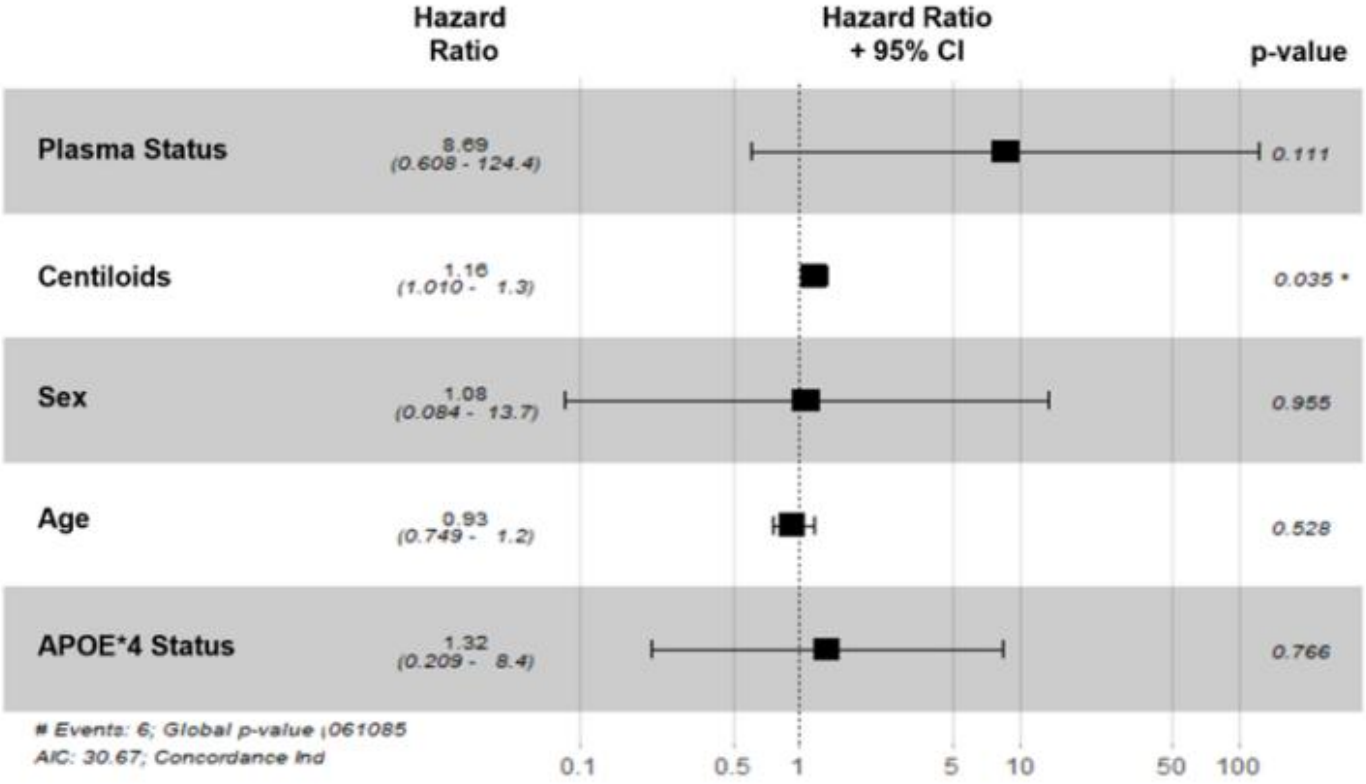


Figure 2. Cox proportional hazards model hazard ratios of all non-demented participants for risk of converting from PET A- to A+ as associated with categorical plasma Aβ42/40, Centiloids, sex, age, and APOE*4 status.

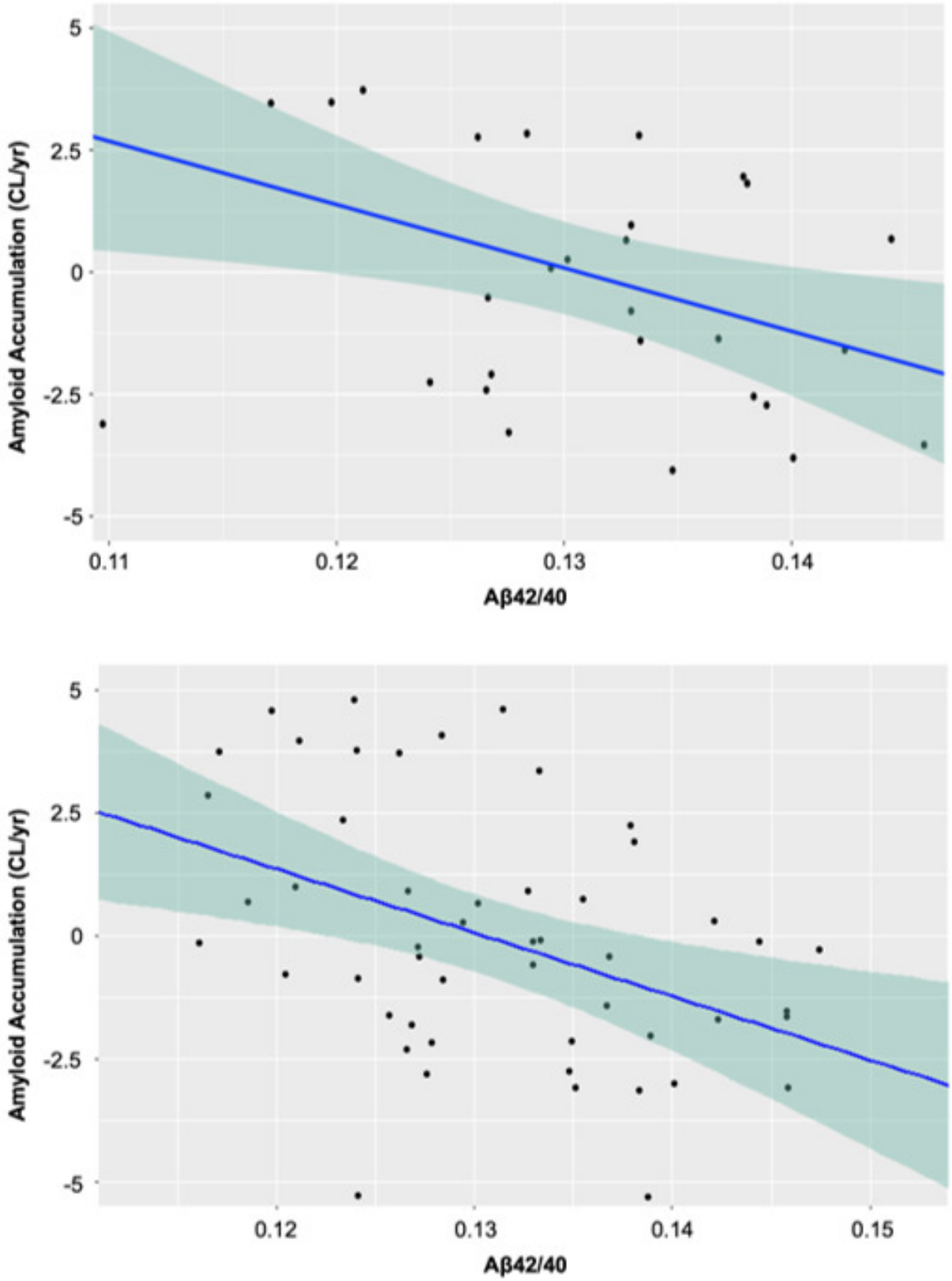


Figure 3. Linear regression of Aβ accumulation, adjusted for Centiloids, sex, age, and APOE*4 status, with plasma Aβ42/40. CU-only are on the top, all non-demented are on the bottom.

Keywords: Plasma Aβ42/40, amyloid PET, amyloid accumulation

22 The relative prevalence of tau severity stages is related to amyloid burden, clinical diagnosis and age

Karly Cody[1], Andrzej Sokolowski[1], Mackenzie Carlson[1], Lucah Medina[1], Joe Winer[1], Christina Young[1], Kyan Younes[1], Alaina Durant[2], Logan Dumitrescu[2], Derek Archer[2], Duygu Tosun-Turgut[3], Sterling Johnson[4], Theresa Harrison[5], Timothy Hohman[2], Elizabeth Mormino[1]

[1]*Department of Neurology and Neurological Sciences, Stanford University, Stanford, CA, US*
[2]*Vanderbilt Memory and Alzheimer's Center, Vanderbilt Genetics Institute, Department of Neurology, Vanderbilt University Medical Center, Nashville, TN, US*
[3]*Department of Radiology, University of California-San Francisco, San Francisco, CA, US*
[4]*Department of Medicine, University of Wisconsin-Madison, Madison, WI, US*
[5]*Neuroscience Department, University of California-Berkeley, Berkeley, CA, US*

Objectives: This study leverages multi-site harmonized PET data from the AD Sequencing Project-Phenotype Harmonization Consortium to characterize the prevalence of tau PET stages along the amyloid continuum.

Methods: Participants (n=2,153; Table 1) from A4, ADNI, SCAN-Prospective, SCAN-Mixed Protocol, and WRAP who underwent amyloid and tau PET imaging were included in this study. PET data corresponding to ligand-specific post-injection windows were processed and harmonized using an MRI-free pipeline. Amyloid PET SUVRs were translated to centiloids (CLs) and regional tau positivity (T+/-) was derived within ligand using gaussian mixture modeling. A hierarchical staging schema was used to classify tau severity (e.g. T-, T12+, T34+, T56+). The cumulative probability of hierarchical tau stages was estimated according to CLs, age, and clinical stage (e.g. CU, MCI, Dementia) using ordinal logistic regression models.

Results: The frequency and spatial extent of T+ generally increased with CL level and clinical stage (Figure 1). Analyses estimating the cumulative prevalence of tau stages indicated significant CL×clinical stage, CL×age, and age×clinical stage interactions, suggesting that the age- and CL-related probability of tau stages differed by clinical stage and that CL-related probability differed by age. Overall, we found that the prevalence of tau stages reflected the expected trend that both increasing CLs and increasing clinical severity corresponded to a higher likelihood of tau PET severity (Figure 2A). Additionally, we observed that the effect of CL and clinical stage was moderated by age (Figure 2B). Among individuals with impairment, the probability of late-stage tau (T56+) was highest among those with younger ages and higher CLs. By contrast, the age effect was diminished in CUs at high CLs as well as at lower CLs in MCI and dementia.

Discussion: Heterogeneity in tau PET severity has important implications for clinical trial design and for inferring contributions of the AD pathway to clinical impairment.

Table 1. Participant Characteristics

Characteristic	Overall N = 2,153	CU N = 1,551	MCI N = 425	Dementia N = 177	p-value[a]
Cohort					<0.001
A4	447 (21%)	447 (29%)	0 (0%)	0 (0%)	
ADNI	917 (43%)	490 (32%)	310 (73%)	117 (66%)	
NACC[b]	487 (23%)	327 (21%)	102 (24%)	58 (33%)	
WRAP	302 (14%)	287 (19%)	13 (3%)	2 (1%)	
Tau PET Tracer					<0.001
FTP	1,563 (73%)	1,026 (66%)	373 (88%)	164 (93%)	
MK	590 (27%)	525 (34%)	52 (12%)	13 (7%)	
Age (yrs)	72 (8)	71 (8)	75 (8)	75 (9)	<0.001
Education (yrs)	16 (3)	16 (3)	16 (3)	16 (3)	0.008
Sex					<0.001
Female	1,223 (57%)	949 (61%)	196 (46%)	78 (44%)	
Male	930 (43%)	602 (39%)	229 (54%)	99 (56%)	
APOE e4 status					<0.001
e4-	1,105 (58%)	853 (60%)	192 (58%)	60 (39%)	
e4+	803 (42%)	572 (40%)	139 (42%)	92 (61%)	
Centiloids	31 (42)	26 (37)	35 (48)	69 (50)	<0.001
Tau PET stage[c]					<0.001
T-	1,573 (73%)	1,275 (82%)	250 (59%)	48 (27%)	
T12+	222 (10%)	151 (10%)	53 (12%)	18 (10%)	
T34+	111 (5%)	48 (3%)	42 (10%)	21 (12%)	
T56+	175 (8%)	35 (2%)	60 (14%)	80 (45%)	
Discordant	72 (3%)	42 (3%)	20 (5%)	10 (6%)	

Values shown as n (%) or Mean (SD)

[a]Pearson's Chi-squared test; Kruskal-Wallis rank sum test

[b]NACC included PET data from SCAN-Prospective and SCAN-Mixed Protocol

[c]Tau PET positivity was quantified in regions corresponding to Braak staging and individuals were assigned a hierarchical tau PET stage, where later stages could only be achieved if the individual was tau positive in previous stages. Individuals who did not follow the hierarchical staging were classified as discordant.

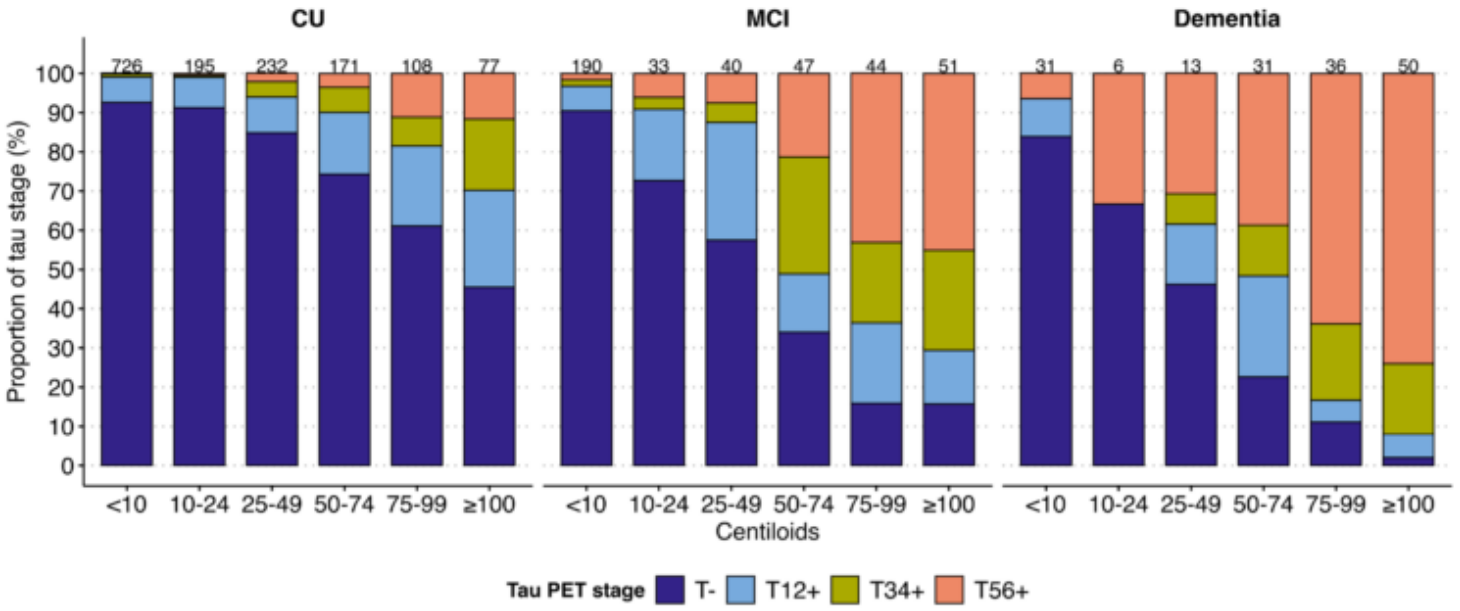


Figure 1. The observed frequency of hierarchical tau PET stages is shown across amyloid levels, measured by centiloids, and by clinical stage. Among individuals with a hierarchical pattern of tau PET positivity (n=2081 (97% of the total sample), the percentage of tau negative (e.g. T-) and tau positive (e.g. T12+, T34+,T56+) individuals is shown in stacked bar plots across centiloids bins and clinical stages. The spatial extent of regional T+ generally increased with both increasing CL level and with increasing clinical severity. Notably, within a single amyloid level, like 50-74 CL, all tau stages were observed in each clinical stage, indicating heterogeneity in tau severity along the Alzheimer's disease continuum. CU = cognitively unimpaired; DEM = dementia; MCI = mild cognitive impairment.

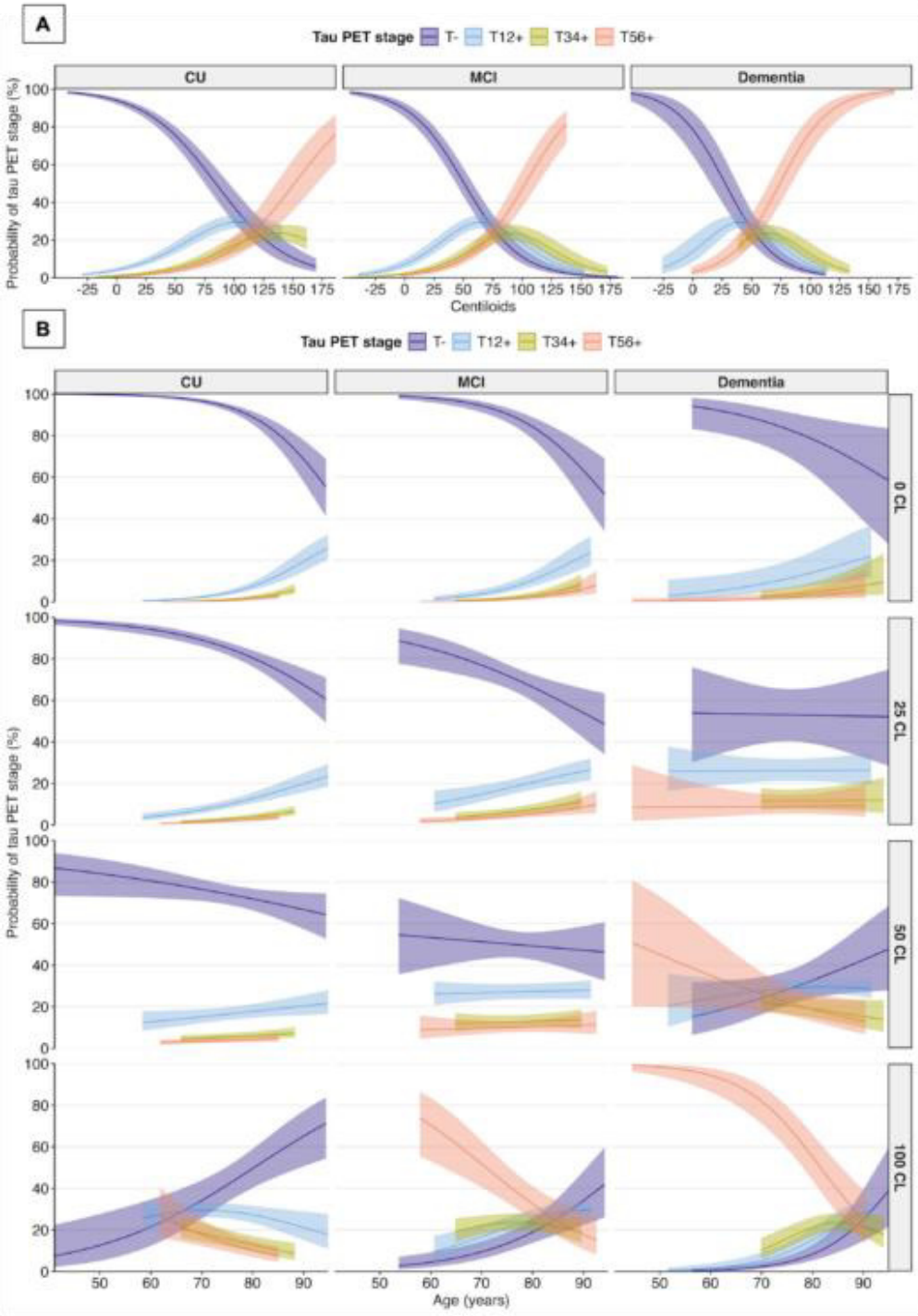


Figure 2. The cumulative prevalence of hierarchical tau PET stages was modeled using centiloids (P<.001), age (P<.001), clinical stage (P<.001), cohort (P<.001), centiloids by clinical stage (P<.001), and centiloids by age (P<.001) and age by clinical stage (P<.001) as risk factors. Shaded areas indicate the 95% CI's for the probability estimates for the ranges of centiloids (Panel A) or ages (Panel B) observed in each tau PET and clinical stage. **Panel (A)** shows the estimated amyloid-related prevalence of tau stages. Across clinical stages, the pattern of amyloid-related prevalence curves for each tau PET stage were similar, such that the prevalence estimates of remaining T- decreased with increasing CLs, estimates for T12+ and T34+ peaked, and estimates of T56+ increased with increasing CLs. While the peak probabilities for T12+ and T34+ were similar across all clinical stages (~30% T12+,~24% T34+), the CL value at which the prevalence curve peaked for T12+ and T34+ differed considerably by clinical stage. On average, T12+ peaked earlier than T34+ and the peak CL value progressively decreased with increasing clinical stage (CU> MCI>Dementia; Peak T12+ 103CL > 65CL> 41CL; Peak T34+ 137CL > 91CL > 64CL). **Panel (B)** details the age-related prevalence of tau stages by amyloid level across clinical stages. The estimated probability of T12+, T34+, and T56+ generally increased with increasing age in CU and MCI, indicating a higher likelihood of tau positivity with older age prior to dementia. Additionally, we observed that the effect of age was moderated by amyloid level and diagnosis. At higher CLs in MCI and dementia, the probability of late-stage tau (T56+) decreased with age, such that the likelihood of T56+ was highest in the presence of clinical impairment among those with younger ages and higher CLs.

Keywords: amyloid PET, tau PET

23 Head-to-head trajectories of tau PET and plasma p-tau217 as a function of Aβ

Bruna Bellaver[1], Guilherme Povala[1], Pamela L. Ferreira[1], Guilherme Bauer-Negrini[1], Firoza Lussier[1], Livia Amaral[1], Carolina Soares[1], Andreia Rocha[1], Joseph Masdeu[2], Dana Tudorascu[1], David Soleimani-Meigooni[4], Juan Fortea[5], Val Lowe[6], Hwamee Oh[7], Belen Pascual[2], Brian A. Gordon[8], Pedro Rosa-Neto[9], Suzanne Baker[3], Tharick A. Pascoal[1]

[1]*University of Pittsburgh, Department of Psychiatry, PA, United States of America, Pittsburgh, PA, US*
[2]*Houston Methodist Research Institute, Department of Neurology, Houston, TX, United States of America, Houston, TX, US*
[3]*Lawrence Berkeley National Laboratory, Berkeley, CA, United States of America, Berkeley, CA, US*
[4]*University of California San Francisco, Memory and Aging Center, San Francisco, CA, United States of America, San Francisco, CA, US*
[5]*Hospital de la Santa Creu i Sant Pau, Sant Pau Memory Unit, Department of Neurology, Barcelona, Spain, Barcelona, ES*
[6]*Mayo Clinic, Department of Radiology, Rochester, MN, United States of America, Rochester, MN, US*
[7]*Brown University, Department of Psychiatry and Human Behavior, Providence, RI, United States of America, Providence, RI, US*
[8]*Washington University in St. Louis, Department of Radiology, St. Louis, MO, United States of America, St. Louis, MO, US*
[9]*Translational Neuroimaging Laboratory, McGill University Research Centre for Studies in Aging, Douglas Research Institute, Montréal, QC,, Montreal, CA*

Background: Tau PET tracers present distinct binding characteristics that might influence their trajectories and relationship with other biomarkers along the AD continuum. In a head-to-head study, we investigated the relationship between the emergence of PET tracers MK6240 and Flortaucipir, and plasma p-tau217 abnormalities as a function of Aβ PET deposition. We further assessed the concordance between tau PET and plasma p-tau217 positivity.

Methods: We assessed 353 individuals from the HEAD study (205 cognitively unimpaired and 148 cognitively impaired) with Aβ PET, MK6240 and Flortaucipir tau PET, and plasma p-tau217 (AlzPath) measures. Tau PET and plasma p-tau217 trajectories were modeled as functions of Aβ burden (Centiloid scale) using the Lowess method. Biomarkers were z-scored using young individuals (n=19, <25 years old) as anchors. Tau PET (Braak 1 region) and plasma p-tau217 were considered positive/abnormal when surpassing 2.5 z-score.

Results: Among the tested markers, MK6240 was the earliest to show abnormality as a function of Centiloid, occurring at Centiloid 21, followed by plasma p-tau217 at Centiloid 37 and Flortaucipir at Centiloid 54 (Fig. 1). Tau PET and plasma p-tau217 positivity showed an overall high concordance (~81% for both tracers; Fig. 2). In MK6240 discordant cases, most individuals were MK6240+/p-tau217- (13.1%), while 6.6% were MK6240-/p-tau217+ (Fig. 2A). For Flortaucipir, 15.4% of discordant cases were Flortaucipir-/p-tau217+, while 4.3% were Flortaucipir+/p-tau217- (Fig. 2B). Most individuals were concordant for tau PET and p-tau217 at Centiloid levels above 50 (>90%; Fig. 2C). Fig. 3 shows representative images of four cases with discordant tau PET/p-tau217 status.

Conclusions: MK6240 becomes abnormal at lower levels of Aβ burden compared to plasma p-tau217 and Flortaucipir. The relatively high prevalence of discordant tau PET positive or plasma p-tau217 positive suggests that some individuals may show tau PET positivity first, while others may exhibit plasma p-tau217 positivity first.

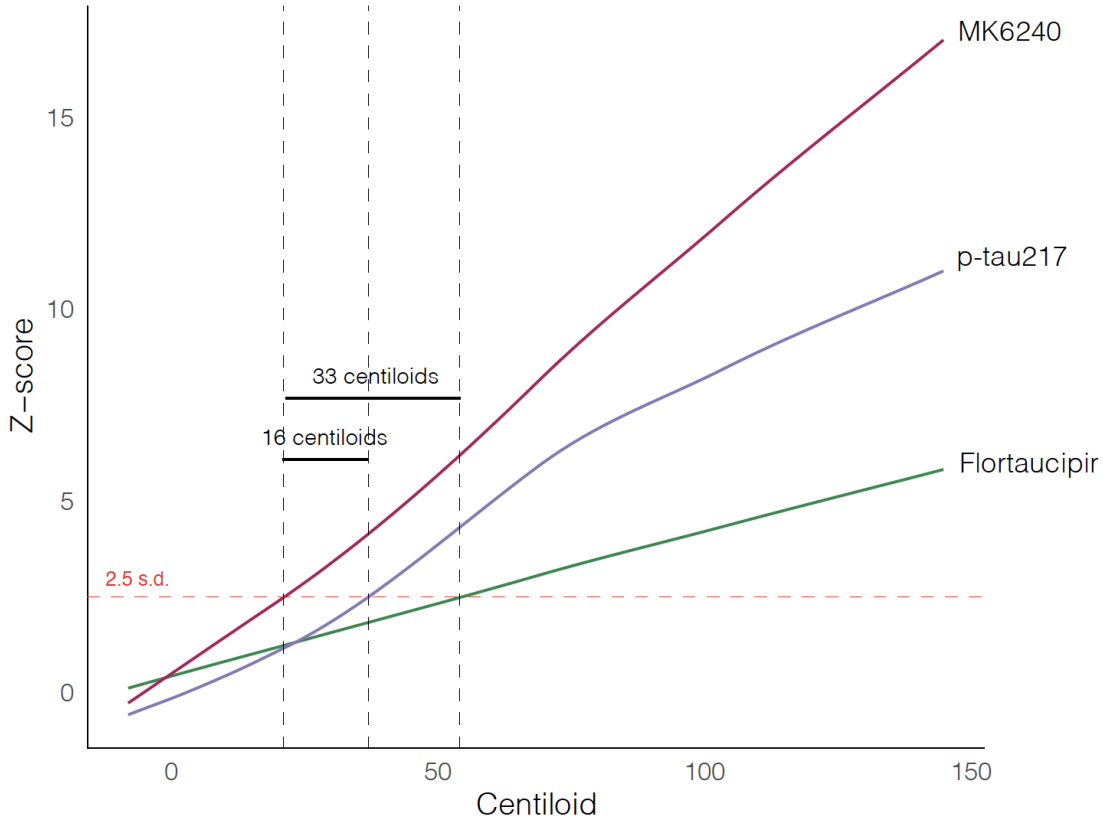


Fig. 1. Robust linear regressions show [18F]MK6240 (Braak 1 region), [18F] Flortaucipir (Braak 1 region) and plasma p-tau217 increases as a function of Aβ burden (n = 353). Young individuals (n=19, <25 years old) were used as anchors to z-scores.

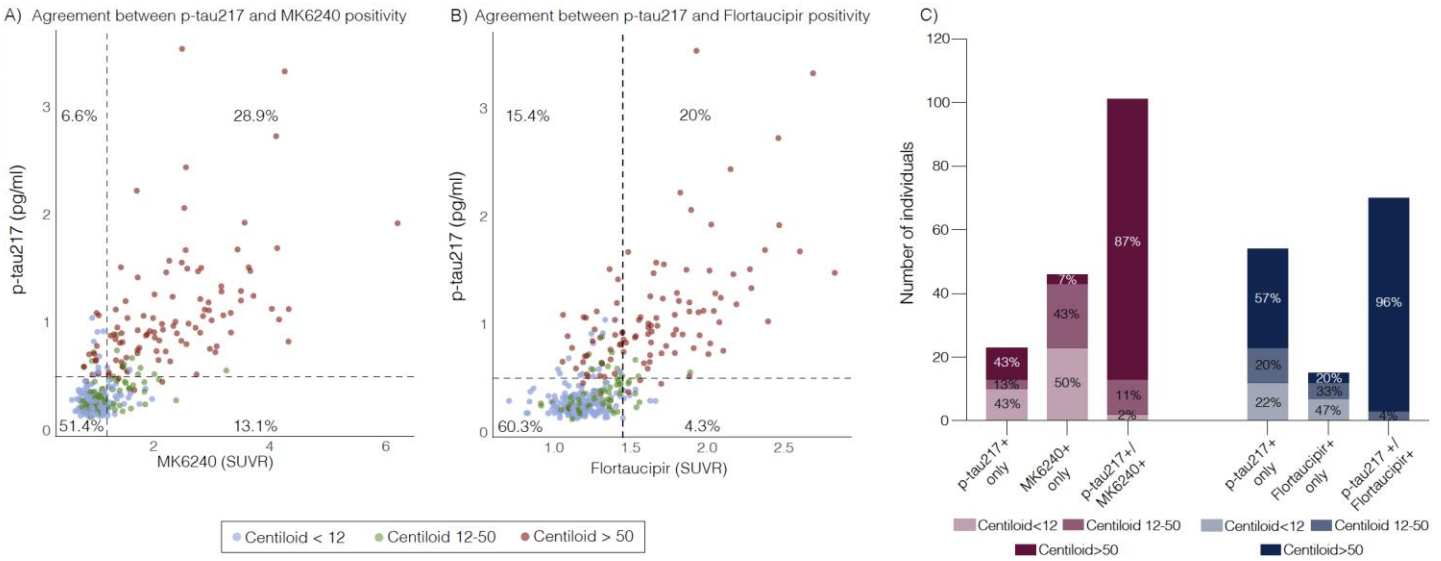


Fig. 2. Agreement between plasma p-tau217 and (A) MK6240 or (b) Flortaucipir postivity. The dotted lines represent cutoff for plasma p-tau217 and tau PET (in Braak 1 region) defined as 2.5 s.d. higher than the mean of young individuals. (C) Number of individuals according to their p-tau217, MK6240 and Flortaucipir status and Centiloid distribution.

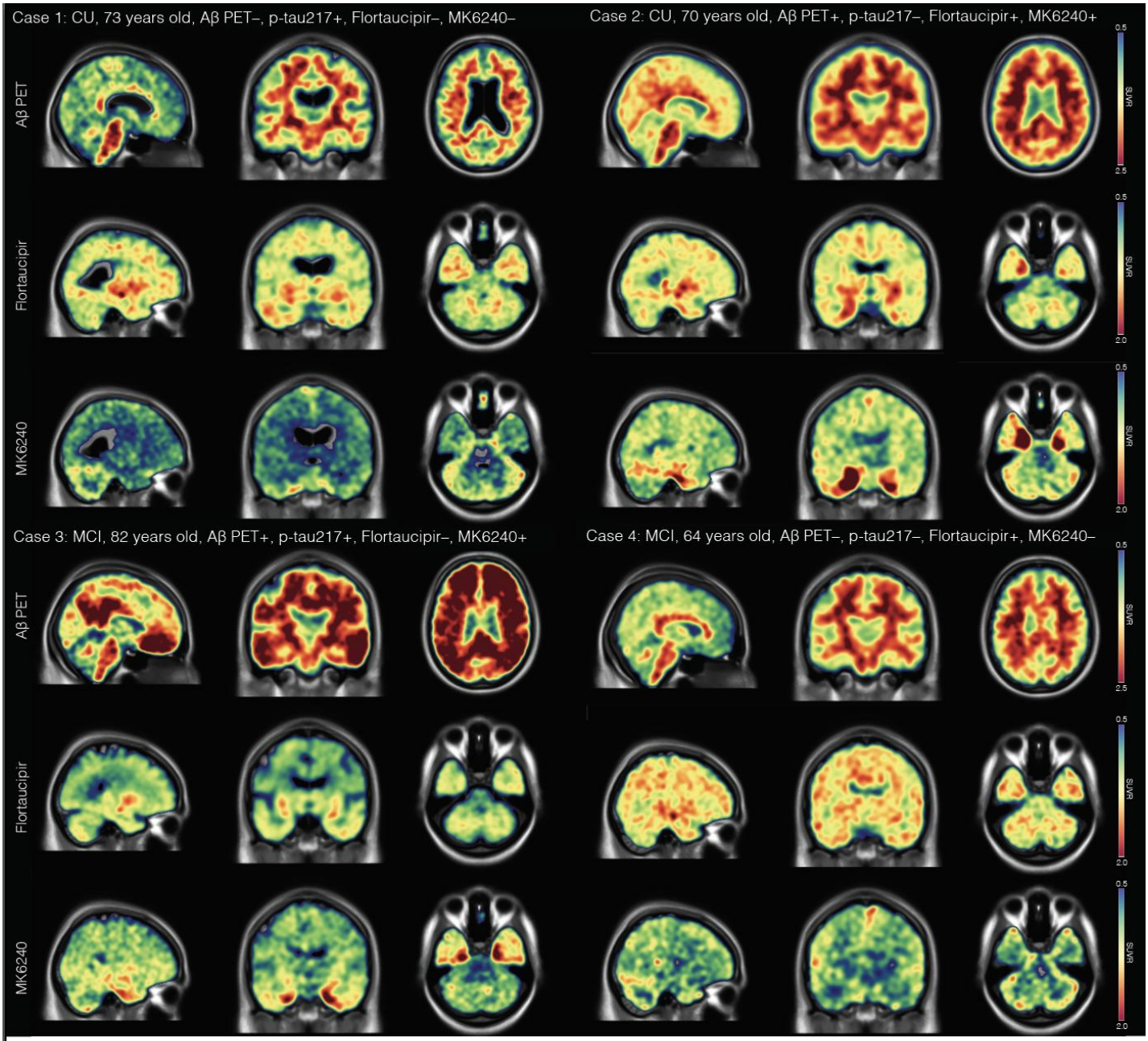


Fig 3 shows four cases of discordant tau PET and plasma p-tau217 individuals. Case 1: cognitively unimpaired (CU), 73 years old plasma p-tau217 positive individual with negative scan for Aβ PET (PIB), Flortaucipir and MK6240. Case 2: CU 70 years old individual plasma p-tau217 negative (0.28 pg/ml measured in duplicate; threshold for positivity = 0.504 pg/ml) with positive Aβ PET (AZD4694), Flortaucipir and MK6240. Case 3: MCI, 82 years old positive for plasma p-tau217, Aβ PET (PIB) and MK6240 but negative for Flortaucipir. Case 4: MCI, 64 years old negative for plasma p-tau217, Aβ PET (AZD4694) and MK6240 but positive for Flortaucipir.

Keywords: biomarkers; tau PET; plasma p-tau

24 Functional submodules in the human locus coeruleus are differentially susceptible to tau pathology

Timothy Lawn[1], Prokopis C. Prokopiou[1], Maxime Van Egroo[1,2], Nicholas J. Ashton[3,4,5,6], Shorena Janelidze[7], Kaj Blennow[8,9], Oskar Hansson[7,10], Henrik Zetterberg[3,11,12,13,14], Heidi I. L. Jacobs[1,2]

[1]*Athinoula A. Martinos Center for Biomedical Imaging, Department of Radiology, Massachusetts General Hospital and Harvard Medical School, 02129, Boston, MA, USA, Boston, MA, US*
[2]*Faculty of Health, Medicine and Life Sciences, School for Mental Health and Neuroscience, Alzheimer Centre Limburg, Maastricht University, Maastricht, The Netherlands, Maastricht, NL*
[3]*Department of Psychiatry and Neurochemistry, Institute of Neuroscience and Physiology, The Sahlgrenska Academy at the University of Gothenburg, Mölndal, Sweden, Mölndal, SE*
[4]*Centre for Age-Related Medicine, Stavanger University Hospital, Stavanger, Norway, Stavanger, NO*
[5]*King's College London, Institute of Psychiatry, Psychology and Neuroscience, Maurice Wohl Institute Clinical Neuroscience Institute, London, UK, London, GB*
[6]*NIHR Biomedical Research Centre for Mental Health and Biomedical Research Unit for Dementia at South London and Maudsley NHS Foundation, London, UK, London, GB*
[7]*Clinical Memory Research Unit, Department of Clinical Sciences Malmö, Lund University, Lund, Sweden, Lund, SE*
[8]*Department of Psychiatry and Neurochemistry, Institute of Neuroscience and Physiology, The Sahlgrenska Academy at the University of Gothenburg, Mölndal, Sweden, Mölndal, SE*
[9]*Clinical Neurochemistry Laboratory, Sahlgrenska University Hospital, Mölndal, Sweden, Mölndal, SE*
[10]*Memory Clinic, Skåne University Hospital, Malmö, Sweden, Malmö, SE*
[11]*Clinical Neurochemistry Laboratory, Sahlgrenska University Hospital, Mölndal, Sweden, Mölndal, SE*
[12]*Department of Neurodegenerative Disease, UCL Institute of Neurology, Queen Square, London, UK, London, GB*
[13]*UK Dementia Research Institute at UCL, London, UK, London, GB*
[14]*Hong Kong Center for Neurodegenerative Diseases, Clear Water Bay, Hong Kong, China, Hong Kong, CN*

Background: The locus coeruleus(LC) is amongst the earliest brain regions to accrue tau pathology in Alzheimer's disease(AD), with its dorso-rostral portion being more vulnerable. This pathology may diminish LC neurons capacity to deploy their full repertoire of varying tonic and brief phasic activity to meet task demands. Here, we examine functional vulnerability within the LC, hypothesising dorso-rostral activity shows selectively reduced task-related variability with increasing tau pathology.

Methods: 87 individuals from a lifespan-cohort(table-1) underwent 7T task-fMRI(high/low arousal images), provided samples for plasma biomarkers(pTau181, pTau217, and pTau231), and completed the Preclinical Alzheimer Cognitive Composite(PACC). We utilised Hursts exponent(HE) to quantify the temporal structure of BOLD fluctuations in each voxel across the entire timeseries, with higher values representing lower variability. Agglomerative hierarchical clustering was applied to within-LC connectivity matrices to delineate functionally similar submodules. Robust linear models tested if submodular or caudo-rostral gradients of HE were related to(or moderated the relationship between) pTau and PACC, controlling for age, sex, education, and framewise displacement.

Results: Rostral HE was positively associated with pTau231 and pTau181, and this was stronger than middle/caudal HE for pTau231(fig-1B/C). Rostral HE was negatively associated with PACC(fig-1D), but did not moderate the relationship between pTau231 or pTau181 and PACC(fig-1E/F). The caudo-rostral HE gradient(fig-2A) was also associated with both pTau231(fig-2B) and pTau181(fig-2C), with lower caudal-vs-rostral values corresponding to elevated pTau levels. Whilst HE gradients did not directly relate to PACC, higher gradients were associated with worse cognitive performance at higher pTau231 and pTau181(fig-2D/E). No relationships were found for pTau217.

Conclusion: The human LC shows selectively lower rostral BOLD signal variability with higher tau pathology and worse cognitive performance, potentially reflecting a reduced capacity to modulate its activity to meet task-related demands. Together, these findings suggesting LC (dys)function may be an early marker of AD-related processes.

Table-1: Demographic, plasma biomarker, and imaging values within the study sample.

Overall, 87 participants were included, but due to missing data some analyses utilise only a subset, as denoted by the number of subjects column. Continuous variables are presented as mean ± SD (range) and categorical variables are presented as count (percentage).

Demographics	**Summary**	**Number of subjects**
Age (years)	60.14 ± 13.49 (31- 87)	87
Sex	F 47 (54.0%), M 40 (46.0%)	87
E4 status	Non-carrier 54 (62.8%), Carrier 32 (37.2%)	86
Education (years)	14.23 ± 2.03 (6 - 20)	86
PACC	0.07 ± 0.61 (-1.70 - 1.20)	86
Plasma biomarkers		
pTau217 (pg/ml)	0.27 ± 0.119 (0.11 - 0.81)	82
pTau231 (pg/ml)	8.64 ± 3.956 (3.292 - 28.94)	82
pTau181 (pg/ml)	1.69 ± 0.80 (0.80 - 6.44)	77
Imaging		
Framewise displacement (mm)	0.036 ± 0.019 (0.014 - 0.110)	87
Hursts exponent (rostral)	0.516 ± 0.030 (0.453 - 0.652)	87
Hursts exponent (middle)	0.519 ± 0.025 (0.477 - 0.584)	87
Hursts exponent (caudal)	0.526 ± 0.023 (0.475 - 0.626)	87
Hursts exponent caudo-rostral gradient	-0.001 ± 0.003 (-0.008 - 0.008)	87

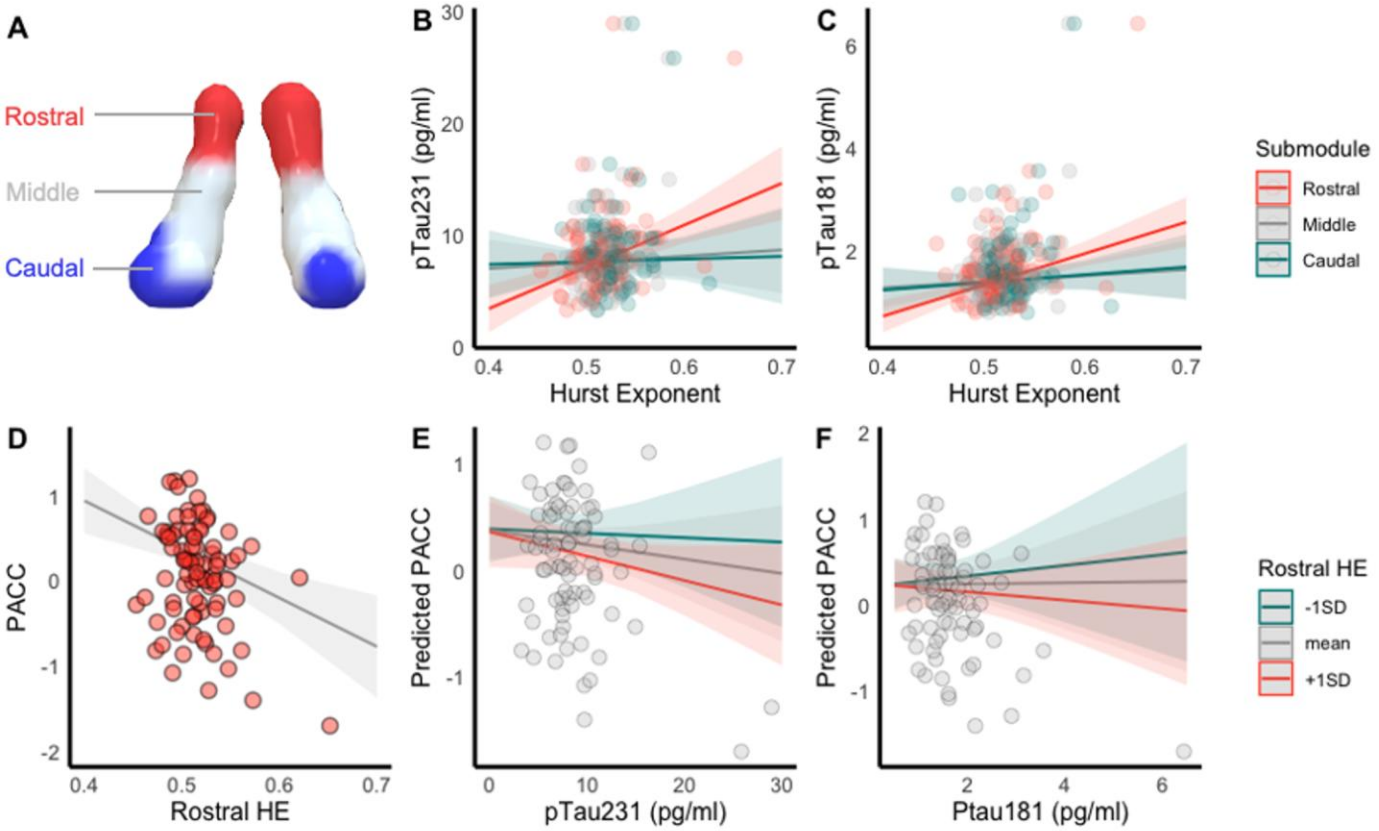


Figure-1: Relationships between voxelwise HE, plasma tau, and cognition.

(A) Hierarchical clustering applied to within-LC connectivity matrices delineated a 6 cluster solution which we bilateralised to give three rostral (red), middle (grey), and caudal (blue) submodules. **(B, C)** HE within these submodules showed differential relationships to plasma tau, with stronger relationships between HE and ptau231 in the rostral compared to both the middle (β = -31.90, SE = 14.19, t(236) = -2.25, p = 0.037) and caudal (β = -35.01, SE = 15.33, t(236) = -2.28, p = 0.033) submodules. There was also a trend towards stronger relationships between HE and pTau181 in the rostral compared to both the middle (β = -4.93, SE = 2.47, t(221) = -2.00, p = 0.075) and caudal (β = -4.63, SE = 2.68, t(221) = -1.73, p = 0.122) submodules. **(D)** Rostral HE values were negatively associated with PACC scores (β = -5.70, SE = 1.61, t(80) = -3.55, p < 0.001). Shaded area represents the 95% confidence interval. **(E, F)** Rostral HE did not moderate the relationship between plasma tau markers and PACC scores for pTau231 (β = -0.31, SE = 0.25, t(74) = -1.27, p = 0.212) or pTau181 (β = -1.84, SE = 1.07, t(69) = -1.73, p = 0.088). Lines represent the relationship between tau levels and PACC scores at different levels of rostral HE: mean (grey), 1 standard deviation below the mean (green), and 1 standard deviation above the mean (orange). Shaded areas represent 95% confidence intervals.

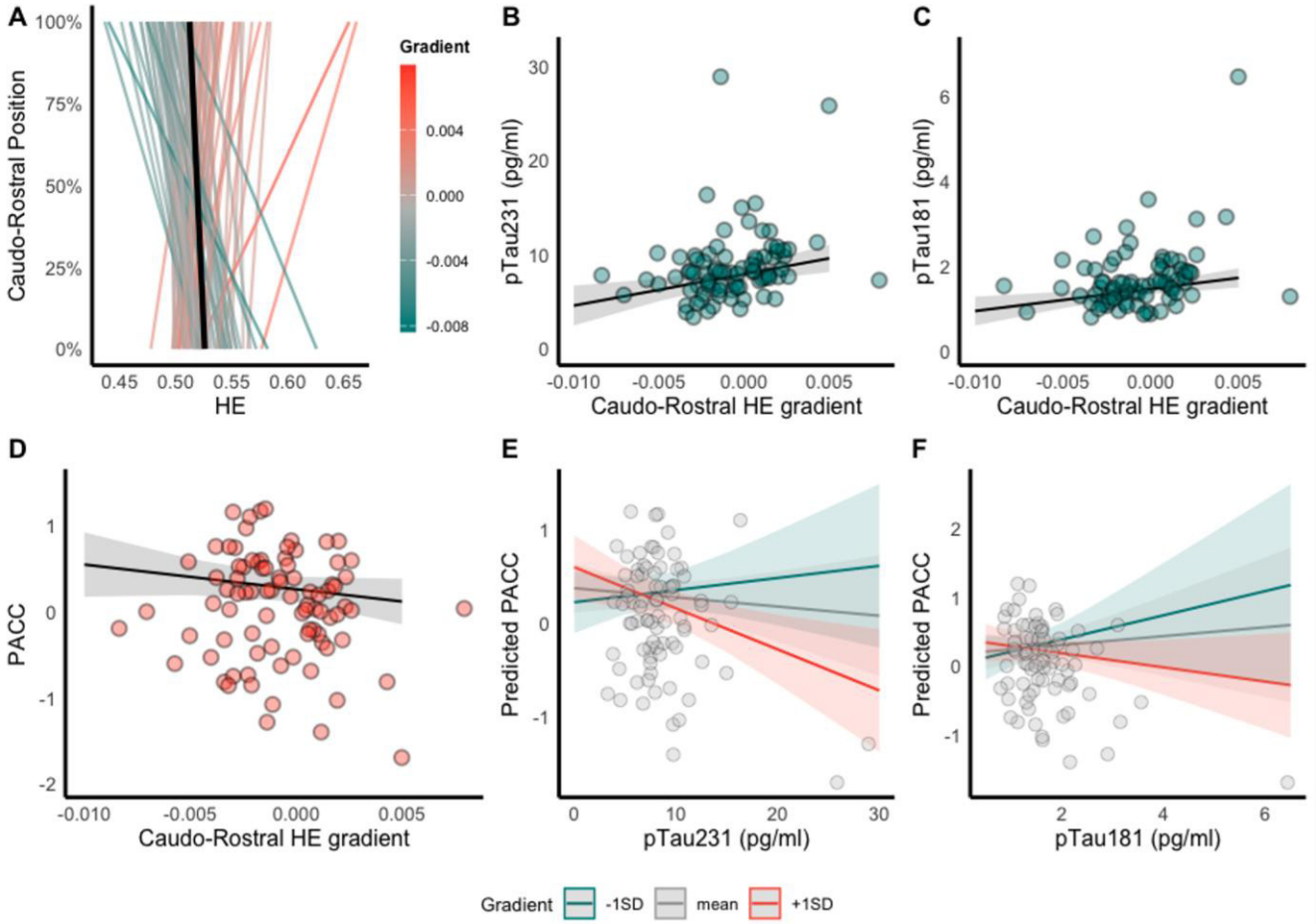


Figure-2: Relationships between the caudo-rostral gradient of HE, tau biomarkers, and cognition.

(A) Caudo-rostral gradients of Hurst Exponent (HE) across the Locus Coeruleus (LC). Each line represents an individual subject, showing the relationship between Z-coordinates and HE values across all LC voxels. Lines therefore depict the change in HE values along the Z (caudo-rostral) axis of the LC. The y-axis represents the normalized position along the caudo-rostral axis, from most caudal (0%) to most rostral (100%). The average gradient is shown in black. **(B, C)** The caudo-rostral HE gradient was positively associated with pTau231 (β = 336.01, SE = 110.05, t(76) = 3.05, p = 0.004) and pTau181 (β = 51.91, SE = 19.59, t(71) = 2.65, p = 0.016). Shaded areas represent 95% confidence intervals. **(D)** The caudo-rostral HE gradient was not related to PACC (β = -28.70, SE = 20.48, t(80) = -1.40, p = 0.168). **(E, F)** Higher caudo-rostral HE gradients were associated with lower PACC scores in the presence of greater tau pathology for both pTau231 (β = -11.39, SE = 4.49, t(74) = -2.53, p = 0.016) and pTau181 (β = -56.07, SE = 21.69, t(69) = -2.59, p = 0.012). Lines represent the relationship between tau levels and PACC scores at different levels of the HE gradient: mean (grey), 1 standard deviation below the mean (green), and 1 standard deviation above the mean (orange). Shaded areas represent 95% confidence intervals.

Keywords: Locus Coeruleus, Cognition, Tau, Preclinical Alzheimer's disease, fMRI

25 Sex-specific associations of BMI, amyloid, and regional tau deposition in community-dwelling cognitively normal older adults

Joshua Gills[1], Oliver Cesar[1], Joanna Dominguez[1], Anamarie Sogade[1], Laurel Browne[1], Elizabeth Weisgerber[1], Julian McBride[1], Elena Valkanova[2], Alfred Mbah[2], Luisa Figueredo[1], Girardin Jean-Louis[3], Arjun Masurkar[1], Ricardo Osorio[1], Omonigho Michael Bubu[1]

[1]*New York University Grossman School of Medicine, New York City, NY, US*
[2]*University of South Florida, Tampa, FL, US*
[3]*Miami University Miller School of Medicine, Miami, FL, US*

Introduction: Increased body mass index (BMI) in mid-life is associated with a higher risk of Alzheimer's disease (AD). Neurofibrillary tangles (NFTs), comprised of hyperphosphorylated aggregated tau protein, are the pathological hallmark of neurodegenerative tauopathies including Alzheimer's Disease (AD). The relationship between sex-dependent adiposity in late adulthood and tau NFT pathology remain inconclusive. We examined sex differences between BMI and PET tau pathology among cognitively normal individuals.

Methods: This cross-sectional analysis consisted of 104 community-dwelling cognitively normal older adults (mean±SD; males (*n*=42): age=72.8±6.5y; females (*n*=62): age=72.6±6.8y) from ongoing NYU longitudinal studies on memory and aging. Subjects completed clinical assessments and two PET scans (FBB and ^{18}F- PI2620). Standard uptake value ratio (SUVR) values from images were computed using FreeSurfer, and normalizing to cerebellar grey matter. For tau, data were analyzed from composite regions corresponding to Braak pathological stages I–VI, and control brain regions not expected to contain NFTs including the pericalcarine cortex, corpus callosum, and caudate nucleus. Linear mixed effects regression models examined association between BMI, sex, BMI*sex, PET SUVR amyloid & tau. Models were adjusted for age, race, and ApoE status.

Results: Relative to females, males were on average slightly more educated (males, females; 17.0±2.4y, 16.6±2.1y), had similar BMI (29.6±10.3 kg/m^2, 29.5±10.8 kg/m^2), and had higher blood pressure (Systolic/diastolic; 168.4/116.3 mmHg, 156.9/100.7 mmHg). Sex and BMI were each associated with both SUVR amyloid and tau (p<0.05 for all). Males with higher BMI, showed increased SUVR tau (β[IV]= β[SE]; β[BMI*sex]=0.0054[0.0025],p=0.031), corresponding to Braak stage I (β[BMI*sex]=0.0122[0.0055],p=0.032), Braak stage III (β[BMI*sex]=0.0054[0.0025],p=0.034), Braak stage IV (β[BMI*sex]=0.0058[0.0020],p=0.006), Braak stage V (β[BMI*sex]=0.0048[0.0019],p=0.014), and Braak stage VI (β[BMI*sex]=0.0039[0.0017],p=0.026).

Conclusion: In this sample of community-dwelling cognitively normal older adults, higher BMI in males was associated with increased tau NFT burden. Thus, excessive adiposity in late-life may contribute to Alzheimer's disease pathology for males.

Keywords: Body Mass Index, Sex, Amyloid, Tau

26 Assessment of ATN with a single dynamic [18]F-PI-2620 recording

Johannes Gnörich[1,2], Julia Kusche-Palenga[1], Agnes Kling[1], Artem Zatcepin[1,2], Amir Dehsarvi[3], Angela Bronte[4], Mirlind Zaganjori[1], Lukas Frontzkowski[1,3], Sebastian Roemer[3,5], Mattes Groß[1], Florian Schöberl[5], Maximilian Scheifele[1], Theresa Bauer[1], Alexander Bernhardt[2,5], Alexander Jäck[2,5], Thilo van Eimeren[6,7], Alexander Drzezga[6,7], Robert Perneczky[11], Katharina Bürger[3], Johannes Levin[5], Peter Bartenstein[1], Osama Sabri[10], Henryk Barthel[10], Michael Rullmann[10], Sophia Stöcklein[8], Günter Höglinger[5,9], Nicolai Franzmeier[3,9,12], Matthias Brendel[1,2,9]

[1]*Department of Nuclear Medicine, University Hospital, LMU Munich, Munich, DE*
[2]*German Center for Neurodegenerative Diseases (DZNE) Munich, Munich, DE*
[3]*Institute for Stroke and Dementia Research, LMU Munich, Munich, DE*
[4]*Universidad de Navarra, Pamplona, Pamplona, ES*
[5]*Department of Neurology, LMU Munich, Munich, Munich, DE*
[6]*Department of Nuclear Medicine, University Hospital Cologne, Cologne, DE*
[7]*German Center for Neurodegenerative Diseases (DZNE), Bonn, Bonn, DE*
[8]*Department of Radiology, LMU Hospital, Ludwig-Maximilians-University of Munich, Munich, DE*
[9]*Munich Cluster for Systems Neurology (SyNergy), Munich, DE*
[10]*University Hospital Leipzig, Department of Nuclear Medicine, Leipzig, DE*
[11]*Department of Psychiatry and Psychotherapy, Ludwig-Maximilians-University,, Munich, DE*
[12]*University of Gothenburg, The Sahlgrenska Academy, Institute of Neuroscience and Physiology, Department of Psychiatry and Neurochemistry, Mölndal and Gothenburg, SE*

Patients with neurodegenerative diseases are classified molecularly using the A/T/N classification system. Apart from fluid biomarkers and structural MRI, the three-dimensional A/T/N system utilizes characteristic features from amyloid-PET (A), tau-PET (T), and FDG-PET (N), requiring multiple imaging sessions. Thus, we evaluated the value of dynamic tau-PET with [^{18}F]PI-2620 to assess A/T/N in individual patients during a single imaging session. Cortical tissue clearance (K2a) of [^{18}F]PI-2620 was validated as a surrogate of the β-amyloid status against amyloid-PET and cerebrospinal fluid (CSF) $A\beta_{42/40}$ ratio, demonstrating remarkable positive (91.5%) and negative (95.1%) predictive values at an AUC of 0.99 ($P<0.0001$). K2a outperformed cortical tau burden (DVR) as a surrogate for β-amyloid status in 47 participants with a clinical diagnosis of probable AD (3/4-repeat(R)-tauopathy) and 82 amyloid-negative controls with possible or probable corticobasal syndrome (CBS) and progressive supranuclear palsy (PSP) (4R-tauopathies). Perfusion [^{18}F]PI-2620 images (R1) were validated as a surrogate marker for neuronal injury, exhibiting strong quantitative and visual correlations with FDG-PET and early-phase amyloid-PET, as well as with volumetric MRI and CSF total tau levels. Our results suggest that [^{18}F]PI-2620 imaging has the potential to facilitate the assessment of PET-based A/T/N during a single dynamic PET session.

Keywords: ATN, tau-PET, tauopathies, amyloid

27 Tau-PET detects advanced primary age-related tauopathy mimicking early-stage AD

Michel Grothe[1], Alexis Moscoso[2], Miguel Labrador-Espinosa[2], Jesús Silva-Rodríguez[1], Fiona Heeman[2], Alejandro Costoya-Sánchez[3], Valle Camacho[4], Martijn van Essen[5], Ismini Mainta[6], Andrés Perissinotti[7], Omar Rodríguez-Fonseca[8], Federica Ribaldi[9], Michael D. Devous, Sr.[10,11], Michael J. Pontecorvo[10,11], Giovanni B. Frisoni[9], Valentina Garibotto[6], Michael Schöll[2,5]

[1]*Reina Sofia Alzheimer Center, CIEN Foundation, ISCIII, Madrid, ES*
[2]*Wallenberg Center for Molecular and Translational Medicine, University of Gothenburg, Gothenburg, SE*
[3]*Nuclear Medicine Department, Instituto de Investigación Sanitaria de Santiago de Compostela, Santiago de Compostela, ES*
[4]*Department of Nuclear Medicine, Hospital de la Santa Creu i Sant Pau, Universitat Autònoma de Barcelona, Barcelona, ES*
[5]*Department of Clinical Physiology, Sahlgrenska University Hospital, Gothenburg, SE*
[6]*Division of Nuclear Medicine, Geneva University Hospitals, Geneva, CH*
[7]*Nuclear Medicine Department, Hospital Clínic Barcelona, Barcelona, ES*
[8]*Nuclear Medicine Department, Lucus Augusti University Hospital, Lugo, ES*
[9]*Geneva Memory Center, Department of Rehabilitation and Geriatrics, Geneva University Hospitals, Geneva, CH*
[10]*Avid Radiopharmaceuticals, Philadelphia, PA, US*
[11]*Eli Lilly and Company, Indianapolis, IN, US*

Background: Primary age-related tauopathy (PART) is typically limited to the medial temporal lobe, but in rare cases it can show a more extensive distribution that associates with cognitive deficits mimicking Alzheimer's disease (AD), a condition that has been termed tangle-dominant disease. It remains unknown whether these advanced forms of PART can be detected in-vivo using PET imaging.

Methods: We first studied the ante-mortem tau- and Aβ-PET imaging ([18F]flortaucipir, [18F]florbetapir), CSF biomarker, and cognitive characteristics of an autopsy case with neuropathologically-confirmed tangle-dominant disease (Braak V, Thal 0, CERAD 0). We then used a large in-vivo cohort of 2402 older individuals to screen Aβ-PET-negative ('A-'; <24.4 Centiloids) individuals for those with elevated neocortical tau-PET ([18F]flortaucipir) signal ('T+', positive visual read), and studied their cognitive, genetic, and CSF biomarker characteristics.

Results: In PET scans acquired 1.8 years before death, the tangle-dominant autopsy case had a negative Aβ-PET (-7 Centiloids) but showed clearly elevated tau-PET signal in temporo-parietal regions, leading to a positive visual read (Fig-1). Repeated CSF measurements (N=8, 2-13 years before death) were constantly negative for $A\beta_{42}$ (>2000 pg/ml) but positive for p-tau_{181} (>30 pg/ml)(Fig-1). Last clinical diagnosis before death was aMCI. In the in-vivo cohort, only 3.6% (45/1264) of A- individuals were T+, but this proportion was significantly higher (9.9%) in cognitively impaired individuals (aMCI/AD dementia). A-T+ showed a temporo-parietal tau-PET signal that was spatially similar but less pronounced compared to A+T+ (Fig-2). CSF p-tau181 levels were significantly elevated in A-T+ compared to A-T- (p=0.01), but Aβ42 levels did not differ (p=0.60). APOE-ε4 frequency in A-T+ (37%) was markedly lower than for A+T+ (69%, p<0.001).

Conclusions: We provide converging neuropathologic and fluid biomarker evidence that tau-PET can detect advanced forms of PART (i.e., tangle-dominant disease), a condition that is phenotypically similar to early-stage AD but may have a different genetic background.

Keywords: PART, tangle-dominant disease, autopsy, tau pet, CSF p-tau

28 Amyloid status moderates associations between hippocampal microstructure, PET tau burden, and memory in dementia-free older adults

Daniel Callow[1], Nisha Rani[1], Kylie Alm[1], Corinne Pettigrew[2], Anja Soldan[2], Michael Miller[3], Marilyn Albert[2], Arnold Bakker[1,2]

[1]*Johns Hopkins School of Medicine Department of Psychiatry and Behavioral Sciences, Baltimore, MD, US*
[2]*Johns Hopkins School of Medicine Department of Neurology, Baltimore, MD, US*
[3]*Johns Hopkins University Department of Biomedical Engineering, Baltimore, MD, US*

Growing evidence suggests that hippocampal gray matter microstructure, assessed through diffusion-weighted imaging (DWI), is a sensitive marker of neurodegeneration in Alzheimer's disease (AD). While hippocampal atrophy is a characteristic feature of AD, microstructural changes may precede tissue atrophy, offering important insights into the early phases of disease. This study assessed the relationships between hippocampal microstructure (assessed with DWI) tau pathology [by positron emission tomography (PET)], and episodic memory performance, focusing on the moderating role of Aβ status assessed by PET imaging. The study included 192 participants without dementia (14 with mild cognitive impairment [MCI]) from the BIOCARD cohort (mean age = 68), of which 52 (27%) were Aβ positive. Multiple linear regression analyses tested whether Aβ status moderated associations between hippocampal mean diffusivity (MD), Braak-staged tau accumulation on PET, and an episodic memory composite score. Results showed that Aβ significantly moderated the associations between higher hippocampal MD and poorer episodic memory (β = -0.24, SE = 0.12, p = 0.039), and greater tau accumulation (β = .29, SE = .08, p < 0.001; β = .26, SE = .08, p = 0.002; β = .19, SE = .08, p = 0.018 for Braak stages II-IV respectively). These interactions indicated that increased hippocampal MD was associated with worse memory and greater tau deposition, but only in individuals who were Aβ positive. Moreover, tau pathology in Braak stages II-IV mediated (indirect effects with 95% CI: β = 0.25 [-0.47, -0.04]; β = 0.19 [-0.38, -0.01]; β = 0.22 [-0.43, -0.02]) the relationship between elevated hippocampal MD and memory decline, independent of hippocampal volume. These effects were attenuated when excluding MCI participants. These findings suggest hippocampal microstructure reflects AD-related neurodegeneration, particularly in the early symptomatic phase, and is more closely associated with tau pathology and cognitive decline than with volumetric atrophy.

Keywords: Diffusion Weighted Imaging; Cognition, Magnetic Resonance Imaging, PET, Hippocampus

29 Performance of an MR-independent analysis pipeline for quantification of tau abnormality using [18F]flortaucipir PET

Alexander DelBene[1], Alexandra Gogola[1], Alexandria Reese[1], Cristy Matan[1], Ming-Hsuan Chiang[1], Beth Snitz[2], Ann Cohen[3], Oscar Lopez[2], Victor Villemagne[3], Brian Lopresti[1]

[1]*Department of Radiology, University of Pittsburgh School of Medicine, Pittsburgh, PA, US*
[2]*Department of Neurology, University of Pittsburgh School of Medicine, Pittsburgh, PA, US*
[3]*Department of Psychiatry, University of Pittsburgh School of Medicine, Pittsburgh, PA, US*

Background: Magnetic resonance (MR) imaging contraindications commonly limit participation in PET neuroimaging studies because most analysis methods require structural MR. An analysis method that accurately indexes the level of tau abnormality using only PET image data could broaden participant inclusion. CapAIBL, an MR-independent method, was compared against SPM-generated CenTauRz (CTRz).

Methods: 150 participants (age 71.1±8.4 years, 44% female, 92% nHW) from the University of Pittsburgh ADRC underwent 3T MR, amyloid [^{11}C]PiB PET, and tau [^{18}F]flortaucipir (FTP) PET scans. PET images were corrected for motion and summed (PiB=50-70 min, FTP=80-100 min). FTP scans were processed using the CenTauR masks through both the SPM and CapAIBL pipelines. Both pipelines were sampled in template space. In the SPM pipeline, a linear PET to MR transformation is done before normalizing. Meta-Temporal (MT) FTP was expressed in CTRz. A global CL ≥20 was used to determine A status for additional evaluation. Linear regressions determined the level of agreement between the two pipelines.

Results: CapAIBL and SPM pipelines showed a high level of agreement (Figure 1) between MT CTRz scores across the entire cohort (β=0.933, r^2=0.976), and for subsets of A+ participants (β=0.954, r^2=0.982, n=70) and A- participants (β=0.855, r^2=0.927, n=80). Compared to CapAIBL, SPM-pipeline CTRz values showed a small, positive bias in A- participants (0.08±0.88 CTRz) that grew more pronounced in A+ participants (0.43±0.91 CTRz; Figure 2). However, comparing T status based on CTRz scores (T+: MT CTRz≥2) between pipelines, this bias had a minimal effect on T classification (97.4% concordance).

Conclusions: MR-less CapAIBL CTRz values show robust agreement with the MR-based SPM pipeline, particularly when Aβ pathology is present. Future work will evaluate the concordance when native-space FTP images are analyzed through both pipelines, assess additional regions of interest, and determine if the FTP CTRz equations require updating/refinement.

Figure 1. Relationships between CapAIBL and SPM CTRz for Meta Temporal region

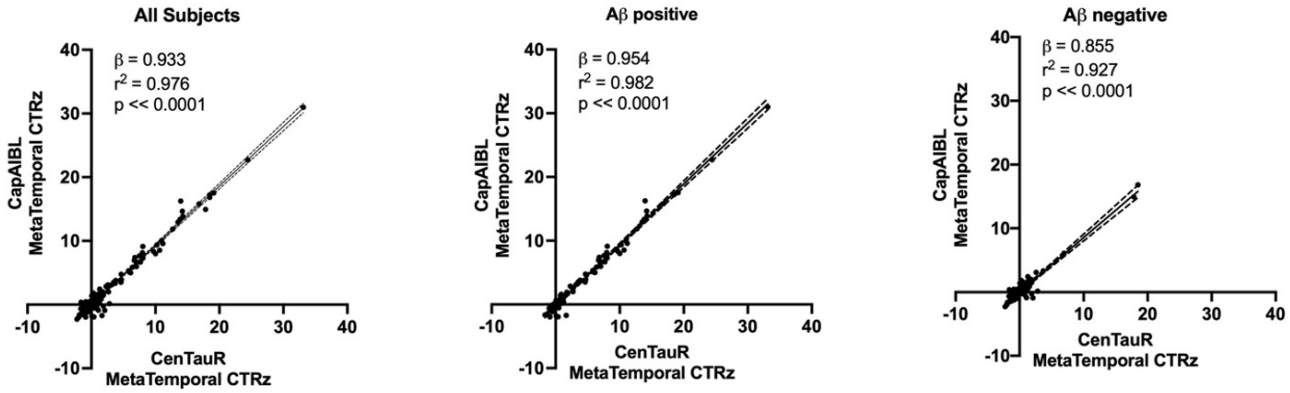
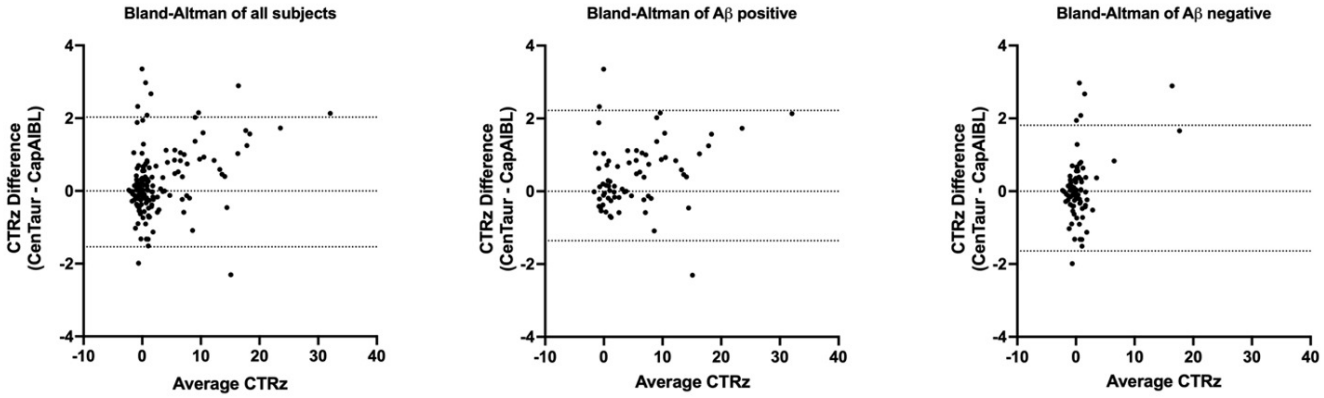


Figure 2. Bland-Altman plots of Meta region CTRz for all cohort, amyloid positive, and amyloid negative participants



Keywords: tau, CapAIBL, SPM, CenTauRz

30 Functional and structural connectivity patterns predict longitudinal tau spreading in asymptomatic individuals expressing Aβ pathology

Jonathan Gallego-Rudolf[1,2], Ting Qiu[1], Mohammadali Javanray[1], Alex Wiesman[2], Frédéric St-Onge[1], Alfonso Fajardo-Valdez[1], Sylvain Baillet[2], Sylvia Villeneuve[1]

[1]*Douglas Research Centre, Montreal, QC, CA*
[2]*Montreal Neurological Institute, Montreal, QC, CA*

Alzheimer's disease (AD) is defined by the pathological accumulation of amyloid-beta (Aβ) and tau proteins in the brain. Animal studies have demonstrated that tau can spread trans-synaptically, propagating from early accumulating regions (epicenters) to the rest of the cortex. This process seems to be aggravated by the presence of Aβ pathology. Non-invasive human neuroimaging studies also suggest tau spreads across structural and functional brain networks, but further longitudinal multimodal neuroimaging studies during the preclinical stage of AD are needed to understand how brain connectivity shapes proteinopathy spreading, the synergistic influence of Aβ and its implications for clinical progression.

We estimated brain connectivity using task-free Magnetoencephalography (MEG), Diffusion Weighted Imaging (DWI), and resting-state functional Magnetic Resonance Imaging (fMRI) and quantified Aβ deposition and longitudinal accumulation of tau using Positron Emission Tomography (PET) in a sample of 76 cognitively unimpaired older adults with a family history of sporadic AD (Figure 1). We assessed whether functional (MEG, fMRI) and structural (DWI) connectivity patterns of individual-specific tau epicenter regions predicted longitudinal tau spreading across the cortex, the interactive effect of global neocortical Aβ pathology on this association, and whether tau accumulation within epicenter-connected regions predicted progression to mild cognitive impairment (MCI).

Cortical regions showing stronger functional (MEG alpha-band, fMRI) and structural (DWI) connectivity with individual-specific tau epicenters had higher longitudinal accumulation of tau in individuals expressing greater levels of neocortical Aβ deposition (Figure 2). Longitudinal tau accumulation within epicenter-connected regions was associated with clinical progression to MCI (Figure 3).

We report consistent findings using three state-of-the-art imaging modalities for estimating brain connectivity, showing that Aβ pathology facilitates tau spreading across functional and structural brain networks, which in turn relates to clinical progression to MCI. These findings advance our understanding of the neuropathological mechanisms underlying early proteinopathy spread during the preclinical stage of AD.

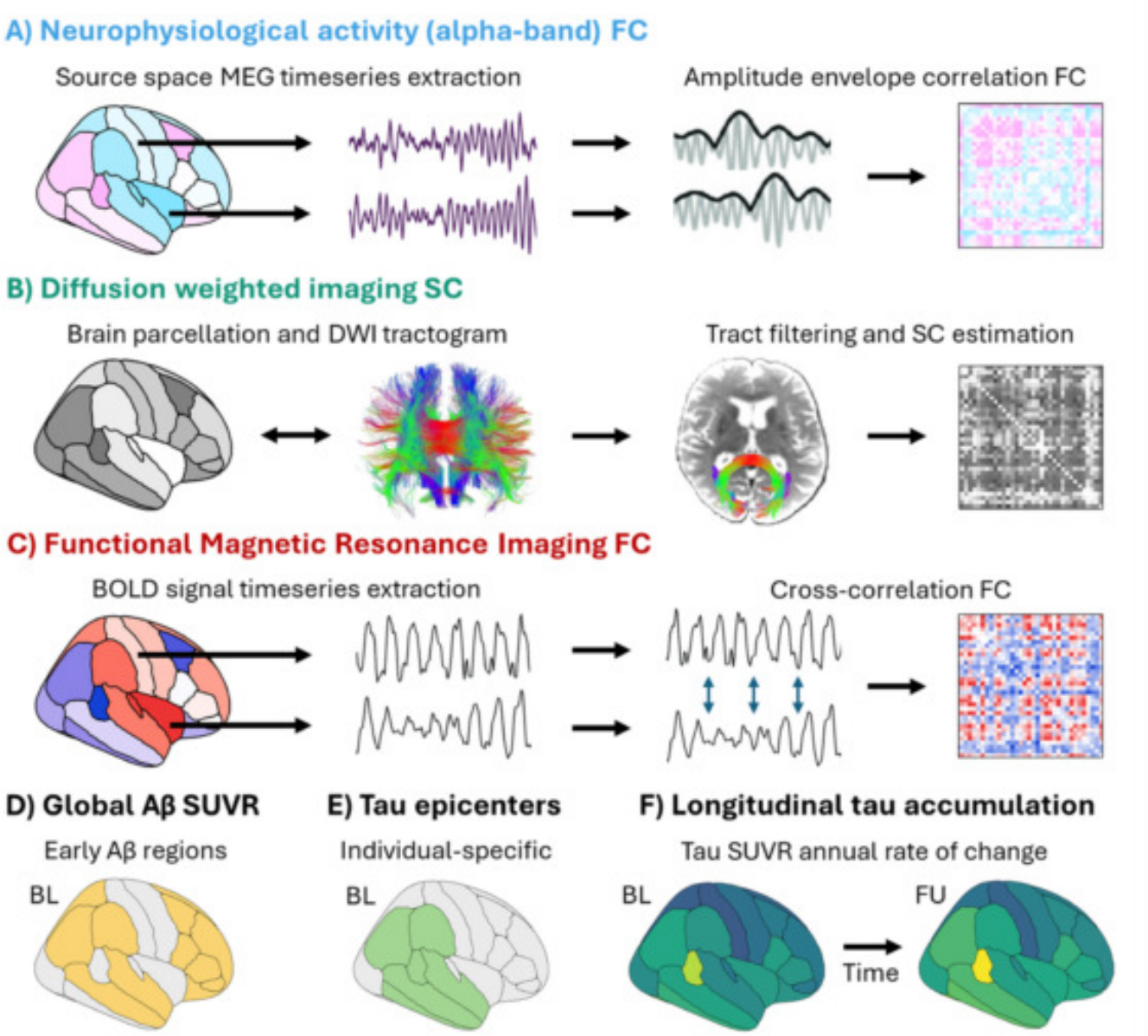


Figure 1. Estimation of functional and structural brain connectivity, global baseline Aβ pathology, tau epicenters and longitudinal tau accumulation. We computed connectivity matrices from the neurophysiological activity MEG timeseries (A), the diffusion weighted image-derived tractogram (B) and the resting-state BOLD fMRI signals (C) across all pairs of the 68 cortical regions of the Desikan-Killiany atlas. D) Baseline global Aβ burden was estimated by calculating the weighted average of SUVR values across a set of early Aβ accumulating cortical regions. E) Individual-specific tau epicenters were defined by selecting the top ten percent of the cortical regions (6 regions) with higher SUVR values from the baseline tau PET scan. F) Longitudinal tau accumulation within each cortical region was estimated by calculating the annual SUVR rate of change between the baseline and follow-up tau PET scans.

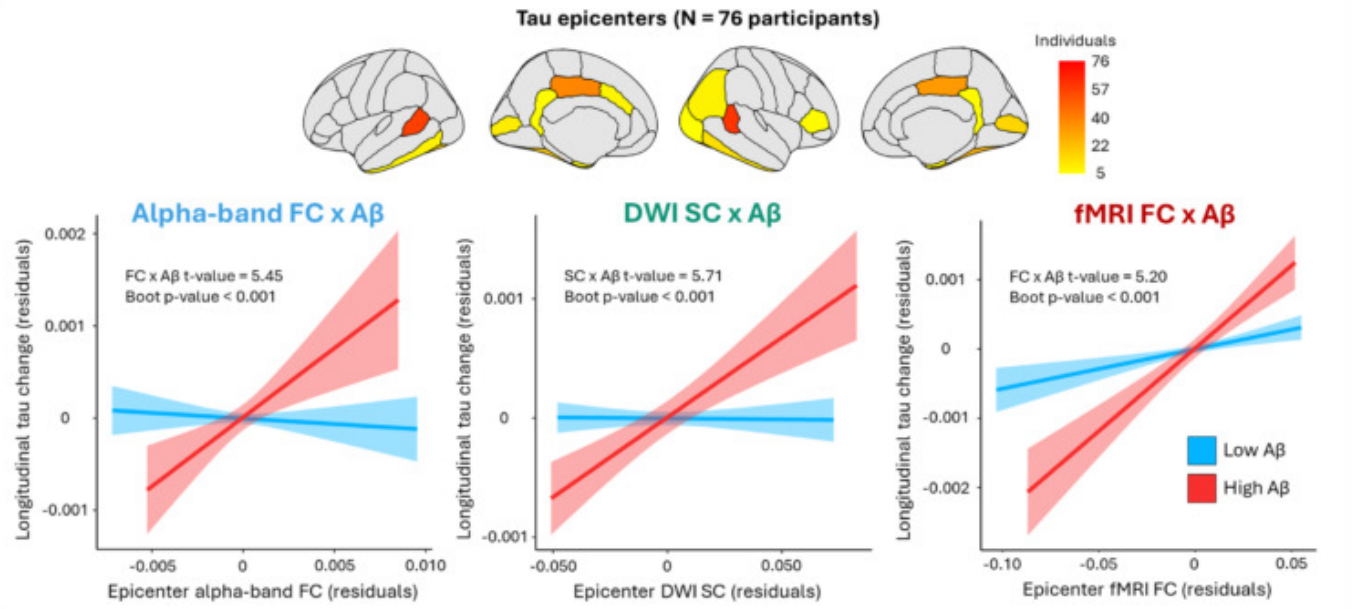


Figure 2. Stronger functional and structural connectivity with individual-specific tau epicenters predicts longitudinal tau accumulation in individuals expressing Aβ pathology. Top panel shows the number of individuals in which each cortical region was selected as one of the six individual-specific tau epicenters. Cortical regions showing stronger neurophysiological activity alpha-band FC (left), DWI SC (middle), and fMRI FC (right) with the individual-specific tau epicenters had increased longitudinal tau accumulation in individuals expressing higher levels of global Aβ pathology. The interaction plots show the residual values after regressing out the cofounding effects of age, sex and years of education. For visualization of the FC/SC x Aβ interaction effect, we plotted the average line of fit across the regression slopes obtained for the top quartile of individuals with higher levels of Aβ (high Aβ; red) and the rest of the group (low Aβ; blue), although continuous SUVR values were used for the statistical analysis.

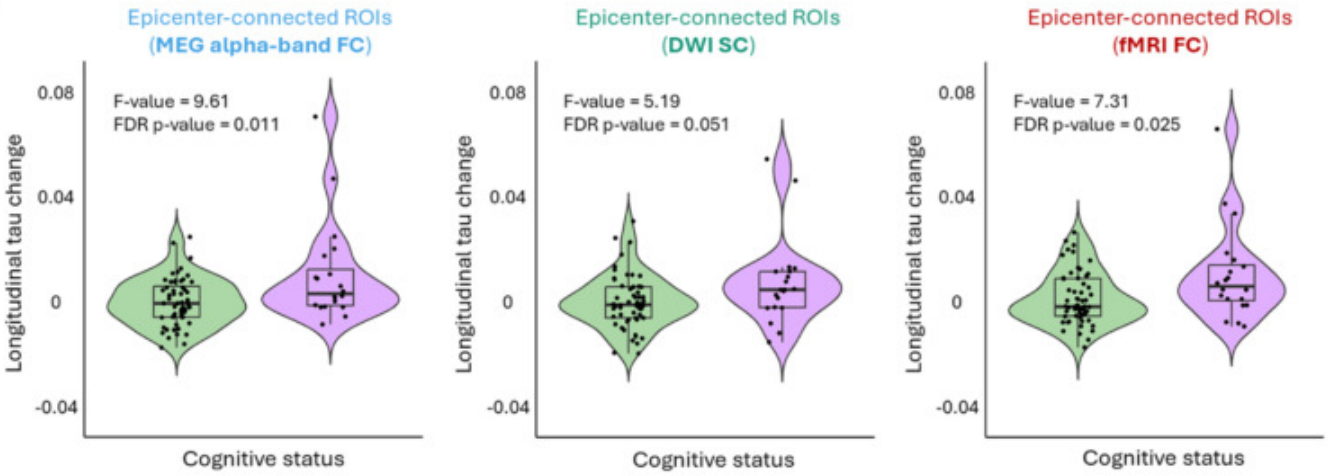


Figure 3. Longitudinal tau accumulation within individual-specific tau epicenter-connected cortical regions predicts clinical progression to Mild Cognitive Impairment. Individuals that progressed to mild cognitive impairment showed higher levels of longitudinal tau accumulation within tau epicenter-connected cortical regions based on the MEG alpha-band FC (left), DWI SC (middle) and fMRI FC (right) profiles, as compared to individuals that remained cognitively stable. Longitudinal tau accumulation is expressed as the residual values of the annual tau SUVR rate of change after regressing out the cofounding effects of age, sex and years of education.

Keywords: Tau spreading, structural and functional connectivity, amyloid, preclinical AD, MCI progression

31 Plasma phospho-tau 217, neurofilament-light, and glial fibrillary acidic protein are differentially associated with longitudinal neuropsychiatric symptoms across the early cognitive spectrum

Jennifer Gatchel[1,2,3], Kexin Yu[4,5], Phebe Palmer[3,4], Chao-Yi Wu[3,4,5], Jacqueline Beltran[1,4,6], Catherine Munro[1,3,7], Pia Webb[3,4], Deborah Blacker[1,3,4], Steven Arnold[1,3,4], Gad Marshall[3,4,7], Hiroko Dodge[3,4,5]

[1]*Massachusetts General Hospital, Department of Psychiatry, Boston, MA, US*
[2]*McLean Hospital, Belmont, MA, US*
[3]*Harvard Medical School, Boston, MA, US*
[4]*Massachusetts General Hospital, Department of Neurology, Boston, MA, US*
[5]*Oregon Health & Science University, Portland, OR, US*
[6]*Northeastern University, Boston, MA, US*
[7]*Brigham and Women's Hospital, Department of Neurology, Boston, MA, US*

Introduction: Neuropsychiatric symptoms (NPS) are common in the preclinical and prodromal stages of Alzheimer's Disease and Related Dementias (ADRD) and are associated with greater cognitive and functional decline. However, the neurobiology of these symptoms and prognostic markers of their emergence are not well understood. We sought to examine the associations between established baseline plasma biomarkers of ADRD and the longitudinal trajectory of NPS in older adults.

Methods: Participants were from the Massachusetts Alzheimer's Disease Research Center longitudinal cohort. A subset, spanning consensus diagnoses of cognitively normal (CN) (n=282, age: 68(10) years) to mild cognitive impairment (MCI) (n=331, age:74(8) years), had baseline plasma samples assayed for phospho-tau ^{217} (p-Tau^{217}), neurofilament-light (NfL) and glial fibrillary acidic protein (GFAP) (Table 1). The average length of follow-up was 8.6±4.2 years for the CN and 7.2±4.1 years for the MCI participants. NPS were measured annually using the self-reported 15-item Geriatric Depression Scale (GDS-15) and the study-partner-reported Neuropsychiatric Inventory Questionnaire (NPI-Q). Plasma biomarkers were log-transformed and z-scores were derived using baseline sample values (CN + MCI). In longitudinal linear mixed-effects models, we examined the NPS measures as the dependent variable in relation to time, plasma biomarkers, and the plasma biomarker × time interaction, controlling for age and sex.

Results: In CN participants, baseline plasma NfL and GFAP were associated with longitudinal GDS, but not with NPI-Q (Figure 1). In MCI participants, baseline plasma p-Tau^{217} and NfL were associated with GDS longitudinally, whereas all three biomarkers (p-Tau^{217}, NfL, GFAP) predicted increasing NPI-Q score over time (Figure 2).

Conclusions: Findings suggest differential plasma biomarker-NPS associations across the early ADRD spectrum. Further work examining plasma biomarkers in relation to specific NPS will provide insight into the prognostic value of these measures in predicting NPS trajectories over the course of ADRD--an area of high potential clinical-translational impact.

Table 1. The cohort's demographic, clinical and plasma biomarker profiles, shown for cognitively normal (CN) and mild cognitive impairment (MCI) participants.

Table 1.1 Cognitively Normal: cohort characteristics

Characteristic	N = 282[1]
PTau 217 (Log 10)	0.59 (0.27)
GFAP (Log 10)	1.82 (0.22)
NFL (Log 10)	2.16 (0.23)
NPI-Q Sum (Max = 36)	0.64 (1.54)
Unknown	9
GDS Total	0.99 (1.61)
Unknown	4
Age (Years)	68 (10)
Sex	
Female	196 (70%)
Male	86 (30%)

[1] Mean (SD); n (%)

Table 1.2 MCI: cohort characteristics

Characteristic	N = 331[1]
PTau 217 (Log 10)	0.72 (0.35)
GFAP (Log 10)	1.92 (0.22)
NFL (Log 10)	2.28 (0.22)
NPI-Q Sum (Max = 36)	1.58 (2.27)
Unknown	24
GDS Total	1.78 (2.35)
Unknown	11
Age (Years)	74 (8)
Sex	
Female	175 (53%)
Male	156 (47%)

[1] Mean (SD); n (%)

p-Tau^{217} = plasma phospho-tau^{217}, NfL = plasma neurofilament light, GFAP = plasma glial fibrillary acidic protein, NPI-Q = Neuropsychiatric Inventory Questionnaire, GDS= Geriatric Depression Scale-15 item

Figure 1. Results from cognitively normal participants

Biomarker Model	Term	NPI-Q Total		GDS Total	
		Beta (95% CI)	p-value	Beta (95% CI)	p-value
P-Tau 217 (Log 10 Z-score)	Years from Baseline	0.08 [0.06-0.11]	**<0.001*** **	0.11 [0.08-0.13]	**<0.001*** **
	P-Tau 217	0.11 [-0.12-0.34]	0.351	0.01 [-0.23-0.25]	0.927
	P-Tau 217 * Years from Baseline	0.00 [-0.02-0.03]	0.816	0.02 [-0.00-0.04]	0.116
GFAP (Log 10 Z-score)	Years from Baseline	0.09 [0.07 - 0.12]	**<0.001*** **	0.11 [0.08-0.13]	**<0.001*** **
	GFAP	0.07 [-0.16-0.30]	0.541	-0.02 [-0.27-0.22]	0.858
	GFAP * Years from Baseline	0.02 [-0.00-0.04]	0.075	-0.02 [0.01-0.04]	**0.002****
NFL (Log 10 Z-score)	Years from Baseline	0.09 [0.07-0.12]	**<0.001*** **	0.13 [0.10-0.15]	**<0.001*** **
	NFL	0.08 [-0.14-0.30]	0.453	0.25 [0.02-0.49]	**0.031***
	NFL * Years from Baseline	0.01 [-0.00-0.03]	0.135	0.02 [0.01-0.03]	**0.007****

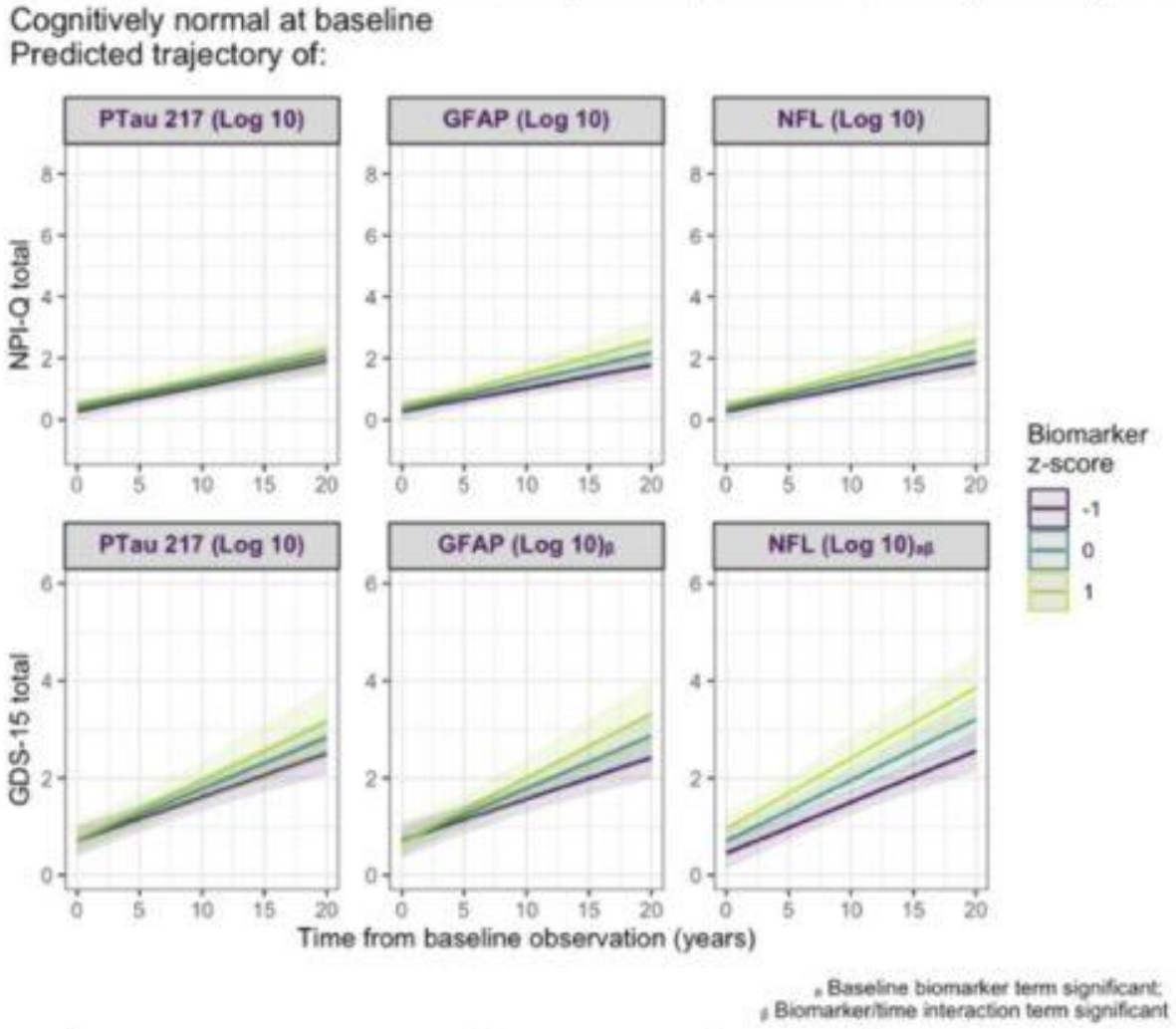


Figure 1. Results of longitudinal mixed effects models for participants cognitively normal at baseline. Separate models were run for each plasma biomarker (P-tau-217 (phospho-tau^{217}), glial fibrillary acidic protein (GFAP), and neurofilament light (NfL)): Neuropsychiatric measure (NPI-Q or GDS) ~ plasma biomarker + time (years from baseline) + (plasma biomarker * time (years form baseline)) + age + sex. The top panel shows model outputs (beta values, 95% confidence intervals, and p-values), with significant terms in bold. The bottom panel provides visualization of these outputs (y axis: neuropsychiatric measure, x-axis: years from baseline). In visualizations, z-transformed biomarker values are colored at sample mean (blue), one standard deviation above mean (yellow), and one standard deviation below mean (purple). NPI-Q: Neuropsychiatric Inventory Questionnaire (NPI-Q); GDS Geriatric Depression Scale-15 item.

Figure 2. Results from participants with mild cognitive impairment

Biomarker Model	Term	NPI-Q Total		GDS Total	
		Beta (95% CI)	p-value	Beta (95% CI)	p-value
P-Tau 217 (Log 10 Z-score)	Years from Baseline	0.20 [0.16-0.24]	**<0.001*** **	0.14 [0.10-0.17]	**<0.001*** **
	P-Tau 217	0.02 [-0.23-0.27]	0.878	-0.06 [-0.28-0.16]	0.610
	P-Tau 217 * Years from Baseline	0.09 [0.07-0.12]	**<0.001*** **	0.02 [0.00-0.04]	**0.045***
GFAP (Log 10 Z-score)	Years from Baseline	0.19 [0.15-0.24]	**<0.001*** **	0.13 [0.10-0.17]	**<0.001*** **
	GFAP	0.06 [-0.24-0.36]	0.708	-0.04 [-0.31-0.22]	0.748
	GFAP * Years from Baseline	0.07 [0.04-0.10]	**<0.001*** **	0.01 [-0.01-0.03]	0.174
NFL (Log 10 Z-score)	Years from Baseline	0.21 [0.16-0.25]	**<0.001*** **	0.15 [0.12-0.19]	**<0.001*** **
	NFL	0.44 [0.13-0.75]	**0.006****	0.28 [0.01-0.56]	**0.045***
	NFL * Years from Baseline	0.03 [0.00-0.06]	**0.025***	0.02 [0.00-0.04]	**0.020***

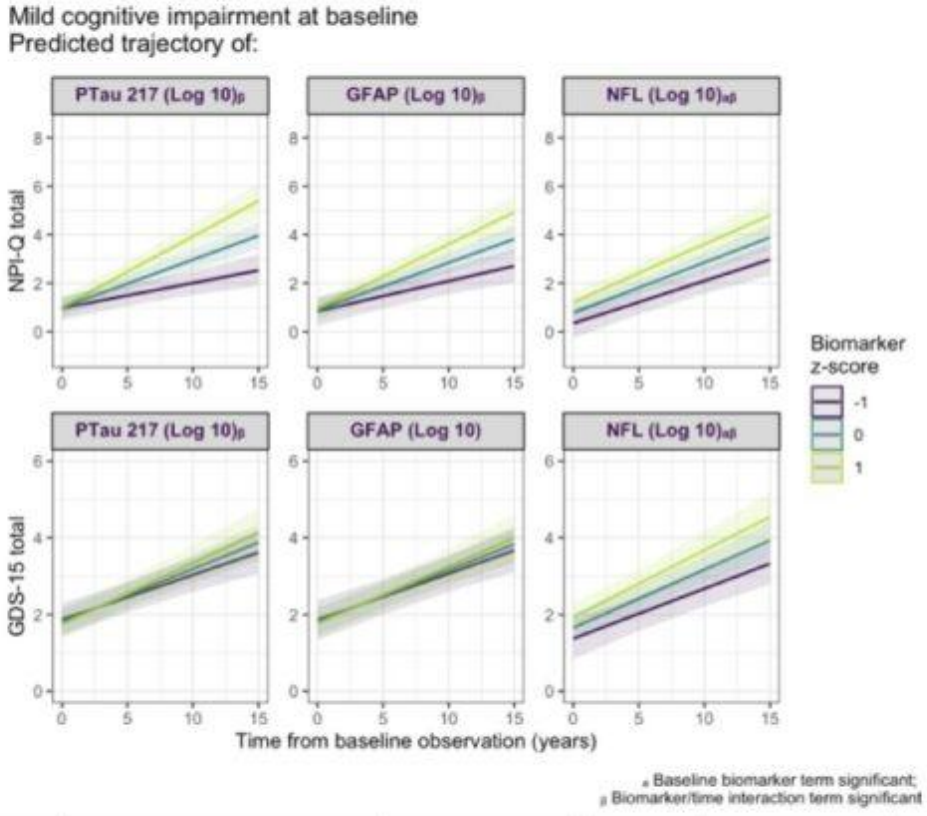


Figure 2. Results of longitudinal mixed effects models for participants with mild cognitive impairment (MCI) at baseline. Separate models were run for each plasma biomarker (P-tau-217 (phospho-tau^{217}), glial fibrillary acidic protein (GFAP), and neurofilament light (NfL)): Neuropsychiatric measure (NPI-Q or GDS) ~ plasma biomarker + time (years from baseline) + (plasma biomarker * time (years form baseline)) + age + sex. The top panel shows model outputs (beta values, 95% confidence intervals, and p-values), with significant terms in bold. The bottom panel provides visualization of these outputs (y axis: neuropsychiatric measure, x-axis: years from baseline). In visualizations, z-transformed biomarker values are colored at sample mean (blue), one standard deviation above mean (yellow), and one standard deviation below mean (purple). NPI-Q: Neuropsychiatric Inventory Questionnaire (NPI-Q); GDS Geriatric Depression Scale-15 item.

Keywords: plasma, phospho-Tau217, neurofilament-light (NfL), glial fibrillary acidic protein (GFAP), neuropsychiatric symptoms (NPS)

32 An assessment of the utility of flortaucipir PET to detect four-repeat tau pathology in a globular glia tauopathy case-series

Rodolfo Gatto[1], Hossam Youssef[1], Sujala Ghatamaneni[3], Gokhan Uruk[1], Paul Min[3], Mu-Hui Fu[1], R. Ross Reichard[2], Val Lowe[3], Dennis Dickson[4], Jennifer Whitwell[3], Keith Josephs[1]

[1]*Department of Neurology, Mayo Clinic, Rochester, MN, US*
[2]*Department of Laboratory Medicine and Pathology, Mayo Clinic, Rochester, MN, US*
[3]*Department of Radiology, Mayo Clinic, Rochester, MN, US*
[4]*Department of Neuropathology, Mayo Clinic, Jacksonville, FL, US*

Introduction: Glial globular tauopathy (GGT) represents a rare neuropathological form of frontotemporal lobar degeneration characterized by four-repeat tau-positive astrocytic and globular glial inclusions. However, little is known about antemortem tau-PET imaging in GGT and whether tau-PET can detect four-repeat tau inclusions in GGT.

Objective: To investigate whether uptake is observed on antemortem tau-PET, using the flortaucipir ligand, in patients with GGT and determine whether uptake represents underlying four-repeat tau or other neuropathological targets.

Materials and Methods: Three patients with neuropathologically confirmed GGT who underwent antemortem flortaucipir PET were investigated. Neuropathological analyses focused on grey and white matter (GM & WM) from the superior medial frontal gyrus (S/M-MG) and superior lateral temporal gyrus (S/L-TG). Immunohistochemical staining was performed with antibodies to tau (AT8, PHF-1, RD4), astrocytic glial fibrillary acidic protein (GFAP), and microglia (Iba1). Beta-amyloid was assessed with Thioflavin-T. Flortaucipir binding was indirectly assessed using a histopathological fluorescent flortaucipir analog (T726). Regional standard uptake value ratios (SUVRs) were calculated from premortem tau-PET images matched to the neuropathological region. Autoradiography studies with a flortaucipir radioligand were performed on consecutive slides.

Results: In all three GGT cases, T726 colocalization was observed in WM than in GM. In WM, T726 colocalization was greatest with PHF-1, followed by RD4 and GFAP, and minimal with Iba1. Elevated antemortem tau-PET SUVRs were observed in S/M-FG and S/L-TG WM regions in all GGT cases. In-vitro flortaucipir autoradiography studies demonstrated no binding to tau in GM or WM.

Conclusions: Although autoradiographic findings were negative, there is some evidence that flortaucipir PET uptake in GGT represents an underlying four-repeat tau burden, especially in the WM.

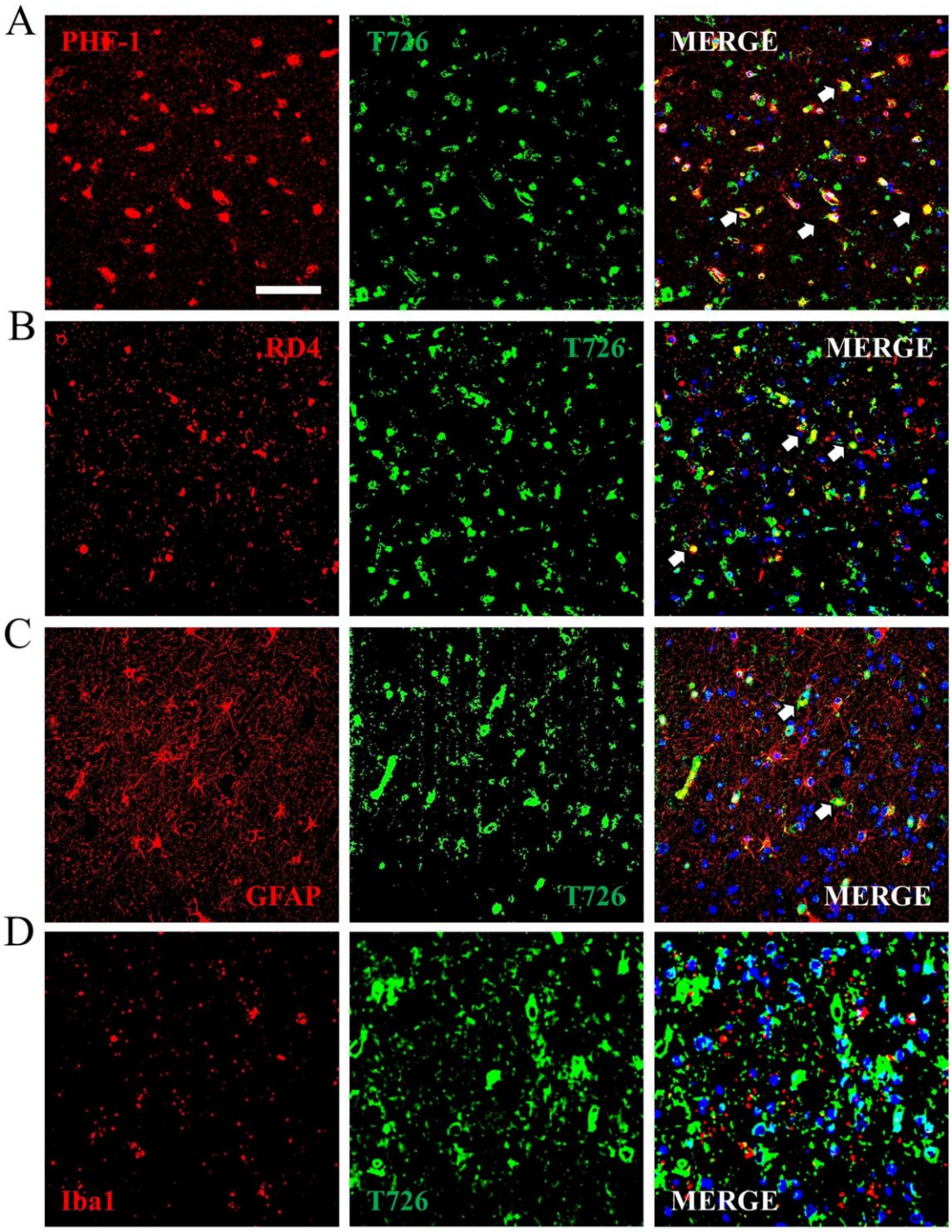


Figure: Confocal microscopy fluorescence from a GGT case. Slides were stained for T726 and phosphorylated tau by PHF-1 (A), four-repeat Tau by RD4 (B), astrocyte staining by GFAP (C), and microglia stainings by Iba1 (D).

Keywords: Globular Glial Tauopathy, Flortaucipir, T726, Four-Repeat Tauopathies, Confocal Fluorescence Microscopy

33 Molecular imaging of neurodegeneration – mitochondria, associated proteins and synapses (MIND-MAPS) in frontotemporal dementia

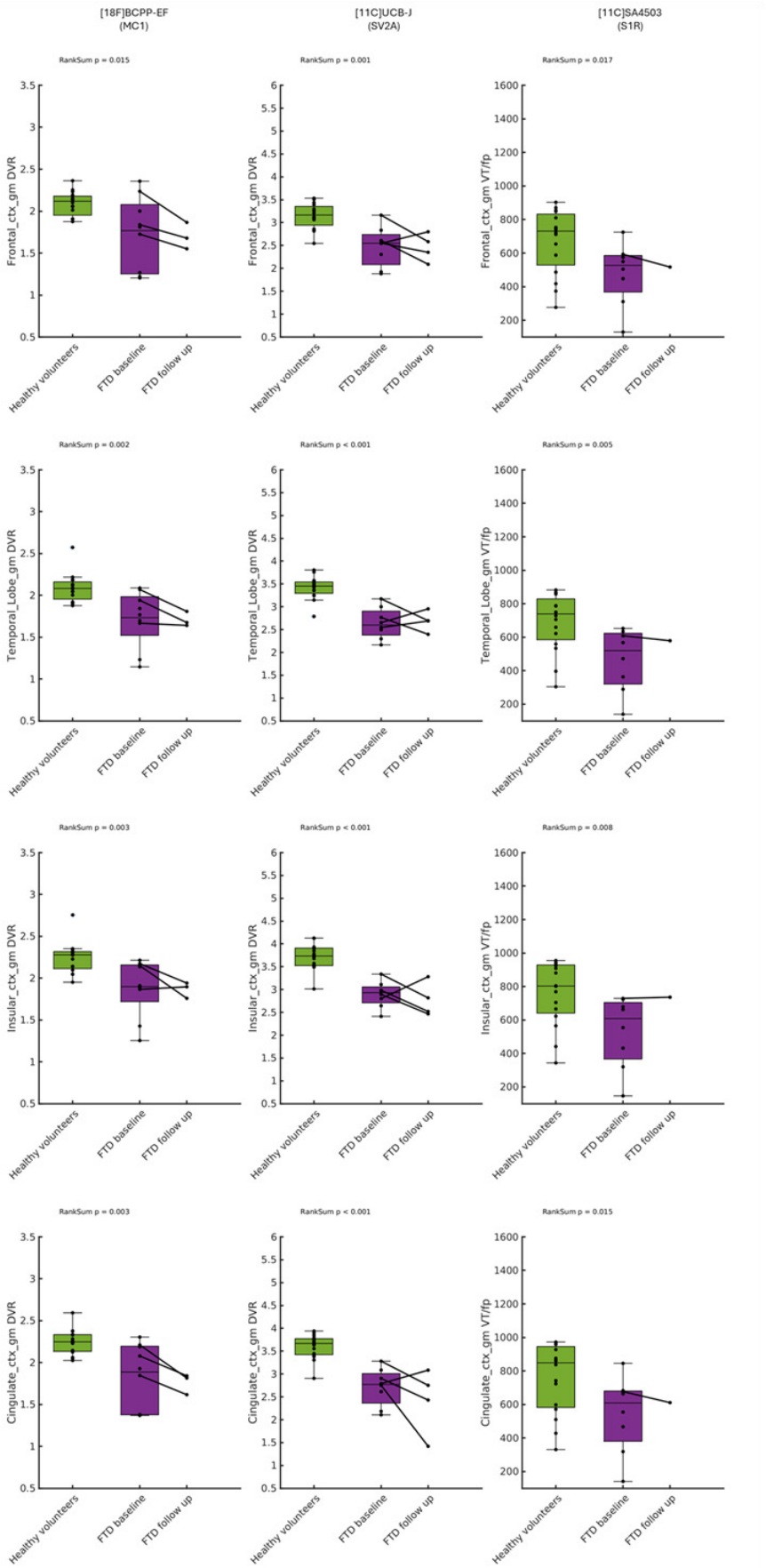
Mica Clarke[1], Alexander Whittington[1], Jan Passchier[1], Yvonne Lewis[1], Luca Passamonti[2], Laigao Chen[3], Cristian Salinas[4], Hideo Tsukada[5], David Cash[6], Eugenii Rabiner[1], Jonathan Rohrer[6]

[1]*Perceptive, London, GB*
[2]*Biogen, Boston, MA, US*
[3]*Pfizer, Boston, MA, US*
[4]*Takeda Pharmaceuticals, Boston, MA, US*
[5]*Hamamatsu Photonics, Hamamatsu, JP*
[6]*Dementia Research Centre, UCL Queen Square Institute of Neurology, London, GB*
[7]*MIND-MAPS Consortium, London, GB*

Mitochondrial and synaptic dysfunction are key features of multiple neurodegenerative disorders. The expression of synaptic vesicle protein 2A (SV2A) quantified using [^{11}C]UCB-J has been established as an index of expression of pre-synaptic terminals, while mitochondrial complex I (MC1) has been quantified using [^{18}F]BCPP-EF as a marker of mitochondrial density. The expression of sigma 1 receptor (S1R) measured using [^{11}C]SA4503 has been proposed as a marker of mitochondrial-associated membranes (MAMs) connecting mitochondria to the endoplasmic reticulum. This is the first study to combine the evaluation of these molecular markers in frontotemporal dementia (FTD).

Ten participants with behavioural variant FTD (age mean 64.2, SD 5.9; disease duration 5.0 years, 5.2; MMSE 22.7, 5.5) and 16 cognitively normal controls (age 63.0, 11.6; MMSE 28.9, 1.1) underwent 90-minute dynamic PET scans following injection of each of the tracers, with arterial blood collected to generate metabolite-corrected arterial input function. Five of the FTD group underwent the same procedures 12 months later. Regions of interest (ROIs) were defined on individual MR images using the CIC anatomical atlas. Regional density was evaluated using the volume of distribution (VT) corrected for the plasma free fraction (VT/fP) for [^{11}C]SA4503, and the regional VT normalised to the VT in the centrum semiovale (DVR) for [^{11}C]UCB-J and [^{18}F]BCPP-EF. Group comparisons used non-parametric Mann-Whitney tests.

Regional density of SV2A, MC1 and S1R was significantly reduced in FTD compared to controls in multiple ROIs including: frontal, temporal, parietal, insular, anterior cingulate and posterior cingulate cortices and the hippocampus, amygdala, thalamus, caudate, putamen and cerebellum. The magnitude of the differences between control and FTD groups is reduced by partial volume correction but not abolished, suggesting reductions are not entirely driven by atrophy. Follow up data revealed further reductions in MC1 and SV2A. Longitudinal investigation of these molecular changes requires replication in a larger cohort.



Keywords: FTD, synaptic, mitochondrial, biomarkers

34 Evaluating tVNS effects on cognitive outcomes and modulating factors in asymptomatic older adults: study design of the WALLe Trial

Nina Engels-Domínguez[1,2], Jill Grube[1], Haley Fenlon[1], Emma Wiklund[1], Lukas Heinrich[1,2], Marion Baillet[1], Maxime van Egroo[1,2], Kathryn Papp[3,4], Joost Riphagen[1], Ronald Garcia[1,5], Roberta Sclocco[1,6,7], Keith Johnson[3,4,8], Vitaly Napadow[1,6,7], Heidi Jacobs[1,2]

[1]*The Athinoula A. Martinos Center for Biomedical Imaging, Department of Radiology, Massachusetts General Hospital, Harvard Medical School, Boston, MA, US*
[2]*Faculty of Health, Medicine and Life Sciences, School for Mental Health and Neuroscience, Alzheimer Centre Limburg, Maastricht University, Maastricht, NL*
[3]*Center for Alzheimer Research and Treatment, Department of Neurology, Brigham and Women's Hospital, Harvard Medical School, Boston, MA, US*
[4]*Department of Neurology, Massachusetts General Hospital, Harvard Medical School, Boston, MA, US*
[5]*Department of Psychiatry, Massachusetts General Hospital, Harvard Medical School, Boston, MA, US*
[6]*Department of Radiology, Logan University, Chesterfield, MO, US*
[7]*Department of Physical Medicine and Rehabilitation, Spaulding Rehabilitation Hospital, Harvard Medical School, Boston, MA, US*
[8]*Gordon Center for Medical Imaging, Department of Radiology, Massachusetts General Hospital, Harvard Medical School, Boston, MA, US*

Background: The locus coeruleus (LC) is among the earliest regions to harbor tau, and the associated aberrant activity patterns may promote Alzheimer's disease (AD) pathology. Transcutaneous vagus nerve stimulation (tVNS), a non-invasive neuromodulation technique stimulating the auricular vagus nerve branch, modulates LC activity and shows potential for delaying cognitive decline in older individuals. The WALLe Trial aims to evaluate the impact of tVNS on cognitive outcomes and identify demographic, neurophysiological, and blood-based biomarker factors predicting positive tVNS-responses in asymptomatic older adults (Table 1).

Study Design: This ongoing single-site trial, enriched for *APOE*-e4 carriage, compares respiration-gated tVNS versus sham stimulation. Its enrollment target is 140 asymptomatic adults aged 60-85, recruited via online and printed advertisements and the MGB-Biobank. After consent and eligibility screening, participants are randomized into one of four arms, receiving sham or tVNS in a cross-over design during LC-dedicated 7T-MR-imaging (visits 2-3). After a 3-to-5-week wash-out period, participants are quasi-randomized to either daily sham or tVNS sessions for 10 days (visits 4-13). Visits 14-15 are cognitive follow-ups. Blood sampling, cognitive testing, pupillometry and other autonomic measurements are collected (Figure 1). The primary outcome is change in face-name association performance (FNAME; Figure 2), evaluated during fMRI (visits 2-3) and behavioral assessments (visits 4-15). Participants remain blinded to study condition and receive remuneration.

Results: To date, 89 participants (age: mean=68.17, SD=5.46, range=60.0-85.9; education: mean=17.01, SD=2.01, range=10-20; female=51.7%; *APOE*-e4 carrier=29.2%) have enrolled, with n=52 completing the trial. Current non-completion rates are 12.4% for screen-fails, 7.9% for drop-outs and 1.1% for no-shows. No serious adverse events or stopping rules occurred. The next expected milestone is reaching 75% of the enrollment target.

Conclusion: The WALLe Trial investigates tVNS effects on cognitive outcomes in AD by integrating cognitive, neuroimaging and blood-based biomarker measures, holding promise to inform the design and target population of preventive intervention strategies in preclinical stages.

	Aims	Outcomes	Relevance
Primary	1. Investigate the short and long-term effects of tVNS on different cognitive domains	*Primary* Change in FNAME score *Secondary* Cognitive testing scores (including composite scores)	Monitor and determine outcome measures of future trials Establish long-term tVNS effects
Secondary	2. Identify demographic characteristics as well as functional brain and AD-related markers that can predict beneficial responses to tVNS	Being a responder on FNAME change scores	Identify target engagement and eligibility markers
	3. Understand biological pathways contributing to beneficial responses to tVNS	Change in FNAME score	Identify potential stratification factors for clinical trials

Table 1. WALLe Trial aims and corresponding outcomes and relevance. Abbreviations: tVNS, transcutaneous vagus nerve stimulation; FNAME, face-name associative memory task (Figure 2a).

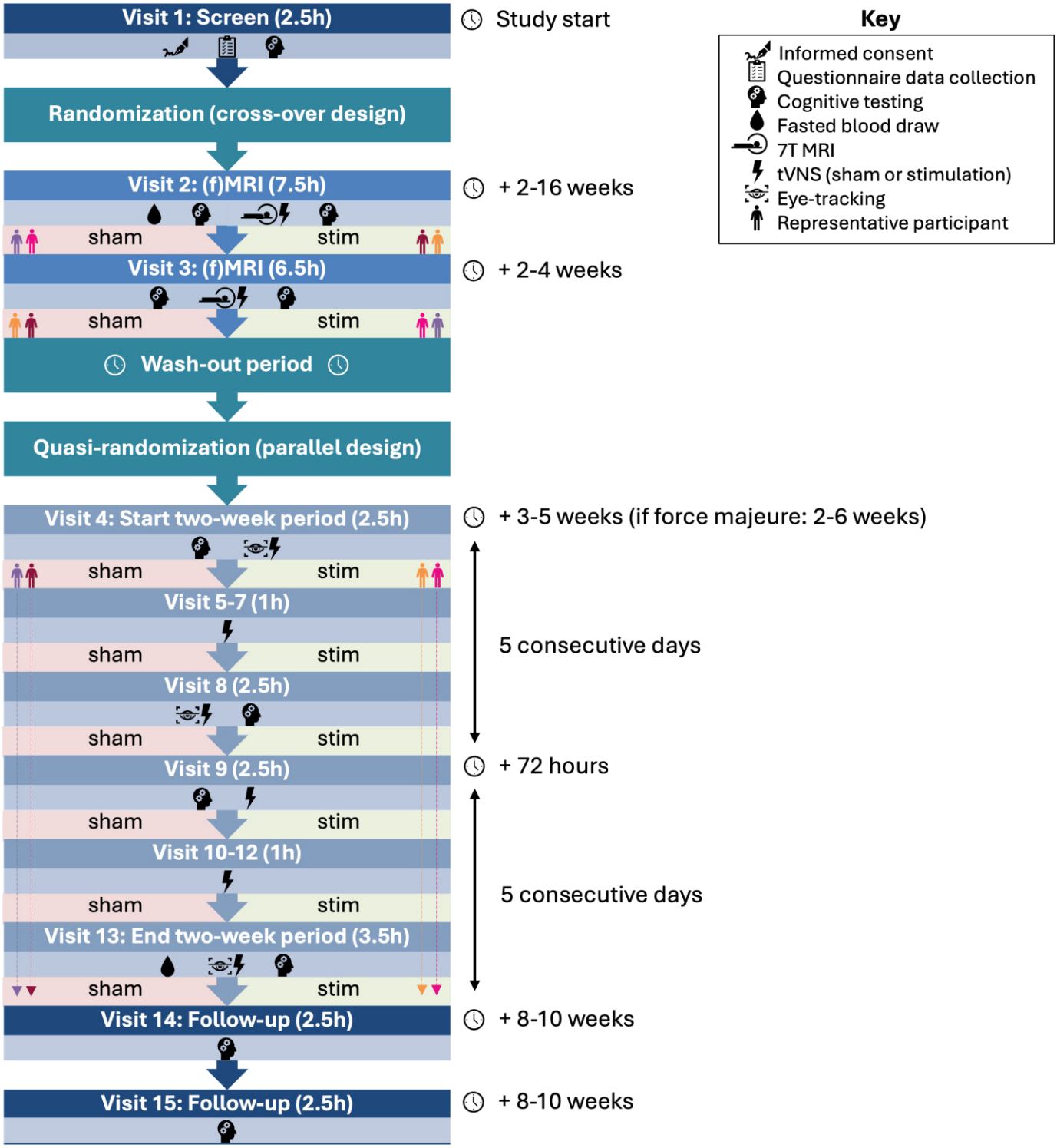


Figure 1. Study design of the WALLe Trial: overview of randomization, visit procedures, and timeline with associated visit durations and windows. The participant flow through the study begins with a screening, followed by randomization into a cross-over design for visit 2 and 3, where tVNS (sham or stimulation, dependent on assigned condition) is paired with the functional FNAME task on the 7T-MRI scanner. After a wash-out period, participants are quasi-randomized into a parallel design for a two-week period of daily weekday visits. During these visits, tVNS (sham or stimulation) is paired either with the behavioral FNAME task alone (visits 5-7 and 10-12) or while measuring pupil dilation with the eye-tracker (visits 4, 8 and 13). The study concludes with two cognitive testing follow-up visits. Visit windows are listed on the right of the flowchart, and colored icons represent participants across different arms. Abbreviations: h, hour(s); stim, stimulation; FNAME, face-name associative memory task.

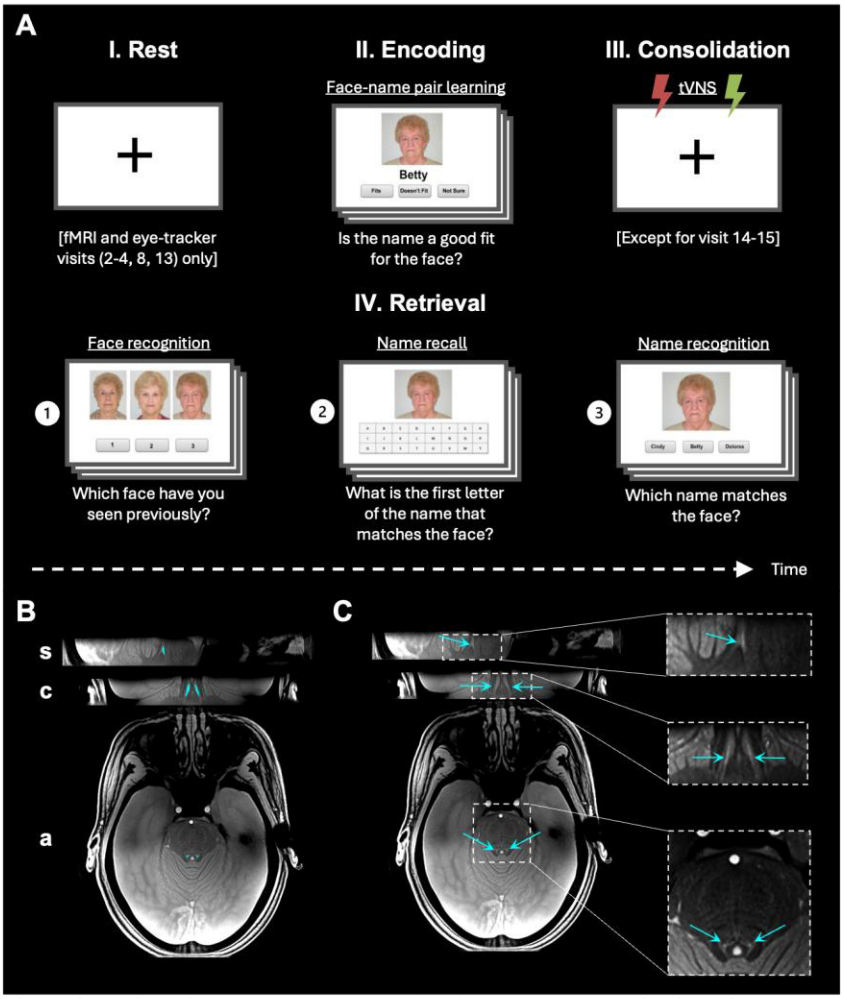


Figure 2. Design of the FNAME task and *in vivo* structural localization of the locus coeruleus using 7T magnetization transfer-weighted turbo flash MRI. a Participants perform the FNAME task across four phases: rest (for (f)MRI and eye-tracking visits only), encoding, consolidation, and retrieval. During the encoding phase, participants learn face-name pairs. In the consolidation phase, participants are instructed to focus on a fixation cross for 20 minutes while receiving either tVNS or sham stimulation in the cymba concha of the left ear. The intervention is gated to respiration differently for each condition, using a biphasic symmetric rectangular waveform at a frequency of 100 Hz. Stimulation intensity is individualized to a 5/10 numeric pain rating scale, ensuring a moderate to strong (but not painful) sensation, with the same intensity applied in subsequent visits. During the consolidation phase of visits 14-15, participants do not receive tVNS or sham stimulation and are not required to focus on a fixation cross. In the retrieval phase, participants complete three different tasks assessing their ability to recognize faces, as well as to recall and recognize the names matching the presented faces. Two distinct sets of faces are used for the FNAME task throughout the study: one for (f)MRI visits (visits 2-3) and another for behavioral visits (visits 4-15), with all faces presented in randomized order. **b** An LC mask (blue) overlaid on the mean magnetization transfer-weighted turbo flash MRI brain image from the WALLe trial cohort to date, shown in sagittal (top), coronal (middle), and axial (bottom) planes. **c** Depiction of the same planes as in panel b, but without the LC mask overlay, featuring a zoomed-in box. Blue arrows highlight the hyperintense LC signal for reference. Abbreviations: tVNS, transcutaneous vagus nerve stimulation; s, sagittal; c, coronal; a, axial; FNAME, face-name associative memory task; LC, locus coeruleus.

Keywords: neuromodulation, tVNS, locus coeruleus, cognition, study design

35 Cerebral perfusion indices from early-phase [18F]-MK6240 dynamic Tau PET imaging in brain regions associated with Alzheimer's disease progression in an aging population.

Maeva Dhaynaut[1], Cristina Lois[3], Amal Tiss[3], Emma Thibault[3], Jessie Fanglu Fu[4], Jinsong Ouyang[1], Keith A. Johnson[3], Georges El Fakhri[1,2], Marc D. Normandin[1], Nicolas J. Guehl[1]

[1]*Yale PET Center, Department of Radiology & Biomedical Imaging, Yale University School of Medicine, New Haven, CT, US*
[2]*Yale PET Center, Department of Bioinformatics & Data Science, Yale University School of Medicine, New Haven, CT, US*
[3]*Gordon Center for Medical Imaging, Department of Radiology, Massachusetts General Hospital, Harvard Medical School, Boston, MA, US*
[4]*Athinoula A. Martinos Center for Biomedical Imaging, Department of Radiology, Massachusetts General Hospital, Harvard Medical School, Boston, MA, US*

Background: Radiotracers with sufficient extraction fraction can provide insights into cerebral blood flow (CBF). Recent findings highlight the utility of early-phase [^{18}F]-MK6240 PET in deriving quantitative perfusion indices, providing information on Tau load and perfusion from the same dynamic scan. Since the relationship between CBF changes and Alzheimer's disease (AD) remains unclear, this study examines cerebral perfusion indices across brain regions mapping AD progression and their relationships with Aβ and Tau.

Methods: Ninety-five aging adults (twenty-four cognitively unimpaired with PIB positive status (CU PIB+), fifty-five with PIB negative status (CU PIB-), sixteen MCI/AD) underwent dynamic [^{11}C]-PiB and [^{18}F]-MK6240 PET scans on a Discovery MI-5, with structural MRI on a 3T Tim Trio. Braak regions (I-VI) were segmented using FreeSurfer to extract regional brain time-activity curves. Early [^{18}F]-MK6240 frames were analyzed with the simplified reference tissue model 2 to estimate the relative delivery rate R_1. Aβ and Tau burdens were quantified using distribution volume ratios (DVR) with Logan method. Aβ burden was defined in a large neocortical aggregate (FLR). All analyses used the cerebellum grey matter as reference. Correlation analyses explored relationships between R_1, age, Aβ, and Tau.

Results: R_1 parameter distribution followed the regional advancement of Braak stages (n=95, p<0.0001 stages I-V). In CU PiB+, R_1 inversely correlated with Aβ burden (p=0.0057) in FLR regions and Tau (p=0.0044) in medial temporal cortex, region linked to early stages. A significant relationship emerged between R_1 and Tau in individuals with MCI or AD within the inferior temporal cortex (n=16, p=0.03), region associated with intermediate stages.

Conclusion: Findings suggest reduced CBF occurs in brain regions representing early AD stages and is linked to Aβ and Tau accumulation in CU individuals with positive PiB status. Correlations between R_1 and Tau in individuals with MCI or AD may emphasize cerebral perfusion deficits in advanced stages.

Keywords: Cerebral Blood Flow, [18F]-MK6240 Tau PET, Alzheimer's Disease, Perfusion Indices, R1 parameter

36 Transcutaneous auricular vagus nerve stimulation improves learning and sleep-wake quality in older APOE-ε4 carriers

Marion Baillet[1,2], Maxime Van Egroo[1,2,3], Nina Engels-Domínguez[1,3], Jill Grube[1], Haley Fenlon[1], Emma E. Wiklund[1], Lukas Heinrich[1,3], Joost M. Riphagen[1,2], Kathryn V. Papp[2,4,5], Ronald G. Garcia[1,2,6], Roberta Sclocco[1,2,7,8], Vitaly Napadow[1,2,7,8], Heidi I. L. Jacobs[1,2,3]

[1]*Athinoula A. Martinos Center for Biomedical Imaging, Department of Radiology, Massachusetts General Hospital, Boston, MA, US*
[2]*Harvard Medical School, Boston, MA, US*
[3]*Faculty of Health, Medicine and Life Sciences, Mental Health and Neuroscience Research Institute, Alzheimer Centre Limburg, Maastricht University, Maastricht, NL*
[4]*Center for Alzheimer Research and Treatment, Department of Neurology, Brigham and Women's Hospital, Boston, MA, US*
[5]*Department of Neurology, Massachusetts General Hospital, Boston, MA, US*
[6]*Department of Psychiatry, Massachusetts General Hospital, Boston, MA, US*
[7]*Department of Radiology, Logan University, Chesterfield, MO, US*
[8]*Department of Physical Medicine and Rehabilitation, Spaulding Rehabilitation Hospital, Boston, MA, US*

Background: The locus coeruleus (LC) constitutes a critical site of initial tau accumulation, and modulates cognitive processes and sleep, which are affected early on in Alzheimer's disease. Here, we investigated the potential of transcutaneous auricular vagus nerve stimulation (taVNS), a neuromodulatory technique presumed to indirectly target LC activity, to improve learning and sleep-wake quality in asymptomatic older individuals.

Methods: Fifty-nine participants from WALLe, an ongoing single-site randomized intervention study comparing repeated sham vs. stimulation, were included (**Fig.1**). Participants were invited for 10 separate visits over the course of two weeks during which they received either sham or stimulation and completed the same version of a Face-Name Associative Memory Exam (FNAME) to assess daily learning. A subset of participants had *APOE* genotype (n=51) and objective measures of sleep-wake quality (n=50) derived from actigraphy recordings before and during/after the intervention. Nonlinear mixed-effects models and paired t-tests were used to investigate intervention-related changes in learning and in sleep-wake quality, respectively.

Results: While we did not observe an effect of taVNS on FNAME metrics (time*condition, all $p>0.05$), we found that *APOE*-ε4 carriers receiving the stimulation exhibited greater practice effects on response times in recalling the first letter of names compared to *APOE*-ε4 carriers in the sham condition, while no difference was observed for non-carriers (time*condition**APOE*, $p=0.0002$, **Fig.2**). Regarding sleep-wake quality, participants receiving the stimulation displayed a decrease in the number of nocturnal awakenings compared to the sham condition ($p=0.032$), and this effect was stronger among *APOE*-ε4 carriers ($p=0.014$, **Fig.3**).

Conclusions: Our findings indicate that repeated taVNS is beneficial for *APOE*-ε4 carriers by improving learning and sleep-wake quality, suggesting taVNS may be an effective non-invasive intervention approach to modulate cognition and sleep in at-risk individuals. Considering that this study is still ongoing, these preliminary results will be reassessed in a larger sample.

Variables	Sham condition	Stimulation condition
N	28	31
Demographics		
Age (years)	68.1 ± 6.2	67.6 ± 4.7
Sex (n, %)		
Female	16 (57%)	17 (55%)
Male	12 (43%)	14 (45%)
Education (years)	16.8 ± 1.9	17.9 ± 1.6
APOE-ε4 carriers (n, %)†	8 (36%)	13 (45%)
MMSE score*	29.3 ± 0.9	29.2 ± 0.7
TICS score#	35.8 ± 2.2	35.8 ± 1.8

Mean ± standard deviation
† Available for 51 participants (22 sham condition / 29 stimulation condition)
* Available for 37 participants (17 sham condition / 20 stimulation condition)
# Available for 22 participants (11 sham condition / 11 stimulation condition)
APOE: apolipoprotein E; MMSE: Mini-Mental State Examination; TICS: Telephone Interview for Cognitive Status

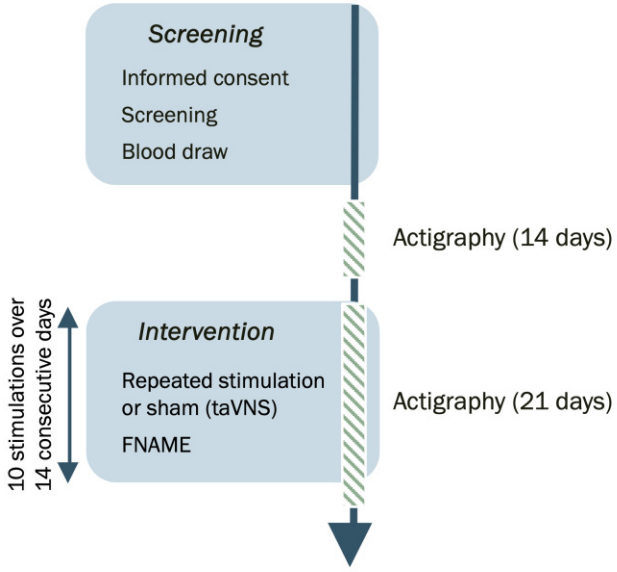


Figure 1. Participants characteristics and simplified study design. The electrode is placed in the cymba conchae of the left ear for both sham and stimulation conditions, with the intervention gated to respiration differently for each condition. Stimulation intensity is individualized to a 5/10 numeric pain rating scale, ensuring a moderate to strong (but not painful) sensation, and the same intensity is used in subsequent sessions. Each taVNS session lasts 20 minutes, with a biphasic symmetric rectangular waveform at a frequency of 100 Hz. The same set of faces is presented during the FNAME task, which includes a face recognition, a first letter name recall (face-name recall) and a face-name matching trial, to capture daily learning. Triaxial accelerometer data are measured for a continuous period of up 21 days at 50Hz with a dynamic range of +-8g while following a habitual sleep-wake schedule.

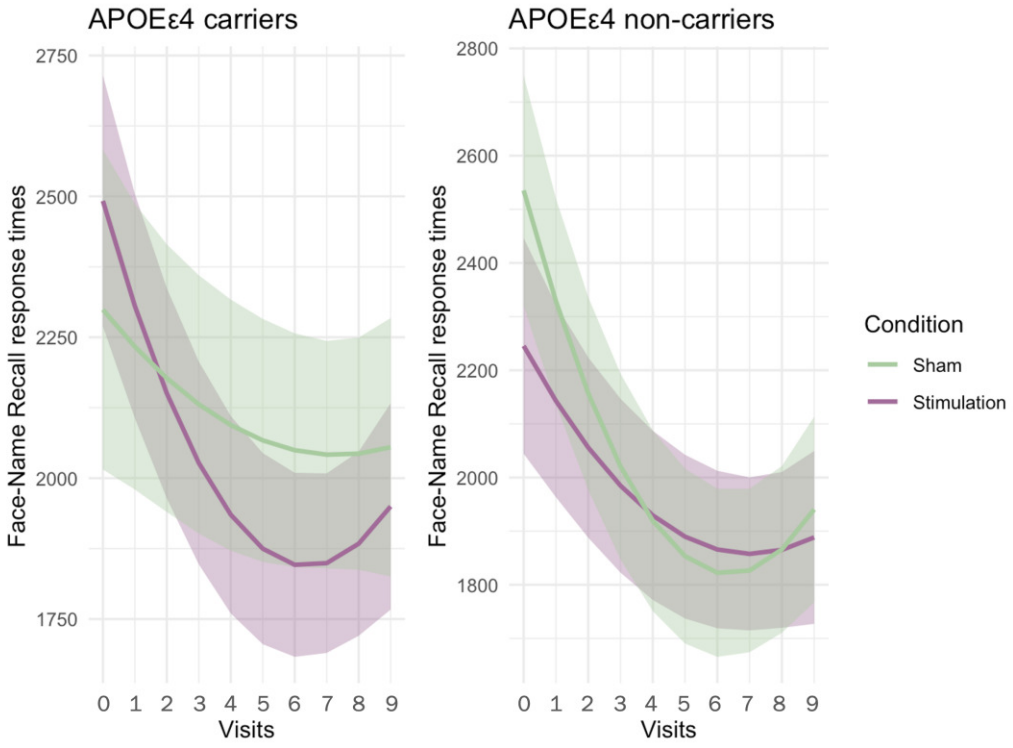


Figure 2. Effects of repeated serial stimulation or sham for two weeks on the Face-Name recall response times stratified according to *APOE* status. *APOE*-ε4 carriers receiving the stimulation exhibited greater practice effects on the Face-Name recall response times compared to *APOE*-ε4 carriers receiving the sham condition, while no difference was observed for non-carriers (non-linear mixed model, time*condition**APOE*, F=8.9, p=0.0002). Shaded areas represent 95% confidence interval.

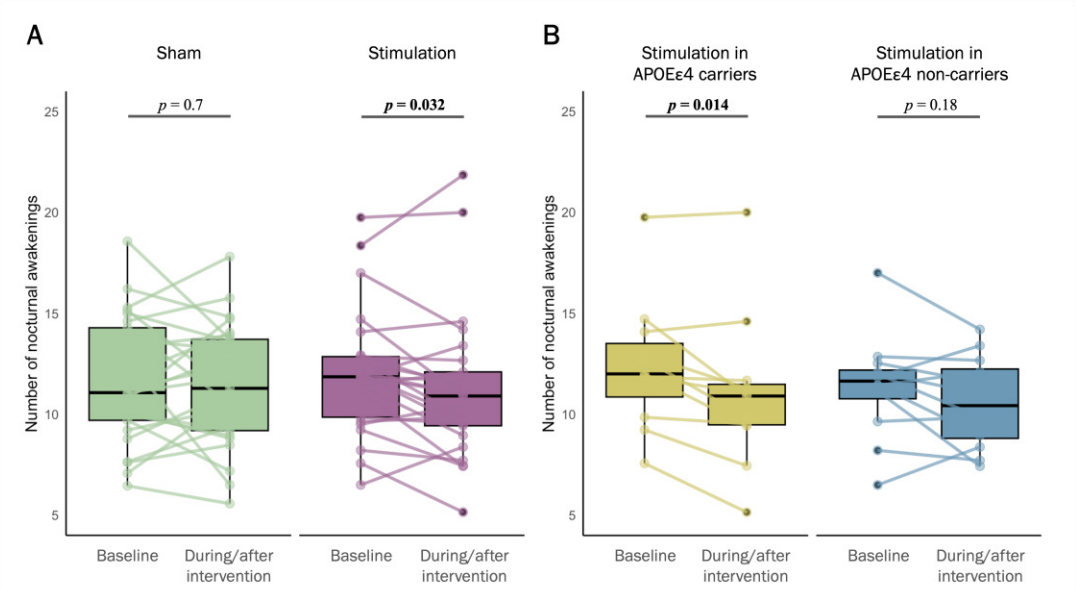


Figure 3. (A) Effects of repeated serial stimulation or sham for two weeks on the number of nocturnal awakenings, and (B) stratified according to *APOE* status in the stimulation condition. A significant decrease in the number of nocturnal awakenings was observed in the stimulation condition (paired *t*-test, $t = 2.3$, $p = 0.032$, purple) but not in the sham condition (paired *t*-test, $t = 0.4$, $p = 0.7$, green). Analysis stratified according to *APOE* genotype revealed that the decrease in the number of nocturnal awakenings was particularly expressed in *APOE*-ε4 carriers who received the stimulation (Wilcoxon test, $V = 60$, $p = 0.014$, yellow; $V = 57$, $p = 0.18$ in *APOE*-ε4 non-carriers, blue).

Keywords: Locus coeruleus, transcutaneous auricular vagus nerve stimulation, learning, sleep, APOE

37 Biological-clinical mismatch reflects co-pathology and vulnerability to neurodegeneration

Christopher Brown[1], Sandhitsu Das[1], Long Xie[3], Ilya Nasrallah[2], John Detre[1], Paul Yushkevich[2], Corey McMillan[1], David Wolk[1]

[1]*Department of Neurology, University of Pennyslvania, Philadelphia, PA, US*
[2]*Department of Radiology, University of Pennsylvania, Philadelphia, PA, US*
[3]*Siemens Healthineers, Princeton, NJ, US*

The dissociation of clinical and biological staging in the revised Alzheimer's Association criteria for Alzheimer's disease highlight the concept of clinical-biological mismatch as a reflection of resilience/vulnerability factors (e.g. co-pathologies). We sought to evaluate the usefulness of this concept by specifically assessing mismatch between Tau-PET and cognitive scales in the ADNI dataset. There were 365 Aβ+ (based on Core 1 biomarkers) participants with Tau-PET and cognitive testing with CDR-SB, measuring global function, and ADAS-13, primarily measuring amnestic impairment. We used Tau-MaX, our recently developed measure which quantifies global tau magnitude and extent, to measure tau burden. We used linear regression to predict CDR-SB or ADAS13 using Tau-MaX controlling for age, sex, and education. Results demonstrated moderate association between Tau-MaX and CDR-SB and ADAS13 (Figure 1A). Standardized residuals (SR) were calculated for each participant, with SR > 0.6 defining vulnerable groups, SR < -0.6 resilient, and -0.6 ≤ SR ≤ 0.6 canonical. Tau-MaX was similar between groups, but there was higher clinical stage, using Alzheimer's Association criteria, in vulnerable groups and lower stage in resilient groups (Figure 1B). We compared differences in cortical thickness, white matter hyperintensity (WMH) volume, and presence of α-synuclein between these groups controlling for age, sex, and Tau-MaX. CDR-vulnerable participants showed reduced thickness in a diffuse set of brain regions with the strongest effects in the temporal lobe (Figure 2A-B), while ADAS-vulnerable had reduced thickness primarily in temporo-limbic regions, suggestive of concomitant LATE (Figure 3A-B). CDR-vulnerable participants showed higher levels of α-synuclein+ compared to canonical and CDR-resilient participants (Figure 2C), while ADAS-vulnerable had higher levels of α-synuclein+ than ADAS-resilient (Figure 3C). Overall, these findings point to the value of clinical-biological mismatch to identify those with greater neurodegeneration and/or likely co-pathology (α-synuclein and LATE). Further, cognitive domain-based mismatch may allow for detection of more specific co-pathologies.

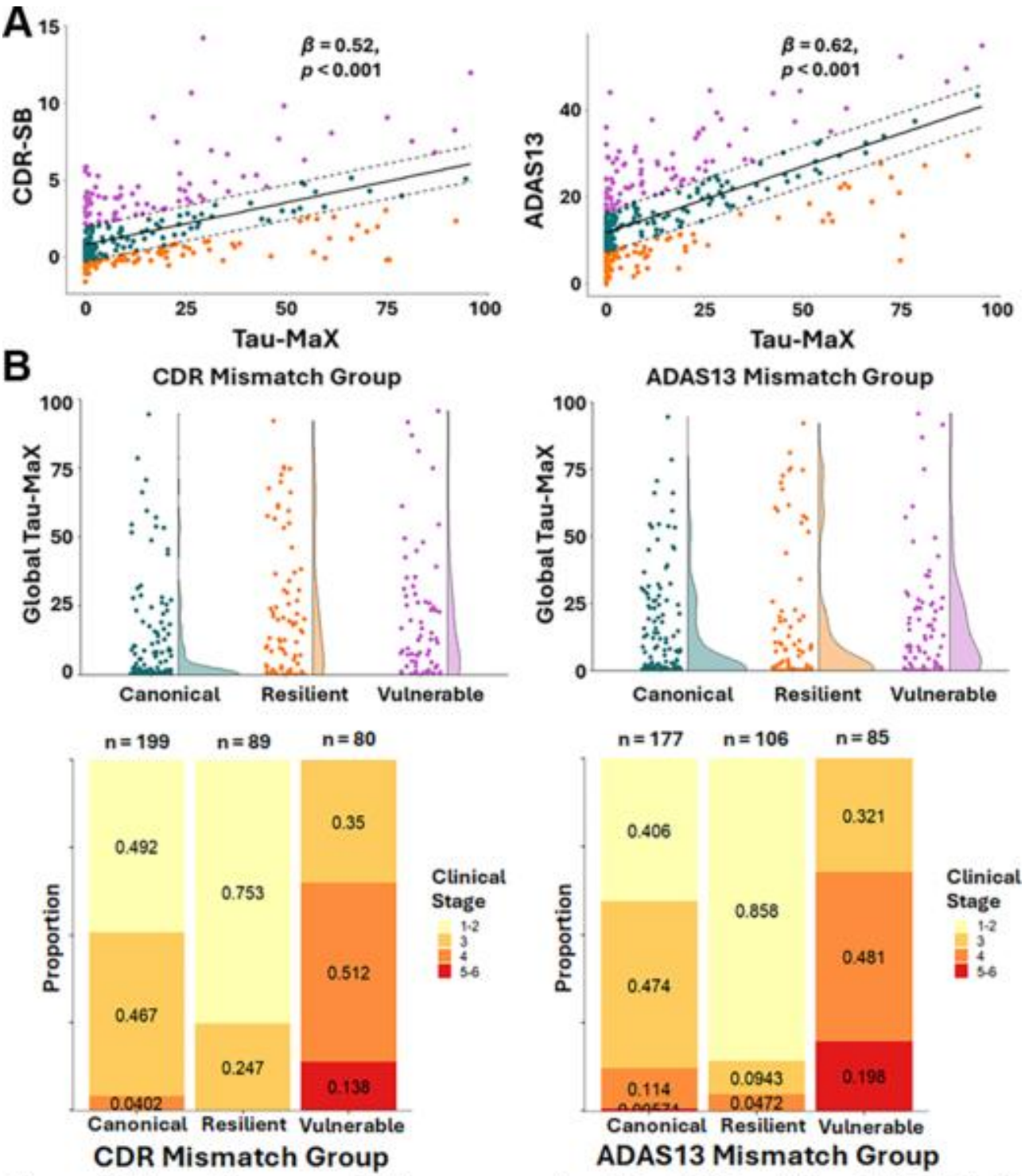


Figure 1. Mismatch groups. A: Linear regression of Tau-MaX predicting CDR-SB (left) and ADAS13 (right) with solid line representing linear-best fit and dashed lines representing standardized residual ± 0.6. Participants falling within these lines are considered canonical (green), above are vulnerable (purple) and below are resilient (orange). **B:** Tau severity (top) and clinical severity (bottom) plotted for CDR (left) and ADAS13 (right) mismatch groups. CDR resilient and vulnerable had higher Tau-MaX than canonical groups. For both CDR and ADAS, resilient groups had lower clinical stage and vulnerable groups had higher clinical stage.

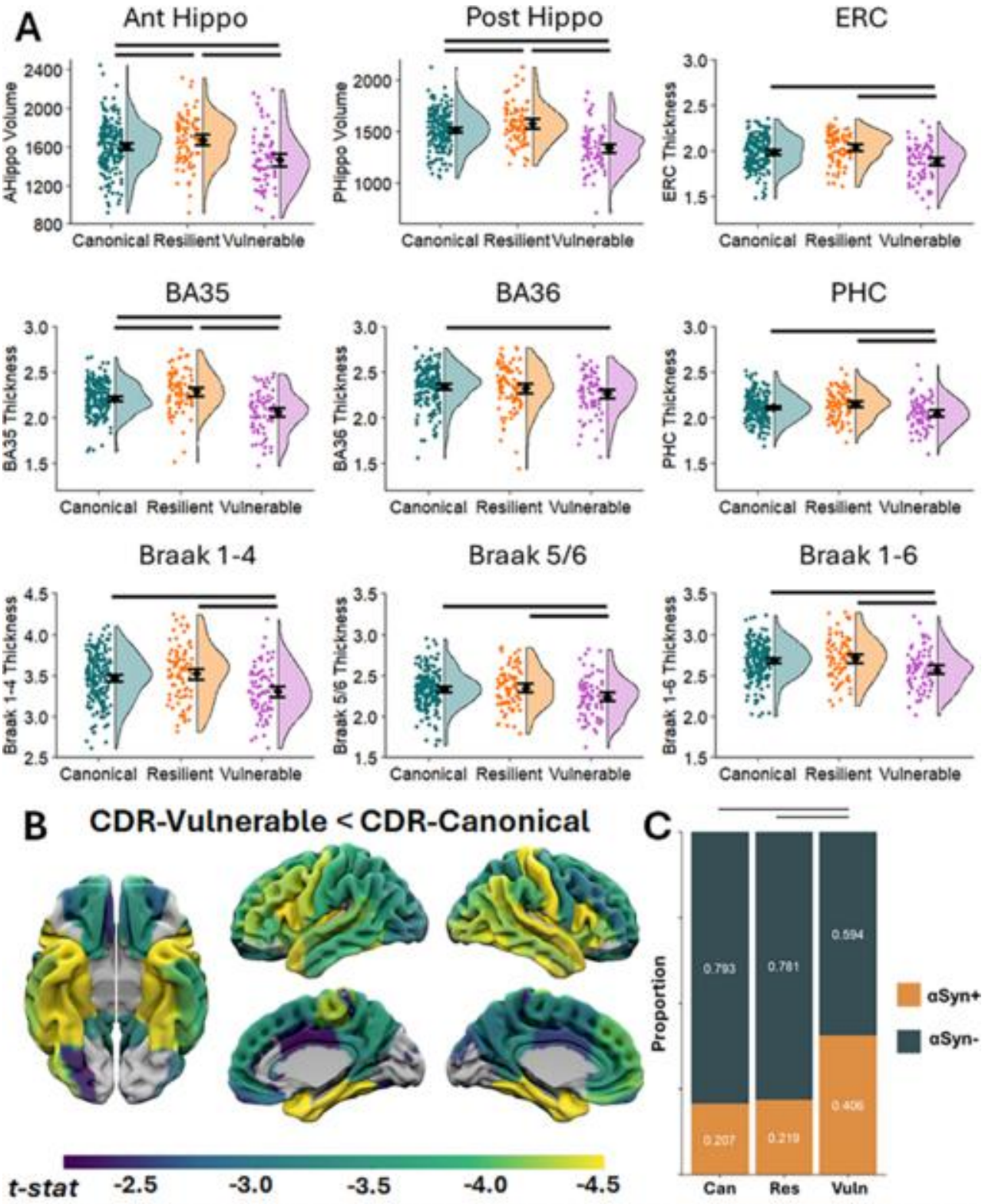


Figure 2. CDR-SB Mismatch. A: Differences in hippocampal volume, medial temporal lobe thickness from T1-ASHS,and ANTs cortical thickness measures in Braak meta-ROIs between canonical (green), resilient (orange), and vulnerable (purple) groups controlling for age, sex, education, and Tau-MaX. Significant differences are shown by lines above groups. **B**: Whole brain region-wise analysis of ANTS cortical thickness comparing CDR-vulnerable with CDR-canonical groups controlling for age, sex, education, and Tau-MaX. The color scale depicts the t-statistic for the contrast with only those with FDR-corrected $p < 0.05$ shown. **C**: Differences in proportion of αSyn+ participants in each group are shown with more αSyn+ participants in CDR-vulnerable than in CDR-canonical or CDR–resilient.

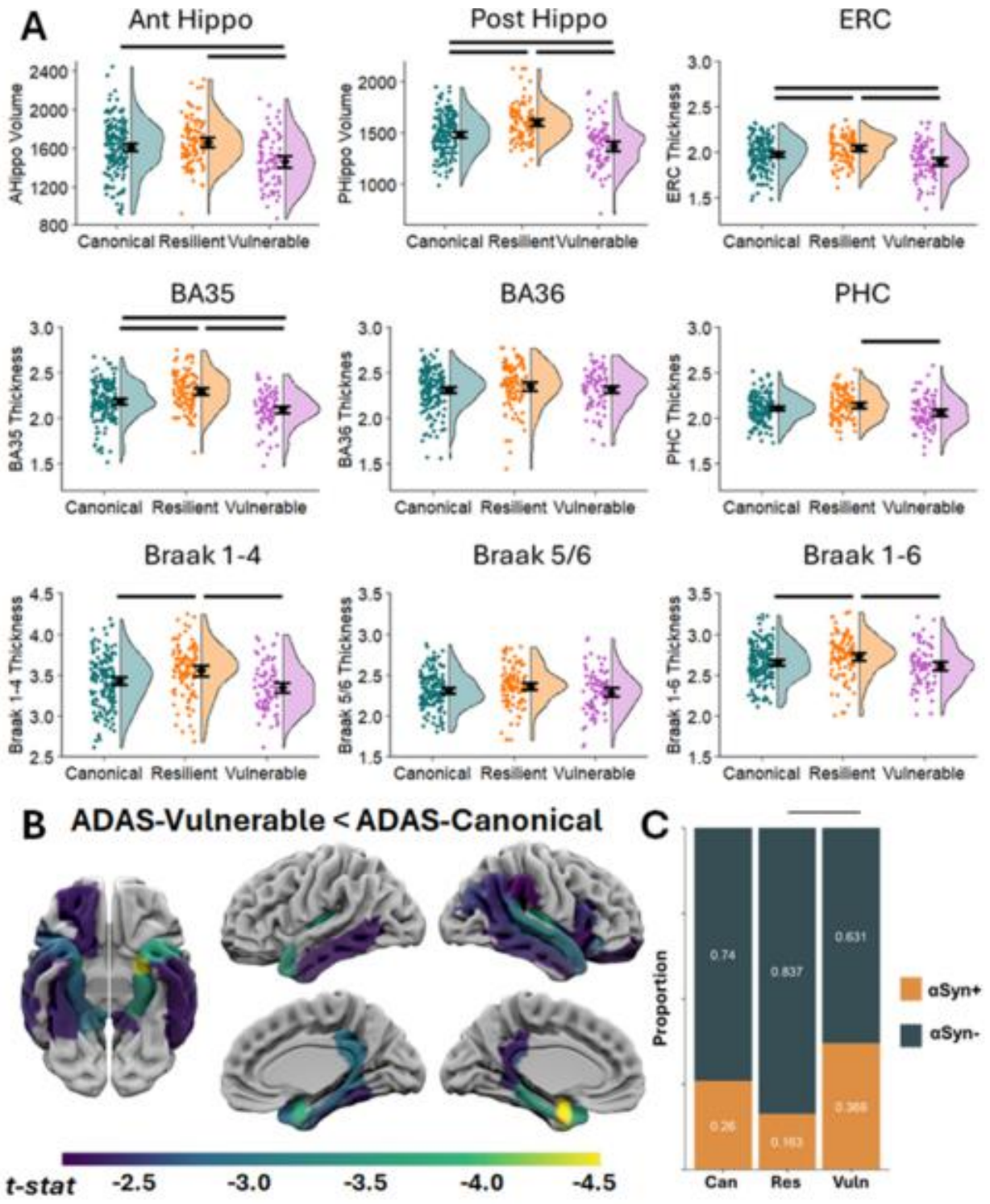


Figure 3. ADAS13 Mismatch. A: Differences in hippocampal volume, medial temporal lobe thickness from T1-ASHS,and ANTs cortical thickness measures in Braak meta-ROIs between canonical (green), resilient (orange), and vulnerable (purple) groups controlling for age, sex, education, and Tau-MaX. Significant differences are shown by lines above groups. **B:** Whole brain region-wise analysis of ANTS cortical thickness comparing ADAS13-vulnerable with ADAS13-canonical groups controlling for age, sex, education, and Tau-MaX. The color scale depicts the t-statistic for the contrast with only those with FDR-corrected $p < 0.05$ shown. **C:** Differences in proportion of αSyn+ participants in each group are shown with more αSyn+ participants in ADAS-vulnerable than in ADAS–resilient.

Keywords: Tau PET, cognition, Alzheimer's staging, flortaucipir

38 Validation of PET spatial extent as sensitive amyloid biomarker in early stages of amyloidosis

Grace Del Carmen Montenegro[1], Emma G Thibault[1], Jessie Fanglu Fu[1,4], Julie C Price[1], Bernard J Hanseeuw[2,3], Heidi I.L. Jacobs[4], Reisa A. Sperling[2,5], Keith A. Johnson[1,5], Michelle E. Farrell[1]

[1]*Department of Radiology, Massachusetts General Hospital, Harvard Medical School, Boston, MA, US*
[2]*Department of Neurology, Massachusetts General Hospital, Harvard Medical School, Boston, MA, US*
[3]*Department of Neurology, Cliniques Universitaires Saint-Luc, Université Catholique de Louvain, Bruxelles, BE*
[4]*Athinoula A. Martinos Center for Biomedical Imaging, Charlestown, MA, US*
[5]*Center for Alzheimer Research and Treatment, Department of Neurology, Brigham and Women's Hospital, Harvard Medical School, Boston, MA, US*

	A4/LEARN			Tau Subsample		
	EXT- (N=435)	EXT+ (N=337)	EXT++ (N=345)	EXT- (N=61)	EXT+ (N=80)	EXT++ (N=104)
Global FBP SUVR						
Mean (SD)	0.671 (0.0274)	0.759 (0.0441)	0.934 (0.0778)	0.673 (0.0297)	0.763 (0.0410)	0.921 (0.0702)
Median [Min, Max]	0.673 [0.591, 0.728]	0.752 [0.673, 0.903]	0.915 [0.802, 1.24]	0.677 [0.592, 0.728]	0.768 [0.688, 0.880]	0.903 [0.816, 1.13]
Sex						
F	266 (61.1%)	209 (62.0%)	208 (60.3%)	34 (55.7%)	51 (63.8%)	66 (63.5%)
M	169 (38.9%)	128 (38.0%)	137 (39.7%)	27 (44.3%)	29 (36.3%)	38 (36.5%)
APOE Status						
Carrier	90 (20.7%)	143 (42.4%)	232 (67.2%)	13 (21.3%)	31 (38.8%)	79 (76.0%)
Non-carrier	343 (78.9%)	194 (57.6%)	113 (32.8%)	48 (78.7%)	49 (61.3%)	25 (24.0%)
Missing	2 (0.5%)	0 (0%)	0 (0%)	0 (0%)	0 (0%)	0 (0%)
Age						
Mean (SD)	70.3 (4.22)	70.9 (4.48)	72.7 (5.17)	69.2 (3.63)	71.1 (4.62)	72.2 (4.90)
Median [Min, Max]	69.4 [65.0, 85.6]	70.0 [65.0, 84.5]	72.0 [65.0, 85.7]	68.1 [65.1, 80.4]	70.6 [65.1, 84.5]	71.9 [65.0, 85.5]
Education						
Mean (SD)	16.7 (2.55)	16.6 (2.83)	16.6 (2.93)	16.6 (2.58)	16.2 (3.03)	15.8 (2.63)
Median [Min, Max]	16.0 [8.00, 30.0]	16.0 [8.00, 27.0]	16.0 [9.00, 30.0]	16.0 [11.0, 20.0]	16.0 [9.00, 26.0]	16.0 [9.00, 21.0]
Total Time - Cognitive						
Mean (SD)	4.47 (1.57)	4.23 (1.65)	4.21 (1.55)	4.90 (1.34)	4.36 (1.43)	4.38 (1.44)
Median [Min, Max]	5.00 [0.129, 7.25]	4.91 [0.123, 6.67]	4.89 [0.167, 5.83]	5.26 [0.238, 6.87]	4.97 [0.192, 5.69]	4.98 [0.167, 5.53]
Total Time - Tau						
Mean (SD)	3.36 (1.66)	3.16 (1.91)	3.40 (1.93)	3.36 (1.66)	3.16 (1.91)	3.43 (1.91)
Median [Min, Max]	3.21 [0, 5.51]	3.67 [0, 5.39]	4.58 [0, 5.37]	3.21 [0, 5.51]	3.67 [0, 5.39]	4.58 [0, 5.37]

Table 1: Sample Demographics. This table presents baseline demographic and clinical characteristics for the full A4/LEARN sample and the tau subsample, stratified by amyloid stage using spatial extent into EXT- (<5%, Aβ-), EXT+ (5-84%, spreading Aβ), and EXT++ (>85%, widespread Aβ).

			Independent Models						Combined Models					
Outcome	Sample	n	Aβ term	β	SE	p	η^2	AIC	β	SE	p	AIC	$\chi2$	p
MTL TAU	All tau	244	SUVR	0.006	0.001	<.001	0.097	-1828	0.002	0.003	0.635	-1828	3.200	0.202
	All tau	244	EXT	0.007	0.001	<.001	0.106	-1826	0.005	0.003	0.122		5.712	0.058
	EXT > 85%	103	SUVR	0.003	0.004	0.397	0.010	-628						
	EXT < 85%	141	SUVR	0.004	0.003	0.202	0.014	-1278	-0.008	0.007	0.295	-1277	3.118	0.210
	EXT < 85%	141	EXT	0.004	0.002	0.061	0.032	-1279	0.010	0.006	0.087		2.790	0.248
	EXT < 50%	110	SUVR	0.005	0.004	0.211	0.018	-973	-0.015	0.007	0.043	-981	12.049	0.002
	EXT < 50%	110	EXT	0.012	0.004	0.004	0.106	-981	0.023	0.007	0.001		4.511	0.105
NEO TAU	All tau	244	SUVR	0.016	0.002	<.001	0.266	-1959	0.021	0.005	<.001	-1957	2.596	0.273
	All tau	244	EXT	0.014	0.002	<.001	0.196	-1935	-0.005	0.005	0.306		26.732	0.000
	EXT > 85%	103	SUVR	0.024	0.006	<.001	0.145	-647						
	EXT < 85%	141	SUVR	0.011	0.003	0.001	0.108	-1430	-0.004	0.008	0.558	-1431	5.066	0.079
	EXT < 85%	141	EXT	0.010	0.002	<.001	0.150	-1434	0.013	0.006	0.028		0.688	0.709
	EXT < 50%	110	SUVR	0.008	0.003	0.021	0.061	-1147	-0.010	0.005	0.057	-1159	16.125	0.000
	EXT < 50%	110	EXT	0.012	0.003	<.001	0.212	-1159	0.020	0.005	<.001		4.356	0.113
PACC	All	1113	SUVR	-0.218	0.019	<.001	0.123	44371	-0.312	0.050	<.001	44366	8.704	0.013
	All	1113	EXT	-0.187	0.019	<.001	0.090	44415	0.102	0.050	0.042		53.033	0.000
	EXT > 85%	343	SUVR	-0.402	0.074	<.001	0.092	14502						
	EXT < 85%	770	SUVR	-0.123	0.037	0.001	0.018	29606	0.064	0.089	0.469	29604	6.427	0.040
	EXT < 85%	770	EXT	-0.116	0.029	<.001	0.026	29604	-0.162	0.070	0.021		4.185	0.123
	EXT < 50%	651	SUVR	-0.071	0.052	0.170	0.004	24741	0.104	0.086	0.226	24738	6.925	0.031
	EXT < 50%	651	EXT	-0.146	0.055	0.009	0.014	24738	-0.235	0.092	0.011		4.277	0.118

Table 2 Caption: This table summarizes the results of linear mixed-effects models examining the predictive power of baseline amyloid burden (SUVR) and spatial extent (EXT) on 3 outcomes: cognitive decline (PACC) and tau accumulation (MTL and NEO). For each outcome, 3 models were performed. First, independent models were run to test the association between each Aβ metric at baseline and on each outcome over time (Model 1: time*SUVR, Model 2: time*EXT). EXT and SUVR were standardized to allow for direct comparison of the β estimates and standard error between models. Effect sizes (partial η^2) and Akaike Information Criterion (AIC) are reported to provide estimates of EXT and SUVR's effect on each outcome and overall model fit. Next, we conducted a combined model including the time*EXT and time*SUVR terms in the same model to see which measure (if either) was a better fit to the data. AIC for the combined model is also reported, allowing comparison against the independent models for EXT SUVR to determine which model is the best fit (lowest AIC). Finally, $\chi2$ statistics and their associated p-values from a likelihood-ratio test (ANOVA) between independent SUVR/EXT models and the combined model are reported to indicate whether adding EXT (or SUVR) explains additional variance in predicting PACC or tau accumulation (i.e. for SUVR rows a $p<0.05$ for the $\chi2$ test indicates EXT explained significant additional variance in the outcome measure, while $p<0.05$ in EXT rows indicate SUVR explained significant additional variance). This set of analyses were repeated within different subsamples representing different stages of amyloidosis.

Background: We recently demonstrated the sensitivity of PET spatial extent (EXT) measures of amyloid-beta (Aβ) when targeting the earliest stage of preclinical Alzheimer's disease (AD). In cognitively-unimpaired older adults from the Harvard Aging Brain Study (HABS), [^{11}C]PiB spatial extent (% neocortex with elevated uptake) was a better predictor of subsequent tau proliferation and cognitive decline than traditional measures of neocortical uptake. We sought to validate the PET EXT approach through replication in an independent sample with a different Aβ radioligand.

Methods: 1,117 cognitively-unimpaired older adults (Table1) were included from A4 Study (n=537, placebo) and LEARN (n=576) with baseline Aβ-PET ([^{18}F]florbetapir) and longitudinal cognitive assessments using Preclinical Alzheimer's Cognitive Composite (PACC, median=4.9 years). A subsample of 245 participants (n_{A4}=189, n_{LEARN}=55) also had longitudinal [^{18}F]flortaucipir (FTP) Tau-PET. We quantified Aβ using SUVR and EXT within a neocortical aggregate. Linear mixed-effects models assessed how well SUVR and EXT predicted three outcomes over time: cognition and tau SUVR in the medial temporal lobe (MTL) and temporal neocortex (NEO). Further analysis within subsamples assessed the relative performance of EXT and SUVR at different stages of amyloidosis.

Results: In the full sample (Table2), EXT was a stronger predictor of MTL tau accumulation while SUVR was a better predictor of changing PACC and NEO tau due to their association with increasing SUVR after Aβ was widespread (EXT>85%). Conversely, EXT was the stronger predictor for all three outcomes in earlier Aβ-EXT stages (EXT<85%, EXT<50%, Table2).

Conclusion: We replicated Aβ EXT's superior prediction of future cognitive decline and tau proliferation during the early stages of preclinical AD, when Aβ is still spreading. In contrast with our previous findings, increasing Aβ SUVR was still associated with tau and cognition after Aβ EXT was saturated. These results underscore the importance of adapting the choice of Aβ metrics to disease stage.

Keywords: Early Detection, Preclinical AD, Spatial Extent, Cognitive Decline, Tau

39 Developing a novel reference region for PI-2620-PET imaging to facilitate assessment of 4-repeat tauopathies

Lukas Frontzkowski

L. Frontzkowski*; M. Gross*; J. Gnörich, A. Dewenter; A. Desharvi; M. Malpetti; S. Roemer; A. Steward; F. Wagner; M. Brendel*; N. Franzmeier*

[1|2|3|4]*Institute for Stroke and Dementia Research (ISD) | Department of Neurology, LMU University Hospital | Department of Nuclear Medicine, LMU University Hospital | Department of Clinical Neurosciences and Cambridge University Hospitals NHS Trust*

Background: Neurodegenerative 4-repeat (4R) tauopathies commonly manifest as progressive supranuclear palsy (PSP). PSP patients show elevated PI-2620-PET in subcortical 4R tau predilection sites (e.g., globus pallidus), suggesting PI-2620-PET as a promising 4R tau neuroimaging candidate. However, optimal quantification of PI-2620-PET in 4R tauopathies remains challenging, as conventional cerebellar tau-PET reference regions also accumulate 4R tau. We aimed to use unbiased image-derived input function (IDIF) PET data to determine an optimized PET reference region for in vivo quantification of 4R tau.

Methods: We obtained 60-minute dynamic PI-2620-PET in 54 PSP Richardson Syndrome (PSP-RS) patients and 19 healthy controls (HC), applying IDIF-modeling using carotid timeseries to assess unbiased PI-2620-PET binding and determine total distribution volume (VT). Through an iterative approach, we intensity-normalized VT-images against white-matter regions in the Hammers brain atlas, identifying regions where intensity-normalized pallidum PET values showed the largest PSP-RS vs. HC differences. White-matter regions with strongest PSP-RS vs. HC differences surviving multiple-comparison correction were summarized into a single reference region spanning bilateral temporal white-matter. This ROI was then used to determine SUVRs using conventional 20-40 minute PI-2620-PET data in PSP-RS, a PSP-non-RS validation sample (n=63), as well as non-tau disease controls (i.e., alpha-synucleinopathies, n=20; Alzheimer's disease, n=23).

Results: Using PI-2620 SUVRs obtained with the temporal-lobe white-matter reference, we detected strong PSP-RS vs. HC group differences in basal ganglia SUVRs using voxel-wise comparisons ($p<0.001$, FWE-cluster corrected, Fig. 1). Similar basal ganglia differences were detected for PSP-non-RS vs. HC, but not for alpha-syn or AD vs. HC (cortical AD-like group differences). Minimal group differences were found using a conventional inferior cerebellar grey matter reference region (Fig. 2).

Conclusions: Our findings suggest temporal white-matter is superior to inferior cerebellum as a reference region for PI-2620-PET imaging in 4R tauopathies due to increased sensitivity and specificity for 4R tau.

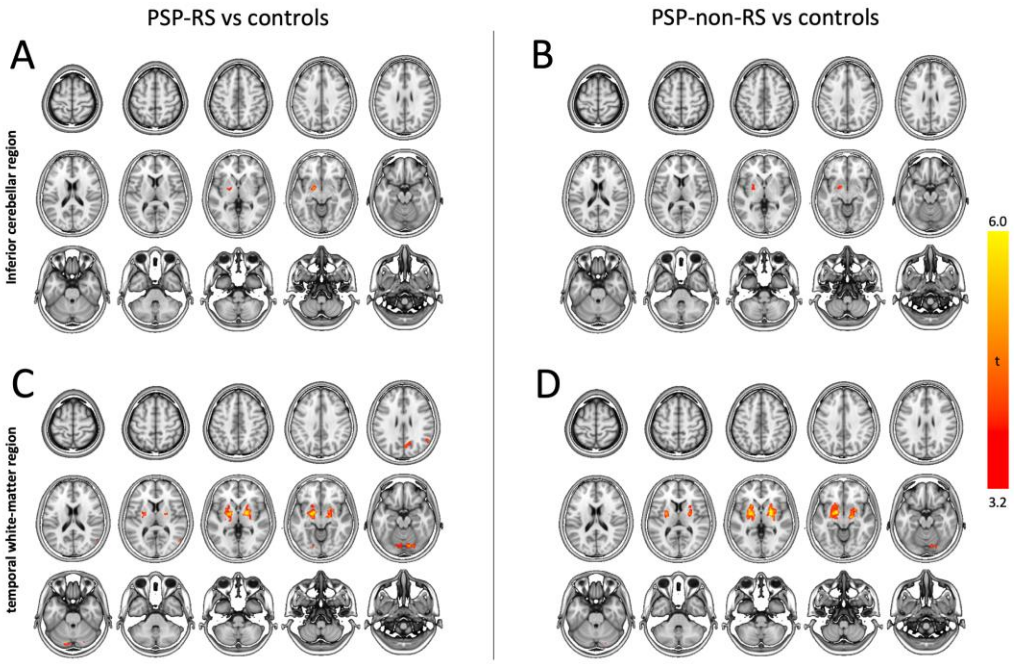


Figure 1: Results of cluster-corrected group comparisons (FWE, p < 0.001) for 20-40 minute PI-2620 SUVR data between PSP-RS and controls (A, B) and PSP-non-RS and controls (C, D). SUVR data was either intensity normalized using temporal white-matter region (A, C) or the conventionel inferior cerebellum as reference region (B, D).

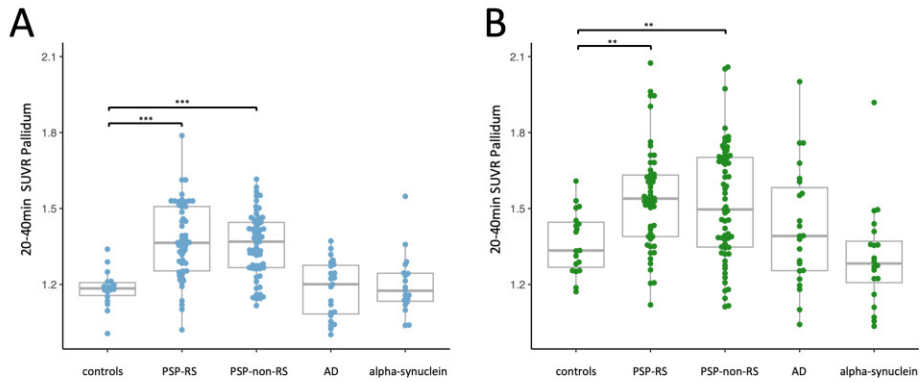


Figure 2: Boxplots illustrating the mean 20-40 minute PI-2620-PET SUVR from the pallidum for each group. SUVR data was either intensity-normalized via a temporal white matter region (A) or the conventional inferior cerebellum region (B). Asteriks are used to illustrate level of significance *** = p < 0.0001, ** = p < 0.001.

Keywords: PI-2620, tau-PET, 4R-tauopathies, PSP, Neurodegeneration

40 P-TAU217, GFAP, and NFL plasma biomarker associations with demographic, medical and neurocognitive features from middle-aged through older adulthood

Steven Arnold[1], Pia Kivisakk[1], Hadia Fatima[1], Jennifer Gentsch[2], Carlos Cruchaga[2], Chao-Yi Wu[1], Hiroko Dodge[1], Beau Ances[1,2], David Salat[1]

[1]*Massachusetts General Hospital, Harvard Medical School, Boston, MA, US*
[2]*Washington University in St. Louis, Saint Louis, MO, US*

The Adult Aging Brain Connectome (AABC) study follows healthy adults, ages 36-100+ from diverse backgrounds at four sites across the U.S.A., evaluating demographic, genetic, molecular, neurocognitive and anatomic/functional brain imaging characteristics. Its principal goals are to identify and understand risk and resilience factors for cognitive brain aging across the mature adult lifespan. Here we present current baseline data on phospho-tau 217 (pTau217), glial fibrillary acidic protein (GFAP) and neurofilament light (NfL) plasma biomarkers in the AABC and their associations with age, race and ethnicity, cardiovascular-metabolic health factors and global indices of cognition in different stages of adulthood.

The sample for analysis consisted of 652 individuals with a mean age 65.9 (s.d.15.4, range 36-100+), roughly equally distributed in three age categories - Younger Mature (36-55), Older (56-75), and Oldest (76+). 54.1% were Female and 45.9% Male. Racial identities included Asian 4.9%, Black/African-American 15.2%, Multi/Other 6.3%, and White 73.6%. 11.5% identified as Hispanic/Latino.

In univariate analyses, age was strongly correlated with all three biomarkers across the entire sample and within each age category, most highly in the Older (56-75) category. Across the age spectrum, women had lower levels of pTau217, higher GFAP, and no differences in NfL compared to men. There were significant differences for all biomarkers by race and ethnicity with higher values in Whites and Non-Hispanics overall and within each age category. In linear regression models adjusted for age, sex, race and ethnicity, differing indices of cardiovascular-metabolic factors were significantly associated with pTau217, GFAP and NfL. Finally, in fully adjusted models, higher pTau217 and NfL were significantly associated with lower cognitive performance overall, and especially in the Older and Oldest categories.

These data on robust blood-based biomarkers of AD and neurodegeneration identify early changes in AD biomarkers and their associations with cardiovascular-metabolic factors and cognition across the mature adult lifespan.

Keywords: p-tau, gfap, nfl, lifespan, cardiovascular

41 DeepSUVR: Using temporal constraints to improve tau quantification

Pierrick Bourgeat[1], Jurgen Fripp[1], Ashley Gillman[1], Azadeh Feizpour[2], Christopher Schwarz[4], Clifford R. Jack[4], Val Lowe[4], Michael W. Weiner[3], Colin L. Masters[5], Victor L. Villemagne[6], Christopher C. Rowe[2,5], Vincent Dore[1,2]

[1]*CSIRO Health and Biosecurity, Brisbane, AU*
[3]*Department of Molecular Imaging & Therapy, Austin Health, Melbourbe, AU*
[4]*San Francisco Veterans Affairs Medical Center, San Francisco, CA, US*
[5]*Department of Radiology, Mayo Clinic and Foundation, Rochester, MN, US*
[5]*The Florey Institute of Neuroscience and Mental Health, University of Melbourne, Parkville, AU*
[6]*Department of Psychiatry, University of Pittsburgh, Pittsburgh, PA, US*

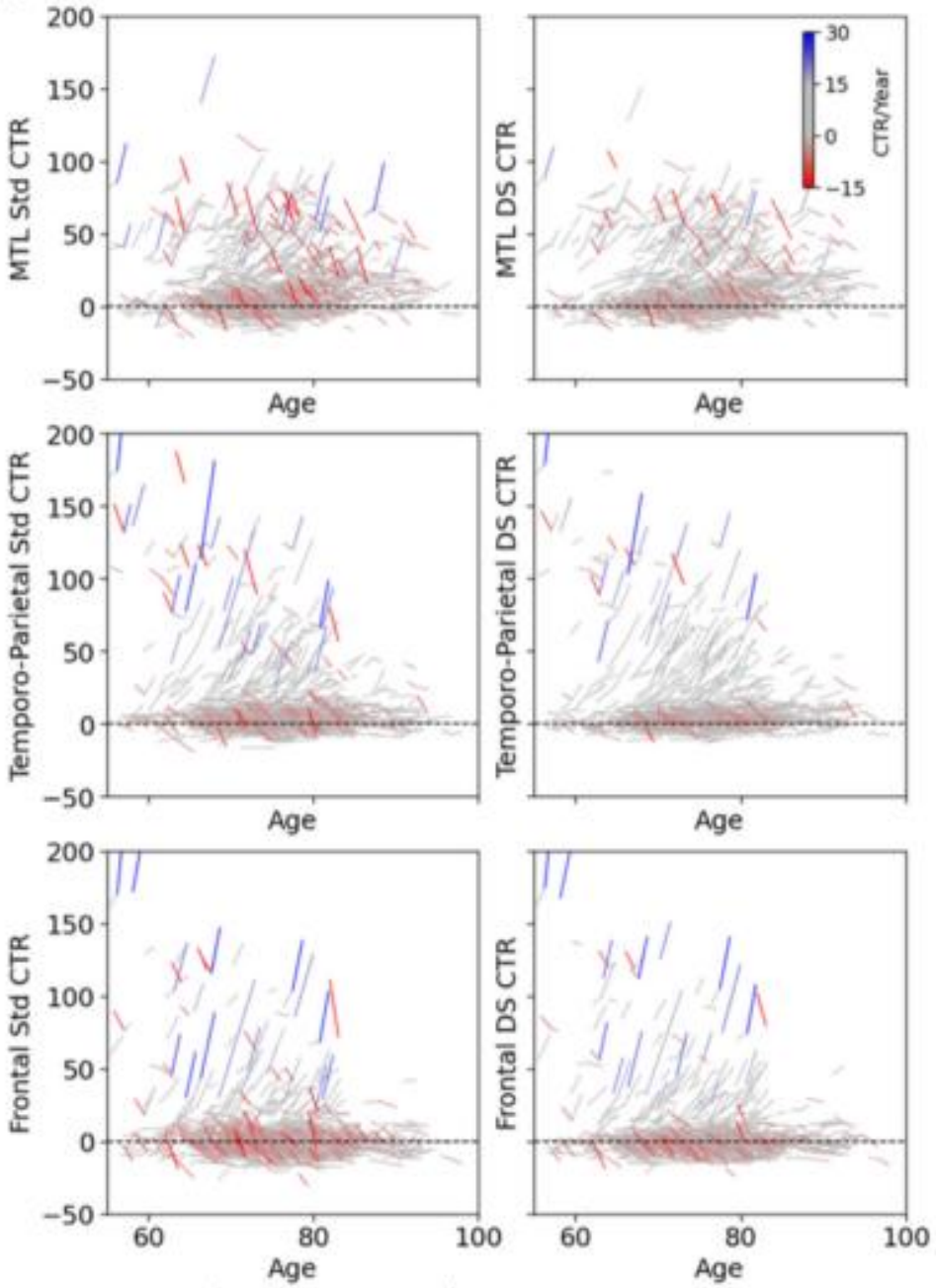
Background: Tau PET quantification using SUVR is affected by noise, spill in, and non-specific binding in the reference and target regions. We evaluated a novel deep learning method which learns from noise in longitudinal trajectories to correct the SUVR and improve quantification.

Method: 730 participants imaged at two or more visits using Flortaucipir (FTP=474) or MK6240 (MK=597) in AIBL+ADNI (N=1771 scans) had their tau PET images spatially normalised and quantified using the CenTauR (CTR) SPM8 pipeline. A deep learning network (DeepSUVR) was trained to predict a SUVR correction factor (CF) for each spatially normalised image. For each iteration, the prediction was run on 2 random visits from the same participant, resulting in 2 Adjusted CTR computed using SUVR*CF and each tracer's CTR transform. A loss function was defined to penalise unexpected temporal changes like CTR decreasing over time, CTR deviating from the CTR/Year vs mean CTR curve. The model was trained using 5-fold cross-validation on AIBL+ADNI. Once trained, the inference is performed on each visit independently. The model was evaluated on the out-of-fold test-sets, using the percentage of outliers (defined as changes <-5CTR/Yr or >15CTR/Yr), and comparing the rate of change in the CU-/CU+/MCI+/AD+ using a matched subset of MK and FTP. The model was further evaluated on an independent longitudinal test set from the Mayo Clinic comparing the rate of change in the CU/AD.

Results: In AIBL+ADNI, DeepSUVR reduced outliers by 44% on average in the MTL, Temporo-Parietal and Frontal regions (Fig1). It also increased the separation in CTR/Yr between clinical groups in both AIBL+ADNI (Fig2) and in the Mayo dataset (Fig3).

Conclusions: We have developed a novel technique to improve CTR quantification. While a larger dataset is essential to better optimise the model, the preliminary results are promising and show potential to reduce sample-sizes required in anti-tau trials.

(a)



(b)

	MTL		Temporo-Parietal		Frontal	
	Std	DS	Std	DS	Std	DS
CTR < -5CTR/Y	6.40%	**3.90%**	3.80%	**1.40%**	5.90%	**3.10%**
CTR > 15CTR/Y	1.90%	**0.80%**	1.90%	**1.50%**	2.20%	**1.80%**

Figure 1. (a) Longitudinal trajectories in the combined AIBL+ADNI dataset using the standard CTR quantification pipeline (left) and the DeepSUVR approach (right) in the MTL (top), Temporo-Parietal (middle) and Frontal (bottom) with a colormap highlighting negative rates of changes in red and changes above 15CTR/Yr in blue. (b) The table shows the percentage of trajectories between 2 consecutive visits with changes below −5CTR/Yr or above 15CTR/Yr when using the Standard approach (Std) or DeepSUVR (DS). Bold values indicate the lower number of outliers between the 2 quantification methods.

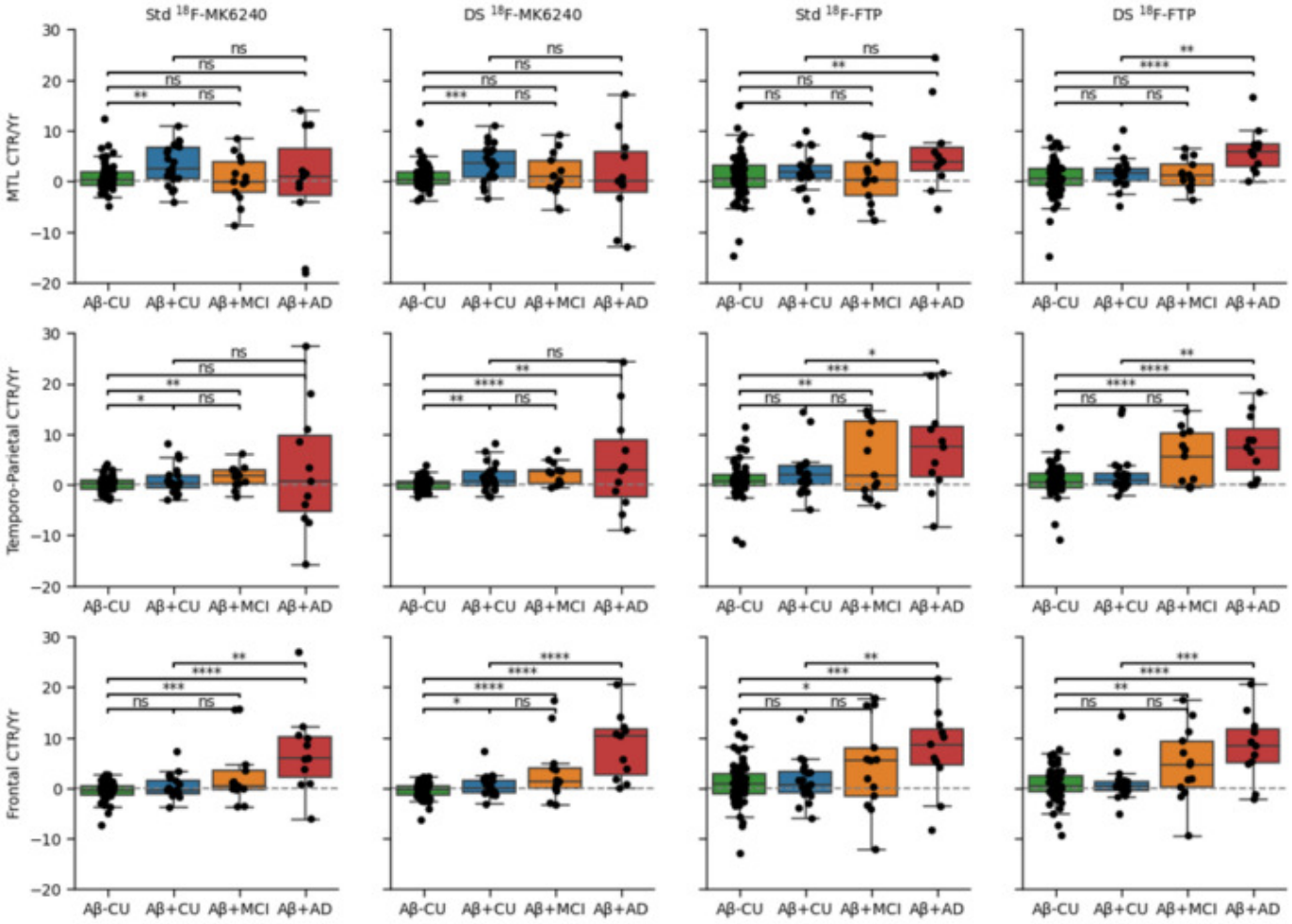


Figure 2. Boxplot showing the CTR/Yr in the MTL (top), Temporo-Parietal (middle) and Frontal (bottom) in 4 diagnosis groups (Aβ- CU, Aβ+ CU, Aβ+ MCI and Aβ+ AD) from a subset of MK (left) and FTP (right) from AIBL+ADNI. The MK and FTP subsets were matched for Age, Centiloid, MMSE and time between baseline and follow-up. For each tracer, the first column shows the CTR/Yr computed using the Standard CTR approach (Std) and the second column shows the CTR/Yr computed using DeepSUVR (DS). The significance of the group separation is denoted using ns: not significant; *: p<0.5; **:p<0.1; ***:p<0.01; ****:p<0.001.

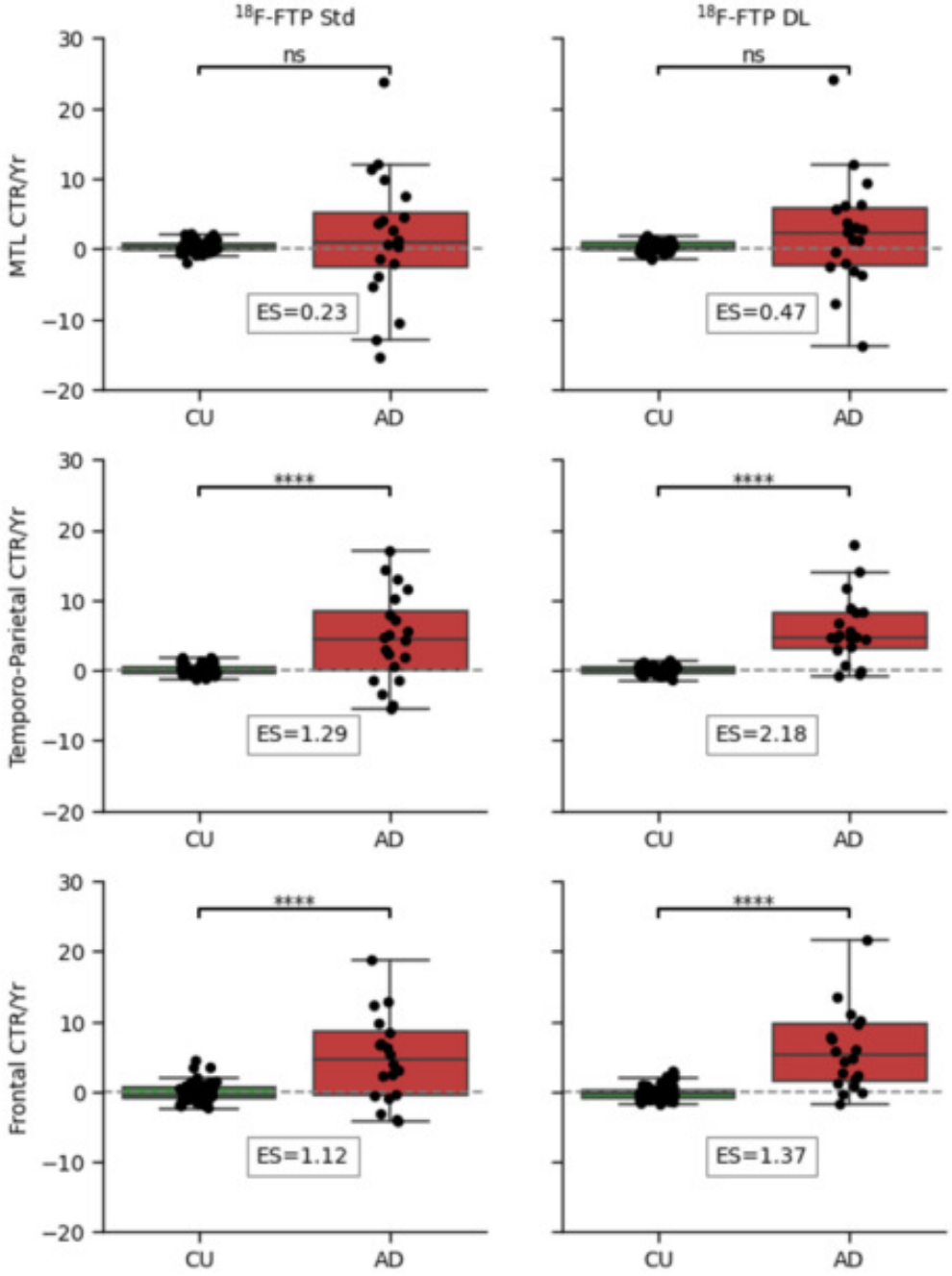


Figure 3. Boxplot showing the CTR/Yr in the MTL (top), Temporoparietal (middle) and Frontal (bottom) in CU (N=50) and AD (N=35) from a subset of FTP from the Mayo Clinic Study of Aging and Mayo Clinic Alzheimer's Disease Research Center (https://www.gaain.org/centaur-project). The CTR/Yr computed using the Standard CTR approach (left) and DeepSUVR (right). The significance of the group separation is denoted using ns: not significant; ****:p<0.001. The effect size (ES) between CU and AD is computed using Cohen's d.

Keywords: CenTauR, Flortaucipir, MK6240, quantification

42 Increasing the granularity of tau-PET Braak staging using medial temporal lobe segmentations to detect early memory impairment

Etienne Aumont[1,2], Brandon Hall[1,2,3], Lydia Trudel[1,2,3], Tevy Chan[1,2,3], Ali Hosseini[1,2,3], Arthur Macedo[1,2,3], Jaime Fernandez Arias[1,2,3], Nesrine Rahmouni[1,2,3], Joseph Therriault[1,2,3], Stijn Servaes[1,2,3], Gleb Bezgin[1,2,3], Jenna Stevenson[1,2,3], Pedro Rosa-Neto[1,2,3]

[1]*McGill University Research Centre for Studies in Aging, Montréal, QC, CA*
[2]*Montreal Neurological Institute, Montréal, QC, CA*
[3]*Department of neurology and neurosurgery, Montréal, QC, CA*

Transforming brain images to a standard template has been a staple of tau PET processing. However, this transformation comes at the cost of spatial specificity, which might be particularly important to study the small medial temporal lobe (MTL) regions. This study aims to supplement traditional tau-PET Braak staging with native space MTL tau-PET to identify early memory impairment better.

We segmented 6 MTL regions using T1-weighted images from 356 participants (60.1% female, aged 53-85 years) using the Automatic Segmentation of Hippocampal Subfields algorithm (ASHS). With this, we generated native space stages for [^{18}F]MK6240 tau-PET images based on 2.5 standard deviation above the mean of 40 participants aged 18-25. The three stages were based on 1) transentorhinal and entorhinal cortices; 2) anterior and posterior hippocampus; 3) perirhinal and parahippocampal cortices. These stages were compared to standard-space-based Braak stages. They were then combined to show differences in memory impairment measured with the Rey Auditory Verbal Learning Test (RAVLT).

Native space stages tended to show earlier tau stages, with 14 participants reaching stage 1 while at Braak 0, and 21 at stage 3 and Braak II (Figure 1A). These two subgroups were designated as Braak stages 0.5 and 2.5, respectively. The validity of these stages was supported by temporal meta-ROI elevation at stage 0.5 and 2.5 (Figure 1B). Stage 2.5 was the earliest showing significant impairment at the RAVLT delayed recall and learning scores ($p < 0.01$; Figure 2).

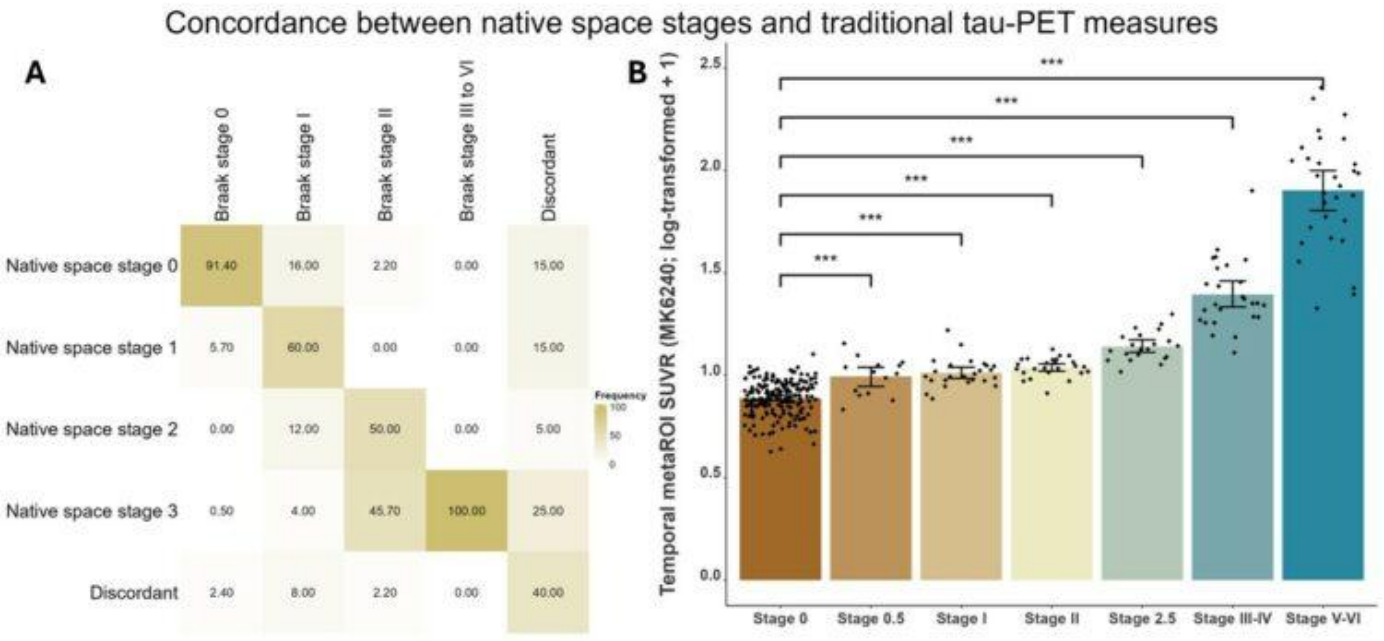


Figure 1: **A)** Correspondence of traditional tau-PET Braak stages with native space stages based on ASHS medial temporal lobe (MTL) subregion . Note that Braak stage 0 has the highest count (N = 209 out of a total of N = 356). Fourteen participants were ASHS 1+/Braak 0 (Stage 0.5) and 21 were ASHS 3/Braak II. **B)** Stages 0.5 shows a significant temporal metaROI tau-PET elevation, comparable to stage I. Stage 2.5 shows an intermediate elevation between stages II and III. Standard error bars are shown. ***: $p < 0.001$.

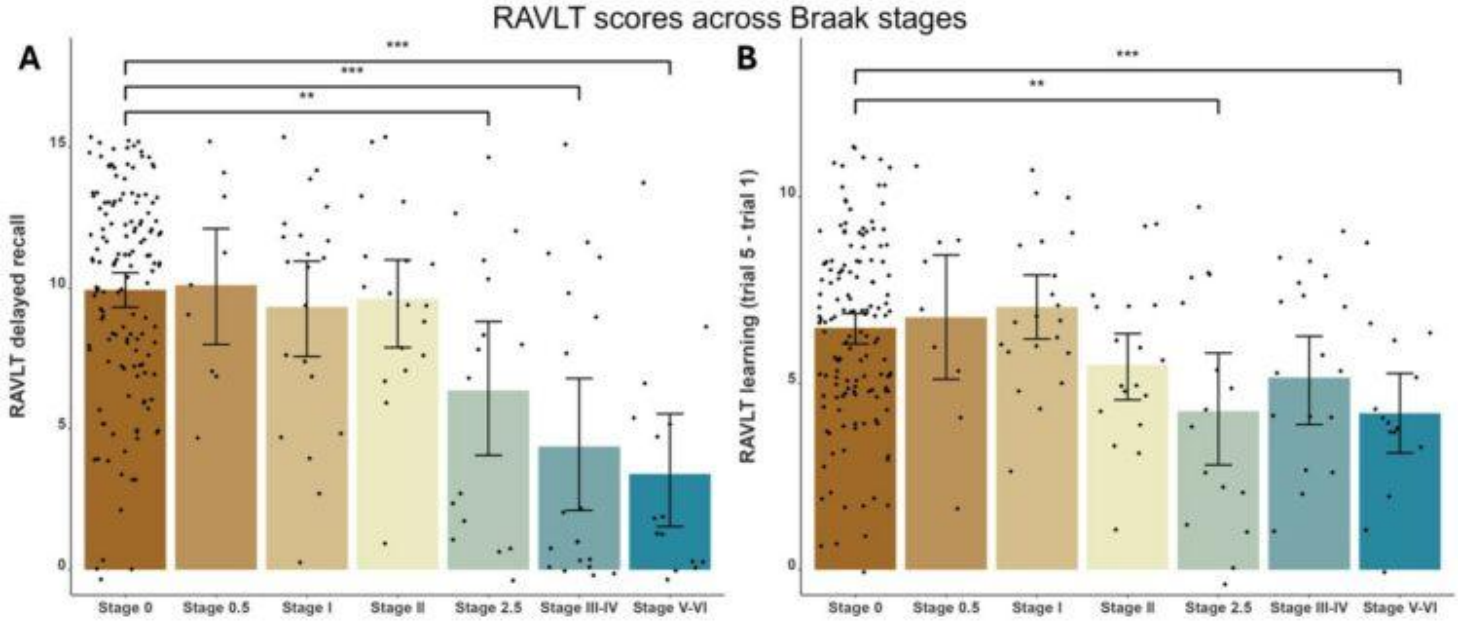


Figure 2: RAVLT scores across the Braak stages supplemented by the ASHS-designated stages 0.5 and 2.5. **A)** RAVLT delayed recall scores are significantly lower at stages 2.5, III-IV and V-VI compared to stage 0. **B)** The total learning (difference between trial 5 and trial 1) are significantly lower at stages 2.5 and V-VI. Standard error bars are shown. ***: $p < 0.001$; **: $p < 0.01$.

Using native space tau-PET images may allow us to identify the earliest tau pathology with better sensitivity than standard space. The intermediate stage 2.5 putatively marks the earliest propagation of tau outside of the hippocampus and transentorhinal and entorhinal cortices. This suggests that hippocampal tau pathology is insufficient to explain the AD-associated memory impairment.

Keywords: Braak stages, Tau-PET, tau, automatic segmentation, memory

43 The universal tau PET scale (Uniτ) for Flortaucipir, MK6240, PI2620 and RO948 harmonization

Guilherme Povala[1], Guilherme Bauer-Negrini[1], Bruna Bellaver[1], Firoza Z. Lussier[1], Livia Amaral[1], Pamela Lukasewicz Ferreira[1], Dana L. Tudorascu[1], Quentin Finn[2], Joseph Masdeu[2], David Soleimani-Meigooni[3], Juan Fortea[4], Val Lowe[5], Hwamee Oh[6], Belen Pascual[2], Brian A. Gordon[7], Pedro Rosa-Neto[8], Suzanne Baker[9], Tharick A. Pascoal[1]

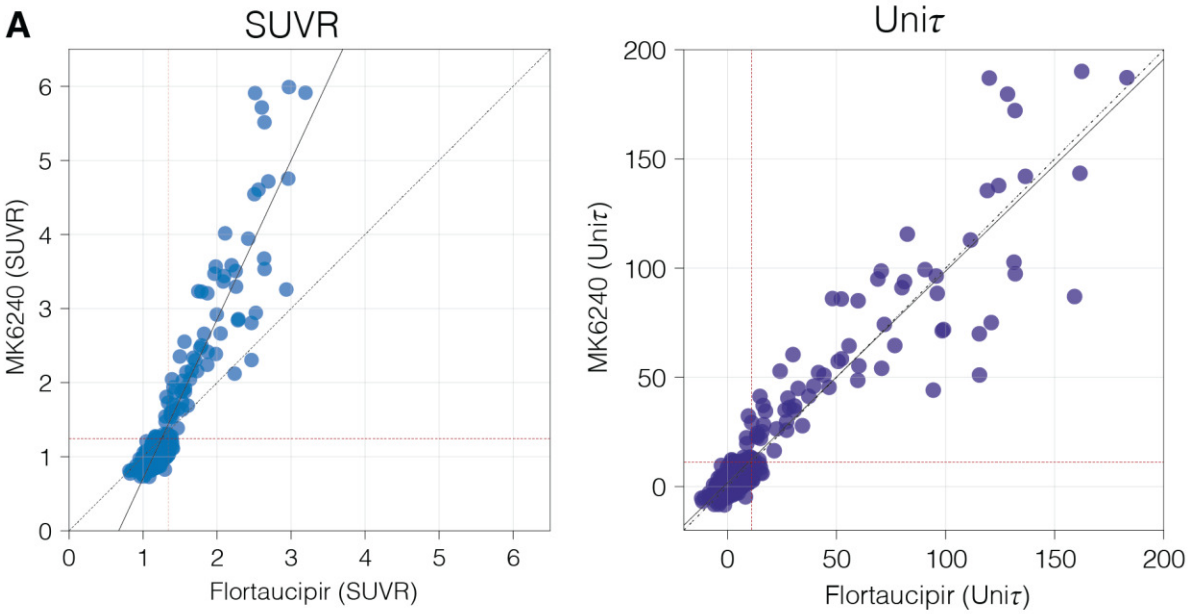
[1]*University of Pittsburgh, Department of Psychiatry, Pittsburgh, PA, US*
[2]*Houston Methodist Research Institute, Department of Neurology, Houston, TX, US*
[3]*University of California San Francisco, Memory and Aging Center, San Francisco, CA, US*
[4]*Hospital de la Santa Creu i Sant Pau, Sant Pau Memory Unit, Department of Neurology, Barcelona, ES*
[5]*Mayo Clinic, Department of Radiology, Rochester, MN, US*
[6]*Brown University, Department of Psychiatry and Human Behavior, Providence, RI, US*
[7]*Washington University in St. Louis, Department of Radiology, Saint Louis, MO, US*
[8]*Translational Neuroimaging Laboratory, McGill University Research Centre for Studies in Aging, Douglas Research Institute, Montréal, QC, CA*
[9]*Lawrence Berkeley National Laboratory, Berkeley, CA, US*

Objective: HEAD is a longitudinal, multi-site, observational, non-randomized head-to-head study of tau-PET tracers. Here, we tested the hypothesis that the Uniτ scale can accurately harmonize the tau-PET tracers Flortaucipir, MK6240, PI2620, and RO948 onto a universal tau-PET measurement.

Methods: We assessed 402 individuals across aging and AD spectrum scanned head-to-head with Flortaucipir and MK6240, and a subset of 67 also with PI2620 and RO948. Tau-PET SUVRs were processed to a common 8mm FWHM using inferior cerebellar gray matter as reference. We previously estimated Uniτ parameters on a training set (n=200) fitting a single-step smoothed hyperbolic tangent mathematical model to the CenTauR Meta-Temporal ROI SUVRs anchored in the mean SUVR of young participants and the 90th percentile from cognitively impaired individuals. We compared tau positivity classifications of the tracers on Uniτ with the classification derived from the original SUVRs (mean + 3 SD from young participants).

Results: Uniτ was able to successfully harmonize Flortaucipir and MK6240 by aligning the values of both tracers (**Fig.1**). For Flortaucipir, the tau positivity classifications of the Uniτ scale matched those from the original SUVRs (ground truth). For MK6240, there was one mismatched case (**Fig.1**). Additionally, by utilizing tracer-specific parameters, Uniτ successfully harmonized PI2620 and RO948 with both Flortaucipir and MK6240, achieving regression lines close to unity, confirming its applicability across multiple tau-PET tracers (**Fig.2**). Finally, upon applying the Uniτ transformation to all brain voxels, Uniτ reasonably harmonized 3D images to the Uniτ scale, substantially reducing visual variabilities (**Fig.3**).

Conclusion: Our results indicate that tau PET tracers can be harmonized to a common scale using anchor points from a large head-to-head dataset. It remains to be seen how Uniτ will perform in the ongoing 18-month follow-up of the HEAD study. Uniτ is freely available on multiple platforms (www.unitau.app) for ROI or voxel-wise tau PET harmonization.



B

	SUVR-	SUVR+
MK6240	307	95
Flortaucipir	315	87

	Unitau-	Unitau+
MK6240	308 (0.3%)	94 (-1.1%)
Flortaucipir	315 (0%)	87 (0%)

Figure 1. Comparison of SUVR estimates (left) and Unitau estimates (right) between MK6240 and Flortaucipir tau PET tracers. (A) The original SUVR data shows important variability in tracer associations, while the Unitau scale aligned them more closely, with a regression line near unity (RMSE: 10.78, R2: 0.89, y=0.97x+1.62). (B) Individuals' positivity classification based on the Unitau scale are also presented. For MK6240, there is 1 mismatch classification in Unitau compared to the SUVR, whereas for Flortaucipir the positivity classifications remain the same of SUVRs. Unitau harmonization reduces systematic differences preserving tracers' characteristics, resulting in a more consistent relationship between tau tracers.

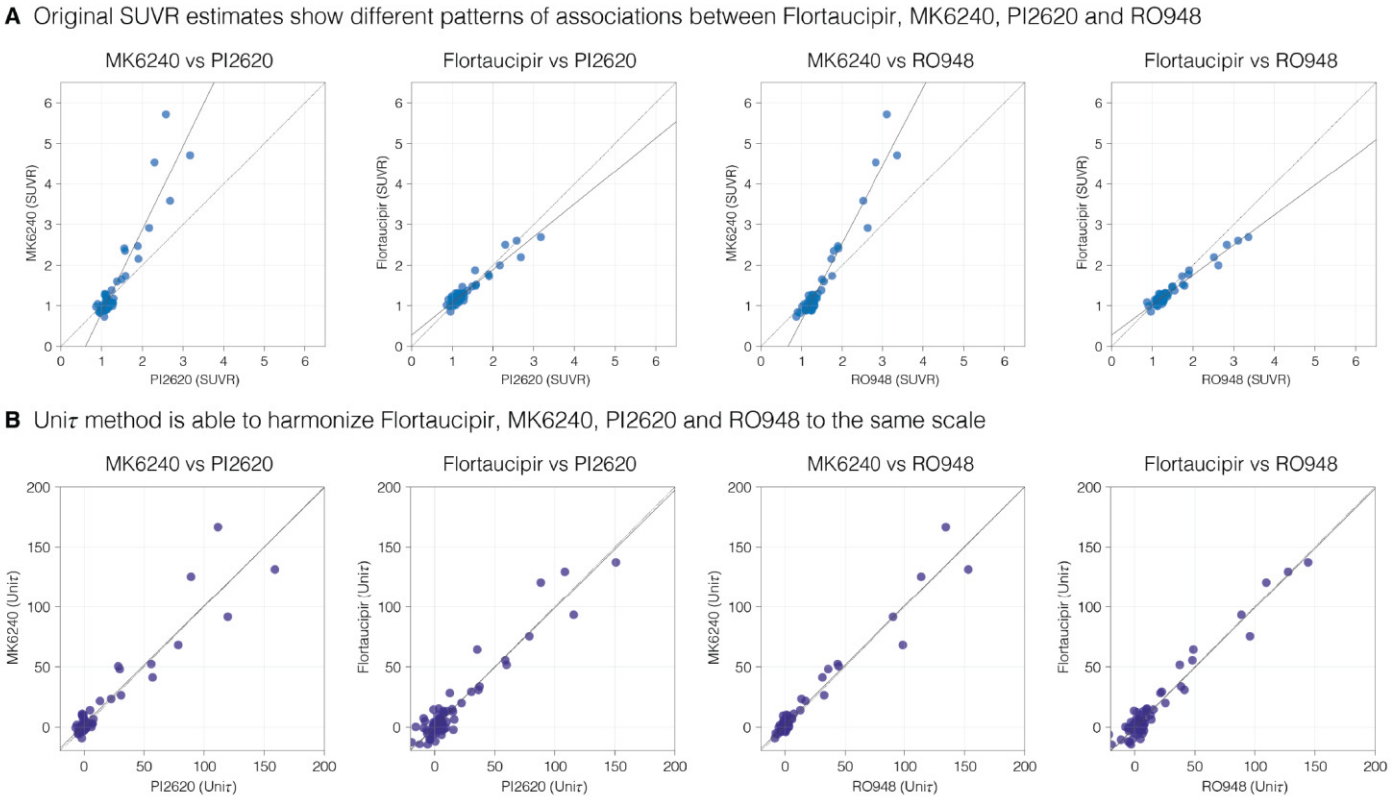


Figure 2. Comparison of SUVR estimates and Unitau harmonization using MK6240, Flortaucipir, PI2620, and RO948 tau PET tracers. (A) Original SUVR estimates reveal substantial differences in associations between tracers in the scatter plots. The diagonal line represents perfect agreement. (B) The Unitau method harmonized SUVR values into a unified scale with regression lines overlapping with the diagonal line, reducing variability and enhancing consistency between tracers.

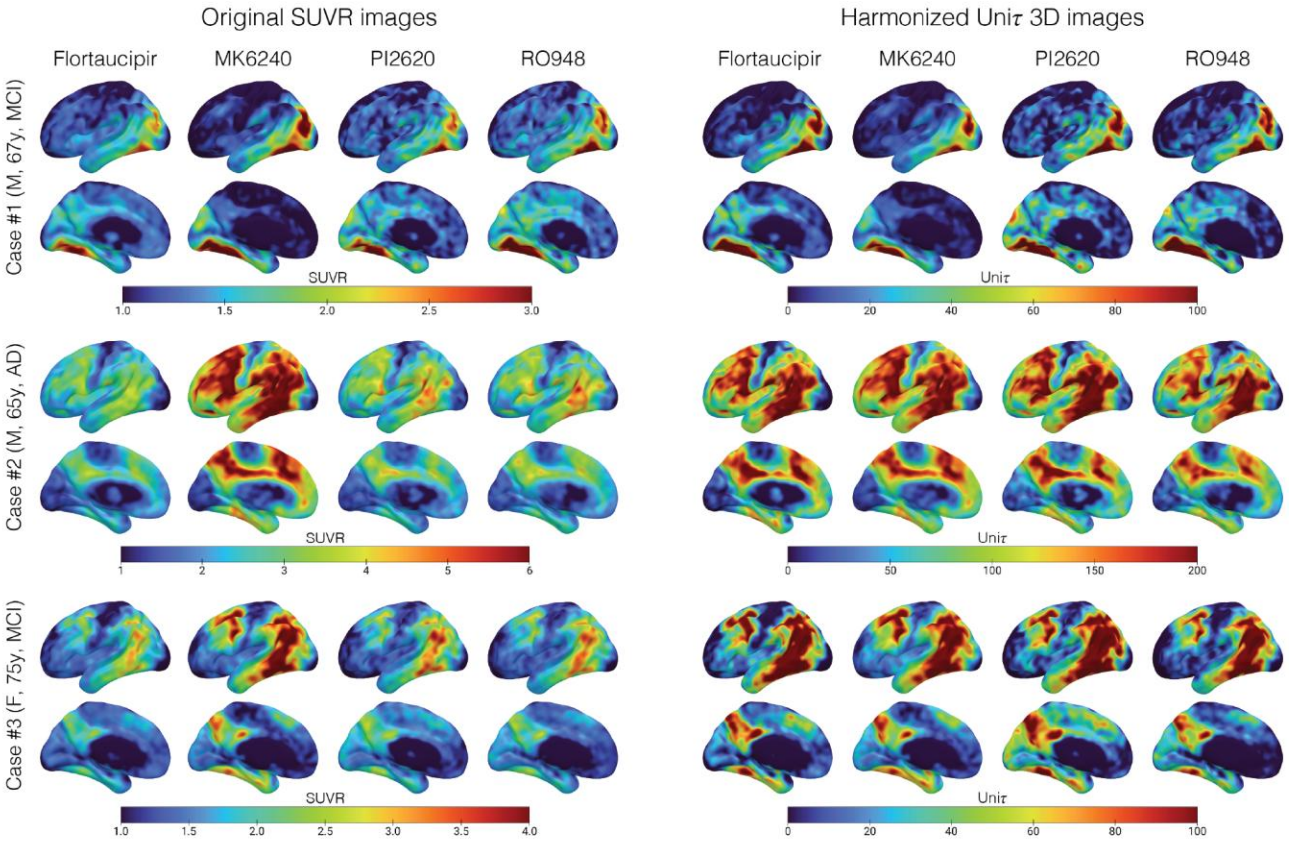


Figure 3. 3D visualization of SUVR and Uniτ harmonization results using Flortaucipir, MK6240, PI2620, and RO948 tau-PET tracers for representative cases. The left panel shows SUVR images, while the right panel displays the harmonized Uniτ images, reducing visual differences and providing a consistent view of tau distribution. Color bars indicate SUVR values (left) and Uniτ units (right).

Keywords: tau, PET, harmonization, Unitau, head-to-head

44 Assessing the relationship between neuropsychiatric symptoms, amyloid and tau pathology, and white matter hyperintensity volume across sexes in preclinical Alzheimer's disease

Aurélie Garrone[1], Yara Yakoub[1,2], Alfonso Fajardo-Valdez[1,2], Ting Qiu[1,2], Valentin Ourry[1,2], Sylvia Villeneuve[1,2,3]

[1]*Douglas Mental Health University Institute, Montreal, QC, CA*
[2]*Integrated Program in Neuroscience, Faculty of medicine, McGill University, Montreal, QC, CA*
[3]*Department of Psychiatry, Faculty of medicine, McGill University, Montreal, QC, CA*

Introduction: Neuropsychiatric symptoms (NPS) are highly prevalent in Alzheimer's disease (AD) and may constitute both risk factors and early signs of the disease. Cross-sectional and longitudinal studies have shown that NPS are associated with increased Ab and tau burden in preclinical AD populations. The amygdala, a brain region involved in emotion modulation and processing, is among the most vulnerable regions to exhibit early tau deposition. Further, white matter hyperintensity (WMH) volume, another neurological correlate of AD, has been linked to worsening NPS, especially in frontotemporal regions. Interestingly, sex may also affect the incidence and prevalence of NPS in AD. We assessed the associations between NPS and 1) Aβ, 2) amygdala tau and 3) frontal WMH burden in cognitively unimpaired older adults.

Methods: 208 participants from the longitudinal PREVENT-AD cohort received amyloid (^{18}F-NAV4694) and tau (^{18}F-Flortaucipir) PET-scans. We conducted linear regressions using sex as an interaction term to assess the effect of NPS (apathy, anxiety, depression, stress, perseverative thinking and neuroticism) on global Aβ-PET standard uptake values ratio (SUVr), tau-PET SUVr in the amygdala, and WMH volume in the frontal lobe. These associations were also examined separately in males and females. All models were corrected for age.

Results: Despite females having slightly more NPS than males, the associations between depression and amyloid and between WMH volume and neuroticism were stronger in males as compared to females. Several other associations, particularly with WMH volume, were found in males but not in females.

Conclusions: We found associations between NPS and both MRI and PET markers of AD in cognitively unimpaired individuals at risk of AD. Some of these associations were stronger in males, despite females being at increased risk of AD and known to exhibit a higher prevalence of NPS. These findings will need to be replicated in an independent cohort.

	Female	Male	χ^2	*df*	*p*
Sex (%)	142 (68%)	66 (32%)	27.77	1	< **.001*** **
ApoE4 Carrier (%)	55 (26%)	27 (13%)	0.02	1	.8835
			t	*df*	*p*
Mean Age at PET Scan (SD)	67.66 (4.79)	69.125 (5.38)	-1.85	114.79	.0668
NPS					
Mean Apathy Score (SD)	25.34 (5.80)	26.95 (6.69)	-2.35	216.27	**.0196***
Mean GAI Score (SD)	2.78 (4.02)	1.79 (3.48)	2.57	292.27	**.0107***
Mean GDS Score (SD)	1.54 (1.94)	1.36 (2.34)	0.76	208.45	.4473
Mean Stress Score (SD)	5.58 (5.91)	5.20 (5.53)	0.62	260.49	.5354
Mean Neuroticism Score (SD)	19.43 (7.05)	17.44 (6.78)	2.65	251.36	**.0085****
Mean Perseverative Thinking Score (SD)	18.31 (10.32)	14.22 (9.07)	4.12	300.06	< **.001*** **
Mean Global Amyloid SUVr (SD)	1.33 (0.30)	1.28 (0.28)	1.83	288.85	.0608
Mean Tau SUVr in the Amygdala (SD)	1.27 (0.15)	1.26 (0.14)	0.85	288.45	.3978
Mean Frontal WMH Volume (SD) (mm^3)	594.30 (1054.00)	475.43 (498.56)	1.51	387.91	0.1313

Table 1. Demographic Characteristics and Results of Neuropsychiatric and Biomarker Measures (Global Aβ-PET SUVr, Amygdala tau-PET SUVr and Frontal WMH Volume). *Abbreviations.* ApoE4 = Apolipoprotein E4; PET = Positron Emission Tomography; SUVr = Standardized Uptake Value Ratio; WMH = White Matter Hyperintensity; GAI = Geriatric Anxiety Inventory; GDS = Geriatric Depression Scale. * $p < 0.05$; ** $p < 0.01$; *** $p < 0.001$.

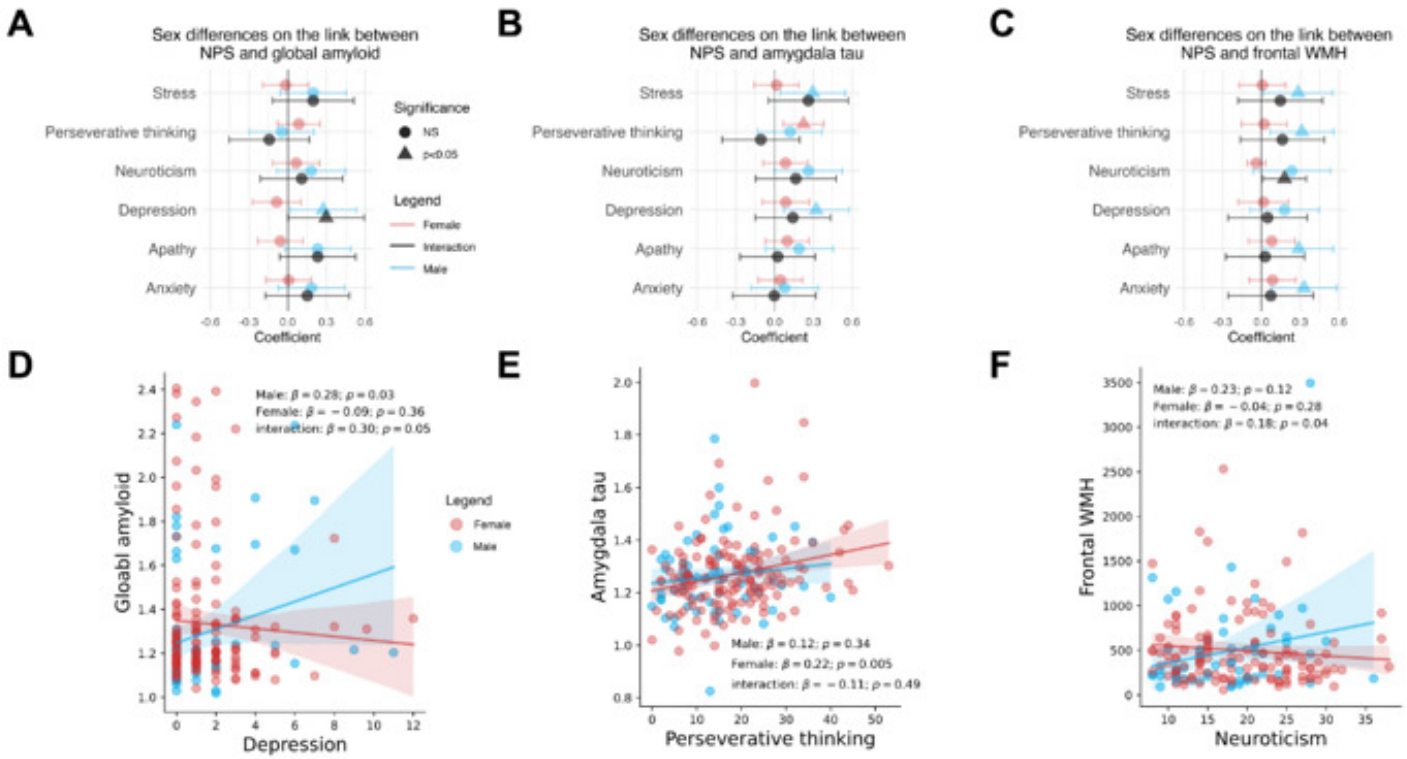


Figure 1. Summary of Sex Differences in the Relationship Between Neuropsychiatric Symptoms (NPS) and Biomarkers of Alzheimer's Disease. Males are represented in blue, females in red, and interaction effect of sex on the relationship between NPS and pathology in black. Plots display associations between NPS and global Aβ-PET SUVr (A), NPS and amygdala tau-PET SUVr (B), and NPS and frontal WMH volume (C) across sexes. Panels D-F represent plots of some of the significant associations demonstrated between NPS and the aforementioned markers of AD pathology. In males, higher depression score was linked with greater global Aβ-PET SUVr (D), while in females, increased perseverative thinking was associated with higher tau-PET SUVr (E). The significant interaction effect of sex on the relationship between neuroticism and frontal WMH volume (F) suggests that neuroticism affects WMH volume differently in males and females. Sex indeed seemed to have the greatest impact on the relationship between NPS and frontal WMH volume, with several associations being observed in males but not in females.

Keywords: Tau, Amyloid, Alzheimer's disease, White matter hyperintensity, Neuropsychiatric symptoms

45 Unveiling the heterogeneity of tau spreading in aging and Alzheimer's disease using polygenic combinations: Towards personalized models

Ibai Diez[1,2,3,4], Cristina Lois[1], Jorge Garcia Condado[3,5], Michelle E Farrell[5], Emma G Thibault[1], Heidi I.L. Jacobs[2], Rachel F. Buckley[5,6], Bernard J Hanseeuw[1,7], Michael J. Properzi[5], Hyun-Sik Yang[5,8], Reisa Sperling[2,5,8], Jesus M. Cortes[3,4,9], Yakeel T. Quiroz[5,10,11], Jorge Sepulcre[12], Keith Johnson[1,2,5,8], Teresa Gomez-Isla[5,13]

[1]*Gordon Center for Medical Imaging, Department of Radiology, Massachusetts General Hospital, Harvard Medical School, Boston, MA, USA, Boston, MA, US*
[2]*Athinoula A. Martinos Center for Biomedical Imaging, Department of Radiology, Massachusetts General Hospital, Harvard Medical School, Charlestown, MA, USA, Charlestown, MA, US*
[3]*Computational Neuroimaging Lab, Biobizkaia Health Research Institute, Barakaldo, Spain, Barakaldo, ES*
[4]*IKERBASQUE Basque Foundation for Science, Bilbao, Spain, Bilbao, ES*
[5]*Department of Neurology, Massachusetts General Hospital, Harvard Medical School, Boston, Massachusetts, USA, Boston, MA, US*
[6]*Melbourne School of Psychological Sciences, University of Melbourne, Melbourne, VIC, Australia, Melbourne, AU*
[7]*Department of Neurology, Cliniques Universitaires Saint-Luc, Université Catholique de Louvain, Bruxelles, Belgium, Bruxelles, BE*
[8]*Center for Alzheimer Research and Treatment, Department of Neurology, Brigham and Women's Hospital, Boston, MA, USA, Boston, MA, US*
[9]*Department of Cell Biology and Histology, University of the Basque Country, Leioa, Bizkaia, Spain, Leioa, ES*
[10]*Department of Psychiatry, Massachusetts General Hospital, Harvard Medical School, Boston, Massachusetts, USA, Boston, MA, US*
[11]*The Neuroscience Group of Antioquia, University of Antioquia, Medellín, Colombia, Medllin, CO*
[12]*Yale PET Center, Yale Medical School, Yale University, New Haven, CT, USA, New Haven, CT, US*
[13]*Mass General Institute for Neurodegenerative Disease, Charlestown, MA, USA., Charlestown, MA, US*

Tau pathology spreading in the brain was traditionally thought to be consistent across individuals with Alzheimer's disease (AD). However, recent neuroimaging, clinical and neuropathologic studies suggest high inter-individual variability in tau spreading patterns. This variability could explain the observed differences in clinical presentation, age of onset, disease progression, and affected cognitive domains (like memory, language, or visuospatial or executive function). We hypothesize that distinct polygenic combinations of 98 genetic risk loci for late-onset AD can provide a more precise characterization of the observed heterogeneity.

In this study, we analyzed genetic information and Flortaucipir PET data from 792 individuals from ADNI (n=478) and A4/ELearn (n=314) studies (619 cognitively normal, 153 mild cognitive impairment (MCI), and 20 AD; age 74.0 ± 6.8; 55% female) to investigate the association between different polygenic combinations and tau spreading patterns in aging and AD. As PET outcome, we used partial volume corrected (three-compartment Muller-Gartner MG Method) SUVr (reference: inferior cerebellar grey matter). Using tau spreading models, we identified a tau spreading backbone network and observed four distinct tau spreading subnetworks consistent with previously reported AD subtypes: limbic, medial temporal lobe sparing, lateral temporal, and posterior (Fig 1). Additionally, we identified genetic variants linked to specific subtypes of tau pathology and unique patterns of tau spreading (Fig 2). Moreover, combinations of these genetic factors revealed mixed subtypes.

This study offers new observations that connect individual genetics to the diverse manifestations of tau pathology in AD, providing a more comprehensive explanation for the variations in tau spread severity and spatial distribution among individuals. While incorporating individual genetic makeup could enhance current AD

diagnostic criteria and enable personalized and predictive models, further research is necessary to explore the role of additional genetic variants and the influence of different environmental factors.

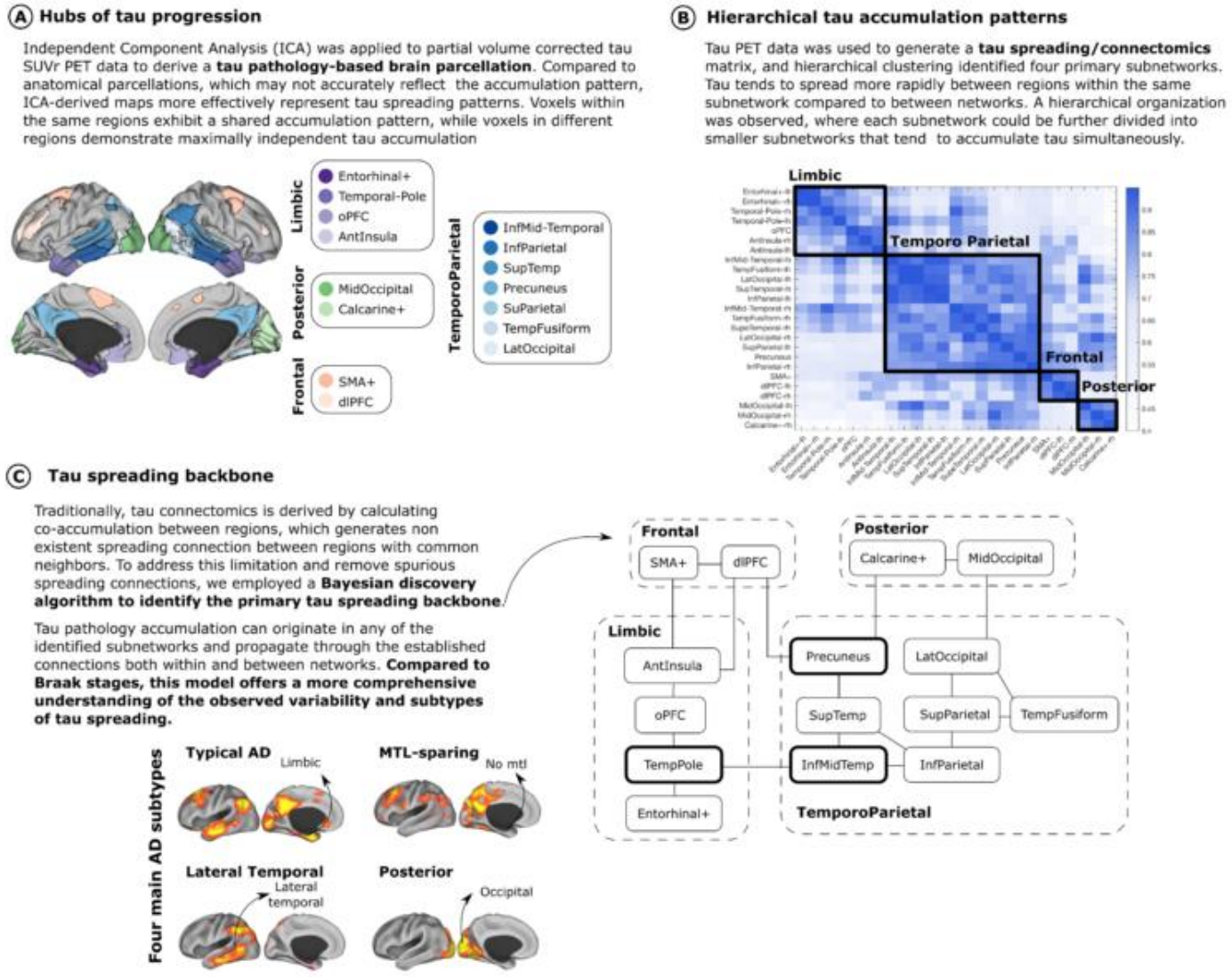


Fig1: Tau Spreading Backbone

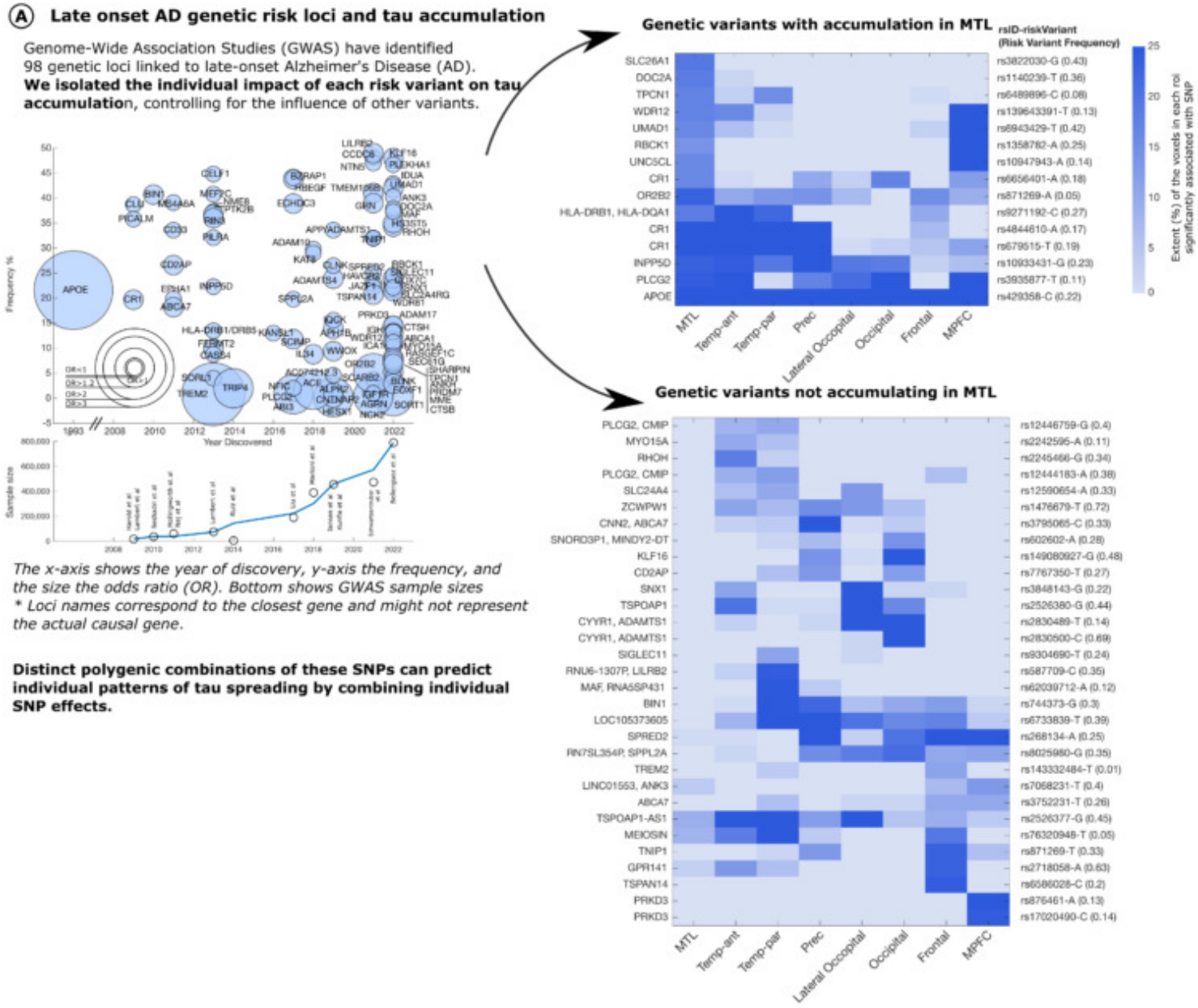


Fig2: Genetics and Tau Spreading

Keywords: Tau Spreading, Aging, Alzheimer's disease, genetic risk

46 Regional amyloid and tau: Exploring regional sex-based differences in a middle-aged community-based cohort

Diana S Guzmán[1], Froogh Aziz[1], Anna C Smith[1], Hannah Houlihan[1], Thairi C Sanchez[1], José A Luchsinger[1], Patrick J Lao[1]

[1]*Columbia University Medical Center, New York, NY, US*

Background: As previously reported in the Northern Manhattan Study of Metabolism and Mind (NOMEM) study, women have greater global amyloid and tau burden, yet less neurodegeneration in AD signature regions compared to men. We sought to characterize regional sex differences in amyloid and tau burden in this middle-aged community-based cohort.

Methods: 541 NOMEM participants underwent Florbetaben PET and 391 NOMEM participants underwent MK-6240 PET (Table 1). Florbetaben SUVR was assessed in Thal phase regions (parietal cortex, frontal cortex, temporal cortex, cingulate gyrus, and striatum) and MK-6240 SUVR in Braak stage regions (I-VI). ROI-level and voxelwise sex differences were adjusted for age, APOE4, and for global amyloid in tau models.

Results: On the ROI-level, women had greater amyloid across Thal phase regions and greater tau across all Braak stage regions without much regional variability. On the voxel-level, women had greater amyloid in Thal phase regions and the occipital cortex. Women had greater tau in Braak stage regions, with a right sided laterality in the temporal cortex. Non-brain uptake in the leptomeninges, scalp, and ventricles was greater in women for Florbetaben and MK-6240.

Conclusion: Women had greater amyloid burden diffusely across the brain, extending to the occipital cortex, and greater tau burden in the right temporal cortex. Cerebral amyloid angiopathy and verbal memory should be further explored in relation to occipital cortex involvement from amyloid and relative sparing of the left temporal cortex from tau in women. Differential partial volume effect (i.e., men had lower cortical thickness and greater ventricular volume) or off-target binding profiles should also be considered when assessing sex differences.

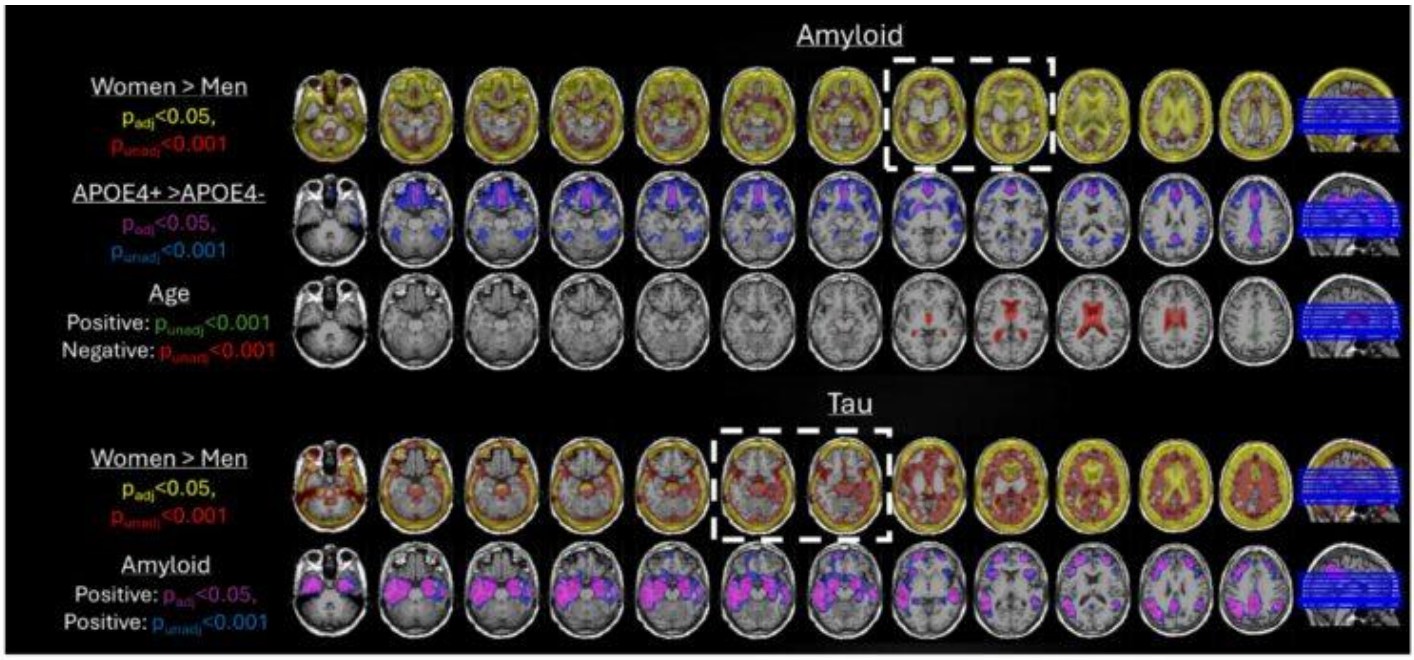


Figure 1. Voxelwise sex effects for Amyloid and Tau PET. Clusters within extracerebral and ventricular regions may be related to differential partial volume effect (i.e., more neurodegeneration in men compared to women) or off-target binding patterns. Known covariate effects are also shown. Dotted white boxes highlight clusters that extended beyond Thal phase regions for amyloid (e.g., occipital cortex) and right sided laterality in Braak stage regions for tau (e.g., temporal cortex). Color indicates different significance thresholds or different direction of association (e.g., age on amyloid).

	Florbetaben PET		MK-6240 PET	
	Female (N = 352)	Male (N = 189)	Female (N = 253)	Male (N = 138)
Age	64 (3)	64 (3)	64 (3)	64 (3)
Education	12 (4)	13 (4)	12 (4)	12 (4)
Race/Ethnicity				
Non-Hispanic Black/African American	61 (17%)	57 (30%)	44 (17%)	36 (26%)
Non-Hispanic White	39 (11%)	37 (20%)	28 (11%)	27 (20%)
Hispanic	252 (72%)	95 (50%)	181 (72%)	75 (54%)
AD Signature Regions [mm]	2.69 (0.10)	2.64 (0.11)	2.69 (0.10)	2.64 (0.11)
Intracranial Volume [cm^3]	1,374 (131)	1,538 (152)	1,365 (133)	1,538 (154)

Table 1. Demographic characteristics for participants who underwent Florbetaben -PET and MK6240 -PET. Mean (SD) are reported for continuous variables. N (%) are reported for categorical variables.

Keywords: Sex, PET, Amyloid, Tau

47 Comparison of topographical patterns of abnormalities of the tau PET tracers [18F]Flortaucipir, [18F]MK6240, [18F]PI2620, and [18F]RO948

Livia Amaral[1], Guilherme Povala[1], Guilherme Bauer-Negrini[1], Emma Ruppert[1], Bruna Bellaver[1], Firoza Lussier[1], Pamela L. Ferreira[1], Joseph Masdeu[2], Dana L. Tudorascu[1], David Soleimani-Meigooni[3], Juan Fortea[4], Val Lowe[5], Hwamee Oh[6], Belen Pascual[2], Brian A. Gordon[7], Pedro Rosa-Neto[8], Suzanne Baker[9], Tharick A. Pascoal[1]

[1]*University of Pittsburgh, Department of Psychiatry, Pittsburgh, PA, US*
[2]*Houston Methodist Research Institute, Department of Neurology, Houston, TX, US*
[3]*University of California San Francisco, Memory and Aging Center, San Francisco, CA, US*
[4]*Hospital de la Santa Creu i Sant Pau, Sant Pau Memory Unit, Department of Neurology, Barcelona, ES*
[5]*Mayo Clinic, Department of Radiology, Rochester, MN, US*
[6]*Brown University, Department of Psychiatry and Human Behavior, Providence, RI, US*
[7]*Washington University in St. Louis, Department of Radiology, St. Louis, MO, US*
[8]*Translational Neuroimaging Laboratory, McGill University Research Centre for Studies in Aging, Douglas Research Institute, Montréal, QC, CA*
[9]*Lawrence Berkeley National Laboratory, Berkeley, CA, US*

Objective: Multiple tau PET tracers have been shown to accurately capture tau tangle deposition in the human brain. However, single-tracer studies have demonstrated different uptake patterns across the AD spectrum. This study uses head-to-head acquired tau PET tracers (the HEAD study) to compare the topographical spread of tau pathology across the four most widely used tau PET tracers.

Methods: We studied 66 individuals (30 CU (10% A+) and 36 CI (33% A+)) with [^{18}F]Flortaucipir, [^{18}F]MK6240, [^{18}F]PI2620, and [^{18}F]RO948 tau PET tracers. PET SUVR was calculated using the inferior cerebellar grey matter as the reference region at 8mm FWHM. PET topographical spread was assessed using the percentage of abnormal voxels (PAV) above the mean + 2.5 SD of CU amyloid-negative individuals. ROC AUCs were used to compare the performance of SUVR and PAV in the meta-temporal ROI for identifying the presence of cognitive impairment (CU versus CI).

Results: PAV demonstrated a slightly higher AUC than SUVR in identifying cognitive impairment across all four tau PET tracers (**Figure 1**). PAV progressively increased from CU to MCI and dementia, partially following Braak stage patterns across the four tracers (**Figure 2**). Probabilistic 3D maps indicated that MCI subjects exhibited the highest concentrations of tau abnormality (20-40%), mostly confined to the entorhinal cortex and laterally (**Figure 3**). Individuals with dementia showed a higher concentration of tau PET abnormalities in the parietal and temporal lobes, with very similar patterns across tracers.

Conclusion: In this preliminary analysis, we found that tau PET topographical spread (measured with PAV) was associated with cognitive impairment. [^{18}F]MK6240 exhibited the most consistent regional abnormality patterns in individuals in early disease stages within Braak I-II regions. All four PET tracers showed substantial tau abnormality regional spread in individuals with dementia, with the highest concentrations in the temporoparietal regions.

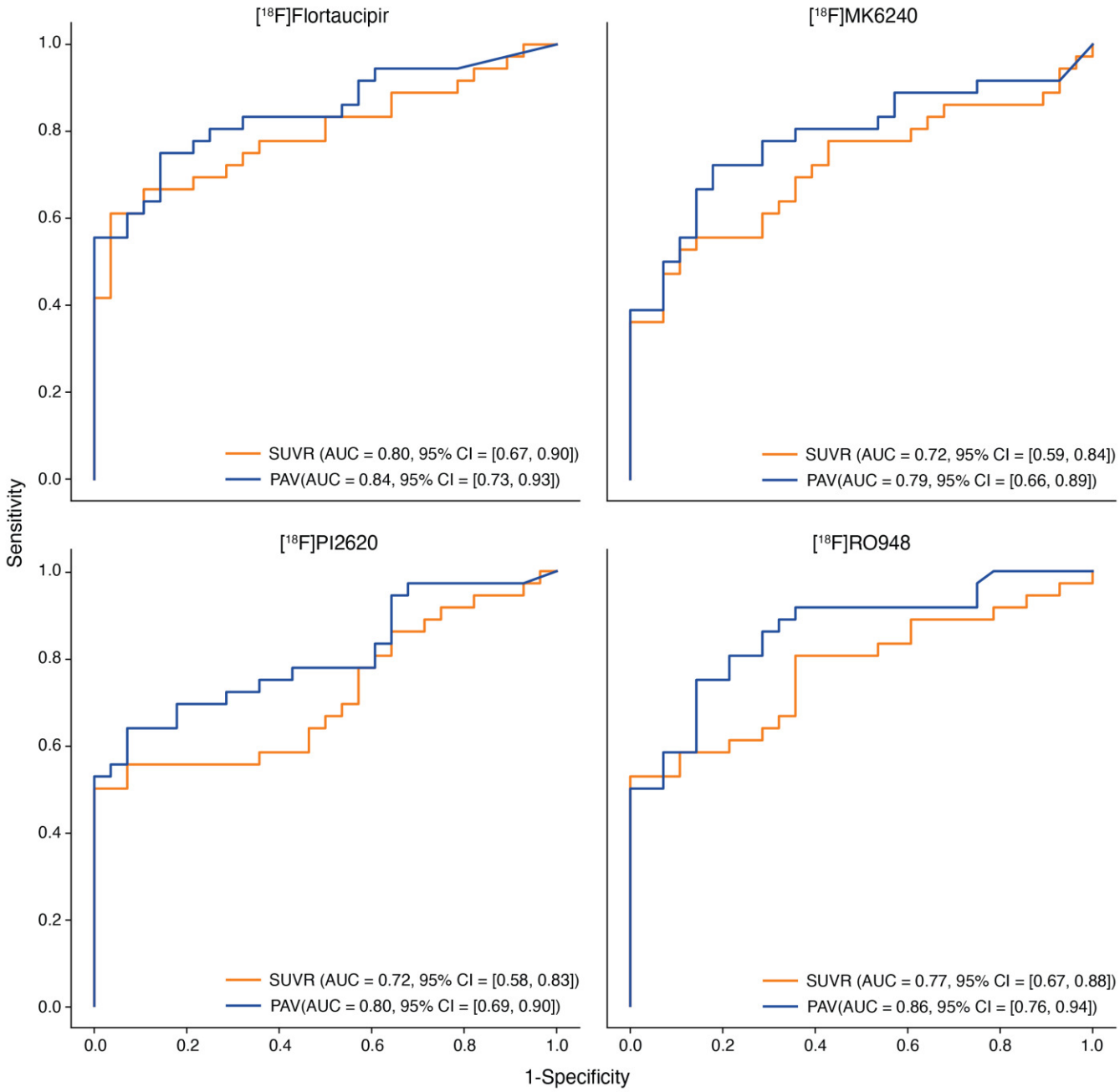


Figure 1. ROC AUC of SUVR and percentage of abnormal voxels (PAV) in the meta-temporal region for identifying cognitive impairment (CU versus CI) using Flortaucipir, MK6240, PI2620, and RO948

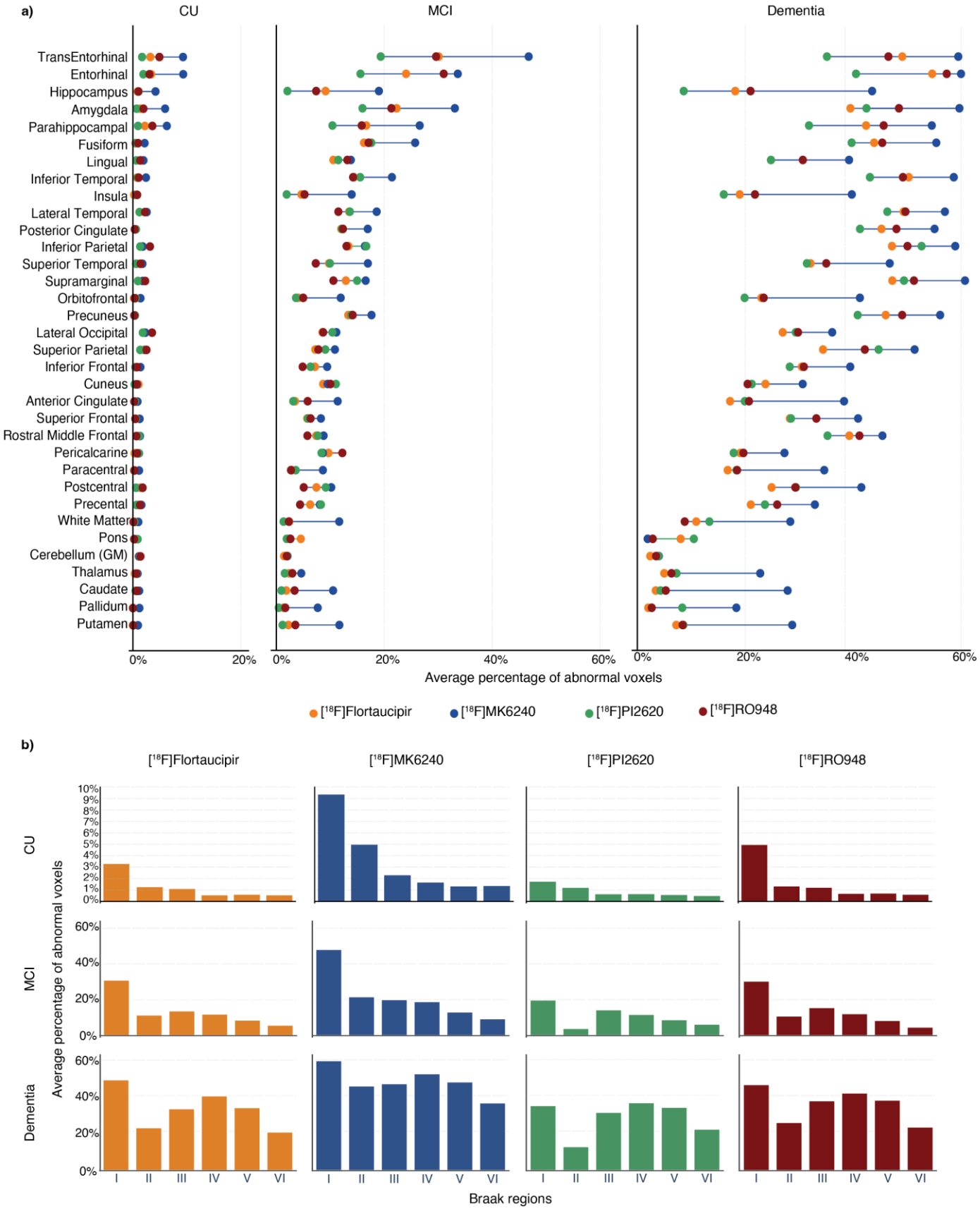


Figure 2. Average percentage of abnormal voxels (PAV) for Flortaucipir, MK6240, PI2620, and RO948 Tau PET tracers across different regions and groups: a) DKT Atlas regions and b) Braak regions. CU = Cognitively Unimpaired; MCI = Mild Cognitive Impairment.

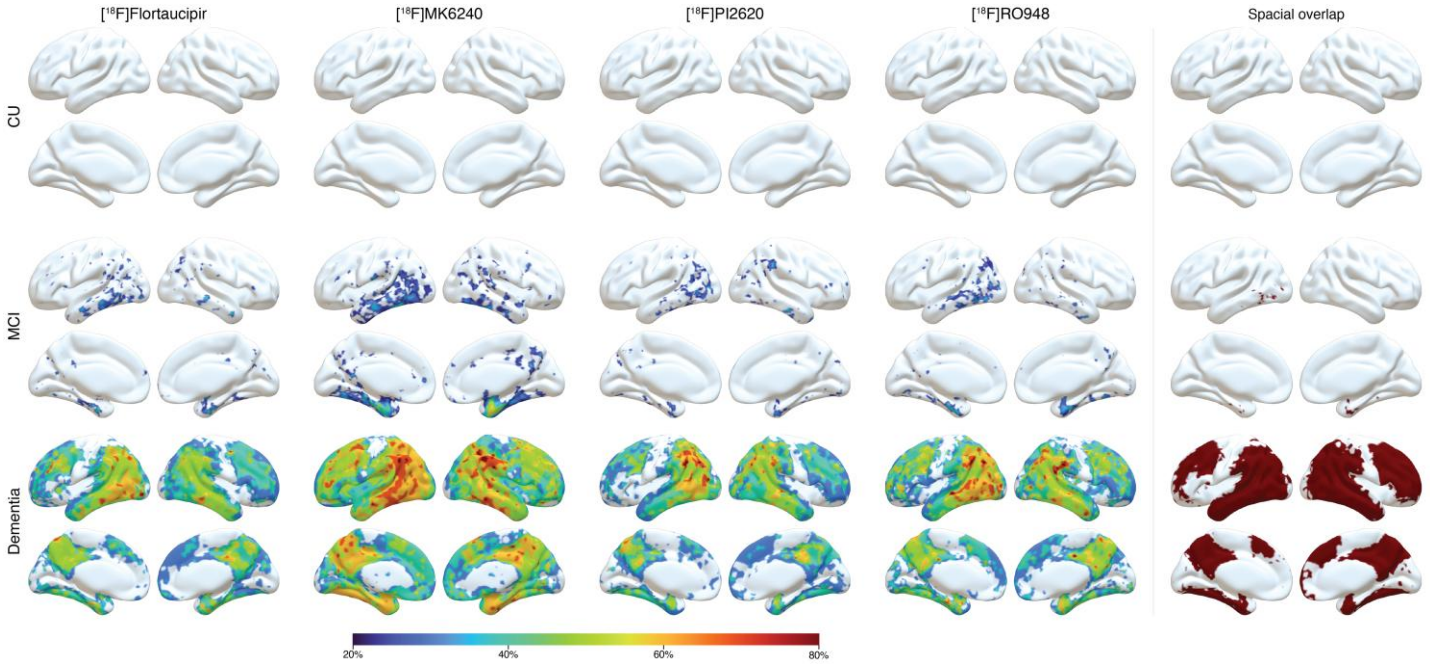


Figure 3. 3D probabilistic maps showing the averaged percentage of abnormal voxels across groups for the four tau PET tracers. A spatial overlap map (right side) indicates the voxels where all four tracers showed abnormalities using the tested method. CU = Cognitively unimpaired, MCI = Mild Cognitive Impairment.

Keywords: tau, PET, tracer, Alzheimer, cognition

48 Subtle cognitive deficits detected through routine in-office tests are associated with global Aβ and temporal tau in cognitively unimpaired individuals

Cynthia Felix[1], George Rebok[2], Felix Kollasserry[3], Beth Snitz[4], Pamela Ferreira[1], Dana Tudorascu[1], Guilherme Povala[1], Pampa Saha[1], Livia Amaral[1], Firoza Lussier[1], Joseph Masdeu[5], David Soleimani-Meigooni[6], Juan Fortea[7], Val Lowe[8], Hwamee Oh[9], Brian Gordon[10], Pedro Rosa-Nato[11], Suzanne Baker[12], Ziad Nasreddine[13], Tharick Pascoal[1,4]

[1]*Department of Psychiatry, University of Pittsburgh, Pittsburgh, PA, US*
[2]*Johns Hopkins School of Public Health, Baltimore, MD, US*
[3]*Indian Statistical Institute, Bangalore, IN*
[4]*Department of Neurology, University of Pittsburgh, Pittsburgh, PA, US*
[5]*Houston Methodist Research Institute, Houston, TX, US*
[6]*University of California San Francisco, San Francisco, CA, US*
[7]*Hospital de la Santa Creu i Sant Pau, Barcelona, ES*
[8]*Mayo Clinic, Rochester, MN, US*
[9]*Brown University, Providence, RI, US*
[10]*Washington University in St. Louis, St. Louis, MO, US*
[11]*Translational Neuroimaging Laboratory, McGill University Research Centre for Studies in Aging, Montreal, QC, CA*
[12]*Lawrence Berkeley National Laboratory, Berkeley, CA, US*
[13]*MoCA Cognition, Greenfield Park, QC, US*

Background: Studies show that individuals classified as cognitively unimpaired (CU) can exhibit a heterogeneous pattern of subtle clinical abnormalities, potentially linked to early Alzheimer's disease (AD). Identifying subtle cognitive deficits in this population using widely used cognitive tests is crucial, as early treatment for AD has been increasingly recognized to be potentially more effective. In this study, we aim to evaluate the link between Montreal Cognitive Assessment (MoCA) scores and AD pathology in CU individuals.

Methods: We studied 204 cognitively unimpaired (CU) older adults who underwent both ^{18}F-FTP and ^{18}F-MK6240 scans. These individuals were stratified based on their amyloid PET status, determined by visual reading, into CU Aβ+ (n = 35) and CU Aβ- (n = 137), as part of the ongoing HEAD study. CU adults had MMSE scores between 24-30 and Clinical Dementia Rating (CDR) of 0 and were clinically identified as non-MCI and non-demented. Voxel-wise linear regression models tested the association between MoCA and tau pathology.

Results: CU Aβ+/TAU+ had significantly lower total MoCA scores than Aβ-/TAU- individuals (Fig. 1). Lesser MoCA total score was significantly associated with greater mediobasal temporal tau deposition, using both ^{18}F-MK6240 and ^{18}F-FTP [Fig. 2]. When we separated the population by Aβ status, we found that these results were driven by the CU Aβ+ group (Fig. 3A) and were not present in CU Aβ- individuals (Fig. 3B).

Discussion: These findings indicate that the MoCA, a simple routine in-office clinical test, can detect subtle cognitive dysfunction associated with AD in CU older adults. This suggests that simple cognitive testing can play a role in the early detection of AD in clinical settings, potentially pre-screening individuals currently identified as preclinical AD for early intervention.

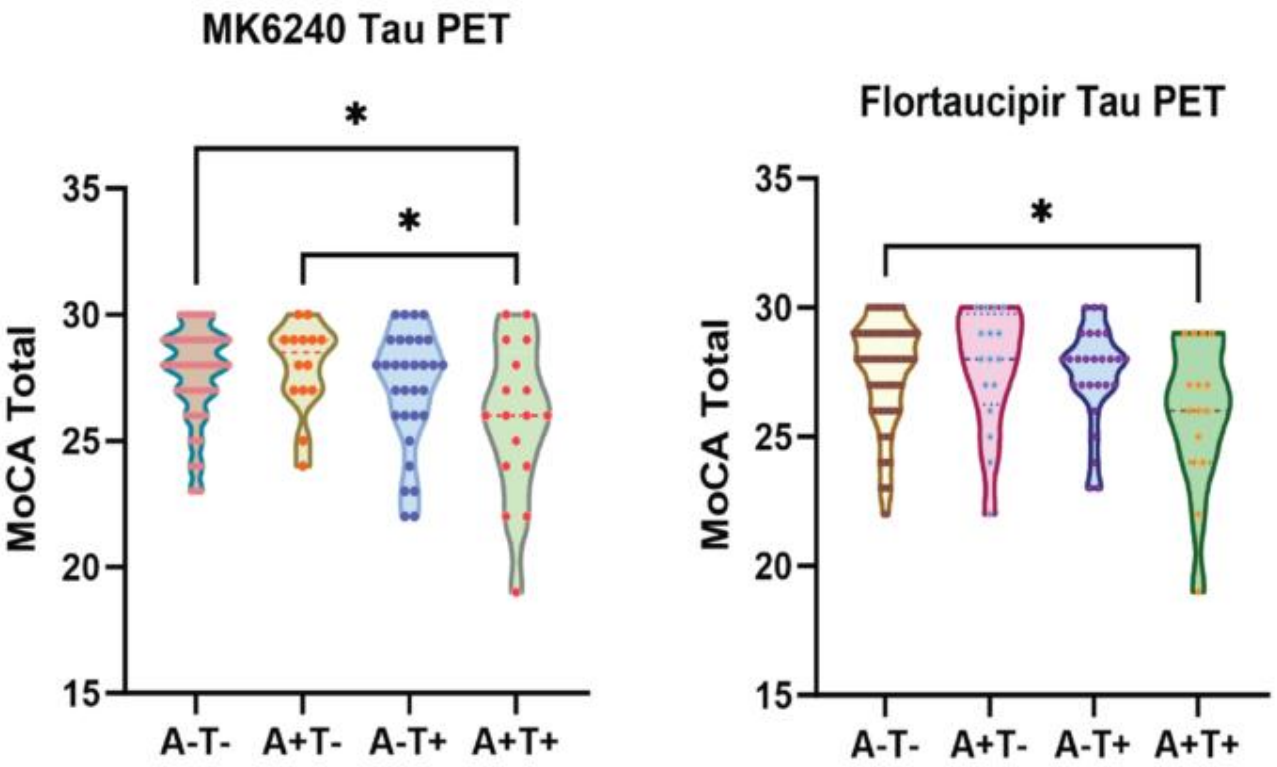


Fig 1. Violin Plots showing MoCA score distribution in cognitively unimpaired older adults based on amyloid and tau pathologies detected using PET imaging. MoCA total score distribution (n = 147) in CU Aβ+/TAU+ older adults is significantly lower compared to Aβ-/TAU- individuals. MK6240 and FTP tau-PET tracers are compared.

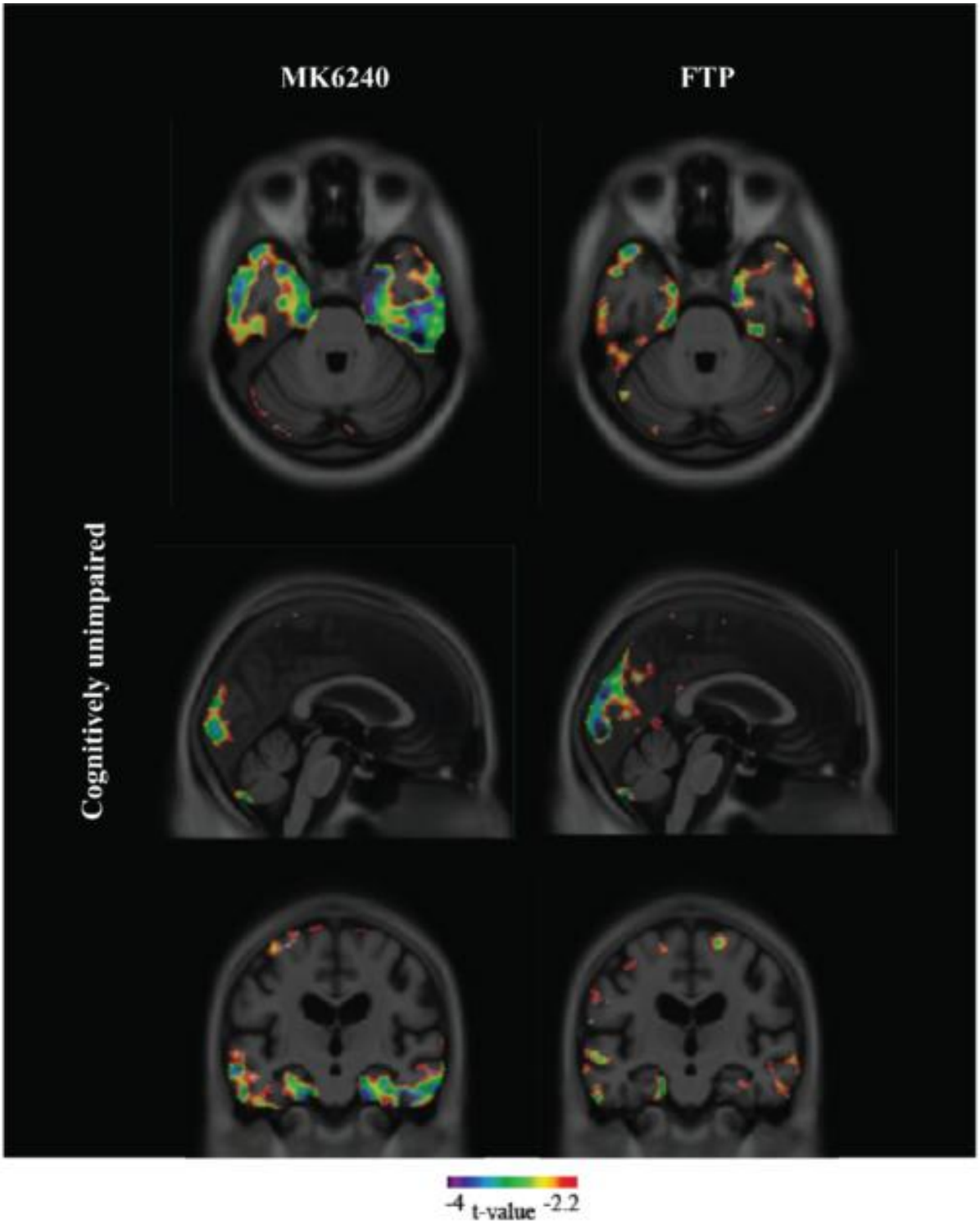


Fig 2. Greater tau PET pathology is associated with lower MoCA scores in cognitively unimpaired individuals. In the entire CU group (n = 204), tau PET SUVR was negatively associated with global cognition (MoCA total). The two tau PET tracers, MK6240 and Flortaucipir (FTP), showed associations in similar topographical regions.

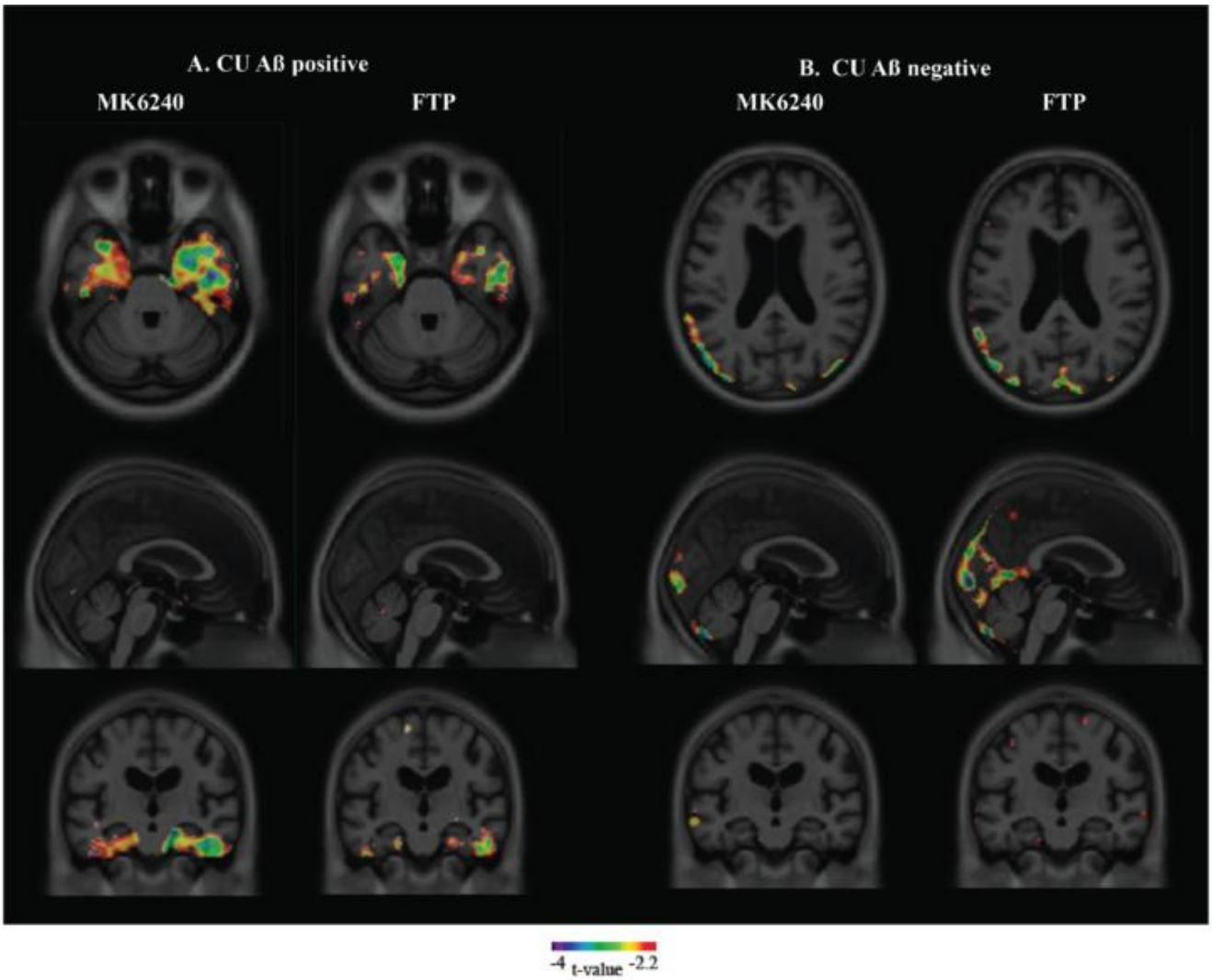


Fig 3. Greater tau PET pathology is associated with lower MoCA scores in cognitively unimpaired Aß-positive individuals. In the CU Aß-positive group (n = 35) [Fig. 3A], tau PET SUVR was negatively associated with global cognition (MoCA total). In the CU Aß-negative group (n = 137) [Fig. 3B], neither tau-PET tracer (MK6240 nor FTP) showed an association with cognition in target regions.

Keywords: Cognitively unimpaired (CU), cognition, tau-PET, MK6240, Flortaucipir

49 Estradiol-dependent associations between sleep complaints and tau deposition in women at elevated AD risk

Kitty Lui[1,2,4], Xin Wang[2], Pam Deyong[3], Atul Malhotra[3], Erin Sundermann[4], Sarah Banks[2,4]

[1]*SDSU/UC San Diego Joint Doctoral Program in Clinical Psychology, San Diego, CA, US*
[2]*UC San Diego, Dept. of Neurosciences, La Jolla, CA, US*
[3]*UC San Diego, Dept. of Medicine, La Jolla, CA, US*
[4]*UC San Diego, Dept. of Psychiatry, La Jolla, CA, US*

Background: Poor sleep has a complex, likely bidirectional relationship with Alzheimer's Disease (AD) pathology, yet is often overlooked in the work up for dementia risk. Older women are more vulnerable to AD, and report worse sleep quality than men. Estradiol levels are predictive of sleep quality in premenopausal and perimenopausal women, but are rarely assessed in older women. In older women at elevated risk for AD, we examined the relationship between sleep complaints and pathological tau, and whether this was moderated by estradiol levels.

Methods: 50 women (72.5±4.2y) participating in the Women: Inflammation Tau Study; Inclusion criteria were elevated polygenic risk for AD, or family history of dementia, and mild cognitive impairment on screening. The Pittsburgh Sleep Quality Index assessed subjective sleep quality. They also underwent 18F-MK6240 positron emission tomography to determine tau deposition. Standardized uptake value ratios were calculated in Braak stage III/IV regions, using eroded cerebellum grey matter as the reference. Estradiol was measured using liquid chromatography with tandem mass spectrometry in plasma samples, and results were divided into tertiles withing this cohort. We tested the associations between sleep and tau, and the estradiol's moderating effect, controlling for age, body mass index, and years of education.

Results: Worse subjective sleep quality was associated with more pathological tau (b=0.06, p=0.048), and lower levels of estradiol (b=-3.66, p<0.01). There was a moderating effect of estradiol (p=0.09) such that the sleep-tau relationship was only significant in women with average or below-average levels (ps<0.02), but not in women with higher-than-average levels (p=0.30;Figure).

Conclusion: Poor self-reported sleep quality was linked to greater tau only in those with average or low-average estradiol. This study highlights potential modifiable risk targets ofpoor sleepand low estradiol in women at high-risk of AD.

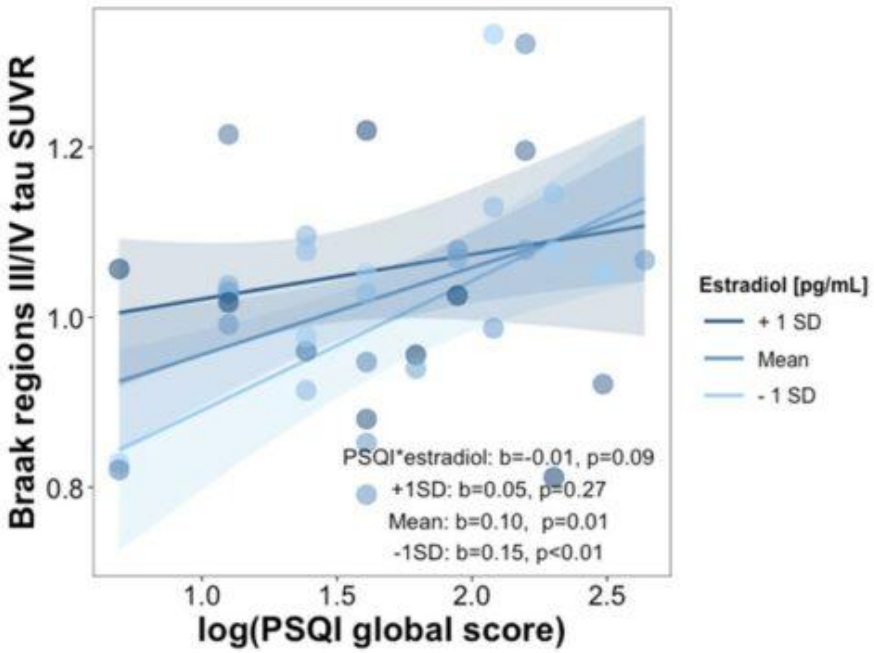


Figure 1: Scatter plot showing relationship of sleep complaints to tau by estradiol tertile

---

Keywords: sex hormones, sleep, modifiable risk factor, women

50 Impact of age and sex on extra-cerebral off-target binding in tau PET scans (18F-FTP)

Sujala Ghatamaneni[3], Daniel Kim[3], Marin Nycklemoe[3], Emily S Lundt[4], Christopher G Schwarz[3], Mahathi Kandimalla[3], David Jacobson[3], Sabrina Albertson[3], Clifford R Jack[3], Jeffrey Gunter[3], Ronald Peterson[3], Tiffany kung[3], Vamika sharma[3], Lim Seokbeen[3], Val Lowe, Hoon-ki Min

[2]*Department of Radiology, Mayo Clinic, Rochester, MN, US*
[2]*Department of Clinical trials and Biostatistics, Mayo Clinic, Rochester, MN, US*
[3]*Department of Cardiology, Mayo Clilnc, Rochester, MN, US*
[4]*Department of Neurology, Mayo Clinic, Rochester, MN, US*

Background: Tau PET imaging with 18F-flortacipir (18F-FTP) has directed interest in accurately tracking longitudinal tau changes with Alzheimer's disease, thus minimizing variability is critical. Off-target signal has the potential to complicate interpretation of 18F-FTP imaging due to potential spillover effects, with increased effect seen in later stages of Alzheimer's due to cerebral atrophy and proximity of off-target areas to relevant cortical areas. Previously, we demonstrated the effect of uptake period activity on 18F-FTP signal. With increasing recent interest in demographic factors that may affect off-target binding, we investigated the effect of age and sex in extra-cerebral off-target signal in 18F-FTP PET imaging.

Method: Standard 18F-FTP PET protocol was performed in 330 participants. Two independent readers measured tau uptake in predetermined off-target regions, including extraocular muscle, meninges, and occipital bone among others. Correlation and grouped assessed the relationship between participants' age with off-target tau uptake (SUV) and sex with SUV.

Result: Age had a significant effect on off-target in most brain regions, with variable positive or negative correlation based on area. Notably, SUV in the oculomotor muscles, masseter muscle, and pterygoid all showed significant positive correlation with age, but SUV in meninges and occipital bone showed significant negative correlation with age (n=330, $p<0.001$). Grouped comparison between sexes showed 'male' status was generally associated with lower SUV. The greatest effect of sex was observed in the internal carotid artery, occipital bone and superior cranial meninges. (n=330, $p<0.01$).

Conclusion: We observed that age and sex significantly affect extra-cerebral off-target signal in 18F-FTP PET imaging, adding to previous evidence of off-target binding within brain regions. As a result, the variability introduced by age and sex may pose challenges to studying tau accumulation, especially considering age with longitudinal tracking.

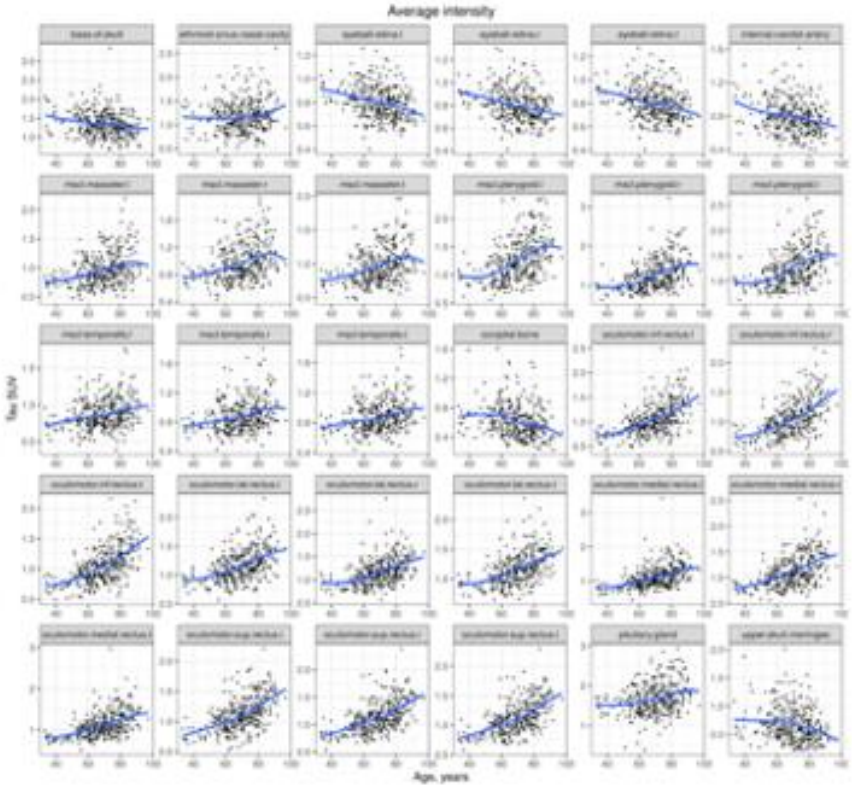


Figure 1. Tau average SUV relationship to age of participant categorized by off-target region of interest. Local polynomial regression curve as well as 95% confidence band is shown. When applicable, laterality is given as well as combined left and right sides.

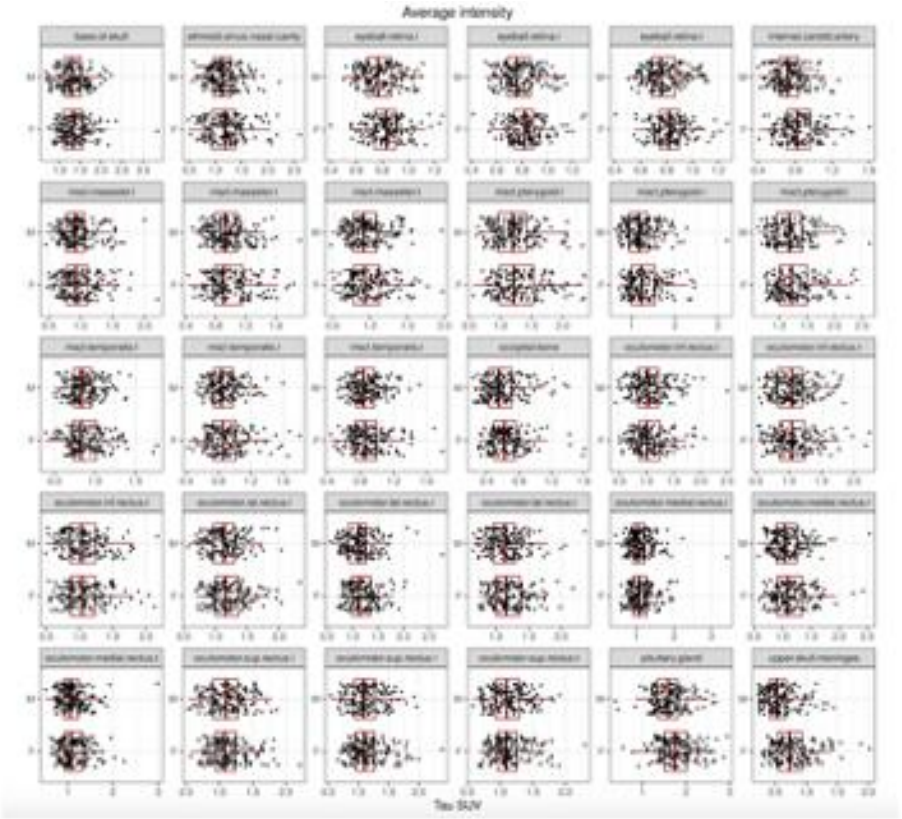


Figure 2. Tau average SUV in relation to sex of participant by off-target region of interest. When applicable, laterality is given as well as combined left and right sides

Keywords: Tau extra cerebral, Tau off target binding, impact of age and sex, Tau PET, 18F-FTP

51 Metabolic inefficiency is associated with regional vulnerability to tau deposition

Jenna Adams[1], Dana Parker[1], Irene Zhao[1], Michael Yassa[1]

[1]*University of California, Irvine, Irvine, CA, US*

Background: Increased metabolic demand may predispose brain regions to the accumulation of pathology in Alzheimer's disease. Here, we tested if metabolic inefficiency is associated with regional patterns of tau deposition in older adults.

Methods: We characterized patterns of glucose metabolism using 18F-Fluorodeoxyglucose-PET (FDG) in relation to structural connectivity and tau deposition in older adults from ADNI. 482 FDG scans were warped to MNI space. The mean SUVR of 218 cortical ROIs from the Brainnetome Atlas were extracted and averaged across cognitively normal participants (Fig1A). Multishell diffusion MRI from 40 cognitively normal, amyloid-negative participants was used to create whole brain tractograms. The average number of streamlines between each ROI pair was extracted to create a healthy structural connectome. The density of structural connections to each region, normalized by regional volume, was computed (Fig1B). The ratio of mean FDG SUVR to the density of structural connections was calculated for each region and used as a measure of metabolic demand, with higher values representing inefficiency (higher FDG than expected for structural density). 18F-Flortaucipir SUVR was averaged across 1,628 scans across diagnoses to obtain regional patterns of tau-PET uptake.

Results: Regions demonstrating the greatest metabolic inefficiency (top 5% of regions) were primarily found within the medial temporal lobe, including the transentorhinal/perirhinal cortex, entorhinal cortex, temporal agranular cortex, and amygdala (Fig1C). We next tested associations between metabolic inefficiency and regional vulnerability to tau deposition. Metabolic inefficiency values were highest for regions classified within earlier Braak stages ($r = 0.39$, $p<0.001$; Fig1D), and higher metabolic inefficiency was associated with greater average regional values of FTP SUVR ($r = 0.27$, $p = 0.03$; Fig1E).

Conclusions: Metabolic inefficiency, defined as increased metabolic demand compared to the density of structural connections, may lead to greater susceptibility to early tau accumulation in medial temporal lobe regions.

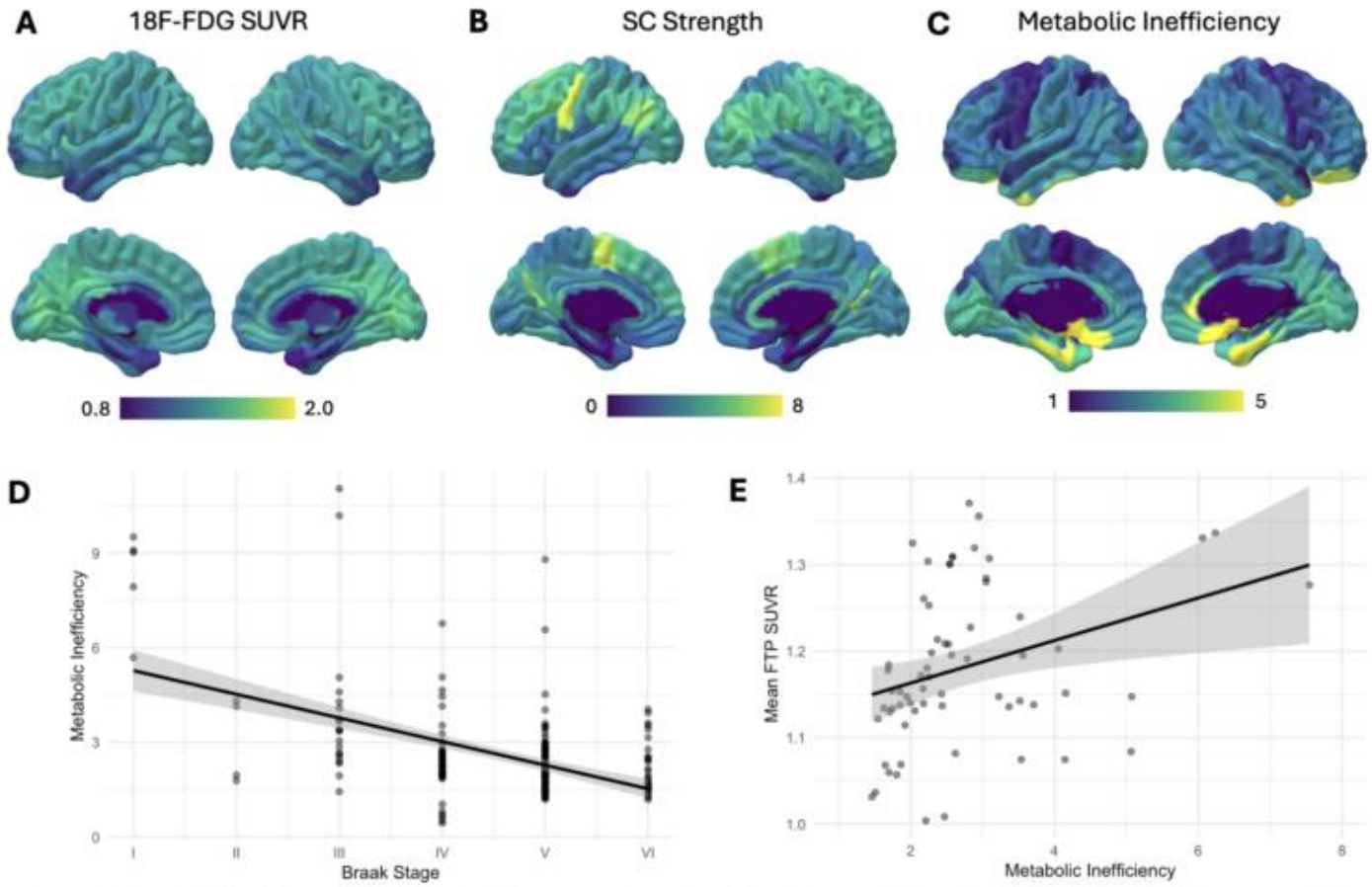


Figure 1. Metabolic inefficiency is associated with patterns of tau deposition. A, Mean 18F-Fluorodeoxyglucose (FDG) PET across cognitively normal older adults. **B**, Mean structural connectivity (SC) density of each brain region computed from an average healthy connectome. **C,** Metabolic demand, calculated by the regional proportion of FDG to SC density (controlling for regional volume), in which higher values indicate metabolic inefficiency (greater FDG compared to structural density). **D,** Higher metabolic inefficiency in regions classified in earlier Braak Stages. **E,** Higher metabolic inefficiency was associated with higher regional 18F-Flortaucipir (FTP).

Keywords: tau, glucose metabolism, structural connectivity, PET

52 Relationship between Polygenetic Risk Score of BrainAge and plasma biomarkers in the A4/Elearn Study

Jorge Garcia Condado[1,2,3], Colin Birkenbihl[3], Jesus M Cortes[1,4], Rachel F Buckley[3,5], Ibai Diez[1,4,6,7]

[1]*Computational Neuroimaging Lab, Biobizkaia Health Research Institute, Barakaldo, ES*
[2]*Universidad del Pais Vasco (UPV/EHU), Leioa, ES*
[3]*Massachusetts General Hospital, Department of Neurology, Boston, MA, US*
[4]*IKERBASQUE Basque Foundation for Science, Bilbao, ES*
[5]*Melbourne School of Pyschological Sciences, University of Melbourne, Melbourne, AU*
[6]*Gordon Center for Medical Imaging, Department of Radiology, Boston, MA, US*
[7]*Athinoula A. Martinos Center for Biomedical Imaging, Boston, MA, US*

Increasing research is studying the interplay between genetic factors, brain aging, and neurodegeneration, particularly in the context of Alzheimer's disease. Tools such as Brain Age Gap, which measures the discrepancy between chronological and predicted brain age based on neuroimaging, and Polygenic Risk Scores (PRS), which quantify genetic predisposition to specific traits like accelerated brain aging, are proving valuable in elucidating the genetic underpinnings of neurodegeneration.

We analyzed genetic information and plasma biomarkers from the A4/ELearn study on 3014 cognitively normal subjects (71.4 ± 4.6 age; 40.3% male). PRS of BrainAge models were calculated for each subject using the summary GWAS statistics of Wen et. al, Nature Communications 2024 for three types of BrainAge models: Grey Matter (GM), White Matter (WM) and Functional Connectivity (FC). We focused on plasma biomarkers from the study: pTau217 (N=736), FP42/FP40 (N=2429), plasma APOE4 prtoein levels (N=588), GFAP (N=1641), Neuro Filament Light Chain (N=1643) and pTauC2 (N=1163). We used a general linear model to study the association between the biomarkers with PRS and with the interaction between age and PRS for each BrainAge model.

We found that the interaction between age and GM PRS, was positively associated with pTAU217 (p-value=0.0073) and pTauC2 (p-value=0.040). The GM PRS alone was also associated with pTauC2 after adjusting for age and the interaction (p-value=0.042). Moreover, the interaction between age and WM PRS was associated positively with FP42/40 (p-value=0.020) and pTauC2 (p-value=0.043). We did not find significant differences in PRS values splitting by amyloid positivity, by APOE4 genotype or using FC PRS.

This study highlights the significance of genetic factors contributing to accelerated brain aging and its association with neurodegenerative biomarkers. The effects of these genetic predispositions become apparent when combined with aging, suggesting that the interaction between genetics and age may better reflect the role of genetic factors in neurodegeneration.

Keywords: Brain Age, Polygenetic Risk Score, Aging, Alzheimer's disease, Plasma Biomarkers

53 Combined impact of plasma phospho-tau 217 and NfL on longitudinal domain-specific cognitive decline

Hiroko Dodge[1], Chao-Yi Wu[1], Liu Chen[1], Jennifer Gatchel[1], Sudeshna Das[1], Pia Kivisäkk[1], Steven Arnold[1]

[1]*Harvard Medical School, Boston, MA, US*

Introduction: Plasma p-tau217, an indicator of tau pathology with strong associations to amyloid-beta pathology, and NfL, a marker of axonal damage and neurodegeneration, are promising diagnostic and prognostic tools. Their combined use could offer more accurate diagnostic or prognostic insights than either biomarker alone. To enhance the clinical utility of these plasma biomarkers, we examined the trajectories of domain-specific cognitive functions by stratifying participants based on plasma p-tau217 (quantiles) and NfL levels (high/low), among those with normal cognition (NC) and mild cognitive impairment (MCI).

Methods: Participants from the Massachusetts Alzheimer's Disease Research Center longitudinal cohort, with either normal cognition (CN) or MCI and available plasma p-tau217 and NfL samples, were included (Table 1). Cognitive functions were assessed longitudinally using the National Alzheimer's Coordinating Center Uniform Data Set V1, V2, and V3: general cognition (MMSE, MoCA converted to MMSE in V3), memory (Logical Memory), executive functions (Trail Making B, Log-transformed and reverse-coded) and language-based executive function (Category Fluency Animals). We used linear mixed-effects models with 8 groups combining p-tau217 (quantiles) and NfL (low/high) to predict cognitive trajectories over 7 years, controlling for age.

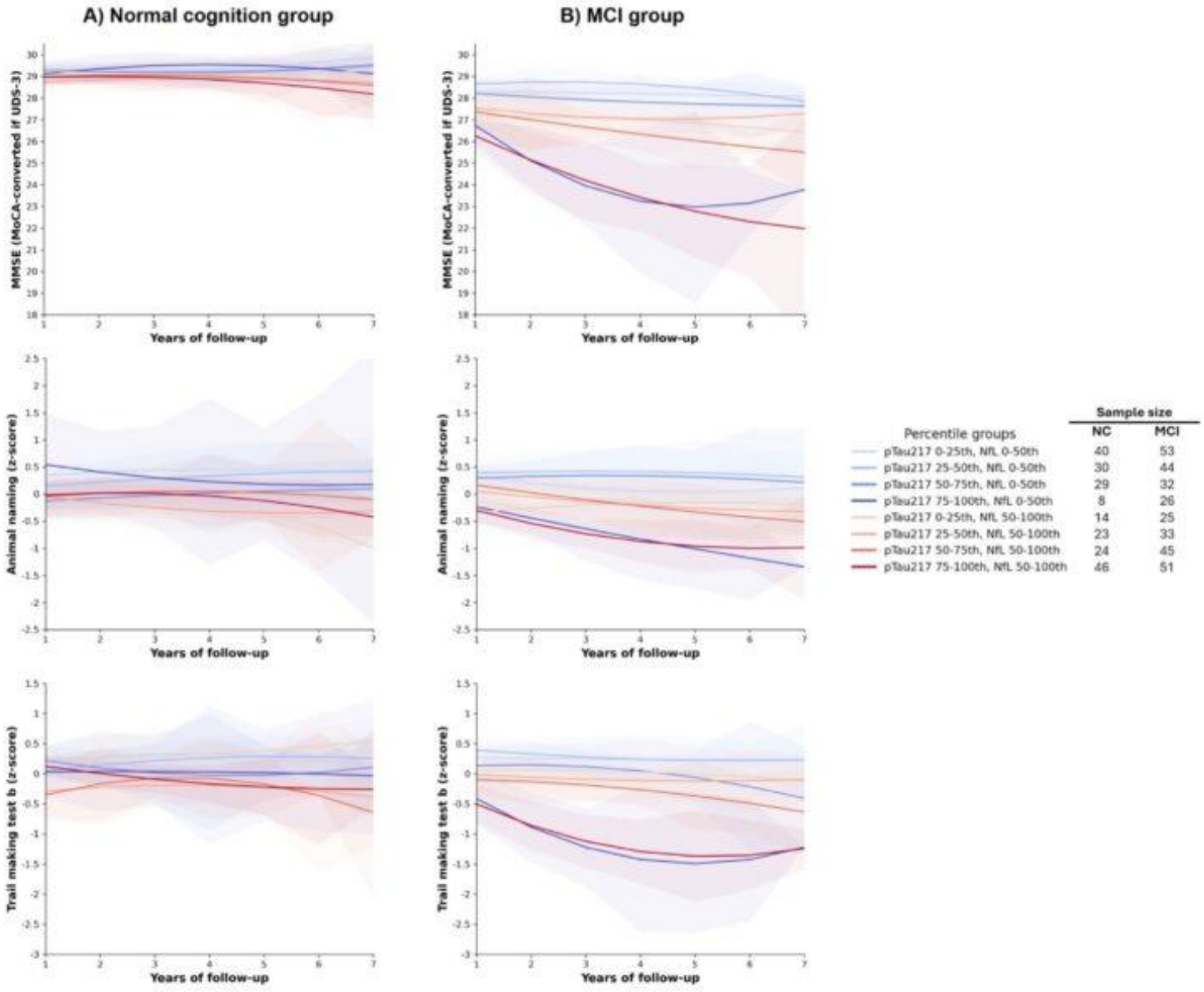
Results: Visual inspection of trajectory plots (Figure 1) shows that among participants with normal cognition, higher NfL levels are associated with worse cognitive trajectories across all domains, irrespective of p-tau217 levels. On the other hand, in MCI participants, the highest p-tau217 group exhibits the worst cognitive outcomes, regardless of NfL levels. This pattern persisted across all cognitive domain outcomes. Despite the small sample size, statistically significant differences were observed between some groups.

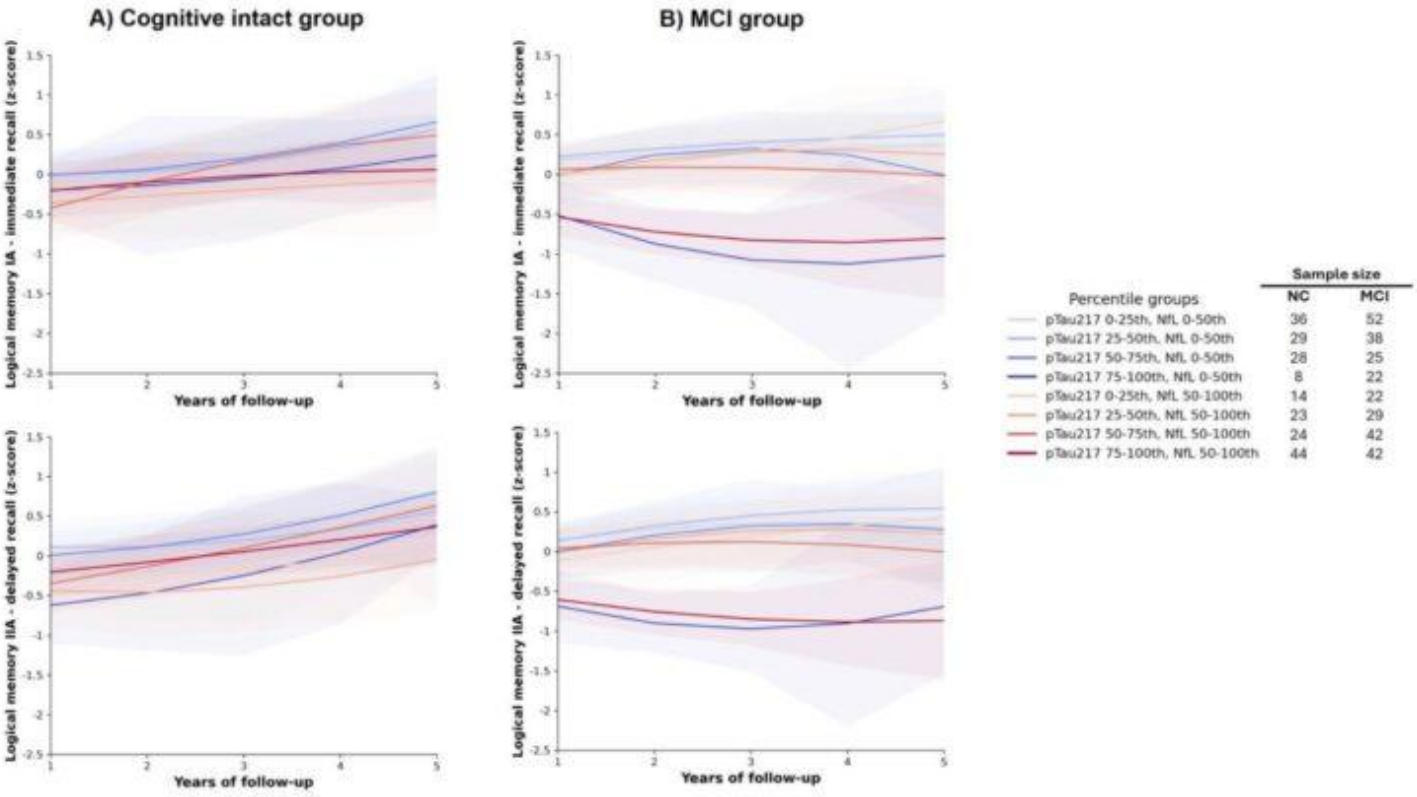
Conclusions: NfL levels are linked to cognitive outcomes when p-tau217 is lower. The combination of these plasma biomarkers provides a promising approach for predicting domain-specific cognitive decline. Future research should focus on identifying the optimal cutpoints for biomarker combinations to enhance prognostic accuracy.

Table 1. Baseline characteristics of participants

MADRC samples	Cognitively unimpaired (n=214)	Mild cognitive impairment (n=309)
Age (years), mean±SD	73.61±6.48	76.29±6.43
Female, n(%)	143(66.8)	156(50.8)
Education (years), mean±SD	16.41±2.56	16.19±2.64
MMSE (total score), mean±SD	29.13±1.06	27.68±2.49
Animal naming (counts), mean±SD	20.54±5.34	17.37±5.96
Trail Making Test B (secs), mean±SD	76.52±33.78	111.89±64.60
Logical Memory IA, mean±SD	15.18±3.52	11.90±4.75
Logical Memory IIA, mean±SD	14.29±3.74	10.30±5.24
pTau217 (pg/ml), mean±SD		
0-25th	2.04±0.48	2.28±0.61
25-50th	3.16±0.27	3.96±0.58
50-75th	4.44±0.46	7.27±1.31
75-100th	11.51±8.05	17.25±7.45
NfL (pg/ml), mean±SD		
0-50th	117.54±25.76	141.33±30.91
50-100th	257.18±172.68	300.32±149.47

Figure 1: Longitudinal domain-specific cognitive outcomes by combinations of baseline pTau217 and NfL levels





The follow-up duration for Logical Memory Tests is limited to 5 years because they were not assessed in UDS V3.

Keywords: p-tau217, NfL, trajectories of cognitive decline, domain-specific cognition, MCI

54 Comparison of distribution volume and standardized uptake value ratio for a MAO-B tracer in mild cognitive impairment

Gleb Bezgin[1], Nesrine Rahmouni[1], Ryuichi Harada[2], Nobuyuki Okamura[2], Andrea Lessa Benedet[3], Nicholas Ashton[3], Henrik Zetterberg[3], Kaj Blennow[3], Pedro Rosa-Neto[1]

[1]*McGill University, Montreal, QC, CA*
[2]*Tohoku Medical and Pharmaceutical University, Sendai, JP*
[3]*University of Gothenburg, Gothenburg, SE*

Introduction: SMBT-1 is a promising PET tracer for Monoamine Oxidase-B (MAO-B) imaging[1]. While selective and sensitive for Alzheimer's disease (AD), methods to quantify this family of tracers are being improved. Here, using a sample of subjects from an AD cohort, we compare results obtained using distribution volume (DV) and standardized uptake value ratio (SUVR). Using both techniques, we explore the association between these PET metrics and several plasma biomarkers (GFAP, p-tau-217, p-tau-231 YKL-40 and Abeta42/40 ratio).

Methods: We administered SMBT-1 on fourteen subjects from the TRIAD cohort[2] (7 cognitively normal (CN), 4 with mild cognitive impairment (MCI), 2 with non-AD pathology; mean age 71.9). The scanning was performed using High-Resolution Research Tomograph (HRRT), and the MRI was done on a SIEMENS Prisma scanner. For the PET images, we computed DV and SUVR, using cerebellar grey as reference region. Proteomics data for plasma GFAP, p-tau-217, p-tau-231, Abeta40, Abeta42 and YKL-40 were obtained using NULISA[3]. The association between DV/SUVR images and fluid biomarkers was assessed using VoxelStats[4].

Results: Time activity curves for MCI had more sustained tracer retention than those of CN subjects, resulting in generally higher DV values (Fig.1A). VoxelStats analyses showed that DV and SUVR were generally consistent in capturing association between PET data and plasma biomarkers (Fig.1B). GFAP, p-tau-217 and p-tau-231 showed association with voxels around precuneus and medial frontal, whereas YKL-40 was most associated with periventricular white matter. Abeta42/40 relationship with DV had scattered cortical distribution; this association was moderate and marginally significant (r=-0.5; p=0.07; Fig.1C-left). GFAP correlated with the whole cortex average of SUVR (r=0.7; p<0.05; Fig.1C-right).

Conclusions: Even with a current modestly powered sample, we saw associations between SMBT-1 and several AD fluid biomarkers; these associations were consistent between DV and SUVR. We expect to show these results with a largely extended sample at the conference.

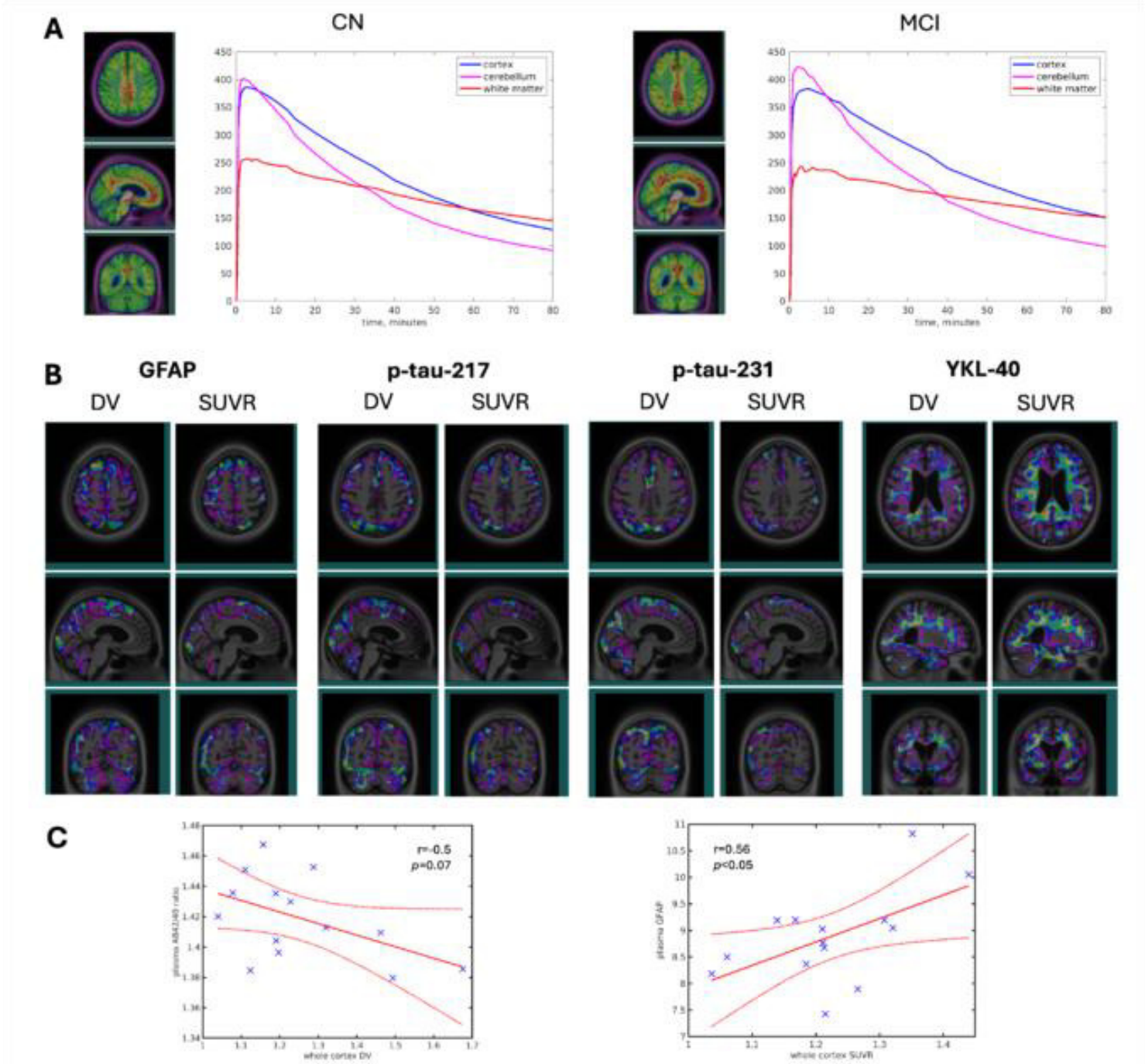


Figure 1. Analysis of SMBT-1 data in the TRIAD cohort. A: average images and time activity curves (TACs) for the CN (left) and MCI (right) subjects. B: VoxelStats results showing t-maps for the association in the linear model with plasma biomarkers as response variables, DV and SUVR as independent variable, and age and sex as covariates. C: correlations between SUVR/DV measurements across the whole cortex and Abeta42/40 ratio (left) and GFAP (right).

References:
1. Harada R et al. J Nucl Med 2021, 62 (2):253-58.
2. Stevenson et al. Alzheimer's & Dementia 2020, 16(Suppl.4):e043982.
3. Feng W et al. Nat Commun 2023, 14:7238.
4. Mathotaarachchi S et al. Front Neuroinform 2016, 10:20.

Keywords: positron emission tomography, kinetic modeling, monoamine oxidase B, plasma biomarkers

55 Association between early and late tau aggregation across tau imaging agents: The HEAD Study

Nesrine Rahmouni[1], Cécile Tissot[2], Joseph Therriault[1], Ali Hosseini[1], Arthur Macedo[1], Stijn Servaes[1], Firoza Lussier[3], Lydia Trudel[1], Brandon Hall[1], Jaime Fernandez-Arias[1], Yi-Ting Wang[1], Jenna Stevenson[1], Serge Gauthier[1], Suzanne Baker[2], Tharick A. Pascoal[3], Pedro Rosa-Neto[1]

[1]*McGill University, Montreal, QC, CA*
[2]*Lawrence Berkeley National Laboratory, Berkeley, CA, US*
[3]*University of Pittsburgh, Pittsburgh, PE, US*

Background: The association between medial temporal and neocortical SUVR depends on availability of cortical tau. However, tracer differences in affinity and off-target binding might interfere in these associations. Here, we examined the association between medial temporal and neocortical SUVR using voxel-based approach.

Methods: We included 68 individuals (46 Cognitively Unimpaired and 22 Cognitively Impaired) from the HEAD Study recruited at McGill University. All individuals were assessed for amyloid-β (Aβ) deposition using [^{18}F]AZD4694-PET and four tau-PET ligands ([^{18}F][^{18}F]MK6240, [^{18}F]Flortaucipir, [^{18}F]RO948 and [^{18}F]PI-2620). Correlation maps evaluated the relationship between PET tracers' uptake in the entorhinal cortex (EC), in the inferior temporal gyrus and in the posterior cingulate and their association with the tracer's uptake in later Braak regions. Correlations coefficients were compared across Braak Stages.

Results: Positive associations were observed between tau-PET SUVR in the EC (Figure1). [^{18}F]MK6240 EC was correlated with tracer uptake in the whole cortex. [^{18}F] Flortaucipir was associated with tracer uptake in similar regions, albeit showing a lower t-value. [^{18}F]PI2620 EC uptake correlated with binding in regions Braak II-V. Finally, [^{18}F]RO948 was associated with uptake. Across Braak regions, entorhinal seed covariance maps are restricted to early Braak regions in Aβ- individuals, while encompassing neocortical regions in Aβ+ individuals (Figure 2). Finally, seeds outside the MTL reflected advanced tau covariance patterns in Aβ+ individuals, with [^{18}F]MK6240 showing stronger correlation patterns in all Braak regions, followed by [^{18}F] Flortaucipir, [^{18}F]RO948 and [^{18}F]PI2620 (Figure 3).

Conclusion: [^{18}F]MK6240 showed higher and more widespread correlations between early and late tau pathology, potentially due to this tracer's higher affinity for tau tangles. Results were concordant at the voxel and region-on-interested levels. [^{18}F] Flortaucipir, [^{18}F]RO948 and [^{18}F]PI-2620 showed similar results, in lower magnitude.

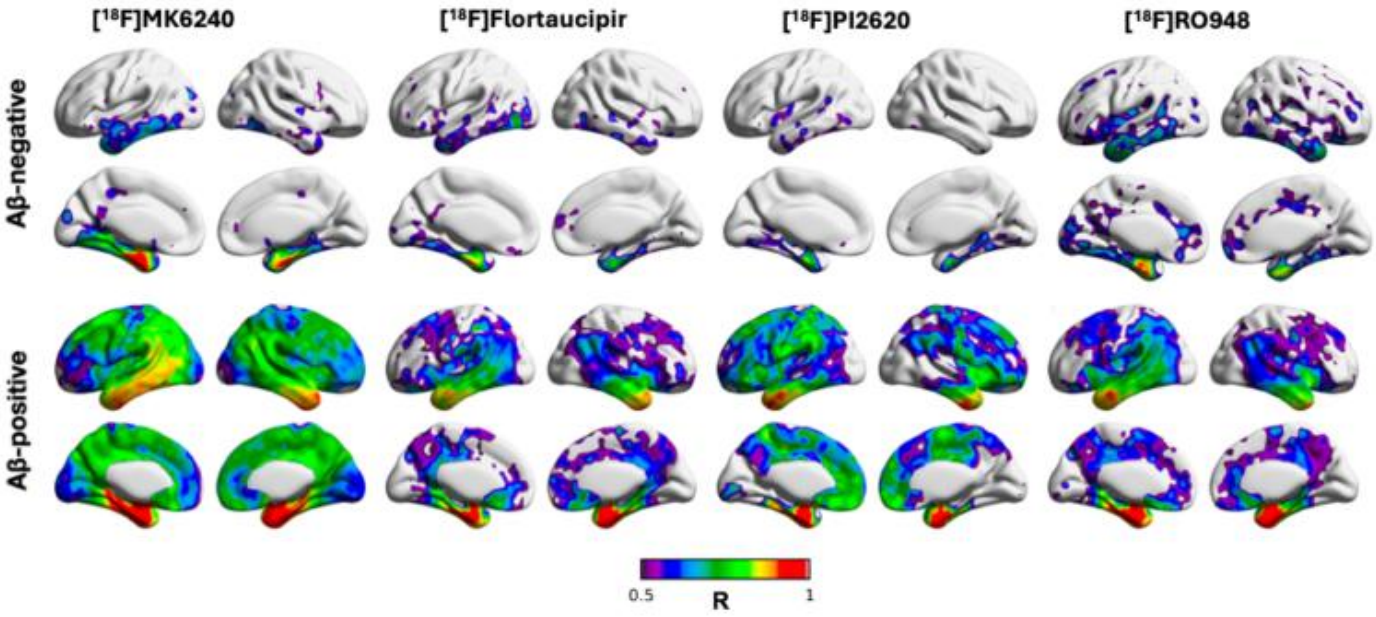


Figure 1: Patterns of Entorhinal cortex-Neocortical tau covariance.

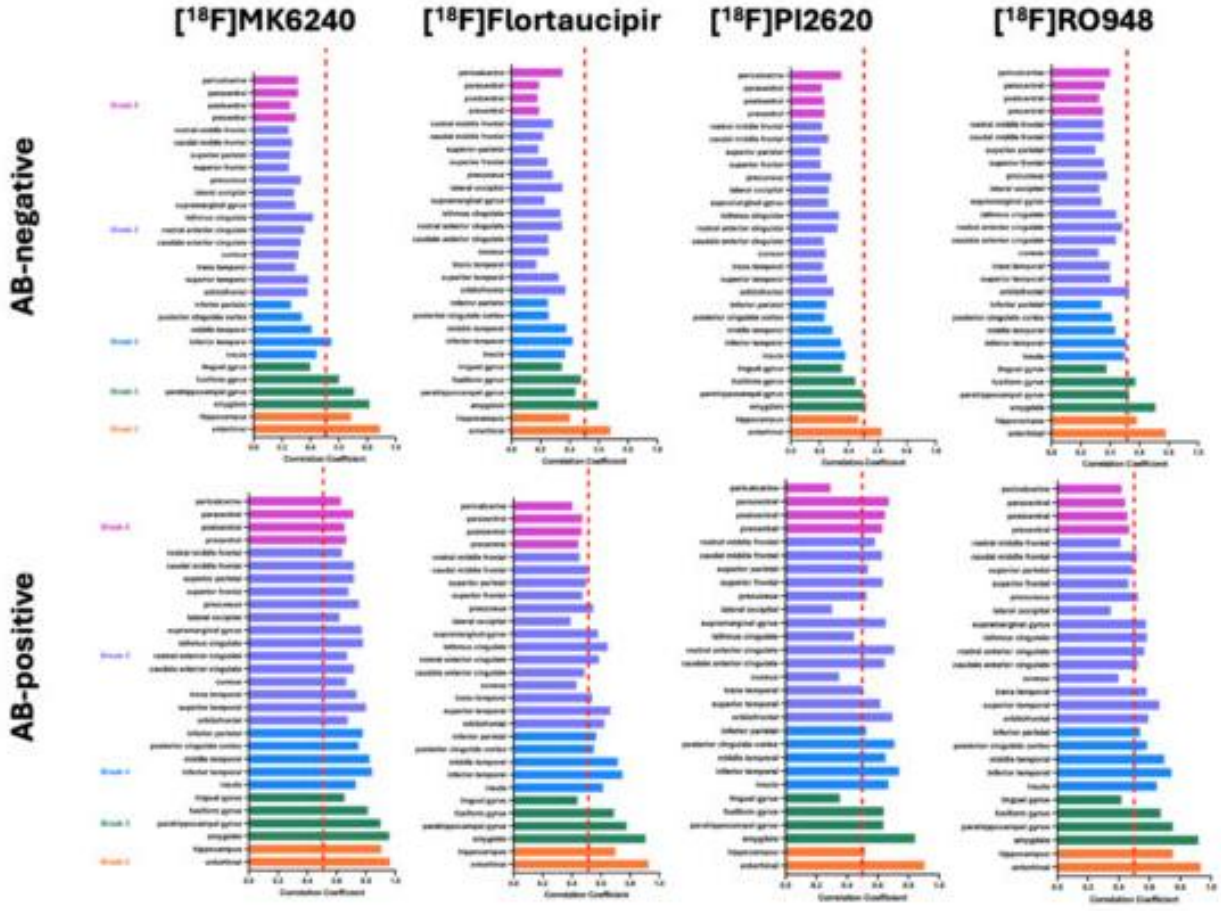


Figure 2: Entorhinal seed covariance maps across Braak Stages

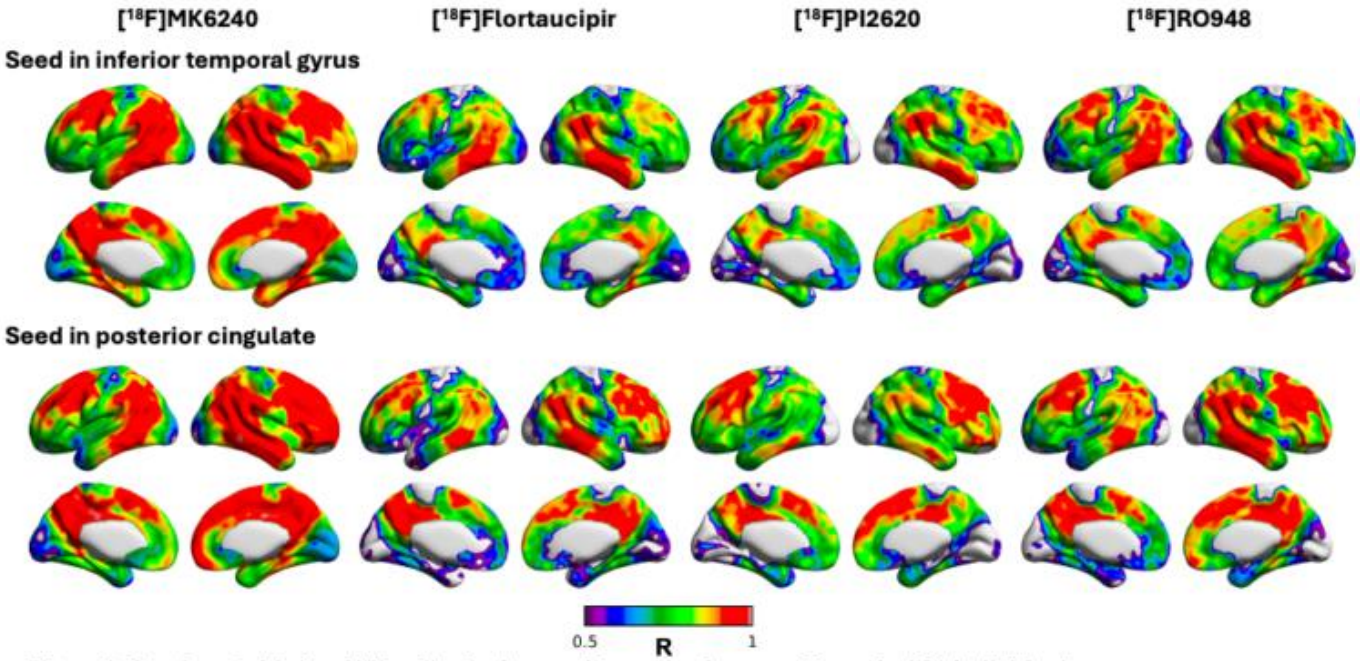


Figure 3: Seeds outside the MTL reflect advanced tau covariance patterns in Aβ+ individuals

Keywords: Tau, PET Imaging, Biomarkers, Head-to-head

56 The impact of spatial smoothing on the accuracy of Centiloid thresholds

Alfonso Fajardo-Valdez[1,2], Ting Qiu[1,2], Jonathan Gallego-Rudolf[1,2], Mohammadali Javanray[1,2], Sylvia Villeneuve[1,3,4]

[2]*Douglas Mental Health University Institute, Montreal, Quebec, Canada, Montreal, QC, CA*
[2]*Integrated Program in Neuroscience, Faculty of medicine, McGill University, Montreal, Canada, Montreal, QC, CA*
[3]*Montreal Neurological Institute, McGill University, Montreal, Canada, Montreal, QC, CA*
[4]*Department of Psychiatry, Faculty of medicine, McGill University, Montreal, Canada, Montreal, QC, CA*

Introduction: The Centiloid (CL) scale was developed to harmonize amyloid-beta (Aβ) values across tracers, preprocessing methods and scanners. CLs are useful to derive comparable cut-off thresholds to assess Aβ positivity across sites. For CLs to be reliable, the linear model output evaluating ground truth vs obtained CLs needs to respect some criteria. Here, we examined differences due to spatial smoothing (SS), a common procedure in PET preprocessing, on SUVR-to-CL conversion, CL-based thresholds, and group-level SUVR statistics.

Methods: We obtained CLs and 50-70 min ^{18}F-NAV4694 PET scans from 55 subjects (10 young, 45 AD) from the GAAIN website. Preprocessing was conducted via the VilleneuveLab pipeline (Vlpp; see Qiu et al., 2024) using 4 distinct Vlpp SS Spatial Smoothing (FWHM) kernels: 0mm, 4mm, 8mm and 12mm. We extracted Aβ SUVRs from the GAAIN cortical mask (whole-cerebellum as reference region) and we calculated CLs using the standard GAAIN ^{18}F-NAV4694 CL equation:

$$CL_{NAV4694} = 100 \times (SUVR_{NAV4694} - 1.031) / 1.172$$

Throughout linear models, we evaluated the accuracy of CLs. We then classified older individuals as Aβ- or Aβ+ based on CL12 or CL20 thresholds. Finally, we calculated the effect size (Cohen's D) when comparing SUVR means of Desikan-Killiany (DK) regions or global amyloid index (average of 40 DK regions) between groups. Analyses were reproduced in a sample of n=45 older adults from the PREVENT-AD cohort (fig 2).

Results: No SS resulted in higher accuracy of CLs (fig 1a / table 1). At C12 threshold, greater SS increased the number Aβ+ individuals, whereas at CL20, classifications outcomes were highly similar. Despite these, a significant effect of SS was found when comparing Aβ+ vs Aβ- SUVRs in both datasets.

Conclusions:

- More reliable CLs were obtained with non-smoothed data.
- SUVRs are influenced by SS.
- Evaluation with other tracers and pipelines is needed.

Figures:

Table1: Fitted linear model's coefficients (GAAIN CL ~ Vlpp CL) under distinct spatial smoothing kernels. For deeming predicted CLs as accurate, the following criteria (Klunk et al., 2015) must be fulfilled: Intercept [0.98 – 1.02]; Slope [-2 – 2]; $R^2 > 0.98$.

Vlpp Spatial Smoothing (FWHM)	Intercept	Slope	R-Squared	R-squared Passed?	Slope Passed?	Intercept Passed?	Passed?
00 mm	0.013	1.01	0.996	Yes	Yes	Yes	Yes
04 mm	-0.170	1.031	0.996	yes	No	Yes	No
08 mm	-0.912	1.09	0.995	Yes	No	Yes	No
12 mm	-2.23	1.091	0.953	No	No	No	No

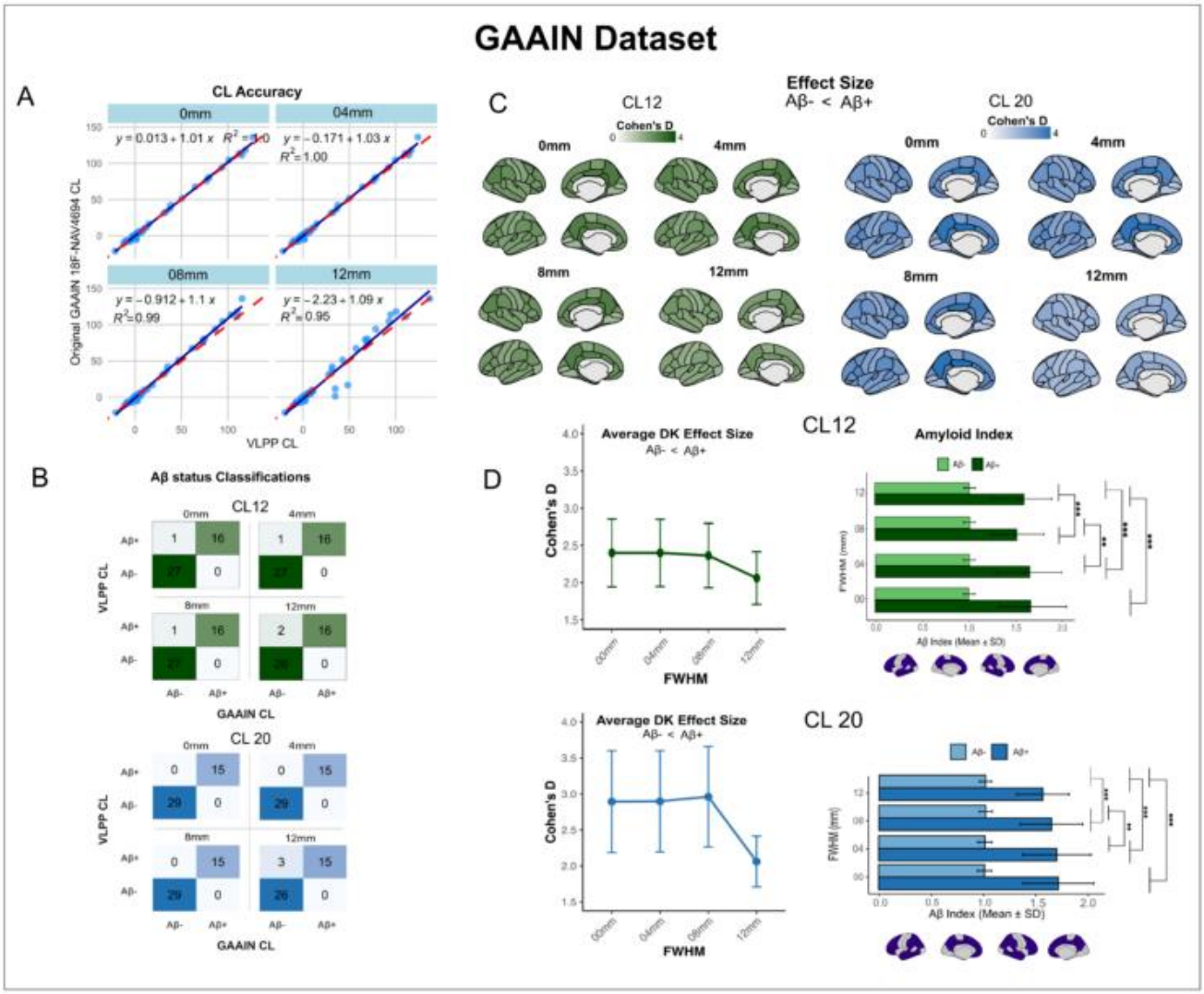


Figure 1: A) Accuracy of predicted GAAIN values from Vlpp CLs with distinct spatial smoothing levels. In scatterplots blue lines correspond to obtained regression lines whereas red-dotted lines depict a perfect model fit (intercept = 0, slope = 1. B) Aβ status classification labels in GAAIN vs Vlpp at distinct spatial smoothing kernels. In both CL12 (green) and CL20 (blue) classification outcomes were similar, slightly differing in the 12 mm Vlpp Spatial Smoothing (FWHM). Based on CL12 and CL20 classifications, we evaluated the Aβ- vs Aβ+ effect size when comparing the mean SUVR values. C) depicts ¬¬effect size in DK atlas regions whereas in D) lineplots display de average DK effect size. Barplots show the Aβ indexes as a function SS kernels and group. Main effects of SS were found. Significant p-values (uncorrected) are illustrated as ** p-value < 0.01 and *** p-value <0.001.

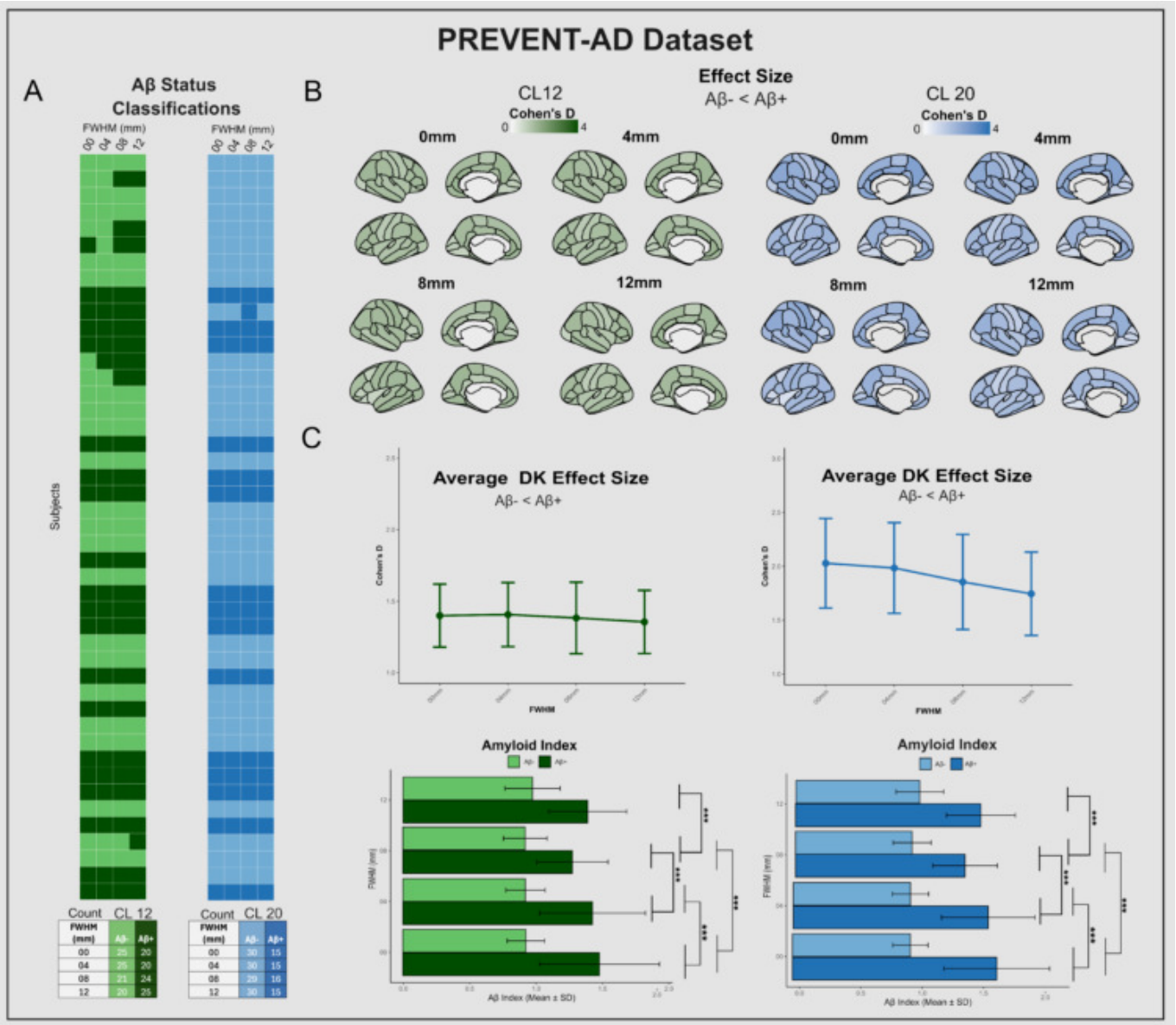


Figure 2: CL12 (green) and CL20 (blue) classifications in the PREVENT-AD cohort (n = 45). In A) heatmaps show classification labels for each subject at different SS levels. B) Aβ- vs Aβ+ effect size in the DK regions and in C) lineplots show average size, whereas barplots show Aβ index per group at the distinct Vlpp Spatial Smoothing (FWHM) kernels. Main effects of SS were found. Significant p-values (uncorrected) are illustrated as *** p-value < 0.001.

Keywords: Centiloid, PET, amyloid-beta, preprocessing, SUVR

57 Longitudinal amyloid PET trajectories in the HABS-HD cohort

Tobey Betthauser[1], Jacob Morse[1], Margo Heston[1], Rebecca Langhough[1,2], Finnuella Carey[1], Julie Wisch[3], Beau Ances[3], Annie Cohen[4], Arthur Toga[5], Meredith Braskie[5], Megan Zuelsdorff[1,6], Sid O'Bryant[7], Karin Meeker[7]

[1]*University of Wisconsin-Madison, School of Medicine and Public Health, Department of Medicine, Madison, WI, US*
[2]*University of Wisconsin-Madison, Wisconsin Alzheimer's Institute, Madison, WI, US*
[3]*Washington University School of Medicine, Department of Neurology, St Louis, MO, US*
[4]*University of Pittsburgh, Department of Psychiatry, Pittsburgh, PA, US*
[5]*Mark and Mary Stevens Neuroimaging and Informatics Institute, Keck School of Medicine, University of Southern California, Los Angeles, CA, US*
[6]*University of Wisconsin-Madison, School of Medicine and Public Health, Department of Nursing, Madison, WI, US*
[7]*University of North Texas Health Science Center, Institute for Translational Research, Fort Worth, TX, US*

Background: Amyloid PET and longitudinal accumulation trajectories are well-characterized in cohorts primarily comprised of non-Hispanic White (NHW) participants. This work investigates whether sampled iterative local approximation (SILA), previously validated for amyloid trajectory modeling in NHW cohorts, generalizes to other ethnoracial groups from the HABS-HD-ATN study.

Methods: 556 participants with longitudinal Florbetataben PET SUVR were included (**Table 1**). Cortical amyloid was quantified averaging SUVR across FreeSurfer-defined regions (whole cerebellum reference region, 90-110 min). A+ was defined as global SUVR>1.076 based on GMM. SILA was applied across the entire sample to model longitudinal amyloid accumulation and estimate individualized A+ age and time (A+ age minus age at scan) using each person's last scan as a reference. SILA SUVR residuals were calculated at the first scan to investigate amyloid accumulation trajectories differences. ANOVA/Chi^2 tested for differences in age, %A+, global SUVR, and for SUVR prediction residual differences between groups stratified by A+/- and secondarily within A- and A+ strata. LME tested for possible differences in amyloid accumulation rates between groups, stratified by A+/- (ageXgroupXA+/-).

Results: Ethnoracial groups differed on age, FBB SUVR, and %A+ (age: NHW >Hispanic >Black). NHW had higher SUVR and higher %A+ than Black and Hispanic groups (**Table 1, Figure 1**). ANOVA indicated main effects of A+/- and group for SILA prediction residuals, which were lower for NHW and for A- groups (**Figure 2**). No significant group differences were observed for SUVR residuals within A+/- strata (p(A-)=0.10, p(A+)=0.10. LME indicated no significant group differences in amyloid accumulation rates (interaction p=0.75).

Discussion: Preliminary analyses suggest SILA is amenable to amyloid trajectory modeling across ethnoracial groups and amyloid PET trajectories are similar across groups but require further investigation with larger longitudinal samples and more statistical power. Further work will investigate possible differences in A+ onset age and possible differential effects of *APOE*.

	Black	Hispanic	NHW	p(group)	Pairwise
n	137	206	213	-	-
Age at last scan mean [95% CI]	64.96 [63.67, 66.24]	67.57 [66.47, 68.67]	71.99 [71.09, 72.88]	<0.001	1 < 2 < 3
FBB Global SUVR mean [95% CI]	1.02 [1.00, 1.04]	1.04 [1.02, 1.06]	1.09 [1.07, 1.12]	<0.001	3 > 1 and 2
A+/- at last scan n (%)	23 (16.8%)	39 (18.9%)	71 (33.3%)	<0.001	3 > 1 and 2
Years of A PET follow-up Mean [95% CI]	2.15 [2.11, 2.18]	2.15 [2.10, 2.19]	2.20 [2.16, 2.25	0.13	-
Global CDR				<0.001	
0	85 (62.0%)	157 (76.2%)	186 (87.3%)		
0.5	49 (35.8%)	46 (22.3%)	22 (10.3%)		
1	3 (2.2%)	2 (1.0%)	3 (1.4%)		
2	0 (0.0%)	1 (0.5%)	2 (0.9%)		

Table 1: HABS-HD-ATN participant summary by ethnoracial group. FBB and A+/- are established at the last available scan.

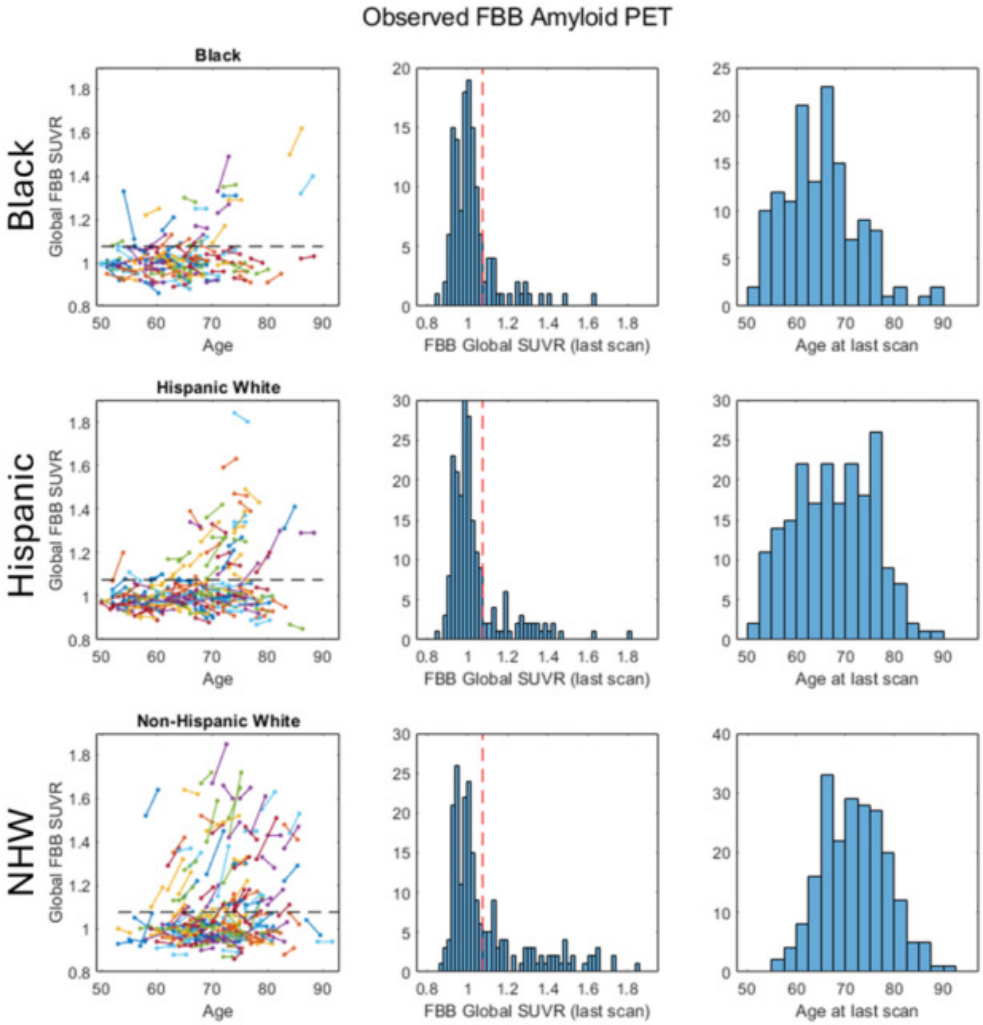


Figure 1: Observed amyloid PET vs. age (left column), SUVR distribution at last observation (middle column), and age at last scan (right column) by race/ethnicity group (rows). NHW = non-Hispanic White

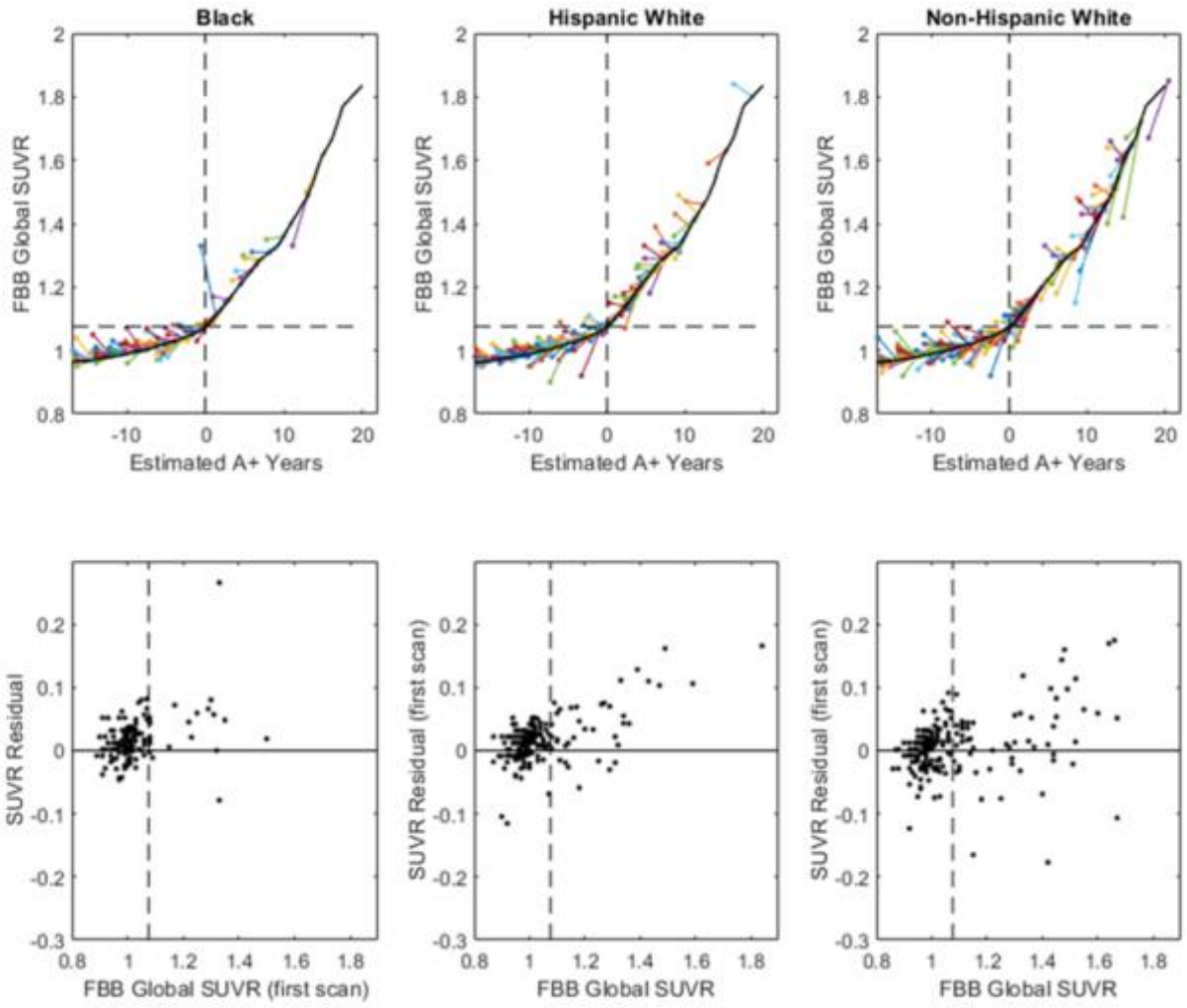


Figure 2: SILA-estimated trajectories (top) and backwards SUVR prediction residuals (bottom) by ethnoracial groups (columns). Positive residuals indicate a lower slope (i.e., slower rate) relative to the SILA-modeled amyloid trajectory function.

Keywords: amyloid, trajectory, diverse, SILA

58 Lower microstructural integrity of the locus coeruleus to entorhinal cortex pathway is related to elevated astrocyte reactivity and tau burden in cognitively unimpaired individuals: a 7T dMRI study

Yuliya Patsyuk[1], Maxime Van Egroo[1,2], Elise Beckers[1,3], Nicholas J. Ashton[4,5,6,7], Shorena Janelidze[8], Kaj Blennow[4,9], Oskar Hansson[8,10], Henrik Zetterberg[4,9,11,12,13], Benedikt A. Poser[14,15], Heidi I.L. Jacobs[1,2]

[1]*Faculty of Health, Medicine and Life Sciences, Mental Health and Neuroscience Research Institute, Alzheimer Centre Limburg, Maastricht University, Maastricht, NL*
[2]*Athinoula A. Martinos Center for Biomedical Imaging, Department of Radiology, Massachusetts General Hospital and Harvard Medical School, Boston, MA, US*
[3]*GIGA-Cyclotron Research Centre-In Vivo Imaging, University of Liège, Liège, BE*
[4]*Department of Psychiatry and Neurochemistry, Institute of Neuroscience and Physiology, The Sahlgrenska Academy at the University of Gothenburg, Mölndal, SE*
[5]*Centre for Age-Related Medicine, Stavanger University Hospital, Stavanger, NO*
[6]*King's College London, Institute of Psychiatry, Psychology and Neuroscience, Maurice Wohl Institute Clinical Neuroscience Institute, London, GB*
[7]*NIHR Biomedical Research Centre for Mental Health and Biomedical Research Unit for Dementia at South London and Maudsley NHS Foundation, London, GB*
[8]*Clinical Memory Research Unit, Department of Clinical Sciences Malmö, Lund University, Lund, SE*
[9]*Clinical Neurochemistry Laboratory, Sahlgrenska University Hospital, Mölndal, SE*
[10]*Memory Clinic, Skåne University Hospital, Malmö, SE*
[11]*Department of Neurodegenerative Disease, UCL Institute of Neurology, Queen Square, London, GB*
[12]*UK Dementia Research Institute at UCL, London, GB*
[13]*Hong Kong Center for Neurodegenerative Diseases, Clear Water Bay, Hong Kong, CN*
[14]*Department of Cognitive Neuroscience, Faculty of Psychology and Neuroscience, Maastricht University, Maastricht, NL*
[15]*Maastricht Brain Imaging Centre, Faculty of Psychology and Neuroscience, Maastricht University, Maastricht, NL*

Introduction: Pre-tangle tau inclusions from the locus coeruleus (LC) are hypothesized to propagate to the initial cortical site of tau pathology –the entorhinal cortex (EC)– via neuron-to-neuron transmission along its projections. Examining the LC-EC pathway integrity *in vivo* might shed light on the mechanisms underlying the earliest processes contributing to disease progression. Here, we investigated the relationship between microstructural integrity of the LC-EC pathway and plasma AD-related biomarkers in cognitively normal adults along the adult lifespan.

Methods: Forty-seven cognitively unimpaired participants (mean age=60.4±15.1y.; 23 females) (**Table 1**) underwent a 7T MRI session including LC imaging and a multi-shell high-angular resolution diffusion imaging protocol. The LC-EC pathway was reconstructed using probabilistic tractography. Microstructural integrity of the LC-EC pathway was assessed with Fractional Anisotropy (FA), Mean Diffusivity (MD), and NODDI-derived metrics of Neurite Density Index (NDI) and Orientation Dispersion Index (ODI). A control tract originating from the LC and reaching prefrontal/frontal areas was also included. Additionally, blood samples were processed for plasma AD-related biomarkers, including $A\beta_{42/40}$ ratio, GFAP, NfL, $pTau_{181}$, $pTau_{217}$ and $pTau_{231}$.

Results: Multiple robust linear regressions adjusted for age, sex and volume showed that lower FA in the LC-EC tract associated with elevated levels of GFAP (p=.03) and $pTau_{217}$ (p=.043). Conversely, MD was positively associated with GFAP (p<.001), $pTau_{217}$ (p=.031) and $pTau_{181}$ (p=.019). Higher ODI values related to higher $pTau_{231}$ (p=.017) and $pTau_{181}$ (p=.041) (**Figure 1**). In the control tract, lower FA (p=.003) and NDI (p=.039) values were

associated with lower $A\beta_{42/40}$ ratio, and lower MD values associated with higher $A\beta_{42/40}$ ratio (p=.003)(**Figure 2**).

Conclusion: Our results suggest that microstructural integrity of the LC-EC tract is associated with astrocyte reactivity and elevated tau burden in the earliest asymptomatic stages of the disease, consistent with *postmortem* reports. Future analyses will investigate the topography of these associations along the LC-EC tract.

Table 1. Summary statistics for demographic characteristics, diffusion metrics and plasma biomarker levels in the study sample (N = 47).

	N = 47
Demographic characteristics	
Age, years	60.43 ± 15.11 (30 - 85)
Sex, No. (%)	
Female	23 (48.94)
Male	24 (51.06)
APOE ε4 carrier, No. (%)	11 (23.40)
Volume LC-EC, bilateral (mm^3)	4490.46 ± 1775.49 (1364.52 – 10552.68)
Volume control tract, bilateral (mm^3)	65753.31 ± 17393.89 (31364.53 - 105552.07)
Diffusion metrics	
LC-EC tract (bilateral)	
FA	0.38 ± 0.02 (0.34 - 0.55)
MD (10^3)	0.64 ± 0.026 (0.59 - 0.71)
NDI	0.59 ± 0.04 (0.49 - 0.67)
ODI	0.23 ± 0.02 (0.18 - 0.27)
Control tract (bilateral)	
FA	0.45 ± 0.02 (0.38 - 0.51)
MD (10^3)	0.58 ± 0.03 (0.53 - 0.67)
NDI	0.65 ± 0.05 (0.51 - 0.72)
ODI	0.22 ± 0.02 (0.15 - 0.25)
Plasma biomarkers	
$A\beta_{42/40}$ ratio	0.09 ± 0.01 (0.05 - 0.12)
GFAP (pg/mL)	154 ± 64 (54 - 389)
NfL (pg/mL)	18.10 ± 7.68 (6.56 - 43.43)
$pTau_{181}$ (pg/mL)	1.68 ± 0.86 (0.86 - 6.44)
$pTau_{217}$ (pg/mL)	0.27 ± 0.13 (0.11 – 0.81)
$pTau_{231}$ (pg/mL)	8.34 ± 3.87 (3.29 - 25.85)

Note: values for each continuous variables are presented as mean ± SD (range).

APOE ε4 = apolipoprotein ε4, LC = locus coeruleus, EC = entorhinal cortex, FA = fractional anisotropy, MD = mean diffusivity (10^3), NDI = neurite density index, ODI = orientation dispersion index, Aβ = amyloid beta, GFAP = glial fibrillary acidic protein, NfL = neurofilament light polypeptide.

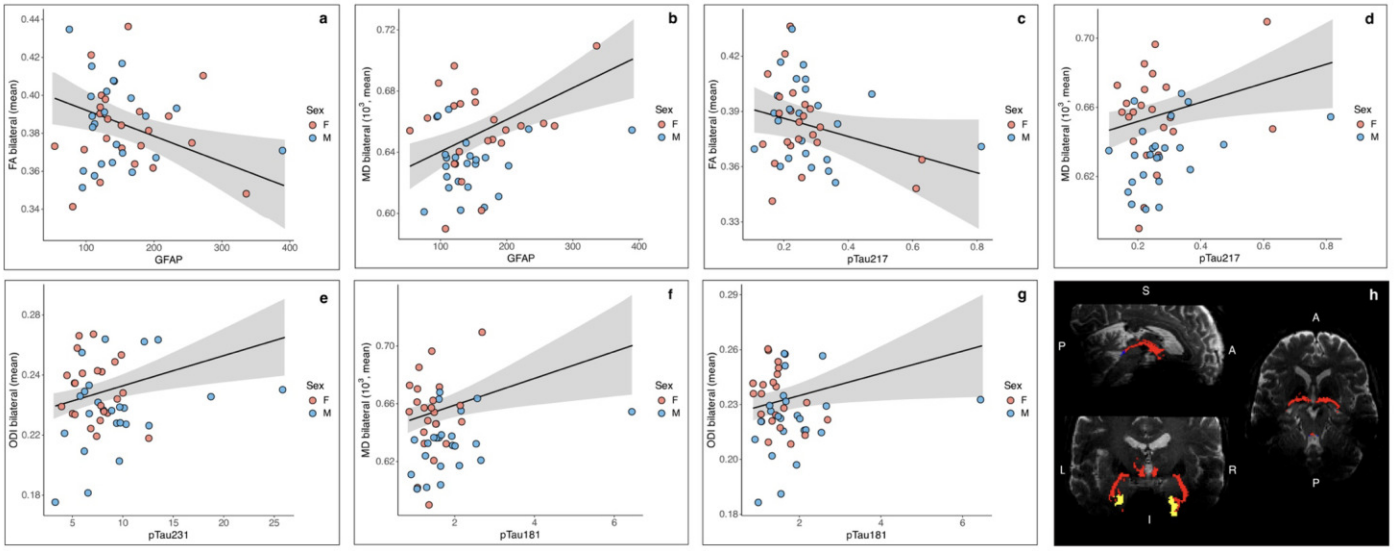


Figure 1. Associations between microstructural integrity of the LC-EC tract and plasma AD-related biomarkers (*N* = 47). Lower fractional anisotropy (FA) (**a**, t = -2.77, p = .03) and higher mean diffusivity (MD) (**b**, t = 2.77, p < .001) values were associated with higher astroglial activation, as captured by GFAP plasma concentration. Similarly, lower FA (**c**, t = -2.07, p = .043) and higher MD (**d**, t = 2.21, p = .031) values were associated with higher pTau217 levels. MD values were also positively associated with pTau181 burden (**f**, t = 2.40 p = .019). Mean values for the orientation dispersion (ODI) index were positively linked to both higher pTau231 (**e**, t = 2.49, p = .017) and pTau181 levels (**g**, t = 2.09, p = .041). However, it is worth mentioning that, although not detected as an influential value by means of Cook's Distance analysis, after removing one participant the associations with pTau181 became only trending with respect to MD values (t = 2.0051, p = 0.052) and lost significance in case of ODI (t = 1.3523, p = 0.182). All robust linear regression models were adjusted for age, sex and tract volume. The LC (in blue)-EC (in yellow) tract (in red) is shown for one representative participant in subject-specific diffusion space (**h**).

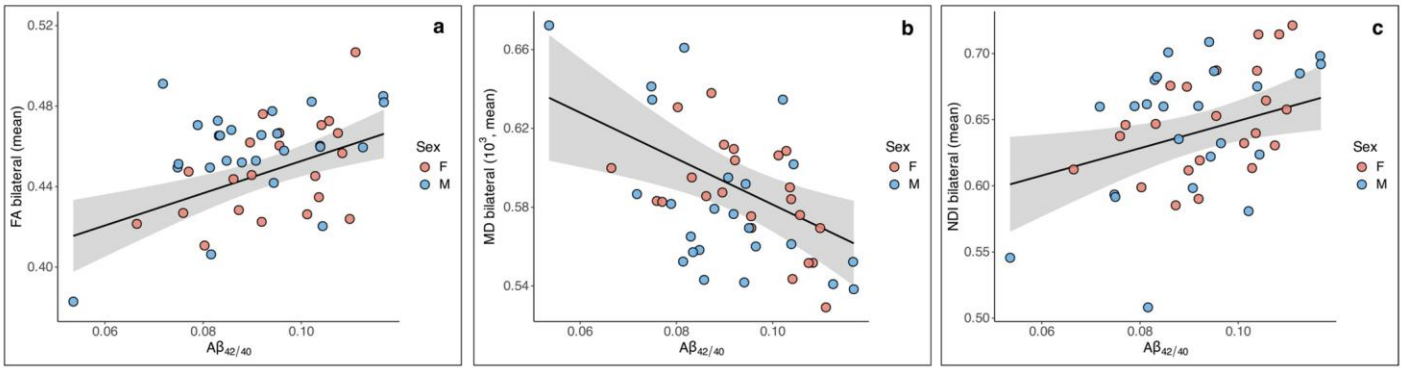


Figure 2. Associations between microstructural integrity of the LC-prefrontal/frontal cortex tract and plasma AD-related biomarkers (*N* = 47). Lower fractional anisotropy (FA) (**a**, t = 3,32, p = .003) and neurite density index (NDI) (**b**, t = 2.19, p = .039) values were associated to lower $A\beta_{42/40}$ ratio, while the inverse relationship was observed between mean diffusivity (MD) values and $A\beta_{42/40}$ ratio (**c**, t = -3,20, p = .003). All robust linear regression models were adjusted for age, sex and tract volume.

Keywords: locus coeruleus, entorhinal cortex, microstructural integrity, AD-related biomarkers, preclinical AD

Wednesday, January 15, 2025 - 11:35 am - 01:00 pm

Podium Session

SESSION II: Spatial Patterns

CHAIRS: Ansel Hillmer, Pedro Rosa-Neto

Wednesday, January 15, 2025		
11:35 am – 01:00 pm	**SESSION II** Spatial Patterns	**Ansel Hillmer,** University of Michigan, Ann Arbor, MI, USA **Pedro Rosa-Neto,** McGill University, Montreal, QC, Canada
11:35 am – 11:40 am	Session Overview	**Chairs**
11:40 am	The interaction of initial medial temporal lobe tauopathy and amyloid-beta spatial extent in driving caTAUstrophe	**Michelle Farrell**, Massachusetts General Hospital, Boston, MA, US
11:55 am	Mapping spatial white matter integrity linked to tau accumulation: Insights from tractometry with multi-shell diffusion imaging	**Jenna Adams**, University of California Irvine, Irvine, CA, US
12:10 pm	Spatial patterns of voxel-wise tau accumulation across the Alzheimer's disease spectrum	**Corrina Fonseca**, Department of Neuroscience, University of California Berkeley, Berkeley, CA, US
12:25 pm	PET astroglia and microglia follow tau propagation patterns in Alzheimer's disease	**Nesrine Rahmouni**, McGill University, Montreal, QC, CA
12:40 pm – 01:00 pm	Discussion	

The interaction of initial medial temporal lobe tauopathy and amyloid-beta spatial extent in driving caTAUstrophe

Michelle Farrell[1], Emma G. Thibault[1], Grace Del Carmen Montenegro[1], Jessie Fanglu Fu[1], Elliott Slade[1], Michael J Properzi[1], Julie C. Price[1], Bernard Hanseeuw[1,2], Rema Raman[3], Michael Donohue[3], Paul Aisen[3], Reisa A. Sperling[1,4], Keith A. Johnson[1,4]

[1]*Massachusetts General Hospital, Boston, MA, US*
[2]*Cliniques Universitaires Saint-Luc, Université Catholique de Louvain, Brussels, BE*
[3]*Keck School of Medicine, University of Southern California, Los Angeles, CA, US*
[4]*Brigham & Women's Hospital, Boston, MA, US*

Background: The accelerated spread of medial temporal lobe (MTL)-tau into the neocortex in the presence of amyloid-beta (Aβ) is a key event in Alzheimer's disease (AD) pathogenesis, dubbed 'caTAUstrophe'. We sought to assess whether the onset of caTAUstrophe varies based on initial MTL tauopathy level and the extent of Aβ in the neocortex and MTL.

Methods. 246 cognitively-unimpaired older adults were included (Table1) from the A4 trial (n=191, placebo) and the LEARN study (n=55) with baseline Aβ-PET (florbetapir) and 1-4 tau-PET scans (flortaucipir) over up to 5.5 years. Baseline Aβ was quantified using neocortical spatial extent (EXT; %florbetapir+) and classified into stages: EXT-0 (Aβ-,<5%), EXT-1 (spreading, 5-85%), EXT-2 (widespread, >85%). MTL and neocortical temporal (NeoT) tau SUVR were computed, and individuals were grouped by high/low baseline MTL-tau. Linear mixed models assessed the time*baseline-Aβ-EXT stage*MTL-tau-group interaction on MTL and NeoT tau SUVR. Additional analyses evaluated MTL-Aβ and its association with changing MTL-tau.

Results. MTL and NeoT tau proliferation diverged based on initial MTL-tau level (Figure1). In MTL-low participants (Figure2A), increased MTL and NeoT tau proliferation were not observed until the widespread Ab-EXT-stage2. These accelerated tau changes were associated with baseline MTL-Aβ elevations (Figure2B). Conversely, tau proliferation started earlier in those with initially high MTL-tau (Figure2C), with accelerated MTL-tau change and the onset of NeoT-tau with spreading Aβ in EXT-stage1. These earlier MTL-tau changes were not associated with elevations in MTL-Aβ but rather with proximal lateral temporal regions (Figure2D).

Conclusions. The timeline to caTAUstrophe differed based on the level of existing MTL-tau, with rapid tau proliferation at the first signs of Aβ when high but delayed tau proliferation until after Aβ was widespread when low. While MTL Aβ was detectable after Aβ became widespread, it was proximal lateral temporal regions that predicted the earlier, rapid tau proliferation seen in spreading Aβ stage.

	n	Age	Education	Sex	APOE	BI NeoT FTP SUVR
EXT-0/MTLlow	45	69.3 (4.0)	16.4 (2.4)	26 (58%)	8 (18%)	1.13 (0.06)
EXT-0/MTLhigh	16	68.9 (2.3)	17.1 (3.1)	8(50%)	5 (31%)	1.19 (0.04)*
EXT-1/MTLlow	29	71.5 (5.7)*	15.8 (2.9)	19 (59%)	10 (35%)	1.13 (0.05)
EXT-1/MTLhigh	51	70.9 (4.0)^{t}	16.4 (3.1)	35 (64%)	21 (41%)*	1.20 (0.07)***
EXT-2/MTLlow	29	73.1 (5.6)**	15.7 (2.8)	17 (65%)	23 (79%)***	1.13 (0.06)
EXT-2/MTLhigh	76	72.0 (4.7)**	15.9 (2.4)	46 (64%)	57 (75%)***	1.30 (0.14)***

Table 1. Sample Demographics by baseline Aβ-EXT-stage/MTL-tau. Means and standard deviations are reported for continuous variables (Age and Education in years) and categorical variables are n and proportions (Sex= n(%) female, APOE, n(%) carrier). Significance is shown for comparison across groups. ^{t}p<.10, *p<.05,**p<.05, ***p<.001

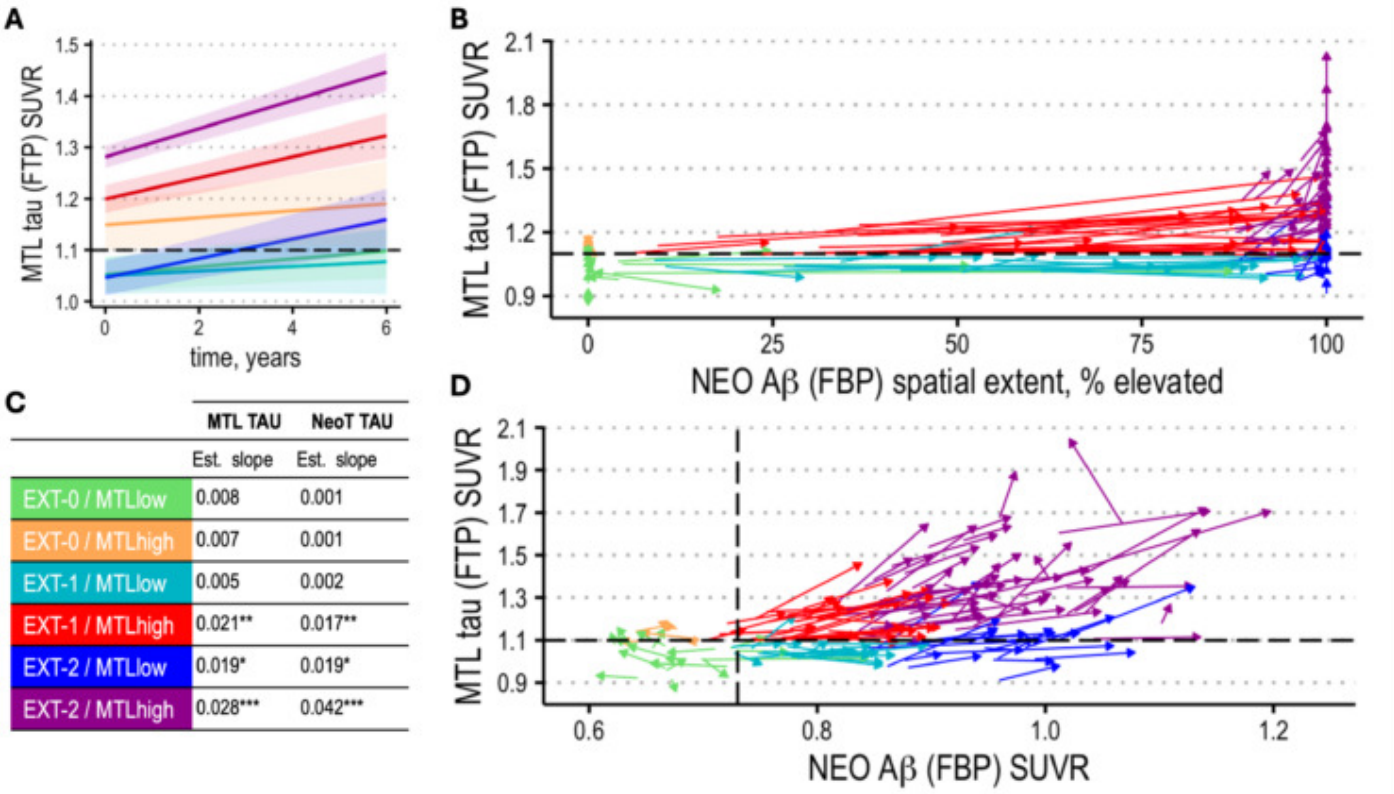


Figure 1. Tau proliferation in the medial temporal lobe differs as a function of baseline Aβ-EXT-stage and MTL-tau group. A, C) Results are shown from linear mixed effects models testing the time* baseline Aβ-EXT-stage* baseline MTL-tau group interaction on MTL-tau SUVR. Similar results were obtained for NeoT tau SUVR. Models covaried for baseline age, sex, education, and APOE (and their interactions with time) and included random participant intercept and slope. A) Estimated marginal means are reported for MTL-tau for the 6 baseline Aβ-EXT-stage*baseline MTL-tau groups for the average participant in the model (a 71.8 year old female APOE non-carrier with 16 years of education). Group colors are shown in the table (B) and model estimates of the fixed effect slopes are reported each group. Significance is reported for each group based on whether change in each group was significantly different from the reference group of EXT-0 /MTL-low participants. MTL-tau SUVR increased over time for all groups, but accelerated change over time was observed for EXT-1/MTL-high, EXT-2/MTL-low and EXT-2/ MTL-high participants. NeoT-tau SUVR did not exhibit change over time until EXT-stage 1 in those with initially high MTL-tau and EXT-stage 2 for those with initially low MTL-tau. B,D) Individual trajectories of change in Aβ and change in tau over time are shown and color-coded by baseline EXT-stage/MTL-tau group (legend in table, B), with Aβ measured using B) spatial extent (EXT) and C) mean SUVR over the same neocortical (NEO) aggregate.

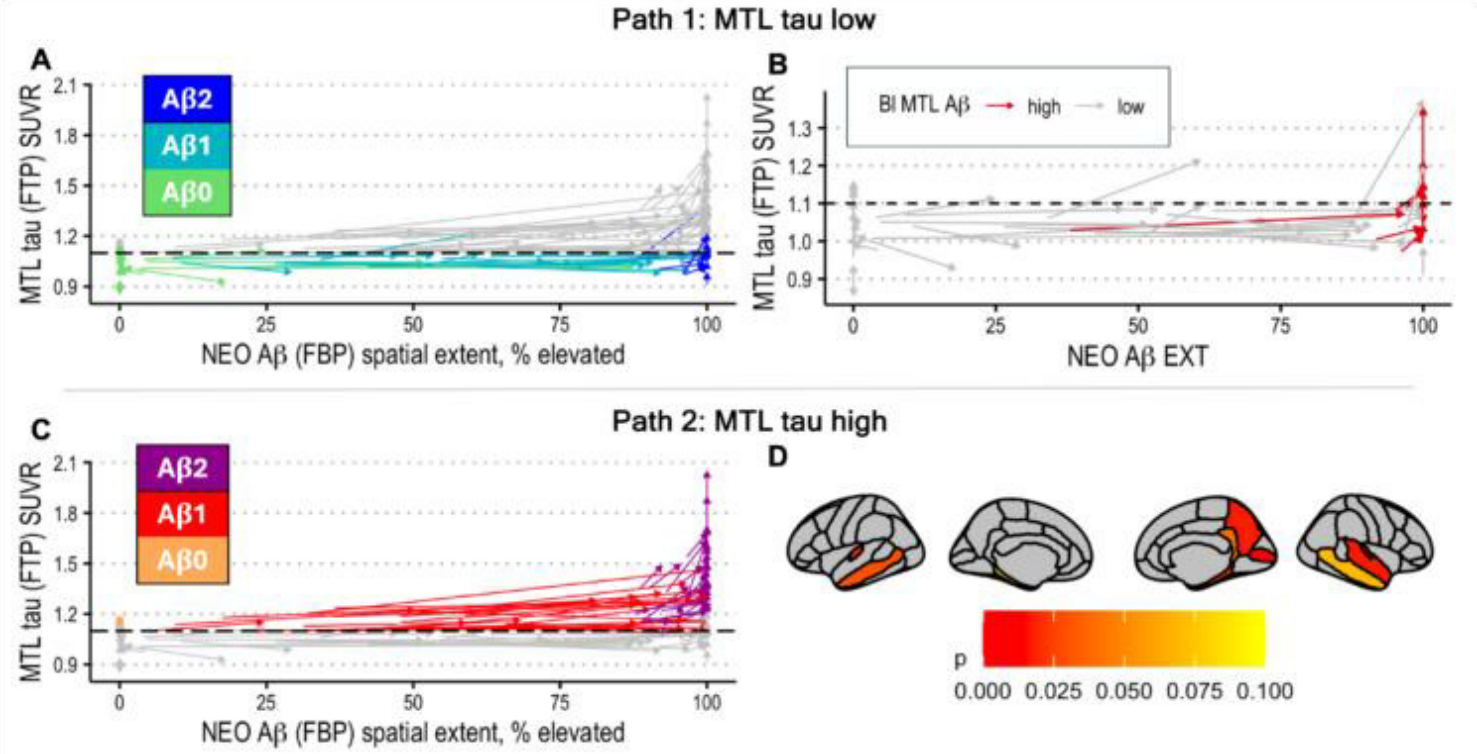


Figure 2. Two trajectories of changing Aβ and tau diverge by baseline MTL tau level. A,C) Individual trajectories for for Aβ EXT and MTL tau are shown (same as Figure 1B) but highlighting two diverging paths based on whether initial MTL tau was low (A) or high (C). A) There is slow but significant change in the MTL-low group even in those without evidence of Aβ (Aβ EXT Stage 0) that is likely age-related, but this slow increase in tau does not change as Aβ spreads throughout EXT stage 1. MTL tau SUVR only accelerates after individuals reach widespread Aβ in EXT Stage 2. B) Elevated Aβ MTL SUVR (red) was not observed until individuals reached widespread Aβ in EXT Stage 2 in all but 1 participant. This is consistent with hypothesis that Aβ reaches the MTL after Aβ has spread throughout the neocortex, where it accelerates tau proliferation. C) Conversely, those starting with high MTL tau exhibited accelerated change in MTL tau with the first signs of Aβ in the spreading EXT Stage 1. D) Elevated baseline MTL Aβ was not significantly associated with these early changes in EXT Stage1, but they were associated with baseline Aβ elevations in nearby neocortical temporal regions and the precuneus. A series of linear mixed effects models were performed assessing the association between baseline Aβ ROI elevation (ROI SUVR> local ROI threshold) and change in MTL-tau over time within individuals in EXT-Stage 1. The color scale in the brain plot shows standardized β coefficients for significant ROIs ($p<.05$).

Keywords: early detection, preclinical, tau, medial temporal lobe, spatial extent

Mapping spatial white matter integrity linked to tau accumulation: Insights from tractometry with multi-shell diffusion imaging

Dana Parker[1], Jenna Adams[1], Liv Mcmillan[1], Michael Yassa[1]

[1]*University of California Irvine, Irvine, CA, US*

Introduction: Tau pathology has the potential to disrupt white matter (WM) integrity. Previous work has shown global disruption to these tracks. However, the specific spatial locations along the impacted tracts has yet to be investigated in depth. Tractometry utilizes tractography to quantify WM integrity by placing equidistant nodes along the length of white matter bundles. We assessed WM integrity along the spatial extent of medial temporal lobe (MTL) tracts and investigated if tau pathology or cognitive impairment is associated with spatially-specific patterns of WM integrity.

Methods: 159 older adults from ADNI3 (101 cognitively normal and 58 cognitively impaired (MCI/AD) participants) received tau-PET (FTP) and multishell dMRI. Fractional anisotropy was calculated for each unilateral tract (uncinate fasciculus [UF], inferior longitudinal fasciculus [ILF], inferior fronto-occipital fasciculus [IFOF]) along 100 equidistant nodes using pyAFQ. Tau-PET composite SUVRs within entorhinal cortex and amygdala (MTL tau) and meta-temporal regions were extracted. A mixed effects model was performed to test for both main effects of tau and diagnosis on WM integrity, and interactions between these factors by node, which indicate spatially specific effects.

Results: When analyzing spatial WM integrity with tractometry, all tracts showed significant three-way interactions between tau, diagnosis, and node location (ps<0.001), and both tau by node (ps<0.001) and diagnosis by node location interactions (ps<0.001), suggesting these factors impact WM integrity differentially along the tracts. Critically, these models revealed no significant main effects of tau or diagnosis, confirming spatial analyses have improved sensitivity to these effects. Post-hoc analyses identified specific nodes within these tracts that showed significant associations with tau levels.

Discussion: Our results show that tau accumulation along different regions of the tract can be a useful measure of early preclinical AD pathology. Notably, these vulnerable WM nodes overlapped with areas known for tau deposition, providing valuable insights into effects of tau pathology.

Keywords: Diffusion MRI, White Matter Integrity, Tractometry, Alzheimer's disease

Spatial patterns of voxel-wise tau accumulation across the Alzheimer's disease spectrum

Corrina Fonseca[1], Renaud La Joie[2], Yishu Chao[1], Gil Rabinovici[2], William Jagust[1], Theresa Harrison[1]

[1]*Department of Neuroscience, University of California Berkeley, Berkeley, CA, US*
[2]*Memory and Aging Center, Department of Neurology, Weill Institute for Neuroscience, University of California San Francisco, San Francisco, CA, US*

Background: Cross-sectional tau deposition has been described by Braak staging, but how patterns of tau spread evolve over time and the factors driving longitudinal changes remain unclear. We used whole-brain voxel-wise analyses to examine longitudinal tau accumulation patterns and their associations with demographics, *APOE*, and baseline Alzheimer's disease (AD) pathology across the spectrum from normal aging to clinical AD.

Methods: 1,426 flortaucipir (FTP) scans in 583 participants were included from 4 studies: BACS, ADNI, HABS, and UCSF (Table 1). Voxel-wise FTP SUVR slope maps were generated to explore whole-brain tau accumulation patterns within clinical diagnostic groups and associations with age, sex, APOEε4, baseline Aβ and tau status, and baseline global Aβ and tau (entorhinal cortex [ERC] and inferior temporal gyrus [ITG]). T-tests and multiple regression were performed in cognitively normal participants and full sample separately.

Results: Longitudinal voxel-wise tau accumulation patterns resembled Braak staging, progressing from the medial temporal lobe to temporoparietal and frontal regions in more advanced clinical stages (Figure 1). APOEε4, Aβ positivity, and ERC tau positivity were associated with faster tau accumulation in temporal, parietal, and frontal regions. Baseline global Aβ, ERC tau, and ITG tau were key predictors of tau accumulation in progressively higher neocortical Braak regions (Figure 2). Interactions between Aβ and ERC and ITG tau suggested synergistic effects on tau accumulation in downstream Braak regions across the spectrum. Voxel-wise tau accumulation in temporoparietal and frontal regions was more strongly linked to lower hippocampal volume and MMSE at the end of the tau follow-up period compared to baseline measures.

Conclusions: This data-driven, voxel-wise approach to spatially map tau accumulation revealed that the evolution of the typical pattern of tau deposition is driven by APOE genotype, Ab, and tau in ERC and ITG. These findings may guide future trials targeting the accumulation tau pathology.

Characteristic	Full Sample n = 583	CN Aβ- n = 274	CN Aβ+ n = 162	MCI Aβ+ n = 81	AD Aβ+ n = 66
Age, yrs [a,d,e]	73.9 ± 7.4	73.5 ± 6.7	75.5 ± 6.0	73.4 ± 8.6	72.2 ± 10.6
Sex, M/F n	261/322	118/156	65/97	42/39	36/30
Education, yrs [c]	16.5 ± 2.5	16.7 ± 2.7	16.5 ± 2.2	16.5 ± 2.6	15.9 ± 2.6
APOEε4, +/- n [a-c]	232/341	56/214	90/71	50/29	36/27
Tau+, % [a-e]	26.1	4.0	24.7	61.7	77.3
Baseline to Follow-up FTP, yrs [a-c,e,f]	2.8 ± 1.3	3.2 ± 1.3	2.7 ± 1.2	2.6 ± 1.2	1.6 ± 0.6
Baseline Aβ CL [a-f]	40.2 ± 43.1	4.4 ± 8.5	61.2 ± 34.5	75.8 ± 32.7	93.6 ± 33.1
Baseline ERC FTP SUVR [a-f]	1.4 ± 0.4	1.2 ± 0.2	1.4 ± 0.3	1.7 ± 0.5	2.0 ± 0.6
Baseline ITG FTP SUVR [a-f]	1.5 ± 0.6	1.3 ± 0.1	1.4 ± 0.3	1.8 ± 0.7	2.5 ± 1.1
Baseline Hippo Volume, cm^3 [b-f]	7.8 ± 0.9	8.0 ± 0.8	7.8 ± 8.2	7.4 ± 0.9	7.1 ± 1.1
Final Hippo Volume, cm^3 [b-f]	7.5 ± 1.0	7.8 ± 0.8	7.6 ± .08	7.0 ± 1.0	6.5 ± 1.2
Baseline MMSE [a-f]	28.1 ± 2.6	29.2 ± 1.0	28.9 ± 1.3	27.4 ± 2.3	22.4 ± 3.7
Final MMSE [a-f]	27.0 ± 4.5	29.0 ± 1.2	28.3 ± 1.9	24.8 ± 4.9	18.5 ± 6.4
Cohort, %					
ADNI	57	50	52	85	64
BACS	15	18	23	--	--
HABS	22	32	25	--	--
UCSF	6	--	--	15	36

Table 1 Participant Characteristics
Values represent mean ± standard deviation for continuous variables and participant count (n) for categorical variables. Tau positivity and cohort is represented as percentage (%) of each subgroup. There were no APOE genotype data for 5 CN, 2 MCI, and 3 AD participants. Aβ status was determined using the Aβ-PET scan closest to tau-PET baseline (± 1 year). Data from four independent studies were included: Alzheimer's Disease Neuroimaging Initiative (ADNI), Berkeley Aging Cohort Study (BACS), Harvard Aging Brain Study (HABS), and University of California San Francisco (UCSF). Because the Aβ-PET tracer varied by study, we used PiB mean distribution volume ratio (DVR) or FBB/FBP standard uptake value ratio (SUVR) cutoffs determined within each study (BACS & UCSF PiB DVR>1.065; HABS PiB DVR>1.20; ADNI FBB SUVR>1.08; ADNI FBP SUVR>1.11). Tau status was determined by a cutoff defined as two standard deviations above the mean FTP SUVR within the Freesurfer-derived ERC ROI in Aβ- CN participants (ERC FTP SUVR>1.52). 11.7% of CN participants were tau+ and 68.7% of MCI or AD patients were tau+; *yrs: years; M: Male; F: Female; APOEε4: apolipoprotein ε4 allele; FTP: Flortaucipir; PiB: Pittsburgh Compound-B; FBB: Florbetaben; FBP: Florbetapir; Aβ: beta-amyloid; CL: Centiloids; ERC: entorhinal cortex; ITG: inferior temporal gyrus; hippo: hippocampal; MMSE: Mini-Mental Status Exam. Comparisons at p<0.05 a. CN Aβ- vs. CN Aβ+; b. CN Aβ- vs. MCI; c. CN Aβ- vs. AD; d. CN Aβ+ vs. MCI; e. CN Aβ+ vs. AD; f. MCI Aβ+ vs. AD*

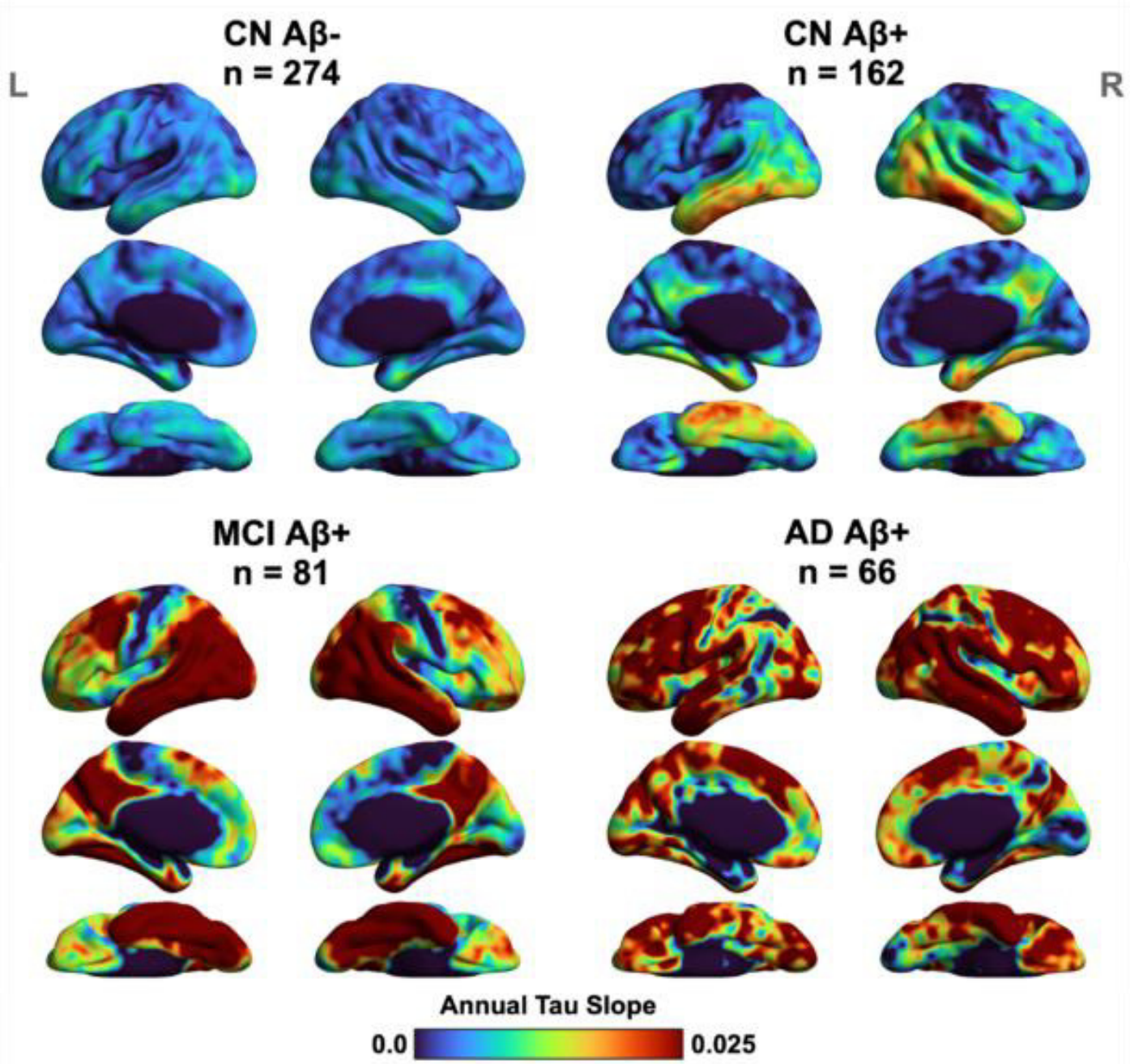


Figure 1. Average group-level voxel-wise tau slope maps by diagnostic group
Voxel-wise patterns of tau accumulation are shown as average tau slope at each voxel within each group. Voxel-wise tau (FTP SUVR) slope maps were generated by fitting linear regressions for FTP SUVR by time from baseline at each voxel in native subject space. Maps were then warped to MNI space, smoothed by 6 mm FWHM kernel, and masked by cortical gray matter. Tau accumulation patterns resemble characteristic progression of tau pathology following Braak stages I-IV in CN, Braak stages I-VI in MCI and AD patients. *CN: Cognitively normal; MCI: Mild cognitive impairment; AD: Alzheimer's disease; FTP: flortaucipir; FWHM: Full width at half maximum.*

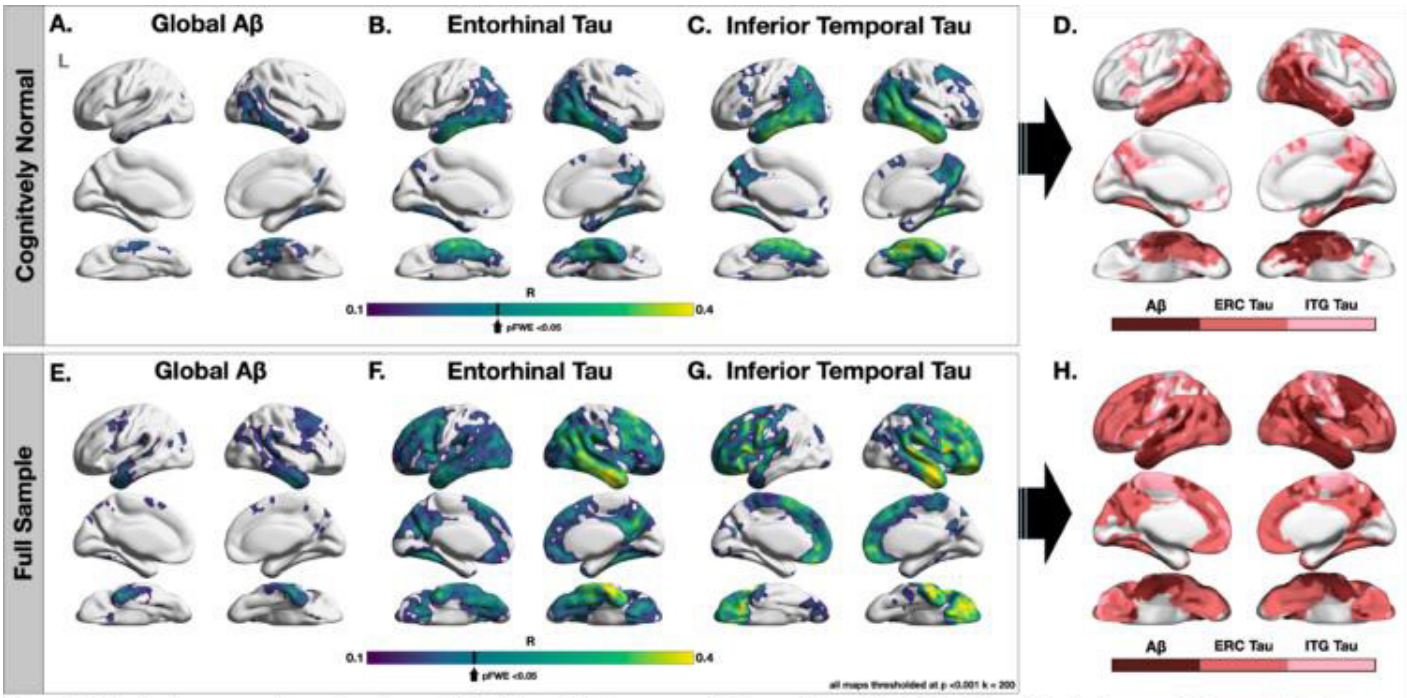


Figure 2. Voxel-wise regressions showing relationships with tau accumulation and baseline Aβ and tau. Voxel-wise correlation coefficient maps showing the relationship between baseline global Aβ, ERC and ITG tau and patterns of voxel-wise tau accumulation in CN only group (**A-D**) and the full sample (**E-H**). All maps are thresholded at of $p_{voxel} < 0.001$, cluster k=200 with pFWE<0.05 shown on color bar. The specific tau accumulation patterns associated with each advancing stage of baseline pathology measure (i.e., Aβ → ERC tau → ITG tau) mirror the canonical AD progression of tau in both the CN group and the full sample. A binarized summary of the regression maps showing overlap between patterns of significant tau accumulation for each predictor. Each shade of red indicates patterns of tau associated with each predictor (Aβ=dark red; ERC tau=lighter red; ITG tau=pink) within the CN only group (top) and full sample (bottom) (**C**). *Aβ: beta-amyloid; ERC: entorhinal cortex; ITG: inferior temporal gyrus; CN: cognitively normal*

Keywords: flortaucipir, longitudinal tau-PET, voxel-wise analyses

PET astroglia and microglia follow tau propagation patterns in Alzheimer's disease

Nesrine Rahmouni[1], Ali Hosseini[1], Lydia Trudel[1], Etienne Aumont[1], Arthur Macedo[1], Gleb Bezgin[1], Brandon Hall[1], Joseph Therriault[1], Yi-Ting Wang[1], Jaime Fernandez Arias[1], Stijn Servaes[1], Jenna Stevenson[1], Ryuichi Harada[5], Nobuyuki Okamura[5], Andrea Lessa Benedet[3], Eduardo R. Zimmer[4], Tharick Pascoal[2], Pedro Rosa-Neto[1]

[1]*McGill University, Montreal, QC, CA*
[2]*University of Pittsburgh, Pittsburgh, PE, US*
[3]*University of Gothenburg, Gothenburg, SE*
[4]*Universidade Federal do Rio Grande do Sul, Porto Alegre, BR*
[5]*Tohoku Medical and Pharmaceutical University, Sendai, JP*

Background: Glial responses affect Alzheimer's disease (AD) pathophysiology. However, prior studies of in-vivo typically provide partial appraisals of tau distribution focusing either on microglia or astrocytes. Here, we investigated the associations between astroglia and microglia with amyloid and tau, across the AD spectrum using PET.

Methods: We included 18 individuals from the TRIAD cohort (8 Aβ positive). Aβ deposition, tau tangles, microglial activation (TSPO) and astrocyte reactivity (MAO-B) were assessed via [^{18}F]AZD4694-PET, [^{18}F]MK6240-PET, [^{11}C]PBR28- PET and [^{18}F]SMBT-1-PET respectively. Voxel-based regression models evaluated the association of [^{18}F]SMBT-1-PET in the precuneus with amyloid-PET, tau-PET and TSPO-PET. We explored the voxelwise colocalization of microglial activation and astrocytes reactivity's spatial extent by seeding in Braak I and V. Finally, we ran network analysis for the 4 tracers using SUVR uptake in (1) Braak regions and (2) amyloid-PET staging regions.

Results: Tau-PET and [^{18}F]SMBT-1 SUVR in the precuneus were positive associated through the whole cortex, most strongly in Braak V and VI. Positive associations with TSPO-PET were mainly restricted to the frontal cortex. No associations with amyloid-PET were significant **(Fig.1)**. Similar spatial extent signatures were found between MAO-B-PET and TSPO-PET when seeding in Braak I and V **(Fig.2A,B)**, with the highest associations in mid-to-late Braak regions. Network matrices revealed that the rates of cross-sectional tau propagation correlated hierarchically with each other according to the Braak stages for microglia- astroglia- and tau-PET and the elements of each matrix positively correlated with each other **(Fig.3A)**. Microglia and astroglia matrices' elements did not correlate with amyloid-PET matrix elements**(Fig.3B)**.

Conclusion: This is the first PET study addressing the associations between amyloid, tau, TSPO and MAO-B in the same individuals. Our study highlights the colocalization between microglial activation, astrocytes reactivity and tau accumulation within specific Braak stages.

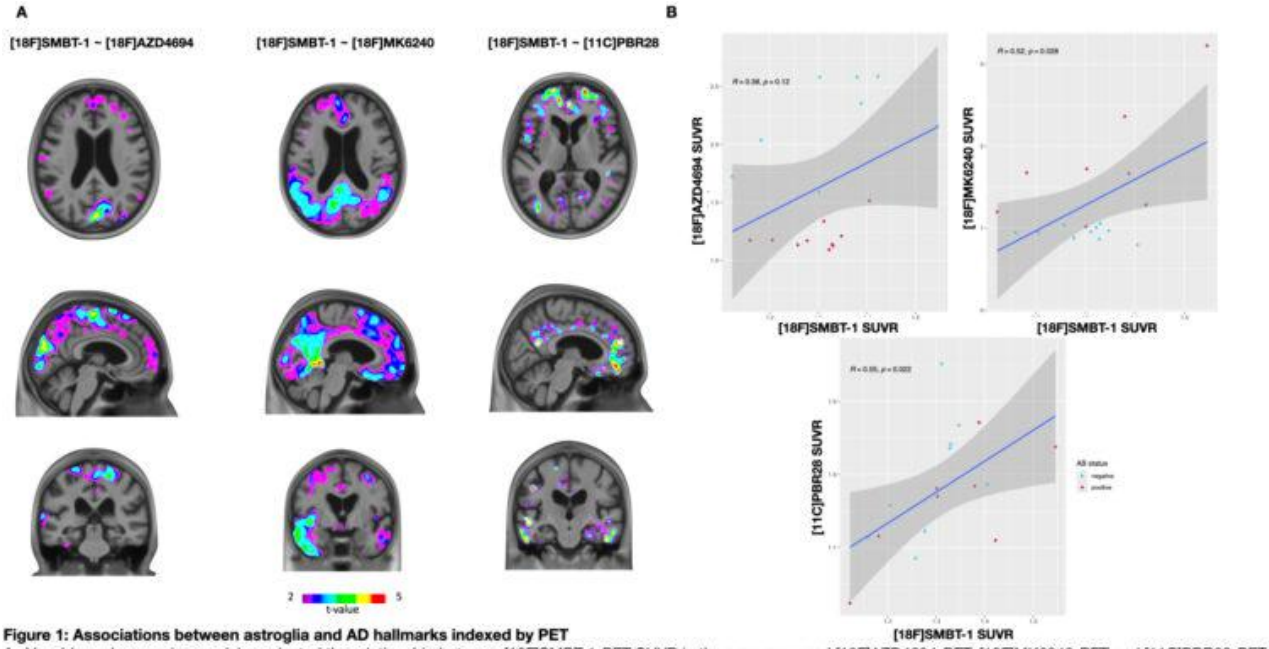


Figure 1: Associations between astroglia and AD hallmarks indexed by PET

A. Voxel-based regression models evaluated the relationship between [18F]SMBT-1-PET SUVR in the precuneus and [18F]AZD4694-PET, [18F]MK6240-PET and [11C]PBR28-PET

B. Linear regression models using Spearman correlation coefficients evaluated the relationship [18F]SMBT-1 SUVR in the precuneus and Global [18F]AZD4694 SUVR, metaROI [18F]MK6240 SUVR and posterior cingulate [11C]PBR28 SUVR

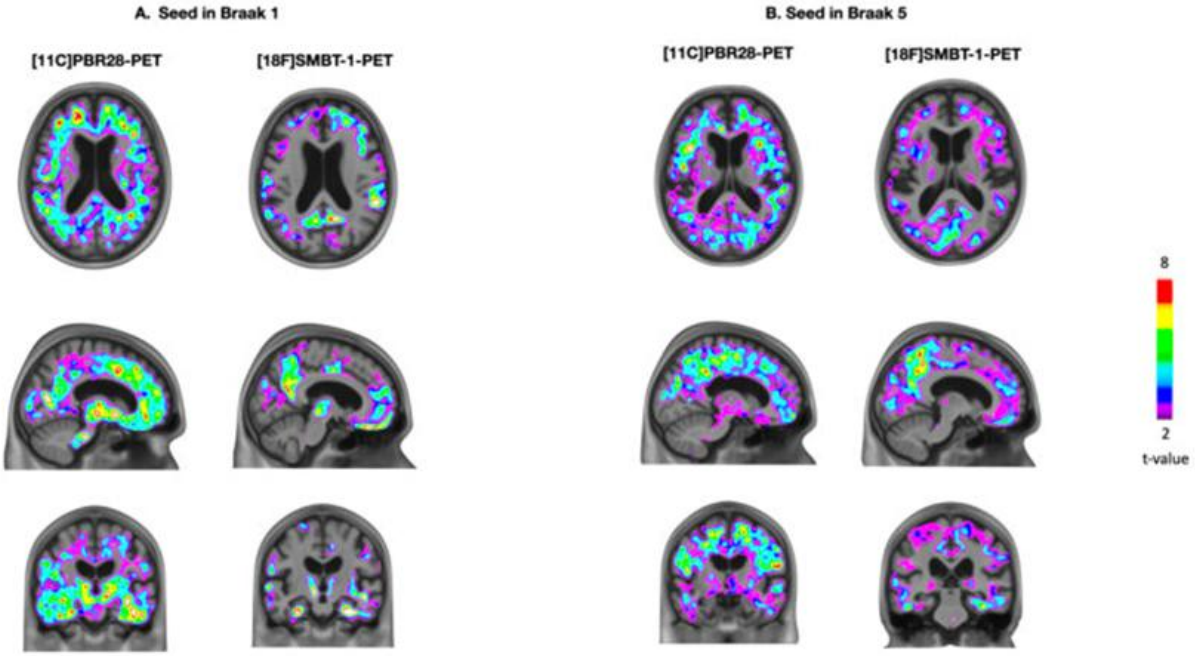


Figure 2: Colocalization of microglial activation and astrocytes reactivity's spatial extent .

A. Voxel-based regression models evaluated the relationship between voxelwise PET and PET SUVR in Braak 1 using [11C]PBR28-PET and [11C]SMBT-1-PET

B. Voxel-based regression models evaluated the relationship between voxelwise PET and PET SUVR in Braak 5 using [11C]PBR28-PET and [11C]SMBT-1-PET

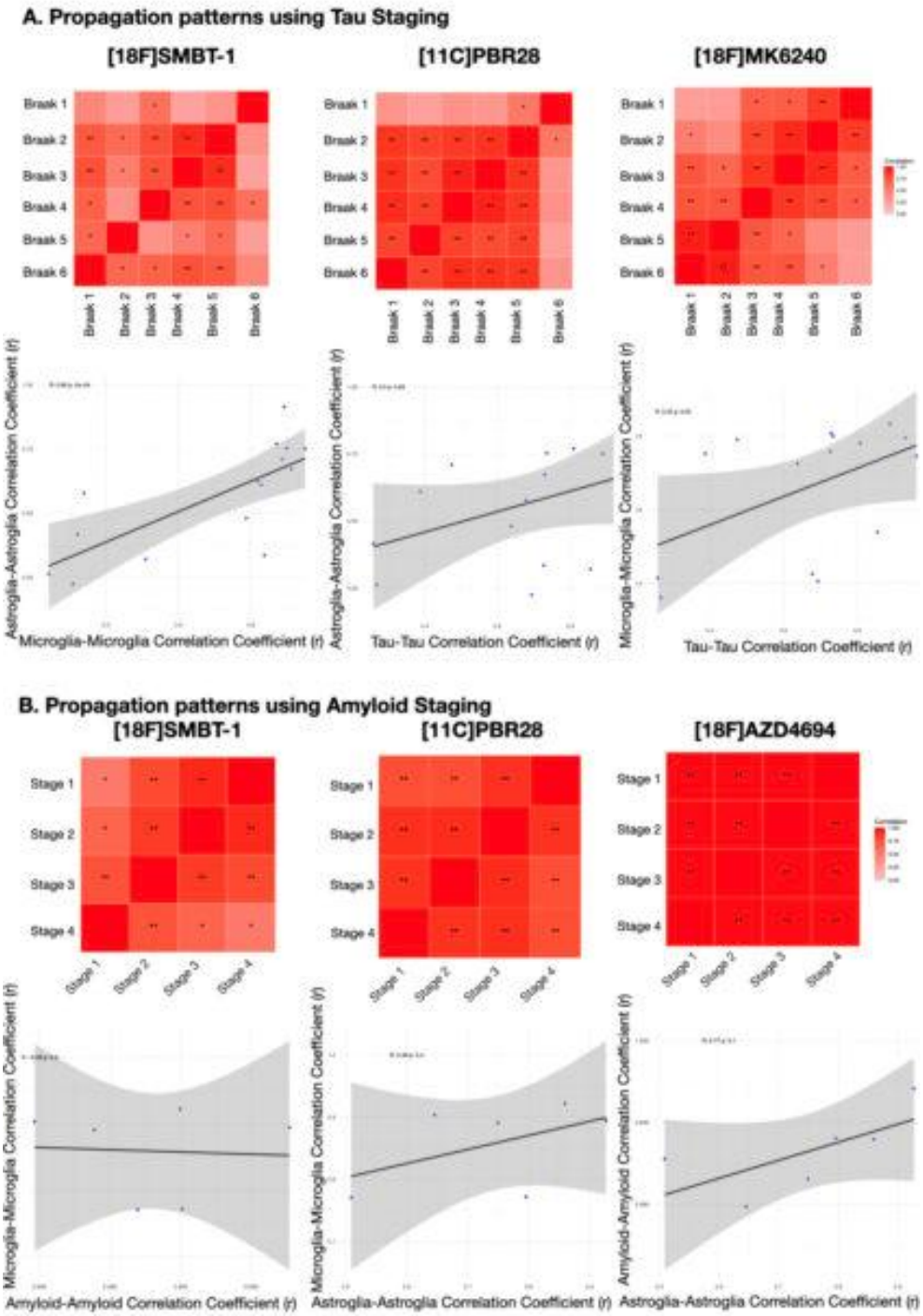


Figure 3: Astroglia and Microglia follow similar propagation patterns to tau tangles

A. **Tau Staging :** Matrices revealed that the rates of cross-sectional tau propagation correlated hierarchically with each other according to the Braak stages for microglia-astroglia- and tau-PET. Spearman correlation coefficients (r) with P<0.05 are highlighted with a single asterisk. Scatterplots show that the elements of each matrix are positively correlated with each other.

B. **Amyloid Staging :** Matrices revealed that the rates of cross-sectional amyloid spreading correlated hierarchically with each other according to the Amyloid stages for microglia-astrocyte and amyloid-PET. Spearman correlation coefficients (r) with P<0.05 are highlighted with a single asterisk. Scatterplots show that the elements of each matrix are not positively correlated with each other.

Keywords: Astroglia, Microglia, Tau, PET, imaging

Wednesday, January 15, 2025 - 02:00 pm - 02:30 pm

Kolb, Hartmuth

Keynote: From click chemistry to precision neuroscience

Hartmuth Kolb

Enigma Biomedical Group

This presentation highlights the transformative role of click chemistry in the development of molecular imaging probes, including the Tau PET tracers, ^{18}F-T807 (aka AV1451, Flortaucipir, Tauvid) and ^{18}F-T808. PET imaging of Alzheimer's disease pathology has been instrumental for developing the biomarker-driven framework for diagnosis and staging of the disease, which has catalyzed the advent of the first disease-modifying therapies. We will discuss the integration of fluid assays and imaging workflows into clinical trials and how some of these measurements even function as reasonably likely surrogate endpoints. Looking forward, emerging imaging techniques targeting pathological proteins such as TDP-43 and a-Synuclein, as well as neuroinflammatory processes, promise to expand the scope of neurodegenerative disease research. Together, these advances empower patient-centric precision medicine, driving innovation in neuroscience diagnostics and therapeutics.

Dr. Hartmuth Kolb received his PhD in Organic Chemistry in 1991 at Imperial College of Science, Technology and Medicine, London. He joined Ciba-Geigy in 1993 and in 1997 became VP of Chemistry at Coelacanth Corporation to work with K. Barry Sharpless on pioneering Click Chemistry.

Dr. Kolb was the first author of the first publication on this topic (2022 Chemistry Nobel Prize for Sharpless, Meldal and Bertozzi). He then became head of Siemens Biomarker Research, where he and his team developed PET tracers using Click Chemistry. The PET tracer [18F]-T807 (aka "Flortaucipir", "Tauvid") is currently the only FDA-approved agent for imaging a distinctive characteristic of Alzheimer's disease in the brain called tau pathology. After joining Janssen in January 2014, he worked on developing PET tracers for all therapeutic areas, and on precision medicine approaches in Neuroscience. His lab developed one of the first p217Tau blood tests for detecting the presence of Alzheimer's pathology in patients.

In March 2024, he joined Enigma Biomedical Group (EBG) as their CSO to focus on the development of CNS imaging tracers. Dr. Kolb has served as co-chair of the Neuroscience Steering Committee of the Foundation of NIH Biomarkers consortium. He has over 100 peer reviewed scientific papers and over 40 patents.

Wednesday, January 15, 2025 - 02:45 pm - 04:25 pm

Podium Session

SESSION III: Neuropath I

CHAIRS: Tobey Betthauser, Teresa Gomez-Isla

Wednesday, January 15, 2025		
02:45 pm - 04:25 pm	**SESSION III** Neuropath I	**Tobey Betthauser,** University of Wisconsin School of Medicine and Public Health, Madison, WI, USA **Teresa Gomez-Isla,** Massachusetts General Hospital, Boston, MA, USA
02:45 pm – 02:50 pm	Session Overview	**Chairs**
02:50 pm	Correlation between in vivo 18F-flortaucipir PET and whole brain postmortem histological tau signals in Alzheimer's Disease	**Yishu Chao**, University of California Berkeley, Berkeley, CA, US
03:05 pm	Tau-PET, structural MRI, and cognitive measures are differentially correlated with tangle and neuritic pathology across the neurofibrillary tangle lifespan	**Christina M. Moloney**, Department of Neuroscience, Mayo Clinic, Jacksonville, FL, US
03:20 pm	Binding of [3H]MK-6240 to different tau lesions: a brain autopsy study	**Milos Ikonomovic**, University of Pittsburgh School of Medicine, Department of Psychiatry, Pittsburgh, PA, US
03:35 pm	Plasma extracellular vesicle TDP-43 and hippocampal volume as complementary biomarkers for LATE-NC and hippocampal sclerosis: a pathologic validation study	**Michel Grothe**, Reina Sofia Alzheimer Center, CIEN Foundation, ISCIII, Madrid, ES
03:50 pm	Discovery and preclinical development of [18F]ACI-19626, a first-in-class TDP-43 PET tracer	**Francesca Capotosti**, AC Immune SA, EPFL Innovation Park, Building B, Lausanne, OTHER, CH
04:05 pm – 04:25 pm	Discussion	

Correlation between in vivo 18F-flortaucipir PET and whole brain postmortem histological tau signals in Alzheimer's disease

Yishu Chao[1], Yuheng Chen[2], Trevor A. Chadwick[1], Theresa M. Harrison[1], Helmut Heinsen[3], Daniela Ushizima[4], Duygu Tosun[2], William J. Jagust[1], Lea T. Grinberg[2]

[1]*University of California Berkeley, Berkeley, CA, US*
[2]*University of California San Francisco, San Francisco, CA, US*
[3]*University of Würzburg, Würzburg, DE*
[4]*Lawrence Berkeley National Laboratory, Berkeley, CA, US*

Background: Studies correlating in vivo FTP signals with postmortem immunohistochemical (IHC) assessments are often limited by their methods, either using qualitative approaches or comparing limited ROIs. We created whole-brain, quantitative AD-tau density heatmaps to investigate which AD-related tau subtype correlates best with FTP signal in vivo and regional differences in correlation strength.

Methods: We processed two human brains (Case1 neuropathologic change score: A2B2C1; Case2: A3B3C3) through our deep-learning histology pipeline to generate 3D tau density heatmaps for 3 tau antibodies: AT8 (p-tau S202/205), AT100 (p-tau Th212/214), and MC1 (conformational change). Heatmaps and FTP-PET were coregistered to postmortem MRIs. Heatmaps were smoothed to 6mm isotropic resolution, matching that of FTP-PET. FTP-PET was inferior cerebellar gray normalized. SUVRs and histological signals were displayed at the voxel level and averaged in Desikan-Killiany ROIs. We compared signal intensities between cases with paired Welch's t-tests, correlated ROI-wise and voxel-wise FTP and histological signals with Spearman's rank correlation and Pearson correlation, respectively.

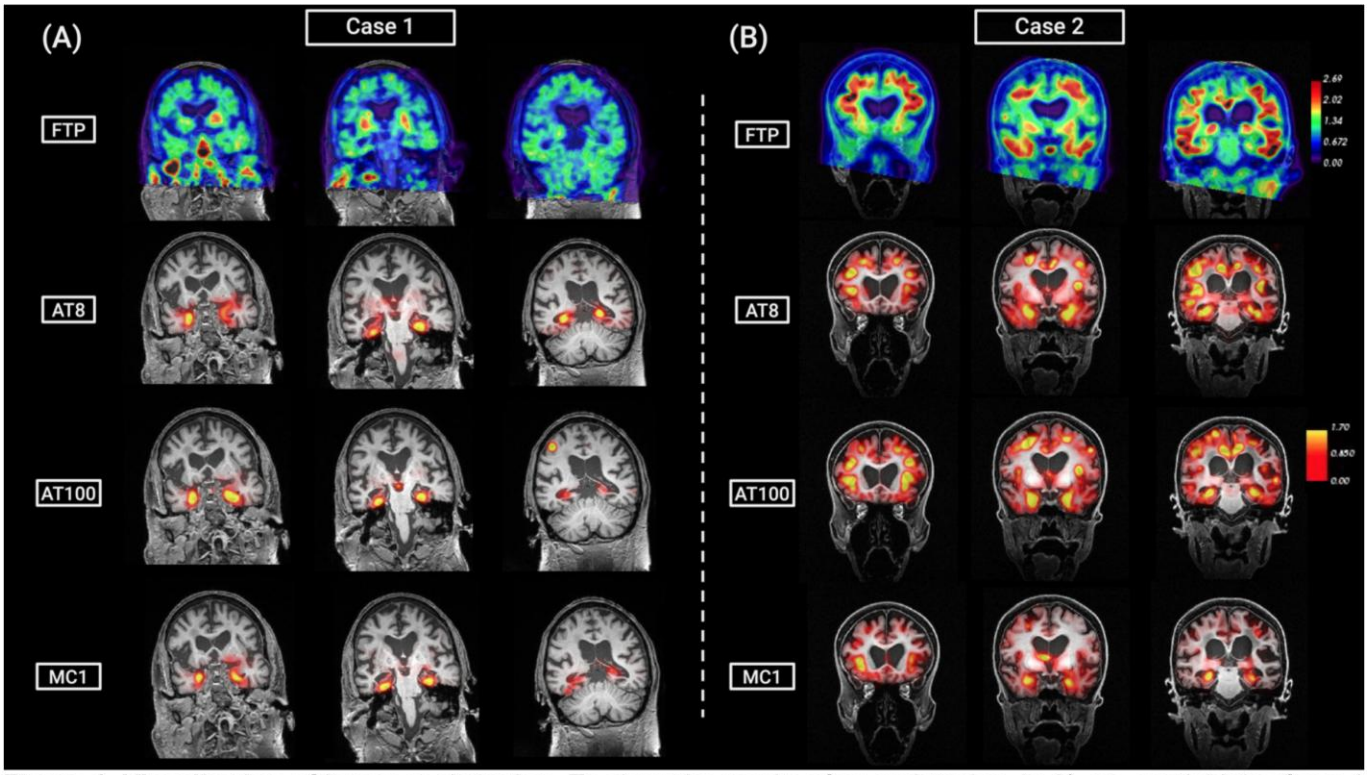


Figure 1. Visualization of image registration. To show the results of co-registration, in A), we overlaid the Case 1 FTP scan and histological heatmaps with Case 1 postmortem MRI at 3 different voxel locations (columns). Case 1 belonged to an 88-year-old cognitively normal donor with AD neuropathologic change score of A2B2C1 (Braak 4 case). Similarly, we overlaid case 2 FTP scan and histological heatmaps with the Case 2 postmortem MRI in B). Case 2 belonged to a 76-year-old donor with AD dementia and neuropathologic change score of A3B3C3 (Braak 6 case). FTP SUVRs were inferior-cerebellar normalized and scaled from 0-2.7, and all 6 heatmaps were scaled from 0-1.7 to allow for visual comparison. As expected, Case 2 FTP scan and heatmaps all showed elevated signal in neocortical areas when compared to Case 1 images. Paired Welch's t-tests confirmed visual findings and showed significant higher FTP and histological signals in case 2 ROIs than case 1 (n=47 ROIs, DF=46; $p<0.001$ for all tests. FTP: t=-12.06; AT8: t=-8.954; AT100:t=-8.51; MC1: t=-3.590). FTP=flortaucipir; ROIs=regions of interest; SUVR=standardized uptake value ratio; DF=degrees of freedom.

Results: Fig.1 shows coregistration between all modalities. Paired t-tests showed significantly higher FTP and histological signals in Case2 ROIs (Fig.1). In ROI-wise analyses, only AT8 in Case2 significantly correlated with FTP SUVRs (n=64 ROIs, r_s= 0.461, $p<0.001$) (Fig.2). FTP SUVRs failed to capture medial-temporal lobe (MTL) tau burden. Voxel-wise distributions of FTP and histological signals were visualized in 4 early-Braak ROIs (Fig.3) and were significantly correlated in all ($p<0.001$), though a ceiling effect of FTP SUVRs was observed. ROI-wise and voxel-wise analyses revealed regional variations in signal distribution.

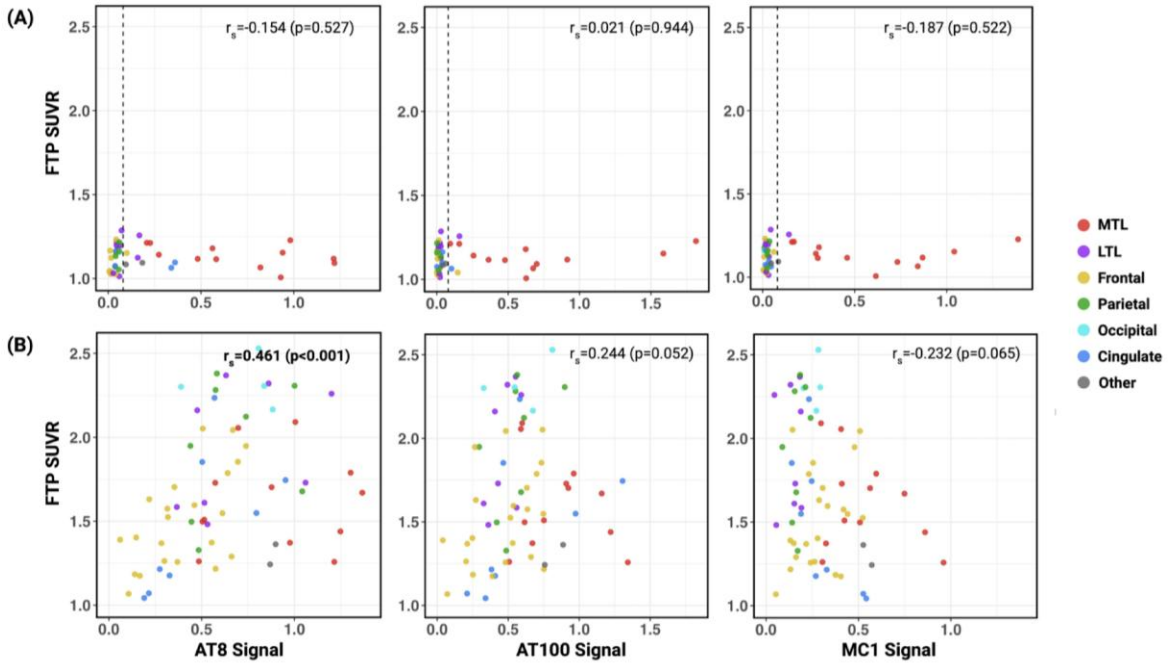


Figure 2: ROI-wise FTP-histological signal correlation. A) scatter plots of Case 1 histological tau signals vs. FTP SUVRs. As expected for a Braak stage 4 case, tau burden outside the medial temporal lobe (MTL) was minimal. However, FTP signal was detected at varying levels in several non-MTL regions, likely due to noise or off-target binding. These regions were therefore excluded from the ROI-wise statistical analyses through a uniform threshold of 0.08 (ROIs left of the black dashed line were excluded). After thresholding, n=19 ROIs for AT8, n=15 ROIs for AT100, and n=14 ROIs for MC1. Spearman's rank correlation coefficients were computed, and no significant correlation was found. B) scatter plots of histological tau signals vs. FTP SUVRs for case 2 (Braak 6). n=64 ROIs for all 3 analyses. Spearman rank order correlation coefficients were computed, and a direct significant correlation was found between AT8 and FTP measures. FTP=flortaucipir, MTL=medial temporal lobe; ROI=region of interest; SUVR=standardized uptake value ratio.

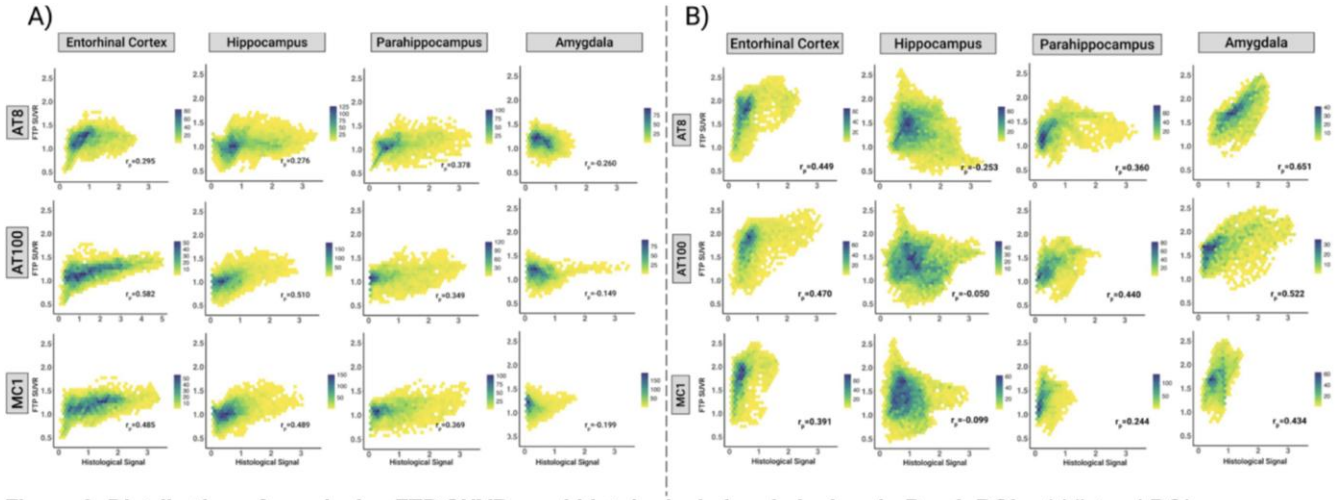


Figure 3. Distribution of voxel-wise FTP SUVRs and histological signals in 4 early-Braak ROIs. 4 bilateral ROIs that are early sites of tau accumulation— entorhinal cortex, hippocampus, Freesurfer-defined parahippocampus, and the amygdala—were selected. Voxel-wise signal distributions were visualized for Cases 1(Braak 4 case) in (A) and Case 2 (Braak 6 case) in (B). All Pearson correlations were significant (p<0.001). The distributions of FTP vs. histological signals are visualized as hex bin plots, where darker color indicates that more voxels fall within the range of FTP and histological signals. Each row represents the signal distributions of a different antibody, and each column a different ROI. In all ROIs, FTP SUVRs are noisy when histological signals are low and gradually plateau as the histological signals increase. FTP=flortaucipir; ROI=region of interest; SUVR=standardized uptake value ratio.

Conclusion: In vivo FTP SUVRs correlated best with AT8, which captures tangles and neuropil threads, in Case2 with more severe AD pathology. ROI-wise analyses suggest that FTP-PET is insensitive at low histological burden, with regional variations (e.g. less sensitivity in MTL) while voxel-wise FTP measures are noisy and fail to reflect high histological burden.

Keywords: Deep learning, immunohistochemistry, flortaucipir, correlation

Tau-PET, structural MRI, and cognitive measures are differentially correlated with tangle and neuritic pathology across the neurofibrillary tangle lifespan

Christina M. Moloney[1], Matthew H. Rutledge[2], Zhongwei Peng[2], Ashley C. Wood[1], Darren M. Rothberg[1], Jessica F. Tranovich[1], Scott A. Przybelski[3], Ekaterina I. Hofrenning[3], Mary M. Machulda[4], Ronald C. Petersen[5], Clifford R. Jack Jr[6], Aivi T. Nguyen[7], R. Ross Reichard[7], Prashanthi Vemuri[6], Dennis W. Dickson[1,8], Nicholas M. Kanaan[9], Rickey E. Carter[2], Val J. Lowe[6], Melissa E. Murray[1,8]

[1]*Department of Neuroscience, Mayo Clinic, Jacksonville, FL, US*
[2]*Department of Quantitative Health Sciences, Mayo Clinic, Jacksonville, FL, US*
[3]*Department of Quantitative Health Sciences, Mayo Clinic, Rochester, MN, US*
[4]*Department of Psychiatry and Psychology, Mayo Clinic, Rochester, MN, US*
[5]*Department of Neurology, Mayo Clinic, Rochester, MN, US*
[6]*Department of Radiology, Mayo Clinic, Rochester, MN, US*
[7]*Department of Laboratory Medicine and Pathology, Rochester, MN, US*
[8]*Department of Laboratory Medicine and Pathology, Jacksonville, FL, US*
[9]*Department of Translational Neuroscience, College of Human Medicine, Michigan State University, Grand Rapids, MI, US*

Objectives: The neurofibrillary tangle lifespan is defined by three maturity levels: pretangles, mature tangles, and ghost tangles. A gap in knowledge exists regarding the type of tau pathology and tangle maturity levels the antemortem measures reflect. We aimed to compare tangle and neuritic burden of 15 tau antibodies that range through the tangle lifespan with ^{18}F-Flortaucipir (tau-PET) standard uptake value ratio (SUVr), structural MRI (sMRI), and cognitive measures.

Methods: Posterior hippocampus serial sections of cases (n=27) with antemortem measures acquired within 3 years of death were stained with 15 tau antibodies, which recognize either pan-tau, or specific phosphorylated, conformational, and truncation epitopes. We used GENIE pattern recognition to separately quantify tangle and neuritic pathology burden. Neuroimaging measures included tau-PET SUVr) and sMRI cortical thickness or hippocampal volume. Memory, global cognition, and dementia severity were assessed with the Auditory-Verbal Learning Test (AVLT), Mini-Mental State Exam (MMSE), and Clinical Dementia Rating (CDR), respectively.

Results: Tau-PET correlated moderately to strongly with tangle and neuritic pathology for markers across the tangle lifespan, with the strongest correlations for middling tangle maturity markers (Figure). sMRI correlated moderately with tangle burden of middling/advanced tangle maturity markers, and some early tangle maturity markers. sMRI correlated moderately with neuritic burden for fewer antibodies. AVLT strongly correlated with tangle and neuritic pathology throughout the tangle lifespan. MMSE weakly correlated with antibodies through the tangle lifespan, with most significant correlations in the cortices and with neuritic pathology. CDR significantly correlated with tangle burden of advanced tangle maturity marker MN423 in the fusiform.

Conclusions: These suggest that antemortem measures differentially correlate with specific types of tau pathology along the tangle lifespan. These findings aid in understanding what these antemortem measures reflect, which will have implications when interpreting future treatments.

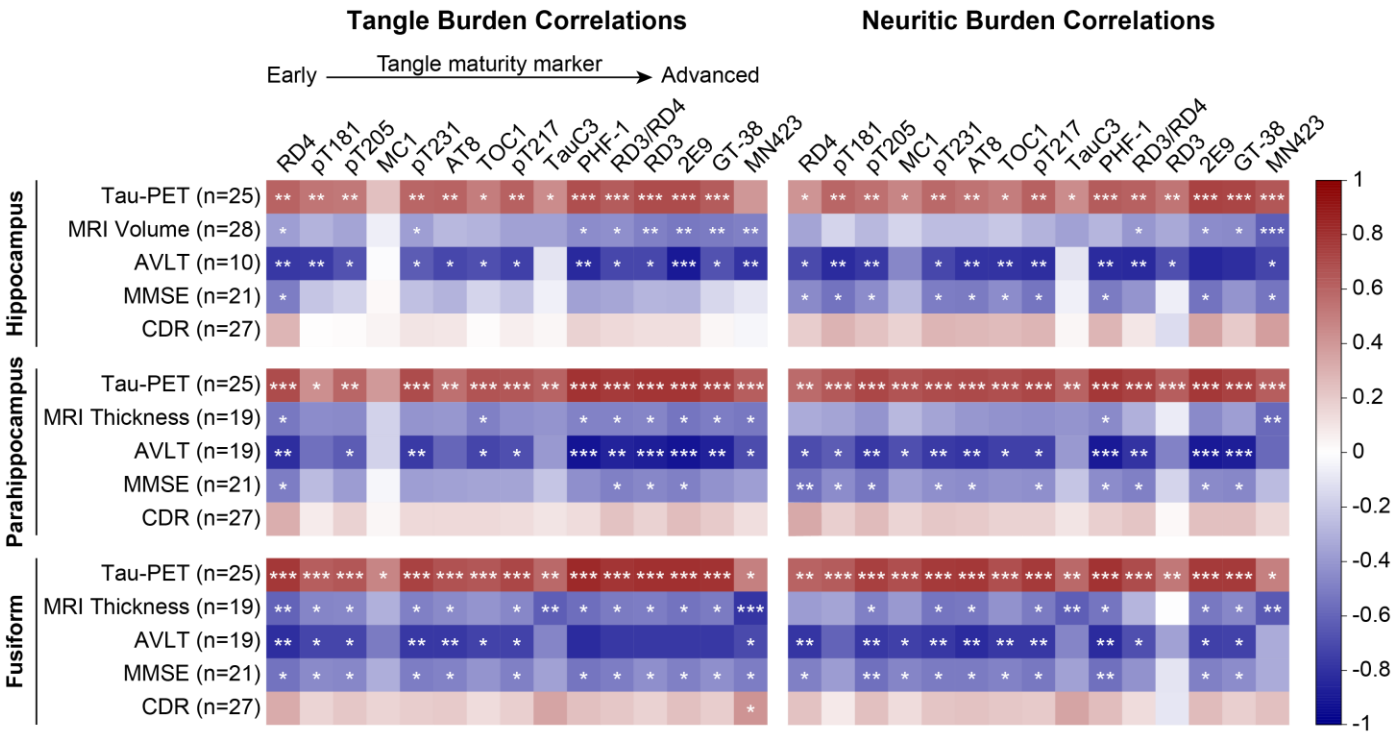


Figure. Heatmap of tangle and neuritic pathology burden correlations with antemortem measures. Data are presented as non-parametric Spearman correlation coefficient (scale bar) and p<0.05 was considered statistically significant (*, p<0.05; ** p<0.01; *** p<0.001). Cases with antemortem measure greater than 3 years to death were excluded from analyses.

Keywords: Neuropathology, neurofibrillary tangle maturity, tau-PET, MRI

Binding of [3H]MK-6240 to different tau lesions: a brain autopsy study

Eric Abrahamson[1,2], Tobey Betthauser[3,4,5], M Shahriar Salamat[3,6], Lan Shao[1], Victor Villemagne[7], Milos Ikonomovic[1,2,7]

[1]*Department of Neurology, University of Pittsburgh, Pittsburgh, PA, US*
[2]*Geriatric Research Education and Clinical Center, VA Pittsburgh HS, Pittsburgh, PA, US*
[3]*Wisconsin Alzheimer's Disease Research Center, University of Wisconsin-Madison, Madison, WI, US*
[4]*Department of Medicine, School of Medicine and Public Health, University of Wisconsin-Madison, Madison, WI, US*
[5]*Department of Medical Physics, School of Medicine and Public Health, University of Wisconsin-Madison, Madison, WI, US*
[6]*Department of Pathology, School of Medicine and Public Health, University of Wisconsin-Madison, Madison, WI, US*
[7]*Department of Psychiatry, University of Pittsburgh, Pittsburgh, PA, US*

Introduction: Monoclonal anti-Aβ antibody treatment reduces brain Aβ deposits in AD, but reductions in tau-PET were also reported. We tested the hypothesis that tau lesions most closely involved with Aβ plaques are an important binding substrate of tau-PET ligands.

Methods: We combined [^{3}H]MK-6240 autoradiography (ARG) with dual immunofluorescence for p-tau (AT8) and Aβ (NAB228) in same tissue sections from autopsy AD brains. We then assessed localization and intensity of [^{3}H]MK-6240 ARG signal relative to tau pathology subtypes including neurofibrillary tangles (NFT), dystrophic neurites in neuritic plaques (DN/NP), and neuropil threads (NT), as well as Aβ plaques using semi-quantitative methods. We also correlated p-tau immunolabeled NFT, DN/NP, and NT load (percent area coverage) with [^{3}H]MK-6240 ARG binding in 10 brain regions from a typical AD case.

Results: The most intense [^{3}H]MK-6240 ARG signal corresponded to AT8-positive DN/NP. No ARG signal was detected in Aβ plaques without AT8-labeled DN. Semi-quantitative rating of ARG signal intensity showed that DN/NP >> NFT > NT, with DN/NP yielding significant ARG signal even at low densities. High densities of NFT and NT also produced significant ARG signal. [^{3}H]MK-6240 ARG correlated with total tau pathology percent area coverage (R=0.69, p=0.035), with trends for NFT (R=0.59, p=0.08) and NT (R=0.53, p=0.12) but not DN/NP (R=0.12, p=0.76).

Conclusion: Tau in DN/NP is a robust binding substrate of MK-6240. However, across brain regions, NFT and NT had greater areal coverage than DN/NP likely driving their better correlations with [^{3}H]MK-6240 ARG. DN/NP densities showed regional variability, with inferior temporal cortex 2-3 times higher than other regions. Thus, both type and regional density of tau lesions contribute to MK-6240 PET signal. Reductions in tau PET seen after Aβ monoclonal antibody treatment could involve DN/NP removal especially in brain regions where their percent area coverage exceeds that of NFT and NT.

Keywords: Alzheimer's disease, autoradiography, neuritic plaques, neurofibrillary tangles, tau

Plasma extracellular vesicle TDP-43 and hippocampal volume as complementary biomarkers for LATE-NC and hippocampal sclerosis: a pathologic validation study

Michel Grothe[1], Linda Zhang[1], Jesús Silva-Rodriguez[1], Francisco López-González[1], Minerva Martinez-Castillo[1], Selçuk Özdemir[2], Alberto Rábano[1], Pascual Sánchez-Juan[1], Anja Schneider[2]

[1]*Reina Sofia Alzheimer Center, CIEN Foundation, ISCIII, Madrid, ES*
[2]*German Center for Neurodegenerative Diseases (DZNE), Bonn, DE*

Background: Plasma extracellular vesicle TDP-43 (EV-TDP-43) has recently been proposed as a molecular biomarker of TDP-43 pathology in frontotemporal dementia. We assessed the ability of EV-TDP-43 to detect limbic-predominant age-related TDP-43 encephalopathy neuropathologic change (LATE-NC) in an autopsy cohort of predominantly AD-type dementia patients. For comparison, we studied hippocampal volume (HV) on MRI as a previously proposed imaging biomarker for LATE-NC and associated hippocampal sclerosis (HS).

Methods: We studied 74 autopsied dementia patients who had ante-mortem blood samples and quality-controlled 3T-MRI available. EV-TDP-43 was measured using size exclusion chromatography and SIMOA as described recently. HV was derived from structural MRI using automated volumetry implemented in SPM12/CAT12. Neuropathological examination included assessment of AD neuropathologic change (ADNC), LATE-NC, and presence of HS.

Results: EV-TDP-43 levels were significantly higher (p=0.005) and HV (p=0.017) was significantly lower in LATE-NC(+)(n=50) compared to LATE-NC(-)(n=24), although group separation in ROC analysis was relatively weak (both AUC=0.67). LATE-NC stage was weakly associated with EV-TDP-43 (r_s=0.25; p=0.04) and more strongly with HV (r_s=-0.41; p<0.001). Group separation increased when combining both biomarkers (AUC=0.72) and particularly when excluding LATE-NC stage-1 cases (AUC=0.75). HV was highly sensitive to HS status (p<0.001, AUC=0.82), whereas EV-TDP-43 was not (p=0.49). EV-TDP-43 also distinguished between LATE-NC(-) and LATE-NC(+) cases without HS (p=0.02, AUC=0.71), whereas HV did not (p=0.38). When limited to cases with high ADNC (N=52), EV-TDP-43 distinguished between those with and without comorbid LATE-NC (p=0.016, AUC=0.65), but HV did not (p=0.28).

Conclusions: Plasma EV-TDP-43 levels and hippocampal volume provide complementary information as biomarkers of LATE-NC and hippocampal sclerosis, respectively. The relatively weak group separation by EV-TDP-43 levels could be due to the comparably low degree of spatially restricted TDP-43 pathology in LATE-NC. Results might have been affected by the characteristics of the study sample focused on end-of-life dementia patients with late-stage disease and multiple comorbidities.

Keywords: Plasma, Extracellular vesicles, limbic-predominant age-related TDP-43 encephalopathy, autopsy, MRI

Discovery and preclinical development of [18F]ACI-19626, a first-in-class TDP-43 PET tracer

Francesca Capotosti[1], Efthymia Vokali[1], Nicolas Dreyfus[1], Elodie Chevallier[1], Dorian Charmey[1], Tania Melly[1], Monisha Rathnam[1], Andreia Monica Serra[1], Thomas Jaquier[1], Carlo Scialo[2], Harro Seelaar[3], Emanuele Buratti[4], Peter Nelson[5], Magdalini Polymenidou[2], Madiha Derouazi[1], Andrea Pfeifer[1], Marie Kosco-Vilbois[1], Tamara Seredenina[1]

[1]*AC Immune SA, EPFL Innovation Park, Building B, Lausanne, CH*
[2]*Department of Quantitative Biomedicine, University of Zurich, Zurich, CH*
[3]*Department of Neurology, Erasmus University Medical Centre, Rotterdam, NL*
[4]*Molecular Pathology, International Centre for Genetic Engineering and Biotechnology, Trieste, IT*
[5]*University of Kentucky, Lexington, KY, US*

Background: Aggregated TDP-43 is a pathological hallmark of amyotrophic lateral sclerosis (ALS), frontotemporal dementia (FTD) and limbic-predominant age-related TDP-43 encephalopathy (LATE), and a co-pathology in other neurodegenerative diseases, including Alzheimer's disease (AD). There are currently no validated biofluid or imaging biomarkers of TDP-43 pathology. Direct detection of TDP-43 aggregates will revolutionize precision medicine via accurate diagnosis, patient stratification and assessment of therapeutic efficacy in clinical trials.

Methods: Using our Morphomer® small molecule library of brain-penetrant and beta sheet binding compounds, initial hits were identified using patients' brain material. Orthogonal radiobinding and autoradiography assays were used to assess binding affinity and target engagement on brain samples from diverse cases with FTLD-TDP, ALS and LATE-NC-ADNC, and selectivity over other aggregation-prone proteins on AD and Parkinson's disease (PD) tissue. Brain pharmacokinetic profiles were obtained in mice, followed by assessment of brain uptake, distribution and washout for selected 18F radiolabeled compounds in non-human primates (NHP).

Results: Medicinal chemistry optimization enabled the discovery of the TDP-43 tracer, ACI-19626, that binds with high affinity (low nM Kd) to human brain-derived aggregated TDP-43, but not soluble physiological TDP-43. It differentiates FTLD-TDP type A and B patient samples from age-matched controls and can visualize target engagement to TDP-43 inclusions in ALS and LATE-NC-ADNC brain tissue. ACI-19626 displays excellent selectivity for TDP-43 over Abeta, Tau and alpha-synuclein aggregates, and no binding to common off-target proteins, including monoamine oxidase A and B. [^{18}F]ACI-19626 rapidly enters the brain of NHPs and shows fast and complete washout, a profile suitable for brain PET imaging. Toxicology studies showed a desired safety profile.

Conclusions: [^{18}F]ACI-19626 was identified as a promising first-in-class TDP-43 PET tracer for the detection and monitoring of TDP-43 pathology in living patients. Based on its excellent profile, it was selected for evaluation in a First-in-Human study.

Keywords: TDP-43, new tracer, ALS, FTD

Wednesday, January 15, 2025 - 04:25 pm - 04:30 pm

Podium Session

Blitz Session 1B: Short Poster Presentations

Wednesday, January 15, 2025		
04:25 pm - 04:30 pm	**Blitz Session 1B**	
04:25 pm – 04:27 pm	Introduction	
04:27 pm	Pathological asymmetry in early onset AD reflects heterogenous disease trajectories	**Jacob Ziontz**, Memory and Aging Center, Department of Neurology, University of California San Francisco, San Francisco, CA, US
04:28 pm	Functional submodules in the human locus coeruleus are differentially susceptible to tau pathology	**Timothy Lawn**, Athinoula A. Martinos Center for Biomedical Imaging, Department of Radiology, Massachusetts General Hospital and Harvard Medical School, 02129, Boston, MA, USA, Boston, MA, US
04:29 pm	The universal tau PET scale (Uniτ) for Flortaucipir, MK6240, PI2620 and RO948 harmonization	**Guilherme Povala**, University of Pittsburgh, Department of Psychiatry, Pittsburgh, PA, US

Pathological asymmetry in early onset AD reflects heterogenous disease trajectories

Jacob Ziontz[1], Piyush Maiti[1], Jiaxiuxiu Zhang[1], Konstantinos Chiotis[1], Ganna Blazhenets[1], Salma Rocha[1], Ranjani Shankar[1], Alinda Amuiri[1], Daniel Schonhaut[1], Dustin Hammers[2], Ani Eloyan[3], Robert Koeppe[4], Maria Carrillo[5], Bradford Dickerson[6], Liana Apostolova[7], Gil Rabinovici[1], Renaud La Joie[1]

[1]*Memory and Aging Center, Department of Neurology, University of California San Francisco, San Francisco, CA, US*
[2]*Department of Neurology, Indiana University School of Medicine, Indianapolis, IN, US*
[3]*Department of Biostatistics, Brown University School of Public Health, Providence, RI, US*
[4]*Department of Radiology, University of Michigan, Ann Arbor, MI, US*
[5]*Medical & Scientific Relations Division, Alzheimer's Association, Chicago, IL, US*
[6]*Department of Neurology, Massachusetts General Hospital and Harvard Medical School, Boston, MA, US*
[7]*Department of Radiology, Mayo Clinic, Rochester, MN, US*

Background: Asymmetrical AD pathology has been observed in atypical variants and even cognitively unimpaired (CU) individuals, but how asymmetry presents and changes over time in early-onset AD (EOAD) is unknown.

Methods: We included 373 amyloid-PET-positive patients under 65 years with MCI or mild dementia and 92 CU individuals (10 amyloid-PET-positive, 82 amyloid-PET-negative) from the Longitudinal Early Onset AD study (LEADS). Patient clinical phenotypes were amnestic or nonamnestic EOAD, primary progressive aphasia (PPA), or posterior cortical atrophy. Participants had florbetaben and flortaucipir PET, MRI, and neuropsychological testing at baseline; 206 individuals had 1-3 follow-up imaging visits. We used Freesurfer7.1 segmentation to compute a global asymmetry index for the three imaging modalities reflecting left/right hemisphere signal difference relative to overall cortical signal. We defined symmetrical, left-, and right-lateralized groups using a threshold of +/-2SD from the CU amyloid-PET-negative mean for each modality.

Results: Asymmetry was observed across modalities, most prevalent in flortaucipir followed by cortical volume and florbetaben. Both left and right asymmetry was evident in all clinical phenotypes, though PPA individuals were systematically left-lateralized. Lateralization and degree of asymmetry between modalities were correlated within individuals, particularly between flortaucipir and atrophy (Figure 1). Adjusting for age, sex, education, and overall cortical signal, individuals with lateralized flortaucipir and atrophy performed worse than those with symmetrical signal across domains (Figure 2). Notably, left-lateralized individuals performed worst in verbal fluency while right-lateralized individuals performed worst in visuospatial processing (all $p < 0.001$). Longitudinally, flortaucipir asymmetry decreased over time while volumetric asymmetry increased. Flortaucipir decline was particularly driven by individuals with greater cortical signal abnormality at baseline (Figure 3).

Conclusion: Asymmetry and resulting cognitive impairment are common across clinical phenotypes in EOAD, reflecting intermediate levels of biomarker abnormality. Asymmetry thus varies with disease progression in amyloid, tau, and finally atrophy, declining longitudinally as pathology accumulates contralaterally.

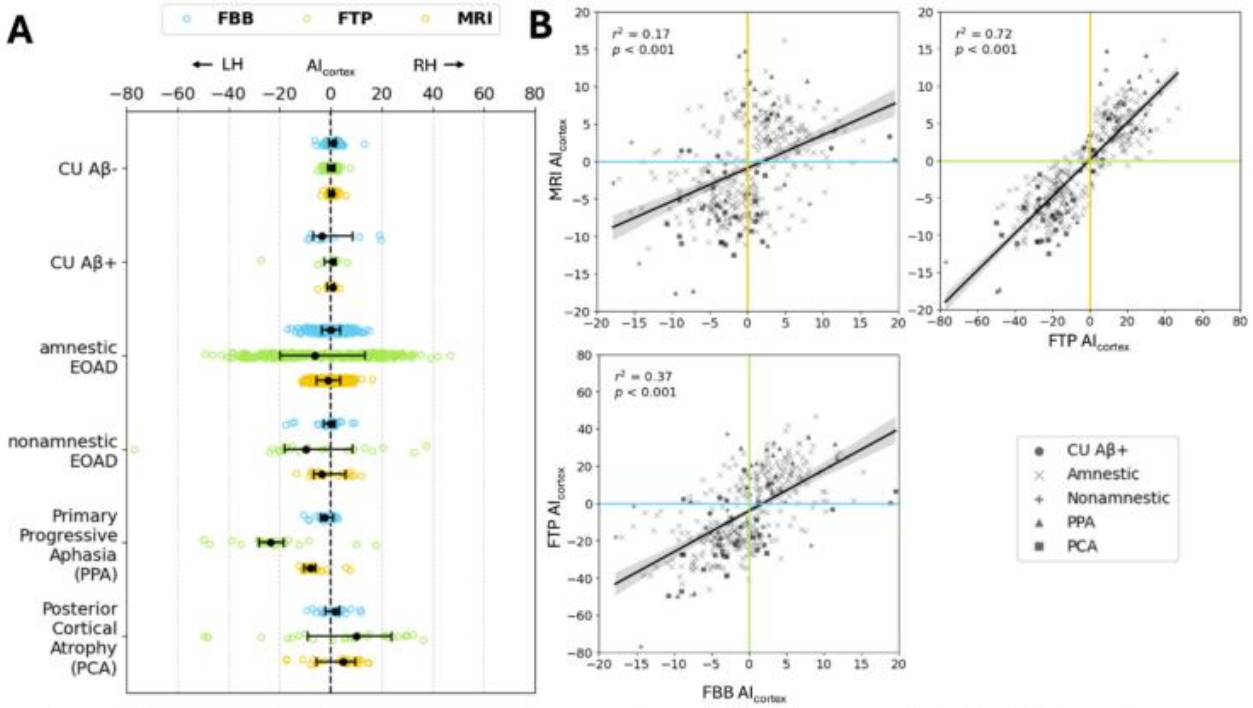


Figure 1. Aβ, tau, and volumetric asymmetry across diagnostic groups in EOAD. (A) Global cortical asymmetry index (AI_{cortex}) for florbetaben (FBB), flortaucipir (FTP), and brain volume (MRI) across diagnostic groups. Negative AI values indicate left-lateralized asymmetry, while positive values indicate right-lateralized asymmetry. Group medians with interquartile range are shown with black dots and confidence bands. **(B)** AI_{cortex} correlations between FBB and MRI *(top left)*, FTP and MRI *(top right)*, and FBB and FTP *(bottom left)*.

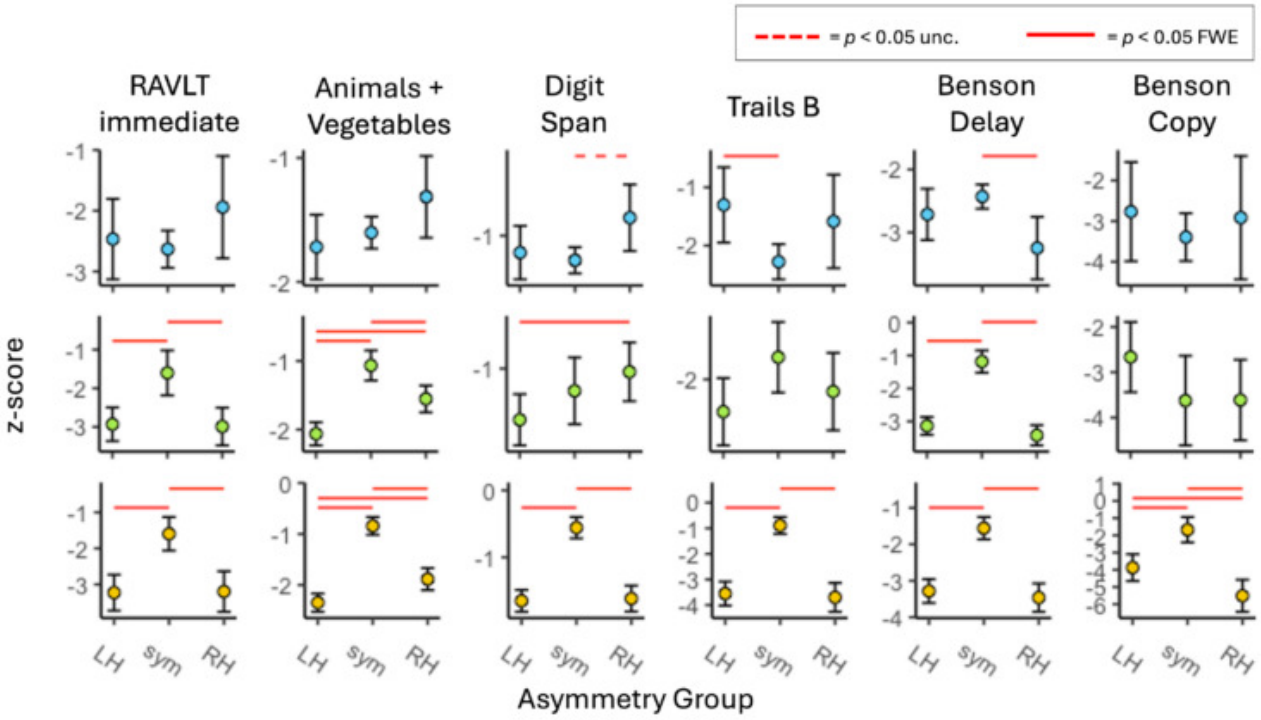


Figure 2. Association between asymmetry and cognitive performance across domains. Group differences between left-lateralized (LH), symmetrical (sym), and right-lateralized (RH) cognitive performance across cognitive tests for florbetaben (*blue*), flortaucipir (*green*), and cortical volume (*yellow*). Z-scores computed with mean and SD of the CU amyloid-PET-negative group. Colored dots visualize estimated marginal means adjusted for age, sex, education, and overall cortical signal. Groups defined using +/-2SD of mean asymmetry in the CU amyloid-PET-negative group.

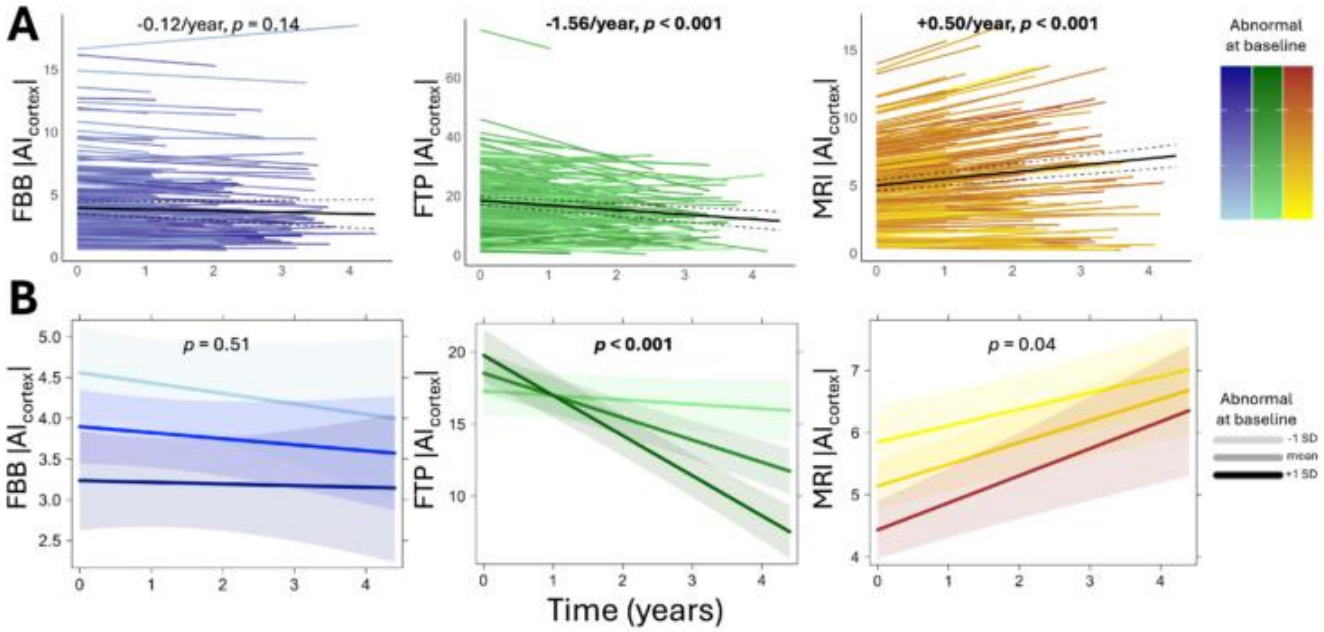


Figure 3. Longitudinal association between absolute cortical asymmetry and baseline abnormality. Y-axis values reflect absolute value of asymmetry index ($|AI_{cortex}|$) to examine asymmetry regardless of left/right lateralization. **(A)** Individualized absolute asymmetry slopes for florbetaben signal *(*FBB, *left)*, flortaucipir signal (FTP, *middle)*, and brain volume (MRI, *right*) from linear mixed effects with random effects of intercept and slope, with intensity colored by abnormality of overall cortical signal at baseline. Black lines and confidence intervals represent the group-level model effect. **(B)** Interaction between baseline cortical signal and change in absolute asymmetry over time. Lines visualize modeled effect at 3 different levels of baseline abnormality (-1SD, mean, +1SD).

Keywords: Early-onset, asymmetry, tau, amyloid, cognition

Functional submodules in the human locus coeruleus are differentially susceptible to tau pathology

Timothy Lawn[1], Prokopis C. Prokopiou[1], Maxime Van Egroo[1,2], Nicholas J. Ashton[3,4,5,6], Shorena Janelidze[7], Kaj Blennow[8,9], Oskar Hansson[7,10], Henrik Zetterberg[3,11,12,13,14], Heidi I. L. Jacobs[1,2]

[1]*Athinoula A. Martinos Center for Biomedical Imaging, Department of Radiology, Massachusetts General Hospital and Harvard Medical School, 02129, Boston, MA, USA, Boston, MA, US*
[2]*Faculty of Health, Medicine and Life Sciences, School for Mental Health and Neuroscience, Alzheimer Centre Limburg, Maastricht University, Maastricht, The Netherlands, Maastricht, NL*
[3]*Department of Psychiatry and Neurochemistry, Institute of Neuroscience and Physiology, The Sahlgrenska Academy at the University of Gothenburg, Mölndal, Sweden, Mölndal, SE*
[4]*Centre for Age-Related Medicine, Stavanger University Hospital, Stavanger, Norway, Stavanger, NO*
[5]*King's College London, Institute of Psychiatry, Psychology and Neuroscience, Maurice Wohl Institute Clinical Neuroscience Institute, London, UK, London, GB*
[6]*NIHR Biomedical Research Centre for Mental Health and Biomedical Research Unit for Dementia at South London and Maudsley NHS Foundation, London, UK, London, GB*
[7]*Clinical Memory Research Unit, Department of Clinical Sciences Malmö, Lund University, Lund, Sweden, Lund, SE*
[8]*Department of Psychiatry and Neurochemistry, Institute of Neuroscience and Physiology, The Sahlgrenska Academy at the University of Gothenburg, Mölndal, Sweden, Mölndal, SE*
[9]*Clinical Neurochemistry Laboratory, Sahlgrenska University Hospital, Mölndal, Sweden, Mölndal, SE*
[10]*Memory Clinic, Skåne University Hospital, Malmö, Sweden, Malmö, SE*
[11]*Clinical Neurochemistry Laboratory, Sahlgrenska University Hospital, Mölndal, Sweden, Mölndal, SE*
[12]*Department of Neurodegenerative Disease, UCL Institute of Neurology, Queen Square, London, UK, London, GB*
[13]*UK Dementia Research Institute at UCL, London, UK, London, GB*
[14]*Hong Kong Center for Neurodegenerative Diseases, Clear Water Bay, Hong Kong, China, Hong Kong, CN*

Background: The locus coeruleus(LC) is amongst the earliest brain regions to accrue tau pathology in Alzheimer's disease(AD), with its dorso-rostral portion being more vulnerable. This pathology may diminish LC neurons capacity to deploy their full repertoire of varying tonic and brief phasic activity to meet task demands. Here, we examine functional vulnerability within the LC, hypothesising dorso-rostral activity shows selectively reduced task-related variability with increasing tau pathology.

Methods: 87 individuals from a lifespan-cohort(table-1) underwent 7T task-fMRI(high/low arousal images), provided samples for plasma biomarkers(pTau181, pTau217, and pTau231), and completed the Preclinical Alzheimer Cognitive Composite(PACC). We utilised Hursts exponent(HE) to quantify the temporal structure of BOLD fluctuations in each voxel across the entire timeseries, with higher values representing lower variability. Agglomerative hierarchical clustering was applied to within-LC connectivity matrices to delineate functionally similar submodules. Robust linear models tested if submodular or caudo-rostral gradients of HE were related to(or moderated the relationship between) pTau and PACC, controlling for age, sex, education, and framewise displacement.

Results: Rostral HE was positively associated with pTau231 and pTau181, and this was stronger than middle/caudal HE for pTau231(fig-1B/C). Rostral HE was negatively associated with PACC(fig-1D), but did not moderate the relationship between pTau231 or pTau181 and PACC(fig-1E/F). The caudo-rostral HE gradient(fig-2A) was also associated with both pTau231(fig-2B) and pTau181(fig-2C), with lower caudal-vs-rostral values corresponding to elevated pTau levels. Whilst HE gradients did not directly relate to PACC, higher gradients were associated with worse cognitive performance at higher pTau231 and pTau181(fig-2D/E). No relationships were found for pTau217.

Conclusion: The human LC shows selectively lower rostral BOLD signal variability with higher tau pathology and worse cognitive performance, potentially reflecting a reduced capacity to modulate its activity to meet task-related demands. Together, these findings suggesting LC (dys)function may be an early marker of AD-related processes.

Table-1: Demographic, plasma biomarker, and imaging values within the study sample.

Overall, 87 participants were included, but due to missing data some analyses utilise only a subset, as denoted by the number of subjects column. Continuous variables are presented as mean ± SD (range) and categorical variables are presented as count (percentage).

Demographics	**Summary**	**Number of subjects**
Age (years)	60.14 ± 13.49 (31- 87)	87
Sex	F 47 (54.0%), M 40 (46.0%)	87
E4 status	Non-carrier 54 (62.8%), Carrier 32 (37.2%)	86
Education (years)	14.23 ± 2.03 (6 - 20)	86
PACC	0.07 ± 0.61 (-1.70 - 1.20)	86
Plasma biomarkers		
pTau217 (pg/ml)	0.27 ± 0.119 (0.11 - 0.81)	82
pTau231 (pg/ml)	8.64 ± 3.956 (3.292 - 28.94)	82
pTau181 (pg/ml)	1.69 ± 0.80 (0.80 - 6.44)	77
Imaging		
Framewise displacement (mm)	0.036 ± 0.019 (0.014 - 0.110)	87
Hursts exponent (rostral)	0.516 ± 0.030 (0.453 - 0.652)	87
Hursts exponent (middle)	0.519 ± 0.025 (0.477 - 0.584)	87
Hursts exponent (caudal)	0.526 ± 0.023 (0.475 - 0.626)	87
Hursts exponent caudo-rostral gradient	-0.001 ± 0.003 (-0.008 - 0.008)	87

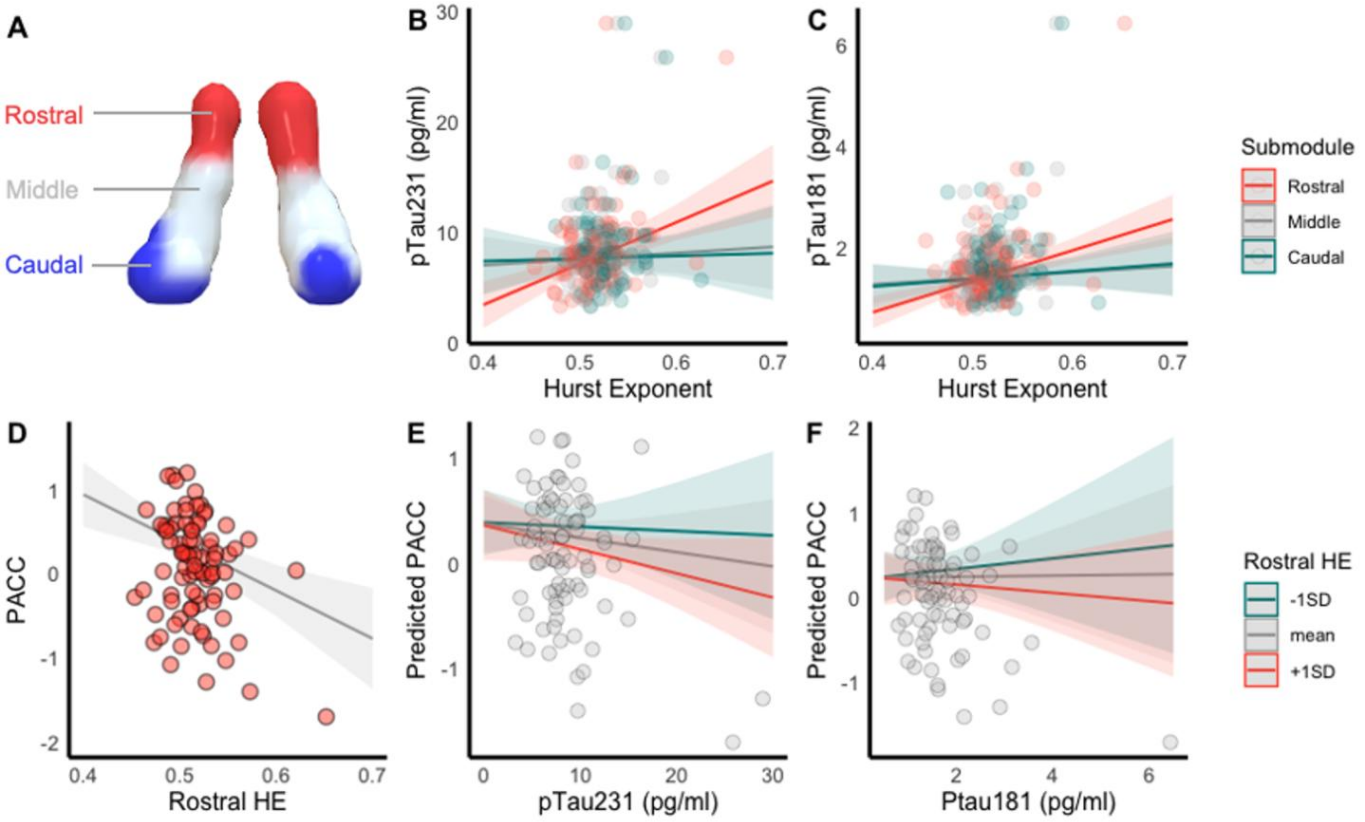


Figure-1: Relationships between voxelwise HE, plasma tau, and cognition.

(A) Hierarchical clustering applied to within-LC connectivity matrices delineated a 6 cluster solution which we bilateralised to give three rostral (red), middle (grey), and caudal (blue) submodules. **(B, C)** HE within these submodules showed differential relationships to plasma tau, with stronger relationships between HE and ptau231 in the rostral compared to both the middle (β = -31.90, SE = 14.19, t(236) = -2.25, p = 0.037) and caudal (β = -35.01, SE = 15.33, t(236) = -2.28, p = 0.033) submodules. There was also a trend towards stronger relationships between HE and pTau181 in the rostral compared to both the middle (β = -4.93, SE = 2.47, t(221) = -2.00, p = 0.075) and caudal (β = -4.63, SE = 2.68, t(221) = -1.73, p = 0.122) submodules. **(D)** Rostral HE values were negatively associated with PACC scores (β = -5.70, SE = 1.61, t(80) = -3.55, p < 0.001). Shaded area represents the 95% confidence interval. **(E, F)** Rostral HE did not moderate the relationship between plasma tau markers and PACC scores for pTau231 (β = -0.31, SE = 0.25, t(74) = -1.27, p = 0.212) or pTau181 (β = -1.84, SE = 1.07, t(69) = -1.73, p = 0.088). Lines represent the relationship between tau levels and PACC scores at different levels of rostral HE: mean (grey), 1 standard deviation below the mean (green), and 1 standard deviation above the mean (orange). Shaded areas represent 95% confidence intervals.

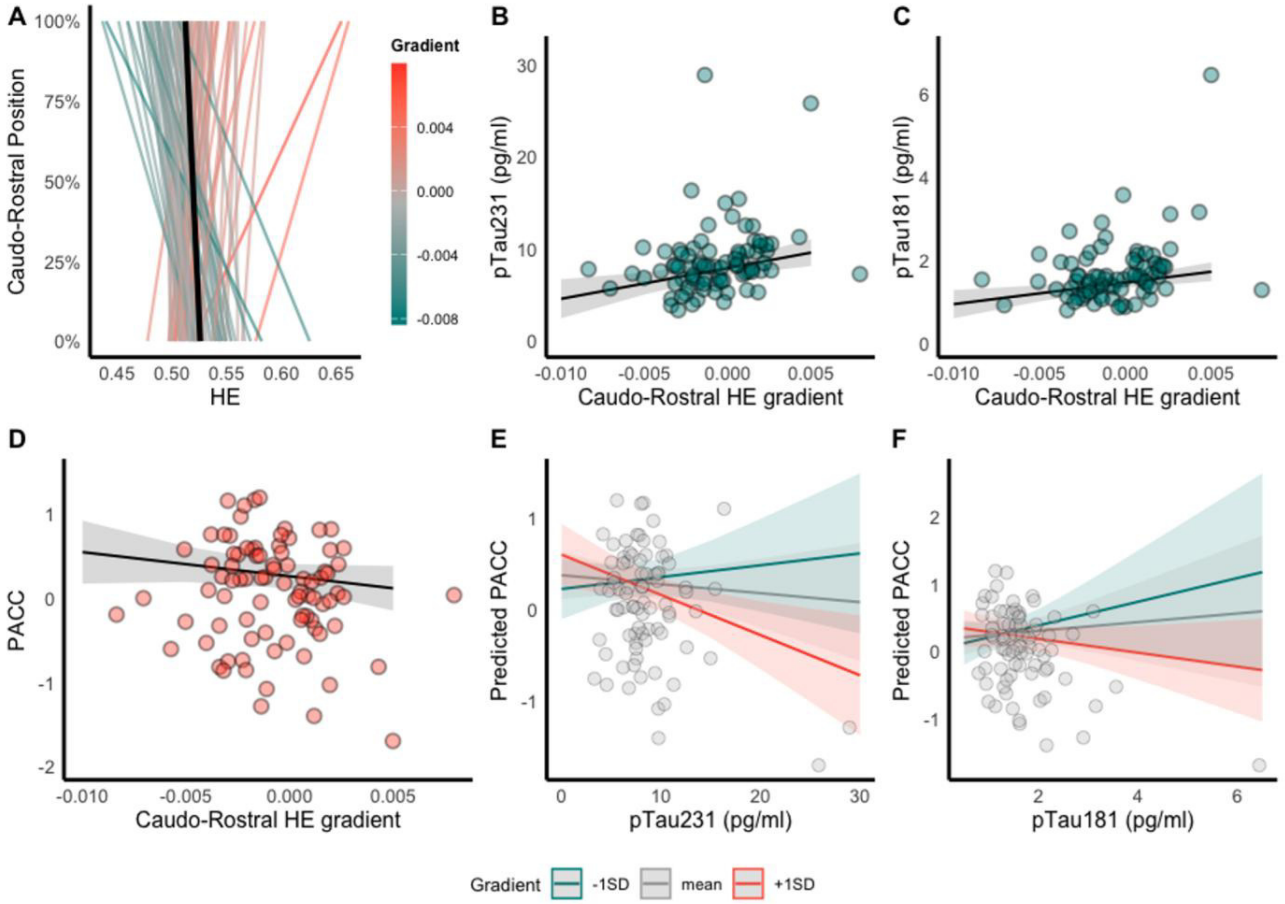


Figure-2: Relationships between the caudo-rostral gradient of HE, tau biomarkers, and cognition.

(A) Caudo-rostral gradients of Hurst Exponent (HE) across the Locus Coeruleus (LC). Each line represents an individual subject, showing the relationship between Z-coordinates and HE values across all LC voxels. Lines therefore depict the change in HE values along the Z (caudo-rostral) axis of the LC. The y-axis represents the normalized position along the caudo-rostral axis, from most caudal (0%) to most rostral (100%). The average gradient is shown in black. **(B, C)** The caudo-rostral HE gradient was positively associated with pTau231 (β = 336.01, SE = 110.05, t(76) = 3.05, p = 0.004) and pTau181 (β = 51.91, SE = 19.59, t(71) = 2.65, p = 0.016). Shaded areas represent 95% confidence intervals. **(D)** The caudo-rostral HE gradient was not related to PACC (β = -28.70, SE = 20.48, t(80) = -1.40, p = 0.168). **(E, F)** Higher caudo-rostral HE gradients were associated with lower PACC scores in the presence of greater tau pathology for both pTau231 (β = -11.39, SE = 4.49, t(74) = -2.53, p = 0.016) and pTau181 (β = -56.07, SE = 21.69, t(69) = -2.59, p = 0.012). Lines represent the relationship between tau levels and PACC scores at different levels of the HE gradient: mean (grey), 1 standard deviation below the mean (green), and 1 standard deviation above the mean (orange). Shaded areas represent 95% confidence intervals.

Keywords: Locus Coeruleus, Cognition, Tau, Preclinical Alzheimer's disease, fMRI

The universal tau PET scale (Uniτ) for Flortaucipir, MK6240, PI2620 and RO948 harmonization

Guilherme Povala[1], Guilherme Bauer-Negrini[1], Bruna Bellaver[1], Firoza Z. Lussier[1], Livia Amaral[1], Pamela Lukasewicz Ferreira[1], Dana L. Tudorascu[1], Quentin Finn[2], Joseph Masdeu[2], David Soleimani-Meigooni[3], Juan Fortea[4], Val Lowe[5], Hwamee Oh[6], Belen Pascual[2], Brian A. Gordon[7], Pedro Rosa-Neto[8], Suzanne Baker[9], Tharick A. Pascoal[1]

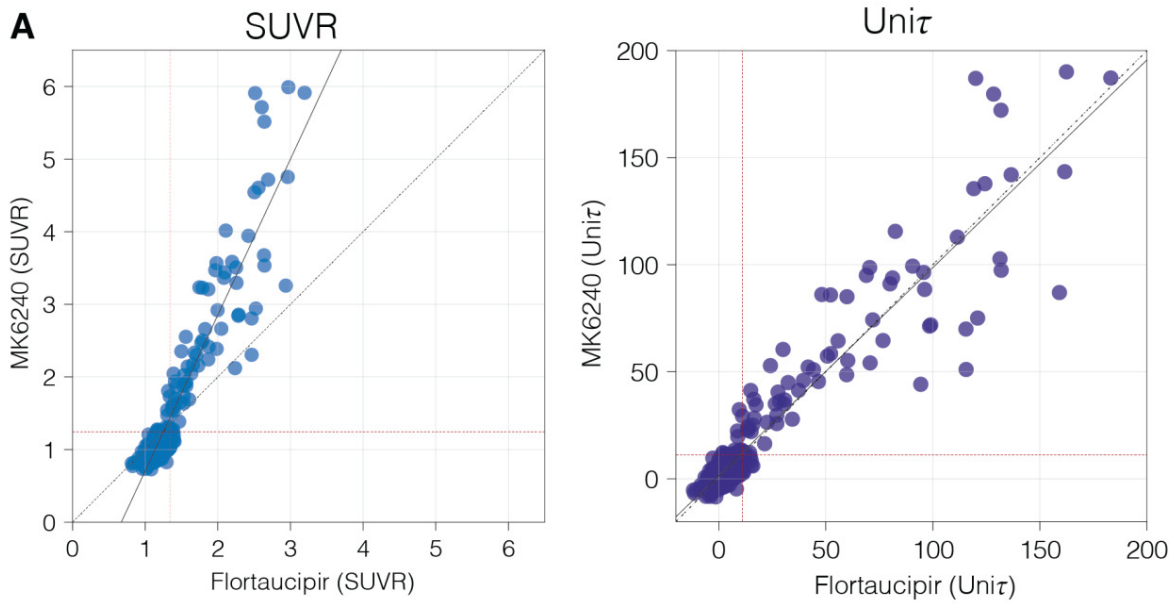
[1]*University of Pittsburgh, Department of Psychiatry, Pittsburgh, PA, US*
[2]*Houston Methodist Research Institute, Department of Neurology, Houston, TX, US*
[3]*University of California San Francisco, Memory and Aging Center, San Francisco, CA, US*
[4]*Hospital de la Santa Creu i Sant Pau, Sant Pau Memory Unit, Department of Neurology, Barcelona, ES*
[5]*Mayo Clinic, Department of Radiology, Rochester, MN, US*
[6]*Brown University, Department of Psychiatry and Human Behavior, Providence, RI, US*
[7]*Washington University in St. Louis, Department of Radiology, Saint Louis, MO, US*
[8]*Translational Neuroimaging Laboratory, McGill University Research Centre for Studies in Aging, Douglas Research Institute, Montréal, QC, CA*
[9]*Lawrence Berkeley National Laboratory, Berkeley, CA, US*

Objective: HEAD is a longitudinal, multi-site, observational, non-randomized head-to-head study of tau-PET tracers. Here, we tested the hypothesis that the Uniτ scale can accurately harmonize the tau-PET tracers Flortaucipir, MK6240, PI2620, and RO948 onto a universal tau-PET measurement.

Methods: We assessed 402 individuals across aging and AD spectrum scanned head-to-head with Flortaucipir and MK6240, and a subset of 67 also with PI2620 and RO948. Tau-PET SUVRs were processed to a common 8mm FWHM using inferior cerebellar gray matter as reference. We previously estimated Uniτ parameters on a training set (n=200) fitting a single-step smoothed hyperbolic tangent mathematical model to the CenTauR Meta-Temporal ROI SUVRs anchored in the mean SUVR of young participants and the 90th percentile from cognitively impaired individuals. We compared tau positivity classifications of the tracers on Uniτ with the classification derived from the original SUVRs (mean + 3 SD from young participants).

Results: Uniτ was able to successfully harmonize Flortaucipir and MK6240 by aligning the values of both tracers (**Fig.1**). For Flortaucipir, the tau positivity classifications of the Uniτ scale matched those from the original SUVRs (ground truth). For MK6240, there was one mismatched case (**Fig.1**). Additionally, by utilizing tracer-specific parameters, Uniτ successfully harmonized PI2620 and RO948 with both Flortaucipir and MK6240, achieving regression lines close to unity, confirming its applicability across multiple tau-PET tracers (**Fig.2**). Finally, upon applying the Uniτ transformation to all brain voxels, Uniτ reasonably harmonized 3D images to the Uniτ scale, substantially reducing visual variabilities (**Fig.3**).

Conclusion: Our results indicate that tau PET tracers can be harmonized to a common scale using anchor points from a large head-to-head dataset. It remains to be seen how Uniτ will perform in the ongoing 18-month follow-up of the HEAD study. Uniτ is freely available on multiple platforms (www.unitau.app) for ROI or voxel-wise tau PET harmonization.



B

	SUVR-	SUVR+
MK6240	307	95
Flortaucipir	315	87

	Uniτ-	Uniτ+
MK6240	308 (0.3%)	94 (-1.1%)
Flortaucipir	315 (0%)	87 (0%)

Figure 1. Comparison of SUVR estimates (left) and Uniτ estimates (right) between MK6240 and Flortaucipir tau PET tracers. (A) The original SUVR data shows important variability in tracer associations, while the Uniτ scale aligned them more closely, with a regression line near unity (RMSE: 10.78, R2: 0.89, y=0.97x+1.62). (B) Individuals' positivity classification based on the Uniτ scale are also presented. For MK6240, there is 1 mismatch classification in Uniτ compared to the SUVR, whereas for Flortaucipir the positivity classifications remain the same of SUVRs. Uniτ harmonization reduces systematic differences preserving tracers' characteristics, resulting in a more consistent relationship between tau tracers.

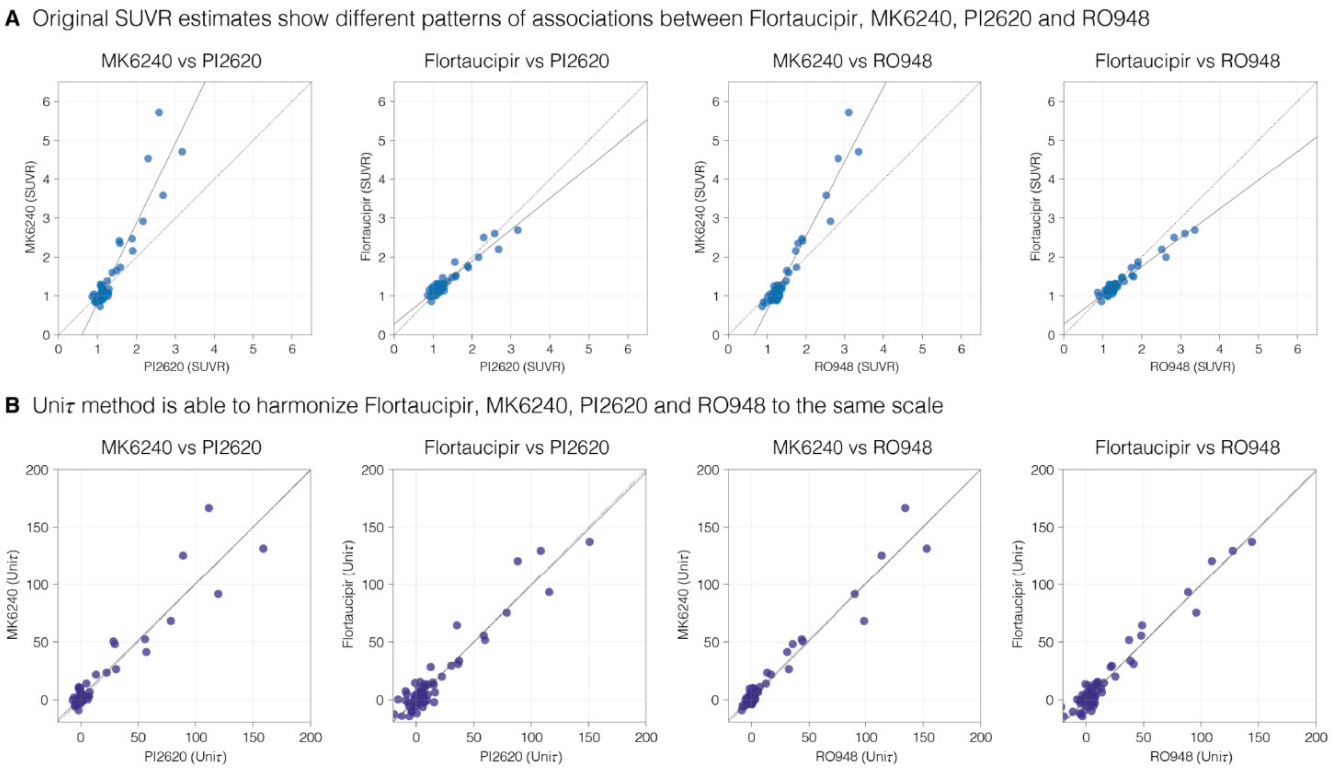


Figure 2. Comparison of SUVR estimates and Uniτ harmonization using MK6240, Flortaucipir, PI2620, and RO948 tau PET tracers. (A) Original SUVR estimates reveal substantial differences in associations between tracers in the scatter plots. The diagonal line represents perfect agreement. (B) The Uniτ method harmonized SUVR values into a unified scale with regression lines overlapping with the diagonal line, reducing variability and enhancing consistency between tracers.

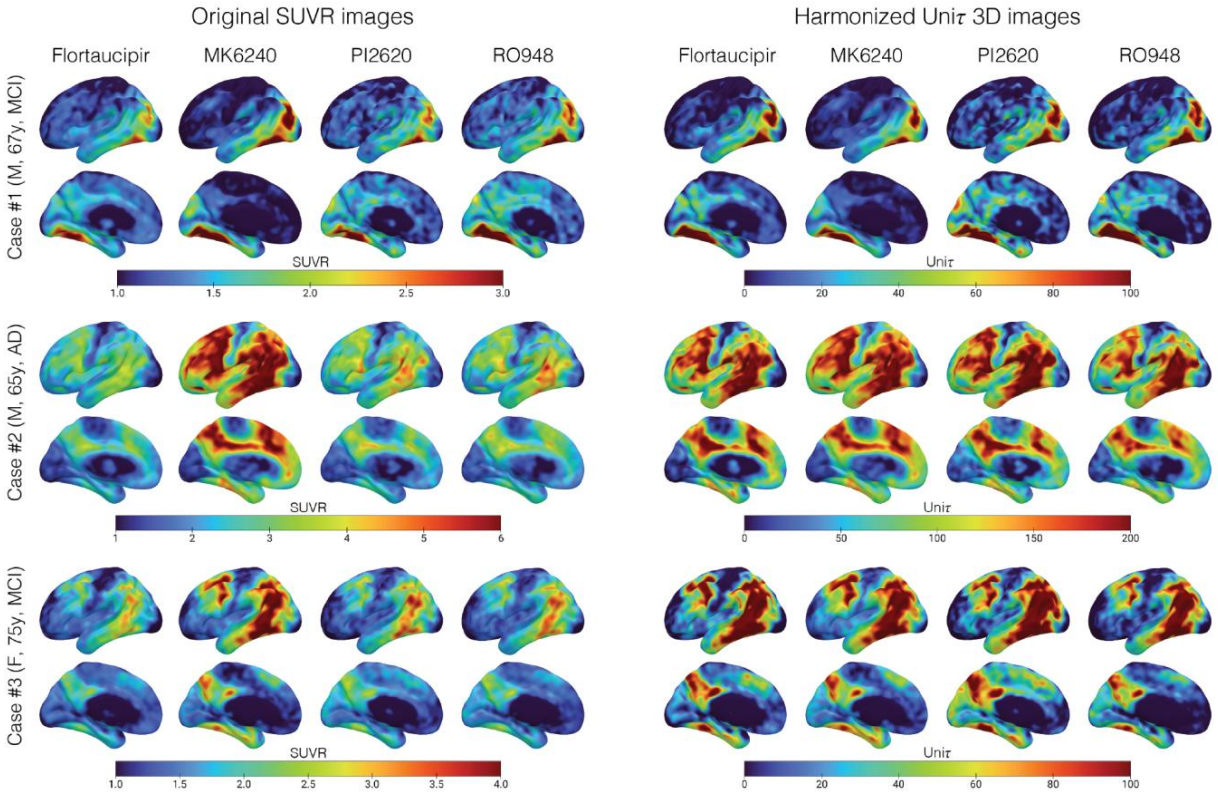


Figure 3. 3D visualization of SUVR and Uniτ harmonization results using Flortaucipir, MK6240, PI2620, and RO948 tau-PET tracers for representative cases. The left panel shows SUVR images, while the right panel displays the harmonized Uniτ images, reducing visual differences and providing a consistent view of tau distribution. Color bars indicate SUVR values (left) and Uniτ units (right).

Keywords: tau, PET, harmonization, Unitau, head-to-head

Thursday, January 16, 2025 - 08:45 am - 10:00 am

Podium Session

ISTAART Collaborations: Addressing Accessibility and Acceptability of Neuroimaging in Diverse Populations

Thursday, January 16, 2025		
08:45 am - 10:00 am	**ISTAART Collaborations Addressing Accessibility and Acceptability of Neuroimaging in Diverse Populations**	**Shana Stites,** University of Pennsylvania, Philadelphia, PA, USA **Tobey Betthauser,** University of Wisconsin, Madison, WI, USA
08:45 am – 08:50 am	Introduction	**Reisa Sperling,** Brigham and Women's Hospital/HMS, Boston, MA, USA
08:50 am	Background and collaboration	**Tobey Betthauser,** University of Wisconsin, Madison, WI, USA
08:55 am	A-Frame: Actionable framework for accessibility, acceptability, and alliance in aging studies using imaging	**Shana Stites,** University of Pennsylvania, Philadelphia, PA, USA
09:05 am	Community-engaged research for increasing representation in brain aging studies – the HABS-HD approach and lessons learned	**Sid O'Bryant,** University of North Texas Health Science Center, Fort Worth, TX, USA
09:15 am	Neuroimaging of older Latino adults in Boston: Linking established and new cohorts	**Yakeel Quiroz,** Massachusetts General Hospital, Boston, MA, USA
09:25 am – 09:55 am	Discussion	
09:55 am - 10:00 am	Concluding remarks and resources	

Neuroimaging and fluid biomarkers for Alzheimer's disease (AD) have had a dramatic influence on our understanding of AD pathophysiology, the development of disease modifying therapies, and prognosis of clinical symptoms. However, most of these discoveries have been made in relatively homogeneous samples. It remains unclear the extent to which these findings will generalize to populations of other races or levels of education, socioeconomic status, or backgrounds. This is in part due to considerable disparities in equity of access and acceptability of AD biomarkers in research studies, clinical trials, and clinical practice across diverse communities, where AD biomarkers are playing an increasingly integral role, particularly with disease-modifying treatments now coming available. While these disparities are acknowledged, practical steps are needed to effectively close these gaps in access and acceptability.

This session is a continuation of a collaborative, multidisciplinary workshop held at AAIC 2024 designed to identify solutions of all kinds to improve accessibility and acceptability of AD biomarkers to members of under recruited groups.

Thursday, January 16, 2025 - 10:00 am - 10:05 am

Podium Session

Blitz Session 2A: Short Poster Presentations

Thursday, January 16, 2025		
10:00 am - 10:05 am	**Blitz Session 2A**	
10:00 am – 10:02 am	Introduction	
10:02 am	The role of cohort heterogeneity in predicting AD/ADRD cognitive decline	**Peiwei Liu**, Department of Neuroscience, University of California, Berkeley, Berkeley, CA, US
10:03 am	Sex moderates the association between regional tau and longitudinal cognitive decline in A4 and LEARN studies	**Annie Li**, Department of Neurology, Massachusetts General Hospital, Harvard Medical School, Boston, MA, US
10:04 am	Low tau in Aβ-positive cognitively impaired individuals: Alzheimer's disease or something more?	**Konstantinos Ioannou**, Karolinska Institutet, Stockholm, SE

The role of cohort heterogeneity in predicting AD/ADRD cognitive decline

Peiwei Liu[1], Jacinda Taggett[1], Theresa Harrison[1], Heather Snyder[3], Charles DeCarli[4], Prashanthi Vemuri[5], Danielle Harvey[6], William Jagust[1], Laura Baker[2], Susan Landau[1]

[1]*Department of Neuroscience, University of California, Berkeley, Berkeley, CA, US*
[2]*Gerontology and Geriatric Medicine, Wake Forest University, Winston-Salem, NC, US*
[3]*Alzheimer's Association, Chicago, IL, US*
[4]*Department of Neurology, University of California, Davis, Sacramento, CA, US*
[5]*Department of Radiology, Mayo Clinic, Rochester, MN, US*
[6]*Public Health Sciences, University of California, Davis, Sacramento, CA, US*

Background: We previously reported that tau PET was more predictive of cognition in ADNI (a clinic-based sample low in comorbidities and ethnoracial diversity) than U.S. POINTER (a community-based sample with high cardiovascular risk and ethnoracial diversity), and this difference was driven by Aβ+ individuals. Here, we investigate the roles of cortical thickness and cardiovascular risk contributing to cohort differences among Aβ+ older individuals.

Methods: U.S. POINTER (N = 775; 68.9 ± 5.2 years, 62.8% female, 30.6% Aβ+) and ADNI (N = 405; 69.9 ± 5.4 years, 58% female, 31.1% Aβ+) were matched by age, sex, Clinical Dementia Rating Scale Sum of Boxes score, and APOE4 status (Table 1). Among the Aβ+ subset, generalized linear models in each cohort examined baseline whole-brain tau PET (MK6240 in U.S. POINTER, FTP in ADNI) and Preclinical Alzheimer's Cognitive Composite (PACC) scores. We also examined cohort-specific cortical thickness associations with PACC scores and cardiovascular risk (Framingham Risk Score (FRS)). Models with PACC controlled for age, sex, education, and PACC exposures, while FRS related models were controlled for education only.

Results: Tau throughout temporal and posterior cingulate regions (Figure 1), and lower cortical thickness in temporal pole, precuneus, and frontal regions (Figure 2A) were associated with poorer cognition (PACC) in ADNI, but these associations were much weaker in U.S. POINTER. However, there were more robust cortical thickness associations throughout frontal, cingulate, parietal, and occipital regions with cardiovascular risk in U.S. POINTER than ADNI (Figure 2B).

Conclusion: In ADNI, cognition is linked to cortical thickness and tau in AD-related regional patterns that have been previously observed in predominantly clinic-based samples. In POINTER, however, these associations were much weaker, and thickness was more closely linked to cardiovascular risk. Cohort recruitment differences, particularly in diversity and cardiovascular risk factors, impact the generalizability of AD-related brain-cognition relationships.

Keywords: Alzheimer's disease, Tau, Cortical thickness, Cognition, Cardiovascular risk

Sex moderates the association between regional tau and longitudinal cognitive decline in A4 and LEARN studies

Annie Li[1], Hannah M. Klinger[1], Mabel Seto[3], Colin J. Birkenbihl[1], Michelle Farrell[1], Emma Thibault[1], Robert A. Rissman[2], Michael Properzi[1], Aaron P. Schultz[1], Diana L. Townsend[1], Hyun-Sik Yang[1,3], Keith A. Johnson[1,3], Rema Reman[2], Oliver Langford[2], Michael Donohue[2], Reisa A. Sperling[1,3], Rachel F. Buckley[1,3,4], Gillian T. Coughlan[1]

[1]*Department of Neurology, Massachusetts General Hospital, Harvard Medical School, Boston, MA, US*
[2]*Alzheimer's Therapeutic Research Institute, University of Southern California, San Diego, CA, US*
[3]*Neurology Department, Brigham and Women's Hospital, Boston, MA, US*
[4]*Melbourne School of Psychological Sciences, University of Melbourne, Melbourne, AU*

Background: Existing literature suggests that women exhibit higher tauopathy relative to men, but evidence for sex moderating the association between tauopathy and cognitive decline is sparse. To address this gap, we investigated sex differences on cognitive trajectories as a function of tau burden.

Methods: The study included 436 clinically normal adults from the Anti-Amyloid Treatment in Asymptomatic Alzheimer's Disease trial (A4) and the companion Longitudinal Evaluation of Amyloid Risk and Neurodegeneration (LEARN) study (Table 1), with at least one baseline tau-positron emission tomography (PET) scan and cognitive follow-ups (mean(SD)=3.34(2.19)years, range=0.03-9.04 years). Four Alzheimer's disease-related tau regions were selected: parahippocampus, amygdala, entorhinal, and inferior temporal gyri. Cognitive outcomes were measured using Preclinical Alzheimer Cognitive Composite (PACC) scores. Random-effects regression models estimated the interaction between sex (men/women) and regional tau (continuous) on longitudinal PACC, adjusting for age and education over time, including participant-specific intercepts and slopes. PACC slopes were extracted, and a linear model was used in the floodlight analysis to identify baseline tau thresholds required to detect sex-divergent cognitive trajectories.

Results: Among those with elevated parahippocampal tau (β=0.08, 95%CI:0.00-0.16, P=0.038), amygdala tau (β=0.11, 95%CI:0.03-0.19, P=0.009), inferior temporal tau (β=0.10, 95%CI:0.02-0.18, P=0.014), and entorhinal tau (β=0.08, 95%CI:0.00-0.16, P=0.043), women exhibited significantly faster rates of cognitive decline relative to men. At low levels of tau, women maintained superior PACC performance. Floodlight analysis identified tau thresholds for a significant association between sex and cognitive change (1.25-1.32 tau-SUVR), except for entorhinal tau. These thresholds were used to categorize participants for visualizing trajectories by sex (Figure). Adjusting for substudy, treatment, and baseline amyloid level did not alter findings (Table 2).

Conclusion: Higher regional tau levels in women may contribute to a greater risk of cognitive decline relative to men. These findings emphasize the importance of considering sex-specific tau levels at the baseline of clinical trials.

Table 1: Demographic Characteristics

Characteristics	A4/LEARN N=436	
	MEN	WOMEN
Total No.	183	253
Baseline tau-PET age, mean (SD)	72.9 (4.9)	71.1 (4.7)
APOE ε4 carriers, No. (%)	97 (53.0)	138 (54.5)
Education yrs, mean (SD)	16.9 (2.8)	15.7 (2.7)
Treatment_Solanezumab, No. (%)	87 (47.5)	105 (41.5)
SUBSTUDY_A4, No. (%)	163 (89.1)	225 (88.9)
SUVR, mean (SD)	1.3 (0.2)	1.3 (0.2)
Tau-PET time, mean (min, max)	3.4 (1.4, 7.1)	3.4 (1.3, 6.8)

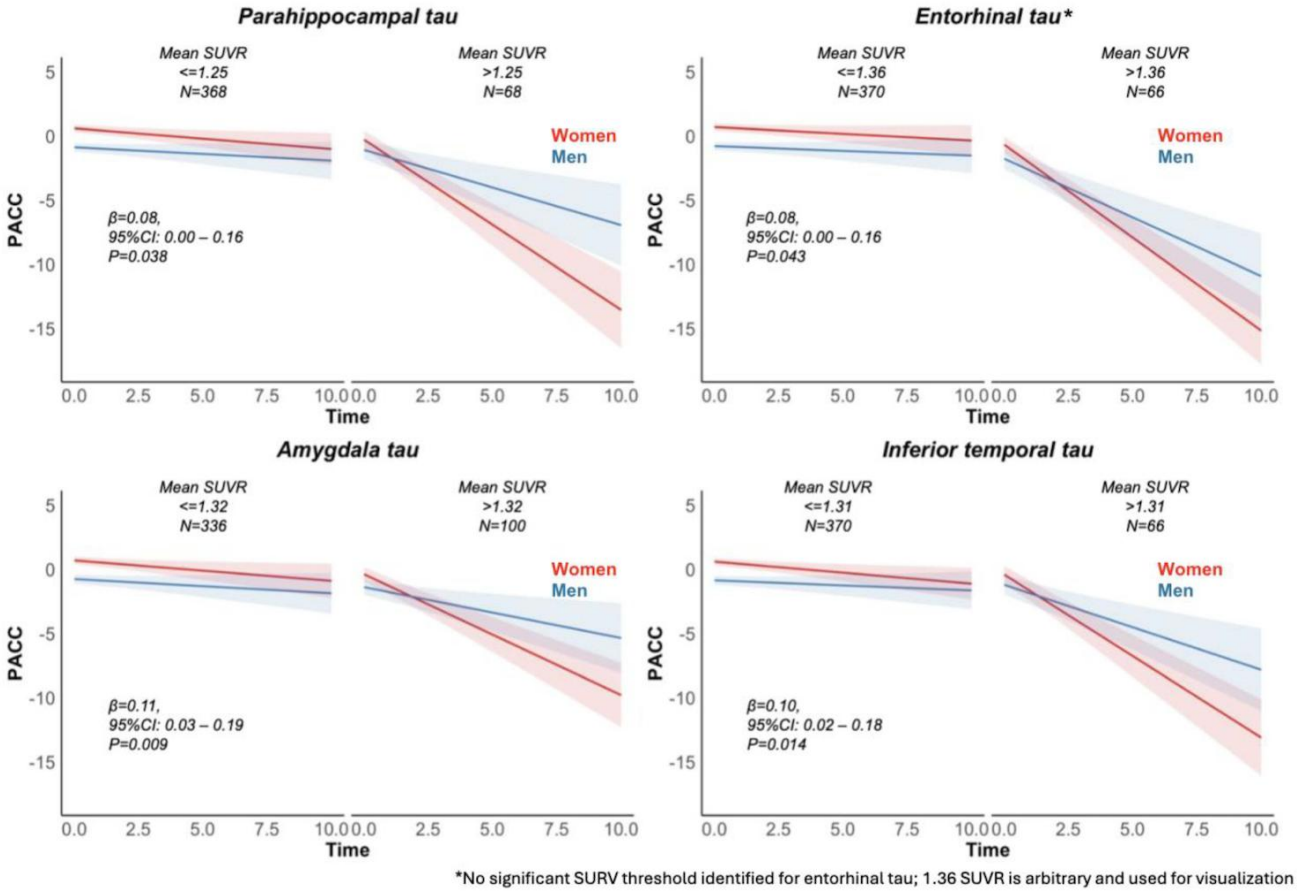
A4/LEARN: Anti-Amyloid Treatment in Asymptomatic Alzheimer's Disease trial and the companion Longitudinal Evaluation of Amyloid Risk and Neurodegeneration study

Table 2: Interaction between sex and regional tau burden on PACC score remains significant after covarying for the effects of substudy, treatment, and baseline amyloid level over time

	Model with Substudy x Time N=436			Model with Treatment x Time N=436			Model with Baseline Amyloid Level x Time N=331		
Predictors	*std. Beta*	*std. CI*	*std. p*	*std. Beta*	*std. CI*	*std. p*	*std. Beta*	*std. CI*	*std. p*
(SEX [Male] × Baseline Parahippocampal) × PACC Time	0.08	0.00 – 0.16	**0.044**	0.09	0.00 – 0.17	**0.040**	0.11	0.01- 0.20	**0.023**
(SEX [Male] × Baseline Amygdala) × PACC Time	0.11	0.03 – 0.19	**0.009**	0.12	0.03 – 0.21	**0.008**	0.15	0.05- 0.24	**0.002**
(SEX [Male] × Baseline Entorhinal) × PACC Time	0.08	0.00 – 0.15	**0.046**	0.09	0.00 – 0.17	**0.041**	0.12	0.03- 0.21	**0.007**
(SEX [Male] × Baseline Inferior temporal) × PACC Time	0.10	0.02 – 0.18	**0.015**	0.11	0.02 – 0.19	**0.013**	0.14	0.04- 0.22	**0.006**

Model with SUBSTUDY x Time: PACC ~ SEX x Baseline Tau x PACC Time + Baseline tau-PET age x PACC Time + Education years x PACC Time + Substudy x PACC Time.
Model with Treatment x Time: PACC ~ SEX x Baseline Tau x PACC Time + Baseline tau-PET age x PACC Time + Education years x PACC Time + Treatment x PACC Time
Model with Baseline Amyloid Level x Time: PACC ~ SEX x Baseline Tau x PACC Time + Baseline tau-PET age x PACC Time + Education years x PACC Time + Baseline Amyloid Level x PACC Time

Figure: Sex moderates the association between regional tau and cognitive decline in A4/LEARN, with cognitive trajectories diverging above a tau threshold of 1.25-1.32 tau-SUVR.



SUVR: standardized uptake value ratio

Keywords: Sex differences, tau-PET, longitudinal, cognitive decline

Low tau in Aβ-positive cognitively impaired individuals: Alzheimer's disease or something more?

Konstantinos Ioannou[1], Khadidzha Abdullaieva[1], Richard J. Perrin[2], Marina Bluma[1], Konstantinos Poulakis[1], Antoine Leuzy[3,4], Dorota Religa[1,5], Elena Rodriguez-Vieitez[1], Konstantinos Chiotis[1,5,6]

[1]*Karolinska Institutet, Stockholm, SE*
[2]*Washington University, Saint Louis, MO, US*
[3]*University of Gothenburg, Gothenburg, SE*
[4]*Sahlgrenska Academy, Region Västra Götaland, SE*
[5]*Karolinska University Hospital, Stockholm, SE*
[6]*University of California, San Francisco, CA, US*

Aims: This study leverages biomarker and autopsy data with the aim to evaluate the impact of mixed pathologies on interpreting cognitive impairment within the AT biomarker system.

Methods: Individuals with at least one instance of antemortem CSF AD biomarkers measurement (Roche, Elecsys ®) and a full postmortem assessment were identified from the ADNI database. Previously validated cut-offs were used to define A+ (Aβ42≤981 pg/mL) and T+ (p-tau181≥24.3 pg/mL). Aβ PET burden was quantified in-house using the Centiloid pipeline. AT groups were compared with respect to cognitive performance, CSF α-synuclein positivity (Amprion, SYNTap ®), Aβ PET burden, clinical comorbidities, and neuropathological evidence of proteinopathies associated with cognitive impairment or vascular brain injury (VBI). Mixed AD was defined as the copresence of Alzheimer's disease neuropathological change (ADNC) and at least another non-AD proteinopathy at autopsy.

Results: We identified and grouped 77 individuals by AT status (median [IQR] interval from CSF sampling to death=3.13 [1.45, 5.69] years). Both A+T- and A+T+ groups were more severely cognitively impaired than the A-T- group at CSF sampling (Table 1). The A+T- and A+T+ groups had similar demographics, frequency of CSF α-synuclein positivity, Aβ PET burden and frequency of clinical comorbidities. The groups showed differences in APOE4 frequency. The A+T+ group showed a higher frequency of ADNC (100% vs 78%, p-value=0.008) than the A+T- group. When ADNC was present, the A+T- group exhibited a higher frequency of mixed AD (79% vs 28%, p-value=0.002) than the A+T+ group, even when taking VBI into consideration (Figure 1).

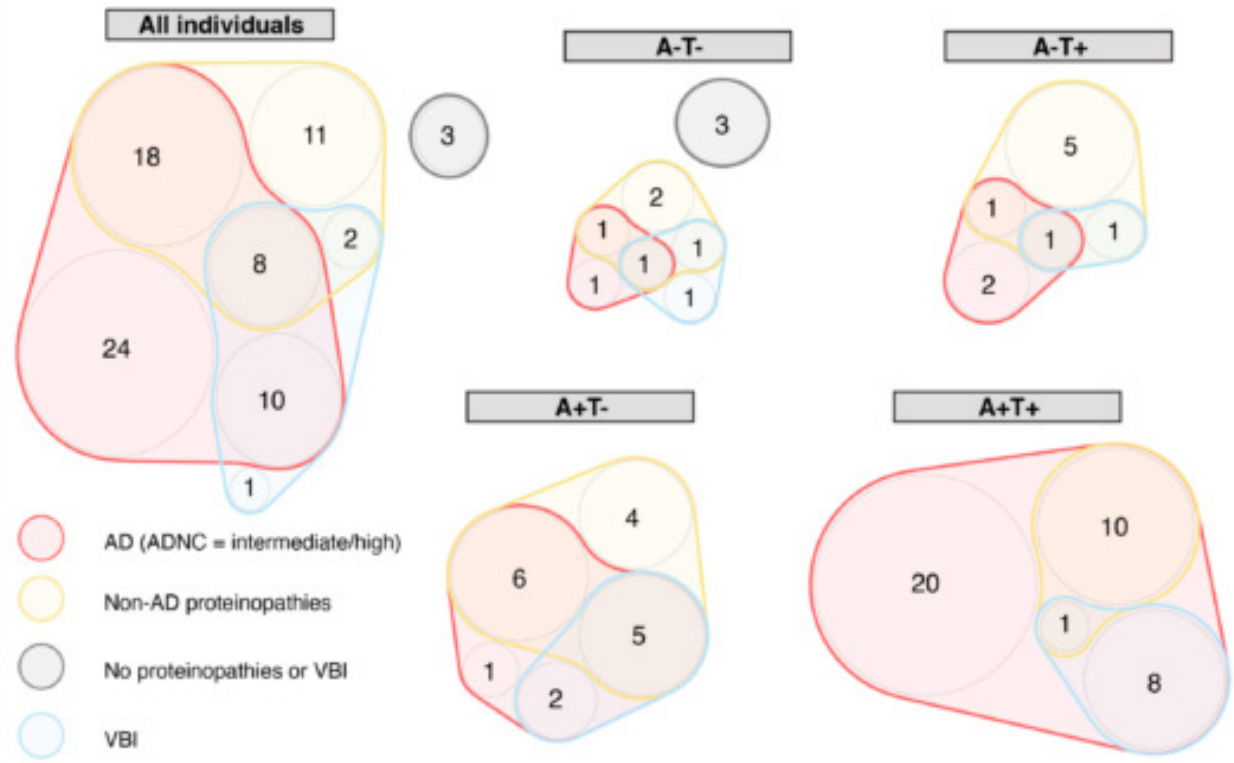
Conclusions: Cognitive impairment associated with Aβ positivity and low tau (A+T-) is linked to mixed AD. These cases deviate from the expected disease path, as proposed by the most recent criteria (Jack CR Jr, et al. Alzheimers Dement. 2024) (Figure 2), and highlight the need for specific biomarkers for non-AD proteinopathies.

Table 1. Demographics, clinical information, and biomarker levels by CSF AT status.

Characteristic	A-T-, N = 10 [1]	A-T+, N = 10 [1]	A+T-, N = 18 [1]	A+T+, N = 39 [1]	p-value [2,3]
Age (y.) [4]	77.5 (72.6, 86.0)	83.0 (80.3, 84.7)	80.5 (76.2, 85.0)	76.3 (73.0, 82.0)	0.2[e]
Sex (Female)	0 / 10 (0%)	5 / 10 (50%)	3 / 18 (17%)	12 / 39 (31%)	**0.042**[a]
Education (y.)	17.5 (15.3, 18.0)	17.0 (14.3, 18.0)	18.0 (16.0, 19.8)	16.0 (15.0, 18.0)	0.5
Presence of APOE4	1 / 10 (10%)	3 / 10 (30%)	4 / 18 (22%)	31 / 39 (79%)	**< 0.001**[c,e,f]
Cognitive status (CI) [4]	5 / 10 (50%)	7 / 10 (70%)	17 / 18 (94%)	38 / 39 (97%)	**< 0.001**[b,c,e]
Neuropsychology [4]					
MMSE	29.0 (28.3, 30.0)	27.0 (26.3, 28.0)	23.0 (20.5, 26.8)	24.0 (19.5, 26.0)	**< 0.001**[a,b,c,e]
Memory score [5]	0.2 (0.0, 1.3)	-0.1 (-0.6, 1.1)	-0.7 (-1.3, 0.4)	-1.1 (-1.5, -0.7)	**< 0.001**[b,c,e]
Biomarkers					
Interval from CSF sampling to death (y.)	3.4 (1.9, 6.4)	1.6 (0.7, 4.7)	2.8 (1.3, 5.7)	3.8 (1.7, 5.2)	0.5
CSF Aβ42 (pg/mL)	1,391.5 (1,230.3, 1,605.8)	2,016.0 (1,061.0, 3,052.3)	480.4 (358.9, 570.6)	540.2 (421.1, 665.9)	**< 0.001**[b,c,d,e]
CSF p-tau181 (pg/mL)	15.6 (13.6, 17.6)	32.8 (30.0, 39.7)	20.4 (17.2, 23.1) [6]	34.3 (28.6, 46.3)	**< 0.001**[a,c,d,f]
CSF α-syn (Type 1) [7]	2 / 9 (22%) [8]	4 / 10 (40%)	9 / 18 (50%)	15 / 39 (38%)	0.8
Aβ PET (CL) [9]	-2.0 (-9.4, 4.8)	-6.8 (-14.6, 61.9)	72.8 (44.8, 85.4)	94.1 (66.8, 113.8)	**< 0.001**[b,c,e]

[1] Median (interquartile range); n / N (%). [2] Kruskal-Wallis rank sum test; Fisher's exact test. [3] a. A-T- vs A-T+; b. A-T- vs A+T-; c. A-T- vs A+T+; d. A-T+ vs A+T-; e. A-T+ vs A+T+; f. A+T- vs A+T+. [4] At the time of CSF sampling. [5] ADNI composite memory score. [6] One A+T- individual was excluded from this statistical analysis due to exceptionally low CSF tau and CSF p-tau181 levels. [7] Positivity Type 1 = αSyn aggregates detected, aggregation profile consistent with Type 1 seeds as seen in Parkinson's disease and Lewy body dementia. [8] One A-T- had no available data for CSF α-syn. [9] Aβ PET scans were available for 51 individuals (A-T-, n = 7; A-T+, n = 6; A+T-, n = 10; A+T+ n = 28). [A-/+ = β-amyloid negativity/positivity, ADNI = Alzheimer's Disease Neuroimaging Initiative, CI = cognitively impaired, CL = centiloids, CSF = cerebrospinal fluid, MMSE = mini mental state examination, PET = positron emission tomography, T-/+ = tau negativity/positivity]

A. Overlap of AD and other pathologies related to cognitive decline



B. Prevalence of AD and other pathologies related to cognitive decline per AT group

Pathologies	A-T- (N = 10) [1]	A-T+ (N = 10) [1]	A+T- (N = 18) [1]	A+T+ (N = 39) [1]	p-value [2,3]
Proteinopathies [4]					
ADNC (intermediate/high)	3 / 10 (30%)	4 / 10 (40%)	14 / 18 (78%)	39 / 39 (100%)	**< 0.001** [b,c,e,f]
LB neocortical (diffuse)	0 / 10 (0%)	2 / 10 (20%)	7 / 18 (39%)	7 / 39 (18%)	0.093 [b]
PSP	1 / 10 (10%)	1 / 10 (10%)	0 / 18 (0%)	0 / 39 (0%)	0.065
AGD	2 / 10 (20%)	6 / 10 (60%)	10 / 18 (56%)	3 / 39 (7.7%)	**< 0.001** [e,f]
FTLD (TDP43)	1 / 10 (10%)	0 / 10 (0%)	1 / 18 (5.6%)	0 / 39 (0%)	0.2
LATE-NC, Stage > 1 + hippocampal sclerosis [5]	0 / 10 (0%)	1 / 9 (11%)	2 / 17 (12%)	1 / 37 (2.7%)	0.2
PART	1 /10 (10%)	2 / 10 (20%)	1 / 18 (5.6%)	0 / 39 (0%)	**0.038** [a]
VBI [4]	3 / 10 (30%)	2 / 10 (20%)	7 / 18 (39%)	9 / 38 (24%) [6]	0.7
Composite neuropathological profile					**< 0.001** [c,e,f]
Pure AD (only ADNC)	1 / 10 (10%)	2 / 10 (20%)	3 / 18 (17%)	28 / 39 (72%)	
Non-AD proteinopathy [7]	3 / 10 (30%)	6 / 10 (60%)	4 / 18 (22%)	0 / 39 (0%)	
Mixed AD (without VBI) [8,9]	2 / 10 (20%)	2 / 10 (20%)	11 / 18 (61%)	11 / 39 (28%)	
Mixed AD as a proportion of ADNC					
Mixed AD (without VBI)/ADNC [8,9]	2 / 3 (67%)	2 / 4 (50%)	11 / 14 (79%)	11 / 39 (28%)	**0.003** [f]
Mixed AD (with VBI)/ADNC [8,10]	2 / 3 (67%)	2 / 4 (50%)	13 / 14 (93%)	19 / 39 (49%)	**0.012** [f]

[1] n / N (%). [2] Fisher's exact test. [3] a. A-T- vs A-T+; b. A-T- vs A+T-; c. A-T- vs A+T+; d. A-T+ vs A+T-; e. A-T+ vs A+T+; f. A+T- vs A+T+. [4] Based on NACC guidelines. [5] Four individuals (A-T+, n = 1; A+T-, n = 1; A+T+ n = 2) did not have data available for either the presence of LATE-NC or hippocampal sclerosis. [6] One A+T+ individual did not have available data regarding the presence of VBI. [7] All proteinopathies except for ADNC. [8] PART was not included in the definition of mixed AD by default. [9] Mixed AD = ADNC + ≥ 1 non-AD proteinopathies related to cognitive decline. [10] Mixed AD = ADNC + ≥ 1 non-AD proteinopathies related to cognitive decline or VBI. [A-/+ = β-amyloid negativity/positivity, AD = Alzheimer's disease, ADNC = AD neuropathologic change, AGD = Argyrophilic grain disease, FTLD = frontotemporal lobar degeneration, LATE-NC = limbic-predominant age-related TDP-43 encephalopathy neuropathologic changes, LB = Lewy bodies, NACC = National Alzheimer's Coordinating Center, PART = primary age-related tauopathy, PSP = progressive supranuclear palsy, T-/+ = tau negativity/positivity, VBI = vascular brain injury].

Figure 1. Presence of overlapping pathologies at autopsy across the AT groups. **A.** Overlap of AD and other pathologies related to cognitive decline. **B.** Prevalence of AD and other pathologies related to cognitive decline per AT group. A+T- individuals had a higher prevalence of mixed pathologies (i.e., mixed AD) compared to A+T+ individuals. The most common co-proteinopathies in A+T- individuals were neocortical LB (39%) and AGD (56%).

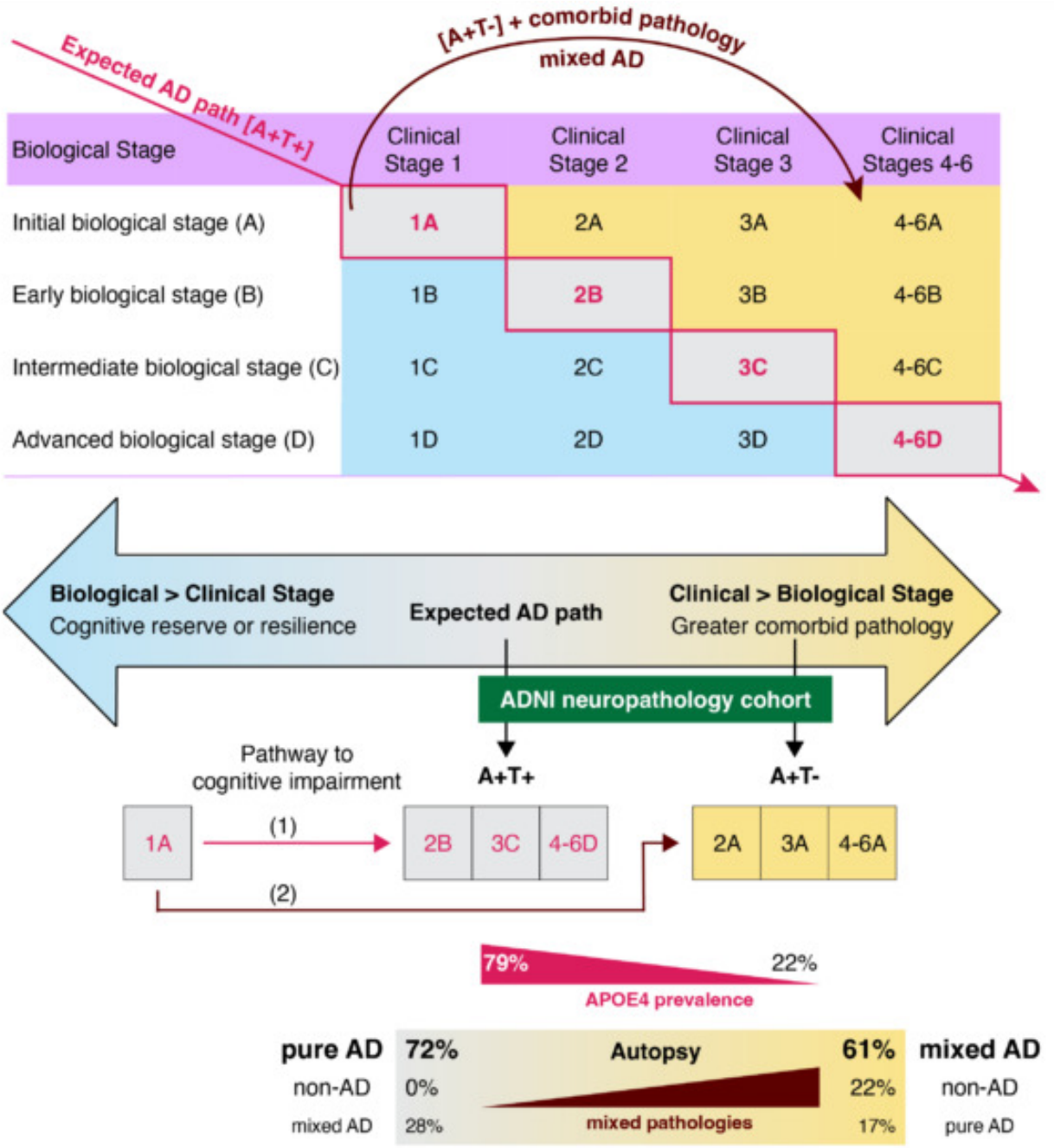


Figure 2. The impact of mixed pathologies on the AT biomarker system with respect to the most recent revised AD criteria (Jack CR Jr, et al. Alzheimers Dement. 2024). The presence of non-AD proteinopathy can influence the clinical interpretation of the AT biomarker system. Cognitively impaired A+T+ individuals have followed the expected AD path (1), but A+T- individuals may have reached severe cognitive impairment through an alternative pathway based on mixed pathologies (2). Mixed AD was defined as the copresence of ADNC and at least one other non-AD proteinopathy related to cognitive decline (VBI is not included here) at autopsy. [A-/+ = β-amyloid negativity/positivity, AD = Alzheimer's disease, ADNC = AD neuropathological change, ADNI = AD neuroimaging initiative,T-/+ = tau negativity/positivity, VBI = vascular brain injury].

Keywords: Alzheimer's disease, mixed pathologies, AT biomarker system

Thursday, January 16, 2025 - 10:05 am - 11:00 am

P2A: Poster Session 2A

Thursday, January 16, 2025			
10:05 am – 11:00 am	**Poster Session 2A** *(repeating in the afternoon as 2B)*		
Board 59	Interpretable prediction of amyloid PET positivity using non-negative matrix factorization	Zhang | Barnard | Gogineni | Corriveau-Lecavalier | Botha | Burkett | Johnson | Lowe | McCarter | Ramanan | Graff-Radford | Knopman | Petersen | Jones	**David T. Jones**, Department of Neurology, Mayo Clinic, ROCHESTER, MN, US
Board 60	Data-driven biomarker discovery nominates novel diagnostic plasma biomarkers and provides insights into Alzheimer's disease pathophysiology in an African American cohort	Kuchenbecker | Thompson | Hurst | Opdenbosch | Heckman | Reddy | Nguyen | Casellas | Sotelo | Redy | Lucas | Day | Willis | Graff-Radford | Ertekin-Taner | Kalari | Carrasquillo	**Lindsey Kuchenbecker**, Department of Neuroscience, Mayo Clinic, Jacksonville, FL, USA, Jacksonville, FL, US
Board 62	Longitudinal multicenter head-to-head harmonization of tau PET tracers: an overview of the HEAD study cohort	Lussier | Povala | Bauer-Negrini | Silva do Amaral | Lukasewicz Ferreira | Bellaver | Masdeu | Tudorascu | Soleimani-Meigooni | Fortea | Lowe | Oh | Pascual | Gordon | Rosa-Neto | Baker | Pascoal	**Firoza Lussier**, University of Pittsburgh, Pittsburgh, PA, US
Board 63	Higher time varying brain functional connectivity is associated with slower tau accumulation at the preclinical stage of Alzheimer's disease	Javanray | St-Onge | Bellec | Misic | Soucy | Villenueve	**Mohammadali Javanray**, McGill University, Montreal, QC, CA
Board 64	Graph convolutional networks to predict cognitive decline at the individual level in Alzheimer's disease	Kang | Heaton | Nyman | Biparva | McSweeney | Ottoy | Masellis | Shirzadi | Johnson | Sperling | Schultz | Jasmeer | Swardfager | Lipsman | Black | Rabin | Goubran	**Min Su Kang**, Artificial Intelligence and Computational Neurosciences lab, Sunnybrook Research Institute, University of Toronto, Toronto, ON, CA
Board 65	Low tau in Aβ-positive cognitively impaired individuals: Alzheimer's disease or something more?	Ioannou | Abdullaieva | J. Perrin | Bluma | Poulakis | Leuzy | Religa | Rodriguez-Vieitez | Chiotis	**Konstantinos Ioannou**, Karolinska Institutet, Stockholm, SE
Board 66	A plasma clock for Alzheimer disease based on %p-tau217	Petersen | Milà-Alomà | Tosun | Li | Shaw | Dage | Zetterberg | Saef | Holtzman | Morris | Xiong | Bateman | Bannon | Potter | Schindler	**Kellen K. Petersen**, Department of Neurology, Washington University in St. Louis, St. Louis, MO, US
Board 67	Network-based amyloid-β pathology predicts subsequent cognitive decline in cognitively normal older adults	He | Razlighi | Gazes | Habeck | Stern	**Hengda He**, Cognitive Neuroscience Division, Department of Neurology, Columbia University, Vagelos College of Physicians and Surgeons, New York, NY, US
Board 68	Associations between APOE-TOMM40 '523 haplotype variants and limbic system white matter microstructure in Black and White individuals	Mooney | Archer | Sathe | Hohman | Kadiri | Lamar | Arfanakis | Yu | Barnes | Deters	**Katelyn Mooney**, University of California Los Angeles, Neuroscience Interdepartmental Program (NSIDP), David Geffen School of Medicine, Los Angeles, CA, USA., Los Angeles, CA, US

Board 69	Multi element MRI template method for analysis of Down syndrome PET	Laymon | Minhas | Heffley | Gilmore | Kondaveeti | Gogola | Royse | Joshi | Lopresti | Luo | Davuluri | Matan | Tudorascu | Christian | Zaman | Beau | Cohen | Handen	**Charles Laymon**, University of Pittsburgh, Pittsburgh, PA, US
Board 70	Whole-blood gene expression associations with Aβ-PET accumulation and cognitive decline	Klinger | Janve | Seto | Brown | Birkenbihl | Coughlan | Townsend | Zyski | Wang | Amariglio | Papp | Rentz | Yang | Chhatwal | Clifton | Donohue | Raman | Rissman | Aisen | Johnson | Sperling | Dumitrescu | Hohman | Buckley	**Hannah Klinger**, Massachusetts General Hospital/Harvard Medical School, Boston, MA, US
Board 71	Longitudinal change in five dominant dimensions of brain aging in relation to brain amyloid status and Alzheimer's-related plasma biomarkers	Bilgel | Shah | Cooper | An | Walker | Moghekar | Yang | Erus | Davatzikos | Resnick	**Murat Bilgel**, Laboratory of Behavioral Neuroscience, National Institute on Aging, Baltimore, MD, US
Board 72	Enrichment of patients with concomitant LATE on the Alzheimer's disease continuum using hippocampal volume	Mundada | Lyu | Sadeghpour | Brown | McCrew | Xie | Yushkevich | Das | Wolk	**Nidhi Mundada**, University of Pennsylvania, Philadelphia, PA, US
Board 73	AT(N) staging of Alzheimer's disease: Comparison of visual interpretation and automated quantification pipelines	Lopresti | Cohen | DelBene | Reese | Matan | Gogola | Chiang | Snitz | Royse | Lopez | Villemagne	**Brian Lopresti**, Department of Radiology, University of Pittsburgh School of Medicine, Pittsburgh, PA, US
Board 74	MK-6240 off-target binding patterns in relation to microglia density, measured through TSPO PET	Heuer | Johnson | Smith | Guzman | Houlihan | Okafor | Sanchez | Talmasov | Dass | Chikwem | Provenzano | Kreisl | Noble | Small | Lao	**Lauren Heuer**, Columbia University Medical Center, New York, NY, US
Board 75	Association between medication use and [18F]MK6240 and [18F]Flortaucipir uptake across the Alzheimer's disease spectrum	Mroué | Lukasewicz Ferreira | Povala | Bellaver | Bauer-Negrini | Lussier | Amaral | Scop Medeiros | Ruppert | Silva da Rocha | Scarpatto Rodrigues | Silva Oliveira | Soares Katz | Teixeira Leffa | Saha | Felix | Masdeu | Soleimani-Meigooni | Fortea | Lowe | Oh | Pascual | Gordon | Rosa-Neto | Baker | Pascoal	**Rayan Mroué**, University of Pittsburgh, Department of Psychiatry, Pittsburgh, PA, US
Board 76	Lower LC-EC tract integrity is associated with entorhinal tau in autosomal-dominant Alzheimer's disease	Koops | Giudicessi | Bonillas-Felix | Medrano | Martinez | Gonzalez | Alvarez | Aguillon | Quiroz | Jacobs	**Elouise Koops**, Martinos Center for Biomedical Imaging, Department of Radiology, Massachusetts General Hospital, Harvard Medical School, Boston, MA, US
Board 77	APOE4 associated with higher off-target meninges signal with [F-18]MK6240 PET	McVea | DiFilippo | McLachlan | Bettcher | Tudorascu | Johnson | Zammit | Betthauser | Christian	**Andrew McVea**, University of Wisconsin - Madison, Madison, WI, US
Board 78	An accurate and automated technique for removing spill-over contamination and off-target retention from a cerebellar reference region for tau PET	Minhas | DelBene | Gogola | Reese | Luo | Laymon | Lopresti | Dore | Pascoal | Baker | Tudorascu | Villemagne	**Davneet Minhas**, University of Pittsburgh, Pittsburgh, PA, US
Board 79	Updated public CenTauR pipelines to measure	Schwarz | Leuzy | Doré | Villemagne | Xiao | Pappas | Przybelski |	**Christopher Schwarz**, Mayo Clinic, Rochester, MN, US

	CenTauR, CenTauRZ, and SUVR tau PET units	Prakaashana | Senjem | Lowe | Gunter | Kantarci | Vemuri | Graff-Radford | Petersen | Knopman | Jack	
Board 80	Predicting regional Alzheimer's disease pathology with plasma p-tau217 in preclinical AD	Moon | Chen	**Hasom Moon**, Stony Brook University, Stony Brook, NY, US
Board 81	TSPO-PET before and after low-dose interleukin-2 in patients with mild to moderate Alzheimer's disease	Pascual | Faridar | Finn | Gamez | Appel | Masdeu	**Belen Pascual**, Houston Methodist Stanley H. Appel Department of Neurology, Houston Methodist Research Institute, Weill Cornell Medicine, Houston, TX, US
Board 82	In low neocortical tau individuals, high amygdala tau predicts faster cognitive decline	Hanseeuw | Thibault | Farell | Buckley | Properzi | Gatchel | Amariglio | Marshall | Beiser | Seshadri | De Carli | Sperling | Jacobs | Johnson	**Bernard Hanseeuw**, Mass General Brigham, Boston, MA, US
Board 83	EOAD-signature atrophy predicts progression to dementia in patients with early-onset MCI due to Alzheimer's disease	Paranhos | Katsumi | Brickhouse | Eckbo | Zaitsev | Du | Eloyan | Nudelman | Foroud | Dage | Carrillo | Rabinovici | Apostolova | Dickerson | Touroutoglou | Consortium	**Yuta Katsumi**, Department of Biostatistics, Center for Statistical Sciences, Brown University, Providence, RI, US
Board 84	FDG reference region selection using PiB amyloid status-guided iterative normalization in a Down syndrome cohort	McLachlan | Keator | Price | Tudorascu | Laymon | Cohen | Lao | Handen | Fryer | Ances | Zaman | Head | Mapstone | Bettcher | Guerrero Gonzalez | LeMerise | McVea | DiFillipo | Zammit | Hartley | Christian	**Max McLachlan**, University of Wisconsin - Madison, Madison, WI, US
Board 85	Microscopic visualization of fluorescent MK-6240	Kunach | S. Smith | I. Antczak | Gupta | Monistrol | Tripathi | Jalapati | Guiot | Stoddard | H. Shahmoradian | K. Shoichet | Vaquer-Alicea | Rosa-Neto | M. Ready | I. Diamond	**Peter Kunach**, Center for Alzheimer's and Neurodegenerative Diseases, Peter O'Donnell Jr. Brain Institute, Dallas, TX, US
Board 86	Conversion of Tau PET SUVR data to CenTauR units using the Joint Propagation Model	Leuzy | Raket | Villemagne | Klein | Tonietto | Olafson | Baker | Saad | Bullich | Lopresti | Sanabria Bohorquez | Lutz | Boada | Betthauser | Charil | Collins | Collins | Gunn | Higuchi | Hostetler | Hutchison | Iaccarino | Insel | Irizarry | Jack Jr | Jagust | Johnson | Johnson | Karten | Marquié | Mathotaarachchi | Mintun | Ossenkoppele | Pappas | Petersen | Rabinovici | Rosa-Neto | Schwarz | Smith | Stephens | Whittington | Carrillo | Pontecorvo | Haeberlein | Dunn | Kolb | Stephenson | Rowe | Hansson | Doré	**Antoine Leuzy**, Clinical Memory Research Unit, Department of Clinical Sciences, Lund University, Lund, SE
Board 87	The role of cohort heterogeneity in predicting AD/ADRD cognitive decline	Liu | Taggett | Harrison | Snyder | DeCarli | Vemuri | Harvey | Jagust | Baker | Landau	**Peiwei Liu**, Department of Neuroscience, University of California, Berkeley, Berkeley, CA, US
Board 88	Differential tau accumulation in early-onset and late-onset Alzheimer's disease: Insights from [18F]-Florzolotau PET	Khurelbaatar | Huang | Lin | Huang | Hsu | Huang | Wu | Huang | Chang | Hsiao	**Bayarjargal Khurelbaatar**, Department of Medical Imaging and Radiological Sciences, Chang Gung University, Taoyuan, Taiwan, ROC., Taoyuan, TW
Board 89	Heterogeneity of FDG-PET patterns among tau-negative amnestic patients	Silva-Rodríguez | Moscoso | Labrador-Espinosa | Sánchez-Juan | Scholl | Grothe	**Jesús Silva-Rodríguez**, Reina Sofia Alzheimer Centre, CIEN Foundation, ISCIII, Madrid, ES

Board 90	Predicting amyloid positivity and tau burden in dementia using a combination of different biomarkers	Huang | Lin | Huang | Huang | Wu | Chang | Hsiao	**Shao-Yi Huang**, Department of Medical Imaging and Radiological Sciences, Chang Gung University, Taoyuan, TW
Board 91	Evaluation of [^{3}H]SynVesT -1 binding in post-mortem brain tissue from control and Alzheimer's disease as a biomarker of synaptic loss	Kulagowska | Lemoine | King | Gladstein | Bevis | Bonsall | Finnema | Spires-Jones | Wells | SV2A project team	**Laura Kulagowska**, Perceptive, London, GB
Board 92	Exploring the predictive power of graph-theoretic metrics for tau pathology in cognitively unimpaired older adults	Johns | Vin | Abuwarda | Fredericks	**Emily Johns**, Department of Neurology, Yale University School of Medicine, New Haven, CT, US
Board 93	Tracking biomarkers accuracy for predicting progression to mild cognitive impairment	Gallego-Rudolf | Wiesman | Baillet | Villeneuve	**Jonathan Gallego-Rudolf**, Douglas Research Centre, Montreal, QC, CA
Board 94	Tau burden across Braak stages is associated with regionally specific amyloid accumulation: insights from the BIOCARD cohort	Rani | Alm | Callow | Pettigrew | Soldan | Miller | Albert | Bakker	**Nisha Rani**, Department of Psychiatry and Behavioral Sciences, Johns Hopkins University School of Medicine, Baltimore, MD, US
Board 95	Relationship between neuroinflammatory ER176-PET and functional connectivity in Progressive Apraxia of Speech	Singh-Reilly | Sintini | Satoh | Duffy | Utianski | Clark | Stephens | Lowe | Josephs | Whitwell	**Neha Singh-Reilly**, Department of Neurology, Mayo Clinic, Rochester, MN, US
Board 96	Sex moderates the association between regional tau and longitudinal cognitive decline in A4 and LEARN studies	Li | Klinger | Seto | Birkenbihl | Farrell | Thibault | Rissman | Properzi | Schultz | Townsend | Yang | Johnson | Reman | Langford | Donohue | Sperling | Buckley | Coughlan	**Annie Li**, Department of Neurology, Massachusetts General Hospital, Harvard Medical School, Boston, MA, US
Board 97	Evaluation of the Uni-tau and CenTauR frameworks in new datasets for tau PET harmonization in Alzheimer's disease	Lutz | Olafson | Tonietto | Klein | Pascoal | Negrini | Povala | Leuzy | Raket | Doren | Sanabria Bohorquez | Teng	**Olivia Lutz**, Research and Early Development (gRED), Genentech, Inc, South San Francisco, CA, US
Board 98	Hemispheric lateralization of tau-related network dysfunction and its association with neuropsychiatric symptoms in preclinical Alzheimer's disease	Moret | Vin | Fredericks	**Sophia Moret**, Yale University, New Haven, CT, US
Board 99	Characterization and correction of extracerebral [18F]MK-6240 tau PET off-target signal in Alzheimer's disease	Olafson | Tonietto | Doren | Sanabria Bohórquez	**Emily Olafson**, Research and Early Development (gRED), Genentech, Inc., South San Francisco, CA, US
Board 100	Investigation of optimal intensity threshold for tau-PET overlap index	Lim | Lee | Min | Moloney | Mester | Ghatamaneni | Senjem | Nguyen | Graff-Radford | Schwarz | Gunter | Kantarci | Boeve | Vemuri | Jones | Jack | Petersen | Murray | Lowe	**Seokbeen Lim**, Department of Radiology, Mayo Clinic, Rochester, MN, US
Board 101	DeepSUVR: Towards redefining the Centiloid	Bourgeat | Fripp | Lebrat | Gillman | Cox | Goyal | Tosun-Turgut | LaMontagne | Benzinger | Weiner |	**Pierrick Bourgeat**, CSIRO Health and Biosecurity, Brisbane, AU

	masks using a data-driven approach	Morris | Villemagne | Masters | Rowe | Dore	
Board 102	Mechanical stress of the entorhinal cortex: A potential driver of tau pathology?	Zhang | Crary | Provenzano	**Frank Provenzano**, Columbia University, New York, NY, US
Board 103	Amyloid-Tau to neurodegeneration mismatch from inter-modality image translation using deep learning	Lyu | Yushkevich | Dong | Khandelwal | Brown | Duong | Li | Xie | Wisse | Das | Wolk	**Xueying Lyu**, University of Pennsylvania, Philadelphia, PA, US
Board 104	Tau PET subgroups differ in network patterns of functional connectivity and amyloid PET	Millar | Doering | Adeyemo | McKay | Metcalf | Roman | Canfield | Jindal | Flores | Strain | Wisch | Hassenstab | Schindler | Morris | Gordon | Ances | Benzinger	**Peter Millar**, Washington University in St. Louis, St. Louis, MO, US
Board 105	Cortical freewater increases with tau tangle aggregation	Hall | Aumont | Rahmouni | Therriault | Hosseini | Trudel | Fernandez-Arias | Macedo | Servaes | Bezgin | Wang | Zheng | Stevenson | Sanjeewa | Benedet | Triana-Baltzer | Kolb | Ashton | Zetterberg | Blennow | Pascoal | Klostranec | Rosa-Neto	**Brandon Hall**, McGill University, Montreal, QC, CA
Board 106	Distinct spatiotemporal patterns of vascular disease in Alzheimer's disease subtypes	Ottoy | Yin | Kang | Gibson | Clappison | Yang | Carver | Rahmouni | Stevenson | Servaes | Therriault | Pascoal | Soucy | Gauthier | Black | Rosa-Neto | Goubran	**Julie Ottoy**, Hurvitz Brain Sciences Program, Sunnybrook Research Institute, University of Toronto, Toronto, ON, CA
Board 107	Annual percent change of microglia density in relation to tau accumulation in older adults	Houlihan | Johnson | Smith | Guzman | Okafor | Heuer | Sanchez | Talmasov | Chikwem | Dass | Noble | Kreisl | Small | Lao	**Hannah Houlihan**, Columbia University Medical Center, New York, NY, US
Board 108	Physical frailty as a risk factor for increased tau accumulation and cognitive decline in cognitively unimpaired older adults	Palmgren | Matos | Kirn | Robinson | Pintucci | Properzi | Schultz | Amariglio | Rentz | Johnson | Sperling | Chhatwal | Yau	**Kailee Palmgren**, Department of Neurology, Massachusetts General Hospital, Boston, MA, US
Board 109	Assessing neuroinflammation in Alzheimer's disease: A TSPO-PET study using ER176 and its correlation with amyloid and tau pathology	Kandimalla | Jacobson | Lim | Lee | Min | Botha | Graff-Radford | Jones | Vemuri | Kantarci | Knopmam | Jack | Petersen | Lowe	**David Jacobson**, Department of Neurology, Mayo Clinic, Rochester, MN, US
Board 110	Two distinct sources of 18F-MK-6240 off-target signal identified by individualized head modeling and PET kinetics	Chen | Fu | Puonti | Thibault | Johnson | Price	**Charles Chen**, Athinoula A. Martinos Center for Biomedical Imaging, Massachusetts General Hospital, Charlestown, MA, US
Board 112	TSPO PET mediates tau-associated neurodegeneration in limbic and temporal regions across clinical variants of Alzheimer's disease	Lao | Johnson | Smith | Guzman | Houlihan | Okafor | Heuer | Sanchez | Talmasov | Chikwem | Dass | Noble | Kreisl | Small	**Patrick Lao**, Columbia University Medical Center, New York, NY, US
Board 114	Tracking plasma biomarker abnormalities with amyloid time accumulation	Bluma | Chiotis | Bucci | Savitcheva | Matton | Kivipelto | Jeromin | De Santis | Di Molfetta | Ashton | Blennow | Zetterberg | Nordberg	**Marina Bluma**, Karolinska Institutet, Department of Neurobiology, Care Sciences and Society, Division of

			Clinical Geriatrics, Center of Alzheimer Research, Stockholm, SE
Board 115	Advancing antibody-based pretargeted PET imaging of protein aggregates in the brain	Gustavsson | Honer | Hvass | Shalgunov | Clausen | Stotz | Wünsche | Lopes van den Broek | Knudsen | Aldana | Niewoehner | Gobbi | Kustermann | Battisti | Kjær | Herth	**Michael Honer**, Cluster for Molecular Imaging, Department of Biomedical Sciences, University of Copenhagen, Copenhagen, DK
Board 116	Longitudinal change in mnemonic discrimination and influence of Aβ burden	Kraft | Nair | Gonen | Skotnicki | Rodrigue | Kennedy	**Jessica Kraft**, Center for Vital Longevity, University of Texas at Dallas, Dallas, TX, US

59 Interpretable prediction of amyloid PET positivity using non-negative matrix factorization

Gemeng Zhang[1], Leland R. Barnard[1], Venkatsampath Gogineni[1], Nick Corriveau-Lecavalier[1,2], Hugo Botha[1], Brian J. Burkett[3], Derek R. Johnson[3], Val J. Lowe[3], Stuart J. McCarter[1], Vijay K. Ramanan[1], Jonathan Graff-Radford[3], David S. Knopman[1], Ronald C. Petersen[1], David T. Jones[1]

[1]*Department of Neurology, Mayo Clinic, ROCHESTER, MN, US*
[2]*Department of Psychiatry and Psychology, ROCHESTER, MN, US*
[3]*Department of Radiology, ROCHESTER, MN, US*

Background: β-amyloid accumulation is a key biomarker in Alzheimer's disease (AD). Standardized uptake value ratio (SUVR) images and the derived Centiloid (CL) values are commonly used to evaluate amyloid PET positivity(A+) alongside visual reading. We propose an interpretable non-negative matrix factorization (NMF) method to assist the visual reading process by decomposing the amyloid PET scans into representative components, facilitating accurate A+ detection while ensuring interpretability for clinical validation.

Method: PET images from the 18F-Florbetapir tracer were analyzed. A total of 2300 amyloid-PET images from Imaging Dementia – Evidence for Amyloid Scanning (IDEAS) study was used for NMF model training (and classification models training (200 A+, 200 A-). The remaining 1700 images (1121 A+, 579 A-) were used as a test set. Two external datasets, the Mayo Clinic Alzheimer's Disease Therapy Clinic (ADTC) (84 A+, 11 A-) and the ADNI4 cohort data (31 A+, 35 A-) are used for validation. Amyloid-PET images were registered to an amyloid-PET template, and whole brain SUVR images were generated using the cerebellum as the reference region. The NMF model was fitted using SUVR images, and logistic regression (LR) model was used for A+/A- prediction. LR weights were further used to interpret the relationship between NMF features and A+/A- classification.

Results: The LR model achieved an AUC of 0.94 (95% CI: 0.93-0.95) on IDEAS test set, 0.98 (95% CI: 0.94-1.00) on Mayo ADTC and 0.97 (95% CI: 0.94-1.00) on ADNI4 (See Fig.1). NMF components C2 (whole-brain SUVR average) and C8 (gray-over-white contrast) were the top influencers for A+ prediction, while C7 (white-over-gray contrast) was most influential for A- prediction (See Fig.2).

Conclusion: The strong prediction performance across two external datasets demonstrates that NMF-based SUVR patterns generalize well and provide interpretable, accurate A+ predictions. Visualizations of key components align with established radiological reading protocols.

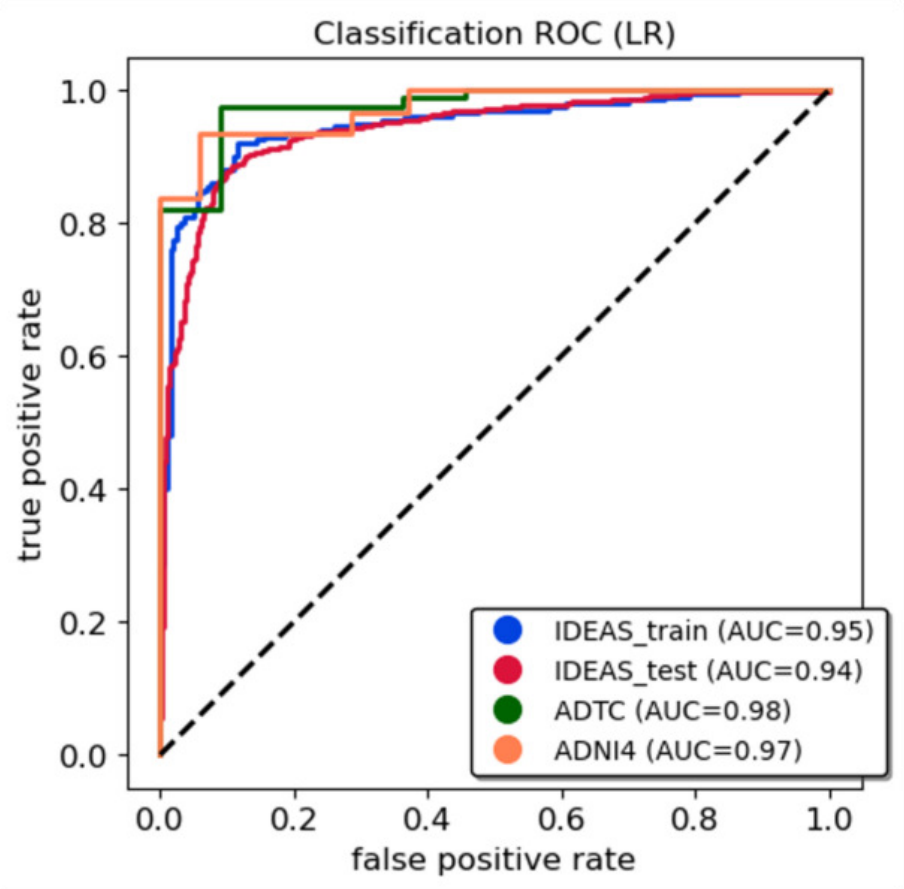


Fig 1. ROC curves of LR model prediction on IDEAS training/testing dataset, ADTC dataset and ADNI4 dataset.

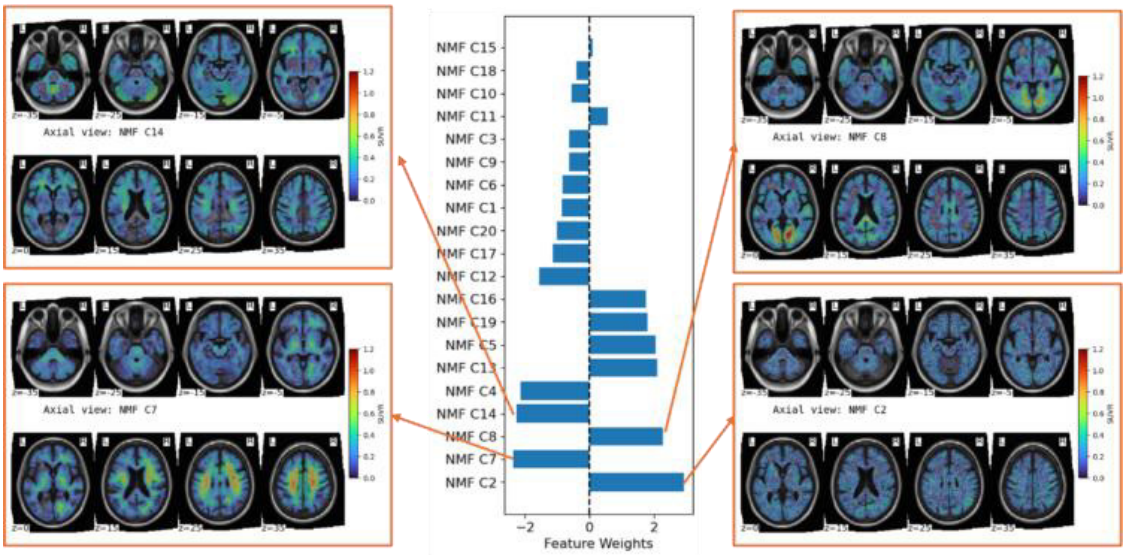


Fig 2. The top 4 NMF components identified by logistic regression. The NMF components are visualized overlaying the T1 image in template space. Left: top 2 NMF components positively correlated to A- prediction. Right: top 2 NMF components positively correlated to A+ prediction. Middle: The weights of all NMF components in LR model.

Keywords: amyloid-PET, interpretable prediction, PET read

60 Data-driven biomarker discovery nominates novel diagnostic plasma biomarkers and provides insights into Alzheimer's disease pathophysiology in an African American cohort

Lindsey Kuchenbecker[1], Kevin Thompson[2], Cheyenne Hurst[1], Bianca Opdenbosch[1], Michael Heckman[3], Joseph Reddy[3], Thuy Nguyen[1], heidi Casellas[1], Katie Sotelo[1], Delila Redy[1], John Lucas[4], Gregory Day[5], Floyd Willis[6], Neill Graff-Radford[5], Niluer Ertekin-Taner[1,5], Krishna Kalari[2], Minerva Carrasquillo[1]

[1]*Department of Neuroscience, Mayo Clinic, Jacksonville, FL, USA, Jacksonville, FL, US*
[2]*Department of Quantitative Health Sciences, Mayo Clinic, Rochester, MN, USA, Rochester, MN, US*
[3]*Department of Quantitative Health Sciences, Mayo Clinic, Jacksonville, FL, USA, Jacksonville, FL, US*
[4]*Department of Psychiatry and Psychology, Mayo Clinic, Jacksonville, FL, USA, Jacksonville, FL, US*
[5]*Department of Neurology, Mayo Clinic, Jacksonville, FL, USA, Jacksonville, FL, US*
[6]*Department of Family Medicine, Mayo Clinic, Jacksonville, FL, USA, Jacksonville, FL, US*

Background: Blood-based biomarker development is of increasing interest due to improved accessibility compared to established diagnostic modalities for Alzheimer's disease (AD). However, current plasma biomarker candidates have not been tested comprehensively in diverse populations, and represent only a fraction of pathways dysregulated in AD. This study seeks to address these knowledge gaps through untargeted plasma biomarker discovery in African Americans (AA), an underrepresented group in AD research despite having a higher risk of developing AD compared to non-Hispanic Whites.

Methods Untargeted proteomics were obtained using the SomaScan 7k assay on plasma samples from AA study participants diagnosed as AD dementia (n=183) or cognitively unimpaired (CU, n=145). Machine learning approaches were implemented to identify an optimal protein panel to discriminate between AD dementia and CU. Predictive models were built using elastic net regression optimized with nested cross-validation on 7,298 proteins and evaluated using the area under the receiver operating curve (AUC). The generalizability of plasma protein predictors was evaluated in non-overlapping plasma and brain proteome datasets.

Results: Thirty-three proteins were identified as predictors. Despite the untargeted selection of predictors, many of these proteins have been linked to core AD pathology and disease-associated pathways, including neuroinflammation, synaptic integrity, and the matrisome. These 33 plasma proteins were able to classify AD dementia versus CU with an AUC of 0.91, a substantial increase compared to a model including age and sex (AUC=0.67). Sixteen of the 33 protein predictors were present in the ANMerge plasma proteomics dataset, and 14/33 predictors were present in the AMP-AD Diverse Cohorts brain proteomics dataset, each achieving AUCs of 0.83 and 0.94 when combined with age, sex, and *APOE*, respectively.

Conclusion: Data-driven biomarker discovery leveraging untargeted proteomics and machine learning identified plasma proteins that could serve as a novel and highly accurate diagnostic plasma biomarker panel for AD in AA.

Keywords: blood-based biomarkers, diagnosis, health disparities, proteomics, machine learning

62 Longitudinal multicenter head-to-head harmonization of tau PET tracers: an overview of the HEAD study cohort

Firoza Lussier[1], Guilherme Povala[1], Guilherme Bauer-Negrini[1], Livia Silva do Amaral[1], Pamela Lukasewicz Ferreira[1], Bruna Bellaver[1], Joseph Masdeu[2], Dana L. Tudorascu[1], David Soleimani-Meigooni[3], Juan Fortea[4], Val Lowe[5], Hwamee Oh[6], Belen Pascual[2], Brian A. Gordon[7], Pedro Rosa-Neto[8], Suzanne Baker[9], Tharick A. Pascoal[1]

[1]*University of Pittsburgh, Pittsburgh, PA, US*
[2]*Houston Methodist Research Institut, Houston, TX, US*
[3]*University of California San Francisco, San Francisco, CA, US*
[4]*Hospital de la Santa Creu i Sant Pau, Barcelona, ES*
[5]*Mayo Clinic, Rochester, MN, US*
[6]*Brown University, Providence, RI, US*
[7]*Washington University in St. Louis, St. Louis, MO, US*
[8]*McGill University, Montreal, QC, CA*
[9]*Lawrence Berkeley National Laboratory, Berkeley, CA, US*

Background: Standardizing tau pathology quantification *in vivo* is challenged by differences in binding characteristics between tau-PET tracers. The HEAD study aims to generate a leading, longitudinal head-to-head dataset of MK-6240, Flortaucipir, RO948, and PI-2620 tau-PET to harmonize tracers' outcomes and develop tools for the generalization of findings across studies and trials.

Methods: The HEAD study comprises nine sites across the US, Canada, and Europe, at which study participants (young/CU/MCI/dementia) undergo tau-PET with at least two tracers, amyloid-PET, MRI, blood collection, and standardized neuropsychological testing, at baseline and 18-month follow-up. PET and MRI acquisition are based on ADNI4 protocols and neuropsychological testing employs the NACC Uniform Data Set. The National Centralized Repository for AD serves as the blood sample biorepository and the Laboratory of Neuroimaging provides a centralized database for imaging/clinical data archiving.

Results: In 24 months (November 2022-October 2024), 594 active study participants were enrolled in HEAD, with 444 (75%) having completed baseline data collection. Mean age of older adults is 71.6 years, and 23% of individuals come from underrepresented groups (race/ethnicity/rurality). Thus far, 1,210 head-to-head tau-PET have been acquired in the HEAD study, using MK-6240, Flortaucipir, PI-2620, and RO948 (mean acquisition window=30.3 days). Over 500 data points of amyloid-PET, MRI, blood, and clinical assessment have additionally been collected (**Fig.1**). Representative cases of head-to-head tau-PET with 4 tracers are shown in **Fig.2**. APOEε4 carriership, plasma biomarkers (Aβ42/40 ratio/NfL/GFAP/PTau217), visual rating of amyloid-PET, and Braak stage classification have been derived from the HEAD cohort, summarized in **Fig.3**.

Conclusions: The HEAD study cohort represents the largest head-to-head tau-PET dataset to date and represents a continued effort in the optimization of AD imaging biomarkers. Results being generated from HEAD study cohort data will provide novel and crucial guidance on the use of tau-PET tracers in research, clinical trials, and prospectively in clinical practice.

Figure 1: The HEAD study cohort

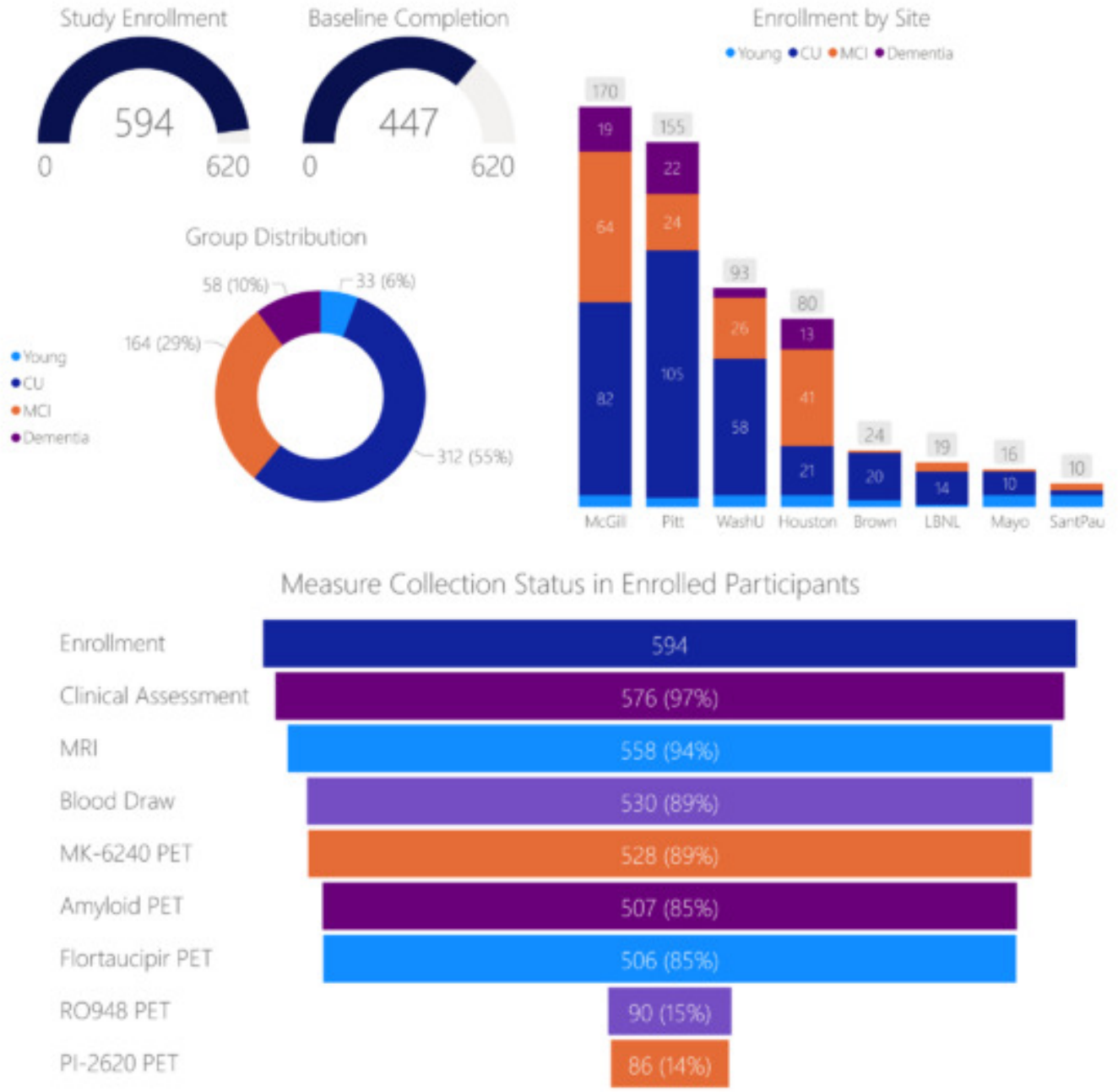


Figure 1: Current progress on building the HEAD study cohort is shown. In 24 months (November 2022 to October 2024), **N=594** active study participants have been enrolled into the HEAD study, with **N=444**, or **75%**, having completed all cross-sectional (baseline) study procedures thus far (top left). Group distribution is shown in the middle left, further characterizing the HEAD cohort as composed of **55%** cognitively unimpaired, **39%** cognitively impaired, and **6%** young healthy control individuals. Study enrollment by performance site is shown on the top right. Data collection in the HEAD study is summarized at the bottom; in just under 24 months, **N=1,210** tau PET scans have been collected in the HEAD study overall (MK-6240, Flortaucipir, PI-2620, RO948) within an average acquisition window between MK-6240 and Flortaucipir PET of 30.3 days. **Over 500 data points** of amyloid-PET, blood samples, and clinical & cognitive assessment have additionally been collected.

Figure 2: HEAD study cases with four head-to-head tau PET

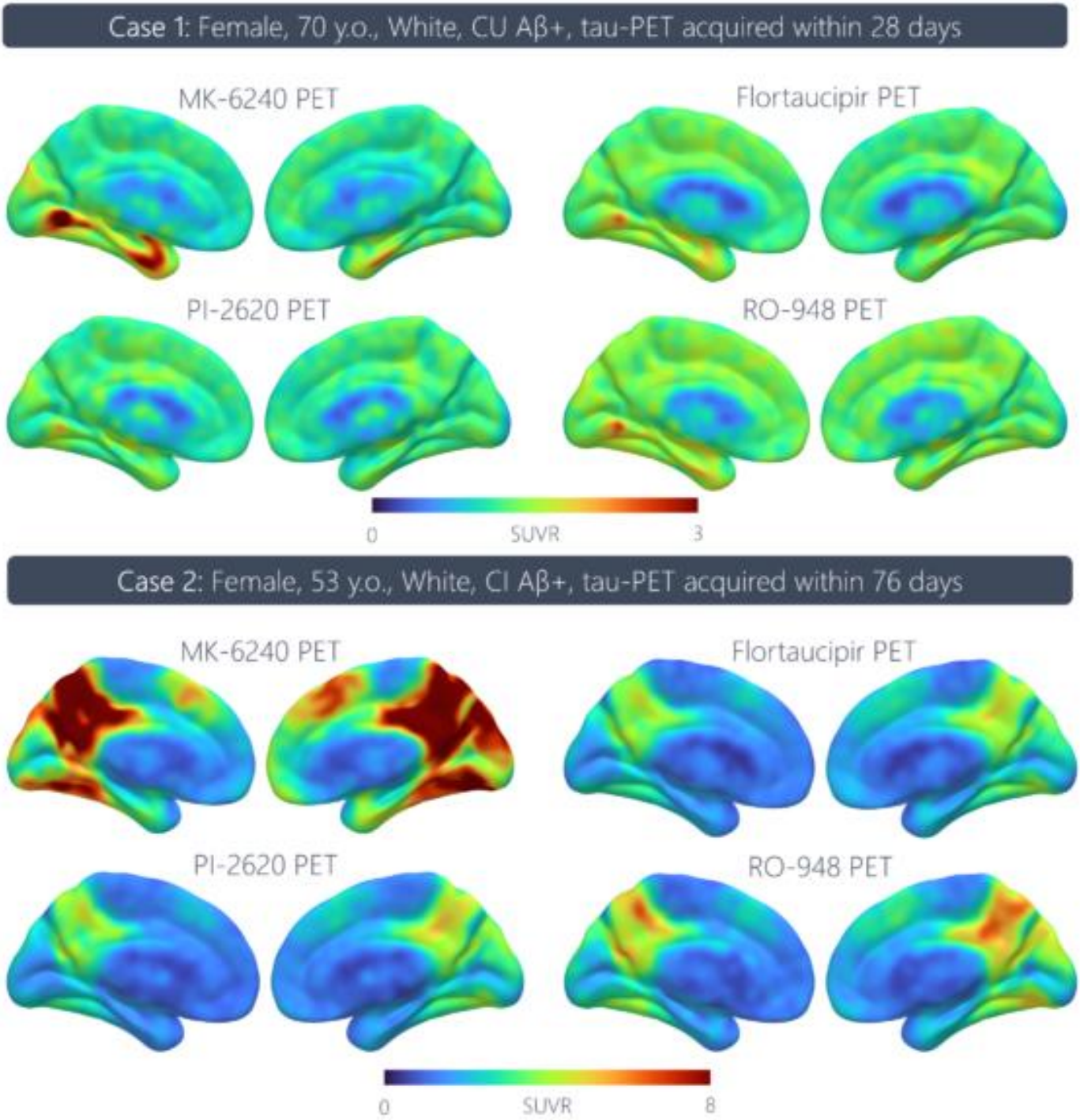


Figure 2: This figure presents some illustrative cases of subjects with head-to-head PET with **4 tau agents acquired in HEAD**. This first case is a 70-year-old CU Aβ+ participant who received tau PET with MK-6240, Flortaucipir, PI-2620, and RO948 within **28 days**. We remark early accumulation of tau pathology in the medial temporal lobe, which importantly is seen in all tracers in this participant. In the second case, a 53-year-old CI Aβ+ participant underwent all 4 tau PET in **76 days**. We observe a much wider spread of tau pathology, and we can see a similar regional distribution of tau PET signal in all 4 tracers. We remark higher uptake in MK-6240 due to its larger dynamic range, with a decreasing intensity in signal observed in this participant in RO-948, PI-2620, and Flortaucipir respectively.

Figure 3: Clinical characteristics of the HEAD study cohort

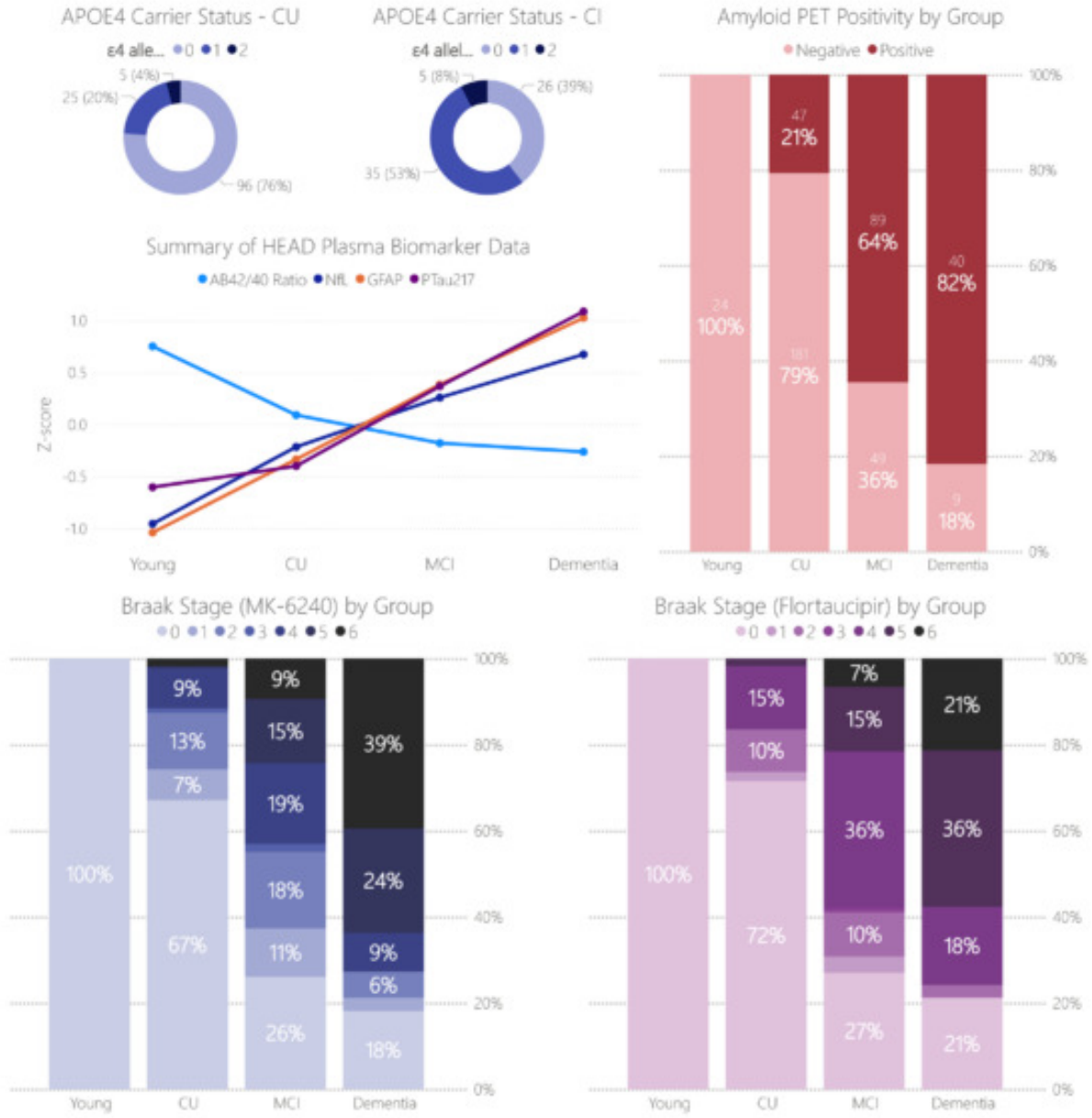


Figure 3: Clinical characteristics of the HEAD study cohort are shown, w.r.t. APOEε4 carrier status, currently measured plasma biomarkers, amyloid-PET positivity from visual rating, and Braak stage classification derived from both MK-6240 and Flortaucipir tau PET. While **24%** of CU individuals are APOEε4 carriers, this increases to **61%** in CI individuals (top left). Plasma AB42/40 ratio, NfL, GFAP, and PTau217 show expected levels across groups, summarized in this figure by z-score (middle left). Visual rating of amyloid-PET shows an increasing rate of positivity from CU (**21%**) to MCI (**64%**) to Dementia (**82%**) participants (top right). Finally, Braak stage classification, using 2.5sd from young controls as a threshold of abnormality, showed similar proportions of individuals classified at Braak stages 1 or above in CU (**~30%**), MCI (**~75%**), and dementia (**~80%**) (bottom).

Keywords: Alzheimer's disease, tau, PET, amyloid, MRI

63 Higher time varying brain functional connectivity is associated with slower tau accumulation at the preclinical stage of Alzheimer's disease

Mohammadali Javanray[1,3], Frédéric St-Onge[1,3], Pierre Bellec[4], Bratislav Misic[1,2,5], Jean-Paul Soucy[1,2,5], Sylvia Villenueve[1,3]

[1]*McGill University, Montreal, QC, CA*
[2]*Montreal Neurological Institute and Hospital, Montreal, QC, CA*
[3]*Douglas Mental Health Research Centre, Montreal, QC, CA*
[4]*Centre de Recherche de l'Institut Universitaire de Gériatrie de Montréal (CRIUGM), Montreal, QC, CA*
[5]*McConnell Brain Imaging Centre, Montreal Neurological Institute and Hospital, McGill University, Montreal, QC, CA*

Background: Amyloid beta (Aβ) and tau accumulations in the brain begin years before clinical symptoms of Alzheimer's disease (AD) emerge, indicating the preclinical stage of AD. The level and accumulation patterns of Aβ and tau have been linked to brain functional connectivity (FC). However, at the AD preclinical stage, studies exhibit inconsistent findings, with both increases and decreases in the FC of resting-state functional networks relative to pathology levels. Given the time-varying nature of FC and its significance for cognition and behavior, Time Varying FC (TVFC) is a candidate for a more sensitive measure of early Aβ and tau accumulation. Accordingly, the relationship of TVFC with Aβ and tau burden and their accumulation at the preclinical phase of AD was assessed.

Methods: Our study focused on 240 cognitively unimpaired individuals at risk of developing AD dementia from the PREVENT-AD cohort with both resting state functional magnetic resonance imaging (rsfMRI) and positron emission tomography (PET). Aβ (NAV4694) and tau (^{18}F-flortaucipir) accumulation were quantified as the average Standardized Uptake Value Ratio (SUVR) within a global ROI and temporal meta-ROI, respectively. TVFC of the Default Mode Network (DMN), limbic and whole brain networks were computed (fig 1), and the relationship of TVFC with cross-sectional levels and longitudinal accumulation rates of Aβ and tau was further assessed.

Results: Higher DMN and whole brain TVFC were associated with slower annual rates of tau accumulation, while no association was observed with Aβ accumulation rate (fig 2). Cross-sectionally, no relationship was observed between Aβ or tau level with TVFC (fig 3).

Conclusion: Our findings highlight the role of time-varying brain FC in relation to Aβ and tau accumulation during the preclinical stage of AD. Greater variability in whole-brain and DMN FC may help slow tau accumulation, emphasizing the significance of TVFC in early AD pathological process.

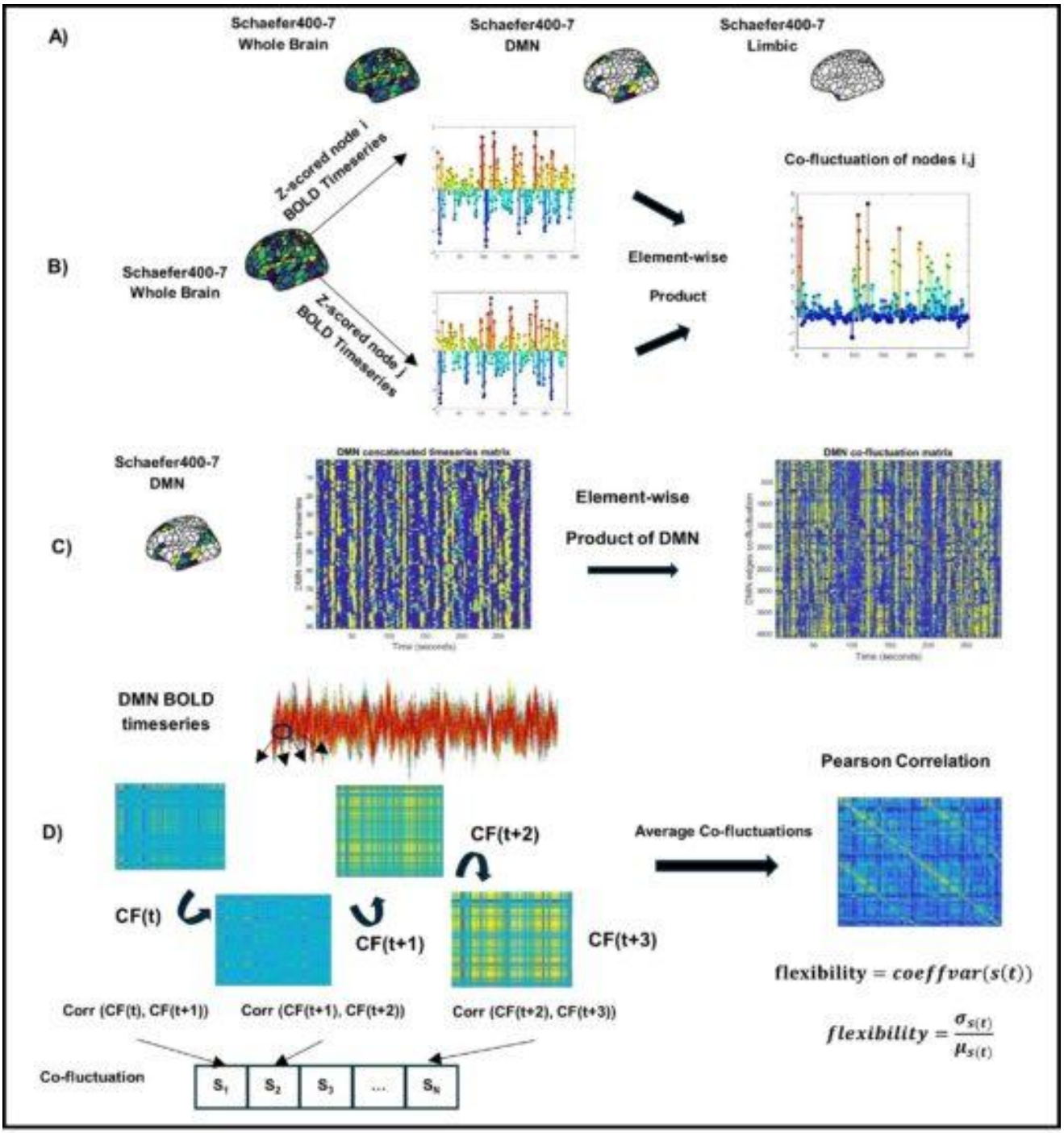


***Figure* 1.** Workflow for computing the proposed Time-Varying Functional Connectivity (TVFC) measure. **A.** The studied networks from the Schaefer 7-400 atlas are shown, including the Default Mode Network (DMN), Limbic, and whole brain networks. **B.** Two nodes from the Schaefer 400-node parcellation were selected to represent possible node pairs among the 400 nodes. For each selected node pair, the element-wise product of the z-scored timeseries is calculated, forming an edge timeseries. This process is repeated for all node pairs within the DMN, limbic, and whole brain networks, generating edge timeseries for each pair. These edge timeseries values, calculated at each time point, form a co-fluctuation matrix for that specific time. **C.** The DMN co-fluctuation matrix formation is shown as an example: First, the z-scored timeseries of all DMN nodes are concatenated. Then, the element-wise product for each timeseries pair is computed, creating a matrix of edge timeseries for each unique DMN node pair. **D.** Four example DMN co-fluctuation matrices are provided to illustrate the TVFC computation. Each co-fluctuation matrix is vectorized, and the Pearson correlation between each pair of consecutive matrices is calculated and stored in a "co-fluctuation similarity vector." The TVFC measure is derived by computing the coefficient of variation of this similarity vector.

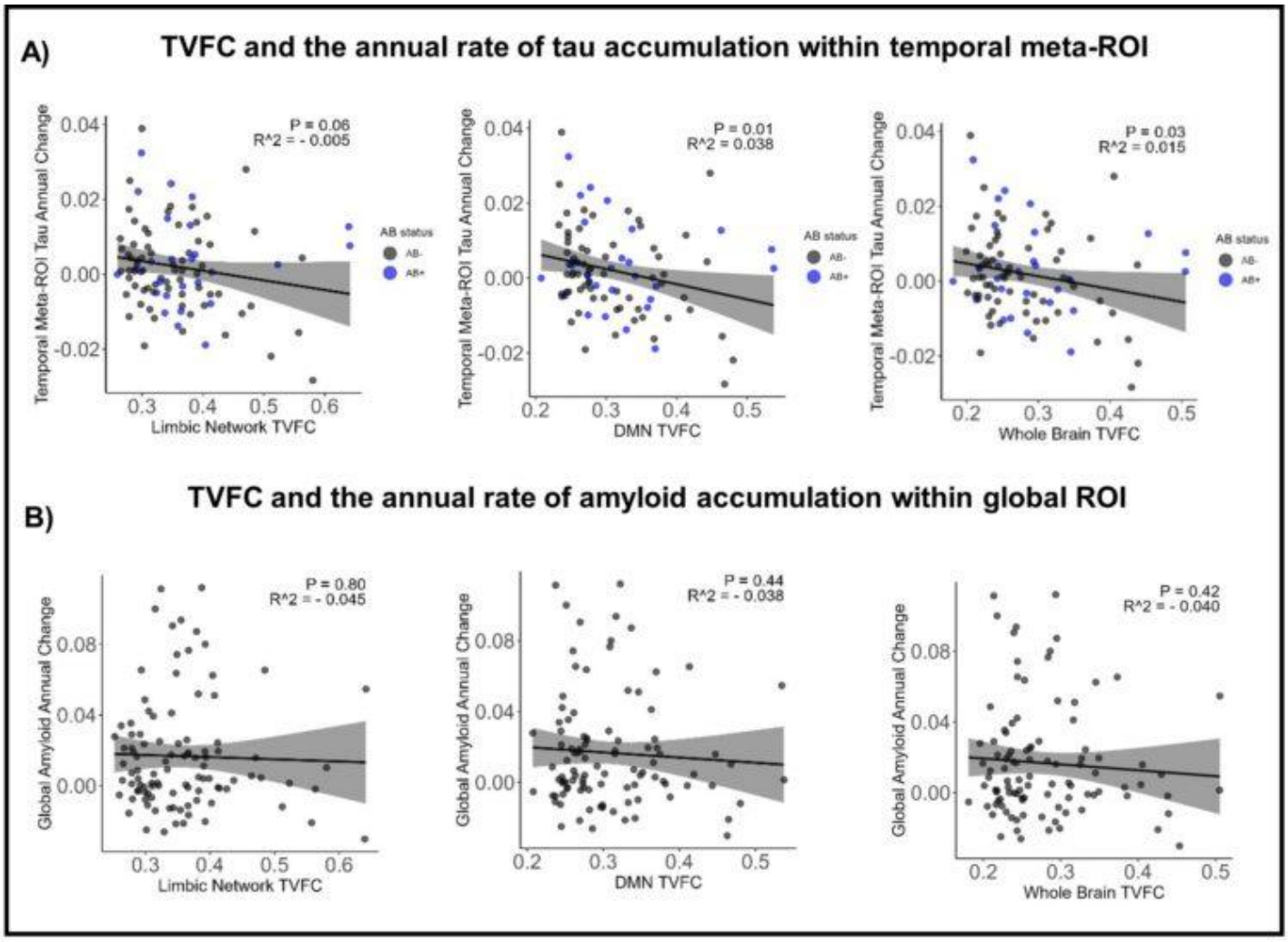


Figure 2. Linear regression models, incorporating age, sex, average framewise displacement (FD), and the time interval between PET and fMRI scans as covariates, were used to assess the relationship between annual changes in global Aβ or tau within the temporal meta-ROI and TVFC in resting-state DMN, Limbic, and whole-brain networks. **A.** Higher TVFC in the DMN and whole-brain networks is associated with a slower annual rate of tau accumulation in the temporal meta-ROI. Individuals are color-coded by their baseline Aβ status, categorized as Aβ+ or Aβ- based on a global amyloid index SUVR threshold of 1.26, determined by Gaussian mixture modeling. **B.** No significant association was observed between annual changes in the global Aβ index and TVFC in the DMN, Limbic, or whole-brain networks.

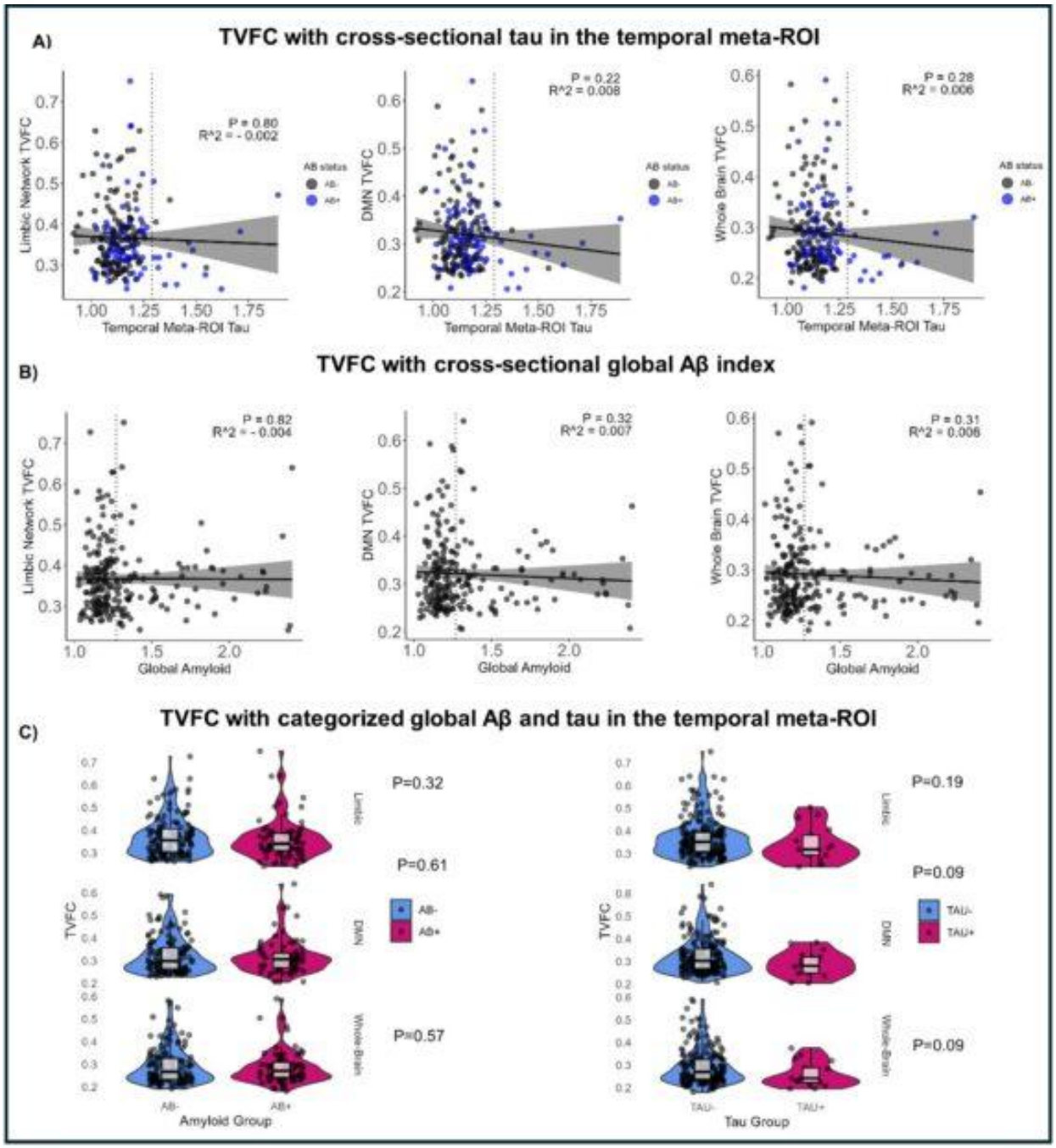


Figure 3. A. Linear regression models examining the relationship between TVFC and tau levels in Limbic, DMN, and whole-brain networks, with age, sex, average FD, and the interval between PET and fMRI scans as covariates. Participants are dichotomized by a 1.29 SUVR threshold for tau in the temporal meta-ROI, indicated by a dotted line, and color-coded by Aβ status, classified using a 1.26 SUVR cutoff. **B.** Linear regression models, including the same covariates as in panel A, assess the relationship between Aβ levels and TVFC across Limbic, DMN, and whole-brain networks. The 1.26 SUVR cutoff for Aβ status is represented by a dotted line. **C.** Violin plots illustrate the distribution of TVFC within the networks of interest. Statistical differences between groups are assessed using ANCOVA tests, with p-values provided for each comparison.

Keywords: Alzheimer's Disease, Time Varying Functional Connectivity, PET, fMRI, Preclinical

64 Graph convolutional networks to predict cognitive decline at the individual level in Alzheimer's disease

Min Su Kang[1,2], Jacquline Heaton[1,2], Alexander J. Nyman[1,2], Mahdi Biparva[1], Melissa McSweeney[1,2], Julie Ottoy[1,2], Mario Masellis[2,3], Zahra Shirzadi[4,5], Keith Johnson[4,5], Reisa Sperling[4,5], Aaron Schultz[4,5], Chhatwal Jasmeer[4,5], Walter Swardfager[2,6], Nir Lipsman[2,7], Sandra E. Black[2,3], Jennifer Rabin[2,3,6], Maged Goubran[1,2,6,8]

[1]*Artificial Intelligence and Computational Neurosciences lab, Sunnybrook Research Institute, University of Toronto, Toronto, ON, CA*
[2]*Hurvitz Brain Sciences Program, Sunnybrook Research Institute, University of Toronto, Toronto, ON, CA*
[3]*Department of Medicine (Division of Neurology), University of Toronto, Toronto, ON, CA*
[4]*Department of Neurology, Massachusetts General Hospital, Harvard Medical School, Boston, MA, US*
[5]*Center for Alzheimer Research and Treatment, Department of Neurology, Brigham and Women's Hospital, Harvard Medical School, Boston, MA, US*
[6]*Department of Pharmacology & Toxicology, University of Toronto, Toronto, ON, CA*
[7]*Harquail Centre for Neuromodulation, Sunnybrook Health Sciences Centre, University of Toronto, Toronto, ON, CA*
[8]*Department of Medical Biophysics, University of Toronto, Toronto, ON, CA*

Background: Cognitive trajectories in Alzheimer's disease (AD) are highly heterogeneous. There is a pressing need to develop biomarker models that predict cognitive trajectories at the individual level. Our goal was to develop advanced deep-learning models to predict cognitive trajectories at the individual level as measured by the Preclinical Alzheimer Cognitive Composite (PACC). We employed graph convolutional networks (GCNs) using multimodal longitudinal biomarkers.

Methods: 597 ADNI participants (245 CN, 252 MCI, 100 AD dementia) and 200 HABS participants (196 CN, 4 MCI) underwent baseline 3T-MRI, Aβ-PET and cognitive assessments. Baseline predictors included demographics (age, sex, education), genetic (APOEe4), cognitive (MMSE, Trails A, Boston naming test and PACC), and imaging variables (Aβ-PET, cortical volume and thickness). The outcome was the longitudinal PACC scores. We trained GCN and GraphSage (a GCN that aggregates features across neighbouring nodes) to predict longitudinal PACC trajectories using 80% of the ADNI data and validated the models in the remaining 20% of ADNI data and the entire HABS dataset. We compared GCNs against a traditional gradient-boosting regressor (GBR).

Results: GraphSage performed the best overall in predicting longitudinal PACC scores with the highest R^2 (GraphSage: 0.89±0.33 vs. GRB: 0.65±0.63) and lowest mean square error (MSE) (**Fig.1**). GraphSage significantly outperformed GBR on both ADNI and HABS ($p<0.02$; **Fig.1**) and maintained high performance with the inclusion of more challenging Aβ- MCI individuals ($p<0.001$; **Fig.2**). Importantly, our model accurately predicted PACC scores at an individual level in the unseen HABS dataset (**Fig1**). Extracted feature importance from the GraphSage model revealed that baseline PACC was the most robust predictor followed by demographics and Aβ-PET features (**Fig.2**).

Conclusion: Our study shows that graph-based models, especially GraphSage, outperform traditional machine learning methods in predicting cognitive decline at the individual level. GCNs promise more accurate and generalizable predictions of *personalized* cognitive trajectories in AD.

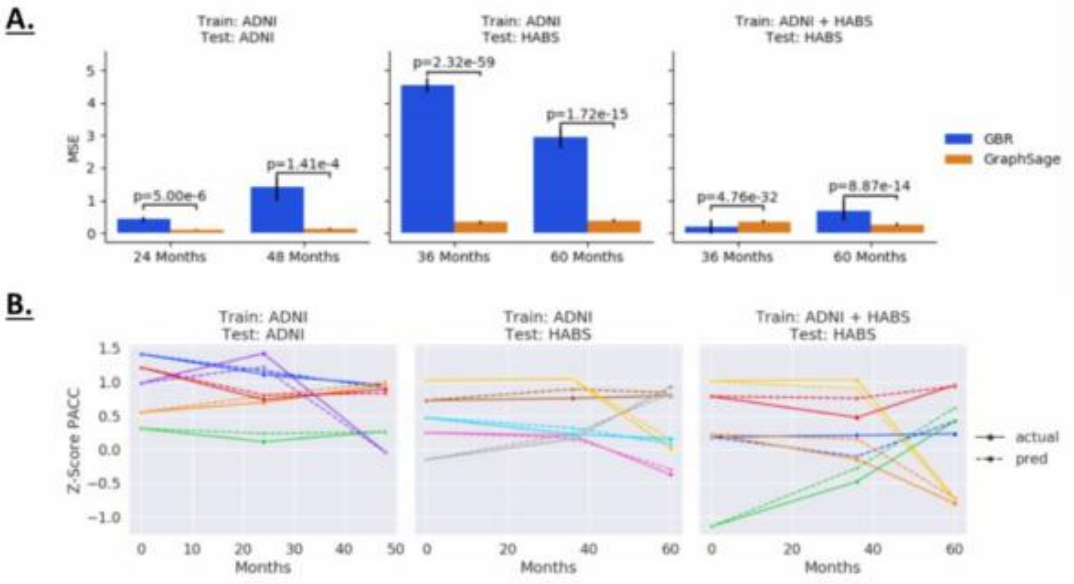


Figure 1. Model performance evaluation and individual-level longitudinal PACC score prediction. A) MSE for GBR (blue) and GraphSage (orange) tested on ADNI at 24 and 48 months, and HABS at 36 and 60 months. The GraphSage model showed significantly lower MSE scores compared to GBR across all time points. B) Individual-level PACC score prediction tested on ADNI or ADNI combined with HABS. The figures show the actual (solid lines, circles) and predicted (dotted lines, squares) trajectories for the five subjects with the lowest prediction error.

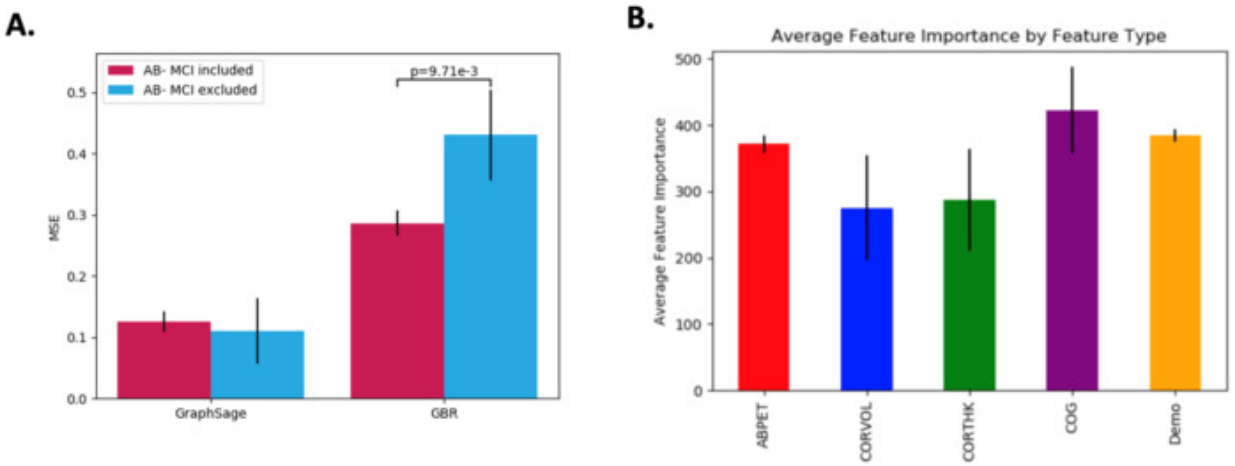


Figure 2. Model stability and feature importance. A) MSE for GBR and GraphSage tested on ADNI with the models trained/tested with and without Aβ-negative MCI patients. The GraphSage MSE scores were not significantly different, while the GBR MSE scores showed a significant difference between the models, suggesting that GraphSage is more stable against more challenging preclinical data. B) The GraphSage feature importance in predicting longitudinal PACC scores when tested in ADNI. The baseline cognitive metrics showed the greatest importance in predicting the future PACC scores, followed by demographics and regional Ab-PET SUVR.

Keywords: personalized longitudinal predictions, cognition, GCNs, machine learning, deep learning

65 Low tau in Aβ-positive cognitively impaired individuals: Alzheimer's disease or something more?

Konstantinos Ioannou[1], Khadidzha Abdullaieva[1], Richard J. Perrin[2], Marina Bluma[1], Konstantinos Poulakis[1], Antoine Leuzy[3,4], Dorota Religa[1,5], Elena Rodriguez-Vieitez[1], Konstantinos Chiotis[1,5,6]

[1]*Karolinska Institutet, Stockholm, SE*
[2]*Washington University, Saint Louis, MO, US*
[3]*University of Gothenburg, Gothenburg, SE*
[4]*Sahlgrenska Academy, Region Västra Götaland, SE*
[5]*Karolinska University Hospital, Stockholm, SE*
[6]*University of California, San Francisco, CA, US*

Aims: This study leverages biomarker and autopsy data with the aim to evaluate the impact of mixed pathologies on interpreting cognitive impairment within the AT biomarker system.

Methods: Individuals with at least one instance of antemortem CSF AD biomarkers measurement (Roche, Elecsys ®) and a full postmortem assessment were identified from the ADNI database. Previously validated cut-offs were used to define A+ (Aβ42≤981 pg/mL) and T+ (p-tau181≥24.3 pg/mL). Aβ PET burden was quantified in-house using the Centiloid pipeline. AT groups were compared with respect to cognitive performance, CSF α-synuclein positivity (Amprion, SYNTap ®), Aβ PET burden, clinical comorbidities, and neuropathological evidence of proteinopathies associated with cognitive impairment or vascular brain injury (VBI). Mixed AD was defined as the copresence of Alzheimer's disease neuropathological change (ADNC) and at least another non-AD proteinopathy at autopsy.

Results: We identified and grouped 77 individuals by AT status (median [IQR] interval from CSF sampling to death=3.13 [1.45, 5.69] years). Both A+T- and A+T+ groups were more severely cognitively impaired than the A-T- group at CSF sampling (Table 1). The A+T- and A+T+ groups had similar demographics, frequency of CSF α-synuclein positivity, Aβ PET burden and frequency of clinical comorbidities. The groups showed differences in APOE4 frequency. The A+T+ group showed a higher frequency of ADNC (100% vs 78%, p-value=0.008) than the A+T- group. When ADNC was present, the A+T- group exhibited a higher frequency of mixed AD (79% vs 28%, p-value=0.002) than the A+T+ group, even when taking VBI into consideration (Figure 1).

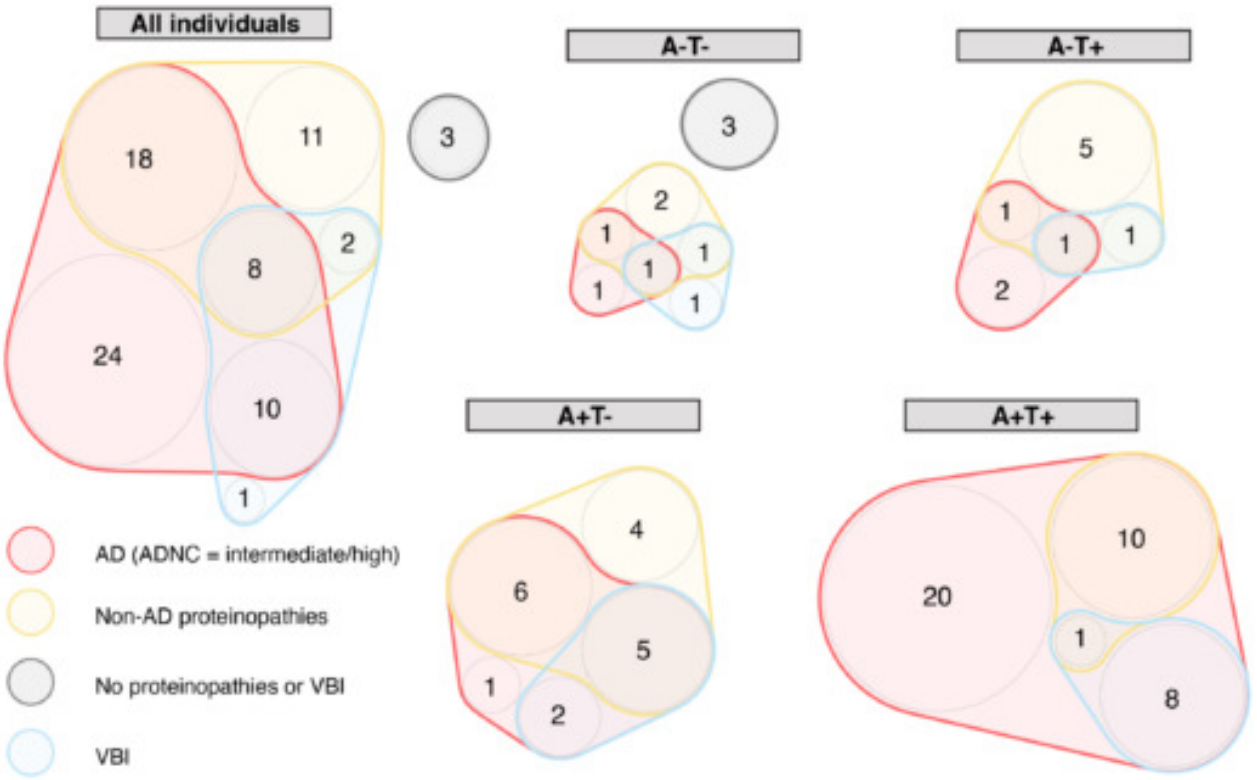
Conclusions: Cognitive impairment associated with Aβ positivity and low tau (A+T-) is linked to mixed AD. These cases deviate from the expected disease path, as proposed by the most recent criteria (Jack CR Jr, et al. Alzheimers Dement. 2024) (Figure 2), and highlight the need for specific biomarkers for non-AD proteinopathies.

Table 1. Demographics, clinical information, and biomarker levels by CSF AT status.

Characteristic	A-T-, N = 10 [1]	A-T+, N = 10 [1]	A+T-, N = 18 [1]	A+T+, N = 39 [1]	p-value [2,3]
Age (y.) [4]	77.5 (72.6, 86.0)	83.0 (80.3, 84.7)	80.5 (76.2, 85.0)	76.3 (73.0, 82.0)	0.2[e]
Sex (Female)	0 / 10 (0%)	5 / 10 (50%)	3 / 18 (17%)	12 / 39 (31%)	**0.042**[a]
Education (y.)	17.5 (15.3, 18.0)	17.0 (14.3, 18.0)	18.0 (16.0, 19.8)	16.0 (15.0, 18.0)	0.5
Presence of APOE4	1 / 10 (10%)	3 / 10 (30%)	4 / 18 (22%)	31 / 39 (79%)	**< 0.001**[c,e,f]
Cognitive status (CI) [4]	5 / 10 (50%)	7 / 10 (70%)	17 / 18 (94%)	38 / 39 (97%)	**< 0.001**[b,c,e]
Neuropsychology [4]					
MMSE	29.0 (28.3, 30.0)	27.0 (26.3, 28.0)	23.0 (20.5, 26.8)	24.0 (19.5, 26.0)	**< 0.001**[a,b,c,e]
Memory score [5]	0.2 (0.0, 1.3)	-0.1 (-0.6, 1.1)	-0.7 (-1.3, 0.4)	-1.1 (-1.5, -0.7)	**< 0.001**[b,c,e]
Biomarkers					
Interval from CSF sampling to death (y.)	3.4 (1.9, 6.4)	1.6 (0.7, 4.7)	2.8 (1.3, 5.7)	3.8 (1.7, 5.2)	0.5
CSF Aβ42 (pg/mL)	1,391.5 (1,230.3, 1,605.8)	2,016.0 (1,061.0, 3,052.3)	480.4 (358.9, 570.6)	540.2 (421.1, 665.9)	**< 0.001**[b,c,d,e]
CSF p-tau181 (pg/mL)	15.6 (13.6, 17.6)	32.8 (30.0, 39.7)	20.4 (17.2, 23.1) [6]	34.3 (28.6, 46.3)	**< 0.001**[a,c,d,f]
CSF α-syn (Type 1) [7]	2 / 9 (22%) [8]	4 / 10 (40%)	9 / 18 (50%)	15 / 39 (38%)	0.8
Aβ PET (CL) [9]	-2.0 (-9.4, 4.8)	-6.8 (-14.6, 61.9)	72.8 (44.8, 85.4)	94.1 (66.8, 113.8)	**< 0.001**[b,c,e]

[1] Median (interquartile range); n / N (%). [2] Kruskal-Wallis rank sum test; Fisher's exact test. [3] a. A-T- vs A-T+; b. A-T- vs A+T-; c. A-T- vs A+T+; d. A-T+ vs A+T-; e. A-T+ vs A+T+; f. A+T- vs A+T+. [4] At the time of CSF sampling. [5] ADNI composite memory score. [6] One A+T- individual was excluded from this statistical analysis due to exceptionally low CSF tau and CSF p-tau181 levels. [7] Positivity Type 1 = αSyn aggregates detected, aggregation profile consistent with Type 1 seeds as seen in Parkinson's disease and Lewy body dementia. [8] One A-T- had no available data for CSF α-syn. [9] Aβ PET scans were available for 51 individuals (A-T-, n = 7; A-T+, n = 6; A+T-, n = 10; A+T+ n = 28). [A-/+ = β-amyloid negativity/positivity, ADNI = Alzheimer's Disease Neuroimaging Initiative, CI = cognitively impaired, CL = centiloids, CSF = cerebrospinal fluid, MMSE = mini mental state examination, PET = positron emission tomography, T-/+ = tau negativity/positivity]

A. Overlap of AD and other pathologies related to cognitive decline



B. Prevalence of AD and other pathologies related to cognitive decline per AT group

Pathologies	A-T- (N = 10) [1]	A-T+ (N = 10) [1]	A+T- (N = 18) [1]	A+T+ (N = 39) [1]	p-value [2,3]
Proteinopathies [4]					
ADNC (intermediate/high)	3 / 10 (30%)	4 / 10 (40%)	14 / 18 (78%)	39 / 39 (100%)	**< 0.001** [b,c,e,f]
LB neocortical (diffuse)	0 / 10 (0%)	2 / 10 (20%)	7 / 18 (39%)	7 / 39 (18%)	0.093 [b]
PSP	1 / 10 (10%)	1 / 10 (10%)	0 / 18 (0%)	0 / 39 (0%)	0.065
AGD	2 / 10 (20%)	6 / 10 (60%)	10 / 18 (56%)	3 / 39 (7.7%)	**< 0.001** [e,f]
FTLD (TDP43)	1 / 10 (10%)	0 / 10 (0%)	1 / 18 (5.6%)	0 / 39 (0%)	0.2
LATE-NC, Stage > 1 + hippocampal sclerosis [5]	0 / 10 (0%)	1 / 9 (11%)	2 / 17 (12%)	1 / 37 (2.7%)	0.2
PART	1 /10 (10%)	2 / 10 (20%)	1 / 18 (5.6%)	0 / 39 (0%)	**0.038** [e]
VBI [4]	3 / 10 (30%)	2 / 10 (20%)	7 / 18 (39%)	9 / 38 (24%) [6]	0.7
Composite neuropathological profile					**< 0.001** [c,e,f]
Pure AD (only ADNC)	1 / 10 (10%)	2 / 10 (20%)	3 / 18 (17%)	28 / 39 (72%)	
Non-AD proteinopathy [7]	3 / 10 (30%)	6 / 10 (60%)	4 / 18 (22%)	0 / 39 (0%)	
Mixed AD (without VBI) [8,9]	2 / 10 (20%)	2 / 10 (20%)	11 / 18 (61%)	11 / 39 (28%)	
Mixed AD as a proportion of ADNC					
Mixed AD (without VBI)/ADNC [8,9]	2 / 3 (67%)	2 / 4 (50%)	11 / 14 (79%)	11 / 39 (28%)	**0.003** [f]
Mixed AD (with VBI)/ADNC [8,10]	2 / 3 (67%)	2 / 4 (50%)	13 / 14 (93%)	19 / 39 (49%)	**0.012** [f]

[1] n / N (%). [2] Fisher's exact test. [3] a. A-T- vs A-T+; b. A-T- vs A+T-; c. A-T- vs A+T+; d. A-T+ vs A+T-; e. A-T+ vs A+T+; f. A+T- vs A+T+. [4] Based on NACC guidelines. [5] Four individuals (A-T+, n = 1; A+T-, n = 1; A+T+ n = 2) did not have data available for either the presence of LATE-NC or hippocampal sclerosis. [6] One A+T+ individual did not have available data regarding the presence of VBI. [7] All proteinopathies except for ADNC. [8] PART was not included in the definition of mixed AD by default. [9] Mixed AD = ADNC + ≥ 1 non-AD proteinopathies related to cognitive decline. [10] Mixed AD = ADNC + ≥ 1 non-AD proteinopathies related to cognitive decline or VBI. [A-/+ = β-amyloid negativity/positivity, AD = Alzheimer's disease, ADNC = AD neuropathologic change, AGD = Argyrophilic grain disease, FTLD = frontotemporal lobar degeneration, LATE-NC = limbic-predominant age-related TDP-43 encephalopathy neuropathologic changes, LB = Lewy bodies, NACC = National Alzheimer's Coordinating Center, PART = primary age-related tauopathy, PSP = progressive supranuclear palsy, T-/+ = tau negativity/positivity, VBI = vascular brain injury].

Figure 1. Presence of overlapping pathologies at autopsy across the AT groups. **A.** Overlap of AD and other pathologies related to cognitive decline. **B.** Prevalence of AD and other pathologies related to cognitive decline per AT group. A+T- individuals had a higher prevalence of mixed pathologies (i.e., mixed AD) compared to A+T+ individuals. The most common co-proteinopathies in A+T- individuals were neocortical LB (39%) and AGD (56%).

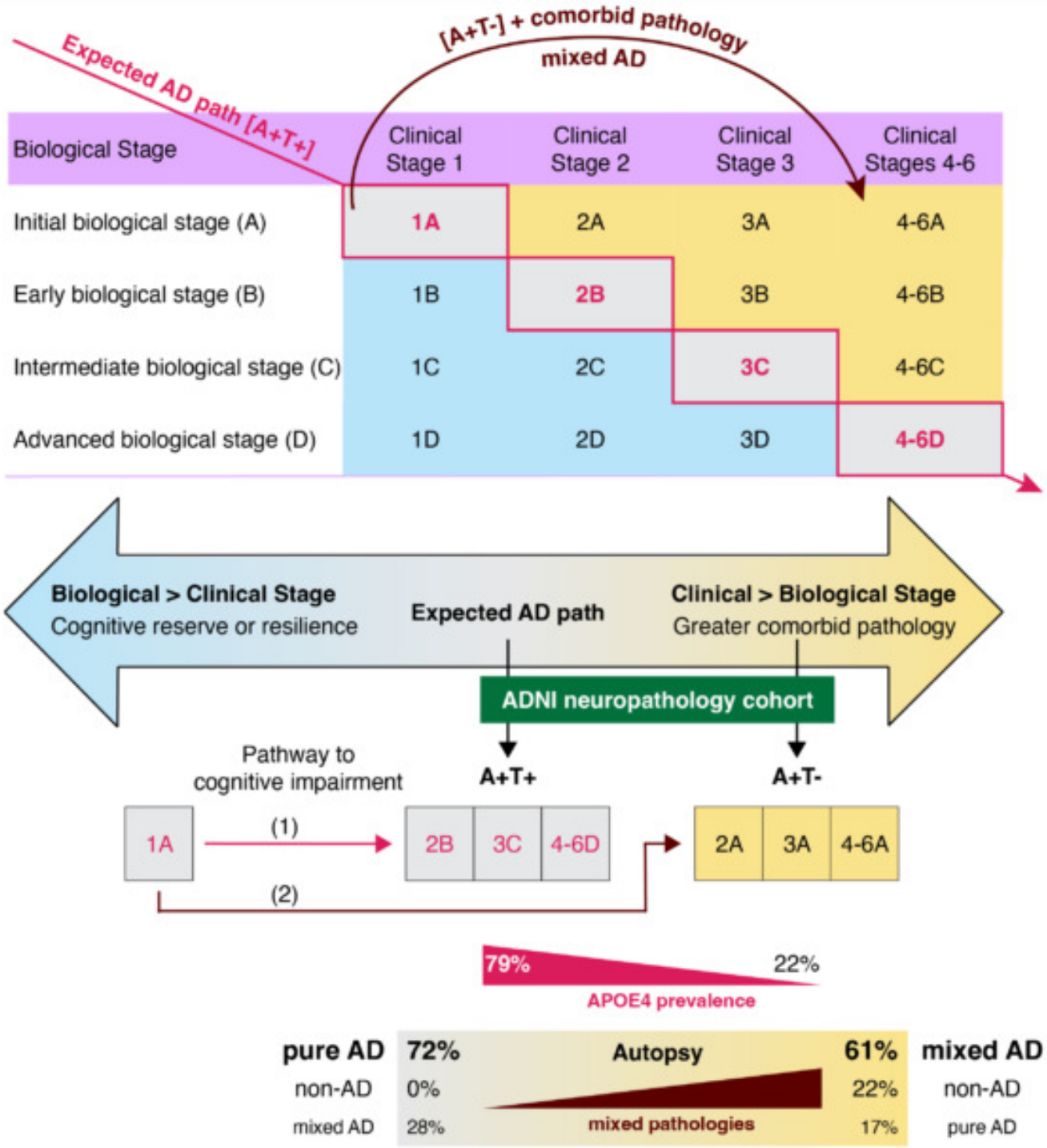


Figure 2. The impact of mixed pathologies on the AT biomarker system with respect to the most recent revised AD criteria (Jack CR Jr, et al. Alzheimers Dement. 2024). The presence of non-AD proteinopathy can influence the clinical interpretation of the AT biomarker system. Cognitively impaired A+T+ individuals have followed the expected AD path (1), but A+T- individuals may have reached severe cognitive impairment through an alternative pathway based on mixed pathologies (2). Mixed AD was defined as the copresence of ADNC and at least one other non-AD proteinopathy related to cognitive decline (VBI is not included here) at autopsy. [A-/+ = β-amyloid negativity/positivity, AD = Alzheimer's disease, ADNC = AD neuropathological change, ADNI = AD neuroimaging initiative,T-/+ = tau negativity/positivity, VBI = vascular brain injury].

Keywords: Alzheimer's disease, mixed pathologies, AT biomarker system

66 A plasma clock for Alzheimer disease based on %p-tau217

Kellen K. Petersen[1], Marta Milà-Alomà[2,3], Duygu Tosun[2,3], Yan Li[1], Leslie M. Shaw[4], Jeffrey L. Dage[5,6], Henrik Zetterberg[7,8,9,10,11,12], Benjamin Saef[1], David M. Holtzman[1], John C. Morris[1], Chengjie Xiong[1,13], Randall J. Bateman[1], Anthony W. Bannon[14], William Z. Potter[15], Suzanne E. Schindler[1]

[1]*Department of Neurology, Washington University in St. Louis, St. Louis, MO, US*
[2]*Northern California Institute for Research and Education, San Francisco, CA, US*
[3]*Department of Radiology and Biomedical Imaging, University of California San Francisco, San Francisco, CA, US*
[4]*Department of Pathology and Laboratory Medicine, Perelman School of Medicine, University of Pennsylvania, Philadelpia, PA, US*
[5]*Department of Neurology, Indiana University School of Medicine, Indianapolis, IN, US*
[6]*Stark Neurosciences Research Institute, Indiana University School of Medicine, Indianapolis, IN, US*
[7]*Institute of Neuroscience and Physiology, Department of Psychiatry and Neurochemistry, The Sahlgrenska Academy at University of Gothenburg, Mölndal, SE*
[8]*Clinical Neurochemistry Laboratory, Sahlgrenska University Hospital, Mölndal, SE*
[9]*UK Dementia Research Institute Fluid Biomarkers Laboratory, UK DRI at UCL, London, GB*
[10]*Department of Neurodegenerative Disease, UCL Queen Square Institute of Neurology, London, GB*
[11]*Hong Kong Center for Neurodegenerative Diseases, Clear Water Bay, Units 1501-1502, 1512-1518, 15/F Building 17W, 17 Science Park W Ave, Science Park, Hong Kong, CN*
[12]*Wisconsin Alzheimer's Disease Research Center, University of Wisconsin School of Medicine and Public Health, University of Wisconsin-Madison, Madison, WI, US*
[13]*Division of Biostatistics, Washington University in St. Louis, St. Louis, MO, US*
[14]*AbbVie, Chicago, IL, US*
[15]*Highly qualified expert, Philadelphia, PA, US*

Background: Amyloid PET-based time proxies have provided valuable insights into the timing of biomarker and clinical changes in Alzheimer disease (AD). However, compared to PET imaging, collection of blood is much more accessible and a "plasma clock" could be very useful.

Methods: Data from individuals in the Knight ADRC and ADNI who had longitudinal plasma %p-tau217 measures were used to create separate plasma clocks. The %p-tau217 measures were transformed into a time scale by integrating the inverse of the modeled rate of change. A %p-tau217 value of 4.06%, which has high correspondence with an amyloid PET Centiloid of 20, was used as time zero for the clock. Plasma clock performance was evaluated using associations between estimated time based on the clock and actual time measures.

Results: Cognitively unimpaired and impaired individuals from the Knight ADRC (n=511) and ADNI (n=392) were included. The rate of change for %p-tau217 was relatively consistent between 1.19-10.37% (**Figure 1**) and was used to develop plasma %p-tau217 clocks (**Figure 2**). The Knight ADRC plasma clock showed strong correlations between estimated and actual time since conversion (i.e., %p-tau217=4.06%) (R2=0.544, Pearson r=0.738), estimated plasma time intervals and actual time intervals (R2=0.327, r=0.575), and estimated and actual age at conversion (R2=0.706, r=0.842). The ADNI plasma clock showed similar correlations between estimated and actual time since conversion (i.e., %p-tau217=4.06%) (R2=0.484, r=0.698), estimated plasma time intervals and actual time intervals (R2=0.301, r=0.551), and estimated and actual age at conversion (R2=0.771, r=0.880) (**Figure 3**).

Conclusion: The %p-tau217 plasma clock exhibits strong associations with actual temporal timeline, suggesting that %p-tau217 may be useful in understanding the time course of AD including biomarker changes and symptom

onset. Plasma clocks may enable a more accessible and cost-effective alternative to amyloid PET-based timelines, with implications for early identification, disease staging, and monitoring of progression for AD.

Figure 1. Generalized Additive Models (GAM) with cubic spline interpolation were used to model the relationship between %p-tau217 rate of change and %p-tau217 level using the data from the Knight ADRC (top row) and ADNI (bottom row). GAMs were used to model the rate of change for the entire range of %p-tau217 values (left). Residual variance across estimated %p-tau217 values were then calculated with the horizontal dashed red line representing the 90th percentile variance cutoff (middle). GAMs were then fit on the restricted range of values (where residual variance was below the 90th percentile variance cutoff for both cohorts (right). For the x-axes, the %p-tau217 value was estimated at the midpoint of the follow-up interval.

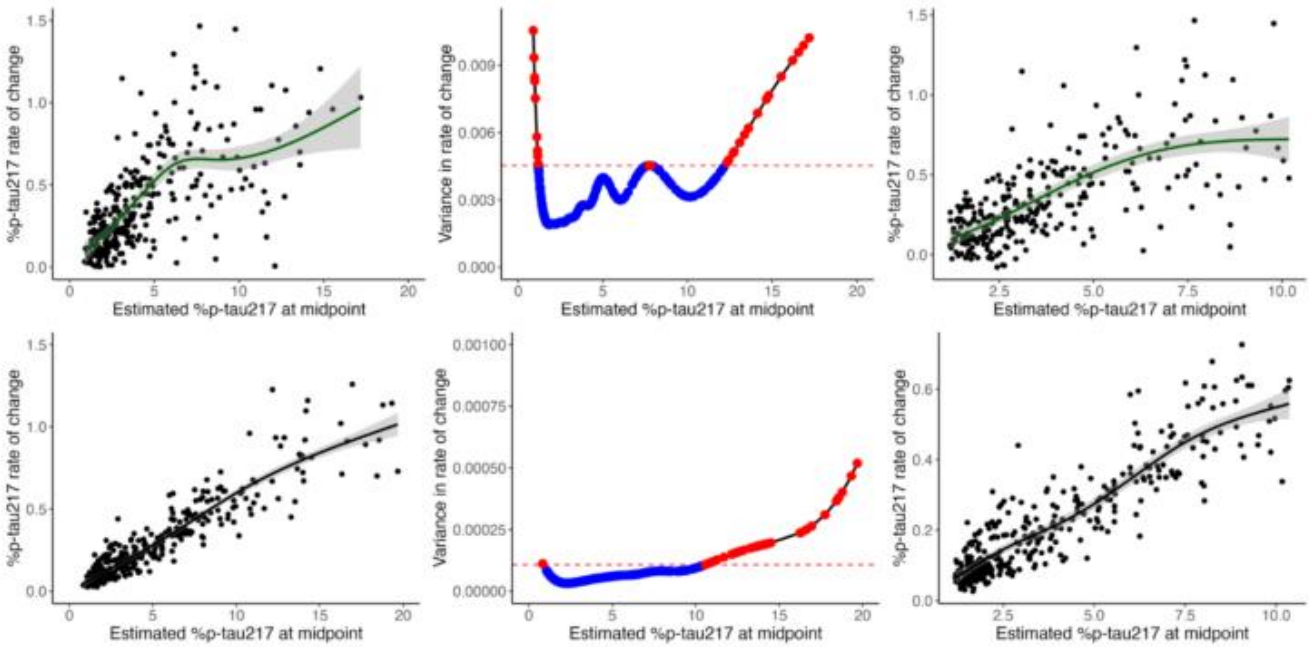


Figure 2. Plasma %p-tau217 trajectories as a function of age (left panels) and estimated time from %p-tau217 positivity (middle panels) for the data from Knight ADRC (top row) and ADNI (bottom row). The "time zero" was set at the %p-tau217=4.06%, which has high correspondence with an amyloid PET Centiloid value of 20. Colors represents global CDR score where blue is 0, yellow is 0.5, and red is ≥1. The right figure depicts plasma clock time for Knight ADRC and ADNI data.

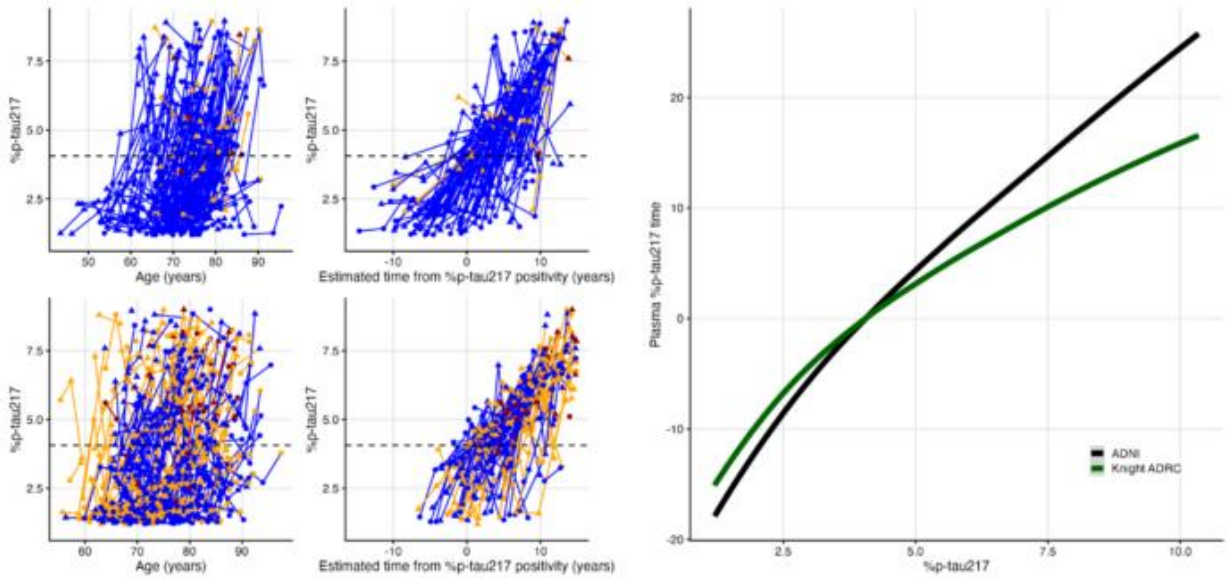
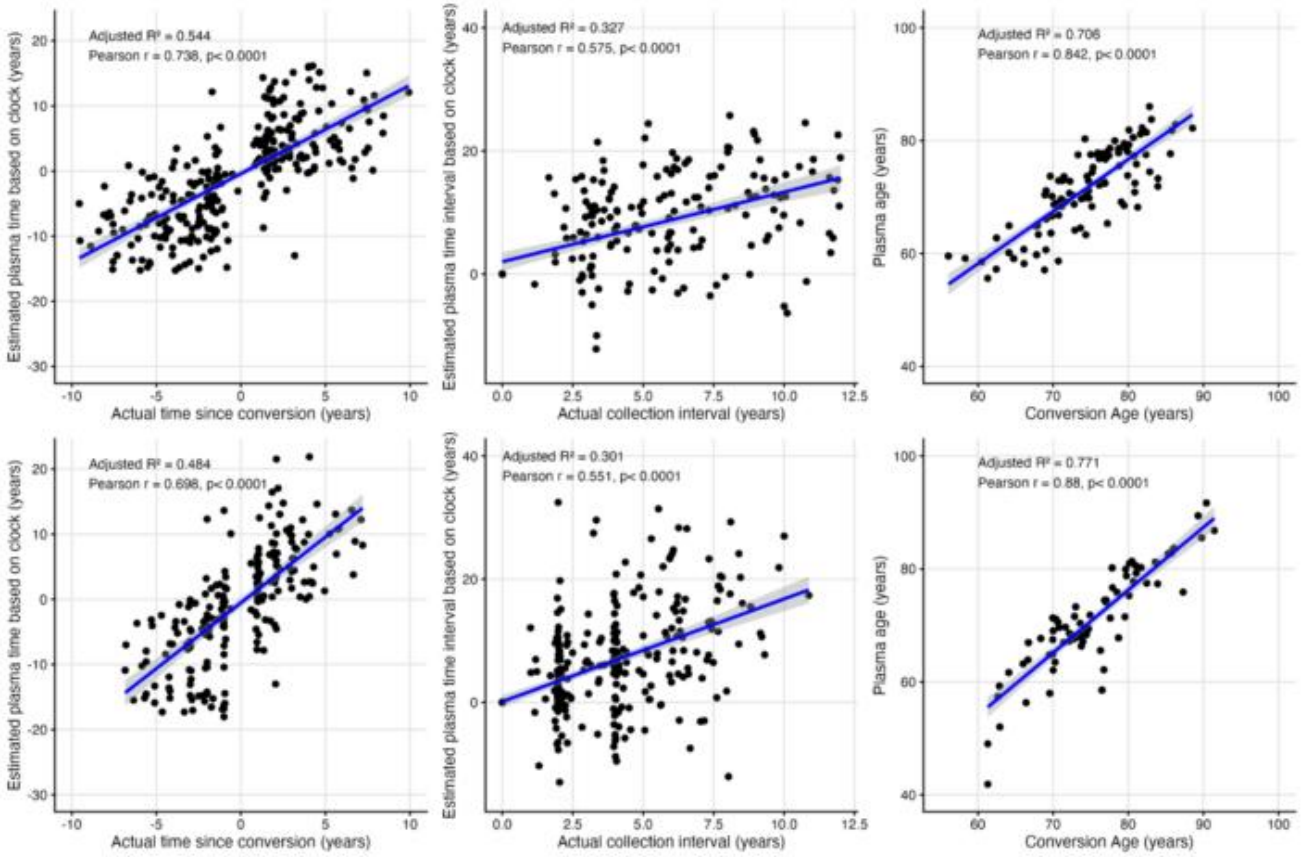


Figure 3. The figure shows results from %p-tau-217 plasma clock models using data from Knight ADRC (top row) and ADNI (bottom row). Moving left to right, panels illustrate the correlation between estimated plasma time and actual time since %p-tau217 positivity conversion, the relationship between estimated plasma time intervals and actual collection intervals, and the correlation between estimated plasma positivity age and actual conversion age. The actual age of conversion was the average of the age at the last negative %p-tau217 and the age at the first positive %p-tau217.



Keywords: p-tau217, plasma biomarkers, disease progression, diagnostics

67 Network-based amyloid-β pathology predicts subsequent cognitive decline in cognitively normal older adults

Hengda He[1], Qolamreza Razlighi[2], Yunglin Gazes[3], Christian Habeck[1,4,5], Yaakov Stern[1,4,5]

[1]*Cognitive Neuroscience Division, Department of Neurology, Columbia University, Vagelos College of Physicians and Surgeons, New York, NY, US*
[2]*Quantitative Neuroimaging Laboratory, Brain Health Imaging Institute, Department of Radiology, Weill Cornell Medicine, New York, NY, US*
[3]*Center for Biomedical Imaging & Neuromodulation, Nathan S. Kline Institute for Psychiatric Research, Orangeburg, NY, US*
[4]*Taub Institute for Research in Alzheimer's Disease and the Aging Brain, Columbia University, New York, NY, US*
[5]*Gertrude H. Sergievsky Center, Columbia University, New York, NY, US*

Background: The deposition of amyloid-β protein in the human brain is a hallmark of Alzheimer's disease and is often related to cognitive decline. However, the relationship between early amyloid-β deposition and future cognitive impairment remains poorly understood, particularly concerning its network-level effects. Here, we employ a cross-validated machine learning approach, and aim to investigate whether integrating subject-specific brain connectome into regional amyloid-β pathology (RAP; standardized uptake value ratio in PET) measures improves predictive validity for cognitive decline.

Methods: Diffusion and resting-state functional MRI were acquired from eighty-five cognitively normal older adults (age 65.56±3.35). We first obtained subject-specific structural connectivity (SC) and functional connectivity (FC)(Fig.1). Then, we developed two network-based amyloid-β pathology (NAP) measures: 1) connectivity-weighted NAP scores quantified both RAP and amyloid-β in all other connected regions, weighted by its connection strength; 2) centrality-scaled NAP scores quantified the RAP in the region scaled by its centrality in the connectivity matrix. Using a cross-validated predictive model (Fig.2), we evaluated the performance of NAP measures in predicting longitudinal cognitive decline in global cognition (4.51±0.68 years follow-up). We compared these results with those from RAP measures that did not include connectome information, and a benchmark model with only connectome measures.

Results: Baseline RAP significantly predicted subsequent cognitive decline (permutation $p<0.05$). Incorporating SC, but not FC, information into pathology measures significantly improved predictive performance (SC: $p<0.01$; FC: $p>0.59$; Fig.3). We further identified a neuropathological signature pattern linked to cognitive decline, involving regions within the default mode, cognitive control, visual, limbic, and salience networks. External validation in the ADNI cohort confirmed the neuropathological signature's association with cognitive decline in delayed memory recall tests, demonstrating its generalizability.

Conclusion: These findings advance our understanding of how amyloid-β pathology relates to brain networks. They highlight the potential of network-based metrics for amyloid-β-PET imaging for identifying individuals at risk for cognitive decline.

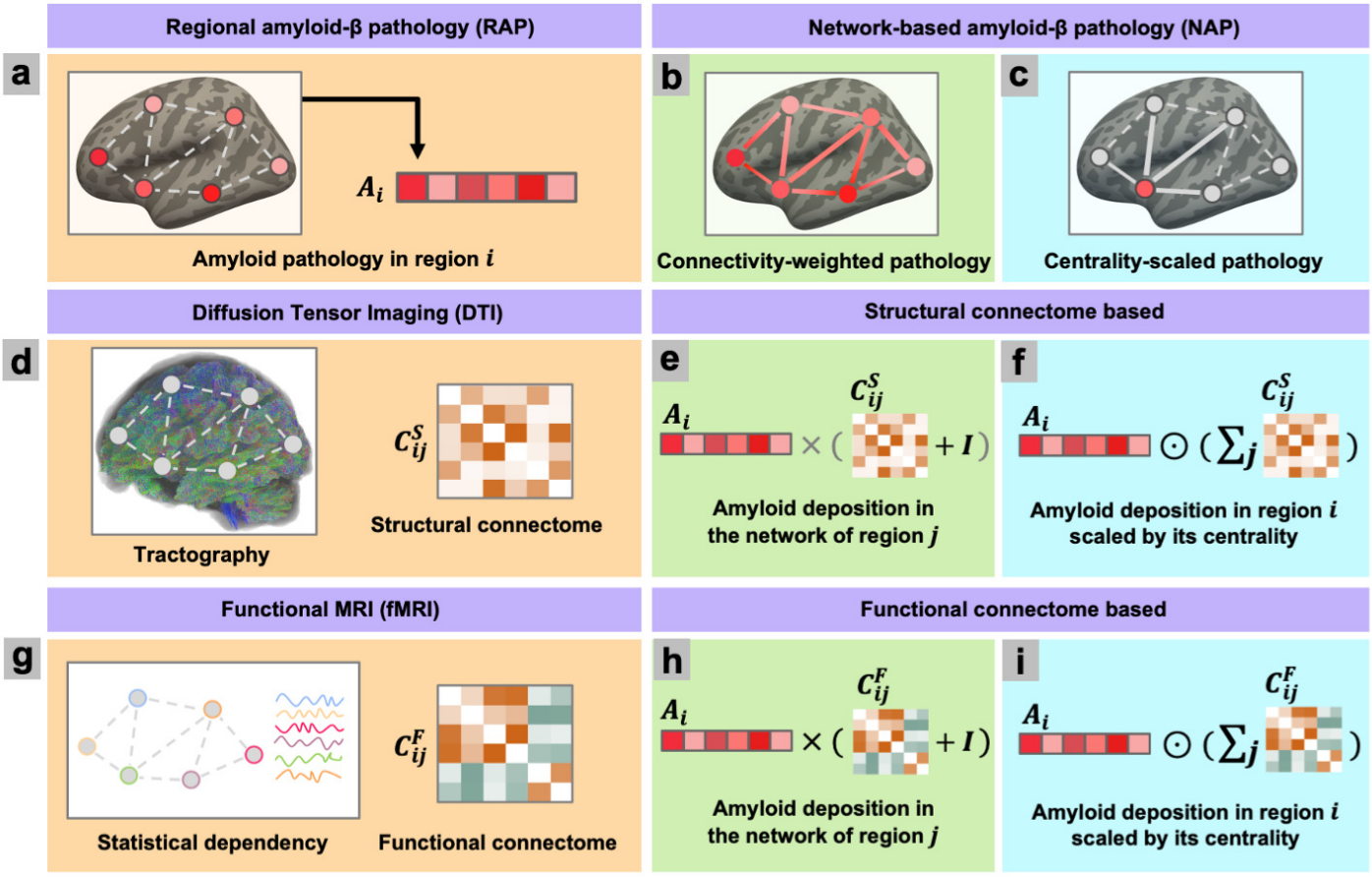


Fig. 1: Regional amyloid-β pathology (RAP) and network-based amyloid-β pathology (NAP). In addition to RAP, the proposed NAP scores incorporate connectome information by using either a connectivity-weighted or centrality-scaled approach. Here, we show a six-region toy network. **a** Illustration of RAP deposition A_i in region i *(i = 1, ..., 6)*. **b** Connectivity-weighted NAP score quantified the influence of Amyloid-β deposition within the connected networks. **c** Centrality-scaled score quantifies the Amyloid-β deposition in the region and scaled it by its centrality in the connectome. Network connectome information can be generated based on either structural connectome (SC) or (**d**) functional connectome (FC) (**g**). **d** SC is derived from tractography on diffusion tensor imaging data. **e** SC based connectivity-weighted NAP score of region j quantifies both the Amyloid-β in region j and a weighed sum of Amyloid-β in all other regions based on connectivity values, where the whole process was denoted as matrix multiplication. **f** SC based centrality-scaled NAP score of region i is quantified by a Hadamard product of RAP measure and connectivity centrality. **g** FC is computed from statistical dependency on functional MRI data. **h, i** For the connectivity-weighted (**h**) and centrality-scaled pathology (**i**), FC based NAP scores are computed the same as SC based approach but with FC.

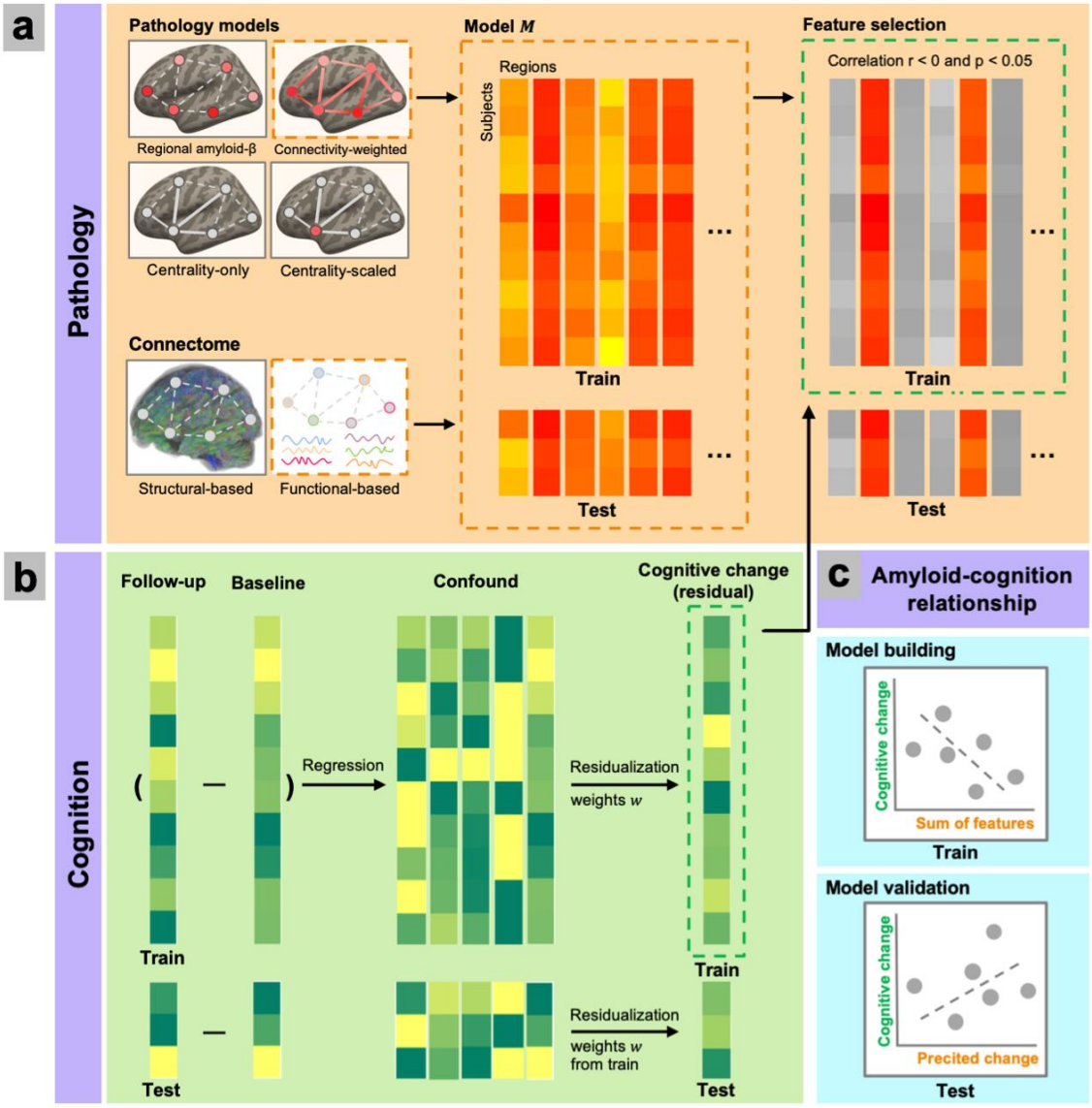


Fig. 2: Cross-validated predictive modeling analysis overview. The figure illustrates an example of using connectivity-weighted network-level amyloid-β pathology (NAP) with functional-based connectome. **a** *Feature selection on the input of pathology models and connectome.* Regional amyloid-β pathology (RAP) or NAP (either connectivity-weighted or centrality-scaled) can be used as input. Individualized network connectomes can be defined based on either structural or functional imaging data. RAP measures do not need the input of connectome information, and the centrality-only model has only connectome information (serving as a benchmark for NAP measures). Since higher pathology is expected to associate with worse cognitive performance, a feature (i.e. regional measures of pathology) is selected if it shows a negative correlation with cognitive change residual score at an uncorrected $p < 0.05$ in the training set. **b** *Computation of longitudinal cognitive change scores.* Subjects are randomly split into a training set and test set. In the training set, we regress out covariate confounds from the longitudinal cognitive change. The covariate-related variability is also removed from the test set using the same weights. **c** *Regression of selected amyloid pathology features in the train set and prediction of cognitive decline in the test set.* The sum of selected features is regressed against cognitive change residual scores from the training sample to obtain model weights. The obtained weights are then applied to the features from test set to predict cognitive decline scores, which were then compared to actual scores to evaluate model prediction performance.

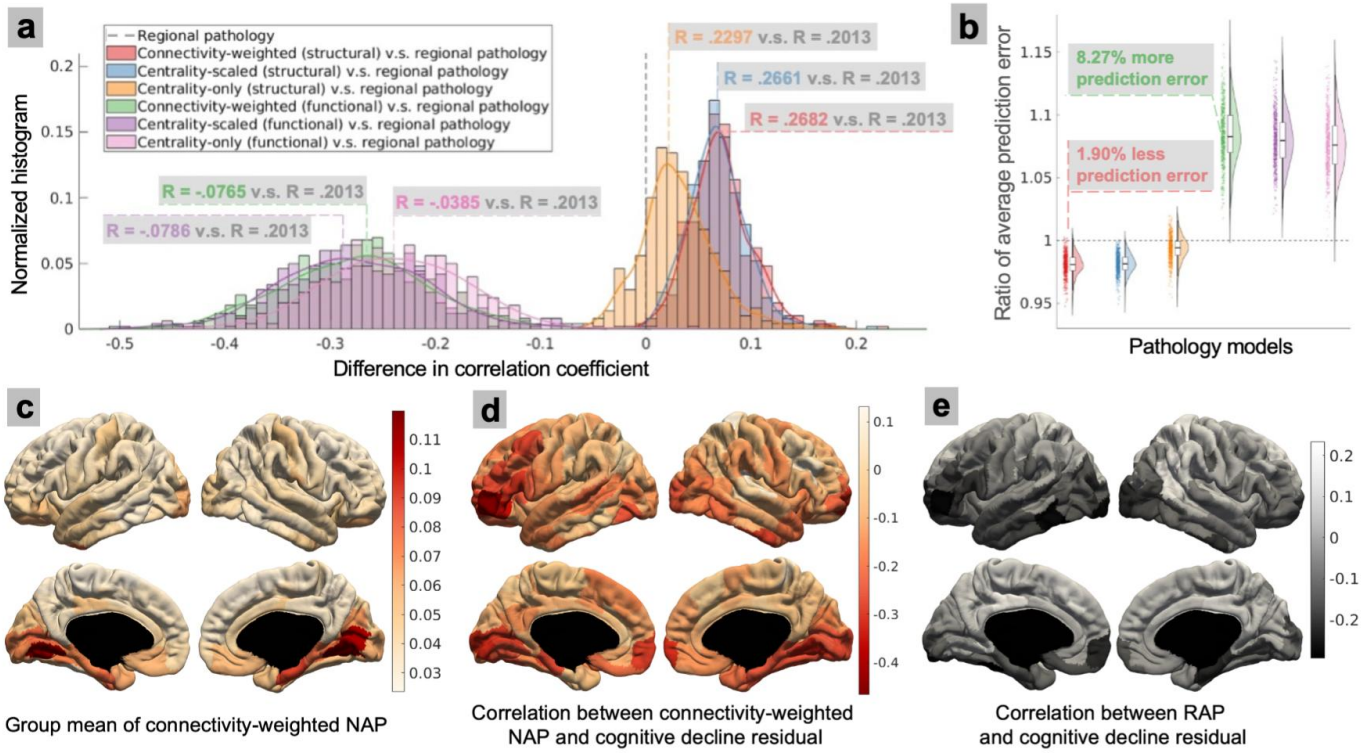


Fig. 3: Performance of cognitive decline predicting using different pathology models across cross-validation repetitions. a Distributions of difference in correlation coefficients between predicted and actual cognitive decline scores across different pathology models. Prediction performance was compared across cross-validation repetitions with regional amyloid-β pathology (RAP) model as the benchmark. Incorporating structural connectome (SC) with connectivity-weighted network-based amyloid-β pathology (NAP) achieved the highest performance (median R = 0.2682), and outperformed ($p < 0.004$; test on difference in correlation coefficients against zero) the prediction performance of RAP measures (median R = 0.2013). **b** Comparison of ratio of average prediction error (*Ratio*) performance between pathology models. Compared to RAP measures, connectivity-weighted NAP measure of SC had *Ratio* = 1.90% less prediction error, whereas connectivity-weighted NAP measures of functional connectome (FC) had *Ratio* = 8.27% more prediction error. **c** Group averaged SC connectivity-weighted NAP scores. **d** Correlation coefficient between cognitive decline and SC connectivity-weighted NAP scores across cortical regions of interest (ROIs) (Spearman partial correlation, controlling for age, sex, education, baseline cognition, and hemispherical mean cortical thickness). **e** Correlation coefficient between cognitive decline and RAP scores across cortical ROIs. NAP scores have higher values in basal cortex regions (**c**). Individual variability in NAP scores in basal cortex regions and the left dorsolateral prefrontal cortex scales with cognitive decline (**d**), showing a stronger negative correlation with subsequent cognitive change compared to RAP scores (**e**).

Keywords: Amyloid-β, cognitive decline, functional MRI, diffusion MRI, connectivity

68 Associations between APOE-TOMM40 '523 haplotype variants and limbic system white matter microstructure in Black and White individuals

Katelyn Mooney[1,2], Derek Archer[3,4,5], Aditi Sathe[3], Timothy Hohman[3,4,6], Ose Kadiri[2], Melissa Lamar[7,8], Konstantinos Arfanakis[7,9,10], Lei Yu[7], Lisa Barnes[7,11], Kacie Deters[2]

[1]*University of California Los Angeles, Neuroscience Interdepartmental Program (NSIDP), David Geffen School of Medicine, Los Angeles, CA, USA., Los Angeles, CA, US*
[2]*University of California Los Angeles, Department of Integrative Biology and Physiology, Los Angeles, CA, USA., Los Angeles, CA, US*
[3]*Vanderbilt Memory and Alzheimer's Center, Vanderbilt University Medical Center, Nashville, TN, USA., Nashville, TN, US*
[4]*Department of Neurology, Vanderbilt University Medical Center, Nashville, TN, USA., Nashville, TN, US*
[5]*Vanderbilt Genetics Institute, Vanderbilt University School of Medicine, Nashville, TN, USA., Nashville, TN, US*
[6]*Vanderbilt Department of Pharmacology, Vanderbilt University Medical Center, Nashville, TN, USA., Nashville, TN, US*
[7]*Rush Alzheimer's Disease Center, Rush University Medical Center, Chicago, USA., Chicago, IL, US*
[8]*Department of Psychiatry and Behavioral Sciences, Rush University Medical Center, Chicago, USA, Chicago, IL, US*
[9]*Department of Biomedical Engineering, Illinois Institute of Technology, Chicago, IL, USA, Chicago, IL, US*
[10]*Department of Diagnostic Radiology and Nuclear Medicine, Rush University Medical Center, Chicago, IL, USA, Chicago, IL, US*
[11]*Departments of Neurological Sciences, and Psychiatry and Behavioral Sciences, Rush University Medical Center, Chicago, USA, Chicago, IL, US*

Background: APOE-TOMM40-'523 haplotype variants influence cognitive decline, where Black APOE-ε3-'523-S carriers experience faster decline, but Black APOE-ε4-'523-S carriers show slower decline. Little is known about how APOE-TOMM40-'523 haplotypes are associated with brain microstructure, which is particularly important as such changes may precede cognitive impairment. This study examines associations between APOE-TOMM40-'523 haplotypes and white matter microstructure (WMM) in limbic tracts involved in memory and cognition in non-Hispanic Black and White individuals.

Methods: Non-Hispanic-White (N=500) and non-Hispanic-Black (N=144) participants from the Rush Memory and Aging Project and Minority Aging Research Study were included. WMM was measured via diffusion MRI (dMRI), preprocessed with PreQual, and analyzed using DTIFIT and MATLAB. Data was harmonized using Longitudinal ComBat. Free-water (FW) and FW-corrected fractional anisotropy (FA_{FWcorr}) were assessed in five limbic tracts, including the cingulum bundle, uncinate fasciculus, fornix, inferior longitudinal fasciculus, and inferior temporal gyrus transcallosal tract. TOMM40-'523-S copy-number associations with FW and FA_{FWcorr} were analyzed via linear regression models, stratified by APOE and racialized group, adjusting for age, sex/gender, education, and clinical diagnosis.

Results: Black-ε4+-one-'523-S carriers had lower FW in the cingulum and inferior longitudinal fasciculus compared to Black-ε4+-no-'523-S carriers. They also had lower FW in the cingulum, uncinate, and fornix, and higher FA_{FWcorr} in the uncinate compared to Black-ε4+-'523-S/S carriers. White-ε3/ε3-'523-S/S carriers had lower FA_{FWcorr} in the cingulum and inferior temporal gyrus compared to White-ε3/ε3-no-'523-S carriers, and lower FA_{FWcorr} in the cingulum compared to White-ε3/ε3-one-'523-S carriers.

Conclusion: This is the first study examining APOE-TOMM40-'523 on WMM in Black participants, and the first to use FW-corrected metrics. Results support that '523-S is deleterious in White-ε3/ε3 carriers but protective in Black-ε4+ carriers, indicating a differential effect of APOE on brain integrity by racialized background.

Figure 1. Plot of '523-S Copy Number and WMM Metrics across Limbic System Tracts in non-Hispanic Black ε4+ participants, with limbic tracts residualized by age, sex, education, and clinical diagnosis. P-values < 0.05 are shown with *, p-values < 0.01 are shown with **.

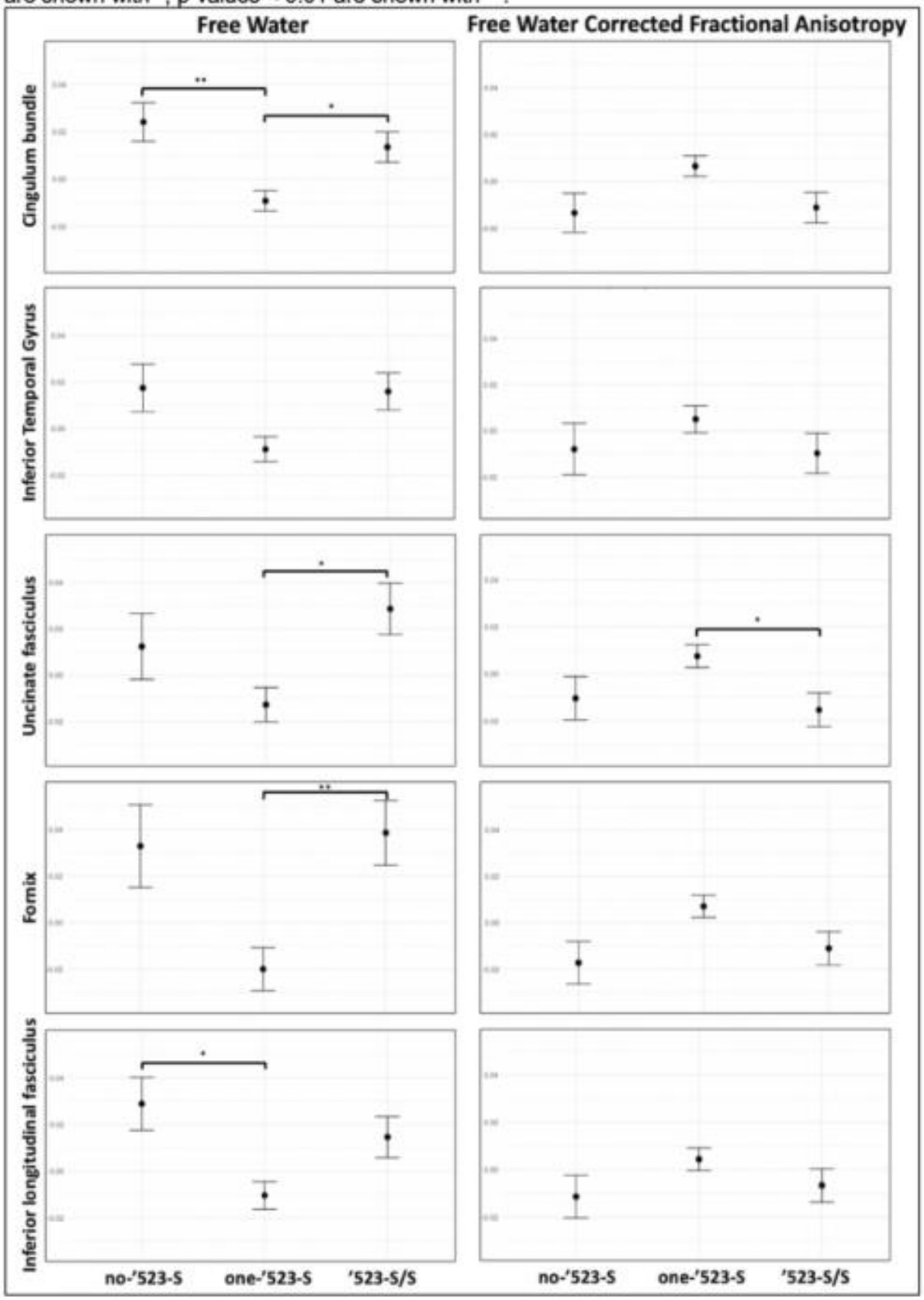
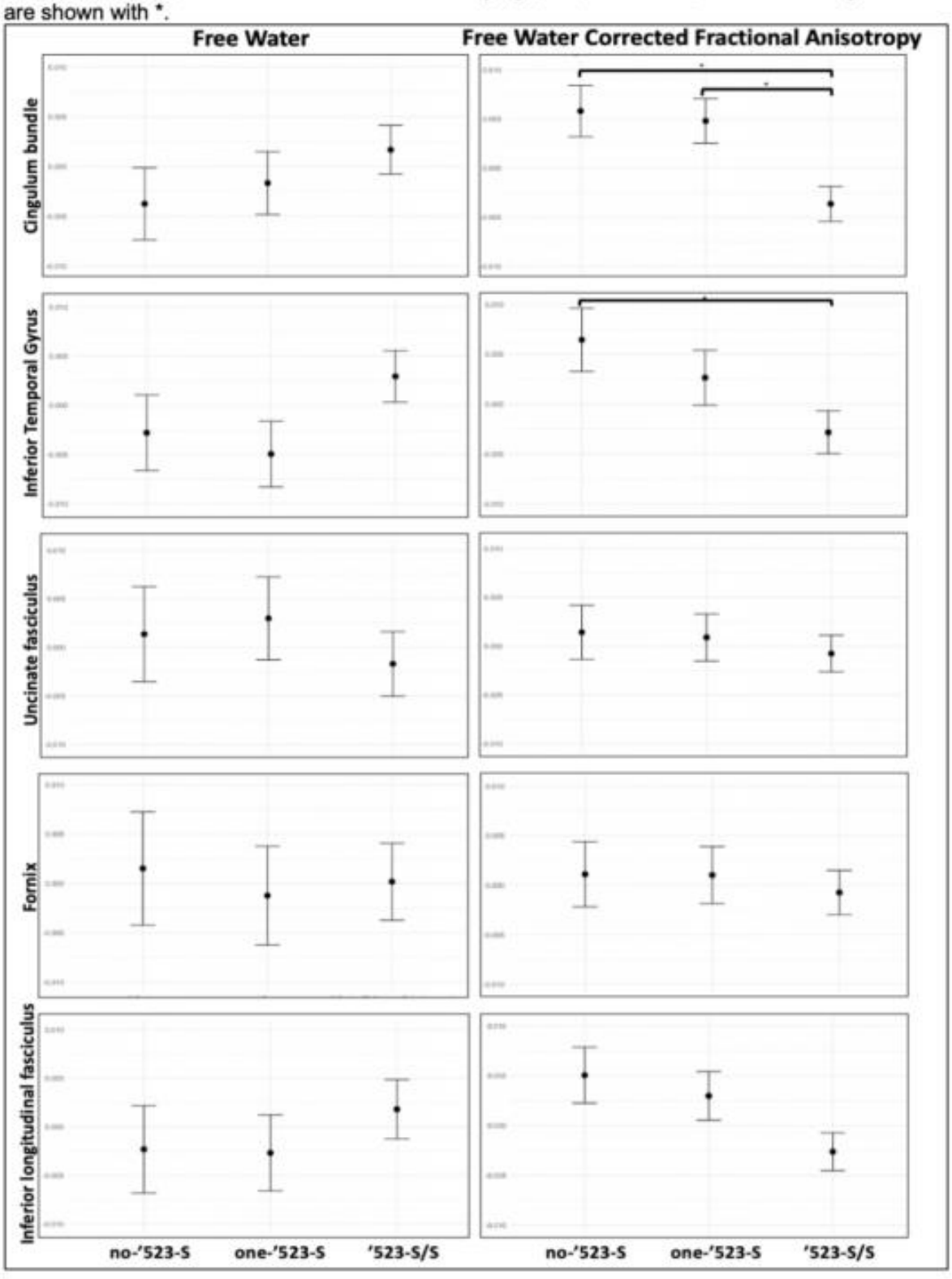


Figure 2. Plot of '523-S Copy Number and WMM Metrics across Limbic System Tracts in non-Hispanic White ε3/ε3 participants, with limbic tracts residualized by age, sex, education, and clinical diagnosis. P-values < 0.05 are shown with *.



Keywords: Diffusion MRI, FW-corrected metrics, Aging, Genetics, Health disparities

69 Multi element MRI template method for analysis of Down syndrome PET

Charles Laymon[1], Davneet Minhas[1], Jaiden Heffley[1], Ally Gilmore[1], Ritvik Kondaveeti[1], Alexandra Gogola[1], Sarah Royse[1], Sai Sravanthi Joshi[1], Brian Lopresti[1], Weiquan Luo[1], Hitesh Davuluri[1], Cristy Matan[1], Dana Tudorascu[1], Bradley Christian[2], Shahid Zaman[3], Ances Beau[4], Ann Cohen[1], Benjamin Handen[1]

[1]*University of Pittsburgh, Pittsburgh, PA, US*
[2]*University of Wisconsin, Madison, MI, US*
[3]*University of Cambridge, Cambridge, GB*
[4]*Washington University, St. Louis, MO, US*

Background: A component of the Alzheimer's Biomarkers Consortium-Down Syndrome (ABC-DS) is tau brain PET. A common analysis method is tracer quantification through application of a subject-space atlas of regions-of-interest (ROIs) determined by parcellating each subject's T1-MR scan using FreeSurfer (FS). There are drawbacks associated with this for Down Syndrome (DS) subjects who exhibit variations in anatomy from FS-atlas priors and are prone to motion during MR acquisition. We evaluate a multi-element template (MET), DS-specific approach for improving results.

Method: In the standard analysis, ABC-DS MR scans were processed through the FS (5.3) pipeline. Parcellation results (atlases) were evaluated by experienced analysts and usually edited to increase conformity with anatomy. The final atlas was either accepted or rejected.

For the MET analysis twelve MR scans (10-DS subjects, 2 controls) were chosen as MR templates based on the quality of their final FS-based atlas from the standard analysis. Subject processing consisted of warping all template MRs to the subject MR using an ANTs-based pipeline and then co-warping each of the 12 associated atlases resulting in the assignment of 12 regional labels to every voxel. A MET atlas for each subject was produced by assigning final voxel labels based on the plurality of template labels. Final MET atlases were accepted or rejected based on ***unedited*** results.

For subjects with acceptable final FS and MET atlases, [^{18}F]AV1451 was sampled using ROIs from both methods and results were compared.

Result: Out of 330 MRs, standard processing resulted in 53 unacceptable atlases whereas the MET processing resulted in 9. Correlation of [^{18}F]AV1451 SUVR between the two methods was high (Figure 1).

Conclusion: Unedited MET is frequently able to provide parcellations for cases in which edited FreeSurfer fails. High correlation between AV1451 measures from the two pipelines suggests that the methods can be used interchangeably.

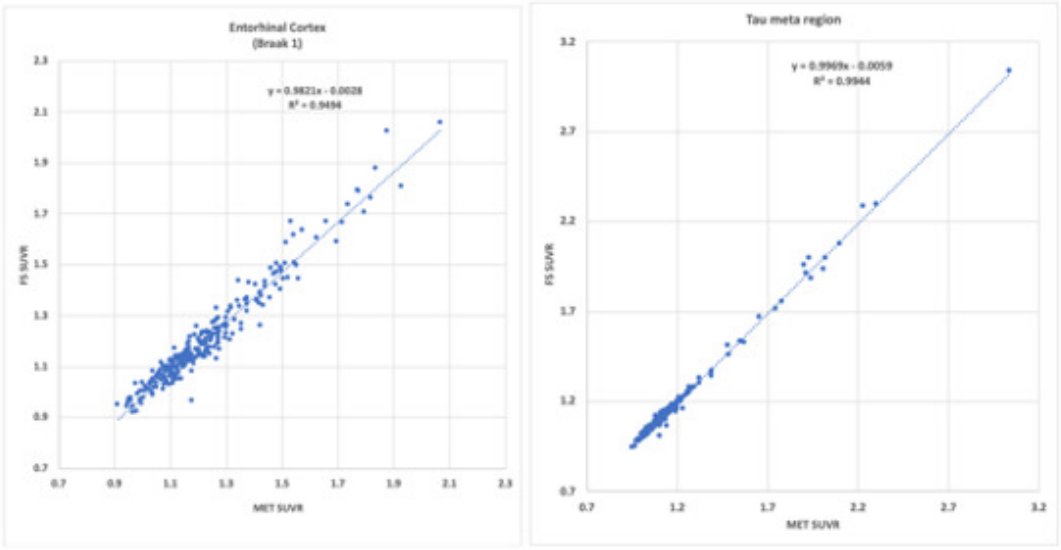


Figure 1. Correlation between AV1451 SUVR using gray matter as reference determined using the FreeSurfer pipeline and MET pipeline for (left) entorhinal cortex, a region of early tau deposition and (right) a tau meta region.

Keywords: Image processing, Down Syndrome, PET

70 Whole-blood gene expression associations with Aβ-PET accumulation and cognitive decline

Hannah M Klinger[1], Vaibhav A Janve[2], Mabel Seto[1,3], Jane A Brown[1], Colin Birkenbihl[1], Gillian Coughlan[1], Diana L Townsend[1], Jane Zyski[2], Ting-Chen Wang[2], Rebecca E Amariglio[3], Kathryn V Papp[3], Dorene M Rentz[3], Hyun-Sik Yang[3], Jasmeer Chhatwal[1], Michelle Clifton[2], Michael C Donohue[4], Rema Raman[4], Robert A Rissman[4], Paul Aisen[4], Keith A Johnson[1], Reisa Sperling[1,3], Logan Dumitrescu[2], Timothy Hohman[2], Rachel Buckley[1]

[1]*Massachusetts General Hospital/Harvard Medical School, Boston, MA, US*
[2]*Vanderbilt Memory & Alzheimer's Center, Vanderbilt University Medical Center, Nashville, TN, US*
[3]*Brigham and Women's Hospital, Boston, MA, US*
[4]*Alzheimer's Therapeutic Research Institute, University of Southern California, San Diego, CA, US*

Objective: Bulk brain-tissue studies of gene expression have discovered novel biological pathways associated with AD neuropathology and pre-morbid cognitive decline. However, these findings are primarily tuned to much older adults and are focused on end-of-life changes. The objective of this study was to ascertain transcriptomic signals from whole-blood associated with Aβ-PET accumulation and cognitive decline in clinically unimpaired older adults from the A4/LEARN studies. Identifying genes in whole-blood that are associated with these *in vivo* AD phenotypes can elucidate biological pathways implicated in these earliest disease processes.

Methods: We selected 1,737 participants ($N_{longitudinal}$=770; 71years(±4.7); 63% Female; 35% *APOE*ε4; 26% Aβ+) from the A4 clinical trial placebo and treatment arms (and screen fail at baseline) and the adjoining LEARN observational study who had Aβ-PET (^{18}F-Florbetapir), cognitive assessments (using PACC), and whole-blood gene expression data from the autosome and X chromosome (20,621 genes) available. Linear mixed-effects models determined the association between gene expression alone and the interactions with sex, *APOE*ε4, and $Aβ_{continuous}$ on longitudinal Aβ-PET and PACC. All analyses included random intercepts/slopes, and is adjusted for age, education level, cohort, and story version. Analyses were FDR corrected.

Results: A SAT1-DT**APOE*ε4 interaction, from a long non-coding (lnc) RNA, was found to weakly associate with Aβ-PET accumulation (Fig.1A & Fig.2A; b=-0.008(0.002),p_{FDR}=0.024). For PACC decline, one gene (TRBV4-2) was moderated by *APOE*ε4*sex, 21 genes by Aβ, and 128 genes by Aβ*sex (Fig.1B-D). Select analyses revealed that lower *ETF1P2* expression, another lncRNA, and higher baseline Aβ was associated with faster cognitive decline (Fig.2B; b_{INT}=2.38(0.5),p_{FDR}=0.003). Lower *ZSCAN2*, implicated in regulating inflammation, resulted in similar patterns, but only in males (b_{INT}=-7.08(1.3),p_{FDR}=0.001; Fig.2C).

Conclusion: Whole-blood transcriptomic signals were not robustly associated with Aβ-PET accumulation but were associated with cognitive decline via interactions with Aβ-PET and sex. Further work and validation in external cohorts will elucidate relevant biological pathways.

Table 1: Participants Demographics					
Characteristic	**Overall** N = 1,737[1]	**A4 Placebo** N = 236 (13.6%)	**A4 Treated** N = 223 (12.8%)	**LEARN** N = 311 (17.9%)	**Screen Fails[2]** N = 967 (55.7%)
Baseline Age	71.31 (4.70)	72.01 (5.15)	71.92 (4.43)	70.36 (4.31)	71.30 (4.72)
Sex					
Female	1,083 (62%)	157 (67%)	134 (60%)	189 (61%)	603 (62%)
Male	654 (38%)	79 (33%)	89 (40%)	122 (39%)	364 (38%)
Years of Education	16.55 (2.75)	16.40 (2.78)	16.74 (2.65)	16.57 (2.46)	16.54 (2.86)
APOEε4 Status					
ε4-	1,116 (65%)	103 (44%)	90 (40%)	232 (75%)	691 (73%)
ε4+	599 (35%)	133 (56%)	133 (60%)	77 (25%)	256 (27%)
Baseline Global Amyloid Burden	1.09 (0.19)	1.32 (0.16)	1.34 (0.17)	0.99 (0.07)	1.01 (0.11)
Baseline PACC	-0.81 (2.33)	-1.24 (2.46)	-1.06 (2.40)	-0.71 (2.24)	-0.68 (2.31)

[1]Mean (SD), n (%); [2]Only baseline data available for these participants

Figure 1. Volcano plots showing the strength and direction of effects of (A) gene*_APOE_ε4 on longitudinal Aβ-PET (B) gene*_APOE_ε4*sex, (C) gene*Aβ, and (D) gene*Aβ*sex associations with longitudinal PACC. The blue dashed line indicates a multiple comparison corrected threshold; the red line indicates an uncorrected significance threshold. Strongest hits are tagged with their gene name.

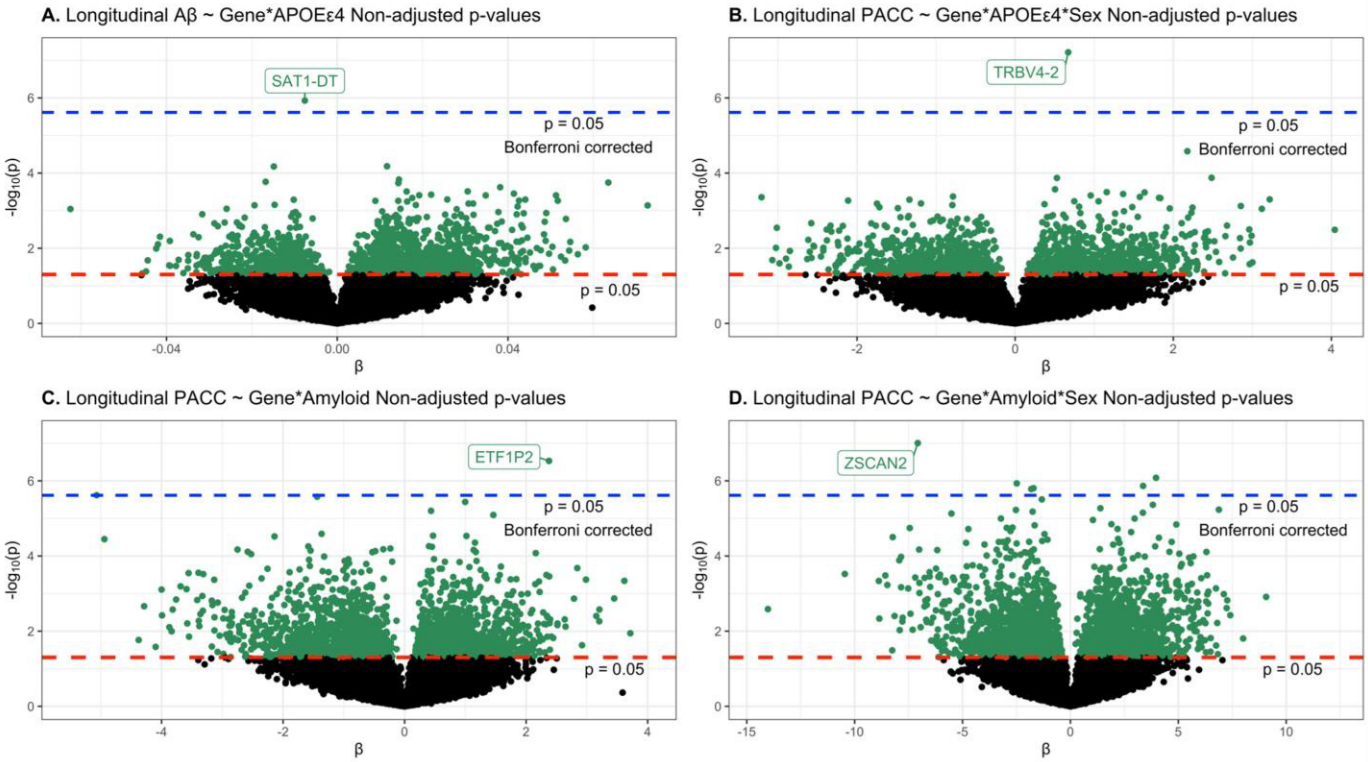
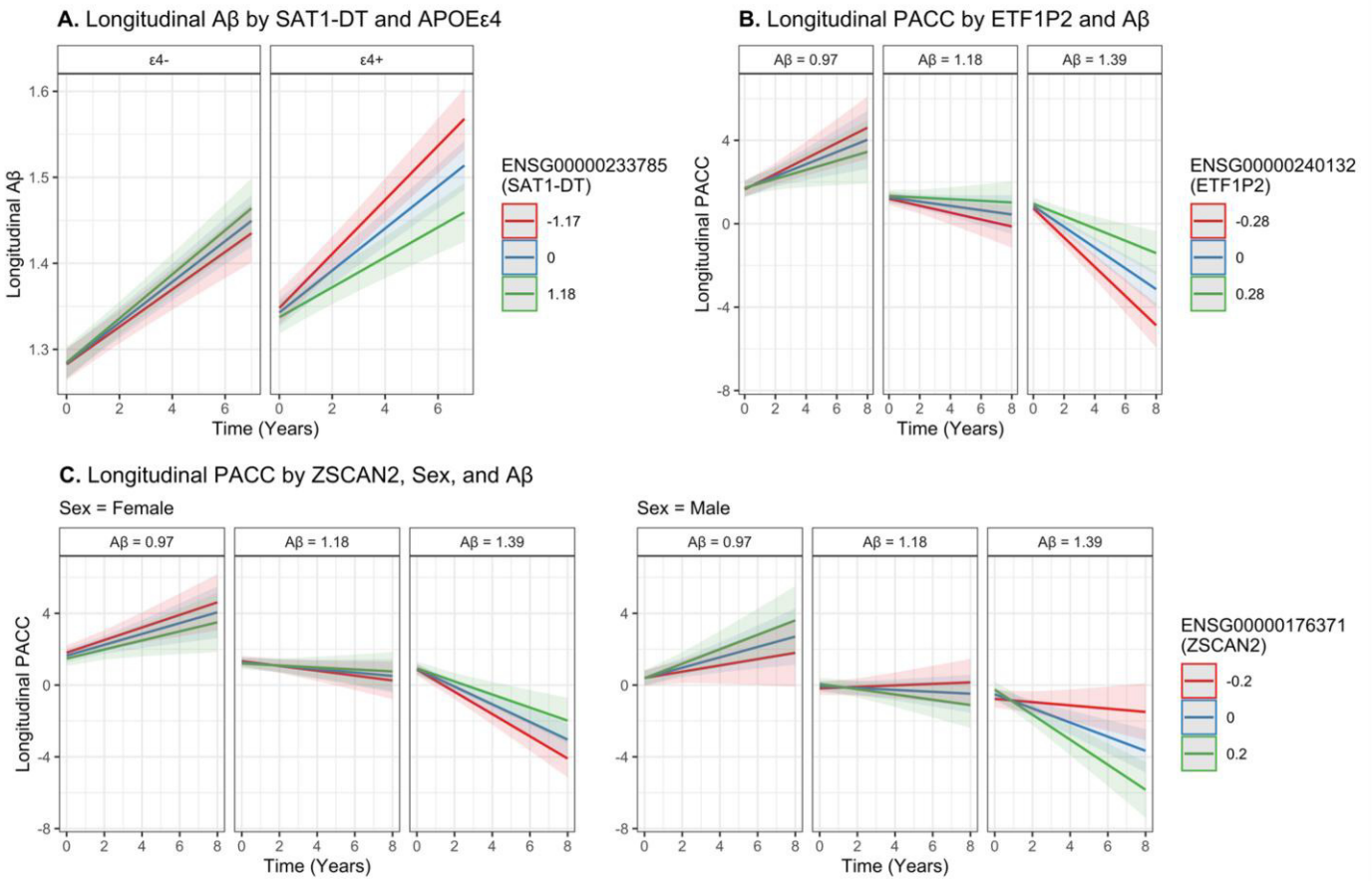


Figure 2. Predicted longitudinal trajectories of (A) Aβ-PET by gene and *APOE*ε4 status over time, (B) PACC by ETF1P2 gene and baseline amyloid burden over time, and (C) PACC by ZSCAN2 gene, sex, and baseline amyloid burden over time.



Keywords: amyloid accumulation, cognitive decline, gene expression

71 Longitudinal change in five dominant dimensions of brain aging in relation to brain amyloid status and Alzheimer's-related plasma biomarkers

Murat Bilgel[1], Ishaan Shah[1], Jasmine Cooper[1,2], Yang An[1], Keenan Walker[1], Abhay Moghekar[3], Zhijian Yang[4], Guray Erus[4], Christos Davatzikos[4], Susan Resnick[1]

[1]*Laboratory of Behavioral Neuroscience, National Institute on Aging, Baltimore, MD, US*
[2]*Department of Psychology, University of Michigan, Ann Arbor, MI, US*
[3]*Department of Neurology, Johns Hopkins University School of Medicine, Baltimore, MD, US*
[4]*Artificial Intelligence in Biomedical Imaging Laboratory (AIBIL), Center for and Data Science for Integrated Diagnostics (AI2D), Perelman School of Medicine, University of Pennsylvania, Philadelphia, PA, US*

Introduction: Plasma biomarkers are associated with regional brain volumes, but it remains unclear if these associations are driven by specific patterns of neurodegeneration among cognitively unimpaired individuals.

Methods: We used data for 179 participants from the Baltimore Longitudinal Study of Aging who were cognitively normal at the time of their plasma Aβ42/Aβ40, GFAP, NfL, and p-tau181 measurements with Quanterix Simoa assays. All participants had undergone at least one assessment with ^{11}C-Pittsburgh Compound B (PiB), allowing for the ascertainment of their amyloid status at the time of plasma biomarker measurements. Structural MRIs concurrent with and following plasma biomarker measurements (707 MRI visits) were used to calculate R-indices describing five dominant dimensions of brain aging: subcortical atrophy (R1), mediotemporal lobe atrophy (R2), parieto-temporal atrophy (R3), diffuse cortical atrophy (R4), and perisylvian atrophy (R5) (Figure 1). Using linear mixed effects models adjusted for baseline age, age^2, sex, age × sex, race, and estimated glomerular filtration rate (eGFR), we examined if baseline plasma biomarkers are associated with longitudinal change in R-indices and whether these associations differ by PiB group.

Results: There were statistically significant differences between PiB− and PiB+ individuals in associations of baseline plasma biomarkers with longitudinal change in R-indices (i.e., PiB group × baseline plasma biomarker × time interaction): among PiB+ vs. PiB− individuals, higher GFAP and NfL at baseline were associated with steeper longitudinal increases in R2 and R3, whereas lower Aβ42/Aβ40 was associated with steeper increases in R2 and R5 (Table, Figure 2).

Discussion: Among individuals with elevated brain amyloid, plasma Aβ42/Aβ40, GFAP, and NfL may be useful for predicting future mediotemporal lobe, parieto-temporal, and perisylvian atrophy, suggesting that these plasma biomarkers may be able to capture impending Alzheimer's-related patterns of neurodegeneration.

Acknowledgments: This study was supported by the National Institute on Aging Intramural Research Program, National Institutes of Health.

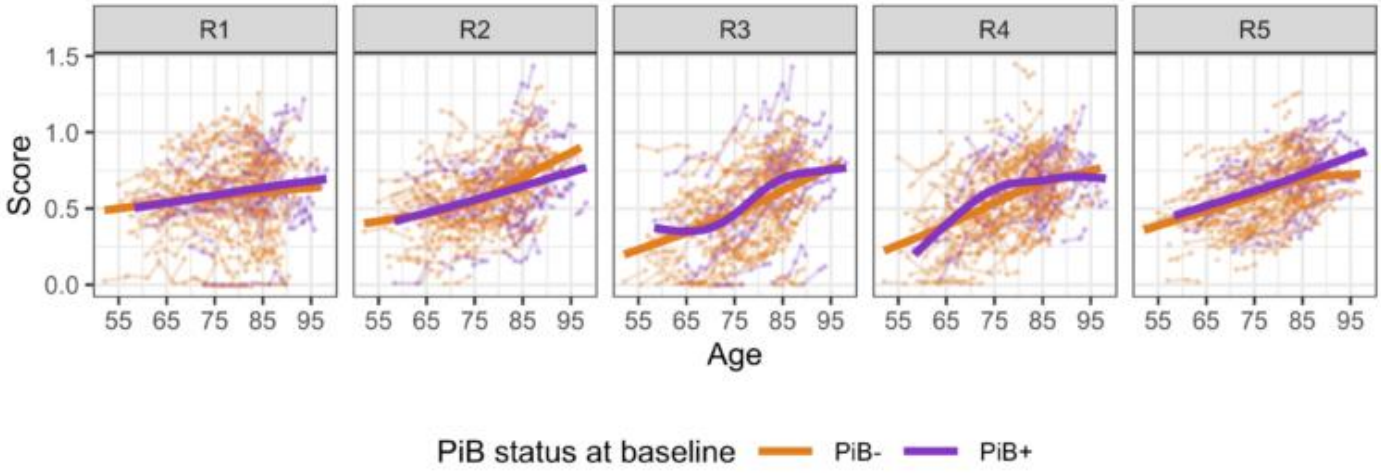


Figure 1: Five dominant dimensions of brain aging (R-indices) vs. age. R1 = subcortical atrophy, R2 = mediotemporal lobe atrophy, R3 = parieto-temporal atrophy, R4 = diffuse cortical atrophy, R5 = perisylvian atrophy.

Table: Estimates of the differences between PiB groups in the associations of baseline plasma biomarkers with longitudinal rates of change in brain atrophy pattern indices.

Biomarker	R1	R2	R3	R4	R5
$A\beta_{42}/A\beta_{40}$	0.00186	**-0.00501***	-0.00194	-0.000837	**-0.00313***
	SE = 0.00254	**SE = 0.00204**	SE = 0.00194	SE = 0.00266	**SE = 0.00146**
GFAP	0.000444	**0.00503***	**0.00547****	-0.00239	0.0012
	SE = 0.00275	**SE = 0.00221**	**SE = 0.00209**	SE = 0.00289	SE = 0.00159
NfL	-0.000129	**0.00748****	**0.00553***	-0.00126	-0.000157
	SE = 0.00304	**SE = 0.00241**	**SE = 0.00231**	SE = 0.00318	SE = 0.00175
p-tau181	-0.000285	-0.00368	0.00173	-0.00261	0.000218
	SE = 0.00297	SE = 0.0028	SE = 0.00268	SE = 0.00359	SE = 0.00203

Abbreviations: Aβ, amyloid-beta; GFAP, glial fibrillary acidic protein; NfL, neurofilament light chain; p-tau, phosphorylated tau; SE, standard error. * $p < 0.05$, ** $p < 0.01$, *** $p < 0.001$

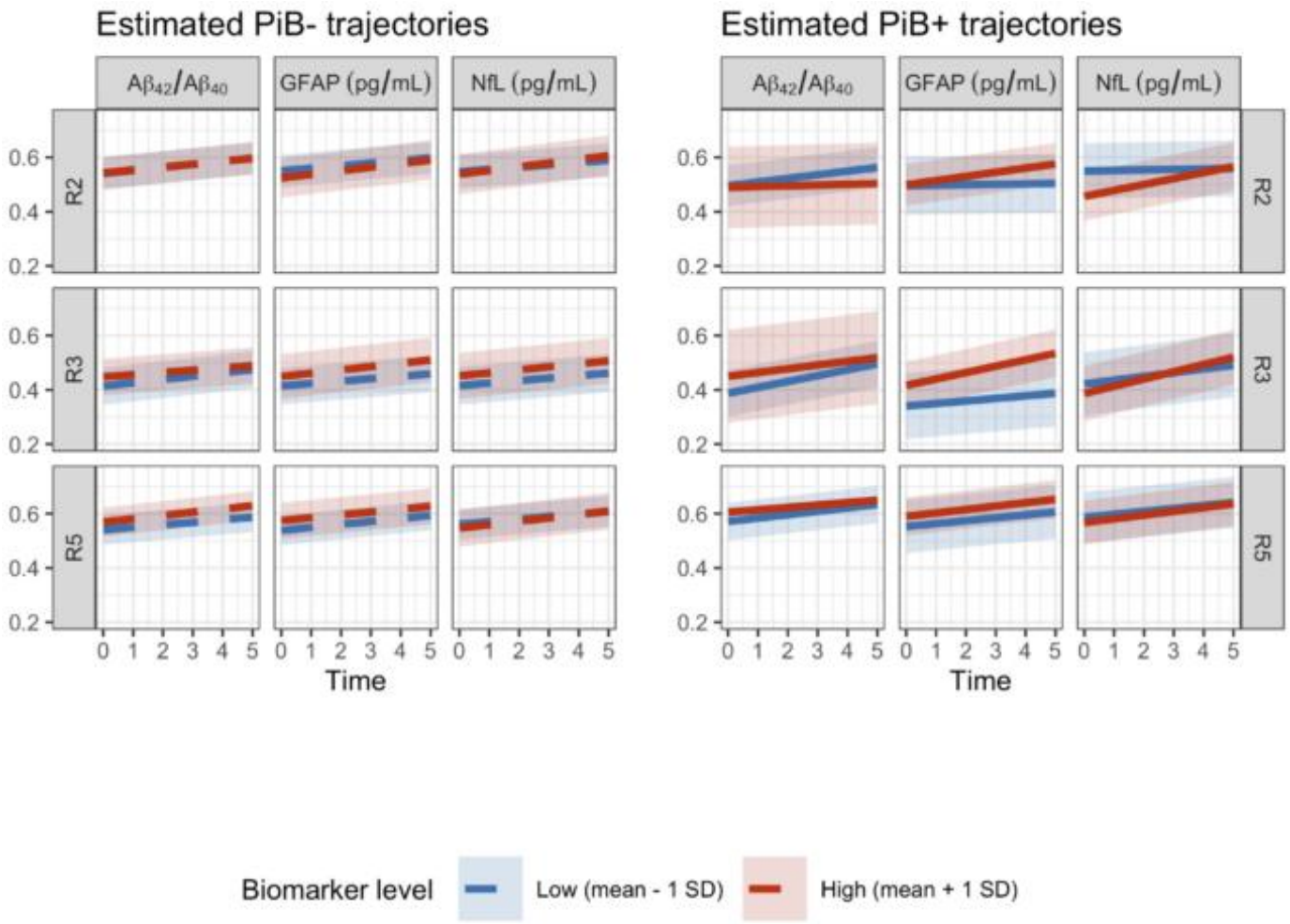


Figure 2: Longitudinal trajectories by baseline biomarker level, estimated using covariate-adjusted linear mixed effects models. Panels on the left illustrate trajectories for PiB- participants (dashed lines) and panels on the right for PiB+ (solid lines). PiB- participants tend not to exhibit differences in the rates of change in R-indices by baseline plasma biomarker level, wheres among PiB+ participants, there are statistically significant differences. Only the R-indices with statistically significant PiB group differences are shown.

Keywords: longitudinal, plasma, neurodegeneration, amyloid

72 Enrichment of patients with concomitant LATE on the Alzheimer's disease continuum using hippocampal volume

Nidhi Mundada[1], Xueying Lyu[1], Niyousha Sadeghpour[1], Christopher Brown[1], Emily McCrew[1], Long Xie[1], Paul Yushkevich[1], Sandhitsu Das[1], David Wolk[1]

[1]*University of Pennsylvania, Philadelphia, PA, US*

Objective: We aimed to identify patients along the AD continuum enriched for concomitant Limbic-predominant age-related TDP-43 encephalopathy (LATE) by defining the lower quartile of hippocampal volume (HV) as a biomarker for possible LATE and AD and explore atrophy pattern differences.

Methods: 164 cognitively impaired participants from ADNI with T1-MRI, amyloid-PET, and tau-PET within 365 days were grouped based on HV quartiles (adjusted for age/intracranial volume) and amyloid status into *suspected* 1) AD-only (HV>50th-percentile, amyloid-positive), 2) LATE-only (HV<25th-percentile, amyloid-negative), 3) AD+LATE (HV<25th-percentile, amyloid-positive). 250 cognitively normal, amyloid-negative participants were also included. Cross-sectional and longitudinal atrophy patterns were examined to determine if AD+LATE showed LATE features beyond hippocampal atrophy. A novel surface-based pointwise regional thickness analysis framework was utilized for MTL.

Results: Suspected-AD+LATE showed imaging features suggestive of LATE (Figure-1B(II)), lower MMSE, CDR, and HV, but higher ITG-tau-SUVR compared to suspected-AD-only (Figure-1A). Suspected-AD-only showed predominant posterior hippocampal atrophy whereas LATE showed more severe anterior hippocampal and amygdala atrophy (Figure-1B(I)) and overlapping tau loads. Cross-sectionally, AD+LATE showed significantly lower thickness in MTL-cortex (Figure-2A) compared to AD-only but primarily in anterior MTL-cortex controlling for tau. Whole brain analysis revealed AD-only had lower thickness in typical AD regions, LATE-only in anterior MTL-cortex (consistent with LATE), and AD+LATE in both AD- and LATE-like regions. Controlling for global tau revealed similar atrophy patterns in anterior hippocampus extending into temporal pole (Figure-2B). Longitudinally, LATE showed slower atrophy than AD (stronger effects in Figure-3A(I)>Figure-3A(II)). AD+LATE showed faster atrophy than AD, however, the effect weakened when controlling for tau. AD+LATE showed increased rate of temporopolar atrophy (Figure-3B(V)).

Conclusions: Patients in lower quartile of HV on the AD continuum exhibit LATE-like patterns, suggesting underlying LATE pathology. A simple hippocampal volume percentile-based metric may help identify patients with concomitant LATE and AD with potential relevance for clinical trials and anti-amyloid therapies.

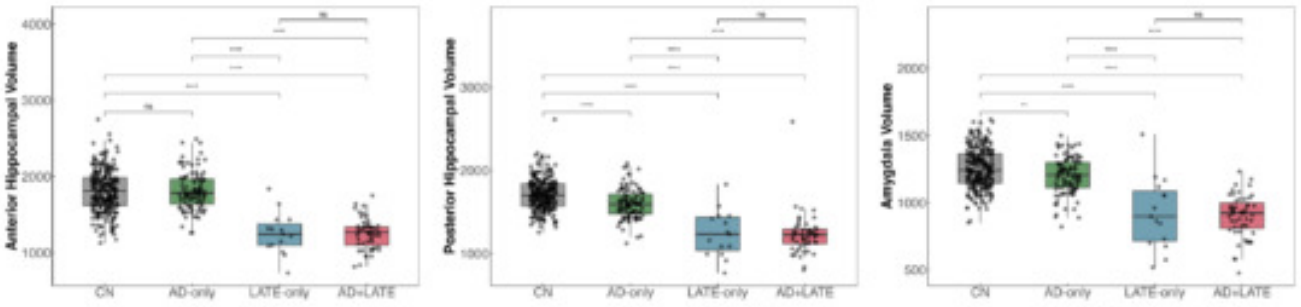
Figure 1: Demographics and Cohort Description

A. Demographics

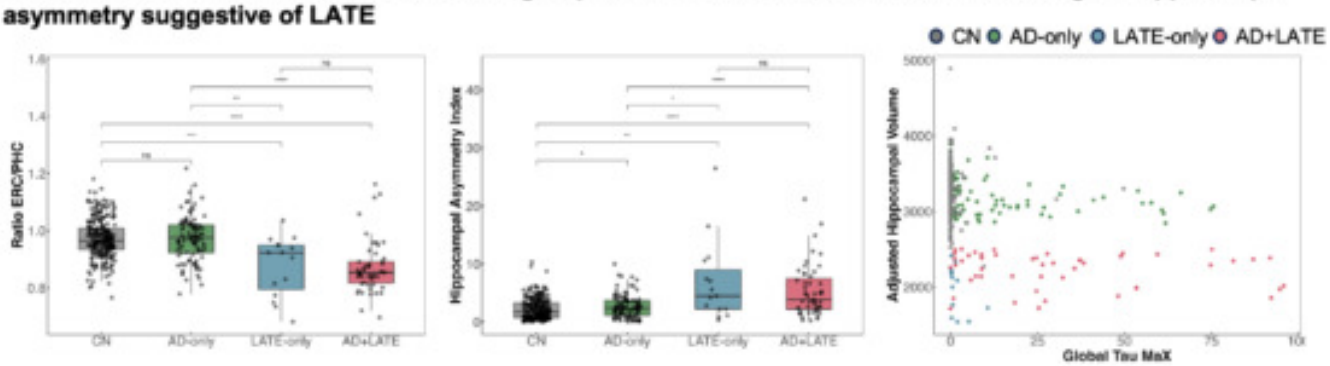
	CN (n=250)	AD-only (n=100)	LATE-only (n=14)	AD+LATE (n=50)	*p*-value
Age	71.5 (6.7)	75.6 (8.1)	74.6 (7.6)	74.8 (7.9)	<0.001
Sex (M/F)	106/144	57/43	26/24*	13/1	<0.001
Education (SD)	16.8 (2.3)	15.9 (2.8)	17.0 (2.9)	15.7 (2.4)	0.003
MMSE (SD)	29.1 (1.2)	26.8 (2.8)***	25.9 (2.6)	23.2 (4.1)	<0.001
CDRSB (SD)	0.05 (0.2)	2.0 (1.8)***	3.2 (2.1)	4.3 (2.9)	<0.001
Hippocampal Vol (SD)	3286 (317)	3227 (255)***	1995 (301)*	2234 (226)	<0.001
ITG-Tau-SUVR (SD)	1.1 (0.1)	1.3 (0.3)***	1.2 (0.1)***	1.7 (0.5)	<0.001

B. Volume, Global Tau and Additional LATE-like features across groups

I: Volumetric group differences pronounced in anterior region of the MTL in patients with suspected AD+LATE

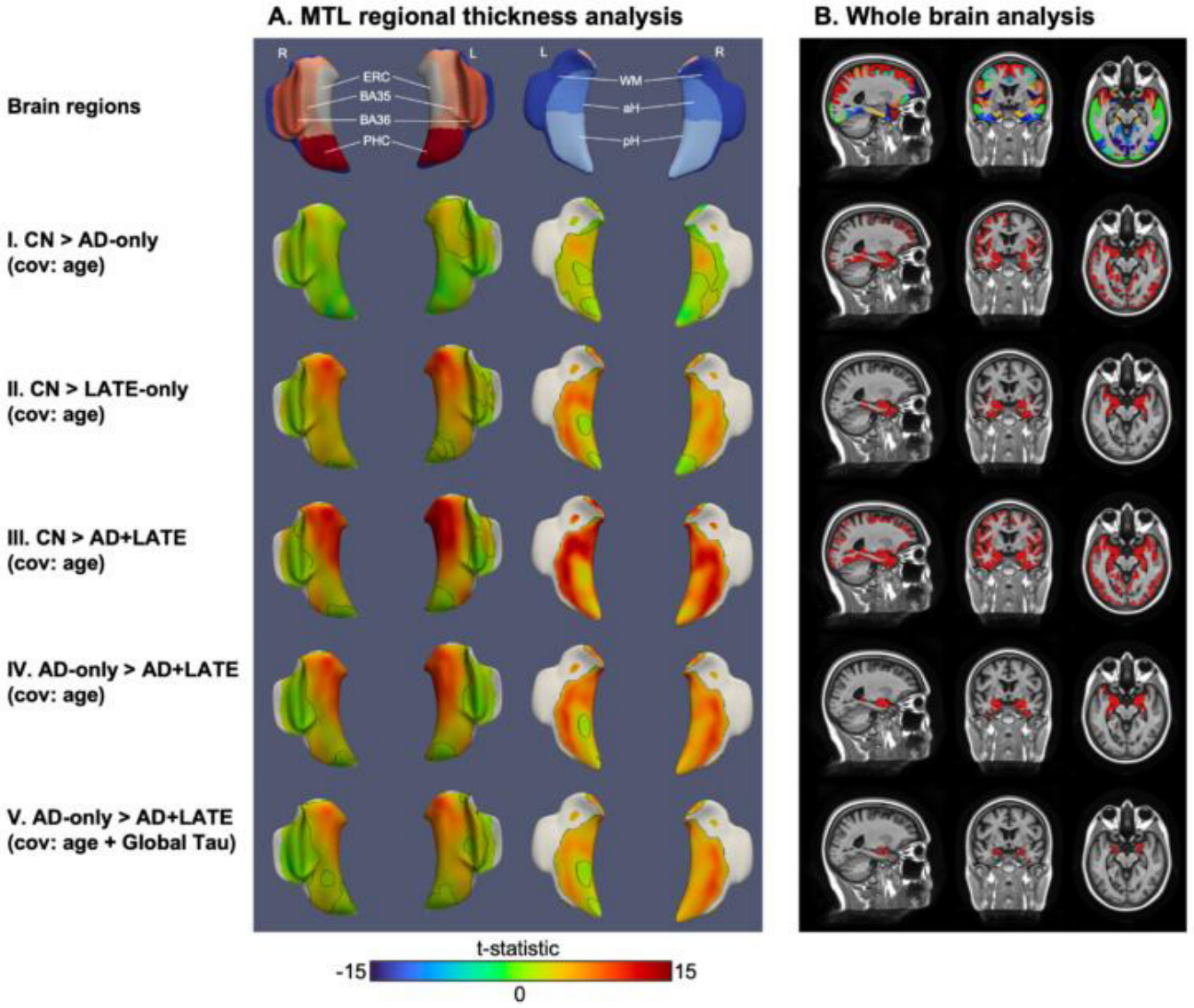


II: Additional Features of LATE – AD+LATE group shows lower ratio of ERC to PHC and higher hippocampal asymmetry suggestive of LATE



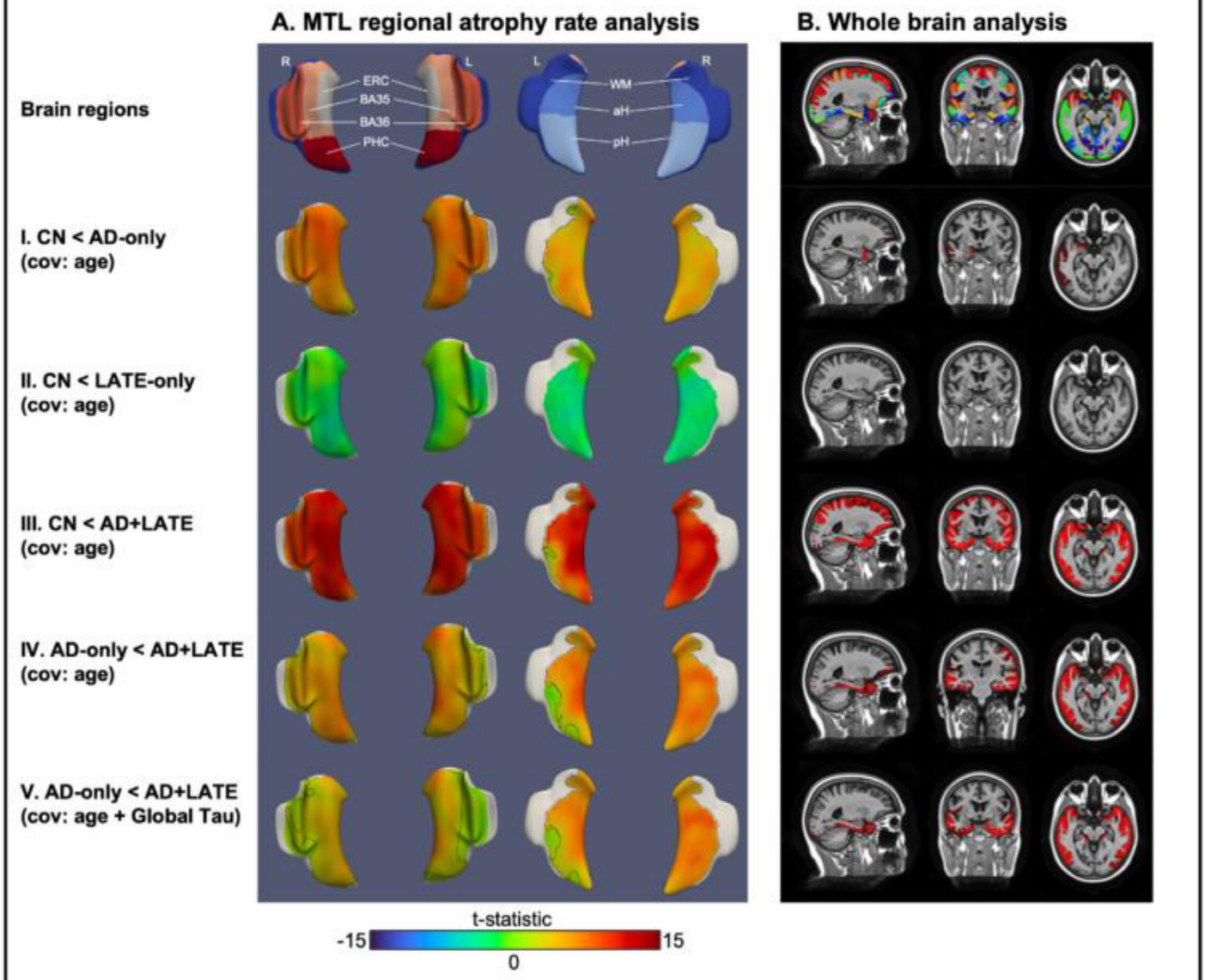
*A. Overall group effects (p-values in last row) were tested using Kruskal-Wallis test. Pairwise group comparisons are reported for AD-only vs AD+LATE (asterisk in AD-only column) and LATE-only vs AD+LATE group (asterisk in LATE-only column) - *p<0.05, ***p<0.001. B. I. Distribution of anterior and posterior hippocampal volume and amygdala volume across groups. II. Distribution of additional features suggestive of LATE, from prior work, ratio of ERC to PHC, and hippocampal asymmetry calculated as (|(L-R)| / (L+R))*100 and the association between Global Tau MaX and total hippocampal volume (adjusted for age and intracranial volume). Global TauMaX is measure of global tau which accounts for both amount and extent of tau burden).*

Figure 2: Cross-sectional group differences in thickness



A. *Maps represent group differences in thickness obtained using a novel pipeline, CRASHS, which builds on top of the ASHS pipeline and adapts tools from the Nighres and CRUISE packages to allow for surface analysis of the MTL. Black lines represent clusters significant at p<0.05. aH=anterior hippocampus, pH=posterior hippocampus.* ***B.*** *Voxelwise group comparisons for controls vs patient groups are shown at p<0.01 FDR corrected, and between patient groups are shown at p<0.05 FDR corrected.*

Figure 3: Longitudinal group differences in atrophy rate



A. *Pointwise annualized atrophy rate maps were created for each participant and then group differences were assessed using generalized linear models. Age (I-V) and global tau max (IV-V) at baseline were used as covariates. Black lines represent clusters significant at p<0.05. aH=anterior hippocampus, pH=posterior hippocampus.* ***B.*** *Linear mixed-effects models were run in all ROIs in the whole brain. P-value of the interaction between group*time for controls vs patient groups are shown at p<0.01 FDR corrected, and between patient groups are shown at p<0.05 FDR corrected.*

Keywords: LATE, TDP-43, co-pathology, MRI

73 AT(N) staging of Alzheimer's disease: Comparison of visual interpretation and automated quantification pipelines

Brian Lopresti[1], Ann Cohen[2], Alex DelBene[1], Alexandria Reese[1], Cristy Matan[1], Alexandra Gogola[1], Michelle Chiang[1], Beth Snitz[3], Sarah Royse[1], Oscar Lopez[3], Victor Villemagne[2]

[1]*Department of Radiology, University of Pittsburgh School of Medicine, Pittsburgh, PA, US*
[2]*Department of Psychiatry, University of Pittsburgh School of Medicine, Pittsburgh, PA, US*
[3]*Department of Neurology, University of Pittsburgh School of Medicine, Pittsburgh, PA, US*

Background: Biomarker standardization methods for PET Aβ (Centiloids, CL) and tau (CenTauRz, CTRz) load in Alzheimer's disease (AD) are used in AT(N) staging. Without post-mortem confirmation, visual interpretation is a practical "gold standard" for evaluating the performance of analytic methods. Here, we compared the performance of analytic and visual methods of AT(N) staging.

Methods: 149 ADRC participants (Table 1) underwent 3T MR, [^{11}C]PiB, and [^{18}F]flortaucipir (FTP) PET imaging. Two raters performed independent visual interpretation of images for Aβ (A), medial temporal lobe tau (T-MTL), neocortical tau (T-NEO), and neurodegeneration (N) status. Discordant ratings were resolved by consensus. Standardized analytic methods were applied to [^{11}C]PiB (CL) and [^{18}F]FTP (CTRz) PET images. AD-signature composite cortical thickness (CCT) and hippocampal volumes normalized to intracranial volume (nHPV) were derived using FreeSurfer. Conventional positivity thresholds were applied to analytic outcomes: CL>20 for A, CTRz>1.5 for T-MTL, CTRz>2 for T-NEO, and CCT<2.8mm or nHPV<0.0049 for N. Logistic regression and ROC analyses were used to determine sensitivity and specificity of analytic status against visual interpretation. The two-graph ROC method (TGROC) was used to identify optimized thresholds for each biomarker.

Results: The CL pipeline showed excellent agreement with visual interpretation (sensitivity=0.902, specificity=1.0; Table 2). CTRz showed excellent specificity but poor sensitivity for T-MTL (MesialTemporal; sensitivity=0.648, specificity=0.948) and T-NEO (MetaTemporal; sensitivity=0.489, specificity=1.0) tau, with frequent false negatives attributed to factors including heterogeneous FTP retention outside the CTRz standard regions or focal and/or asymmetric tau presentations. nHPV was a more accurate predictor of visual N than CCT (accuracy=0.745 vs. 0.671).

Conclusion: The CL pipeline is very reliable for A staging, but further CTRz pipeline optimization may be needed to account for the more heterogeneous/asymmetric presentations of tau. Optimizations will require the determination of more sensitive tau thresholds and refinement of sampling strategies outside of the CenTauR standard regions.

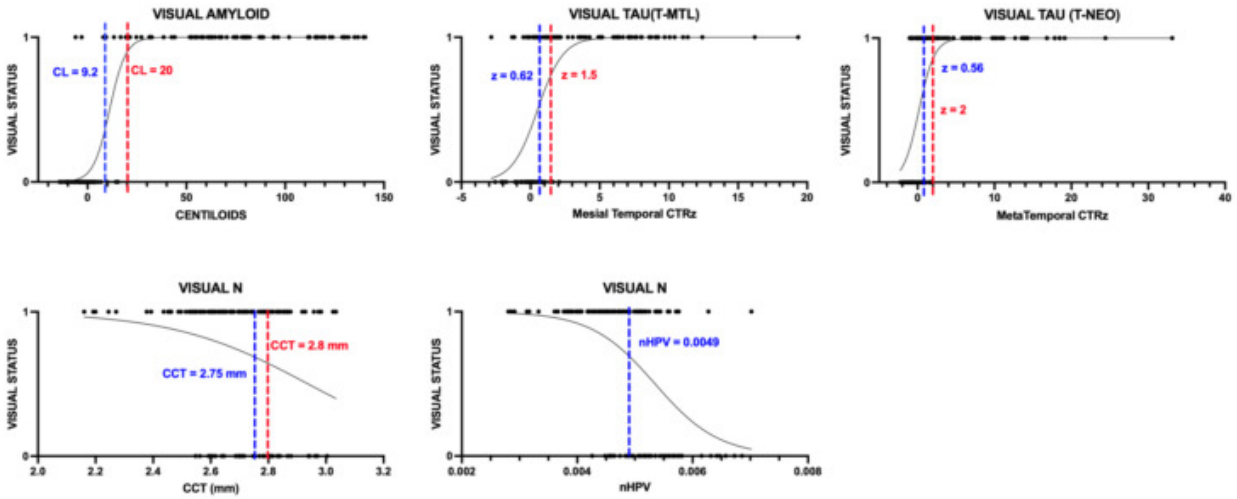
Table 1. Participant characteristics

Demographics		Cognition		APOE Status	
Sex	80M, 69F	CDR		22	1 (0.7%)
Age	71.1±8.6 y	0	24 (16.1%)	23	11 (7.4%)
Education	16.5±8.6 y	0.5	98 (65.8%)	24	5 (3.4%)
Race	140 nHW, 7 AA, 2 other	1	22 (14.8%)	33	78 (52.3%)
		2	5 (3.4%)	34	42 (28.2%)
		MMSE	25.7±4.4	44	10 (6.7%)
		MOCA	22.7±5.7	unknown	2 (1.3%)

Table 2. Performance of analytical methods against visual interpretation

	A	T-MTL	T-NEO	N (CCT)	N (HPV)
Sensitivity (Se)	0.902	0.648	0.489	0.779	0.76
Specificity (Sp)	1.000	0.948	1.000	0.422	0.727
AUC (95% CI)	0.981 (0.957-1.0)	0.876 (0.821-0.931)	0.855 (0.796-0.913)	0.666 (0.575-0.757)	0.821 (0.753-0.889)
Applied Threshold	20 CL	1.5 CTRz	2.0 CTRz	2.8 mm	0.0049
Optimal Threshold for Cohort (TGROC)	9.2 CL	0.62 CTRz	0.56 CTRz	2.75 mm	0.0049

Figure 1. Logistic regression plots showing the predicted probability of visually positive biomarker status for a continuous biomarker range and both conventional and optimal positivity thresholds.



Keywords: AT(N) staging, visual rating, centiloid, CenTauRz

74 MK-6240 off-target binding patterns in relation to microglia density, measured through TSPO PET

Lauren Heuer[1], Aubrey Johnson[1], Anna Smith[1], Diana Guzman[1], Hannah Houlihan[1], Amarachukwu Okafor[1], Thairi Sanchez[1], Daniel Talmasov[1], Dina Dass[1], Nbdusi Chikwem[1], Frank Provenzano[1], William Kreisl[1], James Noble[1], Scott Small[1], Patrick Lao[1]

[1]*Columbia University Medical Center, New York, NY, US*

Background: Tau PET tracers have distinct off-target binding profiles, which may confound quantification. Microglia and border macrophages are involved in blood-brain-barrier permeability and glymphatic clearance mechanisms. We investigated patterns (not magnitude) of off-target leptomeningeal binding profiles of MK-6240 in relation to microglia density, as measured by translocator protein (TSPO) PET signal, across Alzheimer's disease and related dementias.

Methods: Participants (n=35; age=70±8 years, 49% female, BMI=25±4, education=17±3, 83% White, 94% Non-Hispanic, 19% low TSPO affinity, 35% APOE4) from the Longitudinal Imaging of Microglial Activation in Different Clinical Variants of Alzheimer's Disease study completed baseline amyloid PET (Florbetaben), tau PET (MK-6240), and TSPO PET (ER176). Amyloid positivity was determined by visual read (26%), tau positivity as >2SD+mean in controls for early Braak regions (31%), and TSPO positivity as >mean in controls for a global composite (69%). Clinical groups were determined by case consensus (19 controls, 4 aMCI/MCI, 5 AD, 1 LATE, 1 FTD, 1 lvPPA, 4 PCA). Low (29%), variable (11%), and high (60%) extent of MK-6240 off-target binding was visual assessed (fixed range and colorbar across scans; minimal adjustments as necessary). We compared regional ER176 SUVR across MK-6240 off-target binding patterns, adjusting for TSPO affinity and diagnosis [yes/no].

Results: Notably, MK-6240 off-target binding was present in a range of participants including amyloid-negative, tau-negative, TSPO-negative, and individuals with cognitive impairment beyond MCI/AD. Across MK-6240 off-target binding patterns, there was no difference by demographic characteristics (Figure 1A). ER176 was greater in the striatum and prefrontal cortex for the variable MK-6240 off-target binding pattern (Figure 1B).

Conclusion: TSPO PET may capture aspects of regional blood-brain-barrier permeability and/or glymphatic clearance related to the pattern, not necessarily the magnitude, of incomplete (i.e., variable) off-target signal in the leptomeninges. Larger, longitudinal studies with more direct measures of underlying biological mechanisms of off-target binding are needed.

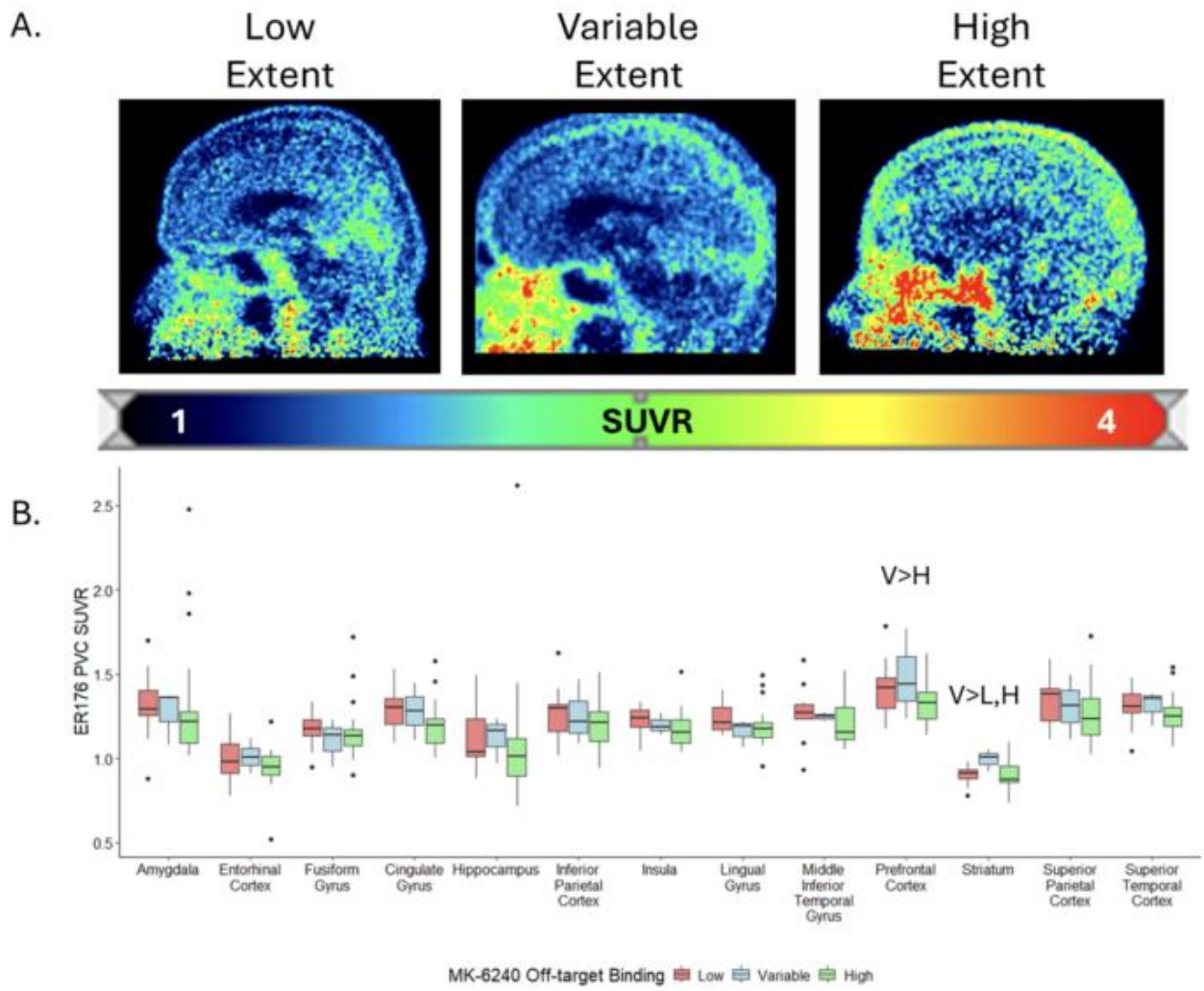


Figure 1. (A) Representative images of low, variable, and high extent of MK-6240 off-target binding patterns in the leptomeninges. (B) Regional ER176 SUVR across MK-6240 off-target binding patterns.

Keywords: microglia, TSPO PET, MK-6240 off-target binding, blood-brain-barrier permeability, leptomeninges

75 Association between medication use and [18F]MK6240 and [18F]Flortaucipir uptake across the Alzheimer's disease spectrum

Rayan Mroué[1], Pamela Lukasewicz Ferreira[1], Guilherme Povala[1], Bruna Bellaver[1], Guilherme Bauer-Negrini[1], Firoza Lussier[1], Livia Amaral[1], Marina Scop Medeiros[1], Emma Ruppert[1], Andreia Silva da Rocha[1], Matheus Scarpatto Rodrigues[1], Markley Silva Oliveira[1], Carolina Soares Katz[1], Douglas Teixeira Leffa[1], Pampa Saha[1], Cynthia Felix[1], Joseph Masdeu[2], David Soleimani-Meigooni[3], Juan Fortea[4], Val Lowe[5], Hwamee Oh[6], Belen Pascual[2], Brian A. Gordon[7], Pedro Rosa-Neto[8], Suzanne Baker[9], Tharick A. Pascoal[1]

[1]*University of Pittsburgh, Department of Psychiatry, Pittsburgh, PA, US*
[2]*Houston Methodist Research Institute, Department of Neurology, Houston, TX, US*
[3]*University of California San Francisco, Memory and Aging Center, San Francisco, CA, US*
[4]*Hospital de la Santa Creu i Sant Pau, Sant Pau Memory Unit, Department of Neurology, Barcelona, ES*
[5]*Mayo Clinic, Department of Radiology, Rochester, MN, US*
[6]*Brown University, Department of Psychiatry and Human Behavior, Providence, RI, US*
[7]*Washington University in St. Louis, Department of Radiology, St. Louis, MO, US*
[8]*Translational Neuroimaging Laboratory, McGill University Research Centre for Studies in Aging, Douglas Research Institute, Montréal, QC, CA*
[9]*Lawrence Berkeley National Laboratory, Berkeley, CA, US*

Background: Quantifying tau aggregates in the human brain can be achieved using Positron Emission Tomography (PET) techniques, which can potentially be affected by binding competition due to medication use. Patients with dementia often have high rates of comorbidities and polypharmacy. Therefore, this study aims to investigate the potential influence of multiple medications on the uptake of the tau tracers MK6240 (MK) and Flortaucipir (FTP).

Methods: 246 individuals, 140 cognitively unimpaired (CU) Aβ-negative and 106 cognitively impaired (CI) Aβ-positive, from the HEAD study were included in the analyses (Table 1). Five classes of medications were evaluated: Anti-Hypertensives, Statins, Anti-Diabetics, Psychoactive drugs, and NSAIDs (Table 2). We compared MK and FTP SUVR in the Medial Temporal Lobe (MTL) and Neotemporal Cortex (NTC) in individuals on and off medications. The linear regressions that tested associations were corrected for confounding factors, including age, sex, education, and MoCA score. Correction for multiple comparisons was applied using the Bonferroni method (adjusted p-value at 0.00125).

Results: Among CI Aβ-positive individuals, Anti-Diabetics were associated with lower FTP SUVR in the NTC and lower MK SUVR in both the MTL and NTC. Psychoactive medications were linked to lower MK SUVR in the MTL. In CU Aβ-negative individuals, NSAIDs and Statins were associated with higher SUVR in the NTC for FTP and MK, respectively. However, none of these associations remained significant after correction for multiple comparisons (Table 3).

Conclusion: Our findings indicate that there are no significant associations between the use of the medications studied and MK or FTP uptake when accounting for covariates and applying multiple comparison corrections.

Table 1: Demographic Characteristics and Medication Use

	% on Medication	% Female on medication†	% Male on medication†	Mean Age ± SD (Years)	Mean MoCA Score ± SD	Mean CDR ± SD	Mean Years of Education ± SD
Medication	**Amyloid Negative, CU (n=140)**						
Anti-Hypertensives	39.3	33.3	49.1	65.6 ± 8.8	27.2 ± 2.3	0	16 ± 2.6
Statins	42.9	36.8	52.8	**67.2 ± 7.5***	27.2 ± 2.1	0	16.2 ± 2.9
Anti-Diabetics	18.6	17.2	20.8	62.6 ± 7.4	27 ± 2.2	0	16.2 ± 2.6
Psychoactives	28.6	33.3	20.8	63.4 ± 8.2	27 ± 2.3	0	15.8 ± 3.2
NSAIDs	15.7	**10.3***	**24.5***	66.3 ± 8.8	26.5 ± 2.3	0	16 ± 2.9
Medication	**Amyloid Positive, CI (n=106)**						
Anti-Hypertensives	50.9	46.2	55.6	**74.2 ± 6.2***	20.4 ± 5.5	3.5 ± 2.4	15.1 ± 3.1
Statins	50	**38.5***	**61.1***	**74.5 ± 6***	20.6 ± 6.1	3.5 ± 2.4	15.4 ± 2.8
Anti-Diabetics	9.4	3.8	14.8	69.6 ± 7.7	20.8 ± 5.2	3 ± 1.9	16.4 ± 2.5
Psychoactives	44.3	**55.8***	**33.3***	71.5 ± 6.3	21.4 ± 5.3	3.2 ± 2.3	15.7 ± 3.1
NSAIDs	24.5	28.8	20.4	72.7 ± 5.8	21.3 ± 6.1	3.3 ± 2.8	15.8 ± 2.9

Abbreviations: CU = Cognitively Unimpaired; CI = Cognitively Impaired; CDR = Clinical Dementia Rating

* = $p < 0.05$

† = Percentages for females and males on medications are calculated relative to the total number of females and males in each group

Table 2: Medications Included by Class

Anti-Hypertensives
Lisinopril, Enalapril, Ramipril, Trandolapril, Perindopril, Benazepril, Losartan, Valsartan, Irbesartan, Candesartan, Olmesartan, Telmisartan, Azilsartan, Metoprolol, Atenolol, Carvedilol, Bisoprolol, Nebivolol, Nadolol, Propranolol, Labetalol, Amlodipine, Nifedipine, Diltiazem, Hydrochlorothiazide, Indapamide, Chlorthalidone, Spironolactone, Eplerenone, Doxazosin, Olmesartan-hydrochlorothiazide, Telmisartan-amlodipine, Telmisartan-hydrochlorothiazide, Irbesartan-Hydrochlorothiazide, Hydrochlorothiazide-triamterene
Statins
Lovastatin, Pravastatin, Simvastatin, Fluvastatin, Atorvastatin, Rosuvastatin, Pitavastatin
Anti-Diabetics
Semaglutide, Dulaglutide, Liraglutide, Tirzepatide, Empagliflozin, Canagliflozin, Dapagliflozin, Saxagliptin, Sitagliptin, Linagliptin, Insulin Glargine, Insulin Lispro, Insulin Aspart, Glimepiride, Glipizide, Gliclazide, Glyburide, Metformin, Metformin-Empagliflozin, Metformin-Sitagliptin, Semaglutide, Dulaglutide, Liraglutide, Tirzepatide
Psychoactives
Escitalopram, Sertraline, Fluoxetine, Citalopram, Paroxetine, Desvenlafaxine, Duloxetine, Venlafaxine, Amitriptyline, Nortriptyline, Trimipramine, Desipramine, Trazodone, Mirtazapine, Bupropion, Vortioxetine, Buspirone, Risperidone, Aripiprazole, Olanzapine, Quetiapine, Lumateperone, Lithium, Pregabalin, Gabapentin, Levetiracetam, Phenytoin, Topiramate, Lamotrigine
NSAIDs
Nepafenac, Diclofenac, Aspirin, Ibuprofen, Naproxen, Meloxicam, Celecoxib

The medications listed were selected based on their use within the sample population

Table 3: Effect of Medication Use on Tracer SUVR in Aβ Negative and Aβ Positive Groups

	MTL FTP Beta Estimate [95% CI], p-value	Neotemporal FTP Beta Estimate [95% CI], p-value	MTL MK Beta Estimate [95% CI], p-value	Neotemporal MK Beta Estimate [95% CI], p-value
Medication	**Amyloid Negative, CU (n=140)**			
Anti-Hypertensives	0.02 [-0.02, 0.06], p = (0.317415)	0.01 [-0.02, 0.03], p = (0.587929)	0.04 [-0.01, 0.09], p = (0.137378)	0.02 [-0.01, 0.05], p = (0.260645)
Statins	0.01 [-0.03, 0.05], p = (0.566808)	0.01 [-0.02, 0.03], p = (0.543757)	0.02 [-0.03, 0.07], p = (0.443978)	0.04 [0, 0.07], p = (0.040594)
Anti-Diabetics	0 [-0.05, 0.05], p = (0.913421)	0 [-0.03, 0.03], p = (0.996517)	-0.02 [-0.09, 0.04], p = (0.482590)	0 [-0.05, 0.04], p = (0.905185)
Psychoactives	0.04 [-0.01, 0.08], p = (0.105185)	0.02 [-0.01, 0.05], p = (0.124770)	0.01 [-0.05, 0.06], p = (0.721950)	0.01 [-0.02, 0.05], p = (0.435352)
NSAIDs	0.02 [-0.03, 0.08], p = (0.429552)	0.04 [0, 0.07], p = (0.027999)	0.01 [-0.06, 0.08], p = (0.861997)	0.03 [-0.01, 0.08], p = (0.171425)
Medication	**Amyloid Positive, CI (n=106)**			
Anti-Hypertensives	-0.06 [-0.16, 0.05], p = (0.317852)	-0.06 [-0.2, 0.07], p = (0.343800)	-0.25 [-0.53, 0.03], p = (0.084778)	-0.15 [-0.48, 0.19], p = (0.384923)
Statins	-0.04 [-0.15, 0.07], p = (0.496290)	-0.08 [-0.22, 0.05], p = (0.223626)	-0.09 [-0.38, 0.2], p = (0.543031)	-0.13 [-0.47, 0.22], p = (0.465085)
Anti-Diabetics	-0.11 [-0.3, 0.08], p = (0.239643)	-0.24 [-0.46, -0.01], p = (0.036777)	-0.53 [-1.01, -0.06], p = (0.027720)	-0.78 [-1.33, -0.23], p = (0.005834)
Psychoactives	-0.05 [-0.16, 0.06], p = (0.367629)	-0.07 [-0.2, 0.07], p = (0.338805)	-0.3 [-0.59, -0.02], p = (0.036018)	-0.28 [-0.62, 0.05], p = (0.095588)
NSAIDs	0.05 [-0.07, 0.18], p = (0.384735)	0.01 [-0.14, 0.17], p = (0.863990)	0.15 [-0.17, 0.47], p = (0.345166)	0.16 [-0.21, 0.54], p = (0.392081)

Abbreviations: MTL = Medial Temporal Lobe; FTP = Flortaucipir; CU = Cognitively Unimpaired; CI = Cognitively Impaired
p values are nominal
p value threshold adjusted for multiple comparison is set at 0.00125

Keywords: tau-PET, medications, Alzheimer

76 Lower LC-EC tract integrity is associated with entorhinal tau in autosomal-dominant Alzheimer's disease

Elouise Koops[1], Averi Giudicessi[2], Nikole Bonillas-Felix[2], Randy Medrano[2], Lusiana Martinez[2], Isabella Gonzalez[2], Sergio Alvarez[4], David Aguillon[3], Yakeel T. Quiroz[2,3,6], Heidi Jacobs[1,5]

[1]*Martinos Center for Biomedical Imaging, Department of Radiology, Massachusetts General Hospital, Harvard Medical School, Boston, MA, US*
[2]*Department of Psychiatry, Massachusetts General Hospital, Harvard Medical School, Boston, MA, US*
[3]*Neuroscience Group of Antioquia, Medicine School, University of Antioquia, Medellín, CO*
[4]*Department of Radiology, Hospital Pablo Tobón Uribe, Medellín, CO*
[5]*Faculty of Health, Medicine and Life Sciences, School for Mental Health and Neuroscience, Alzheimer Centre Limburg, Maastricht University, Maastricht, NL*
[6]*Department of Neurology, Massachusetts General Hospital, Harvard Medical School, Boston, MA, US*

Background: Autopsy studies indicate that the locus coeruleus (LC) is one of the first regions accumulating tau in autosomal and sporadic AD before it becomes detectable in the entorhinal cortex (EC). As tau is assumed to spread trans-axonally, it can be hypothesized that this process is associated with LC-EC tract degradation. While LC-EC tract degradation has been reported in sporadic AD, it remains unknown whether LC-EC tract degradation occurs in autosomal-dominant Alzheimer's disease (ADAD) and is associated with entorhinal tau pathology.

Methods: We investigated the LC-EC white matter tract with diffusion-weighted imaging in the COLombia-BOSton cohort with PSEN1-E280A mutation (n=30) and healthy controls (n=33;Table 1) using fixel-based analyses and tractography. Clinical status was defined with the Functional Assessment Staging Test (FAST). The MMSE and the CERAD Word List were used to measure cognition. Multiple linear regressions related LC-EC tract characteristics to age to disease onset, sex, PET-derived entorhinal tau burden, and cognition.

Results: Fiber-bundle cross-section (FC) of the LC-EC tract was lower for female than male participants ($p<0.0001$;Fig 1A). In mutation carriers, the combined fiber-bundle density and cross-section metric (FDC) ($p=0.032$) and FC ($p=0.019$;Fig 1B) of the LC-EC tract were lower in those closer to disease onset. Lower tract integrity (Fig 2A;Fig 2B) was associated with higher entorhinal tau in mutation carriers but not controls, with lower FC being associated with higher entorhinal tau in asymptomatic mutation carriers (n=22, FAST=1&2) as disease-onset approaches ($p=0.037$;Fig 2C). Lower FC, not FDC, was associated with worse memory performance in mutation carriers ($p=0.038$) but not in controls ($p=0.11$;Fig 2D).

Conclusion: We observed a female vulnerability to LC-EC tract degradation. Furthermore, degradation of the LC-EC tract was associated with worse cognition and higher entorhinal tau in asymptomatic PSEN1-E280A mutation carriers, suggesting that LC-EC tract integrity may be predictive of entorhinal tau accumulation in ADAD.

Table 1. Characteristics of participants. Per PSEN1-E280A mutation carrier status, the mean and standard deviation are given for age, education level, MMSE score, and entorhinal tau. Participants who underwent a Tau-PET (FTP), PiB-PET, Diffusion Weighted Imaging scan, and 3T-MRI scan were extracted from the COLombia-BOSton (COLBOS) cohort. In the mutation carrier group, n = 23 were asymptomatic, and n = 7 were symptomatic. In this cohort, the FAST was used to define clinical status, and the MMSE and CERAD Word List were used to measure cognition. *Abbreviations: MMSE = Mini-Mental State Examination, FAST = Functional assessment staging test, FTP = [^{18}F]Flortaucipir, SUVr = Standard Uptake Value referenced to cerebellar gray matter, PiB = Pittsburgh Compound B, PET = Positron Emission Tomography, CERAD = Consortium to Establish a Registry for Alzheimer's Disease.*

	Control, N = 33[1]	**E280A carrier**, N = 30[1]	**p-value**[2]
Age	35.30 (4.52)	38.92 (6.06)	**0.009**
Sex			0.9
Male	15 (45.45%)	12 (40.00%)	
Female	18 (54.55%)	18 (60.00%)	
Education (years)	11.64 (3.98)	9.33 (4.19)	**0.029**
MMSE	28.91 (0.91)	27.10 (3.02)	**0.002**
FAST			**<0.001**
1	32 (96.97%)	16 (53.33%)	
2	1 (3.03%)	7 (23.33%)	
3	0 (0.00%)	6 (20.00%)	
4	0 (0.00%)	1 (3.33%)	
PiB status			**<0.001**
PIB-	33 (100.00%)	6 (20.00%)	
PIB+	0 (0.00%)	24 (80.00%)	
FTP entorhinal (SUVr)	1.06 (0.22)	1.74 (0.69)	**<0.001**

[1]Mean (SD); n (%)
[2]One-way ANOVA; Pearson's Chi-squared test; Fisher's exact test

Figure 1. Macro and microstructural characteristics of the LC-EC tract in relation to sex and age to onset.
(A) Fiber-bundle cross-section (FC) of the LC-EC tract was significantly lower for female than for male participants (t=-5.99, p < 0.0001). This sex effect was present in both the mutation carrier (*t*=-4.8, *p*<0.0001) and control subgroups (*t*=-3.6, *p*=0.001). The inserted image shows the LC-EC tract in green, with the LC depicted in blue and the EC in orange. (B) Being closer to the age to onset (median ~44 years) was associated with lower 'fiber bundle density and cross-section' metric (FDC) (*t*=-2.3, *p*=0.032) and FC (*t*=-2.5, *p*=0.019) of the LC-EC tract in mutation carriers. *Abbreviations: E280A+ = individuals with the PSEN1 E280A mutation, E280A- = individuals from the same kindred without the PSEN1 E280A mutation, log FC = fiber-bundle cross-section, FDC = combined fiber density and fiber-bundle cross-section, LC-EC = locus coeruleus-entorhinal cortex.*

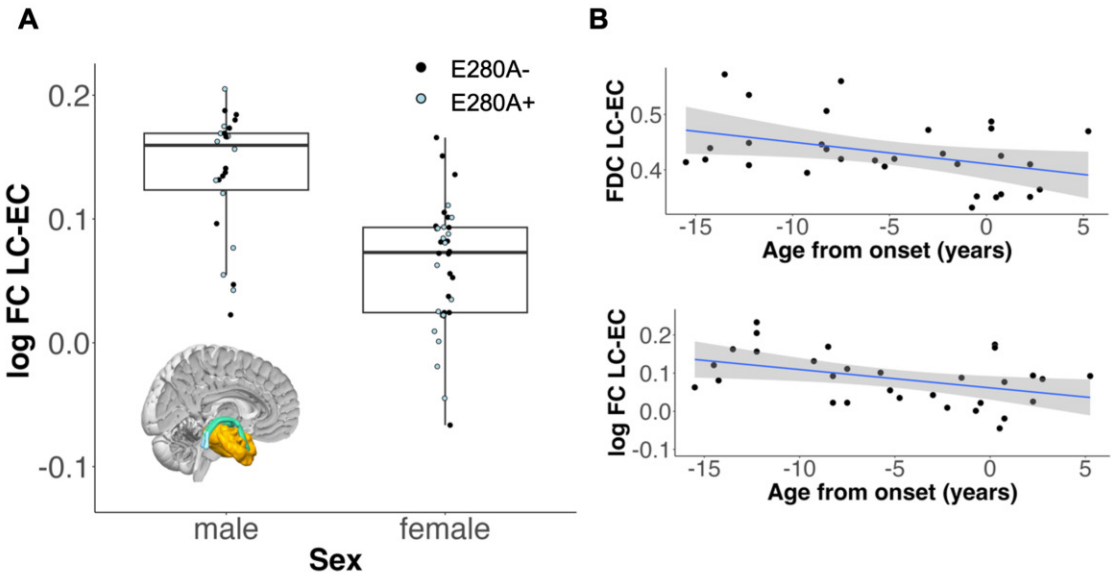
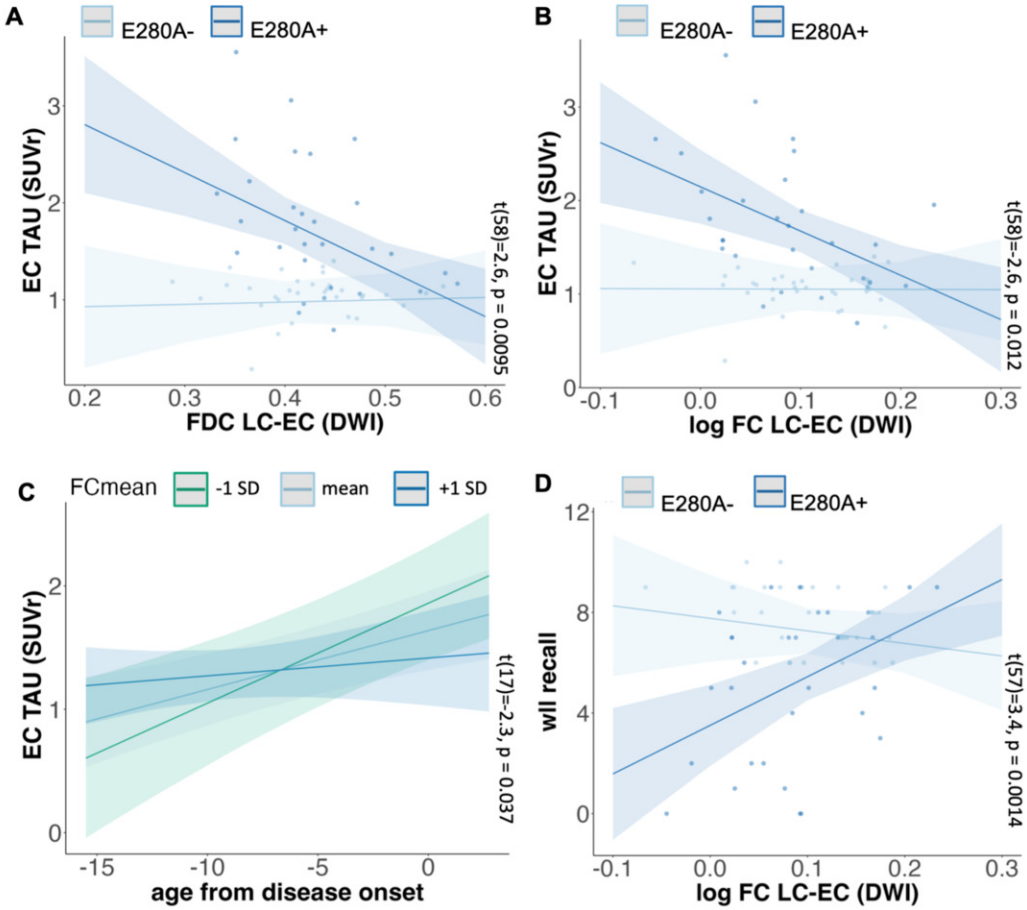


Figure 2. Macro and microstructural characteristics of the LC-EC tract in relation to entorhinal tau and cognition. Interaction analyses showed that lower FDC (A) and FC (B) were associated with higher entorhinal tau (Flortaucipir; PVC-corrected; cerebellar reference) in mutation carriers (t=-2.4, p=0.026; t=-2.2, p=0.037) but not in controls (t=0.22, p=0.83; t=-0.52, p=0.61), with sex as covariate in the models. (C) In asymptomatic mutation carriers (FAST scores 1 and 2), lower FC, but not FDC, of the LC-EC tract is associated with a steeper increase in entorhinal tau as the age of onset of the disease approaches (t=-2.3, p=0.037). (D) Interaction analyses showed that lower FC, but not FDC, was associated with worse memory performance in mutation carriers (t=2.2, p=0.038) but not in controls (t=-1.66, p=0.11), as indexed by the recall element of the word list learning task. This association also exists in the asymptomatic mutation carriers (t=4.4, p=0.0009). Sex and education were entered as covariates in the model.* Age was not included as a covariate due to the close association with disease trajectory, but the effects remained if we additionally included age as a covariate. Statistics in the figures reflect the interaction effect. *Abbreviations: E280A-=control participants, E280A+=mutation carriers, EC=entorhinal cortex, SUVr=standardized uptake value referenced to cerebellar gray, FDC=fiber density and cross-section, log FC=fiber bundle cross-section, DWI=diffusion-weighted imaging, wll recall= CERAD word list learning task, recall element.*



Keywords: Autosomal Dominant Alzheimer's Disease, PET, tau, locus coeruleus, Diffusion Weighted Imaging

77 APOE4 associated with higher off-target meninges signal with [F-18]MK6240 PET

Andrew McVea[1], Alexandra DiFilippo[1], Max McLachlan[1], Brecca Bettcher[1], Dana Tudorascu[2], Sterling Johnson[1], Matthew Zammit[1], Tobey Betthauser[1], Bradley Christian[1]

[1]*University of Wisconsin - Madison, Madison, WI, US*
[2]*University of Pittsburgh, Pittsburgh, PA, US*

Background: Individuals with the APOE4 allele have an enhanced risk of Alzheimer's disease (AD) and APOE4 carriage is associated with earlier onset of AD pathology including tau aggregation. [F-18]MK6240 is a PET radioligand that binds to tau aggregates in AD with variable off-target signal surrounding the cortex in the meninges that can influence quantification. Previous studies examining MK6240 signal have shown significantly higher meninges uptake in females and PET signal dependence on scanner model. The goal of this investigation is to evaluate meninges MK6240 signal in a large cohort to study the relationship between APOE4 carriage and meninges uptake.

Method: Participants were scanned at the University of Wisconsin–Madison on a Biograph Horizon mCT or ECAT HR+ (Table 1). MK6240 PET images were smoothed using a 6mm^3 gaussian kernel then processed using a standardized pipeline to generate SUVR images using the inferior cerebellar grey matter reference region. A meninges ROI was created by diluting the MNI-152 cortical brain mask by 5mm and then subtracting the original mask (Fig. 1). Statistical comparisons were made using a multiple regression model examining the association between meninges SUVR and APOE4 carriage with sex, scanner model and the interaction terms between variables as covariates.

Results: Higher average meninges signal was observed for APOE4 carriers ($p = 0.03$), and similar to previous results, for females ($p < 0.001$) and participants imaged on the mCT ($p < 0.001$). The interaction term between scanner and sex was significant ($p = 0.02$), while interactions between sex and APOE status ($p = 0.34$) and scanner and APOE4 carriage were non-significant ($p = 0.42$).

Conclusions: Meninges signal is a highly variable factor in MK6240 imaging that can bias tracer uptake outcomes. The relationships between APOE4 carriage and sex on meninges uptake should be accounted for in MK6240 quantification and population-based comparisons.

	mCT (n = 551)	HR+ (n = 501)	Total (n = 1051)
Age	68.4±7.6	69.7±7.1	69.0±7.4
Sex (%)	68%	70%	69%
APOE4+ (%)	39%	41%	40%
APOE2+ (%)	11%	13%	12%
Aβ+ (%)	29%	22%	24%
Tau+ (%)	20%	17%	18%
CI (%)	19%	14%	17%

Table 1: Description of the University of Wisconsin-Madison [F-18]MK6240 PET imaging cohort inlcluded in this study. A subset of this cohort had their amyloid (n = 282), tau (n = 285) and cognitive statuses (n = 828) available.

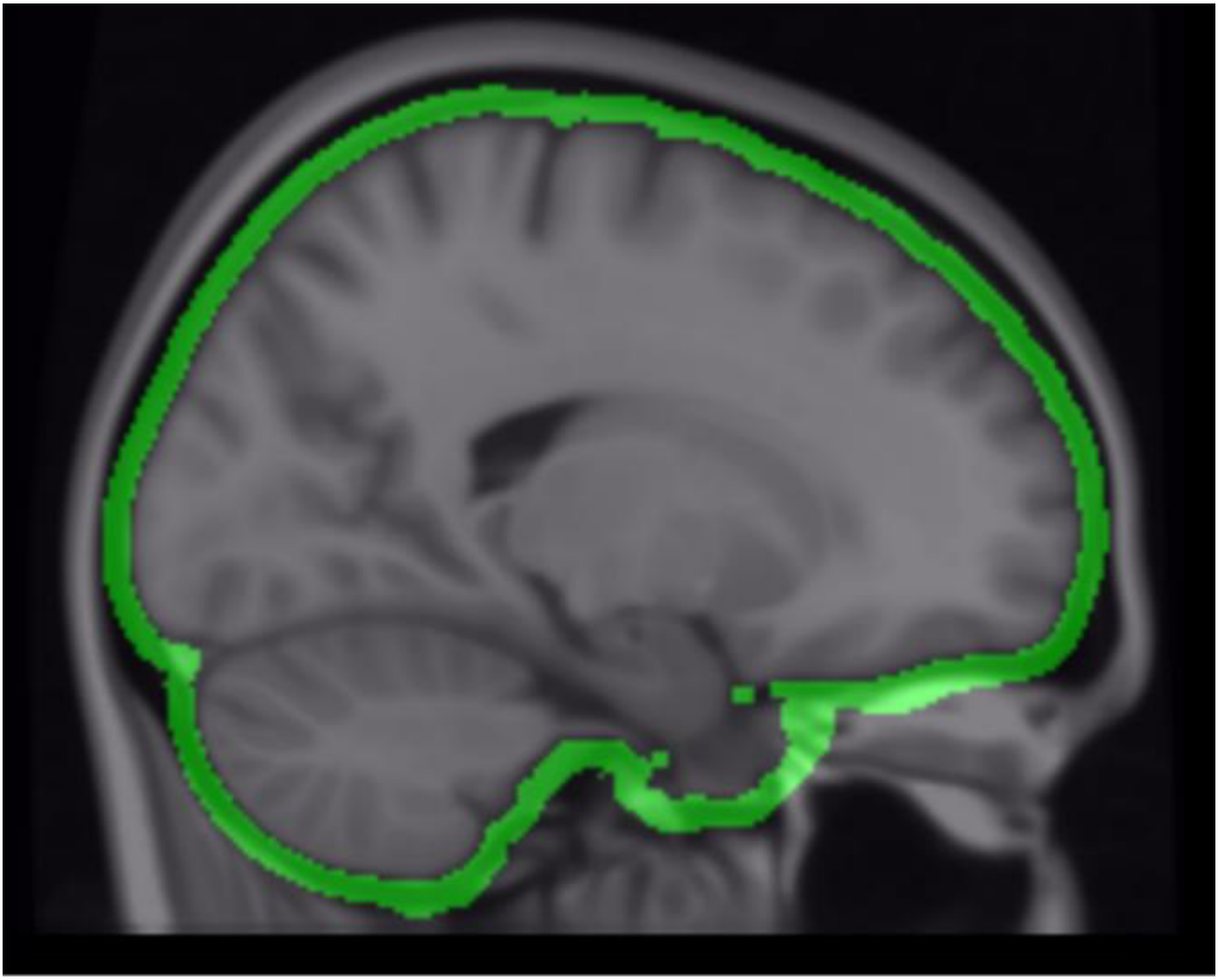


Fig. 1: Meninges ROI defined for this study circumscribing the cortex. Comparisons of meninges SUVR were all made in standard space using a uniform PET image processing pipeline for both scanner types.

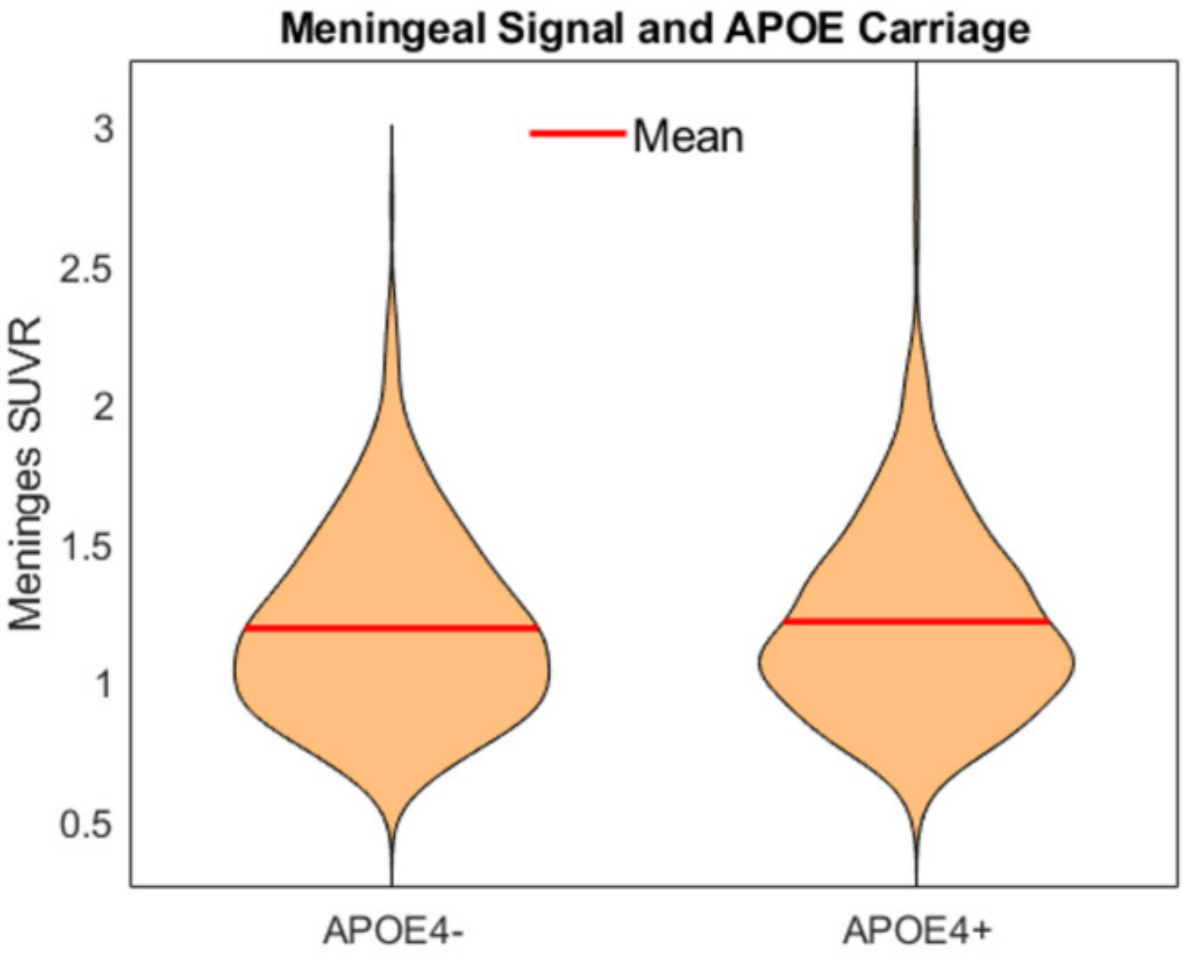


Fig. 2: Violin plots comparing the association between meninges signal and APOE carriage. APOE4 carriers had a significantly higher meningeal [F-18]MK6240 SUVR (1.21±0.35) than non-carriers (1.19±0.33) in our linear mixed effects model ($p = 0.03$).

Keywords: Meninges, [F-18]MK6240, APOE4 carriage, multiple regression, off-target signal

78 An accurate and automated technique for removing spill-over contamination and off-target retention from a cerebellar reference region for tau PET

Davneet Minhas[1], Alex DelBene[1], Alexandra Gogola[1], Alexandria Reese[1], Weiquan Luo[1], Charles Laymon[1], Brian Lopresti[1], Vincent Dore[2], Tharick Pascoal[1], Suzanne Baker[3], Dana Tudorascu[1], Victor Villemagne[1]

[1]*University of Pittsburgh, Pittsburgh, PA, US*
[2]*Austin Health, Melbourne, AU*
[3]*Lawrence Berkeley National Laboratory, Berkeley, CA, US*

Background: Reference region (RR) definition impacts tau PET quantification. In this work, we explore methods of optimizing the RR by minimizing spillover and off-target signal.

Methods: We developed CerTauSeg, an algorithm that identifies clusters of contamination in an individual subject's whole cerebellar gray tau PET scan with no a priori knowledge. CerTauSeg accuracy was evaluated against standard RRs using simulations, which included varying sources of off-target contamination (superior cerebellum, meninges) and sinogram-added noise, constructed with Siemens E7 Tool Projector software.

CerTauSeg was applied to 338 ADNI FTP-PET scans in template space to generate subject-specific "clean" cerebellar GM masks. A "Universal" ADNI FTP RR (UTCer) was created by averaging all "clean" cerebellar GM masks and thresholding at 95%. Cohen's d effect sizes were calculated across cognitive and Aβ status groups of CenTauR SUVRs based on CerTauSeg, UTCer, and standard cerebellar RRs.

Results: CerTauSeg outperformed existing RR quantification methods in accurately quantifying uncontaminated cerebellar radioactivity concentrations (Figure 1). Based on visual inspection, 21 (6.2%) ADNI FTP-PET scans failed CerTauSeg refinement, likely due to gross misregistration, excessive motion artifact, or smoothing. Successful application of CerTauSeg resulted in subject-specific masks free of superior cerebellar off-target retention, cortical spillover, cerebellar atrophy/CSF dilution, and scanner FOV cutoff (Figure 2). The UTCer is presented in Figure 2I.

The UTCer outperformed subject-specific CerTauSeg and standard cerebellar masks in discriminating CenTauR universal and mesial SUVRs between CN Aβ+ and CN Aβ- groups, and between MCI Aβ+ and CN Aβ- groups (Table 1). However, whole cerebellar GM and inferior cerebellar GM RRs outperformed the UTCer in discriminating ADs from CN Aβ- across all CenTauR regions, potentially due to excessive sampling of atrophied CSF space in ADs, which may disproportionately inflate AD SUVRs.

Conclusion: UTCer outperformed CerTauSeg and existing RR methods. Multi-tracer and longitudinal evaluations of CerTauSeg and UTCer are ongoing.

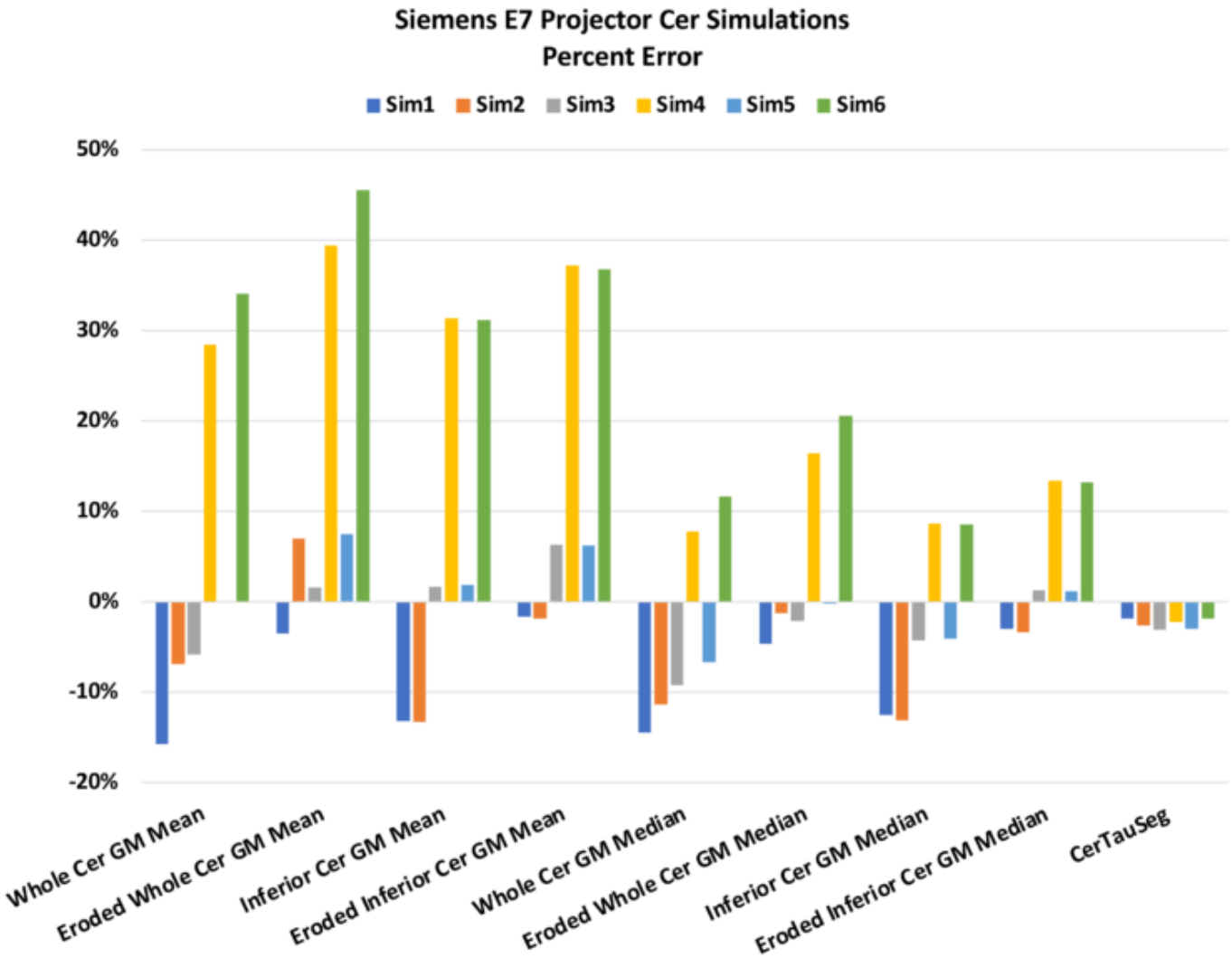


Figure 1. Accuracy (% Error, lower is better) of morphological and statistical cerebellar sampling techniques in assessing “true” cerebellar reference radioactivity concentrations across 6 different cerebellar tau PET simulations (Sim1-Sim6), consisting of varying patterns and magnitudes of superior cerebellar off-target retention and meningeal spillover contamination.

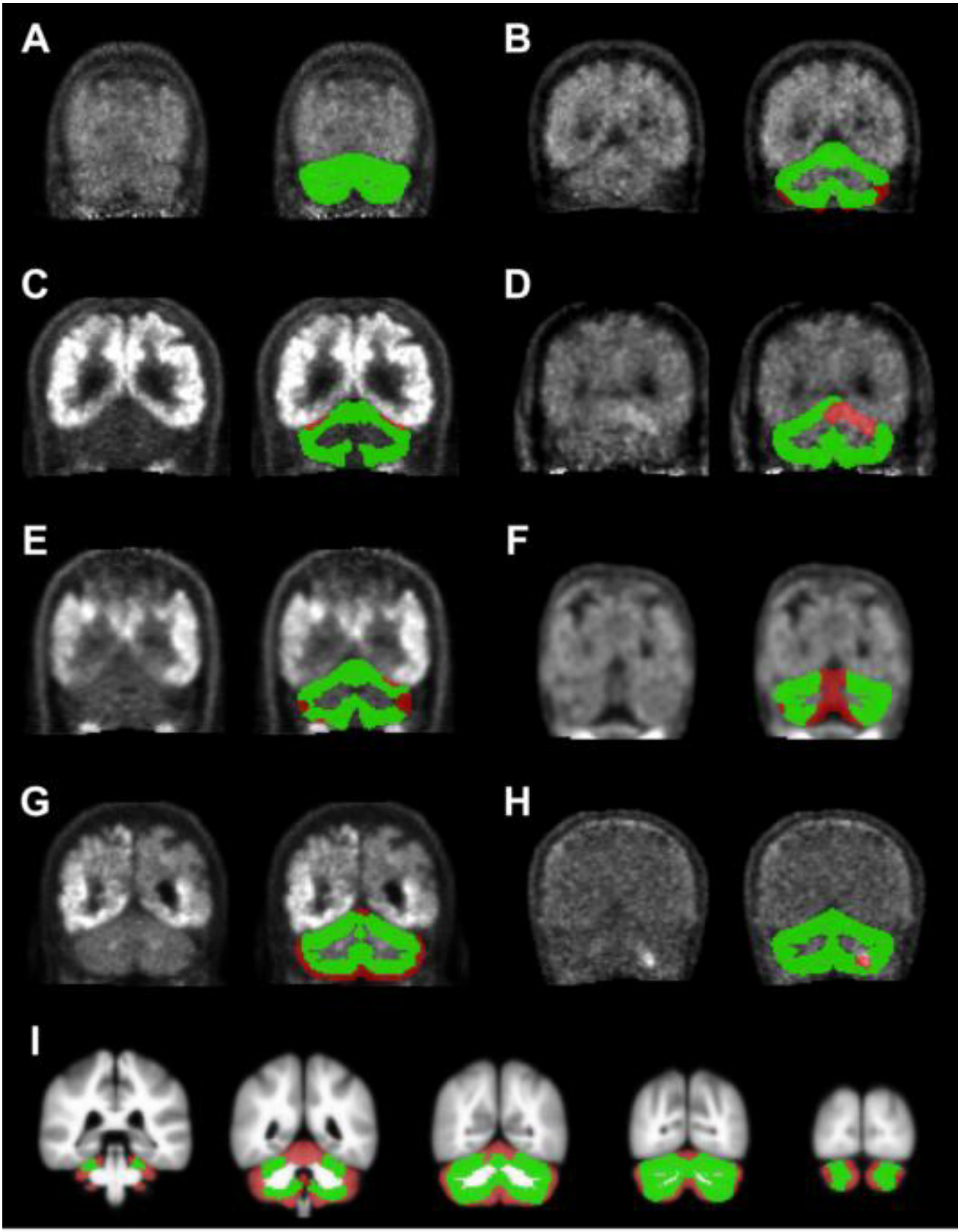


Figure 2. (A)-(H) Coronal slices of eight different ADNI FTP PET scans with subject-specific CerTauSeg cerebellar segmentation results, in which green voxel were classified as "clean" cerebellar reference and red voxels removed due to off-target contamination or CSF dilution. (I) Five coronal slices of the "Universal" ADNI FTP reference region in green, overlaid on on the whole cerebellar GM mask in red.

Table 1. Cohen's d effect sizes of CenTauR region SUVRs between cognitive and amyloid status groups according to cerebellar reference region

		Whole Cer GM	Eroded Whole Cer GM	Inferior Cer GM	Eroded Inferior Cer GM	CenTauR Cer	Subject-specific CerTauSeg Cer	Universal ADNI FTP Cer
Universal	CN Aβ+ vs CN Aβ-	0.251	0.217	0.222	0.178	0.150	0.197	0.251
	MCI Aβ+ vs CN Aβ-	1.340	1.299	1.348	1.305	1.340	1.292	1.372
	AD vs CN Aβ-	1.852	1.800	1.857	1.796	1.833	1.788	1.788
Mesial	CN Aβ+ vs CN Aβ-	0.445	0.418	0.409	0.378	0.353	0.404	0.461
	MCI Aβ+ vs CN Aβ-	2.024	2.005	2.048	2.038	2.074	2.033	2.118
	AD vs CN Aβ-	2.719	2.646	2.654	2.581	2.581	2.672	2.699
Temporo-Parietal	CN Aβ+ vs CN Aβ-	0.264	0.229	0.237	0.193	0.165	0.211	0.261
	MCI Aβ+ vs CN Aβ-	1.317	1.276	1.329	1.284	1.321	1.270	1.343
	AD vs CN Aβ-	1.793	1.744	1.802	1.742	1.779	1.734	1.731
Frontal	CN Aβ+ vs CN Aβ-	0.262	0.229	0.232	0.188	0.155	0.202	0.258
	MCI Aβ+ vs CN Aβ-	0.931	0.915	0.977	0.928	0.965	0.905	0.946
	AD vs CN Aβ-	1.522	1.500	1.535	1.490	1.513	1.488	1.469

Note: Green highlights are largest effect sizes for a given CenTauR region and group comparison, and yellow denotes the 2nd largest effect size.

Keywords: tau, PET, reference, cerebellum, FTP

79 Updated public CenTauR pipelines to measure CenTauR, CenTauRZ, and SUVR tau PET units

Christopher Schwarz[1], Antoine Leuzy[2,3,4], Vincent Doré[5], Victor L. Villemagne[6], Cally Xiao[7], Ioannis Pappas[7], Scott A. Przybelski[1], Carl M. Prakaashana[1], Matthew L. Senjem[1], Val J. Lowe[1], Jeffrey L. Gunter[1], Kejal Kantarci[1], Prashanthi Vemuri[1], Jonathan Graff-Radford[1], Ronald C. Petersen[1], David S. Knopman[1], Clifford R. Jack[1]

[1]*Mayo Clinic, Rochester, MN, US*
[2]*Clinical Memory Research Unit, Department of Clinical Sciences, Lund University, Lund, SE*
[3]*Critical Path for Alzheimer's Disease (CPAD) Consortium, Critical Path Institute, Tucson, AZ, US*
[4]*Enigma Biomedical Group, Knoxville, KY, US*
[5]*Austin Health, Melbourne, AU*
[6]*University of Pittsburgh, Pittsburgh, PA, US*
[7]*Laboratory of Neuro Imaging, USC Stevens Neuroimaging and Informatics Institute, Keck School of Medicine of USC, University of Southern California, Los Angeles, CA, US*

Background: The CenTauR project provides universal measurement scales and regions-of-interest (ROIs) for standardizing tau PET quantification units across tracers and pipelines. At HAI 2024, we released two fully automated software pipelines on the Global Alzheimer's Association Interactive Network (GAAIN) CenTauR website (https://www.gaain.org/centaur-project) to compute numeric CenTauR$_Z$ and CenTauR SUVR values for input pairs of T1-w MRI and late-uptake summed tau PET NIfTI files from 6 different tracers: FTP (AV-1451), MK-6240, RO948, GTP1, PI2620, or PM-PBB3, with 5 different CenTauR regions of interest (ROIs): universal (global), mesial temporal, meta-temporal, temporoparietal, and frontal. CenTauR$_Z$ units use a Z-score approach to allow binary classification (+/-) of images from across all these tau PET tracers, using a common threshold. The first pipeline implements the SPM8-based "Centiloid Standard" approach, which is also standard for CenTauR calibration. The second pipeline implements a more modern approach that quantifies images in MRI space incorporating SPM12 tissue-class segmentations and the Mayo Clinic Adult Lifespan Template. Both automatically apply included calibration equations.

The CenTauR group have recently released new calibration (slope and intercept) equations for "CenTauR" units, determined using their Joint Propagation Model (JPM) (Leuzy et al., 2024). Unlike CenTauR$_Z$, CenTauR units are designed to allow quantitative comparison of continuous values across tracers at all levels of pathology, analogous to the typical usage of Centiloid units for amyloid PET.

Methods: We have updated both GAAIN.org CenTauR pipelines with the new "CenTauR" calibration equations to now additionally output values in "CenTauR" units.

Results: These updated pipelines will be publicly released on https://www.gaain.org/centaur-project on or before HAI 2025.

Discussion: These pipelines allow researchers all over the world to easily quantify tau PET scans in CenTauR standardized units, enabling greater harmonization across tracers and across research groups.

Keywords: CenTauR,tau PET,standardization,harmonization

80 Predicting regional Alzheimer's disease pathology with plasma p-tau217 in preclinical AD

Hasom Moon[1], Xi Chen[1]

[1]*Stony Brook University, Stony Brook, NY, US*

Background: Plasma p-tau217 is recognized as a promising biomarker with high sensitivity and specificity for detecting Alzheimer's disease (AD). However, its value in inferring regional and longitudinal AD pathology is largely unstudied. This study aimed to examine how plasma p-tau217 can reflect regional tau burden and longitudinal change, in comparison to Aβ, in PET.

Methods: Using data from the Anti-Amyloid Treatment in Asymptomatic Alzheimer's disease (A4) study, 333 Aβ+ cognitively unimpaired older adults (age ≥ 65 years, 190 Females) underwent repeated 18-F Florbetapir Aβ PET and 18-F Flortaucipir tau PET, with baseline plasma p-tau217 measured using an Eli Lilly electrochemiluminescence immunoassay. Associations between p-tau217 and regional SUVRs were examined using correlations with Bonferroni correction.

Results: Plasma p-tau217 was associated with concurrent tau in early-to-mid Braak regions, primarily restricted to temporal-parietal regions and precuneus (Figure 1a-b) and Aβ burden across cortical regions, particularly in precuneus (Figure 2a-b). When predicting tau PET distribution using a single measure of p-tau217, we found the predicted tau burden was largely similar to the observed pattern (Figure 3). Longitudinally, baseline plasma p-tau217 predicted tau accumulation across broader cortical regions (Figure 1c-d), extending beyond temporal regions further to medial-lateral frontal regions. However, plasma p-tau217 had little prediction for Aβ change (Figure 2c-d), probably reflecting Aβ plateau in late preclinical AD.

Conclusion: We found evidence highlighting the potential of using a single measurement of plasma p-tau217 to infer regional pathology burden in preclinical AD. Plasma p-tau217 reflects concurrent tau pathology in temporal-parietal regions and cortical amyloid burden. Furthermore, its strong prediction for future tau accumulation, but not Aβ, suggests that elevation of p-tau217 may be an earlier event reflecting emerging tau pathology prior to measurable PET changes, offering support for clinical utility of plasma p-tau217 for disease monitoring, early detection, and timely intervention of AD.

Figure 1. Relationship between p-tau217 and tau PET. (a) Significant correlation between p-tau217 and concurrent regional tau PET. (b) Correlation between p-tau217 and concurrent early tau composite. (c) Significant correlation between p-tau217 and slope of longitudinal regional tau PET. (d) Correlation between p-tau217 and slope of early tau composite. The slopes for longitudinal tau PET in Figure 1(c) and 1(d) were extracted using linear mixed-effects models (N = 296). Only regions with family-wise error (FWE)-corrected p value < .05 were presented in Figure 1(a) and 1(c). All results remained consistent after controlling for age and amyloid composite.

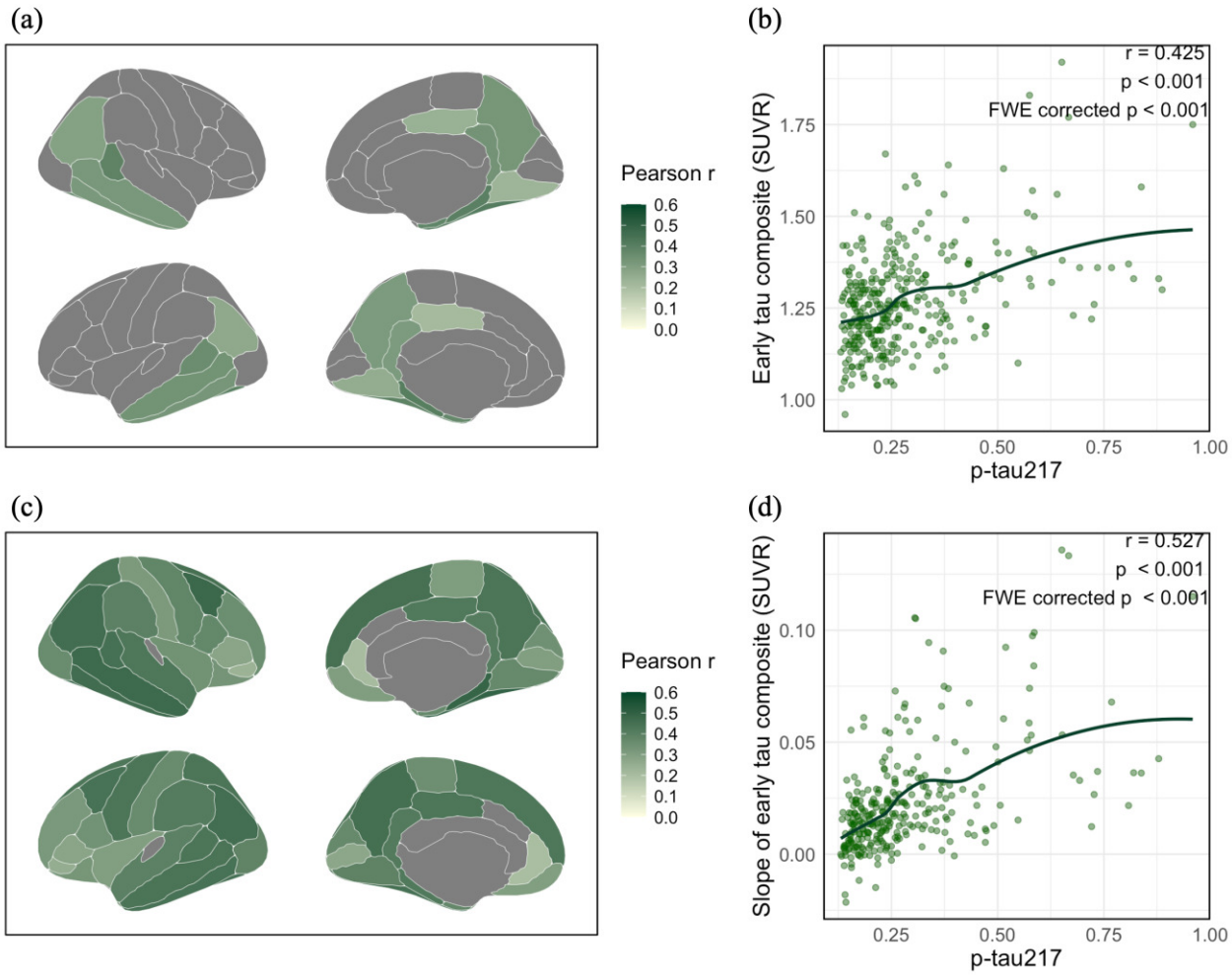


Figure 2. Relationship between p-tau217 and amyloid PET. (a) Correlation between p-tau217 and concurrent amyloid composite. (b) Correlation between p-tau217 and precuneus amyloid. (c) Correlation between p-tau217 and slope of amyloid composite change. (d) Correlation between p-tau217 and slope of precuneus amyloid change. The slopes for amyloid PET changes in Figure 2(c) and 2(d) were calculated as the change in SUVRs between two time points divided by the time lag (in years) (N = 280). All results remained consistent after controlling for age and early tau composite.

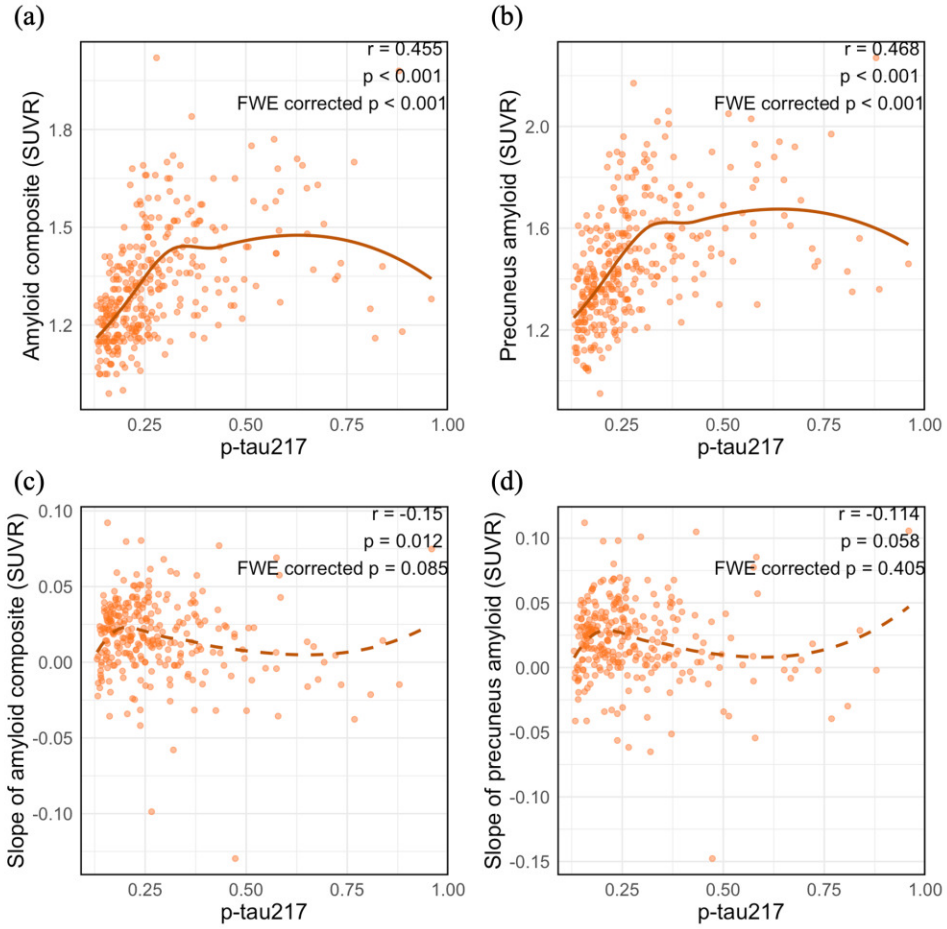
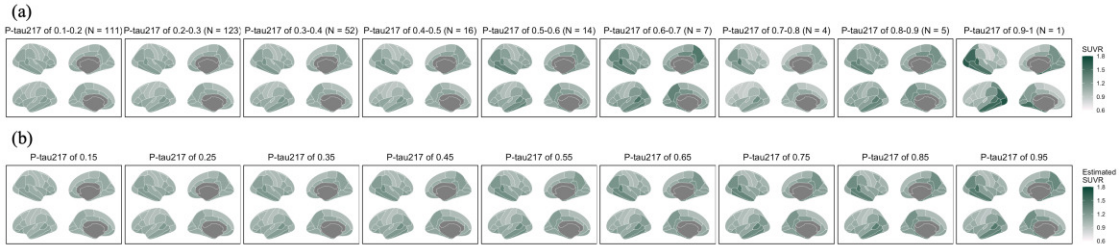


Figure 3. High similarities between the observed (a) and estimated (b) concurrent regional tau PET pattern across the levels of p-tau217.



Keywords: plasma p-tau217, amyloid, tau, PET, preclinical Alzheimer's disease

81 TSPO-PET before and after low-dose interleukin-2 in patients with mild to moderate Alzheimer's disease

Belen Pascual[1], Alireza Faridar[1], Quentin Finn[1], Nazaret Gamez[1], Stanley Appel[1], Joseph Masdeu[1]

[1]*Houston Methodist Stanley H. Appel Department of Neurology, Houston Methodist Research Institute, Weill Cornell Medicine, Houston, TX, US*

Background: Brain inflammation can be assessed using translocator protein (TSPO) PET. TSPO is highly expressed by microglia, peripherally-derived macrophages, and astrocytes. However, TSPO PET does not distinguish between M1 (neurotoxic) and M2 (neuroprotective) microglial phenotypes. Since the applicability of TSPO PET to study the evolution of brain inflammation in AD clinical trials targeting inflammation has not been studied, we performed TSPO-PET in a clinical trial using ^{11}C-ER176, which has high specific binding, a favorable metabolite profile, and is increased in brain areas with high tau levels.

Methods: Thirty-eight AD patients (ages 50-86, MMSE scores 12-26) participated in a phase 2a, randomized, double-blind, placebo-controlled trial evaluating two dosing frequencies of Interleukin-2 (IL-2). Over a 21-week period, 9 participants received IL-2 every 4 weeks (IL-2 q4wks), 10 received IL-2 every 2 weeks (IL-2 q2wks), and 19 received placebo. ^{11}C-ER176 PET (using standard methods and an arterial-input function), blood/CSF biomarkers, and clinical scores were obtained before and after treatment.

Results: Group analyses did not show TSPO-PET binding differences before and after the different IL-2 dosing regimens or placebo. At the individual level, TSPO-PET binding was reduced in the hippocampus after treatment in most participants on IL-2 but not in those on placebo. Both IL-2 dosing regimens increased Treg numbers and function, but IL-2 q4wks was superior in enhancing Treg counts and Foxp3 mean fluorescent intensity. In the IL-2 q4wks group, CSF Aβ42 levels improved significantly (p=0.045), with a promising trend toward stabilized CSF-NfL levels (p=0.061) and slowed cognitive decline compared to placebo.

Conclusions: While IL-2 immunotherapy every 4 weeks enhanced Treg populations, showing promising trends in AD biomarkers and clinical scales, TSPO-PET was largely unchanged over the 21 weeks of the trial. A longer follow-up, a larger sample or, more likely, PET tracers specific for M1 and M2 are needed for clinical trials.

Keywords: TSPO, 11C-ER176 PET, Inflammation, IL-2 immunotherapy, Alzheimer's disease

82 In low neocortical tau individuals, high amygdala tau predicts faster cognitive decline

Bernard Hanseeuw[1,2], Emma Thibault[1], Michelle Farell[1], Rachel Buckley[1], Michael Properzi[1], Jennifer Gatchel[1], Rebecca Amariglio[1], Gad Marshall[1], Alexa Beiser[4], Sudha Seshadri[3], Charles De Carli[5], Reisa Sperling[1], Heidi Jacobs[1], Keith Johnson[1]

[1]*Mass General Brigham, Boston, MA, US*
[2]*Cliniques Universitaires Saint-Luc, Brussels, BE*
[3]*University of Texas Health San Antonio, San Antonio, TX, US*
[4]*Boston University, Boston, MA, US*
[5]*University of California Davis, Davis, CA, US*

Background: Recent clinical trials have used low signal in temporal neocortex (tau-PET stage<3) to identify individuals with early tauopathy. However, clinically normal (CN) adults with tau pathology restricted to the entorhinal cortex (stage=1) have slow clinical progression. Identifying tau-PET stage=2 –early progressive tauopathy– may thus hasten prevention trials. Post-mortem studies define intermediate Braak-stages as tau pathology in the medial temporal lobe, including hippocampus and amygdala, without neocortical tauopathy. We investigated amygdala Flortaucipir data, as off-target binding blurs hippocampal signal.

Methods: ^{F18}-Flortaucipir data were collected at Mass General Brigham in 490CN older than 55 and 48MCI patients. We used a sample of 100 low-amyloid individuals younger than 55 (mean age=47.8) to define thresholds for low and high tau-PET signal in three regions-of-interest: entorhinal (EC), amygdala (AMYG), and inferior temporal (IT) cortex. We defined thresholds as mean+2SD of the younger group, which were slightly lower, but overall consistent with Gaussian mixture models. Tau-PET staging was proposed following the proportion of participants with positive signal in each region. Linear mixed-models adjusted for age, sex, and education predicted subsequent cognition (PACC5) with PET stages.

Results: Across the 538 participants, we observed 12.7% EC+ (n=68), 9.1% AMYG+ (n=49), 8.4% IT+ (n=41). Tau-PET staging classified 98% of participants, including 86.3% as stage=0 (EC-/AMYG-/IT-), 3.0% as stage=1 (EC+/AMYG-/IT-), 3.0% as stage=2 (EC+/AMYG+/IT-), and 5.9% as stage=3 (EC+/AMYG+/IT+). The proportion of MCI/AD and high-amyloid participants increased with stages (Fig.1), with evidence that stage=2 were mostly high-amyloid CN. In CN, higher tau-PET stages predicted faster cognitive decline, with stage=2 declining faster than stage=1 (p=0.05), and slower than stage=3 (p=0.03, Fig.2). After excluding stage 3 individuals (red dots, Fig.3), amygdala tau was still associated with cognitive decline (p=0.05), whereas neocortical regions was not.

Conclusions: Amygdala tau-PET signal identifies clinically normal individuals at-risk for cognitive decline before neocortical tauopathy is apparent.

Fig.1: Characteristics of the participants

Mean value *(SD)*	All N=538	Stage 0 N=466	Stage 1 N=16	Stage 2 N=16	Stage 3 N=32	Two-tail p-value
Age at tau-PET Years	68.6 *(10.0)*	69.5 *(10.6)*	75.3* *(13.8)*	76.8* *(8.1)*	69.1* *(8.9)*	**<0.001**
Education Years	16.3 *(2.8)*	16.3 *(2.8)*	15.9 *(3.0)*	17.3 *(2.2)*	16.3 *(2.1)*	0.80
Female (%)	54.2%	55.4%	43.7%	62.5%	46.9%	0.20
E4 carriers (%)	25.7%	22.2%	12.5%	75.0%**	68.8%**	**<0.001**
% Clinically Impaired	7.9%	3.8%	6.3%	18.7%*	59.4%***	**<0.001**
% High-PiB individuals	23.4%	15.7%	18.7%	75.0%**	96.9%***	**<0.001**
Annual PACC5 change z-score/year	-0.06 *(0.10)*	-0.05 *(0.08)*	-0.08* *(0.09)*	-0.15** *(0.11)*	-0.22*** *(0.20)*	**<0.001**
Cognitive Follow-up Years	6.3 *(4.0)*	6.3 *(4.0)*	5.9 *(4.1)*	5.0 *(3.5)*	7.3 *(4.4)*	0.31

Fig.2: Cognitive decline by tau-PET stages

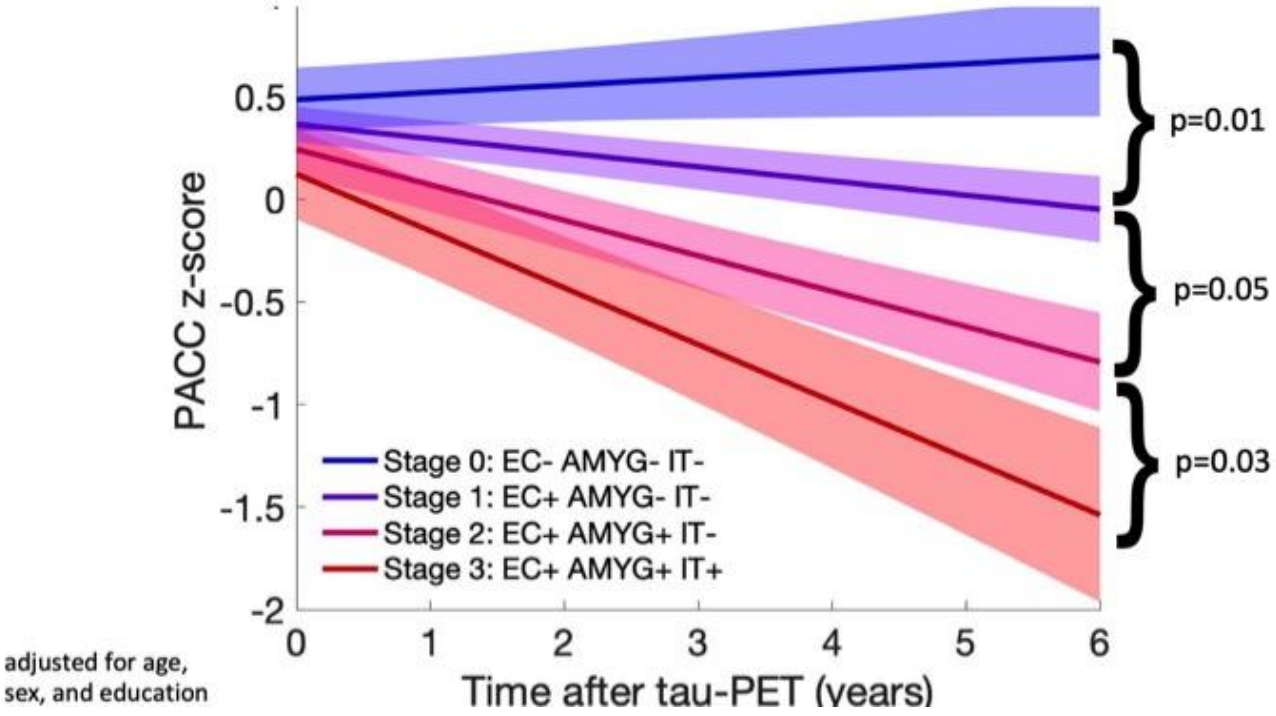
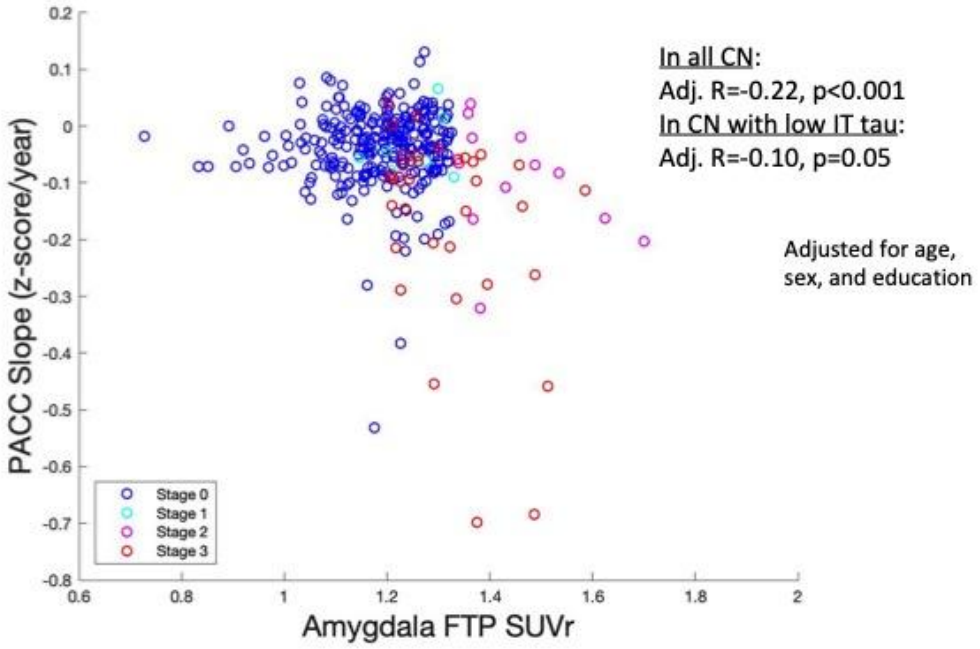


Fig.3: Scatter plot of amygdala Flortaucipir SUVr versus subsequent cognitive decline



Keywords: Amygdala, tau-PET, Braak staging, cognitive decline

83 EOAD-signature atrophy predicts progression to dementia in patients with early-onset MCI due to Alzheimer's disease

Thiago Paranhos[1], Yuta Katsumi[1], Michael Brickhouse[1], Ryan Eckbo[1], Alexander Zaitsev[1], Anna Du[1], Ani Eloyan[2], Kelly N. Nudelman[3], Tatiana Foroud[3], Jeffrey L. Dage[3,4], Maria C. Carrillo[5], Gil D. Rabinovici[6], Liana Apostolova[3,4,7], Bradford C. Dickerson[1], Alexandra Touroutoglou[1], LEADS Consortium[3]

[1]*Frontotemporal Disorders Unit and Massachusetts Alzheimer's Disease Research Center, Department of Neurology, Massachusetts General Hospital and Harvard Medical School, Boston, MA, US*
[2]*Department of Biostatistics, Center for Statistical Sciences, Brown University, Providence, RI, US*
[3]*Department of Neurology, Indiana University School of Medicine, Indianapolis, IN, US*
[4]*Department of Medical and Molecular Genetics, Indiana University School of Medicine, Indianapolis, IN, US*
[5]*Medical & Scientific Relations Division, Alzheimer's Association, Chicago, IL, US*
[6]*Department of Neurology, University of California – San Francisco, San Francisco, CA, US*
[7]*Department of Radiology and Imaging Sciences, Center for Neuroimaging, Indiana University School of Medicine Indianapolis, Indianapolis, IN, US*

Prognostic risk stratification for patients at the mild cognitive impairment (MCI) stage of early-onset Alzheimer's disease (EOAD) would allow professionals and loved ones to make better-informed medical and life planning decisions. While research including our own (Bakkour, Morris, Dickerson, 2009) has demonstrated the prognostic value of MRI-based measures of brain structure in late-onset amnestic AD, its utility for predicting progression to dementia in EOAD remains unclear. Here, we measured the magnitude of cortical atrophy within our recently described EOAD signature regions (Touroutoglou et al. 2023) in patients with EOAD at the MCI stage (N=84) recruited in LEADS. The main goal of the study was to evaluate the utility of this measure as a predictor of time to subsequent progression to dementia. Our second goal was to examine the independent or synergistic contributions of EOAD signature of atrophy and standard clinical severity measures used in clinical trials. For each patient, we measured the time between baseline visit and subsequent visit at which progression to mild dementia was documented or last observation. Baseline cortical atrophy was measured as *W*-scores (i.e., *Z*-scores adjusted for age and sex relative to a sample of healthy controls) in the EOAD signature. Baseline clinical severity was quantified with the Clinical Dementia Rating Sum-of-Boxes scores (CDR-SB). Simple and multivariable Cox regression models examined the relationship between atrophy in EOAD signature, CDR-SB, and the likelihood of progression to dementia. Greater baseline atrophy in the EOAD signature predicted higher risk of progression to dementia (hazard ratio = 1.2, 95% CI 1.1-1.3) and provided additive value to the CDR-SB (hazard ratio: 2.1, 95% CI:1.7-2.8) in predicting progression. These findings point to the role of EOAD MRI signature as an imaging biomarker to guide prognostication for patients with EOAD and their families and to inform the design of clinical trials.

Keywords: Magnetic Resonance Imaging; Clinical Dementia Rating Scale Sum of Boxes; prognostication; disease-modifying therapies; risk stratification

84 FDG reference region selection using PiB amyloid status-guided iterative normalization in a Down syndrome cohort

Max McLachlan[1], David Keator[2], Julie Price[3], Dana Tudorascu[4], Charles Laymon[4], Annie Cohen[4], Patrick Lao[5], Ben Handen[4], Tim Fryer[6], Beau Ances[7], Shahid Zaman[6], Elizabeth Head[2], Mark Mapstone[2], Brecca Bettcher[1], Jose Guerrero Gonzalez[1], Lisette LeMerise[1], Andrew McVea[1], Alexandra DiFillipo[1], Matthew Zammit[1], Sigan Hartley[1], Bradley Christian[1]

[1]*University of Wisconsin - Madison, Madison, WI, US*
[2]*University of California, Irvine, Irvine, CA, US*
[3]*MGH Martinos Center, Harvard, Boston, MA, US*
[4]*University of Pittsburgh, Pittsburgh, PA, US*
[5]*Columbia University Irving Medical Center, New York, NY, US*
[6]*University of Cambridge, Cambridge, GB*
[7]*Washington University in St. Louis, St. Louis, MO, US*

Background: Individuals with Down syndrome (DS) carry a genetic risk for Alzheimer's disease, resulting in an accelerated AT[N] timeline. The heterogeneity of glucose metabolism and definition of a suitable FDG reference region has not been fully characterized in DS. In the neurotypical population, many FDG PET studies implement whole brain (WB) intensity normalization, despite evidence for underestimation of metabolic change. Yakushev et al. (2008) proposed a data-driven method for reference region selection by leveraging false-positive hypermetabolism generated from WB normalization. The goal of this work is to investigate the data-driven method in a DS cohort, using amyloid status as a general predictor for metabolism.

Methods: Cross-sectional FDG scans were acquired in a cohort of 92 participants with DS. Each participant completed cognitive consensus testing at time of FDG scan and amyloid (Aβ) PiB PET imaging ~1.5 years prior. FDG scans were realigned, summed 30-60min, smoothed by 6mm, spatially normalized to a DS-specific template, and intensity-normalized using WB average. Participants were grouped by Aβ status (Table 1). Voxel-level statistics were performed in SPM12, using Welch's t-test as the statistical comparison between groups. The T-map for the Aβ+ > Aβ- contrast (hypermetabolism) was thresholded to $p<0.05$ (FWE corrected); the surviving clusters were masked (Figure 1) and used for the second-pass iterative normalization.

Results: Figure 2 displays hypometabolism between amyloid groups after FWE correction. Iterative normalization detects larger significant clusters, primarily in the angular gyri, precuneus, cingulate, and temporal cortices. Figure 3 compares FDG SUVR across methods and cognitive status. Iterative normalization shows significant hypometabolism between CS and Dementia groups in all regions; WB normalization only detects differences for the whole cortex and parietal lobe.

Conclusion: Data-driven iterative normalization demonstrates greater discriminative power than WB normalization in the DS population. This method can be explored for other radiotracers without validated reference regions.

	Aβ-	Aβ+	Entire Cohort
Cohort Size (n)	78	14	92
Average Age at Scan (yrs)	38.5 (SD = 7.6)	48.8 (SD = 7.2)	40.0 (SD = 8.4)
Sex (M/F)	40/38	8/6	48/44
Cognitive Status			
CS	72	6	78
MCI	5	1	6
Dementia	1	7	8

Table 1 – Participant demographics. Aβ positivity was determined using a threshold of 18.1 CL.
Abbreviations: CS = cognitively stable; MCI = mild cognitive impairment

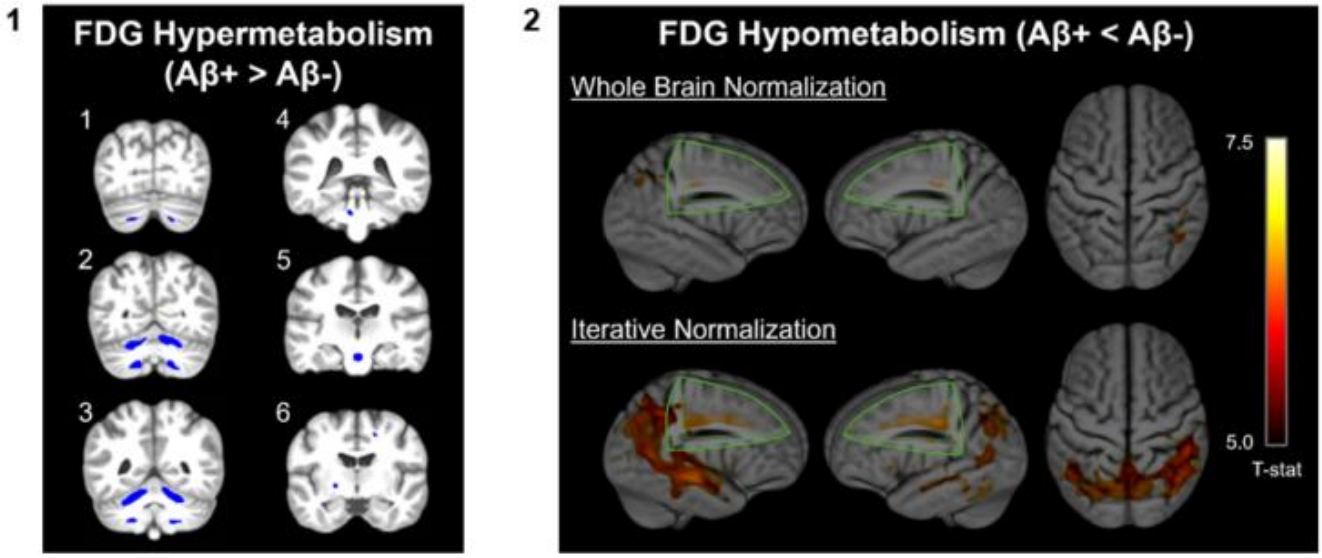


Figure 1 – Clusters of significant FDG hypermetabolism (Aβ+ > Aβ-) detected with whole brain normalization, using p<0.05 after FWE correction. Clusters are predominately in the cerebellum and pons. Whole brain normalization has been shown to detect false-positive hypermetabolism in preserved brain regions when compared across AD stages (Herholz et al. 1990; Herholz et al. 2002; Buchert et al. 2005). Therefore, these clusters were masked and then used as reference region for the iterative normalization technique.

Figure 2 – Clusters of significant hypometabolism (Aβ+ < Aβ-) for each normalization method, using p<0.05 after FWE correction. Hypometabolism is biologically expected in the Aβ+ group. Whole brain normalization detects small clusters of hypometabolism in the cingulate cortex and angular gyrus. Iterative normalization detects much larger clusters throughout the temporal and parietal lobes. Sensitivity analysis (by age and sex matching across amyloid groups) replicates these findings to a lower degree of significance.

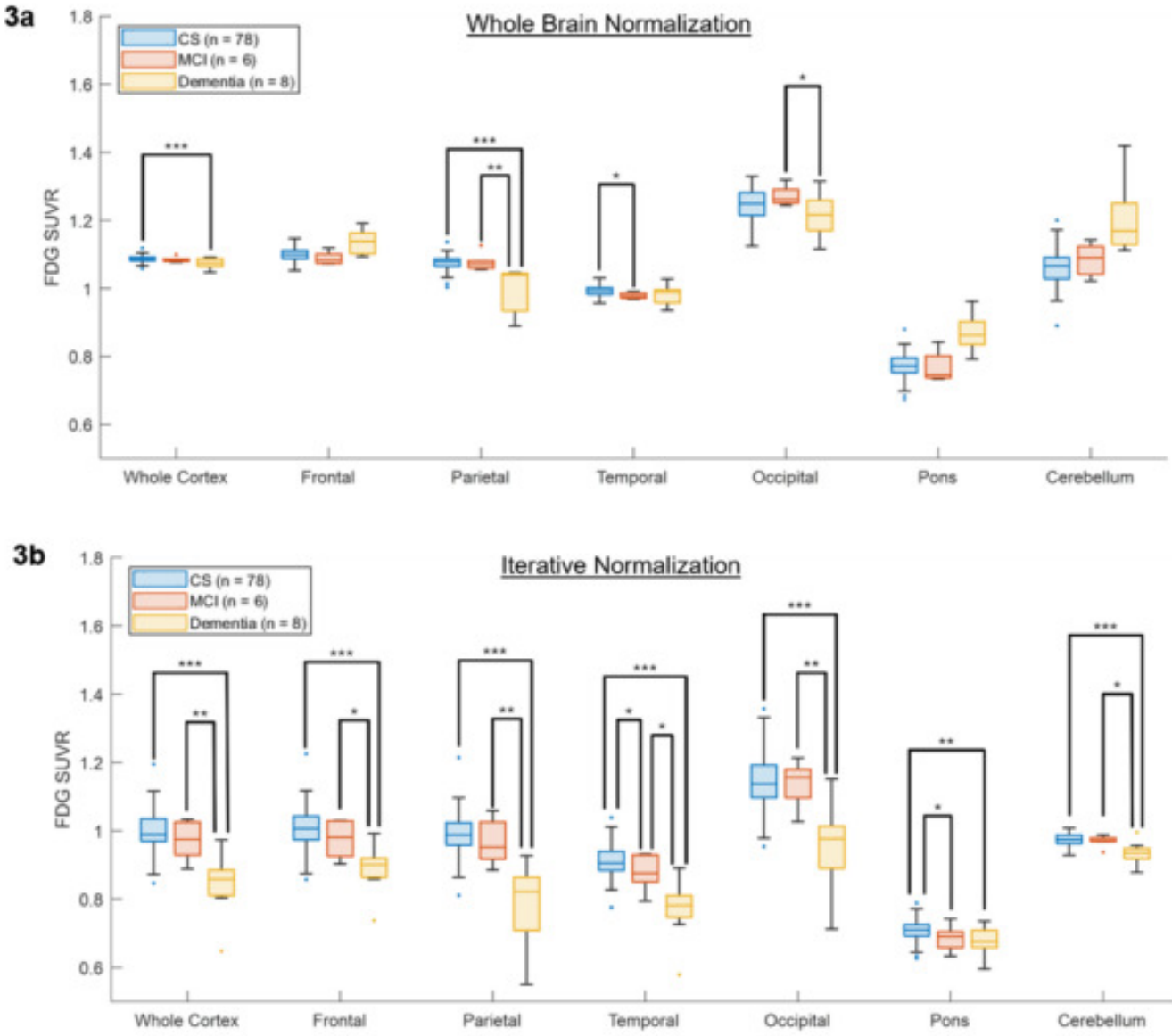


Figure 3a – FDG SUVR after whole brain normalization, separated by brain region and cognitive status. One-tailed t-tests were performed assuming greater hypometabolism coincides with greater cognitive impairment. Significant hypometabolism is detected between CS and Dementia groups in the whole cortex and parietal lobe.

Figure 3b – FDG SUVR after iterative normalization, separated by brain region and cognitive status. One-tailed t-tests were performed assuming greater hypometabolism coincides with greater cognitive impairment. Significant hypometabolism is detected between CS and Dementia groups in all observed brain regions. Most brain regions also demonstrate significant hypometabolism between MCI and Dementia groups.

Abbreviations: CS = cognitively stable; MCI = mild cognitive impairment

Keywords: Amyloid, Alzheimer's disease, Down syndrome, PET, FDG

85 Microscopic visualization of fluorescent MK-6240

Peter Kunach[1,2], Matthew S. Smith[3], Monika I. Antczak[3], Ankit Gupta, Jim Monistrol, Parth Tripathi, Varun Jalapati, Marie-Christine Guiot, Daniel Stoddard, Sarah H. Shahmoradian, Brian K. Shoichet, Jaime Vaquer-Alicea, Pedro Rosa-Neto, Joseph M. Ready, Marc I. Diamond

[1]*Center for Alzheimer's and Neurodegenerative Diseases, Peter O'Donnell Jr. Brain Institute, Dallas, TX, US*
[2]*Department of Neurology, McGill University, Montreal, QC, CA*
[3]*Department of Pharmaceutical Chemistry, University of California San Francisco, San Francisco, CA, US*
[4]*Program of Biophysics, University of California San Francisco, San Francisco, CA, US*
[5]*Department of Biochemistry, University of Texas Southwestern Medical Center, Dallas, TX, US*
[6]*Department of Biophysics, University of Texas Southwestern Medical Center, Dallas, TX, US*

The Positron Emission Tomography (PET) ligand, MK-6240, binds tau filaments from Alzheimer's disease (AD). Cryogenic electron microscopy (cryo-EM) has revealed a stacked binding mode for MK-6240 facilitated by homotypic pi-pi interactions, and a hydrogen bond with the fibril. We leveraged this information to design a fluorescent analog based on the MK-6240 scaffold. We produced an MK-6240 analog containing a fluorescent moiety, that binds both recombinant and *ex vivo* tau filaments. We determined the precise mode of interaction by cryo-EM. Akin to the parental compound, the analog binds in a columnated fashion via pi-pi interactions, but forms hydrogen bonds with different tau residues. Fluorescent MK-6240 specifically labels AD tau pathology in fixed tissue slices. This novel conformation-specific dye may improve development of agents for diagnosis and therapy of AD.

Keywords: PET, Fluorescence, Cryo-EM, Alzheimer Disease, Tau

86 Conversion of Tau PET SUVR data to CenTauR units using the Joint Propagation Model

Antoine Leuzy[1,2,3], Lars Lau Raket[1,6], Victor L Villemagne[7,8,9], Gregory Klein[10], Matteo Tonietto[10], Emily Olafson[11], Suzanne Baker[12], Ziad S Saad[13], Santiago Bullich[14], Brian Lopresti[15], Sandra Sanabria Bohorquez[11], Olivia Lutz[11], Mercè Boada[16,17], Tobey J Betthauser[18,19,20], Arnaud Charil[21], Emily C Collins[6], Jessica A Collins[22], Roger N Gunn[24], Makoto Higuchi[25], Eric Hostetler[26], R Matthew Hutchison[22], Leonardo Iaccarino[6], Philip S Insel[27], Michael C Irizarry[21], Clifford R Jack Jr[28], William J Jagust[29], Keith A Johnson[30,31], Sterling C Johnson[18,19,20], Yashmin Karten[2], Marta Marquié[16,17], Sulantha Mathotaarachchi[3], Mark A Mintun[6], Rik Ossenkoppele[1,32], Ioannis Pappas[33], Ronald C Petersen[34], Gil D Rabinovici[35], Pedro Rosa-Neto[37], Christopher G Schwarz[28], Ruben Smith[1,39], Andrew W Stephens[14], Alex Whittington[23], Maria C Carrillo[40], Michael J Pontecorvo[6], Samantha Budd Haeberlein[3], Billy Dunn[41], Hartmuth C Kolb[3], Diane Stephenson[2], Christopher C Rowe[8,9,42], Oskar Hansson[1,39], Vincent Doré[9,44]

[1]*Clinical Memory Research Unit, Department of Clinical Sciences, Lund University, Lund, SE*
[2]*Critical Path for Alzheimer's Disease (CPAD) Consortium, Critical Path Institute, Tucson, AZ, US*
[3]*Enigma Biomedical USA, Knoxville, TN, US*
[4]*Wallenberg Centre for Molecular and Translational Medicine, University of Gothenburg, Gothenburg, SE*
[5]*Department of Psychiatry and Neurochemistry, University of Gothenburg,, Gothenburg, SE*
[6]*Eli Lilly and Company, Indianapolis, IN, US*
[7]*Department of Neurology, University of Pittsburgh School of Medicine, Pittsburgh, PA, US*
[8]*Florey Department of Neuroscience, University of Melbourne, Victoria, AU*
[9]*Department of Molecular Imaging & Therapy, Austin Health, Victoria, AU*
[10]*F. Hoffmann-La Roche Ltd, Basel, CH*
[11]*Clinical Imaging Group, Genentech, Inc., San Francisco, CA, US*
[12]*Lawrence Berkeley National Laboratory, Berkeley, CA, US*
[13]*Janssen Research & Development, San Diego, USA;, San Diego, CA, US*
[14]*Life Molecular Imaging GmbH, Berlin, DE*
[15]*Department of Radiology, University of Pittsburgh School of Medicine, Pittsburgh, PA, US*
[16]*Ace Alzheimer Center Barcelona, Barcelona, ES*
[17]*Networking Research Center on Neurodegenerative Diseases (CIBERNED), Madrid, ES*
[18]*Wisconsin Alzheimer's Disease Research Center, University of Wisconsin-Madison School of Medicine and Public Health, madison, WI, US*
[19]*Department of Medicine Division of Geriatrics, University of Wisconsin-Madison School of Medicine and Public Health, Madison, WI, US*
[20]*Department of Medical Physics, University of Wisconsin-Madison, Madison, WI, US*
[21]*Eisai, Inc., Nutley, NJ, US*
[22]*Biogen, Cambridge, MA, US*
[23]*Perceptive Discovery, London, GB*
[24]*Xing Imaging – A Mitro Company, London, GB*
[25]*Advanced Neuroimaging Center, Institute for Quantum Medical Science, National Institutes for Quantum Science and Technology, Chiba, JP*
[26]*Merck & Co., West Point, PA, US*
[27]*Department of Psychiatry and Behavioral Sciences, University of California, San Francisco, CA, US*
[28]*Department of Radiology, Mayo Clinic, Rochester, MI, US*
[29]*University of California Berkeley; Lawrence Berkeley National Laboratory, Berkeley, CA, US*

[30]*Harvard Medical School, Department of Radiology, Boston, MA, US*
[31]*Gordon Center for Medical Imaging, Massachusetts General Hospital, Boston, MA, US*
[32]*Amsterdam University Medical Center, Neuroscience Campus Amsterdam, Alzheimercenter, Amsterdam, NL*
[33]*Laboratory of Neuro Imaging, USC Stevens Neuroimaging and Informatics Institute, Keck School of Medicine of USC, University of Southern California, Los Angeles, CA, US*
[34]*Department of Neurology, Mayo Clinic, Rochester, MI, US*
[35]*Department of Neurology, Memory and Aging Center, Weill Institute for Neurosciences, University of California, San Francisco, CA, US*
[36]*Department of Radiology & Biomedical Imaging, University of California, San Francisco, CA, US*
[37]*Translational Neuroimaging Laboratory, Department of Neurology and Neurosurgery, Faculty of Medicine, The McGill University Research Centre for Studies in Aging, McGill University, Montreal, QC, CA*
[38]*Montreal Neurological Institute, McGill University, Montreal, QC, CA*
[39]*Department of Neurology, Skåne University Hospital, Lund, SE*
[40]*Alzheimer's Association, Chicago, IL, US*
[41]*Senior advisor to CPAD Consortium, Critical Path Institute, Tucson, AZ, US*
[42]*The Australian Dementia Network (ADNeT), The University of Melbourne, Melbourne, AU*
[43]*Memory Clinic, Skåne University Hospital, Malmö, SE*
[44]*Health and Biosecurity Flagship, The Australian eHealth Research Centre, CSIRO, Melbourne, AU*

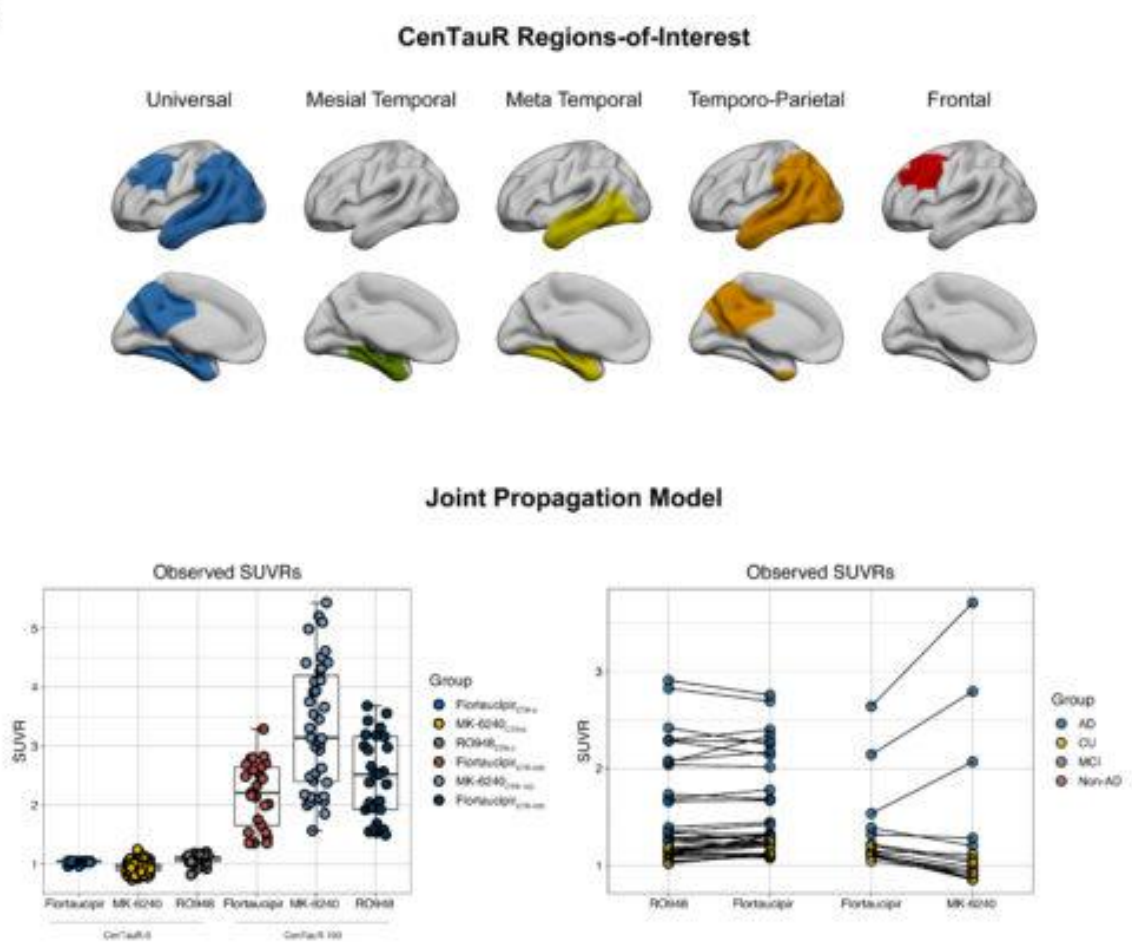
Objectives: The CenTauR scale has been recently proposed for between-tracer harmonization of tau-PET images. Here, we studied how CenTauRs enhance the comparability of tau-PET quantification by comparing the prevalence of CenTauR-defined tau-PET positivity across two matched cohorts scanned with different tau-PET tracers.

Methods: The Joint Propagation Model (JPM) is a statistical model developed within the Critical Path for Alzheimer's Consortium (CPAD) led Tau PET Harmonization Working Group (Leuzy et al., Alzheimers Dement. 2024; Figure 1A). The JPM simultaneously models the relationships of data from anchor point subjects and data from subjects in head-to-head studies with the CenTauR scale, providing conversion equations for multiple tracers. We applied these JPM equations to convert [^{18}F]flortaucipir SUVR (Meta-temporal ROI) data from 561 cognitively impaired participants from the ADNI and OASIS-3 studies into CenTauRs. We then used ROC analysis to find the CenTauR cut-off for positivity (T+) that best discriminated between FDA-approved positive/negative visual reads.. The prevalence of T+ was compared across two matched cohorts consisting of Aβ-positive cognitively impaired (MCI and AD dementia) individuals scanned with either [^{18}F]flortaucipir (ADNI) or [^{18}F]MK-6240 (AIBL). The cohorts were matched at the individual level based on age, MMSE, and Centiloids.

Results: A cut-off of 18 CenTauRs was found to optimally classify [^{18}F]flortaucipir PET visual reads (Figure 1B). The matching procedure identified 46 cases in total (23 [^{18}F]flortaucipir, 23 [^{18}F]MK-6240). The prevalence of T+ using the 18 CenTauRs cut-off for the Meta-temporal ROI was found to be highly comparable across tracers ([^{18}F]flortaucipir, n=19; 83%; [^{18}F]MK-6240, n=17; 74%). Further analyses involving other ROIs, tracers and cohorts along with SUVR-to-CenTauR conversion equations, will be presented.

Conclusions: Implementation of standardized methodologies is key to harmonizing Tau-PET results across distinct AD research and interventional clinical trials. These preliminary analyses suggest that JPM-derived CenTauR equations are suitable for harmonization of tau-PET outcome data.

A



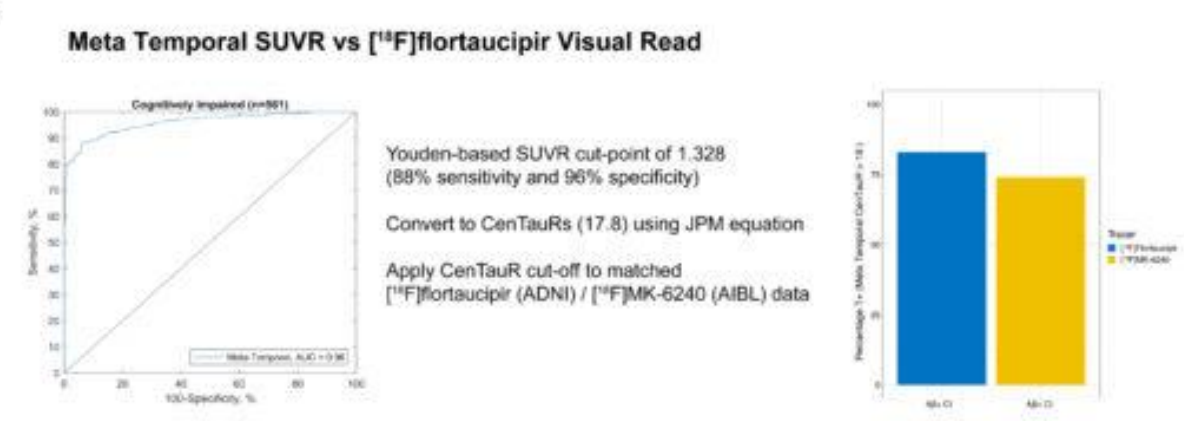
$SUVR_{ij} = a_j \cdot c_i + b_j + \varepsilon_{ij}$

Subject i's SUVR with tracer t is a linear transformation of the subject's true CenTauR status, c_i

ε_{ij} is normally distributed measurement noise that may depend on the tracer

Model has two unknowns, a_j and c_i multiplied together - there is structure to c_i requiring modelling

B



Keywords: Tau PET, Harmonization, CenTauR, Joint Propagation Model

87 The role of cohort heterogeneity in predicting AD/ADRD cognitive decline

Peiwei Liu[1], Jacinda Taggett[1], Theresa Harrison[1], Heather Snyder[3], Charles DeCarli[4], Prashanthi Vemuri[5], Danielle Harvey[6], William Jagust[1], Laura Baker[2], Susan Landau[1]

[1]*Department of Neuroscience, University of California, Berkeley, Berkeley, CA, US*
[2]*Gerontology and Geriatric Medicine, Wake Forest University, Winston-Salem, NC, US*
[3]*Alzheimer's Association, Chicago, IL, US*
[4]*Department of Neurology, University of California, Davis, Sacramento, CA, US*
[5]*Department of Radiology, Mayo Clinic, Rochester, MN, US*
[6]*Public Health Sciences, University of California, Davis, Sacramento, CA, US*

Background: We previously reported that tau PET was more predictive of cognition in ADNI (a clinic-based sample low in comorbidities and ethnoracial diversity) than U.S. POINTER (a community-based sample with high cardiovascular risk and ethnoracial diversity), and this difference was driven by Aβ+ individuals. Here, we investigate the roles of cortical thickness and cardiovascular risk contributing to cohort differences among Aβ+ older individuals.

Methods: U.S. POINTER (N = 775; 68.9 ± 5.2 years, 62.8% female, 30.6% Aβ+) and ADNI (N = 405; 69.9 ± 5.4 years, 58% female, 31.1% Aβ+) were matched by age, sex, Clinical Dementia Rating Scale Sum of Boxes score, and APOE4 status (Table 1). Among the Aβ+ subset, generalized linear models in each cohort examined baseline whole-brain tau PET (MK6240 in U.S. POINTER, FTP in ADNI) and Preclinical Alzheimer's Cognitive Composite (PACC) scores. We also examined cohort-specific cortical thickness associations with PACC scores and cardiovascular risk (Framingham Risk Score (FRS)). Models with PACC controlled for age, sex, education, and PACC exposures, while FRS related models were controlled for education only.

Results: Tau throughout temporal and posterior cingulate regions (Figure 1), and lower cortical thickness in temporal pole, precuneus, and frontal regions (Figure 2A) were associated with poorer cognition (PACC) in ADNI, but these associations were much weaker in U.S. POINTER. However, there were more robust cortical thickness associations throughout frontal, cingulate, parietal, and occipital regions with cardiovascular risk in U.S. POINTER than ADNI (Figure 2B).

Conclusion: In ADNI, cognition is linked to cortical thickness and tau in AD-related regional patterns that have been previously observed in predominantly clinic-based samples. In POINTER, however, these associations were much weaker, and thickness was more closely linked to cardiovascular risk. Cohort recruitment differences, particularly in diversity and cardiovascular risk factors, impact the generalizability of AD-related brain-cognition relationships.

Keywords: Alzheimer's disease, Tau, Cortical thickness, Cognition, Cardiovascular risk

88 Differential tau accumulation in early-onset and late-onset Alzheimer's disease: Insights from [18F]-Florzolotau PET

Bayarjargal Khurelbaatar[1], Shao-Yi Huang[1], Kun-Ju Lin[1,2], Chin-Chang Huang[3], Jung-Lung Hsu[3], Kuo-Lun Huang[3], Hsiu-Chuan Wu[3], Chi-Wei Huang[4], Chiung-Chih Chang[4], Ing-Tsung Hsiao[1,2]

[1]*Department of Medical Imaging and Radiological Sciences, Chang Gung University, Taoyuan, Taiwan, ROC., Taoyuan, TW*
[2]*Molecular Imaging Center and Nuclear Medicine, Chang Gung Memorial Hospital, Taoyuan, Taiwan, ROC., Taoyuan, TW*
[3]*Neurology, Chang Gung Memorial Hospital, Taoyuan, Taiwan, ROC., Taoyuan, TW*
[4]*Neurology, Chang Gung Memorial Hospital, Kaohsiung, Taiwan, ROC., Kaohsiung, TW*

Objective: We investigated the longitudinal changes in cortical tau accumulations and their correlation in different brain regions among patients in the Alzheimer's disease (AD) continuum using [^{18}F]-Florzolotau PET.

Methods: This study included 55 participants (age 69.8±2.3 y; 22 men, 33 women): 18 with mild cognitive impairment (MCI), and 37 with Alzheimer's disease (AD). All participants completed [^{18}F]-Florzolotau PET and [^{18}F]-Florbetapir PET, MRI, and neuropsychological tests at baseline and after follow-up. Amyloid-β (Aβ) PET images were visually scored as positive (+) or negative (-). Patients on the AD continuum, including Aβ+ MCI and AD, were classified into early-onset (EO+ <65 y) or late-onset (LO+ ≥65 y) groups. The mean MMSE scores of EOAD and LOAD were 24.2±1.2 and 25.6±0.8 for baseline, 22.5±0.9 and 23.8±1.5 for follow-up, separately. Tau PET SUV ratios (SUVRs) were calculated for each Braak stage VOI using the inferior cerebellum as the reference region.

Results: Significant differences were observed in tau accumulation, with EO+ patients showing rapid global cortical tau accumulation, particularly in Braak stages III-VI compared to LO+. The global cortical [^{18}F]-Florzolotau PET SUVR were 1.67±0.72 in 40 LO+ patients (75.8±4.1 y), and 1.87±0.9 in 15 EO+ patients (63.8±2.3 y; P<0.001) at baseline. The global cortical SUVR increased by 2% and 25.6% in the LO+ and EO+ groups, respectively and the EO+ group showed higher regional tau deposition than the LO+ groups (P<0.005 for each), with rapid accumulation in Braak stage III-IV (17.7±13.92%; P<0.006), Braak stage V-VI (16.5±11.5%; P<0.005), and global SUVR (P<0.005) compared with the LO+ group.

Conclusion: The findings suggest a more rapid progression of tau pathology in EOAD compared to LOAD, particularly in later Braak stages. Further longitudinal studies are warranted to elucidate the relationship between tau accumulation and long-term cognitive decline in Alzheimer's disease.

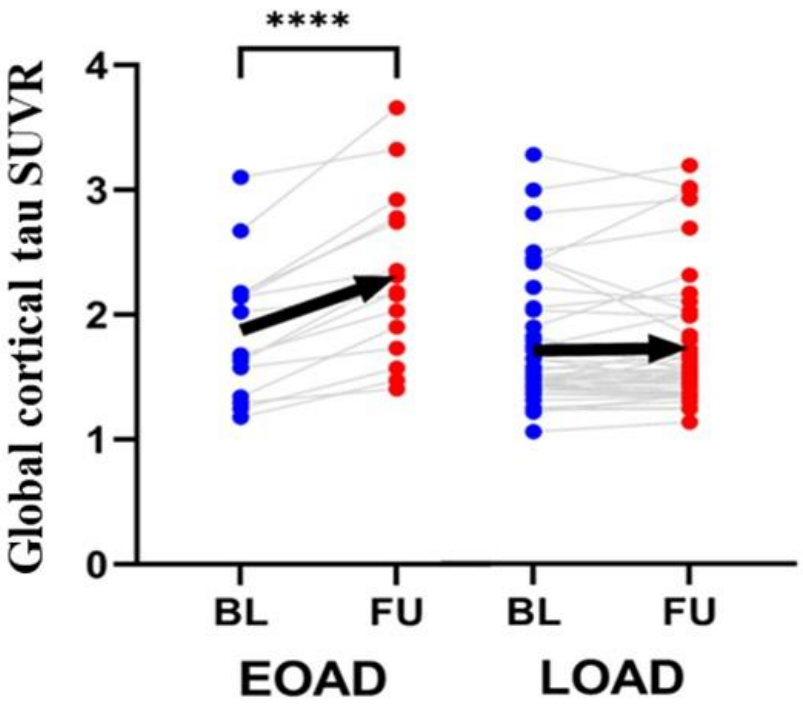


FIGURE 2. Changes in the global cortical [^{18}F]-Florzolotau PET SUVR in EOAD and LOAD. BL=baseline; FU=follow-up

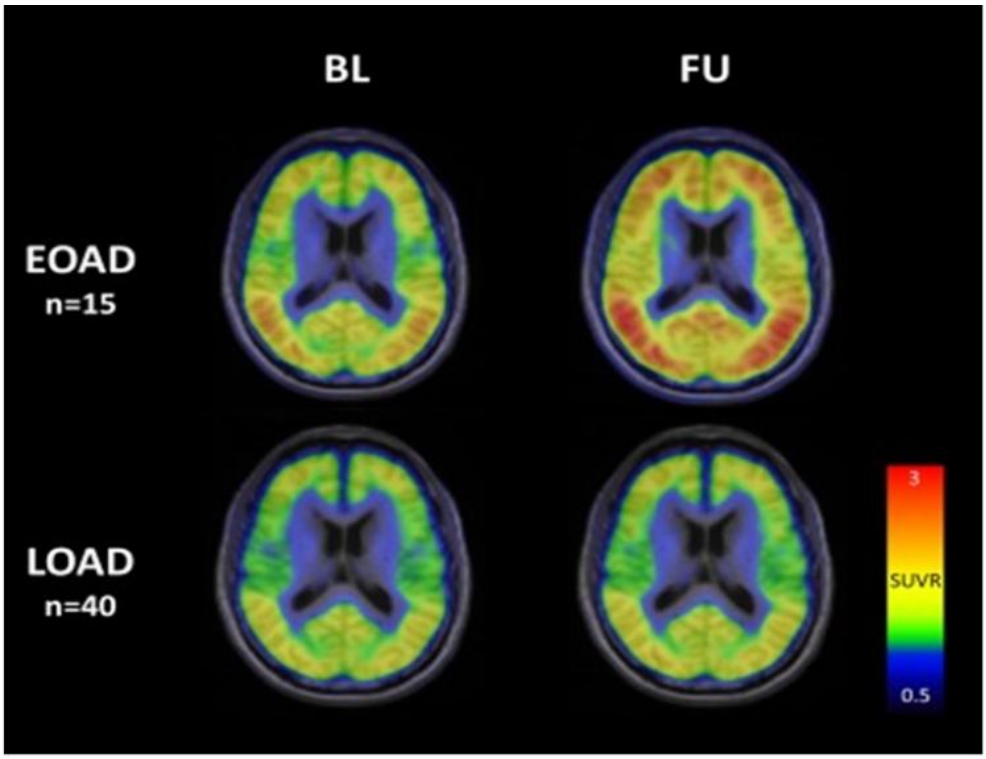


FIGURE 1. Average[^{18}F]-Florzolotau PET images of EOAD and LOAD at baseline (BL) and at 1.6-y follow-up (FU).

Keywords: Tau accumulation, Early-Onset Alzheimer's Disease, Late-Onset Alzheimer's Disease, [18F]-Florzolotau PET, MMSE score

89 Heterogeneity of FDG-PET patterns among tau-negative amnestic patients

Jesús Silva-Rodríguez[1], Alexis Moscoso[2], Miguel A. Labrador-Espinosa[2], Pascual Sánchez-Juan[1], Michael Scholl[2], Michel J. Grothe[1]

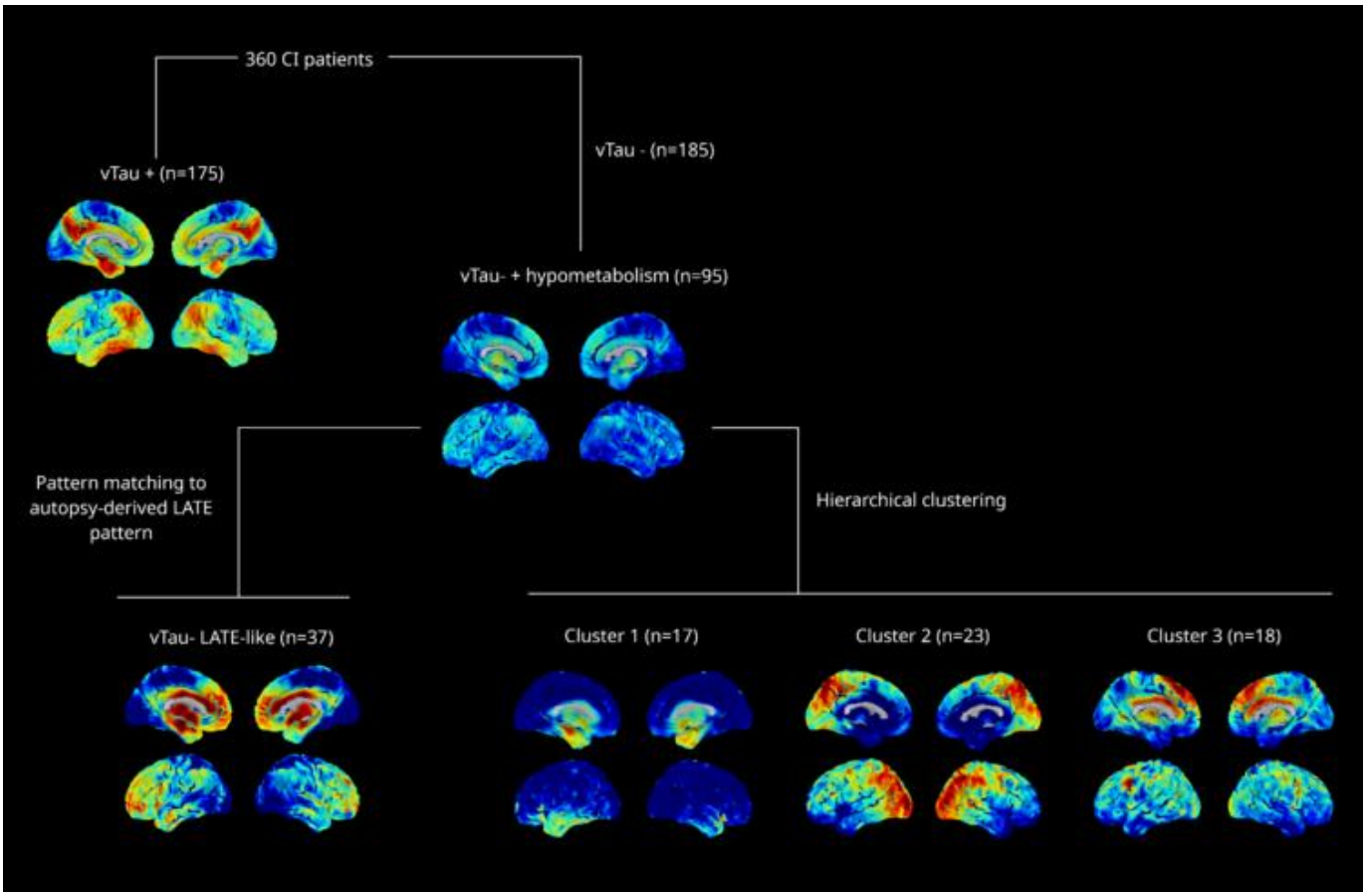
[1]*Reina Sofia Alzheimer Centre, CIEN Foundation, ISCIII, Madrid, ES*
[2]*Wallenberg Center for Molecular and Translational Medicine and Department of Psychiatry and Neurochemistry, University of Gothenburg, Gothenburg, SE*

Introduction: Approximately 20-30% of patients diagnosed with Alzheimer's disease (AD) dementia do not meet pathological criteria for AD, with an even higher proportion in amnestic mild cognitive impairment (aMCI). Among tau-negative (Tau-) patients, limbic-predominant age-related TDP-43 encephalopathy (LATE) emerges as a key diagnostic alternative, particularly in older individuals. LATE is associated with a characteristic temporo-limbic hypometabolic pattern on FDG-PET imaging. However, the heterogeneity of hypometabolic patterns among Tau- amnestic patients remains poorly understood.

Methods: 360 patients (261 aMCI, 99 AD dementia) from the Alzheimer's Disease Neuroimaging Initiative (ADNI) underwent both 18F-Flortaucipir and 18F-FDG-PET scans. Participants were classified as Tau+ or Tau- based on a visual assessment. Tau- patients were further screened for hypometabolism. LATE-like patterns were identified through automated pattern-matching to autopsy-confirmed cases. Additional FDG-PET patterns were explored using hierarchical clustering. Differences in age, hippocampal volume, and cognitive measures were analyzed between groups.

Results: 185 patients (162 aMCI) were classified as Tau-. Among these, 37 patients (39%) showed a LATE-like pattern (see Fig.1). Hierarchical clustering of the remaining patients identified three distinct clusters: a left-lateralized temporal pole pattern suggestive of semantic dementia (C1, 18%), a posterior-occipital pattern typical for dementia with Lewy bodies (C2, 24%), and a diffuse frontal pattern of unknown origin (C3, 19%). LATE-like patients were significantly older (p=0.02) and had greater memory impairment (p=0.02) and hippocampal atrophy (p=0.03) compared to other Tau- individuals. When applying the newly proposed clinical criteria for probable LATE, i.e. Tau- amnestic profile at elevated age (>75y) and significant hippocampal atrophy, most patients (59%) showed a LATE-like pattern, although other patterns remained present (C1=19%, C2=9%, C3=13%).

Conclusions: FDG-PET provides valuable diagnostic insights after a negative Tau-PET scan. In older Tau- amnestic patients with hippocampal atrophy, LATE-like temporo-limbic hypometabolism is most common, but distinct hypometabolic patterns suggestive of other neurodegenerative conditions are also present.



Keywords: tau-PET, FDG-PET, LATE

90 Predicting amyloid positivity and tau burden in dementia using a combination of different biomarkers

Shao-Yi Huang[1], Kun-Ju Lin[1,2,3], Chin-Chang Huang[4], Kuo-Lun Huang[4], Hsiu-Chuan Wu[4], Chiung-Chih Chang[5], Ing-Tsung Hsiao[1,2,3]

[1]*Department of Medical Imaging and Radiological Sciences, Chang Gung University, Taoyuan, TW*
[2]*Molecular Imaging Center and Nuclear Medicine, Chang Gung Memorial Hospital, Taoyuan, TW*
[3]*Healthy Aging Center, Chang Gung University, Taoyuan, TW*
[4]*Neurology, Chang Gung Memorial Hospital, Taoyuan, TW*
[5]*Neurology, Chang Gung Memorial Hospital, Kaohsiung, TW*

Purpose: Amyloid status and tau burden are essential factors in determining the effectiveness of anti-amyloid treatments for Alzheimer's disease. This work aims to predict amyloid positivity and tau burden from different combinations of biomarkers.

Materials and methods: In this study, a total of 37 CU, 77 MCI, and 105 Dementia were included with T1-MRI, [^{18}F]Florbetapir, [^{18}F]Florzolotau, plasma biomarkers (i.e. pTau217, pTau181, Aß42/40, GFAP, and NfL), and neuropsychological testing. Amyloid positivity (A+/-) from visual reading was applied, and in addition the amyloid Centiloid (CL) was calculated. The global tau SUVr was generated within a data-driven AD-vulnerable VOI to derive tau burdens (low, intermediate, high) using the Gaussian mixture model from a cohort of CU A- and dementia A+. The comparison of each biomarker value among different tau burden groups was performed. The logistic regression analysis was conducted to predict the amyloid positivity and tau burden.

Results: In dementia/MCI with A+ cases, a significantly higher CL (low= 44.32±28.73; intermediate= 68.24±37.08; high=96.81±15.48) was observed with increasing tau burden. The level of pTau217 is significantly higher in the high tau group as compared to the low and intermediate tau group (Figure 1). For the prediction of amyloid positivity, pTau217 as a predictor performs well for classifying A+ and A- (AUC=0.93; R^2=0.54; p<0.0001). As for the tau burden, combining amyloid CL and pTau217 with two-way interaction (AUC= 0.90; R^2=0.33; p<0.0001) provides a better model to predict low/intermediate and high tau burden in the A+ groups as compared to other models (Figure 2).

Conclusions: Consistent with previous literatures, the pTau217 biomarker shows robust efficacy in predicting amyloid positivity. Furthermore, combining amyloid CL with pTau217 as a predictive model presents significant potential for estimating tau burden.

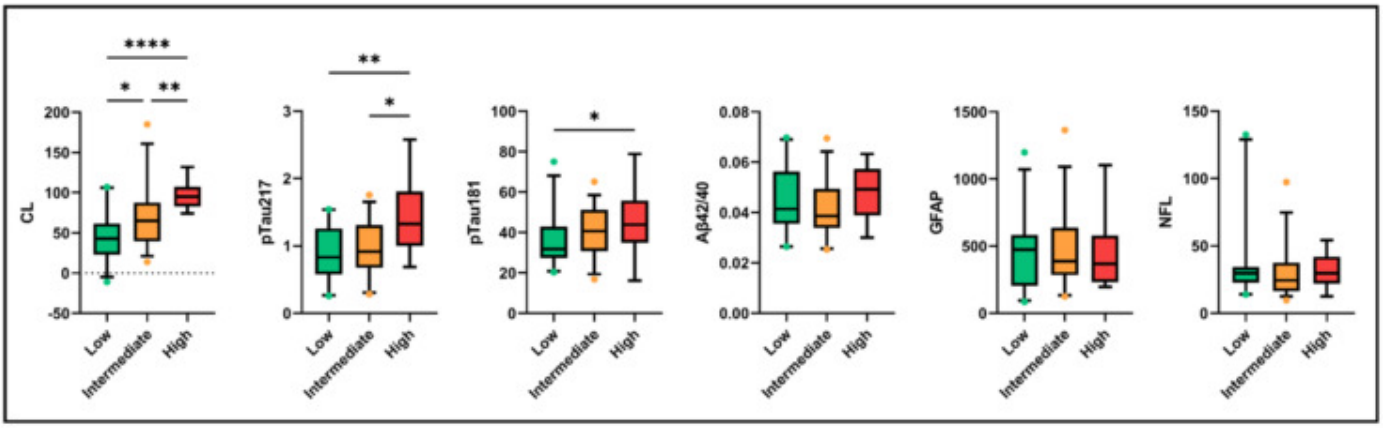


Figure 1. The comparison of amyloid CL and plasma biomarkers among different tau burdens in amyloid+ Dementia/MCI groups.

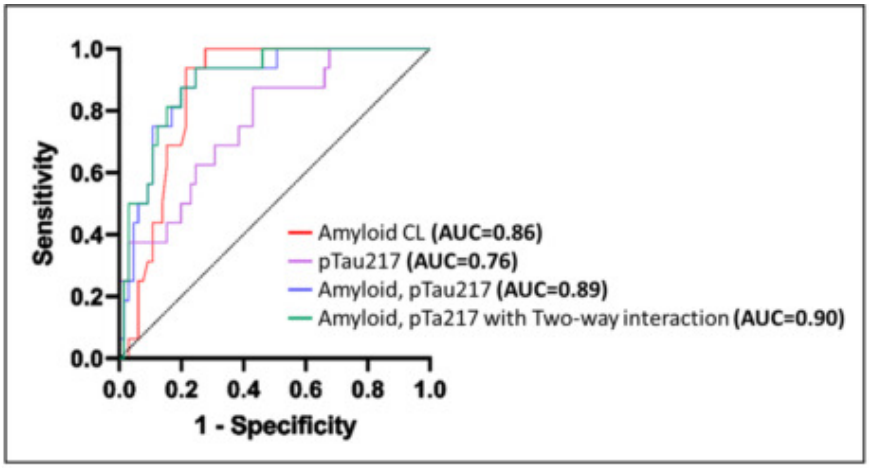


Figure 2. The ROC curve of predicting low/intermediate and high tau burden using different combinations of amyloid CL and pTau217 in Dementia/MCI with A+ groups.

Keywords: Alzheimer's disease, plasma biomarkers, tau burden

91 Evaluation of [^{3}H]SynVesT - 1 binding in post-mortem brain tissue from control and Alzheimer's Disease as a biomarker of synaptic loss

Laura Kulagowska[1], Laetitia Lemoine[1], Declan King[2], Scott Gladstein[3], Amanda Bevis[4], David Bonsall[1], Sjoerd Finnema[3], Tara Spires-Jones[2], Lisa Wells[1], FNIH SV2A project team[4]

[1]*Perceptive, London, GB*
[2]*University of Edinburgh, Edinburgh, GB*
[3]*AbbVie, Chicago, IL, US*
[4]*Foundation for the National Institutes of Health, Rockville, MD, US*

Backgrounds and Methods: This study aims to use homogenate binding techniques to evaluate [^{3}H]SynVesT-1 binding to synaptic vesicle glycoprotein 2A (SV_{2A}), found in the pre-synaptic terminals, to understand its potential as a synaptic density biomarker. Binding parameters (binding affinity (K_D), and maximal binding sites (B_{MAX})) from 412 postmortem samples (70 subjects, 3 regions) were analysed. Subjects were divided into 3 groups: control (BS 0-II), early Alzheimer's Disease (E-AD) (BS III-IV) and Alzheimer's Disease (AD) (BS V-VI). Three regions were analysed: entorhinal cortex (EC), cerebellum and centrum semiovale; for each total homogenate (TH) and synaptoneurosome.

Results: Initial results show a saturable specific binding signal of [^{3}H]SynVesT-1 in EC and cerebellum homogenates from all three subject groups. The centrum semiovale does not fit a suitable binding curve, with less specific binding observed, and greater variability across cases. The binding affinity of [^{3}H]SynVesT-1 was comparable across groups and homogenate preparations (TH and synaptoneurosome).

The K_D ranged from 3-7 nM. In EC TH, B_{MAX} ranged from 2320 ± 104 fmol/mg protein in AD, to 2788 ± 109 fmol/mg protein in control. In EC synaptoneurosome homogenates, B_{MAX} ranged from 3969 ± 200 fmol/mg protein in AD, to 5380 ± 319 fmol/mg protein in E-AD. In cerebellum TH, B_{MAX} ranged from 2274 ± 91 fmol/mg protein in control, to 2997 ± 224 fmol/mg protein in E-AD. In cerebellum synaptoneurosome homogenates, B_{MAX} ranged from 2725 ± 148 fmol/mg protein in AD, to 4469 ± 284 fmol/mg protein in E-AD.

Conclusions: Initial results show group-wise differences in the B_{MAX} of [^{3}H]SynVesT-1 in EC, with E-AD subjects showing a greater binding signal. This trend could suggest a compensatory mechanism early in the progression of the disease. This is part of the SV2A PET Project, a program of the FNIH Biomarker Consortium.

Keywords: Biomarker, Synaptic loss, Neurodegeneration, radioligand binding

92 Exploring the predictive power of graph-theoretic metrics for tau pathology in cognitively unimpaired older adults

Emily Johns[1,2], Raina Vin[1,2,3], Hamid Abuwarda[1,2], Carolyn Fredericks[1,2]

[1]*Department of Neurology, Yale University School of Medicine, New Haven, CT, US*
[2]*Interdepartmental Neuroscience Program, Yale University School of Medicine, New Haven, CT, US*
[3]*Department of Psychiatry, Yale University School of Medicine, New Haven, CT, US*

Background: Tau pathology is a hallmark feature of Alzheimer's disease (AD), yet its impact on brain network organization in cognitively unimpaired older adults remains unclear. Resting-state functional MRI (rs-fMRI) allows for assessing brain connectivity through graph-theoretic metrics, quantifying network structure and function. This study evaluated the predictive power of these metrics and moderating factors in key networks affected in AD such as the default mode network (DMN) and salience network (SN) for tau pathology in cognitively unimpaired amyloid-positive and amyloid-negative older adults.

Methods: Functional connectivity matrices were generated from Pearson correlations between regions of interest defined by the Brainnetome Atlas in 380 participants in the A4 study. Graph-theoretic metrics—local efficiency, degree, betweenness centrality, and closeness centrality—were calculated for each network. Regression models assessed the relationship of these metrics for regional tau SUVRs. Additionally, we explored the moderating effects of age, sex, education, amyloid PET burden, ethnicity, and APOE genotype on these relationships.

Results: In the DMN, higher local efficiency in the hippocampus, cingulate, precuneus, superior frontal, parahippocampal, and temporal gyri was consistently associated with lower tau PET signal in Braak stage 5 (adjusted-pvalue=0.047). In the SN, higher betweenness centrality in the medial amygdala predicted early-stage Braak pathology (Braak stage 1/2, $p<0.001$). Conversely, increased degree in the cingulate, insular, and lateral occipital gyri was associated with reduced tau PET (adjusted-pvalues=0.001 to 0.022). Moderation analyses revealed that in the lateral occipital cortex of the SN, the negative relationship between degree and tau was moderated by higher amyloid burden (interaction-p=0.014) and greater years of education (interaction-p=0.042).

Conclusion: These findings suggest that enhanced local network connectivity may confer resilience against Alzheimer's pathology in key brain networks. The moderating effects of amyloid deposition and education highlight the complex interplay between neuropathological burden, cognitive reserve, and network integrity.

Keywords: graphy theory, tau PET, default mode network, salience network

93 Tracking biomarkers accuracy for predicting progression to mild cognitive impairment

Jonathan Gallego-Rudolf[1,2], Alex Wiesman[2], Sylvain Baillet[2], Sylvia Villeneuve[1]

[1]*Douglas Research Centre, Montreal, QC, CA*
[2]*Montreal Neurological Institute, Montreal, QC, CA*

The Alzheimer's disease (AD) continuum includes a wide preclinical phase in which neuropathological events take place decades before symptom onset. Identifying early biomarkers for predicting the risk of progression from the asymptomatic to the mild cognitive impairment (MCI) stage is crucial for improving patient prognosis, as therapeutic interventions might be more promising at this stage.

We assessed spectral power features from task-free magnetoencephalographic (MEG) recordings, magnetic resonance imaging (MRI) derived hippocampal volume, plasma biomarkers, and positron emission tomography (PET) measures of Aβ and tau deposition in a group of cognitively unimpaired older adults with a family history of AD (N=99). From this sample, 30 individuals developed MCI based on a multidisciplinary consensus who had access to longitudinal neuropsychological assessments and were blind to AD biomarkers. We benchmark these biomarkers using a series of logistic regression models to assess the temporal evolution of their accuracy for predicting MCI progression, in combination with clinical information (Figure 1).

Neurophysiological activity features were as good as Aβ and tau PET for predicting progression to MCI when acquired close to symptom onset but showed a steeper decrease in accuracy at larger intervals compared to PET and plasma biomarkers, which remained the most accurate over time (Figure 2). When incorporating all features into the same model, Aβ-PET proved to be sensitive for predicting MCI progression up to 6 years before clinical onset, while MEG and tau-PET (along with age and sex) were good predictors 3-4 years prior to MCI progression (Figure 3).

Our results delineate a timeline evolution for the accuracy of distinct biomarkers for predicting progression from the asymptomatic to the prodromal stage of the AD continuum. These results highlight the dynamic sensitivity of different biomarkers for predicting symptom onset and might serve as a reference for future work in clinical settings and trials.

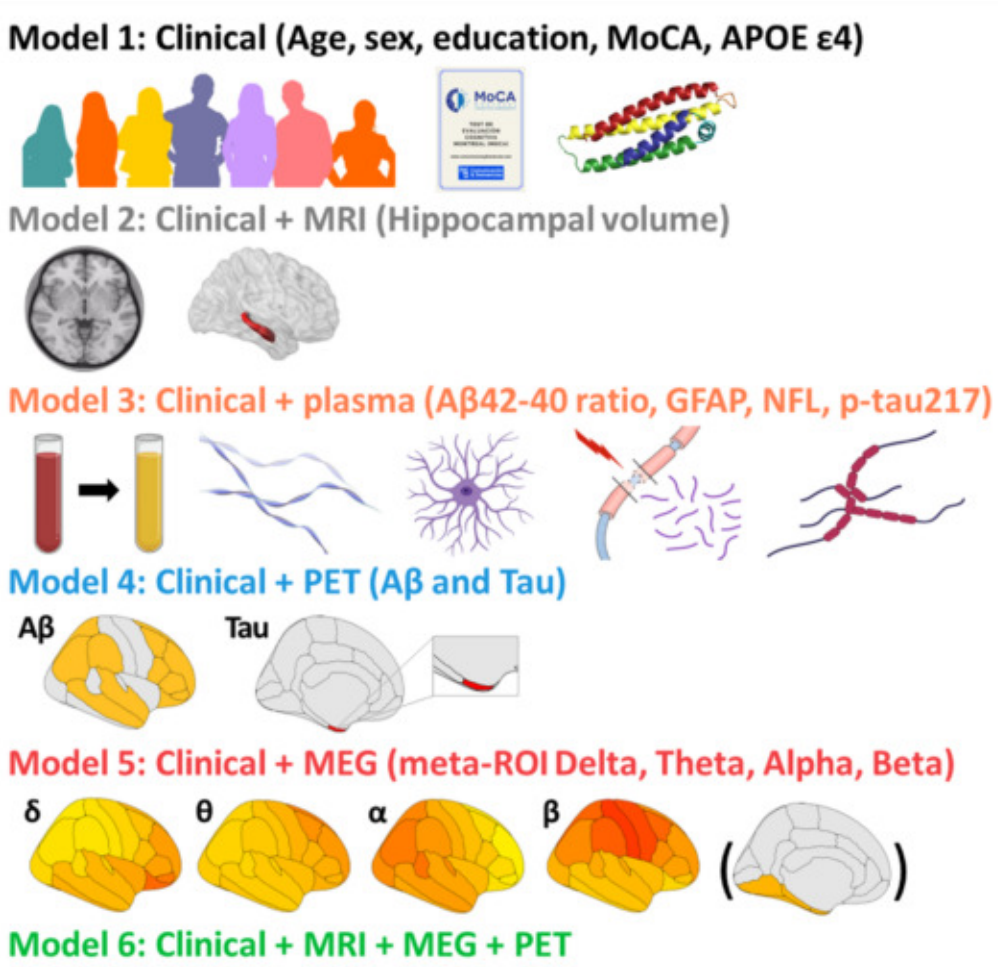


Figure 1. Logistic regression models for predicting MCI progression. We defined a series of logistic regression models for predicting MCI progression. The base model (Model 1) included demographic, clinical and genetic information from the participants. Subsequent models combined these clinical biomarkers with hippocampal volumes extracted from structural MRI (Model 2), Aβ42/40 ratio, GFAP, NFL and p-tau217 plasma biomarkers (Model 3), Aβ and tau PET SUVR values from early accumulating regions (Model 4) or neurophysiological spectral power extracted from temporal lobe regions (Model 5). Finally, model 6 included all features.

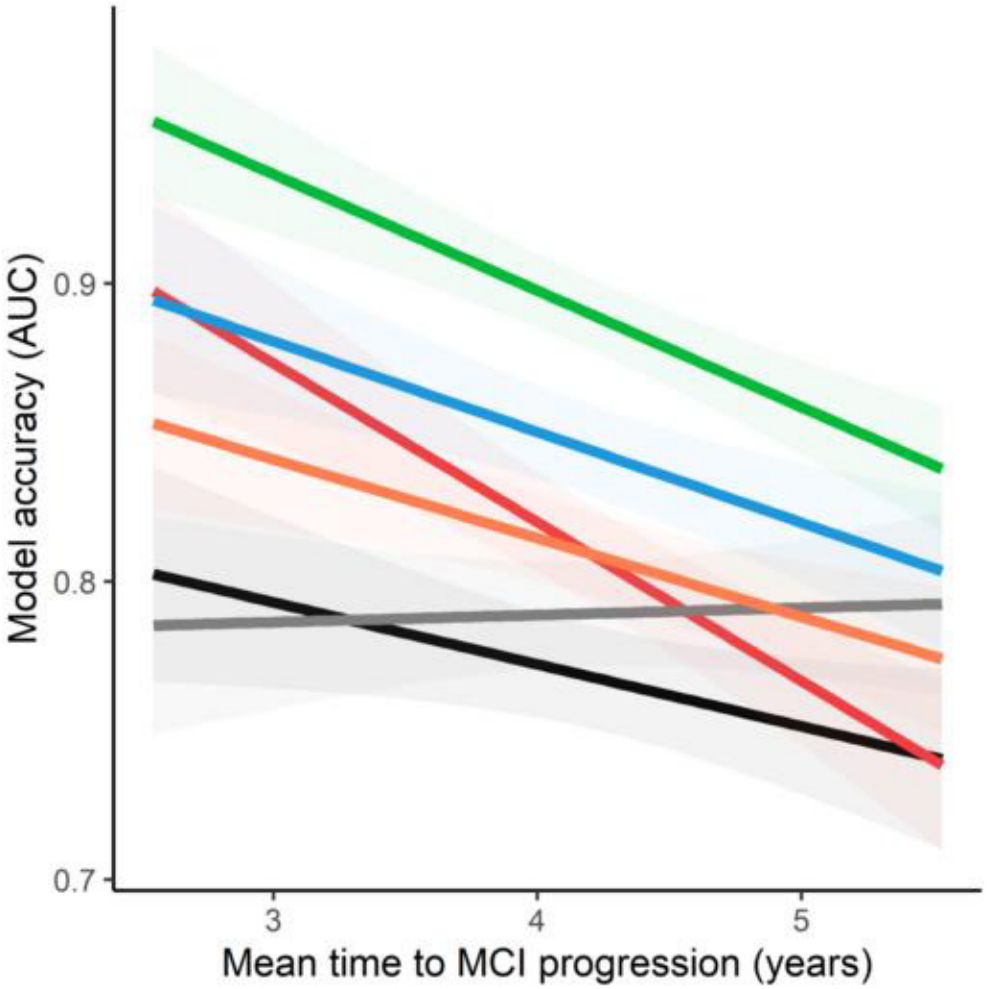


Figure 2. Model accuracy decreases with increasing time between biomarker collection and MCI diagnosis. A linear regression model was fitted to the area under curve (AUC) values obtained from running the logistic regression models using a sliding-window approach to assess the impact of time between biomarker collection and MCI diagnosis. The accuracy of all models except for the clinical + MRI model significantly decreased as time between biomarker collection and MCI diagnosis increased.

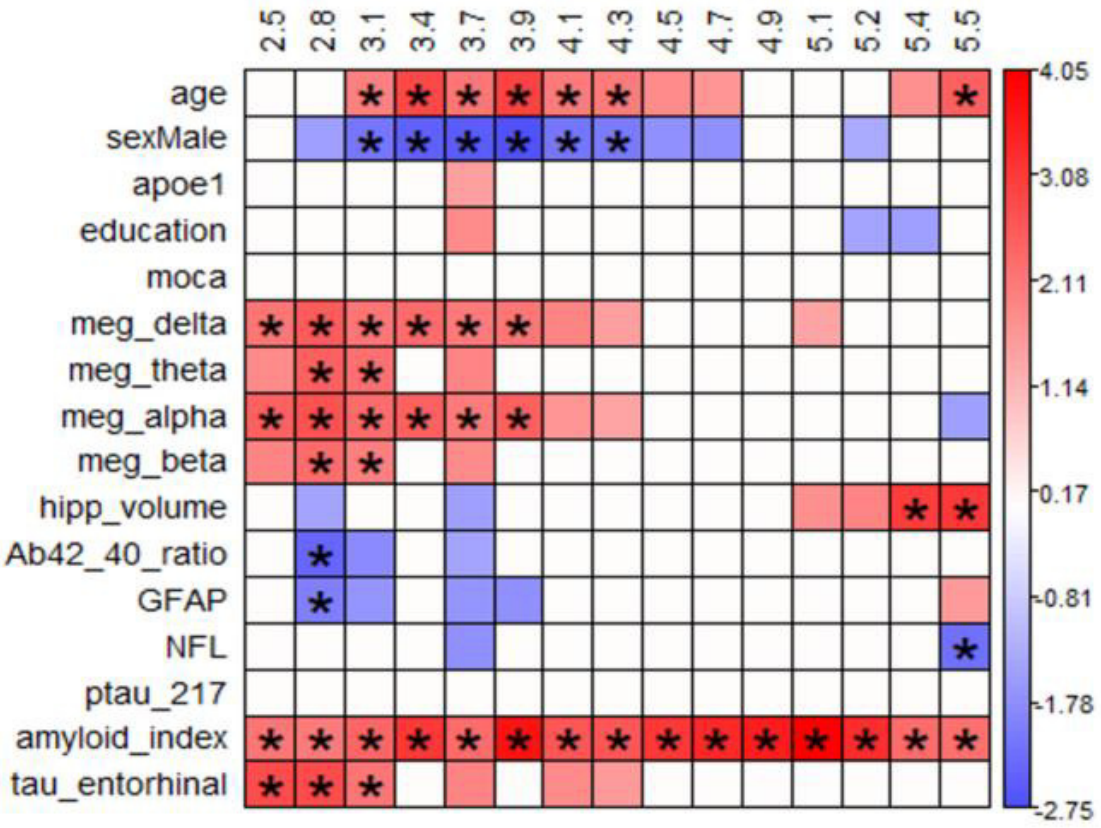


Figure 3. Different biomarkers are more sensitive for predicting progression to MCI depending on the time between biomarker collection and MCI diagnosis. Stepwise logistic regression was applied to the models including all biomarkers to assess which features were more important for predicting MCI progression depending on the time between biomarker collection and diagnosis. High levels of Aβ were consistently identified as a strong predictor for MCI progression up to 6 years before symptom onset, while older age, being female, having higher tau SUVR and higher MEG delta and alpha power were also identified as strong predictors 3-4 years prior to MCI diagnosis.

Keywords: Preclinical AD, progression to MCI, biomarkers, multimodal neuroimaging, plasma

94 Tau burden across Braak stages is associated with regionally specific amyloid accumulation: insights from the BIOCARD cohort

Nisha Rani[1], Kylie H Alm[1], Daniel D. Callow[1], Corinne Pettigrew[2], Anja Soldan[2], Michael Miller[3], Marilyn Albert[2], Arnold Bakker[1,2]

[1]*Department of Psychiatry and Behavioral Sciences, Johns Hopkins University School of Medicine, Baltimore, MD, US*
[2]*Department of Neurology, Johns Hopkins School of Medicine, Baltimore, MD, US*
[3]*Department of Biomedical Engineering, Johns Hopkins University, Baltimore, MD, US*

Alzheimer's disease is characterized by accumulation of amyloid-β (Aβ) plaques and tau tangles. Aβ deposition typically begins in neocortical regions years before onset of cognitive decline, while tau pathology spreads systematically through select brain regions, typically described as Braak stages (I-VI). The impact of regional Aβ on tau propagation remains a key research focus. We examined the associations between regional Aβ and tau burden measured by positron emission tomography (PET) in 192 participants without dementia (14 with mild cognitive impairment [MCI]) in the BIOCARD cohort, of whom 52 (27%) were Aβ positive. Amyloid status was assessed using standardized uptake value ratios (SUVR) obtained from the medial orbitofrontal cortex (OFC), lateral OFC, precuneus, posterior cingulate, anterior cingulate, parietal, temporal, and superior frontal regions using 11C-PIB PET. Tau burden was quantified using 18F-MK6240 PET across 29 brain regions, assigned to each of the Braak stages. Associations were examined with stepwise and hierarchical regressions, covarying for age, sex, education, and ApoE4 status. In stepwise regression analyses for Braak stages (I-II), amyloid in the medial OFC emerged as significantly associated with tau burden (β = 1.45, t = 4.75, p <.001 for Braak-I; β = 0.80, t = 3.58, p <.001 for Braak-II), while in later Braak stages, amyloid in the precuneus emerged as significantly associated with tau burden (β = 0.57, t = 9.59, p <.001 for Braak-III; β = 1.54, t = 3.76, p <.001 for Braak-IV; β = 0.39, t = 5.90, p <.001 for Braak-V; and β = 0.17, t = 2.30, p <.05 for Braak-VI). Hierarchical regression confirmed the selective and significant contribution of medial OFC and precuneus specific amyloid to tau burden across Braak stages. These findings suggest that localized measures of amyloid burden show utility in understanding amyloid and tau dynamics.

Keywords: 11C-PIB PET, 18F-MK6240 PET, Mild cognitive impairment, Braak stages, amyloid burden

95 Relationship between neuroinflammatory ER176-PET and functional connectivity in Progressive Apraxia of Speech

Neha Singh-Reilly[1], Irene Sintini[2], Ryota Satoh[2], Joseph Duffy[1], Rene Utianski[1], Heather Clark[1], Yehkyoung Stephens[1], Val Lowe[2], Keith Josephs[1], Jennifer Whitwell[2]

[1]*Department of Neurology, Mayo Clinic, Rochester, MN, US*
[2]*Department of Radiology, Mayo Clinic, Rochester, MN, US*

Background: Progressive apraxia of speech (PAOS) is a neurodegenerative disease affecting programming or planning of speech that most commonly results from a four-repeat tauopathy. Neuroinflammation plays an important role in accelerating the disease process and has a close relationship with tau. Little is known about the relationship between neuroinflammation and functional connectivity disruptions and the spread of neuroinflammation across functionally connected regions.

Methods: Sixteen PAOS patients were recruited by the Neurodegenerative Research group from the Department of Neurology, Mayo Clinic, Rochester, MN and underwent neuroinflammatory (ER176)-PET, tau (^{18}F-flortaucipir)-PET and a resting state functional MRI. Images were parcellated using the Schaefer 200 atlas for cortical regions and the Harvard-Oxford atlas for subcortical regions. Graph theory was applied to functional connectivity matrices to extract degree and clustering coefficients. Group-average graph theory metrics were correlated with regional ER176-PET and flortaucipir-PET SUVRs. PET patient-specific epicenters were identified as the 2.5% regions with the highest SUVR. To investigate connectivity-based spreading of inflammation and tau, linear regression was applied on each patient relating the connectivity to the epicenter and the SUVR in the rest of non-epicenter regions.

Results: At the group level, both ER176-PET and flortaucipir-PET SUVRs showed a positive correlation to degree and a negative correlation to clustering coefficient across regions. These associations were strong within cortical regions and attenuated when subcortical regions were included (Figure 1). Patient-specific analysis showed that stronger connectivity to flortaucipir epicenters was associated with higher regional ER176-PET signal. It was also noted that stronger connectivity to ER176 epicenters was associated with higher regional ER176-PET signal (Figure 2).

Discussion: Neuroinflammatory ER176-PET and flortaucipir-PET uptake were higher in regions with low clustering coefficient, implying that both inflammation and tau are associated with disrupted local connectivity. Tau may play an important role in facilitating the spread of neuroinflammation through connectivity.

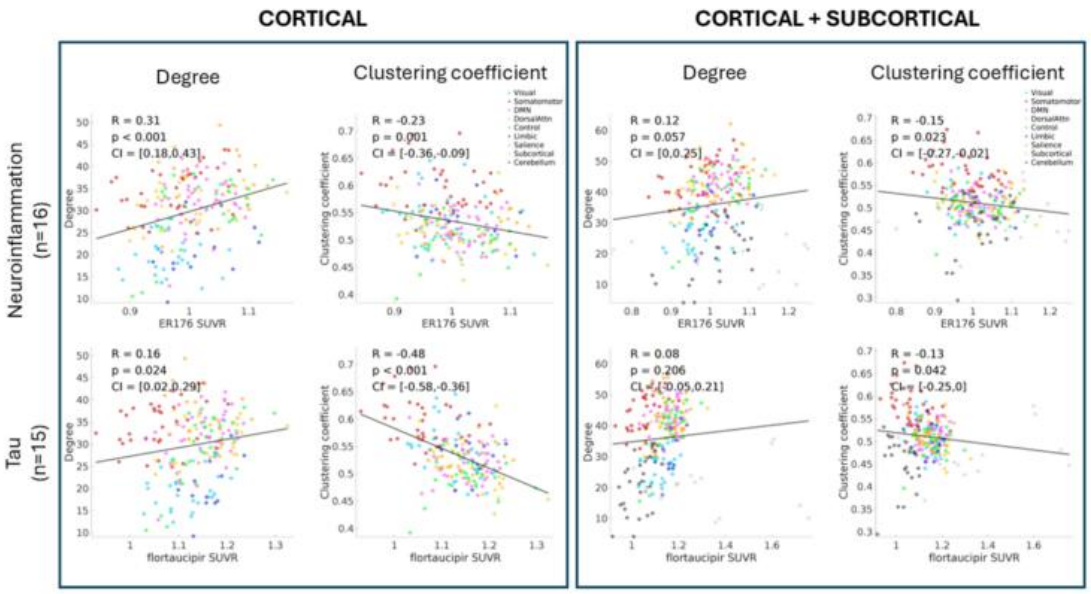


Figure 1: Graph theory metrics. These plots show group-average graph theory metrics and their relationship to PET measures. Separate plots were generated for cortical only and both cortical and subcortical regions.

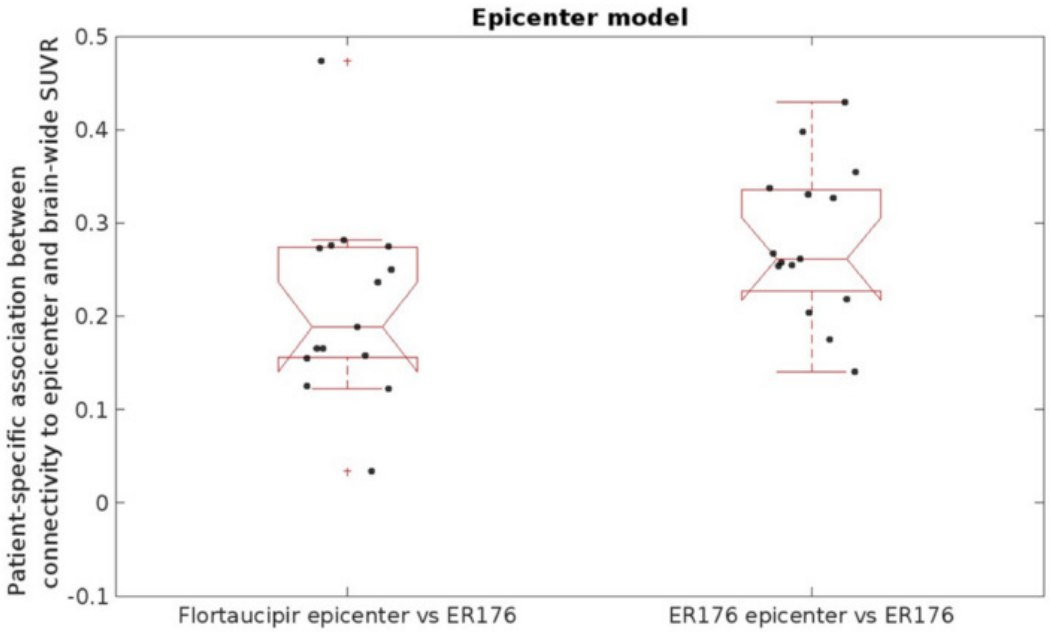


Figure 2: Patient specific epicenter analysis. These plots show patient-specific beta-values between i) connectivity to flortaucipir epicenter and ER176-PET SUVR of brain regions and ii) connectivity to ER176 epicenter and ER176-PET SUVR of brain regions

Keywords: Progressive apraxia of speech, neuroinflammatory ER176 PET, flortaucipir-PET

96 Sex moderates the association between regional tau and longitudinal cognitive decline in A4 and LEARN studies

Annie Li[1], Hannah M. Klinger[1], Mabel Seto[3], Colin J. Birkenbihl[1], Michelle Farrell[1], Emma Thibault[1], Robert A. Rissman[2], Michael Properzi[1], Aaron P. Schultz[1], Diana L. Townsend[1], Hyun-Sik Yang[1,3], Keith A. Johnson[1,3], Rema Reman[2], Oliver Langford[2], Michael Donohue[2], Reisa A. Sperling[1,3], Rachel F. Buckley[1,3,4], Gillian T. Coughlan[1]

[1]*Department of Neurology, Massachusetts General Hospital, Harvard Medical School, Boston, MA, US*
[2]*Alzheimer's Therapeutic Research Institute, University of Southern California, San Diego, CA, US*
[3]*Neurology Department, Brigham and Women's Hospital, Boston, MA, US*
[4]*Melbourne School of Psychological Sciences, University of Melbourne, Melbourne, AU*

Background: Existing literature suggests that women exhibit higher tauopathy relative to men, but evidence for sex moderating the association between tauopathy and cognitive decline is sparse. To address this gap, we investigated sex differences on cognitive trajectories as a function of tau burden.

Methods: The study included 436 clinically normal adults from the Anti-Amyloid Treatment in Asymptomatic Alzheimer's Disease trial (A4) and the companion Longitudinal Evaluation of Amyloid Risk and Neurodegeneration (LEARN) study (Table 1), with at least one baseline tau-positron emission tomography (PET) scan and cognitive follow-ups (mean(SD)=3.34(2.19)years, range=0.03-9.04 years). Four Alzheimer's disease-related tau regions were selected: parahippocampus, amygdala, entorhinal, and inferior temporal gyri. Cognitive outcomes were measured using Preclinical Alzheimer Cognitive Composite (PACC) scores. Random-effects regression models estimated the interaction between sex (men/women) and regional tau (continuous) on longitudinal PACC, adjusting for age and education over time, including participant-specific intercepts and slopes. PACC slopes were extracted, and a linear model was used in the floodlight analysis to identify baseline tau thresholds required to detect sex-divergent cognitive trajectories.

Results: Among those with elevated parahippocampal tau (β=0.08, 95%CI:0.00-0.16, P=0.038), amygdala tau (β=0.11, 95%CI:0.03-0.19, P=0.009), inferior temporal tau (β=0.10, 95%CI:0.02-0.18, P=0.014), and entorhinal tau (β=0.08, 95%CI:0.00-0.16, P=0.043), women exhibited significantly faster rates of cognitive decline relative to men. At low levels of tau, women maintained superior PACC performance. Floodlight analysis identified tau thresholds for a significant association between sex and cognitive change (1.25-1.32 tau-SUVR), except for entorhinal tau. These thresholds were used to categorize participants for visualizing trajectories by sex (Figure). Adjusting for substudy, treatment, and baseline amyloid level did not alter findings (Table 2).

Conclusion: Higher regional tau levels in women may contribute to a greater risk of cognitive decline relative to men. These findings emphasize the importance of considering sex-specific tau levels at the baseline of clinical trials.

Table 1: Demographic Characteristics

	A4/LEARN N=436	
Characteristics	**MEN**	**WOMEN**
Total No.	183	253
Baseline tau-PET age, mean (SD)	72.9 (4.9)	71.1 (4.7)
APOE ε4 carriers, No. (%)	97 (53.0)	138 (54.5)
Education yrs, mean (SD)	16.9 (2.8)	15.7 (2.7)
Treatment_Solanezumab, No. (%)	87 (47.5)	105 (41.5)
SUBSTUDY_A4, No. (%)	163 (89.1)	225 (88.9)
SUVR, mean (SD)	1.3 (0.2)	1.3 (0.2)
Tau-PET time, mean (min, max)	3.4 (1.4, 7.1)	3.4 (1.3, 6.8)

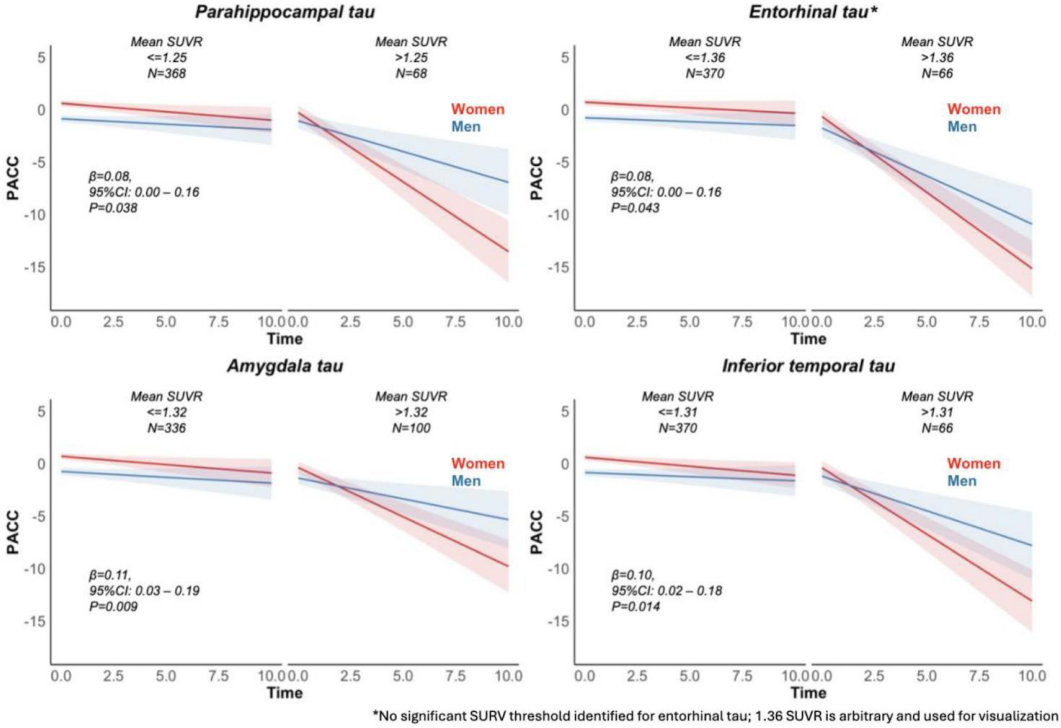
A4/LEARN: Anti-Amyloid Treatment in Asymptomatic Alzheimer's Disease trial and the companion Longitudinal Evaluation of Amyloid Risk and Neurodegeneration study

Table 2: Interaction between sex and regional tau burden on PACC score remains significant after covarying for the effects of substudy, treatment, and baseline amyloid level over time

	Model with Substudy x Time N=436			Model with Treatment x Time N=436			Model with Baseline Amyloid Level x Time N=331		
Predictors	*std. Beta*	*std. CI*	*std. p*	*std. Beta*	*std. CI*	*std. p*	*std. Beta*	*std. CI*	*std. p*
(SEX [Male] × Baseline Parahippocampal) × PACC Time	0.08	0.00 – 0.16	**0.044**	0.09	0.00 – 0.17	**0.040**	0.11	0.01- 0.20	**0.023**
(SEX [Male] × Baseline Amygdala) × PACC Time	0.11	0.03 – 0.19	**0.009**	0.12	0.03 – 0.21	**0.008**	0.15	0.05- 0.24	**0.002**
(SEX [Male] × Baseline Entorhinal) × PACC Time	0.08	0.00 – 0.15	**0.046**	0.09	0.00 – 0.17	**0.041**	0.12	0.03- 0.21	**0.007**
(SEX [Male] × Baseline Inferior temporal) × PACC Time	0.10	0.02 – 0.18	**0.015**	0.11	0.02 – 0.19	**0.013**	0.14	0.04- 0.22	**0.006**

Model with SUBSTUDY x Time: PACC ~ SEX x Baseline Tau x PACC Time + Baseline tau-PET age x PACC Time + Education years x PACC Time + Substudy x PACC Time.
Model with Treatment x Time: PACC ~ SEX x Baseline Tau x PACC Time + Baseline tau-PET age x PACC Time + Education years x PACC Time + Treatment x PACC Time
Model with Baseline Amyloid Level x Time: PACC ~ SEX x Baseline Tau x PACC Time + Baseline tau-PET age x PACC Time + Education years x PACC Time + Baseline Amyloid Level x PACC Time

Figure: Sex moderates the association between regional tau and cognitive decline in A4/LEARN, with cognitive trajectories diverging above a tau threshold of 1.25-1.32 tau-SUVR.



SUVR: standardized uptake value ratio

Keywords: Sex differences, tau-PET, longitudinal, cognitive decline

97 Evaluation of the Uni-tau and CenTauR frameworks in new datasets for tau PET harmonization in Alzheimer's disease

Olivia Lutz[1], Emily Olafson[1], Matteo Tonietto[2], Gregory Klein[2], Tharick Pascoal[3], Guilherme Negrini[3], Guilherme Povala[3], Antoine Leuzy[4], Lars Lau Raket[5], Nick Doren[2], Sandra Sanabria Bohorquez[1], Edmond Teng[1]

[1]*Research and Early Development (gRED), Genentech, Inc, South San Francisco, CA, US*
[2]*Research and Early Development (pRED), Hoffmann-La Roche, Basel, CH*
[3]*Department of Psychiatry, University of Pittsburgh, Pittsburgh, PA, US*
[4]*Critical Path for Alzheimer's Disease (CPAD) Consortium, Critical Path Institute, Tucson, AZ, US*
[5]*Eli Lilly and Company, Indianapolis, IN, US*

Introduction: Several tau-PET tracers are used in Alzheimer's disease (AD) research and therapy, but SUVR metrics are not directly comparable across tracers. To date, two methods, CenTauR and Uni-tau, have been developed to transform SUVR values into a harmonized tau-PET scale. Neither has been evaluated in independent data. Our objective was to evaluate the CenTauR and Uni-tau scale by evaluating whether tracer bias was detectable in harmonized data.

Methods: [^{18}F]FTP tau-PET images from the Alzheimer's Disease Neuroimaging Initiative (ADNI) and [^{18}F]MK-6240 tau-PET images from the Lantheus database were used to create matched samples of AD/Aβ+ and cognitively unimpaired (CU)/Aβ- individuals (**Table 1**). Samples were matched on age, sex, and MMSE. SUVRs calculated using the inferior cerebellum as a reference were converted to CenTauR/Uni-tau using equations for the meta temporal region. Tracer effect was estimated with the F-statistic, comparing linear models with SUVR/CenTauR/Uni-tau as the dependent variable with and without 'tracer' as an independent variable, controlling for age/sex/MMSE. Low-high tau-PET cut-offs were determined by fitting Gaussian mixture models on the combined AD/Aβ+ and CU/Aβ- samples.

Results: In SUVR, a strong tracer effect was detectable in the AD/Aβ+ and CU/Aβ- samples (**Figure 1**). In CenTauR and Uni-tau, no tracer effect was detected in the AD/Aβ+ samples. In CU/Aβ- samples, there was a large tracer effect for CenTauR ($F = 56.5$, $p < 0.001$) and a small tracer effect for Uni-tau ($F = 4.46$, $p = 0.04$) (**Figure 1**). Cut-offs were more similar in Uni-tau than CenTauR (Table 2).

Conclusion: Our study found that while both harmonization methods remove tracer bias in AD/Aβ+ patients, Uni-tau appears to more effectively harmonize CU/Aβ- individuals than CenTauR. This was also indicated by more consistent low-high tau-PET cut-offs using Uni-tau.

		[^{18}F]MK-6240 (Lantheus)	[^{18}F]FTP (ADNI)	Statistic[a]	p
Cognitively unimpaired Aβ- n = 142	Age*	73.7 (7.6)	72.2 (6.6)	1.2	0.23
	Sex (F/M)	35/36	41/30	0.56	0.45
	MMSE*	29.2 (0.8)	29.1 (1.0)	0.47	0.64
AD/Aβ+ N = 70	Age*	72.8 (7.4)	72.6 (7.6)	0.09	0.92
	Sex (F/M)	23/12	16/19	1.45	0.22
	MMSE*	21.9 (5.3)	23.9 (2.9)	-1.98	0.05

Table 1. Demographics of matched samples and differences in demographics across samples. *Mean (SD). Differences between counts of sex assessed between tracers by Chi-squared test (χ^2), differences in means assessed with an unpaired T-test (T-statistic)[a]. Aβ = amyloid beta, AD = Alzheimer's disease.

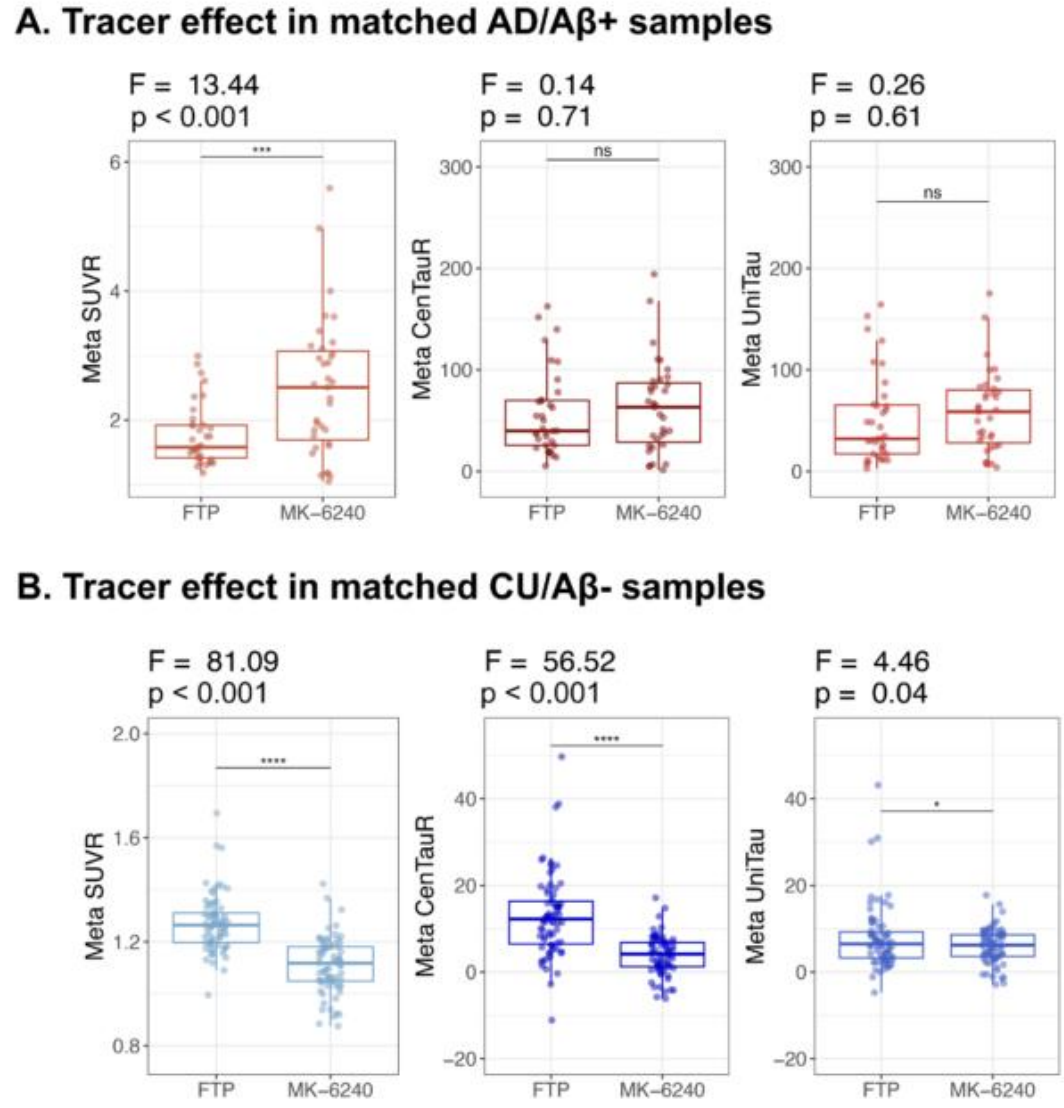
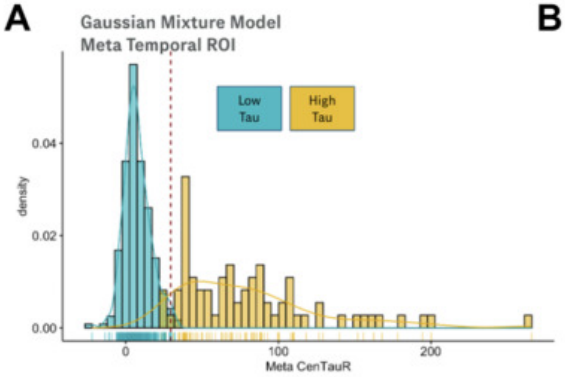


Figure 1. Boxplots of SUVR, CenTauR, and Uni-tau data, split by cohort, with F-statistics and corresponding p-values representing the variance in the data attributable to the original tracer, after controlling for age, sex, and MMSE. **A**, Alzheimer's Disease (AD) Aβ+ individuals, **B,** cognitively unimpaired (CU) Aβ- individuals with zoomed y-axes. F = F-statistic of the tracer effect. ****, p < 0.0001, ***, p < 0.001, *, p < 0.05, n.s. = not significant.

A



B

	[^{18}F]FTP	[^{18}F]MK-6240
SUVR	1.5	1.47
CenTauR	33.39	18.68
Uni-tau	22.0	19.07

Figure 2. A. Visualization of Gaussian mixture modeling (GMM) approach to deriving low-high tau-PET cutoffs. Gaussian mixture models were fit on the full sample (AD/Aβ+ and CU/Aβ-) and the cut-off was defined as the point at which the distributions overlap. **B.** Table with low-high tau-PET cut-offs derived from GMM in SUVR, CenTauR, and Uni-tau.

Keywords: tau PET, PET imaging, harmonization, Alzheimer's disease

98 Hemispheric lateralization of tau-related network dysfunction and its association with neuropsychiatric symptoms in preclinical Alzheimer's disease

Sophia Moret[1], Raina Vin[1], Carolyn Fredericks[1]

[1]*Yale University, New Haven, CT, US*

Background: Neurofibrillary tau tangles are one of the hallmark biomarkers of Alzheimer's Disease (AD). In symptomatic AD, tau pathology shows temporal lobe asymmetry, with greater right-hemisphere tau linked to more severe behavioral symptoms on the Neuropsychiatric Inventory (NPI) (Younes et al., 2024). However, the effects of tau on hemispheric connectivity and its direct relationship with neuropsychiatric symptoms in the preclinical stages remain unclear.

Methods: We used a preclinical dataset (n=260 amyloid-positive participants in the Anti-Amyloid Treatment in Asymptomatic Alzheimer's Disease (A4) study) to investigate hemispheric differences in regional tau uptake, functional connectivity, and their associations with anxiety and depression severity. Structural and functional MRI and tau PET data were parcellated using the Human Brainnetome Atlas. We computed a novel graph-theoretic metric, tau-weighted node strength (NS), defined as the product of each node's regional tau uptake and its functional connectivity with regions in the ipsilateral hemisphere. Spearman correlations were performed between tau-weighted NS and anxiety and depression scores and were repeated using tau uptake alone. All correlations were corrected for multiple comparisons using false discovery rate.

Results: Our results show significant correlations between depression scores and tau-weighted NS particularly in limbic regions, including the caudal temporal thalamus (p=0.003)**,** anterior hippocampus (p=0.006), and paracentral lobule (p = 0.003)**.** Anxiety scores significantly correlated in limbic and somatosensory regions, such as the anterior hippocampus (p=0.002)**,** paracentral lobule (p=0.003)**,** and postcentral gyrus (p=0.050)**.** Notably, there were more significant correlations in the right hemisphere (Figure 1). Regional tau uptake alone did not exhibit significant correlations with either metric.

Conclusions: These findings suggest that tau-related network disruptions are associated with specific neuropsychiatric symptoms. Our work reveals an association between hemispheric lateralization of tau pathology and neuropsychiatric symptoms. Future analyses will explore whether similar tau-driven hemispheric lateralization connectivity patterns are associated with neuropsychiatric scores in symptomatic AD.

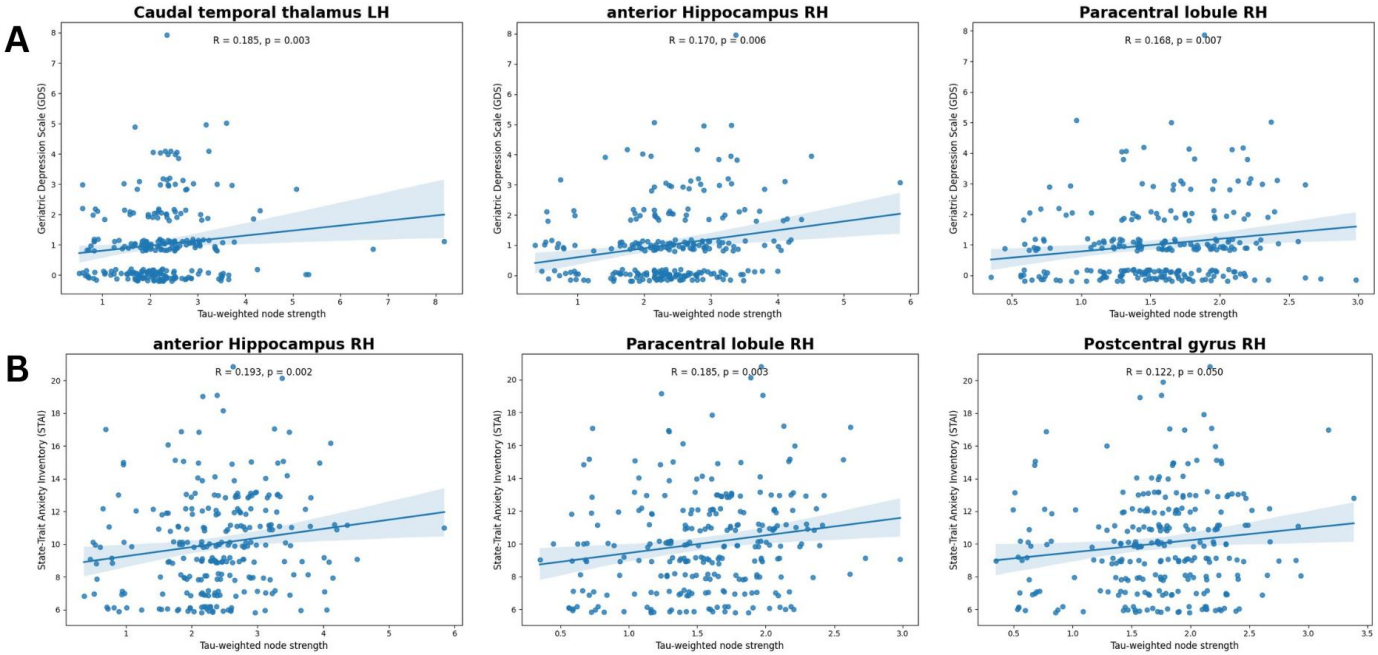


Figure 1. Spearman correlations taken ipsilaterally and corrected for multiple comparisons using False Discovery Rate (FDR). **(A)** Geriatric Depression Scale (GDS) scores correlated with computed tau-weighted node strength. **(B)** State-Trait Anxiety Inventory (STAI) correlated with computed tau-weighted node strength.

Keywords: PET, Alzheimer's, hemisphere, neurology, dementia

99 Characterization and correction of extracerebral [18F]MK-6240 tau PET off-target signal in Alzheimer's disease

Emily Olafson[1], Matteo Tonietto[2], Nick Doren[2], Sandra Sanabria Bohórquez[1]

[1]*Research and Early Development (gRED), Genentech, Inc., South San Francisco, CA, US*
[2]*Research and Early Development (pRED), Hoffmann-La Roche, Basel, CH*

Introduction: [18F]MK-6240 is a next-generation tau-PET tracer with high affinity for tau aggregates in Alzheimer's disease (AD). It exhibits off-target signals in extracerebral regions such as the meninges and sinus that may impact signal quantification. In this study, we aimed to characterize the extracerebral [18F]MK-6240 signal and to develop a method to mitigate its impact on tau-PET quantification.

Methods: We analyzed [18F]MK-6240 PET images from the Lantheus database (**Table 1**). Non-negative matrix factorization (NMF) was used to identify interpretable clusters of the extracerebral signal in cognitively unimpaired amyloid negative subjects (CU/Aβ-). Eroded regions of interest (ROIs) for the meta temporal (MT) and cerebellum were created to measure cerebral signal without influence from extracerebral compartments (see **Figure 1A**). Spill-over was quantified as the percent difference in SUV (calculated using subject weight and injected dose) between the full and eroded (%Δ[eroded-full]) (**Figure 1A**). Using the eroded cerebellum as a reference, coefficients capturing the meningeal spill-over into the MT were calculated by modeling %Δ[eroded-full] as a function of the meninges SUVR (**Figure 2A, B**). SUVRs in the MT in amyloid positive (Aβ+) subjects were adjusted using the meninges coefficients derived from CU/Aβ- subjects (**Figure 2B**). The similarity between the eroded and adjusted MT SUVR was calculated with R2.

Baseline Cohort	**Aβ- (amyloid negative) subjects**	**Aβ+ (amyloid positive) subjects**		
		CU	**MCI**	**AD**
Total number	113	46	14	19
Number of females (%)	62 (55%)	28 (62%)	9 (64%)	12 (63%)
Mean Age (std)	74.5 (8.5)	78.1 (6.3)	73.7 (8.6)	72.3 (6.6)
Mean MMSE [min-max]	29.1 [25-30]	28.9 [24-30]	24.3 [13-30]	20.2 [9-29]
Mean Meta Temporal SUVR (std)	1.02 (0.10)	1.16 (0.33)	2.11 (0.84)	2.35 (0.84)

Table 1. Population characteristics. CU = cognitively unimpaired, MCI = mild cognitive impairment, AD = Alzheimer's disease.

Results: NMF identified four components, with the meninges and sinus clustering separately (**Figure 1B**). In both ROIs, the %Δ[eroded-full] was significantly related to weights for only the meningeal NMF component. Applying

the equation improved the R2 between full and eroded SUVRs from 0.91 to 0.97 in Aβ+ subjects with low cortical tau (**Figure 2C**).

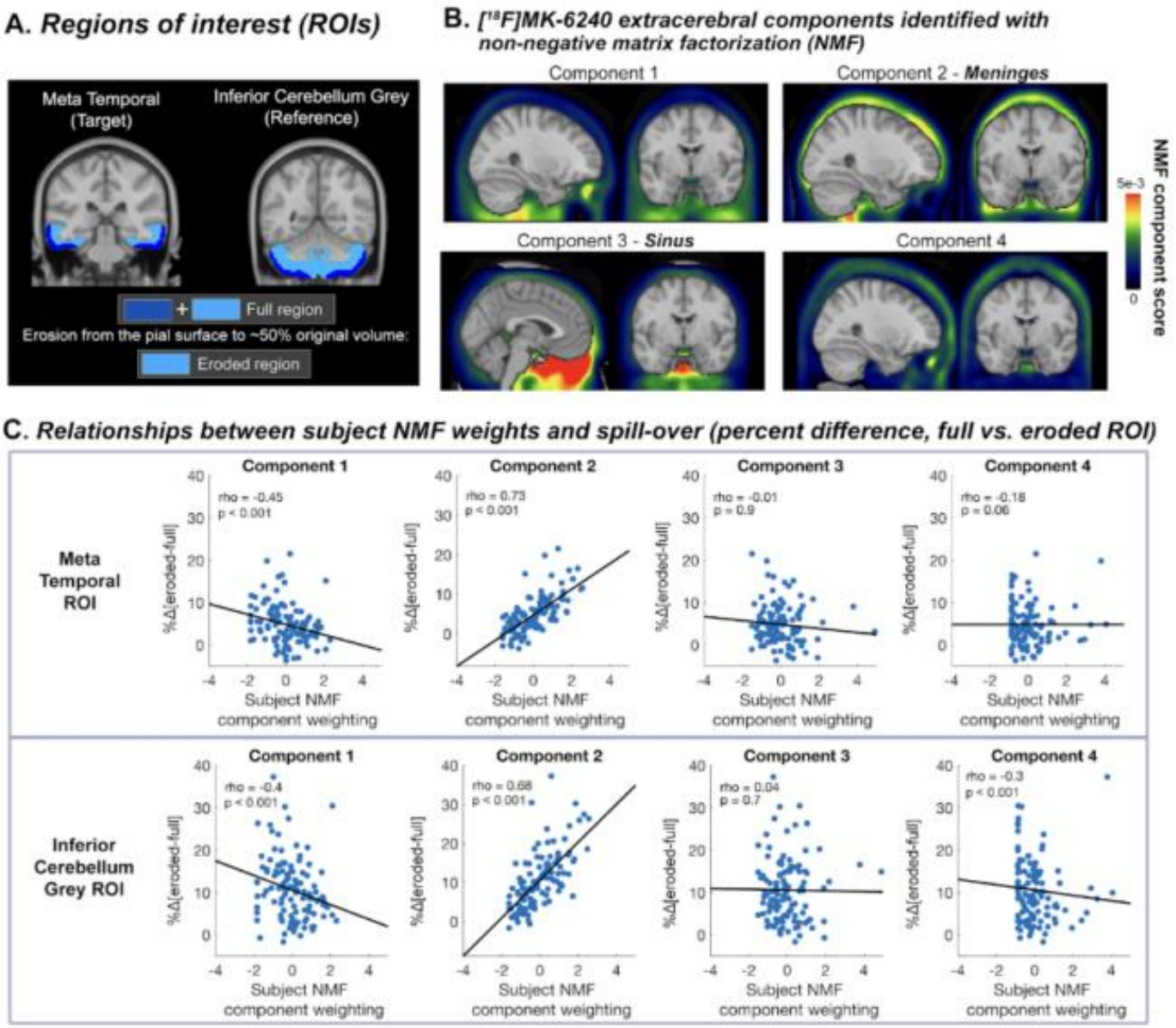


Figure 1. NMF-derived extracerebral components and their impact on target & reference region signals. **A.** NMF components 1-4, each plotted separately and overlaid with a template extracted brain. Component 3 is recognized as the meninges; component 3 is recognized as the frontal/ethmoid/sagittal sinus. **B**. Coronal views of the full and eroded meta temporal and cerebellum regions of interest used in the analyses. **C.** Scatterplots showing the relationship between subject-specific weightings for component 2 and 3 from NMF and the percent difference between full and eroded regions with Spearman rank correlation coefficients and corresponding p-values.

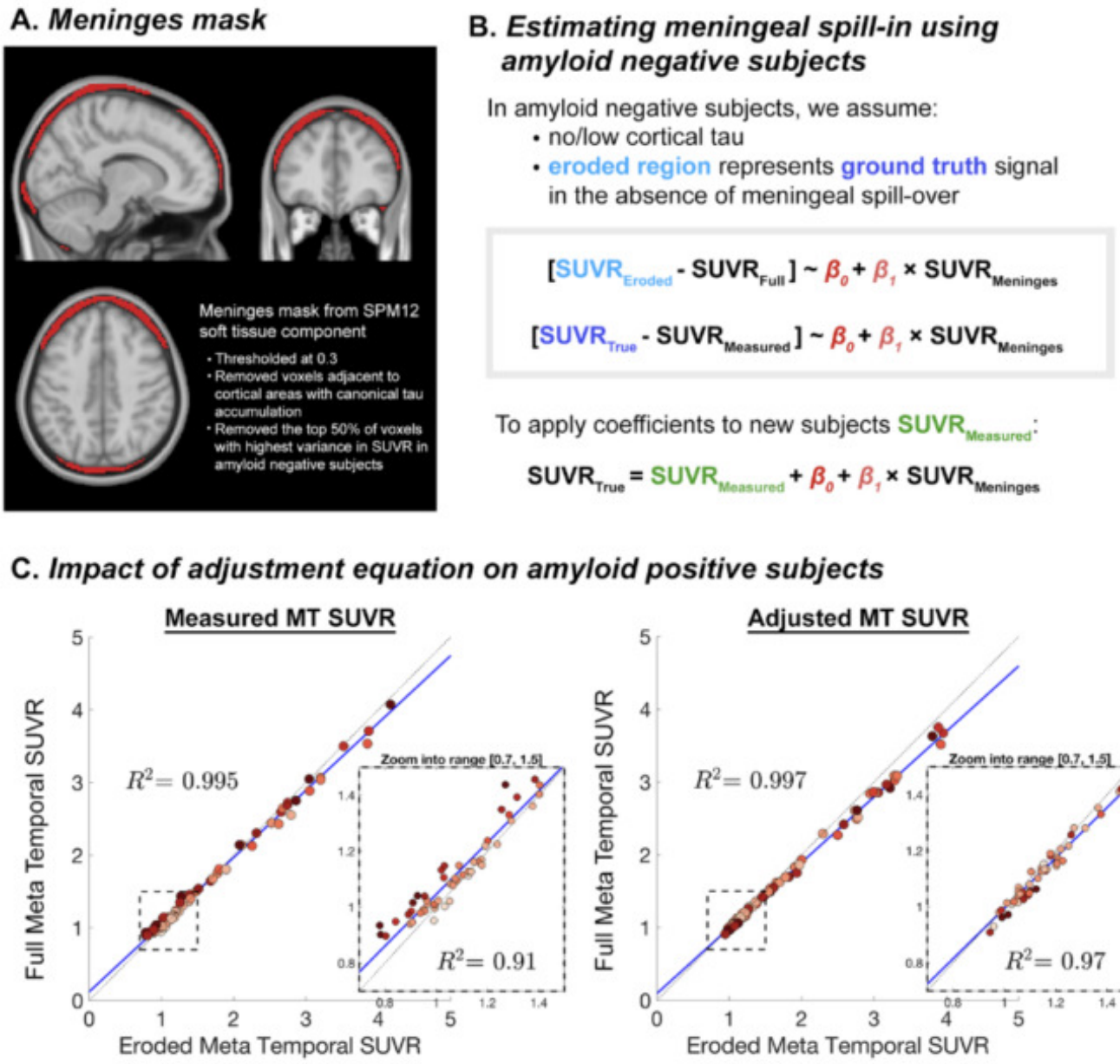


Figure 2. Estimation and application meningeal spill-over correction method. **A.** Meninges mask used to quantify meningeal SUVR. **B.** Assumptions of the modeling and proposed method of estimating correction coefficients (β_0 and β_1) in amyloid negative cognitively unimpaired subjects. **C.** Impact of correction in all baseline amyloid positive subjects and in the subset of subjects with low tau (i.e., SUVR < 1.5).

Conclusion: Our study suggests that the meninges and sinus are distinct sources of off-target [18F]MK-6240 signal. The proposed method for correcting meningeal spill-over mitigates extracerebral spill-over in new subjects.

Keywords: MK-6240, meninges, off-target signal, quantification, harmonization

100 Investigation of optimal intensity threshold for tau-PET overlap index

Seokbeen Lim[1], Jeyeon Lee[2], Hoon-Ki Min[1], Christina M. Moloney[3], Carly T. Mester[4], Sujala Ghatamaneni[1], Matthew L. Senjem[5], Aivi T. Nguyen[6], Jonathan Graff-Radford[7], Christopher G. Schwarz[1], Jeffrey L. Gunter[1], Kejal Kantarci[1], Bradley Boeve[7], Prashanthi Vemuri[1], David T. Jones[7], Clifford R. Jack[1], Ronald C. Petersen[7], Melissa E. Murray[3], Val J. Lowe[1]

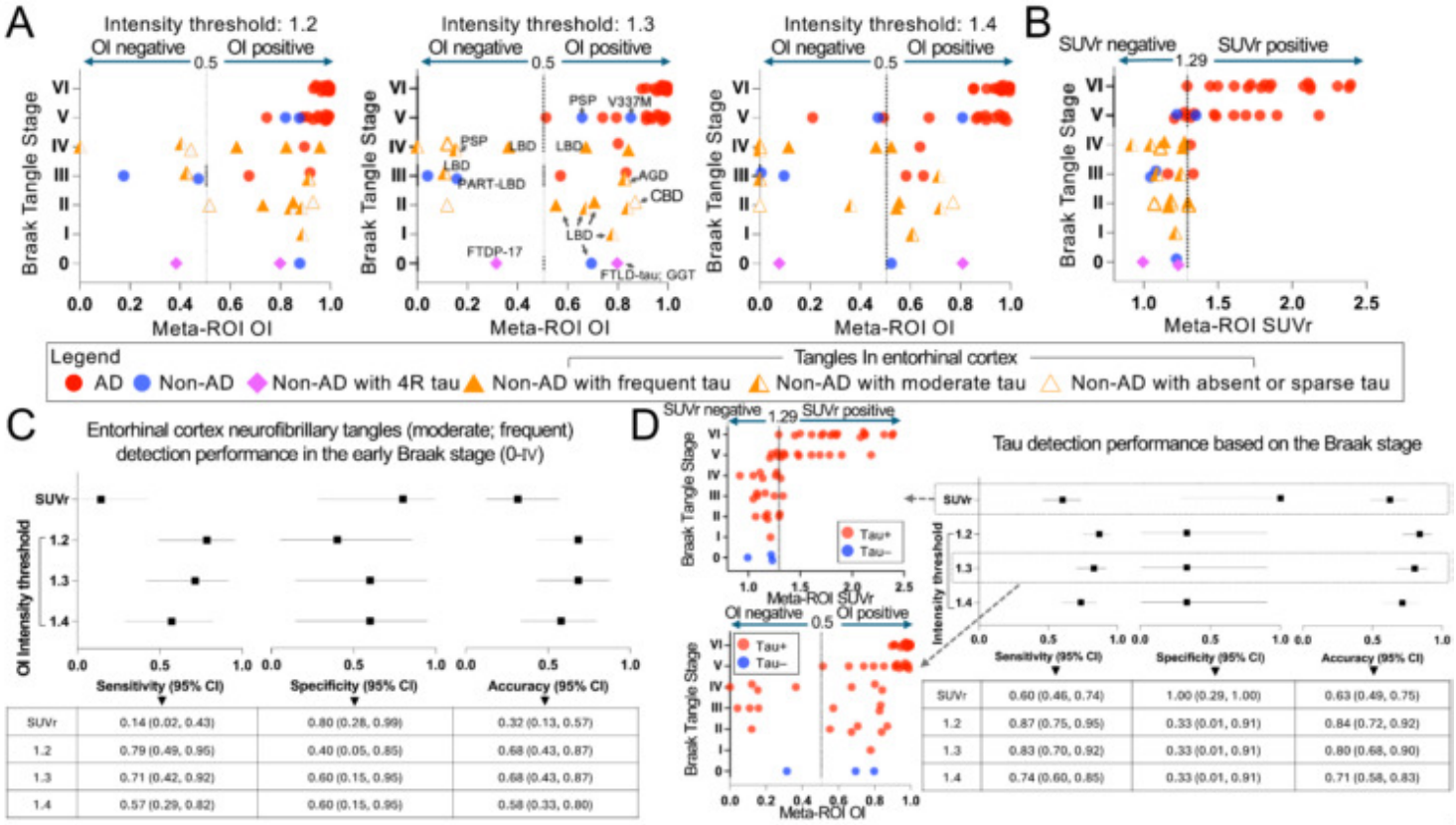
[1]*Department of Radiology, Mayo Clinic, Rochester, MN, US*
[2]*Department of Biomedical Engineering, Hanyang University, Seoul, KR*
[3]*Department of Neuroscience, Mayo Clinic, Jacksonville, FL, US*
[4]*Department of Health Sciences Research, Mayo Clinic, Rochester, MN, US*
[5]*Information Technology, Mayo Clinic, Rochester, MN, US*
[6]*Laboratory Medicine and Pathology, Mayo Clinic, Rochester, MN, US*
[7]*Department of Neurology, Mayo Clinic, Rochester, MN, US*

Background: The Overlap Index (OI) we previously published (Lee et al., 2022) is a reliable method for detecting tau accumulation using tau-PET imaging (flortaucipir; AV1451). It identifies voxel-wise standardized uptake value ratio (SUVr) elevations across serial scans. Previous studies selected OI intensity thresholds based on OI and SUVr relationships. However, parameter optimization is needed to confirm correlations between neuropathologic Braak stages and Meta-ROI OI. This study aims to optimize the OI intensity threshold in tau-PET by comparing it to neuropathologic Braak staging.

Methods: This study included 57 participants from the Mayo Clinic Study of Aging or Mayo Alzheimer's Disease Research Center, all of whom underwent autopsy and at least two serial AV1451 tau-PET scans and 3T T1-weighted MRI within and average of 16 months. Tau-PET SUVr images were normalized to cerebellar crus grey matter, and MR images were co-registered to a single-subject MRI mean. Tau-PET scans were resampled into this space, and OI was calculated by selecting a ROI and applying intensity thresholds (1.2–1.4). Clusters with fewer than 20 contiguous voxels were excluded. Neuropathologic Braak staging was determined using AT8 immunohistochemistry. Sensitivity, specificity, and accuracy were calculated to compare detection performance between OI and SUVr.

Results: OI demonstrated higher sensitivity and accuracy than meta-ROI SUVr across all thresholds in detecting tau pathology, particularly in early Braak stages (I-IV). OI identified NFTs in the entorhinal cortex, especially in moderate to frequent NFT cases, outperforming SUVr. OI detected FTLD-tau and GGT pathology in individuals at Braak stage 0, which SUVr didn't. While SUVr had higher specificity, OI at an intensity threshold of 1.3 offered balanced performance for early tau pathology detection.

Conclusion: The OI in serial tau PET imaging outperforms SUVr in detecting localized tau accumulation by capturing elevated signals in voxel subsets within the ROI, with a 1.3 optimal threshold.



	Sensitivity (95% CI)	Specificity (95% CI)	Accuracy (95% CI)
SUVr	0.14 (0.02, 0.43)	0.80 (0.28, 0.99)	0.32 (0.13, 0.57)
1.2	0.79 (0.49, 0.95)	0.40 (0.05, 0.85)	0.68 (0.43, 0.87)
1.3	0.71 (0.42, 0.92)	0.60 (0.15, 0.95)	0.68 (0.43, 0.87)
1.4	0.57 (0.29, 0.82)	0.60 (0.15, 0.95)	0.58 (0.33, 0.80)

	Sensitivity (95% CI)	Specificity (95% CI)	Accuracy (95% CI)
SUVr	0.60 (0.46, 0.74)	1.00 (0.29, 1.00)	0.63 (0.49, 0.75)
1.2	0.87 (0.75, 0.95)	0.33 (0.01, 0.91)	0.84 (0.72, 0.92)
1.3	0.83 (0.70, 0.92)	0.33 (0.01, 0.91)	0.80 (0.68, 0.90)
1.4	0.74 (0.60, 0.85)	0.33 (0.01, 0.91)	0.71 (0.58, 0.83)

Figure 1. Association of OI according to intensity threshold with Braak tangle stage. (A) Association between meta-ROI OI and Braak tangle stage at intensity thresholds of 1.2, 1.3, and 1.4. Red circles represent AD patient groups, while non-AD cases associated with 4R tau based on autopsy reports are shown in purple. The degree of NFT distribution in the entorhinal cortex, as reported in autopsy, is classified as frequent, moderate, sparse, or absent represented by three different types of triangles. Among non-AD individuals, those without a record of NFT distribution at autopsy are represented by blue circles. Major pathological diagnoses were labeled for non-AD cases in the 1.3 intensity threshold graph. Abbreviations include: LBD (Lewy body disease), FTDP-17 (Frontotemporal degeneration with Parkinsonism linked to chromosome 17), FTLD-tau GGT (Frontotemporal lobar degeneration with 4R-tauopathy, consistent with Globular Glial Tauopathy), AGD (Argyrophilic grain disease), CBD (Corticobasal degeneration), PSP (Progressive supranuclear palsy), PART (Primary Age-Related Tauopathy), and V337M (tau mutation) (B) Association between meta-ROI SUVr and Braak tangle stages. OI demonstrates better detection of individuals with tau pathology in early Braak stages (I-IV) compared to meta-ROI SUVr. Additionally, OI could identify individuals with FTLD-tau GGT pathology among patients with 4R tau at Braak stage 0 (C) OI exhibits higher sensitivity accuracy than SUVr in detecting moderate and frequent NFT cases in the entorhinal cortex during early Braak stages. While SUVr demonstrates greater specificity than OI, the overall balanced performance for early diagnosis indicates that the 1.3 intensity threshold for OI provides optimal performance (D) Investigation of tau detection performance between OI and SUVr. We assumed that Braak stages I-IV are tau positive and Braak stage 0 is tau negative. OI demonstrates better sensitivity and accuracy than SUVr at all three intensity thresholds. In contrast, SUVr shows superior specificity compared to OI. In conclusion, the OI offers better performance over SUVr in detecting localized tau accumulation by capturing elevated signals in a subset of voxels within the ROI, while SUVr could average out these signals across the entire ROI or meta-ROI. An intensity threshold of 1.3 is recommended for optimal early tau pathology detection, providing a balanced approach to sensitivity, specificity, and accuracy.

Keywords: Tau-PET, Overlap Index, Neuropathologic Braak stage, Optimize parameter

101 DeepSUVR: Towards redefining the Centiloid masks using a data-driven approach

Pierrick Bourgeat[1], Jurgen Fripp[1], Leo Lebrat[1], Ashley Gillman[1], Timothy Cox[1], Manu Goyal[5], Duygu Tosun-Turgut[4], Pamela LaMontagne[5], Tammie Benzinger[3], Michael Weiner[4], John Morris[3], Victor L Villemagne[6], Colin Masters[7], Christopher Rowe[2,7], Vincent Dore[1,2]

[1]*CSIRO Health and Biosecurity, Brisbane, AU*
[2]*Department of Molecular Imaging & Therapy, Austin Health, Melbourne, AU*
[3]*Knight Alzheimer Disease Research Center, St. Louis, MO, US*
[4]*San Francisco Veterans Affairs Medical Center, San Francisco, CA, US*
[5]*Mallinckrodt Institute of Radiology, Washington University School of Medicine, St. Louis, MO, US*
[6]*Department of Psychiatry, University of Pittsburgh, Pittsburgh, PA, US*
[7]*The Florey Institute of Neuroscience and Mental Health, University of Melbourne, Melbourne, AU*

Background: PET quantification using the Standardised Uptake Value Ratio (SUVR) is hindered by noise, spill in, and specific binding in the reference region. We evaluated a novel deep learning method which learns from noise in longitudinal trends to correct SUVR quantification and use it to derive new optimized Centiloid masks.

Method: 2281 participants with 2+ visits in AIBL/ADNI (7380 scans) had their Amyloid PET images spatially normalised and quantified usinon-g the Centiloid SPM8 pipeline. A deep learning network (DeepSUVR) was trained to predict a SUVR correction factor (CF) for each spatially normalised image. For each iteration, the prediction was run on 2 random timepoints from the same participant, resulting in 2 Adjusted Centiloids computed using SUVR*CF and each tracer's standard Centiloid transform. A loss function was defined to penalise unexpected temporal changes: Centiloid decreasing over time, Centiloid deviating from the Centiloid/Year vs mean Centiloid curve. The model was trained using 5-fold cross-validation on ADNI+AIBL. For each tracer, new reference and target masks were generated through optimisation to maximise the correlation with the corrected SUVRs in ADNI+AIBL. The resulting masks were evaluated on the OASIS and GAAIN calibration datasets.

Results: The new target masks were similar to the original Centiloid masks, but the new reference masks showed greater variability across tracers and included more white matter. Both DeepSUVR and the masks increased the inter-tracer correlation in the GAAIN dataset while reducing the variance in the young controls. They also increased the correlation between Centiloid/Year vs mean Centiloid in AIBL+ADNI (from ρ=0.41 to ρ=0.52) and OASIS (ρ=0.49 to ρ=0.58).

Conclusions: We evaluated a new technique to correct SUVR estimation based on noise in longitudinal trends, which was used to define new masks. These masks provide an insight into the inner-workings of DeepSUVR and could inform the development of new Centiloid masks.

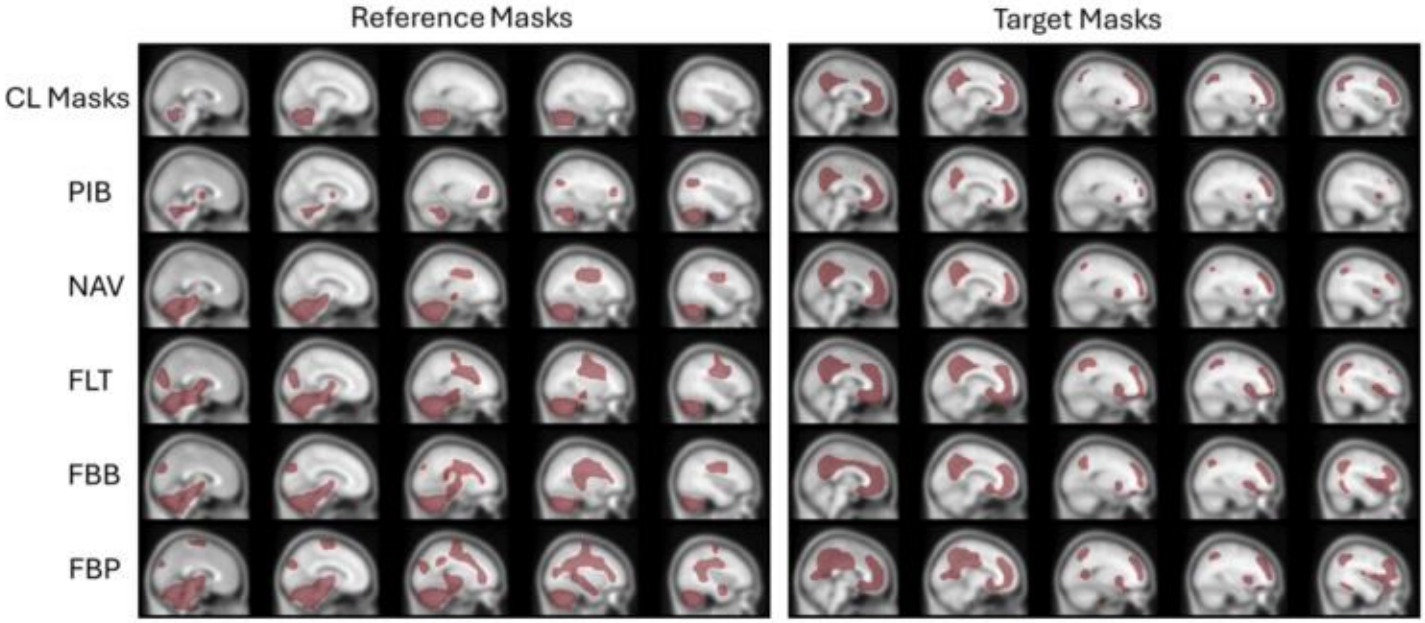
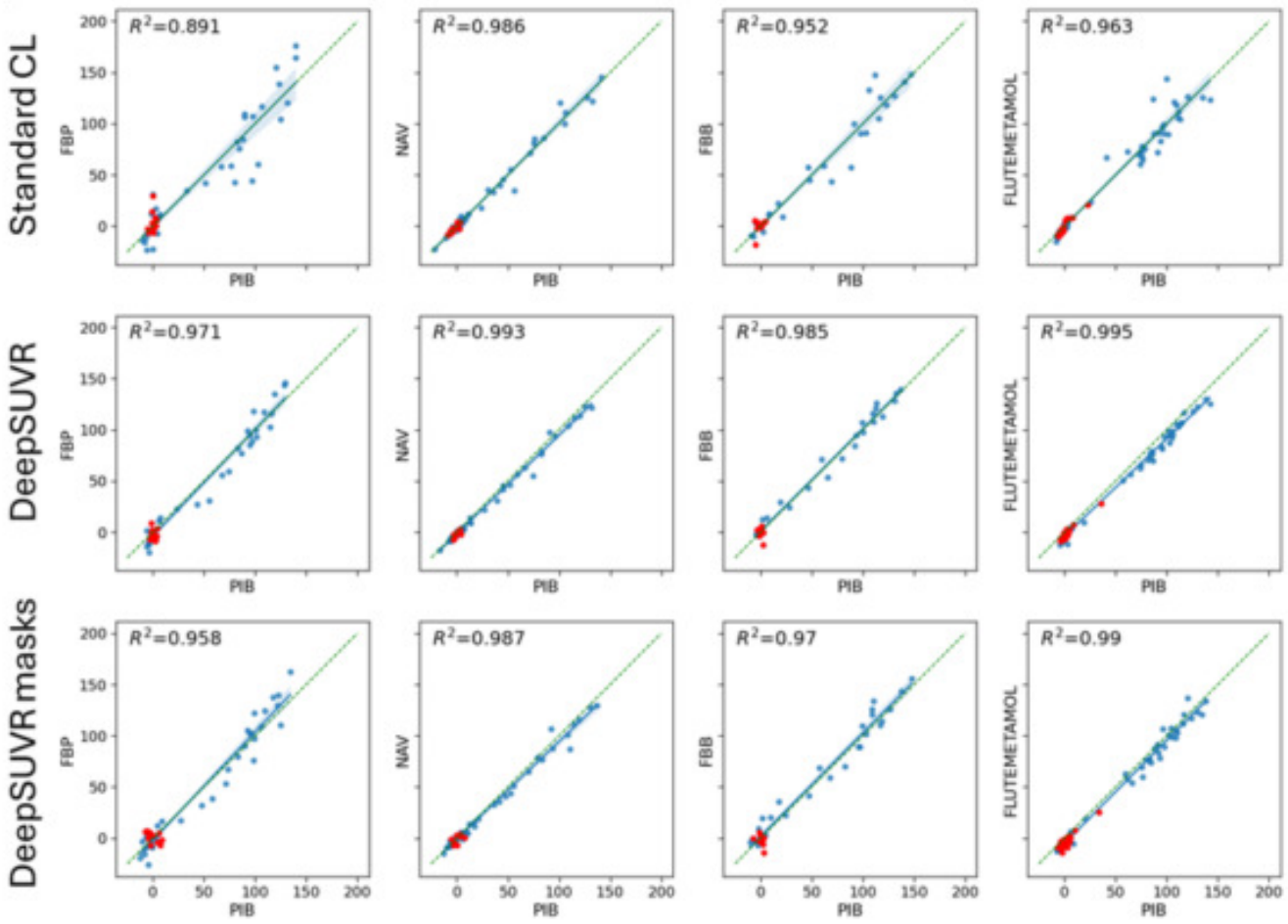


Figure 1. Original Centiloid reference and target masks (top row) and the newly derived Centiloid masks for PIB, NAV, Flutemetamol (FLT), Florbetaben (FBB) and Florbetapir (FBP)

a)



b)

Tracer	Standard	DeepSUVR	DeepSUVR Mask
FBP	9.95	4.51	5.08
FBB	6.90	4.88	5.43
FLUTE*	5.59	3.88	4.82
NAV	4.35	3.48	4.15
PIB	4.38	4.08	5.19

Figure 2. a) Agreement, assessed using the coefficient of determination R^2, between PIB and each ^{18}F tracer in the GAAIN calibration dataset using the Standard masks (top), DeepSUVR (middle) and the new DeepSUVR derived masks (bottom). Young controls are highlighted in red. b) Standard deviation in the young controls for each tracer and quantification method. *One YC was excluded from the calculation as their CL was >20 using both tracers.

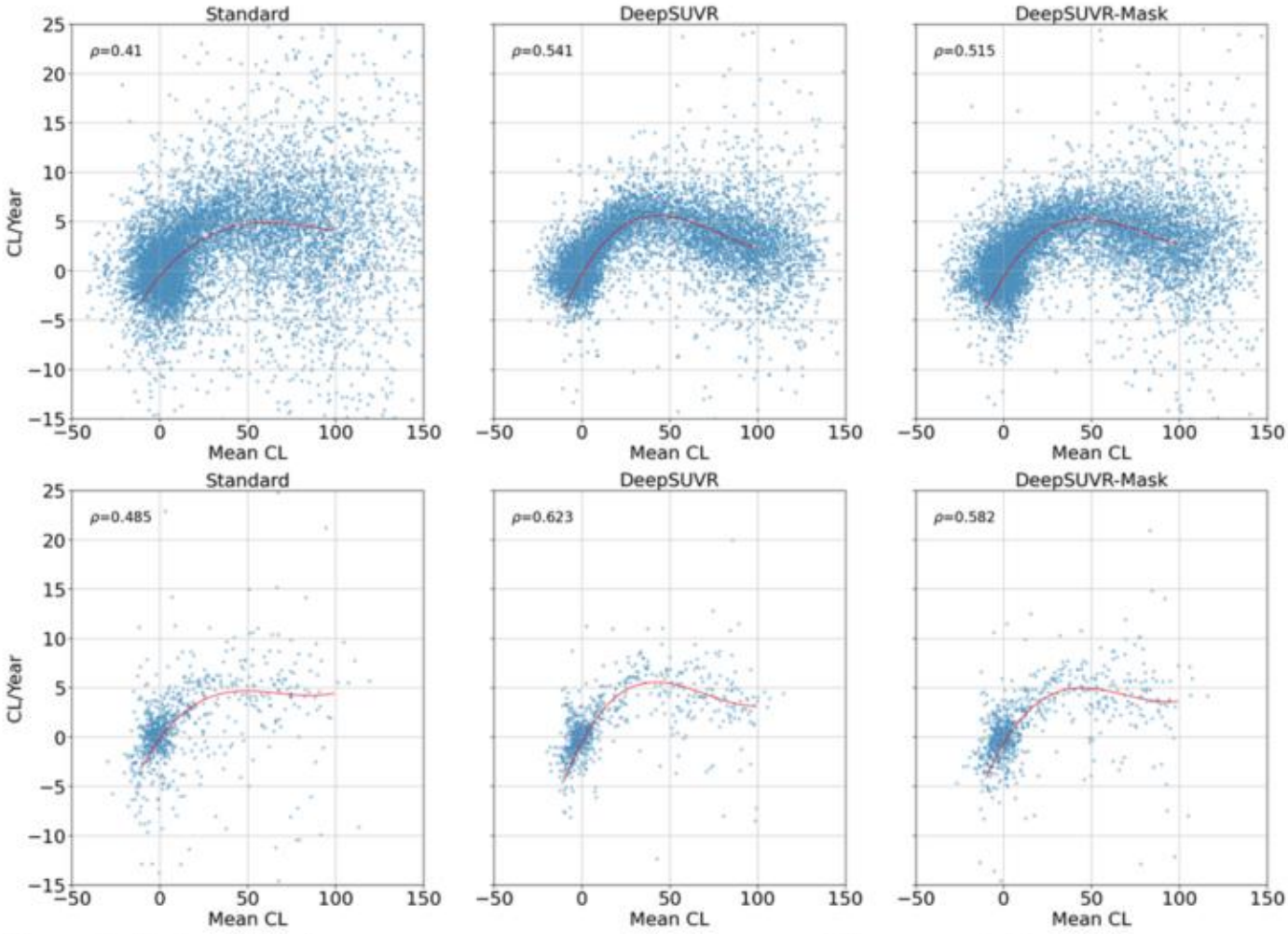


Figure 3. Rate of CL change per year compared to mean CL computed using the Standard masks (left), DeepSUVR (middle) and the new DeepSUVR derived masks (Right) in the AIBL/ADNI dataset (top) and the independent OASIS dataset (Bottom). Each point represents the mean/rate of change based on a pair of images from the same participant. The Spearman rank correlation is denoted using ρ.

Keywords: Centiloid, quantification

102 Mechanical stress of the entorhinal cortex: A potential driver of tau pathology?

Luyue Zhang[1], John Crary[2], Frank Provenzano[1]

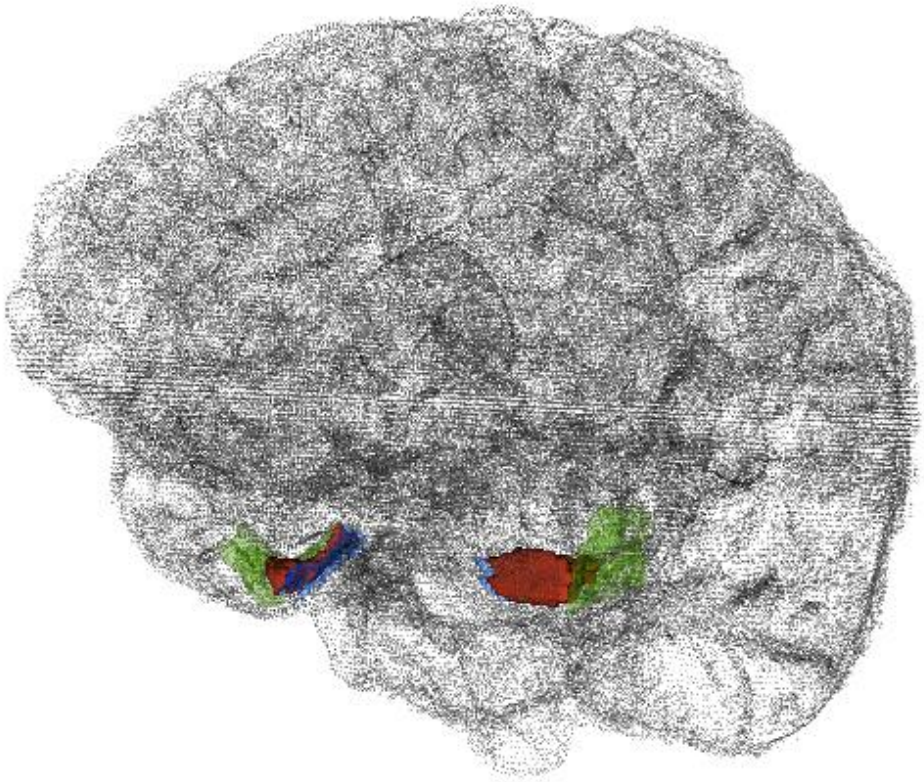
[1]*Columbia University, New York, NY, US*
[2]*Ichan School of Medicine, New York, NY, US*

Introduction: Taupathic changes, namely neurofibrillary tangle deposition in the temporal lobe, are a hallmark of Alzheimer's disease (AD). Tangle deposition is associated with multiple neurodegenerative conditions, as well as traumatic brain injury (TBI). There are several intrinsic mechanisms that have been suggested to initiate the spread of tau in Alzheimer's disease, however less is known about external or structural contributions, specifically in the entorhinal cortex where tau is first shown to accumulate.

Methods: In a cohort of 47 MCI individuals with structural MRI and Tau PET who do (n=24) and do not (n=23) go on to convert to AD, we develop a metric for measuring the proximity between the entorhinal cortex (EC) and tentorial incisor. We do so using FreeSurfer and manual ROIs and then model the volume of this channel using a space index. We then heuristically divide the groups using a threshold of the space index into close and distant proximity. We then test relationships between the proximity measure, conversion and tau PET entorhinal cortex SUVr.

Results: We discovered a significant relationship between entorhinal tau PET and conversion, agnostic of amyloid status, in the close-proximity group (p=0.017), but not in the-proximity group (p=0.467). Proximity measure was not correlated with conversion, tau EC SUVr, nor entorhinal or hippocampal volume.

Discussion: The data presented in a well-characterized cohort with structural imaging and measures of regional tau uptake suggest a possible relationship between the closeness of the entorhinal cortex with a stiff structure medial to it that may be a source of repeated compressive action. This measure can be applied to any reasonable quality structural MRI scan and posits a potential physical mechanism and source of tau deposition. This suggests a potential chronic cause of tau deposition and AD risk.



A glass brain with EC(green), distance between(red) and incisura tentorii(blue).

Keywords: tau, tau pet, entorhinal cortex, trauma, mci

103 Amyloid-Tau to neurodegeneration mismatch from inter-modality image translation using deep learning

Xueying Lyu[1], Paul Yushkevich[2], Mengjin Dong[3], Pulkit Khandelwal[4], Christopher Brown[5], Michael Duong[6], Yue Li[7], Long Xie[8], Laura Wisse[9], Sandhitsu Das[10], David Wolk[11]

[1]*University of Pennsylvania, Philadelphia, PA, US*
[2]*University of Pennsylvania, Philadelphia, PA, US*
[3]*University of Pennsylvania, Philadelphia, PA, US*
[4]*University of Pennsylvania, Philadelphia, PA, US*
[5]*University of Pennsylvania, Philadelphia, PA, US*
[6]*University of Pennsylvania, Philadelphia, PA, US*
[7]*University of Pennsylvania, Philadelphia, PA, US*
[8]*University of Pennsylvania, Philadelphia, PA, US*
[9]*Lund University, Lund, SE*
[10]*University of Pennsylvania, Philadelphia, PA, US*
[11]*University of Pennsylvania, Philadelphia, PA, US*

Background: Prior work demonstrated the mismatch between tau pathology (T) and neurodegeneration (N) can reveal co-pathologies (e.g., vascular disease, TDP-43) and resilience to Alzheimer's disease (AD). Tau is considered the driver of neurodegeneration, but its interaction with amyloid (A) may jointly contribute to brain atrophy in a spatially complex manner. This study advanced exploration of AD pathology and neurodegeneration *mismatch by c*reating synthetic images of N based on *both* T and A using inter-modality image translation, allowing a neural network to model non-linear, spatial relationships between tau, amyloid, and neurodegeneration. Predicted images were compared to actual images to quantify *mismatch*.

Method: We studied 184 amyloid-positive (A+) symptomatic patients from ADNI, each with paired Tau PET and MRI scans representing T and N, alongside Centiloid values for A. We trained a 3D-UNet to learn AT-N relationship by synthesizing cortical thickness map from Tau SUVR and Centiloid-derived images (Figure 1). The reconstruction error (predicted versus actual thickness) across 100 regions of interest (ROIs) was used to quantify the AT-N mismatch.

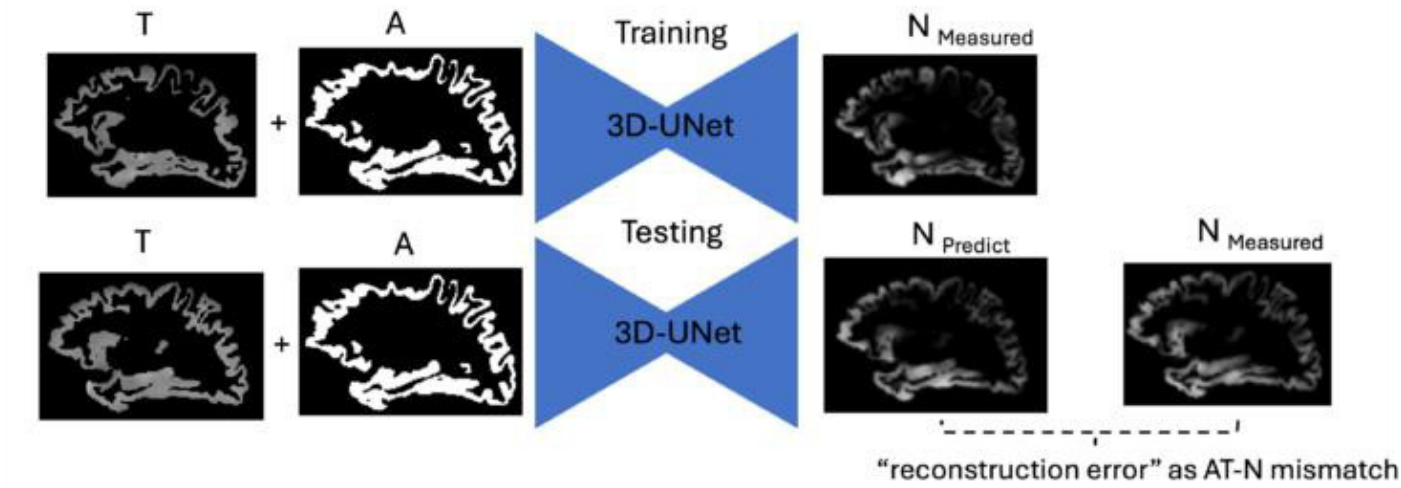


Figure 1. Schematic of AT-N image translation. The model predicts cortical thickness (N) based on tau SUVR from ^{18}F-flortaucipir tracer uptake (T) and amyloid levels quantified using Centiloid values (A). The "reconstruction error," representing the difference between predicted and actual thickness, is used as the AT-N mismatch metric. .

Results: The voxel-wise mean absolute error for cortical thickness prediction across 40 test patients was 0.38 mm, with an average correlation (rho) of 0.80 (±0.1) between predicted and actual thickness across the brain. Tau correlated more strongly with predicted than actual thickness, especially in regions with high tau deposition (Figure 2). Additionally, the model incorporating amyloid displayed stronger tau-thickness correlations than without amyloid, suggesting greater reliance on AD molecular pathology for N prediction. A global mismatch metric, derived from reconstruction error, was significantly associated with worse cognition and increased white matter hyperintensities, but not with global tau levels, suggesting sensitivity to non-AD modulators of N (Figure 3).

Conclusion: The AT-N mismatch, captured through image translation, was linked to clinical and pathological features. Future work will refine this approach for broader clinical application.

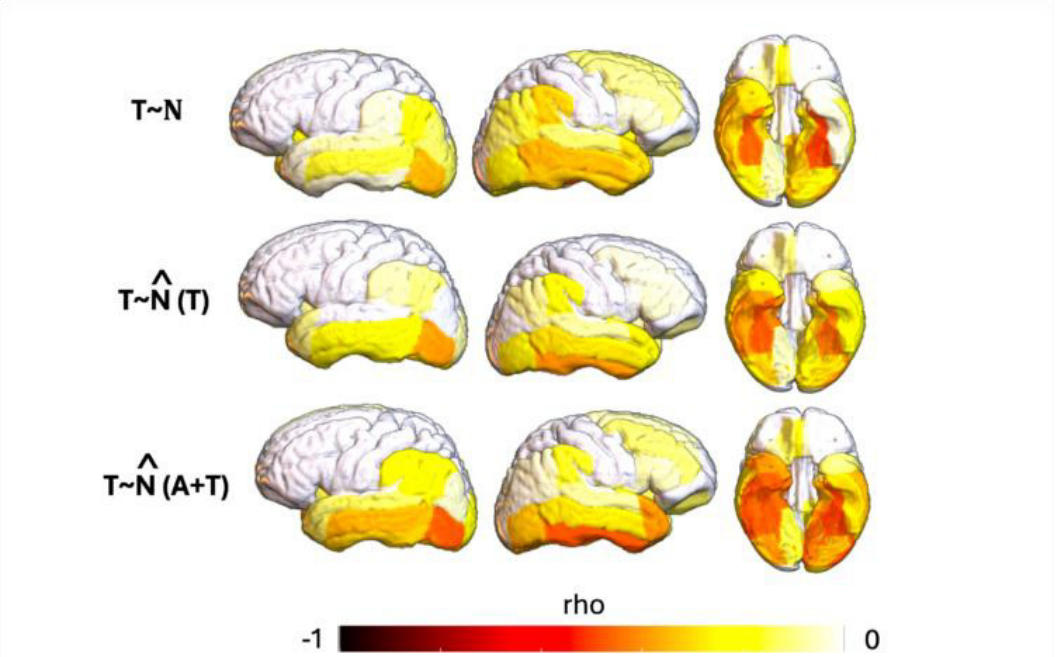


Figure 2. Associations between tau and cortical thickness, visualized in regions showing a negative correlation. The top row shows the associations between tau and measured thickness. The middle row displays the associations between tau and predicted thickness based on tau SUVR alone. The bottom row shows the associations between tau and predicted thickness based on both tau SUVR and Centiloid values.

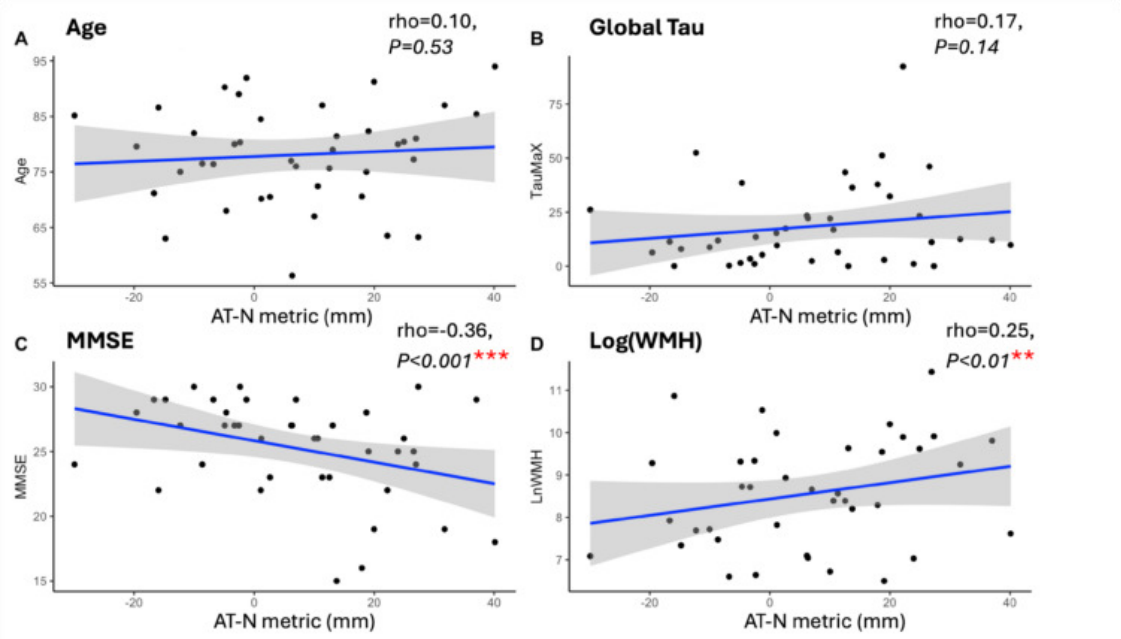


Figure 3. Associations between AT-N mismatch metric and clinical characteristics. Panels show the relationship between T-N mismatch and age (A), global tau severity measured by TauMaX which accounts both amount and extent of tau burden (B), MMSE (C), and log-transformed white matter hyperintensities (LnWMH, D). Associations with MMSE and LnWMH were adjusted for age, sex, and TauMaX. Abbreviations: WMH=white matter hyperintensities.

Keywords: amyloid imaging, Tau PET imaging, Neurodegeneration, co-pathologies, Deep Learning

104 Tau PET subgroups differ in network patterns of functional connectivity and amyloid PET

Peter Millar[1], Stephanie Doering[1], Babatunde Adeyemo[1], Nicole McKay[1], Nicholas Metcalf[1], June Roman[1], Pete Canfield[1], Saurabh Jindal[1], Shaney Flores[1], Jeremy Strain[1], Julie Wisch[1], Jason Hassenstab[1], Suzanne Schindler[1], John Morris[1], Brian Gordon[1], Beau Ances[1], Tammie Benzinger[1]

[1]*Washington University in St. Louis, St. Louis, MO, US*

Background: Spatiotemporal patterns of tau accumulation differ between distinct presentations of Alzheimer disease (AD) and can be identified with PET. Tau accumulation may be driven in part by trans-neuronal spreading through network connections, which can be estimated using resting-state-functional-connectivity MRI (RSFC), and by amyloid-β (Aβ) deposition. We aimed to replicate tau-PET subtypes and tested subtype-specific differences in RSFC and Aβ-PET.

Method: We used the Subtype-and-Stage-Inference (SuStaIn) model to identify spatiotemporal patterns in 820 tau-PET scans (^{18}F-flortaucipir) from 629 Knight-ADRC participants (mean age=70.3, SD=8.6, N=690 CDR®-0, N=130 CDR>0). RSFC correlations were analyzed using seeds in primary-visual-cortex (V1) and precuneus/posterior-cingulate-cortex (PCC). Aβ-PET SUVRs using ^{11}C-Pittsburgh-compound-B (N=365) or ^{18}F-florbetapir (N=423) were harmonized using a Centiloid transformation.

Result: We identified three tau-PET subtypes, resembling previously-reported patterns: limbic-predominant (N=157), posterior-predominant (N=27), and medial-temporal-lobe (MTL)-sparing (N=52), Figure 1. The remaining scans were tau-negative (N=570) or had unstable classifications (N=14). MTL-sparing participants were younger, more severely impaired, and had greater levels of Aβ-PET than other groups (p's<0.001). Posterior-predominant participants were less frequently *APOE* ε4 carriers than other groups (p's<0.001). Although posterior-predominant participants exhibited lower levels of Aβ-PET than limbic-predominant participants in anterior regions and global summaries, Aβ-PET was slightly greater in occipital regions, Figure 2. Compared to limbic-predominant participants, V1 RSFC correlations were greater in cingulo-opercular and fronto-parietal regions in posterior-predominant participants and in cingulo-opercular regions in MTL-sparing participants, Figure 3. PCC RSFC correlations were greater in default-mode regions in posterior-predominant participants and MTL-sparing participants. MTL-sparing participants also exhibited stronger anti-correlations between PCC and cingulo-opercular and fronto-partietal regions.

Conclusion: We replicated three distinct spatiotemporal subtypes of tau-PET accumulation and their associations with individual differences and AD severity in an independent sporadic AD cohort. We identified differences in spatial patterns of Aβ-PET and RSFC, which may contribute to unique patterns of tau spreading within these subtypes.

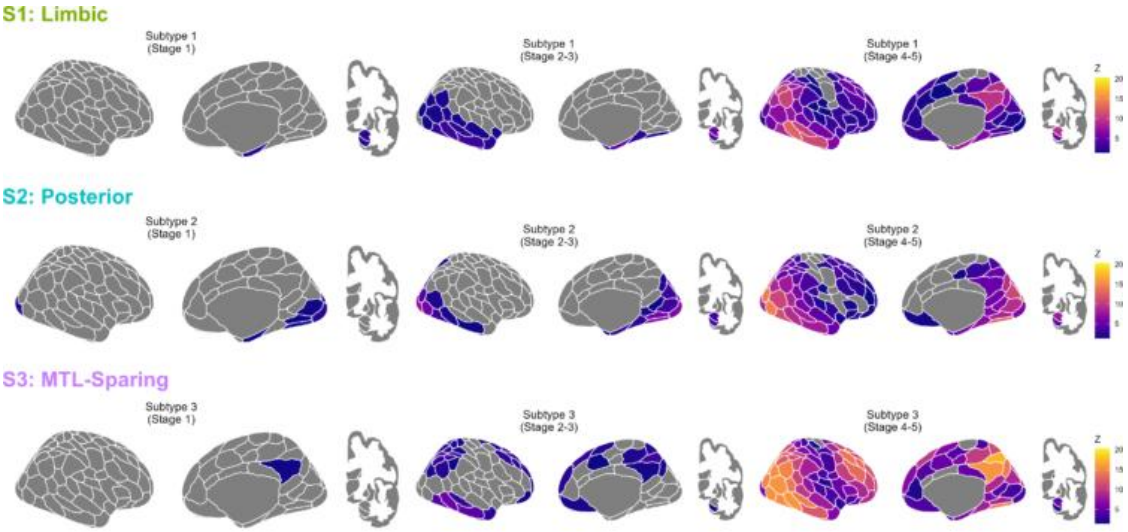


Figure 1. Tau-PET spatiotemporal patterns identified by the SuStaIn model. **Subtype 1 (S1)** appears as "limbic-predominant." **Subtype 2 (S2)** appears as "posterior-predominant." **Subtype 3 (S3)** appears as "medial-temporal-lobe (MTL)-sparing." Scans were merged between Stages 2 and 3 and between Stages 4 and 5 to increase sample size per bin. Regional standardized uptake value ratios (SUVRs) were standardized relative to a low-SUVR distribution, identified for each region using a Gaussian mixture model (GMM). Values are thresholded at z = 1.4 for visualization.

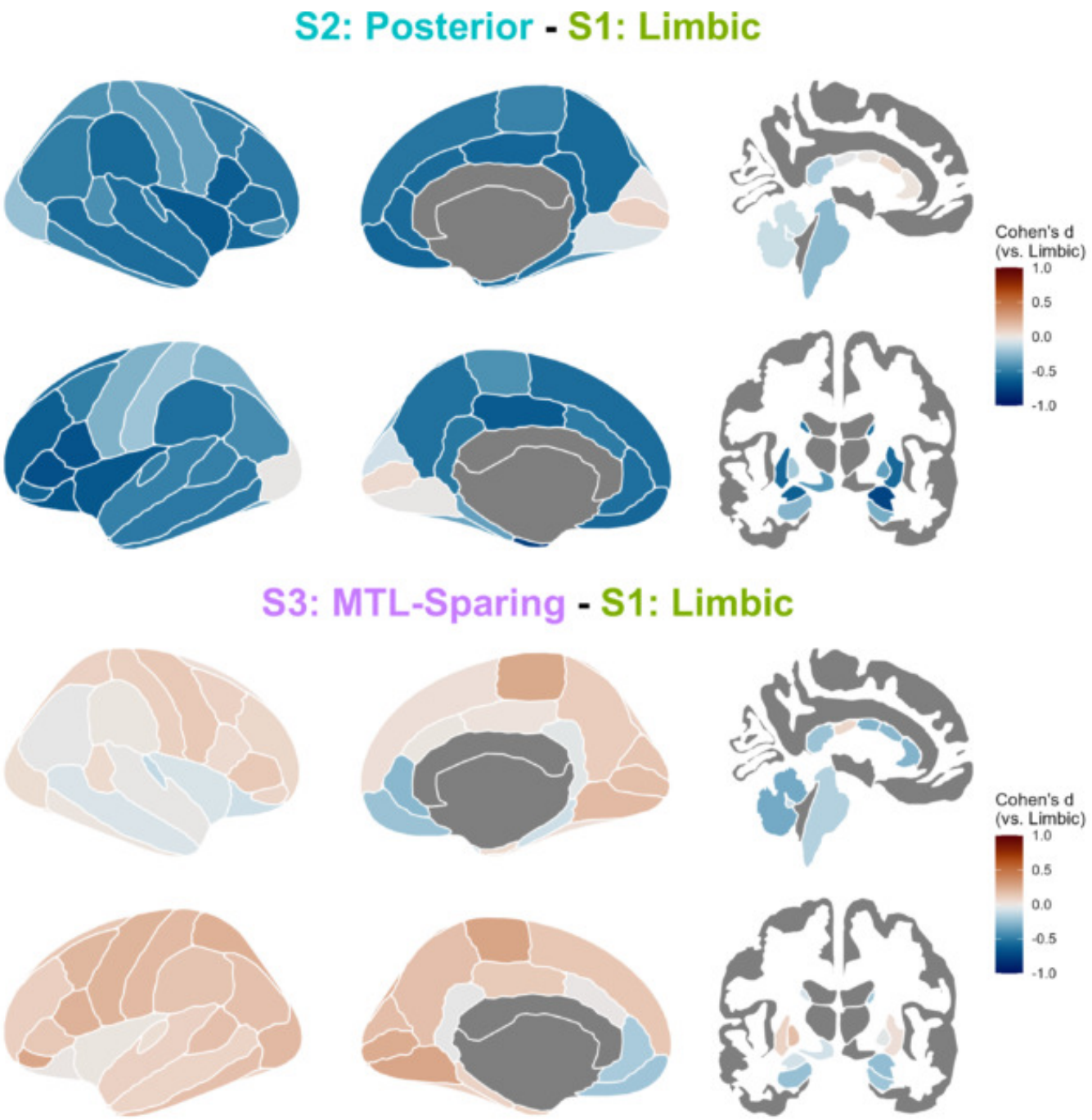


Figure 2. Differences in regional Aβ-PET between Tau-PET subtypes. Effect sizes (Cohen's d) of the group differences in regional Aβ-PET between each "atypical" subgroup (**S2: Posterior** and **S3: MTL-Sparing**) and the "typical" subgroup (**S1: Limbic**).

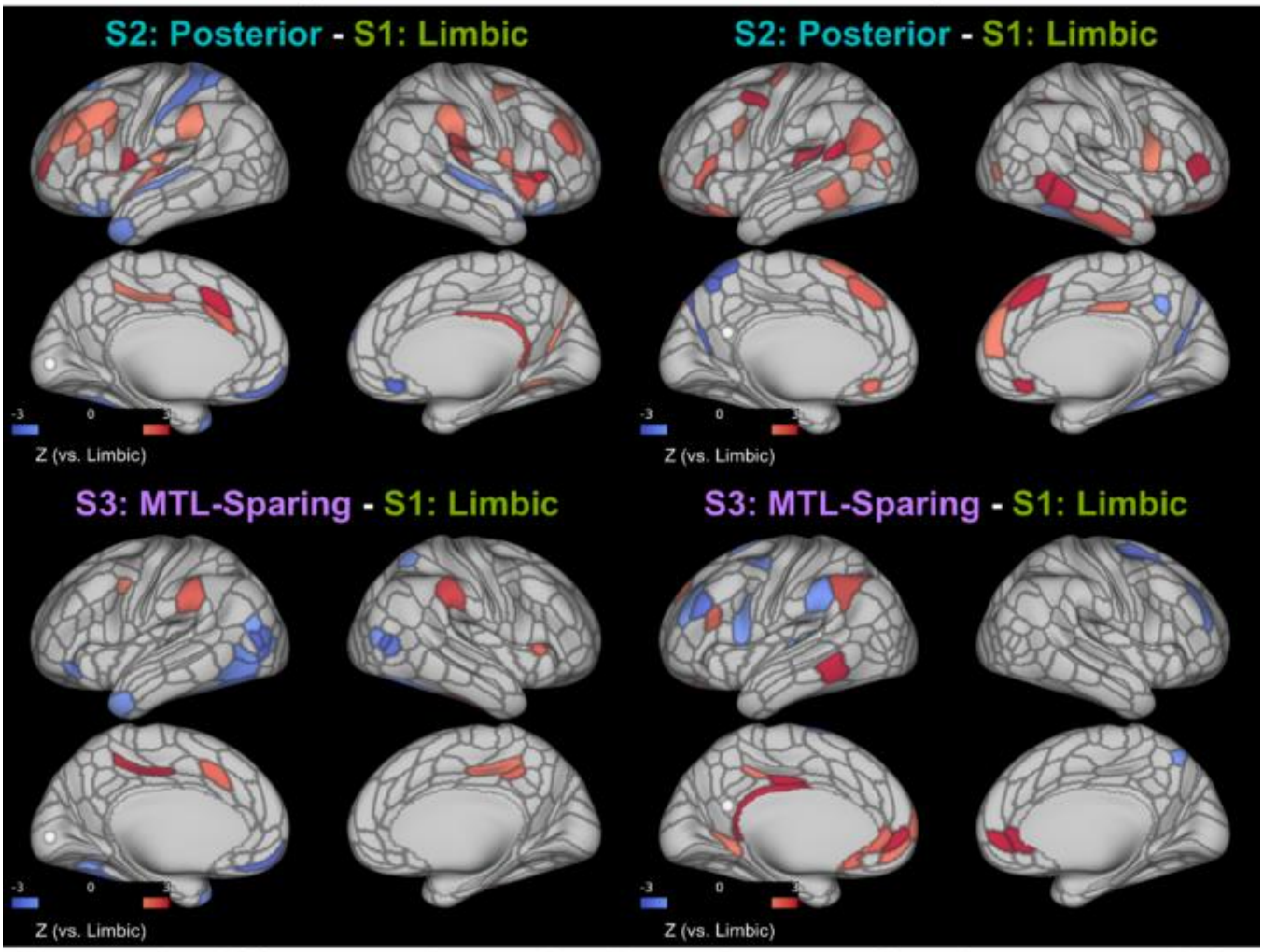


Figure 3. Differences in regional resting-state-function connectivity (RSFC) between Tau-PET subtypes. RSFC correlation maps are plotted using seeds (white spheres) in (**A**) primary-visual-cortex (V1) and (**B**) precuneus / posterior-cingulate-cortex (PCC). RSFC correlation values in each "atypical" subgroup (**S2: Posterior** and **S3: MTL-Sparing**) were standardized relative to a bootstrapped distribution of RSFC correlation values generated by randomly sampling 33 scans from the "typical" subgroup (**S1: Limbic**) 10,000 times. Values are thresholded at z = 2 for visualization.

Keywords: tau PET, atypical Alzheimer disease, resting-state functional connectivity, amyloid PET, brain networks

105 Cortical freewater increases with tau tangle aggregation

Brandon Hall[1,2], Etienne Aumont[1,2], Nesrine Rahmouni[1,2], Joseph Therriault[1,2], Seyyed-Ali Hosseini[1,2], Lydia Trudel[1,2], Jaime Fernandez-Arias[1,2], Arthur Macedo[1,2], Stijn Servaes[1,2], Gleb Bezgin[1,2], Yi-Ting Wang[1,2], Yansheng Zheng[1,2], Jenna Stevenson[1,2], Sulantha Sanjeewa[1,2], Andrea Benedet[5], Gallen Triana-Baltzer[6], Hartmuth Kolb[6], Nicholas Ashton[7], Henrik Zetterberg[5], Kaj Blennow[8], Tharick Pascoal[4], Jesse Klostranec[1,9], Pedro Rosa-Neto[1,2,3]

[1]*McGill University, Montreal, QC, CA*
[2]*Translational Neuroimaging Laboratory, The McGill University Research Centre for Studies in Aging, Montreal, QC, CA*
[3]*Douglas Hospital Research Centre, Verdun, QC, CA*
[4]*University of Pittsburg, Pittsburg, PA, US*
[5]*Department of Psychiatry and Neurochemistry, Institute of Neuroscience and Physiology, The Sahlgrenska Academy, Gothenburg, SE*
[6]*Neuroscience Biomarkers, Janssen Research & Development, La Jolla, CA, US*
[7]*Wallenberg Centre for Molecular and Translational Medicine, University of Gothenburg, Gothenburg, SE*
[8]*Clinical Neurochemistry Laboratory, Sahlgrenska University Hospital, Mölnda, SE*
[9]*Division of Diagnostic and Interventional Neuroradiology, Montreal Neurological Institute and Hospital, Montreal, QC, CA*

It is unclear how cortical microstructure changes across biological stages of Alzheimer's disease (AD), and how this occurs in response to amyloid plaques, tauopathy, and inflammation. We hypothesize that tauopathy is chiefly responsible. To test this, we investigated how different measures of tauopathy influence microstructural integrity in the whole brain, temporal meta-ROI, and hippocampus.

We sampled 301 participants (59% female, age 67±10) from the TRIAD cohort with T1 MRI, diffusion-weighted MRI, amyloid PET (F^{18}-NAV4694), tau PET (F^{18}-MK6240), and plasma biomarkers. We used the NODDI MATLAB toolbox to derive voxelwise freewater images, wherein higher cortical values represent inflammation and decreased microstructural integrity. We used FreeSurfer 7 to derive temporal meta-ROI) and hippocampal masks, and Standard Uptake Value Ratio (SUVR) to calculate amyloid and tau PET images. Plasma biomarkers were measured by Simoa assay. We stratified participants by amyloid SUVR positivity, plasma ptau 217 positivity (T1), and tau SUVR positivity (T2). We performed voxelwise correlations between freewater and tau SUVR via VoxelStats MATLAB toolbox. Voxelwise regressions between freewater and plasma biomarkers and the mediation analyses performed in R 4.4.1. Models covaried for amyloid SUVR, age, sex, and APOE4 genotype status. Multiple comparisons correction performed by random field theory method.

Tau PET and plasma p-tau217 positively correlated with freewater in temporal and occipital regions (**Fig1A**, **Fig2A**). However, the effect of p-tau217 is only present in participants positive for tau tangles (**Fig 2C)**. Freewater increased only in the A+T2+ group in the meta-ROI and hippocampus (**Fig1B,C)**. Tau SUVR in meta-ROI mediated the correlations between both GFAP and p-tau217 with freewater in the A+T+ group (**Fig3**).

In neocortical and allocortical AD-relevant regions, increased freewater correlates with tau tangle accumulation. Our results suggest that while astrogliosis is involved with inflammation and decreasing microstructural integrity,

this only occurs due to neurofibrillary tangles.

Figure 1. Increased tau is correlated with increased freewater independent of amyloid

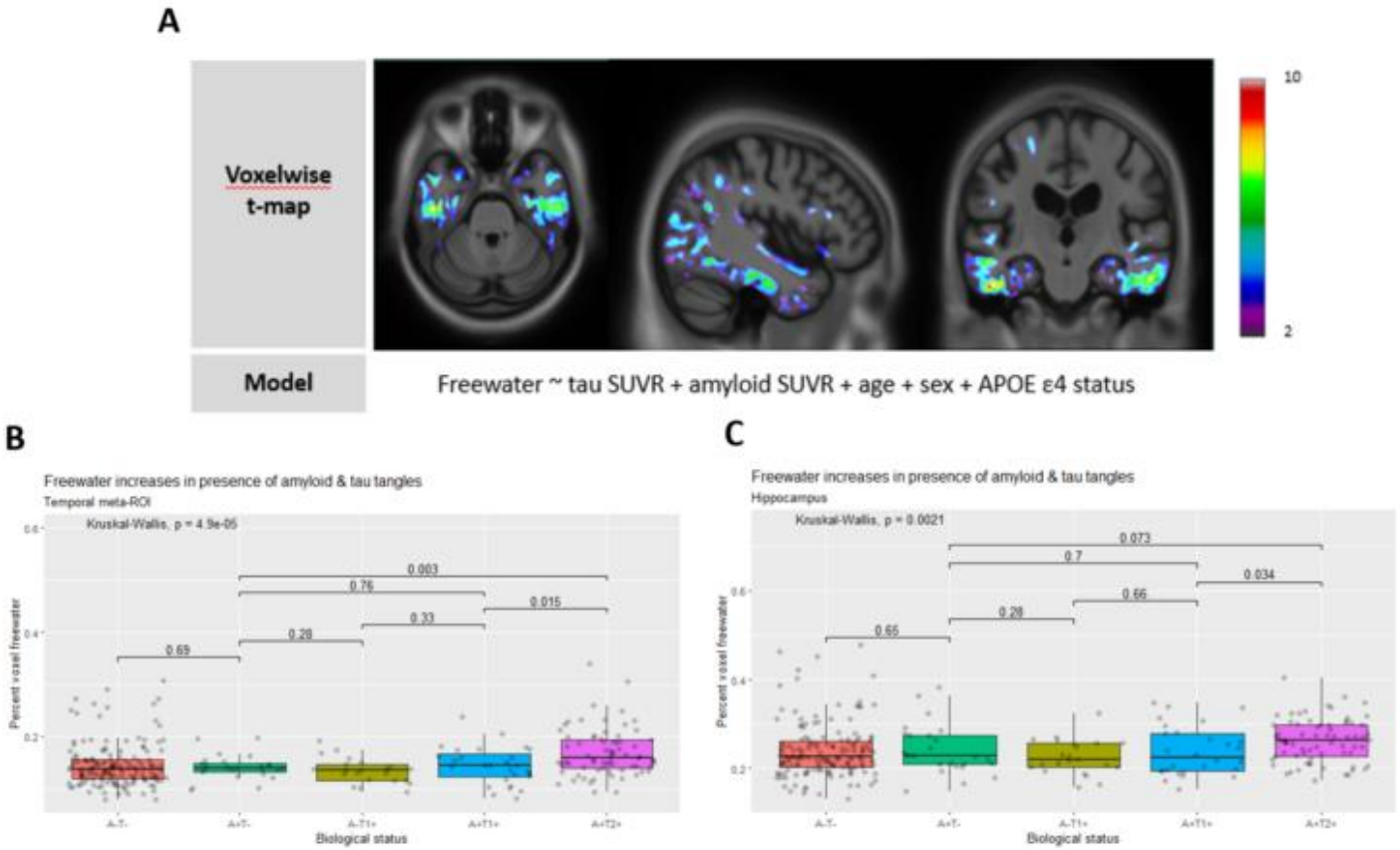


Figure 1. A) Voxelwise t-value maps of positive associations between freewater and tau PET after correction for amyloid PET, age, sex, and APOE4 allele frequency. Negative correlations did not survive multiple comparisons correction. Of note, the spatial distribution and intensity of positive correlations between tau PET and freewater closely resembles that found in the correlation of plasma ptau 217 and freewater. **B)** Boxplots of freewater in the temporal meta-ROI across different biological stages of AD-associated proteinopathy: amyloid-negative tau-negative (A-T-), amyloid-positive tau-negative (A+T-), amyloid-negative tau-plasma217-positive (A-T1+), amyloid-positive tau-plasma217-positive (A+T1+), amyloid-positive tau-PET-positive (A+T2+). **C)** As B, but instead showing freewater in the hippocampus across the biological stages.

Figure 2. Plasma ptau 217 correlates with freewater independent of amyloid in meta-ROI and hippocampus

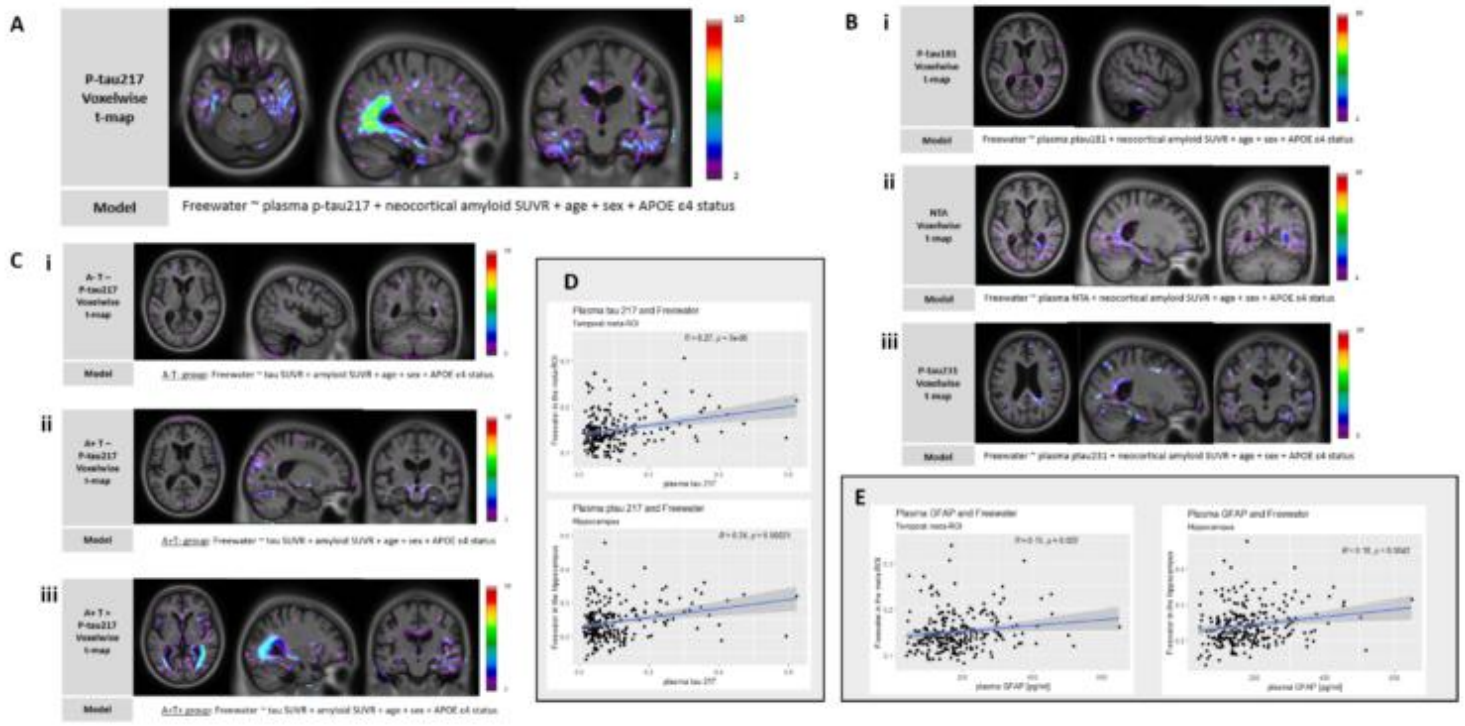


Figure 2. A) Voxelwise t-value maps of positive correlations between the plasma p-tau217 and freewater adjusting for average neocortical amyloid SUVR age, sex, and APOE4 allele frequency. **B)** As A, but instead showing the correlations between freewater and i) plasma p-tau181 ii) plasma N-terminal containing Tau fragments iii) plasma p-tau231. **C)** As A, but instead showing the correlations between the freewater and p-tau217 in participants grouped by biological stage, as defined by PET positivity: i) amyloid negative, tau negative ii) amyloid positive, tau negative iii) amyloid positive tau positive. **D)** Scatterplots depicting the correlation between plasma p-tau217 and freewater in the temporal meta-ROI and the hippocampus. **E)** Scatterplots depicting the correlation between plasma GFAP and freewater in the temporal meta-ROI and the hippocampus. Participants are grouped into three categories based on PET positivity for amyloid and tau due to group size restraints imposed by stratification used earlier in **Fig1**.

Figure 3. The effect of plasma GFAP on Freewater is mediated by tau

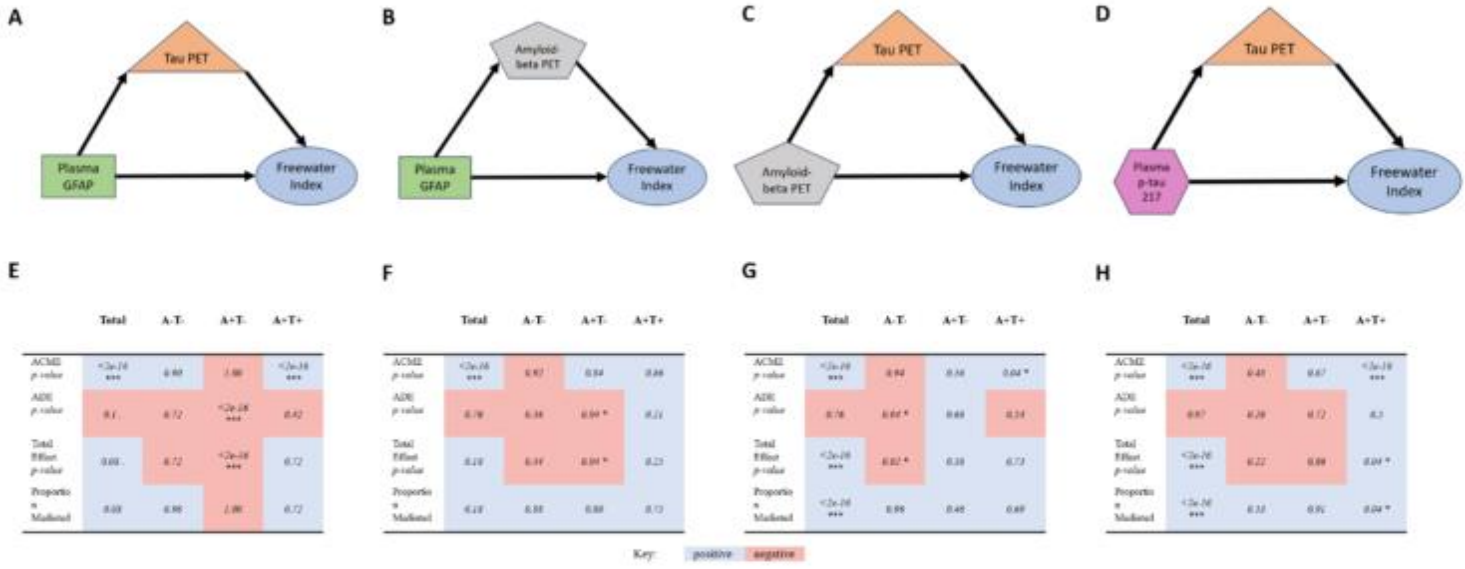


Figure 3. A) Schematic representation of the mediation analysis between plasma GFAP predicting the freewater index in the temporal meta-ROI, mediated by average tau SUVR in the temporal meta-ROI. This model was replicated across participants by biological stage. **B)** Schematic representation of the mediation analysis between plasma GFAP predicting the freewater index in the meta-ROI, mediated by neocortical amyloid SUVR. There was no significant mediation. **C)** Schematic representation of the mediation analysis between neocortical amyloid SUVR predicting the freewater index in the meta-ROI, mediated average tau SUVR in the temporal meta-ROI. **D)** Schematic representation of the mediation analysis between plasma p-tau217 predicting the freewater index in the meta-ROI, mediated plasma tau SUVR. Summary statistics and effect direction of mediation model from **A** across biological stages. **E)** Summary statistics and effect direction of mediation model from **B** across biological stages. **F)** Summary statistics and effect direction of mediation model from **C** across biological stages. **H)** Summary statistics and effect direction of mediation model from **D** across biological stages. Participants are grouped into three categories based on PET positivity for amyloid and tau due to group size restraints imposed by stratification used earlier in **Fig1**.
P-value 0.1 – 0.05: .
P-value 0.05 – 0.01: *
P-value 0.009 – 0.001: **
P-value < 0.0009: ***

Keywords: tau, PET, plasma, inflammation, microstructure

106 Distinct spatiotemporal patterns of vascular disease in Alzheimer's disease subtypes

Julie Ottoy[1], Eric Yin[1], Min Su Kang[1], Erin Gibson[1], Andrew Clappison[1], Ying Yang[1], Katrina Carver[1], Nesrine Rahmouni[2], Jenna Stevenson[2], Stijn Servaes[2], Joseph Therriault[2], Tharick Pascoal[2], Jean-Paul Soucy[3], Serge Gauthier[2], Sandra Black[1], Pedro Rosa-Neto[2,3], Maged Goubran[1]

[1]*Hurvitz Brain Sciences Program, Sunnybrook Research Institute, University of Toronto, Toronto, ON, CA*
[2]*Translational Neuroimaging laboratory, McGill Centre for Studies in Aging, Montreal, QC, CA*
[3]*Montreal Neurological Institute, McGill University, Montreal, QC, CA*

Background: Alzheimer's disease (AD) is a heterogeneous disorder that is often comorbid with cerebral small vessel disease (SVD). However, the spatiotemporal patterns of SVD imaging markers remain not well understood. Here, we evaluated 1) spatiotemporal effects of microstructural white matter injury on MRI-visible lesion progression, and 2) whether distinct patient subtypes and stages exist based on regional SVD and AD biomarkers.

Methods: The longitudinal TRIAD cohort comprised cognitively normal, MCI, and AD dementia (baseline, y1, y2: *N*=202, 100, 70). We quantified both global and regional imaging markers of microstructural injury (DTI-based free water; fractional anisotropy; mean diffusivity in normal-appearing white matter) as well as MRI-visible lesions (white matter hyperintensities 'WMH'; perivascular spaces 'PVS'). We studied baseline and longitudinal associations of DTI-markers with WMH and PVS in (1) amyloid-negative (Aβ-) vs. Aβ+ individuals, and (2) subtypes of individuals with distinct baseline SVD patterns, identified through the Subtype and Stage Inference (SuStaIn) algorithm.

Results: At baseline, higher free water was associated with both higher WMH and PVS volume (*P<0.001*), irrespective of Aβ status. Longitudinally, higher free water predicted faster WMH growth (both globally and regionally) but slower centrum-semiovale PVS growth, particularly in Aβ+ (**Fig.1a**). Free water in the occipital cortex mediated the relationship between Aβ and WMH growth. Finally, SustaIn identified 3 subtypes (**Fig.1b**). Subtype-1 ("AD") had Aβ accumulation first, followed by greater free water that was associated with an increase in vascular lesion growth (**Fig.1c**). Subtype-2 ("mixed") had early involvement of SVD markers with later changes in free water. Subtype-3 ("SVD") demonstrated pure vascular characteristics.

Conclusions: Higher free water predicted vascular lesion progression in AD, with distinct spatiotemporal patterns identifiable through subtyping and staging. Patient subtyping based on underlying pathobiological changes can enable identifying subgroups of patients to which vascular- vs. Aβ-specific treatment mechanisms may apply.

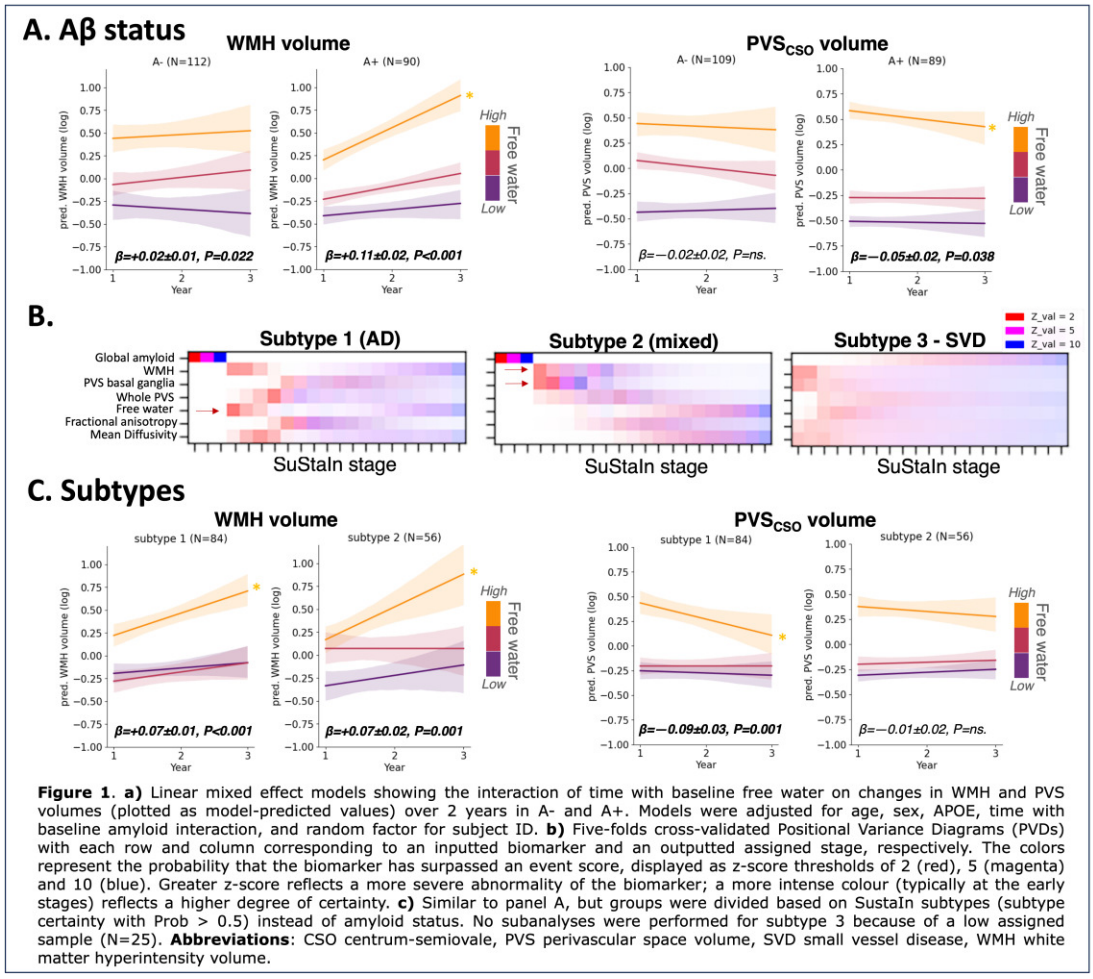


Figure 1. **a)** Linear mixed effect models showing the interaction of time with baseline free water on changes in WMH and PVS volumes (plotted as model-predicted values) over 2 years in A- and A+. Models were adjusted for age, sex, APOE, time with baseline amyloid interaction, and random factor for subject ID. **b)** Five-folds cross-validated Positional Variance Diagrams (PVDs) with each row and column corresponding to an inputted biomarker and an outputted assigned stage, respectively. The colors represent the probability that the biomarker has surpassed an event score, displayed as z-score thresholds of 2 (red), 5 (magenta) and 10 (blue). Greater z-score reflects a more severe abnormality of the biomarker; a more intense colour (typically at the early stages) reflects a higher degree of certainty. **c)** Similar to panel A, but groups were divided based on SustaIn subtypes (subtype certainty with Prob > 0.5) instead of amyloid status. No subanalyses were performed for subtype 3 because of a low assigned sample (N=25). **Abbreviations**: CSO centrum-semiovale, PVS perivascular space volume, SVD small vessel disease, WMH white matter hyperintensity volume.

Keywords: Alzheimer's disease, Vascular disease, Neuroimaging, Free water, SuStaIn

107 Annual percent change of microglia density in relation to tau accumulation in older adults

Hannah Houlihan[1], Aubrey Johnson[1], Anna Smith[1], Diana Guzman[1], Amarachukwu Okafor[1], Lauren Heuer[1], Thairi Sanchez[1], Daniel Talmasov[1], Ndubisi Chikwem[1], Dina Dass[1], James Noble[1], William Kreisl[1], Scott Small[1], Patrick Lao[1]

[1]*Columbia University Medical Center, New York, NY, US*

Background: We sought to quantify regional annual percent change in ER176, a novel TSPO PET radiotracer, and tau accumulation in older adults.

Methods: Participants (n=13 amyloid-negative controls without cognitive impairment; n=1 amyloid-positive individual with Posterior Cortical Atrophy (PCA); Table 1) from the Longitudinal Imaging of Microglial Activation in Different Clinical Variants of Alzheimer's Disease study underwent amyloid (Florbetaben), tau (MK6240), and TSPO PET (ER176). Annual percent change in partial volume corrected TSPO and tau SUVR for 13 AD-related ROIs were assessed by demographic characteristics and baseline biomarker values in controls.

Results: TSPO change ranged from -4.6±2% in hippocampus to +3.3±2% in superior temporal lobe for controls, and from -5.8% in hippocampus to +4.1% in middle inferior temporal lobe in PCA (Figure 1A). Tau change ranged from -0.4±5% in inferior parietal cortex to +5.2±3% in entorhinal cortex in control, and from -1.4% in hippocampus to +9.5% in entorhinal cortex in PCA (Figure 1B). Older age was associated with a greater TSPO change in lingual (0.17 [0.01, 0.33], p=0.04) and fusiform gyrus (0.6 [0.07, 1.1], p=0.03). Greater baseline MK6240 was associated with a greater TSPO change in lingual gyrus (5.5 [1.7, 9.2], p=0.01). Greater baseline TSPO was associated with greater MK6240 change in superior parietal cortex (42 [24, 60], p=0.001) and cingulate gyrus (66 [2.2, 129], p=0.04).

Conclusion: Compared to previous generation TSPO tracers, ER176 had a similar but slightly greater range in percent change per year and had the added benefit of including low affinity binders. Longitudinally, TSPO demonstrated both increases and decreases across the brain in controls and one individual with PCA, whereas tau demonstrated mostly increases, which was greatest in the entorhinal cortex. These longitudinal ER176 PET data relative to tau PET reflect the dynamic role of TSPO in aging and disease.

	Controls
N	13
Age	69.8±6 years
Sex	62% Women
Education	16.5±2 years
Race	85% White
Ethnicity	83% Non-Hispanic
TSPO Affinity	54% Low Affinity
APOE4 Carrier	23% APOE4
Follow-up	2.28 ± 0.10 years

Table 1: Demographic information for 13 amyloid-negative controls without cognitive impairment. Demographics for the 1 amyloid-positive individual with Posterior Cortical Atrophy (PCA) were omitted to prevent potential identification, but the demographics were similar to that of the controls.

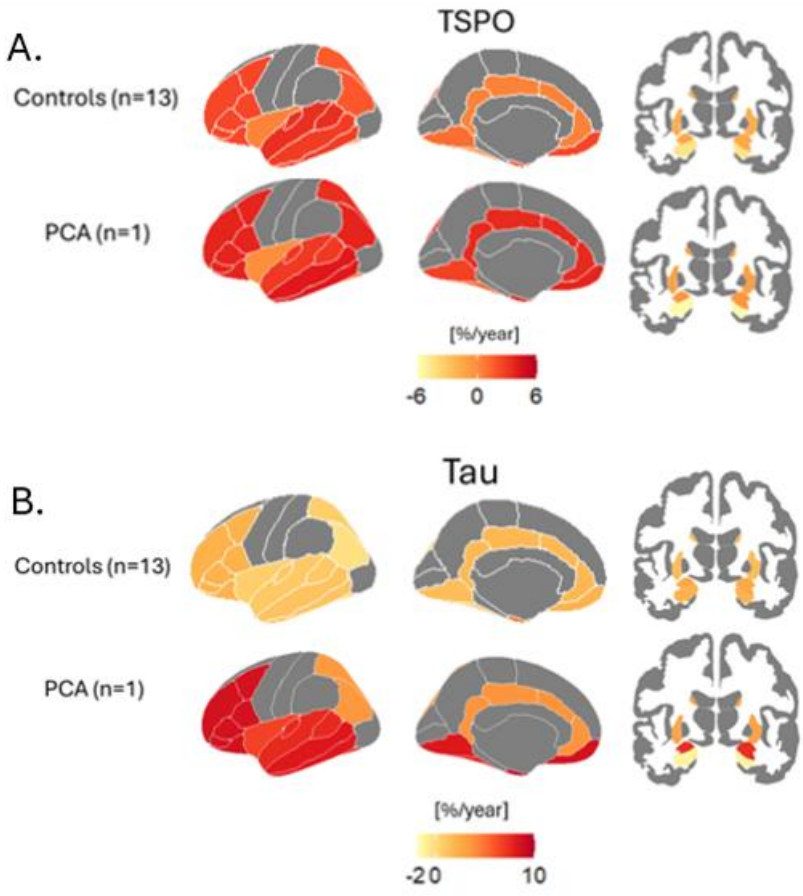


Figure 1: Annual percent change in controls and 1 individual with PCA for TSPO PET (A) and MK6240 PET (B). Gray regions were not quantified.

Keywords: Microglia, Tau, PET

108 Physical frailty as a risk factor for increased tau accumulation and cognitive decline in cognitively unimpaired older adults

Kailee Palmgren[1], Paola Matos[1], Dylan Kirn[1,2], Talia Robinson[1,2], Eva Pintucci[1], Michael Properzi[1,4], Aaron Schultz[1,3,4], Rebecca Amariglio[1,2,3], Dorene Rentz[1,2,3], Keith Johnson[1,2,3], Reisa Sperling[1,2,3], Jasmeer Chhatwal[1,2,3], Wai-Ying Wendy Yau[1,2,3]

[1]*Department of Neurology, Massachusetts General Hospital, Boston, MA, US*
[2]*Department of Neurology, Brigham and Women's Hospital, Boston, MA, US*
[3]*Harvard Medical School, Boston, MA, US*
[4]*Athinoula A. Martinos Center for Biomedical Imaging, Department of Radiology, Massachusetts General Hospital, Charlestown, MA, US*

Background: Frailty is an age-related syndrome of reduced physiological reserve and increased vulnerability to adverse health outcomes. Physical frailty is a risk factor for dementia, including Alzheimer's disease (AD). However, its impact on the accumulation of amyloid and tau pathology, especially during the preclinical period, is unclear, limiting development of prevention/intervention strategies.

Method: We examined older adults from the Harvard Aging Brain Study who were cognitively unimpaired at baseline with longitudinal cognition (N=327), amyloid (Pittsburgh Compound-B; N=269), and tau (Flortaucipir; N=193) PET (Table 1). Physical frailty was measured using the cumulative deficit model with a 30-item frailty index (FI; higher indicate greater frailty) (Table 2). Sensitivity analyses were performed using a modified 4-criteria Fried frailty phenotype (shrinking, slowness, exhaustion, inactivity). Using linear mixed effects models, we examined the impact of baseline frailty on longitudinal amyloid burden and the interactive associations between frailty and baseline amyloid on longitudinal inferior temporal cortex (ITC) tau and cognitive decline (Preclinical Alzheimer Cognitive Composite-5).

Result: Adjusting for age and sex, there were no significant associations between FI and baseline amyloid, tau, or cognition ($p>0.15$). FI was not associated with longitudinal amyloid burden ($p=0.42$; Figure 1A). By contrast, higher FI and elevated baseline amyloid were synergistically associated with faster ITC tau accumulation ($t=2.64$, $p=0.01$), with no additional main effect of FI on longitudinal tau ($p=0.50$). There was a concordant interaction of higher FI and amyloid on faster cognitive decline ($t=-2.11$, $p=0.04$), along with a modest main effect of higher FI on faster decline independent of amyloid ($t=-2.49$, $p = 0.01$). Sensitivity analyses using modified Fried frailty phenotype yielded similar results (Figure 1B).

Conclusion: Our findings suggest that targeting physical frailty in cognitively unimpaired older adults may help slow amyloid-related tau accumulation and cognitive decline, as well as have a modest benefit on non-amyloid-related cognitive aging.

Table 1. Participant characteristics

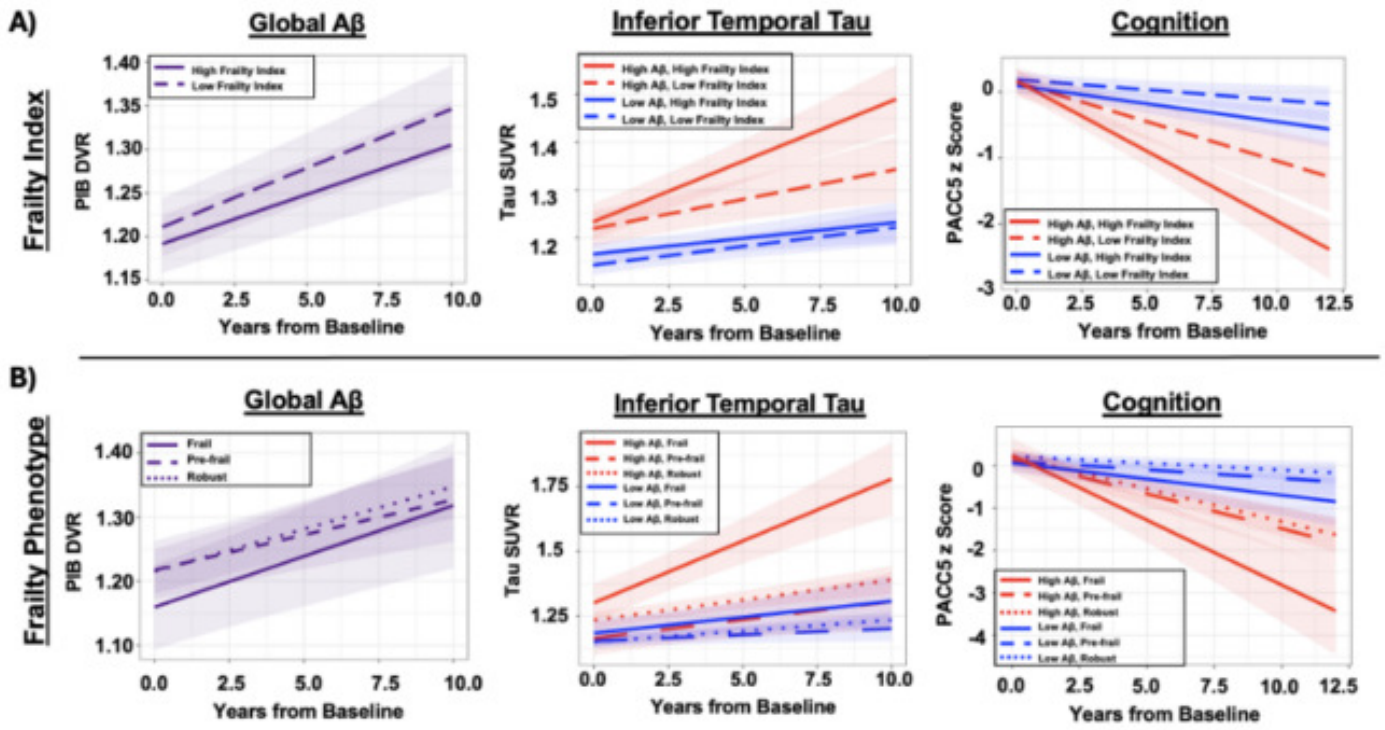
	All Participants N=327	Longitudinal PIB Subgroup N=269	Longitudinal Tau Subgroup N=193
Age at baseline, yr, mean (SD)	71.8 (7.9)	71.4 (8.04)	70.3 (8.2)
Females, n (%)	198 (61)	165 (61)	118 (61)
Education, yr, mean (SD)	15.9 (2.95)	16.0 (2.9)	16.1 (2.9)
APOE ε4 carriers, n (%)	90 (28)	73 (27)	52 (27)
Frailty Index, mean (SD)	0.16 (0.1)	0.16 (0.1)	0.15 (0.1)
Baseline PiB PET FLR DVR, mean (SD)	1.17 (0.2)	1.16 (0.2)	1.15 (0.2)
Baseline Aβ positive, n (%)	77 (24)	59 (22)	40 (21)
# longitudinal PIB PET scans, median (IQR; range)	N/A	3 (2-4; 2-6)	N/A
Duration of PIB PET follow up, yr, median (IQR; range)	N/A	5 (3-8; 2-13)	N/A
Baseline ITC tau PET SUVR, mean (SD)	N/A	N/A	1.19 (0.1)
# longitudinal tau PET scans, median (IQR; range)	N/A	N/A	3 (2-3; 2-5)
Duration of tau PET follow up, yr, median (IQR; range)	N/A	N/A	5 (3-6; 1-11)
Time between baseline and first tau PET, yr, mean (SD)	N/A	N/A	2.1 (1.6)
# longitudinal PACC assessments, median (IQR; range)	9 (6-10; 2-14)	9 (7-11; 3-14)	10 (7-12; 4-14)
Duration of cognitive follow up, yr, median (IQR; range)	8 (5-11; 1-14)	10 (6-12; 2-14)	10 (7-12; 3-14)

APOE ε4 = apolipoprotein E ε4 allele; DVR = distribution volume ratio; FLR = frontal, lateral temporal and parietal, and retrosplenial regional uptake; IQR = interquartile range; ITC = inferior temporal cortex; PACC5 = Preclinical Alzheimer's Cognitive Composite-5; PET = positron emission tomography; PIB = Pittsburgh compound-B; SD = standard deviation; SUVR = standardized uptake value ratio

Table 2. 30-item Physical Frailty Index

Physical Health	**Shrinking**
Compared to other people your own age, how would you rate your physical health?	Weight loss >10 lbs over 1 year
How often do health problems stand in the way of your doing the things that you want to do?	
How many times have you been hospitalized overnight in the last five years?	
Cancer (other than skin cancer)	
Chronic liver disease	**Slowness/mobility**
Diabetes	Gait speed
Elevated Cholesterol	Gait abnormality
Hearing problems	Do you need help to walk?
Heart attack or bypass surgery	Have you fallen recently
Angina or atrial fibrillation	
Hypertension	
Joint disease	
Kidney disease	**Exhaustion**
Pulmonary embolism or blood clot	During your waketime, do you feel tired, fatigued, or not up to par?
Sleep disorder	How often do you feel tired or fatigued after your sleep?
Spine disease	
Stroke or TIA	
Thyroid disease	
Vision problems	**Inactivity**
Polypharmacy	Pedometer step count
Overweight or obese	
Underweight	

Figure 1. Associations of baseline frailty index (A) and modified Fried frailty phenotype (B) with longitudinal Aβ burden, tau accumulation, and cognitive decline. (A) Linear mixed effects models revealed no associations between baseline frailty index and longitudinal Aβ burden (β=-0.01 [-0.04 to 0.02], p=0.42; Panel A). By contrast, individuals with high frailty index and elevated Aβ (solid red line) exhibited faster inferior temporal cortex (ITC) tau accumulation (β=0.01 [0.00 to 0.02], p=0.01), and faster cognitive decline measured with the Preclinical Alzheimer's Cognitive Composite-5 (PACC5) (β=-0.06 [-0.12 to -0.004], p=0.04). There was additionally an independent main effect of higher frailty on faster PACC5 decline (β=-0.07 [-0.12 to -0.01], p=0.01). For visualization, the estimated trajectories based on representative levels of low versus high baseline frailty index and (for tau and PACC5 models) low versus high baseline Aβ burden are presented. Low and high frailty is represented by -1 and +1 SD relative to the mean (low = 0.07, high = 0.26). Low and high Aβ are represented by the mean Aβ burden of Aβ-negative (PIB DVR 1.08) and Aβ-positive (PIB DVR 1.46) individuals. (B) Sensitivity analyses were performed with a modified 4-criteria Fried frailty phenotype (shrinking, slowness, exhaustion, inactivity). Individuals meeting none of the criteria were classified as "Robust", one as "Prefrail", and two or more as "Frail". Results were overall similar, with frail but not prefrail individuals associated with faster ITC tau accumulation and cognitive decline relative to the robust group. Aβ = β-amyloid; DVR = distribution volume ratio; PIB = Pittsburgh compound-B; SUVR = standardized uptake value ratio.



Keywords: physical frailty, tau accumulation, cognitive decline

109 Assessing neuroinflammation in Alzheimer's disease: A TSPO-PET study using ER176 and its correlation with amyloid and tau pathology

Mahathi Kandimalla[1], David Jacobson[1], Seokbeen Lim[1], Jeyeon Lee[1,3], Hoon-Ki Min[1], Hugo Botha[2], Jonathan Graff-Radford[2], David Jones[2], Prashanthi Vemuri[1], Kejal Kantarci[1], David Knopmam[2], Clifford Jack[1], Ronald Petersen[2], Val Lowe[1]

[1]*Department of Radiology, Mayo Clinic, Rochester, MN, US*
[2]*Department of Neurology, Mayo Clinic, Rochester, MN, US*
[3]*Department of Biomedical Engineering, Seoul, KR*

Objective: Neuroinflammation plays a crucial role in neuronal damage, synaptic dysfunction, and impaired neurogenesis, significantly contributing to Alzheimer's Disease (AD) progression. In this study, we evaluated ER176's effectiveness in detecting neuroinflammation across a spectrum of disease with CU A–, CU A+, MCI, and AD participants, with particular attention to amyloid and tau status.

Methods: Participants from the Mayo Clinic Study of Aging were recruited for this study. The study included four participant groups: cognitively unimpaired with normal amyloid (CU A–, n=25), cognitively unimpaired with high amyloid (CU A+, n=25), mild cognitive impairment with increased amyloid (MCI A+, n=25), and AD dementia (AD, n=15). We explored the variations in Neuroinflammation PET results among different groups.

Results: We conducted surface-based ROI analysis, incorporating age, sex, and rs6971 polymorphism genotype as covariates. Our results did not indicate significant differences in neuroinflammation between CU A+ and CU A–. However, when compared to CU A–, both MCI and AD groups displayed significant differences, with AD exhibiting a broader range of affected areas. No significant difference was observed between MCI and CU A+, while AD showed significant differences compared to CU A+. Comparing AD to MCI did not reveal significant differences. The comparison of amyloid-positive and amyloid-negative groups showed significant differences (Figure 1a). The comparison between tau-positive (tau>=1.29) and tau-negative (tau<1.29) was even more significant (Figure 1b).

Conclusion: Our findings demonstrate that ER176 uptake is associated with neuroinflammatory changes in AD, particularly in relation to tau pathology. This suggests that ER176 may serve as a more effective marker for tau-mediated neuroinflammation than for amyloid-driven processes. Also, while significant differences were observed between CU A–, MCI, and AD groups, there was no substantial difference between MCI and AD, indicating a possible plateau in neuroinflammation.

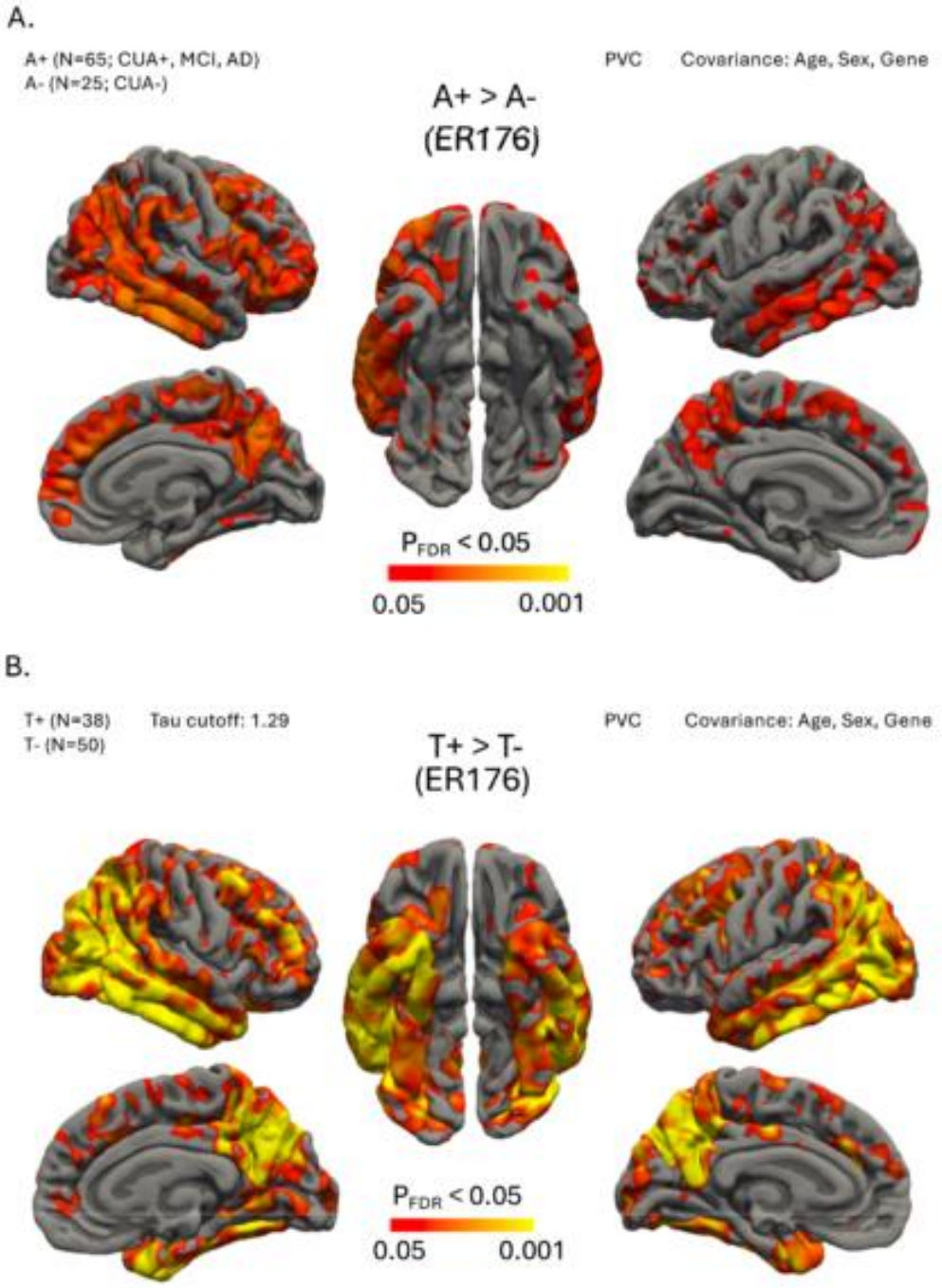


Figure 1: Surface-based analysis using the Müller-Gärtner method, one of the partial volume correction (PVC) methods, was performed with age, sex, and rs6971 polymorphism genotype as covariates. A color scale was applied based on the p-value from FDR multiple correction, where significance is represented by deeper red for a significance level of 0.05 and yellow for a significance level approaching 0.01. (A) Group-wise analysis with amyloid comparing CU A+ (MCI/AD, n=65) to CU A– (n=25). (B) Group-wise analysis with tau using a threshold of 1.29, with 38 tau+ and 50 tau– participants.

Keywords: Neuroinflammation, ER176, Alzheimer's Disease, Tau pathology, TSPO-PET

110 Two distinct sources of 18F-MK-6240 off-target signal identified by individualized head modeling and PET kinetics

Charles Chen[1], Jessie Fanglu Fu[1], Oula Puonti[1], Emma Thibault[2], Keith Johnson[2], Julie Price[1]

[1]*Athinoula A. Martinos Center for Biomedical Imaging, Massachusetts General Hospital, Charlestown, MA, US*
[2]*Gordon Center for Medical Imaging, Massachusetts General Hospital, Boston, MA, US*

Background: ^{18}F-MK-6240 PET is a powerful tool for visualizing neurofibrillary tangles (NFTs) in aging and Alzheimer disease (AD). However, ^{18}F-MK-6240 PET off-target signal (OTS) in the meninges can spill into brain parenchyma. Partial volume correction of OTS spill-in is challenging due to the thin structure of the meninges; prior approaches have used the FreeSurfer-defined skull mask to approximate the meningeal OTS, as this is a readily available parcellation. Herein, we describe an approach that uses individualized head modeling and PET kinetics to more precisely identify meningeal OTS.

Methods: We applied the Complete Head Anatomy Reconstruction Method (CHARM, Puonti et al. NeuroImage 2020) to segment the whole head from T1-weighted (T1w), T2w, and T2w FLAIR MRI in our test-retest dataset of dynamic (0-120 minutes) ^{18}F-MK-6240 PET/MRI in seven older adults (one diagnosed with AD; Table 1). We use the T1w/T2w ratio to separate meninges from CSF. This enables us to generate time-activity curves (TACs) for cerebral and cerebellar cortices, CSF, meninges, and skull (cortical and cancellous bone), and compare these to TACs generated using FreeSurfer-defined skull. The Diebold-Mariano test was used to determine which CHARM+T1w/T2w-defined TAC (meningeal or cortical bone) is a more accurate predictor of FreeSurfer-defined skull TAC.

Results: FreeSurfer-defined skull overlaps inconsistently with CHARM+T1w/T2w-defined meninges, especially near the tentorium (Fig.1). CHARM+T1w/T2w-defined meningeal and bone TACs show differing kinetics: the meninges/bone show high/low initial uptake that increases/decreases over time (Fig.2A). FreeSurfer-defined skull TAC is more similar to the CHARM+T1w/T2w-defined cortical bone than meningeal TAC (Diebold-Mariano p-values<0.01, Fig.2B). Findings are consistent across participants and test/retest studies.

Conclusion: In this work, the meninges and bone were found to represent two spatiotemporally distinct sources of OTS in ^{18}F-MK-6240 PET. Future efforts will use this information to more precisely correct for partial volume averaging and assess impact on quantification of ^{18}F-MK-6240 tau burden.

Table 1: Participant demographics.

	Cognitively normal (n=6)	Alzheimer disease diagnosis (n=1)
Test-retest interval (days)	25 [14 30]	30
Age (years)	66 [63 71]	54
Sex	Male=4, Female=2	Male=1
MMSE	29.5 [29 30]	22

Continuous values are summarized as median [first quartile third quartile]. MMSE=mini-mental state examination.

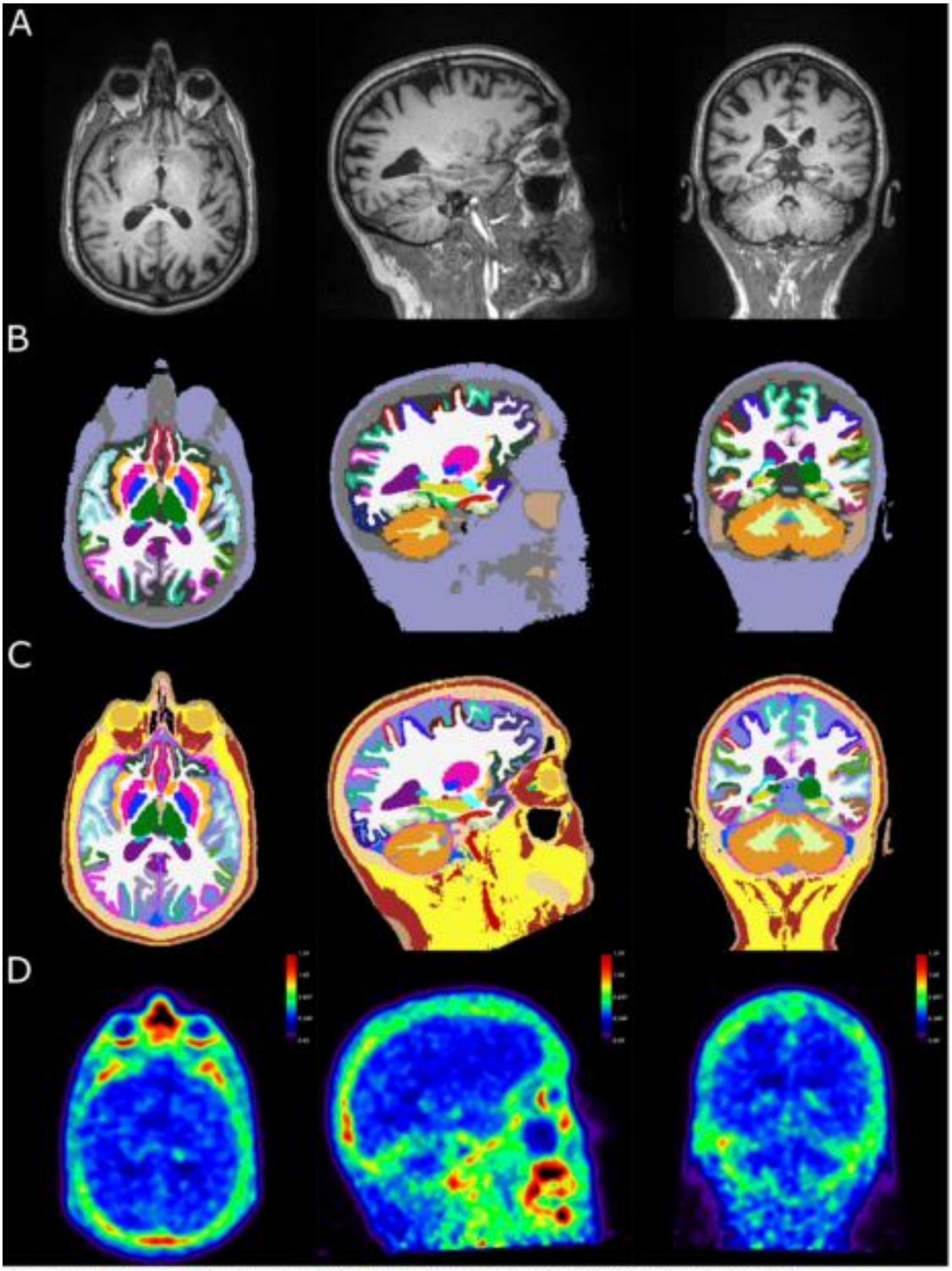


Figure 1: Comparing T1-weighted MRI, FreeSurfer skull segmentation, CHARM+T1w/T2w segmentation, and 18F-MK-6240 SUV90-110 in an exemplar individual with low tau and no cognitive impairment (participant #1). (A) A T1-weighted MRI shown in axial, sagittal, and coronal views. (B) The corresponding FreeSurfer segmentation (skull=light grey). (C) The corresponding CHARM+T1w/T2w segmentation (skull=light tan (cortical bone), which surrounds medium tan (cancellous bone), meninges (magenta), CSF (periwinkle)). Note the tentorium cerebelli, which are labeled as meninges in CHARM+T1w/T2w segmentation but are included in cerebral cortex or cerebellar cortex in FreeSurfer. (D) A 18F-MK-6240 SUV image (time window=90-110 minutes). Note the OTS in the meninges (tentorium), but also in the bone, retina, choroid plexus, and mucosa, among others.

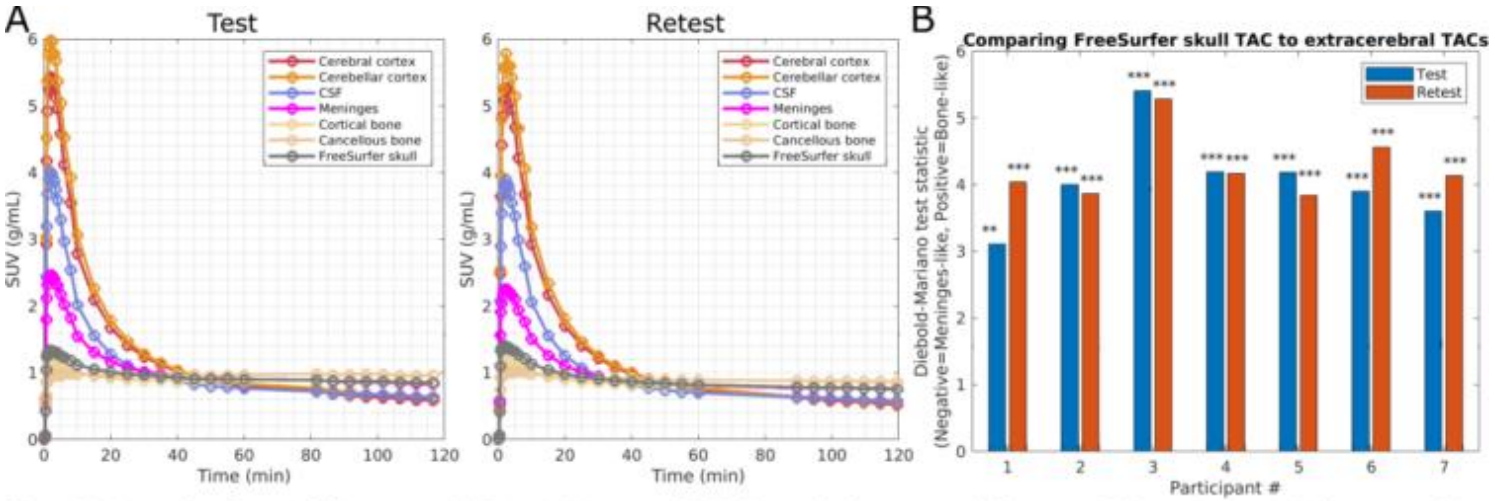


Figure 2: Comparing time activity curves. (A) Time activity curves (TACs) for cerebral cortex, cerebellar cortex, CSF, meninges, cortical bone, cancellous bone, and FreeSurfer-defined skull in a cognitively normal participant (participant #4) across test and retest studies. (B) Diebold-Mariano test statistics comparing which CHARM+T1w/T2w-defined TAC (meningeal or cortical bone) is more accurate predictor of FreeSurfer-defined skull TAC (null hypothesis=no difference in accuracy, negative values=CHARM+T1w/T2w meningeal TAC is a more accurate predictor of FreeSurfer-defined skull TAC, positive values=CHARM+T1w/T2w cortical bone TAC is a more accurate predictor of FreeSurfer-defined skull TAC, *=p-value<0.05, **=p-value<0.01, ***=p-value<0.001). Participants #1, 2, 4, 5, 6, and 7 are cognitively normal; participant #3 has an AD diagnosis.

Keywords: Tau PET, off-target, head model, kinetics, meninges

112 TSPO PET mediates tau-associated neurodegeneration in limbic and temporal regions across clinical variants of Alzheimer's disease

Patrick Lao[1], Aubrey Johnson[1], Anna Smith[1], Diana Guzman[1], Hannah Houlihan[1], Amarachukwu Okafor[1], Lauren Heuer[1], Thairi Sanchez[1], Daniel Talmasov[1], Ndubisi Chikwem[1], Dina Dass[1], James Noble[1], William Kreisl[1], Scott Small[1]

[1]*Columbia University Medical Center, New York, NY, US*

Background: Microglia surveil the brain microenvironment and respond in neuroprotective and neurotoxic ways. We investigated the role of microglia in individuals with ADRD, and hypothesized that microglia mediate progressive associations between amyloid, tau, and neurodegeneration.

Methods: Participants (21 controls, 25 individuals with ADRD) from the Longitudinal Imaging of Microglial Activation in Different Clinical Variants of Alzheimer's Disease study underwent baseline amyloid PET (Florbetaben SUVR), tau PET (MK6240 SUVR), TSPO PET (ER176 SUVR), and structural MRI (gray matter volume). Consensus diagnosis (e.g., MCI, AD, PCA, FTD, LATE) was performed at the CUIMC ADRC. We assessed regional TSPO mediations along key ATN pathways, adjusting for multiple comparisons. Sensitivity analyses were performed stratified by amyloid positivity.

Results: TSPO mediated the association between tau and neurodegeneration in limbic and temporal regions (-0.27 to -0.39, $p<0.02$; 43% to 89% of total effect; Figure 1). However, TSPO also had a positive mediation in the cingulate gyrus (0.26, $p=0.04$; 63%) suggesting TSPO was neuroprotective. TSPO mediated tau-associated neurodegeneration in limbic regions even in amyloid-negative ADRD (-0.42 to -0.58, $p<0.01$; 60% to 65%), and further mediated the association between amyloid and tau in temporal and parietal regions (0.18 to 0.25, $p<0.04$; 29% to 52%) as well as tau across progressive Braak stages (0.1 to 0.13, $p<0.01$; 10% to 16%), but only in amyloid-positive ADRD.

Conclusion: Across ADRD diagnoses that have different underlying brain microenvironments to which microglia are sensitive, microglia mediated tau-associated neurodegeneration, even in the context of low amyloid. In the context of elevated amyloid, microglia may also be involved in the link between amyloid to tau and in tau spreading. These findings have potential implications for anti-amyloid treatments, where amyloid burden is normalized, but inflammatory alterations may continue to contribute to tau and tau-induced neurodegeneration.

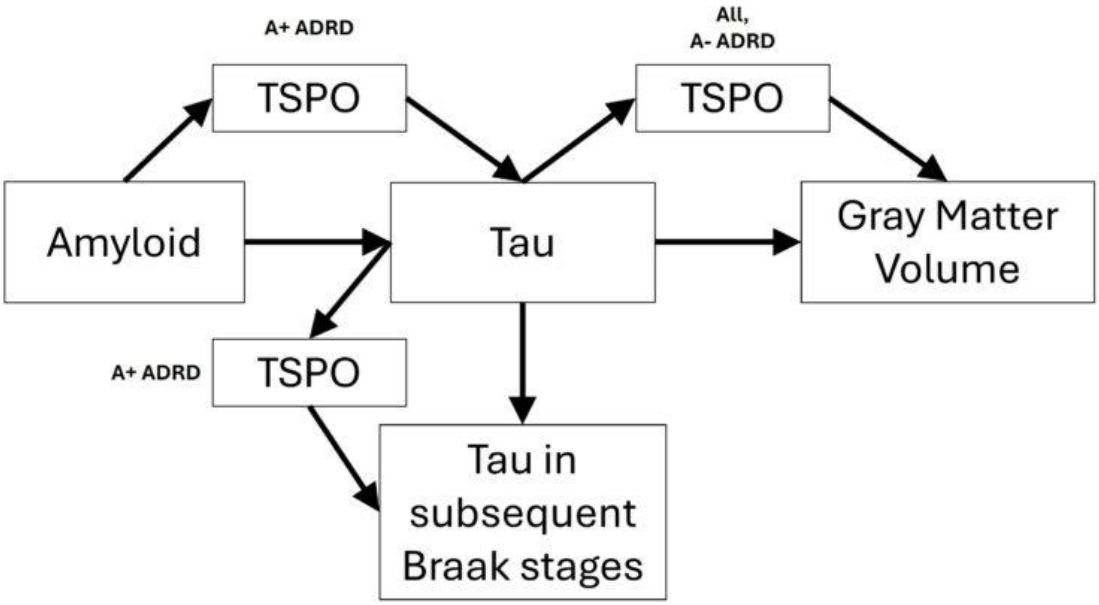


Figure 1. TSPO Mediations from Amyloid to Tau, Tau to Tau in subsequent Braak stages, and Tau to Neurodegeneration.

Keywords: TSPO PET, microglia, tau, neurodegeneration

114 Tracking plasma biomarker abnormalities with amyloid time accumulation

Marina Bluma[1], Konstantinos Chiotis[1,6,7], Marco Bucci[1,2], Irina Savitcheva[5], Anna Matton[1], Miia Kivipelto[1,2], Andreas Jeromin[3], Giovanni De Santis[4], Guglielmo Di Molfetta[4], Nicholas J. Ashton[4], Kaj Blennow[4], Henrik Zetterberg[4], Agneta K Nordberg[1,2]

[1]*Karolinska Institutet, Department of Neurobiology, Care Sciences and Society, Division of Clinical Geriatrics, Center of Alzheimer Research, Stockholm, SE*
[2]*Karolinska University Hospital, Theme Inflammation and Aging, Stockholm, SE*
[3]*ALZPath, Inc, ALZPath, Inc, Carlsbad, CA, US*
[4]*University of Gothenburg, Department of Psychiatry and Neurochemistry, Molndal, SE*
[5]*Karolinska University Hospital, Medical Radiation Physics and Nuclear Medicin, Stockholm, SE*
[6]*Department of Neurology, Karolinska University Hospital, Stockholm, SE*
[7]*Memory and Aging Center; Department of Neurology;University of California, San Francisco, CA, US*

Aim: Plasma pTau fragments and GFAP are potential candidates for early detection and screening of patients for anti-amyloid therapies. Although it has been shown that these plasma biomarkers change early, the specific timing at which these changes become significant to identify Aβ+ individuals has yet to be determined.

Methods: Data were acquired from a memory clinic cohort (N=138) assessed at the Memory Clinic, Karolinska University Hospital, Stockholm, Sweden. Using a nonlinear model of relationship between amyloid accumulation time and load (Schindler et al., (2021)), we estimated the duration of amyloid accumulation (AmyloidTime) based on centiloid values from amyloid PET scans. We then predicted the AmyloidTime linked with the threshold of plasma biomarkers becoming abnormal to detect individuals with Aβ+ scan with 90% sensitivity. By subtracting AmyloidTime from each patient's age, we estimated their amyloid accumulation onset age ('age-of-Aβ-onset'), identifying young accumulators as those with age-of-Aβ-onset under 50 years, which would correspond to a minimum of 15 years of Aβ-accumulation at age 65.

Results: The AmyloidTime corresponding to 100% accuracy of positive visual read for Aβ-PET scan was 4.8 years (and 90%-1year before 0 AmyloidTime). The AmyloidTime required for plasma biomarker levels become abnormal enough to provide 90% sensitivity in identifying amyloid positive PET scans was: 5.4 years for pTau217, 8.7 - for GFAP, 9.2 - for pTau181, and 10.5 - for pTau231 (Fig.1). Plasma pTau217 and pTau181 levels, but not plasma GFAP or pTau231, were significantly higher in early amyloid accumulators, even after adjusting for the effect of amyloid load or AmyloidTime (Fig.2).

Conclusions: Plasma pTau217 levels show a significant change, enabling the identification of Aβ+ individuals with 90%sensitivity 5.4 years after reaching the Aβ-accumulation tipping point. Young-age Aβ-accumulators showed higher levels of pTau217 and pTau181, suggesting an exacerbation of tau pathology within this patient subgroup.

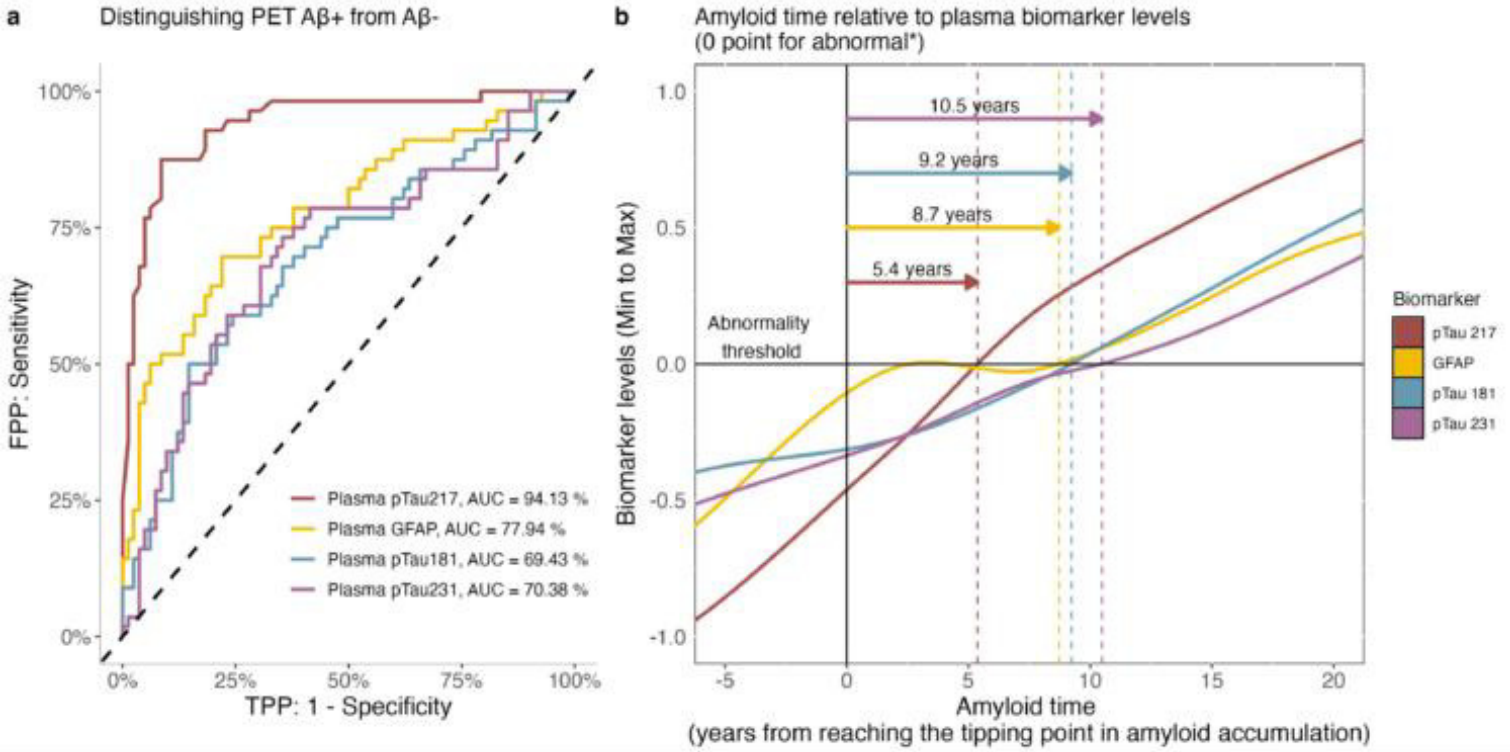


Figure 1. **(a)** Plasma biomarkers as predictors for amyloid PET visual read positivity: ROC curves show plasma pTau217 with the highest area under the curve (AUC, 94%), followed by GFAP (78%), pTau231 (70%), and pTau181 (69%). **(b)** Fitted trajectories of scaled biomarker data show different timing of abnormality onset with respect to the time of amyloid accumulation. Plasma pTau217 reached the abnormality at 5.4 years, GFAP at 8,7 years, pTau118 at 9.2 years, and pTau231 at 10.5 years. Biomarkers centred to the point of reaching the abnormal level corresponding to 90% sensitivity for amyloid positivity. Curves were fit with locally estimated scatterplot smoothing (LOESS) regression.

*Abnormality defined as biomarker threshold linked to 90% sensitivity for amyloid positivity.

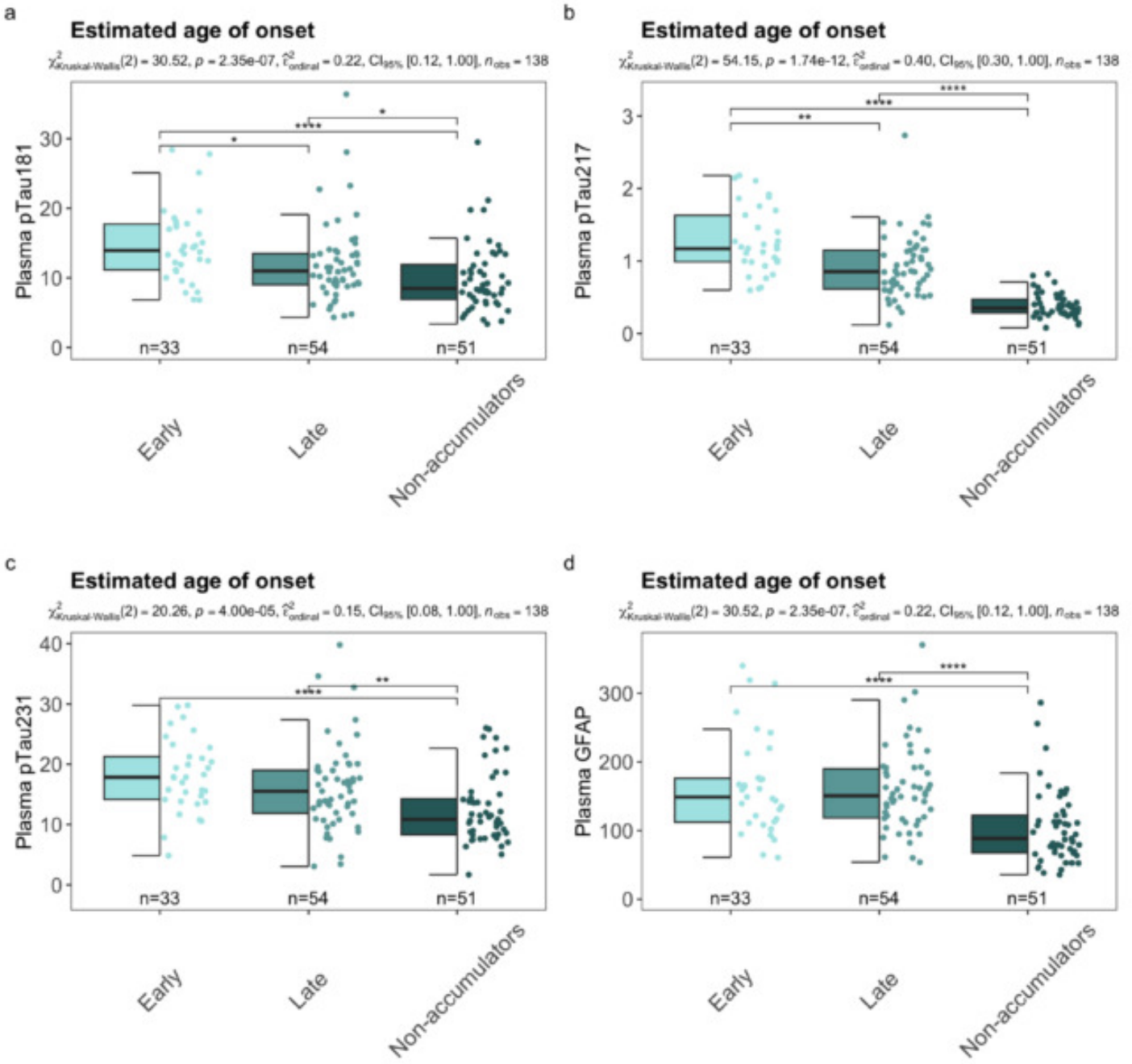


Figure 2. Boxplots showing differences and the post hoc pairwise comparison between the groups of early, late and non- accumulators. **(a)** Levels of pTau181 are increased in early amyloid accumulators. **(b)** Also, pTau217 levels are also significantly higher in early accumulators. (c-d) Plasma pTau231 and GFAP did not show significant differences between early and late accumulators. **(a-d)** All biomarkers were increased in accumulators compared to non-accumulators. The p values in the subtitles indicate the results from an analysis of variance conducted with the Kruskal–Wallis test. Post hoc analysis was carried out using Dunn's test, and corrections for multiple comparisons were made using the false discovery rate. *p < 0.05, **p < 0.01, ***p < 0.001, ****p < 0.0001.

Keywords: Plasma, biomarkers, Amyloid, PET, accumulation

115 Advancing antibody-based pretargeted PET imaging of protein aggregates in the brain

Tobias Gustavsson[1], Michael Honer[5], Lars Hvass[2], Vladimir Shalgunov[3], Anne Skovsbo Clausen[2], Sophie Stotz[1], Thomas Wünsche[1], Sara Lopes van den Broek[1], Gitte Moos Knudsen[4], Blanca Aldana[1], Jens Niewoehner[5], Luca Gobbi[5], Thomas Kustermann[5], Umberto Battisti[1], Andreas Kjær[2,3], Matthias M. Herth[1,3]

[1]*Department of Drug Design and Pharmacology, University of Copenhagen, Copenhagen, DK*
[2]*Cluster for Molecular Imaging, Department of Biomedical Sciences, University of Copenhagen, Copenhagen, DK*
[3]*Department of Clinical Physiology, Nuclear Medicine & PET, Rigshospitalet, Copenhagen, DK*
[4]*Neurobiology Research Unit and Center for Integrated Molecular Brain Imaging, Rigshospitalet, Copenhagen, DK*
[5]*Pharma Research and Early Development, Roche Innovation Center Basel, F. Hoffmann-La Roche Ltd., Basel, CH*

The discovery of small molecule PET tracers for certain forms of protein aggregates has proven challenging. Monoclonal antibodies (mAbs) with their excellent specificity along with improved blood-brain barrier (BBB) penetration upon modification may offer an alternative approach. In particular, the pretargeted imaging strategy, uncoupling the long pharmacokinetic half-life of mAbs from the shorter physical half-life of the radionuclide, may result in higher imaging contrast and lower radiation burden. Several pretargeting approaches are based on bioorthogonal reactions, the tetrazine (Tz) ligation between a trans-cyclooctene (TCO) and a Tz being the most prominent one.

We evaluated whether an in-house developed BBB-penetrable Tz ([18F]BBB-Tz) with rapid TCO ligation kinetics can be used for imaging Aβ pathology in the 5xFAD mouse model using a TCO-modified bispecific construct of the antibody BS-mAb31 (TCO-bsAb), which targets both Aβ fibrils and the mouse transferrin receptor (mTfR).

TCO-bsAb (10 TCOs per bsAb on average) exhibited minor affinity alteration to Aβ and mTfR, and no change in antibody integrity. On-section Tz-TCO ligation on 5xFAD brain sections generated three days after TCO-bsAb injection revealed a [18F]BBB-Tz binding pattern colocalizing with Aβ pathology and yielded cortical/thalamic-to-cerebellar ratios of 3-6. Conversely, in wildtype mice, no region-specific binding of [18F]BBB-Tz was detected, with a cortical/thalamic-to-cerebellar ratio of 1. This data indicated that TCOs on BS-mAb remained reactive three days post injection.
Intravenous injection of [18F]BBB-Tz in 5xFAD mice three days after administration of TCO-bsAb showed successful Tz-TCO ligation in vivo and specific visualization of Aβ-bound TCO-bsAb by revealing a [18F]BBB-Tz binding pattern colocalizing with Aβ pathology and demonstrating a ~1.4-higher cortical and hippocampal tracer retention in 5xFAD mice compared to wildtypes.

Pre-treatment with a peripheral, non-BBB-penetrable Tz reduced blood plasma retention of [18F]BBB-Tz by 77% highlighting the possibility of using masking agents to improve target-to-blood ratios.

Keywords: Pretargeting, tetrazine, TCO, 5xFAD

116 Longitudinal change in mnemonic discrimination and influence of Aβ burden

Jessica Kraft[1], Jahnavi Nair[1], Chen Gonen[1], Marci Skotnicki[1], Karen Rodrigue[1], Kristen Kennedy[1]

[1]*Center for Vital Longevity, University of Texas at Dallas, Dallas, TX, US*

Introduction: The ability to remember and discriminate among highly similar objects, a function of the hippocampus, declines with healthy aging, but is abjectly impaired in Alzheimer's disease. Mnemonic discrimination tasks may serve as early indicators of incipient pathology. Indeed, our group found that increasing beta-amyloid (SUVR) was associated with decreasing discrimination. To be useful for disease prediction, longitudinal follow-up performance must be assessed; however, no longitudinal studies to date exist examining within-person change. Thus, the current study assessed longitudinal change in mnemonic similarity task (MST) performance in relation to Aβ deposition in cognitively-healthy adults.

Methods: 133 adults (aged 53-92 years at baseline) completed the MST, with 64 returning an average of 42.37 months later. MST requires participants to encode object pairs and their locations on the screen, followed by a recognition memory task ("same", "different", or "new" judgments). Difficulty is modulated by altering distance (5, 10 or 15cm away from original target) during recall in the "different" condition. ^{18}F-Florbetapir PET images were obtained at baseline. SUVR was calculated from the mean of 7 cortical ROIs (normalized to cerebellum) to index Aβ burden.

Results: Linear mixed-effects models demonstrated that discrimination performance was stable across 4-years within-person, regardless of age or difficulty. Cross-sectionally, discrimination performance was poorer with increasing age and lure distance (difficulty). Significant lure*SUVR interaction indicated that higher Aβ-SUVR was associated with poorer discrimination, particularly at the highest distance.

Discussion: This study presents the first report of longitudinal MST performance, demonstrating that unlike the steep "age declines" estimated from cross-sectional research, mnemonic discrimination appears to be stable across 4 years in cognitively-normal adults. Cross-sectionally, Aβ-burden is associated with level of performance, but not change. Individuals with elevated amyloid burden show lower discriminability on pattern separation performance. Future studies with longer lags will clarify the extent and duration of this effect.

Keywords: amyloid, cognition, mnemonic similarity task, PET

Thursday, January 16, 2025 - 11:00 am - 12:40 pm

Podium Session

SESSION IV: Neuropath II

CHAIRS: Keith Johnson, Christina Moloney

Thursday, January 16, 2025		
11:00 am - 12:40 pm	**SESSION IV** Neuropath II	**Keith Johnson,** Massachusetts General Hospital, Boston, MA, USA **Christina Moloney,** Mayo Clinic, Jacksonville, FL, USA
11:00 am – 11:05 am	Session Overview	**Chairs**
11:05 am	Understanding the mechanisms of synaptic vesicle glycoprotein 2A change in Alzheimer's disease	**Laetitia Lemoine**, Perceptive, London, GB
11:20 am	Association of [18F]Flortaucipir-PET and plasma p-tau217 with tau neuropathology in AD and other neurodegenerative disorders	**Agathe Vrillon**, University of California San Francisco, San Francisco, CA, US
11:35 am	Tau-related cortical thinning is concentrated in sulcal depths	**Samira Maboudian**, Department of Neuroscience, University of California, Berkeley, Berkeley, CA, US
11:50 am	Comparison of [3H]MK-6240 and [3H]AV-1451 binding in relation to brain concentrations of p-tau: A postmortem biochemistry study	**Tobey Betthauser**, University of Wisconsin-Madison, School of Medicine and Public Health, Department of Medicine, Madison, WI, US
12:05 pm	In vitro binding of the tau PET tracer [3H]JSS20-183A and its comparison with PI-2620, T807 and PM-PBB3 in human postmortem brain tissue	**Dinahlee Saturnino Guarino**, Department of Radiology, University of Pennsylvania, Philadelphia, PA, US
12:20 pm – 12:40 pm	Discussion	

Understanding the mechanisms of synaptic vesicle glycoprotein 2A change in Alzheimer's disease

Declan King[1], David Bonsall[2], Scott Gladstein[3], Laetitia Lemoine[2], Amanda Bevis[4], Sjoerd J Finnema[3], Tara L Spires-Jones[1], FNIH SV2A Project Team[4]

[1]*University of Edinburgh, Edinburgh, GB*
[2]*Perceptive, London, GB*
[3]*AbbVie, Chicago, IL, US*
[4]*Foundation for the National Institutes of Health, Rockville, MD, US*

Background & Methods: Synaptic vesicle glycoprotein 2A (SV2A) levels are decreased in Alzheimer's disease (AD) brains, as revealed by Positron Emission Tomography (PET). Whether this decrease is due to synapse loss or SV2A protein loss remains unclear, hindering treatment development and interpretation of SV2A PET as a biomarker for neurodegenerative diseases. Radioligand binding, array tomography, and electron microscopy were each applied to post-mortem entorhinal cortex (EC) and cerebellum from control (BS 0-II; n=23), early-AD (BS III-VI; n=21) and AD (BS V-VI; n=25) cases to understand how changes in binding signal may relate to structural changes and PET signal.

Results: All samples showed similar binding affinity using [^{3}H]SynVesT-1 (K_D range 3-7 nM). In the EC synaptoneurosomes, the E-AD group showed a higher B_{MAX} compared to the other groups (5380 ± 319 fmol/mg protein). Array tomography of a sub-population of AD vs Control cases showed SV2A puncta density strongly correlated with synaptophysin puncta density in both brain regions ($p<0.001$). Regional differences in SV2A densities were observed between cerebellum and EC. SV2A puncta density was lower in AD EC ($p=0.03$) and higher in AD cerebellum ($p=0.003$) compared to controls. No differences were found in the proportion of synaptophysin puncta labelled with SV2A. Electron microscopy showed SV2A protein localized to presynaptic vesicles, with no difference in immuno-gold labelled SV2A particles per synapse ($p=0.53$).

Conclusion: Our findings suggest temporal changes in SV2A B_{MAX} with disease progression, and that loss of SV2A PET signal in AD patients is likely caused by synapse loss rather than SV2A protein loss within remaining synapses. This indicates that strategies for reversing synaptic loss may be crucial in treating AD and other synaptopathies and supports the interpretation of SV2A PET imaging as biomarker of synaptic loss. This is part of the SV2A PET Project, a program of the FNIH Biomarker Consortium.

Keywords: biomarker, radioligand binding, array tomography, electron microscopy, synaptopathies

Association of [18F]Flortaucipir-PET and plasma p-tau217 with tau neuropathology in AD and other neurodegenerative disorders

Agathe Vrillon[1,3], Salvatore Spina[1,3], Jhony Mejia-Perez[1], Tia Lamore[1], Daniel Schonhaut[1], Claire Yballa[1], David Soleimani-Meigooni[1], Adam Boxer[1], Julio Rojas[1], Argentina Lario Lago[1], William Jagust[1], Bruce Miller[1,3], Howard Rosen[1,3], William Seeley[1,3], Lea Grinberg[1,3], Gil Rabinovici[1], Lawren VandeVrede[1], Renaud La Joie[1,3]

[1]*University of California San Francisco, San Francisco, CA, US*
[2]*University of California Berkley, Berkley, CA, US*
[3]*Global Brain Health Institute, San Francisco, CA, US*

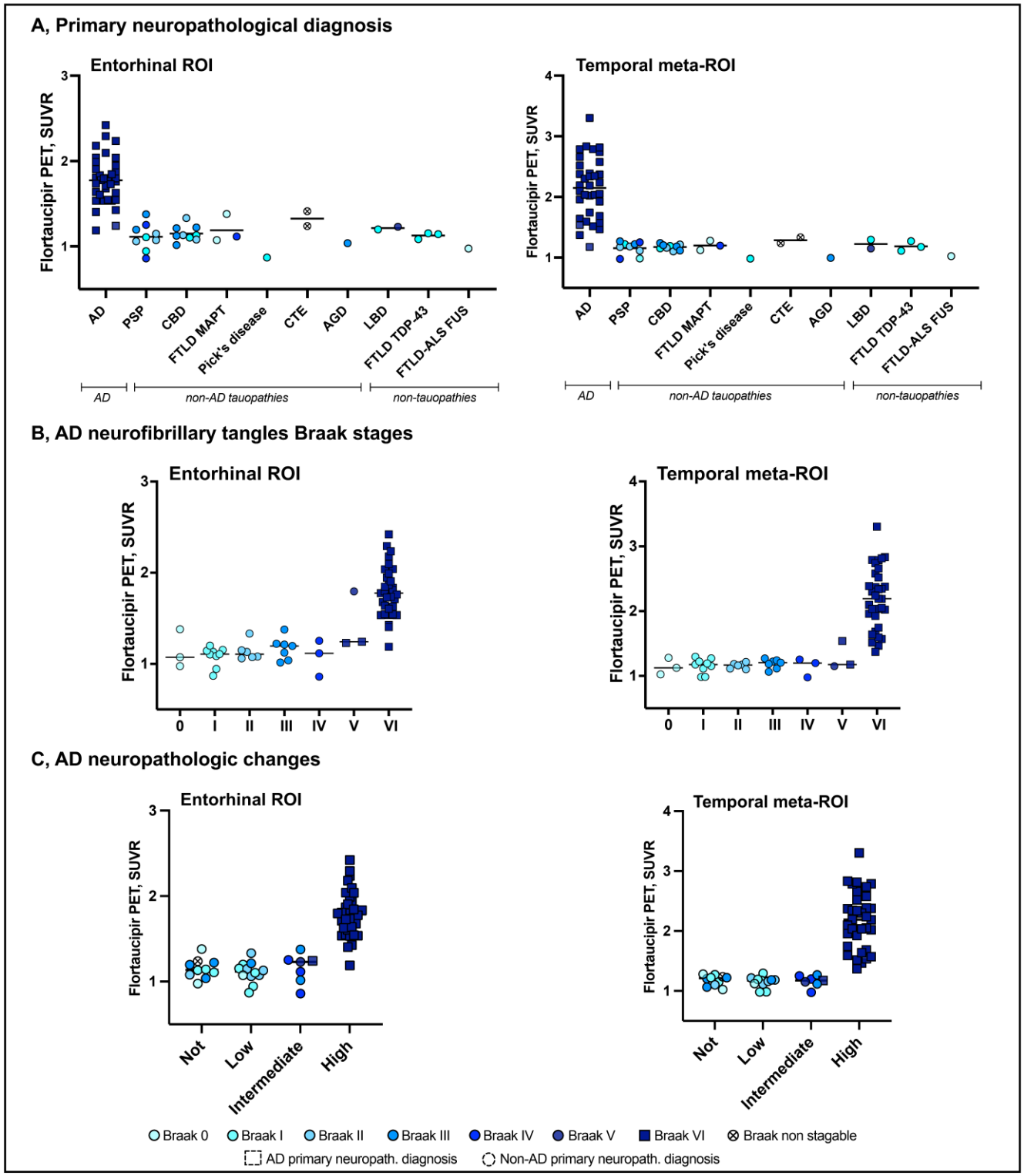
Background: Evaluating the relationships between tau imaging and fluid biomarkers with autopsy data is critical for validating their sensitivity and specificity for Alzheimer's disease neuropathologic change (ADNC). We aimed to examine the association between Flortaucipir-PET and AD neuropathology and to characterize the association between Flortaucipir-PET and plasma ptau-217 levels in autopsy cases.

Method: We analyzed Flortaucipir-PET (acquisition 80-100 minutes post-injection) from 66 patients with a clinical diagnosis of various neurodegenerative diseases who underwent autopsy at the UCSF Alzheimer's Disease Research Center (median age 66 years [range 34-96], 39% female, median PET-to-autopsy delay 3.8 years [range 0.3-8.2]). SUVRs were calculated (reference: inferior cerebellar cortex) in the entorhinal cortex (early tau region) and the temporal meta-ROI (AD signature region). Semi-quantitative rating of tau neuropathology in six brain regions was available for n=38 participants. Plasma p-tau217 was measured using Simoa (Janssen®) in n=54 participants (median PET-to-plasma delay 1.4 months [range 0-7]).

Results: Our cohort included 35 patients with autopsy-confirmed AD, 25 with non-AD tauopathies, and 6 with non-tau neurodegenerative diseases. Flortaucipir-SUVRs were elevated in patients with a primary neuropathological diagnosis of AD compared with non-AD patients (**Fig.1A**). Consistently elevated PET signal was detected in both the entorhinal cortex and temporal meta-ROI of patients with neurofibrillary tangle (NFT) Braak stage VI (**Fig.1B**) and high ADNC levels (**Fig.1C**). Semi-quantitative levels of NFTs and AD tau gray matter threads were correlated with local Flortaucipir-SUVRs across cortical regions (**Fig.2**). Plasma p-tau217 levels were increased in patients with advanced AD neuropathology (**Fig.3A**). P-tau217 levels were strongly correlated with Flortaucipir-SUVRs across ROIs ($r \geq 0.75$), fully driven by Braak V-VI cases **(Fig.3B).** Flortaucipir-SUVRs and plasma p-tau217 levels discriminated AD from non-AD neuropathological diagnosis with similarly high performance (AUC=0.95-0.99 **Fig.3C**).

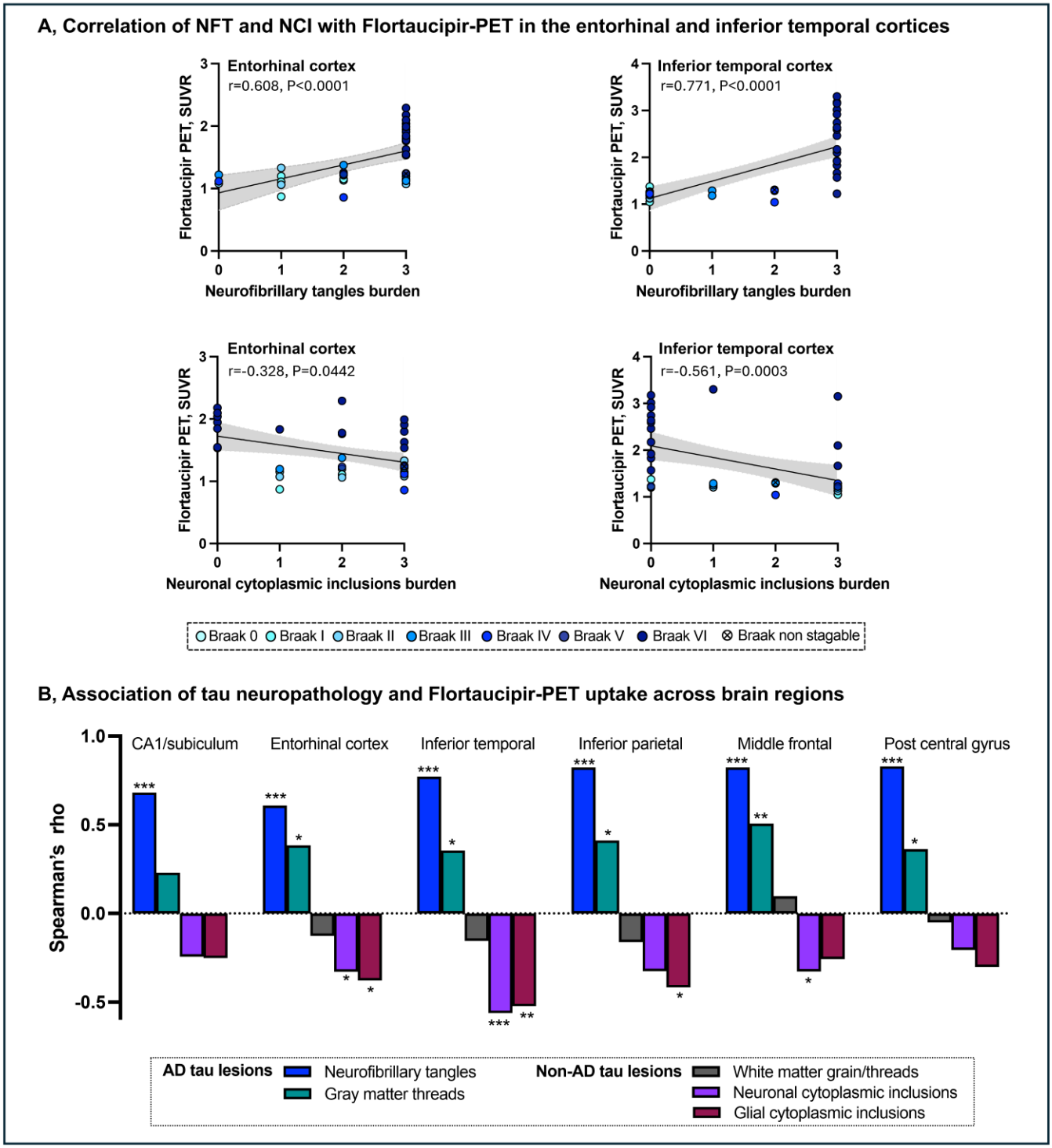
Conclusion: Flortaucipir-PET and plasma p-tau217 both displayed strong specificity to advanced AD tau neuropathology but lacked sensitivity to early AD tau stages.

Figure 1, Association of Flortaucipir-PET with neuropathological findings



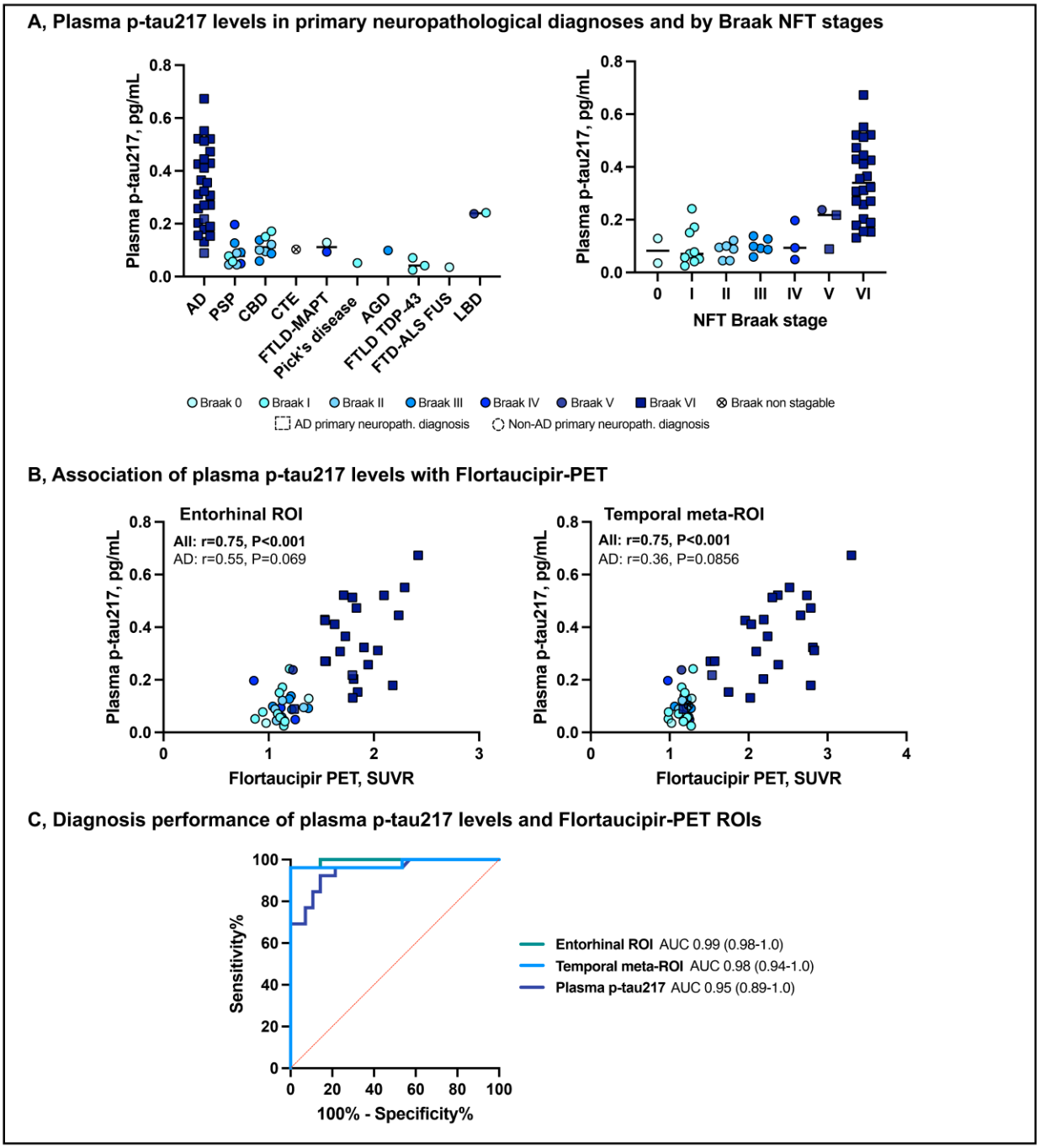
Flortaucipir entorhinal and temporal meta-ROI SUVRs **A,** across primary neuropathological diagnoses. **B,** across AD neurofibrillary tangles (NFT) Braak stages. **C,** across levels of AD neuropathologic changes (ADNC). ALS, amyotrophic lateral sclerosis; AGD, argyrophilic grain disease; CBD, corticobasal degeneration; CTE, chronic traumatic encephalopathy; FTLD, frontotemporal lobar degeneration; LBD, Lewy body dementia; PSP: progressive supranuclear palsy.

Figure 2, Association of Flortaucipir-PET with tau neuropathology burden



A, Correlation of tau neurofibrillary tangles (NFT) and tau neuronal cytoplasmic inclusions (NCI) burden with Flortaucipir-PET SUVRs across entorhinal and inferior temporal cortices; **B,** Bar charts indicating Spearman's rho correlation between tau pathologies and Flortaucipir-PET SUVRs in cortical brain regions (*P<0.05, **P<0.001, ***P<0.0001). Semi-quantitative analysis of tau neuropathology (visually rated from 0 to 3 by immunohistochemistry using CP13 staining) was performed in a subsample of n=38.

Figure 3, Association of plasma p-tau217 levels with Flortaucipir-PET



A, Plasma p-tau217 levels across primary neuropathological diagnoses and neurofibrillary tangles (NFT) Braak stages (n=54). **B**, Correlation of plasma p-tau217 levels with Flortaucipir-SUVR in entorhinal and temporal meta-ROI. **C**, ROC analysis comparing Flortaucipir entorhinal SUVR, temporal meta-ROI SUVR, and plasma ptau-217 levels performance to discriminate between AD and non-AD primary neuropathological diagnosis. AUCs comparison (Delong test): entorhinal ROI SUVR versus plasma p-tau217, P=0.05; temporal meta-ROI SUVR versus plasma p-tau217, P=0.11.

Keywords: Alzheimer's disease; PET; flortaucipir; autopsy, plasma p-tau217

Tau-related cortical thinning is concentrated in sulcal depths

Samira Maboudian[1,2], Corrina Fonseca[1,2], Yishu Chao[1,2], Duygu Tosun[3], Lea Grinberg[4,5], Kevin Weiner[1,2,6], William Jagust[1,2,7]

[1]*Department of Neuroscience, University of California, Berkeley, Berkeley, CA, US*
[2]*Helen Wills Neuroscience Institute, University of California, Berkeley, Berkeley, CA, US*
[3]*Department of Radiology, University of California, San Francisco, San Francisco, CA, US*
[4]*Department of Neurology, University of California, San Francisco, San Francisco, CA, US*
[5]*Weill Institute for Neurosciences Memory and Aging Center, University of California, San Francisco, San Francisco, CA, US*
[6]*Department of Psychology, University of California, Berkeley, Berkeley, CA, US*
[7]*Molecular Biophysics and Integrated Bioimaging, Lawrence Berkeley National Laboratory, Berkeley, CA, US*

Background: Prior studies suggest sulci are unique markers of age- and Alzheimer's disease (AD)-related morphological changes, but the pattern of regional vulnerability to tau pathology is incompletely understood. We performed this study to determine whether tau-related atrophy preferentially affects sulci and specifically the deepest areas (sulcal pits), which are hypothesized connectivity hubs.

Methods: We used MRI, amyloid and tau (FTP) PET scans from ADNI participants: 94 AD, 113 Aβ+ MCI, 468 cognitively normal (166 Aβ+). Correlation between vertex-wise cortical thickness and whole-brain tau SUVR was performed using FreeSurfer's GLM pipeline, generating an ROI of significant clusters ("clusters;" Fig.1). We calculated the overlap between the clusters and the following ROIs: whole-brain gyri vs. sulci, sulcal pits vs. rest of sulci. We used mixed-effects ANOVAs to examine effects of ROI (sulci/gyri, pits/rest) and hemisphere on the amount of overlap with the clusters. In a postmortem Braak 6 case, we calculated the amount of tau (AT8) in sulci compared to gyri. We also examined resting state connectivity strength between the hippocampus and sulcal vs. gyral regions of an "AD signature" ROI (Fig.3C), in a sample of 120 older (OA, age 60-94) and 64 younger adults (YA, age 18-33) from the Berkeley Aging Cohort Study.

Results: Clusters of significant negative tau-thickness correlation overlapped more with sulci than gyri ($p<.0001$, Fig.2B), and more with sulcal pits ($p<.0001$, Fig.2C). AT8 tau signal in the postmortem case was higher in sulci than gyri, and higher in pits (Fig.3A-B). Hippocampal connectivity strength was higher in sulci than gyri for YA, but not OA (Fig.3C-D).

Conclusions: We find that tau-related thinning occurs mostly in sulci, particularly in sulcal pits. This may occur because sulci accumulate more tau, potentially due to higher connectivity to the hippocampus throughout the lifecourse.

Figures

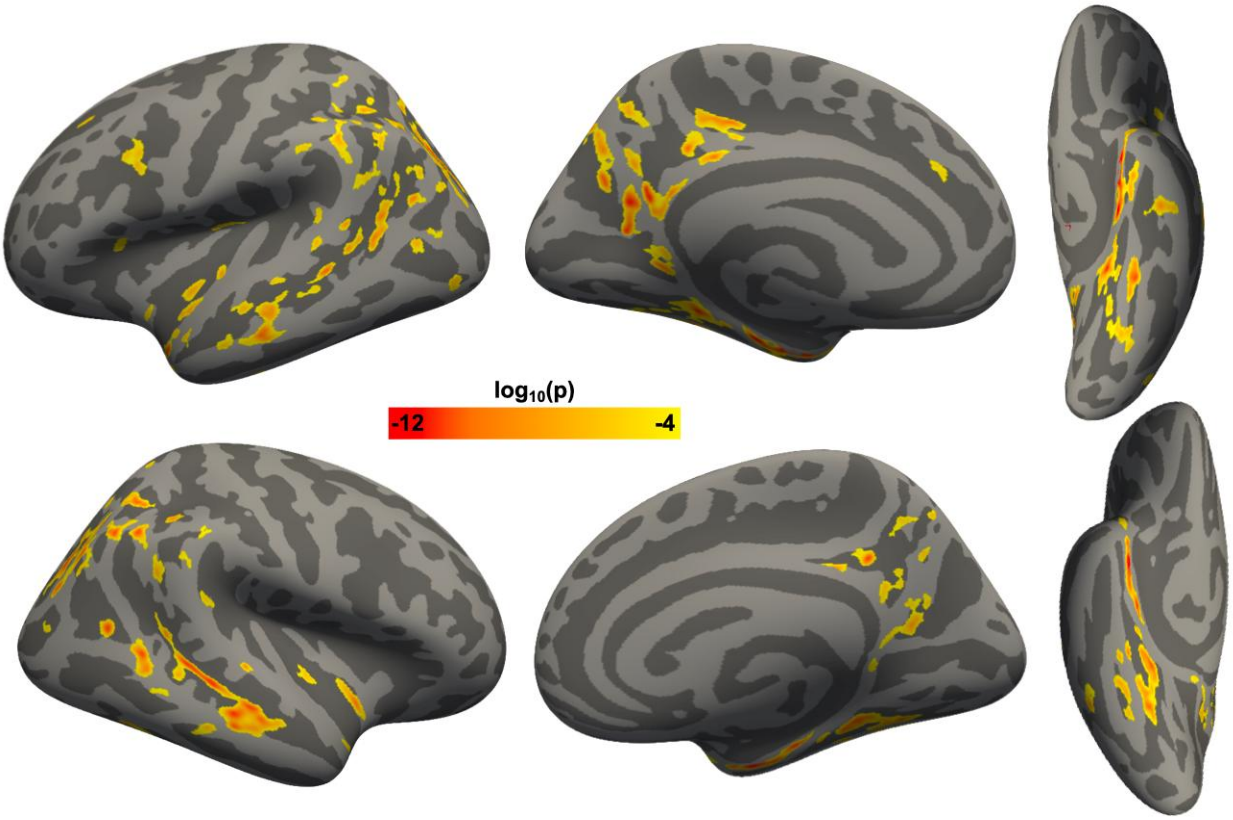


Figure 1. Tau-thickness correlation clusters. Clusters of significant correlation between vertex-wise cortical thickness and whole-brain (Braak 1,3-6) tau (FTP) SUVR projected onto the *fsaverage* surface. Surface overlay shows significance values (uncorrected) masked by clusters that survive correction for multiple comparisons (with a vertex-wise cluster threshold of 0.0001 and a cluster-wise p-value threshold of 0.05). These clusters were used as the binary "cluster" ROI. Top row: left hemisphere; bottom row: right hemisphere.

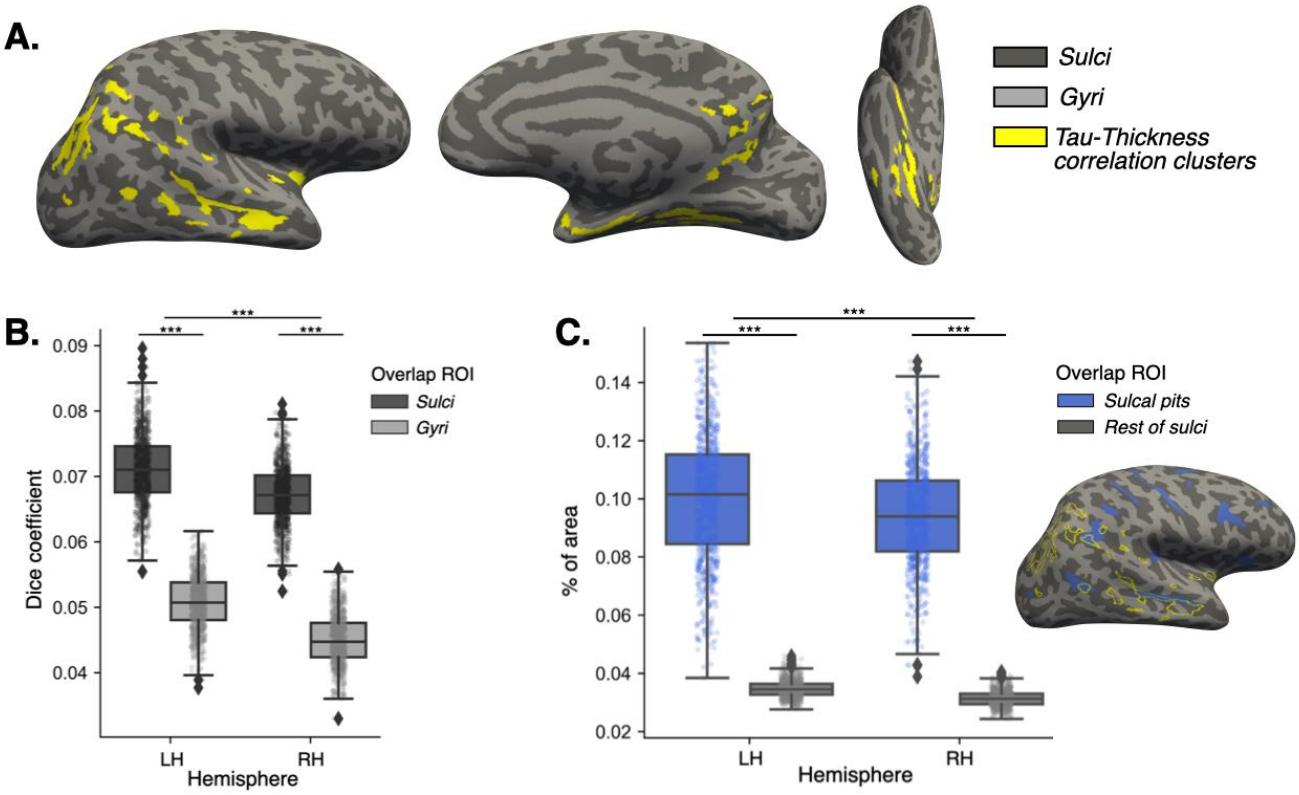


Figure 2. Clusters of significant negative tau-thickness correlation overlap more with sulci. (**A**) Binary ROI of clusters with significant correlation cortical thickness and whole-brain tau (see Fig.1) projected onto an example participant surface. (**B**) Overlap (dice coefficient) between tau-thickness cluster and whole-brain sulcal or gyral ROI. A mixed-effects ANOVA with ROI (sulcal/gyral) as a between-subject variable and hemisphere (LH/RH) as a within-subject variable shows a main effect of ROI ($p<.0001$), hemisphere ($p<.0001$) and a hemisphere x ROI interaction ($p<.0001$). (**C**) Overlap (% of ROI area covered by cluster) between tau-thickness cluster and the deepest 5% of sulcal points or the remaining 95% of sulcal points. A mixed-effects ANOVA with ROI (deepest 5% / remaining 95%) as a between-subject variable and hemisphere (LH/RH) as a within-subject variable shows a main effect of ROI ($p<.0001$), hemisphere ($p<.0001$) and a hemisphere x ROI interaction ($p<.001$). LH=left hemisphere, RH=right hemisphere. ***=$p<0.0001$.

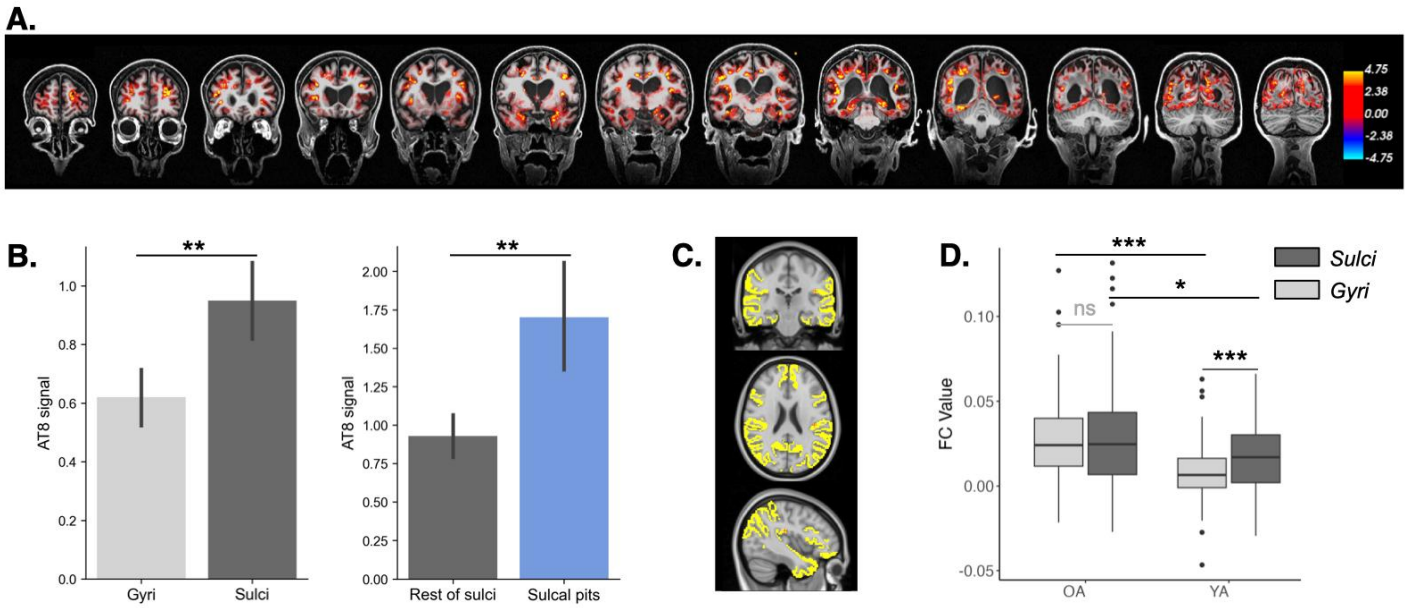


Figure 3. Tau accumulates more in sulci, potentially due to higher sulcal connectivity to the hippocampus in young adults. (**A**) MRI sections from a postmortem case with Braak 6 tau pathology, with an AT8 (p-Tau Ser202, Thr205 Monoclonal Antibody) heat map overlayed. (**B**) Average AT8 signal intensity across Desikan-Killiany atlas regions masked by sulci vs. gyri (left) or sulcal pits vs. the rest of sulci (right). Error bars = 95% CI. (**C**) Cortical "AD signature" region ROI used for functional connectivity (FC) analyses in (D), consisting of the following regions: entorhinal, inferior temporal, parahippocampal, temporal pole, precuneus, supramarginal, superior+inferior parietal, superior frontal, pars opercularis, pars triangularis, pars orbitalis. (**D**) Average hippocampus seed-to-voxel FC values in sulcal vs. gyral areas of AD signature ROI. P-values report results of mixed-effects ANOVA with fixed effects of group [older adult (OA)/younger adult (YA)] and ROI (sulci/gyri). *** p<0.0001, ** p< 0.001, * p<0.01

Funding: AG024904 (ADNI), AG034570 (BACS), Avid Radiopharmaceuticals.

Keywords: tau, atrophy, sulci, neuroanatomy, MRI

Comparison of [3H]MK-6240 and [3H]AV-1451 binding in relation to brain concentrations of p-tau: A postmortem biochemistry study

Tobey Betthauser[1], Eric Abrahamson[2], Manik Debnath[3], William Paljug[3], Shahriar Salamat[4], Thomas Karikari[3], Victor Villemagne[3], Milos Ikonomovic[2,3]

[1]*University of Wisconsin-Madison, School of Medicine and Public Health, Department of Medicine, Madison, WI, US*
[2]*University of Pittsburgh, Department of Neurology, Pittsburgh, PA, US*
[3]*University of Pittsburgh, Department of Psychiatry, Pittsburgh, PA, US*
[4]*University of Wisconsin-Madison, School of Medicine and Public Health, Department of Pathology, Madison, WI, US*

Background: Validation studies of tau PET radioligands require assessment of tracer's binding in relation to regional neuropathology. Additionally, quantitative biochemical assays of regional p-tau concentrations can facilitate interplay between imaging and plasma biomarker studies. We performed parallel analyses of [^{3}H]MK-6240 and [^{3}H]AV-1451 in-vitro binding for comparison with p-tau concentrations in same postmortem brain tissue extracts from autopsy cases with a range of Alzheimer's disease (AD) neuropathologic change severity.

Methods: Study cohort consisted of 8 autopsy cases from the University of Wisconsin and University of Pittsburgh ADRC brain banks, including cognitively unimpaired controls and AD cases with intermediate and high AD neuropathologic changes. In all cases, frozen tissues from eleven brain regions were processed to quantify [^{3}H]MK-6240 and [^{3}H]AV-1451 in-vitro binding as well as concentrations of tau pThr181, pThr231, pSer199, and pSer396 determined by tau phospho-epitope specific ELISA.

Results: Correlations between higher [^{3}H]MK-6240 binding and higher p-tau concentrations were strongest for pSer396 ($R=0.62$, $p<0.0001$) and pThr231 ($R=0.59$, $p<0.0001$), followed by pSer199 ($R=0.39$, $p=0.0004$) and pThr181 ($R=0.28$, $p=0.0141$). In contrast, correlations between higher [^{3}H]AV-1451 binding and higher p-tau concentrations were strongest for pThr181 ($R=0.52$, $p<0.0001$), followed by pSer396 ($R=0.25$, $p<0.0026$), and no significant correlations were observed with pThr231 or pSer199.

Conclusion: Higher [^{3}H]MK-6240 binding (and likely higher [^{18}F]MK-6240 PET tracer retention) may reflect this ligand's interaction with tau molecules containing greater abundance of phosphorylated epitopes at pSer396 > pThr231 > pSer199 > pThr181. In contrast, higher [^{3}H]AV-1451 binding appears to be influenced by greater phosphorylation at pThr181 and pSer396, but not pThr231 or pSer199. Depending on the role and abundance of these phosphorylated epitopes across tau maturation and aggregation, such differences may have implications for each ligand's *in vivo* PET detection and monitoring of tau pathology progression and their relationship with plasma p-tau markers.

Keywords: pathology, tau, MK-6240, FTP, biochemistry

In vitro binding of the tau PET tracer [3H]JSS20-183A and its comparison with PI-2620, T807 and PM-PBB3 in human postmortem brain tissue

Dinahlee Saturnino Guarino[1], Jeffrey Stehouwer[2], John L. Robinson[3], Theresa Schuck[3], Edward B. Lee[3,4], Virginia M. Lee[3,4], Neil Vasdev[5,6], Chester A. Mathis[2], Robert H. Mach[1]

[1]*Department of Radiology, University of Pennsylvania, Philadelphia, PA, US*
[2]*Department of Radiology, University of Pittsburgh, Pittsburgh, PA, US*
[3]*Department of Pathology and Laboratory Medicine, Center for Neurodegenerative Disease Research, Institute on Aging, University of Pennsylvania, Philadelphia, PA, US*
[4]*Penn Center for Neurodegenerative Disease Research, University of Pennsylvania School of Medicine, Philadelphia, PA, US*
[5]*Azrieli Centre for Neuro-Radiochemistry, Brain Health Imaging Centre, Centre for Addiction and Mental Health, Toronto, ON, CA*
[6]*Department of Psychiatry, University of Toronto, Toronto, ON, CA*
[7]*Department of Pathology and Laboratory Medicine, University of Pennsylvania School of Medicine, Philadelphia, PA, US*

Objectives: Imaging of tau inclusions will help in the diagnosis, prevention and treatment of neurodegenerative disorders. The goals of this study were to evaluate the utility of [^{3}H]JSS20-183A and to compare its binding properties with three tau positron emission tomography (PET) tracers, PI-2620, T807 (AV-1451, flortaucipir, Tauvid) and PM-PBB3, in the same human postmortem tissue to understand the binding profile of each radiotracer.

Methods: [^{3}H]JSS20-183A in vitro autoradiography and immunohistochemistry studies were conducted in postmortem samples from patients with Alzheimer's disease, AD with Lewy bodies, frontotemporal lobar degeneration-tau (Pick's disease, progressive supranuclear palsy and corticobasal degeneration), frontotemporal lobar degeneration-Tar DNA-binding protein 43 (TDP-43), Parkinson's disease, Parkinson's disease with dementia, Dementia with Lewy Bodies, Multiple system atrophy and elderly controls free of pathology. Brain sections were stained for tau, Aβ and α-synuclein and compared to JSS20-183A autoradiography on adjacent sections. Binding and competition assays to compare the regional distribution of the four tau tracers were also conducted using autoradiography.

Results: The binding profile of JSS20-183A with respect to tau isoforms in various neurodegenerative diseases was: 3R/4R tau (AD) > 3R tau (Pick's disease) > 4R tau (CBD) > 4R tau (PSP). There is no evidence of binding to lesions containing α-synuclein or TDP-43. [^{3}H]JSS20-183A, [^{3}H]PI-2620, [^{3}H]T807, [^{3}H]PM-PBB3 autoradiography in AD brains showed similar binding for the four tracers. Results from CBD, PSP and Pick's cases showed high binding of [^{3}H]JSS20-183A and [^{3}H]PM-PBB3 and lower specific binding of [^{3}H]PI-2620 and [^{3}H]T807.

Discussion: Our results suggest that JSS20-183A holds promise as a radiotracer for the detection of tau pathology in AD and the non-AD tauopathies. We also demonstrated the different binding properties among the second-generation tau PET tracers, which may assist in further understanding of tau heterogeneity in neurodegenerative disorders.

Keywords: Alzheimer's disease, non-AD-tauopathies, autoradiography,Tau imaging, Tau PET tracers

Thursday, January 16, 2025 - 01:40 pm - 02:10 pm

Grinberg, Lea

Keynote: From neuropathology to biomarkers: Novel strategies for detecting and monitoring Early Alzheimer's disease in vivo

Grinberg, Lea

University of California, San Francisco

Neuropathology has revealed key insights into Alzheimer's disease (AD) that have driven biomarker discovery, enabling the detection and, to some extent, monitoring of AD hallmarks in vivo. This talk will delve into neuropathological observations that represent underexplored opportunities for biomarker development, focusing on those with the potential to enable even earlier detection and monitoring. By bridging tissue-based discoveries with imaging and fluid biomarkers, modern neuropathology is well positioned to address gaps in current biomarker development strategies and improve the early diagnosis and tracking of neurodegenerative conditions.

Dr. Lea Tenenholz Grinberg is a neuropathologist specializing in brain aging and associated disorders, most notably, Alzheimer's and neurological basis of sleep disturbances in neurodegenerative diseases.

Currently, she is a Full Professor and a John Douglas French Alzheimer's Foundation Endowed Professor at the UCSF Memory and Aging Center, part of the Executive Board of the Global Brain Health Institute and member of the Medical Scientific Advisory Group for the Alzheimer Association. She is also a Professor of Pathology at the University of Sao Paulo.

In 2003, Dr. Grinberg was among the founders of a brain bank in São Paulo, focusing on brain aging. This brain bank which she had since developed into an extremely prolific and highly regarded institution, helped Dr. Grinberg prove that contrary to what has been accepted previously, the brainstem and not the cortex, harbors the first detectable neurodegeneration in Alzheimer's disease. In 2009, she was the recipient of the UNESCO-L'Oréal Award "For Women in Science," and in 2010 she received the John Douglas French Alzheimer Foundation "Distinguished Research Scholar Award." Currently, Dr. Grinberg is the Co-Leader of the UCSF/Neurodegenerative Disease Brain Bank, where she conducts neuropathological diagnosis of neurodegenerative diseases. She also directs the Human Biology Validation Core for the NIH/U54 Tau Centers Without Walls, is a principal investigator from the Tau Consortium and colead the Neuropathology Core for the LEADS project.

Thursday, January 16, 2025 - 02:25 pm - 03:50 pm

Podium Session

SESSION V: Clinically Relevant Applications

CHAIRS: Renaud La Joie, Reisa Sperling

Thursday, January 16, 2025		
02:25 pm - 03:50 pm	**SESSION V** Clinically Relevant Application	**Renaud La Joie,** University of California, San Francisco, San Francisco, CA, USA **Reisa Sperling,** Brigham and Women's Hospital/HMS, Boston, MA, USA
02:25 pm - 02:30 pm	Session Overview	**Chairs**
02:30 pm	Neuropathologic and ARIA-related findings in aducanumab-treated Alzheimer's disease: a postmortem analysis of superficial cortical Aβ clearance	**Baayla D.C. Boon**, Department of Neuroscience, Mayo Clinic, Jacksonville, FL, US
02:45 pm	Robustness of the centiloid scale across research and commercial software using [18F]flutemetamol PET images	**Adam Schwarz**, GE HealthCare, Chalfont St. Giles, GB
03:00 pm	Impact of ARIA on cerebral volume changes with Gantenerumab	**Matteo Tonietto**, Research and Early Development (pRED), Hoffmann-La Roche, Basel, CH
03:15 pm	Independent effects of baseline white matter hyperintensity and APOE ε4 on future ARIA-H emergence in A4 trial	**Zahra Shirzadi**, Department of Neurology, Massachusetts General Hospital, Brigham and Women's Hospital, Harvard Medical School, Boston, MA, US
03:30 pm – 3:50 pm	Discussion	

Neuropathologic and ARIA-related findings in aducanumab-treated Alzheimer's disease: a postmortem analysis of superficial cortical Aβ clearance

Baayla D.C. Boon[1,2], Yoav Piura[3], Jessica L. Chalk[1], Christina M. Moloney[1], Sarah J. Lincoln[1], Matthew H. Rutledge[4], Derek R. Johnson[5,7], Dennis W. Dickson[1], Aivi T. Nguyen[6], R. Ross Reichard[6], Jonathan Graff-Radford[7], David S. Knopman[7], Neill Graff-Radford[3], Melissa E. Murray[1]

[1]*Department of Neuroscience, Mayo Clinic, Jacksonville, FL, US*
[2]*Department of Neurology, Alzheimer Center Amsterdam, Amsterdam University Medical Center, location Vrije Universiteit Medical Center, Amsterdam, NL*
[3]*Department of Neurology, Mayo Clinic, Jacksonville, FL, US*
[4]*Department of Quantitative Health Sciences, Mayo Clinic, Jacksonville, FL, US*
[5]*Department of Radiology, Mayo Clinic, Rochester, MN, US*
[6]*Department of Laboratory Medicine and Pathology, Mayo Clinic, Rochester, MN, US*
[7]*Department of Neurology, Mayo Clinic, Rochester, MN, US*

Background: Several monoclonal amyloid-β (Aβ) antibodies, including aducanumab, have been tested to treat Alzheimer's disease (AD). Limited data is available on neuropathology after treatment or amyloid-related imaging abnormalities (ARIA) side effects. We report on such data from five aducanumab-treated study participants with AD.

Methods: Aducanumab-treated study participants who came to autopsy (n=5) were matched to AD controls (n=12) based on the presence/type of autosomal dominant AD mutation, *APOE* genotype, age at cognitive symptom onset, and sex. We assessed cognitive measures, ^{18}F-florbetapir PET composite SUVr, ARIA risk factors, and AD neuropathologic change. Brain regions affected along Thal amyloid phases were stained for Aβ isoforms using multiplex immunofluorescence. ARIA-affected brain regions were assessed using Perl's Prussian blue, Aβ, fibrinogen for blood brain barrier integrity, membrane attack complex (C5b-C9) for complement activation, and activated microglia (IBA1, CD68).

Results: Study participants included four males and one female, each carrying at least one *APOE ε4* allele. Two carried a *PSEN1 NM_000021.4:c.817G>A*, p.Glu273Lys mutation. Two had ARIA on MRI. None cognitively benefitted from the drug. In four study participants, the composite ^{18}F-florbetapir SUVr declined by 0.3-0.4. Cumulative dosage ranged between 5–241 mg/kg and time between last infusion and death 5-41 months. In study participants, Aβ was cleared in cortical layer I ($p<0.05$) but not in the total cortex (**Fig. 1**). When assessing distinct Aβ deposits, the burden of diffuse plaques was reduced only in cortical layer I ($p<0.05$). Hemosiderin was not distinct for ARIA and was present in non-treated AD controls. However, in study participants with ARIA-H, hemosiderin was seen in superficial cortical layers near CAA-laden meningeal and penetrating vessels that showed complement and microglial activation (**Fig. 2**).

Conclusions: We observed Aβ clearance and ARIA-related findings localized in the superficial cortical layers, suggesting that aducanumab biodistribution is more significant in superficial rather than deep cortical layers.

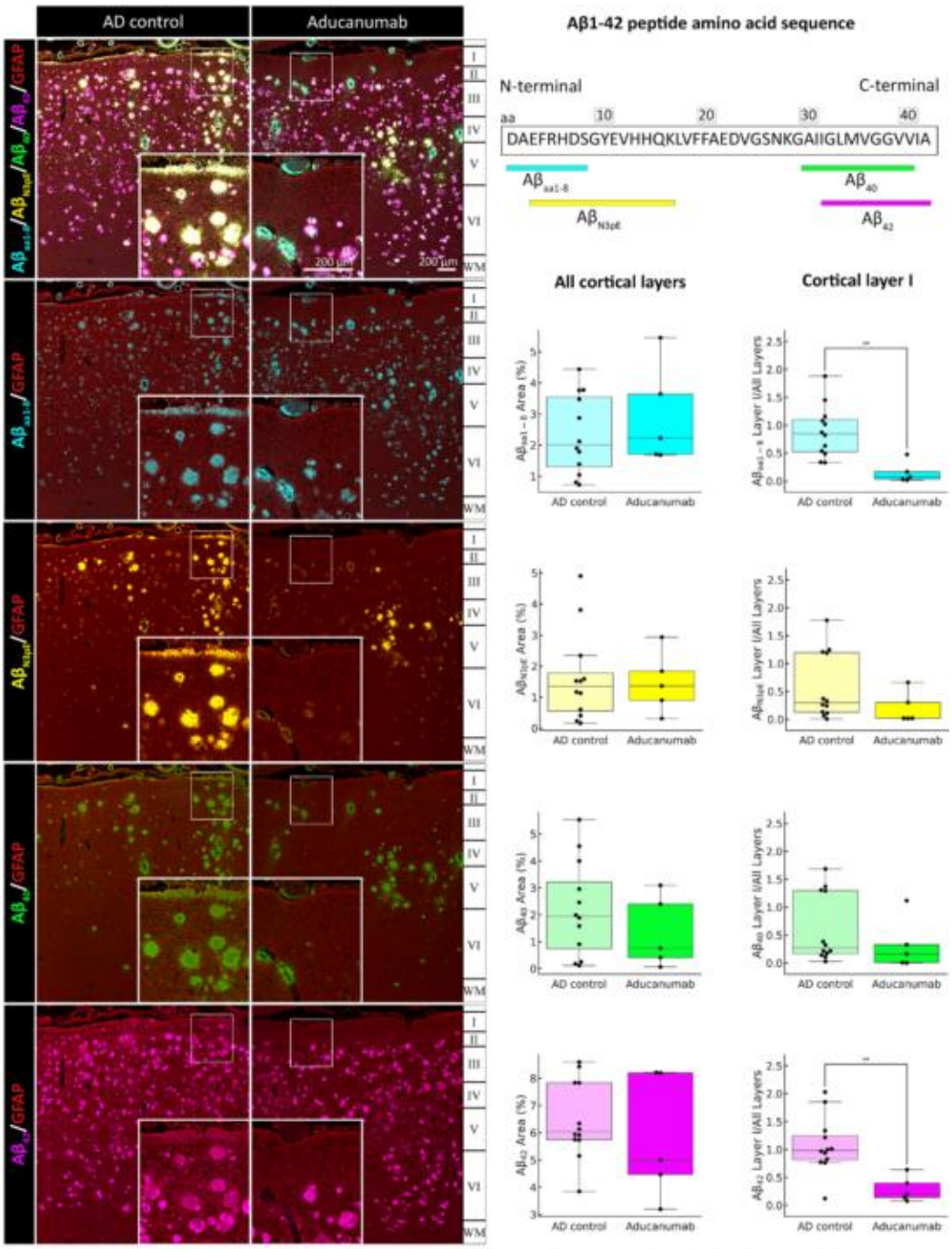


Fig. 1. Distribution of Aβ isoforms in aducanumab-treated participants versus non-treated AD controls. The left panels display representative immunofluorescent images for each Aβ isoform listed. The right panels present boxplots depicting the immunoreactive area for Aβ isoforms in 1) all six cortical layers and 2) cortical layer I/all six cortical layers.

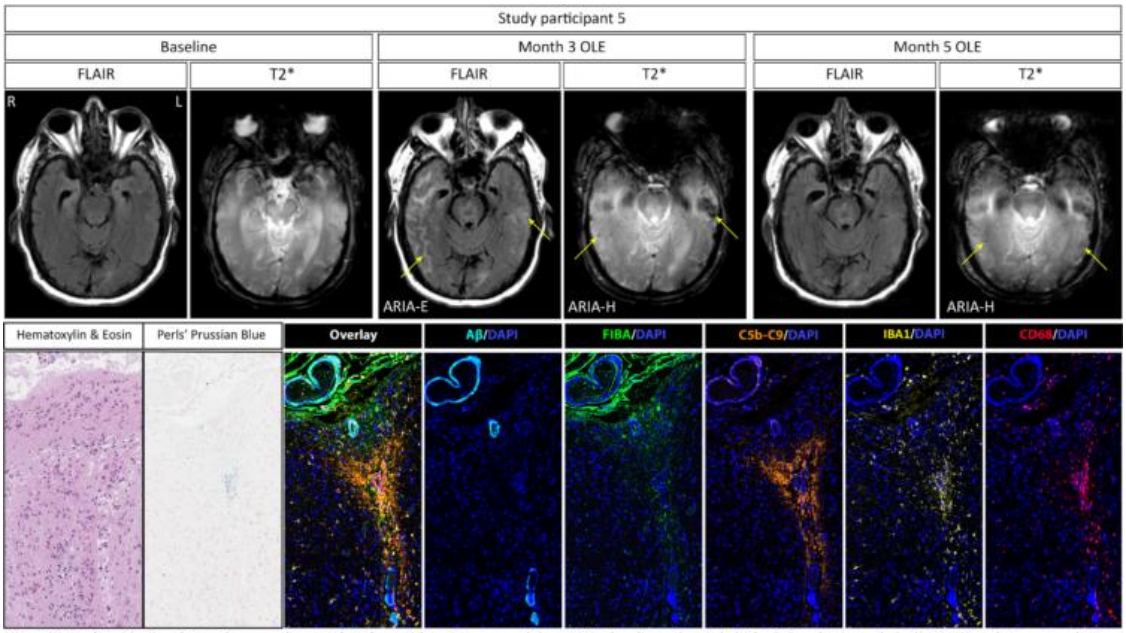


Fig. 2. ARIA-related findings in an aducanumab-treated study participant. Upper panel shows MRI at baseline, at 3 months in the OLE, and at 5 months in the OLE. Note the two pre-existing microbleeds at baseline in the T2* sequence (white arrow). At 3 months in the OLE, ARIA-E is present in FLAIR sequence and ARIA-H in T2* sequence (yellow arrows). At 5 months in the OLE, ARIA-E is resolved, but ARIA-H has increased. Bottom panel depicts histologic findings in ARIA-affected regions. Microinfarcts (H&E) with hemorragic component (Prussian Blue) are present along penetrating CAA-laden (Aβ) vessels. Blood brain barrier is breached (FIBA) with complement activtaion (C5b-C9) and microglia activation (IBA1, CD68). FIBA=fibrinogen α, OLE=open label extension phase.

Keywords: ARIA, amyloid targeting therapies, aducanumab, neuropathology, amyloid-beta

Robustness of the centiloid scale across research and commercial software using [18F]flutemetamol PET images

Adam Schwarz[3], Ariane Bollack[1,2], Chris Buckley[1], Mark Battle[1], Oskar Hansson[4], Pierrick Bourgeat[5], Vincent Dore[5,6], Jurgen Fripp[5], Lennart Thurfjell[7], Will Balhorn[8], Mike Haas[8], Chris Page[1], Gill Farrar[1]

[1]*GE HealthCare, Chalfont St. Giles, GB*
[2]*UCL, London, GB*
[3]*GE HealthCare, Holliston, MA, US*
[4]*Lund University, Lund, SE*
[5]*CSIRO, Brisbane, AU*
[6]*Austin Health, Melbourne, AU*
[7]*Combinostics, Tampere, FI*
[8]*MIM Software Inc., Cleveland, OH, US*

Background: Amyloid PET quantification using the Centiloid (CL) metric is becoming more prevalent and may have a role in clinical decision-making. To evaluate the robustness and interchangeability of CL values obtained from different software, we systematically assessed repeatability, reproducibility, and reliability across six CL quantification pipelines applied to 210 [^{18}F]flutemetamol scans.

Methods: Three datasets were used: (1) An AD test-retest cohort (N=10x2); (2) an aMCI cohort (N=80); (3) cases from the BioFINDER-1 cohort enriched for amyloid loads around common positivity thresholds (0-50CL) (N=110). Two regulatory-approved software (cPET, MIMneuro) and four research pipelines (CapAIBL, rPOP, Amypype, SPM8) were evaluated. Dataset 1 was used to assess repeatability. Dataset 2 was used to assess reproducibility in terms of absolute agreement in continuous CL values. Datasets 2 and 3 were used to assess reliability for dichotomizing amyloid scans into positive and negative. The latter was performed for three thresholds of 11, 25 and 37 CL.

Results: The test-retest analysis revealed an absolute bias of <5 CL for all pipelines. Within-subject coefficients of variation ranged from 2.6 to 4.2% and repeatability coefficients from 8.1 to 16.1 CL (Table 1). Strong associations in continuous CL estimates were observed across pairs of software (R^2≥0.93, Figure 1). Agreement in +/- status between software was 92-99% (kappa 0.84-0.97) in dataset 2 and 75-97% (kappa 0.48-0.93) in dataset 3. For the two regulatory-approved software, agreement at the three CL thresholds was 94%, 97% and 97% in dataset 2 and 86%, 94% and 93% in dataset 3.

Conclusions: CL quantification was generally repeatable and reproducible across the software packages evaluated, with high inter-software reliability around thresholds of 11, 25 and 37 CL. Uncertainty estimates should always be considered when interpreting results.

Table 1 Summary Statistics for the Test-Retest Dataset Processed with Six Software

	A*	B	C	D	E*	F
N	10	10	10	5†	8†	10
R^2	0.97	0.96	0.94	0.93	0.96	0.97
Mean Test	90.6	91.6	96.7	102.9	96.5	96.4
Mean Retest	89.9	91.3	96.6	105.6	95.9	97.7
Mean difference	-0.7	-0.3	-0.1	2.7	-0.5	1.4
Absolute mean difference	3.3	3.7	4.3	4.8	3.9	2.9
wSD	2.8	3.4	4.1	4.1	3.6	2.5
wCV (%)	3.1	3.7	4.2	3.9	3.7	2.6
RC	8.8	10.8	13.2	16.1	11.8	8.1
ICC	0.99 [0.95, 1]	0.98 [0.93, 1]	0.97 [0.89, 0.99]	0.96 [0.76, 1]	0.98 [0.91, 1]	0.99 [0.94, 1]

* Denotes commercial, regulatory-approved software package; † Some scans were excluded following processing errors; Mean difference between test and retest values computed as (CL_{retest} - CL_{test}); wSD = within-individual standard deviation; wCV = within-individual coefficient of variation; RC = repeatability coefficient (minimum amount of change between two measurements in the same individual needed to be 95% confident that the observed difference corresponds to true change rather than variability); ICC = intraclass correlation coefficient, corresponding to ICC(2,1) (two-way, absolute agreement, single rater).

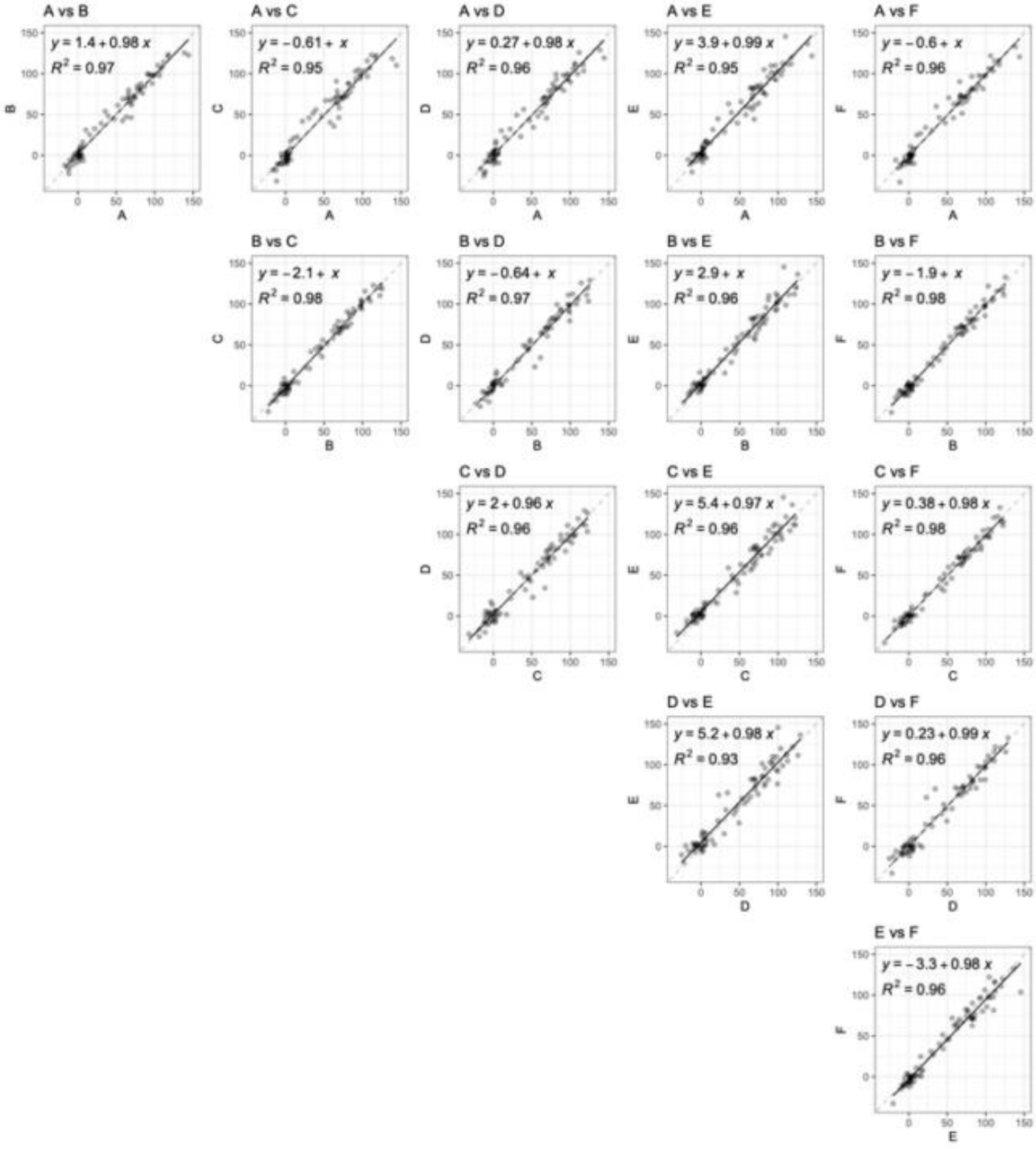


Figure 1: Correlation of Centiloid Values across Six Software Applications

Keywords: Vizamyl, Flutemetamol, Centiloids, Quantification

Impact of ARIA on cerebral volume changes with Gantenerumab

Matteo Tonietto[1], Erica Silvestri[1], Christopher Belder[2,3], Frederik Barkhof[2,4], Nick Fox[2], Janice Smith[5], Gregory Klein[1]

[1]*Research and Early Development (pRED), Hoffmann-La Roche, Basel, CH*
[2]*Dementia Research Centre, UCL Queen Square Institute of Neurology, London, GB*
[3]*Adelaide Medical School, University of Adelaide, Adelaide, AU*
[4]*Department of Radiology & Nuclear Medicine, Amsterdam UMC, Vrije Universiteit, Amsterdam, NL*
[5]*Roche Products Ltd, Hoffmann-La Roche, Welwyn Garden City, GB*

Introduction: Gantenerumab is a monoclonal antibody targeting aggregated forms of amyloid-beta. The phase III GRADUATE investigational studies aimed to assess the efficacy and safety of gantenerumab in early AD. Similarly to other anti-Aβ immunotherapies, participants treated with Gantenerumab 1) exhibited accelerated brain volume loss compared to placebo and 2) in some cases, also developed amyloid-related imaging abnormalities (ARIA). In this study, we investigated the relationship between ARIA and brain volume loss.

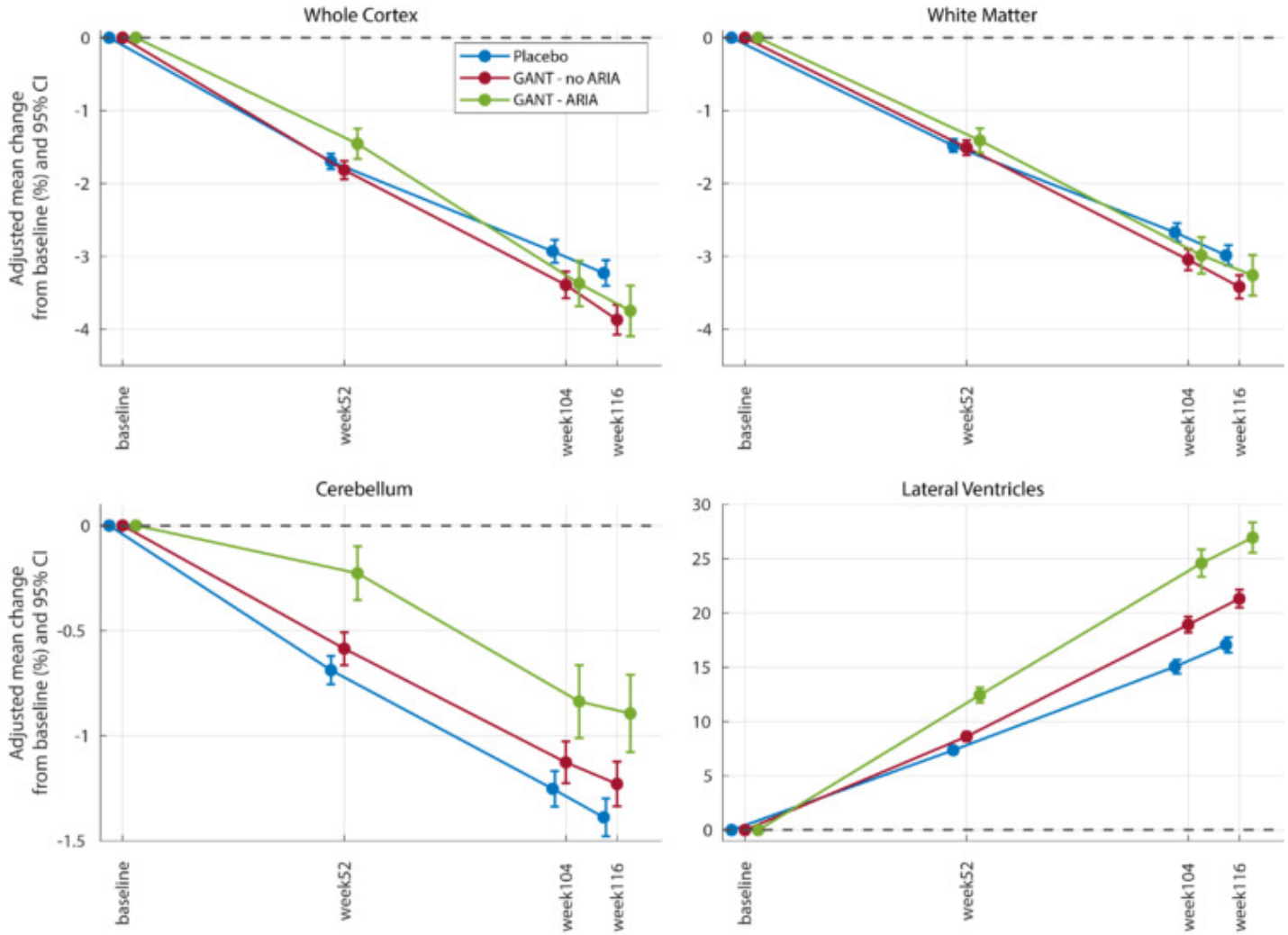
Methods: Volumetric MRI changes in the whole cortex, white matter, lateral ventricles, and cerebellum regions were calculated using Tensor-Based-Morphometry and compared between placebo, and gantenerumab-treated participants both with and without ARIA. Additionally, the study investigated the association between volumetric changes and the maximum Barkhof Grand Total Scale (BGTS) score of ARIA severity in the ARIA group, as well as the relationship between volume changes and clinical/cognitive scores in all three groups.

Results: At the end of the study, relative to no ARIA, the group with ARIA showed no significant difference in whole cortex or white matter volume loss but had greater lateral ventricular volume expansion and lower cerebellar volume loss (Figure 1).

At week 52, in the ARIA group higher BGTS scores were associated with smaller regional volume changes, and greater ventricular volume expansion. By the study's end, only ventricular volume expansion was still associated with the ARIA BGTS score (Figure 2)

Participants with ARIA exhibited less clinical/cognitive change for the same amount of ventricular expansion compared to those on Gantenerumab without ARIA and placebo (Figure 3).

Conclusion: ARIA effect on cortical volume change was transient and resolved by the end of the studies. The lower volume loss in the cerebellum and higher expansion of the ventricles in the ARIA group suggest an alteration of the CSF dynamics due to ARIA, which was not associated with accelerated clinical/cognitive worsening.



Number of participants included in each group at each time point:

	Week 52	Week 104	Week 116
Placebo	756	636	660
GANT – no ARIA	569	461	461
GANT – ARIA	213	142	147

Figure 1: Shown is the adjusted mean relative change from baseline (CFB) in the whole cortex, white matter, cerebellum, and lateral ventricles volumes through week 116.

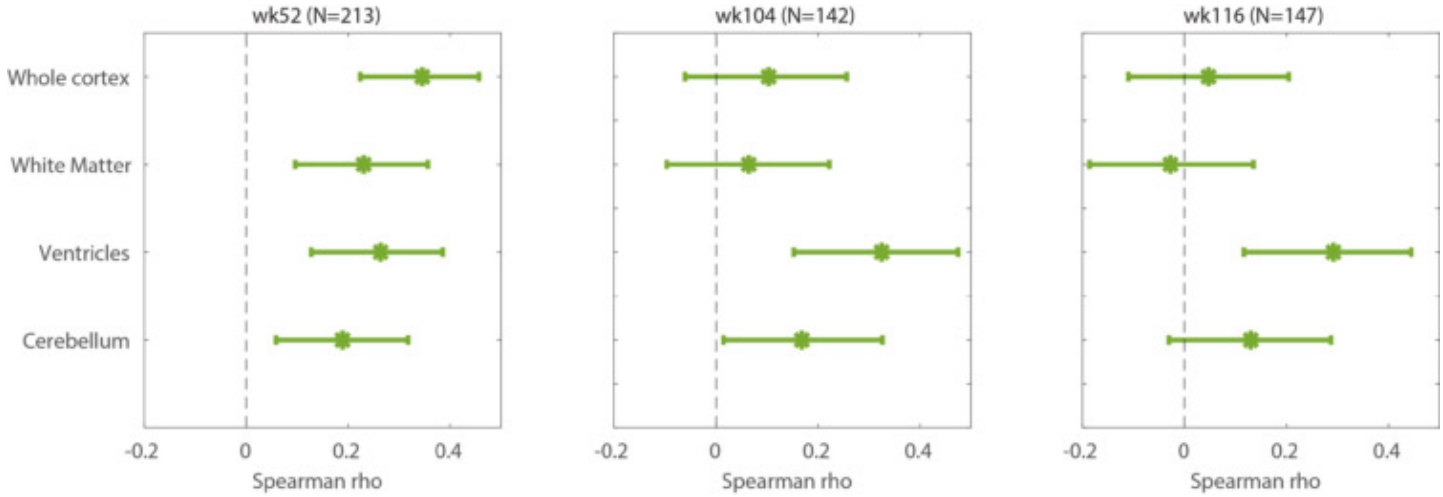


Figure 2: Shown is the Spearman correlation coefficient between the maximum BGTS score and relative volumetric changes from baseline of the whole cortex, white matter, ventricles, and cerebellum in the gantenerumab-treated participants with ARIA. Error bars represent the 95% confidence interval calculated with bootstrap (N=10000). A positive correlation means that participants with more severe ARIA had lower volume loss (or bigger volume expansion in case of ventricles)

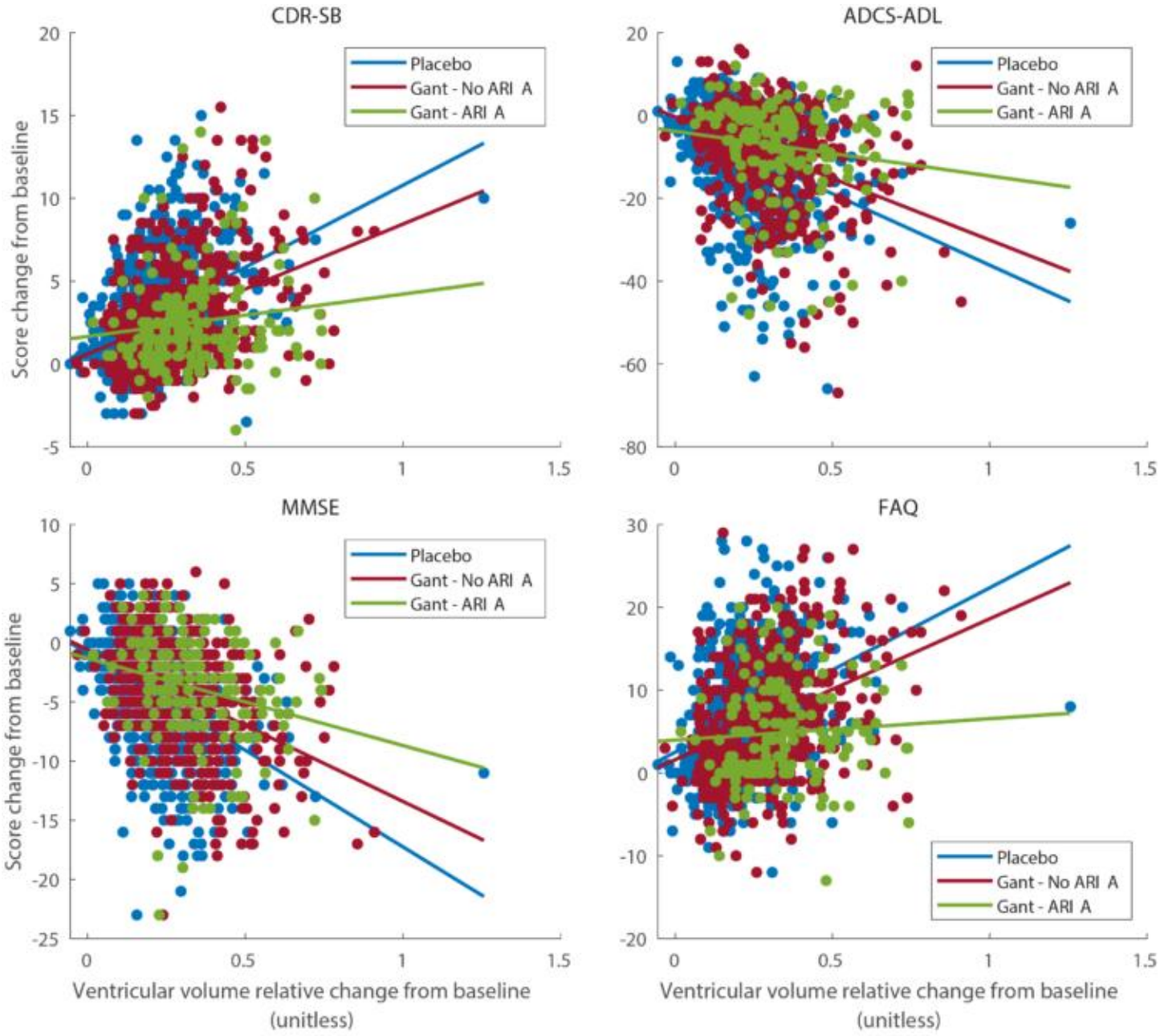


Figure 3: Shown is the scatter plot between the ventricular volume relative change from baseline and the CDR-SB, ADCS-ADL, MMSE, and FAQ changes from baseline for placebo (blue), gantenerumab-treated participants without ARIA (red), and gantenerumab-treated participants with ARIA (green). Lines represent the least square linear fit.

Keywords: Gantenerumab, ARIA, amyloid

Independent effects of baseline white matter hyperintensity and APOE ε4 on future ARIA-H emergence in A4 trial

Zahra Shirzadi[1], Aaron Schultz[1], Nazila Loghmani[1], Michael Properzi[1], Michael Rafii[2], Michael Donohue[2], Shunran Wang[2], Clifford Jack Jr[3], Steven Greenberg[1], Rema Raman[2], Paul Aisen[2], Reisa Sperling[1], Jasmeer Chhatwal[1]

[1]*Department of Neurology, Massachusetts General Hospital, Brigham and Women's Hospital, Harvard Medical School, Boston, MA, US*
[2]*Alzheimer's Therapeutic Research Institute, University of Southern California, San Diego, CA, US*
[3]*Mayo Clinic, Radiology, Rochester, MN, US*

Background: Increased white matter hyperintensity volume (WMH) visible on MRI is a common but non-specific finding in Alzheimer's disease (AD). Recent evidence shows that elevated WMH correlates with cerebral amyloid angiopathy (CAA), and may precede ARIA-H manifestations, including microhemorrhages (MCH) and superficial siderosis (SS). We hypothesized that people with preclinical AD who had increased WMH would have a greater likelihood of developing ARIA-H lesions during longitudinal follow-up. We examined this hypothesis using longitudinal data from the Anti-Amyloid Treatment in Asymptomatic Alzheimer's study (A4).

Methods: ARIA-H lesions (MCH and SS) were identified by experienced radiologists at Mayo Clinic. People were categorized as having 0, 1, or 2+ lesions based on Boston criteria for CAA, and WMH volume was categorized using tertiles. Focusing on people with 0 or 1 lesion at baseline (i.e., those without probable CAA), we examined age, sex, amyloid, WMH, APOE ε4, cardiovascular risk, and treatment group as predictors of whether people would develop 2+ ARIA-H lesions (emergence of probable CAA) by the time of their last MRI (4.5y post-baseline).

Results: Among 1097 individuals with 0 or 1 ARIA-H lesions at baseline, 120 had 2+ ARIA-H lesions observed on their last MRI. Elevated baseline WMH (OR= 2.16, p=.004) and APOE ε4 carriage (OR=1.72, p=.01) independently predicted membership in this group (Figure 1). 7% of individuals developed 1+ new ARIA-H lesion every two years, and elevated baseline WMH volume (OR= 2.99, p=.001) and APOE ε4 carriage (OR=2.5, p=.001) independently predicted membership in this group (Figure 2).

Conclusion: These results suggest that both elevated WMH and APOE ε4 carriage are associated with a greater likelihood and rate of ARIA-H emergence in people with preclinical AD. More broadly, these results support the hypothesis that increased WMH volume may be an early marker for CAA pathophysiologic changes.

Table 1: *Participants' demographics and study information. Mean ± Standard deviation or number (percentage) is reported.*

	Participants (N=1156)
Age at baseline (years)	71.9 ± 4.8
APOE ε4 (yes)	679 (59%)
Sex (Female)	685 (59%)
Race (White / Black/Asian / other)	1087 / 28 / 24 / 17 (94 % / 2.4 % / 2.1 % / 1.5%)
Amyloid at baseline (PET SUVR)	1.5 ± 0.2
Definite MCH+SS count at baseline (0/1/≥2)	938 / 159 / 59 (81% / 14% / 5%)
Definite MCH+SS count at the last visit (0/1/≥2)	775 / 202 / 179 (67% / 17% / 15%)
Group (solanezumab / placebo)	570 / 586 (49 % / 51 %)
Cardiovascular risk score	27 ± 16
WMH volume at baseline, normalized to an intracranial volume of 1300 cm^3	4.9 ± 6.3

APOE ε4: Apolipoprotein E allele ε4 status
MCH: microhemorrhages
SS: superficial siderosis
WMH: white matter hyperintensity

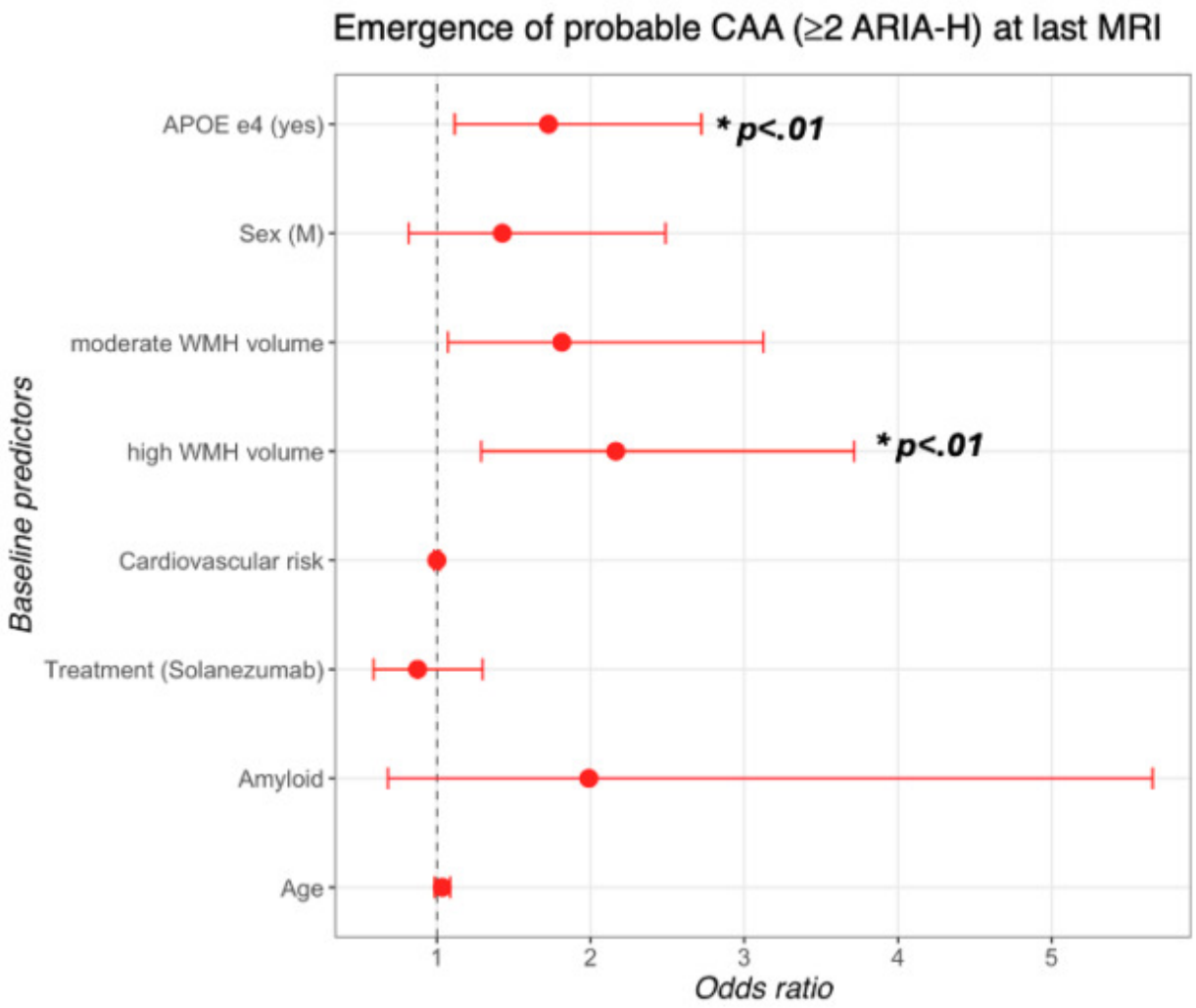


Figure 1: Contribution of baseline predictors to the risk of emergence of probable CAA (≥2 ARIA-H) in people with 0 or 1 ARIA-H lesions at baseline (i.e., without probable CAA at baseline). APOE ε4 and high baseline WMH volume independently explained the risk of future CAA emergence.

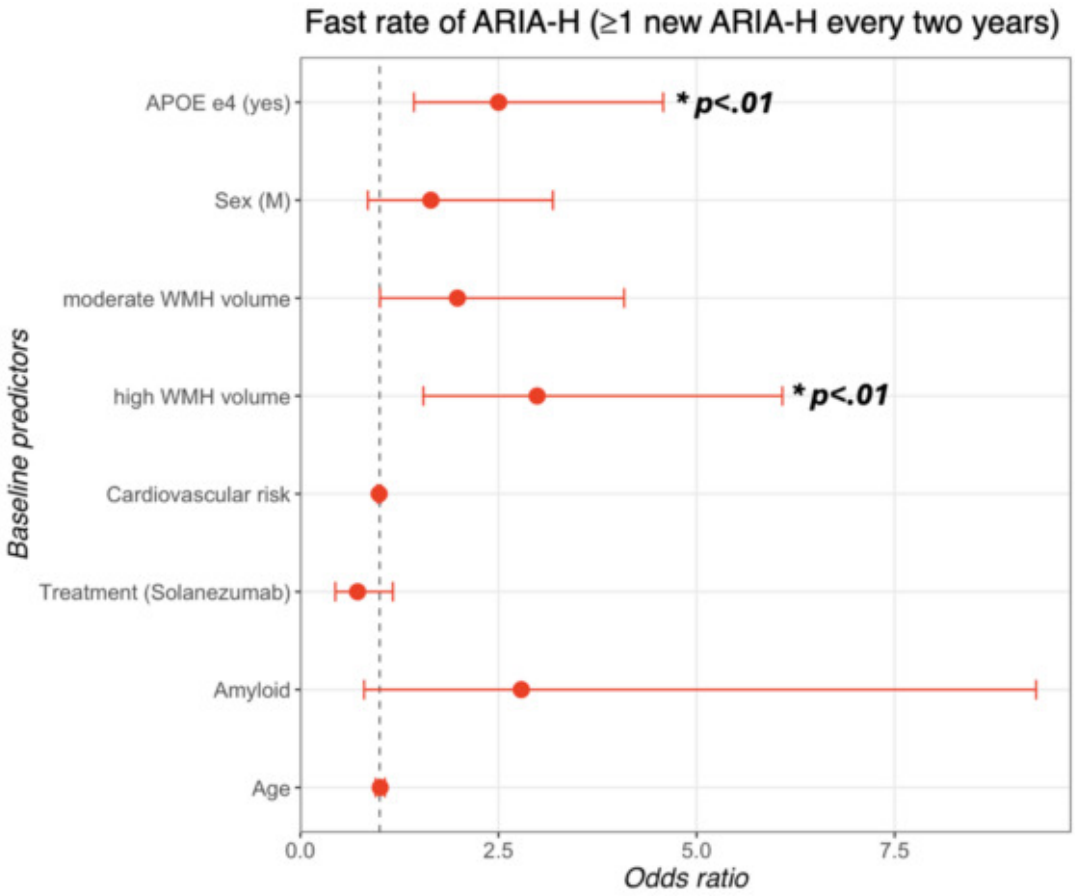


Figure 2: Contribution of baseline predictors to a fast rate of longitudinal new ARIA-H accumulation (i.e., ≥1 lesion every two years). APOE ε4 and high baseline WMH volume independently explained the risk of fast ARIA-H accumulation.

Keywords: White matter hyperintensity, cerebral microhemorrhages, cerebral amyloid angiopathy, Amyloid related imaging abnormalities

Thursday, January 16, 2025 - 03:50 pm - 03:55 pm

Podium Session

Blitz Session 2B: Short Poster Presentations

Thursday, January 16, 2025		
03:50 pm - 03:55 pm	**Blitz Session 2B**	
03:50 pm – 03:52 pm	Introduction	
03:52 pm	Cortical freewater increases with tau tangle aggregation	**Brandon Hall**, McGill University, Montreal, QC, CA
03:53 pm	Two distinct sources of 18F-MK-6240 off-target signal identified by individualized head modeling and PET kinetics	**Charles Chen**, Athinoula A. Martinos Center for Biomedical Imaging, Massachusetts General Hospital, Charlestown, MA, US
03:54 pm	Tracking plasma biomarker abnormalities with amyloid time accumulation	**Marina Bluma**, Karolinska Institutet, Department of Neurobiology, Care Sciences and Society, Division of Clinical Geriatrics, Center of Alzheimer Research, Stockholm, SE

Cortical freewater increases with tau tangle aggregation

Brandon Hall[1,2], Etienne Aumont[1,2], Nesrine Rahmouni[1,2], Joseph Therriault[1,2], Seyyed-Ali Hosseini[1,2], Lydia Trudel[1,2], Jaime Fernandez-Arias[1,2], Arthur Macedo[1,2], Stijn Servaes[1,2], Gleb Bezgin[1,2], Yi-Ting Wang[1,2], Yansheng Zheng[1,2], Jenna Stevenson[1,2], Sulantha Sanjeewa[1,2], Andrea Benedet[5], Gallen Triana-Baltzer[6], Hartmuth Kolb[6], Nicholas Ashton[7], Henrik Zetterberg[5], Kaj Blennow[8], Tharick Pascoal[4], Jesse Klostranec[1,9], Pedro Rosa-Neto[1,2,3]

[1]*McGill University, Montreal, QC, CA*
[2]*Translational Neuroimaging Laboratory, The McGill University Research Centre for Studies in Aging, Montreal, QC, CA*
[3]*Douglas Hospital Research Centre, Verdun, QC, CA*
[4]*University of Pittsburg, Pittsburg, PA, US*
[5]*Department of Psychiatry and Neurochemistry, Institute of Neuroscience and Physiology, The Sahlgrenska Academy, Gothenburg, SE*
[6]*Neuroscience Biomarkers, Janssen Research & Development, La Jolla, CA, US*
[7]*Wallenberg Centre for Molecular and Translational Medicine, University of Gothenburg, Gothenburg, SE*
[8]*Clinical Neurochemistry Laboratory, Sahlgrenska University Hospital, Mölnda, SE*
[9]*Division of Diagnostic and Interventional Neuroradiology, Montreal Neurological Institute and Hospital, Montreal, QC, CA*

It is unclear how cortical microstructure changes across biological stages of Alzheimer's disease (AD), and how this occurs in response to amyloid plaques, tauopathy, and inflammation. We hypothesize that tauopathy is chiefly responsible. To test this, we investigated how different measures of tauopathy influence microstructural integrity in the whole brain, temporal meta-ROI, and hippocampus.

We sampled 301 participants (59% female, age 67±10) from the TRIAD cohort with T1 MRI, diffusion-weighted MRI, amyloid PET (F^{18}-NAV4694), tau PET (F^{18}-MK6240), and plasma biomarkers. We used the NODDI MATLAB toolbox to derive voxelwise freewater images, wherein higher cortical values represent inflammation and decreased microstructural integrity. We used FreeSurfer 7 to derive temporal meta-ROI) and hippocampal masks, and Standard Uptake Value Ratio (SUVR) to calculate amyloid and tau PET images. Plasma biomarkers were measured by Simoa assay. We stratified participants by amyloid SUVR positivity, plasma ptau 217 positivity (T1), and tau SUVR positivity (T2). We performed voxelwise correlations between freewater and tau SUVR via VoxelStats MATLAB toolbox. Voxelwise regressions between freewater and plasma biomarkers and the mediation analyses performed in R 4.4.1. Models covaried for amyloid SUVR, age, sex, and APOE4 genotype status. Multiple comparisons correction performed by random field theory method.

Tau PET and plasma p-tau217 positively correlated with freewater in temporal and occipital regions (**Fig1A**, **Fig2A**). However, the effect of p-tau217 is only present in participants positive for tau tangles (**Fig 2C)**. Freewater increased only in the A+T2+ group in the meta-ROI and hippocampus (**Fig1B,C)**. Tau SUVR in meta-ROI mediated the correlations between both GFAP and p-tau217 with freewater in the A+T+ group (**Fig3**).

In neocortical and allocortical AD-relevant regions, increased freewater correlates with tau tangle accumulation. Our results suggest that while astrogliosis is involved with inflammation and decreasing microstructural integrity, this only occurs due to neurofibrillary tangles.

Figure 1. Increased tau is correlated with increased freewater independent of amyloid

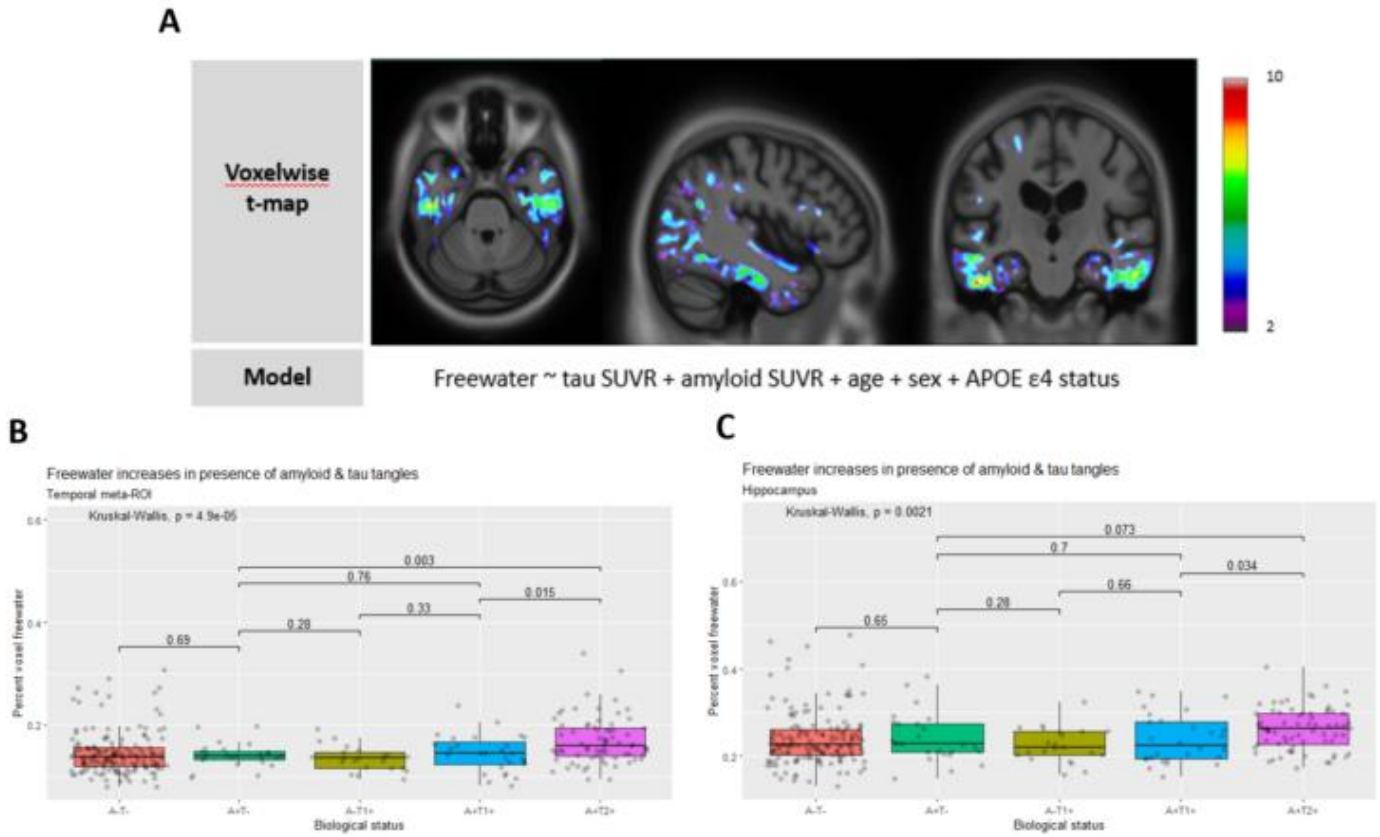


Figure 1. A) Voxelwise t-value maps of positive associations between freewater and tau PET after correction for amyloid PET, age, sex, and APOE4 allele frequency. Negative correlations did not survive multiple comparisons correction. Of note, the spatial distribution and intensity of positive correlations between tau PET and freewater closely resembles that found in the correlation of plasma ptau 217 and freewater. **B)** Boxplots of freewater in the temporal meta-ROI across different biological stages of AD-associated proteinopathy: amyloid-negative tau-negative (A-T-), amyloid-positive tau-negative (A+T-), amyloid-negative tau-plasma217-positive (A-T1+), amyloid-positive tau-plasma217-positive (A+T1+), amyloid-positive tau-PET-positive (A+T2+). **C)** As B, but instead showing freewater in the hippocampus across the biological stages.

Figure 2. Plasma ptau 217 correlates with freewater independent of amyloid in meta-ROI and hippocampus

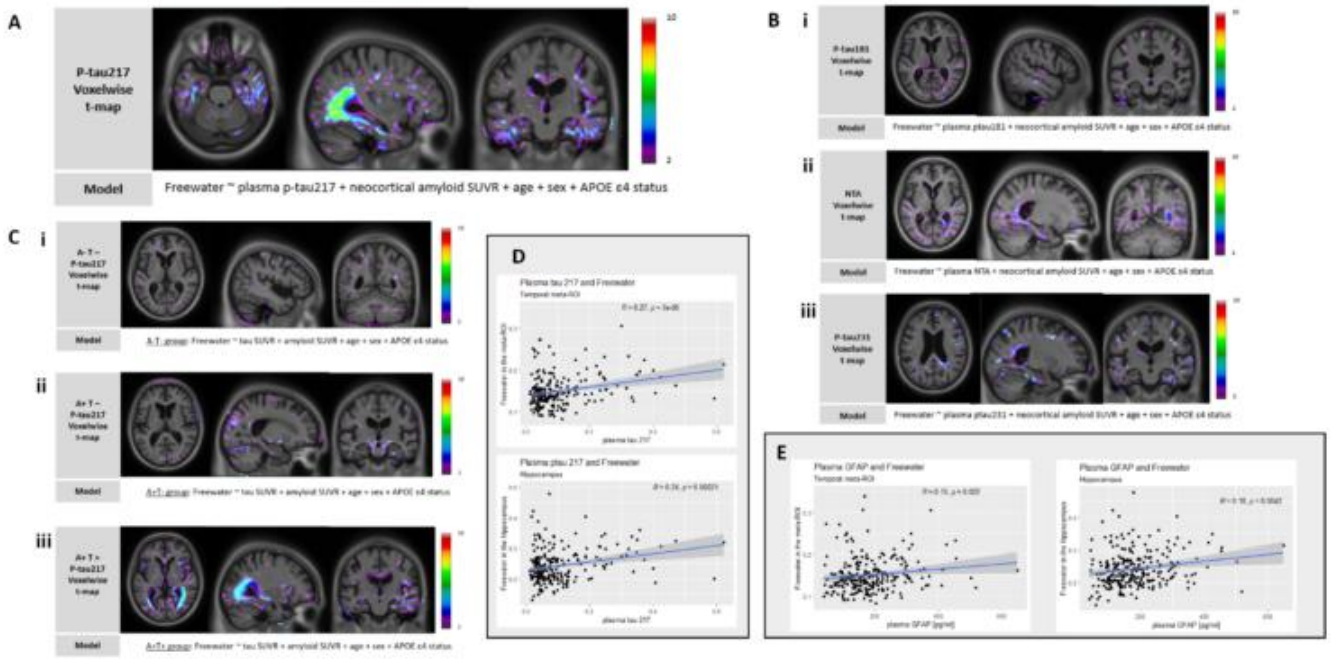


Figure 2. A) Voxelwise t-value maps of positive correlations between the plasma p-tau217 and freewater adjusting for average neocortical amyloid SUVR age, sex, and APOE4 allele frequency. **B)** As A, but instead showing the correlations between freewater and i) plasma p-tau181 ii) plasma N-terminal containing Tau fragments iii) plasma p-tau231. **C)** As A, but instead showing the correlations between the freewater and p-tau217 in participants grouped by biological stage, as defined by PET positivity: i) amyloid negative, tau negative ii) amyloid positive, tau negative iii) amyloid positive tau positive. **D)** Scatterplots depicting the correlation between plasma p-tau217 and freewater in the temporal meta-ROI and the hippocampus. **E)** Scatterplots depicting the correlation between plasma GFAP and freewater in the temporal meta-ROI and the hippocampus. Participants are grouped into three categories based on PET positivity for amyloid and tau due to group size restraints imposed by stratification used earlier in **Fig1**.

Figure 3. The effect of plasma GFAP on Freewater is mediated by tau

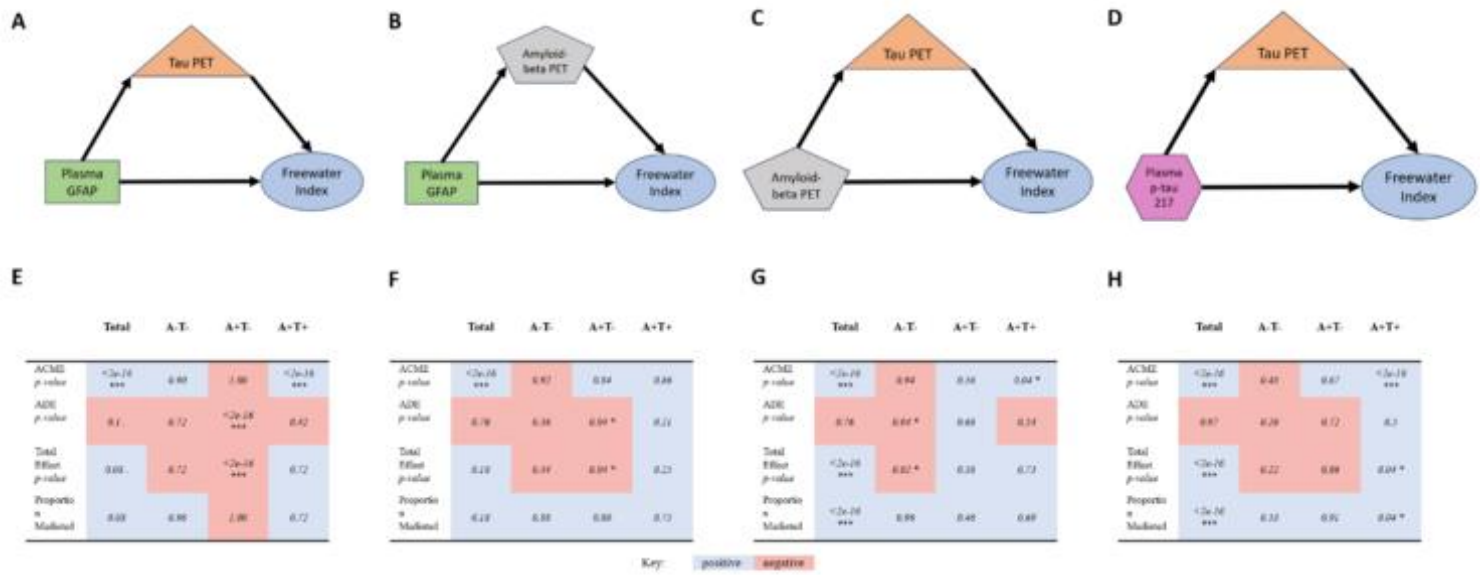


Figure 3. A) Schematic representation of the mediation analysis between plasma GFAP predicting the freewater index in the temporal meta-ROI, mediated by average tau SUVR in the temporal meta-ROI. This model was replicated across participants by biological stage. **B)** Schematic representation of the mediation analysis between plasma GFAP predicting the freewater index in the meta-ROI, mediated by neocortical amyloid SUVR. There was no significant mediation. **C)** Schematic representation of the mediation analysis between neocortical amyloid SUVR predicting the freewater index in the meta-ROI, mediated average tau SUVR in the temporal meta-ROI. **D)** Schematic representation of the mediation analysis between plasma p-tau217 predicting the freewater index in the meta-ROI, mediated plasma tau SUVR. Summary statistics and effect direction of mediation model from **A** across biological stages. **E)** Summary statistics and effect direction of mediation model from **B** across biological stages. **F)** Summary statistics and effect direction of mediation model from **C** across biological stages. **H)** Summary statistics and effect direction of mediation model from **D** across biological stages. Participants are grouped into three categories based on PET positivity for amyloid and tau due to group size restraints imposed by stratification used earlier in **Fig1**.
P-value 0.1 – 0.05: .
P-value 0.05 – 0.01: *
P-value 0.009 – 0.001: **
P-value < 0.0009: ***

Keywords: tau, PET, plasma, inflammation, microstructure

Two distinct sources of 18F-MK-6240 off-target signal identified by individualized head modeling and PET kinetics

Charles Chen[1], Jessie Fanglu Fu[1], Oula Puonti[1], Emma Thibault[2], Keith Johnson[2], Julie Price[1]

[1]*Athinoula A. Martinos Center for Biomedical Imaging, Massachusetts General Hospital, Charlestown, MA, US*
[2]*Gordon Center for Medical Imaging, Massachusetts General Hospital, Boston, MA, US*

Background: ^{18}F-MK-6240 PET is a powerful tool for visualizing neurofibrillary tangles (NFTs) in aging and Alzheimer disease (AD). However, ^{18}F-MK-6240 PET off-target signal (OTS) in the meninges can spill into brain parenchyma. Partial volume correction of OTS spill-in is challenging due to the thin structure of the meninges; prior approaches have used the FreeSurfer-defined skull mask to approximate the meningeal OTS, as this is a readily available parcellation. Herein, we describe an approach that uses individualized head modeling and PET kinetics to more precisely identify meningeal OTS.

Methods: We applied the Complete Head Anatomy Reconstruction Method (CHARM, Puonti et al. NeuroImage 2020) to segment the whole head from T1-weighted (T1w), T2w, and T2w FLAIR MRI in our test-retest dataset of dynamic (0-120 minutes) ^{18}F-MK-6240 PET/MRI in seven older adults (one diagnosed with AD; Table 1). We use the T1w/T2w ratio to separate meninges from CSF. This enables us to generate time-activity curves (TACs) for cerebral and cerebellar cortices, CSF, meninges, and skull (cortical and cancellous bone), and compare these to TACs generated using FreeSurfer-defined skull. The Diebold-Mariano test was used to determine which CHARM+T1w/T2w-defined TAC (meningeal or cortical bone) is a more accurate predictor of FreeSurfer-defined skull TAC.

Results: FreeSurfer-defined skull overlaps inconsistently with CHARM+T1w/T2w-defined meninges, especially near the tentorium (Fig.1). CHARM+T1w/T2w-defined meningeal and bone TACs show differing kinetics: the meninges/bone show high/low initial uptake that increases/decreases over time (Fig.2A). FreeSurfer-defined skull TAC is more similar to the CHARM+T1w/T2w-defined cortical bone than meningeal TAC (Diebold-Mariano p-values<0.01, Fig.2B). Findings are consistent across participants and test/retest studies.

Conclusion: In this work, the meninges and bone were found to represent two spatiotemporally distinct sources of OTS in ^{18}F-MK-6240 PET. Future efforts will use this information to more precisely correct for partial volume averaging and assess impact on quantification of ^{18}F-MK-6240 tau burden.

Table 1: Participant demographics.

	Cognitively normal (n=6)	Alzheimer disease diagnosis (n=1)
Test-retest interval (days)	25 [14 30]	30
Age (years)	66 [63 71]	54
Sex	Male=4, Female=2	Male=1
MMSE	29.5 [29 30]	22

Continuous values are summarized as median [first quartile third quartile]. MMSE=mini-mental state examination.

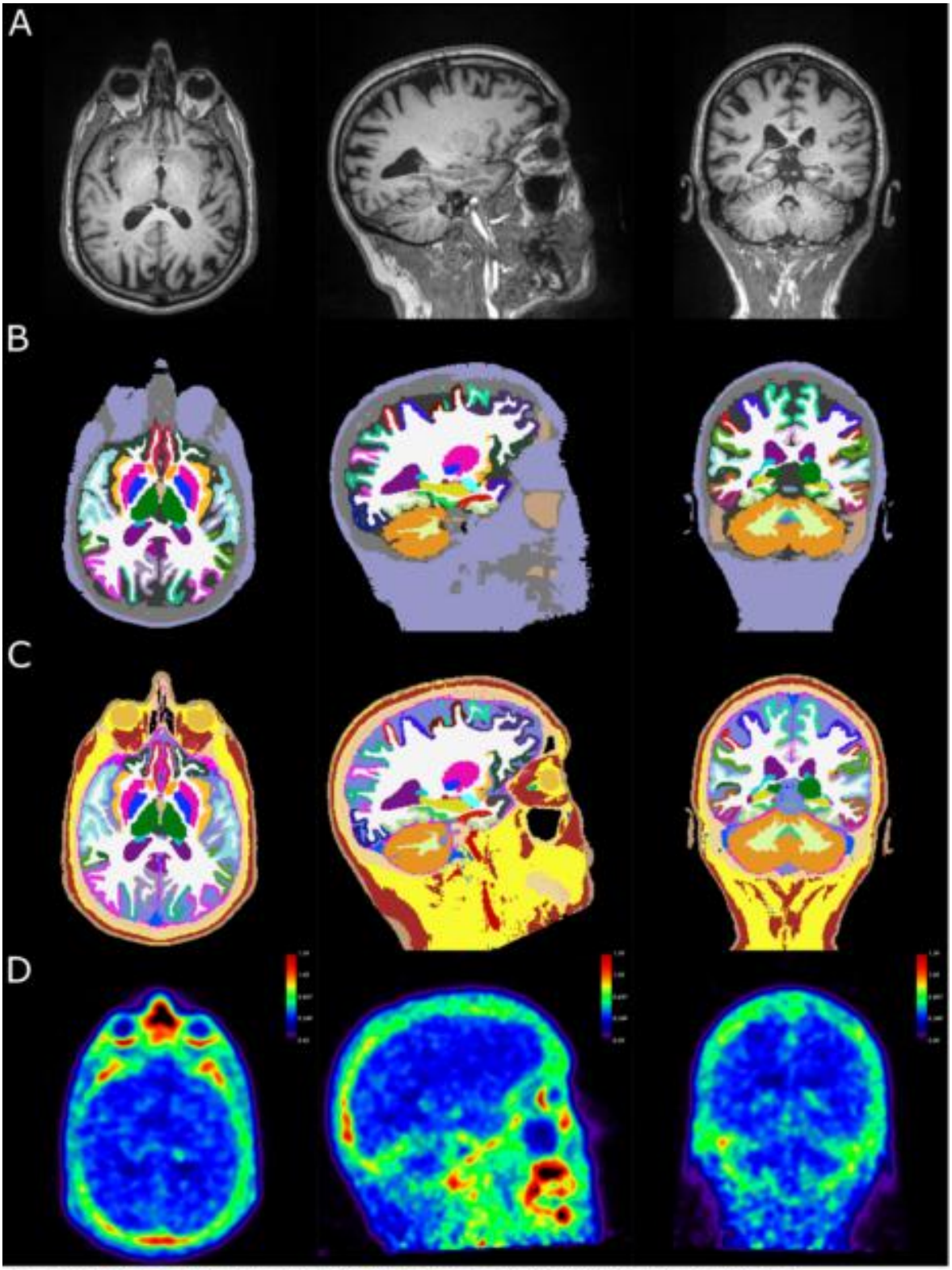


Figure 1: Comparing T1-weighted MRI, FreeSurfer skull segmentation, CHARM+T1w/T2w segmentation, and 18F-MK-6240 SUV90-110 in an exemplar individual with low tau and no cognitive impairment (participant #1). (A) A T1-weighted MRI shown in axial, sagittal, and coronal views. (B) The corresponding FreeSurfer segmentation (skull=light grey). (C) The corresponding CHARM+T1w/T2w segmentation (skull=light tan (cortical bone), which surrounds medium tan (cancellous bone), meninges (magenta), CSF (periwinkle)). Note the tentorium cerebelli, which are labeled as meninges in CHARM+T1w/T2w segmentation but are included in cerebral cortex or cerebellar cortex in FreeSurfer. (D) A 18F-MK-6240 SUV image (time window=90-110 minutes). Note the OTS in the meninges (tentorium), but also in the bone, retina, choroid plexus, and mucosa, among others.

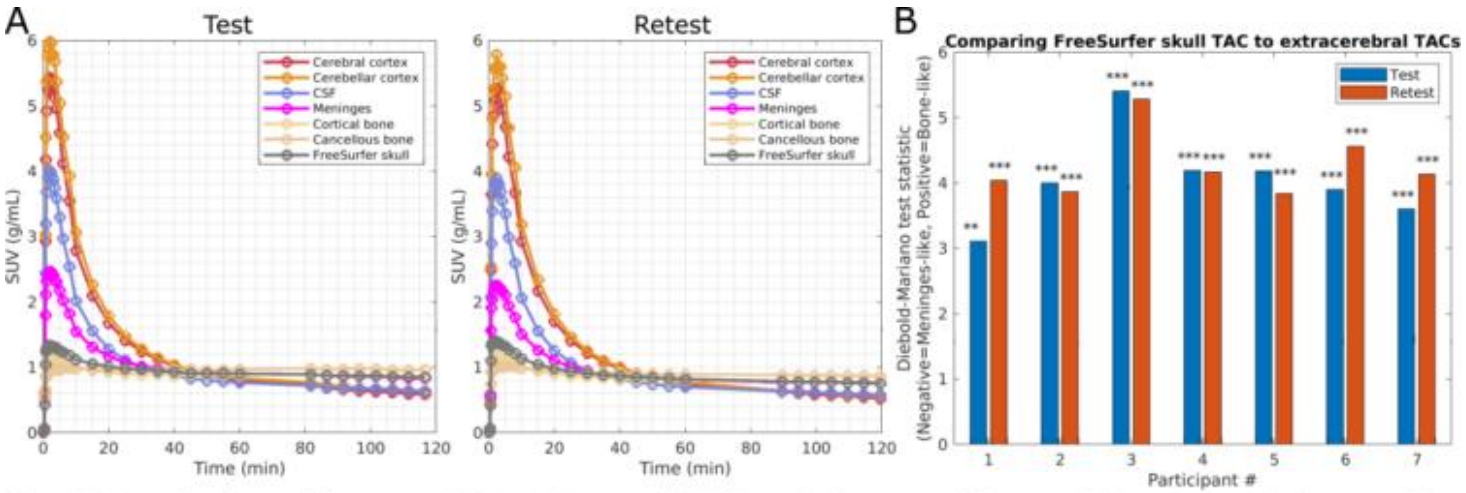


Figure 2: Comparing time activity curves. (A) Time activity curves (TACs) for cerebral cortex, cerebellar cortex, CSF, meninges, cortical bone, cancellous bone, and FreeSurfer-defined skull in a cognitively normal participant (participant #4) across test and retest studies. (B) Diebold-Mariano test statistics comparing which CHARM+T1w/T2w-defined TAC (meningeal or cortical bone) is more accurate predictor of FreeSurfer-defined skull TAC (null hypothesis=no difference in accuracy, negative values=CHARM+T1w/T2w meningeal TAC is a more accurate predictor of FreeSurfer-defined skull TAC, positive values=CHARM+T1w/T2w cortical bone TAC is a more accurate predictor of FreeSurfer-defined skull TAC, *=p-value<0.05, **=p-value<0.01, ***=p-value<0.001). Participants #1, 2, 4, 5, 6, and 7 are cognitively normal; participant #3 has an AD diagnosis.

Keywords: Tau PET, off-target, head model, kinetics, meninges

Tracking plasma biomarker abnormalities with amyloid time accumulation

Marina Bluma[1], Konstantinos Chiotis[1,6,7], Marco Bucci[1,2], Irina Savitcheva[5], Anna Matton[1], Miia Kivipelto[1,2], Andreas Jeromin[3], Giovanni De Santis[4], Guglielmo Di Molfetta[4], Nicholas J. Ashton[4], Kaj Blennow[4], Henrik Zetterberg[4], Agneta K Nordberg[1,2]

[1]*Karolinska Institutet, Department of Neurobiology, Care Sciences and Society, Division of Clinical Geriatrics, Center of Alzheimer Research, Stockholm, SE*
[2]*Karolinska University Hospital, Theme Inflammation and Aging, Stockholm, SE*
[3]*ALZPath, Inc, ALZPath, Inc, Carlsbad, CA, US*
[4]*University of Gothenburg, Department of Psychiatry and Neurochemistry, Molndal, SE*
[5]*Karolinska University Hospital, Medical Radiation Physics and Nuclear Medicin, Stockholm, SE*
[6]*Department of Neurology, Karolinska University Hospital, Stockholm, SE*
[7]*Memory and Aging Center; Department of Neurology;University of California, San Francisco, CA, US*

Aim: Plasma pTau fragments and GFAP are potential candidates for early detection and screening of patients for anti-amyloid therapies. Although it has been shown that these plasma biomarkers change early, the specific timing at which these changes become significant to identify Aβ+ individuals has yet to be determined.

Methods: Data were acquired from a memory clinic cohort (N=138) assessed at the Memory Clinic, Karolinska University Hospital, Stockholm, Sweden. Using a nonlinear model of relationship between amyloid accumulation time and load (Schindler et al., (2021)), we estimated the duration of amyloid accumulation (AmyloidTime) based on centiloid values from amyloid PET scans. We then predicted the AmyloidTime linked with the threshold of plasma biomarkers becoming abnormal to detect individuals with Aβ+ scan with 90% sensitivity. By subtracting AmyloidTime from each patient's age, we estimated their amyloid accumulation onset age ('age-of-Aβ-onset'), identifying young accumulators as those with age-of-Aβ-onset under 50 years, which would correspond to a minimum of 15 years of Aβ-accumulation at age 65.

Results: The AmyloidTime corresponding to 100% accuracy of positive visual read for Aβ-PET scan was 4.8 years (and 90%-1year before 0 AmyloidTime). The AmyloidTime required for plasma biomarker levels become abnormal enough to provide 90% sensitivity in identifying amyloid positive PET scans was: 5.4 years for pTau217, 8.7 - for GFAP, 9.2 - for pTau181, and 10.5 - for pTau231 (Fig.1). Plasma pTau217 and pTau181 levels, but not plasma GFAP or pTau231, were significantly higher in early amyloid accumulators, even after adjusting for the effect of amyloid load or AmyloidTime (Fig.2).

Conclusions: Plasma pTau217 levels show a significant change, enabling the identification of Aβ+ individuals with 90%sensitivity 5.4 years after reaching the Aβ-accumulation tipping point. Young-age Aβ-accumulators showed higher levels of pTau217 and pTau181, suggesting an exacerbation of tau pathology within this patient subgroup.

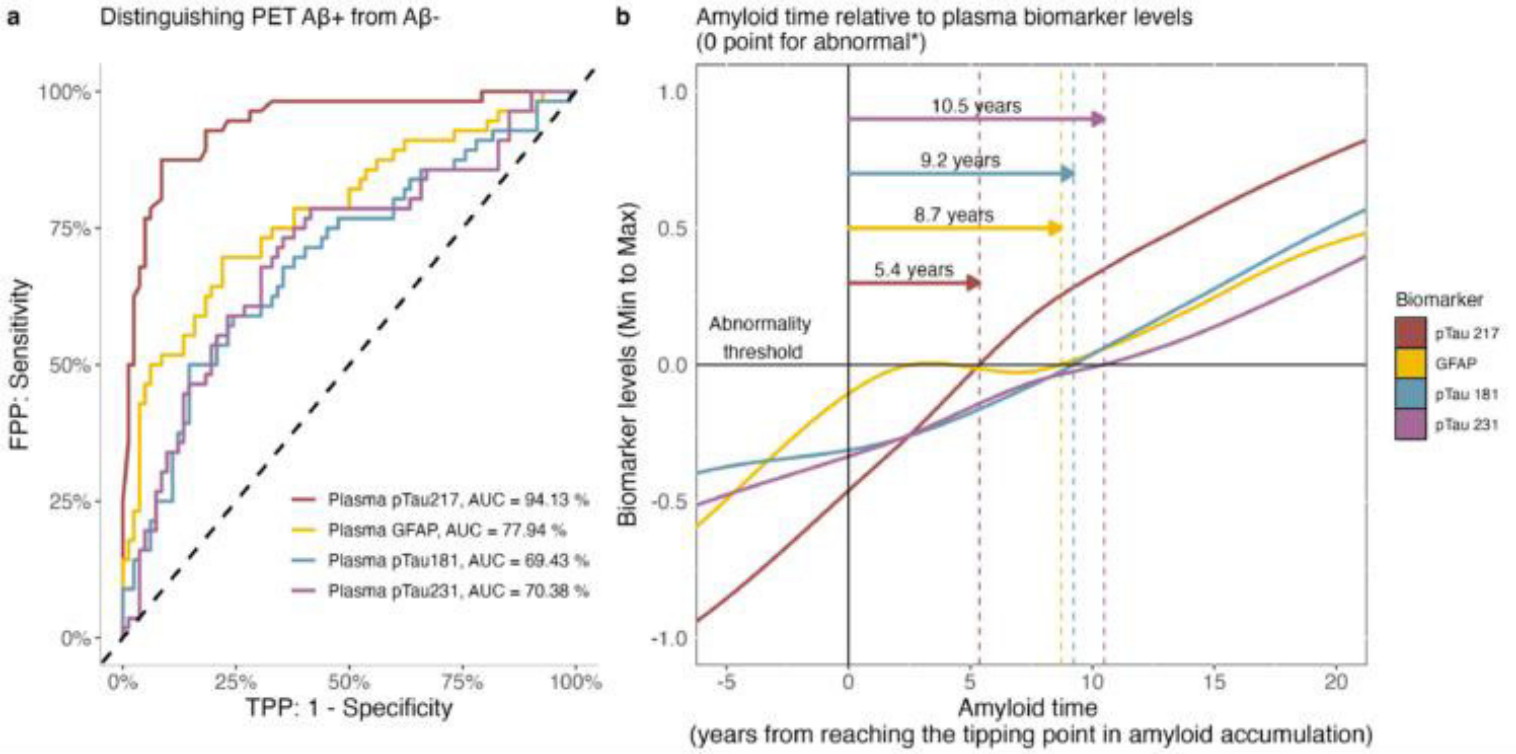


Figure 1. **(a)** Plasma biomarkers as predictors for amyloid PET visual read positivity: ROC curves show plasma pTau217 with the highest area under the curve (AUC, 94%), followed by GFAP (78%), pTau231 (70%), and pTau181 (69%). **(b)** Fitted trajectories of scaled biomarker data show different timing of abnormality onset with respect to the time of amyloid accumulation. Plasma pTau217 reached the abnormality at 5.4 years, GFAP at 8,7 years, pTau118 at 9.2 years, and pTau231 at 10.5 years. Biomarkers centred to the point of reaching the abnormal level corresponding to 90% sensitivity for amyloid positivity. Curves were fit with locally estimated scatterplot smoothing (LOESS) regression.

*Abnormality defined as biomarker threshold linked to 90% sensitivity for amyloid positivity.

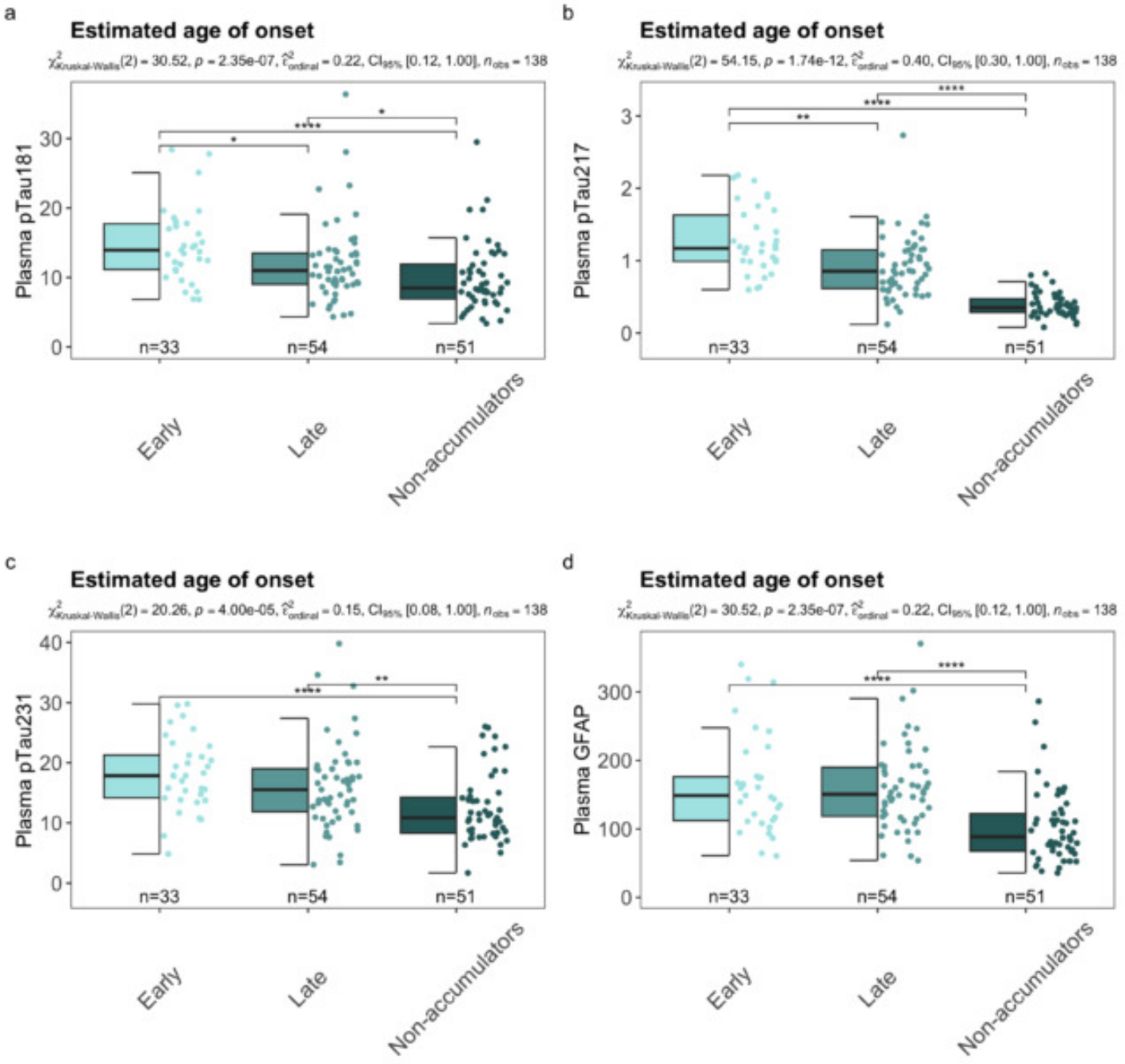


Figure 2. Boxplots showing differences and the post hoc pairwise comparison between the groups of early, late and non- accumulators. **(a)** Levels of pTau181 are increased in early amyloid accumulators. **(b)** Also, pTau217 levels are also significantly higher in early accumulators. (c-d) Plasma pTau231 and GFAP did not show significant differences between early and late accumulators. **(a-d)** All biomarkers were increased in accumulators compared to non-accumulators. The p values in the subtitles indicate the results from an analysis of variance conducted with the Kruskal–Wallis test. Post hoc analysis was carried out using Dunn's test, and corrections for multiple comparisons were made using the false discovery rate. *p < 0.05, **p < 0.01, ***p < 0.001, ****p < 0.0001.

Keywords: Plasma, biomarkers, Amyloid, PET, accumulation

Thursday, January 16, 2025 - 04:50 pm - 06:15 pm

Podium Session

SESSION VI: Heterogeneity

CHAIRS: Sylvia Villeneuve, David Wolk

Thursday, January 16, 2025		
04:50 pm - 06:15 pm	**SESSION VI** Heterogeneity	**Sylvia Villeneuve,** McGill University, Montreal, QC, Canada **David Wolk,** Penn Memory Center, Philadelphia, PA, USA
04:50 pm – 04:55 pm	Session Overview	**Chairs**
04:55 pm	Improving history-based prediction of biomarker and clinical progression of autosomal dominant Alzheimer's disease using mutation-level analysis of Aβ production	**Stephanie Schultz**, Harvard Medical School, Cambridge, MA, US
05:10 pm	Tau PET load in early- and late-onset Alzheimer's disease: A cross-sectional and longitudinal comparison of the LEADS and ADNI cohorts	**Konstantinos Chiotis**, University of California San Francisco, San Francisco, CA, US
05:25 pm	Regional tau quantification methodologies in early symptomatic participants with presence of tau pathology	**Diana Otero Svaldi**, Eli Lilly and Company, Indianapolis, IN, US
05:40 pm	Alpha Synuclein co-pathology accelerates amyloid associated tau accumulation in Alzheimer's disease	**Nicolai Franzmeier**, Institute for Stroke and Dementia Research (ISD), LMU University Hospital, Munich, DE
05:55 pm – 06:15 pm	Discussion	

Improving history-based prediction of biomarker and clinical progression of autosomal dominant Alzheimer's disease using mutation-level analysis of Aβ production

Stephanie Schultz[1], Yiwen Rao[1], Courtney Maa[1], Jean-Pierre Bellier[1], Lei Liu[1], Dennis Selkoe[1], Eric McDade[2], Richard Perrin[2], Brian Gordon[2], John Morris[2], Jorge Llibre-Guerra[2], Celeste Karch[2], Tammie Benzinger[2], Cahngjie Xiong[2], Johannes Levin[3], Mathias Jucker[11], Takeshi Ikeuchi[5], Nick Fox[6], Peter Schofield[7], Edward Huey[4], Ralph Martins[9], Gregory Day[8], Pedro Rosa-Neto[10], Randall Bateman[2], Jasmeer Chhatwal[1]

[1]*Harvard Medical School, Cambridge, MA, US*
[2]*Washington University in St. Louis, St. Louis, MO, US*
[3]*German Center for Neurodegenerative Diseases, Munich, DE*
[4]*Butler Hospital, Providence, RI, US*
[5]*Brain Research Institute, Niigata University, Niigata, JP*
[6]*Dementia Research Centre, UCL, London, GB*
[7]*Neuroscience Research Australia, Sydney, AU*
[8]*Mayo Clinic, Jacksonville, FL, US*
[9]*Edith Cowan University, Perth, AU*
[10]*McGill University, Montreal, QC, CA*
[11]*University of Tuebingen, Tuebingen, DE*

Introduction: In autosomal dominant Alzheimer's disease (ADAD) mutation carriers, age at symptom onset (AAO) is similar across families, enabling prediction of carriers' AAO from family history. However, comprehensive family histories are not available for all carriers. Furthermore, history-derived AAO, though informative, does not fully capture the clinical and biomarker heterogeneity seen in ADAD. We hypothesized that mutation-level measures of altered Aβ production may augment history-derived AAO in predicting disease course. Leveraging a cell-culture model that assesses Aβ production by individual mutations, we summarized mutation-level Aβ production. Notably, mutation-level Aβ production measurements are derived outside the context of family polygenic factors, age, and demographics, thereby potentially providing unique information regarding ADAD. Here, we examined whether this Aβ production composite can improve the prediction of ADAD clinical and biomarker progression using data from the Dominantly Inherited Alzheimer's Network study (DIAN).

Methods: 161 *PSEN1* variants were co-transfected with APP into HEK293 cells deficient in PSEN1/2, and Aβ-37/40/42 production was quantified for each variant. The composite measure of Aβ production was derived out-of-sample and then applied to 56 *PSEN1* variants with available clinical and biomarker data from DIAN (Figure 1, n=190 carriers).

Results: Mutation-level Aβ production was strongly associated with PiB-PET, grey-matter volume, and clinical measures, above and beyond APOE4, age, sex, and history-derived AAO, and improved the prediction of all clinical and biomarker measures assessed (Tables 1+2). History-derived AAO and the Aβ production composite were independently associated with amyloid-PET and grey-matter, and the inclusion of the Aβ production composite particularly improved the prediction of subcortical pathologic change (Figure 2).

Conclusions: Incorporation of a mutation-level cellular Aβ production measure improves prediction regarding the clinical and biomarker course of ADAD. Incorporating Aβ production measures may greatly improve our understanding of inter-individual heterogeneity in ADAD and improve the design and execution of ADAD clinical trials.

Table 1. Comparison of models including history-derived AAO and mutation-level composite of Aβ production.

	Cortical PiB-PET			Hippocampal GM Volume			CDR-SB		
	AIC	AIC Wt	Adj-R^2	AIC	AIC Wt	Adj-R^2	AIC	AIC Wt	Adj-R^2
Model 1	467.31	0.02	0.33	457.40	0.00	0.37	477.32	0.04	0.30
Model 2	439.71	0.00	0.23	442.53	0.00	0.41	477.20	0.04	0.30
Model 3	**459.84**	**0.98**	**0.36**	**426.69**	**1.00**	**0.46**	**470.83**	**0.93**	**0.33**

Comparison of Akaike Information Criterion (AIC), AIC weight (Wt), and adjusted- R-squared from a set of three linear regression models (lm):

Model 1: lm (Outcome ~ Covariates + history-derived AAO)
Model 2: lm (Outcome ~ Covariates + cell-based composite of Aβ production)
Model 3: lm (Outcome ~ Covariates + history-derived AAO + cell-based composite of Aβ production)

Outcome = Cortical PiB-PET SUVR, ICV-adjusted bilateral hippocampal grey matter (GM) volume (mm^3), or clinical Dementia Rating® Sum Boxes (CDR®-SB).
Covariates = APOE4 status, self-reported sex, and age for all models. Years of education included as additional covariate for CDR-SB model.

Best fitting model for each outcome is bolded.

Table 2. History-derived AAO and mutation-level composite of Aβ production predict cross-sectional PiB-PET, grey-matter volume, and clinical measures.

	Cortical PiB-PET		Hippocampal Grey Matter Volume		CDR-SB	
	β (SE)	P-value	β (SE)	P-value	β (SE)	P-value
Intercept	0.04 (0.12)	0.760	-0.09 (0.11)	0.383	0.02 (0.12)	0.864
Education	-	-	-	-	**-0.14 (0.06)**	**0.032**
APOE4 status	0.06 (0.13)	0.617	0.02 (0.12)	0.848	0.08 (0.13)	0.572
Sex	-0.19 (0.12)	0.105	0.18 (0.11)	0.093	-0.17 (0.12)	0.153
Age	**0.56 (0.06)**	**< 0.001**	**-0.64 (0.06)**	**< 0.001**	**0.55 (0.07)**	**< 0.001**
History-derived AAO	**-0.42 (0.07)**	**< 0.001**	**0.27 (0.06)**	**< 0.001**	**-0.21 (0.07)**	**0.004**
Aβ production comp.	**-0.20 (0.06)**	**0.002**	**0.34 (0.06)**	**< 0.001**	**-0.19 (0.07)**	**0.004**

Standardized estimates (SE) and p-values from linear regression models with dependent variables of interest for mean cortical PiB-PET (SUVR), bilateral hippocampal volume (mm^3; ICV-corrected), or CDR-SB and independent variables for APOE4 status, self-reported sex, age, history-derived AAO, and a cell-based composite of Aβ production. The model examining CDR Sum of Boxes (CDR-SB) was additionally adjusted for years of education. Terms were z-scored prior to being entered into the model. Terms with p-value < 0.05 are bolded.

Figure 1. Schematic overview of study design

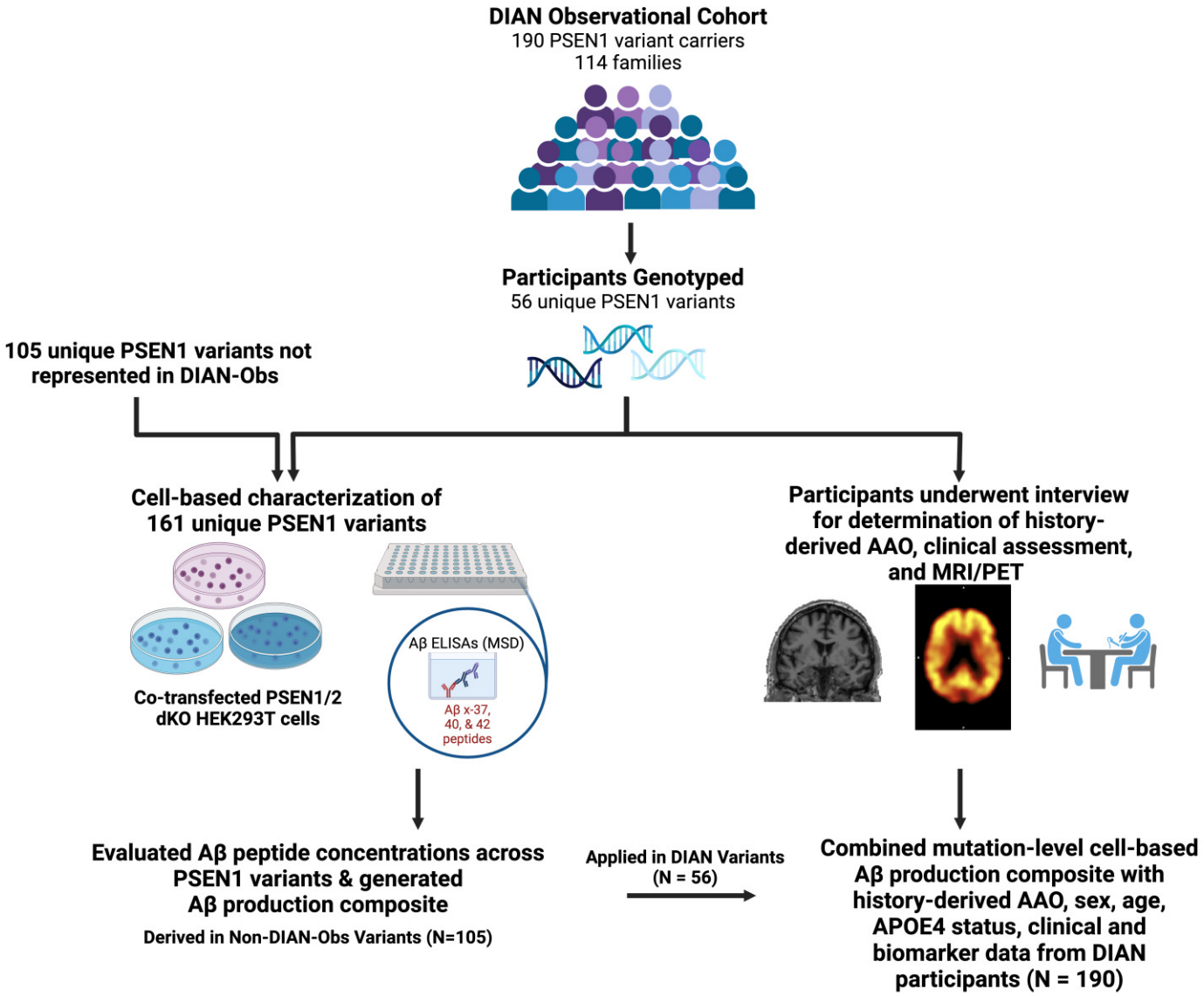
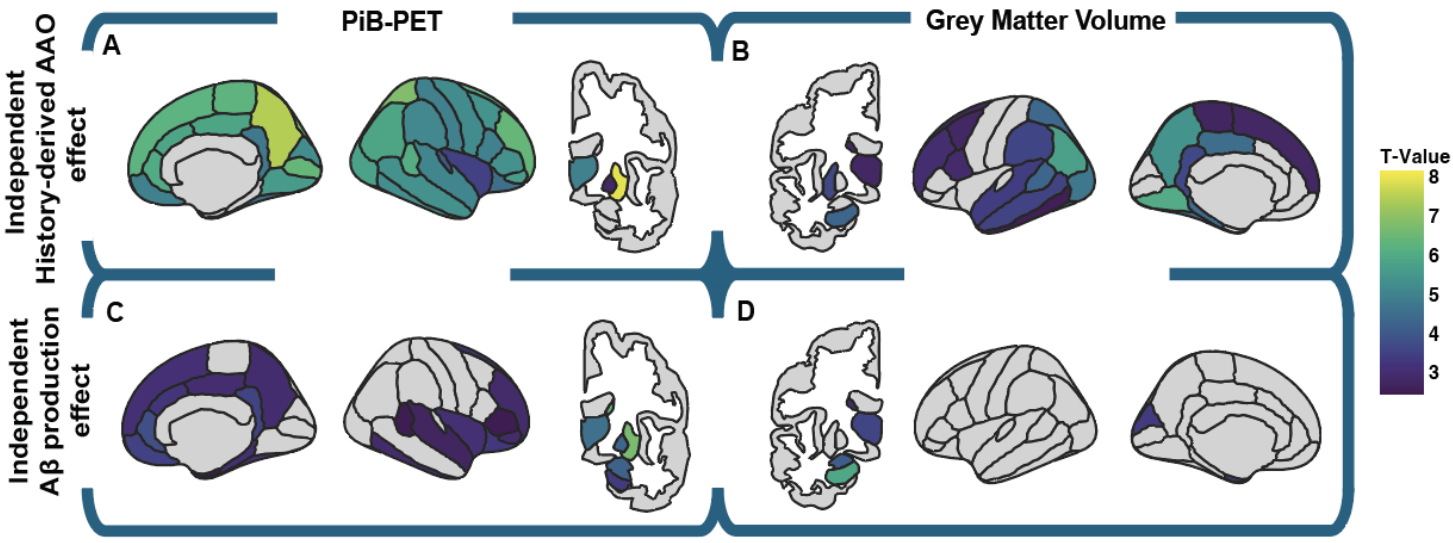


Figure 2. Mutation-level composite of Aβ production and history-derived AAO are independently associated with regional Aβ burden and grey matter volume



Linear regression models with dependent terms of interest for regional bilateral PiB-PET (SUVR) and regional bilateral grey-matter volume (mm3; ICV-corrected) and independent terms for APOE4 status, self-reported sex, age, history-derived AAO, and a cell-based composite of Aβ production were fitted (see Table 1 Model 3). T-values from history-derived AAO (A,B) and a cell-based composite of Aβ production (C,D) terms evaluating independent effects on regional PiB-PET (A,C) and grey-matter volumes (B,D) are depicted. The T-value scale for PiB-PET analyses was inverted. Regions where history-derived AAO or composite of Aβ production terms were not significant ($p > 0.05$) are depicted as grey.

Keywords: Gamma-secretase, heterogeneity, autosomal dominant Alzheimer's disease, Aβ production, cellular

Tau PET load in early- and late-onset Alzheimer's disease: A cross-sectional and longitudinal comparison of the LEADS and ADNI cohorts

Konstantinos Chiotis[1], Ganna Blazhenets[1], Daniel R. Schonhaut[1], Julien Lagarde[1], David Soleimani-Meigooni[1], Piyush Maiti[1], Jiaxiuxiu Zhang[1], Ranjani Shankar[1], Alinda Amuiri[1], Salma Rocha[1], Dustin B. Hammers[2], Ani Eloyan[3], Robert Koeppe[4], Maria C. Carrillo[5], Bradford C. Dickerson[6], Liana G. Apostolova[2], Renaud La Joie[1], Gil D. Rabinovici[1]

[1]*University of California San Francisco, San Francisco, CA, US*
[2]*Indiana University, Indianapolis, IN, US*
[3]*Brown University, Providence, RI, US*
[4]*University of Michigan, Ann Arbor, MI, US*
[5]*Alzheimer's Association, Chicago, IL, US*
[6]*Massachusetts General Hospital and Harvard Medical School, Boston, MA, US*

Aims: We aimed to assess differences in baseline and longitudinal tau PET tracer binding between early-onset Alzheimer's disease (EOAD) and late-onset Alzheimer's disease (LOAD) in the LEADS and ADNI cohorts, respectively.

Methods: We analyzed amyloid-beta PET-positive, cognitively impaired participants from the LEADS (EOAD; n=383) and ADNI (LOAD; n=196) cohorts with available ^{18}F-Flortaucipir tau PET data (Table 1). A subset had longitudinal ^{18}F-Flortaucipir PET data from LEADS (n=232) and ADNI (n=94) with average follow-up intervals of 1.95 and 2.44 years, respectively. All ^{18}F-Flortaucipir PET scans were processed using the CenTauR pipeline. Cognitively normal participants from LEADS (n=94) and ADNI (n=421) with baseline ^{18}F-Flortaucipir and amyloid-beta PET scans were also analyzed for comparison. We performed EOAD vs. LOAD comparisons using multivariate linear and linear mixed-effects models for cross-sectional and longitudinal analyses, respectively.

Table 1. Clinical characteristics of the patient sample

Characteristics	EOAD (LEADS), n = 383 [1]	LOAD (ADNI), n = 196 [1]	EOAD vs LOAD p-value [2]
Age in years at baseline	59.15 (4.03)	77.71 (6.62)	<0.001
Gender, female	208 (54%)	76 (39%)	<0.001
ApoE ε4 carriers	207 (56%) [3]	119 (63%) [3]	0.12
Clinical stage at baseline			<0.001
MCI	105 (27%)	123 (63%)	
Dementia	278 (73%)	73 (37%)	
Centiloids	97.73 (27.10)	85.59 (34.07)	<0.001
Education	15.62 (2.42)	15.99 (2.60)	0.10
CDR-SB at baseline	3.87 (1.99) [4]	2.58 (2.00) [4]	<0.001
MMSE at baseline	21.34 (5.40) [5]	25.61 (3.74)	<0.001
Follow-up interval in years	1.95 (0.97) [6]	2.44 (1.36) [6]	0.002

[1] Mean (SD); n (%), [2] Welch Two Sample t-test; Pearson's Chi-squared test; [3] Twelve cases with EOAD and seven with LOAD did not have available APOE genotyping; [4] Four cases with EOAD and four with LOAD did not have a CDR-SB assessment at baseline; [5] Seven cases with EOAD did not have MMSE assessment at baseline. [6] Longitudinal data were available for 232 cases with EOAD and 96 with LOAD.

Results: Baseline comparisons revealed large effect-size, significant differences in ^{18}F-Flortaucipir binding between EOAD and LOAD (Fig. 1). EOAD participants had higher ^{18}F-Flortaucipir levels in widespread neocortical regions compared to LOAD, after adjusting for covariates. In both groups, tau load was negatively associated with age. In EOAD, a significantly steeper slope was found in the association between amyloid-beta and ^{18}F-Flortaucipir load, as well as between cognitive scores and ^{18}F-Flortaucipir load. Longitudinally, EOAD participants exhibited a faster increase in ^{18}F-Flortaucipir binding than LOAD, predominantly in frontal and occipital areas (Fig. 2), with both groups showing an inverse linear relationship between ^{18}F-Flortaucipir accumulation rates and age.

Conclusion: EOAD patients demonstrate significantly higher tau loads, broader neuroanatomical involvement and faster tau accumulation over time compared to LOAD, independent of disease stage. These findings suggest that earlier age-of-onset in AD is linked to a more aggressive tauopathy. The early, extensive tau spread in symptomatic EOAD, even at an early clinical stage, may also limit the efficacy of anti-amyloid-beta therapies in this population.

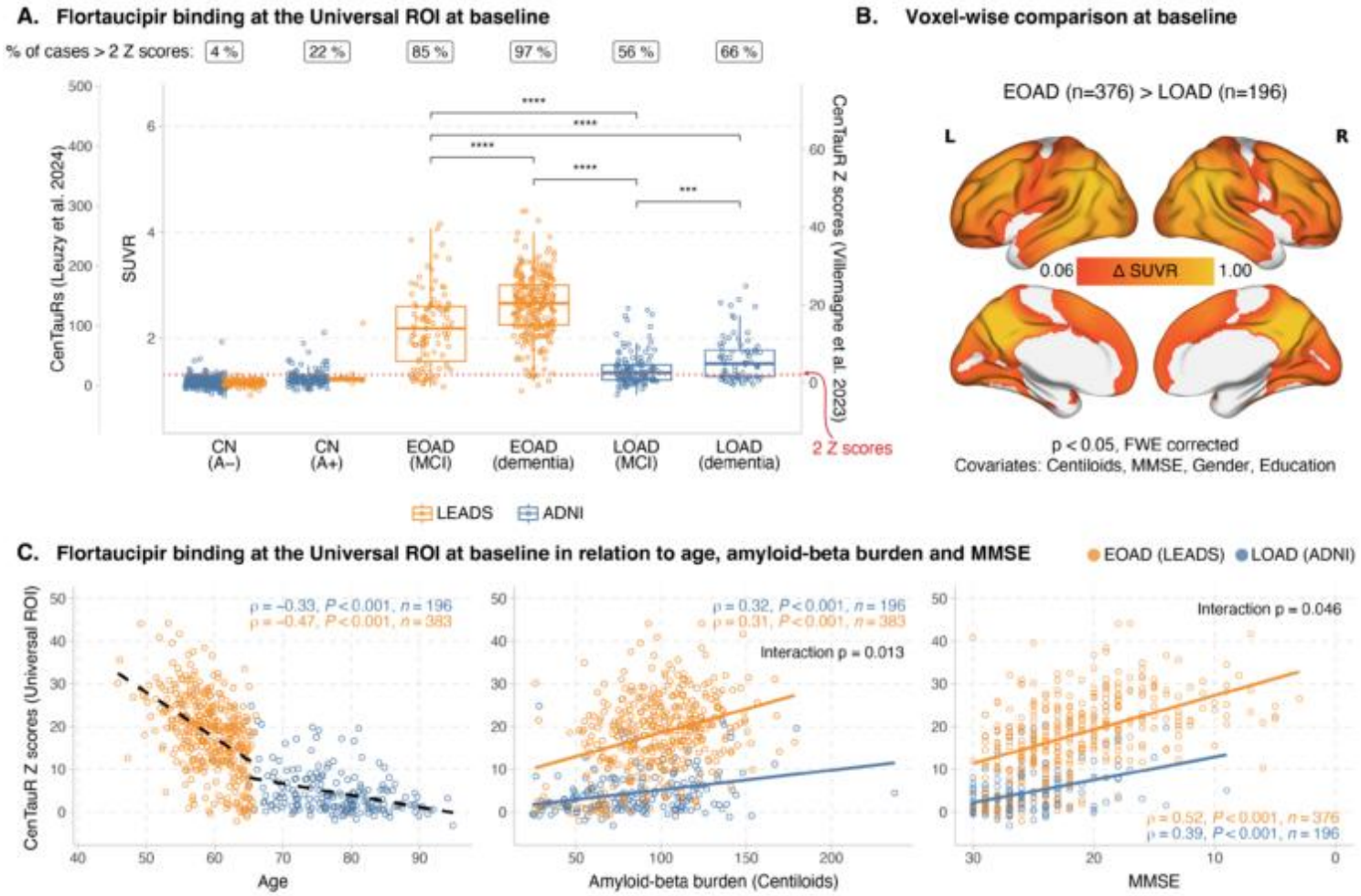


Figure 1. Group comparisons of cross-sectional ^{18}F-Flortaucipir binding in the CenTauR Universal region of interest (A), and using voxel-wise t-test (B). Association of ^{18}F-Flortaucipir binding with age, amyloid-beta burden and MMSE at baseline in EOAD and LOAD (C). Linear models assessing the association with amyloid-beta burden and MMSE were adjusted for gender, education, as well as MMSE and amyloid-burden, respectively. All models excluded data from n=7 patients with EOAD and missing baseline MMSE data.

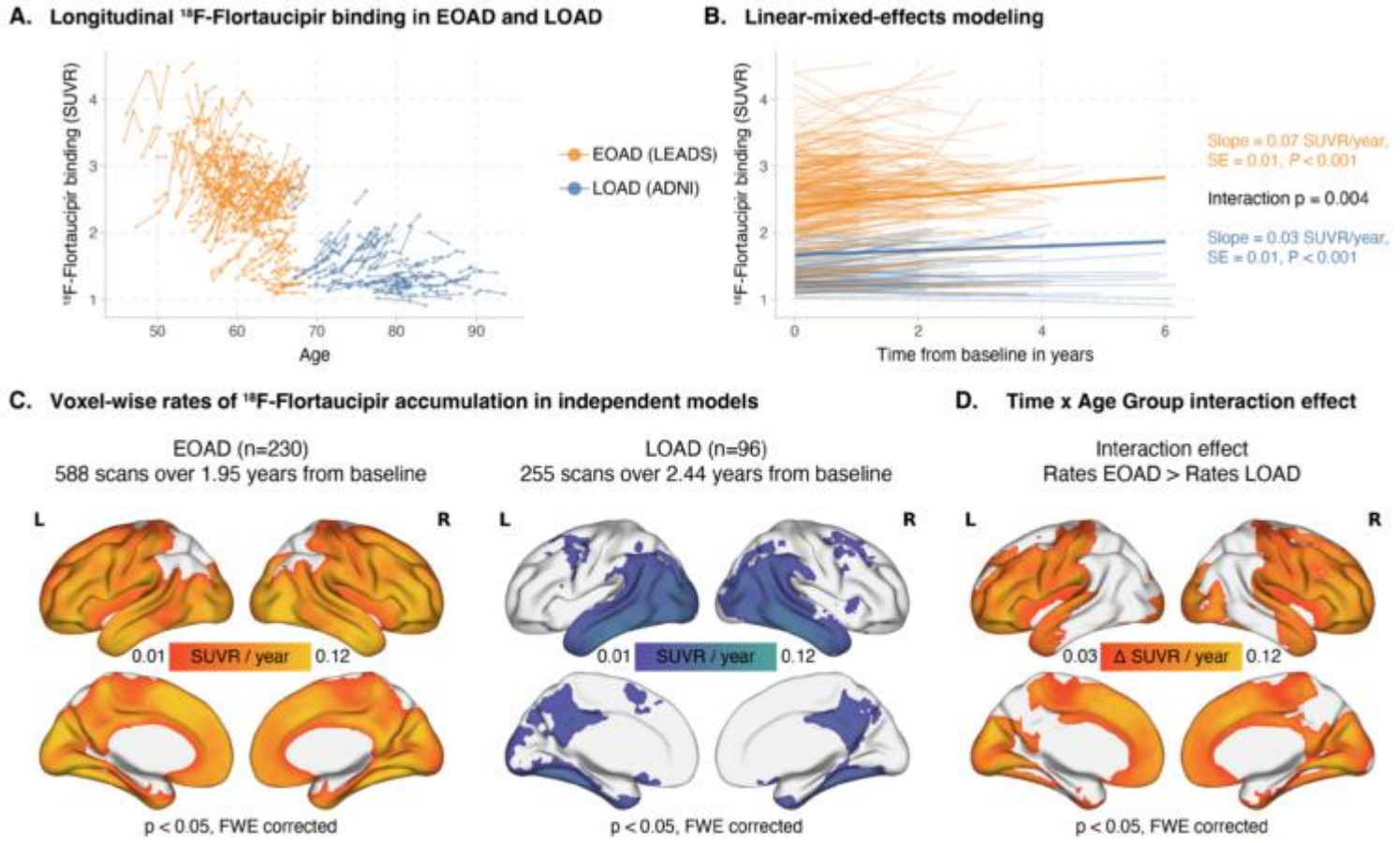


Figure 2. Longitudinal ^{18}F-Flortaucipir binding in the CenTauR Universal region of interest (A) and linear mixed-effects modeling in the same area (B). Voxel-wise linear mixed-effects models of increases in longitudinal ^{18}F-Flortaucipir binding separately in EOAD and LOAD (C), and when assessing the interaction term of time with age group (D). The linear mixed-effects models were adjusted for baselime amyloid-beta burden (Centiloids), MMSE, gender and education. The models included a random intercept (i.e., ID) and slope (i.e., time from baseline). All models excluded data from n=2 patients with EOAD with longitudinal tau PET data and missing baseline MMSE data.

Keywords: tau PET, EOAD, LOAD, age, amyloid

Regional tau quantification methodologies in early symptomatic participants with presence of tau pathology

Diana Otero Svaldi[1], Leonardo Iaccarino[1], Ixavier Alonzo Higgins[1], Nicolai Franzmeier[2], Michael Ewers[2], Sergey Shcherbinin[1]

[1]*Eli Lilly and Company, Indianapolis, IN, US*
[2]*Institute for Stroke and Dementia Research, University Hospital, Ludwig Maximilian University of Munich, Munich, DE*

Background: This study compares approaches for defining target regions in their ability to consistently capture tau progression relative to anatomical composites used in Alzheimer's disease trials.

Methods: Paired, baseline and 18-month regional flortaucipir data were included from TRAILBLAZER-ALZ2 (NCT04437511, Low/Medium/High Tau) and TRAILBLAZER-ALZ (NCT03367403, Low/Medium Tau) placebo participants. Regional SUVRs were combined into four composite regions according to individual- versus group-level and anatomical- versus data-driven approaches. Composites were defined and ranked according to hypothetical longitudinal spatial gradients based on descending mean regional SUVR (Q1→Q4). Anatomical composites were defined by lobes, whereas data-driven composites (quartiles) were defined by either baseline SUVR or functional connectivity (FC) to the highest baseline SUVR quartile. Group-level methodologies used mean regional SUVRs across participants, whereas individual-level used single participant regional SUVRs. Finally, the minimum positive composite (lowest SUVR>2 standard deviations (SD) above amyloid-negative cohort mean) was considered a target region. Longitudinal signal-to-noise (SNR) for each composite (mean/SD of change) and mean SNR across composites were compared to group lobar composites (reference method, Figure1A). Homogeneity between individual-level spatial gradients and across trial-level spatial gradients were evaluated for methods showing similar/superior SNR to reference.

Results: Group-level, data driven approaches exhibited lower mean SNR relative to the reference but provided increases in Q1 SNR (Figure1). Individualized methods exhibited similar/higher mean SNR, increased Q3-Q4 SNR (Figure1), and increased spatial homogeneity between participants (Figure2) and across trials (Figure3) versus the reference. Minimum positive composites exhibited superior SNR across individualized and anatomical methodologies (Figure1B). Spatial gradients were similar between SUVR-based and FC-based methodologies (Figures1-3).

Conclusions: Participant specific target regions may improve consistency in longitudinal tau PET analyses. For each participant, focusing on regions that have recently reached positivity may improve SNR. The similarity between SUVR-based and FC-based methods continues to suggest connectivity between regions is a significant mechanism contributing to tau spread.

Figure 1

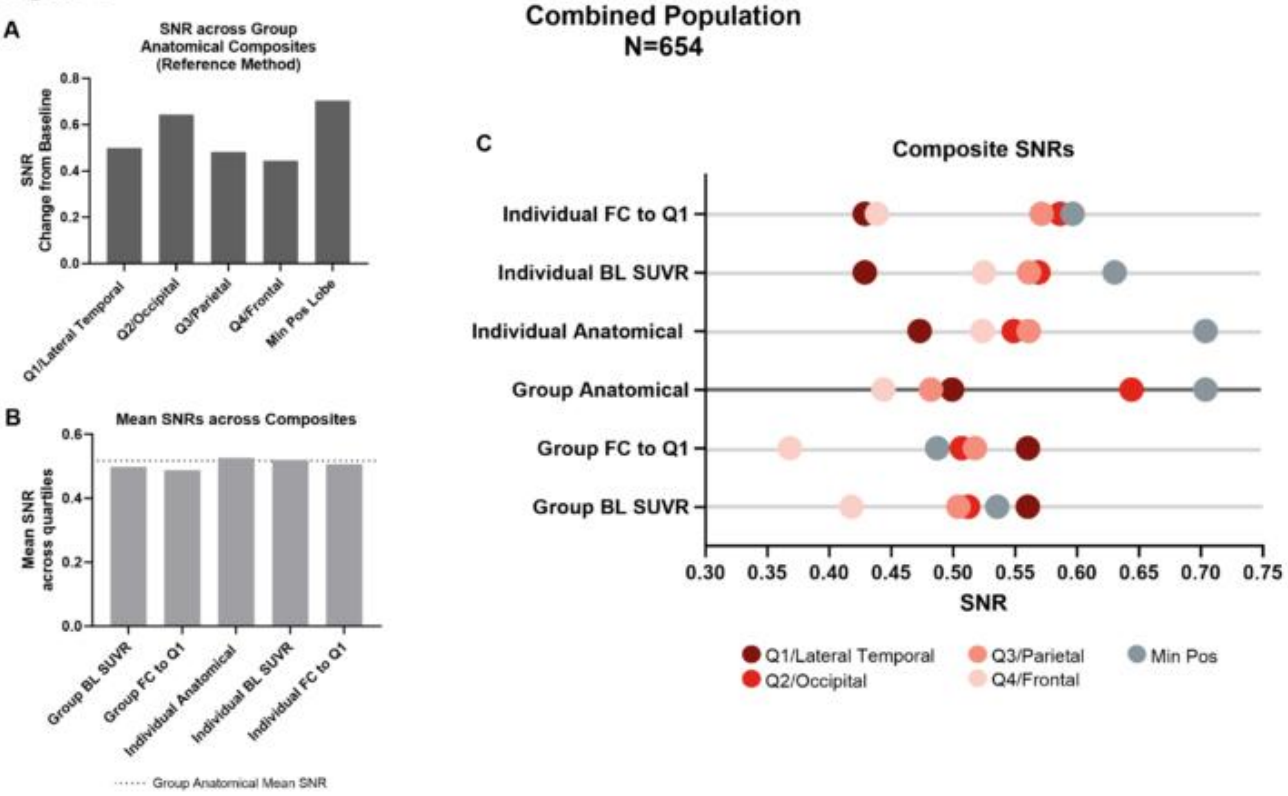
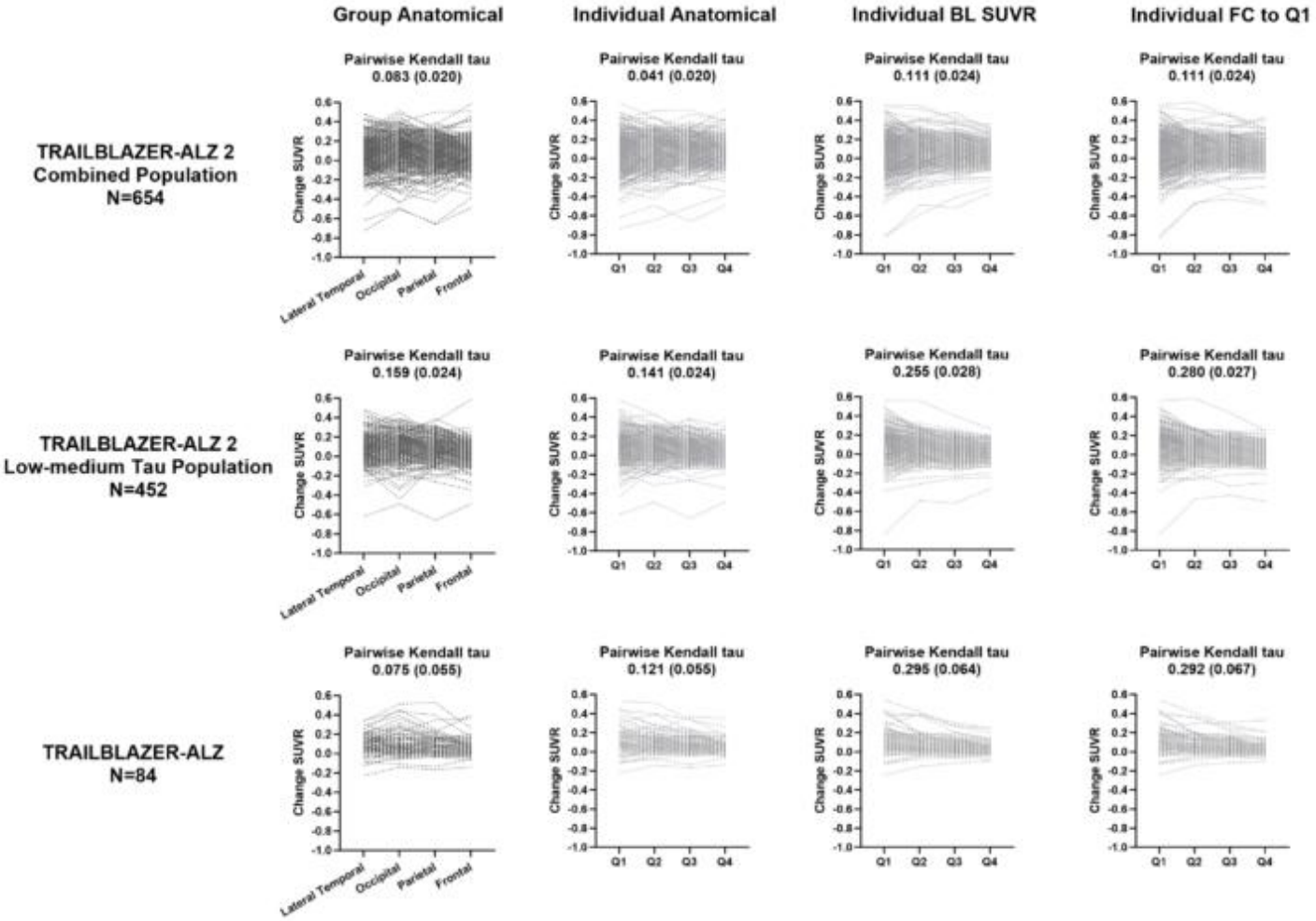
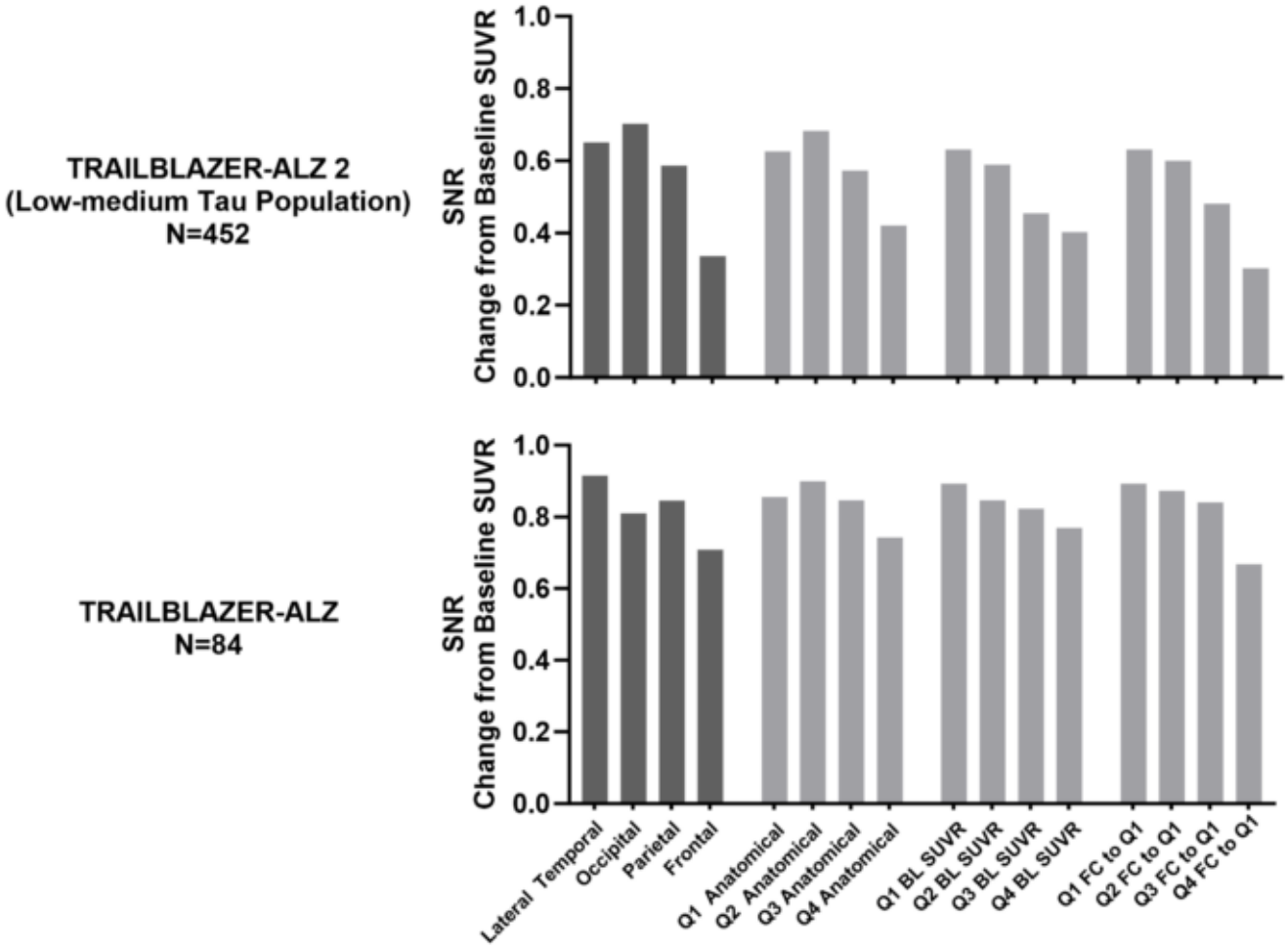

A
SNR across Group Anatomical Composites (Reference Method)
SNR Change from Baseline
0.0
0.2
0.4
0.6
0.8
Q1/Lateral Temporal
Q2/Occipital
Q3/Parietal
Q4/Frontal
Min Pos Lobe
B
Mean SNRs across Composites
Mean SNR across quartiles
0.0
0.2
0.4
0.6
Group BL SUVR
Group FC to Q1
Individual Anatomical
Individual BL SUVR
Individual FC to Q1
Group Anatomical Mean SNR
TRAILBLAZER-ALZ 2
Combined Population
N=654
C
Composite SNRs
Individual FC to Q1
Individual BL SUVR
Individual Anatomical
Group Anatomical
Group FC to Q1
Group BL SUVR
0.30
0.35
0.40
0.45
0.50
0.55
0.60
0.65
0.70
0.75
SNR
Q1/Lateral Temporal
Q2/Occipital
Q3/Parietal
Q4/Frontal
Min Pos

Figure 2. Pairwise Kendall's Tau of Hypothesized Spatial Tau Gradients Between Particiapants



Pairwise Kendall tau=mean (SE)

Figure 3. Composite SNRs in Order of Hypothesized Tau Spatial Gradient across Trials



Keywords: Tau PET, clinical trials, tau progression, target regions, functional connectivity

Alpha Synuclein co-pathology accelerates amyloid associated tau accumulation in Alzheimer's disease

Nicolai Franzmeier[1,2,3], Sebastian N Roemer[1,4], Alexander Bernhardt[4], Amir Amir Dehsarvi[1], Anna Dewenter[1], Anna Steward[1], Lukas Frontzkowski[1,5], Zeyu Zhu[1], Johannes Gnörich[5], Julia Pescoller[1], Fabian Wagner[1], Fabian Hirsch[1,2,3], Hannah DeBruin[6], Rik Ossenkoppele[6,7], Carla Palleis[4], Michael Schöll[3,8,9], Johannes Levin[2,4,10], Matthias Brendel[2,5,10], Guenter Hoeglinger[2,4,10]

[1]*Institute for Stroke and Dementia Research (ISD), LMU University Hospital, Munich, DE*
[2]*Munich Cluster for Systems Neurology (SyNergy), Munich, DE*
[3]*University of Gothenburg, The Sahlgrenska Academy, Institute of Neuroscience and Physiology, Department of Psychiatry and Neurochemistry, Gothenburg, SE*
[4]*Department of Neurology, LMU University Hospital, Munich, DE*
[5]*Department of Nuclear Medicine, University Hospital, LMU Munich, Munich, DE*
[6]*Alzheimer's Center, VU University Medical Center Amsterdam, Amsterdam, NL*
[7]*Clinical Memory Research Unit, Lund University, Lund, SE*
[8]*Wallenberg Centre for Molecular and Translational Medicine, University of Gothenburg, Gothenburg, SE*
[9]*Dementia Research Centre, Queen Square Institute of Neurology, University College London, London, GB*
[10]*German Center for Neurodegenerative Diseases (DZNE), Munich, DE*

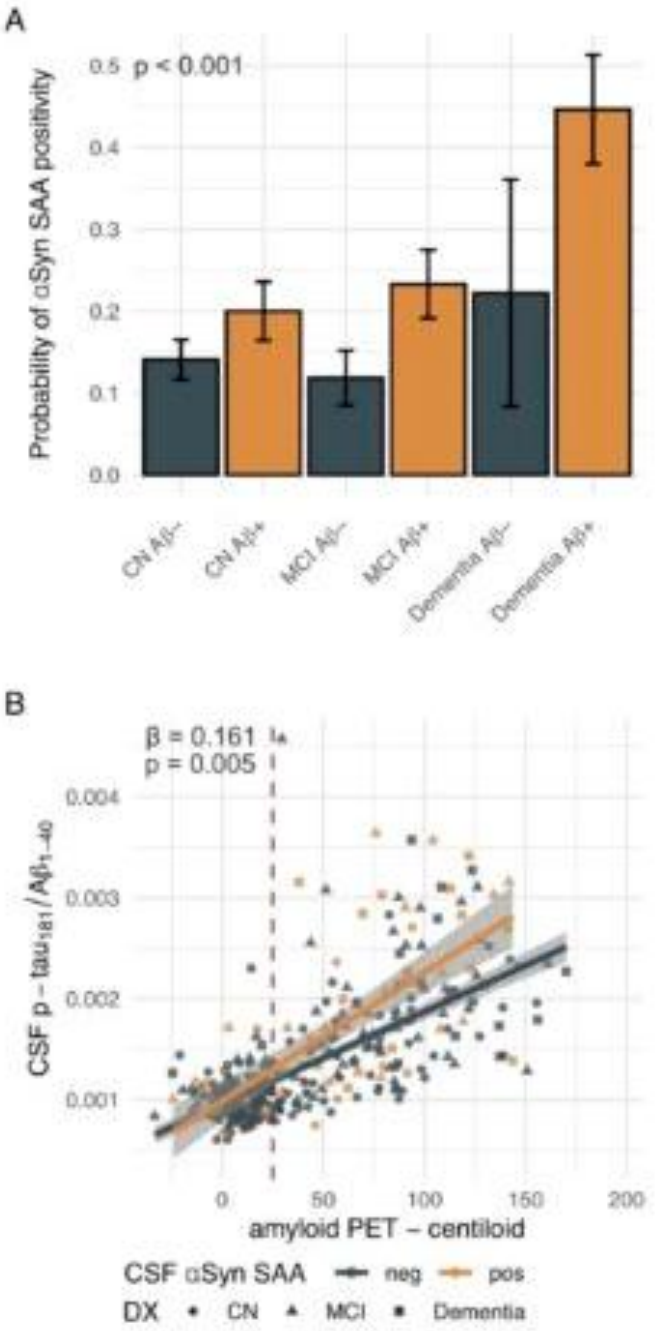
Objectives: Alpha-Synuclein (α-Syn) is a hallmark pathology in Parkinson's disease but also the most common co-pathology in Alzheimer's disease (AD). Preclinical studies suggest that α-Syn can amplify amyloid-beta (Aβ)-associated tau aggregation, implying that α-Syn co-pathology may contribute to the Aβ-induced tau aggregation observed in AD. To investigate this, we combined a novel CSF-based seed-amplification assay (SAA) to determine α-Syn positivity with PET neuroimaging in a large cohort ranging from cognitively normal individuals to those with dementia, examining whether α-Syn co-pathology accelerates Aβ-driven tau accumulation and cognitive decline.

Methods: In 284 Aβ-positive and 308 Aβ-negative subjects, we employed amyloid-PET, Flortaucipir tau-PET, and a CSF-based α-Syn SAA assay to detect in vivo α-Syn aggregation. CSF p-tau181 measures were available for 410 subjects to assess early tau abnormalities. A subset of 155 Aβ-positive and 135 Aβ-negative subjects underwent longitudinal tau-PET over approximately 2.5 years. Using linear regression models, we analyzed whether α-Syn positivity was linked to stronger Aβ-related increases in baseline fluid and PET tau biomarkers, faster Aβ-driven tau-PET increase, and more rapid cognitive decline.

Results: α-Syn positivity was more common in Aβ+ subjects (CN/MCI/Dementia: CN/MCI/Dementia: 20/23/45%, Fig.1A) and increased with clinical severity compared to Aβ- subjects (14/12/22%; $p<0.001$). α-Syn positivity was associated with stronger Aβ-related p-tau181 increases ($p=0.005$, Fig.1B), tau-PET uptake ($p<0.006$, Fig.2A-E), and faster Aβ-driven tau-PET increases ($p=0.024$, Fig.2F-J) over time in tau-vulnerable brain regions. Additionally, α-Syn positivity was linked to faster Aβ-related ($p<0.001$), but not tau-related, cognitive decline ($p=0.972$).

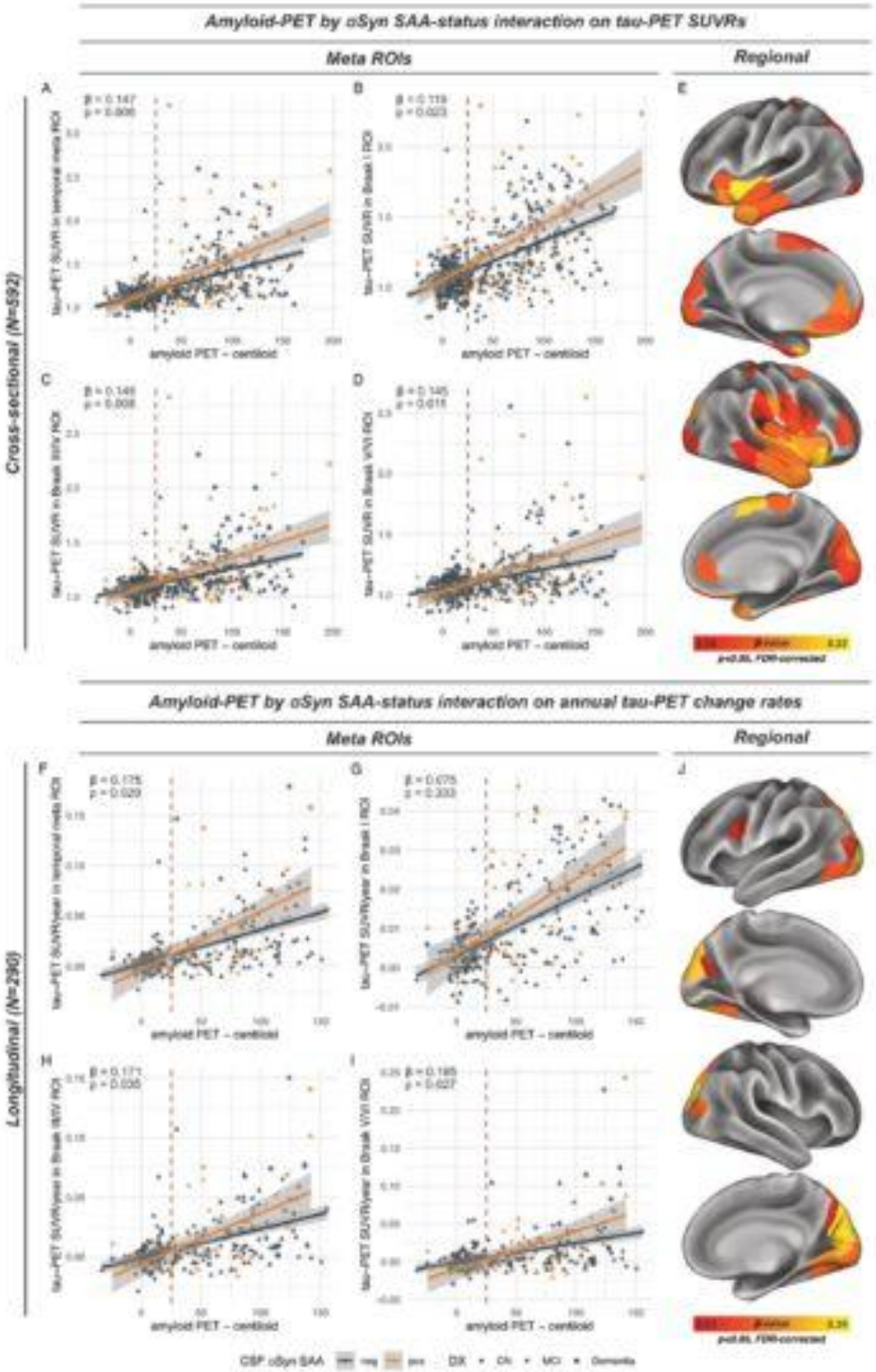
Conclusion: These findings suggest that α-Syn co-pathology, detectable via CSF-based SAA, is more prevalent in advanced AD and is associated with accelerated tau pathology which drives faster cognitive decline. This highlights that a-Syn co-pathology may accelerate amyloid-driven AD pathophysiology.

Figure 1:



Barplot, illustrating the probability of αSyn SAA positivity stratified by amyloid status and clinical syndrome severity (A). Scatterplot illustrating the interaction effect between amyloid-PET and αSyn SAA status on cross-sectional levels of CSF p-Tau$_{181}$/Aβ$_{1-40}$ as an indicator of earliest tau pathophysiology. Diagnostic groups are indicated by shape, the cut-point of amyloid-PET positivity is indicated by the dashed red line at 25 centiloids. The beta value indicates the strength of the amyloid-PET x CSF αSyn SAA interaction effect.

Figure 2:



Scatterplots illustrating the interaction effect between global amyloid-PET (i.e. centiloid) and aSyn SAA status on tau-PET SUVRs for meta ROIs (A-D) and regional analyses (E), as well as for annual tau-PET SUVR change rates (F-J). Diagnostic groups are indicated by shape, the cut-point of amyloid-PET positivity is indicated by the dashed red line at 25 centiloids. Beta value indicates the strength of the amyloid-PET x CSF aSyn SAA interaction effect.

Keywords: Amyloid, tau, alpha synuclein, tau aggregation

Friday, January 17, 2025 - 09:00 am - 10:40 am

Podium Session

SESSION VII: Factors which Influence ATN

CHAIRS: Heidi Jacobs, Suzanne Schindler

Friday, January 17, 2025		
09:00 am - 10:40 am	**SESSION VII** Factors which Influence ATN	**Heidi Jacobs,** Massachusetts General Hospital, Boston, MA, USA **Suzanne Schindler**, Washington University School of Medicine in St Louis, St Louis, MO, USA
09:00 am – 09:05 am	Session Overview	**Chairs**
09:05 am	Evaluating the ATN framework in a racially and ethnically diverse cohort: Preliminary analysis from the Health Aging Brain Study- Health Disparities Study	**Ann D. Cohen**, University of Pittsburgh School of Medicine, Department of Psychiatry, Pittsburgh, PA, US
09:20 am	Racial and ethnicity differences in plasma biomarker eligibility prior to amyloid PET imaging in the AHEAD 3-45 Study	**Doris Molina-Henry**, Alzheimer's Therapeutic Research Institute, University of Southern California, San Diego, CA, US
09:35 am	Examining neighborhood disadvantage as a factor explaining amyloid onset age	**Margo B. Heston**, Wisconsin Alzheimer's Disease Research Center, University of Wisconsin School of Medicine and Public Health, Madison, WI, US
09:50 am	Intersections of sex and neighborhood disadvantage on Alzheimer's disease pathology	**Alexandria Reese**, Department of Epidemiology, University of Pittsburgh, Pittsburgh, PA, US
10:05 am	Sex moderates relationships between P-Tau217 and longitudinal tau-PET: A multi-cohort study	**Gillian Coughlan**, Department of Neurology, Massachusetts General Hospital, Harvard Medical School, Boston, MA, US
10:20 am – 10:40 am	Discussion	

Evaluating the ATN framework in a racially and ethnically diverse cohort: Preliminary analysis from the Health Aging Brain Study- Health Disparities Study

Ann D. Cohen[1], Michael C. Donohue[2], Beau Ances[3], Karin L. Meeker[4], Julie Wisch[3], Meredith N. Braskie[5], Melissa Petersen[4], Leigh A Johnson[4], Robert A. Rissman[2], Arthur W. Toga[5], Kristine Yaffe[6], Sid O'Bryant[4]

[1]*University of Pittsburgh School of Medicine, Department of Psychiatry, Pittsburgh, PA, PA, US*
[2]*Alzheimer's Therapeutic Research Institute, University of Southern California, San Diego, CA, US*
[3]*Washington University School of Medicine Department of Neurology, St. Louis, MO, US*
[4]*University of North Texas, Health Science Center, Fort Worth, TX, US*
[5]*University of Southern California, Stevens Neuroimaging and Informatics Institute, Los Angeles, CA, US*
[6]*University of California, San Francisco; Weill Institute for Neurosciences, San Francisco, CA, US*

A key concept underlying Alzheimer's disease (AD) is the presence of Aβ (A). This preclinical stage of AD is expected to progress to neocortical Tau (T), neurodegeneration (N), and dementia. However, this "ATN" progression remains to be fully validated in diverse populations. The goal of Health Aging Brain Study- Health Disparities (HABS-HD), is to conduct an assessment of ATN imaging biomarkers across adulthood . Here, we explore whether the temporal ordering of ATN in HABS-HD differs across racialized groups.

In 1,833 participants underwent MRI (N), [18F]Florbetaben (A), [^{18}F]PI-2620 (T) PET, white matter hyperintensities, and HPACC scores (Table 1). To estimate disease progression curves in each group we estimated the predominant sequence of AT(N), WMH, and cognitive trajectories and compare them. We utilized the latent time joint mixed effect model (LTJMM). A latent time parameter is used to estimate where individuals reside on the long-term time scale. This latent time parameter is estimated by considering all five markers in a "joint" model.

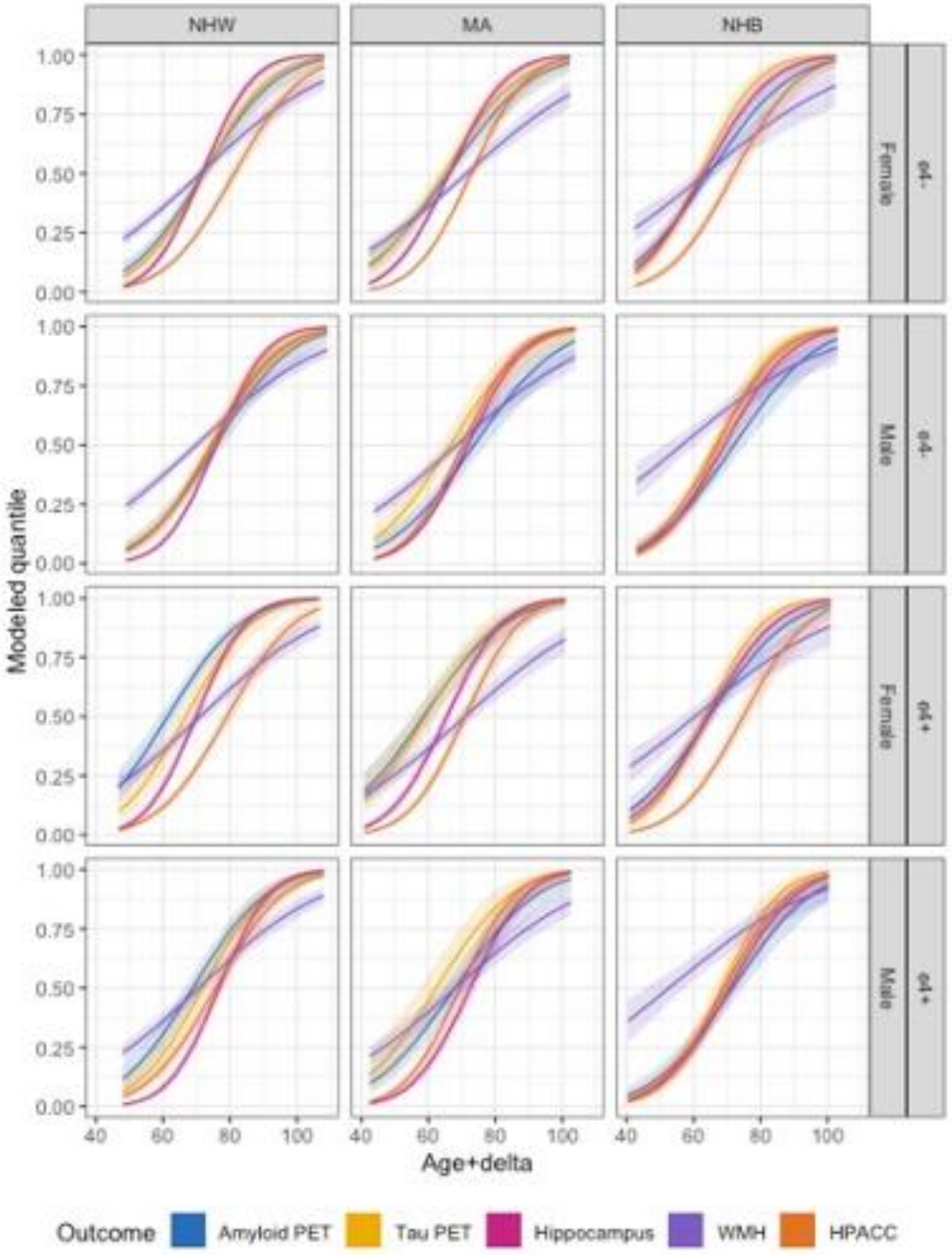
NHW participants demonstrated the highest proportion of cognitively unimpaired participants but also the highest proportion of amyloid-positive participants (25% vs 13% MA vs 15% NHB). LTJMM prediction models demonstrate among NHW participants, A increases earliest, followed by T and N, as previously reported. However, among MA and NHB participants, there is very little distinction between the temporal increases in ATN (Figure 1). Unlike NHW participants, in MA APOE4 carriers, tau appears to be the earliest pathology to increase while there is very little temporal distinction in NHB APOE4 carriers (Figure 1).

Among a racially/ ethnically diverse group of individuals ATN curves differ substantially suggesting that the ATN model may not be generalizable across diverse populations.

Table 1

	NHW (N=1082)	MA (N=1079)	NHB (N=605)	Total (N=2766)	p value
Ethnicity/Language					< 0.001[1]
NHW	1082 (100.0%)	0 (0.0%)	0 (0.0%)	1082 (39.1%)	
MA-English	0 (0.0%)	368 (34.1%)	0 (0.0%)	368 (13.3%)	
MA-Spanish	0 (0.0%)	711 (65.9%)	0 (0.0%)	711 (25.7%)	
Other	0 (0.0%)	0 (0.0%)	605 (100.0%)	605 (21.9%)	
DX					< 0.001[1]
CN	882 (81.5%)	787 (72.9%)	359 (59.3%)	2028 (73.3%)	
MCI	144 (13.3%)	219 (20.3%)	197 (32.6%)	560 (20.2%)	
Dementia	56 (5.2%)	73 (6.8%)	49 (8.1%)	178 (6.4%)	
Age					< 0.001[2]
Mean (SD)	68.5 (8.7)	63.3 (8.0)	62.9 (7.8)	65.2 (8.7)	
Range	50.0 - 92.0	50.0 - 91.0	50.0 - 90.0	50.0 - 92.0	
Gender					< 0.001[1]
male	462 (42.7%)	362 (33.5%)	211 (34.9%)	1035 (37.4%)	
female	620 (57.3%)	717 (66.5%)	394 (65.1%)	1731 (62.6%)	
HPACC					< 0.001[2]
Missing	18	40	4	62	
Mean (SD)	0.6 (4.0)	-3.2 (4.7)	-1.9 (4.3)	-1.4 (4.7)	
Range	-18.8 - 11.8	-24.1 - 7.8	-19.6 - 7.4	-24.1 - 11.8	
APOEe4					< 0.001[1]
Negative	763 (70.5%)	868 (80.4%)	365 (60.3%)	1996 (72.2%)	
Positive	319 (29.5%)	211 (19.6%)	240 (39.7%)	770 (27.8%)	
ABeta positive					0.002[1]
Missing	819	876	23	1718	
Mean (SD)	0.2 (0.4)	0.1 (0.4)	0.2 (0.4)	0.2 (0.4)	
Range	0.0 - 1.0	0.0 - 1.0	0.0 - 1.0	0.0 - 1.0	
First TAU Med Temp SUVR					0.301[2]
Missing	657	782	275	1714	
Mean (SD)	1.1 (0.1)	1.2 (0.1)	1.1 (0.2)	1.1 (0.2)	
Range	0.9 - 2.1	0.8 - 2.1	0.8 - 2.6	0.8 - 2.6	
First Hippocampus (scanner adjusted)					< 0.001[2]
Missing	2	4	3	9	
Mean (SD)	6367.9 (870.3)	6414.7 (792.9)	6224.6 (779.9)	6354.9 (824.2)	
Range	2952.7 - 8785.9	3207.6 - 8904.7	2311.7 - 8220.7	2311.7 - 8904.7	
Average ICV (scanner adjusted)					< 0.001[2]
Mean (SD)	1459657.7 (145251.5)	1376203.2 (130068.5)	1409040.0 (129189.7)	1416031.1 (140942.2)	
Range	1070578.2 - 1967786.6	1036566.4 - 1772465.9	1095237.5 - 1783949.5	1036566.4 - 1967786.6	

Participant demographics



LTJMM prediction plots by sex and e4 status

Keywords: Health disparities, ATN, PET

Racial and ethnicity differences in plasma biomarker eligibility prior to amyloid PET imaging in the AHEAD 3-45 Study

Doris Molina-Henry[1,8], Rema Raman[1,8], Andy Liu[1,8], Oliver Langford[1,8], Joel Braunstein[2], Shobha Dhadda[3], Michael Irrizary[3], Joshua Grill[4,5,8], Keith Johnson[6,7,8], Robert Rissman[1,8], Paul Aisen[1,8], Reisa A Sperling[6,7,8], AHEAD 3-45 Study Team[8]

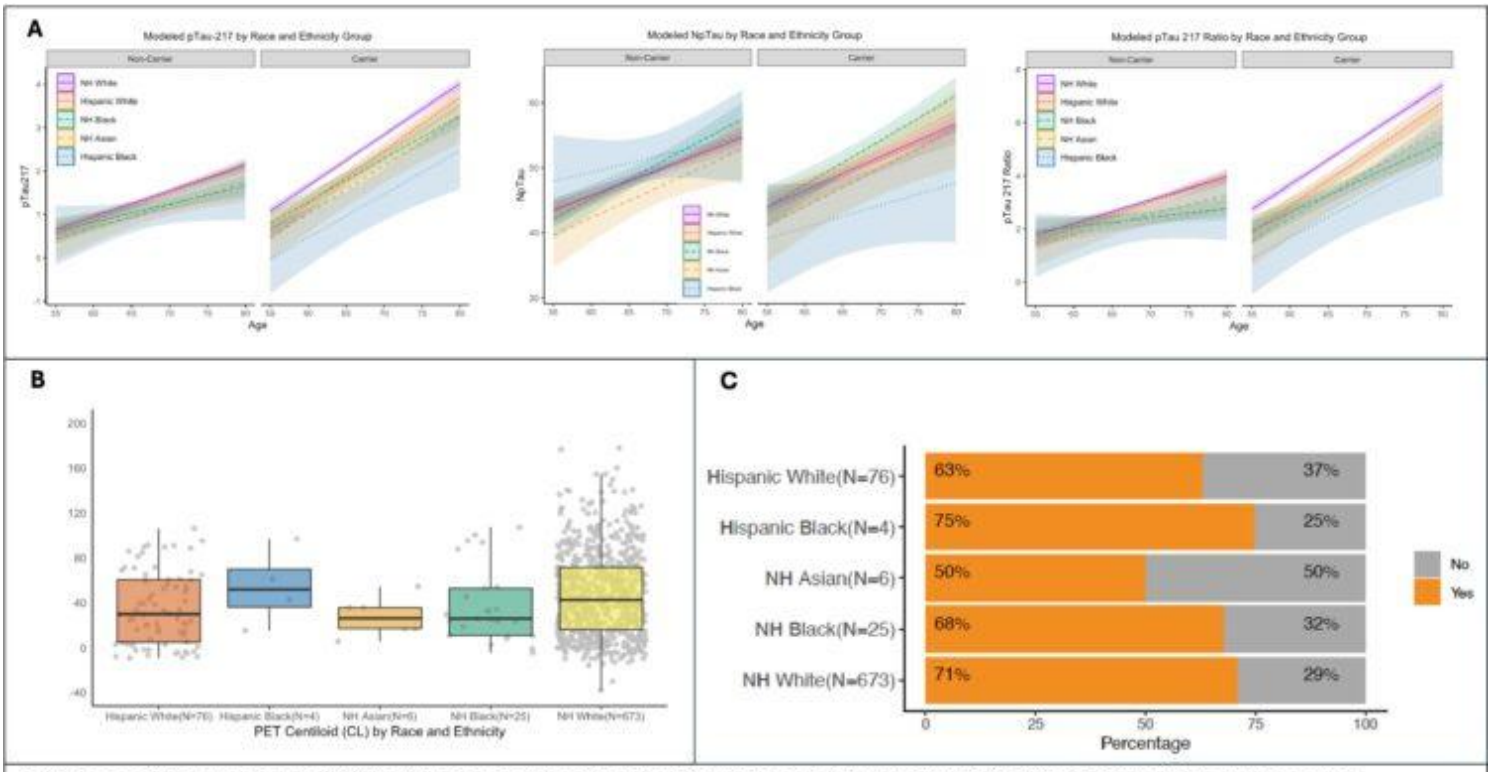
[1]*Alzheimer's Therapeutic Research Institute, University of Southern California, San Diego, CA, US*
[2]*C2N Diagnostics, St. Louis, MO, US*
[3]*Eisai Inc., Nutley, NJ, US*
[4]*Institute for Memory Impairments and Neurological Disorders, University of California Irvine, Irvine, CA, US*
[5]*University of California Irvine, Irvine, CA, US*
[6]*Massachusetts General Hospital, Harvard Medical School, Boston, MA, US*
[7]*Brigham and Women's Hospital, Boston, MA, US*
[8]*Alzheimer's Clinical Trials Consortium, https://www.actcinfo.org/, US*

The AHEAD 3-45 Study utilized a shared screening algorithm to enroll cognitively unimpaired individuals into two sister trials (A3 and A45) testing targeted dosing of lecanemab based on screening amyloid PET. A major goal of the AHEAD Study recruitment process was to improve the inclusion of racial and ethnic under-represented groups (RE-URG). A plasma screening algorithm was introduced as the first step to minimize potential bias in cognitive and clinical eligibility criteria that disproportionately exclude these groups prior to PET.

We assigned participants in North America to mutually exclusive groups based on self-reported race and ethnicity: Hispanic Black (HB), Hispanic White (HW), Non-Hispanic Asian (NHA), Non-Hispanic Black (NHB) and Non-Hispanic White (NHW). A plasma algorithm utilized C2N mass spectrometry for Ab 42/40 and phosphorylated-tau 217 (p-tau217)/non-phosphorylated-tau (np-tau) ratio, and included age and APOE. Participants who were "plasma eligible" underwent amyloid PET imaging (^{18}F-NAV4694) to determine trial eligibility.

In North America, 11,678 individuals underwent plasma screening. NHW APOE e4 carriers showed higher levels of p-tau217 at almost all ages compared to NHB and HB e4 carriers (Figure 1A). A steeper age-related rise in np-tau was observed in NHB, which lowered the p-tau217 ratio at older ages. Overall RE-URG participants had significantly lower rates of plasma eligibility (p=0.001). Among participants who met plasma eligibility, mean CL values tended to be lower among RE-URG (Figure 1B) but amyloid PET eligibility (>20CL) rates were similar (Figure 1C).

RE-URG showed lower rates of plasma biomarker eligibility, with evidence of an age delay in accumulation compared to NHW, particularly among APOE e4 carriers. Among plasma eligible participants, PET eligibility rates were similar across groups, suggesting that the same plasma prediction algorithms were appropriately applied across race and ethnic groups. These findings support prior evidence suggesting that prevalence of amyloid pathology may be lower in some RE-URG.



A. Cross-sectional plasma p-tau217 (Left), non-phosphorylated tau (Center) and p-tau217/np-tau (Right) in 11,678 AHEAD screens across race/ethnicities by age divided by APOE4 carrier status. Interestingly, the p-tau217 suggests parallel accumulation but with different intercepts (potential age offset for positivity) but non-phosphorylated tau (and the ratio) shows increasing slope associated with age in some URG, consistent with greater contribution of co-morbidities, such as impaired renal clearance. **B.** PET Centiloids (CL) levels by RE-URG in a subgroup of plasma eligible individuals who underwent PET neuroimaging (n=784). Most RE-URG trended toward lower PET CL levels, with slightly higher levels in NH White. (p=0.04). **C.** Bar plots reflecting PET eligibility rates among participants who were plasma eligible. PET eligibility rates are not different by race and ethnicity (p=0.4) supporting our previous data suggesting that the same plasma prediction algorithms were appropriately applied across race and ethnic groups.

Keywords: plasma, biomarkers, ethnicity, amyloid, race

Examining neighborhood disadvantage as a factor explaining amyloid onset age

Margo B. Heston[1,2], Rebecca E. Langhough[1,3], Will R. Buckingham[2], Jacob Morse[1], Elena Ruiz de Chavez[1], Richard J. Chappell[1,4], Sterling C. Johnson[1,3], Sanjay Asthana[1], Brian A. Gordon[5], Carey E. Gleason[1], Lindsay R. Clark[1], Barbara B. Bendlin[1,2,3], W. Ryan Powell[2], Megan L. Zuelsdorff[1,2,6], Tobey J. Betthauser[1,2]

[1]*Wisconsin Alzheimer's Disease Research Center, University of Wisconsin School of Medicine and Public Health, Madison, WI, US*
[2]*Center for Health Disparities Research, University of Wisconsin School of Medicine and Public Health, Madison, WI, US*
[3]*Wisconsin Alzheimer's Institute, University of Wisconsin School of Medicine and Public Health, Madison, WI, US*
[4]*Department of Biostatistics and Medical Informatics, University of Wisconsin School of Medicine and Public Health, Madison, WI, US*
[5]*Knight Alzheimer's Disease Research Center, Washington University School of Medicine in St. Louis, St. Louis, MO, US*
[6]*University of Wisconsin-Madison School of Nursing, Madison, WI, US*

Background: Social factors including neighborhood disadvantage have shown associations with higher postmortem amyloid burden, lower hippocampal volume, and accelerated trajectories of cortical thinning and cognitive decline, but it is unknown if disadvantage affects when AD pathology begins. This work investigates whether amyloid onset age differs between most and least disadvantaged neighborhood groups.

Methods: We included amyloid PET data from the Wisconsin ADRC (WADRC)/Wisconsin Registry for Alzheimer's Prevention (WRAP) and Washington University Knight ADRC (WashU) (Ns=787 and 738; **Table 1**). Cortical amyloid was quantified averaging ^{11}C-Pittsburgh compound B DVR_{LGA} across AAL3-defined regions (WADRC) and ^{11}C-PiB $SUVR_{30\text{-}60}$/^{18}F-Florbetapir $SUVR_{50\text{-}70}$ across Freesurfer-defined regions (WashU, cerebellar cortex reference); WashU SUVRs were converted to Centiloids. We applied sampled iterative local approximation (SILA) across cohorts separately to model amyloid accumulation and estimate individual A+ onset age (EAOA). A+ was defined as global DVR>1.16 (CL>17.10) and CL>14.76 using GMM. Area deprivation index (ADI) measured neighborhood disadvantage (2020 vintage), binarizing state decile rankings to compare EAOA between participants in the 30% most and 70% least disadvantaged neighborhoods. Cox proportional hazards regression tested ADI effects on A+ risk, controlling for *APOE*, sex, and baseline age; Kaplan-Meier curves illustrated risk model effects.

Results: Cohort differences were observed for proportion of A+, baseline age, and composition across diagnosis, sex and race, but not ADI (**Table 1, Figure 1 bottom**). Cox regression **(Figure 2**) indicated ADI was not associated with A+ risk or EAOA (**Figure 1 top**, *p*s=.43,.09) while confirming *APOE* main effects. Female sex was associated with earlier EAOA in WashU (*p*=.01; WADRC/WRAP *p*=.44), however ADI-by-sex effects were nonsignificant in exploratory testing (*p*s=.57,.13).

Discussion: Results in two cohorts suggest neighborhood disadvantage does not influence A+ onset age, however samples had low representation of highly disadvantaged neighborhoods. Future work in larger samples will investigate whether ADI affects time from A+ onset to dementia.

Table 1. Participant demographics stratified by study cohort

Characteristic	WADRC and WRAP N = 787	WashU (OASIS) N = 738	*P* value
A+ at/before last PET scan, n (%)	264 (34)	315 (43)	<0.001†
Age at baseline, mean (SD) years	66.0 (8.02)	68.9 (8.72)	<0.001*
Neighborhood disadvantage exposure, n (%)			0.11†
30% most disadvantaged	104 (13)	78 (11)	
70% least disadvantaged	683 (87)	660 (89)	
Clinical diagnosis, n (%)			<0.001‡
Cognitively unimpaired	649 (83)	539 (74)	
Mild cognitive impairment	106 (13)	30 (4.1)	
Dementia	25 (3.2)	157 (22)	
Impaired: not AD	6 (0.8)	0 (0)	
Unknown	1	12	
Sex, n (%)			<0.001†
Female	536 (68)	410 (56)	
Male	251 (32)	328 (44)	
APOE genotype, n (%)			
ε2ε2	0 (0)	5 (0.7)	
ε2ε3	78 (10)	88 (12)	
ε2ε4	19 (2.5)	24 (3.3)	
ε3ε3	384 (50)	359 (49)	
ε3ε4	233 (30)	221 (30)	
ε4ε4	54 (7.0)	36 (4.9)	
Unknown	19	5	
Race, n (%)			<0.001‡
White	495 (92)	623 (84)	
Black or African American	35 (6.5)	107 (14)	
American Indian or Alaska Native	7 (1.3)	1 (0.1)	
Asian	1 (0.2)	5 (0.7)	
More than one	0 (0)	2 (0.3)	
Unknown	249	0	

*Wilcoxon rank sum test †Pearson's Chi-squared test ‡Fisher's exact test. Abbreviations: A+, amyloid positivity assessed using ^{11}C-Pittsburgh compound B or ^{18}F-Florbetapir PET neuroimaging; AD, Alzheimer's disease; *APOE*, apolipoprotein E; SD, standard deviation.

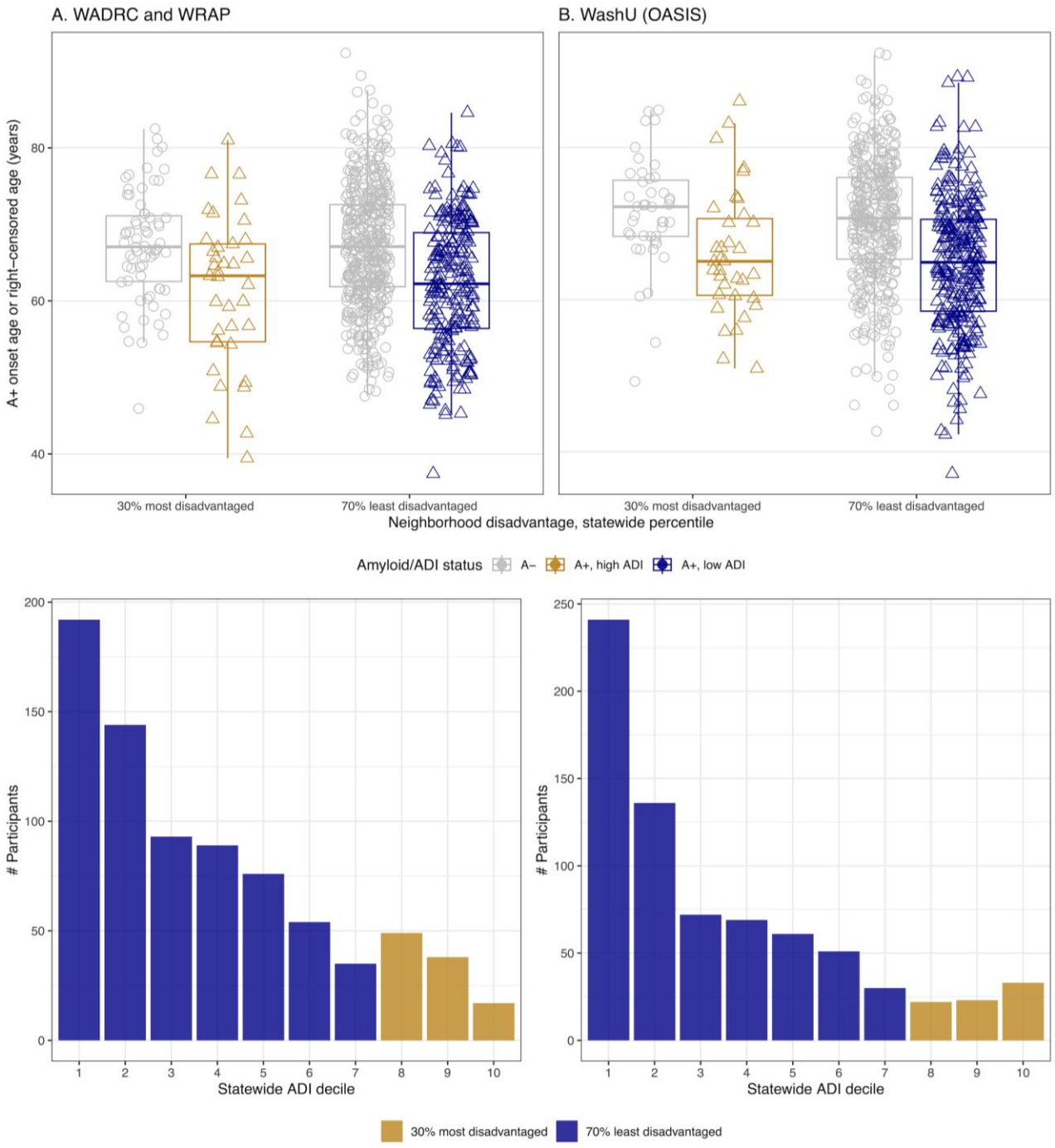


Figure 1. Distribution of EAOA across neighborhood disadvantage. Estimated age at A+ in global cortical ROIs across high and low ADIs (top), and participant distributions across ADI (bottom) shown for (A) Wisconsin ADRC/WRAP and (B) WashU OASIS samples. Plot color indicates level of neighborhood disadvantage for A+ cases, and age at censor is shown with gray circles for A-. Abbreviations: A+, amyloid positive status assessed using PET neuroimaging with ^{11}C-Pittsburgh compound B (DVR_{LGA} for Wisconsin, $SUVR_{30\text{-}60}$ for WashU) and ^{18}F-Florbetapir $SUVR_{50\text{-}70}$ (WashU) radiotracers; ADI, area deprivation index; OASIS, Open Access Series of Imaging Studies; WADRC, Wisconsin Alzheimer's Disease Research Center; WRAP, Wisconsin Registry for Alzheimer's Prevention; WashU, Washington University Knight ADRC.

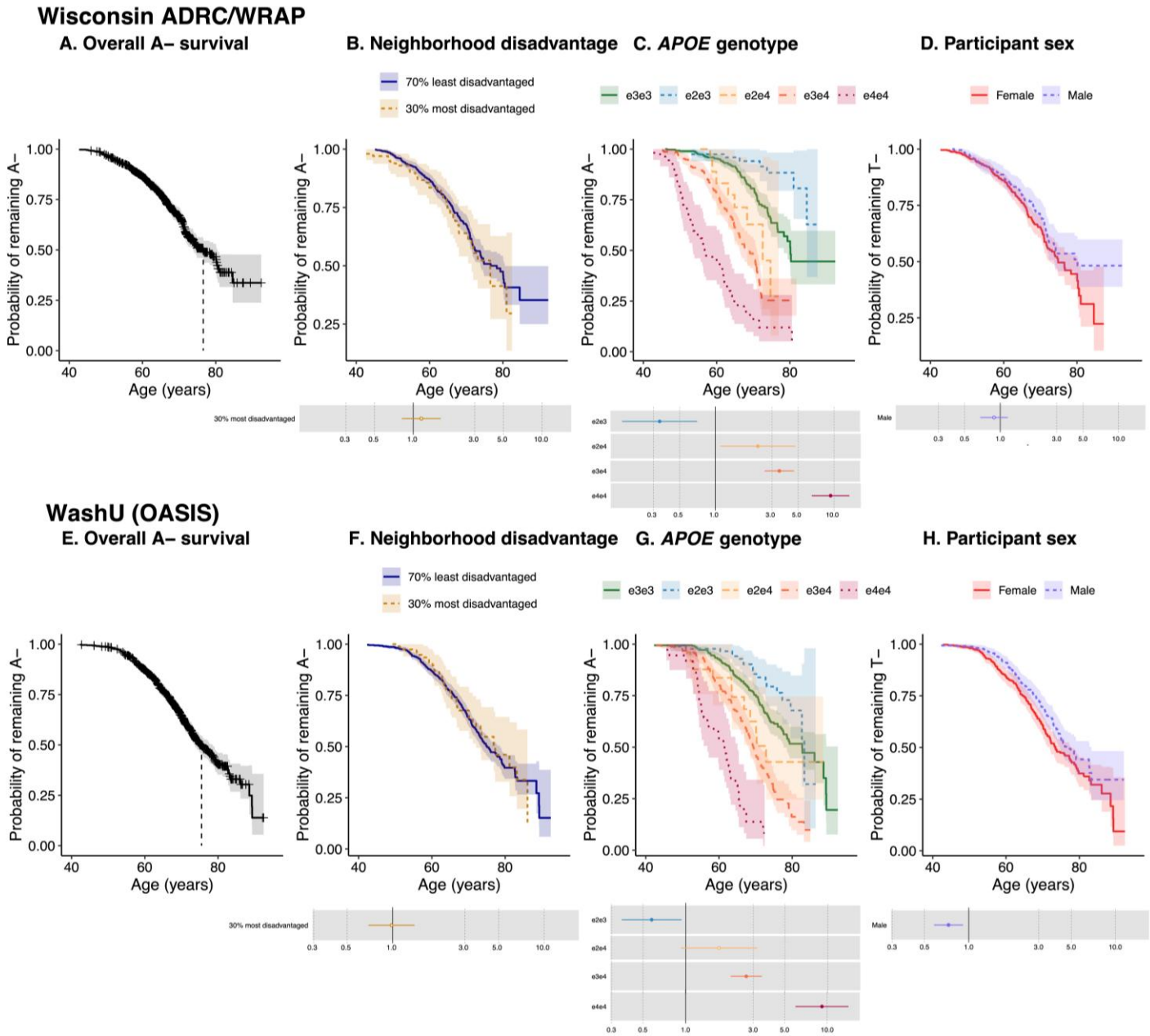


Figure 2. A- survival stratified across risk factors and cohort. Kaplan-Meier curves depicting the probability of remaining A- as a function of age (**A, E**), and stratified across levels of main effects included in the Cox proportional hazards model (Wisconsin **B-D**, WashU **F-H**). Main effect hazard ratios from Cox proportional hazards regression are shown in forest plots below each variable's stratified Kaplan-Meier curve. Abbreviations: A-, amyloid negative status assessed using PET neuroimaging with ^{11}C-Pittsburgh compound B (DVR_{LGA} for Wisconsin, $SUVR_{30\text{-}60}$ for WashU) and ^{18}F-Florbetapir $SUVR_{50\text{-}70}$ (WashU) radiotracers; ADI, area deprivation index; OASIS, Open Access Series of Imaging Studies; WADRC, Wisconsin Alzheimer's Disease Research Center; WRAP, Wisconsin Registry for Alzheimer's Prevention; WashU, Washington University Knight ADRC.

Keywords: Sampled iterative localized approximation, neighborhood disadvantage, individualized amyloid PET onset age, Wisconsin ADRC, Washington University Knight ADRC

Intersections of sex and neighborhood disadvantage on Alzheimer's disease pathology

Alexandria Reese[1,2], Sarah Royse[2,3], Beth Snitz[3,4], Nirupama Natarajan[5,6], James Hengenius[7], Theodore Huppert[8], Rebecca Roush[6], Geraldine Cisneros[6], Alexandra Gogola[2], Brian Lopresti[2], Oscar Lopez[3,4,6], James Becker[3,6], Ann Cohen[3,6], C. Elizabeth Shaaban[1,3]

[1]*Department of Epidemiology, University of Pittsburgh, Pittsburgh, PA, US*
[2]*Department of Radiology, University of Pittsburgh, Pittsburgh, PA, US*
[3]*Alzheimer's Disease Research Center, University of Pittsburgh, Pittsburgh, PA, US*
[4]*Department of Neurology, University of Pittsburgh, Pittsburgh, PA, US*
[5]*Department of Pathology, University of Pittsburgh, Pittsburgh, PA, US*
[6]*Department of Psychiatry, University of Pittsburgh, Pittsburgh, PA, US*
[7]*CHU Sainte-Justine Research Centre, Université de Montréal, Montréal, QC, CA*
[8]*Department of Electrical and Computer Engineering, University of Pittsburgh, Pittsburgh, PA, US*

Background: Differences in Alzheimer's disease (AD) biomarkers have been reported by sex, but their intersection with neighborhood disadvantage is not understood.

Methods: Participants were enrolled in the Connectomics in Brain Aging study. Neighborhood disadvantage was assessed using the area deprivation index (ADI) national rank, where higher scores indicate greater disadvantage. β-amyloid (A) was measured via global ^{11}C-PiB SUVR. Our vascular (V) measure was lobar unhealthy white matter connectivity (UWMC), a novel measure indicating the proportion of white matter (WM) connections affected by WM hyperintensities. Neurodegeneration (N) was measured via cortical thickness from an AD-specific meta-region. Intersectional effects of sex and ADI on AV(N) were examined on the multiplicative and additive scale via robust and log-binomial regressions, respectively.

Results: The sample included N=182 participants (age 62 years; female sex 66%; Black racialization 49%; education 14 years; *APOE4+* 31%; cognitively impaired 27%; Table 1). In robust regressions, female participants had greater frontal UWMC (β=0.06, SE=0.02, p=0.0005) and lower occipital UWMC (β=-0.05, SE=0.02, p=0.02) versus male participants, and high ADI participants had greater frontal (β=0.04, SE=0.02, p=0.04) and temporal UWMC (β=0.04, SE=0.02, p=0.01) versus low ADI participants (Table 2). Intersectional effects were found such that female participants with high ADI had the greatest temporal UWMC on the additive (relative excess risk due to interaction=0.72, 95% CI=[0.11,1.32]) and multiplicative (p-interaction=0.04) scales. Sex-stratified regressions indicated that high ADI was associated with greater temporal UWMC in female participants (β=0.07, SE=0.02, p=0.001), but not male participants (β=-0.002, SE=0.03, p=0.96; Figure 1). Results of sensitivity analyses with temporal WMH instead of UWMC were similar.

Conclusion: We confirmed differences in AV(N) by sex and ADI. Intersectional effects were found on temporal UWMC, such that women with high ADI had the greatest burden. Understanding the role of neighborhood disadvantage on V is important for future interventions, especially for women.

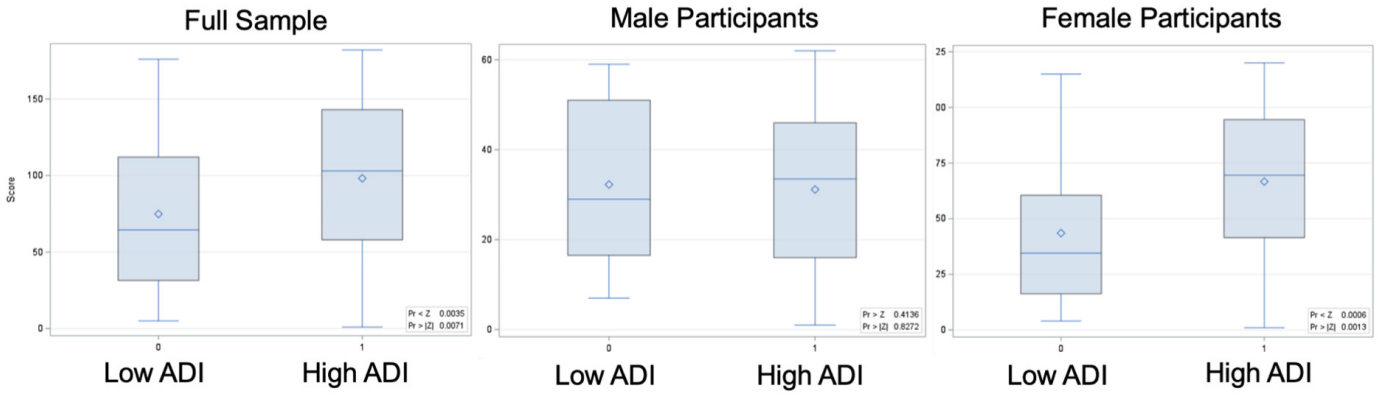
Table 1. Participant characteristics, N=182
N(%) for categorical variables and median (25^{th} %ile, 75^{th} %ile) for continuous.

	Overall	**Male participants N=62 (34.07%)**	**Female participants N=120 (65.93%)**	**Low ADI N=52 (28.57%)**	**High ADI N=130 (71.43%)**
Age, years	62 (57,71)	63.50 (59, 72)	62 (56, 70)	66.50 (60, 72.50)	60 (56, 70)
Racialized Black	89 (48.90%)	28 (45.16%)	61 (50.83%)	11 (21.15%)	78 (60.00%)
Education, years	14 (12,16)	14 (12, 16)	14 (12, 16)	16 (13, 18)	14 (12, 16)
APOE4+	56 (30.77%)	23 (37.10%)	33 (27.50%)	14 (26.92%)	42 (32.31%)
MoCA score	25 (23,27)	25 (23,27)	26 (23, 27)	26 (23,27.50)	25 (23,27)
Cognitively impaired	49 (26.92%)	19 (30.65%)	30 (25.00%)	16 (30.77%)	33 (25.38%)
Amyloid PET, SUVR	1.11 (1.06, 1.20)	1.10 (1.05, 1.51)	1.11 (1.06, 1.18)	1.15 (1.08, 1.48)	1.09 (1.05, 1.17)
UWMC					
Frontal	0.14 (0.09,0.25)	0.11 (0.08, 0.15)	0.17 (0.10, 0.33)	0.11 (0.08, 0.17)	0.16 (0.09, 0.29)
Parietal	0.06 (0.02, 0.15)	0.08 (0.02, 0.14)	0.05 (0.01, 0.15)	0.05 (0.01, 0.13)	0.06 (0.02, 0.17)
Temporal	0.18 (0.10, 0.26)	0.16 (0.08, 0.24)	0.19 (0.10, 0.27)	0.13 (0.07, 0.21)	0.20 (0.11, 0.27)
Occipital	0.06 (0.02, 0.21)	0.10 (0.04, 0.23)	0.05 (0.01, 0.20)	0.07 (0.03, 0.22)	0.06 (0.01, 0.21)
Cortical thickness, mm	2.74 (2.66, 2.80)	2.74 (2.66, 2.80)	2.73 (2.67, 2.79)	2.74 (2.67, 2.79)	2.74 (2.66, 2.80)
ADI National Index	74.50 (46.00, 91.00)	74.00 (44.00, 87.00)	75.50 (48.00, 93.00)	---	---

*Note: N for amyloid PET SUVR=164, Cortical thickness =164

Table 2: Association of ADI (binarized), sex, and their interactions with brain health outcomes.					
	Model 1: Sex + ADI		**Model 2: Sex + ADI + Sex*ADI**		
	Sex	**ADI**	**Sex**	**ADI**	**Interaction**
	Est (SE), p-value	**Est (SE), p-value**	**Est (SE), p-value**	**Est (SE), p-value**	**p-value**
Frontal UWMC	0.06 (0.02), **0.0005**	0.04 (0.02), **0.04**	0.06 (0.033), **0.09**	0.03 (0.03), 0.31	0.78
Parietal UWMC	-0.02 (0.01), 0.13	0.01 (0.01), 0.60	-0.03 (0.02), 0.28	0.0020 (0.02), 0.93	0.77
Temporal UWMC	0.02 (0.02), 0.26	0.04 (0.02), **0.01**	-0.03 (0.03), 0.30	-0.002 (0.03), 0.95	**0.04**
Occipital UWMC	-0.05 (0.02), **0.02**	-0.01 (0.02), 0.63	-0.05 (0.04), 0.18	-0.01 (0.03), 0.75	0.98
Amyloid	0.02 (0.01), 0.06	-0.02 (0.01), 0.12	0.01 (0.02), 0.82	-0.04 (0.02), 0.08	0.36
Cortical Thickness	-0.01 (0.02), 0.76	0.003 (0.02), 0.87	-0.01 (0.03), 0.86	0.002 (0.03), 0.93	0.99

Figure 1: Boxplots and Mann-Whitney-Wilcoxon tests of ADI differences and the intersection of sex and ADI on temporal UWMC



Keywords: beta-amyloid, white matter, neurodegeneration

Sex moderates relationships between P-Tau217 and longitudinal tau-PET: A multi-cohort study

Gillian Coughlan[1], Hannah Klinger[1], Tobey Betthauser[6], Rebecca Langhough[6], Karly Cody[6], Mabel Seto[3], Colin Birkenbihl[1], Annie Li[1], Michelle Farrell[1], Emma Thibault[1], Robert Rissman[2], Michael Properzi[1], Aaron Schultz[1], Diana Townsend[1], Hyun-Sik Yang[3], Keith Johnson[1,4], Rema Raman[2], Oliver Langford[2], Michael C. Donohue[2], Sterling Johnson[6], Reisa Sperling[1,3], Rachel Buckley[1,3,5]

[1]*Department of Neurology, Massachusetts General Hospital, Harvard Medical School, Boston, MA, US*
[2]*Alzheimer's Therapeutic Research Institute, University of Southern California, San Diego, CA, US*
[3]*Brigham and Women's Hospital, Boston, MA, US*
[4]*Gordon Center for Medical Imaging, Department of Radiology, Boston, MA, US*
[5]*Melbourne School of Psychological Sciences, University of Melbourne, Melbourne, AU*
[6]*Department of Medicine, University of Wisconsin-Madison, USA, Madison, WI, US*

Background: Women exhibit elevated insoluble tau aggregates and greater tau proliferation relative to age-matched men. Whether this is due to sex differences in upstream soluble phosphorylated tau(p-tau) is unclear. We examined whether sex and amyloid-β(Aβ) predict baseline soluble p-tau217 and whether baseline p-tau217 predicts tau positron emission tomography(PET) trajectories in a sex-specific manner.

Methods: 796 clinically normal individuals (mean-age:70; 311 *APOE*ε4 carriers; 450 Aβ-positive; Table) from the Anti-Amyloid Treatment in Asymptomatic Alzheimer's Disease trial, the companion Longitudinal Evaluation of Amyloid Risk and Neurodegeneration study(A4/LEARN), the Wisconsin Registry for Alzheimer's Prevention(WRAP) and Harvard Aging Brain Study(HABS) had multiple tau-PET scans and at least one measurement of ptau217 and Aβ-PET. Average tau-PET follow-up time was 3.3 years (range=1.3-8.9years). Cross-sectional sex differences in Aβ dependent soluble pTau217 were characterized using regression models. Longitudinally, random-effects models estimated the sex×baseline-p-tau217×time interaction on each of nine tau-PET regions previously showing cross-sectional sex differences including participant-specific intercepts and slopes. The tau-PET regions included rostral middle frontal gyri, fusiform gyrus, inferior temporal and parietal gyri, the superior parietal lobule, precuneus, lateral occipital cortex, parahippocampal and amygdala. All models adjusted age and education. Women were the reference.

Results: In A4/LEARN, women exhibited elevated p-tau217 concentrations at baseline relative to men, particularly at higher neocortical-Aβ (β=-0.16, *P*=0.008). Longitudinal sex×baseline-p-tau217×time interactions were significant in five, seven and four tau-PET regions in A4/LEARN, WRAP and HABS cohorts, respectively. Across all significant interactions, women showed worse tau trajectories than men, particularly at higher p-tau217 concentrations (see Figure 1 for A4/LEARN and Figure 2 for WRAP and HABS). Additionally, covarying for *APOE*ε4-status and baseline neocortical-Aβ did not alter the longitudinal sex effects (Table 2).

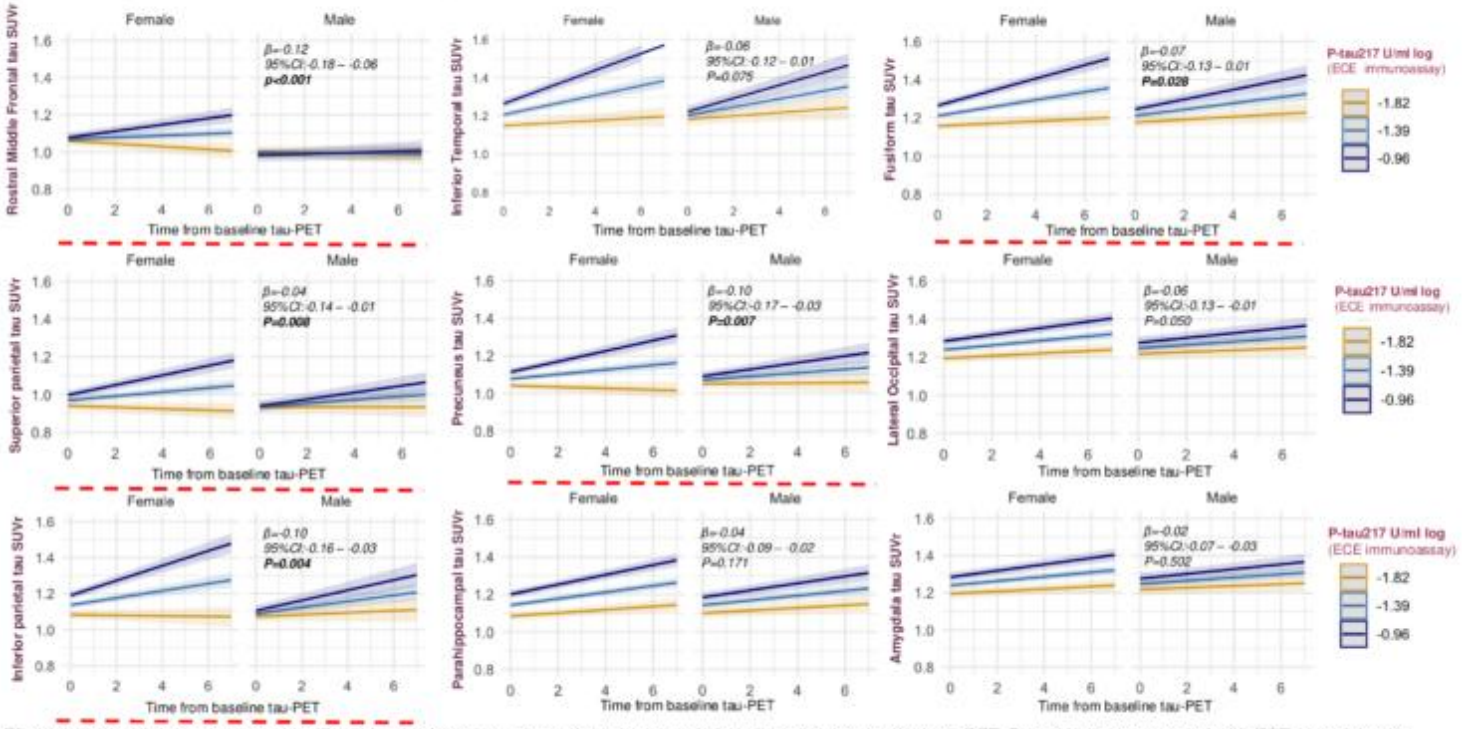
Conclusions: These findings suggest that sex differences in tau proliferation are exacerbated by upstream soluble p-tau levels. Earlier therapeutic approaches reducing soluble p-tau levels might be particularly important in women.

	A4/LEARN		WRAP		HABS	
Charateristics	**Men**	**Women**	**Men**	**Women**	**Men**	**Women**
Total No.	163	213	84	174	57	105
Baseline Tau-PET Age (SD)	72.9 (4.8)	71.5 (4.7)	68.3 (6.9)	67.2 (6.9)	71.4 (8.1)	68.7 (8.8)
APOE ε4 (%)	70 (43)	97 (46)	38 (33)	64 (37)	13 (23)	29 (28)
Aβ Positive (%)	144 (88)	195 (92)	20 (24)	42 (28)	17 (30)	32 (32)
Education Yrs (SD)	16.9 (2.8)	15.8 (2.8)	16.8 (2.2)	15.9 (2.3)	16.4 (2.9)	16.2 (2.6)
Tau-PET Time (SD)	3.4 (1.6)	3.4 (1.6)	2.7 (0.9)	2.7 (0.9)	3.9 (2.7)	3.8 (2.7)

Anti-Amyloid Treatment in Asymptomatic Alzheimer's Disease trial and the companion Longitudinal Evaluation of Amyloid Risk and Neurodegeneration study(A4/LEARN;N=376), the Wisconsin Registry for Alzheimer's Prevention (WRAP) and Harvard Aging Brain Study (HABS). Aβ positivity was determined using pre-defined within study cut-offs.

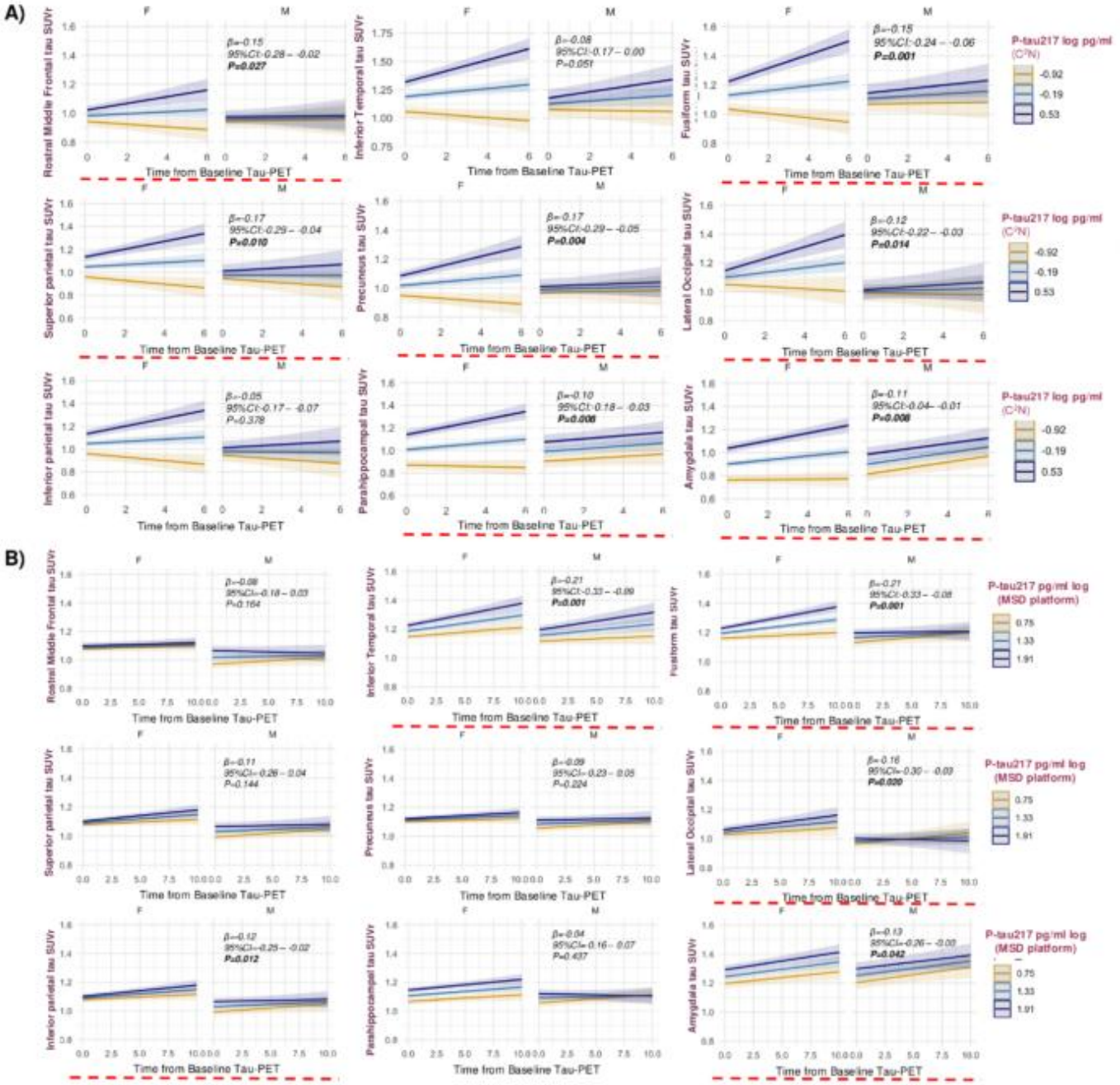
Tau-PET indicated the number of years between the first and last PET scan.

Figure 1: Sex × baseline-p-tau217 × time interactions on regional tau-PET trajectories over time suggesting that associations between elevated p-tau217 and faster regional tau accumulation are more pronounced in women relative to men in A4/LEARN (over 3.5 years, N=376).



The red dashed line represents a significant interaction between sex, baseline p-tau217 and time on longitudinal tau-PET. P-tau217 was measured with ECE immunoassay. P-tau: phosphorylated tau. U/ml: Units per milliliter. Women are the reference.

Figure 2: Sex × baseline-p-tau217 × time interactions on regional tau-PET trajectories over time suggesting that associations between elevated p-tau217 and faster regional tau accumulation are more pronounced in women relative to men in **(A)** WRAP (over 2.1 years, N=258) and **(B)** HABS (over 3.9 years, N=162).



The red dashed line represents a significant interaction between sex, baseline p-tau217 and time on tau-PET. In WRAP and HABS, P-tau217 was measured with mass spectrometry from C²N and MSD from Lilly. P-tau: phosphorylated tau. Pg/ml: Picograms per milliliter.

Keywords: Sex differences, ptau217, tau-PET, longitudinal

Friday, January 17, 2025 - 10:40 am - 10:45 am

Podium Session

Blitz Session 3A: Short Poster Presentations

Friday, January 17, 2025		
10:40 am - 10:45 am	**Blitz Session 3A**	
10:45 am – 10:47 am	Introduction	
10:47 am	Head-to-head comparison of longitudinal plasma assays in relation to longitudinal amyloid pathology in Alzheimer's disease	**Yara Yakoub**, Douglas Mental Health University Institute, Montréal, QC, CA
10:48 am	Calibration of multi-site raters for prospective visual read of amyloid PET scans acquired across the ADRC Consortium for Clarity in ADRD Research Through Imaging (CLARiTI)	**David Soleimani-Meigooni**, Department of Neurology, Memory and Aging Center, Weill Institute for Neurosciences, University of California, San Francisco, CA, US
10:49 am	Plasma phosphorylated tau 217 and longitudinal trajectories of Aβ, tau, and cognition in cognitively unimpaired older adults	**Hyun-Sik Yang**, Brigham and Women's Hospital, Boston, MA, US

Head-to-head comparison of longitudinal plasma assays in relation to longitudinal amyloid pathology in Alzheimer's disease

Yara Yakoub[1,2], Ting Qiu[1,2], Sylvia Villeneuve[1,3,4], Alexa Pichet Binette[5,6,7], Alzheimer's Disease Neuroimaging Initiative (ADNI) ADNI Foundation for the National Institutes of Health (FNIH) Biomarkers Consortium[8]

[1]*Douglas Mental Health University Institute, Montréal, QC, CA*
[2]*Integrated Program in Neuroscience, Faculty of medicine, McGill University, Montréal, QC, CA*
[3]*Montreal Neurological Institute, McGill University, Montréal, QC, CA*
[4]*Department of Psychiatry, Faculty of medicine, McGill University, Montréal, QC, CA*
[5]*Clinical Memory Research Unit, Department of Clinical Sciences Malm., Lund University, Lund, SE*
[6]*Department of Physiology and Pharmacology, Université de Montréal, Montréal, QC, CA*
[7]*Centre de Recherche de l'Institut Universitaire de Gériatrie de Montréal, Montréal, QC, CA*
[8]*Memory and Aging Center, Department of Neurology, Weill Institute for Neurosciences, University of California, San Francisco, CA, US*

Background: Blood-based biomarkers of AD, especially p-tau217, show high concordance with Aβ-PET load and status. While many studies relied on cross-sectional data, assessing dynamic changes in these assays is important for future clinical use and trial outcomes. We evaluated the longitudinal trajectories of multiple plasma biomarkers and their associations with longitudinal changes on Aβ-PET.

Methods: We used data from the ADNI FNIH consortium (**Table 1**). It consists of 404 participants with on average three plasma samples collected over 11 years, in which 14 assays were tested (4 p-tau217, 4 $A\beta_{42/40}$, 2 p-tau181, 2 GFAP, 2 NfL), and with Aβ-PET available over the same period. We first assessed the changes over time for each assay at the group level. Then, we calculated the individual rate of change of each plasma assay and Aβ-PET Centiloids (slope) using linear mixed-effect models. Association between baseline plasma levels and plasma rate of change with Centiloids accumulation were tested using linear regression models.

Results: Across the whole sample, all biomarkers, except for $A\beta_{42/40}$ assays, showed increase over time (**Fig.1A)**, which was similar in the Aβ-positive and Aβ-negative groups assessed separately (**Fig.1B**). Almost all assays showed Aβ-PET dependent changes (time × Aβ status), with the greatest interactions seen with p-tau217 (**Fig.1C**). In the whole group, both baseline plasma levels and plasma slopes were associated with Centiloids accumulation across almost all assays (**Fig.2A-B** for statistics and **C** for scatter plots). In Aβ-positive participants, such associations were no longer significant, except for %p-tau217. In Aβ-negative participants, most of the associations with p-tau assays remained (**Fig.2**).

Conclusion: While all plasma assays levels, except for $A\beta_{42/40}$, increased over time, at higher levels they were no longer associated with insoluble amyloid accumulation. The associations between plasma markers and Centiloid accumulation were also stronger in individuals who had not reached the positivity threshold.

Characteristics	Full sample (N = 404)	Aβ-Negative (N = 249)	Aβ-Positive (N = 155)	P value
Age, years	72.80 (7.27)	71.78 (7.22)	74.43 (7.08)	< 0.001
Education, years	16.29 (2.67)	16.54 (2.69)	15.88 (2.59)	0.02
Sex (n, %)	199 (49.3)	125 (50.2)	74 (47.7)	0.70
***APOE*4 carriers (n, %)**	138 (34.2)	55 (22.1)	83 (53.5)	< 0.001
Aβ-PET Centiloids	24.71 (40.24)	-1.43 (10.70)	66.69 (34.27)	<0.001
Aβ-PET change (Centiloids/year)	2.44 (1.95)	1.44 (1.31)	4.05(1.72)	<0.001
MMSE (/30)	28.51 (1.87)	28.98(1.29)	27.73 (2.35)	<0.001
Clinical diagnosis (n, %)				<0.001
Cognitively normal	210 (52)	145 (58.2)	65 (41.9)	
MCI	184 (45.5)	104 (41.8)	80 (51.6)	
Dementia	10 (2.5)	0 (0)	10 (6.5)	

Table 1. Mean (standard deviation), or where appropriate, count and percentage for both the full and subsample in the ADNI cohort. *P*-values were derived from Kruskal Wallis test for continuous variables and chi-squared for categorical variables. *Abbreviations*: F = female; APOE = apolipoprotein-E genotype; MMMSE = Mini-Mental State Examination; MCI = Mild cognitive impairment.

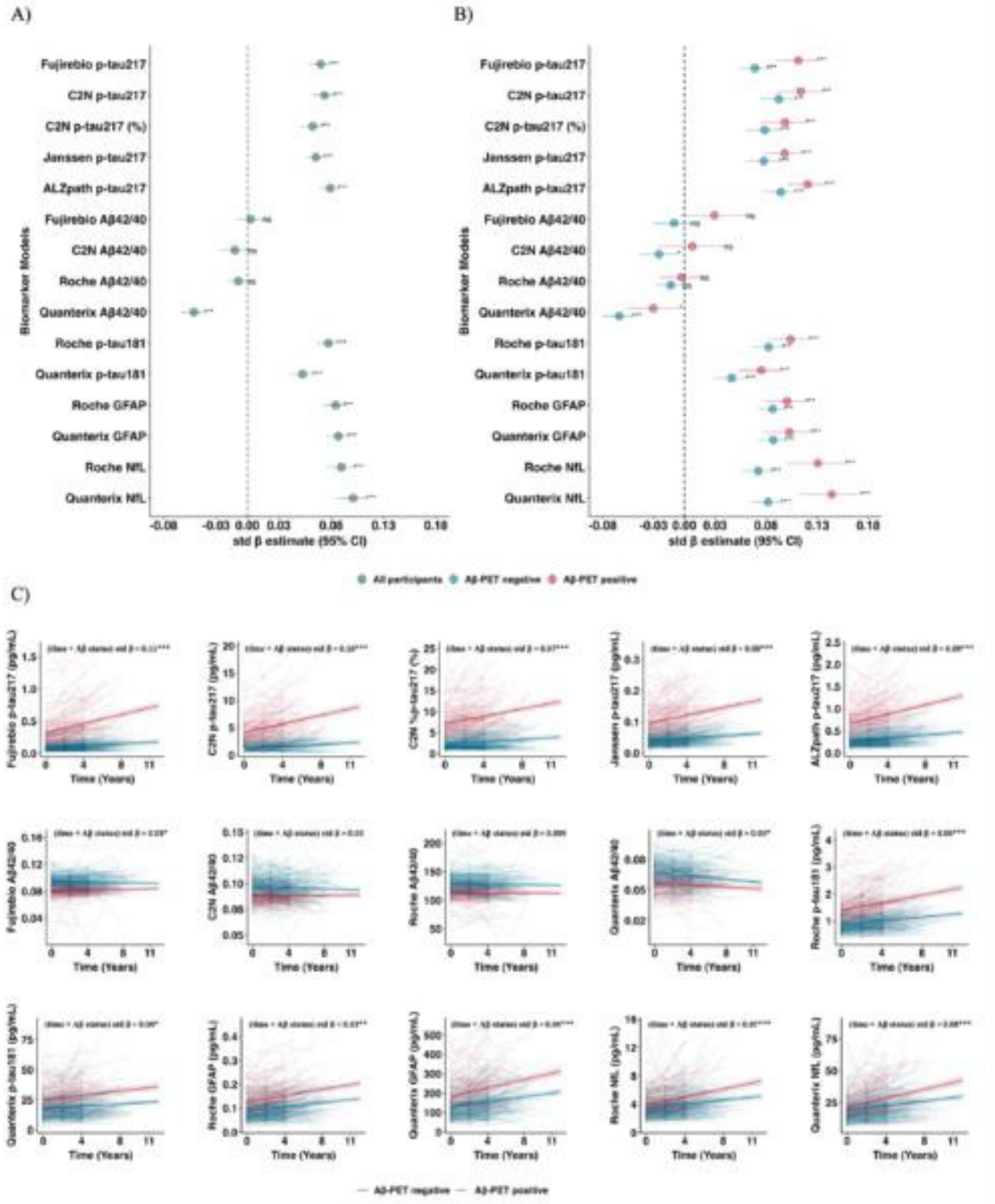


Figure 1. Longitudinal plasma biomarker trajectories across the different assays. Panel A-B) Standardized regression coefficients (std β) and 95% confidence interval (CI) obtained from linear-mixed effect (LME) models of different plasma biomarkers over time (plasma ~ time) for the whole group (A), Aβ-PET positive and negative group (B). **Panel C).** Different plasma biomarkers overtime with the interaction between time and Aβ status at baseline (time × Aβ status), the *x* axis shows time from first plasma biomarker sample. *Notes*: Outliers were removed from both baseline and longitudinal plasma sample using (mean ± 5SD) method. All models were adjusted for age at first plasma timepoint, years of education and sex. * $p < 0.05$, **$p < 0.005$, $p < 0.001$***

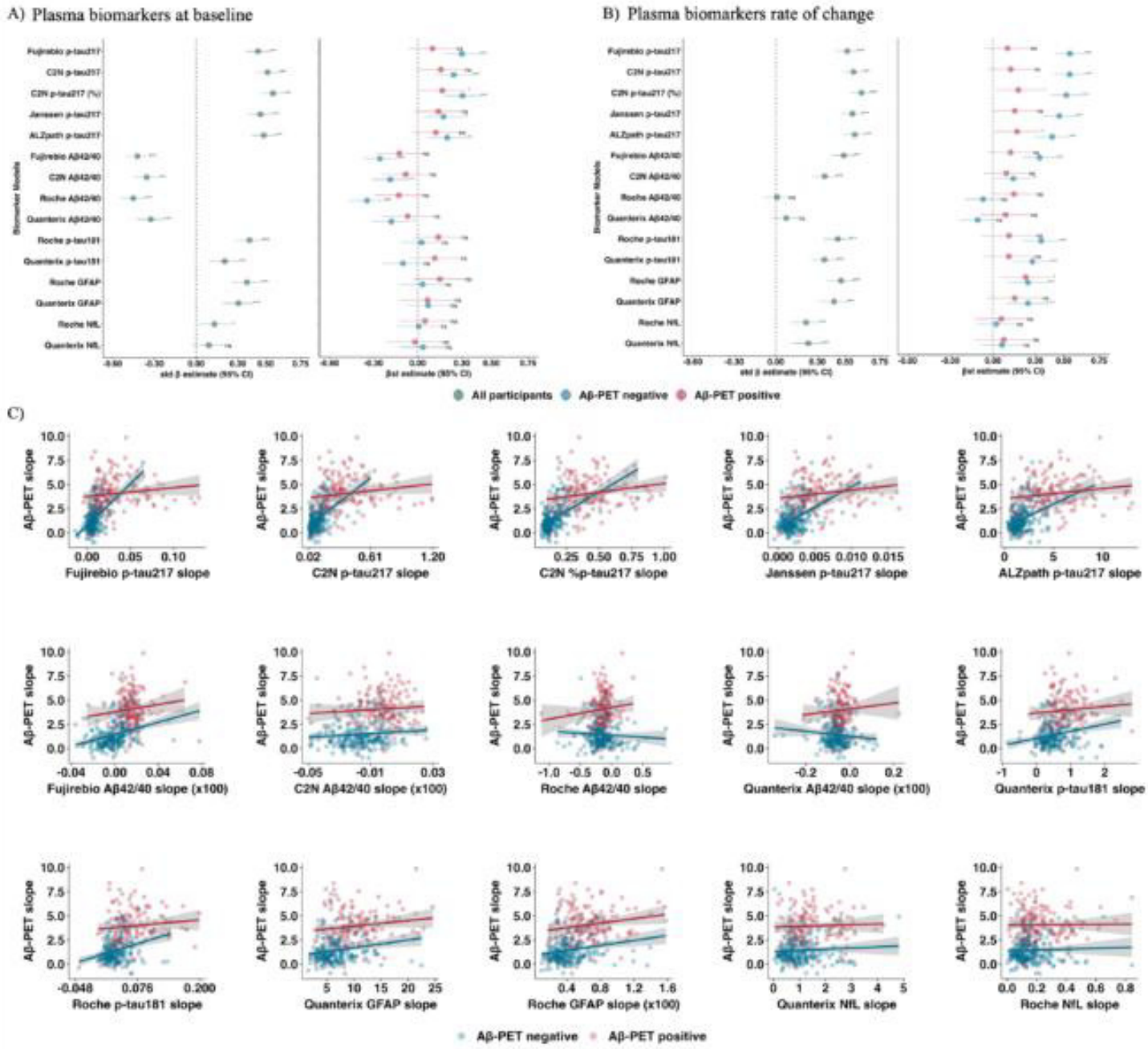


Figure 2. Association between baseline (A) and longitudinal (B-C) plasma biomarkers changes across the different assays with Aβ-PET Centiloids accumulation over time. **Panel A).** The standardized regression coefficients (std β) and 95% confidence intervals (CIs) for all participants (green), the Aβ-PET negative group (blue) and the Aβ-PET positive group (red), derived from the regression models of baseline plasma biomarkers and Aβ-PET slopes. **Panel B).** Std β and 95% CIs for all participants (green), the Aβ-PET negative group (blue) and the Aβ-PET positive group (red), derived from the regression models of plasma biomarkers slopes and Aβ-PET slopes. **Panel C).** Scatterplots illustrating the association between plasma levels rate of change (x-axis) and the Centiloid rate of change (y-axis) in the whole group. *Notes*: Outliers were removed from both baseline and longitudinal plasma sample using (mean ± 5SD) method. All models were adjusted for age at first plasma timepoint, years of education and sex. * $p < 0.05$, ** $p < 0.005$, $p < 0.001$***

Keywords: Plasma, PET, Alzheimer's disease, amyloid, tau

Calibration of multi-site raters for prospective visual read of amyloid PET scans acquired across the ADRC Consortium for Clarity in ADRD Research Through Imaging (CLARiTI)

David Soleimani-Meigooni[1,2], Ganna Blazhenets[1], Renaud La Joie[1], Zoe Lin[1], Carol Soppe[1], Derek Johnson[3], Mary Ellen Koran[4], Jonathan McConathy[5], Ilya Nasrallah[6], Jeremy Tanner[7], Victor Villemagne[8], Charles Windon[1], Michael Zeineh[9], Elizabeth Mormino[10], Sterling Johnson[11], Gil Rabinovici[1,12]

[1]*Department of Neurology, Memory and Aging Center, Weill Institute for Neurosciences, University of California, San Francisco, CA, US*
[2]*Molecular Biophysics and Integrated Bioimaging, Lawrence Berkeley National Laboratory, Berkeley, CA, US*
[3]*Division of Nuclear Medicine, Department of Radiology, Mayo Clinic, Rochester, MN, US*
[4]*Division of Nuclear Medicine, Department of Radiology, Mayo Clinic, Phoenix, AZ, US*
[5]*Division of Molecular Imaging and Therapeutics, Department of Radiology, University of Alabama at Birmingham, Birmingham, AL, US*
[6]*Department of Radiology, University of Pennsylvania, Philadelphia, PA, US*
[7]*Biggs Institute for Alzheimer's and Neurodegenerative Diseases, University of Texas Health Science Center, San Antonio, TX, US*
[8]*Department of Psychiatry, University of Pittsburgh School of Medicine, Pittsburgh, PA, US*
[9]*Department of Radiology, Stanford University School of Medicine, Stanford, CA, US*
[10]*Department of Neurology and Neurological Sciences, Stanford University School of Medicine, Stanford, CA, US*
[11]*Wisconsin Alzheimer's Institute, University of Wisconsin School of Medicine and Public Health, Madison, WI, US*
[12]*Department of Radiology and Biomedical Imaging, University of California, San Francisco, CA, US*

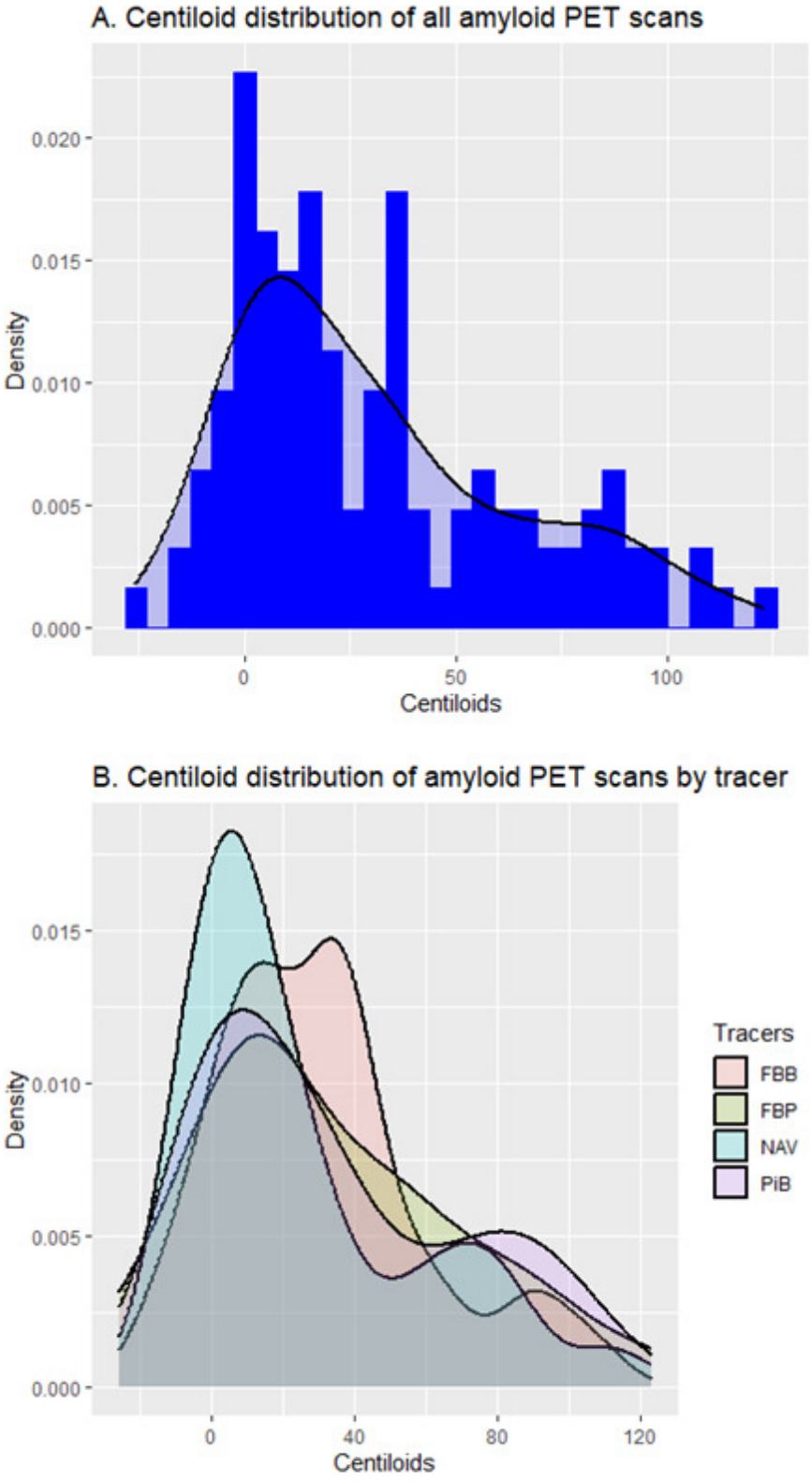
Background: PET visual reads for multi-center studies are conducted centrally by one or a few experts. In CLARiTI, a broader network of raters will perform the reads, necessitating methods to ensure their accuracy and reliability.

Methods: All ADRC sites (N=37) will prospectively acquire amyloid PET scans for 800 cognitively unimpaired and 1200 cognitively impaired participants. Each site can use one of four amyloid PET tracers (^{18}F-florbetapir, ^{18}F-florbetaben, ^{18}F-NAV4694, ^{11}C-PIB). PET scans will be visually interpreted by ten PET neuroimaging experts located across eight ADRCs, using their preferred hardware, software, and file format (DICOM, NIFTI). Calibration requires each reader to perform blinded, independent visual interpretation of 180 amyloid PET scans (30 unique and 15 duplicate scans per tracer), previously read and selected by an expert. An even mix of visually non-elevated and elevated scans were selected, with quantitation spanning -20-120 Centiloids (**Figure 1**), and 15% were visually borderline (similar proportion to ADNI4), with quantitation spanning 4-48 Centiloids (mean 21).

Results: Calibration scans were read by a second expert not serving in CLARiTI. There was 97% concordance and almost perfect agreement between readers (κ=0.932, p<0.001; **Figure 2**). Discordantly read scans were visually borderline elevated (N=2), borderline non-elevated (N=1), and negative (N=1), with quantitation of 8-21 Centiloids (mean 14). Intra-rater reads were 98% concordant and had almost perfect agreement (κ=0.966, p<0.001). These findings hold promise for scaling-up visual reads in CLARiTI, and we expect ≥80% concordance and substantial to almost perfect agreement ($\kappa \geq 0.7$) for inter/intra-rater reliability.

Conclusions: Calibration is essential for accurate/reliable amyloid PET visual reads in large multi-center studies with multiple raters. Involving multiple raters across different sites, who use diverse hardware/software/format combinations, will mirror the natural heterogeneity present in real-world clinical practice. This calibration set can also serve as a standardized training tool for other studies incorporating amyloid PET visual reads.

Figure 1. Centiloid distribution of unique scans in visual read calibration set.



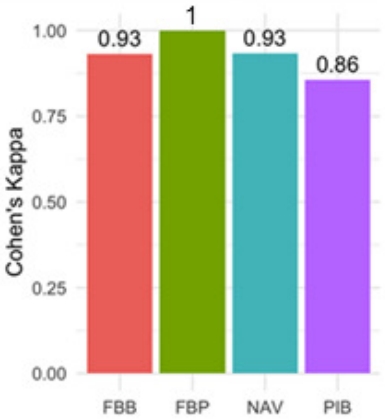
FBB=^{18}F-florbetaben; FBP=^{18}F-florbetapir; NAV=^{18}F-NAV4694; PiB=^{11}C-Pittsburgh Compound B

Figure 2. Inter- and intra-rater agreement of amyloid PET visual reads.

A. Inter-rater agreement

Cohen's kappa for 2 raters
120 subjects, $\kappa = 0.932$

All scans		Rater 2 negative	Rater 2 positive
Rater 1	negative	51	2
	positive	2	65



FBB	Rater 2 negative	Rater 2 positive
Rater 1 negative	12	1
Rater 1 positive	-	17

FBP	Rater 2 negative	Rater 2 positive
Rater 1 negative	14	-
Rater 1 positive	-	16

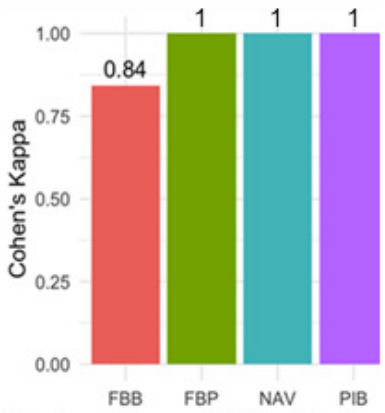
NAV	Rater 2 negative	Rater 2 positive
Rater 1 negative	15	-
Rater 1 positive	1	14

PIB	Rater 2 negative	Rater 2 positive
Rater 1 negative	10	1
Rater 1 positive	1	18

B. Intra-rater agreement

Cohen's kappa for a single rater
60 subjects, $\kappa = 0.966$

All scans		2nd read negative	2nd read positive
1st read	negative	25	-
	positive	1	34



FBB	2nd read negative	2nd read positive
1st read negative	4	-
1st read positive	1	10

FBP	2nd read negative	2nd read positive
1st read negative	6	-
1st read positive	-	9

NAV	2nd read negative	2nd read positive
1st read negative	10	-
1st read positive	-	5

PIB	2nd read negative	2nd read positive
1st read negative	5	-
1st read positive	-	10

FBB=^{18}F-florbetaben; FBP=^{18}F-florbetapir; NAV=^{18}F-NAV4694; PiB=^{11}C-Pittsburgh Compound B

Keywords: amyloid PET, visual reads, multi-site reader calibration

Plasma phosphorylated tau 217 and longitudinal trajectories of Aβ, tau, and cognition in cognitively unimpaired older adults

Hyun-Sik Yang[1,2,3], Juliana Anzai[1,2], Wai-Ying Yau[1,2,3], Andrea Román Viera[1,2], Courtney Maa[1,2], Dylan Kirn[1,2], Michael Properzi[2], Aaron Schultz[2,3], Michelle Farrell[2,3], Heidi Jacobs[2,3], Rachel Buckley[2,3], Kathryn Papp[1,2,3], Gad Marshall[1,2,3], Rebecca Amariglio[1,2,3], Dorene Rentz[1,2,3], Joel Braunstein[4], Keith Johnson[1,2,3], Reisa Sperling[1,2,3], Jasmeer Chhatwal[1,2,3]

[1]*Brigham and Women's Hospital, Boston, MA, US*
[2]*Massachusetts General Hospital, Boston, MA, US*
[3]*Harvard Medical School, Boston, MA, US*
[4]*C2N Diagnostics, St. Louis, MO, US*

Background: Plasma phosphorylated tau 217 (pTau217) reflects the AD pathology burden, but its utility in predicting longitudinal disease progression in cognitively unimpaired (CU) older adults remains unclear.

Methods: Baseline plasma %pTau217 (pTau217/non-phosphorylated-Tau217×100) from n=318 Harvard Aging Brain Study participants (61% female, 81% white, follow-up 8.0±3.9 years, CU at baseline) was quantified by C_2N Diagnostics. We obtained annual Preclinical Alzheimer's Cognitive Composite 5 (PACC5), and Pittsburgh compound B (PiB) and flortaucipir (FTP) PET in Years 1 (baseline), 4, 6, 9, 12. We used cortical PiB DVR (Centiloid [CL]), mesial temporal lobe (MTL), and temporal neocortical (NEO) FTP SUVR composites. Association between %pTau217 and longitudinal Aβ, tau, and cognition were assessed using linear mixed effect models, accounting for age, sex, *APOE* ε4, and education. A log-rank test assessed the "A-" (<24.1 CL) to "A+" progression risk. A path analysis combining baseline %pTau217 and the rates of ΔPiB, ΔNEO-FTP, and ΔPACC5 was performed.

Results: Baseline %pTau217 was associated with longitudinal PiB (n=245, b=0.35, $p=8.9\times10^{-16}$), even in the A- subgroup (n=191, b=0.26, $p=1.6\times10^{-4}$) and the <10 CL subgroup (n=123, b=0.22, p=0.020). Higher baseline %pTau217 tertiles were associated with A- to A+ progression risk (n=189, $\chi^2_{df=2}=14.4$, $p=7.5\times10^{-4}$). Baseline %pTau217 was associated with longitudinal MTL-FTP (n=182, $b=9.4\times10^{-4}$, p=0.030) and NEO-FTP ($b=1.3\times10^{-3}$, $p=4.8\times10^{-5}$), even in the A- subgroup (n=145; MTL-FTP $b=2.6\times10^{-3}$, $p=1.7\times10^{-3}$; NEO-FTP $b=1.2\times10^{-3}$, p=0.043). Baseline %pTau217 was associated with longitudinal PACC5 overall (n=308, b=-0.019, $p=1.5\times10^{-10}$), but this association was not significant in the A- subgroup (n=235, p=0.31). The path analysis suggested that the %pTau217 - ΔPACC5 association is primarily mediated through ΔPiB and ΔNEO-FTP.

Conclusion: Plasma %pTau217 predicted longitudinal Aβ and tau accumulation in CU older adults, even in the A- subgroup, supporting plasma biomarker screening in primary prevention trials. The association of higher baseline %pTau217 with cognitive decline was explained by faster AD pathology progression.

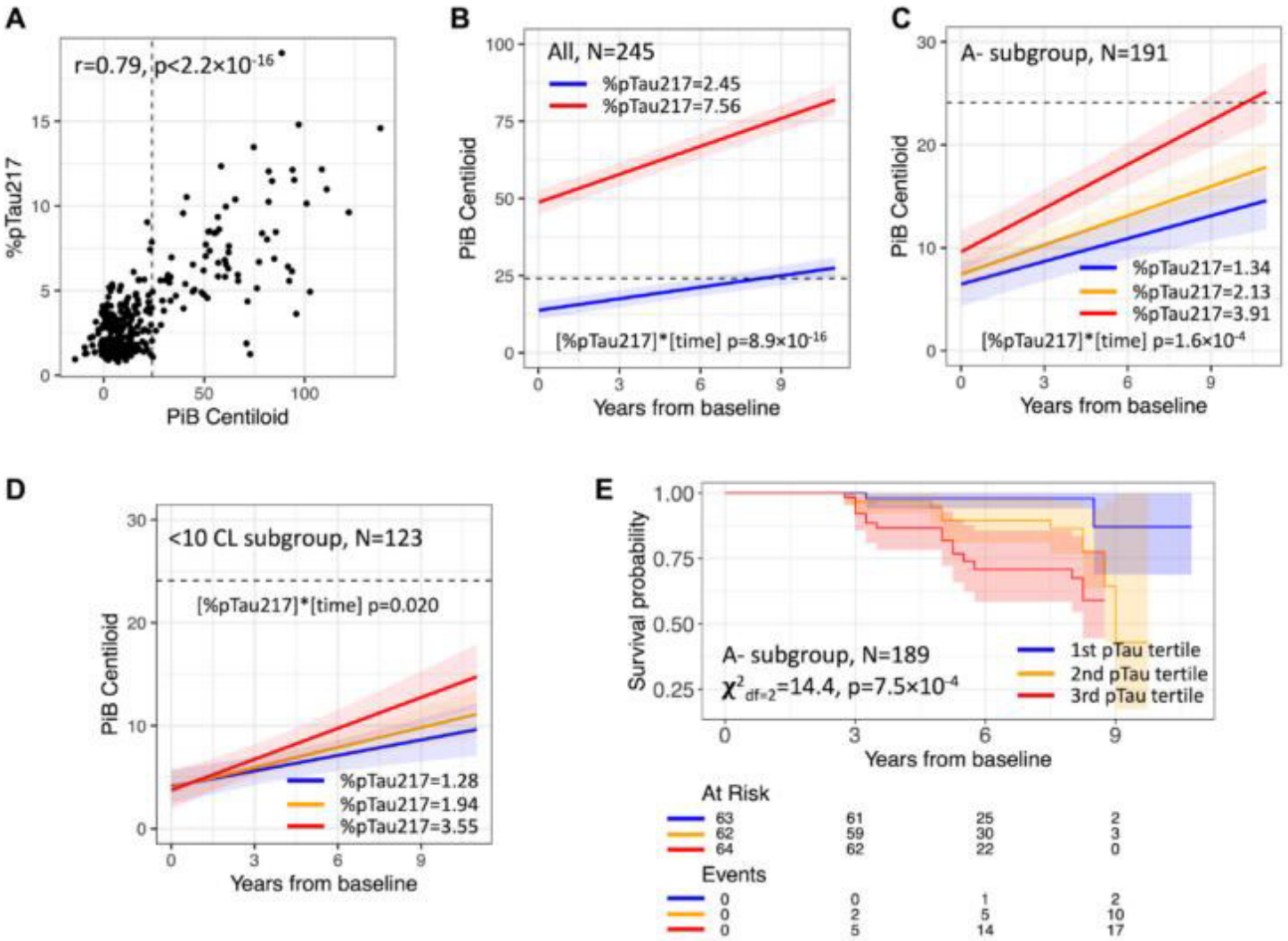


Figure 1. Baseline plasma %pTau217 and cross-sectional and longitudinal cortical Aβ (PiB PET).
(A) Baseline plasma %pTau217 and PiB CL. **(B)** Estimated longitudinal cortical Aβ burden (PIB PET CL) trajectory among all participants with longitudinal PiB PET. Mean values of %pTau217 among A- (2.45) and A+ (7.56) were used for visualization. **(C-D)** Estimated longitudinal cortical Aβ burden (PIB PET CL) trajectory in the A- subgroup (<24.1 CL; **C**) and the <10 CL subgroup (**D**). Mean values of each %pTau217 tertile within each subgroup were used for visualization. Dashed lines indicate the threshold for A+ (24.1 CL). **(E)** The differential risk of A- to A+ progression among CU A- subgroup across the baseline %pTau217 tertile was shown with Kaplan-Meier curves. The log-rank test Chi-square statistic is shown. The number of at-risk and events per group are noted below the plot.

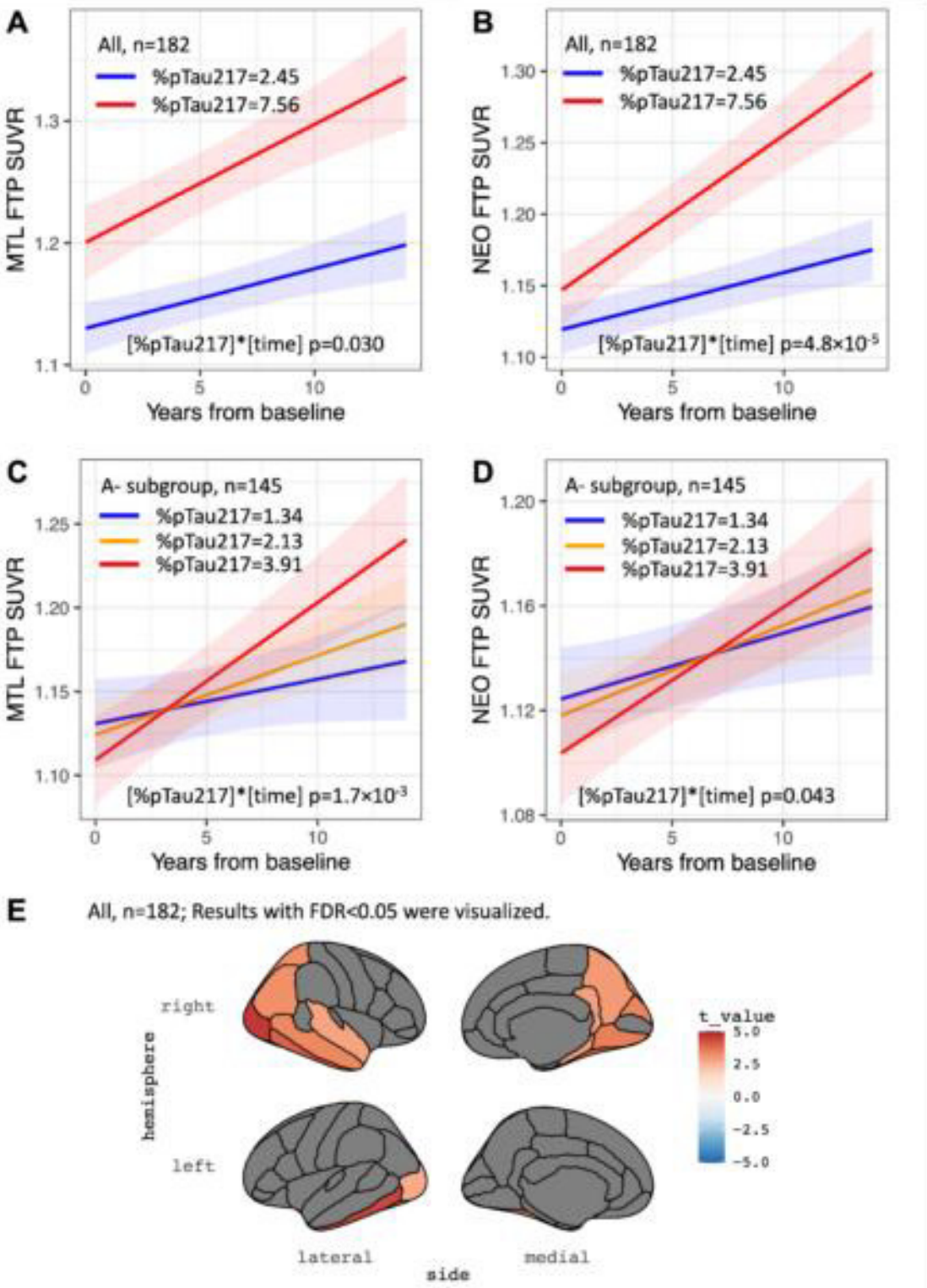


Figure 2. Baseline plasma %pTau217 and cross-sectional and longitudinal tau (FTP PET). (A-B) The estimated longitudinal trajectory of MTL (A) and NEO (B) FTP SUVR. Mean %pTau217 values of A- and A+ subgroups were shown. **(C-D)** The estimated longitudinal trajectory of MTL (C) and NEO (D) FTP SUVR in the baseline A- subgroup. Mean %pTau217 values in each %pTau217 tertile are shown. **(D)** The association between baseline plasma %pTau217 and neocortical (NEO) FTP SUVR from the first FTP PET. **(E)** Exploratory analyses of the baseline %pTau217 – longitudinal tau association in each cortical FTP PET region of interest (ROI). Regions with FDR<0.05 were colored with their association t-values.

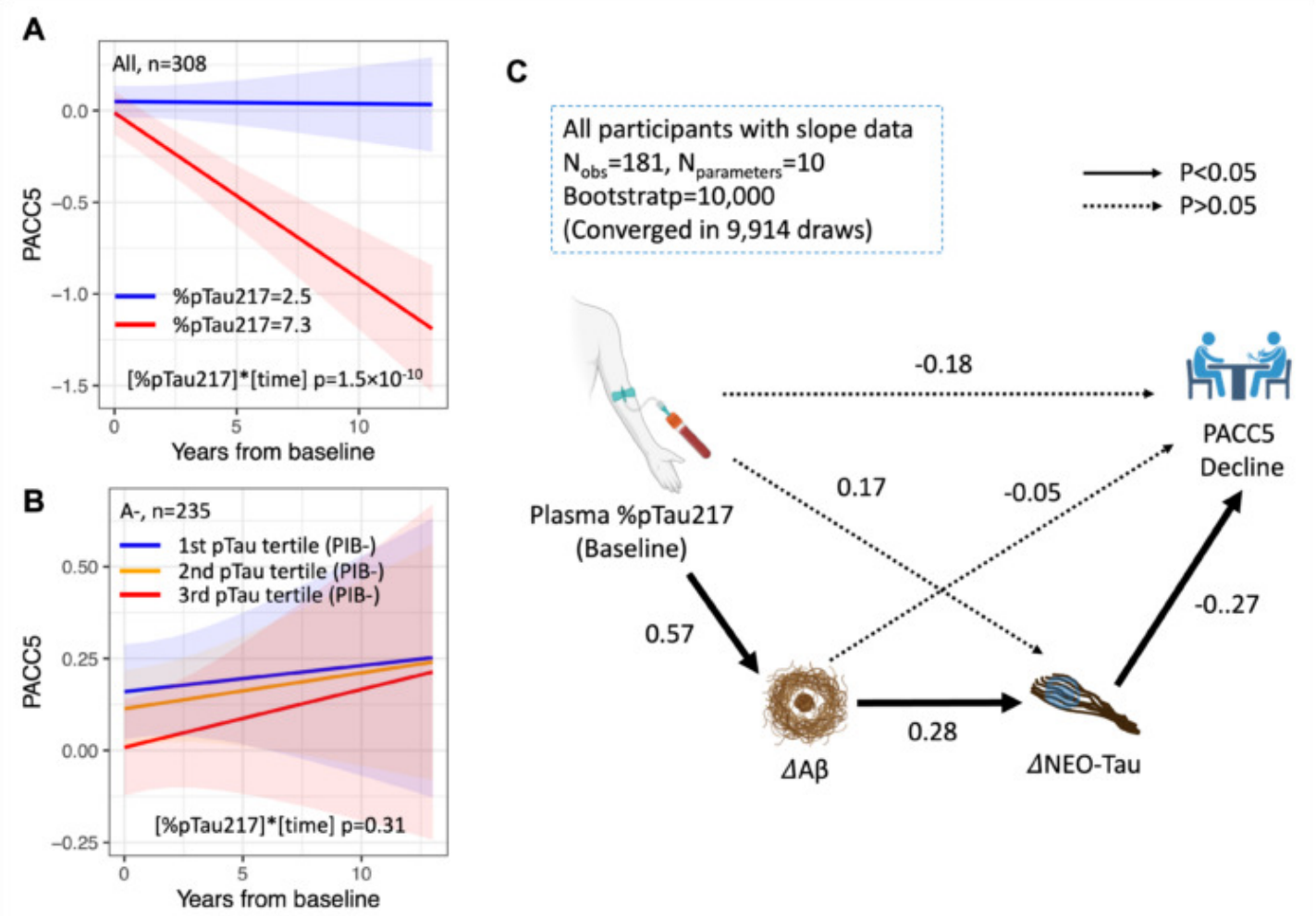


Figure 3. Baseline plasma %pTau217 and longitudinal PACC5. (A-B) The predicted longitudinal trajectory of PACC5 in all participants (A) and the A- subgroup (B). Mean %pTau217 values in the A- (2.5) and A+ (7.5) subgroups were used in (A), and mean %pTau217 values for each tertile among A- subgroup were used in (B) for visualization. **(C)** Path analysis shows that higher baseline %pTau217 is associated with longitudinal Aβ accumulation (ΔAβ; PIB CL slope), which in turn leads to longitudinal neocortical tau accumulation in the neocortex (ΔNEO-Tau; temporal neocortical FTP SUVR slope) and cognitive decline (PACC5 slope). ΔAβ and ΔNEO-Tau explained most of the association between %pTau217 with cognitive decline. Solid arrows indicate significant associations ($p<0.05$); the associations with $p>0.05$ were shown in dashed arrows. Numbers adjacent to each arrow show the relative strength of each association (completely standardized solution).

Keywords: plasma biomarker; phospho-tau217; preclinical Alzheimer's disease; longitudinal PET; disease progression

Friday, January 17, 2025 - 10:45 am - 11:40 am

P3A: Poster Session 3A

Friday, January 17, 2025			
10:45 am – 11:40 am	**Poster Session 3A** *(repeating in the afternoon as 3B)*		
Board 117	Concordance between visual and quantitative amyloid PET and CSF biomarkers in the ADNI-DOD cohort	Vrillon | Blazhenets | Lagarde | Chiotis | Abu Raya | Soleimani-Meigooni | Rabinovici | Weiner | Silbert | Hantke | Schwartz | Livny Ezer | Lesman Segev | Yaffe | Shaw | Landau | La Joie | Gardner	**Agathe Vrillon**, University of California San Francisco, San Francisco, CA, US
Board 118	Calibration of multi-site raters for prospective visual read of amyloid PET scans acquired across the ADRC Consortium for Clarity in ADRD Research Through Imaging (CLARiTI)	Soleimani-Meigooni | Blazhenets | La Joie | Lin | Soppe | Johnson | Koran | McConathy | Nasrallah | Tanner | Villemagne | Windon | Zeineh | Mormino | Johnson | Rabinovici	**David Soleimani-Meigooni**, Department of Neurology, Memory and Aging Center, Weill Institute for Neurosciences, University of California, San Francisco, CA, US
Board 119	Evaluating the effect of APOE genotype in real-world clinical settings: results from the IDEAS-ANGI study	Pezzoli | Jonson | Blazhenets | Schonhaut | Perez | Oddi | Castruita | Casaletto | Hanna | March | Gatsonis | Carrillo | Foroud | La Joie | Yokoyama | Rabinovici	**Stefania Pezzoli**, Memory and Aging Center, Department of Neurology, University of California, San Francisco, San Francisco, CA, US
Board 120	Brain connectivity drives tau distribution while regional vulnerability drives tau load in Alzheimer's disease	Xiao | Bazinet | Strandberg | Hansen | Shafiei | Spotorno | Behjat | Stomrud | Smith | Palmqvist | Mattsson-Carlgren | Dagher | Misic | Hansson | Vogel	**Yu Xiao**, Department of Clinical Sciences Malmö, SciLifeLab, Lund University, Lund, SE
Board 121	Synergistic effects of peripheral inflammation and neuroinflammation on amyloid, vascular, and neurodegeneration markers across the Alzheimer's disease spectrum	Ramirez Tirado | Cohen | Shaaban | Matan | Lopresti | Ikonomovic | Karikari | Villemagne | Lopez	**Laura Alejandra Ramirez Tirado**, Department of Epidemiology, University of Pittsburgh, Pittsburgh, PA, US
Board 122	Impact of amyloid removal on cerebral volume changes with Gantenerumab	Tonietto | Silvestri | Belder | Barkhof | Fox | Smith | Klein	**Matteo Tonietto**, Research and Early Development (pRED), Hoffmann-La Roche, Basel, CH
Board 123	Astrocyte reactivity explains tau-related effects on hippocampal dysfunction and longitudinal atrophy in preclinical Alzheimer's disease	Schweitzer | Iordanova | Chen | Jin | Thurston | Lopresti | Snitz | Tudorascu | Cohen | Kamboh | Halligan-Eddy | Karikari | Villemagne | Aizenstein | Wu	**Noah Schweitzer**, Department of Bioengineering, University of Pittsburgh, Pittsburgh, PA, US
Board 124	Plasma phosphorylated tau 217 and longitudinal trajectories of Aβ, tau, and cognition in cognitively unimpaired older adults	Yang | Anzai | Yau | Román Viera | Maa | Kirn | Properzi | Schultz | Farrell | Jacobs | Buckley | Papp | Marshall | Amariglio | Rentz | Braunstein | Johnson | Sperling | Chhatwal	**Hyun-Sik Yang**, Brigham and Women's Hospital, Boston, MA, US
Board 125	Detection of TDP-43 from plasma-derived astrocyte extracellular vesicles for identification of LATE	Rissman	**Robert Rissman**, University of Southern California, Neuroscience Translational Research Division, Alzheimer's Therapeutic Research Institute, SAN DIEGO, CA, US

Board 126	Short sleep duration is associated with higher subsequent plasma p-tau217 in aging	Winer | Cody | Young | Mormino	**Joseph Winer**, Department of Neurology and Neurological Sciences, Stanford University, Stanford, CA, US
Board 127	Impacts of testing language and rates of amyloid positivity among underrepresented groups in the A4 Study	Sai | D. Grill | C. Mormino | B Young	**Isha Sai**, Department of Neurology and Neurological Sciences, Stanford University, Stanford, CA, US
Board 128	Lower locus coeruleus metabolism is associated with greater year-to-year intraindividual cognitive variability in older individuals with elevated levels of Alzheimer's disease pathology	Wiklund | Van Egroo | Koops | Hanseeuw | Papp | Rentz | Sperling | Johnson | Jacobs	**Emma Wiklund**, The Athinoula A. Martinos Center for Biomedical Imaging, Department of Radiology, Massachusetts General Hospital, Harvard Medical School, Boston, MA, US
Board 129	Long-term cognitive and biomarker trajectories of cognitively unimpaired individuals with elevated plasma ptau-217	Silva-Rodríguez | Zhang | Valeriano-Lorenzo | López-González | Wagner-Reguero | del Ser | Grothe | Sánchez-Juan	**Jesús Silva-Rodríguez**, Reina Sofia Alzheimer Centre, CIEN Foundation, ISCIII, Madrid, ES
Board 130	A large public release of PIB PET and MRI from the Mayo Clinic Study of Aging	Schwarz | Kremers | Prakaashana | Przybelski | Christenson | Williams | Gunter | Senjem | Arani | Reid | Machulda | Fields | Lowe | Kantarci | Graff-Radford | Vemuri | Petersen | Knopman | Jack	**Christopher Schwarz**, Mayo Clinic, Rochester, MN, US
Board 131	Harmonizing visual readings of Flortaucipir and MK-6240 using head-to-head data	Ruppert | Medeiros | Rocha | Soares | Amaral | Povala | Bauer-Negrini | L. Ferreira | Lussier | Oliveira Jr. | Scarpatto Rodrigues | Mroue | Zalzale | Leffa | Saha | Bellaver | L. Tudorascu | Soleimani-Meigooni | Fortea | Lowe | Oh | Pascual | A. Gordon | Rosa-Neto | Baker | A. Pascoal	**Emma Ruppert**, University of Pittsburgh, Department of Psychiatry, Pittsburgh, PA, US
Board 132	Twin-mapping techniques in clinical trials: a proof-of-concept application to the Internet-Based Conversational Engagement Clinical Trial (I-CONECT)	Wu | Chen | Arnold | Dodge	**Chao-Yi Wu**, Neurology, Massachusetts General Hospital (MGH), Harvard Medical School, Charlestown, MA, US
Board 133	Effects of amyloid and tau status on multiplex plasma CNS and inflammatory proteins in a normal aging cohort	Trelle | Cody | Nguyen | Winer | Weiss | Romero | Sai | Wilson | Wagner | Maecker | Mormino	**Karly Cody**, Department of Neurology and Neurological Sciences, Stanford University, Stanford, CA, US
Board 134	Tau imaging thresholds within NIA-AA multilevel tau staging as predictors of tau accumulation and cognitive decline in non-demented individuals	Gogola | Cohen | Snitz | Minhas | Tudorascu | Ikonomovic | Shaaban | Dore | Matan | DelBene | Bourgeat | Leuzy | Aizenstein | Lopez | Lopresti | Villemagne	**Alexandra Gogola**, Department of Radiology, University of Pittsburgh School of Medicine, Pittsburgh, PA, US
Board 135	Multi-morbidity and Alzheimer's disease pathology across the lifespan in adults with Down syndrome	Smith | Edwards | Flores Aguilar | Alshikho | Tudorascu | Rosas | Yassa | Hartley | Handen | Christian | Gutierrez | Wilcock | Head | Brickman | Lao	**Anna Smith**, Columbia University Medical Center, New York, NY, US
Board 136	Cortical atrophy is correlated with the discrepancy between neuroradiological assessment and binary quantitation of florbetapir PET in nondemented older adults	Schwartz | Villamizar Alvarado | Szidonya | Choudhary | Marcoe | Mar | Gillan | Hendricks | Kaye | Silbert	**Daniel Schwartz**, OHSU Neurology, Portland, OR, US

Board 137	Vascular pathology influences the association of tau-PET with neurodegeneration and cognition in Aβ-negative individuals	Silva Oliveira Junior | Bellaver | C.L. Ferreira | Povala | Bauer-Negrini | Lussier | do Amaral | Rodrigues | da Rocha | Saha | Ruppert | Soares | Leffa | Felix | Mroue | Tudorascu | Zalzale | Pascual | Gordon | Lowe | Oh | Soleimani-Meigooni | Fortea | Rosa-Neto | Baker | Pascoal	**Markley Silva Oliveira Junior**, University of Pittsburgh, Department of Psychiatry, Pittsburgh, PA, US
Board 138	Concomitant neurodegeneration of the lateral hypothalamus and locus coeruleus is associated with early Alzheimer's disease-related pathophysiological and cognitive processes	Van Egroo | Baillet | Becker | Price | Properzi | Papp | Rentz | Sperling | Johnson | Jacobs	**Maxime Van Egroo**, Faculty of Health, Medicine and Life Sciences, Mental Health and Neuroscience Research Institute, Alzheimer Center Limburg, Maastricht University, Maastricht, NL
Board 139	Amyloid-associated hyperconnectivity drives tau spreading across connected brain regions in Alzheimer's disease	Roemer-Cassiano | Wagner | Evangelista | Dehsarvi | Steward | Dewenter | Biel | Zhu | Malpetti | Höglinger | Brendel | Jäkel | Scholl | Franzmeier	**Sebastian Niclas Roemer-Cassiano**, Department of Neurology, University Hospital, LMU Munich, Germany, Munich, DE
Board 140	Association of plasma GFAP with tau PET in cognitively unimpaired Aβ-negative subjects	Saha | Bellaver | Povala | Ferreira | Bauer-Negrini | Silva | Lussier | Rodrigues | Oliveira | Rocha | Felix | Ruppert | Medeiros | Katz | Masdeu | Tudorascu | Soleimani-Meigooni | Fortea | Lowe | Oh | Pascual | Gordon | Rosa-Neto | Baker | Pascoal	**Pampa Saha**, University of Pittsburgh, Department of Psychiatry, Pittsburgh, PA, US
Board 141	The striatum is an early, accurate indicator of [C-11]PiB amyloid burden for the Down syndrome population	McLachlan | Price | Tudorascu | Laymon | Lao | Handen | Fryer | Ances | Johnson | Betthauser | Zaman | Head | Mapstone | Bettcher | LeMerise | McVea | DiFillipo | Zammit | Hartley | Christian	**Max McLachlan**, University of Wisconsin - Madison, Madison, WI, US
Board 142	Best practices for tau-PET tracer harmonization in Alzheimer's research	Tissot | Tsai | Giorgio | Blazhenets | Harrison | Olafson | Sanabria | Leuzy | Doré | Jagust | Rosa-Neto | Pascoal | Baker	**Cécile Tissot**, Lawrence Berkeley National Laboratory, Berkeley, CA, US
Board 143	Relationship between metabolic syndrome biomarkers and regional tau accumulation in cognitively unimpaired older adults	Tennant | Luu | Hand | Lee | Toga | O'Bryant | Yaffe | Braskie	**Victoria Tennant**, Mark and Mary Stevens Neuroimaging and Informatics Institute, Keck School of Medicine, Los Angeles, CA, US
Board 144	Association of a unique pattern of white matter T2 FLAIR hyperintensities with plasma and tau PET biomarkers in former American football players	Groh | Farris | Brickman | Alshikho | Miner | Tripodis | Cui | Adler | Balcer | Bernick | Cantu | Coleman | Dodick | Ashton | Zetterberg | Blennow | Peskind | McKee | Mez | Bouix | Cummings | Reiman | Stern | Shenton | Alosco	**Jenna Groh**, Boston University Chobanian & Avedisian School of Medicine, Boston, MA, US
Board 145	Relationship between flortaucipir-PET and quantitative susceptibility mapping in atypical Alzheimer's disease	Singh-Reilly | Satoh | Graff-Radford | Machulda | Lowe | Josephs | Whitwell	**Neha Singh-Reilly**, Department of Neurology, Mayo Clinic, Rochester, MN, US
Board 146	Neuropathological evaluation of the off-target binding of flortaucipir in FTLD subcortical regions: interconnecting tau	Gatto | Youssef | Uruk | Fu | Reichard | Lowe | Whitwell | Josephs	**Rodolfo Gatto**, Department of Neurology, Mayo Clinic, Rochester, MN, US

	aggregates with iron deposition and neuroinflammation		
Board 147	Patterns of cognitive decline in individuals with elevated p-tau217 and low levels (<20 Centiloids) of neocortical Aβ-PET signal	Townsend | Properzi | Klinger | Schultz | Coughlan | Yau | Birkenbihl | Seto | Hanseeuw | Jacobs | Farrell | Yang | Papp | Rentz | Johnson | Sperling | Chhatwal | Amariglio | Buckley	**Diana Townsend**, Department of Neurology, Massachusetts General Hospital, Boston, MA, US
Board 148	Anatomic specificity of inflammation TSPO PET biomarkers in dementia	Finn | Faridar | Toledo | Nakawah | Roman | Masdeu | Pascual	**Belen Pascual**, Houston Methodist Research Institute, Weill Cornell Medicine, Houston, TX, US
Board 149	Head-to-head comparison of longitudinal plasma assays in relation to longitudinal amyloid pathology in Alzheimer's disease	Yakoub | Qiu | Villeneuve | Pichet Binette | ADNI Foundation for the National Institutes of Health (FNIH) Biomarkers Consortium	**Yara Yakoub**, Douglas Mental Health University Institute, Montréal, QC, CA
Board 150	Characterization of PART using MK-6240, Flortaucipir, and plasma p-tau217	Soares | L. Ferreira | Ruppert | S. Medeiros | Rocha | Bellaver | Povala | Bauer-Negrini | Amaral | Bloomquist | Lussier | Masdeu | L. Tudorascu | Soleimani-Meigooni | Fortea | Lowe | Oh | Pascual | A. Gordon | Rosa-Neto | Baker | A. Pascoal	**Carolina Soares**, University of Pittsburgh, Department of Psychiatry, Pittsburgh, PA, US
Board 151	Longitudinal rate of change in CSF biomarkers is associated with subsequent Tau PET burden in Braak stages I and II: Findings from the BIOCARD study	Rani | Moghekar | Callow | Alm | Pettigrew | Soldan | Miller | Wang | Albert | Bakker	**Nisha Rani**, Department of Psychiatry and Behavioral Sciences, Johns Hopkins University School of Medicine, Baltimore, MD, US
Board 152	Head-to-head comparison of four tau-PET tracers for in vivo Braak staging: the HEAD Study	Cassa Macedo | Rahmouni | Tissot | Therriault | Servaes | Wang | Trudel | Aumont | Hall | Chan | Zheng | Lussier | Ferreira | Bellaver | Povala | Pascual | Gordon | Lowe | Oh | Soleimani-Meigooni | Baker | Pascoal | Rosa-Neto	**Arthur Cassa Macedo**, Department of Neurology and Neurosurgery, McGill University, Montreal, QC, CA
Board 153	Astrogliosis in the early-stages of Alzheimer's disease	Dore | Bourgeat | Harada | Furumoto | Mulligan | Xia | Paranawithana | Laws | Feizpour | Bozinovski | Huang | Lopresti | Ikonomovic | Fripp | Okamura | Rowe | Villemagne	**Victor L. Villemagne**, The Australian e-Health Research Centre, The Commonwealth Scientific and Industrial Research Organisation (CSIRO), Melbourne, AU
Board 154	Identifying an optimal aβ cutoff point for progression from mild cognitive impairment to Alzheimer's disease: comparing cognitive performance and aβ pet insights	Shishegar | Bourgeat | Dore | Laws | Porter | Weiner | Masters | Maruff | Sohrabi | Fripp | Villemagne | Rowe	**Pierrick Bourgeat**, School of Psychological Sciences and Turner Institute for Brain and Mental Health, Monash University, Melbourne, Australia, Melbourne, AU
Board 155	Amyloid modifies the association between late-life BMI and longitudinal cognition in cognitively unimpaired individuals	Yau | Raman | Wang | Aggarwal | Brickman | Chhatwal | Cogswell | Graff-Radford | Pillai | Rafii | Aisen | Sperling | A4 and Learn Study Teams	**Wai-Ying Wendy Yau**, Massachusetts General Hospital, Boston, MA, US
Board 156	Amyloid spatial extent captures early tau burden and cognitive deficits, measured by PACC and digital clock drawing test, in preclinical Alzheimer's disease	Thompson | Fu | Farrell | Thibault | Slade | Del Carmen Montenegro | Robinson | Jutten | Davis | Penney | Rodriguez Alonso | Sperling | Rentz | Price | Johnson	**Jackson Thompson**, Massachusetts General Hospital, Harvard Medical School, Boston, MA, US
Board 157	Findings from dynamic [18F]-MK6240 PET imaging after motion and partial volume corrections	Tiss | Gong | Lois | Dhaynaut | Guehl | El Fakhri | Johnson | Ouyang	**Amal Tiss**, Department of Radiology, Massachusetts General Hospital and Harvard

			Medical School, Boston, MA, US
Board 158	Harmonization of MK6240 and Flortaucipir Braak Staging	Rocha | Bellaver | Ruppert | L. Ferreira | Soares | Medeiros | Povala | Amaral | Bauer-Negrini | Lussier | Scarpatto Rodrigues | Oliveira Jr. | Saha | Bloomquist | Masdeu | L. Tudorascu | Soleimani-Meigooni | Fortea | Lowe | Oh | Pascual | A. Gordon | Rosa-Neto | Baker | A. Pascoal	**Andreia Rocha**, University of Pittsburgh, Department of Psychiatry, Pittsburgh, PA, US
Board 159	Comparison of MK-6240 PET and Flortaucipir tau PET imaging for the biological staging of Alzheimer's disease	Scop Medeiros | L. Ferreira | Bellaver | Ruppert | Zalzale | Soares | Povala | Bauer-Negrini | Rocha | S. Rodrigues | Oliveira | Mroue | Saha | Amaral | Lussier | Bloomquist | L. Tudorascu | Masdeu | Soleimani-Meigooni | Fortea | Lowe | Oh | Pascual | A. Gordon | Rosa-Neto | P. Schilling | Baker | A. Pascoal	**Marina Scop Medeiros**, University of Pittsburgh, Pittsburgh, PA, US
Board 160	Impact of early-stage amyloidosis on tau accumulation throughout the medial temporal lobe and neocortex	Slade | Thibault | Thompson | Fu | Becker | Price | Tiss | Gong | Sperling | Johnson | Farrell	**Elliott Slade**, Athinoula A. Martinos Center for Biomedical Imaging, Charlestown, MA, US
Board 161	Associations between age-related tau deposition and neural selectivity in cognitively unimpaired older adults	Sheng | Trelle | Young | Romero | Park | Sai | Vossler | Wagner | Mormino	**Jintao Sheng**, Stanford University, Stanford, CA, US
Board 162	Posterior white matter hyperintensity is related to the emergence of lobar cerebral microbleeds in ADNI	Saukkonen | Yang | Loghmani | Schultz | Greenberg | Sperling | Chhatwal | Shirzadi	**Daniel Saukkonen**, Department of Neurology, Brigham and Women's Hospital, Harvard Medical School, Boston, MA, US
Board 163	Defining the grey zone thresholds for tau PET positivity using the Uniτ scale	Povala | Bellaver | Bauer-Negrini | Ruppert | Medeiros | Amaral | Lussier | Lukasewicz | Soares | Tudorascu | Masdeu | Pascual | Gordon | Lowe | Oh | Soleimani-Meigooni | Rosa-Neto | Baker | A. Pascoal	**Guilherme Povala**, University of Pittsburgh, Department of Psychiatry, Pittsburgh, PA, US
Board 164	Neocortical amyloid spatial extent predicts cognitive decline over time in memory and executive function domains	Thibault | Fu | Thompson | Slade | Jacobs | Price | Rentz | Sperling | Johnson | Farrell	**Emma Thibault**, Massachusetts General Hospital, Boston, MA, US
Board 165	Patterns of tau-PET accumulation and clinical progression according to biological AD stages	Trudel | Therriault | Rahmouni | Cassa Macedo | Servaes | Aumont | Hosseini | Fernandez-Arias | Zheng | Wang | Chan | Hall | Stevenson | Hopewell | Hung-Hsin Hsiao | Gauthier | Vitali | Pascoal | Rosa-Neto	**Lydia Trudel**, Translational Neuroimaging Laboratory, McGill University, Montreal, QC, CA
Board 166	The Tau Progression Index (TPI): an individualized, clinically applicable, multimodally-derived score to predict AD progression	Chiang | Butler | Ghaderi Yazdi | Ozoria | Chernek | Calimag | Blum | Pahlajani | Foldi | Khalafi | Devanand | He | Hojjati | Gholipour Picha | Habeck | Stern | Razlighi	**Qolamreza Razlighi**, Weill Cornell Medicine, New York, NY, US
Board 167	Dried plasma spot optimization for the NULISAseq CNS panel	Wilson | Rea Reyes | Fredricks | team | Rusch | VandenLangenberg | Jensen | Marshall | Keske | Weninger | Jeffers | Huber | Johnson | Zetterberg	**Rachael Wilson**, Wisconsin Alzheimer's Disease Research Center, School of Medicine and Public Health, University of Wisconsin - Madison, Madison, WI, US

Board 168	Clinical validation of the Lumipulse G1200 automated immunoassay for the measurement of Alzheimer's disease plasma biomarkers	Chan | Rahmouni | Zheng | Congalves | Macedo | Aumont | Therriault | Hall | Wang | Trudel | Servaes | Fernandez-Arias | Hopewell | Zetterberg | Pascoal | Benedet | Rosa-Neto	**Tevy Chan**, Translational Neuroimaging Laboratory, The McGill University Research Centre for Studies in Aging, Montréal, QC, Canada, Montreal, QC, CA
Board 169	Sex differences in synaptic loss in early Alzheimer's disease	Galbraith | Abuwarda | O'Dell | Mecca | van Dyck | Fredericks	**Jordan Galbraith**, Department of Neurology, Yale School of Medicine, New Haven, CT, US
Board 170	Assessing the generalizability of AD subtypes across diverse cohorts: HABS-HD and ADNI	An | Gordon | Sotiras | Millar | O'Bryant | Ances | Meeker	**Gordon Zhaoqi An**, Devision of Computational and Data Sciences at Washington University in St. Louis, St. Louis, MO, US
Board 171	Locus coeruleus - medial temporal lobe functional connectivity confers protection against amyloid-related cognitive decline in the context of high cognitive reserve	Heinrich | Prokopiou | Wiklund | Papp | Rentz | Sperling | Johnson | Jacobs	**Lukas Heinrich**, Department of Radiology, Massachusetts General Hospital / Harvard Medical SChool, Boston, MA, US
Board 172	Effect of AD risk factors on tau-PET tracer uptake and its association with amyloid-β pathology	Rodrigues | Bellaver | Povala | Bauer-Negrini | Lussier | Lulasewicz Ferreira | Silva Oliveira Junior | Rocha | Saha | Rupert | Scop Medeiros | Masdeu | Tudorascu | Soleimani-Meigooni | Fortea | Lowe | Oh | Pascual | Gordon | Rosa-Neto | Baker | Pascoal	**Matheus Rodrigues**, University of Pittsburgh, Department of Psychiatry, Pittsburgh, PA, US
Board 173	PI-2620 uptake in the medial temporal lobes discriminates Alzheimer's disease from normal cognition and non-Alzheimer's dementias	Phillips | Temirova | Kamel | Hareras | Ibe | Hlava | Xie | Cousins | Shaw | Das | Maneval | Manning | Brown | Lopez | Keegan | Stephens | McMillan | Irwin | Li | Nasrallah | Wolk	**Jeffrey Phillips**, University of Pennsylvania, Philadelphia, PA, US
Board 174	Characterizing associations with Aβ burden in non-Hispanic Black participants across US POINTER and A4/LEARN cohorts	Robinson | Papp | Harrison | Baker | Snyder | Sperling | Amariglio | Landau | STUDYTEAM | Study Group	**Talia Robinson**, Brigham and Women's Hospital, Boston, MA, US

117 Concordance between visual and quantitative amyloid PET and CSF biomarkers in the ADNI-DOD cohort

Agathe Vrillon[1,6], Ganna Blazhenets[1], Julien Lagarde[1], Konstantinos Chiotis[1], Maison Abu Raya[1,6], David Soleimani-Meigooni[1], Gil Rabinovici[1], Michael Weiner[1], Lisa Silbert[2], Nathan Hantke[2], Daniel Schwartz[2], Abigail Livny Ezer[3], Orit Lesman Segev[3], Kristine Yaffe[1], Leslie Shaw[4], Susan Landau[5], Renaud La Joie[1,6], Raquel Gardner[1,3]

[1]*University of California San Francisco, San Francisco, CA, US*
[2]*Oregon Health & Science University, Portland, OR, US*
[3]*Sheba Medical Center, Tel-Hashomer, Ramat Gan, IL*
[4]*University of Pennsylvania, Philadelphia, PA, US*
[5]*University of California Berkeley, Berkeley, CA, US*
[6]*Global Brain Health Institute, San Francisco, CA, US*

Background: Clinical factors, including comorbidities, may affect visual interpretation of amyloid PET. We evaluated the agreement between PET visual read, centiloid (CL) quantification and CSF AD biomarkers in the ADNI-DOD cohort enrolling US Veterans with a high prevalence of traumatic brain injury (TBI) and post-traumatic stress disorder (PTSD).

Methods: ADNI-DOD participants who underwent [^{18}F]Florbetapir amyloid PET were included (**Figure 1**). Visual reads (VR) were performed by one of five trained neurologists blinded to quantification. CL quantification used an MRI-free pipeline (Landau *et al.*, positivity threshold: CL ≥27). Visually and quantitatively discordant and/or challenging scans were reviewed in consensus meetings to achieve a final read. CSF AD biomarkers measured using Elecsys (Roche®) were examined for a subsample of n=140 individuals. Agreement was evaluated using Cohen's kappa (κ).

Results: We included 274 Veterans (mean age: 70.1 years; 99% male; 84% cognitively unimpaired [CU]; 16% MCI; 60% PTSD, 46% TBI). Overall, 36% (n=100/274) of scans were initially read as positive and 24% (n=67/274) were quantitatively positive (**Figure 2**). Initial visual read and quantification were concordant for 86% of scans (κ=0.67). Agreement tended to be lower in CU participants (85% agreement, κ=0.63, P=0.053) than in MCI (91% agreement, κ=0.82) and lower in the PTSD group than in the TBI group (P=0.036). Discordance (14%) was principally constituted of VR-positive/quantitatively-negative scans (92% [n=36/39 of overall disagreement]). VR-positive/quantitatively-negative scans were characterized mostly by focal tracer uptake or posterior patterns not captured by CL quantification (**Figure 3a**). Among CSF biomarkers, the CSF Ab42/40 ratio showed the highest concordance with PET, with both final VR (84% agreement, κ=0.56) and quantification (85% agreement, κ=0.52) (**Figure 3**).

Conclusion: We observed 14% of visually/quantitatively discordant scans, mostly visually positive with low CL, more common in CU than in MCI participants. PET visual read and quantification had equivalent concordance with CSF-based A status.

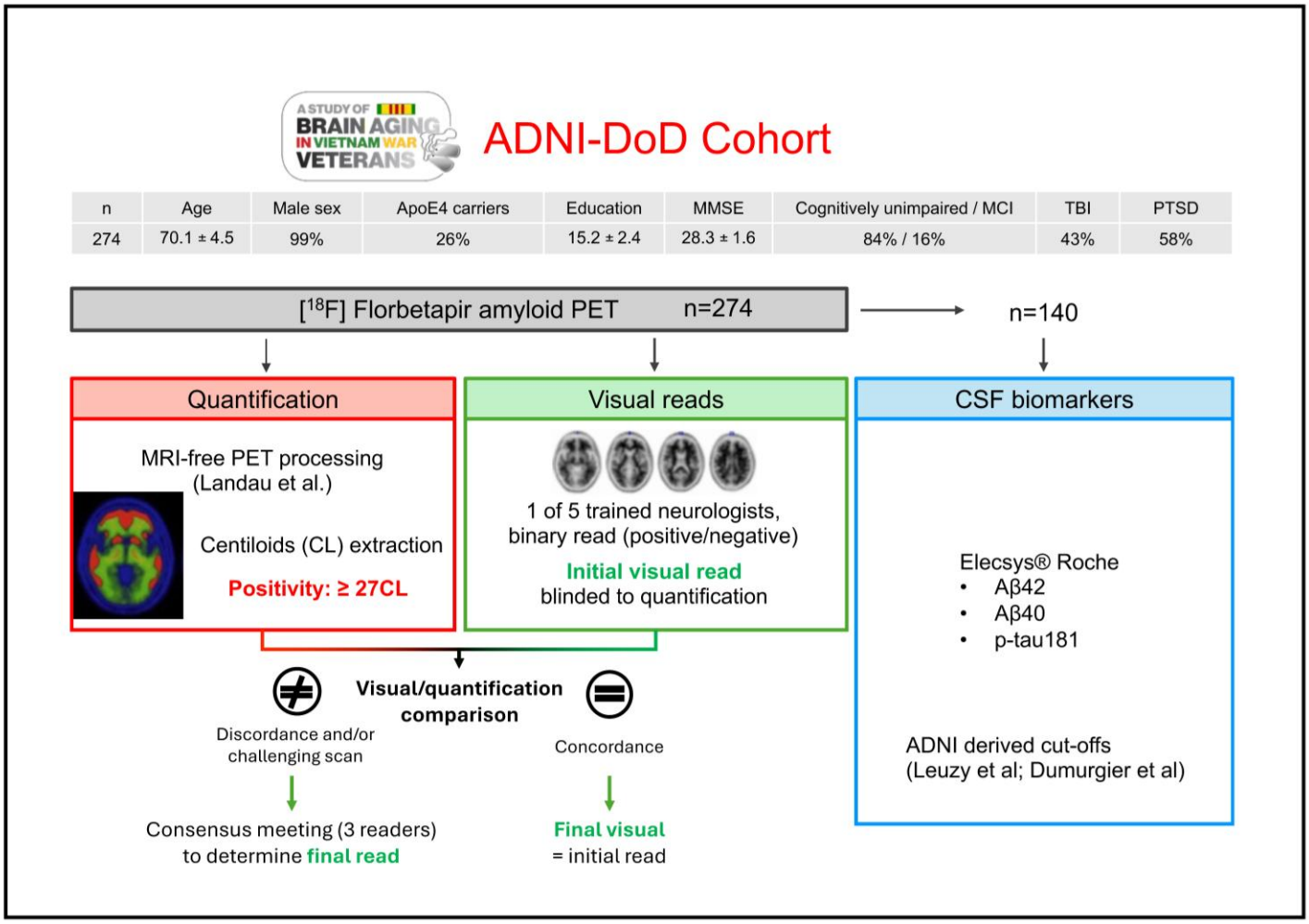


Figure 1, Cohort description and methodology of the study

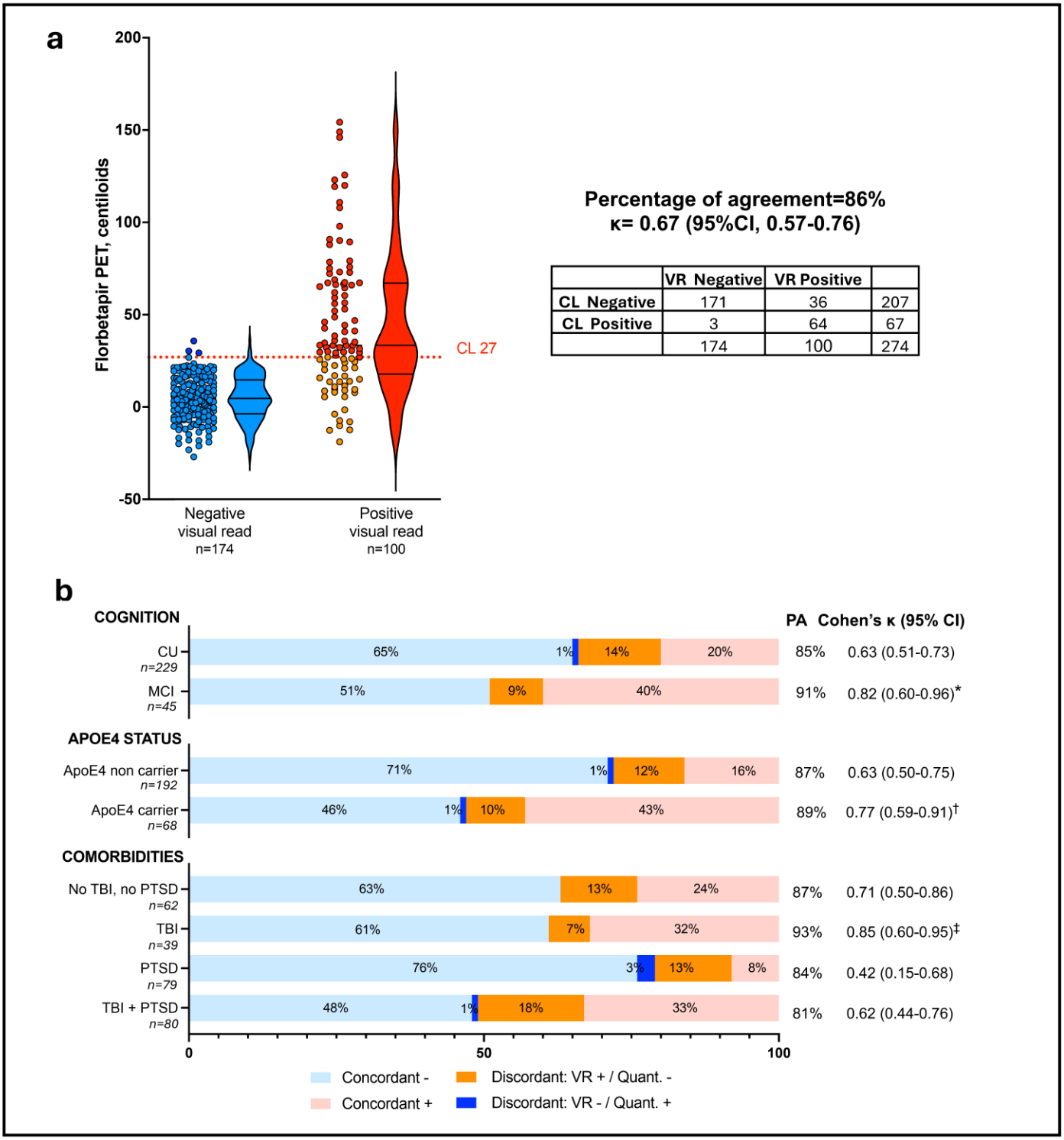


Figure 2, Concordance of initial visual read and centiloids quantification of amyloid PET

a, Centiloid values according to initial visual read in the whole cohort. Agreement of initial visual read and quantification is shown in a contingency table, with the percentage of agreement and Cohen's κ (95% confidence interval).

b, Concordance between quantification and initial visual read of amyloid PET according to clinical variables. Cohen's κ and percentage of agreement (PA) indicated for each subgroup. *Comparison of κ in CU vs. MCI, P=0.053. ‡Comparison of κ in ApoE4 carriers vs. non-carriers P=0.190. ᶜComparison of κ in comorbidities groups: PTSD vs. TBI group, P=0.036.

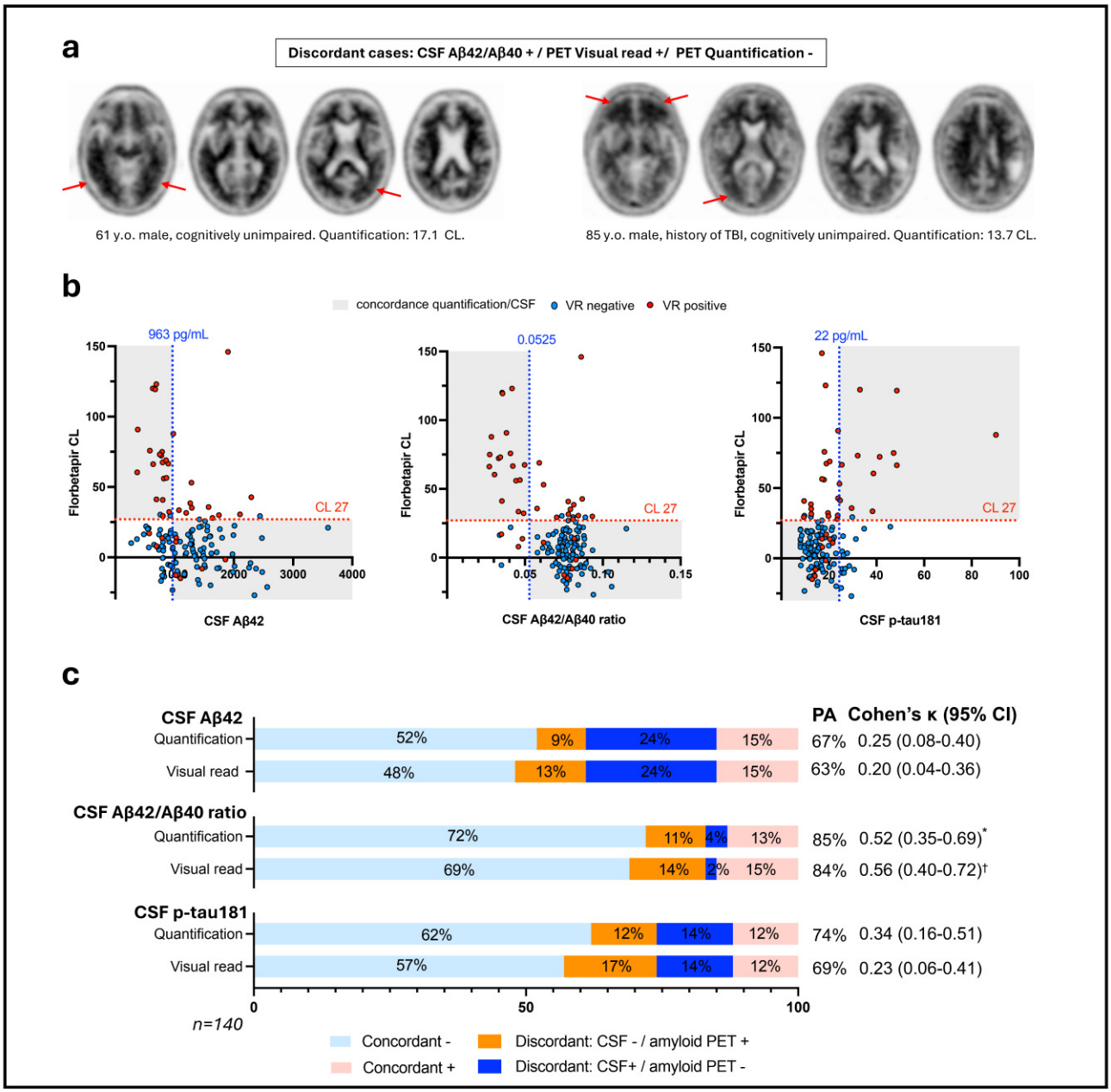


Figure 3, Concordance of CSF AD biomarkers with amyloid PET

a, Amyloid PET in 2 examples of discordant cases. Visual read corresponds to the final read after review in consensus meeting. Red arrows are pointing to cortical tracer uptake.

b, Scatter plots of centiloid quantitation versus CSF biomarkers levels, including Aβ42, Aβ42/Aβ40 ratio, and p-tau181 levels, color-coded by final visual read status. Cut-offs for positivity are indicated as dotted lines, on the y-axis for the centiloid cut-off and on the x-axis for the CSF biomarker.

c, Bar plots displaying concordance between amyloid PET markers (quantification or final visual read) with CSF biomarkers Aβ42, Aβ42/Aβ40 ratio, and p-tau181. Percentage of agreement (PA) and Cohen's κ are indicated for each pair of biomarkers. *Higher concordance of CSF Aβ42/Aβ40 with CL-quantification than that of Aβ42 (P=0.001). †Higher concordance of CSF Aβ42/Aβ40 ratio with amyloid-PET visual read than that of CSF Aβ42 and of p-tau181 (P<0.05).

Keywords: amyloid PET; visual reads; centiloids; CSF biomarkers; veterans

118 Calibration of multi-site raters for prospective visual read of amyloid PET scans acquired across the ADRC Consortium for Clarity in ADRD Research Through Imaging (CLARiTI)

David Soleimani-Meigooni[1,2], Ganna Blazhenets[1], Renaud La Joie[1], Zoe Lin[1], Carol Soppe[1], Derek Johnson[3], Mary Ellen Koran[4], Jonathan McConathy[5], Ilya Nasrallah[6], Jeremy Tanner[7], Victor Villemagne[8], Charles Windon[1], Michael Zeineh[9], Elizabeth Mormino[10], Sterling Johnson[11], Gil Rabinovici[1,12]

[1]*Department of Neurology, Memory and Aging Center, Weill Institute for Neurosciences, University of California, San Francisco, CA, US*
[2]*Molecular Biophysics and Integrated Bioimaging, Lawrence Berkeley National Laboratory, Berkeley, CA, US*
[3]*Division of Nuclear Medicine, Department of Radiology, Mayo Clinic, Rochester, MN, US*
[4]*Division of Nuclear Medicine, Department of Radiology, Mayo Clinic, Phoenix, AZ, US*
[5]*Division of Molecular Imaging and Therapeutics, Department of Radiology, University of Alabama at Birmingham, Birmingham, AL, US*
[6]*Department of Radiology, University of Pennsylvania, Philadelphia, PA, US*
[7]*Biggs Institute for Alzheimer's and Neurodegenerative Diseases, University of Texas Health Science Center, San Antonio, TX, US*
[8]*Department of Psychiatry, University of Pittsburgh School of Medicine, Pittsburgh, PA, US*
[9]*Department of Radiology, Stanford University School of Medicine, Stanford, CA, US*
[10]*Department of Neurology and Neurological Sciences, Stanford University School of Medicine, Stanford, CA, US*
[11]*Wisconsin Alzheimer's Institute, University of Wisconsin School of Medicine and Public Health, Madison, WI, US*
[12]*Department of Radiology and Biomedical Imaging, University of California, San Francisco, CA, US*

Background: PET visual reads for multi-center studies are conducted centrally by one or a few experts. In CLARiTI, a broader network of raters will perform the reads, necessitating methods to ensure their accuracy and reliability.

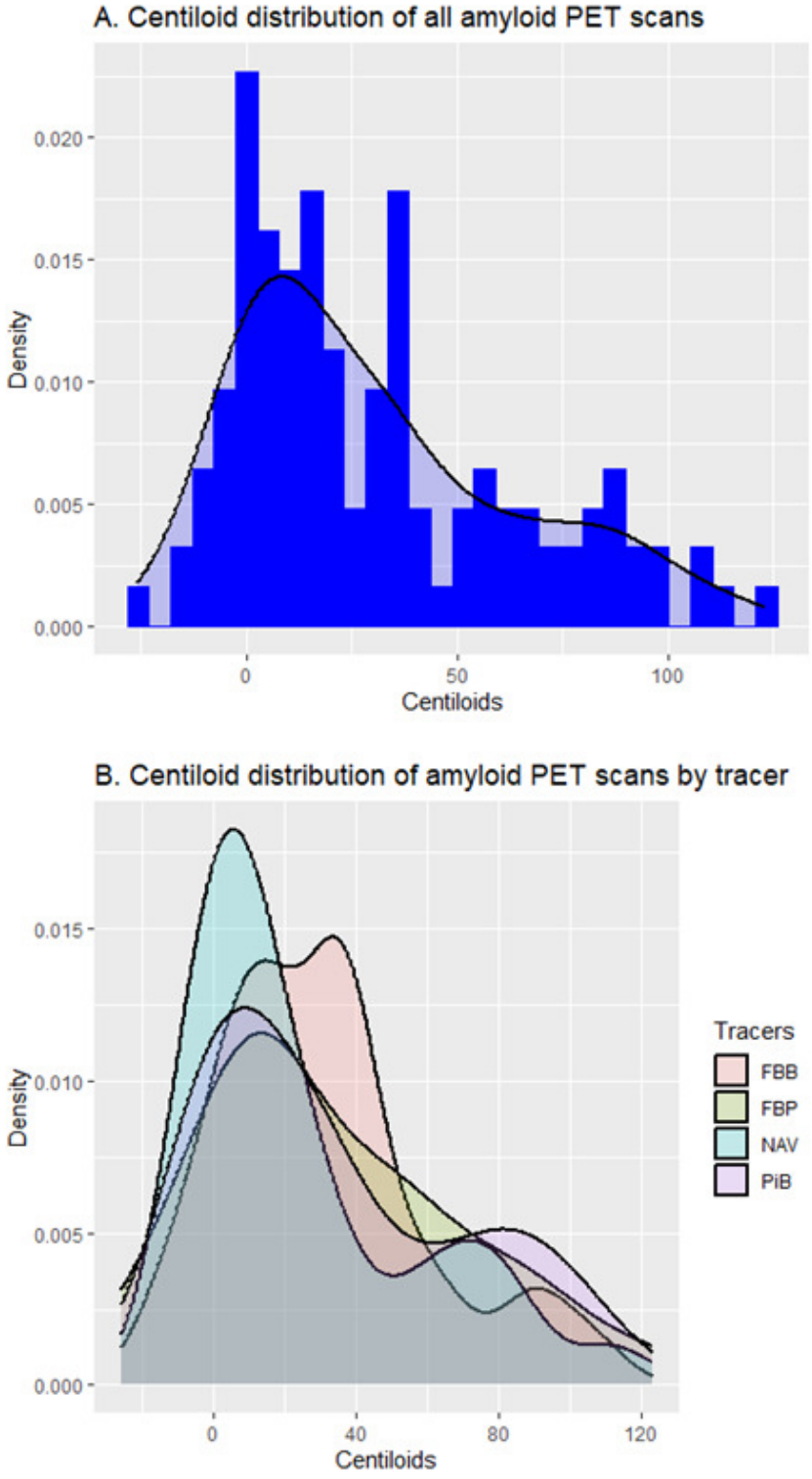
Methods: All ADRC sites (N=37) will prospectively acquire amyloid PET scans for 800 cognitively unimpaired and 1200 cognitively impaired participants. Each site can use one of four amyloid PET tracers (^{18}F-florbetapir, ^{18}F-florbetaben, ^{18}F-NAV4694, ^{11}C-PIB). PET scans will be visually interpreted by ten PET neuroimaging experts located across eight ADRCs, using their preferred hardware, software, and file format (DICOM, NIFTI). Calibration requires each reader to perform blinded, independent visual interpretation of 180 amyloid PET scans (30 unique and 15 duplicate scans per tracer), previously read and selected by an expert. An even mix of visually non-elevated and elevated scans were selected, with quantitation spanning ~20-120 Centiloids (**Figure 1**), and 15% were visually borderline (similar proportion to ADNI4), with quantitation spanning 4-48 Centiloids (mean 21).

Results: Calibration scans were read by a second expert not serving in CLARiTI. There was 97% concordance and almost perfect agreement between readers (κ=0.932, p<0.001; **Figure 2**). Discordantly read scans were visually borderline elevated (N=2), borderline non-elevated (N=1), and negative (N=1), with quantitation of 8-21 Centiloids (mean 14). Intra-rater reads were 98% concordant and had almost perfect agreement (κ=0.966, p<0.001). These findings hold promise for scaling-up visual reads in CLARiTI, and we expect ≥80% concordance and substantial to almost perfect agreement ($\kappa \geq 0.7$) for inter/intra-rater reliability.

Conclusions: Calibration is essential for accurate/reliable amyloid PET visual reads in large multi-center studies with multiple raters. Involving multiple raters across different sites, who use diverse hardware/software/format combinations, will mirror the natural heterogeneity present in real-world clinical practice. This calibration set can

also serve as a standardized training tool for other studies incorporating amyloid PET visual reads.

Figure 1. Centiloid distribution of unique scans in visual read calibration set.



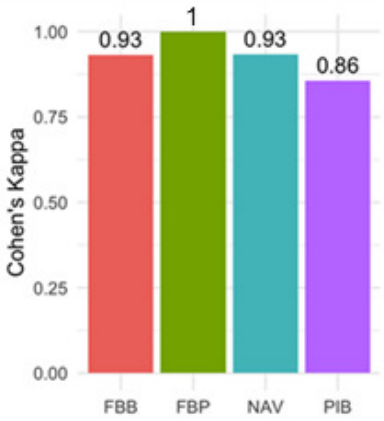
FBB=^{18}F-florbetaben; FBP=^{18}F-florbetapir; NAV=^{18}F-NAV4694; PiB=^{11}C-Pittsburgh Compound B

Figure 2. Inter- and intra-rater agreement of amyloid PET visual reads.

A. Inter-rater agreement

Cohen's kappa for 2 raters
120 subjects, $\kappa = 0.932$

All scans		Rater 2 negative	Rater 2 positive
Rater 1	negative	51	2
	positive	2	65



FBB	Rater 2 negative	Rater 2 positive
Rater 1 negative	12	1
Rater 1 positive	-	17

FBP	Rater 2 negative	Rater 2 positive
Rater 1 negative	14	-
Rater 1 positive	-	16

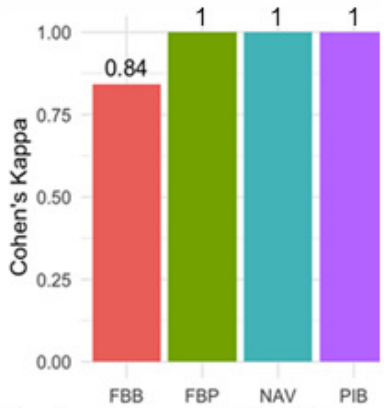
NAV	Rater 2 negative	Rater 2 positive
Rater 1 negative	15	-
Rater 1 positive	1	14

PIB	Rater 2 negative	Rater 2 positive
Rater 1 negative	10	1
Rater 1 positive	1	18

B. Intra-rater agreement

Cohen's kappa for a single rater
60 subjects, $\kappa = 0.966$

All scans		2nd read negative	2nd read positive
1st read	negative	25	-
	positive	1	34



FBB	2nd read negative	2nd read positive
1st read negative	4	-
1st read positive	1	10

FBP	2nd read negative	2nd read positive
1st read negative	6	-
1st read positive	-	9

NAV	2nd read negative	2nd read positive
1st read negative	10	-
1st read positive	-	5

PIB	2nd read negative	2nd read positive
1st read negative	5	-
1st read positive	-	10

FBB=^{18}F-florbetaben; FBP=^{18}F-florbetapir; NAV=^{18}F-NAV4694; PiB=^{11}C-Pittsburgh Compound B

Keywords: amyloid PET, visual reads, multi-site reader calibration

119 Evaluating the effect of APOE genotype in real-world clinical settings: results from the IDEAS-ANGI study

Stefania Pezzoli[1], Caroline Jonson[1], Ganna Blazhenets[1], Daniel Schonhaut[1], Jhony M. Perez[1], Alexis Oddi[1], Ale Castruita[1], Kaitlin B. Casaletto[1], Lucy Hanna[2], Andrew March[3], Constantine Gatsonis[2,4], Maria C. Carrillo[5], Tatiana M. Foroud[6], Renaud La Joie[1], Jennifer S. Yokoyama[1], Gil D. Rabinovici[1]

[1]*Memory and Aging Center, Department of Neurology, University of California, San Francisco, San Francisco, CA, US*
[2]*Center for Statistical Sciences, Brown University School of Public Health, Providence, RI, US*
[3]*Center for Research and Innovation, American College of Radiology, Reston, VA, US*
[4]*Department of Biostatistics, Brown University School of Public Health, Providence, RI, US*
[5]*Alzheimer's Association, Chicago, IL, US*
[6]*Department of Medical and Molecular Genetics, Indiana University, Indianapolis, IN, US*

Background: Real-world data about the clinical utility of *APOE* genotype in memory care are lacking. The ANGI study analyzed DNA from a subset of IDEAS participants. We leveraged this large dataset to assess the predictive value of *APOE* genotype in determining amyloid status and burden in real-world memory care.

Methods: 1637 Medicare beneficiaries with cognitive impairment enrolled in ANGI-IDEAS were included. Amyloid PET positivity was determined using (a) local community visual reads and (b) a Centiloid threshold of 24.4. Centiloids were calculated using a PET-only pipeline in a subset of 1149 participants. Logistic regression assessed the odds of amyloid positivity, while ANCOVA investigated differences in global amyloid burden, measured in Centiloids, adjusting for demographic and clinical characteristics.

Results: Demographics and clinical features are shown in Table 1. Among the total sample, 38% were *APOE4* heterozygotes and 10% were homozygotes. Compared to *APOE3/3*, *APOE3/4 and APOE4/4* carriers showed higher dementia rates ($p<0.001$) and lower MMSE scores ($p<0.001$). Compared to *APOE3/3*, individuals with the *APOE2/4*, *APOE3/4*, and *APOE4/4* genotypes had higher odds of being amyloid positive, following a dose-dependent gradient of increasing risk (Table 2). *APOE2* carriers (*APOE2/2* or *APOE2/3*) had lower odds of being amyloid positive compared to *APOE3/3* (significant only with Centiloid threshold, Table 2). An interaction between *APOE3/4* genotype and sex (male reference) showed an odds ratio of 2.18 (95% CI: 1.29–3.70, $p=0.004$), indicating that *APOE3/4* females had higher odds of amyloid positivity (visual reads). Amyloid burden increased progressively across *APOE* genotypes, with higher-risk genotypes (*APOE3/4* and *APOE4/4*) showing the highest Centiloids (Figure 1).

Conclusion: These findings are particularly important for real-world clinical settings, where genetic risk stratification can inform prevention strategies and treatment decisions. Incorporating genetic information into care may allow for more tailored and personalized interventions, potentially leading to improved clinical outcomes.

Table 1. Demographic and clinical characteristics.

Characteristic	*APOE2+* [a] (N=106)	*APOE3/3* (N=699)	*APOE2/4* (N=45)	*APOE3/4* (N=630)	*APOE4/4* (N=157)
Age, y, Mean (SD)	74.4 (5.74)	74.9 (5.79)	74.2 (6.67)	74.1 (5.20)	71.9 (5.15)
Sex, Female, No. (%)	48 (45.3)	290 (41.5)	20 (44.4)	282 (44.8)	74 (47.1)
Race, No. (%)					
Black or African American	2 (1.9)	7 (1.0)	0 (0)	8 (1.3)	5 (3.2)
White	100 (94.3)	655 (93.7)	45 (100)	590 (93.7)	149 (94.9)
Other race	4 (3.8)	37 (5.3)	0 (0)	32 (5.1)	3 (1.9)
Hispanic ethnicity, No. (%)	0 (0)	15 (2.1)	2 (4.4)	8 (1.3)	2 (1.3)
Highest level of education, No. (%)					
High school graduate or less	22 (20.8)	102 (14.6)	7 (15.6)	139 (22.1)	32 (20.4)
Some college or associate degree	25 (23.6)	159 (22.7)	8 (17.8)	126 (20.0)	31 (19.7)
Bachelor's degree	25 (23.6)	199 (28.5)	14 (31.1)	179 (28.4)	41 (26.1)
Postgraduate degree	34 (32.1)	239 (34.2)	16 (35.6)	186 (29.5)	53 (33.8)
Impairment level, No. (%)					
Mild cognitive impairment	86 (81.1)	550 (78.7)	37 (82.2)	445 (70.6)	98 (62.4)
Dementia	20 (18.9)	149 (21.3)	8 (17.8)	185 (29.4)	59 (37.6)
MMSE [b], Mean (SD)	26.0 (4.05)	26.6 (3.41)	27.0 (2.73)	25.5 (4.33)	24.7 (4.47)
Visual reads, Amyloid positive, No. (%)	42 (39.6)	351 (50.2)	33 (73.3)	510 (81.0)	150 (95.5)
Centiloids [c], Amyloid positive, No. (%)	17 (24.3)	222 (44.8)	25 (83.3)	355 (80.9)	107 (93.9)

[a] *APOE2+* includes four *APOE2/2* carriers and 102 *APOE2/3*; [b] Participants, total n=1229; [c] Participants, total n=1149.

Table 2. *APOE* genotype and amyloid positivity risk.

Aβ positivity	Carriers, No.	OR (95% CI)	*p*-value
Model 1: Visual reads			
APOE2/2 or APOE2/3*	106	0.67 (0.43-1.03)	0.07
APOE3/3	699	[Reference]	NA
APOE2/4	45	3.12 (1.59-6.51)	0.001
APOE3/4	630	4.60 (3.56-5.97)	<0.001
APOE4/4	157	26.71 (13.11-64.30)	<0.001
Model 2: Centiloid-based cut-off			
APOE2/2 or APOE2/3*	70	0.39 (0.21-0.69)	0.002
APOE3/3	496	[Reference]	NA
APOE2/4	30	7.47 (2.98-22.76)	<0.001
APOE3/4	439	5.98 (4.40-8.20)	<0.001
APOE4/4	114	24.74 (11.89-60.41)	<0.001

Logistic regression models were used to predict amyloid positivity based on *APOE* genotype, with results reported as adjusted odds ratios (OR).
Model 1: Visual-reads-based amyloid positivity ~ *APOE* + Sex + Age + Race + Ethnicity + Impairment level
Model 2: Centiloid-based amyloid positivity ~ *APOE* + Sex + Age + Race + Ethnicity + Impairment level
*Including four APOE2/2 carriers in Model 1, and two in Model 2.

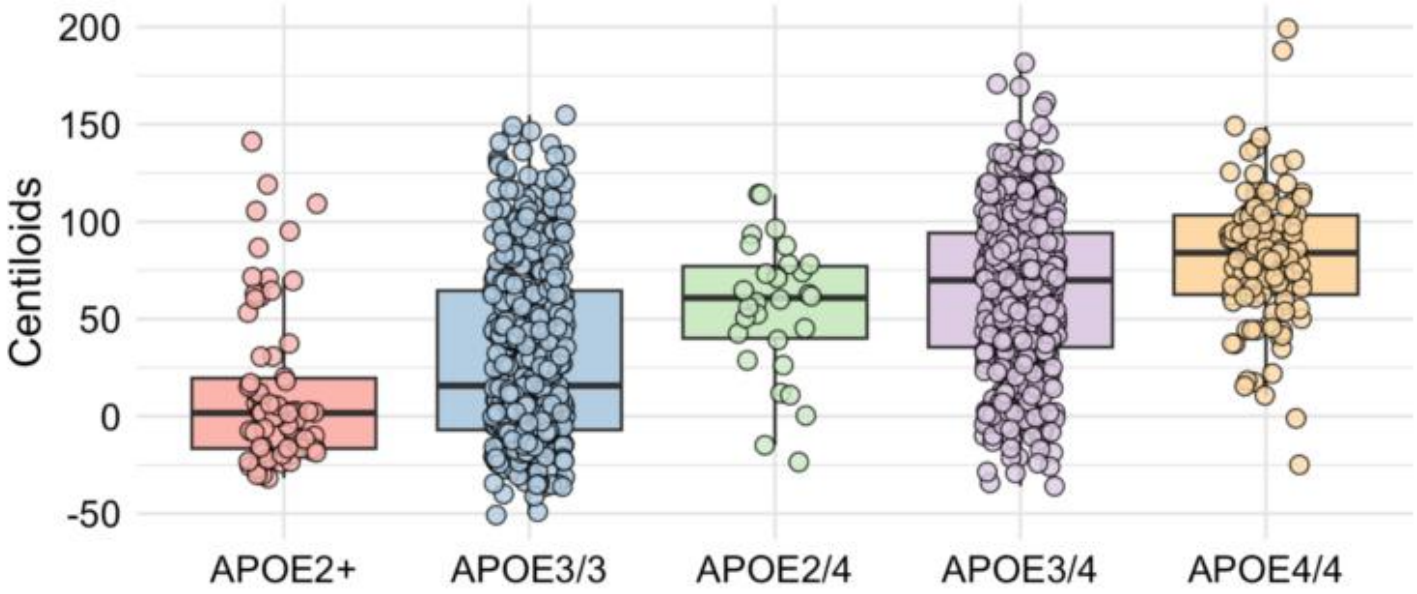


Figure 1. *APOE* genotype and Centiloid values. ANCOVA analyses revealed a significant main effect of *APOE* genotype on global amyloid burden ($p<0.001$), after controlling for age, sex, race, ethnicity and impairment level. Post-hoc comparisons revealed that all *APOE* genotype groups had significantly different amyloid burden levels, except for the comparison between *APOE2/4* and *APOE3/4*, which did not reach significance. *APOE2+* includes two *APOE2/2* and 68 *APOE2/3*.

Keywords: APOE, amyloid PET, dementia, mild cognitive impairment, real-world clinical settings

120 Brain connectivity drives tau distribution while regional vulnerability drives tau load in Alzheimer's disease

Yu Xiao[1], Vincent Bazinet[2], Olof Strandberg[1], Justine Hansen[6], Golia Shafiei[3], Nicola Spotorno[4], Hamid Behjat[4], Erik Stomrud[4], Ruben Smith[4], Sebastian Palmqvist[4], Niklas Mattsson-Carlgren[4], Alain Dagher[6], Bratislav Misic[2], Oskar Hansson[4], Jacob Vogel[1]

[1]*Department of Clinical Sciences Malmö, SciLifeLab, Lund University, Lund, SE*
[2]*McConnell Brain Imaging Centre, Montréal Neurological Institute, McGill University, Montréal, QC, CA*
[3]*Penn Lifespan Informatics and Neuroimaging Center, University of Pennsylvania, Philadelphia, PA, US*
[4]*Clinical Memory Research Unit, Department of Clinical Sciences Malmö, Faculty of Medicine, Lund University, Lund, SE*
[5]*Department of Diagnostic Radiology, Clinical Sciences, Lund University, Lund, SE*
[6]*Department of Neurology and Neurosurgery, McGill University, Montréal, QC, CA*

Objectives: In Alzheimer's disease (AD), tau accumulation is thought to be driven by global transneuronal spread, but selective regional vulnerability likely also plays a role. This study uses computational models to investigate the interplay between network spread and regional vulnerability in influencing tau spread.

Methods: Regional tau-PET data was collected from n=646 amyloid-β (Aβ)-positive elderly participants from the Swedish BioFINDER-2 study (n=219 unimpaired, 212 MCI, 215 AD). Standardized uptake value ratios (SUVR) represented tau load (Fig. 1B). SUVRs were converted to "tau-positive probabilities" (TPP) using two-component Gaussian mixture models, representing tau distribution (Fig. 1C). The Susceptible-Infectious-Recovered (SIR) model (Fig. 1A) simulated tau spread through various brain networks (Fig. 3A) while allowing a priori regional information to influence tau synthesis, clearance, spreading, or misfolding. Regional factors included Aβ-PET, gene expression from the Allen Brain Atlas and various cortical properties (e.g. metabolism, neuroreceptors, myelination, etc) from the neuromaps library. Model performance was evaluated based on the ability to reconstruct observed regional tau TPP or SUVR.

Results: Diffusion through the structural connectome explained tau distribution (TPP) better than tau load (SUVR) (Fig. 2A,B). Across all models, regional factors improved models of tau load more than tau distribution (Fig. 2C-F,3B). Top models for tau load involved structural connectivity and MAPT expression influencing regional misfolding, regional Aβ influencing spread, or cerebral blood flow influencing clearance. Top models for tau distribution involved neuroreceptor covariance and either MAPT expression or ontogenic cortical expansion (Fig 3C-F).

Conclusions: Tau distribution and load are driven by distinct elements. Braak-like tau distribution is mostly explained by structural connectivity and MAPT bioavailability, whereas regional tau load is explained by a combination of brain connectivity and regional factors. Receptor distribution seems to play an important but currently unexplained role in tau spread.

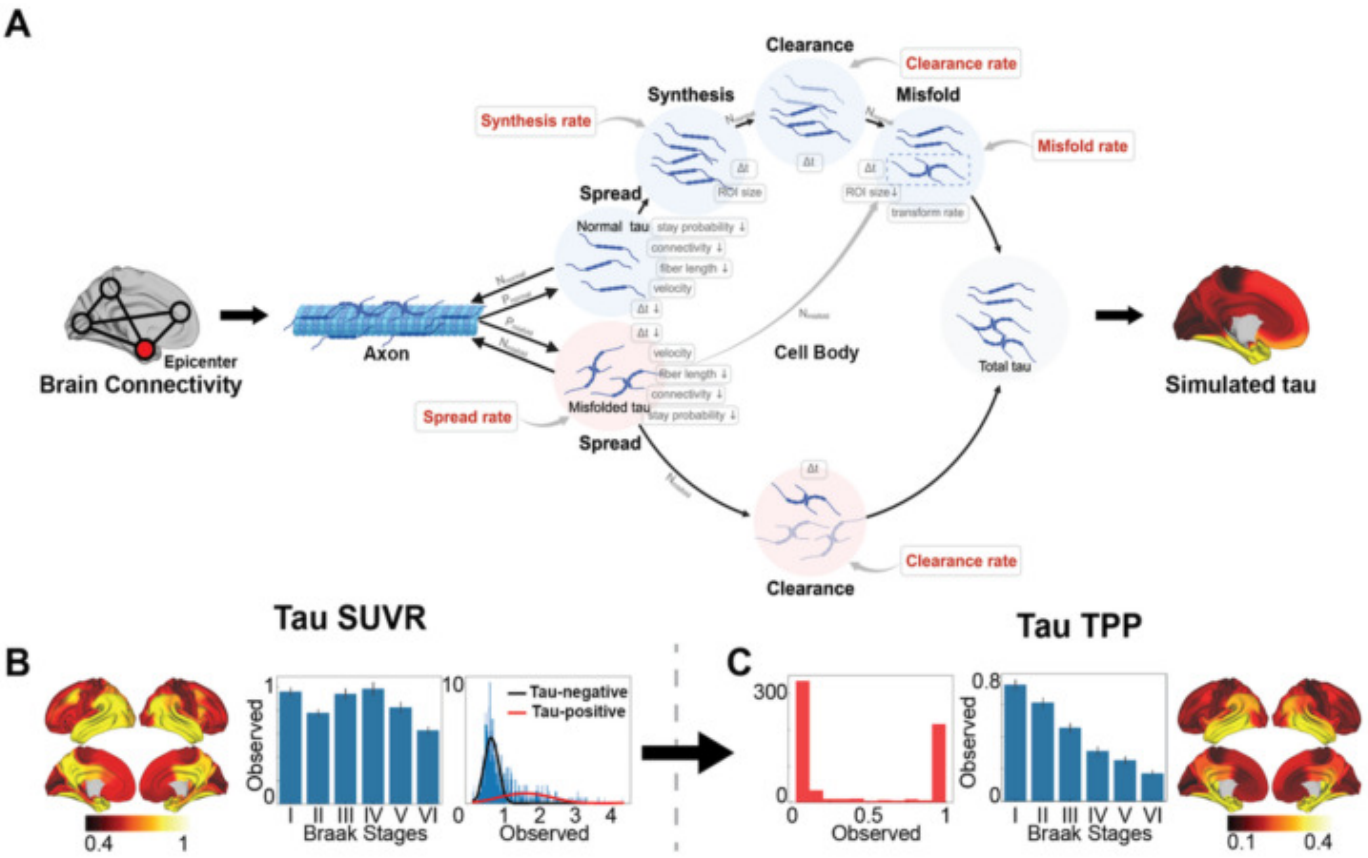


Figure 1: SIR model and tau measurements. A) The simulation process of the Susceptible-Infectious-Recovered Model includes the synthesis, clearance, and misfolding of normal tau (upper blue), and the spread and clearance of misfolded tau (bottom red). Each subprocess is affected by the parameters indicated in the grey squares. Regional biological information can be parameterized through the red highlighted variables: spread rate, synthesis rate, clearance rate, and misfold rate. B) Tau-PET SUVR was used to represent tau load. Brain plot shows average tau SUVR, normalized to a 0-1 scale using cognitively normal Aβ-negative participants as a reference group. Barplot represents mean and SEM of SUVR in Braak stage regions (from Schöll et al., 2016, Neuron) across subjects. Histogram represents SUVR distribution in an example brain region, left fusiform. C) Mixture modeling was run on SUVRs of each brain region. The posterior probabilities were used to calculate the probability that a given subject's value belonged to the tau-positive distribution. This value, tau-positive probability (TPP), was used as an index of tau distribution. This metric indicates whether tau has reached a region, but not the amount present, which is why it reflects tau distribution rather than tau load. TPP better approximates Braak staging.

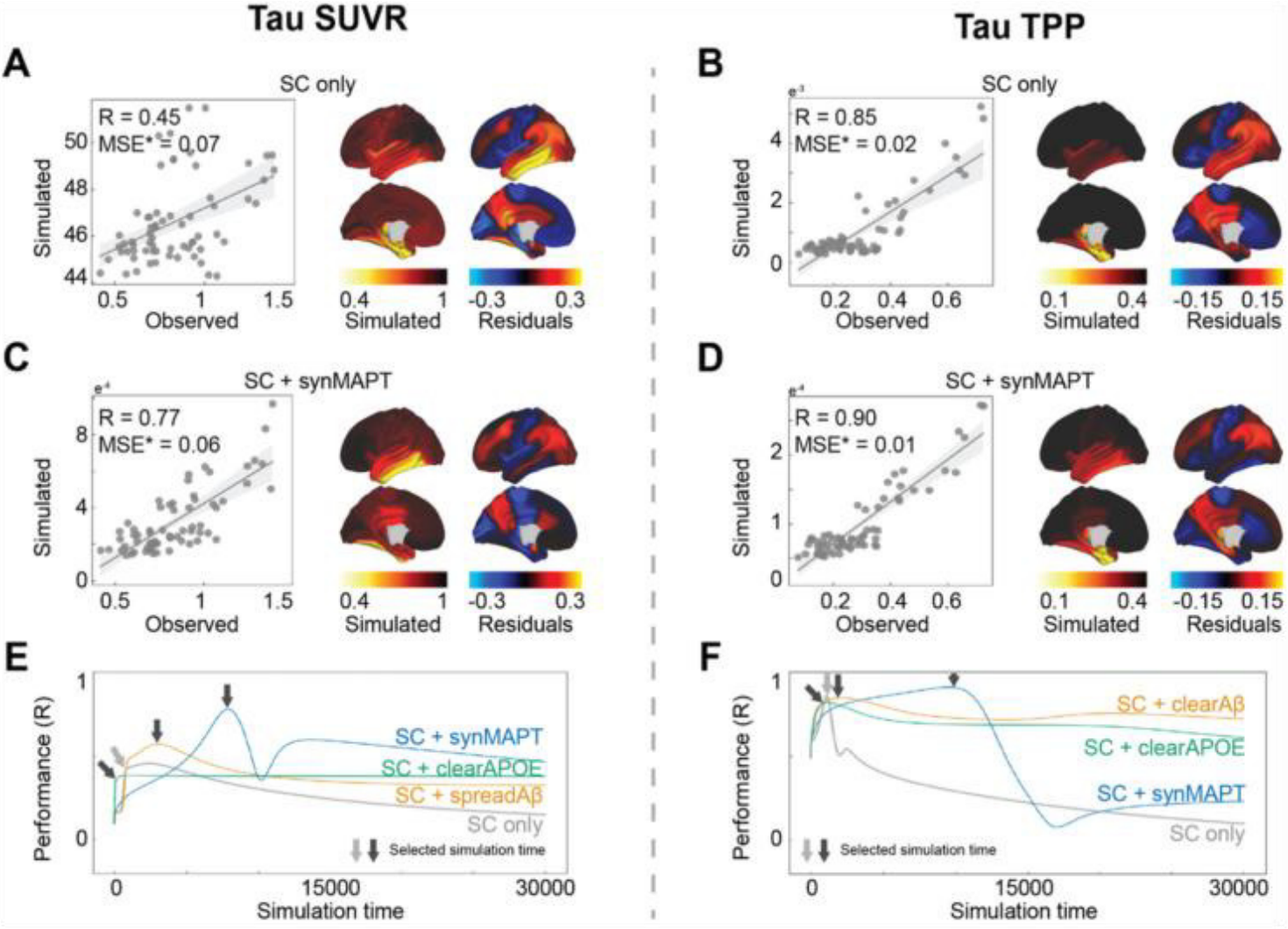


Figure 2. AD-related regional factors improve models of tau load more than models of tau distribution. Results of SIR model simulating diffusion of tau through a structural connectome (derived from healthy young individuals) using an entorhinal cortex epicenter. A) shows model performance on SUVR data, while B) shows performance on TPP data. Scatter plots compare SIR model predictions to observed tau SUVR/TPP. Brain maps project model simulated tau and model residuals. For a hypothesis-driven analysis, four regional factors were used to parameterize the model: MAPT expression influencing regional synthesis, Aβ influencing regional tau spread or APOE gene expression influencing regional tau clearance. C) shows the best-fitting model for SUVR (connectome plus MAPT expression influencing regional synthesis) while D) shows the best-fitting model for TPP (same). E) and F) show each model's performance over simulated time for SUVR and TPP, respectively.

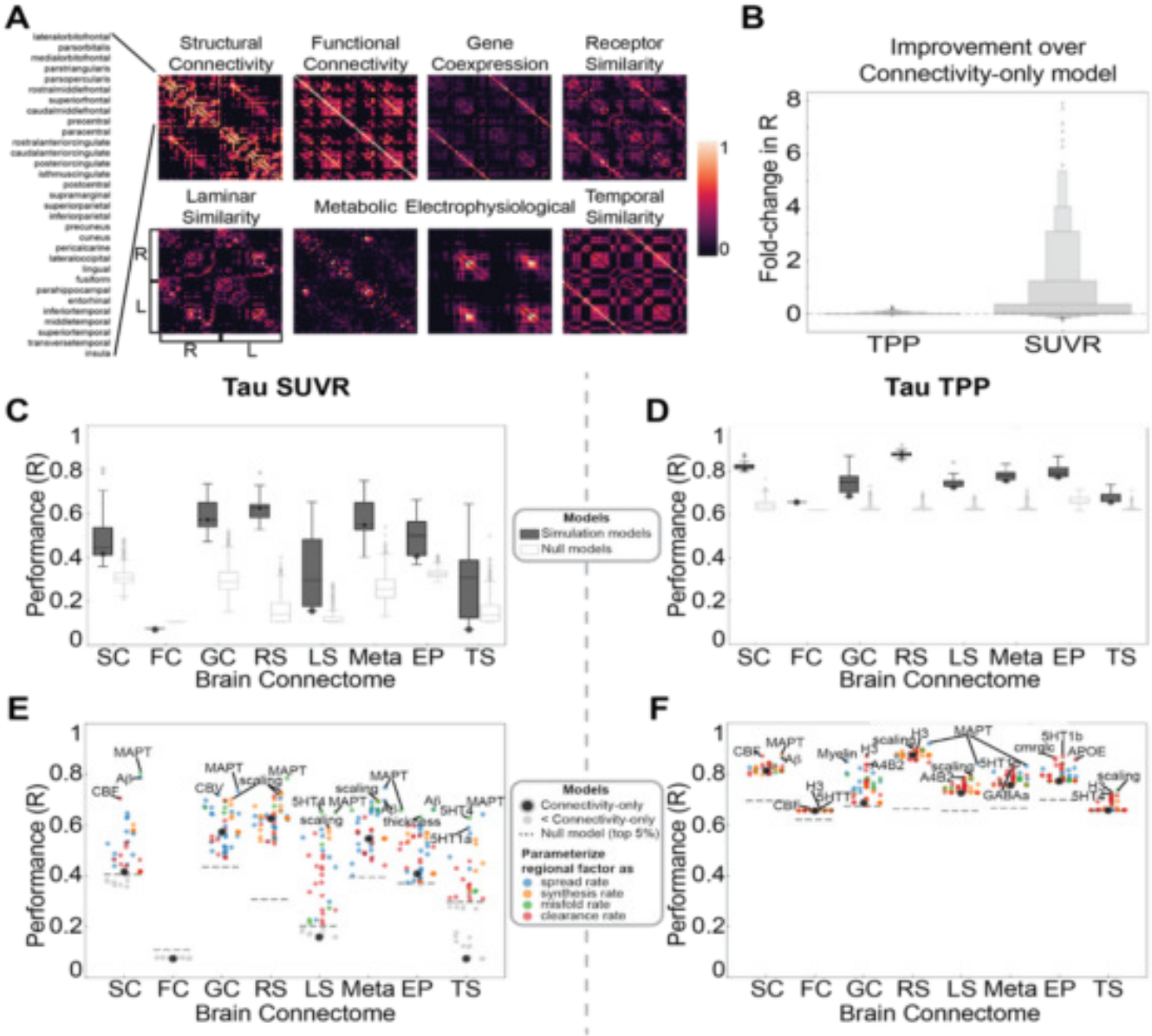


Figure 3. Exploratory analysis of factors contributing to tau spread. A) The SIR model was fit using eight different types of normative connectomes representing different types of regional relationships in the brain, extracted from Hansen et al., 2023 PLoS Biol. This includes structural connectivity (SC) measured with MRI-based diffusion tractography, thresholded MRI-based functional connectivity (FC), regional covariance/similarity in bulk RNA expression across 20,000 genes (GC), regional covariance/similarity in neuroreceptors measured with different PET tracers (RC), regional similarity in laminar profiles (LS), regional covariance in PET-based glucose metabolism (Meta), regional covariance in MEG-based electrophysiological signal across multiple bands (EP) and regional similarity across multiple functional MRI timeseries properties (TS) B) Across 1256 models, SUVR (tau load) models were more improved by the addition of regional factors than TPP (tau distribution) models were. The boxenplot shows the distribution of fold-change increase in model performance across all models. Performance of models across different types of connectomes fitted to C) SUVR and D) TPP data. Models fit TPP data better in general. Across all connectomes, connectome-only models (indicated by gray circles) exceeded chance (95% CI of 1000 models scrambling connectomes but preserving weight and degree distribution). Surprisingly, models using receptor covariance generally performed best, though the top SUVR model often used structural connectivity. E) and F) show the performance of individual models fitted to SUVR and TPP data, respectively. Each dot represents one model. The dot color indicates what parameter the regional information was influencing. Grayed-out dots did not exceed null model performance (indicated by dashed lines). The regional factor added to the model is labeled for the top 3 models of each connectome. These results suggest that widely hypothesized mechanisms do fit the tau data well (i.e. diffusion over structural connectome with MAPT expression influencing tau misfold rate, Aβ influencing regional spread rate or regional cerebral blood flow influencing clearance rate). However, other interesting mechanisms emerge as important for moderating tau load and distribution, such as allometric scaling affecting tau synthesis rate, histamine 3 (H3), vesicular acetylcholine transporter (VAChT), nicotinic acetylcholine (A4B2), and serotonin (5HT1b) receptors influencing tau clearance, serotonin (5HT4) receptor presence driving tau misfolding, and myelination shaping tau spread.

Keywords: Alzheimer's disease, tau-PET, brain connectivity, disease progression model

121 Synergistic effects of peripheral inflammation and neuroinflammation on amyloid, vascular, and neurodegeneration markers across the Alzheimer's disease spectrum

Laura Alejandra Ramirez Tirado[1], Ann D Cohen[2,3], C Elizabeth Shaaban[1,3], Cristy Matan[4], Brian J Lopresti[4], Milos D Ikonomovic[3,5], Thomas K Karikari[2,3], Victor L Villemagne[2,3], Oscar L Lopez[3,5]

[1]*Department of Epidemiology, University of Pittsburgh, Pittsburgh, PA, US*
[2]*Department of Psychiatry, School of Medicine, University of Pittsburgh, Pittsburgh, PA, US*
[3]*Alzheimer's Disease Research Center, University of Pittsburgh, Pittsburgh, PA, US*
[4]*Department of Radiology, University of Pittsburgh, Pittsburgh, PA, US*
[5]*Department of Neurology, University of Pittsburgh, Pittsburgh, PA, US*

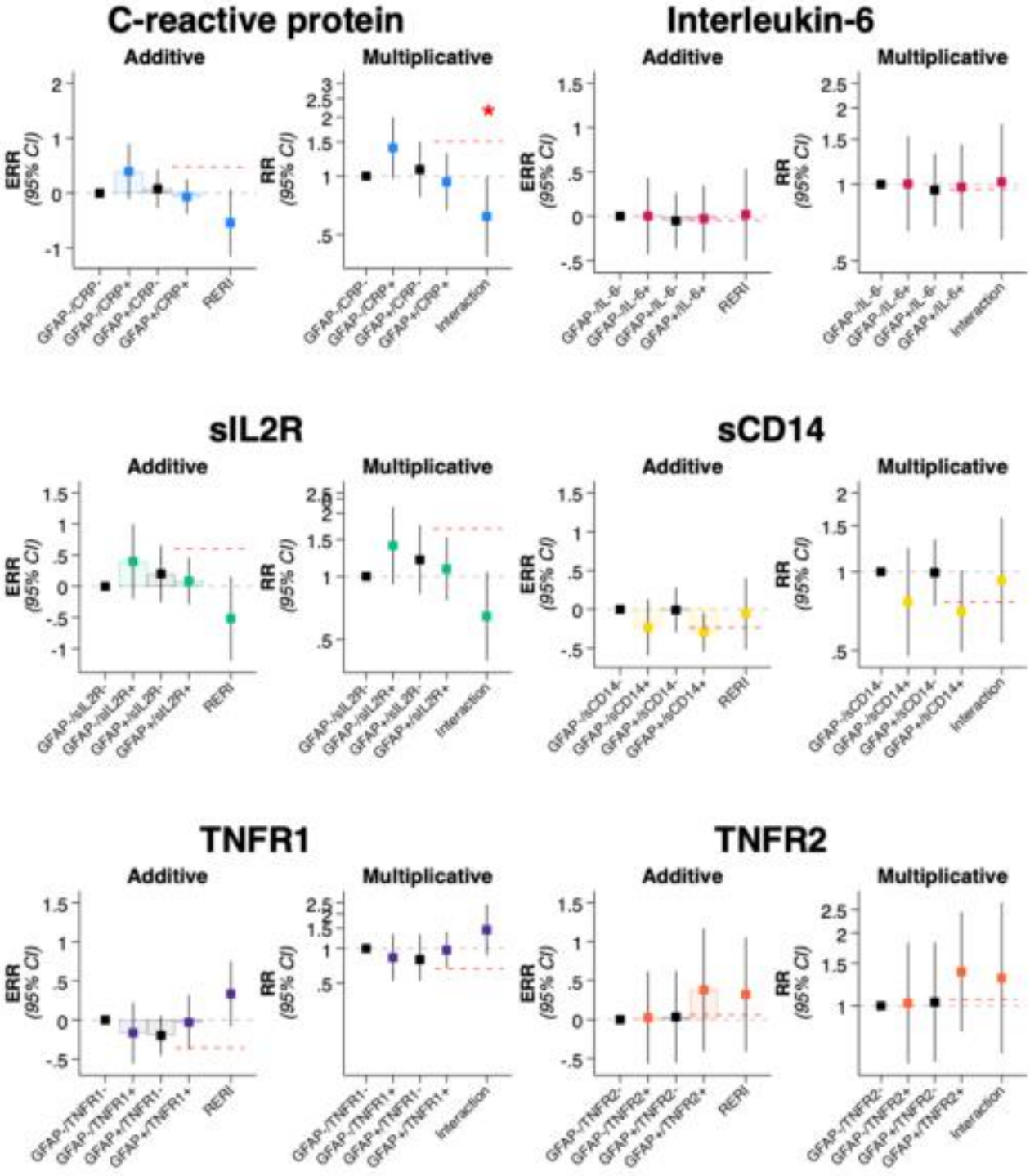
Systemic inflammation and astrogliosis are relevant in Alzheimer's disease (AD). We evaluated whether peripheral inflammation has synergistic effects with astrogliosis on β-amyloid (Aβ), vascular, and neurodegeneration markers.

In the Ginkgo Evaluation of Memory Study, we evaluated the relationship between peripheral inflammation (TNF-R1, TNF-R2, IL-6, IL-2, CRP and sCD14) and astrogliosis (GFAP </≥196pg/mL) as to Aβ burden (</≥20centiloids) and accumulation (centiloids/year), white matter lesion (WML) volume, and neurodegeneration (NfL) across the AD spectrum. Participants underwent PiB-PET scans between 2009-2018. GFAP, NfL, and peripheral inflammatory markers were measured in 2009 by immunoassay; their values were standardized within the cohort. We used negative binomial regression models and adjusted for age, sex, education, *APOEε4*, cystatin C and baseline Aβ status.

190 participants were included (mean age: 86±2.8 yrs., 40.8% women, 96.9% White). GFAP was higher among Aβ+ participants; it did not differ by levels of peripheral inflammation. Aβ accumulation was slower among those with high sCD14, particularly among Aβ+. There was a significant negative multiplicative interaction between GFAP and CRP on Aβ accumulation (RR;95%CI:0.61;.38-.99;p=0.047). WML were larger among GFAP+ individuals. There were significant additive and multiplicative interactions of GFAP with CRP (relative excess risk due to interaction (RERI);95%CI:0.47;0.12-0.83;p=0.008; RR;95%CI:1.76;1.11-2.81;p=0.016, respectively), with TNFR1 (RERI;95%CI:0.63;0.29-0.97;p<.001; RR;95%CI:1.93;1.24-3.01;p=0.004, respectively), and with TNFR2 (RERI;95%CI:0.52;0.22-0.82;p=0.001; RR;95%CI:1.82;1.18-2.82;p=0.006, respectively) on WML. Regarding neurodegeneration, there were significant joint effects of GFAP with CRP, sCD14 and/or TNFR1; and significant additive and/or multiplicative interactions of GFAP with CRP (RERI;95%CI:0.35;0.07-0.62;p=0.012, RR;95%CI:1.37;1.04-1.81;p=0.023,respectively) with TNFR1 (RERI;95%CI:0.29;0.08-0.50;p=.007, RR;95%CI:1.30;1.03-1.63;p=0.023,respectively) and with TNFR2 (RERI;95%CI:0.22;0.005-0.44;p=.045).

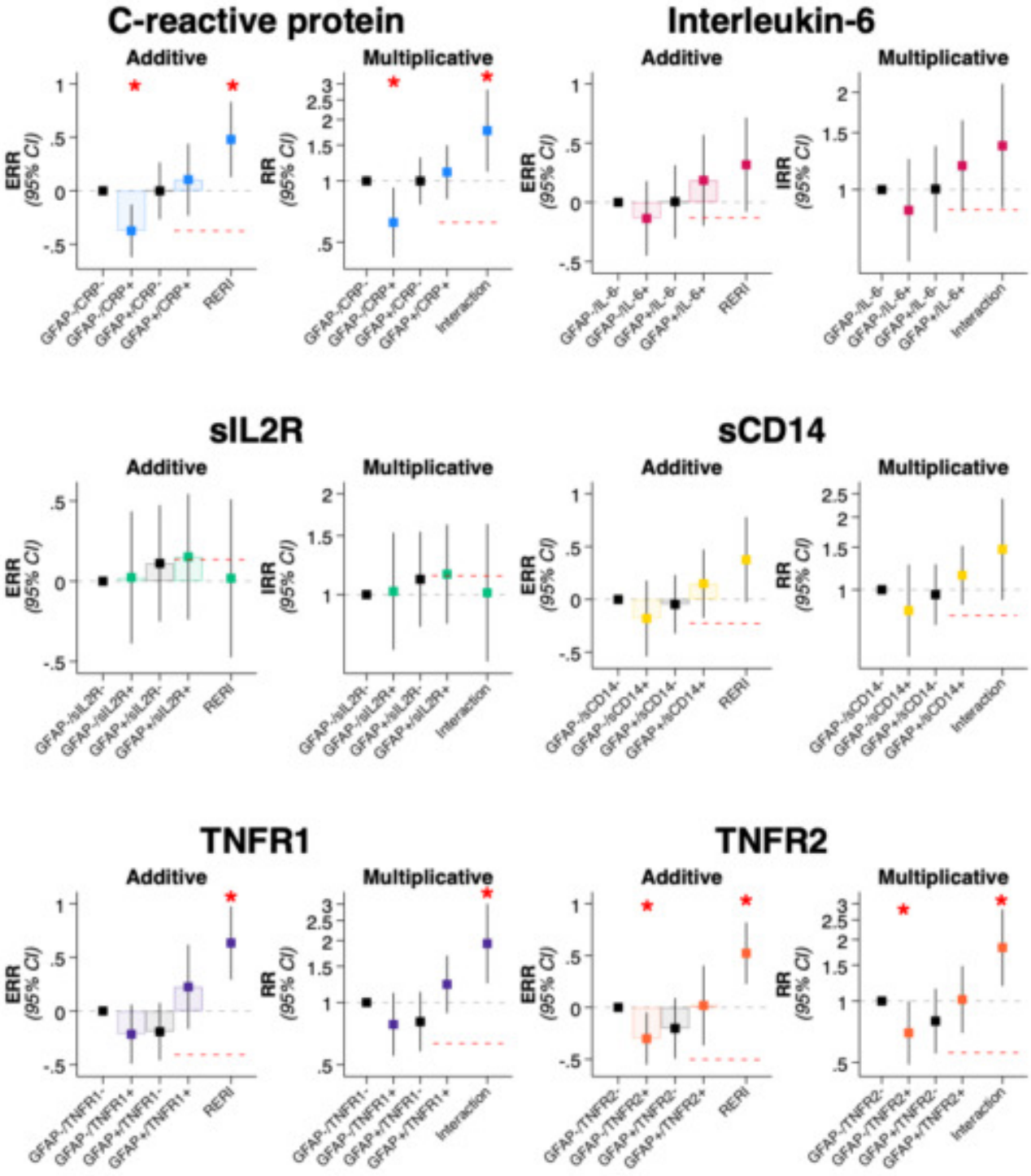
In this 85+ population, with expected high levels of inflammation and more co-pathology; peripheral inflammation (CRP, TNFR1 and/or TNFR2) showed additive/multiplicative synergistic effects with astrogliosis resulting in less amyloid accumulation, greater vascular burden, and more neurodegeneration, particularly in Aβ+ participants. More inflammation may relate with more pathogenesis, bringing participants closer to the amyloid asymptote, slowing Aβ accumulation.

Fig. 1. Interaction between GFAP & Inflammatory markers on Amyloid accumulation (Centiloids/year)



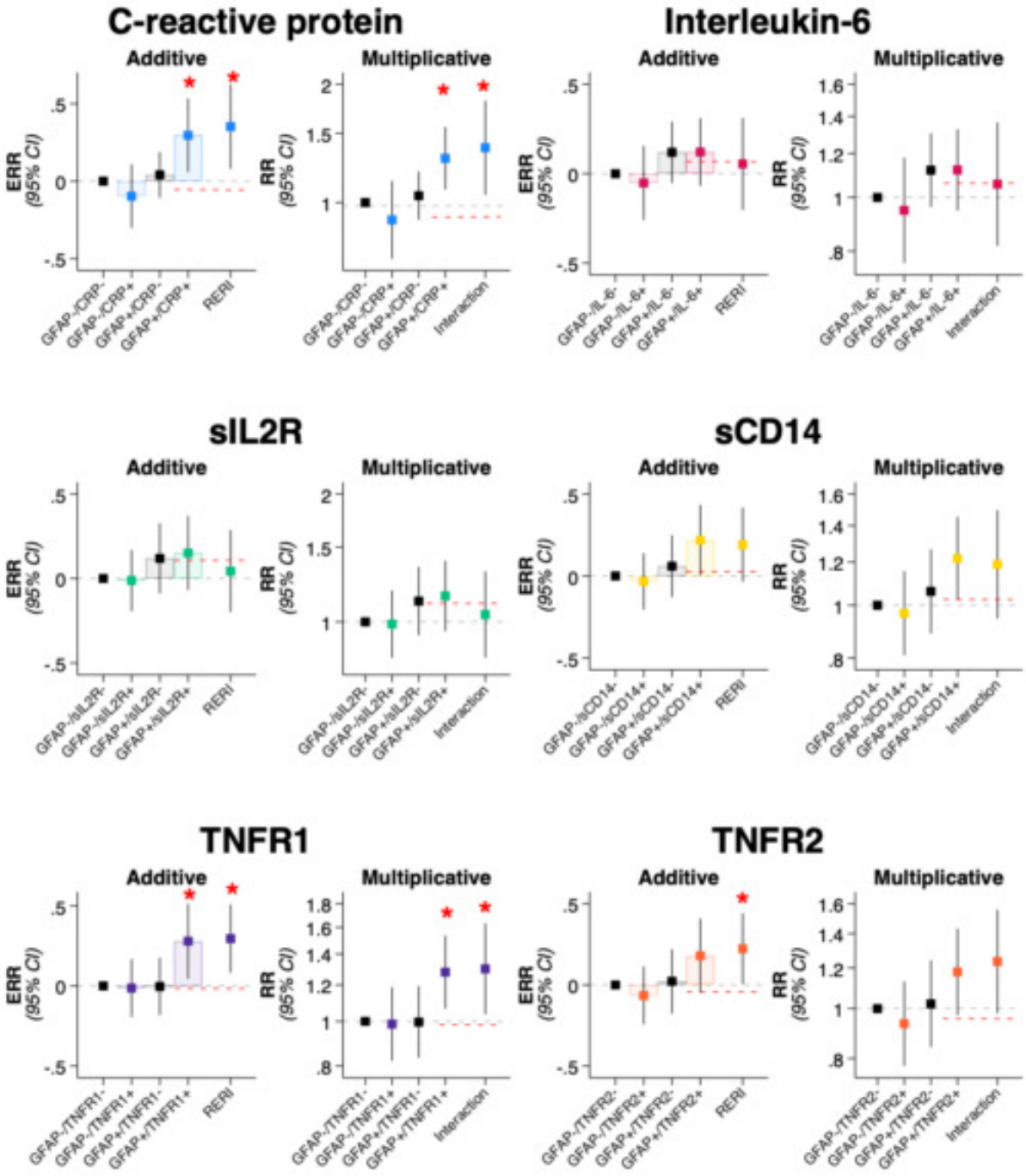
NOTE: Red dash line = expected value for +/+ under either additive or multiplicative model.
In additive=sum of (-/+)plus(+/-); in multiplicative=(-/+)times (+/-).
Adjusted for: *Age, Sex, Education, APOE, Cystatin C and Amyloid status at baseline.*
Abbreviation: *GFAP*: Glial fibrillary acidic protein;*ERR*: Excess relative risk;*RERI*:Relative excess risk due to additive interaction; *95% CI*: 95% Confidence Intervals; *CRP*: C-reactive protein; *IL-6*: Interleukin-6; *sCD14*: soluble Cluster of differentiation 14; *sIL2R*: soluble Interleukin-2 receptor; *TNFR1*: Tumor necrosis factor 1; *TNFR2*: Tumor necrosis factor 2; *red asterisk(*)*: p<.05.

Fig 2.Interaction between GFAP & Inflammatory markers on vascular disease (WML)



NOTE: Red dash line = expected value for +/+ under either additive or multiplicative model.
In additive=sum of (-/+)plus(+/-); in multiplicative=(-/+)times (+/-).
Adjusted for: *Age, Sex, Education, APOE, Cystatin C and Amyloid status at baseline.*
Abbreviation:*GFAP*:Glial fibrillary acidic protein; *ERR*: Excess relative risk;*WML*:White matter lessions; *95% CI*: 95% Confidence Intervals; *CRP*: C-reactive protein; *IL-6*: Interleukin-6; *sCD14*: soluble Cluster of differentiation 14; *sIL2R*: soluble Interleukin-2 receptor; *TNFR1*: Tumor necrosis factor 1; *TNFR2*: Tumor necrosis factor 2;*RERI*:Relative excess risk due to interaction; *red asterisk(*)*: p<.05.

Fig 3. Interaction between GFAP & Inflammatory markers on neurodegeneration (NfL [pg/mL)



NOTE: Red dash line = expected value for +/+ under either additive or multiplicative model.
In additive=sum of (-/+)plus(+/-); in multiplicative=(-/+)times (+/-).
Adjusted for: *Age, Sex, Education, APOE, Cystatin C and Amyloid status at baseline.*
Abbreviation: *GFAP*: Glial fibrillary acidic protein; *ERR*: Excess relative risk; *NfL*: Neurofilament light *95% CI*: 95% Confidence Intervals; *CRP*: C-reactive protein; *IL-6*: Interleukin-6;*sCD14*: soluble Cluster of differentiation 14; *sIL2R*: soluble Interleukin-2; receptor; *TNFR1*: Tumor necrosis factor 1 *TNFR2*: Tumor necrosis factor 2; *RERI*:Relative excess risk due to interaction; *red asterisk(*)*: p<.05.

Keywords: astrogliosis, systemic inflammation, amyloid accumulation, vascular disease, neurodegeneration

122 Impact of amyloid removal on cerebral volume changes with Gantenerumab

Matteo Tonietto[1], Erica Silvestri[1], Christopher Belder[2,3], Frederik Barkhof[2,4], Nick Fox[2], Janice Smith[5], Gregory Klein[1]

[1]*Research and Early Development (pRED), Hoffmann-La Roche, Basel, CH*
[2]*Dementia Research Centre, UCL Queen Square Institute of Neurology, London, GB*
[3]*Adelaide Medical School, University of Adelaide, Adelaide, AU*
[4]*Department of Radiology & Nuclear Medicine, Amsterdam UMC, Vrije Universiteit, Amsterdam, NL*
[5]*Roche Products Ltd, Hoffmann-La Roche, Welwyn Garden City, GB*

Introduction: Gantenerumab is a monoclonal antibody targeting aggregated forms of amyloid-beta. The phase III GRADUATE investigational studies aimed to assess the efficacy and safety of gantenerumab in early AD. Participants treated with Gantenerumab exhibited substantial removal of amyloid plaques and accelerated brain volume loss compared to placebo. In this study we investigated the relationship between amyloid removal and brain volume loss.

Methods: Volume change was estimated using the tensor-based morphometry (TBM) technique, which produced a voxelwise map of relative volume changes for each participant. Spearman correlation was used to assess the association between amyloid removal and cerebral volume loss in gantenerumab-treated participants. Two types of analyses were performed: 1) Global analysis, where amyloid removal was measured in centiloids, and volume change was assessed in the whole brain and whole cortex; 2) Voxelwise analysis, where voxelwise centiloid changes from baseline were computed using centiloid conversion equations applied to amyloid PET SUVR images (Figure 1A), and voxelwise volume changes from baseline were obtained from the TBM method (Figure 1B).

Results: Eighty-eight participants (aged 71.2±8.4, F/M=44/44) in the active arm had both amyloid PET and MRI at screening and at the end of the study. Greater amyloid removal was associated with reduced brain and whole cortex volume loss (Figure 2). Voxelwise analysis revealed a dual pattern: regions typically affected by tau pathology, such as the temporoparietal cortex, followed the global results, while regions usually spared by tau (e.g., thalamus) or those accumulating tau only in later stages of the disease (e.g., Braak VI) exhibited a positive correlation between amyloid removal and volume loss (Figure 3).

Conclusion: The relationship between amyloid removal and brain volume loss with gantenerumab varies between regions typically affected by tau pathology and those that are not. Further analyses are ongoing to better characterize these findings.

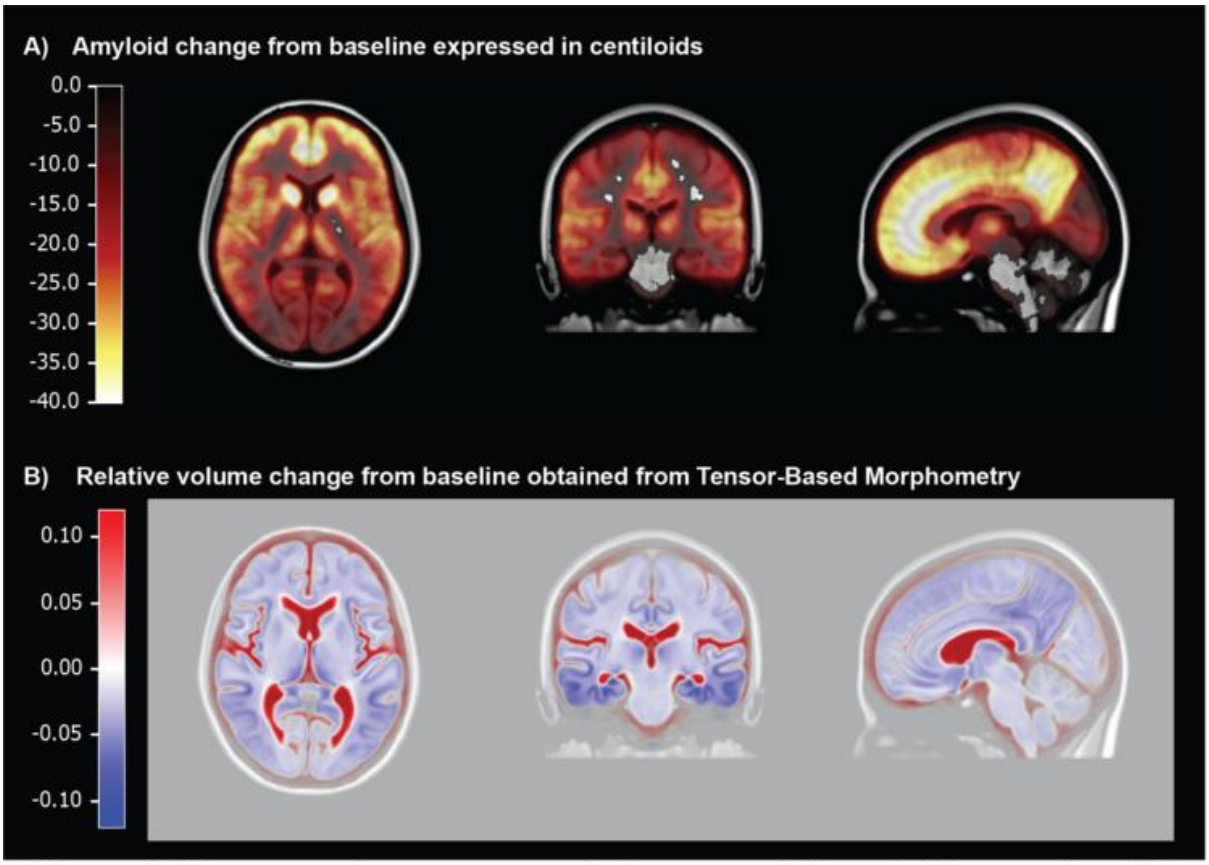


Figure 1: Shown are the average voxelwise maps of A) amyloid removal and B) volume change in gantenerumab-treated participants. Voxelwise centiloid maps were computed using centiloid conversion equations applied to amyloid PET SUVR images. Relative volume change maps were computed using the tensor-based morphometry method.

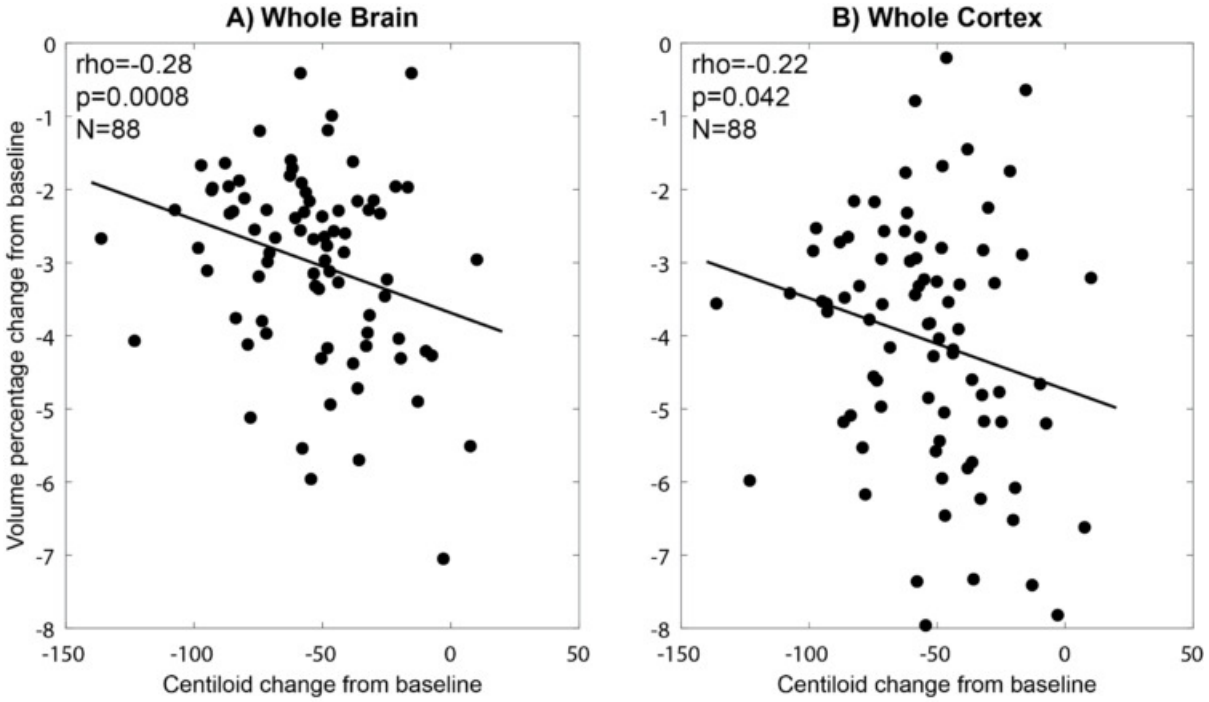


Figure 2: Shown is the scatter plot between the centiloid change from baseline and the whole brain and whole cortex volume percent change from baseline in gantenerumab-treated participants. Line represents the least square linear fit.

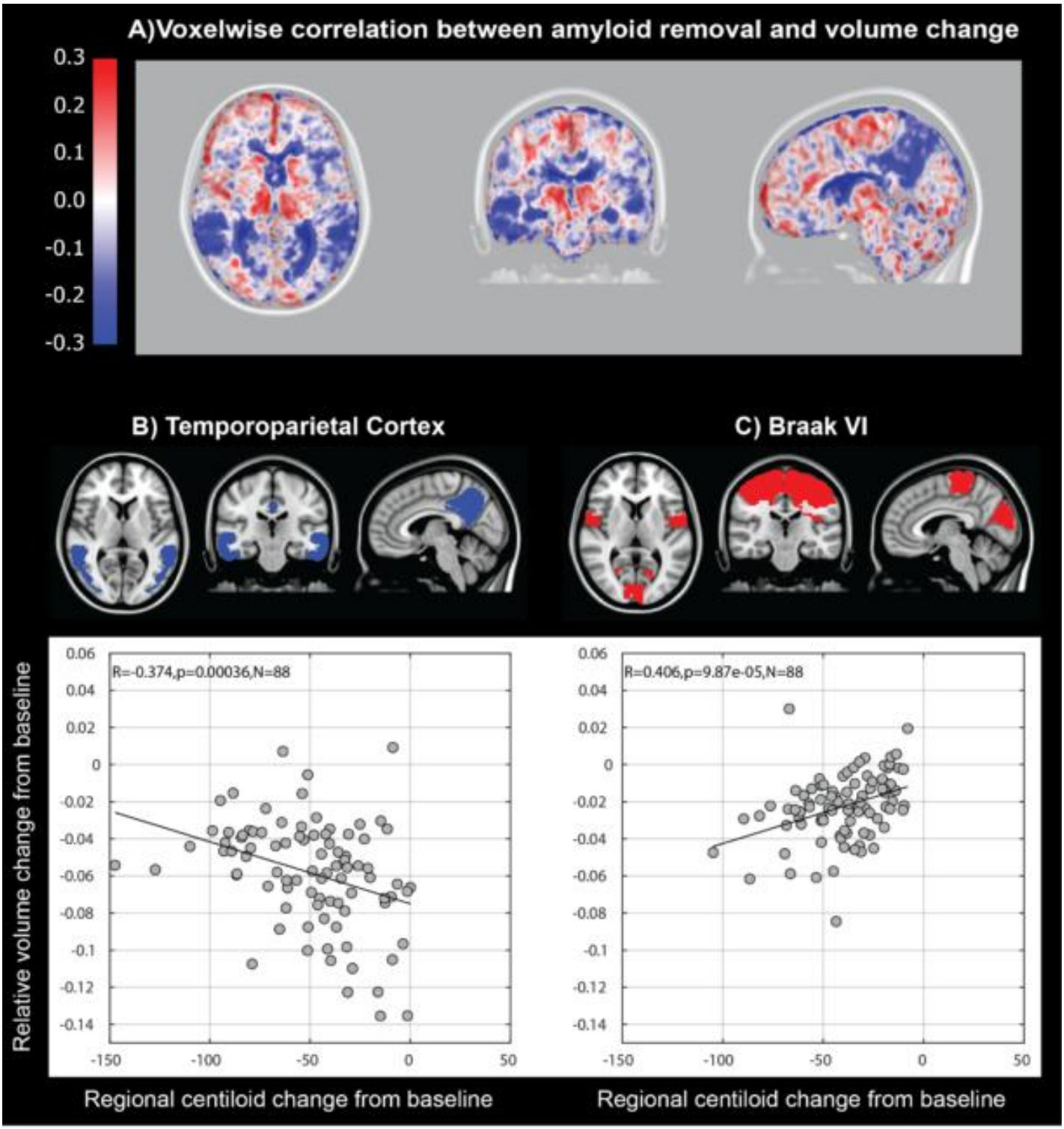


Figure 3: panel A shows the voxelwise Spearman correlation maps between amyloid removal and volume change in participants treated with Gantenerumab. Negative correlations in blue means that greater amyloid removal was associated with lower volume loss in that region, and vice versa for positive correlations in red. Panel B) and C) show the same correlations for two areas: the temporoparietal cortex, likely to be affected by high tau pathology; and the Braak VI region, likely to have low tau pathology. The two regions display opposite behavior.

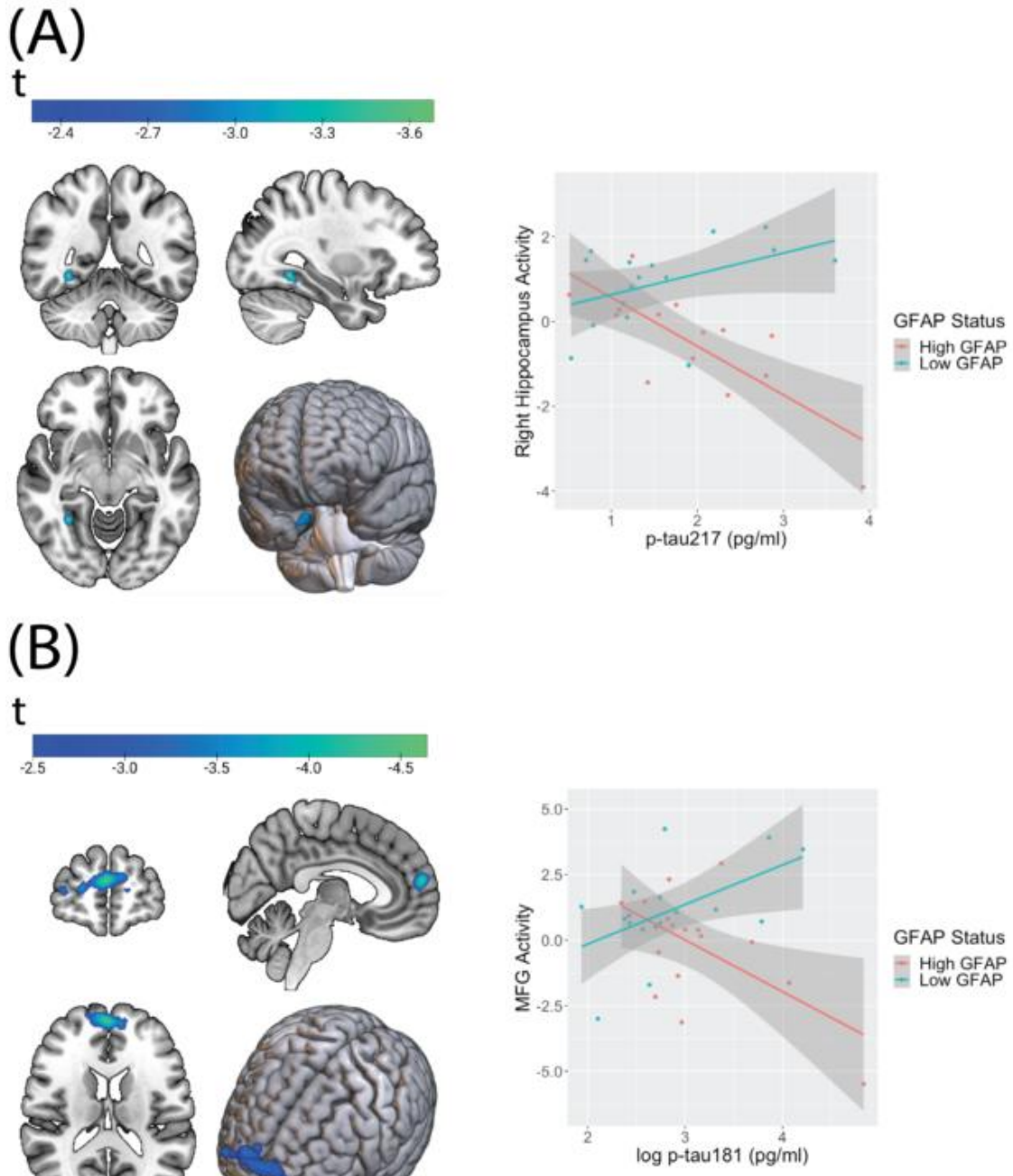
Keywords: volume, amyloid, gantenerumab, tau

123 Astrocyte reactivity explains tau-related effects on hippocampal dysfunction and longitudinal atrophy in preclinical Alzheimer's disease

Noah Schweitzer[1], Bistra Iordanova[1], Chang-le Chen[1], Hecheng Jin[1], Rebecca Thurston[2], Brian Lopresti[3], Beth Snitz[4], Dana Tudorascu[2], Annie Cohen[2], M. Ilyas Kamboh[5], Edythe Halligan-Eddy[2], Thomas Karikari[2], Victor Villemagne[2], Howard Aizenstein[1,2], Minjie Wu[1]

[1]*Department of Bioengineering, University of Pittsburgh, Pittsburgh, PA, US*
[2]*Department of Psychiatry, University of Pittsburgh School of Medicine, Pittsburgh, PA, US*
[3]*Department of Radiology, University of Pittsburgh School of Medicine, Pittsburgh, PA, US*
[4]*Department of Neurology, University of Pittsburgh School of Medicine, Pittsburgh, PA, US*
[5]*Department of Human Genetics, University of Pittsburgh, Pittsburgh, PA, US*

Astrocytes become reactive early in Alzheimer's Disease (AD) as amyloid-β (Aβ) begins to deposit in the brain. Few studies have explored how reactive astrocytes in humans relate to hippocampal activity measured with fMRI in pre-clinical AD. Our study recruited 41 cognitively unimpaired participants (N=22 female, ages 65-82 years) who completed a neuropsychological battery and a face-name associative memory fMRI task and provided blood plasma samples to measure levels of glial fibrillary acidic protein (GFAP), phosphorylated tau217 (p-tau217) and p-tau181. Participants underwent 2-3 follow-up visits where T1-weighted MRIs were acquired 2-3 years apart. A medial split of GFAP was performed and each subject was classified as either "high" or "low GFAP". Regions of interest (ROI) on task fMRI were identified through linear regression models testing for p-tau217 and p-tau181's interaction with GFAP status, controlling for scanner site, sex, age, and Aβ status. Memory learning was calculated from average composite z-scores from the neuropsychological battery results within each domain. Longitudinal T1-weighted images were segmented with FreeSurfer and total hippocampal volume (HV) was normalized by intracranial volume. Linear mixed effects model analyzed the longitudinal association between p-tau and GFAP with HV, including fixed effects of sex, Aβ status, baseline age, and interaction between time from first visit with p-tau level, along with random intercepts and slopes. Compared to low GFAP participants, high GFAP participants experienced decreased right hippocampus and medial frontal gyrus activation with increasing p-tau217, p-tau181 levels (p<0.001; Fig. 1). Decreased hippocampus activity was associated with worse memory learning performance regardless of GFAP status (p=0.018; Fig. 2). Higher p-tau217, p-tau181 levels were associated with a larger decrease in HV over time for high GFAP participants (p=0.0064) but not low GFAP participants (p=0.92; Fig. 3). Our findings highlight how reactive astrocytosis may relate to biologically relevant characteristics



of AD pathogenesis.

Fig.1

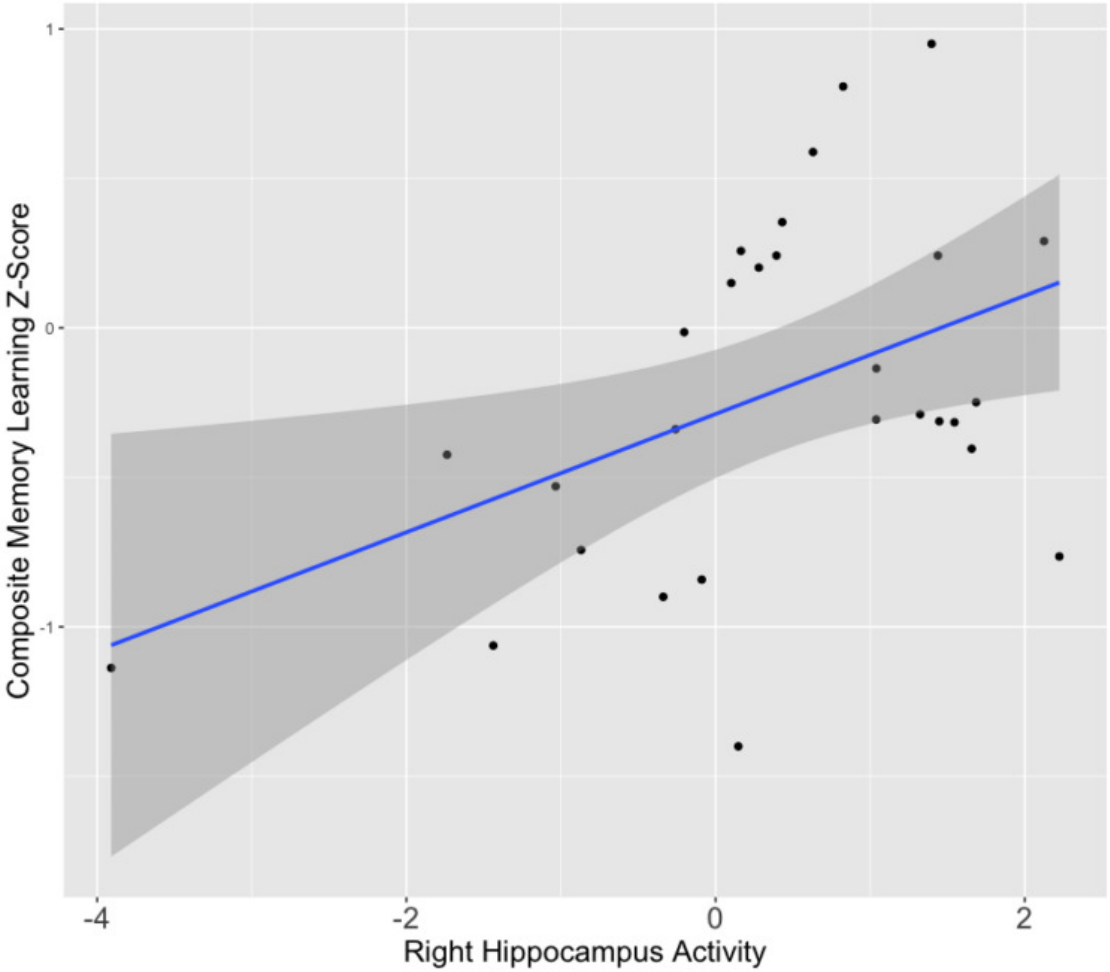


Fig.2

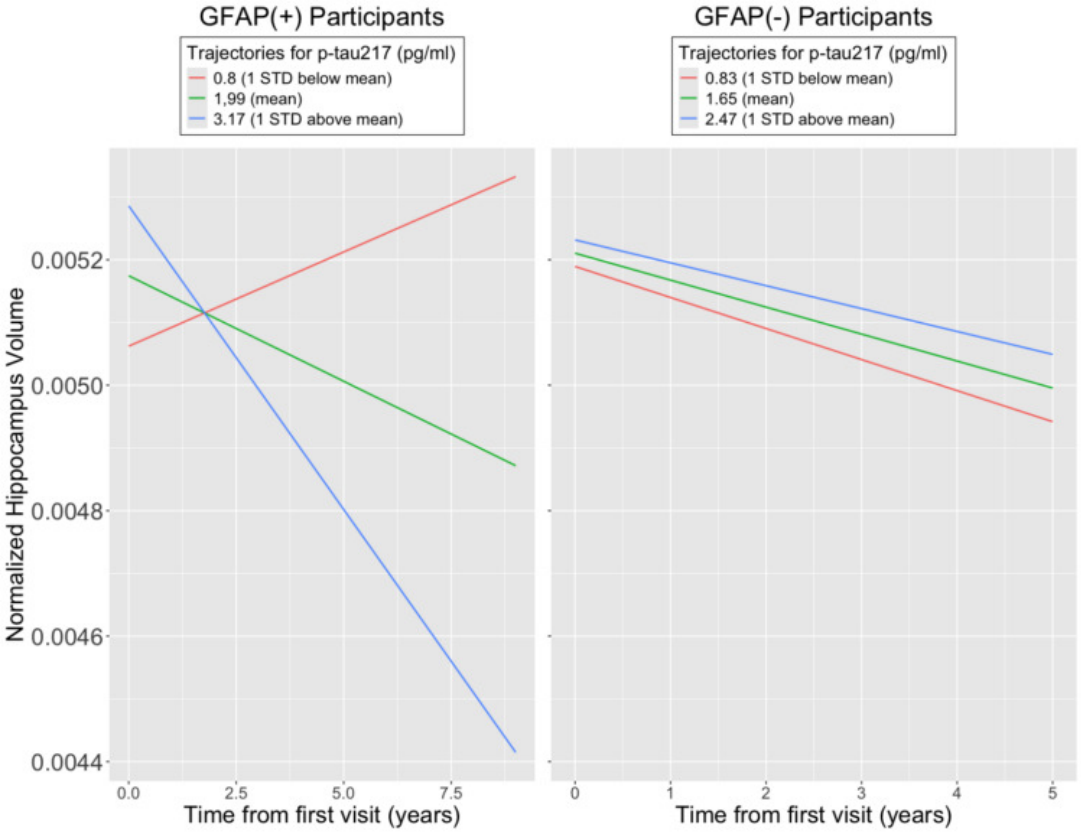


Fig.3

Keywords: plasma tau, astrocytes, fluid biomarkers, fMRI, hippocampus activity

124 Plasma phosphorylated tau 217 and longitudinal trajectories of Aβ, tau, and cognition in cognitively unimpaired older adults

Hyun-Sik Yang[1,2,3], Juliana Anzai[1,2], Wai-Ying Yau[1,2,3], Andrea Román Viera[1,2], Courtney Maa[1,2], Dylan Kirn[1,2], Michael Properzi[2], Aaron Schultz[2,3], Michelle Farrell[2,3], Heidi Jacobs[2,3], Rachel Buckley[2,3], Kathryn Papp[1,2,3], Gad Marshall[1,2,3], Rebecca Amariglio[1,2,3], Dorene Rentz[1,2,3], Joel Braunstein[4], Keith Johnson[1,2,3], Reisa Sperling[1,2,3], Jasmeer Chhatwal[1,2,3]

[1]*Brigham and Women's Hospital, Boston, MA, US*
[2]*Massachusetts General Hospital, Boston, MA, US*
[3]*Harvard Medical School, Boston, MA, US*
[4]*C2N Diagnostics, St. Louis, MO, US*

Background: Plasma phosphorylated tau 217 (pTau217) reflects the AD pathology burden, but its utility in predicting longitudinal disease progression in cognitively unimpaired (CU) older adults remains unclear.

Methods: Baseline plasma %pTau217 (pTau217/non-phosphorylated-Tau217×100) from n=318 Harvard Aging Brain Study participants (61% female, 81% white, follow-up 8.0±3.9 years, CU at baseline) was quantified by C_2N Diagnostics. We obtained annual Preclinical Alzheimer's Cognitive Composite 5 (PACC5), and Pittsburgh compound B (PiB) and flortaucipir (FTP) PET in Years 1 (baseline), 4, 6, 9, 12. We used cortical PiB DVR (Centiloid [CL]), mesial temporal lobe (MTL), and temporal neocortical (NEO) FTP SUVR composites. Association between %pTau217 and longitudinal Aβ, tau, and cognition were assessed using linear mixed effect models, accounting for age, sex, *APOE* ε4, and education. A log-rank test assessed the "A-" (<24.1 CL) to "A+" progression risk. A path analysis combining baseline %pTau217 and the rates of ΔPiB, ΔNEO-FTP, and ΔPACC5 was performed.

Results: Baseline %pTau217 was associated with longitudinal PiB (n=245, b=0.35, $p=8.9\times10^{-16}$), even in the A- subgroup (n=191, b=0.26, $p=1.6\times10^{-4}$) and the <10 CL subgroup (n=123, b=0.22, p=0.020). Higher baseline %pTau217 tertiles were associated with A- to A+ progression risk (n=189, $\chi^2_{df=2}=14.4$, $p=7.5\times10^{-4}$). Baseline %pTau217 was associated with longitudinal MTL-FTP (n=182, $b=9.4\times10^{-4}$, p=0.030) and NEO-FTP ($b=1.3\times10^{-3}$, $p=4.8\times10^{-5}$), even in the A- subgroup (n=145; MTL-FTP $b=2.6\times10^{-3}$, $p=1.7\times10^{-3}$; NEO-FTP $b=1.2\times10^{-3}$, p=0.043). Baseline %pTau217 was associated with longitudinal PACC5 overall (n=308, b=-0.019, $p=1.5\times10^{-10}$), but this association was not significant in the A- subgroup (n=235, p=0.31). The path analysis suggested that the %pTau217 - ΔPACC5 association is primarily mediated through ΔPiB and ΔNEO-FTP.

Conclusion: Plasma %pTau217 predicted longitudinal Aβ and tau accumulation in CU older adults, even in the A- subgroup, supporting plasma biomarker screening in primary prevention trials. The association of higher baseline %pTau217 with cognitive decline was explained by faster AD pathology progression.

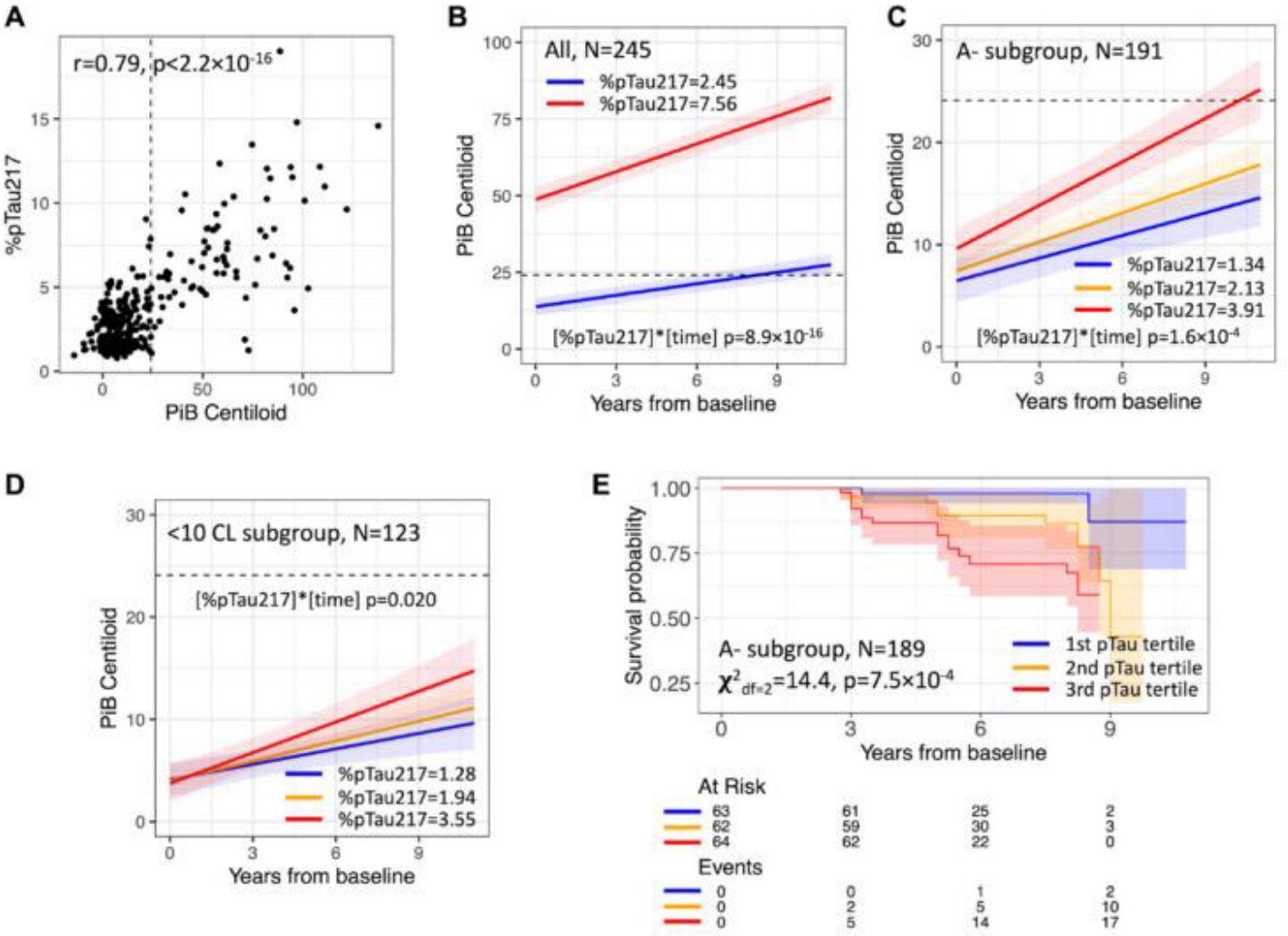


Figure 1. Baseline plasma %pTau217 and cross-sectional and longitudinal cortical Aβ (PiB PET).
(A) Baseline plasma %pTau217 and PiB CL. **(B)** Estimated longitudinal cortical Aβ burden (PIB PET CL) trajectory among all participants with longitudinal PiB PET. Mean values of %pTau217 among A- (2.45) and A+ (7.56) were used for visualization. **(C-D)** Estimated longitudinal cortical Aβ burden (PIB PET CL) trajectory in the A- subgroup (<24.1 CL; **C**) and the <10 CL subgroup (**D**). Mean values of each %pTau217 tertile within each subgroup were used for visualization. Dashed lines indicate the threshold for A+ (24.1 CL). **(E)** The differential risk of A- to A+ progression among CU A- subgroup across the baseline %pTau217 tertile was shown with Kaplan-Meier curves. The log-rank test Chi-square statistic is shown. The number of at-risk and events per group are noted below the plot.

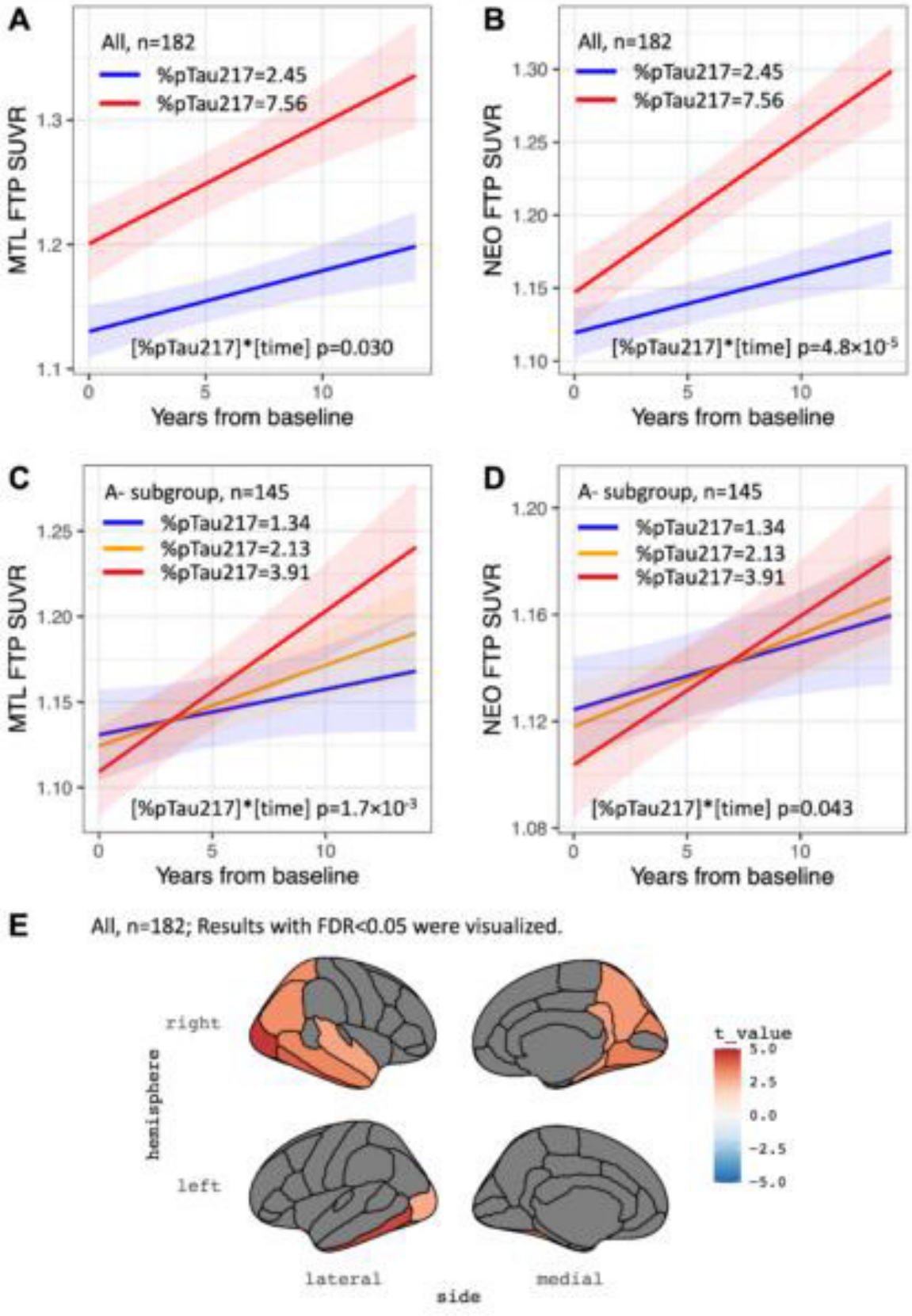


Figure 2. Baseline plasma %pTau217 and cross-sectional and longitudinal tau (FTP PET). (A-B) The estimated longitudinal trajectory of MTL (A) and NEO (B) FTP SUVR. Mean %pTau217 values of A- and A+ subgroups were shown. **(C-D)** The estimated longitudinal trajectory of MTL (C) and NEO (D) FTP SUVR in the baseline A- subgroup. Mean %pTau217 values in each %pTau217 tertile are shown. **(D)** The association between baseline plasma %pTau217 and neocortical (NEO) FTP SUVR from the first FTP PET. **(E)** Exploratory analyses of the baseline %pTau217 – longitudinal tau association in each cortical FTP PET region of interest

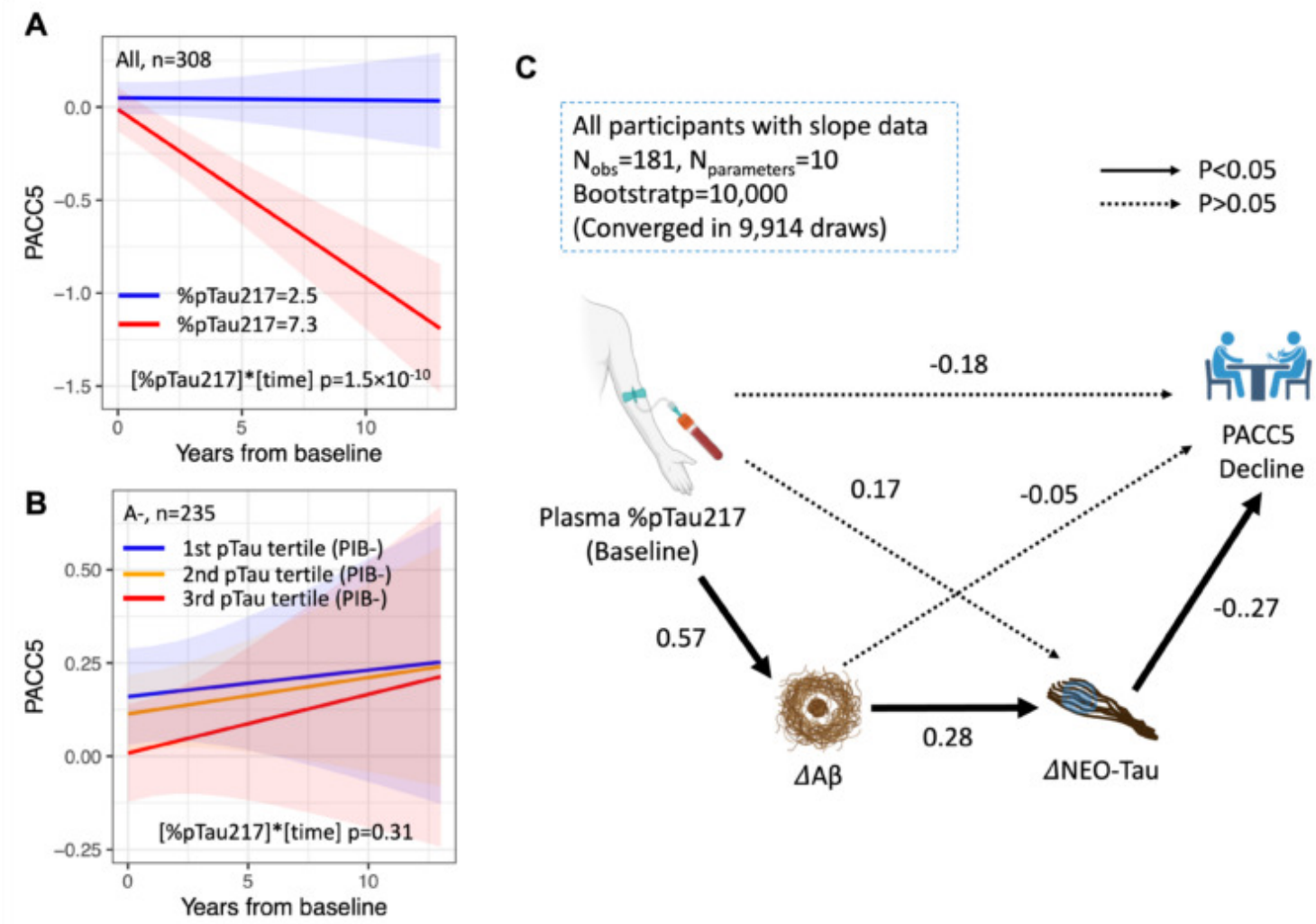


Figure 3. Baseline plasma %pTau217 and longitudinal PACC5. (A-B) The predicted longitudinal trajectory of PACC5 in all participants (A) and the A- subgroup (B). Mean %pTau217 values in the A- (2.5) and A+ (7.5) subgroups were used in (A), and mean %pTau217 values for each tertile among A- subgroup were used in (B) for visualization. **(C)** Path analysis shows that higher baseline %pTau217 is associated with longitudinal Aβ accumulation (ΔAβ; PIB CL slope), which in turn leads to longitudinal neocortical tau accumulation in the neocortex (ΔNEO-Tau; temporal neocortical FTP SUVR slope) and cognitive decline (PACC5 slope). ΔAβ and ΔNEO-Tau explained most of the association between %pTau217 with cognitive decline. Solid arrows indicate significant associations ($p<0.05$); the associations with $p>0.05$ were shown in dashed arrows. Numbers adjacent to each arrow show the relative strength of each association (completely standardized solution).

Keywords: plasma biomarker; phospho-tau217; preclinical Alzheimer's disease; longitudinal PET; disease progression

125 Detection of TDP-43 from plasma-derived astrocyte extracellular vesicles for identification of LATE

Robert Rissman

[1]University of Southern California, Neuroscience Translational Research Division, Alzheimer's Therapeutic Research Institute, SAN DIEGO, CA, US

Background: Limbic predominant age related TDP-43 encephalopathy neuropathological change (LATE-NC) is a neurodegenerative disease characterized brain disease that mimics Alzheimer's disease (AD) clinically. LATE-NC is difficult to diagnose antemortem using clinical information or biomarkers. Recent studies suggest concentrations of extracellular vesicle (EVs) protein cargo derived from neuronal and glial cells may serve as useful diagnostic biomarkers for AD and other neurodegenerative diseases. As an initial step, we developed a high throughout bioassay to detect TDP-43 in plasma derived exosomes for identification of LATE and AD. We will present data on our current efforts on standardization and validation of the assay as well as specifics of the use of RT-QuIC/SAA to identify species of TDP-43 that are unique to LATE.

Method: TDP-43 cargo was detected from astrocyte (ADEVs) using antemortem plasma from participants with autopsy-confirmed diagnoses, including many with LATE (n = 22). =TDP-43 concentrations were compared to a group of brains from healthy controls, mild cognitively impairment (MCI), and AD dementia (n = 42).

Result: TDP-43 levels from plasma ADEVs were diagnostic for identifying LATE subjects, with or without comorbid AD pathology. Measurable levels of TDP-43 were detected in EV-depleted plasma and other EV fractions but these levels were not significantly different amongst the groups. We found no correlation between EV TDP-43 levels with cognition-based variables proximate to death, sex, and APOE carrier status.

Conclusion: TDP-43 in ADEVs may serve as a potential diagnostic tool to rapidly identify subjects with LATE for screening into clinical trials.

Keywords: LATE, TDP-43, Alzheimer's disease, autopsy

126 Short sleep duration is associated with higher subsequent plasma p-tau217 in aging

Joseph Winer[1], Karly Cody[1], Christina Young[1], Elizabeth Mormino[1,2]

[1]*Department of Neurology and Neurological Sciences, Stanford University, Stanford, CA, US*
[2]*Wu Tsai Neurosciences Institute, Stanford University, Stanford, CA, US*

Background: Short sleep duration is associated with elevated amyloid PET burden, but the impact of sleep duration on subsequent biomarker changes is not well understood. We sought to determine whether baseline sleep duration was predictive of longitudinal plasma and imaging biomarkers in cognitively unimpaired older adults.

Methods: We examined 1418 initially unimpaired participants (1071 A+, 347 A-) from the A4/LEARN study with Lilly plasma p-tau217, MRI, and self-reported sleep duration (**Table**). FLAIR MRI was used to quantify white matter hyperintensity (WMH) volume, corrected for intracranial volume. Linear mixed-effects models (random intercept) were used to assess the association between baseline sleep duration and longitudinal change in biomarkers. Models included baseline sleep duration (≤6, 7-8, or ≥9 hours), baseline age, baseline amyloid PET SUVR, and sex and their interactions with time.

Results: Participants were followed for an average of 3.9 ± 2.3 years. Short sleep duration (≤6 hours) at baseline was associated with greater subsequent increase in plasma p-tau217 compared to normal sleep, independent of baseline amyloid PET SUVR (β=0.03 ± 0.009, p=0.004; **Figure 1A**). Both short and long (≥9 hours) sleep durations were associated with greater subsequent increases in WMH volume compared to normal sleep, independent of baseline amyloid PET SUVR (short, β=0.08 ± 0.03, p=0.004; long, β=0.17 ± 0.06, p=0.003; **Figure 1B**).

Conclusions: In this longitudinal study, short sleep was associated with greater increase in AD pathology measured with plasma p-tau217, while both short and long sleep were associated with greater increase in WMH volume, suggesting adequate sleep is important for healthy aging trajectories via multiple pathways.

Variable	Overall	Short sleep (≤6h)	Normal sleep (7-8h)	Long sleep (≥9h)
N	1418	394 (28%)	947 (67%)	77 (5%)
Baseline age (yrs)	71.7 ± 4.8	71.7 ± 4.4	71.6 ± 4.9	72.3 ± 4.9
Female	843 (60%)	209 (53%)	585 (62%)	49 (64%)
Baseline Aβ+	1071 (76%)	306 (78%)	705 (74%)	60 (78%)
Baseline Aβ SUVR	1.25 ± 0.22	1.26 ± 0.21	1.25 ± 0.21	1.29 ± 0.26
# p-tau217 samples	2.4 ± 0.9	2.4 ± 0.9	2.4 ± 0.9	2.3 ± 0.9
# FLAIR MRI	4.3 ± 2.6	4.4 ± 2.3	4.3 ± 2.4	4.3 ± 2.3

Table - Participant demographics.

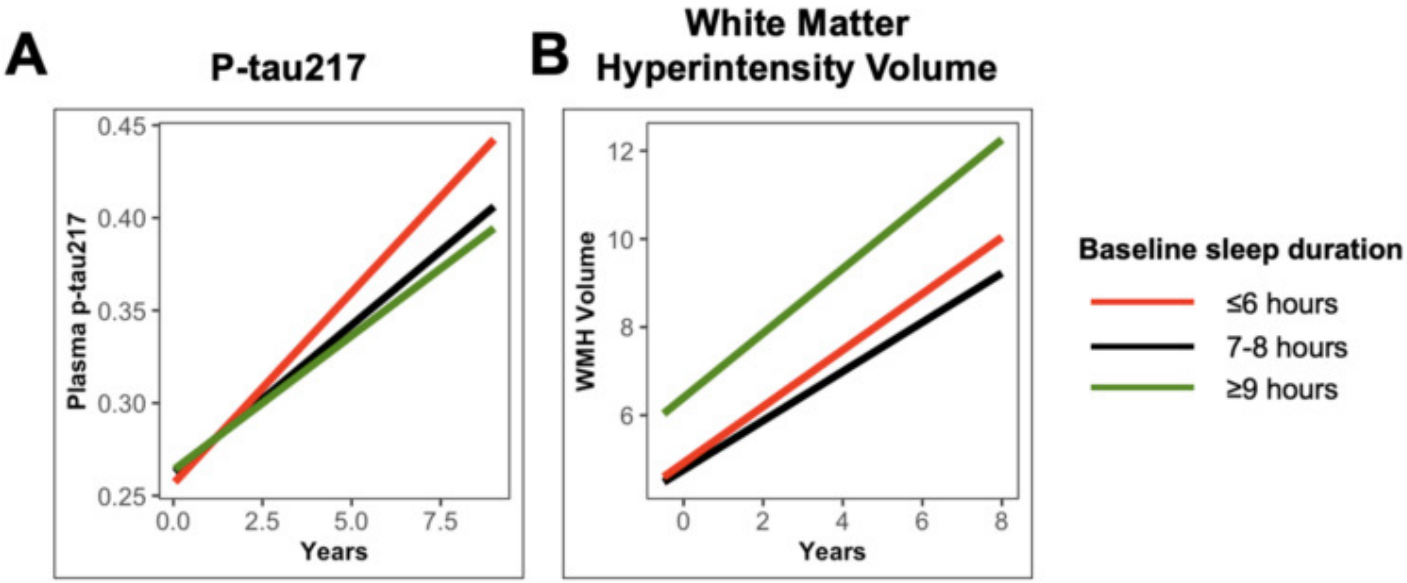


Figure 1 – Plots show estimates from linear mixed models examining increases in A) Lilly plasma p-tau217 and B) white matter hyperintensity volume over time across baseline sleep duration groups. Age, sex, and baseline amyloid PET SUVR were included as covariates in the models. The short sleep duration group showed significantly greater plasma p-tau217 increases over time. Both long and short sleep duration showed significantly greater white matter hyperintensity volume increases over time compared to normal sleep duration.

Keywords: sleep, plasma p-tau, white matter hypertensities, lifestyle, longitudinal

127 Impacts of testing language and rates of amyloid positivity among underrepresented groups in the A4 Study

Isha Sai[1], Joshua D. Grill[2], Elizabeth C. Mormino[1,3], Christina B Young[1]

[1]*Department of Neurology and Neurological Sciences, Stanford University, Stanford, CA, US*
[2]*Institute for Memory Impairments and Neurological Disorders, Departments of Psychiatry and Human Behavior and Neurobiology and Behavior, University of California, Irvine, Irvine, CA, US*
[3]*Wu Tsai Neurosciences Institute, Stanford University, Stanford, Stanford, CA, US*

Objective: To determine whether abnormal amyloid (A+) PET rates in cognitively unimpaired (CU) participants screened for a secondary prevention trial differs across racial/ethnic/testing language groups and identify potential screening biases related to cognition/functioning.

Methods: Data from 6669 participants screened in their primary language for the A4/LEARN Study were divided into race/ethnicity/testing language groups (**Table 1**). Among individuals that passed initial screening and completed the PET visit, differences in A+ rates between race/ethnicity/testing language groups were compared with logistic regression. To probe potential biases in the screening process, we examined rates of screen-failure due to medical/other reasons, cognition/functioning, and normal amyloid PET status (A-). In those who screen-failed due to low cognitive/functioning, we further examined differences between race/ethnicity/language groups in screening and non-screening cognitive tests using logistic, multinomial logistic, and linear regression.

Results: Underrepresented groups [non-Hispanic Black tested in English (NHB-E), non-Hispanic Asian tested in English (NHA-E), and non-Hispanic Asian tested in Japanese (NHA-J)] had significantly lower rates of A+ compared to the non-Hispanic White group tested in English (NHW-E; **Figure 1A**). Of all screened participants, underrepresented groups were significantly more likely to be excluded for medical/other reasons and cognitive/functioning performance prior to the PET visit (**Figure 1B**). Of those who screen-failed due to cognitive/functional performance, the pattern of failure on the three screening tests differed across race/ethnicity/language groups (**Figure 1C**). When probing specific MMSE and CDR items in those who were screened out due to low cognition/functioning, patterns of missed items and endorsed functional domains differed between race/ethnicity/language groups (**Figure 1D-E**). When examining non-screening cognitive tests, performance was comparable between those who screen-failed due to low cognition/functioning and A+ individuals who passed initial screening within NHA-E and NHA-J groups (**Figure 2**).

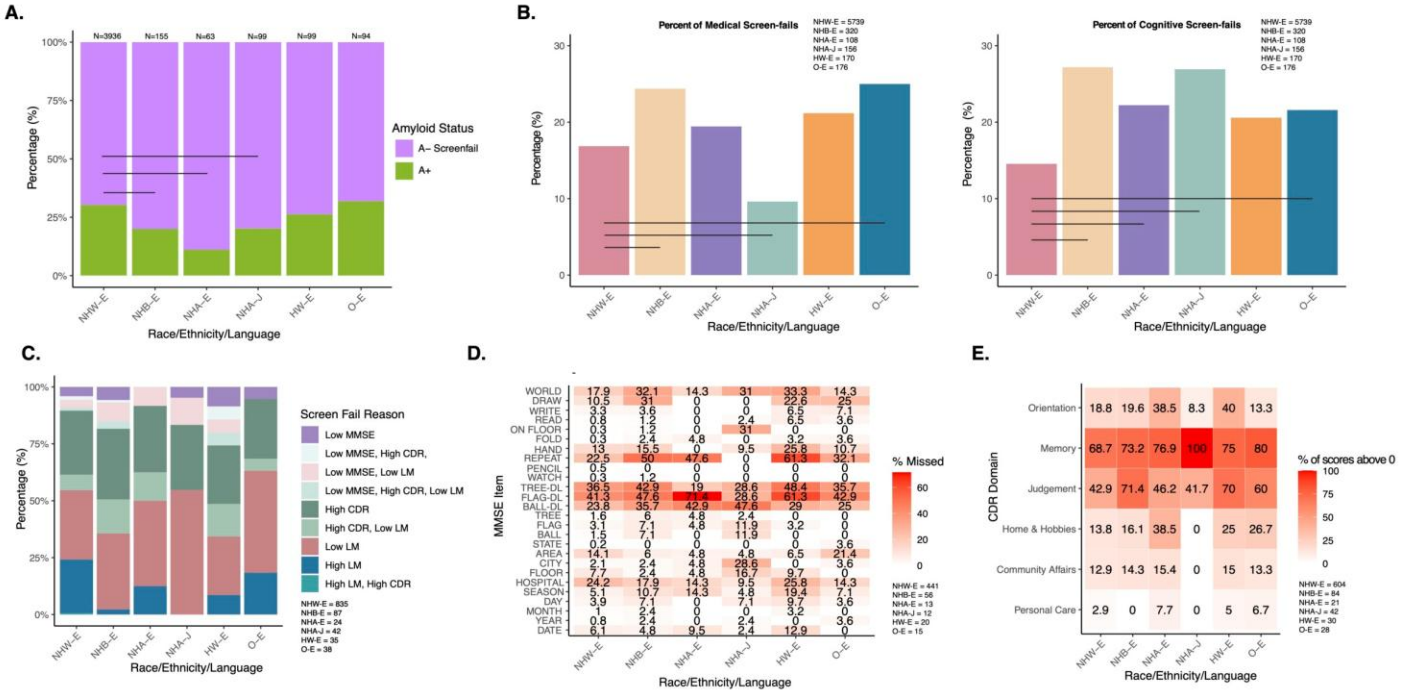
Conclusion: Screening procedure biases may disproportionately reduce the number of participants from underrepresented groups who are eligible for randomization.

Table 1. Demographic information for all A4/LEARN participants that were tested in their primary language. Race, ethnicity, and testing language groups are shown.

	NHW-E (N=5739)	NHB-E (N=320)	NHA-E (N=108)	NHA-J (N=156)	HW-E (N=170)	O-E (N=176)	Overall (N=6669)
Age							
Mean (SD)	71.6 (4.85)	71.3 (4.95)	72.4 (5.38)	72.5 (4.73)	72.0 (4.69)	71.2 (4.67)	71.6 (4.86)
Median [Min, Max]	70.6 [59.8, 86.0]	70.0 [64.5, 86.0]	72.0 [64.1, 85.1]	71.9 [65.1, 85.9]	70.8 [65.0, 83.0]	70.6 [65.0, 85.7]	70.6 [59.8, 86.0]
Sex							
Female	3301 (57.5%)	223 (69.7%)	62 (57.4%)	52 (33.3%)	103 (60.6%)	109 (61.9%)	3850 (57.7%)
Male	2438 (42.5%)	97 (30.3%)	46 (42.6%)	104 (66.7%)	67 (39.4%)	67 (38.1%)	2819 (42.3%)
Years of Education							
Mean (SD)	16.5 (2.94)	15.4 (3.03)	17.0 (2.85)	14.5 (2.31)	15.5 (3.25)	16.3 (3.26)	16.4 (2.97)
Median [Min, Max]	16.0 [0, 36.0]	16.0 [5.00, 30.0]	17.0 [10.0, 26.0]	16.0 [9.00, 20.0]	16.0 [0, 30.0]	16.0 [8.00, 25.0]	16.0 [0, 36.0]
Missing	60 (1.0%)	4 (1.3%)	0 (0%)	0 (0%)	3 (1.8%)	15 (8.5%)	82 (1.2%)
APOE Genotype							
E2/E2	26 (0.5%)	0 (0%)	0 (0%)	0 (0%)	0 (0%)	0 (0%)	26 (0.4%)
E2/E3	475 (8.3%)	37 (11.6%)	5 (4.6%)	15 (9.6%)	6 (3.5%)	13 (7.4%)	551 (8.3%)
E3/E3	2518 (43.9%)	96 (30.0%)	61 (56.5%)	109 (69.9%)	83 (48.8%)	70 (39.8%)	2937 (44.0%)
E2/E4	109 (1.9%)	12 (3.8%)	0 (0%)	2 (1.3%)	4 (2.4%)	2 (1.1%)	129 (1.9%)
E3/E4	1382 (24.1%)	58 (18.1%)	15 (13.9%)	30 (19.2%)	31 (18.2%)	29 (16.5%)	1545 (23.2%)
E4/E4	145 (2.5%)	7 (2.2%)	3 (2.8%)	0 (0%)	3 (1.8%)	3 (1.7%)	161 (2.4%)
Missing	1084 (18.9%)	110 (34.4%)	24 (22.2%)	0 (0%)	43 (25.3%)	59 (33.5%)	1320 (19.8%)
Group							
Other/Medical Screen-fail	968 (16.9%)	78 (24.4%)	21 (19.4%)	15 (9.6%)	36 (21.2%)	44 (25.0%)	1162 (17.4%)
Low Cognitive Screen-fail	633 (11.0%)	85 (26.6%)	21 (19.4%)	42 (26.9%)	32 (18.8%)	31 (17.6%)	844 (12.7%)
High Cognitive Screen-fail	202 (3.5%)	2 (0.6%)	3 (2.8%)	0 (0%)	3 (1.8%)	7 (4.0%)	217 (3.3%)
A- Screen-fail	2744 (47.8%)	124 (38.8%)	56 (51.9%)	79 (50.6%)	73 (42.9%)	64 (36.4%)	3140 (47.1%)
A+	1192 (20.8%)	31 (9.7%)	7 (6.5%)	20 (12.8%)	26 (15.3%)	30 (17.0%)	1306 (19.6%)

Note: NHW-E = Non-Hispanic White participants tested in English, NHB-E = Non-Hispanic Black participants tested in English, NHA-E = Non-Hispanic Asian participants tested in English, NHA-J = Non-Hispanic Asian participants tested in Japanese, HW-E = Hispanic White participants tested in English, O-E = Other (Unknown/Multiple Race-Ethnicities) participants tested in English.

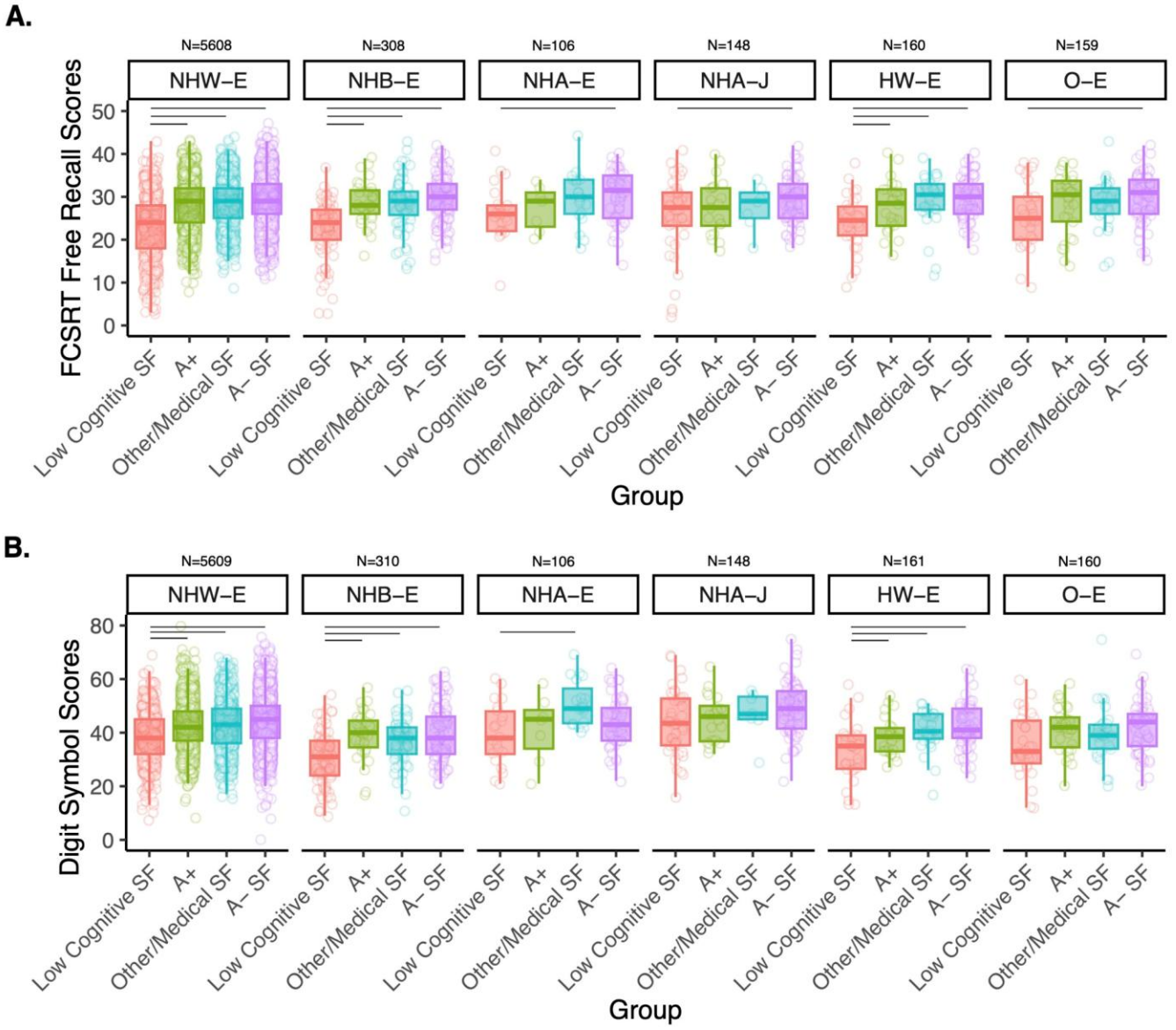
Figure 1. Screen-failure differences between race/ethnicity/testing language groups due to (A) amyloid status in all participants who underwent amyloid PET, (B) percent of medical/other and cognitive/functional screen-fails in all screened participants, (C) neuropsychological performance in those screened out due to cognition/functioning, (D) performance on individual MMSE Items in participants who were screened out due to low cognition/functioning, (E) performance on individual CDR domains in participants who were screened out due to low cognition/functioning.



(A, B) Logistic regressions controlling for age and sex were used to examine group differences. Years of education was additionally controlled for when examining differences in percentage of cognitive screen-fails. (C) Multinomial logistic regression controlling for age, sex, and education was used to examine group differences on screen-failure reason.

Note: NHW-E = Non-Hispanic White participants tested in English, NHB-E = Non-Hispanic Black participants tested in English, NHA-E = Non-Hispanic Asian participants tested in English, NHA-J = Non-Hispanic Asian participants tested in Japanese, HW-E = Hispanic White participants tested in English, O-E = Other (Unknown/Multiple Race-Ethnicities) participants tested in English. MMSE = Mini-Mental State Examination. CDR = Clinical Dementia Rating. LM= Wechsler Memory Scale Logical Memory Delayed Recall.

Figure 2. Performance differences between inclusion/exclusion groups on non-screening cognitive measures of the (A) Free and Cued Selective Reminding Test (FCSRT) Free Recall and (B) Digit Symbol. Raw scores are depicted and horizontal black bars denote significant differences between inclusion/exclusion groups when using linear regression models controlling for age, sex, and education.



Note: NHW-E = Non-Hispanic White participants tested in English, NHB-E = Non-Hispanic Black participants tested in English, NHA-E = Non-Hispanic Asian participants tested in English, NHA-J = Non-Hispanic Asian participants tested in Japanese, HW-E = Non-Hispanic White participants tested in English, O-E = Other (Unknown/Multiple Race-Ethnicities) participants tested in English, SF= screen-fail.

Keywords: Amyloid Positivity, Cognitive Testing, Screening Bias, Underrepresented Groups, Clinical Trial Enrollment

128 Lower locus coeruleus metabolism is associated with greater year-to-year intraindividual cognitive variability in older individuals with elevated levels of Alzheimer's disease pathology

Emma E Wiklund[1], Maxime Van Egroo[1,2], Elouise A Koops[1], Bernard J Hanseeuw[3,4], Kathryn V Papp[7], Dorene M Rentz[6,7], Reisa A Sperling[6,7], Keith A Johnson[3,6,7], Heidi IL Jacobs[1]

[1]*The Athinoula A. Martinos Center for Biomedical Imaging, Department of Radiology, Massachusetts General Hospital, Harvard Medical School, Boston, MA, US*
[2]*Faculty of Health, Medicine and Life Sciences, Mental Health and Neuroscience Research Institute, Alzheimer Centre Limburg, Maastricht University, Maastricht, NL*
[3]*Gordon Center for Medical Imaging, Department of Radiology, Massachusetts General Hospital, Harvard Medical School, Boston, MA, US*
[4]*Department of Neurology, Institute of Neuroscience, Cliniques Universitaires SaintLuc, Université Catholique de Louvain, Brussels, BE*
[5]*Department of Neurology, Massachusetts General Hospital, Harvard Medical School, Boston, MA, US*
[6]*Center for Alzheimer Research and Treatment, Department of Neurology, Brigham and Women's Hospital, Boston, MA, US*

Introduction: Intraindividual variability in cognitive performance is associated with increased risk for Alzheimer's disease (AD) and has been linked to the structure and function of catecholaminergic systems, including the noradrenergic locus coeruleus (LC). Importantly, higher LC metabolism was demonstrated to provide resilience against cognitive decline in preclinical AD. Here, we examined the association between LC metabolism and year-to-year intraindividual variability and assessed the moderating effect of AD pathology on this relationship.

Methods: 155 participants from the Harvard Aging Brain Study **(Figure 1)** underwent structural MRI, Fluorodeoxyglucose (FDG)-, Flortaucipir (FTP)-, Pittsburgh compound B (PiB)-PET scans, and longitudinal cognitive evaluation (mean follow-up 7.74+/-2.34 years). LC FDG-PET signal was extracted using an in-house MRI-based joint-entropy deblurring algorithm with reference to cerebellar white. Year-to-year intraindividual cognitive variability was defined by the coefficient of variation (CoV; SD/mean) within each person for several cognitive tests **(Figure 2).** Entorhinal FTP and neocortical PiB-PET were partial-volume corrected. Multiple linear regressions adjusted for age, sex, and education associated the CoV for each cognitive test with i) LC FDG-PET signal and ii) LC FDG-PET signal interacted with entorhinal FTP-PET or neocortical PiB.

Results: LC FDG-PET signal was not associated with CoV on any cognitive tests **(Figure 2)**. Interaction models indicated that lower LC FDG-PET signal was associated with higher CoV on the DSST (p=0.02) and LM (p=0.02) in individuals with elevated FTP-PET, and higher LM CoV in those with elevated neocortical PiB (p=0.04). Excluding participants with a CDR>0 (N=15) at the time of the FDG-PET did not affect the FTP (DSST: p=0.002, LM: p=0.02) or PiB results (DSST: p=0.03, LM: p=0.02) **(Figure 3).**

Conclusion: Our findings suggest that higher LC metabolism contributes to more stable longitudinal cognitive performance in individuals with elevated AD pathology. These findings therefore have implications for the early detection of individuals at risk for AD trajectories.

Figure 1:

Characteristics of Participants (N = 155)	
Age (years)	75.30 (11.29)
Female (n, %)	92 (59%)
Education (years)	15.97 (2.87)
MMSE score	28.68 (2.16)
CDR Rating = 0[#] (n, %)	135 (87%)
Cognitive follow-up time (years)	7.74 (2.34)
LC FDG-PET (SUVR)	0.84 (0.09)
Entorhinal FTP-PET (SUVR, PVC)	1.35 (0.30)
PiB + [#] (n, %)	44 (28%)

Table 1. *Data is presented as means (standard deviations) or numbers (percentages). Abbreviations: MMSE = Mini-Mental State Examination; CDR = Clinical Dementia Rating; LC = Locus Coeruleus; FTP = Flortaucipir; SUVR = Standardized Uptake Value Ratio; PVC = partial volume correction; PiB = Pittsburgh compound B; [#] at the time of the FDG-PET visit.*

Figure 2:

Cognitive Test	LC Metabolism		
	Estimate	**T-Value**	***P*-Value**
Phonological Fluency (F-A-S)	0.03	0.41	0.68
Digit Symbol Substitution (DSST)	-0.02	-0.23	0.82
Categorical Fluency (CAT)	0.00	0.02	0.98
Free and Cued Selective Reminding Test Free Recall (FCSRT)	0.31	0.85	0.39
Logical Memory Delayed Recall (LM)	-0.02	-0.13	0.89

Table 2: *The relationship between LC metabolism and the coefficient of variation for various cognitive tests. Abbreviations: CoV = Coefficient of Variation (SD/mean); DSST = Digit Symbol Substitution Test; FCSRT = Free and Cued Selective Reminding Test; LC = locus coeruleus; LM = Logical Memory; SUVR = Standardized Uptake Volume Ratio.*

Figure 3:

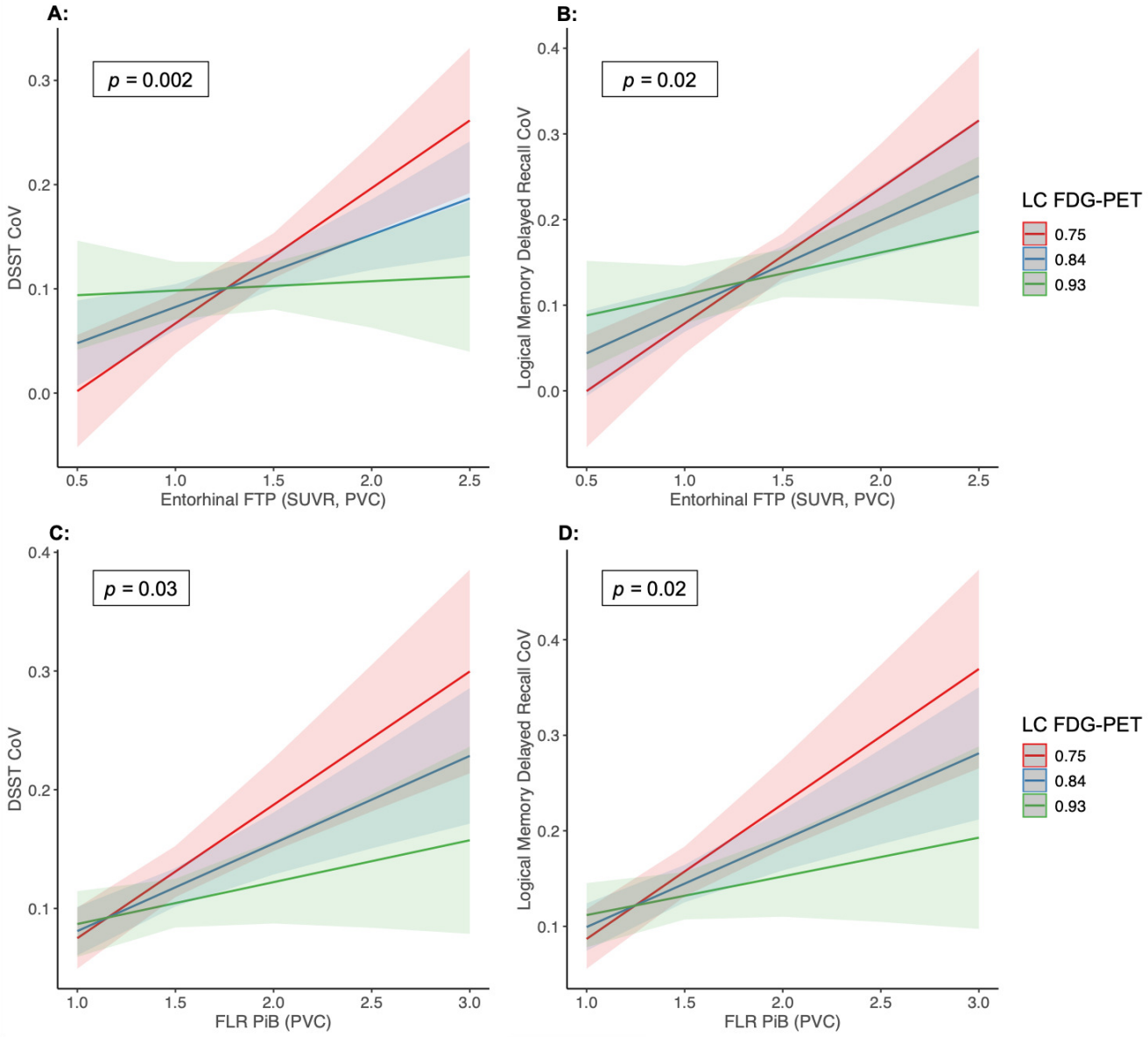


Figure 3. *Interaction between LC FDG-PET signal and entorhinal FTP-PET values on coefficient of variation for A) DSST(t(129) = -3.21; p = 0.002) and B) Logical Memory delayed recall (t(129) = -2.37; p = 0.02). Interaction between LC FDG-PET signal and neocortical (FLR) PiB values on coefficient of variation for C) DSST (t(129) = -2.18; p = 0.03) and D) Logical Memory delayed recall (t(129) = -2.35; p = 0.02).* Results show that at a given level of FTP or PiB, lower LC FDG-PET signal was associated with a higher CoV in the DSST or LM in participants with a CDR=0 . *Abbreviations: CoV = Coefficient of Variation; CDR = Clinical Dementia Rating; DSST = Digit Symbol Substitution Test; FLR = Frontal, Lateral Temporal, and Retrosplenial cortices; FTP = Flortaucipir; LC = Locus Coeruleus; PiB = Pittsburgh compound B; PVC = Partial Volume Correction; SUVR = Standardized Uptake Volume Ratio.*

Keywords: locus coeruleus metabolism, cognitive variability, beta-amyloid, tau, preclinical Alzheimer's disease

129 Long-term cognitive and biomarker trajectories of cognitively unimpaired individuals with elevated plasma ptau-217

Jesús Silva-Rodríguez[1], Linda Zhang[1], Elizabeth L. Valeriano-Lorenzo[1], Francisco J. López-González[1], Sonia Wagner-Reguero[1], Teodoro del Ser[1], Michel J. Grothe[1], Pascual Sánchez-Juan[1]

[1]*Reina Sofia Alzheimer Centre, CIEN Foundation, ISCIII, Madrid, ES*

Introduction: Plasma ptau-217 has demonstrated excellent performance in detecting AD pathology and in distinguishing between AD and non-AD neurodegenerative disorders. However, its value for predicting long-term cognitive decline among cognitively unimpaired (CU) individuals remains unclear.

Methods: We analyzed data from 1044 CU older individuals (75±4yrs, 64% female) enrolled in the Vallecas Project at the CIEN Foundation (Madrid, Spain). Participants underwent annual assessments from 2011 to 2024, including blood sampling, detailed clinical and neuropsychological evaluations, and MRI scanning (average follow-up: 7.2±3.0yrs). Baseline plasma ptau-217 levels were measured using the LUMIPULSE platform (Fujirebio). Subjects were categorized as having either normal (ptau-) or elevated (ptau+) ptau-217 based on a pre-established threshold of 0.247pg/mL. We used linear mixed-effects models to assess longitudinal group differences across three key outcomes: a) cognitive performance, assessed using a modified preclinical Alzheimer's cognitive composite score (mPACC5); b) hippocampal volume, measured on serial MRI using SPM12/CAT12; and c) a blood biomarker of astrocytic activation (GFAP, Simoa® platform, n=506). Additionally, Cox survival analysis was performed to assess the risk of progressing to MCI or dementia. All models were adjusted for sex, baseline age, and APOE4 status.

Results: 16.6% of the participants were classified as ptau+. These individuals showed significantly lower baseline mPACC5 scores (z-score difference: -0.5, $p<0.001$) and a steeper cognitive decline (Δslope = -0.2 z-score/year, $p<0.001$). Ptau+ was also a strong predictor of conversion to MCI/dementia (HR=5.1, CI=[4.1,6.2], $p<0.001$). Ptau+ participants had smaller baseline hippocampal volumes (-3%, $p<0.001$) and experienced faster hippocampal atrophy (Δslope = -0.4%/year, $p<0.002$). Finally, ptau+ was associated with higher baseline levels of GFAP (+33%, $p<0.001$), but rates of change were similar between groups ($p=0.38$).

Conclusions: These findings support the role of plasma ptau-217 as a valuable biomarker for early identification of CU individuals at risk for AD.

Keywords: plasma biomarkers, ptau-217, cognitive trajectories

130 A large public release of PIB PET and MRI from the Mayo Clinic Study of Aging

Christopher G. Schwarz[1], Walter K. Kremers[1], Carl M. Prakaashana[1], Scott A. Przybelski[1], Luke R. Christenson[1], Josie M. Williams[1], Jeffrey L. Gunter[1], Matthew L. Senjem[1], Arvin Arani[1], Robert I. Reid[1], Mary M. Machulda[1], Julie A. Fields[1], Val J. Lowe[1], Kejal Kantarci[1], Jonathan Graff-Radford[1], Prashanthi Vemuri[1], Ronald C. Petersen[1], David S. Knopman[1], Clifford R. Jack[1]

[1]*Mayo Clinic, Rochester, MN, US*

Background: The Mayo Clinic Study of Aging (MCSA) is a longitudinal, population-based study of residents of Olmsted County, Minnesota, USA. MCSA is releasing de-identified clinical and imaging data on GAAIN.org to benefit the research community.

Methods: For our initial release in April 2024, we selected the first imaging visit with 3T GE MRI scanners and concurrent amyloid (PiB) PET from imaging participants 50-90 years of age (average 70.7y). We included 3D T1-weighted, T2-weighted FLAIR, diffusion MRI, and numeric SUVR and Centiloid values from PiB PET.

We also included longitudinal clinical data from all MCSA participants 30-90 years of age (average 70.0y) through the first 15 years of the study. Clinical data includes age, sex, self-reported race/ethnicity, APoE4 allele status, cognitive impairment status (normal, MCI, dementia, or other), height, weight, blood pressure, multi-domain neuropsychological scores, neuroimaging summary measurements, medications, cardiovascular risk factors, social activity, sleep, mood/anxiety, functional measures, and more. All images are released in DICOM format after de-identification with CTP and de-facing with *mri_reface* to further protect participants' privacy, and all de-faced images were visually inspected by a trained data scientist for quality assurance.

Results: Our initial public data release includes clinical data from 5925 unique participants from the Mayo Clinic Study of Aging (MCSA), each ranging from 1-12 visits at roughly 15-month intervals. 1802 of these participants included MR images and PiB PET SUVR+Centiloid values. De-faced DICOM for 1792 accompanying PiB PET studies (4-frame dynamic, late-uptake, smoothed for harmonization) have now been added, and follow-up scans are coming soon. Demographic summaries are given in Table 1.

Discussion: This large, richly characterized, de-identified clinical and imaging dataset is available to the research community at https://www.gaaindata.org/partner/MCSA, and it is suitable for a wide range of research uses. Additional data will be released over time, including longitudinal follow-up imaging.

Table 1. Characteristics table of clinical and imaging participants with the mean (SD) listed for the continuous variables and count (%) for the categorical variables. For the clinical dataset, these values are from the baseline visit.

	Clinical n = 5925	Imaging n = 1802
Age, years	70.0 (13.1)	70.7 (10.0)
Males, no. (%)	3014 (50.9%)	968 (53.7%)
Education, years	14.4 (2.8)	14.7 (2.6)
APOE-4 Carrier, no. (%)	1532 (27.4%)	516 (28.9%)
MMSE	27.8 (2.1)	28.1 (1.7)
Total Visits	3.8 (2.5)	1.0 (0.0)
Primary Diagnosis		
Cognitively Unimpaired, no. (%)	5135 (86.7%)	1573 (87.3%)
MCI, no. (%)	664 (11.2%)	202 (11.2%)
Dementia, no. (%)	87 (1.5%)	22 (1.2%)
Other, no. (%)	14 (0.2%)	2 (0.1%)
Missing/Protocol Deviation, no. (%)	25 (0.4%)	3 (0.2%)
Race		
White, no. (%)	5760 (97.2%)	1765 (97.9%)
Non-European Descent, no. (%)	101 (1.7%)	15 (0.8%)
More than one, no. (%)	38 (0.6%)	14 (0.8%)
Unknown/Not Reported, no. (%)	26 (0.4%)	8 (0.4%)
Ethnicity		
Hispanic/Latino, no. (%)	33 (0.6%)	5 (0.3%)
Non-Hispanic/Latino, no. (%)	5863 (99.0%)	1785 (99.1%)
Unknown/Not Reported, no. (%)	29 (0.5%)	12 (0.7%)

Keywords: PIB,dataset,open science,data sharing,MCSA

131 Harmonizing visual readings of Flortaucipir and MK-6240 using head-to-head data

Emma Ruppert[1], Marina Medeiros[1], Andreia Rocha[1], Carolina Soares[1], Livia Amaral[1], Guilherme Povala[1], Guilherme Bauer-Negrini[1], Pamela L. Ferreira[1], Firoza Lussier[1], Markley Oliveira Jr.[1], Matheus Scarpatto Rodrigues[1], Rayan Mroue[1], Hussein Zalzale[1], Douglas Leffa[1], Pampa Saha[1], Bruna Bellaver[1], Dana L. Tudorascu[1], David Soleimani-Meigooni[4], Juan Fortea[5], Val Lowe[6], Hwamee Oh[7], Belen Pascual[2], Brian A. Gordon[8], Pedro Rosa-Neto[9], Suzanne Baker[10], Tharick A. Pascoal[1]

[1]*University of Pittsburgh, Department of Psychiatry, Pittsburgh, PA, US*
[2]*Houston Methodist Research Institute, Department of Neurology, Houston, TX, US*
[3]*University of California San Francisco, Memory and Aging Center, San Francisco, CA, US*
[4]*Hospital de la Santa Creu i Sant Pau, Sant Pau Memory Unit, Department of Neurology, Barcelona, ES*
[5]*Mayo Clinic, Department of Radiology, Rochester, MN, US*
[6]*Brown University, Department of Psychiatry and Human Behavior, Providence, RI, US*
[7]*Washington University in St. Louis, Department of Radiology, St. Louis, MO, US*
[8]*Translational Neuroimaging Laboratory, McGill University Research Centre for Studies in Aging, Douglas Research Institute, Montréal, QC, CA*
[9]*Lawrence Berkeley National Laboratory, Berkeley, CA, US*

Background: Various visual reading methods for detecting brain tau-PET deposition have been developed for different tracers. However, their comparative performance in the same individuals has not been explored. This study aims to compare the performance of existing visual reading methods using [^{18}F]Flortaucipir(FTP) and [^{18}F]MK-6240(MK) and provide preliminary data toward a unified visual reading approach for all tau-PET tracers.

Methods: We assessed 340 individuals across the AD spectrum from the HEAD cohort (CU-n=175; CI-n=143). A subset of 101 individuals (CU-n=52; CI-n=49) was used to develop a unified visual reading approach. All participants underwent MRI and PET scans with FTP and MK. Visual reads, based on previous methods, were independently performed by two experts blinded to participants' demographics and diagnoses. For FTP, we applied *Sonni's* (PMID-33313377) method, and for MK, we used *Shuping's*(PMID-36873926) method. Inter-rater agreement was evaluated using unweighted Cohen's kappa(κ). Differences between visual reading groups were assessed using ANOVA with post-hoc Tukey tests.

Results: Using previous methods, inter-rater agreement was 72.1% for FTP (κ=0.55[0.48-0.62]) and 83.5% for MK (κ=0.69[0.62-0.76]). Agreement between the two tracers' visual reads(**Fig.1**) ranged from 65.6%-75.3%. These methods classified tau burden as negative, non-AD-like, low or high. In contrast, the developed method achieved an inter-tracer agreement of 87.1% and classified tau burden as negative, low, moderate, or high(**Fig.2**). Additionally, mean differences in tau-PET SUVR in the medial temporal lobe(MTL), plasma p-tau217, and MoCA scores across visual classification groups demonstrated greater statistical significance when using the developed method(**Fig.3**).

Conclusion: This study demonstrates that current visual reading methods produce varying classifications depending on the tracer used, revealing discrepancies below desired clinical performance standards. Our method improved concordance between visual reads by developing a unified, tracer-agnostic approach. Importantly, this method has the potential to create a clinician-friendly single visual reading technique that could be widely adopted for all tau tracers.

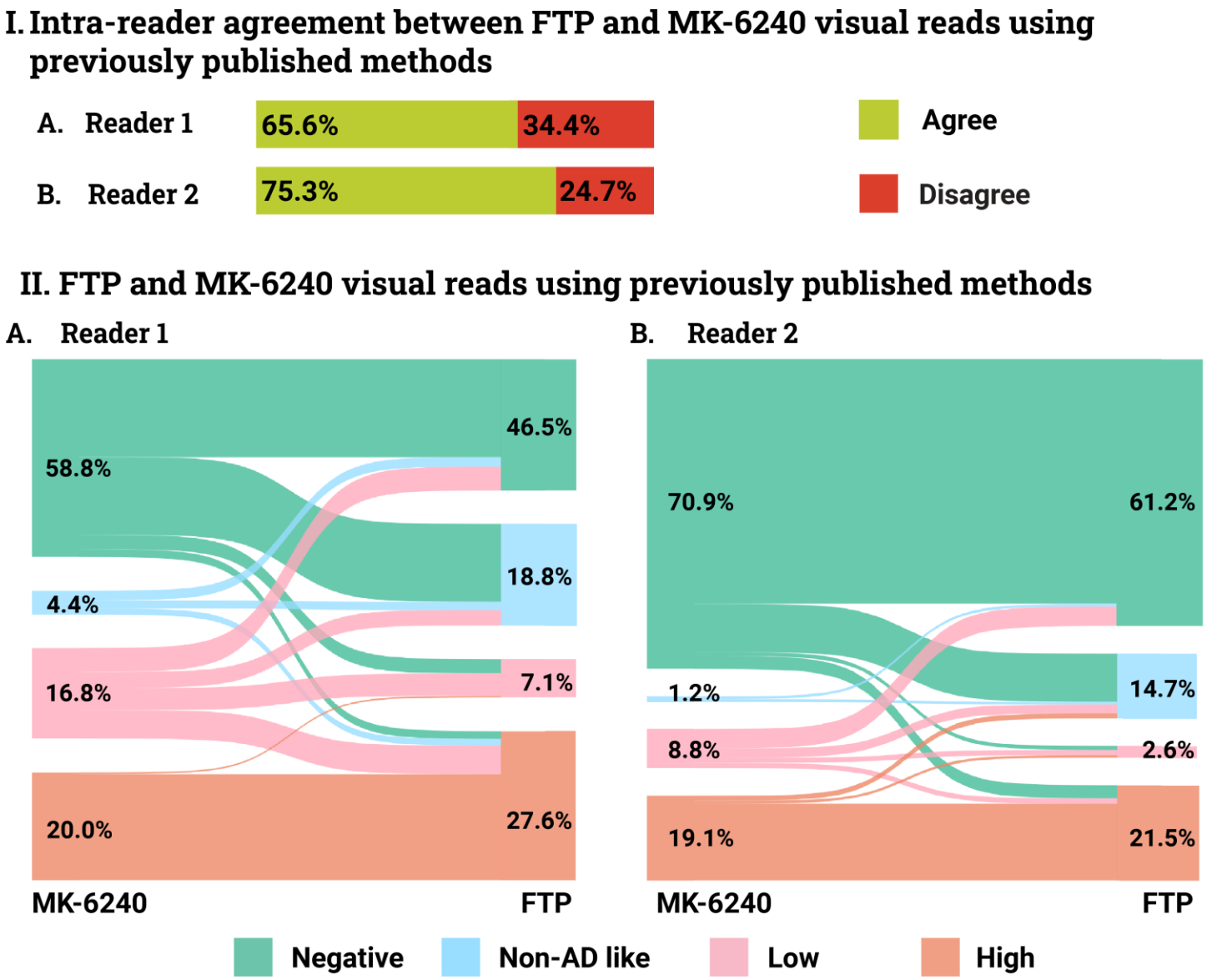


Figure 1. Comparison between FTP and MK visual reads using previously published methods. **I.** Bar plots showing intra-reader agreement for FTP and MK visual classification (n = 340) for Reader 1 (**A**) and Reader 2 (**B**). **II.** Sankey plots illustrating the distribution of each classification group (negative, non-AD like, low and high) for Reader 1 (**A**) and Reader 2 (**B**).The classification groups -negative, non-AD like, low, and high - correspond to the categories described by *Sonni et al.* as *'negative', 'non-AD like', 'MTL only',* and *'AD-like binding'*, and by *Shuping et al.* as '*no uptake', 'MTL only', 'MTL AND*' and '*outside MTL'*.

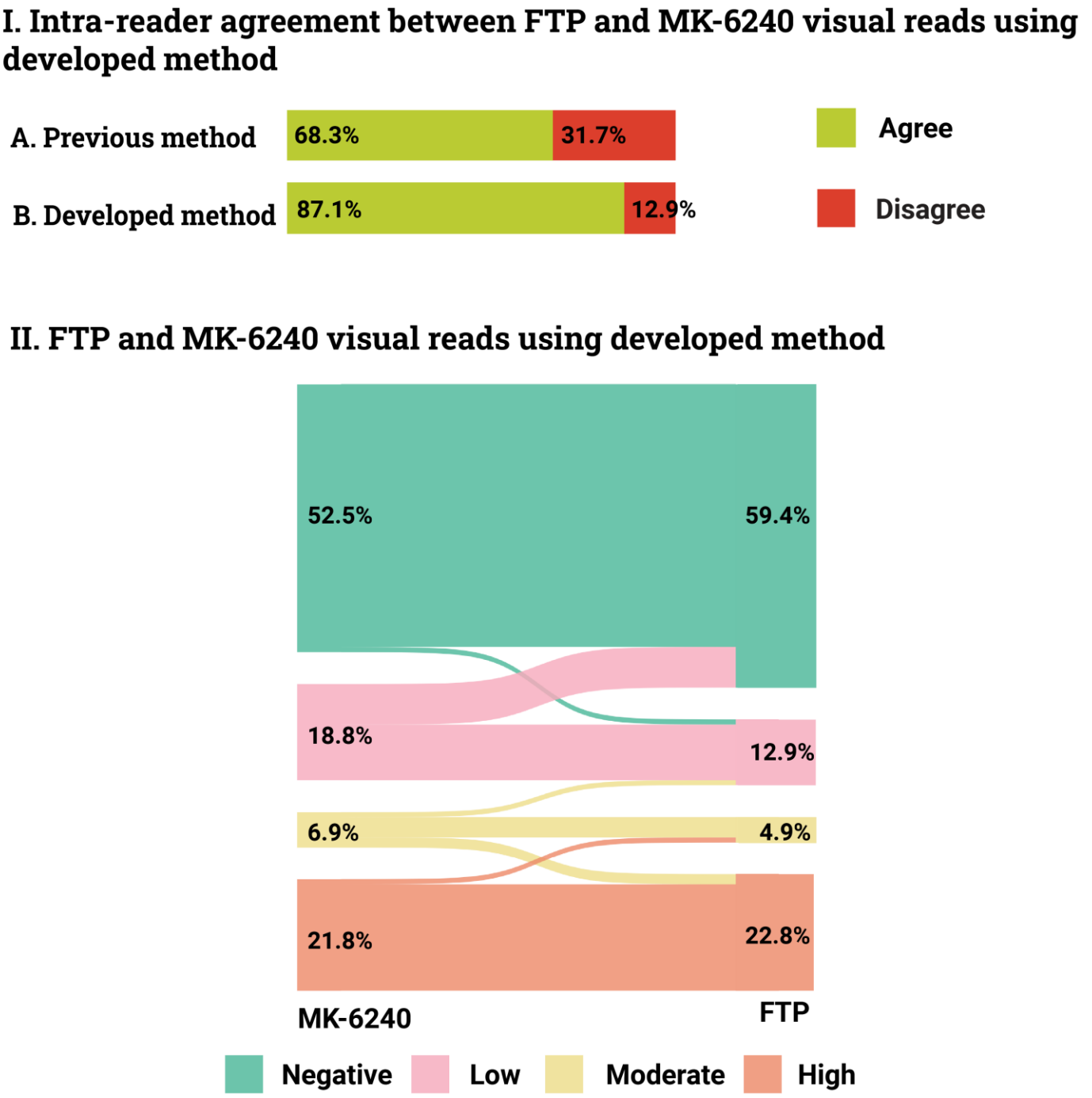
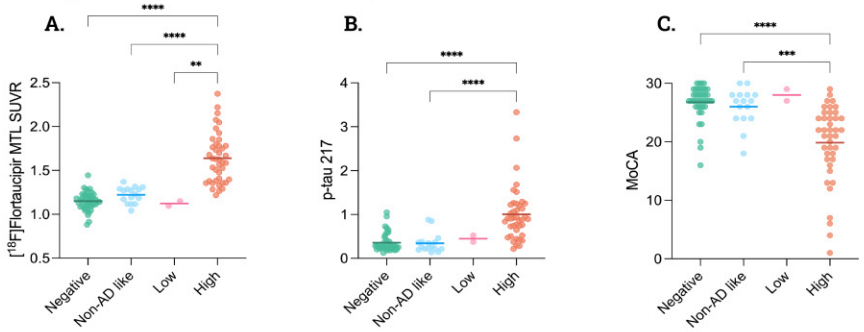


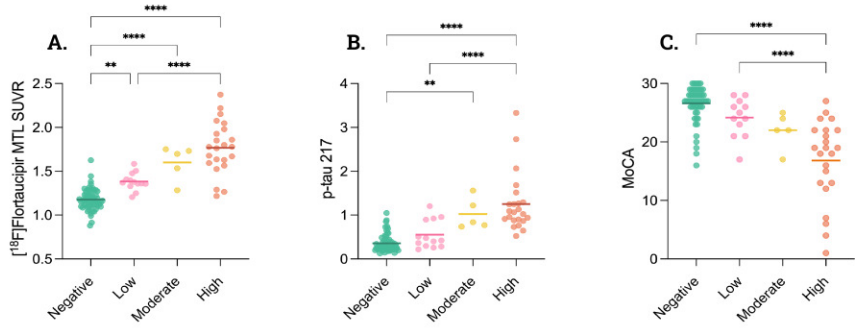
Figure 2. Comparison between FTP and MK visual reads using developed method. **I.** Bar plots showing agreement rates between FTP and MK-6240 visual classification (n = 101) for Reader 1, following previously published methods (**A**) and developed method (**B**). **II.** Sankey plots illustrating the distribution of each classification group (negative, low, moderate and high tau burden) using developed method (n=101).

Scatter plots showing MTL SUVR, p-tau 217 and MoCA grouped by tracer and method

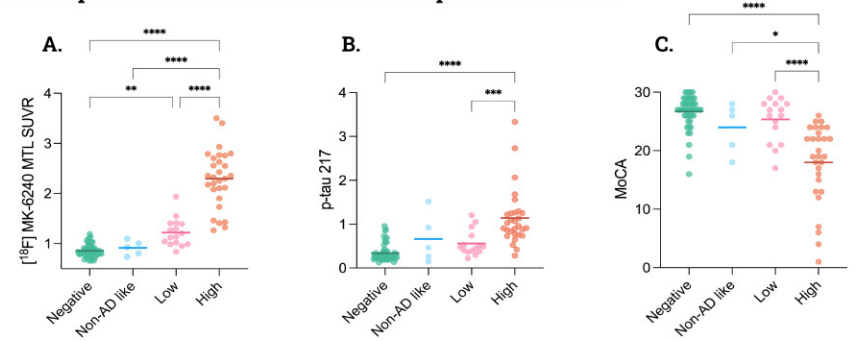
I. Groups based on FTP visual reads previous methods



II. Groups based on FTP visual reads developed method



III. Groups based on MK-6240 visual reads previous methods



IV. Groups based on MK-6240 visual reads developed method

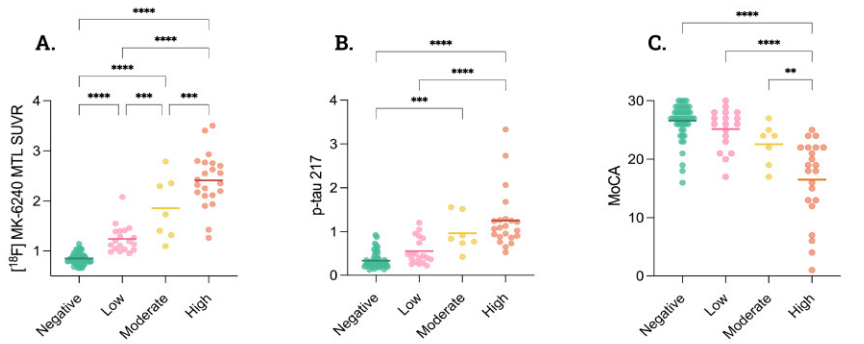


Figure 3. Scatter plots showing the distribution of tau accumulation in the medial temporal lobe (MTL) - measured by tracer's SUVR, plasma p-tau 217 levels, and MoCA scores of the sample subset (n = 101). Tau accumulation in the MTL, measured by FTP SUVR, is shown for groups classified by previous methods (**I.A**) and by the developed method (**II.A**), while the MK MTL SUVR is shown in groups categorized by previous methods (**III.A**) and by developed method (**IV.A**). Scatter plots showing plasma p-tau 217 levels according to visual groups defined by FTP (previous methods in **I.B** and developed method in **II.B**) and by MK (previous methods in **III.B** and in developed method **IV.B**). MoCA scores are presented for groups based on FTP previous methods (**I.C**) and developed method (**II.C**), and for MK previous methods (**III.C**) and developed method (**IV.C**). Mean differences were evaluated using ANOVA with post-hoc Tukey tests. Statistical significance is indicated as *p ≤ 0.05, **p ≤ 0.01, ***p ≤ 0.001, and ****p ≤ 0.0001.

Keywords: visual reads, tau-PET, harmonization, head-to-head, Alzheimer's disease

132 Twin-mapping techniques in clinical trials: a proof-of-concept application to the Internet-Based Conversational Engagement Clinical Trial (I-CONECT)

Chao-Yi Wu[1], Liu Chen[1], Steven Arnold[1], Hiroko Dodge[1]

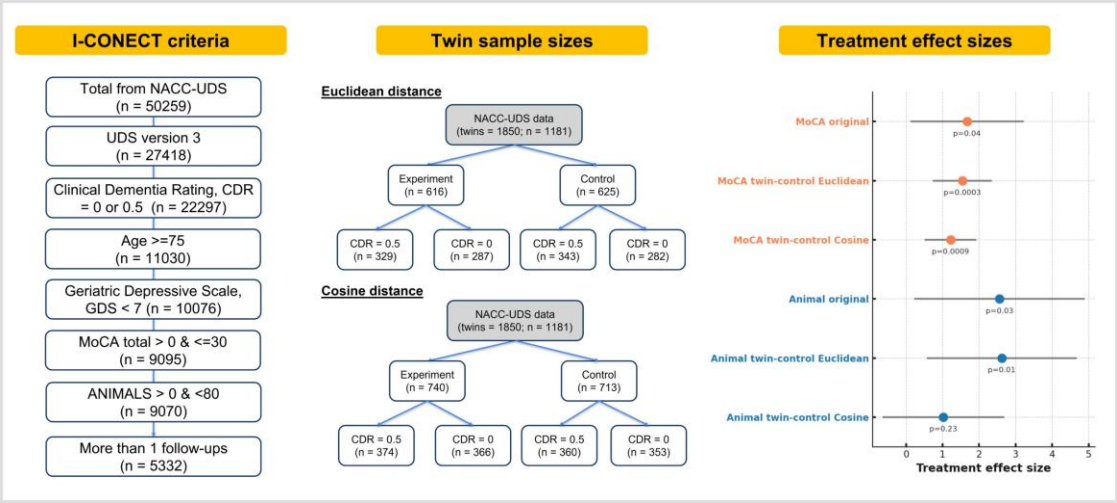
[1]*Neurology, Massachusetts General Hospital (MGH), Harvard Medical School, Charlestown, MA, US*

Objectives: With U.S. Food and Drug Administration (FDA)-approved anti-amyloid, partially disease-modifying treatments now available, the ethical justification for randomly assigning patients to placebo has become controversial. The idea of twin-controls has gained significant attention in recent years, with the aim of creating twin patient cohorts that can be used as a surrogate to predict the effects of treatment on a more personalized level. While promising, the feasibility of twin-mapping techniques remains largely untested.

Methods: I-CONECT is a multi-site randomized controlled trial (RCT) examining the effects of conversational interactions on cognition among socially-isolated subjects aged ≥75 years (normal cognition; mild cognitive impairment). 186 participants were randomized into experimental or control groups. The experimental group engaged in video-chats with study staff 4 times/week for 6 months, while the control group received weekly 10-minute phone calls. The current analysis focused on the efficacy-shown Montreal Cognitive Assessment (MoCA; global cognition) and category fluency animals (language-based executive function) at 6-month follow-up. Ten digital twins were matched to each participant receiving the treatment using data from the National Alzheimer's Coordinating Center Uniform Data Set (NACC-UDS) based on similarity distance metrics (Euclidean;Cosine). Treatment effect sizes and p-values were compared between the original and the twin-control-based result.

Results: Approximately 10% of NACC-UDS participants (5,332 out of 50,259) were eligible for I-CONECT (Figure 1). After twin-mapping, sample sizes for the original control vs. twin-control were 31 vs. 112 for MoCA and 86 vs. 330 for category fluency. Treatment effect sizes showed substantial agreement between original and twin-control results (MoCA: 1.75±0.76 vs. 1.54±0.41; category fluency: 2.56±1.19 vs. 2.62±1.05)(Figure 1). P-values remained significant and smaller when treating the twin samples as controls.

Conclusions: Digital twins from publicly available datasets enhance the rigor of RCTs by providing mapped twins as controls for early-phase dementia trials. Figures 1. Proof-of-concept of twin-mapping technique.



Keywords: virtual twins; synthesized control; anti-amyloid drugs; disease modifying; natural history cohort study

133 Effects of amyloid and tau status on multiplex plasma CNS and inflammatory proteins in a normal aging cohort

Alexandra N Trelle[1], Karly A Cody[1], Tran T Nguyen[2], Joseph R Winer[1], Skylar Weiss[1], America Romero[1], Isha Sai[1], Edward N Wilson[1,3], Anthony D Wagner[3,4], Holden T Maecker[3,5], Elizabeth C Mormino[1,3]

[1]*Neurology & Neurological Sciences, Stanford School of Medicine, Stanford, CA, US*
[2]*Institute for Immunity, Transplantation, and Infection Operations, Stanford University, Stanford, CA, US*
[3]*Wu Tsai Neurosciences Institute, Stanford University, Stanford, CA, US*
[4]*Psychology, Stanford University, Stanford, CA, US*
[5]*Microbiology and Immunology, Stanford University, Stanford, CA, US*

Objective: Scalable plasma markers are needed to capture canonical Alzheimer's disease biomarkers, as well as additional biological pathways relevant for cognitive decline in human aging.

Methods: We evaluated plasma CNS and inflammatory proteins from newly developed multiplex panels (NULISA, Alamar) in clinically unimpaired individuals from the Stanford Aging and Memory Study with available Lumipulse CSF Aβ42/Aβ40 and pTau181 data (n=132; mean (SD) age = 68.8 (5.6) years; 78 female). Cross-sectional fold change differences by A-status (CSF Aβ42/Aβ40<0.075) and T-status (CSF pTau181>50.61) were examined using Wilcoxon rank-sum tests (FDR-corrected, *p*=0.005) across NULISA targets (125 CNS proteins; 250 inflammatory proteins). Spearman correlations assessed continuous associations between NULISA pTau isoforms and CSF proteins. ROC curves evaluated discriminative accuracy of NULISA Aβ and pTau isoforms for amyloid and tau positivity. Linear mixed models assessed change over time of selected NULISA targets in individuals with longitudinal follow-up (n=49; mean (SD) follow-up 5.6 (1.9) years).

Results: Significant differences between A+ and A- individuals were observed for pTau217, pTau231, pTau181, Aβ42, and GFAP (Figure 1A). Significant differences between T+ and T- individuals were observed for CNS panel targets pTau217, pTau231, pTau181, GFAP, TIMP3, SAA1, and inflammatory panel targets TIMP1, CSF3, TREM1, CXCL11, THPO, LGALS9, S100A12 (Figure 1B). Moderate correlations were observed between NULISA pTau isoforms and CSF Aβ42/Aβ40 and pTau181 (Figure 2). NULISA pTau isoforms exhibited high discriminative accuracy for predicting CSF A and T status (Table 1). Among NULISA targets that differed between A or T groups, pTau217, pTau231, and CSF3 exhibited significant increases and Ab42 exhibited significant decreases over time (p<0.05).

Conclusions: NULISA multiplex CNS and inflammatory panels hold promise as a scalable method to measure multiple pathways relevant for human aging and disease processes. Future work is needed to evaluate associations of proteomic changes with cognitive decline and clinical progression.

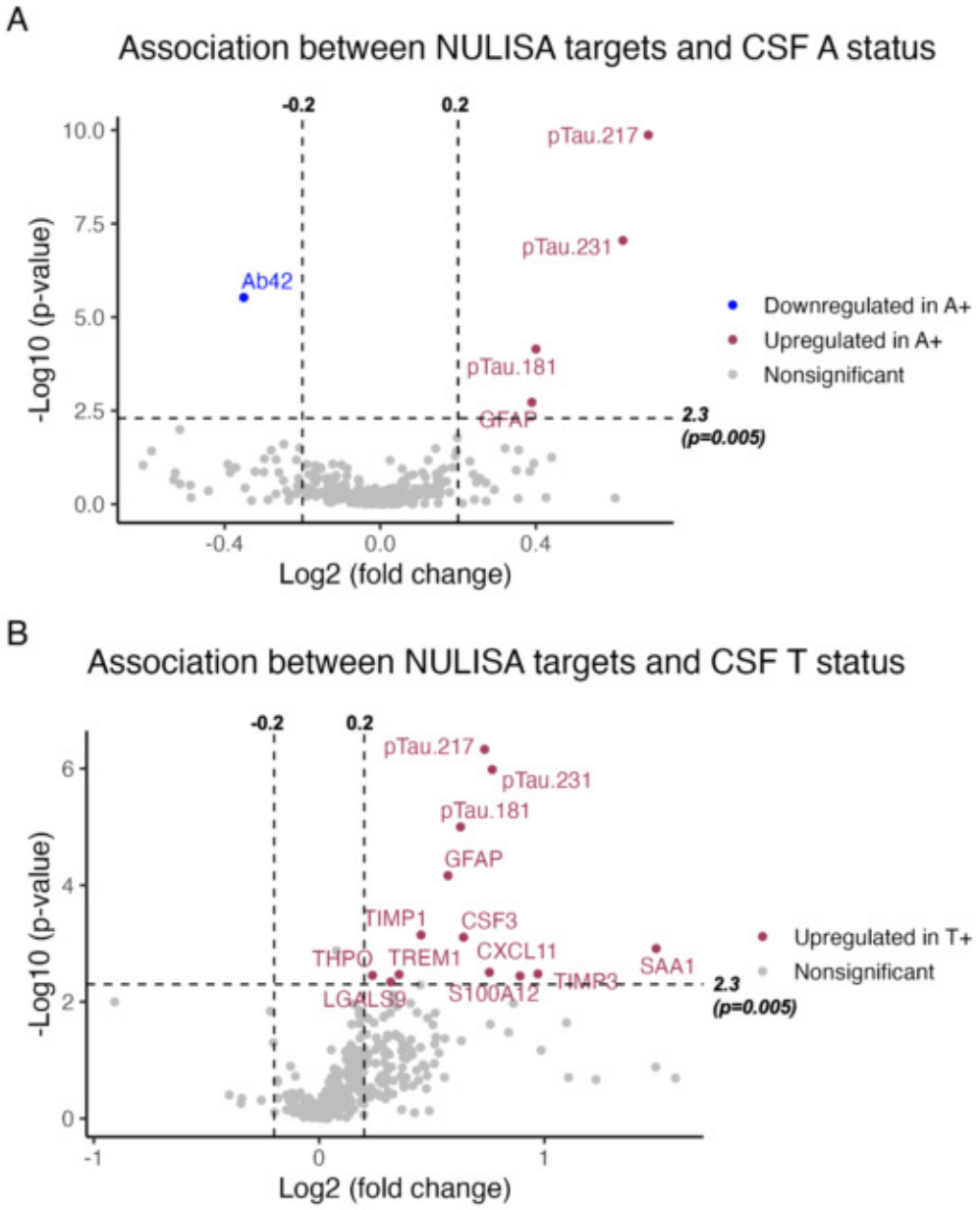


Figure 1. Cross-sectional associations of NULISA targets with CSF A and T status. **A.** Volcano plot of -log10 (p-value) versus log2 (fold change) comparing protein abundances measured in NULISA Protein Quantification (NPQ) units in samples from CSF-defined A+ (n=32) vs A- (n=96) older adults. Significant targets are shown in blue (downregulated) and red (upregulated). **B.** Volcano plot comparing NPQs in samples from CSF-defined T+ (n=21) vs T- (n=111) older adults. Significant targets are shown in red (upregulated).

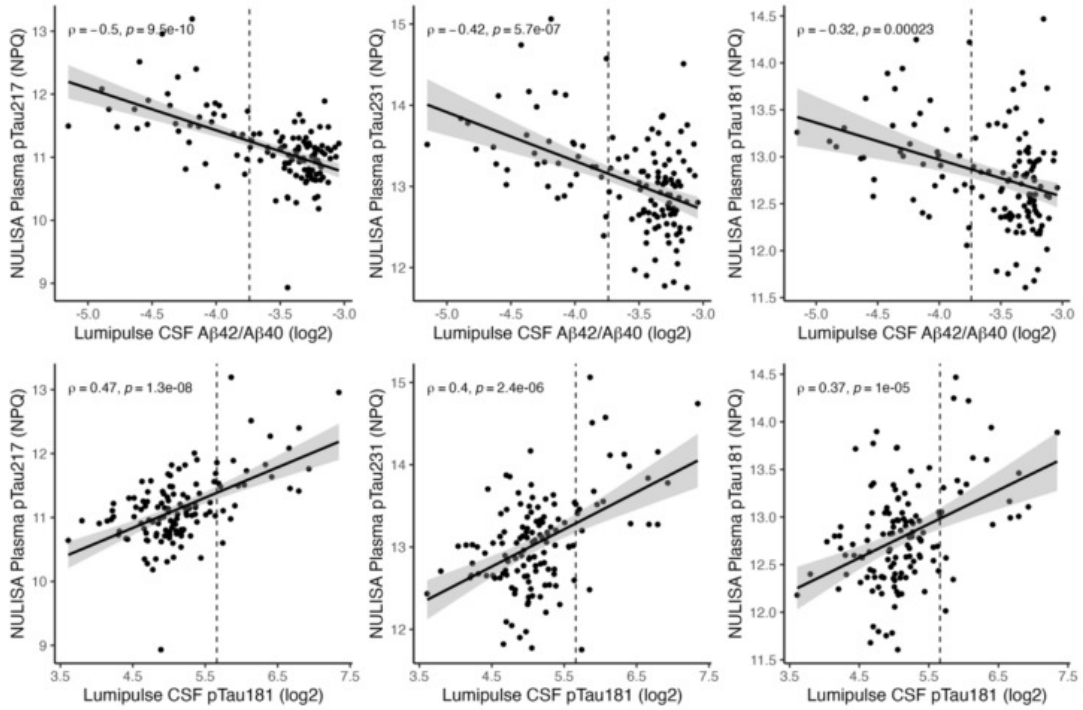


Figure 2. Cross-sectional associations of NULISA pTau isoforms (pTau217, pTau231, pTau181) with CSF Aβ42/Aβ40 (n=132) and CSF pTau181 (n=132). Significant spearman correlations (ρ) and dotted lines corresponding to the positivity threshold for CSF Aβ42/Aβ40 (log2; -3.74) and CSF pTau181 (log2; 5.66) are indicated on each panel. NPQ, NULISA Protein Quantification Units

Table 1: Discriminative accuracy of selected NULISA targets for CSF A and T positivity

NULISA Target	AUC (95% CI) A Status	AUC (95% CI) T Status
pTau217	0.864 (0.779, 0.949)	0.848 (0.745, 0.950)
pTau231	0.803 (0.720, 0.886)	0.837 (0.718, 0.956)
pTau181	0.725 (0.627, 0.823)	0.805 (0.684, 0.926)
Aβ42	0.765 (0.675, 0.855)	0.669 (0.532, 0.805)

A status: CSF Aβ42/Aβ40 < 0.075; T status: CSF pTau181 > 50.61.
The AUC 95% confidence interval (CI) was computed using 2000 bootstrap iterations.

Keywords: Plasma, Multiplex, Amyloid, Tau, Preclinical Alzheimer's disease

134 Tau imaging thresholds within NIA-AA multilevel tau staging as predictors of tau accumulation and cognitive decline in non-demented individuals

Alexandra Gogola[1], Ann Cohen[2,3], Beth Snitz[3,4], Davneet Minhas[1], Dana Tudorascu[2,3], Milos Ikonomovic[3,4,8], C. Elizabeth Shaaban[3,5,8], Vincent Dore[6,7], Cristy Matan[1], Alexander DelBene[1], Pierrick Bourgeat[7], Antoine Leuzy[9], Howard Aizenstein[2,3], Oscar Lopez[3,4], Brian Lopresti[1], Victor Villemagne[2,3,6]

[1]*Department of Radiology, University of Pittsburgh School of Medicine, Pittsburgh, PA, US*
[2]*Department of Psychiatry, University of Pittsburgh, Pittsburgh, PA, US*
[3]*Alzheimer's Disease Research Center, University of Pittsburgh, Pittsburgh, PA, US*
[4]*Department of Neurology, University of Pittsburgh, Pittsburgh, PA, US*
[5]*Department of Epidemiology, Pittsburgh, PA, US*
[6]*Department of Molecular Imaging & Therapy, Austin Health, Melbourne, AU*
[7]*Commonwealth Scientific and Industrial Research Organisation Health & Biosecurity, Melbourne, AU*
[8]*Geriatric Research Education and Clinical Center, Veterans Affairs Pittsburgh Healthcare System, Pittsburgh, PA, US*
[9]*Critical Path for Alzheimer's Disease (CPAD) Consortium, Critical Path institute, Pittsburgh, PA, US*

Background: We evaluated the predictive performance of ^{18}F-flortaucipir (FTP) tau imaging with respect to tau accumulation and cognitive decline in non-demented participants. We also tested the relationships between baseline tau and tau accumulation in relation to different cognitive measures.

Methods: FTP scans from 213 non-demented participants were processed and sampled in Statistical Parametric Mapping software (SPM), version 8, using CenTauR masks. Tau accumulation and cognitive decline associations were assessed longitudinally, with respect to their baseline and most recent evaluations, via survival analysis. Individuals were grouped into 4 groups reflecting the NIA-AA imaging stages: Initial, Early, Intermediate, and Advanced. A "None" group reflecting no pathology was included as a control. Linear regressions were used to compare the longitudinal effects of either baseline tau (SUVR) or tau accumulation (SUVR/year) on cognitive decline.

Results: While the two sets of thresholds yielded slightly different trajectories, both showed that when applying multiple levels of tau positivity, increasing stages of tau predicted both earlier tau accumulation and earlier cognitive decline. Linear regressions revealed that change in global measures of cognition (MMSE, CDR-SB) were significantly associated with baseline tau, while decline in Delayed Recall (DR) was significantly associated with both baseline tau and tau accumulation, where tau accumulation had a greater influence in the model, and Immediate Recall (LM) decline was significantly only associated with tau accumulation.

Conclusions: Implementing the multiple tau stages from the new NIA-AA biological staging framework clearly predicts distinct patterns of tau accumulation and cognitive decline. While baseline tau is predictive of global cognitive decline, tau accumulation is a better predictor of memory decline. Future work is needed in cognitively impaired individuals is needed to determine the suitability of thresholds utilized here in differentiating their trajectories.

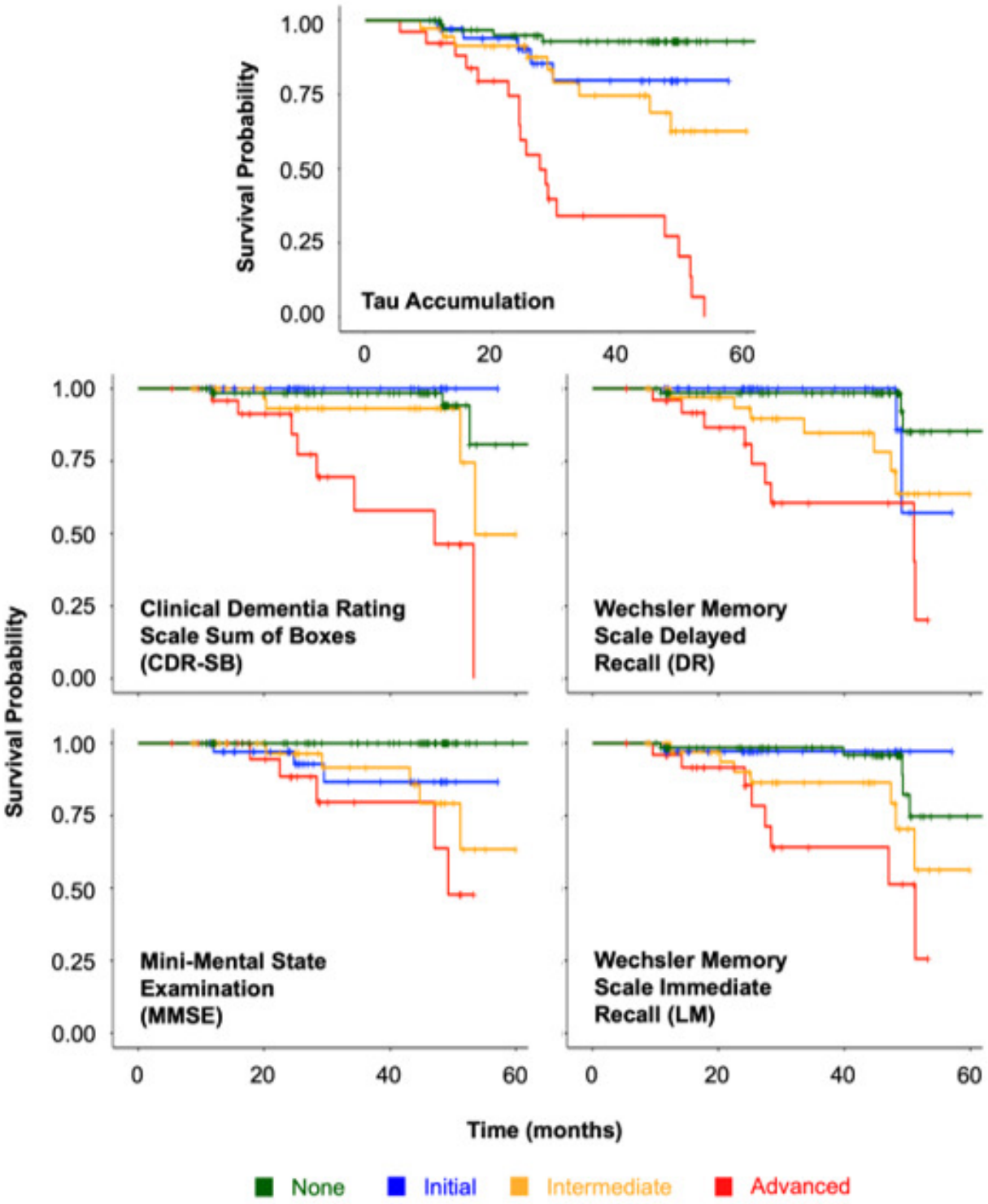


Figure 1. Survival curves of tau accumulation and four cognitive measures for each of the new NIA-AA tau stages based on BETTH thresholds.

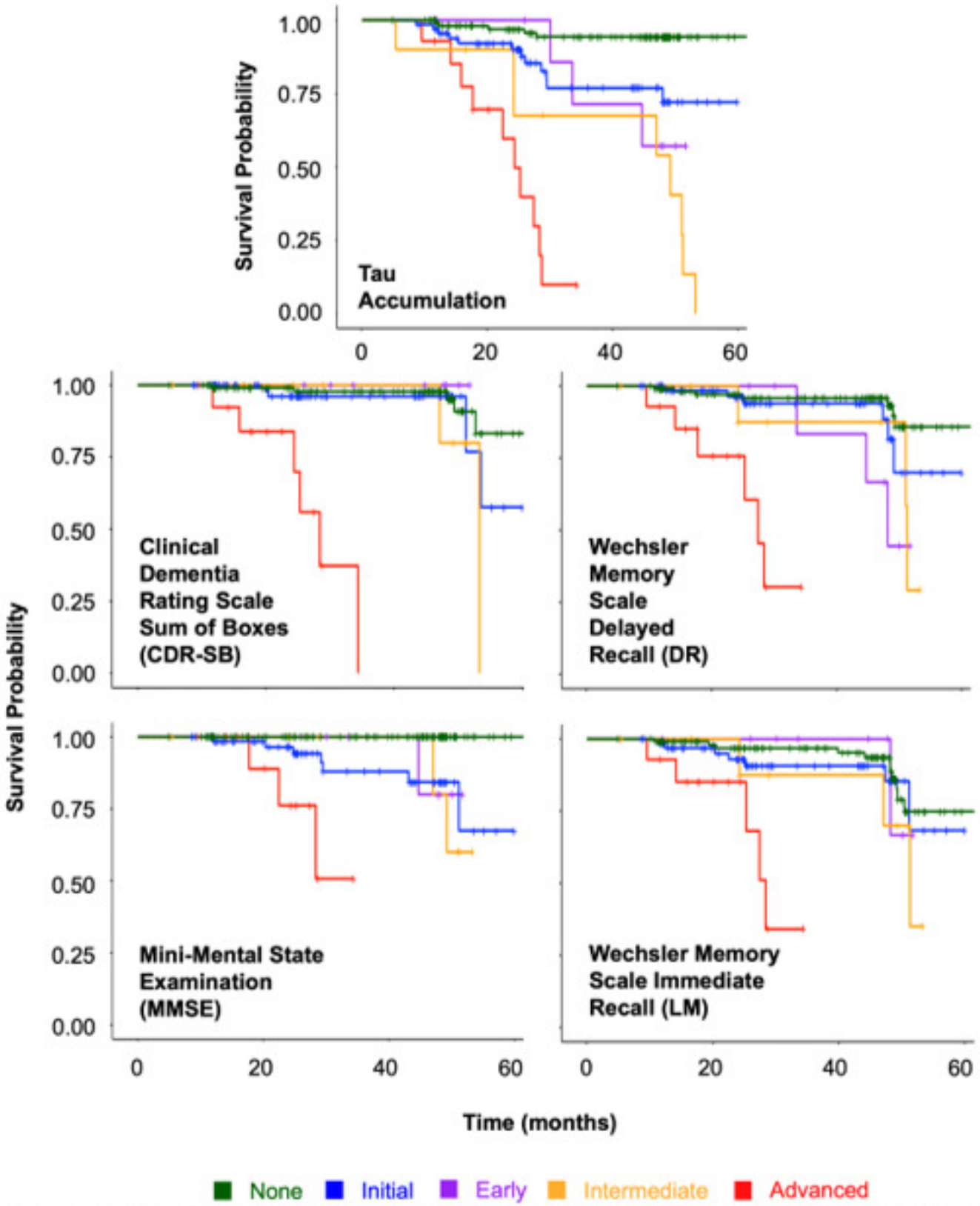


Figure 2. Survival curves of tau accumulation and four cognitive measures for each of the new NIA-AA tau stages based on CenTauRz thresholds.

Table 1. Association of baseline SUVR and tau accumulation (SUVR/year) in the Meta Temporal region with cognitive measures. While baseline tau is predictive of global cognitive (MMSE, CDR-SB) and memory decline (DR), tau accumulation is a much better predictor of memory decline

	Estimate	95% CI	p-value
	Meta Temporal Baseline SUVR		
CDR-SB	1.51	1.02, 2.00	8.01E-09*
DR	-2.55	-4.85, -0.24	3.14E-02*
LM	-1.56	-3.75, 0.63	1.65E-01
MMSE	-2.35	-3.43, -1.27	3.21E-05*
	Meta Temporal Accumulation (SUVR/year)		
CDR-SB	-0.54	-2.04, 0.95	4.78E-01
DR	-8.16	-13.19, -3.12	2.33E-02*
LM	-8.45	-15.10, -1.81	1.35E-02*
MMSE	0.52	-2.77, 3.81	7.55E-01

Keywords: tau PET, tau accumulation, cognitive decline, tau staging

135 Multi-morbidity and Alzheimer's disease pathology across the lifespan in adults with Down syndrome

Anna Smith[1], Natalie Edwards[1], Lisi Flores Aguilar[3], Mohamad Alshikho[1], Dana Tudorascu[4], H. Diana Rosas[6], Michael Yassa[3], Sigan L Hartley[2], Benjamin Handen[4], Bradley Christian[2], Jose Gutierrez[1], Donna Wilcock[5], Elizabeth Head[3], Adam M Brickman[1], Patrick Lao[1]

[1]*Columbia University Medical Center, New York, NY, US*
[2]*University of Wisconsin-Madison, Madison, WI, US*
[3]*University of California-Irvine, Irvine, CA, US*
[4]*University of Pittsburgh, Pittsburgh, PA, US*
[5]*Indiana University, Indianapolis, IN, US*
[6]*Harvard University, Boston, MA, US*

Introduction: People with Down syndrome (DS) have greater risk for certain health conditions compared to the non-DS population, and comorbid contributions to Alzheimer's disease (AD) biomarker developments need to be better understood even in the context of genetic risk. We took a hypothesis-generating approach to explore whether comorbidities are associated with age-related trajectories of AD and cerebrovascular biomarkers in adults with DS.

Methods: Adults with DS (n=259; 45±10 yrs, 43% women, 75% Cognitively-Stable/12% MCI-DS/13%AD-DS/excluded Unable to Determine) from the Alzheimer's Biomarker Consortium-Down syndrome (ABC-DS) underwent MRI (white matter hyperintensity (WMH), enlarged perivascular space (PVS), infarcts, microbleeds), amyloid PET (Florbetapir Centiloids), and tau PET (AV-1451 SUVR). Comorbid conditions were collected from participant's health history. Biomarkers were fit against left-null piecewise regression models with age, adjusting for acquisition parameters across the multisite study. The age-trajectory residuals for each biomarker were then regressed on each comorbidity (i.e., more/less than expected for their age/disease progression).

Results: Congenital heart disease, hypotension, diabetes, sleep apnea, pneumonia, hyperlipidemia, and hypothyroidism were present, but had no associations with biomarker trajectories (Table 1). As previously reported, hypertension was associated with a greater PVS, and lower BMI was associated with greater WMH. Hypertension was further associated with lower early Braak tau. Seizures were associated with greater microbleed likelihood. Visual impairment was associated with greater infarct likelihood, while cataracts were associated with lower tau across Braak stages and lower PVS; hearing impairment was associated with lower late Braak tau. No comorbidity was associated with amyloid.

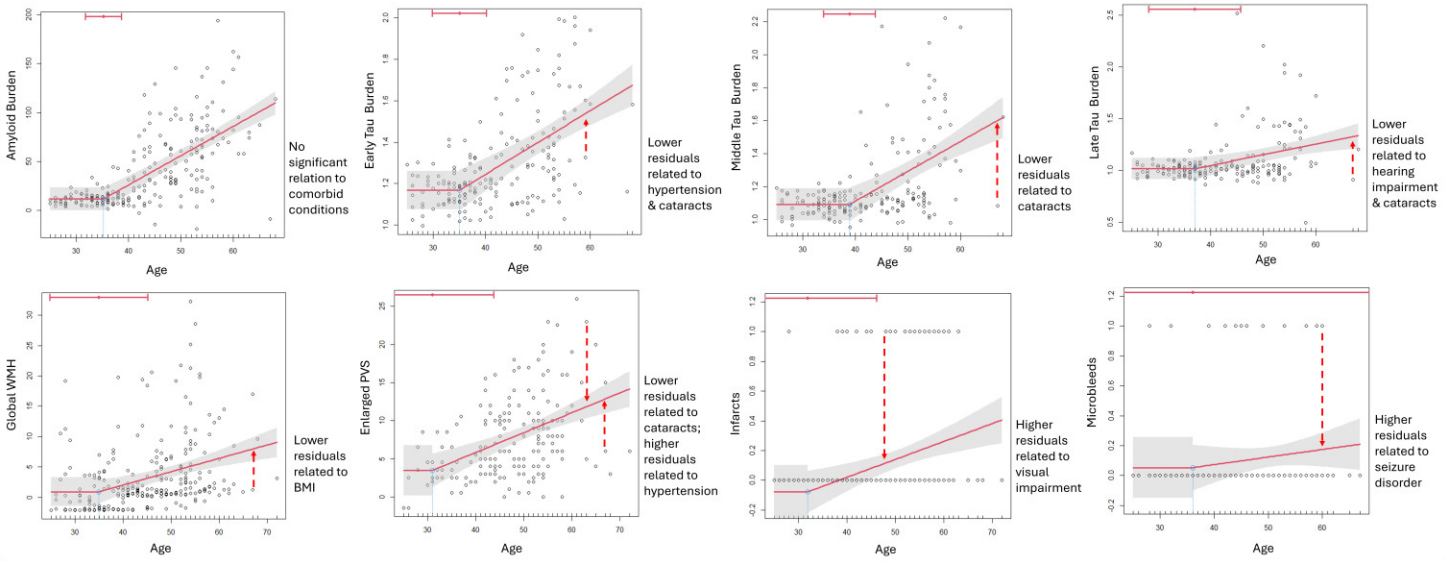
Conclusion: In adults with DS, common comorbidities were not associated with amyloid, suggesting that APP overproduction is a strong driver of amyloid trajectory, approximated by chronological age. Seizures and visual impairment may be related to cerebrovascular burden, and reverse causality is possible. Comorbidity duration/severity/treatment, multimorbidity, AD diagnosis, and selection bias may clarify these patterns.

Table 1. Associations between age-trajectory residuals of each biomarker and co-morbidity.

	Amyloid	Braak I/II	Braak III/IV	Braak V/VI	Global WMH	PVS	Infarcts	Microbleeds
Congenital Heart Disease (35%)	2.8 [-5.5, 11.1] p=0.5	-9e-03 [-0.07, 0.05] p=0.8	-0.02 [-0.08, 0.05] p=0.6	-0.02 [-0.09, 0.05] p=0.6	-0.4 [-2.0, 1.2] p=0.6	-0.9 [-2.6, 0.7] p=0.3	0.7 [-0.3, 1.5] p=0.1	1.0 [-0.3, 2.2] p=0.2
Hypertension (6%)	-0.08 [-19.8, 19.6] p=0.9	**-0.2 [-0.4, -9e-03] p=0.04**	-0.2 [-0.4, 0.04] p=0.1	-0.1 [-0.3, 0.1] p=0.3	-1.0 [-4.2, 2.1] p=0.5	**3.5 [0.2, 6.8] p=0.04**	-0.7 [-2.5, 1.1] p=0.4	-1.3 [-3.9, 1.4] p=0.3
Hypotension (10%)	1.3 [-10.2, 12.8] p=0.8	-0.03 [-0.1, 0.08] p=0.6	-0.04 [-0.2, 0.07] p=0.5	-0.02 [-0.1, 0.1] p=0.7	1.4 [-1.1, 4.0] p=0.3	0.9 [-1.6, 3.5] p=0.5	-0.3 [-1.7, 1.0] p=0.6	0.9 [-1.0, 2.7] p=0.4
Hyperlipidemia (40%)	7.9 [-0.8, 16.7] p=0.08	0.04 [-0.02, 0.1] p=0.2	0.06 [-7e-03, 0.1] p=0.08	0.05 [-0.03, 0.1] p=0.2	-0.7 [-2.2, 0.9] p=0.4	-0.7 [-2.3, 0.9] p=0.4	0.04 [-0.8, 0.9] p=0.9	-0.5 [-1.8, 0.8] p=0.4
Diabetes (6%)	-5.7 [-22.9, 11.5] p=0.5	-0.06 [-0.2, 0.1] p=0.5	-0.06 [-0.2, 0.1] p=0.5	-0.04 [-0.2, 0.2] p=0.7	-1.0 [-4.2, 2.2] p=0.5	-2.0 [-5.3, 1.3] p=0.2	-1.1 [-2.9, 0.6] p=0.2	0.5 [-2.1, 3.1] p=0.7
BMI (53% >30)	0.2 [-0.3, 0.7] p=0.4	2e-04 [-4e-03, 4e-03] p=0.9	3e-04 [-4e-03, 5e-03] p=0.9	2e-03 [-3e-03, 6e-03] p=0.5	**-0.1 [-0.2, -6e-03] p=0.04**	-0.1 [-0.2, 0.01] p=0.08	7e-03 [-0.04, 0.06] p=0.8	-0.04 [-0.1, 0.03] p=0.2
Sleep apnea (41%)	4.5 [-2.2, 11.1] p=0.2	9e-03 [-0.04, 0.06] p=0.7	0.03 [-0.02, 0.09] p=0.3	0.03 [-0.04, 0.09] p=0.4	-0.4 [-1.7, 0.9] p=0.5	-0.2 [-1.6, 0.9] p=0.4	0.07 [-0.7, 0.8] p=0.9	0.6 [-0.4, 1.6] p=0.3
Hypothyroidism (62%)	6.9 [-0.8, 14.6] p=0.08	0.05 [-6e-03, 0.1] p=0.08	0.05 [-7e-03, 0.12] p=0.09	0.04 [-0.02, 0.1] p=0.2	-1.3 [-2.8, 0.2] p=0.08	0.09 [-1.4, 1.6] p=0.9	0.05 [-0.7, 0.9] p=0.9	0.2 [-0.9, 1.3] p=0.7
Pneumonia (34%)	1.4 [-6.9, 9.7] p=0.7	0.02 [-0.04, 0.08] p=0.5	-0.01 [-0.08, 0.05] p=0.7	-0.03 [-0.1, 0.04] p=0.5	0.5 [-1.0, 2.0] p=0.5	-1.0 [-2.5, 0.01] p=0.08	0.6 [-0.2, 1.4] p=0.2	0.8 [-0.3, 1.9] p=0.1
Seizure Disorder (9%)	11.3 [-7.6, 30.2] p=0.2	0.04 [-0.08, 0.2] p=0.5	0.02 [-0.1, 0.2] p=0.8	6e-03 [-0.1, 0.2] p=0.9	1.8 [-0.8, 4.4] p=0.2	-0.03 [-2.6, 2.6] p=0.9	1.3 [-0.2, 2.7] p=0.08	**1.8 [0.08, 3.5] p=0.04**
Hearing Impairment (26%)	4.0 [-4.9, 12.9] p=0.4	-0.03 [-0.1, 0.03] p=0.3	-0.07 [-0.1, 4e-03] p=0.07	**-0.09 [-0.2, -0.01] p=0.03**	-0.6 [-2.2, 1.0] p=0.5	-0.7 [-2.2, 0.9] p=0.4	-1e-03 [-0.8, 0.8] p=1	0.7 [-0.5, 1.8] p=0.3
Visual Impairment (76%)	-4.5 [-13.3, 4.3] p=0.3	-0.03 [-0.1, 0.04] p=0.4	-0.03 [-0.1, 0.04] p=0.4	-0.03 [-0.1, 0.05] p=0.4	0.3 [-1.4, 2.0] p=0.7	-0.6 [-2.3, 1.2] p=0.5	**1.0 [0.1, 1.9] p=0.03**	0.3 [-1.0, 1.5] p=0.7
Cataracts (34%)	-1.7 [-10.1, 6.7] p=0.7	**-0.06 [-0.1, 5e-04] p=0.05**	**-0.09 [-0.2, -0.02] p=0.01**	**-0.1 [-0.2, -0.03] p=4e-03**	0.4 [-1.2, 1.9] p=0.6	**-1.5 [-2.9, -0.04] p=0.05**	0.8 [-0.05, 1.6] p=0.07	-0.3 [-1.4, 0.8] p=0.6

Trajectory-based, age-residual of biomarkers (columns) regressed on comorbidities (rows). Each cell contains the unstandardized slope (B) and associated 95% confidence interval from separate models, adjusted for acquisition parameters. Bold indicates significance (p≤0.05).

Figure 1. Estimated age-trajectories from left-null piecewise regression against age (approximate disease progression in adults with DS). Dotted arrows indicate age-trajectory-residuals, which we then regressed on comorbid conditions.



Keywords: Down syndrome, multimorbidity, Alzheimer's disease pathology, cerebrovascular biomarkers

136 Cortical atrophy is correlated with the discrepancy between neuroradiological assessment and binary quantitation of florbetapir PET in nondemented older adults

Daniel Schwartz[1,3], Ivan E. Villamizar Alvarado[1,3,4], Laszlo Szidonya[2], Gagandeep Choudhary[2], Jennifer Marcoe[1,4], Amanda Mar[1,4], Derrick Gillan[2], Hollie Hendricks[2], Jeffrey Kaye[1,4], Lisa Silbert[1,4,5]

[1]*OHSU Neurology, Portland, OR, US*
[2]*OHSU Radiology, Portland, OR, US*
[3]*OHSU Advanced Imaging Research Center, Portland, OR, US*
[4]*Oregon ADRC, Portland, OR, US*
[5]*Portland Veterans Affairs Healthcare System, Portland, OR, US*

Background: With FDA approval of anti-amyloid therapies and newly proposed biomarker-based Alzheimer's disease (AD) diagnostic criteria[1], accurate assessment of individual cerebral amyloid status in early stage disease is essential. Clinical determination of PET amyloid positivity is complicated by the need to evaluate tracer intensity in neocortical gray matter (GM) relative to white matter (WM) that exhibits non-specific binding[2], an assessment further obfuscated when cortical atrophy results in reduced GM signal. We sought to investigate contributions of cortical thinning to discrepancies in clinical and quantitative amyloid status determinations in dementia-free older adults.

Materials and Methods: A prospective cohort of 119 adults (age 78.5y) underwent florbetapir PET and MRI at Oregon Health & Science University (Table 1). Each was acquired and processed according to ADNI guidelines[3] using SUVR cutoff ≥1.11[4], and clinically assessed by an experienced neuroradiologist. Freesurfer 7.2.0[5] determined cortical thickness and neocortical parcellations.

Table 1	Agree (N=93)	Disagree (N=26)	sig.
Age (y)	76.2	77.4	-
Sex (% female)	63%	73%	-
Education (y)	17.1	17.7	-
MOCA (avg score)	25.0	25.3	-
Global CDR (%>0)	25.8%	23.1%	-

There were no statistically significant differences in these variables between groups.

Results: Fifty-one individuals had an SUVR≥1.11. Twenty-six clinical reads disagreed with quantitative assessment; these participants were significantly closer to the cutoff in those with an SUVR≥1.11 ($t_{(50)}$=3.12,p<.01), and were more likely to have a negative amyloid PET clinical determination (92%). The neocortex was thinner in those with discrepant reads than in those that agreed ($t_{(117)}$=2.05,p<0.05, Figure 2). The groups differed significantly in cortical thickness in each of 9 neocortical parcels averaged across hemisphere; 7 identified as indicators of prodromal AD[6] (Figure 3).

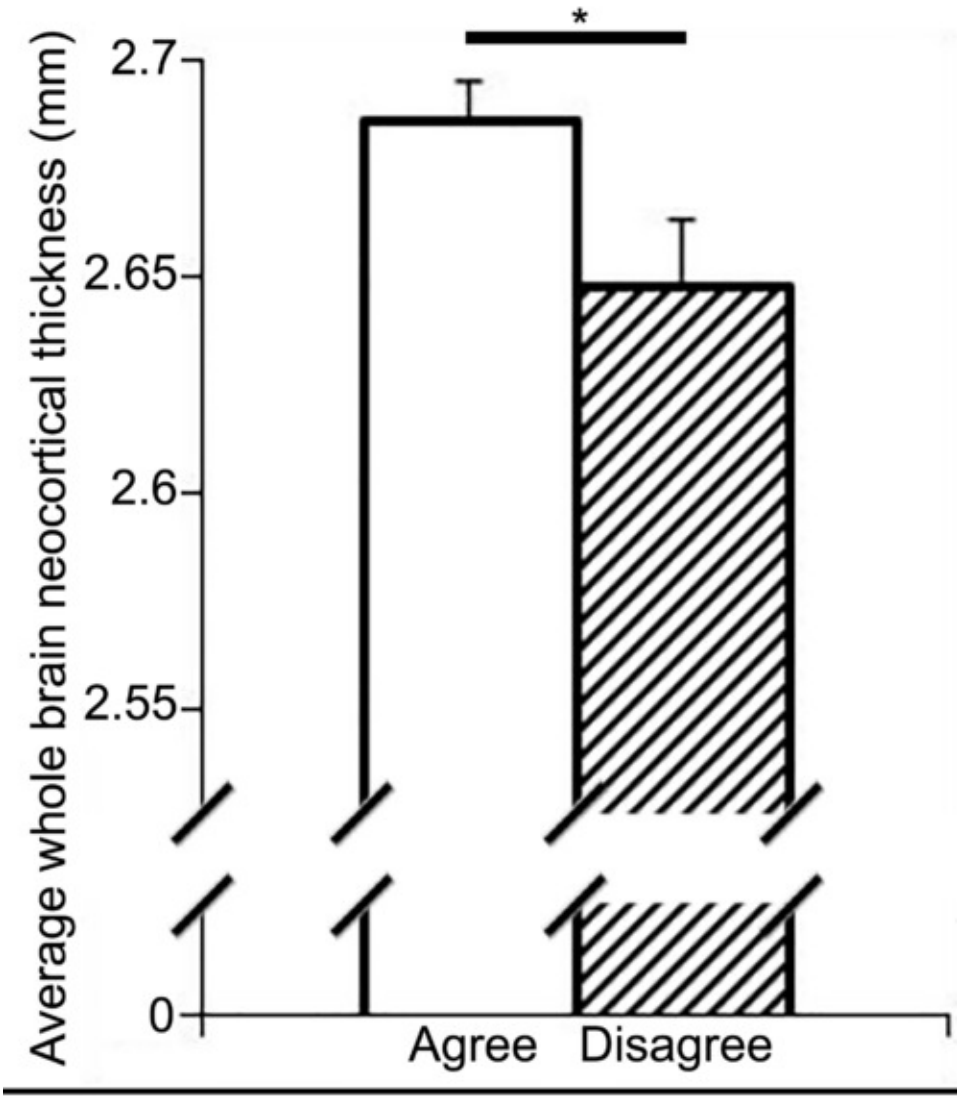


Figure 1. Significant difference ($p<.05$) between participants for which the neuroradiologic read agreed with the quantitative assessment (“agree”) and those that did not agree (“disagree”).

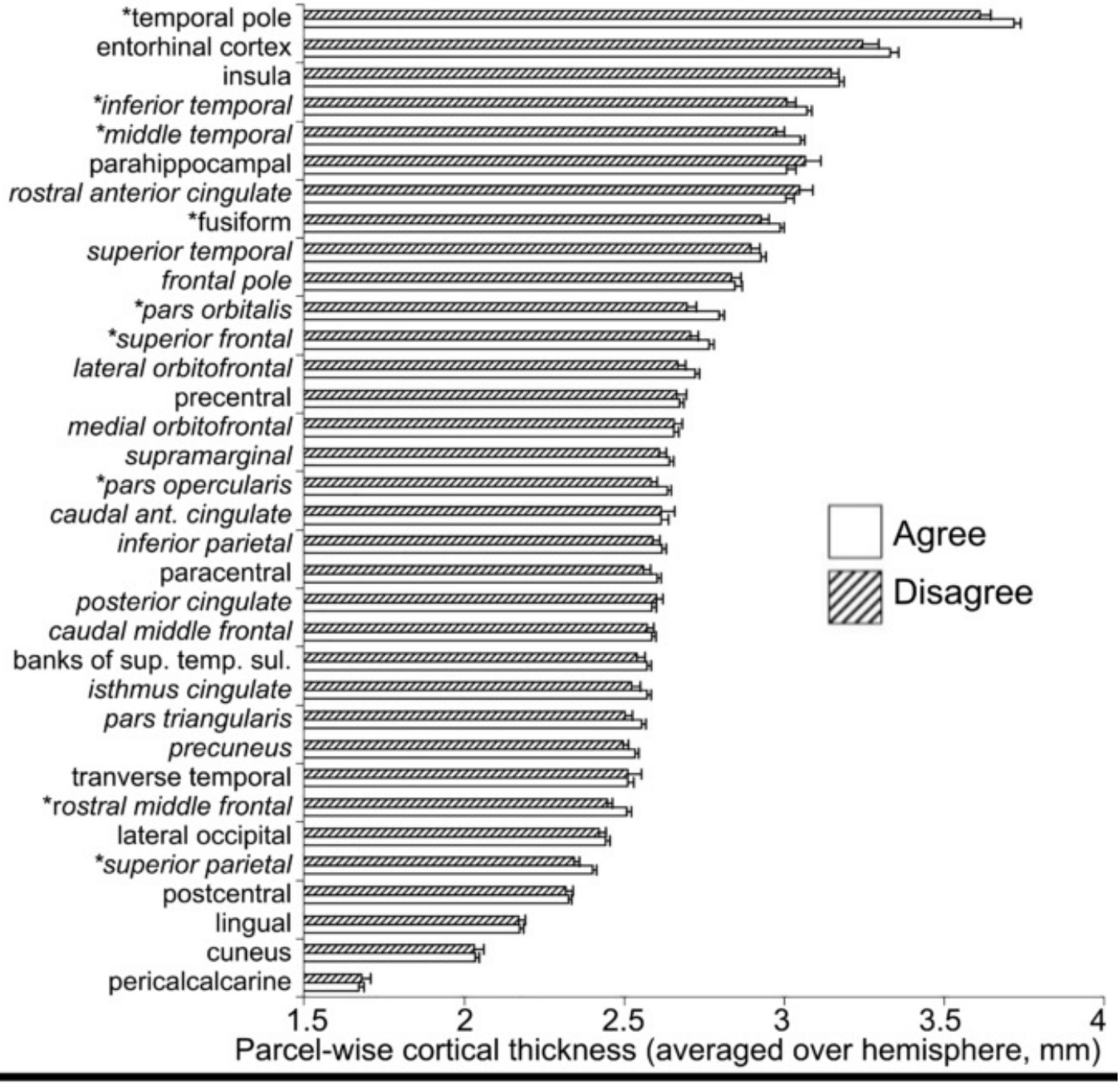


Figure 2. Parcel-wise cortical thickness. Regions implicated in neurodegeneration in prodromal AD[6] are written in italics. Asterisks indicate a significant difference between groups (agree>disagree).

Discussion: Brain atrophy may affect accurate neuroradiological diagnosis and/or quantification of amyloid PET positivity in early AD. Suboptimal sensitivity of amyloid PET clinical assessments may delay care and in research may bias sampling, especially in those participants who are nearest a binary cutoff, early in the disease course. This may present a bias against participants with comorbidities that accelerate the onset of neurodegeneration[1]. Assessment of atrophy is advised especially in those with borderline amyloid positivity.

Keywords: neurodegeneration, PET quantification, clinical PET positivity determination

137 Vascular pathology influences the association of tau-PET with neurodegeneration and cognition in Aβ-negative individuals

Markley Silva Oliveira Junior[1], Bruna Bellaver[1], Pamela C.L. Ferreira[1], Guilherme Povala[1], Guilherme Bauer-Negrini[1], Firoza Lussier[1], Livia do Amaral[1], Matheus Rodrigues[1], Andrea da Rocha[1], Pampa Saha[1], Emma Ruppert[1], Carolina Soares[1], Douglas Leffa[1], Cynthia Felix[1], Rayan Mroue[1], Dana Tudorascu[1], Hussein Zalzale[1], Belen Pascual[2], Brian Gordon[3], Val Lowe[4], Hwamee Oh[5], David Soleimani-Meigooni[6], Juan Fortea[8], Pedro Rosa-Neto[8], Suzanne Baker[9], Tharick Pascoal[1]

[1]*University of Pittsburgh, Department of Psychiatry, Pittsburgh, PA, US*
[2]*Houston Methodist Research Institute, Department of Neurology, Houston, TX, US*
[3]*Washington University in St. Louis, Department of Radiology, St. Louis, MO, US*
[4]*Mayo Clinic, Department of Radiology, Rochester, MN, US*
[5]*Brown University, Department of Psychiatry and Human Behavior,, Providence, RI, US*
[6]*University of California San Francisco, Memory and Aging Center,, San Francisco, CA, US*
[7]*Hospital de la Santa Creu i Sant Pau, Sant Pau Memory Unit, Barcelona, ES*
[8]*Translational Neuroimaging Laboratory, McGill University Research Centre for Studies in Aging, Douglas Research Institute,, Montreal, QC, CA*
[9]*Lawrence Berkeley National Laboratory,, Berkeley, CA, US*

Background: Previous studies have linked the coexistence of amyloid-β (Aβ) and vascular pathology burden (VP) with early tau PET accumulation in Alzheimer's disease (AD). However, the impact of VP on tau PET deposition and its relationship to neurodegeneration and cognitive decline in Aβ-negative individuals remains unclear.

Methods: We analyzed 211 Aβ-PET negative participants (Centiloid < 20) from the HEAD study, including CDR-SB, plasma NfL, ptau217, T1-based volumetrics, [^{18}F]Flortaucipir (FTP), and [^{18}F]MK6240 (MK). VP risk factors tested were hypertension, diabetes, dyslipidemia, tobacco use, and white matter hyperintensity (WMH). Fazekas score 2-3. Participants were categorized into low/negative VP (0-1 risk factors; n = 114) and high/positive VP (2-5 risk factors; n = 97). Group differences were analyzed using ANCOVA, and associations were assessed using linear regressions accounting for age, sex, education, and cognitive status.

Results: Aβ-negative individuals with high VP showed more brain atrophy (Fig. 1A; P = 0.0160), higher plasma NfL (Fig. 1B; P < 0.0001), and elevated ptau217 levels (Fig. 1C; P = 0.0438). Aβ Centiloid levels and FTP uptake were similar between VP groups (Fig. 1D, 1E, 1F, 1H). The high VP group showed lower MTL MK uptake (Fig. 1G; P = 0.0115). FTP levels in the MTL and Neotemporal cortex were significantly associated with cognitive decline (Fig. 3A; β: 0.2618, P = 0.0005) and brain atrophy (Fig. 3B; β: -0.2444, P = 0.0037) only in the high VP group. VP did not alter the association between MK and cognition or atrophy (Fig. 2A-D).

Discussion: VP was associated with brain atrophy, elevated plasma NfL, and ptau217 in Aβ-negative individuals. VP influenced the relationship between FTP, but not MK, with cognitive impairment and brain atrophy. Future analyses should replicate these findings and explore the underlying mechanisms of these differences.

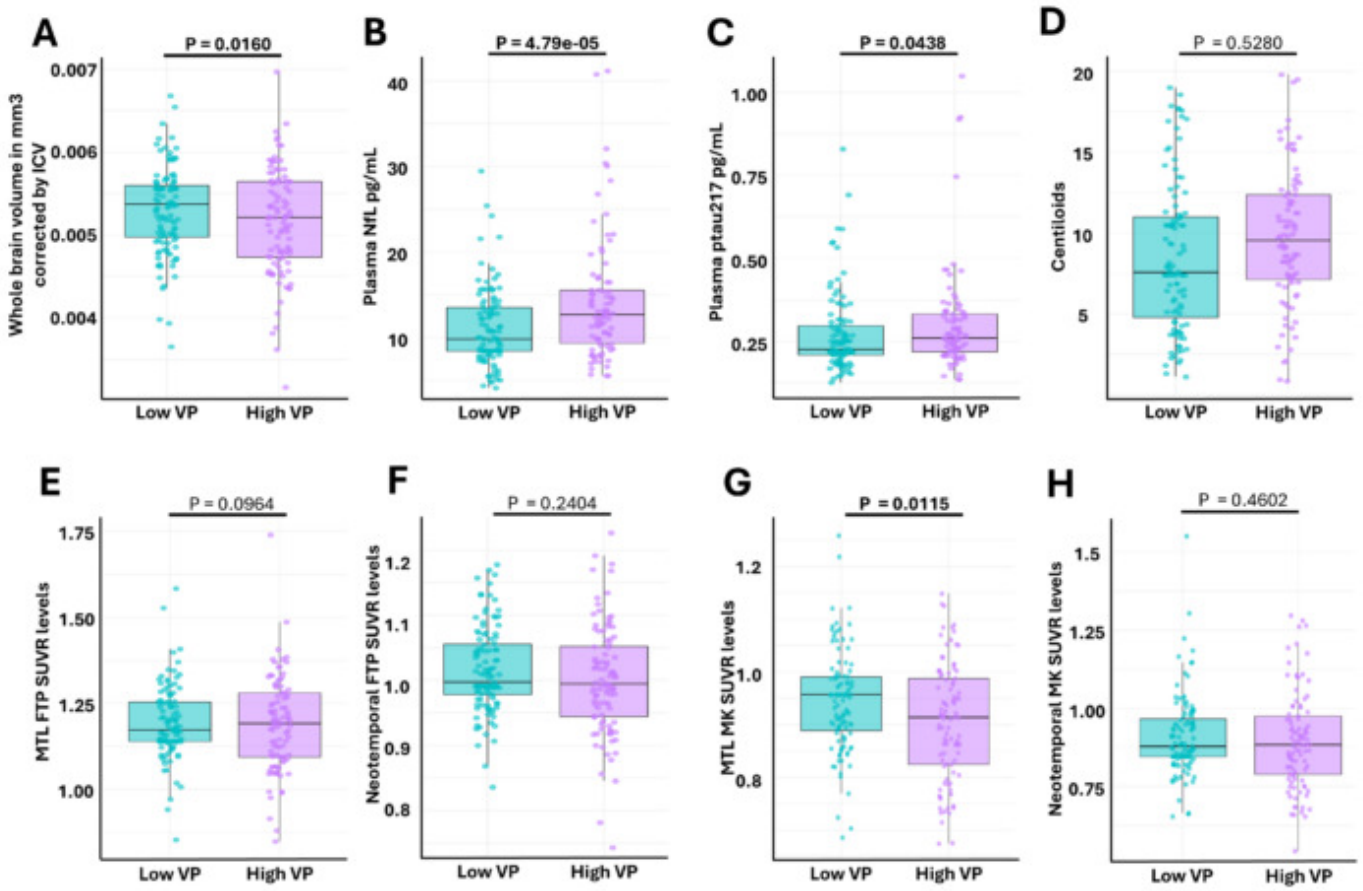


Figure 1: Individuals with high vascular pathology (VP) burden exhibit more brain atrophy and higher plasma NfL and ptau217 levels. Individuals with high VP show greater brain atrophy (A), plasma NfL (B), and plasma ptau217 (C). MTL MK SUVR levels were lower in individuals with high VP (G). Box plots were analyzed utilizing ANCOVA corrected for age, sex, years of education, and cognition. Significant p-values are highlighted in bold.

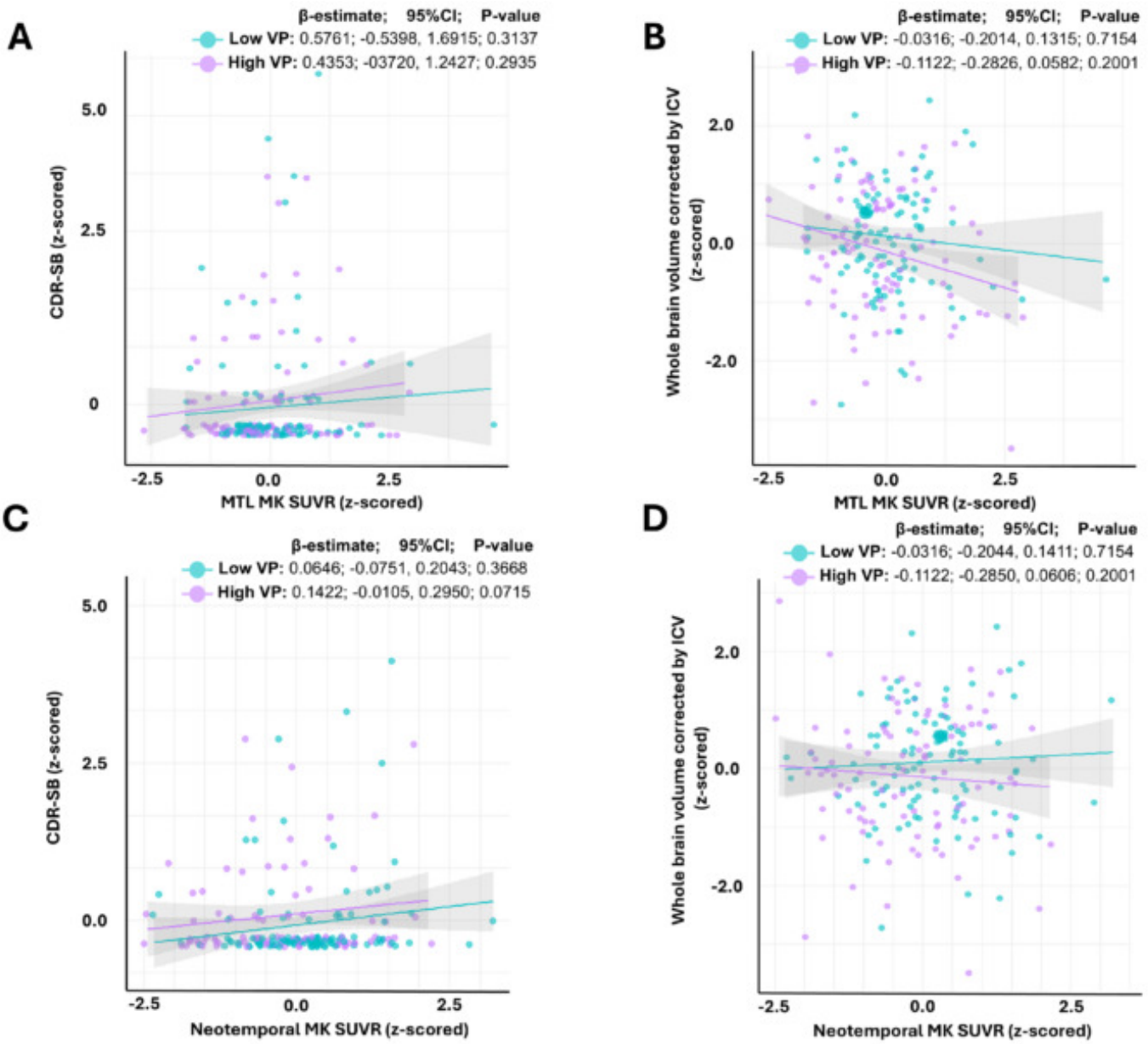


Figure 2: MK6240 uptake in the MTL and neotemporal regions was not associated with cognitive decline or brain atrophy in Aβ-PET negative individuals. MTL MK SUVR uptake is not associated with CDR-SB (A) or brain volume in low or high VP (B). Neotemporal MK SUVR levels are not associated with CDR-SB (C) or brain volume (D) in low or high VP. β-estimates, 95% CI, and P-values were computed using linear regression models adjusted by age, sex, years of education, and cognition status. Significant p-values are highlighted in bold.

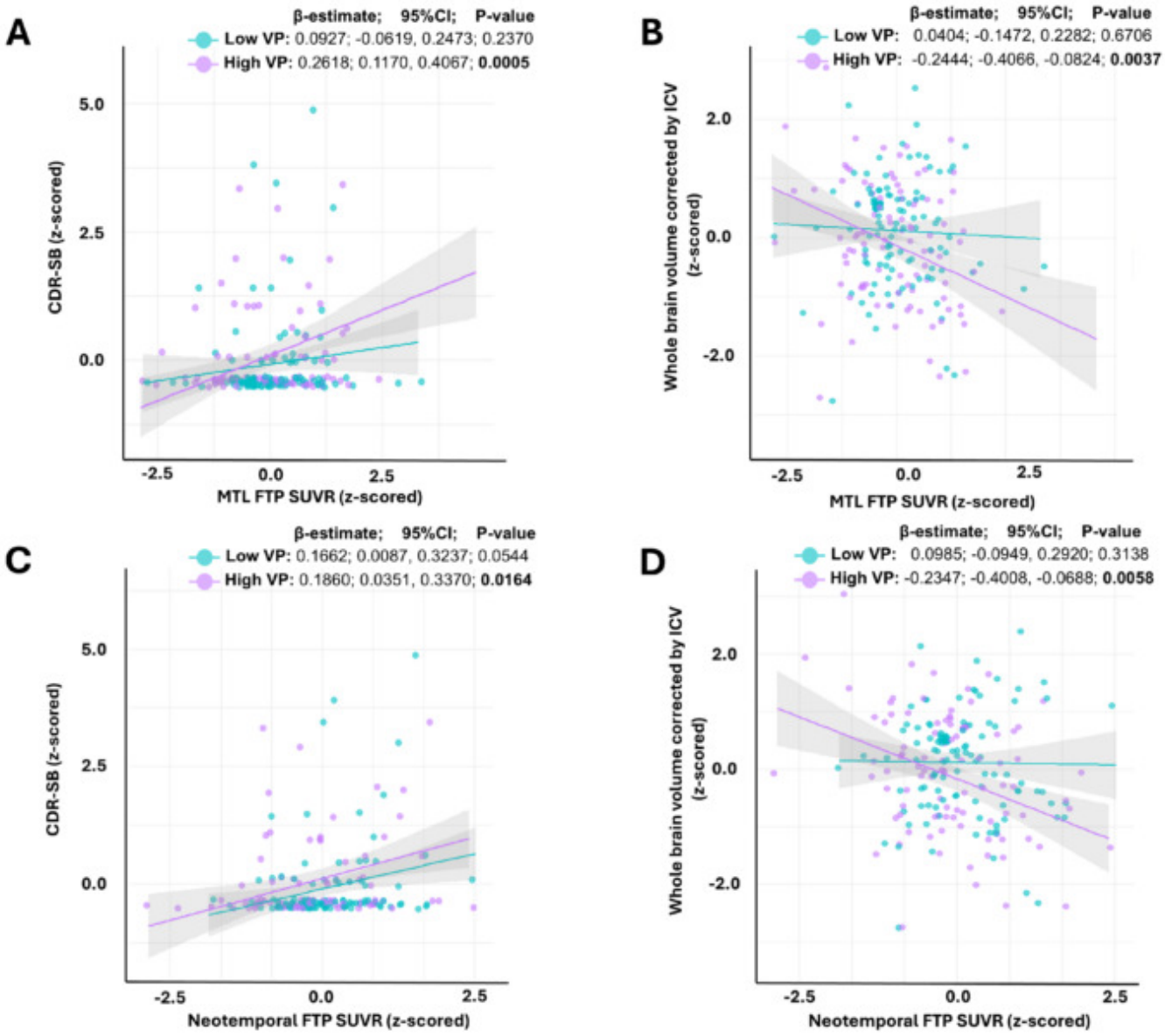


Figure 3: FTP uptake in the MTL and neotemporal regions were linked to cognitive decline and brain atrophy in Aβ-PET negative individuals with risk factors for cerebrovascular pathology. An increase in MTL FTP SUVR levels was associated with cognitive decline (A) and brain atrophy (B) in the high VP group only. Similarly, an increase in neotemporal FTP SUVR levels was associated with cognitive decline (C) and brain atrophy (D) in the high VP group. Beta-estimates, 95% CI, and P-values were computed using linear regression models adjusted by age, sex, years of education, and cognition status. Significant p-values are highlighted in bold.

Keywords: Vascular pathology; tau-pathology; Amyloid-negative; plasma biomarkers; brain volume

138 Concomitant neurodegeneration of the lateral hypothalamus and locus coeruleus is associated with early Alzheimer's disease-related pathophysiological and cognitive processes

Maxime Van Egroo[1,2,3], Marion Baillet[2,3], J. Alex Becker[3,4], Julie C. Price[2,3], Michael J. Properzi[3,5], Kathryn V. Papp[3,6], Dorene M. Rentz[3,6], Reisa A. Sperling[2,3,5,6], Keith A. Johnson[3,4,5,6], Heidi I.L. Jacobs[1,2,3]

[1]*Faculty of Health, Medicine and Life Sciences, Mental Health and Neuroscience Research Institute, Alzheimer Center Limburg, Maastricht University, Maastricht, NL*
[2]*Athinoula A. Martinos Center for Biomedical Imaging, Department of Radiology, Massachusetts General Hospital, Boston, MA, US*
[3]*Harvard Medical School, Boston, MA, US*
[4]*Gordon Center for Medical Imaging, Department of Radiology, Massachusetts General Hospital, Boston, MA, US*
[5]*Department of Neurology, Massachusetts General Hospital, Boston, MA, US*
[6]*Center for Alzheimer Research and Treatment, Department of Neurology, Brigham and Women's Hospital, Boston, MA, US*

Background: The brainstem locus coeruleus (LC) and the lateral hypothalamus (LH) are densely interconnected neuromodulatory subcortical regions that display selective vulnerability to the earliest accumulation of tau pathology in Alzheimer's disease (AD). Recent advances in neuroimaging methods now allow us to quantify the structural integrity of these small brain regions in vivo. Here, we investigated the co-occurrence of neurodegeneration in the LC and LH, and their combined effect on early AD-related pathophysiological and cognitive processes in older individuals.

Methods. 175 participants from the Harvard Aging Brain Study underwent structural MRI including dedicated LC imaging, Flortaucipir (FTP)-PET scan, and longitudinal cognitive evaluations (**Figure 1**). Bilateral volumes of hypothalamic subunits, including the LH, were obtained using FastSurfer-HypVINN segmentation. LC integrity was derived from 5 connected voxels with hyperintense signal, using the pons as a reference region. Thickness of the entorhinal cortex was extracted with FreeSurfer. In addition, entorhinal FTP-PET values were computed and corrected for partial-volume effects. Finally, we used longitudinal Preclinical Alzheimer's Cognitive Composite 5 (PACC5) scores, anchored on the structural LC MRI visit, to assess cognitive decline.

Results. Multiple linear regression models adjusted for age, sex, education, and *APOE* genotype revealed that lower LC MRI signal intensity was specifically linked to smaller LH volumes (p=0.03; **Figure 2**). In addition, interaction models indicated that lower LC MRI signal intensity combined with smaller LH volume were associated with lower entorhinal thickness (p=0.002) and elevated entorhinal FTP-PET values (p=0.04). Linear mixed-effects models further showed that decline in PACC5 was steepest in individuals with both lower LC MRI signal intensity and smaller LH volume (p=0.002; **Figure 3**).

Conclusion. These findings emphasize the importance of considering alterations among multiple subcortical regions collectively to improve early detection of at-risk individuals. Future analyses will integrate additional neuromodulatory subcortical systems such as the cholinergic basal forebrain.

Figure 1. Demographic characteristics and neuroimaging measures in the study sample.

	n = 175
Age at baseline*, years	74.03 ± 9.61
Sex, *n* (%)	
Female	103 (58.86)
Male	72 (41.14)
Education, years	16.42 ± 2.89
Mini-mental state examination, score	28.89 ± 1.54
CDR score > 0 at baseline*, *n* (%)	11 (6.29)
APOE ε4 carrier, *n* (%)	44 (25.14)
Anterior hypothalamus volume, mm^3	236.30 ± 40.54
Medial hypothalamus volume, mm^3	128.05 ± 26.08
Lateral hypothalamus volume, mm^3	134.07 ± 18.49
Posterior hypothalamus volume, mm^3	331.22 ± 61.65
Locus coeruleus signal intensity, ratio	1.33 ± 0.05
Entorhinal cortex thickness, mm	6.67 ± 0.81
Entorhinal cortex FTP, SUVR PVC	1.36 ± 0.35
Cognitive follow-up time#, years	5.03 ± 1.40

Note: Hypothalamic subunits volumes were averaged bilaterally and adjusted for total intracranial volume. *baseline refers to the timepoint of the structural LC MRI session. #starting from the timepoint of the structural LC MRI session. Abbreviations: *APOE* = apolipoprotein E, CDR = Clinical Dementia Rating, FTP = Flortaucipir, PVC = partial-volume corrected, SUVR = standardized uptake value ratio.

Figure 2. Associations between locus coeruleus MRI signal intensity and volumes of hypothalamic subunits for (A) lateral hypothalamus, (B) medial hypothalamus, (C) anterior hypothalamus, and (D) posterior hypothalamus. Hypothalamic subunits volumes were averaged bilaterally and adjusted for total intracranial volume.

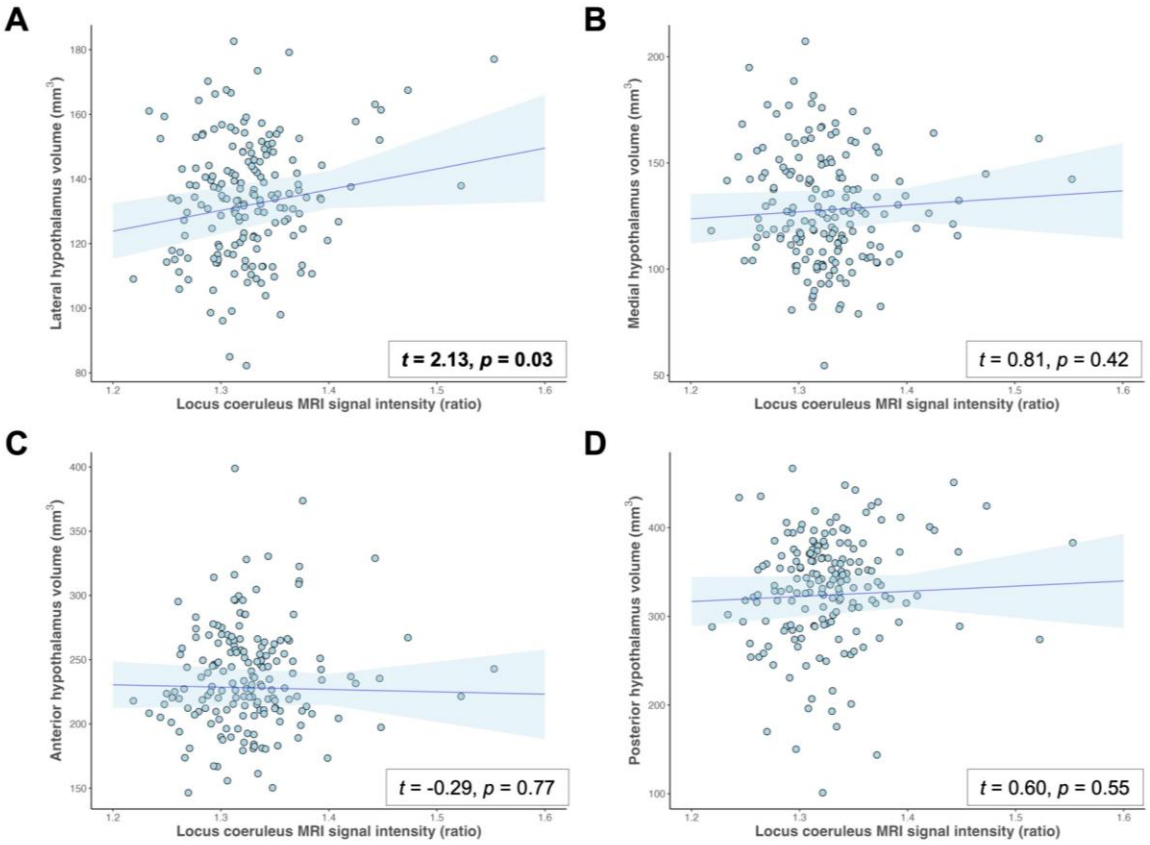
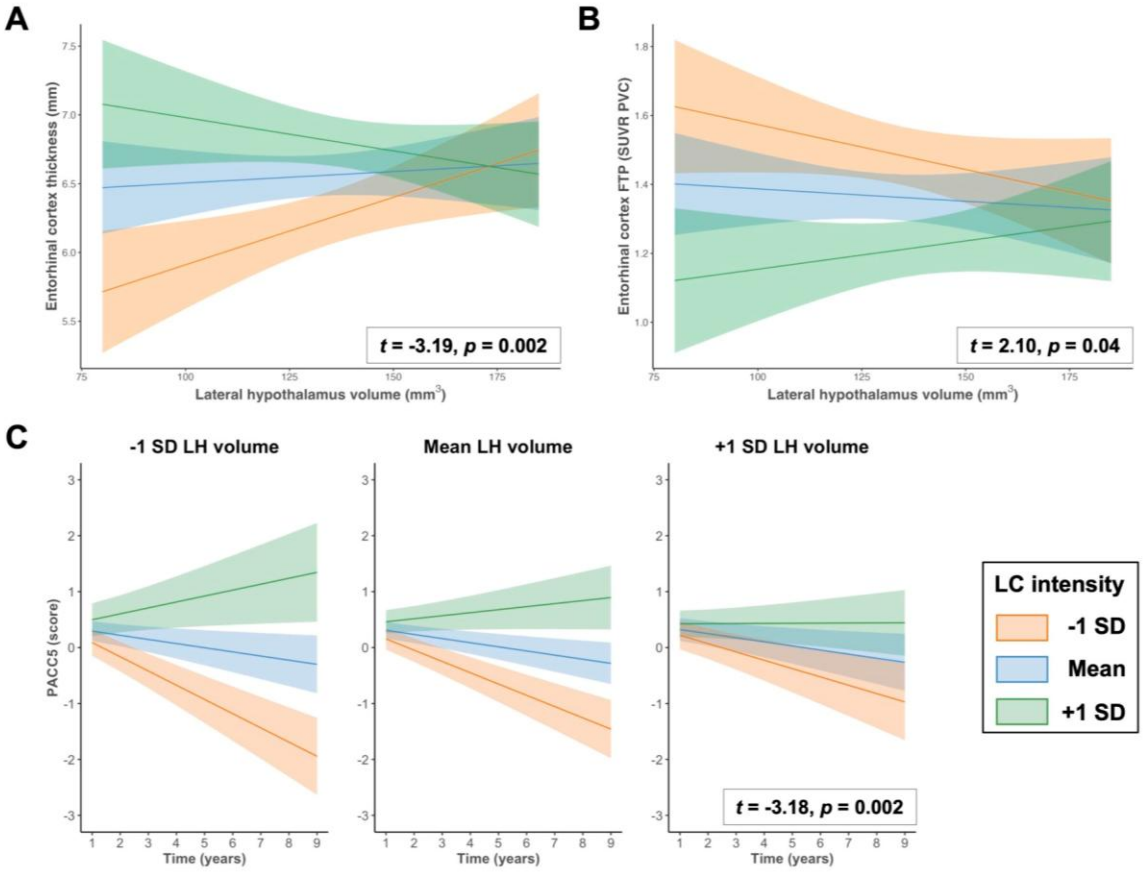


Figure 3. Interactions between lateral hypothalamus volume and locus coeruleus MRI signal intensity on (A) entorhinal thickness, (B) entorhinal FTP-PET values, and (C) longitudinal cognitive decline. Hypothalamic subunits volumes were averaged bilaterally and adjusted for total intracranial volume. The structural LC MRI session serves as the baseline timepoint for the longitudinal cognitive follow-up. Abbreviations: FTP = Flortaucipir, LC = locus coeruleus, LH = lateral hypothalamus, PACC5 = Preclinical Alzheimer's Cognitive Composite 5, PVC = partial-volume corrected, SUVR = standardized uptake value ratio.



Keywords: lateral hypothalamus, locus coeruleus, neuromodulatory subcortical systems, tau, cognitive decline

139 Amyloid-associated hyperconnectivity drives tau spreading across connected brain regions in Alzheimer's disease

Sebastian Niclas Roemer-Cassiano[1,14], Fabian Wagner[2], Lisa Evangelista[2], Amir Dehsarvi[2], Anna Steward[2], Anna Dewenter[2], Davina Biel[2], Zeyu Zhu[2], Maura Malpetti[9], Günter U. Höglinger[1,5,6], Matthias Brendel[5,6,13], Sarah Jäkel[2], Michael Scholl[10,11], Nicolai Franzmeier[2,10,11]

[1]*Department of Neurology, University Hospital, LMU Munich, Germany, Munich, DE*
[2]*Institute for Stroke and Dementia Research (ISD), University Hospital, LMU Munich, Germany, Munich, DE*
[3]*Munich Cluster for Systems Neurology (SyNergy), Munich, Germany, Munich, DE*
[4]*German Center for Neurodegenerative Diseases (DZNE) Munich, Munich, Germany, Munich, DE*
[5]*Department of Clinical Neurosciences, University of Cambridge, Cambridge, UK, Cambridge, GB*
[6]*University of Gothenburg, The Sahlgrenska Academy, Institute of Neuroscience and Physiology, Department of Psychiatry and Neurochemistry, Mölndal and Gothenburg, Sweden, Gothenburg, SE*
[7]*Wallenberg Centre for Molecular and Translational Medicine, University of Gothenburg, Sweden, Gothenburg, SE*
[8]*Department of Nuclear Medicine, University Hospital, LMU Munich, Germany, Munich, DE*
[9]*Max Planck School of Cognition, 04103 Leipzig, Germany, Leipzig, DE*

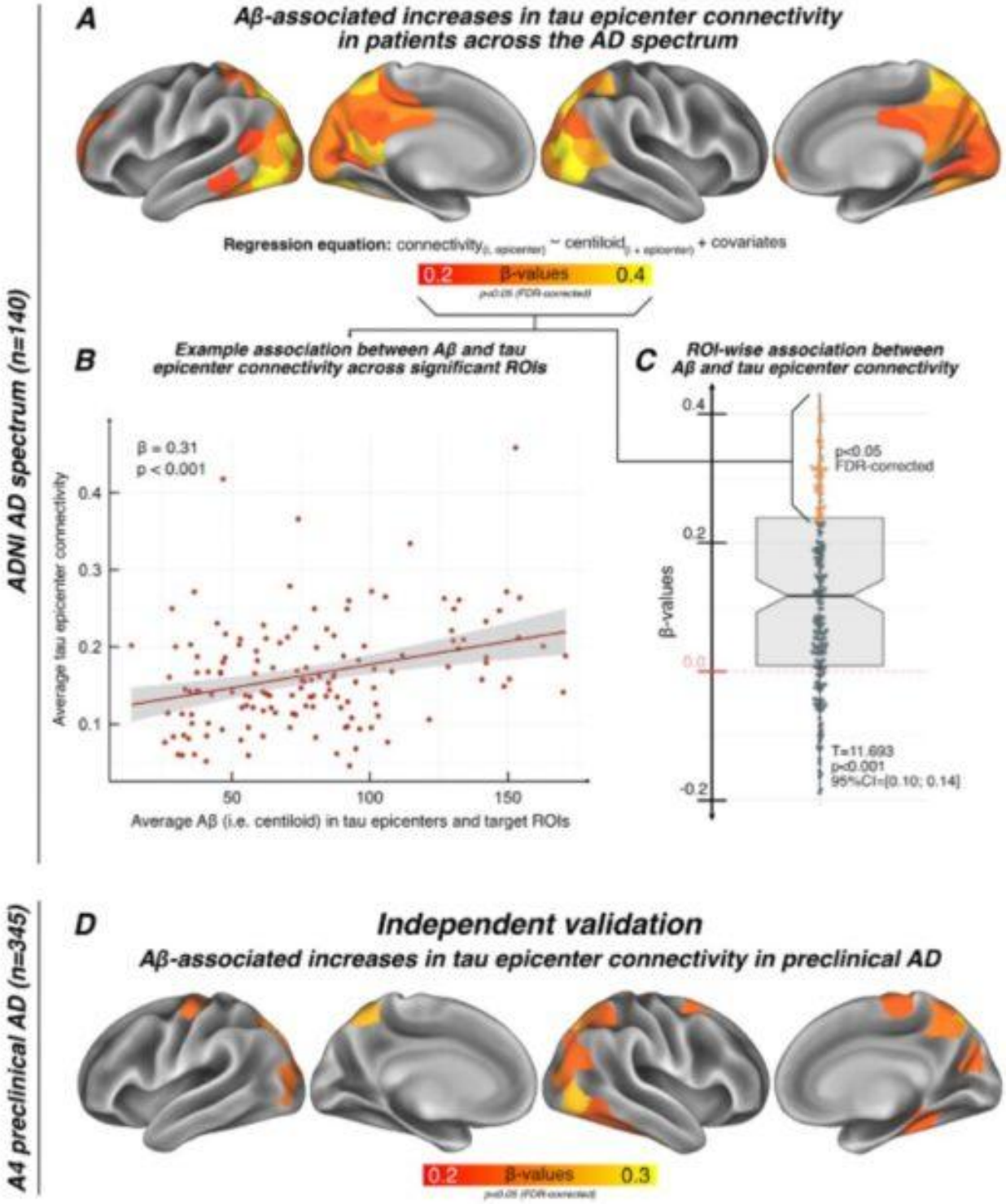
Background: In Alzheimer's disease, Aβ triggers tau spreading which drives neurodegeneration and cognitive decline. Preclinical research found that tau spreads across connected neurons in an activity-dependent manner, and Aβ was shown to trigger neuronal hyperactivity and hyperconnectivity. Therefore, we hypothesized that Aβ induces neuronal hyperactivity and hyperconnectivity, thereby promoting tau spreading from initial epicenters across connected brain regions.

Methods: From ADNI, we included 140 Aβ-positive subjects across the AD spectrum plus 69 Aβ-negative controls, all with baseline amyloid-PET, 3T resting-state fMRI and longitudinal Flortaucipir tau-PET. For validation, we included cross-sectional data of 345 preclinical AD patients from the A4 study. PET and fMRI data were parceled into 200 cortical ROIs and ROI-wise longitudinal tau-PET change rates were computed using linear-mixed models. Further, we included post-mortem brain tissue from 5 AD patients vs. 4 controls stained for Aβ and c-Fos, i.e. a marker of ante-mortem neuronal activity.

Results: In the AD spectrum cohort, we confirmed that Aβ induces hyperconnectivity of temporal lobe tau epicenters to posterior brain regions that are highly vulnerable to tau accumulation in AD (Fig.1A-C). This was replicated in the validation cohort of preclinical AD patients with low cortical tau-PET, suggesting that the emergence of Aβ-related hyperconnectivity precedes neocortical tau spreading (Fig.1D). Supporting that Aβ-associated fMRI-based hyperconnectivity may mirror neuronal hyperactivity, we found that neurons in AD post-mortem tissue expressed higher levels of c-Fos compared to controls, i.e. a marker of ante-mortem neuronal activity (Fig.2). Lastly, using longitudinal tau-PET, we confirmed that Aβ-related connectivity increases of the tau epicenters to posterior brain regions mediated the effect of Aβ on tau accumulation and triggered faster tau spreading (Fig.3).

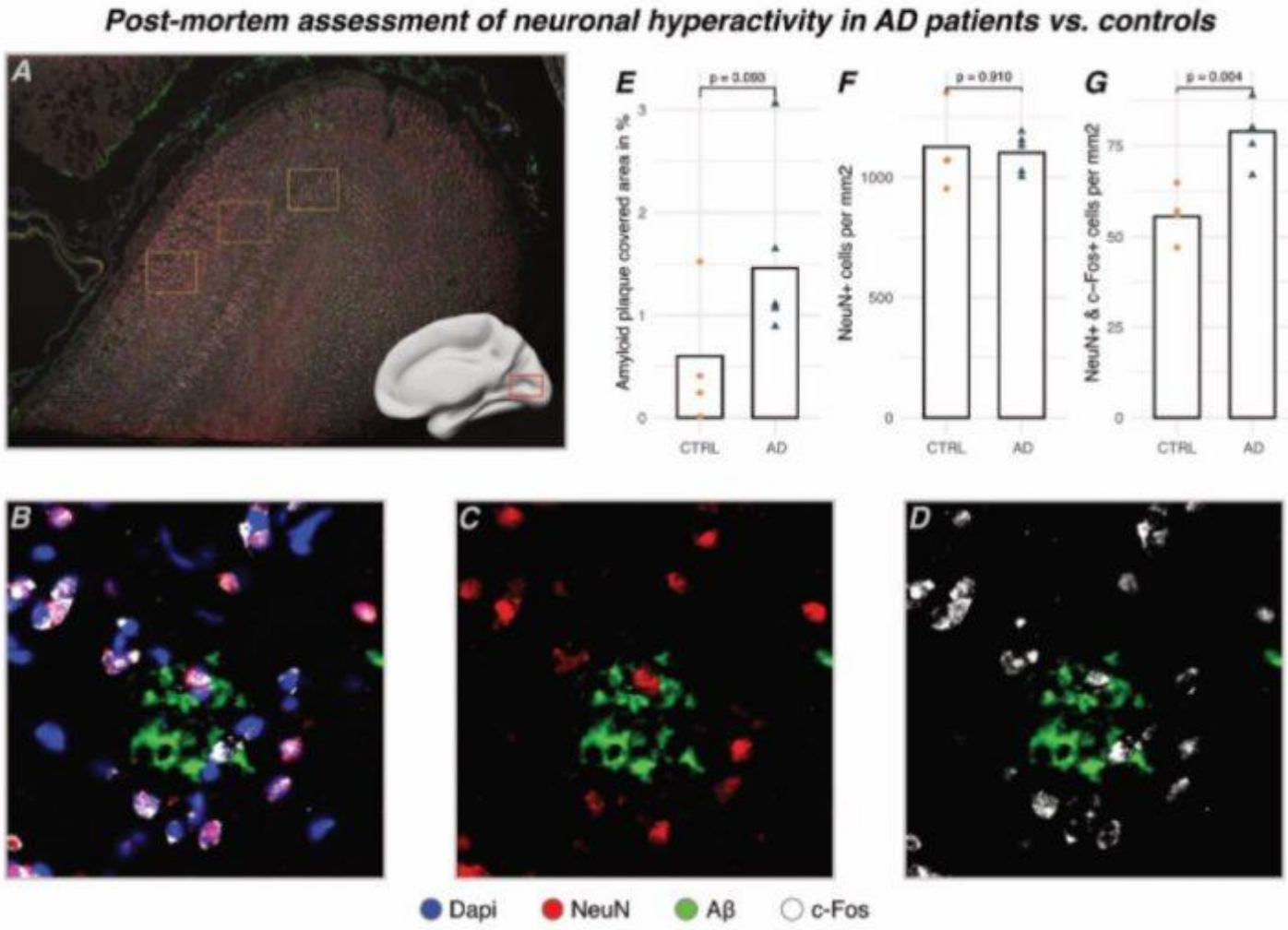
Conclusions: Our translational results suggest that Aβ promotes tau spreading via increasing neuronal activity and connectivity. Therefore, Aβ-associated neuronal hyperexcitability may be a promising target for attenuating tau spreading in AD.

Figure 1



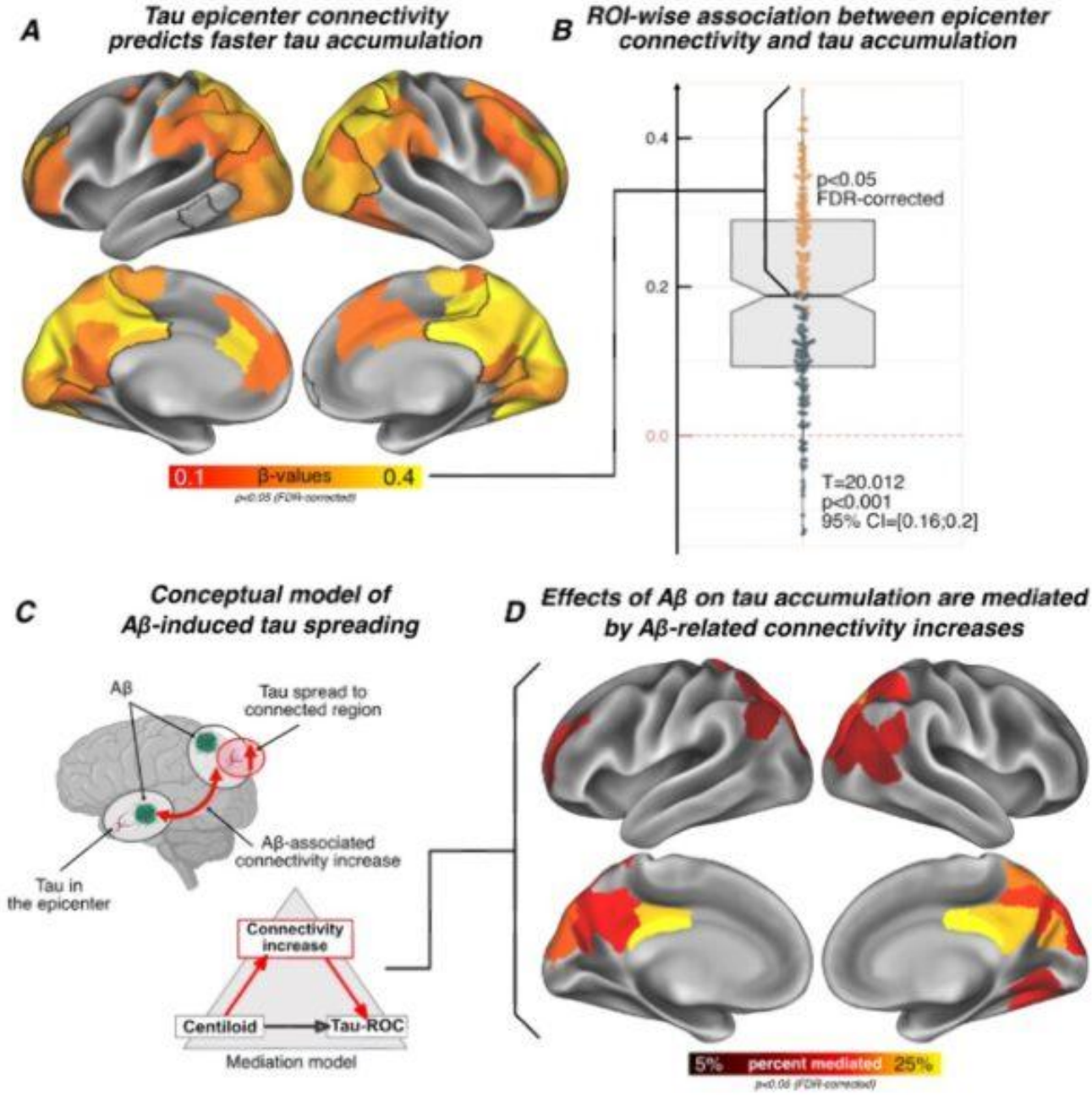
(A) Association between Ab and epicenter connectivity in ADNI. (B) average association between Aβ and connectivity for significant ROIs displayed in panel (A). (C) Un-thresholded distribution of beta values displayed in panel (A) showing that beta-values are overall significantly larger than zero. (D) Validation of the association between Ab and epicenter connectivity in A4.

Figure 2



Post-mortem analyses of AD vs. control (CTRL) brains. (A) Overview of tissue stainings. (B) Merged image of Dapi (cell nuclei), NeuN (Neurons), Ab (amyloid) and c-Fos (marker of ante-mortem neuronal activity), (C) merged image of NeuN and amyloid stainings and (D) merged image of Ab and c-Fos staining. Group differences in (E) Amyloid-Plaque area, (F) neuron count (i.e. NeuN), and (G) the proportion of neurons with c-Fos positive signal.

Figure 3



(A) Association between stronger epicenter connectivity and faster tau accumulation in ADNI, including (B) the unthresholded distribution of beta-values, showing an overall positive association between epicenter connectivity and faster tau accumulation. (C) Conceptual model of Ab-related tau spreading and (D) bootstrapped mediation showing that effects of Ab on tau accumulation are mediated by increased epicenter connectivity.

Keywords: Amyloid-PET, Tau-PET, fMRI, hyperconnectivity

140 Association of plasma GFAP with tau PET in cognitively unimpaired Aβ-negative subjects

Pampa Saha[1], Bruna Bellaver[1], Guilherme Povala[1], Pamela C.L. Ferreira[1], Guilherme Bauer-Negrini[1], Livia Silva[1], Firoza Z. Lussier[1], Matheus S. Rodrigues[1], Markley S. Oliveira[1], Andreia S. Rocha[1], Cynthia Felix[1], Emma Ruppert[1], Marina Scop Medeiros[1], Carolina Soares Katz[1], Joseph Masdeu[2], Dana L. Tudorascu[1], David Soleimani-Meigooni[4], Juan Fortea[5], Val Lowe[6], Hwamee Oh[7], Belen Pascual[2], Brian A. Gordon[8], Pedro Rosa-Neto[9], Suzanne Baker[3], Tharick A. Pascoal[1]

[1]*University of Pittsburgh, Department of Psychiatry, Pittsburgh, PA, US*
[2]*Houston Methodist Research Institute, Houston, TX, US*
[3]*Lawrence Berkeley National Laboratory, Berkeley, CA, US*
[4]*University of California San Francisco, Memory and Aging Center, San Francisco, CA, US*
[5]*Hospital de la Santa Creu i Sant Pau, Sant Pau Memory Unit, Department of Neurology, Barcelona, ES*
[6]*Mayo Clinic, Department of Radiology, Rochester, MN, US*
[7]*Brown University, Department of Psychiatry and Human Behavior, Providence, RI, US*
[8]*Washington University in St. Louis, Department of Radiology, St. Louis, MO, US*
[9]*Translational Neuroimaging Laboratory, McGill University Research Centre for Studies in Aging, Douglas Research Institute, Montreal, QC, CA*

Background: We recently showed that plasma GFAP, a marker for astrocyte reactivity, influences tau PET pathology in cognitively unimpaired Aβ-positive individuals. However, the link between GFAP and tau PET in individuals without detectable Aβ pathology was underexplored. Here, we aim to investigate the association between plasma GFAP and tau PET in cognitively unimpaired Aβ PET-negative individuals.

Methods: We studied 133 cognitively unimpaired (CU) Aβ PET-negative participants from the HEAD cohort with plasma GFAP and p-tau217, as well as tau PET flortaucipir and MK6240 data. Aβ positivity was determined by Aβ PET visual reading or Centiloid 12. Voxel-wise linear regression models tested the association of plasma GFAP and p-tau217 with tau PET. GFAP levels were further stratified into quartiles. SUVR in the entorhinal cortex was compared using ANOVA across GFAP quartiles.

Results: Voxel-wise analysis showed that plasma GFAP levels (but not plasma p-tau217 levels) were associated with tau PET in the medial temporal (e.g., amygdala, entorhinal cortex, hippocampus) and posterior cingulate cortices, predominantly for the tracer flortaucipir (Figure 1A, B, C, D). The association between plasma p-tau217 and tau PET was weak. These results were similar when Aβ positivity was defined based on Centiloid 12. Furthermore, plasma GFAP and tau PET association in the ROI entorhinal region was significant for flortaucipir but not for MK6240 [flortaucipir: β=0.22966, p=0.0081; MK6240: β=0.1296, p=0.1387; Figure 2A, B]. Flortaucipir SUVR was slightly increased in the GFAP 4th quartile compared to the 1st quartile [flortaucipir: p=0.04; MK6240: p=0.38; Figure 2C, D].

Conclusions: We found an association between GFAP levels and tau PET uptake in individuals not expected to exhibit high levels of tau tangle-related tracer uptake. If these preliminary results hold, further studies could be designed to elucidate the underpinning of this association, which could represent low levels of tau pathology, astrogliosis, or other factors.

Figure1:

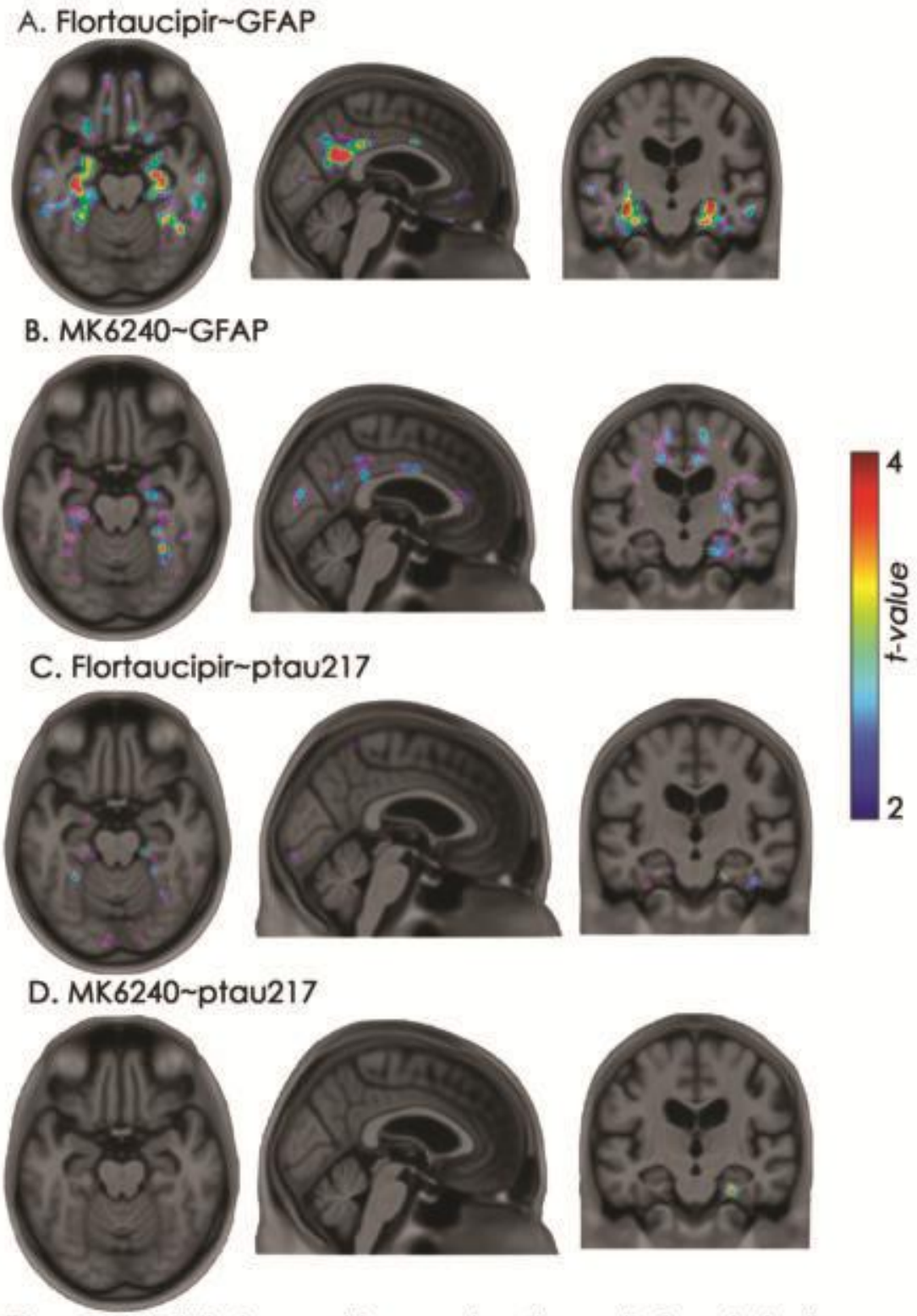


Figure1: T-statistical parametric maps show the result of voxel-wise linear regression testing the regional association of flortaucipir (A: with GFAP and C: with ptau217) and MK6240 (B: with GFAP and D: with ptau217). Heatmap scale is showing the range of t values 2 to 4.

Figure2:

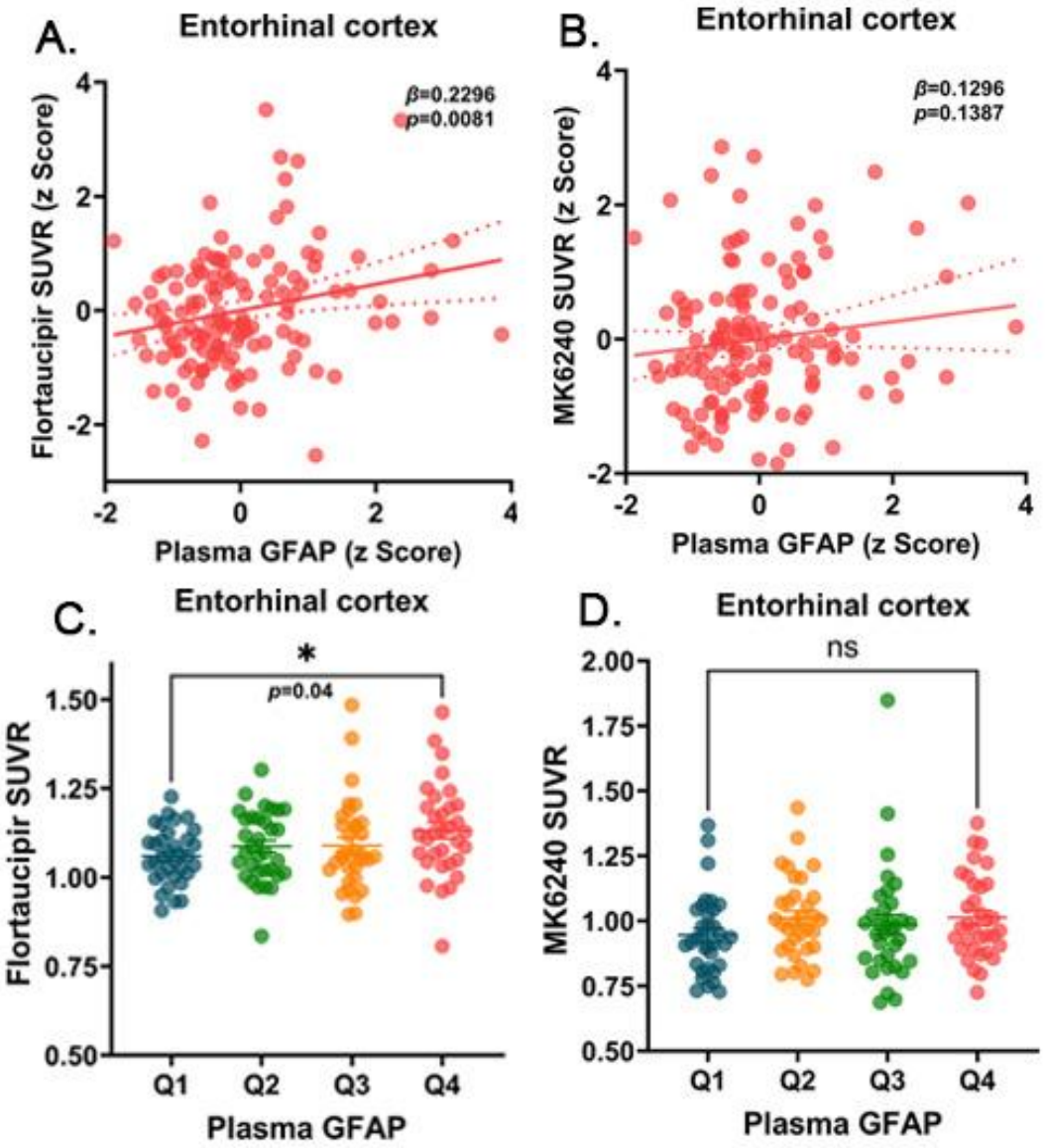


Figure2: Upper panel is representing the linear regression lines showing the association of plasma GFAP with entorhinal MTL SUVR of flortaucipir **(A)** and MK6240 **(B)**. Lower panel is showing the levels of entorhinal MTL SUVR of flortaucipir **(C)** and MK6240 **(D)** in different GFAP quartiles.

Keywords: Alzheimer's, Astrocytes, GFAP, tauPET, ptau217

141 The striatum is an early, accurate indicator of [C-11]PiB amyloid burden for the Down syndrome population

Max McLachlan[1], Julie Price[2], Dana Tudorascu[3], Charles Laymon[3], Patrick Lao[4], Ben Handen[3], Tim Fryer[5], Beau Ances[6], Sterling Johnson[1], Tobey Betthauser[1], Shahid Zaman[5], Elizabeth Head[7], Mark Mapstone[7], Brecca Bettcher[1], Lisette LeMerise[1], Andrew McVea[1], Alexandra DiFillipo[1], Matthew Zammit[1], Sigan Hartley[1], Bradley Christian[1]

[1]*University of Wisconsin - Madison, Madison, WI, US*
[2]*MGH Martinos Center, Harvard, Boston, MA, US*
[3]*University of Pittsburgh, Pittsburgh, PA, US*
[4]*Columbia University Irving Medical Center, New York, NY, US*
[5]*University of Cambridge, Cambridge, GB*
[6]*Washington University in St. Louis, St. Louis, MO, US*
[7]*University of California, Irvine, Irvine, CA, US*

Background: Early detection of amyloid burden will dictate the inclusion criteria of anti-amyloid clinical trials for individuals with Down syndrome (DS). [^{11}C]PiB PET imaging in the DS population has revealed the earliest accumulation of β amyloid (Aβ) in the striatum, though its reliability has not been quantified. This work evaluates the extent and magnitude of striatum-first amyloid accumulation in a DS cohort.

Methods: 175 participants with DS completed a total of 382 longitudinal PiB PET scans (Table 1). PET images were realigned, summed 50-70min, smoothed to 8mm resolution, and spatially normalized to a DS-specific template (Figure 1a). SUVR (whole cerebellum reference) was extracted for the GAINN cortical ROI and striatum-specific ROIs (listed in Figure 1b). Positivity thresholds were calculated for each ROI with a 2-distribution Gaussian mixture model (threshold=μ_{lower}+2*SD_{lower}). Using the sampled iterative local approximation (SILA) method, the average rate of change was calculated within discrete intervals, yielding generalized models for amyloid progression relative to positivity in each ROI. The estimated time-to-amyloid-positivity was calculated by aligning participant trajectories to the models. Paired t-tests evaluated the average differences in time-to-positivity.

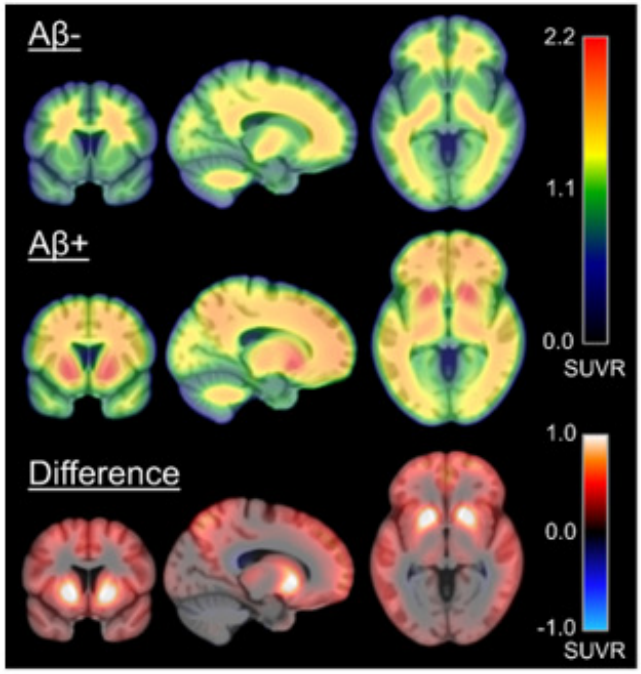
Results: Figure 1b displays the difference in estimated time-to-positivity between the cortex and each striatum-specific ROI. The PET-based striatum shows the earliest sensitivity to amyloid, on average 3.31 (2.50)*** years before the cortex. Figure 2 displays the cortical and striatal SILA models, as well as their ratio along the cortical time-to-positivity axis. On average, the striatum is 16.5% (8.4%) higher than the cortex at time of cortical positivity, and their ratio plateaus at 1.3.

Conclusion: The striatum is an early and accurate indicator of amyloid burden in the DS population. The PET-based striatum ROI shows the greatest sensitivity, while the caudate shows the highest variability, likely from structural atrophy. Striatal amyloid binding is actively being characterized for [^{18}F]florbetapir in DS.

Number of PiB Scans	1 PiB Scan	2 PiB Scans	3 PiB Scans	≥4 PiB Scans	Entire Cohort
Cohort Size (n)	64	59	15	37	175
Average Age at Baseline (yrs)	39.5 (SD = 9.1)	35.0 (SD = 7.4)	37.4 (SD = 6.9)	36.0 (SD = 6.4)	37.1 (SD = 8.0)
Sex (M/F)	36/28	27/32	9/6	20/17	92/83
Aβ-	46	45	6	16	113
Aβ Converter	N/A	7	5	17	29
Aβ+	18	7	4	4	33

Table 1 – Participant demographics. Scans were collected over a period of up to 10 years, with 32 months between scans on average. Aβ positivity was determined using a threshold of 18.1 CL.

1a



1b

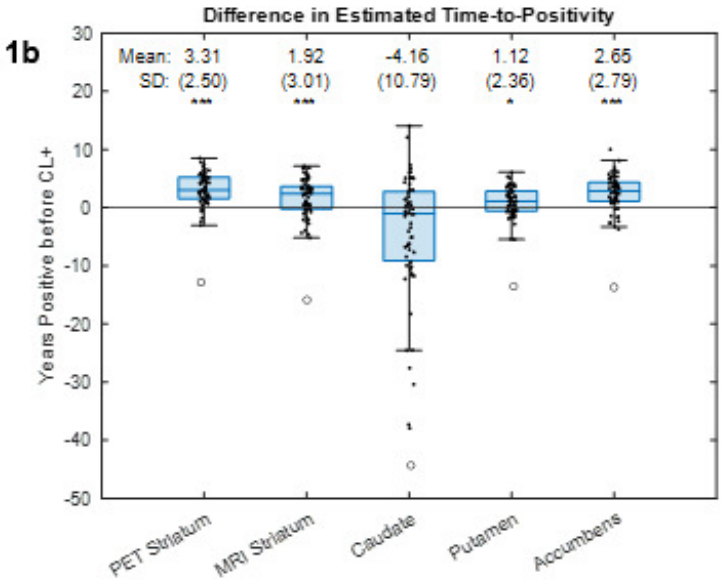


Figure 1a – Average [^{11}C]PiB PET scans for Aβ negative (top) and Aβ positive (middle) groups. The difference image (bottom) demonstrates the highest observed signal in cortical areas, particularly the precuneus and striatum.

Figure 1b – Difference in estimated time-to-positivity between the cortex and each striatum-specific ROI. Since SILA's estimates are most reliable for trajectories that have crossed the positivity threshold, this analysis was only performed for participants with at least one positive scan in each ROI (n=62). ROIs include the caudate, putamen, accumbens, and a composite MRI-based striatum, all generated using the Harvard Oxford Atlas. Additionally, a PET-generated striatum ROI was created by thresholding the difference image in Figure 1a to +0.75 SUVR. Time-to-positivity estimates are calculated by minimizing the sum of squared differences between a participant's amyloid trajectory and the associated SILA model. One individual was deemed an outlier with a Z score < -5 in all ROIs.

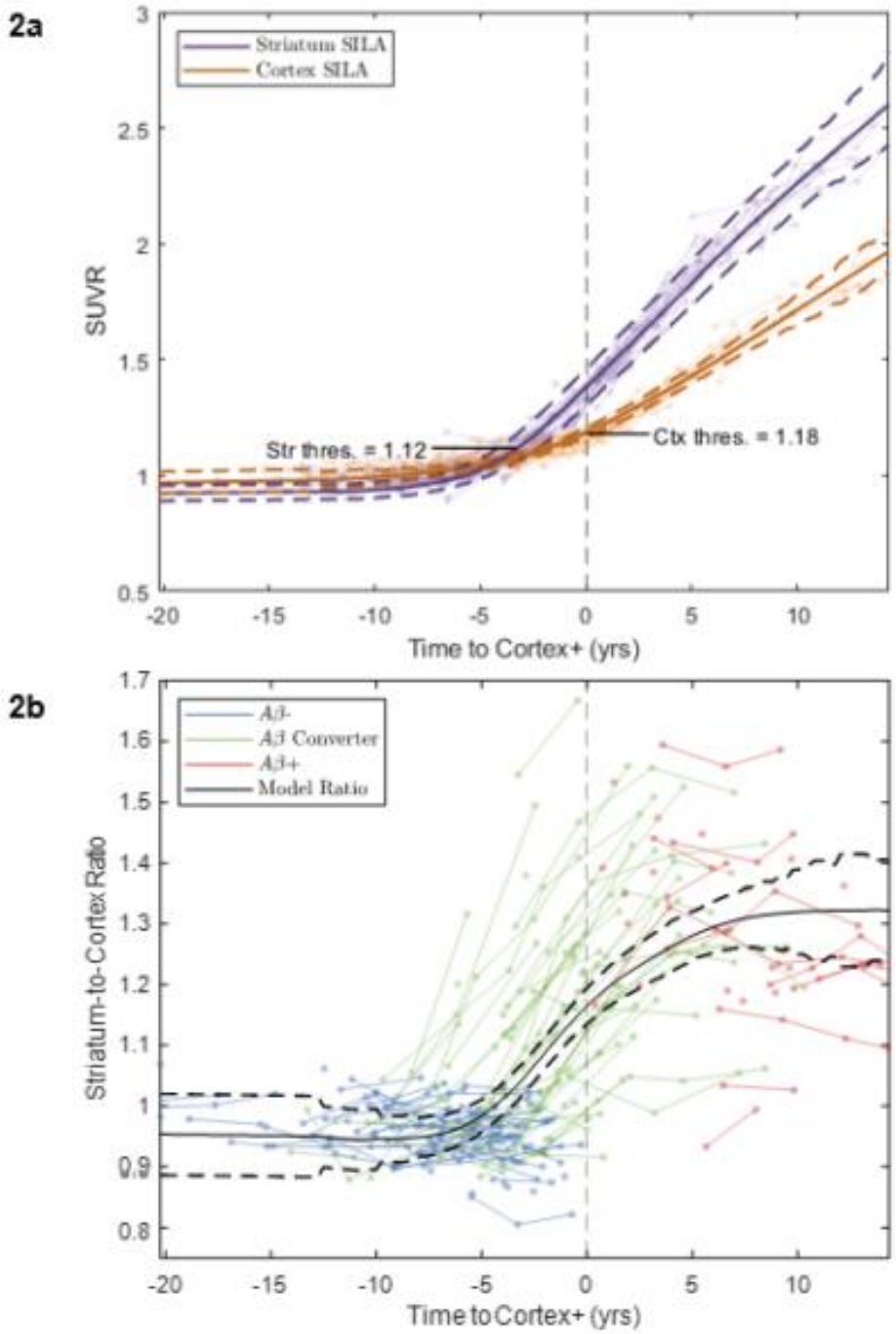


Figure 2a – SILA models for the cortex and PET-based striatum ROIs, with 95% confidence bands. In order to plot the striatum model along the cortex positivity axis, the striatum model was shifted by the average difference found in Figure 1b (3.31 years). Confidence bands were adjusted accordingly. Participant trajectories for each ROI are displayed as semi-transparent markers.

Figure 2b – Ratio of the striatum SILA model to the cortex SILA model, with 95% confidence bands. Participant trajectories are displayed, color-coded by cortical amyloid status. At t=0 (time of cortex positivity), the modeled striatum-to-cortex ratio is 1.165 (0.084).

Keywords: Amyloid, Down syndrome, Alzheimer's disease, PET, Striatum

142 Best practices for tau-PET tracer harmonization in Alzheimer's research

Cécile Tissot[1], Hsin-Yeh Tsai[1], Joseph Giorgio[2], Ganna Blazhenets[3], Theresa Harrison[2], Emily Olafson[4], Sandra Sanabria[4], Antoine Leuzy[5], Vincent Doré[6], William Jagust[1,2], Pedro Rosa-Neto[7], Tharick Pascoal[8], Suzanne Baker[1]

[1]*Lawrence Berkeley National Laboratory, Berkeley, CA, US*
[2]*University of California, Berkeley, Berkeley, CA, US*
[3]*University of California, San Francisco, San Francisco, CA, US*
[4]*Genentech, South San Francisco, CA, US*
[5]*Lund University, Lund, SE*
[6]*Australian e-Health Research Centre, Melbourne, AU*
[7]*McGill University, Montreal, QC, CA*
[8]*University of Pittsburgh, Pittsburgh, PA, US*

Background: Harmonization of tau-PET tracers is critical for consistency in Alzheimer's disease (AD) research. With variability in tracers and their tau pathology affinities, standardized practices are needed to ensure comparability across studies. This consensus paper, based on discussions with PET imaging experts, aims to establish best practices for tracer harmonization, focusing on key performance metrics to be reported.

Methods: Discussions emphasized selecting appropriate metrics to assess harmonization quality. Key metrics include R^2 values, effect sizes between groups (e.g., Aβ+ vs. Aβ-), and test-retest reliability. The voxel-wise versus region-of-interest (ROI) approach was debated, especially for addressing regional asymmetries in tau deposition. The importance of non-linear models to capture early-stage tau accumulation and reduce bias in intermediate tau groups was discussed, along with the relevance of cognitive outcomes for clinical trials.

Results: It was agreed that analyses should include a training dataset to develop harmonization methods, then apply these to a test dataset. In addition to R^2, experts recommend reporting effect sizes and harmonized data slopes as standard metrics to compare tracers and populations and assess harmonization effectiveness. Non-linear models were favored for capturing early tau accumulation and preserving dynamic ranges, particularly in intermediate-to-high tau individuals. Effect sizes and correlations with cognition should be reported before and after transformation. Voxel-wise harmonization was preferred for maintaining regional specificity, though ROI-based methods might suffice for advanced tau stages. Selected ROIs include Braak stages, meta-temporal and whole cortex. Longitudinal stability was emphasized, considering the need for simple yet effective harmonization methods that preserve disease-relevant signals.

Discussion: Experts stressed the importance of reporting key harmonization metrics, including R^2 values and effect sizes, to ensure robust cross-tracer comparisons. Voxel-wise approaches offer precision but must remain flexible, depending on the research question. This supports both academic research and industry applications, promoting effective data integration in AD studies.

Keywords: harmonization, consensus, tau-PET

143 Relationship between metabolic syndrome biomarkers and regional tau accumulation in cognitively unimpaired older adults

Victoria R. Tennant[1], Danielle Luu[1], Maxwell W. Hand[1], Noelle N. Lee[1], Arthur W. Toga[1], Sid E. O'Bryant[3], Kristine Yaffe[2], Meredith N. Braskie[1]

[1]*Mark and Mary Stevens Neuroimaging and Informatics Institute, Keck School of Medicine, Los Angeles, CA, US*
[2]*Department of Psychiatry, Neurology, and Epidemiology and Biostatistics University of California San Francisco, San Francisco, CA, US*
[3]*Institute for Translational Research University of North Texas Health Science Center, Forth Worth, TX, US*

Background: Metabolic syndrome (MetS) is associated with an increased risk of type-II diabetes, stroke, cognitive decline, and dementia in late-life. However, the relationship between specific MetS biomarkers and tau deposition remains unclear.

Methods: We assessed 833 cognitively unimpaired older adults from the Health and Aging Brain Study-Health Disparities (**Table 1**). Linear regression models were run to assess the effect of specific MetS biomarkers on mean ^{18}F-PI-2620 tau standardized uptake value ratio (SUVR) in the medial temporal (MTL), posterior cingulate (PCC), and lateral parietal (LP) regions of interest using the inferior cerebellar gray matter of the posterior cerebellum as the reference region. We then stratified models into non-Hispanic Black (NHB), non-Hispanic White (NHW), and Hispanic subgroups.

Results: In the whole group, higher Aβ-SUVR was associated with more tau in all regions and higher abdominal circumference and triglycerides were associated with more tau in the PCC and LP with a significant ethnoracial group by abdominal circumference interaction on tau. Higher HDL cholesterol was associated with more PCC tau. In the NHB subgroup, higher Aβ-SUVR was associated with more MTL and LP tau, while higher abdominal circumference and triglycerides were associated with more LP and PCC tau. In the NHW and Hispanic subgroups, higher Aβ-SUVR was associated with more tau in all regions. In the NHW subgroup, lower abdominal circumference was associated with more tau in the MTL. In the Hispanic subgroup, higher abdominal circumference was associated with more PCC and LP tau and higher triglycerides and HDL cholesterol were associated with greater PCC tau **(Tables 2-3).**

Conclusions: Our findings suggest that specific MetS biomarkers may relate differently to tau deposition across ethnoracial subgroups, particularly in the PCC and LP where higher abdominal circumference was related to more tau in Hispanic and NHB, but not in NHW older adults.

Table 1. Participant Characteristics	Mean ± Standard dev. (N=833)
Age	65 ± 8.31 (50-90)
Sex M/F	290 (35%) / 543 (65%)
Ethnicity/race	
Non-Hispanic Black/African American	237 (28.5%)
Hispanic	237 (28.5%)
Non-Hispanic White	359 (43%)
Education (years)	15 ± 3.57
Global Aβ SUVR	1.0 ± 0.13
Aβ status -/+	689 (83%) / 144 (17%)
MTL SUVR	1.1 ± 0.11
PCC SUVR	1.0 ± 0.07
LP SUVR	1.0 ± 0.09
Ab. Circumference	41 ± 6.41
Systolic BP	134 ±18.73
Diastolic BP	84 ± 10.31
Triglycerides	123 ± 87.09
Fasting glucose	103 ± 34.26
HDL Cholesterol	57 ± 15.66

Ab. Circumference = abdominal circumference (inches).

Table 2. Results of regression models in all participants

	MTL SUVR		PCC SUVR		LP SUVR	
	β	**p**	**β**	**p**	**β**	**p**
Ab. Circumference	-0.04	0.30	0.17	**<0.001** +	0.15	**<0.001** +
Diastolic BP	0.02	0.70	-0.03	0.53	0.04	0.37
Systolic BP	0.01	0.89	0.04	0.33	-0.03	0.50
Glucose	-0.01	0.73	0.06	0.10	0.05	0.19
HDL Cholesterol	0.03	0.54	0.10	**0.02**	0.04	0.31
Triglycerides	0.05	0.25	0.10	**0.02**	0.10	**0.01**
Age	0.28	**<0.001**	0.19	**<0.001**	0.01	0.78
Education	0.11	**0.002**	0.03	0.43	-0.06	0.10
Sex (F)	0.22	**0.004**	0.36	**<0.001**	0.69	**<0.001**
Global AB SUVR	0.23	**<0.001**	0.11	**0.001**	0.14	**<0.001**
Ethnicity (Hispanic vs NHW)	0.49	**<0.001**	0.17	0.08	0.22	**0.02**
Race (NHB vs NHW)	0.44	**<0.001**	0.09	0.30	-0.10	0.24
Observations	833		833		833	
R^2	0.18		0.12		0.20	
Adjusted R^2	0.17		0.11		0.18	
Residual Std. Error (df = 820)	0.91		0.94		0.90	
F Statistic (df = 12; 820)	15.00***		9.68***		16.63***	

+ Significant interaction between ethnoracial group and abdominal circumference on tau in that larger abdominal circumference was associated with greater tau in NHB and Hispanic participants, but not NHW participants. All continuous variables were scaled. Blood pressure and blood measures were log transformed.

Table 3. Results of regression models in each ethnoracial group

	NHB						NHW						Hispanic					
	MTL SUVR		PCC SUVR		LP SUVR		MTL SUVR		PCC SUVR		LP SUVR		MTL SUVR		PCC SUVR		LP SUVR	
	β	p	β	p	β	p	β	p	β	p	β	p	β	p	β	p	β	p
Ab. Circumference	0.06	0.34	0.24	**0.001**	0.22	**0.001**	-0.13	**0.02**	0.01	0.92	0.04	0.51	0.03	0.63	0.30	**<0.001**	0.22	**<0.001**
Diastolic BP	0.05	0.52	-0.01	0.88	0.02	0.84	0.01	0.89	-0.04	0.55	0.11	0.10	-0.05	0.60	-0.08	0.36	-0.03	0.73
Systolic BP	0.01	0.91	-0.02	0.76	-0.04	0.66	0.01	0.83	0.08	0.24	-0.05	0.45	0.03	0.78	0.07	0.44	-0.02	0.84
Glucose	-0.01	0.88	0.001	0.98	-0.02	0.73	0.01	0.83	0.09	0.12	0.10	**0.06**	-0.07	0.36	0.10	0.16	0.07	0.32
HDL Cholesterol	0.05	0.45	0.10	0.19	0.09	0.22	0.01	0.86	0.03	0.64	-0.03	0.61	0.04	0.68	0.26	**0.002**	0.13	0.13
Triglycerides	0.003	0.96	0.14	**0.03**	0.17	**0.01**	0.01	0.82	0.05	0.42	0.07	0.26	0.15	**0.06**	0.17	**0.03**	0.11	0.16
Age	0.40	**<0.001**	0.25	**<0.001**	0.08	0.25	0.22	**<0.001**	0.18	**0.002**	0.00	0.99	0.18	**0.02**	0.08	0.25	-0.06	0.41
Education	0.15	**0.01**	0.08	0.20	0.01	0.91	0.04	0.42	0.03	0.64	-0.03	0.51	0.08	0.26	-0.04	0.52	-0.12	**0.07**
Sex (F)	0.32	**0.02**	0.54	**<0.001**	0.63	**<0.001**	0.15	0.24	0.37	**0.01**	0.80	**<0.001**	0.02	0.91	-0.06	0.72	0.50	**0.001**
Global AB SUVR	0.15	**0.02**	0.07	0.32	0.13	**0.05**	0.29	**<0.001**	0.11	**0.04**	0.16	**0.002**	0.16	**0.02**	0.16	**0.01**	0.15	**0.02**
N	237		237		237		N	359	359		359		N	237	237		237	
R^2	0.29		0.21		0.20		R^2	0.20	0.10		0.19		R^2	0.10	0.18		0.17	
Adj. R^2	0.26		0.18		0.16		Adj. R^2	0.18	0.07		0.17		Adj. R^2	0.06	0.14		0.14	
Residual Std. Error (df = 226)	0.86		0.91		0.92		Residual Std. Error (df = 348)	0.91	0.96		0.91		Residual Std. Error (df = 226)	0.97	0.93		0.93	
F Statistic (df = 10; 226)	9.22***		6.15***		5.56***		F Statistic (df = 10; 348)	8.64***	3.86***		8.34***		F Statistic (df = 10; 226)	2.46***	4.95***		4.70***	

Keywords: PI-2620, tau, metabolic syndrome, biomarkers

144 Association of a unique pattern of white matter T2 FLAIR hyperintensities with plasma and tau PET biomarkers in former American football players

Jenna R. Groh[1], Chad Farris[1], Adam M. Brickman[2], Mohamad J. Alshikho[2], Annalise E. Miner[1], Yorghos Tripodis[3], Anna Cui[1], Charles H. Adler[4], Laura J. Balcer[5], Charles Bernick[6], Robert C. Cantu[1], Michael J Coleman[8], David Dodick[4], Nicholas Ashton[9], Henrik Zetterberg[9], Kaj Blennow[9], Elaine R. Peskind[10], Ann C. McKee[1], Jesse Mez[1], Sylvain Bouix[11], Jeffrey L. Cummings[12], Eric M. Reiman[13], Robert A. Stern[1], Martha Shenton[8,14], Michael L. Alosco[1]

[1]*Boston University Chobanian & Avedisian School of Medicine, Boston, MA, US*
[2]*Columbia University, Department of Neurology, New York, NY, US*
[3]*Boston University School of Public Health, Boston, MA, US*
[4]*Mayo Clinic College of Medicine, Department of Neurology, Scottsdale, AR, US*
[5]*NYU Grossman School of Medicine, Departments of Neurology, Population Health and Ophthalmology, New York, NY, US*
[6]*Cleveland Clinic Lou Ruvo Center for Brain Health, Las Vegas, NV, US*
[7]*University of Washington, Department of Neurology, Seattle, WA, US*
[8]*Brigham and Women's Hospital, Department of Psychiatry, Psychiatry Neuroimaging Laboratory, Boston, MA, US*
[9]*The Sahlgrenska Academy at the University of Gothenburg, Institute of Neuroscience and Physiology, Department of Psychiatry and Neurochemistry, Mölndal, SE*
[10]*University of Washington School of Medicine, Department of Psychiatry and Behavioral Sciences, Seattle, WA, US*
[11]*École de technologie supérieure, Department of Software Engineering and Information Technology, Montreal, QC, CA*
[12]*University of Nevada Las Vegas, Chambers-Grundy Center for Transformative Neuroscience, Department of Brain Health, School of Integrated Health Sciences, Las Vegas, NV, US*
[13]*Banner Alzheimer's Institute, University of Arizona, Arizona State University, Translational Genomics Research Institute, and Arizona Alzheimer's Consortium, Phoenix, AR, US*
[14]*Brigham and Women's Hospital, Harvard Medical School, Department of Radiology, Boston, MA, US*

Background: Repetitive head impacts (RHI) can lead to long-term white matter injury visualized on FLAIR scans as white matter hyperintensities (WMH). Anecdotally, we observed a distinct pattern of WMH in individuals with RHI exposure: small, punctate, discrete lesions near the cortex at the depths of the sulci (**Figure 1a**). The goal of this study was to empirically characterize this pattern in former elite American football players.

Methods: The sample included 164 male football players (n=111 professional and n=53 college players) and n=55 asymptomatic males without RHI from the DIAGNOSE Project with available MRI, 18F-flortaucipir (FTP), and florbetapir PET data. **(Table 1)**. Visual ratings blind to information about the participant's exposure status and clinical status were conducted to count WMH that were a.) within 1.0cm of the gray/white matter boundary, b.) as bright as the cortex, c.) spherical and d.) less than 1.0cm in size. ANCOVA compared groups on total number of WMH adjusted for age and vascular risk factors. Among football players, multivariable linear regression models assessed relationships between WMH and plasma biomarkers including p-tau181, p-tau231, Aβ42/40 ratio, neurofilament light (NfL), glial fibrillary acidic protein (GFAP) and FTP composite SUVRs.

Results: Number of WMH was greater in football players compared to controls (p=0.007) **(Figure 1b)**. Among former players, elevated p-tau231 (p_{adj}=0.041) and NfL (p_{adj}=0.034) were associated with greater WMH but p-tau181 (p_{adj}=0.295), GFAP (p_{adj}=0.784), and the ratio Aβ42/40 (p_{adj}=0.697) were not **(Figure 2)**. Number of WMH was associated with tau PET composite regions frontal SUVR (p_{adj}=0.046) and left-parietal SUVR (p_{adj}=0.046) but not

mesial-temporal SUVR (p_{adj}=0.285) **(Figure 2)**.

Conclusions: This study provides evidence for a unique pattern of WMH in former elite football players exposed to RHI. The lesion location near the depths of the sulci and gray/white matter junction corresponds to areas susceptible to RHI and tau deposition in CTE.

Table 1. Sample Characteristics

	N	Football N = 164[1]	Control N = 55[1]	p-value[2]
Age (years)	219	57.38 (8.34)	59.67 (8.44)	0.077
Education (years)	219	16.75 (1.46)	17.47 (3.50)	0.68
Race	219			0.96
White		102 (62%)	34 (62%)	
Nonwhite		62 (38%)	21 (38%)	
Total Years of Play	164	15.8 (4.3)	NA (NA)	
Revised Framingham Stroke Risk Profile	208	0.03 (0.03)	0.05 (0.04)	<0.001
Sleep Apnea	215	57 / 161 (35%)	9 / 54 (17%)	0.010
Atrial Fibrillation	216	9 / 162 (5.6%)	0 / 54 (0%)	0.12
Diabetes	217	10 / 162 (6.2%)	5 / 55 (9.1%)	0.54
Hit 6 Total Score	219	46.65 (10.29)	40.09 (5.33)	<0.001
TES Level of CTE Certainty	218			<0.001
No TES		58 (36%)	55 (100%)	
Suggestive of CTE		32 (20%)	0 (0%)	
Possible CTE		21 (13%)	0 (0%)	
Probable CTE		52 (32%)	0 (0%)	
MOCA (Raw Total Score)	218	24.7 (3.4)	26.7 (1.9)	<0.001
Amyloid PET Positive	216	3 (1.8%)	0 (0%)	>0.99
WMH within 0.5cm of the Cortex	219	26 (44)	12 (18)	0.029
WMH within 1.0cm of the Cortex	219	33 (56)	17 (26)	0.038

[1]Mean (SD); n (%); n / N (%)

[2]Wilcoxon rank sum test; Pearson's Chi-squared test; Fisher's exact test

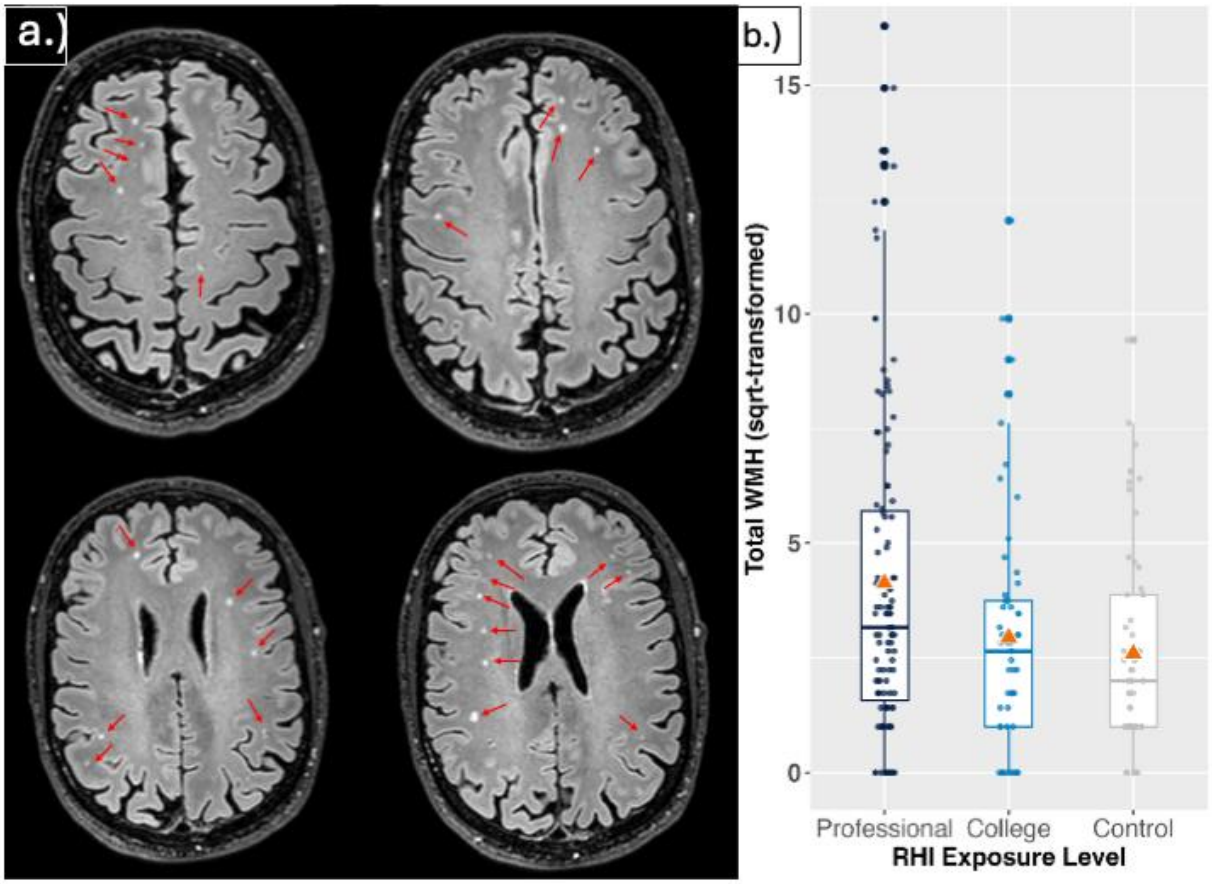


Figure 1.
a.) Exemplar FLAIR scan from a participant with substantial RHI exposure. Red arrows show small, spherical punctate lesions close to the gray matter, distributed throughout the cortex, often in the absence of confluent periventricular lesions. Lesions are also observed in relatively younger aged (e.g., 50s) individual with minimal vascular risk factors. **b.)** Differences in total number of small, punctate, discrete WMH within 0.5cm of the gray matter between former professional American football players, college football players, and unexposed controls. Total number of WMH was greater in former professional players compared to the controls (p=0.001) but not former professional players compared to the college players (p=0.983).

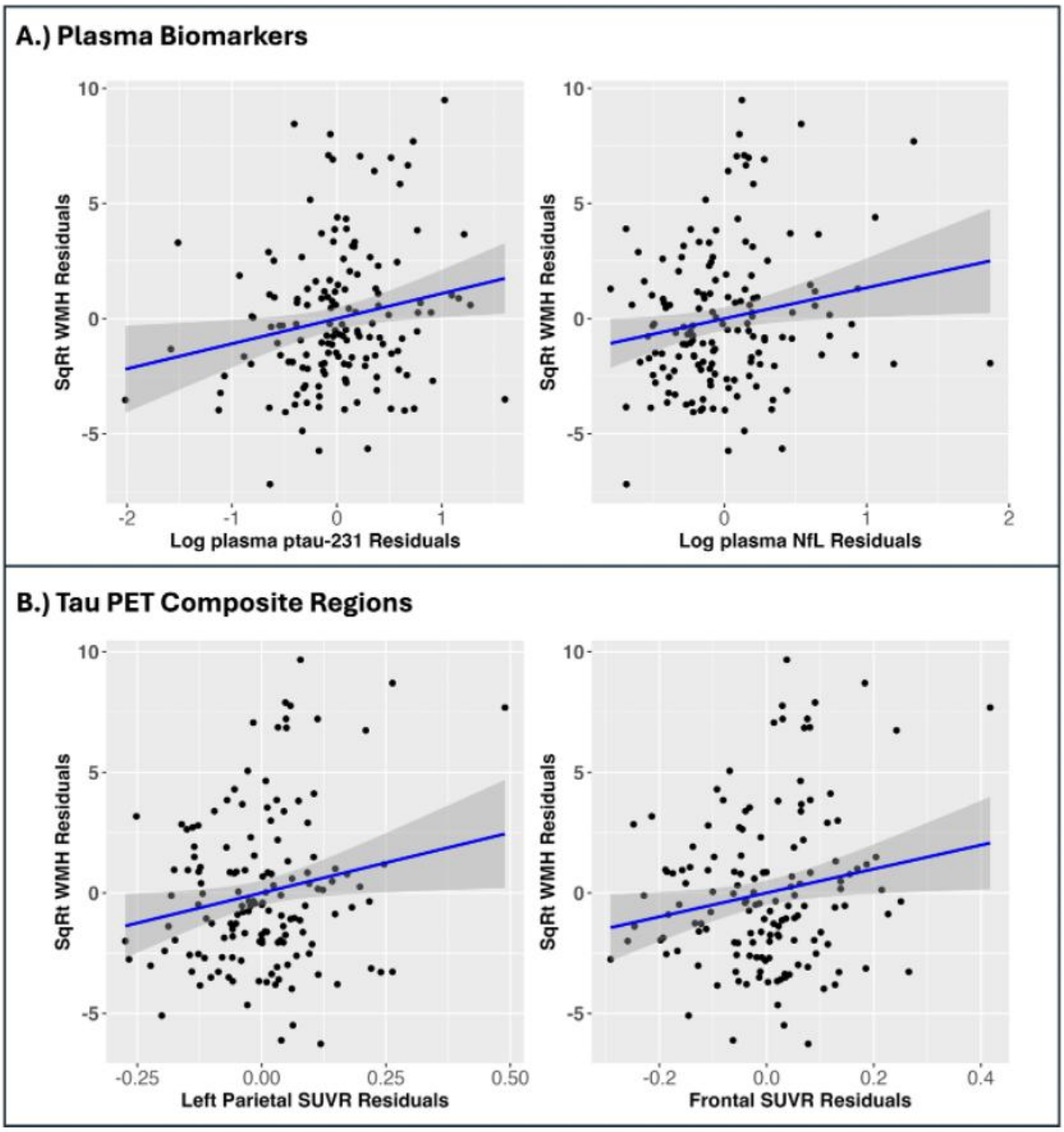


Figure 2.
Adjusted associations between the number of WMH within 0.5cm of the cortex and log-transformed plasma biomarkers/tau PET composite regions in the former American football players. Partial regression plots were adjusted for covariates: age, BMI, race, revised Framingham Stroke Risk Profile score (rFSRP), and sleep apnea. Significant associations include plasma p-tau231 (p_{adj}=0.041)), NfL (p_{adj}=0.034) and FTP composite regions frontal SUVR (p_{adj}=0.046) and left parietal (p_{adj}=0.046).
Abbreviations: white matter hyperintensities (WMH), neurofilament light (NfL), standardized uptake value ratio (SUVR).

Keywords: White matter hyperintensities, aging athletes, repetitive head impacts, flortaucipir, plasma biomarkers

145 Relationship between flortaucipir-PET and quantitative susceptibility mapping in atypical Alzheimer's disease

Neha Singh-Reilly[1], Ryota Satoh[2], Jonathan Graff-Radford[1], Mary Machulda[3], Val Lowe[2], Keith Josephs[1], Jennifer Whitwell[2]

[1]*Department of Neurology, Mayo Clinic, Rochester, MN, US*
[2]*Department of Radiology, Mayo Clinic, Rochester, MN, US*
[3]*Department of Psychiatry & Psychology, Mayo Clinic, Rochester, MN, US*

Background: Quantitative susceptibility mapping (QSM) can detect iron deposition or myelin loss in the brain by estimating magnetic susceptibility properties. Iron is an important component in neurofibrillary tangles and is known to co-localize in regions with tangle burden in Alzheimer's disease (AD). Abnormal magnetic susceptibility measured on QSM has been observed in atypical AD, although it is unclear if susceptibility is regionally related to flortaucipir-PET uptake in atypical AD.

Methods: Forty atypical AD patients (visual variant=24, language variant=7, others=9) were recruited by the Neurodegenerative Research group from the Department of Neurology, Mayo Clinic, Rochester, MN. They underwent a 3T MRI scan with a five-echo gradient echo sequence for calculation of QSM (n=80), Aβ (Pittsburgh Compound-B) and a ^{18}F-flortaucipir PET scan (n=73). All patients showed evidence of Aβ positivity on PET. To assess the relationship between QSM and flortaucipir-PET, two approaches were used i) Voxel-based regression analysis using VoxelStats for the whole brain, and ii) region-of-interest (ROI)-based Spearman's correlation analyses using cortical and subcortical ROIs. All models were adjusted for age and sex as covariates and were corrected for multiple comparisons, specifically the VoxelStats regression maps were corrected using random field theory and the ROI-based correlation plots were corrected using false discovery rate.

Results: At the voxel-level, positive correlations between flortaucipir-PET and QSM were only observed in the left caudate (Figure 1). At the ROI-level, no significant associations were found, although uncorrected data showed a positive association in the occipital lobe (red circle) and a negative association between substantia nigra susceptibility and occipital flortaucipir uptake (blue circle) (Figure 2). Since these findings did not survive corrections, they should be interpreted cautiously.

Discussion: Our data provides little evidence that regional flortaucipir PET uptake is related to susceptibility changes in patients with atypical AD.

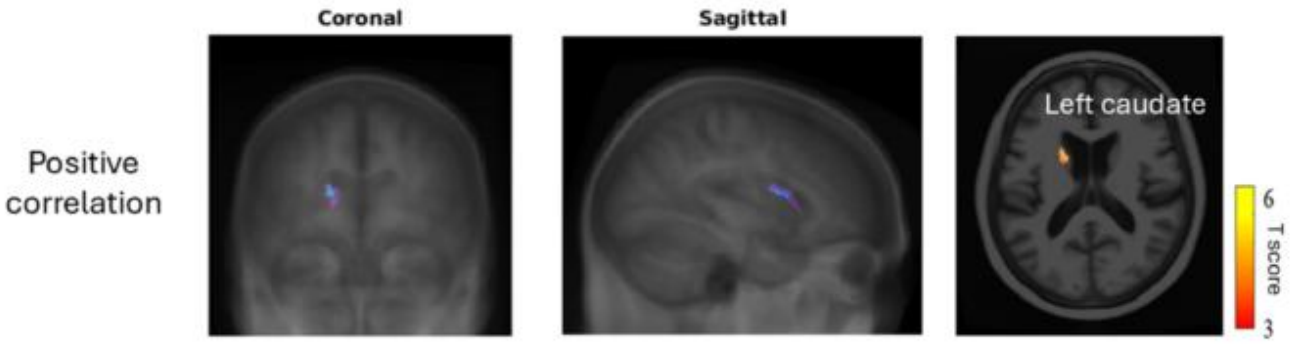


Figure 1: Voxel-based analysis. These maps represent the results for linear regression calculated for each voxel. Results are presented at p<0.001 corrected for multiple comparisons using random field theory. These glass brain visualizations were generated using VoxelStats.

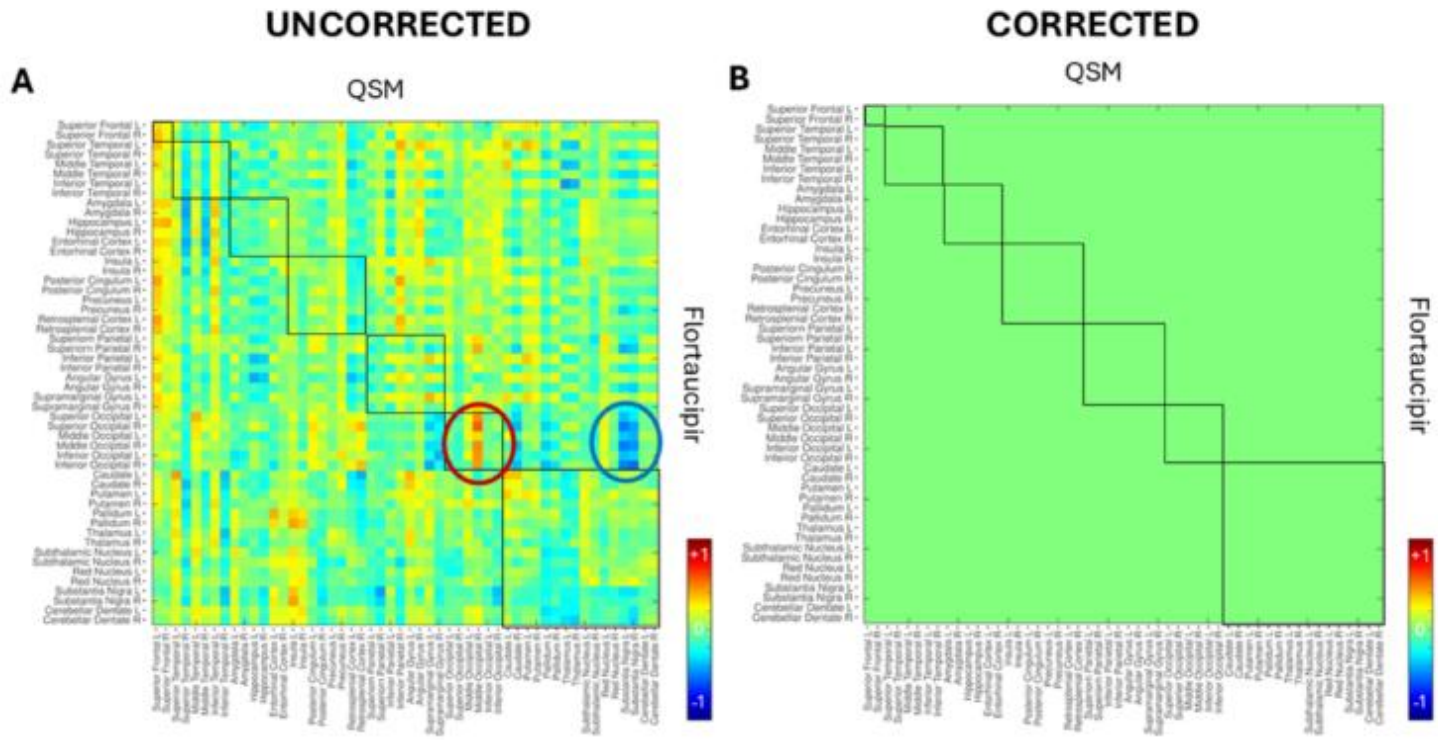


Figure 2: ROI-based analysis. These maps represent the results for spearman correlation. A) Spearman correlations without correction and B) corrected at p<0.05 using false discovery rate. In panel B, correlation coefficients that did not survive the correction were set to 0.

Keywords: Atypical Alzheimer's disease, QSM, flortaucipir-PET

146 Neuropathological evaluation of the off-target binding of flortaucipir in FTLD subcortical regions: interconnecting tau aggregates with iron deposition and neuroinflammation

Rodolfo Gatto[1], Hossam Youssef[1], Gokhan Uruk[1], Mu-Hui Fu[1], R. Ross Reichard[2], Val Lowe[3], Jennifer Whitwell[3], Keith Josephs[1]

[1]*Department of Neurology, Mayo Clinic, Rochester, MN, US*
[2]*Department of Laboratory Medicine and Pathology, Rochester, MN, US*
[3]*Department of Radiology, Rochester, MN, US*

Flortaucipir (FTP) PET uptake can be observed in the basal ganglia (BG) in patients with frontotemporal lobar degeneration (FTLD) and controls, leading to speculation that FTP uptake reflects off-target binding. Increased iron content is observed in FTLD's subcortical brain regions, which appear to correlate with tau aggregates. Iron is an essential component of the oxidative stress in neuroinflammation. We hypothesize that the interplay between tau accumulation and abnormal iron deposition could enhance neuroinflammation and increase the BG's regional (off-target) FTP signal.

Objective: To evaluate whether FTP binding in the BG may be locally exacerbated by the abnormal accumulation of iron and neuroinflammatory processes.

Materials and Methods: We assessed five neuropathologically confirmed cases: two controls, one patient with high-likelihood Alzheimer's disease (H-AD), one with progressive supranuclear palsy (PSP), and one with corticobasal degeneration (CBD). Immunohistochemical staining was performed with antibodies for phosphorylated tau (AT8), 4-repeat tau (RD4), iron using ferritin (Ferr), and neuroinflammatory markers (GFAP/CD68/Iba1) in BG sections. Flortaucipir binding was assessed using a fluorescent analog (T726). The BG was also segmented into the putamen, globus pallidum externum (GPe), and globus pallidum internum (GPi).

Results: Ferritin was increased in the putamen of the H-AD case and the putamen, GPe, and GPi in the PSP and CBD cases. Colocalization between ferritin and T726 was observed in the PSP and CBD cases. Colocalization between GFAP and T726 and CD68 and T726 was seen in the PSP case, while colocalization between Iba1 and T726 was observed in the CBD case.

Conclusions: FTP off-target binding observed in the BG in FTLD cases could be related to iron deposition and locally enhanced by cell-mediated neuroinflammation.

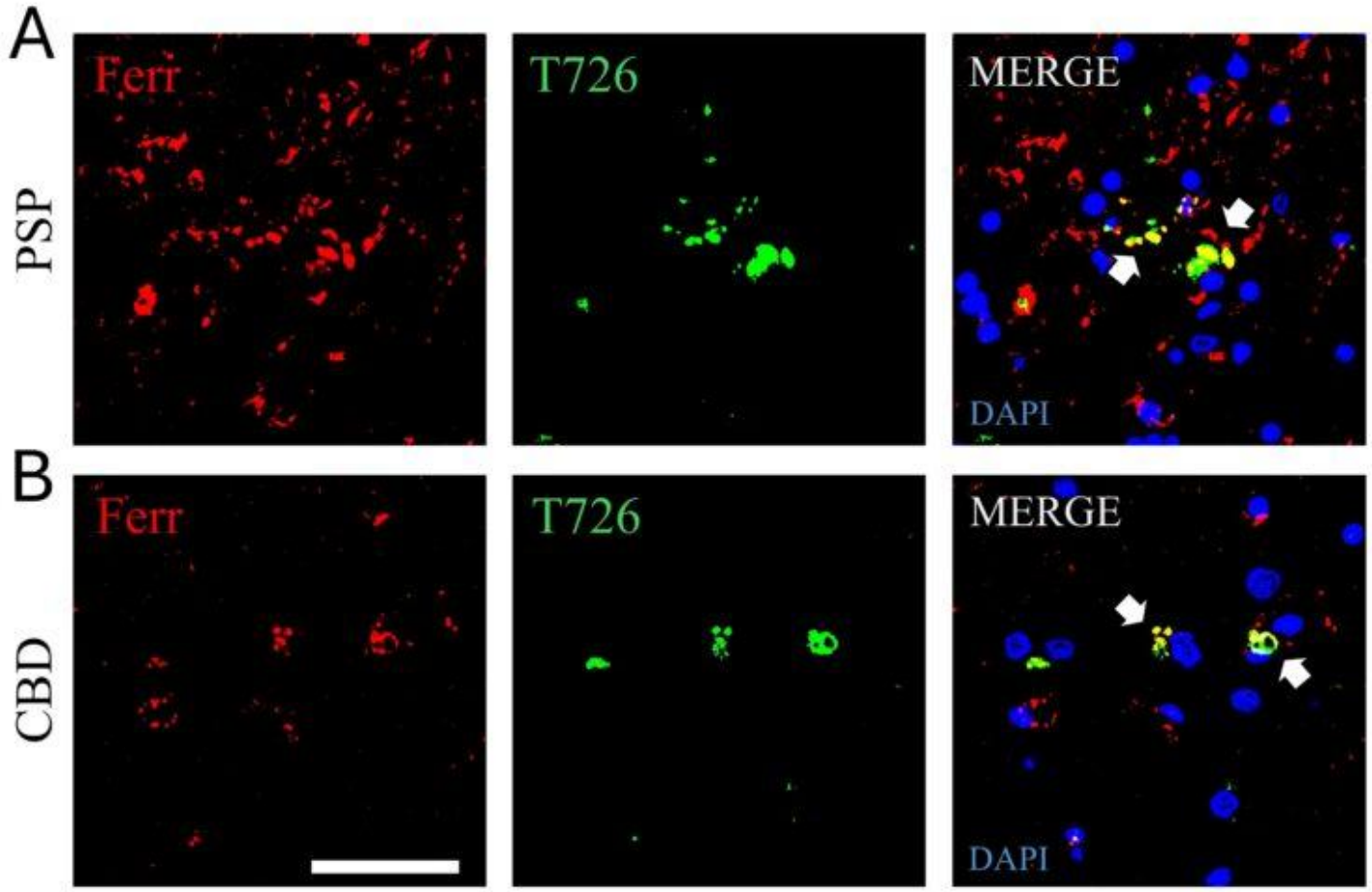


Figure: Confocal microscopy from BG (putamen) in PSP (A) and CBD (B) cases. Staining was performed with ferritin (Ferr) in red and an FTP analog (T726) in green (colocalization by arrows).

Keywords: Frontotemporal Lobar Degeneration, Flortaucipir, T726, Ferritin, Neuroinflammation

147 Patterns of cognitive decline in individuals with elevated p-tau217 and low levels (<20 Centiloids) of neocortical Aβ-PET signal

Diana Townsend[1], Michael Properzi[1], Hannah Klinger[1], Aaron Schultz[1,2], Gillian Coughlan[1], Wai-Ying Yau[1], Colin Birkenbihl[1], Mabel Seto[1], Bernard Hanseeuw[3], Heidi Jacobs[4], Michelle Farrell[4], Hyun-Sik Yang[1], Kathryn Papp[2], Dorene Rentz[2], Keith Johnson[4], Reisa Sperling[1,2], Jasmeer Chhatwal[1,2], Rebecca Amariglio[2], Rachel Buckley[1,2,5]

[1]*Department of Neurology, Massachusetts General Hospital, Boston, MA, US*
[2]*Department of Neurology, Center for Alzheimer Research and Treatment, Brigham and Women's Hospital, Harvard Medical School, Boston, MA, US*
[3]*Department of Neurology, Cliniques Universitaires Saint-Luc, Institute of Neurosciences, UCLouvain, Brussels, BE*
[4]*Department of Radiology, Massachusetts General Hospital, Harvard Medical School, Boston, MA, US*
[5]*Melbourne School of Psychological Sciences, University of Melbourne, Melbourne, AU*

Objective: High baseline plasma p-tau$_{217}$ has been associated with faster rates of cognitive decline in older adults. However, less is known about the impact of p-tau$_{217}$ in individuals with low Aβ-PET (<20CL). We examined associations between p-tau$_{217}$/np-tau$_{217}$ at baseline on cognitive domains of memory, executive function, and semantic fluency in the Harvard Aging Brain Study (HABS).

Method: 230 clinically normal older adults with <20CL Aβ-PET burden, based on ^{11}C-Pittsburgh Compound B (PiB)-PET, were selected from HABS (age=70.3±8years,62% female,17% *APOE*e4+;Table1) and were followed for ~6.2 years (±2.6,range:2.7-8.6 years). All participants underwent a cognitive battery including the MMSE, WMS Logical Memory delayed recall (LMDR), Free and Cued Selective Reminding Test (FCSRT), the Buschke Selective Reminding Test (SRT), Digit Symbol Substitution (DSS), and Categories (Animals, Vegetables, and Fruit). These tests make Preclinical Alzheimer Cognitive Composite (PACC5) and a memory composite. Plasma samples were assayed with C_2N Diagnostics (mass spectrometry) to calculate a p-tau$_{217}$/np-tau$_{217}$ ratio, with tertile cutoffs created based on the entire sample. We ran a series of linear mixed effects models across these tests, adjusting for age, sex, and education over time. We compared these models against those in the full sample.

Results: The highest tertile of p-tau$_{217}$/np-tau$_{217}$ (n=30;>3.7%) was associated with faster rates of cognitive decline (Figure 1A) on FCSRT (Figure 2A), PACC5 and the memory composite, and less practice effects on LMDR (Figure 2B), relative to the lowest tertile (n=104). No effects were found in the middle tertile (n=96). In the full sample, differences appeared across the entire cognitive battery for the highest tertile (Figure 1B). The middle tertile remained unaffected.

Conclusion: In low Aβ-PET burden, high levels of p-tau$_{217}$ are associated with subtle, distinct and localized effects in verbal memory. These findings highlight the contribution that this marker can confer to early detection prior to evidence of preclinical AD.

Table 1. Demographic table, splitting HABS participants with <20CL Aβ-PET burden at baseline into groups based on their baseline p-tau$_{217}$/np-tau$_{217}$ ratio

Characteristic	**Overall**, N = 230[1]	**Low**, N = 104[1]	**Medium**, N = 96[1]	**High**, N = 30[1]
p-tau217/np-tau217 (baseline)				
Mean (SD)	2.36 (1.14)	1.42 (0.29)	2.70 (0.58)	4.58 (0.63)
Range	0.00, 6.10	0.00, 1.83	1.86, 3.73	3.75, 6.10
Age				
Mean (SD)	70.04 (8.24)	68.00 (7.64)	70.87 (8.36)	74.50 (7.85)
Range	50.00, 88.00	50.00, 85.75	50.75, 86.25	58.50, 88.00
Sex				
F	140 (60.87%)	61 (58.65%)	59 (61.46%)	20 (66.67%)
M	90 (39.13%)	43 (41.35%)	37 (38.54%)	10 (33.33%)
Education				
Mean (SD)	15.74 (2.93)	15.63 (3.03)	15.79 (2.84)	15.97 (2.94)
Range	8.00, 20.00	8.00, 20.00	8.00, 20.00	11.00, 20.00
E4 status				
e4-	191 (83.04%)	92 (88.46%)	77 (80.21%)	22 (73.33%)
e4+	39 (16.96%)	12 (11.54%)	19 (19.79%)	8 (26.67%)
PACC (baseline)				
Mean (SD)	0.09 (0.69)	0.18 (0.73)	0.02 (0.63)	0.04 (0.68)
Range	-2.15, 2.06	-2.15, 2.06	-1.82, 1.12	-1.69, 1.15
PiB (baseline)				
Mean (SD)	1.07 (0.04)	1.06 (0.04)	1.07 (0.04)	1.08 (0.04)
Range	0.92, 1.16	0.92, 1.16	0.97, 1.15	1.01, 1.14

[1] n (%)

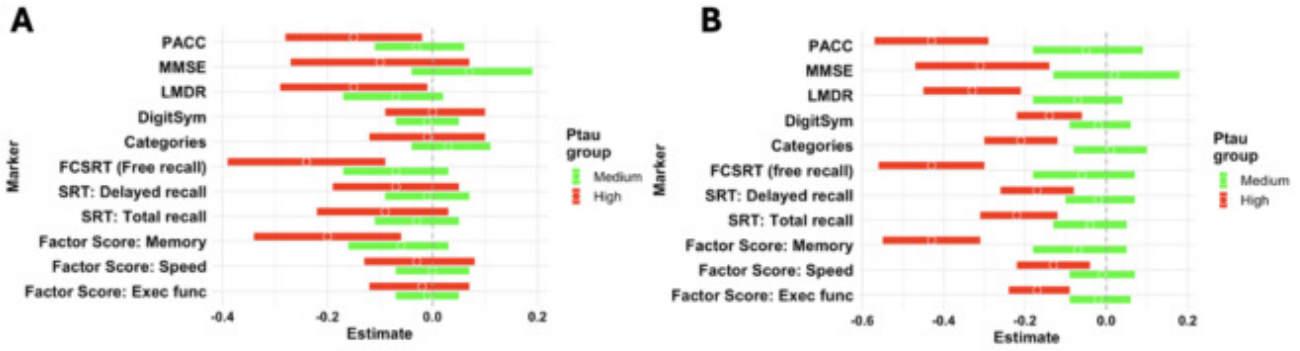


Figure 1. Forest plot of standardized estimates for high and middle p-tau$_{217}$ tertiles over time on each cognitive test relative to the lowest tertile, after adjusting for age, sex, and education levels over time for those with <20CL at baseline (A) versus the entire sample (B).

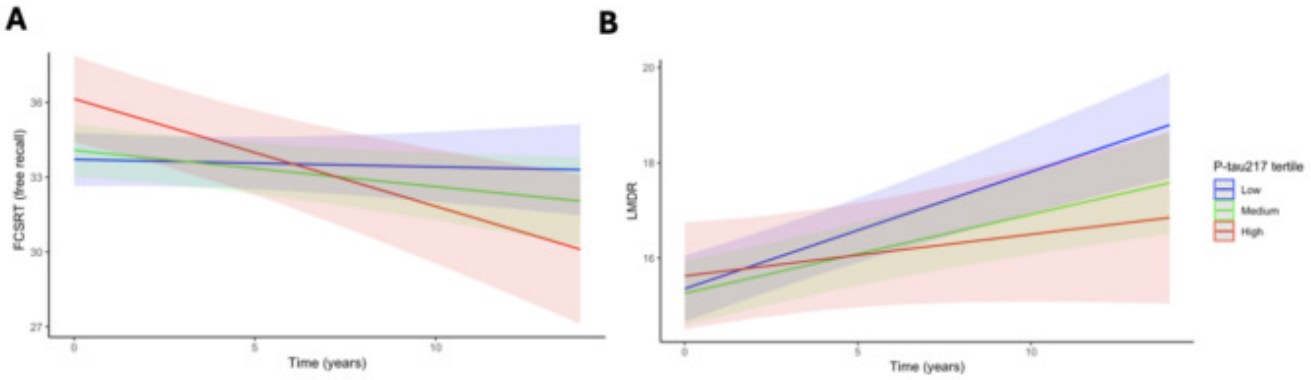


Figure 2. Plot of model estimates from linear mixed effects models predicting (A) Free and Cued Selective Reminding Test scores and (B) Logical Memory Delayed Recall scores from plasma p-tau$_{217}$ levels in older adults with <20CL Aβ-PET after adjusting for age, sex, and education over time.

Keywords: plasma tau, p-tau217, cognitive decline

148 Anatomic specificity of inflammation TSPO PET biomarkers in dementia

Quentin Finn[1], Alireza Faridar[1], Jon B Toledo[1], Obadah Nakawah[1], Gustavo Roman[1], Joseph C Masdeu[1], Belen Pascual[1]

[1]*Houston Methodist Research Institute, Weill Cornell Medicine, Houston, TX, US*

Background: Brain inflammation, a hallmark of neurodegeneration and a potentially important therapeutic target, can be measured *in vivo* with translocator protein 18 kDa (TSPO) PET. Tracers bind to microglia and migrated macrophages. 11C-PBR28 and 11C-ER176 "second-generation" tracers have high TSPO affinity, with 11C-ER176 allowing for the study of all *TSPO* rs6971 genotypes. To assess their anatomical specificity, we used 11C-PBR28 PET and 11C-ER176 PET in frontotemporal lobar degeneration (FTLD) and Alzheimer's disease (AD), respectively. Our goal is to determine whether brain inflammation PET is anatomically specific for the various diseases causing dementia.

Methods: We studied 93 patients and 37 cognitively unimpaired healthy controls. Eighteen non-fluent primary progressive aphasia (nfvPPA)(11/18 women, age 67±6.3 years), 12 semantic variant (svPPA)(7/12 women, 65±7.6 years), and 10 behavioral variant (bvFTD)(5/10 women, 63±8.1 years) patients and 14 controls (5/14 women, 68±6.1 years) had ^{11}C-PBR28 PET. Fifty-three AD patients (27/53 women, age 67±9.2 years) and 23 controls (12/23 women, 68±6.1 years) had ^{11}C-ER176 PET. Total distribution volume (V_T) values for ^{11}C-PBR28 and ^{11}C-ER176 were calculated with the Logan plot and a metabolite-corrected arterial input function. All images were corrected for partial volume effect. A full factorial analysis was performed on V_T values between patients and controls at the voxel level.

Results: V_T values were increased ($p < 0.005$) in areas neuropathologically known to be maximally involved in each one of the FTD variants and AD: nfvPPA (L>R lateral premotor area, precentral gyrus SMA, preSMA) svPPA (left temporal lobe, right temporal pole, left insula), bvFTD (both frontal lobes, anterior temporal lobes, insulae) and AD (precuneus and lateral temporal and parietal association cortex; inflammation topography correlated best with tau topography).

Conclusion: TSPO PET is highly anatomically specific in FTD and AD, providing a biomarker of brain inflammation, a potential therapeutic target in these conditions.

Keywords: TSPO, 11C-ER176 PET, 11C-PBR28 PET, Inflammation, Dementia

149 Head-to-head comparison of longitudinal plasma assays in relation to longitudinal amyloid pathology in Alzheimer's disease

Yara Yakoub[1,2], Ting Qiu[1,2], Sylvia Villeneuve[1,3,4], Alexa Pichet Binette[5,6,7], Alzheimer's Disease Neuroimaging Initiative (ADNI) ADNI Foundation for the National Institutes of Health (FNIH) Biomarkers Consortium[8]

[1]*Douglas Mental Health University Institute, Montréal, QC, CA*
[2]*Integrated Program in Neuroscience, Faculty of medicine, McGill University, Montréal, QC, CA*
[3]*Montreal Neurological Institute, McGill University, Montréal, QC, CA*
[4]*Department of Psychiatry, Faculty of medicine, McGill University, Montréal, QC, CA*
[5]*Clinical Memory Research Unit, Department of Clinical Sciences Malm., Lund University, Lund, SE*
[6]*Department of Physiology and Pharmacology, Université de Montréal, Montréal, QC, CA*
[7]*Centre de Recherche de l'Institut Universitaire de Gériatrie de Montréal, Montréal, QC, CA*
[8]*Memory and Aging Center, Department of Neurology, Weill Institute for Neurosciences, University of California, San Francisco, CA, US*

Background: Blood-based biomarkers of AD, especially p-tau217, show high concordance with Aβ-PET load and status. While many studies relied on cross-sectional data, assessing dynamic changes in these assays is important for future clinical use and trial outcomes. We evaluated the longitudinal trajectories of multiple plasma biomarkers and their associations with longitudinal changes on Aβ-PET.

Methods: We used data from the ADNI FNIH consortium (**Table 1**). It consists of 404 participants with on average three plasma samples collected over 11 years, in which 14 assays were tested (4 p-tau217, 4 $A\beta_{42/40}$, 2 p-tau181, 2 GFAP, 2 NfL), and with Aβ-PET available over the same period. We first assessed the changes over time for each assay at the group level. Then, we calculated the individual rate of change of each plasma assay and Aβ-PET Centiloids (slope) using linear mixed-effect models. Association between baseline plasma levels and plasma rate of change with Centiloids accumulation were tested using linear regression models.

Results: Across the whole sample, all biomarkers, except for $A\beta_{42/40}$ assays, showed increase over time (**Fig.1A)**, which was similar in the Aβ-positive and Aβ-negative groups assessed separately (**Fig.1B**). Almost all assays showed Aβ-PET dependent changes (time × Aβ status), with the greatest interactions seen with p-tau217 (**Fig.1C**). In the whole group, both baseline plasma levels and plasma slopes were associated with Centiloids accumulation across almost all assays (**Fig.2A-B** for statistics and **C** for scatter plots). In Aβ-positive participants, such associations were no longer significant, except for %p-tau217. In Aβ-negative participants, most of the associations with p-tau assays remained (**Fig.2**).

Conclusion: While all plasma assays levels, except for $A\beta_{42/40}$, increased over time, at higher levels they were no longer associated with insoluble amyloid accumulation. The associations between plasma markers and Centiloid accumulation were also stronger in individuals who had not reached the positivity threshold.

Characteristics	Full sample (N = 404)	Aβ-Negative (N = 249)	Aβ-Positive (N = 155)	P value
Age, years	72.80 (7.27)	71.78 (7.22)	74.43 (7.08)	< 0.001
Education, years	16.29 (2.67)	16.54 (2.69)	15.88 (2.59)	0.02
Sex (n, %)	199 (49.3)	125 (50.2)	74 (47.7)	0.70
***APOE*4 carriers (n, %)**	138 (34.2)	55 (22.1)	83 (53.5)	< 0.001
Aβ-PET Centiloids	24.71 (40.24)	-1.43 (10.70)	66.69 (34.27)	<0.001
Aβ-PET change (Centiloids/year)	2.44 (1.95)	1.44 (1.31)	4.05(1.72)	<0.001
MMSE (/30)	28.51 (1.87)	28.98(1.29)	27.73 (2.35)	<0.001
Clinical diagnosis (n, %)				<0.001
Cognitively normal	210 (52)	145 (58.2)	65 (41.9)	
MCI	184 (45.5)	104 (41.8)	80 (51.6)	
Dementia	10 (2.5)	0 (0)	10 (6.5)	

Table 1. Mean (standard deviation), or where appropriate, count and percentage for both the full and subsample in the ADNI cohort. *P*-values were derived from Kruskal Wallis test for continuous variables and chi-squared for categorical variables. *Abbreviations*: F = female; APOE = apolipoprotein-E genotype; MMMSE = Mini-Mental State Examination; MCI = Mild cognitive impairment.

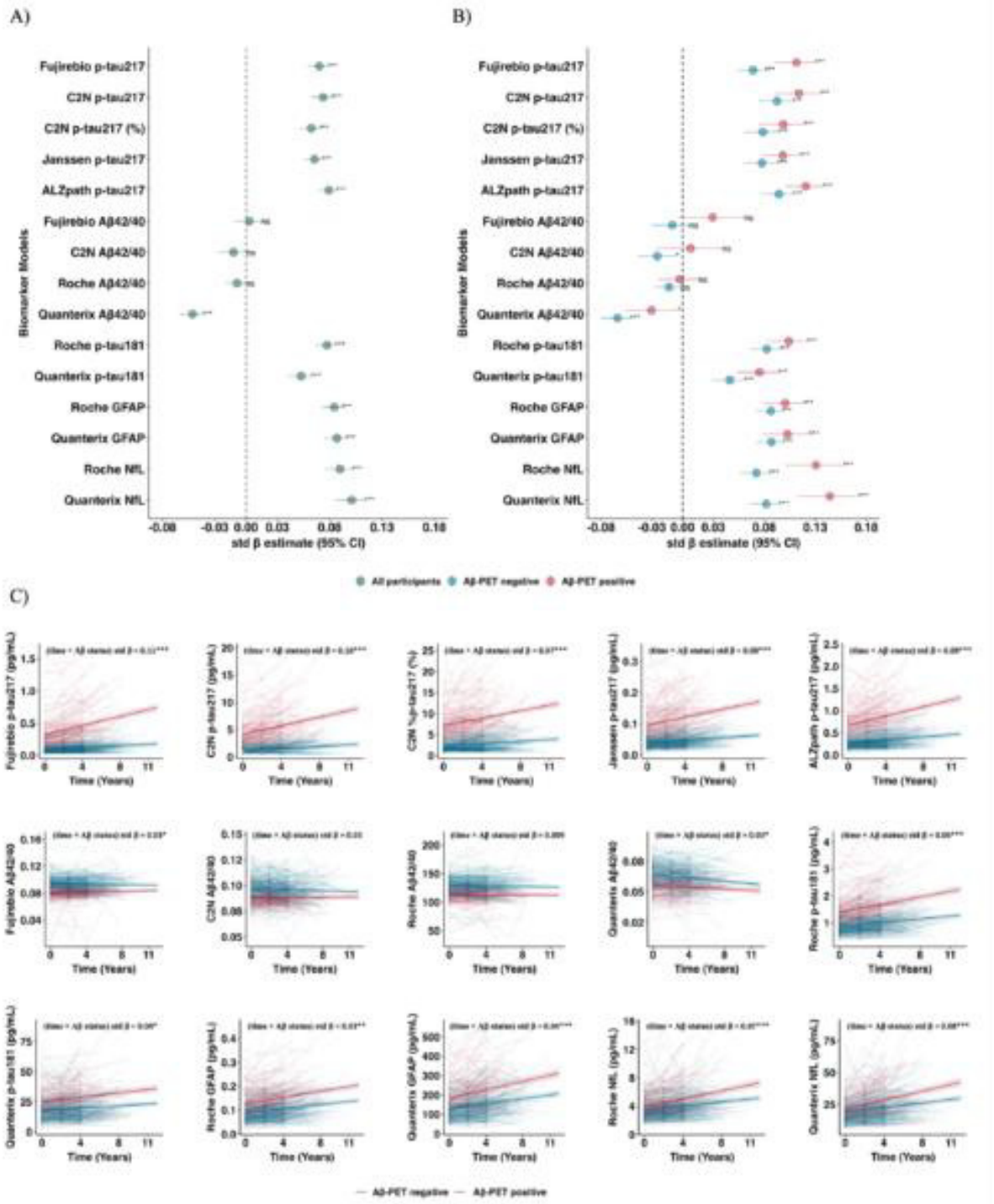


Figure 1. Longitudinal plasma biomarker trajectories across the different assays. Panel A-B) Standardized regression coefficients (std β) and 95% confidence interval (CI) obtained from linear-mixed effect (LME) models of different plasma biomarkers over time (plasma ~ time) for the whole group (A), Aβ-PET positive and negative group (B). **Panel C).** Different plasma biomarkers overtime with the interaction between time and Aβ status at baseline (time × Aβ status), the *x* axis shows time from first plasma biomarker sample. *Notes*: Outliers were removed from both baseline and longitudinal plasma sample using (mean ± 5SD) method. All models were adjusted for age at first plasma timepoint, years of education and sex. * $p < 0.05$, ** $p < 0.005$, $p < 0.001$***

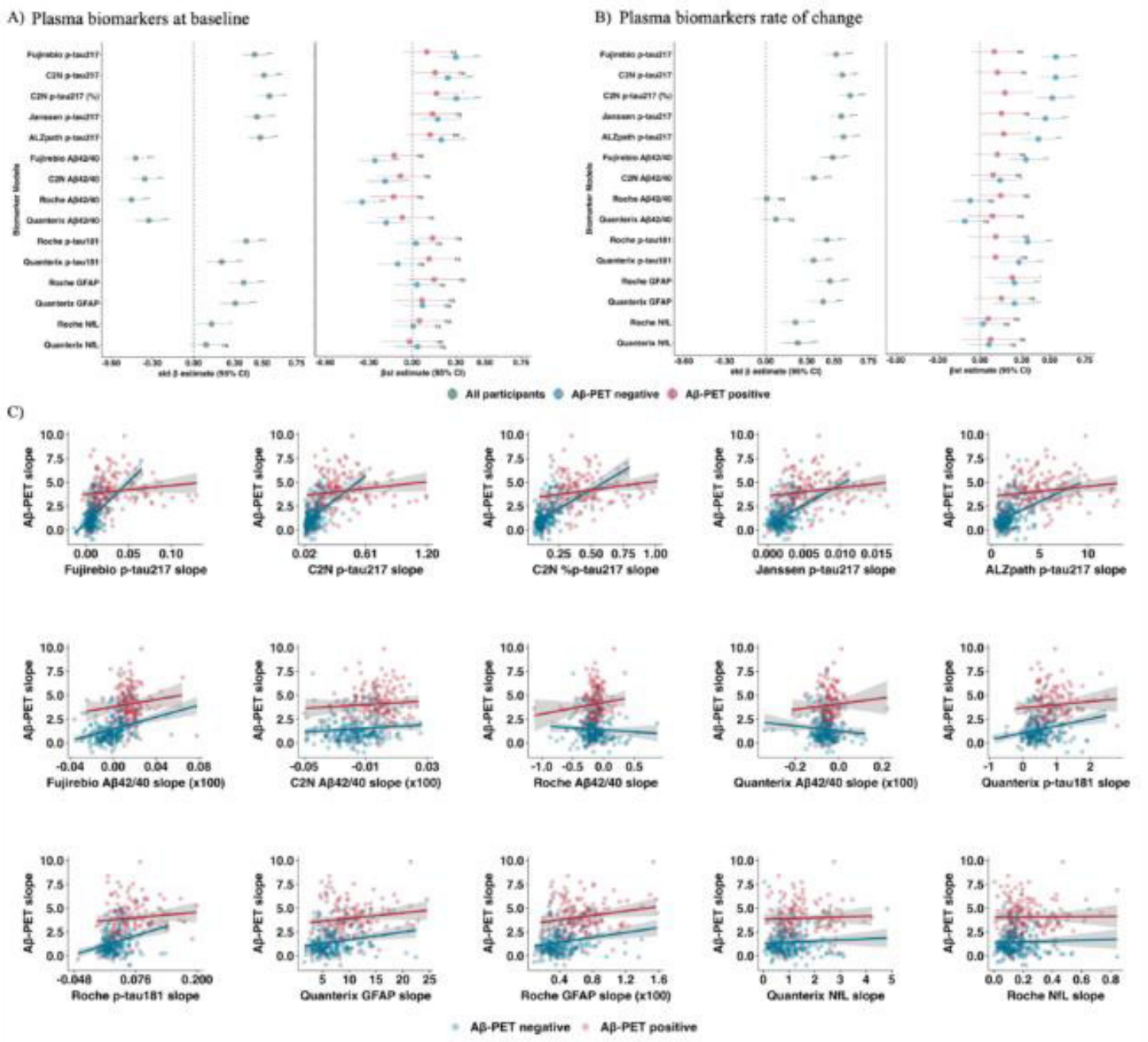


Figure 2. Association between baseline (A) and longitudinal (B-C) plasma biomarkers changes across the different assays with Aβ-PET Centiloids accumulation over time. **Panel A).** The standardized regression coefficients (std β) and 95% confidence intervals (CIs) for all participants (green), the Aβ-PET negative group (blue) and the Aβ-PET positive group (red), derived from the regression models of baseline plasma biomarkers and Aβ-PET slopes. **Panel B).** Std β and 95% CIs for all participants (green), the Aβ-PET negative group (blue) and the Aβ-PET positive group (red), derived from the regression models of plasma biomarkers slopes and Aβ-PET slopes. **Panel C).** Scatterplots illustrating the association between plasma levels rate of change (x-axis) and the Centiloid rate of change (y-axis) in the whole group. *Notes*: Outliers were removed from both baseline and longitudinal plasma sample using (mean ± 5SD) method. All models were adjusted for age at first plasma timepoint, years of education and sex. * $p < 0.05$, ** $p < 0.005$, $p < 0.001$***

Keywords: Plasma, PET, Alzheimer's disease, amyloid, tau

150 Characterization of PART using MK-6240, Flortaucipir, and plasma p-tau217

Carolina Soares[1], Pamela L. Ferreira[1], Emma Ruppert[1], Marina S. Medeiros[1], Andreia Rocha[1], Bruna Bellaver[1], Guilherme Povala[1], Guilherme Bauer-Negrini[1], Livia Amaral[1], Madeleine Bloomquist[1], Firoza Lussier[1], Joseph Masdeu[2], Dana L. Tudorascu[1], David Soleimani-Meigooni[4], Juan Fortea[5], Val Lowe[6], Hwamee Oh[7], Belen Pascual[2], Brian A. Gordon[8], Pedro Rosa-Neto[9], Suzanne Baker[3], Tharick A. Pascoal[1]

[1]*University of Pittsburgh, Department of Psychiatry, Pittsburgh, PA, US*
[2]*Houston Methodist Research Institute, Department of Neurology, Houston, TX, US*
[3]*Lawrence Berkeley National Laboratory, Berkeley, CA, US*
[4]*University of California San Francisco, Memory and Aging Center, San Francisco, CA, US*
[5]*Hospital de la Santa Creu i Sant Pau, Department of Neurology, Barcelona, ES*
[6]*Mayo Clinic, Department of Radiology, Rochester, MN, US*
[7]*Brown University, Department of Psychiatry and Human Behavior, Providence, RI, US*
[8]*Washington University in St. Louis, Department of Radiology, St. Louis, MO, US*
[9]*Translational Neuroimaging Laboratory, McGill University Research Centre for Studies in Aging, Douglas Research Institute, Montreal, QC, CA*

Older adults with brain tau pathology(T) but no evident amyloid-β(A) pathology can be referred to as primary age-related tauopathy(PART).However, in vivo characterization of PART using biomarkers remains unclear, varying based on the method used to define tau pathology(e.g.,fluid or different tau PET tracers). We conducted a head-to-head characterization of PART using two different tau PET tracers and plasma p-tau217.

We studied 345(185 cognitively unimpaired (CU),115 mild cognitively unimpaired (MCI),45 dementia)individuals from the HEAD cohort where all subjects had clinical assessments, MRI, A-PET, and both MK-6240 and Flortaucipir scans in the same visit, and a subset with plasma p-tau217 (n=330).Individuals were conservatively classified as Aβ PET positive (visual readings). Additionally, individuals were classified as tau-positive if their tau PET standard uptake value ratio (SUVR) values in Braak 1 region or plasma p-tau217 levels were above the mean + 2 SD from CU A- individuals. PART individuals were defined as A-T+, and concordance across biomarkers was assessed.Voxel-wise analysis were used to estimate percentage of abnormal voxels.

We found 29(8.40 %) cases of individuals classified as A-T+ (73±7.5 years, 38% females, 17 CU, 10 MCI, 2 dementia).Detection of A-T+ cases varied: Flortaucipir (n=10), MK-6240 (n=14), plasma p-tau217 (n=14). Concordance between biomarkers was low, with the highest overlap (n=4, 14%) between MK-6240 and Flortaucipir (Fig.1A). Interestingly, the number of A-T+ individuals with dementia detected with MK-6240, Flortaucipir and plasma p-tau217, respectively, was 4, 2 and 0 (Fig.1B).

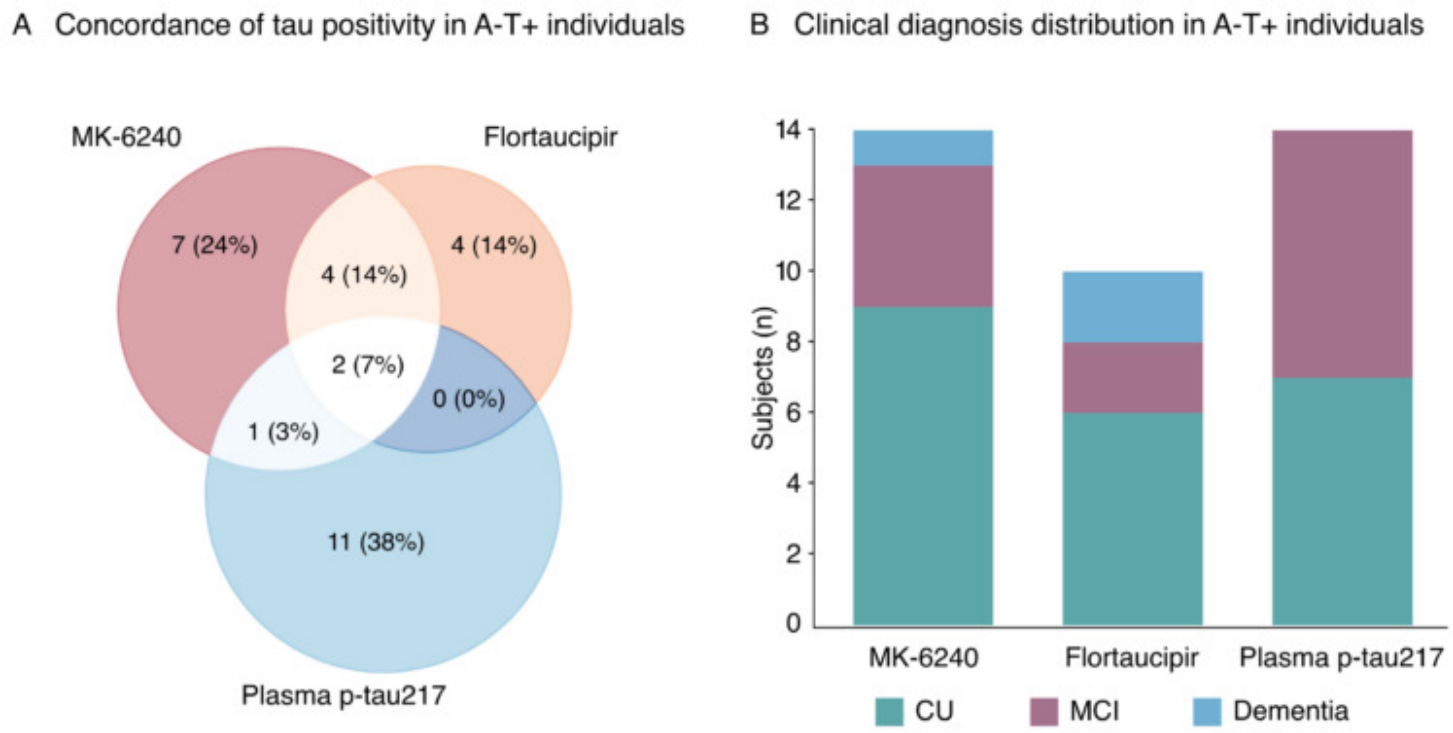


Figure 1. **Low concordance between A-T+ cases defined based on different tau biomarkers.** (**A**)Venn diagram shows the distribution of individuals amyloid-PET negative (A-) and tau-positive (T+), in MK-6240 (left circle), Flortaucipir (right circle) and plasma p-tau217 (lower circle). (**B**) Clinical diagnosis among individuals classified as A-T+. Cognitively unimpaired (CU). Standard deviation (SD). SUVR (standard uptake value ratio). A (amyloid-beta). T (tau).

Tau PET-based PART showed tau-positive in voxels mostly confined to Braak 1 region(Fig.2).

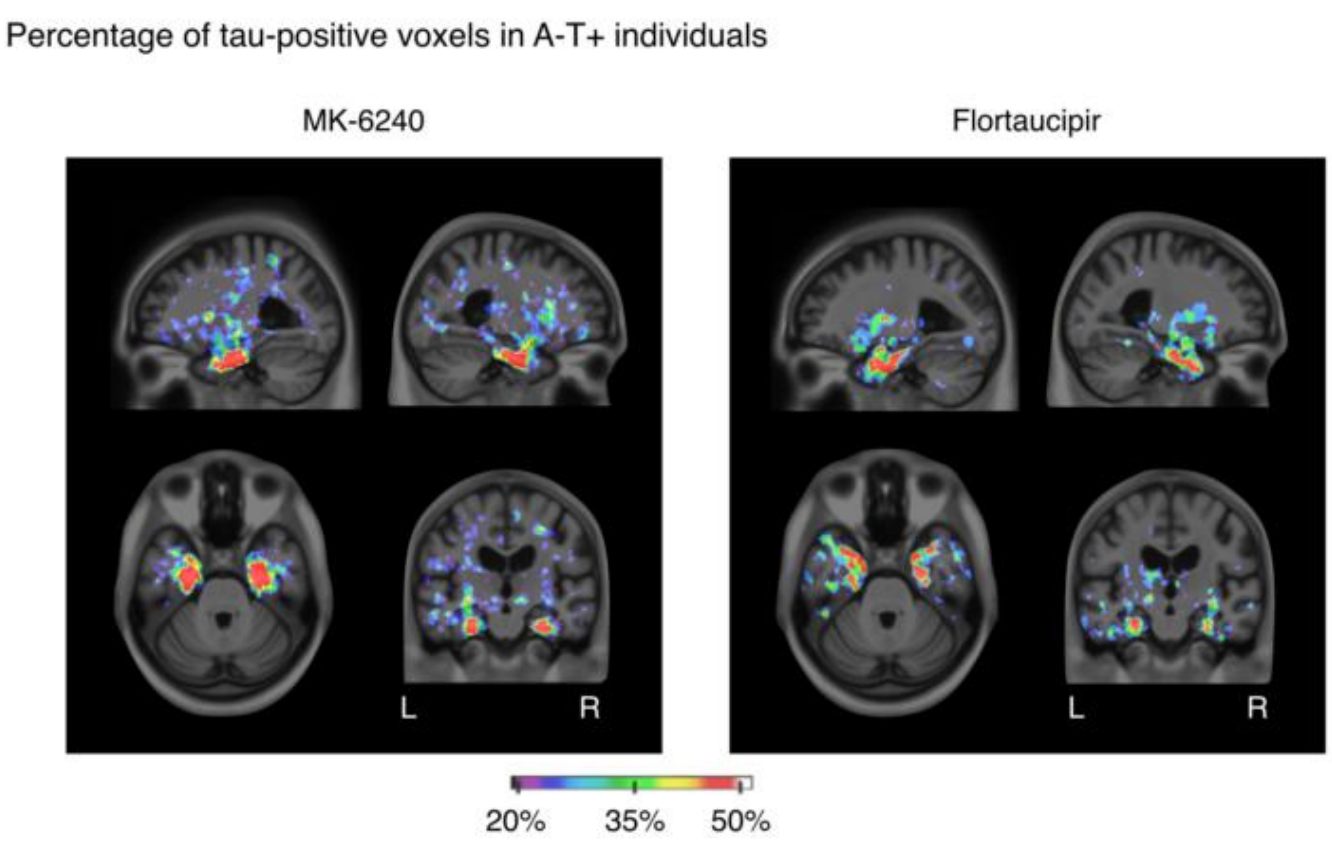


Figure 2. Individuals classified as A-T+ based on tau PET exhibited the highest percentage of tau-positivity confined to early Braak regions. Parametric maps show the percentage of tau abnormality across all brain voxels of individuals classified as A-T+ with MK-6240 (**left**) or with Flortaucipir (**right**). Voxels were considered abnormal when SUVR values exceeded the mean + 2 SD from CU A- in the given voxel. Cognitively unimpaired (CU). Standard deviation (SD). SUVR (standard uptake value ratio). A (amyloid-beta). T (tau).

Representative tau biomarker discordant cases, individuals classified as T+ by only one marker, are illustrated in Fig.3.

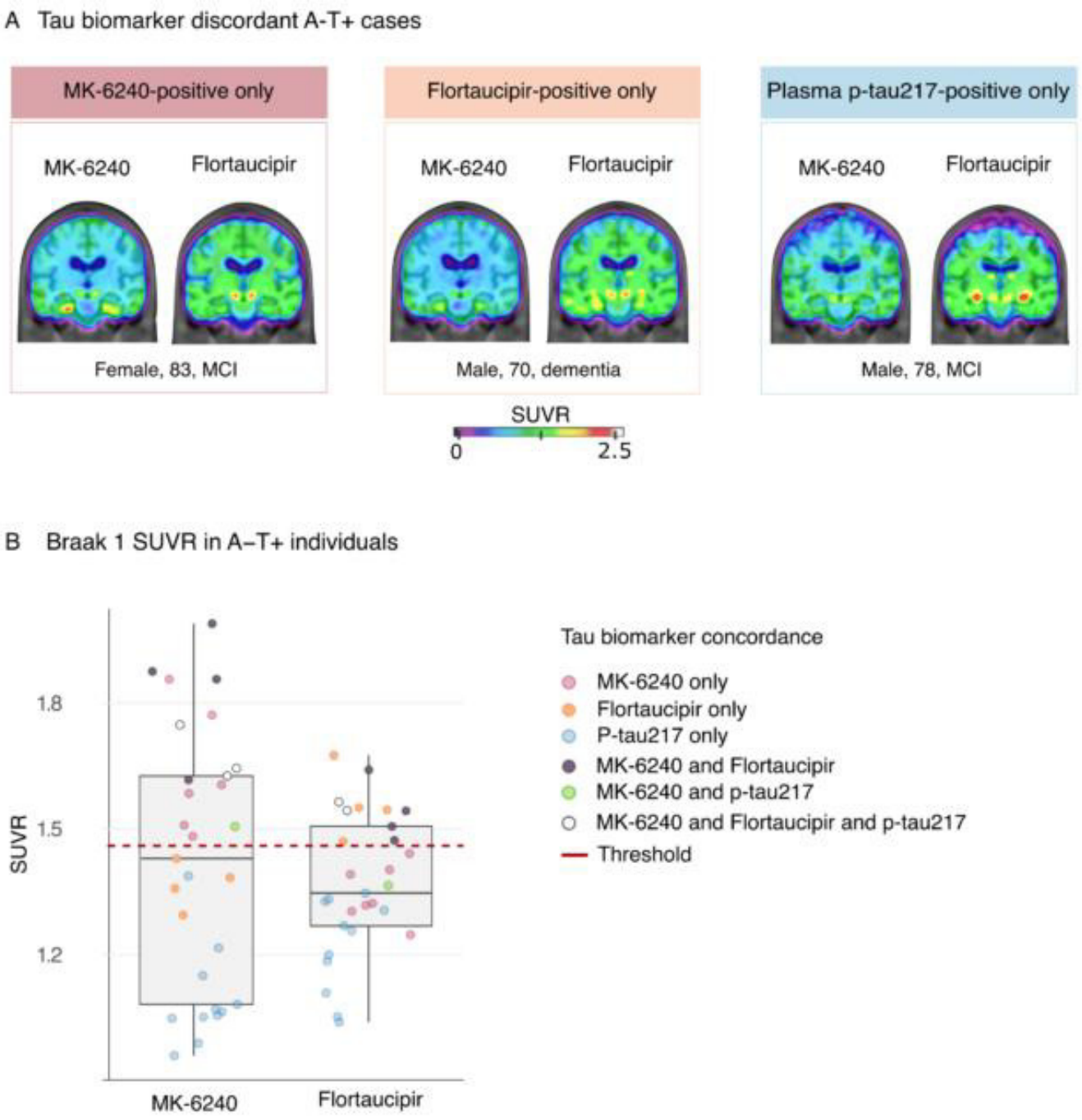


Figure 3. **Tau biomarker discordant cases of A-T+.** (**A**) Parametric maps display SUVR values in amyloid negative (A-) cases where the subject was classified as tau positive (T+) with MK-6240 only (**left**), Flortaucipir only (**center**) or plasma p-tau217 only (**right**). (**B**) Box plots show the SUVR values in Braak 1 region with MK-6240 (**left**) and Flortaucipir (**right**). Each colored circle represents individual SUVR values categorized by the biomarker that defined tau positivity for that subject. The red dashed line indicates the tau positivity threshold (MK-6240: 1.463; Flortaucipir: 1.465)

Our preliminary analysis revealed low concordance among A-T+ cases when determined using MK-6240, Flortaucipir, and plasma p-tau217. Larger studies and longitudinal analyses are necessary to ascertain the pathological trajectories of A-T+ individuals with varying tau biomarker profiles.

Keywords: tau PET, plasma p-tau217, PART

151 Longitudinal rate of change in CSF biomarkers is associated with subsequent Tau PET burden in Braak stages I and II: Findings from the BIOCARD study

Nisha Rani[1], Abhay Moghekar[2], Daniel D. Callow[1], Kylie H Alm[1], Corinne Pettigrew[2], Anja Soldan[2], Michael Miller[3], Jiangxia Wang[4], Marilyn Albert[2], Arnold Bakker[1,2]

[1]*Department of Psychiatry and Behavioral Sciences, Johns Hopkins University School of Medicine, Baltimore, MD, US*
[2]*Department of Neurology, Johns Hopkins School of Medicine, Baltimore, MD, US*
[3]*Department of Biomedical Engineering, Johns Hopkins University, Baltimore, MD, US*
[4]*Department of Biostatistics, Johns Hopkins School of Public Health, Baltimore, MD, US*

Alzheimer's disease (AD) is characterized by the accumulation of amyloid-beta (Aβ) and tau in the brain, years before the onset of cognitive symptoms. Understanding the association between early cerebrospinal fluid (CSF) biomarker changes and subsequent tau pathology based on positron emission tomography (PET) can provide critical insights for early detection and intervention. This study investigates whether longitudinal changes in CSF AD biomarkers are associated with tau deposition in medial temporal lobe (MTL) regions reflecting Braak stages I and II. Analyses included 121 BIOCARD study participants who were cognitively unimpaired at baseline (mean age 57 years). Current tau burden was measured by FMK-6240 PET, and prior levels and trajectories of change in CSF AD biomarkers were measured with p-tau181, total tau (t-tau), and Aβ42/Aβ40 (Lumipulse assay), collected approximately bi-annually over a mean of 12.8 years prior to the tau PET scan. Linear mixed-effect models examined how baseline levels and rates of change in these CSF markers relate to tau PET burden, covarying for age, sex, education, APOE4 genotype, and amyloid positivity. Results indicate significant associations between higher tau PET burden in Braak stages I and II and elevated baseline levels of p-tau181 (β=0.38, p<.001; β=0.23, p<.001) and t-tau (β=0.32, p<.001; β=0.19, p<.001), as well as lower Aβ42/Aβ40 (β=-0.22, p=.002; β =-0.13, p=.001). Additionally, steeper increases in p-tau181 and t-tau over time were associated with greater tau burden in Braak stages I (β=0.009, p=.032; β=0.013, p=.001) and II (β=0.006, p=.024; β=0.008, p=.001). These findings suggest that tau PET burden is preceded by alterations in CSF AD biomarker measures, and that early increases in measures of CSF tau are associated with future MTL tau deposition. This study extends our understanding of the relationship between CSF and PET measures for tracking AD progression.

Keywords: CSF fluid biomarker, Medial temporal lobe, 11C-PIB PET, 18F-MK6240 PET, Braak stages

152 Head-to-head comparison of four tau-PET tracers for in vivo Braak staging: the HEAD Study

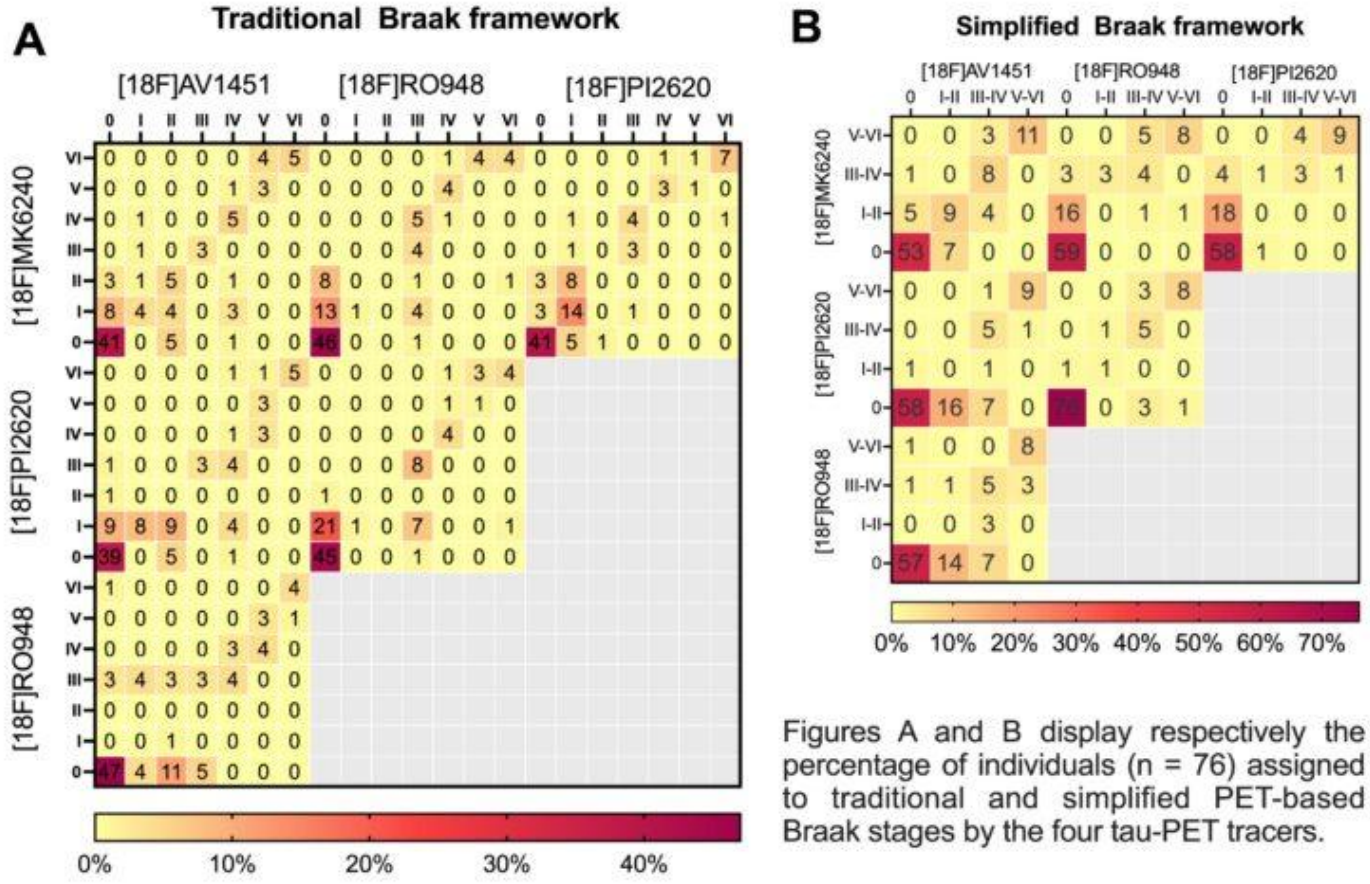
Arthur Cassa Macedo[1], Nesrine Rahmouni[1], Cecile Tissot[2], Joseph Therriault[1], Stijn Servaes[1], Yi-Ting Wang[1], Lydia Trudel[1], Etienne Aumont[1], Brandon Hall[1], Tevy Chan[1], Yansheng Zheng[1], Firoza Z Lussier[3], Pamela CL Ferreira[3], Bruna Bellaver[3], Guilherme Povala[3], Belen Pascual[4], Brian Gordon[5], Val Lowe[6], Hwamee Oh[7], David Soleimani-Meigooni[8], Suzanne Baker[2], Tharick Pascoal[3], Pedro Rosa-Neto[1]

[1]*Department of Neurology and Neurosurgery, McGill University, Montreal, QC, CA*
[2]*Lawrence Berkeley National Laboratory, Berkeley, CA, US*
[3]*Department of Psychiatry, University of Pittsburgh, Pittsburgh, PA, US*
[4]*Department of Neurology, Houston Methodist Research Institute, Houston, TX, US*
[5]*Department of Radiology, Washington University in St. Louis, St. Louis, MO, US*
[6]*Department of Radiology, Mayo Clinic, Rochester, MN, US*
[7]*Department of Psychiatry and Human Behavior, Brown University, Providence, RI, US*
[8]*Memory and Aging Center, University of California San Francisco, San Francisco, CA, US*

Background: Tau-PET tracers allow for *in vivo* Braak staging of individuals in the Alzheimer's disease (AD) continuum. The agreement of different tracers for *in vivo* Braak staging remains unclear. Therefore, we performed a head-to-head comparison of Braak staging using first- and second-generation tau-PET tracers.

Methods: We assessed 42 cognitively impaired and 34 cognitively unimpaired participants (mean [SD] age 67.9 [7.7] years) with four tau-PET tracers ([18F]MK6240, [18F]AV1451, [18F]RO948, and [18F]PI2620) at McGill University, as part of the HEAD study. We calculated standardized uptake value ratio (SUVR) in Braak-like regions of interest (ROI) for each ligand and investigated their Spearman's correlation. Thresholds defined the presence of tauopathy in each Braak ROI, which we used to assign a Braak stage to each participant (Fig.1). Finally, we assessed the agreement between the Braak staging provided by each tracer for the traditional and simplified frameworks (i.e. considering merged Braak ROIs).

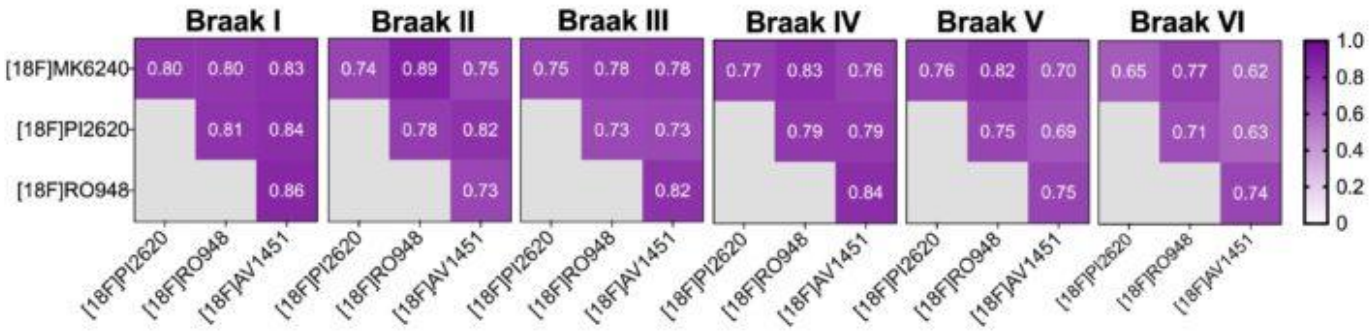
Figure 1. Proportion of participants assigned to each Braak stage by different tau-PET tracers



Figures A and B display respectively the percentage of individuals (n = 76) assigned to traditional and simplified PET-based Braak stages by the four tau-PET tracers.

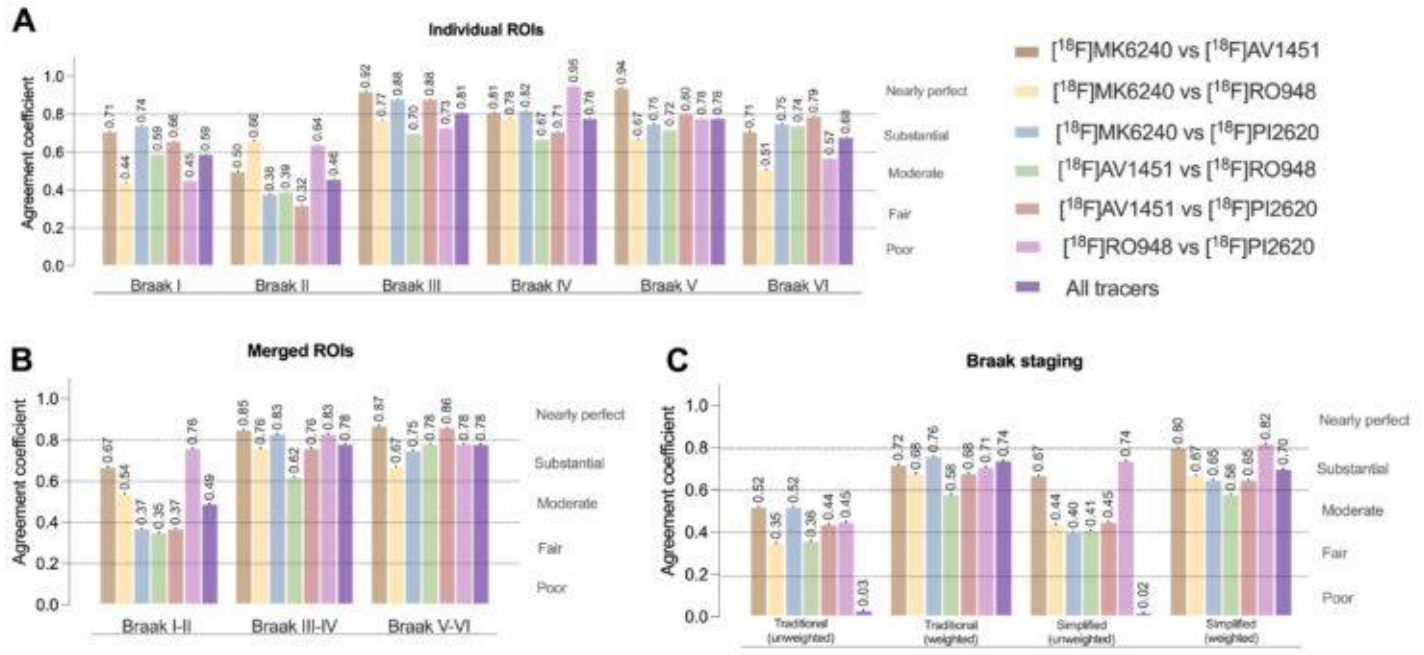
Results: In all Braak ROIs, we found positive correlations between the SUVR values of the four tracers (Fig.2). The strongest correlation was between [18F]MK6240 and [18F]RO948 in Braak II (r=0.89), and the weakest between [18F]MK6240 and [18F]AV1451 in VI (r=0.62). At the ROI level, the worst agreement coefficients were observed in Braak II and I-II, and the best in Braak III (Fig.3A-B). Unweighted agreement among the four tracers regarding the latest abnormal stage was poor (Fig.3C). For both frameworks, weighted agreement was substantial when considering all tracers. Pairwise weighted agreement varied from moderate to substantial in the traditional and from moderate to nearly perfect in the simplified framework.

Figure 2. SUVR values from four different tau-PET tracers show positive correlations across Braak regions



The heatmaps display the Spearman's rho correlation coefficients from the associations between SUVR values obtained in Braak regions with four different tau-PET tracers. All associations are statistically significant (p<.0001).

Figure 3. Braak staging agreement among the four tau-PET tracers



Figures A and B display respectively the agreement coefficients for the presence of tauopathy (tau-PET positivity) in individual (A) and merged (B) Braak regions. In A and B, agreement coefficients were calculated with Cohen's Kappa for pairwise comparisons and with Fleiss Kappa for the comparison among all tracers. Figure C shows the agreement cofficients for the Braak stage assigned to participants, according to both the traditional and simplified Braak staging framework. Both unweighted and weighted Cohen's Kappa coefficients were obtained for pairwise comparisons. The agreement between the four tracers was assessed with Fleiss Kappa, in the unweighted analysis, and with Krippendorff's alpha, in the weighted analysis. Linear weighting was applied in all weighted analyses.

Conclusions: Inter-tracer agreement is especially low in early Braak regions. The four tracers presented substantial ordinal agreement and poor categorical agreement for *in vivo* Braak staging. Slight improvements in agreements were achieved with the simplified framework, as observed in histopathological staging.

Keywords: Braak staging; positron emission tomography; neurofibrillary tangles; Alzheimer's disease; staging

153 Astrogliosis in the early-stages of Alzheimer's disease

Vincent Dore[1,2], Pierrick Bourgeat[1], Ryuichi Harada[3,4], Shozo Furumoto[5], Rachel Mulligan[2], Ying Xia[1], Ishara Paranawithana[1,2], Simon Laws[6], Azadeh Feizpour[2,7], Svetlana Bozinovski[2], Kun Huang[2], Brian J. Lopresti[8], Milos D. Ikonomovic[8,9,10], Jurgen Fripp[1], Nobuyuki Okamura[11], Christopher C. Rowe[2,7], Victor L. Villemagne[2,8]

[1]*The Australian e-Health Research Centre, The Commonwealth Scientific and Industrial Research Organisation (CSIRO), Melbourne, AU*
[2]*Department of Molecular Imaging and Therapy, Austin Health, Melbourne, AU*
[3]*Department of Pharmacology, School of Medicine, Tohoku University, Sendai, JP*
[4]*Institute of Development of Aging and Cancer, Tohoku University,, Sendai, JP*
[5]*Cyclotron and Radioisotope Center, Tohoku University, Sendai, JP*
[6]*School of Medical and Health Sciences, Edith Cowan University, Perth, AU*
[7]*Florey Institute of Neurosciences and Mental Health, University of Melbourne, Melbourne, AU*
[8]*Department of Psychiatry, University of Pittsburgh, Pittsburgh, PA, US*
[9]*Department of Neurology, University of Pittsburgh, Pittsburgh, PA, US*
[10]*Geriatric Research Education and Clinical Center, VA Pittsburgh Healthcare System, Pittsburgh, PA, US*
[11]*Division of Pharmacology, Faculty of Medicine, Tohoku Medical and Pharmaceutical University, Sendai, JP*

Background: Monoamine Oxidase-B (MAO-B) is overexpressed in reactive astrocytes, playing a crucial role in neurodegeneration. Recently, increased binding of the PET MAO-B tracer ^{18}F-SMBT-1 has been shown in preclinical Alzheimer's disease (AD) stages. However, the regional distribution and effect on Aβ of abnormal ^{18}F-SMBT-1 binding along the AD continuum remains unclear.

Method: 133 Cognitively Unimpaired (CU), 24 A+ Mild Cognitive Impairment (MCI), and 20 A+ AD subjects underwent PET imaging with ^{18}F-NAV4694, ^{18}F-MK6240, and ^{18}F-SMBT-1. Aβ and tau PET SUVR were transformed into Centiloid (CL) and CenTauR (CTR) using CapAIBL. A+ was defined as >25CL and T+ >14CTR in the Meta-Temporal. ^{18}F-SMBT-1 scans were spatially normalised using MR-based CapAIBL, scaled to the cerebellar cortex and several cortical regions sampled. The relationship between ^{18}F-SMBT-1 binding and Aβ accumulation was assessed in a subset of 74 CU A-.

Results: Distinct regional ^{18}F-SMBT-1 binding was observed across brain regions (Figure 1). ^{18}F-SMBT-1 binding was higher in CU A+ compared to the CU A- in most regions, while binding in A+ MCI/AD either remained higher (in parietal/cingulate/occipital) or decreased (in frontal/caudate/putamen). Higher ^{18}F-SMBT-1 binding was also significant in CU A+ T- (n=32). In CU A- participants with high ^{18}F-SMBT-1 retention, significantly higher Aβ accumulation rates were observed compared to low ^{18}F-SMBT-1 (1.04CL/yr vs 0.34CL/yr, respectively, p=0.01) (Figure 2). Furthermore, 88% of CU A- individuals with high ^{18}F-SMBT-1 were classified as Aβ accumulators.

Conclusion: ^{18}F-SMBT-1 facilitates quantitative assessment of regional differences in reactive astrogliosis across the AD continuum, as well as longitudinal change. Elevated ^{18}F-SMBT-1 in CU A- predicted Aβ accumulation, highlighting the potential of ^{18}F-SMBT-1 as a prognostic marker in early-stage AD while suggesting modulation of astrocytic function may be a target for AD prevention and treatment.

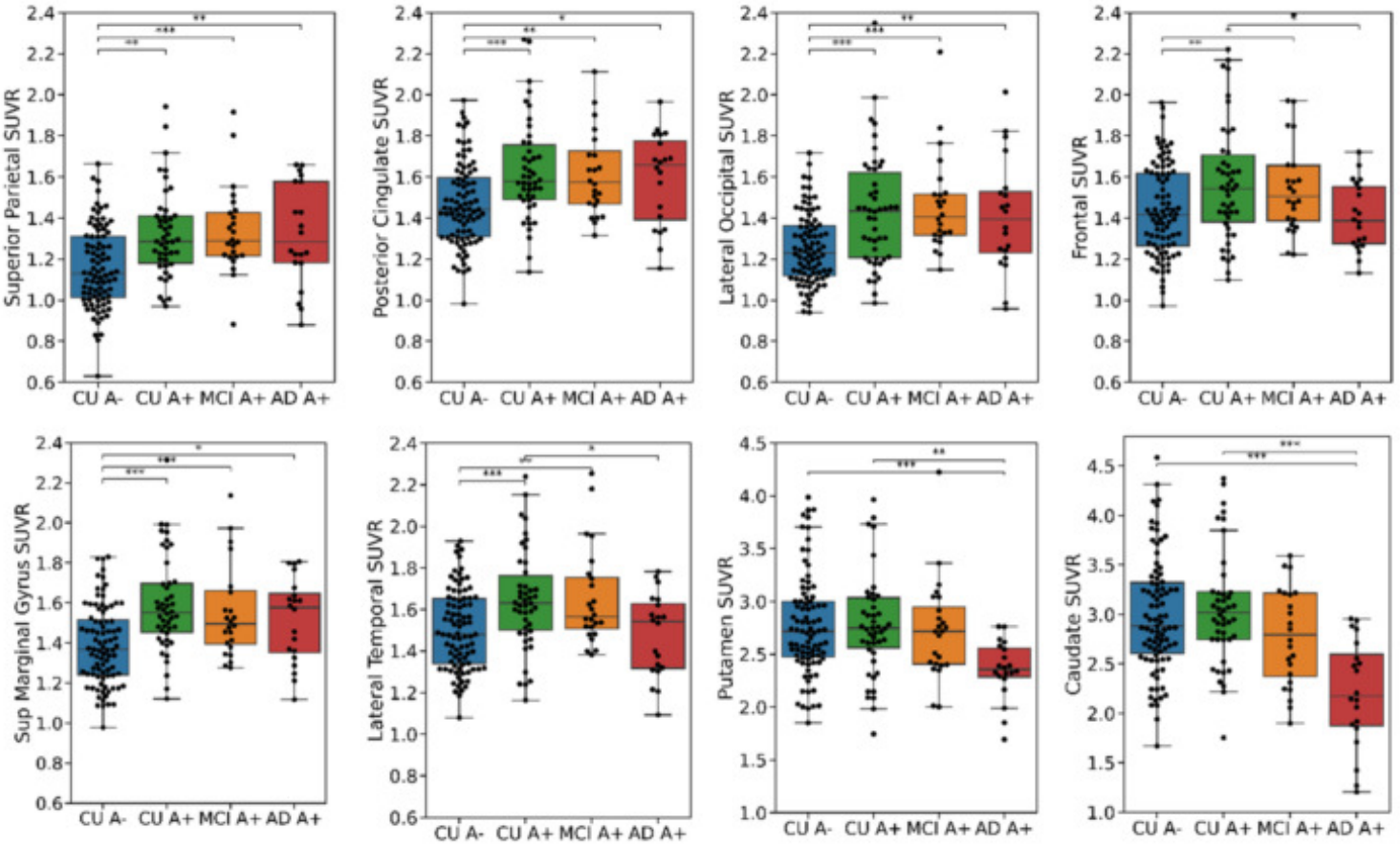


Figure 1: Boxplot showing regional SMBT-1 SUVR for different clinical groups (CU-: cognitively unimpaired Aβ-, CU+: cognitively unimpaired Aβ+, MCI: mild cognitive impairment Aβ+, AD+: Alzheimer's disease Aβ+).

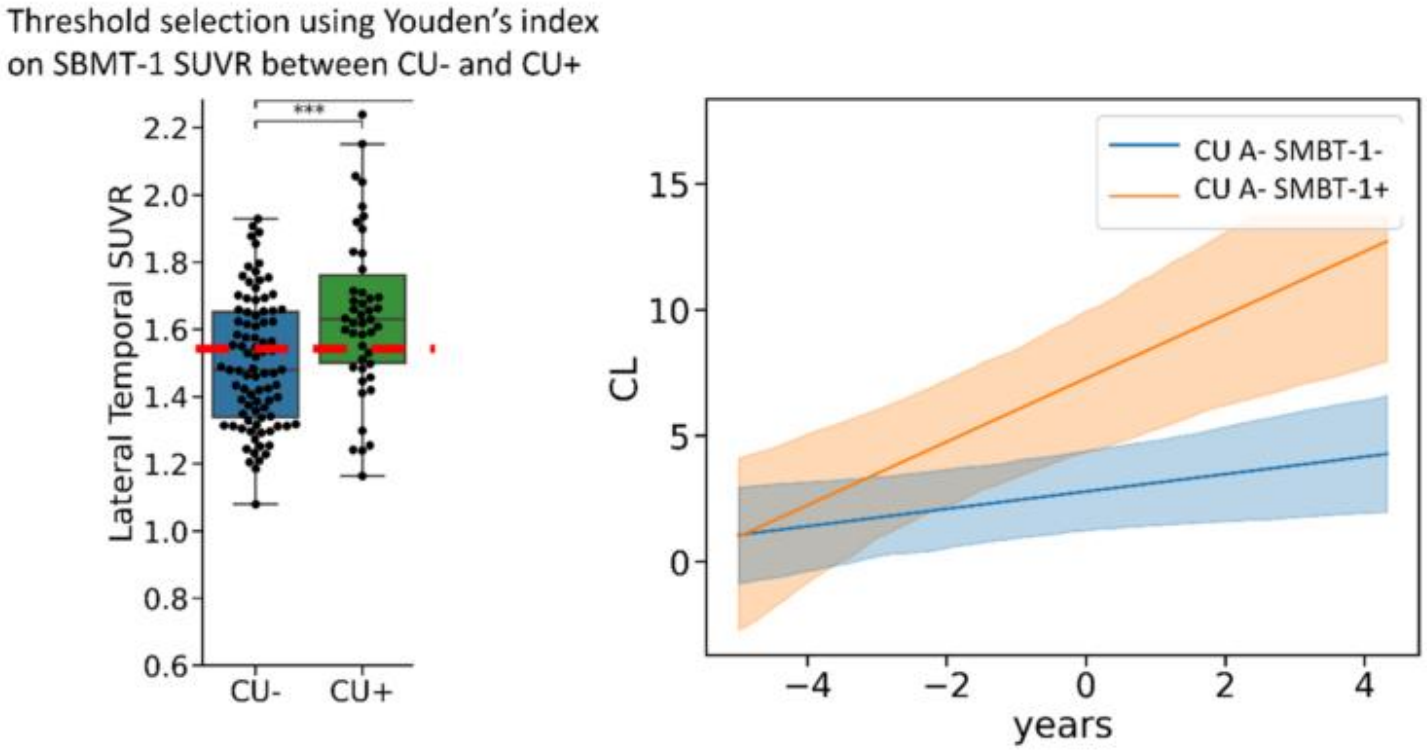


Figure 2: Cognitively unimpaired individual without abnormal Aβ pathology but with elevated SMBT-1 SUVR, accumulate Aβ at a higher rate. Red dashed line shows the cut-off for ^{18}F-SMBT1 positivity in the Lateral Temporal. ^{18}F-SMBT-1 scans were performed at year 0 on the x-axis, with negative years indicative of Aβ PET scans acquired before ^{18}F-SMBT-1.

	CU	MCI A+	AD A+
sample size	133	24	20
Age	75.5 (6.2)	75.0 (7.8)	73.0 (6.7)
Gender, N male	62 (46.6%)	18 (75.0%)*	12 (60.0%)
APOE, N E4	53 (40.5%)	17 (73.9%)*	15 (75.0%)*
CDR.SB	0.0 (0.0)	1.0 (1.6)*	6.0 (3.6)*†
Hippocampal Vol	2.9 (0.3)	2.9 (0.3)	2.5 (0.4)*†
Cortical GM	456.5 (20.7)	447.7 (18.1)	428.9 (16.5)*†
Centiloid	30.7 (46.3)	94.5 (41.4)*	124.6 (28.3)*†
Ab+, N>25CL	46 (34.6%)	24 (100.0%)*	20 (100.0%)*
T+, N>14CTR	16 (12.0%)	11 (46.0%)*	19 (95.0%)*

*Table1: Demographic table, * significantly different from CU, † significantly different from MCI*

Keywords: MAO-B, Astrogliosis, SMBT-1, preclinical, neuroinflammation

154 Identifying an optimal aβ cutoff point for progression from mild cognitive impairment to Alzheimer's disease: comparing cognitive performance and aβ pet insights

Rosita Shishegar[1,2], Pierrick Bourgeat[3], Vincent Dore[1], Simon M. Laws[6], Tenielle Porter[6], Michael Weiner[4], Colin L. Masters[5], Paul Maruff[8], Hamid R. Sohrabi[9], Jurgen Fripp[3], Victor L. Villemagne[7], Christopher Rowe[10]

[1]*The Australian e-Health Research Centre, CSIRO, Melbourne, Australia, Melbourne, AU*
[2]*School of Psychological Sciences and Turner Institute for Brain and Mental Health, Monash University, Melbourne, Australia, Melbourne, AU*
[3]*The Australian e-Health Research Centre, CSIRO, Brisbane, Australia, Brisbane, AU*
[4]*Center for Imaging of Neurodegenerative Diseases, University of California-San Francisco, San Francisco, CA, USA;, San Francisco, CA, US*
[5]*Florey Institute of Neuroscience and Mental Health, The University of Melbourne, Parkville, VIC, Australia, Melbourne, AU*
[6]*Centre for Precision Health, Edith Cowan University, Joondalup, Western Australia;, Joondalup, AU*
[7]*Department of Psychiatry, University of Pittsburgh, Pittsburgh, USA, Pittsburgh, PA, US*
[8]*Cogstate Ltd, Melbourne, VIC, Australia, Melbourne, AU*
[9]*Centre for Healthy Ageing, Health Futures Institute, Murdoch University, Murdoch, Western Australia, Australia, Murdoch, AU*
[10]*Department of Medicine, Austin Health, Heidelberg, VIC, Australia, Heidelberg, AU*

Objectives: To identify the optimal Aβ PET threshold for distinguishing fast progressors to Alzheimer's disease (AD) in individuals with mild cognitive impairment (MCI) and assess whether a cutoff based on Mini-Mental State Examination (MMSE) performance can improve or substitute for the Aβ PET cutoff. This research will refine risk stratification in MCI and guide clinical decision-making regarding early therapeutic interventions.

Methods: We included 690 MCI participants with CDR 0.5 from two cohorts, followed for up to 7 years. Data from AIBL (N=167) and ADNI (N=523) were analyzed using Cox proportional-hazards models, adjusted for age, sex, years of education, and *APOE*-ε4 status, with the event of interest being progression to CDR 1 (plus β-amyloid positivity, Aβ>20 CL). Optimal thresholds for MMSE (27) and Aβ (44 CL) were selected to maximize hazard ratios (HR) at 3 years, categorizing participants into low-risk and high-risk groups based on cognitive performance (188 participants, 27%, MMSE<27 as low-cognition) and Aβ load (364 participants, 52%, as high-Aβ, with 32% overlap with the low-cognition group).

Results: Both 44 CL and MMSE=27 thresholds showed comparable hazard ratios (HR=1.47 and 1.50, respectively; Figure 1). However, the MCI high-cognition group had a significantly higher risk of progressing to AD (risk probability (RP)=1-survival probability; RP=0.10±0.04) than MCI low-Aβ (RP=0.03±0.02). Combining both cutoffs improved risk stratification: 38% of MCI low-cognition, high-Aβ progressed to AD within 3 years (46% survival), while only 6 of 312 of the MCI high-cognition low-Aβ progressed to AD (99% survival).

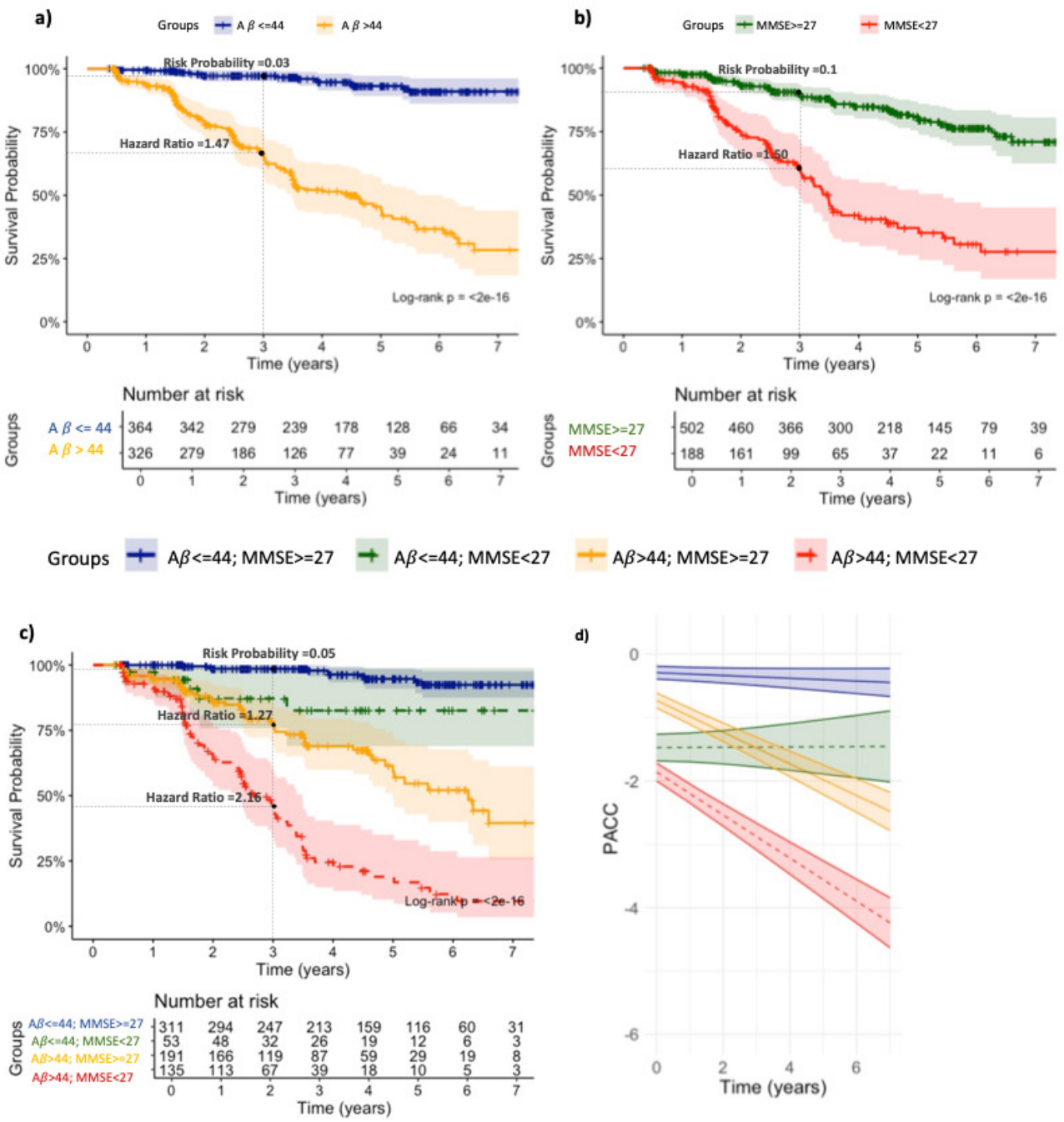


Figure 1. (a-c) Survival curves illustrating the progression from Mild Cognitive Impairment (MCI, CDR=0.5) to Alzheimer's Disease (AD, confirmed by CDR global score=1 and β-amyloid positivity, Aβ>20 CL). Subjects are grouped by: (a) baseline cognitive performance, (b) baseline Aβ status, and (c) a combination of both cognitive performance and Aβ status at baseline. The MMSE score is presented as an example of cognitive performance; similar or even worse results were observed for other cognitive assessments, such as CVLT. (d) Cognitive trajectories over time, represented by harmonized PACC scores from linear mixed models, stratified by combined groups. The effect size for low-cognition, high-Aβ MCIs compared to the high-cognition, low-Aβ group is 0.76, with an annual rate of decline of 0.34 scores.

Conclusion: Cognitive performance alone is not a sufficient substitute for Aβ cutoffs in predicting MCI-to-AD progression. However, binary classification based on Aβ can be improved by combining Aβ with MMSE cutoffs to further stratify the MCI population, providing greater prognostic information on an individual level and aiding in the design of clinical trials and therapeutic interventions for prodromal AD.

Keywords: Clinical trials, MCI-to-AD progression, Aβ PET cutoff, Fast progressors

155 Amyloid modifies the association between late-life BMI and longitudinal cognition in cognitively unimpaired individuals

Wai-Ying Wendy Yau[1,2], Rema Raman[3], Shunran Wang[3], Neelum Aggarwal[4], Adam Brickman[5], Jasmeer Chhatwal[1,2,6], Petrice Cogswell[7], Jonathan Graff-Radford[7], Jay Pillai[7], Michael Rafii[3], Paul Aisen[3], Reisa Sperling[1,2,6], The A4 and Learn Study Teams[8]

[1]*Massachusetts General Hospital, Boston, MA, US*
[2]*Harvard Medical School, Boston, MA, US*
[3]*University of Southern California, San Diego, CA, US*
[4]*Rush University Medical Center, Chicago, IL, US*
[5]*Columbia University, New York, NY, US*
[6]*Brigham and Women's Hospital, Boston, MA, US*
[7]*Mayo Clinic, Rochester, NY, US*
[8]*Alzheimer Clinical Trials Consortium, https://www.actcinfo.org/a4-Study- Team-Lists/, US*

Background: Midlife obesity is linked to increased risk of Alzheimer's disease (AD), but the relationship between late-life obesity and AD is less clear. Given growing interest in combination prevention trials targeting amyloid and vascular risk factors in older individuals, it is critical to understand how late-life BMI and amyloid burden may interact to influence cognitive decline.

Methods: We examined 1668 baseline cognitively unimpaired participants across A4 and LEARN (age 71.5±4.7, 59.9% female, amyloid 47±40 Centiloid, BMI 28±5). Cognition was assessed longitudinally (4.1±1.5 years) using the Preclinical Alzheimer Cognitive Composite (PACC). We examined for interactive effects between baseline BMI and amyloid burden (18F-Florbetapir PET) on cross-sectional (linear regression) and longitudinal (natural cubic spline model) cognition, adjusting for age, sex, education, APOE4, cognitive test version, and study/treatment.

Results: At baseline, higher BMI was associated with lower PACC scores (Standardized β=-0.13, p=0.02; Figure 1), with no interaction between BMI and amyloid on baseline cognition (p=0.70). Longitudinally, we identified a significant interaction between baseline BMI and amyloid burden on cognitive decline (p<0.001). We visualized this interaction across representative levels of BMI and amyloid burden (Figure 2). When baseline amyloid burden was low, lower/normal BMI was associated with a more favorable PACC trajectory. By contrast, when baseline amyloid was high, lower/normal BMI was associated with faster cognitive decline.

Conclusion: In cognitively unimpaired older adults, lower BMI was associated with better baseline cognition irrespective of amyloid burden, suggesting obesity has a negative impact on cognitive aging. Longitudinally, the relationship between BMI and cognitive decline was modified by baseline amyloid. Lower/normal BMI was associated with accelerated rates of cognitive decline as amyloid burden increases, potentially reflecting heightened physiological vulnerability to underlying AD pathology. Taken together, our results suggest that targeting obesity as a prevention strategy for late-life cognitive decline may be most effective before substantial amyloid accumulation.

Table 1. Participant characteristics

	Total	LEARN	A4 Placebo	A4 Solanezumab
	(N=1668)	(N=521)	(N=583)	(N=564)
Age (y)				
Mean (SD)	71.5 (4.7)	70.5 (4.3)	71.9 (5.0)	72.0 (4.7)
Sex				
Female	999 (59.9%)	318 (61.0%)	352 (60.4%)	329 (58.3%)
Male	669 (40.1%)	203 (39.0%)	231 (39.6%)	235 (41.7%)
Education (y)				
Mean (SD)	16.6 (2.7)	16.8 (2.6)	16.6 (2.9)	16.6 (2.7)
APOE e4				
No	402 (77.5%)	241 (41.3%)	231 (41.0%)	874 (52.5%)
Yes	117 (22.5%)	342 (58.7%)	333 (59.0%)	792 (47.5%)
Baseline Amyloid (Centiloid)				
Mean (SD)	46.8 (40.1)	4.3 (12.5)	65.9 (32.1)	66.2 (33.5)
Baseline BMI				
Mean (SD)	27.6 (4.8)	27.5 (5.1)	27.2 (5.0)	27.5 (5.0)

Figure 1. Higher BMI was associated with lower baseline cognition irrespective of amyloid burden. Linear regression revealed no BMI*amyloid interaction on baseline PACC scores (Standardized β=-0.02 [-0.13 to 0.09], p=0.70). Higher BMI was independently associated with lower baseline PACC (Standardized β=-0.13 [-0.24 to -0.02], p=0.02). For visualization, the estimated PACC scores based on representative levels of amyloid burden are presented (25th percentile = 13 Centiloid, 50th percentile = 42 Centiloid, and 75th percentile = 74 Centiloid). Aβ = β-amyloid; CL = Centiloid; PACC = Preclinical Alzheimer Cognitive Composite.

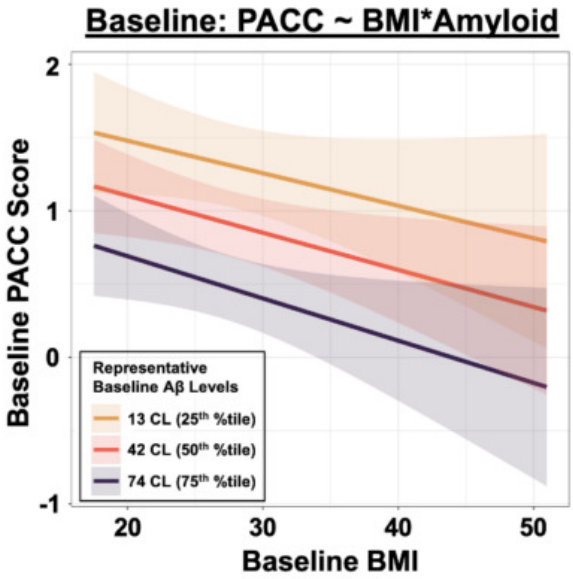
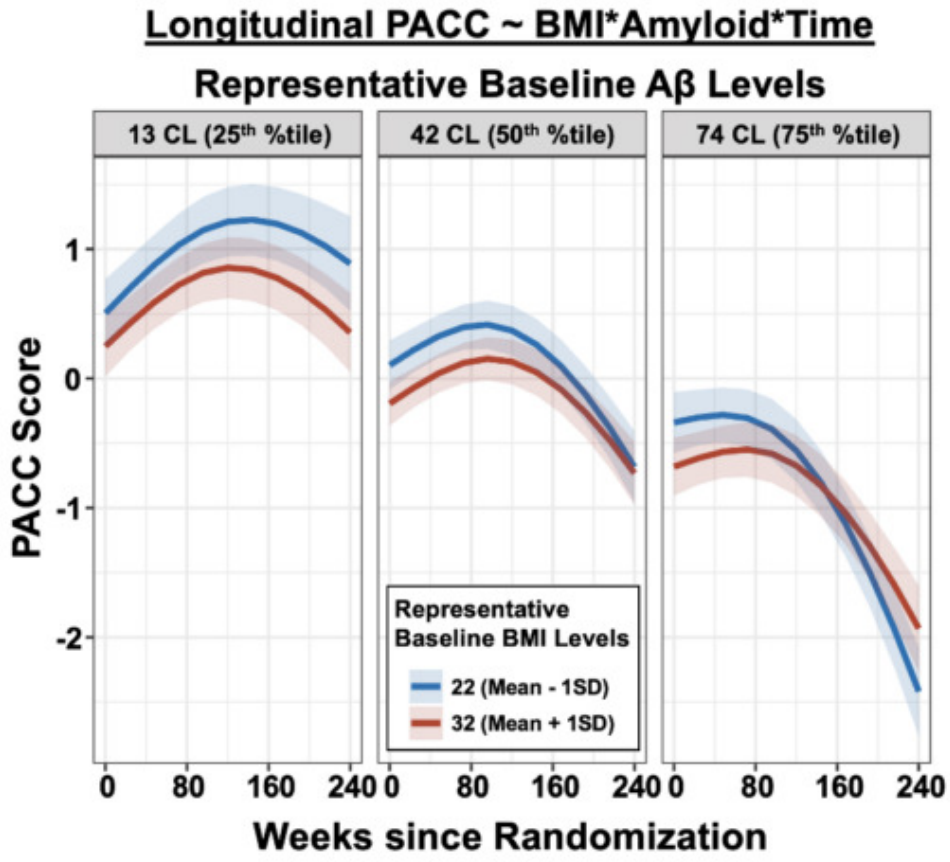


Figure 2. Significant BMI by amyloid interaction on longitudinal cognitive decline. Natural cubic spline model revealed a significant interactive effect of baseline BMI and amyloid burden on longitudinal PACC decline ($p<0.001$). For visualization, the estimated PACC trajectories based on representative levels of baseline BMI and amyloid burden are presented. Low and high BMI are represented by -1 and +1 SD relative to the mean (low = 22, high = 32). Low, moderate and high amyloid burden are represented by 25th (13 Centiloid), 50th (42 Centiloid), and 75th (74 Centiloid) percentiles of baseline amyloid burden in the cohort. As baseline amyloid burden increases, lower BMI was associated with accelerated PACC decline over time. Aβ = β-amyloid; CL = Centiloid; PACC = Preclinical Alzheimer Cognitive Composite.



Keywords: Preclinical AD, BMI, Amyloid, Obesity, Cognitive decline

156 Amyloid spatial extent captures early tau burden and cognitive deficits, measured by PACC and digital clock drawing test, in preclinical Alzheimer's disease

Jackson Thompson[1], Jessie Fanglu Fu[1,2], Michelle Farrell[1], Emma Thibault[1], Elliott Slade[1], Grace Del Carmen Montenegro[1], Talia Robinson[1], Roosmarijn Jutten[1], Randall Davis[4], Dana Penney[3], Marina Rodriguez Alonso[1], Reisa Sperling[1], Dorene Rentz[1], Julie Price[1,2], Keith Johnson[1]

[1]*Massachusetts General Hospital, Harvard Medical School, Boston, MA, US*
[2]*Athinoula A. Martinos Center for Biomedical Imaging, Charlestown, MA, US*
[3]*Lahey Hospital and Medical Center, Burlington, MA, US*
[4]*Massachusetts Institute of Technology, Cambridge, MA, US*

Background: A 2-min digital clock drawing test (DCTclock) was shown to detect early Ab and tau burden in preclinical AD. Spatial extent (EXT) measures the spread of amyloid-b (Ab) and is potentially more sensitive to early Ab burden than the traditional measure of neocortical Ab level. We explored the relationship between DCTclock and PACC5 performance with amyloid-b (Ab) spread using EXT and inferior temporal (IT)/ entorhinal (ERC) FTP.

Methods: 212 cognitively normal older adults underwent baseline cognitive assessments (DCTclock and PACC5), [^{11}C]Pittsburgh Compound B (PiB, DVR) PET, and 186 underwent Flortaucipir (FTP, SUVR) PET (**Table.1**). Ab EXT was calculated as the percentage of Ab-vulnerable neocortex that is PiB+. Participants were separated into 3 EXT groups: EXT- (EXT<7.2%, no Ab), EXT+ (7.2%<EXT<95.6%, early spread), EXT++ (EXT<95.6%, widespread Ab). ANOVA examined EXT group differences in DCTclock and PACC5, corrected for age, education and sex. A series of linear regressions examined the associations between EXT, inferior temporal (IT)/ entorhinal (ERC) FTP, DCTclock, and PACC5.

Results: Both PACC5 and DCTclock showed significant differences between EXT- and EXT++ groups (**Fig.1**). Increasing EXT showed significant association (p=0.0034) with worse DCTclock performance in the EXT+ group. (**Fig.2**). PACC5 scores were significantly associated with IT tau in EXT+ (p<0.001) and EXT++ (p=0.0061), and with ERC tau in EXT+ (p=0.028). Lower DCT scores were linked to IT tau (p=0.0262) and ERC tau (p=0.035) in EXT++.

Conclusion: Ab EXT showed significant association with DCTclock performance in individuals showing early Ab spread but not yet widespread Ab, thus may reflect early deficits in executive function and processing speed. On the other hand, early tau-related cognitive deficits (more memory-related), measured by PACC5, were present in individuals with spreading and widespread Ab. Overall, Ab EXT can potentially provide meaningful measures of early pathological burden reflective of cognitive deficits in preclinical AD.

Characteristic	**Overall**, N = 212[1]	**EXT-**, N = 125[1]	**EXT+**, N = 48[1]	**EXT++**, N = 39[1]
Age	78.59 (6.85)	77.08 (6.93)	81.42 (6.26)	79.97 (5.99)
Education	16.18 (2.91)	16.20 (2.83)	15.96 (3.03)	16.41 (3.08)
Sex				
Female	61%	59%	67%	62%
Male	39%	41%	33%	38%
DCT Score	67.81 (23.44)	73.70 (21.47)	60.97 (23.67)	57.35 (23.83)
PACC5	-0.06 (1.03)	0.23 (0.75)	-0.30 (0.98)	-0.69 (1.46)
Extent (%)	28.48 (40.69)	1.03 (1.99)	42.41 (32.49)	99.31 (1.23)
PiB DVR	1.21 (0.23)	1.07 (0.04)	1.24 (0.12)	1.62 (0.14)
Inferior Temporal FTP PVC	1.53 (0.28)	1.44 (0.14)	1.54 (0.19)	1.81 (0.47)
Entorhinal FTP PVC	1.42 (0.35)	1.30 (0.24)	1.46 (0.24)	1.76 (0.48)
Days Between Clock and PiB Scan	669.23 (687.21)	630.26 (687.26)	759.58 (704.79)	682.90 (671.67)
Days Between Clock and FTP Scan	474.16 (410.48)	466.23 (416.38)	509.46 (406.78)	460.03 (404.62)

[1] Mean (SD); %

Table 1. Population Demographics. Baseline DCTclock tests are paired with the closest PACC5 test and PiB PET scan for which EXT has been calculated. Closest FTP PET scan are chosen to observe cross-sectional data, where the PVC levels are displayed for inferior temporal and entorhinal regions. Aβ burden measured using the PiB DVR levels. First column displays all participants, then separation of groups by EXT- (EXT< 7.2%), EXT+ (7.2% < EXT < 95.6%), and EXT++ (EXT > 95.6%) (Farrell et al., 2024). Mean absolute value between DCT clock test and both PiB scan and FTP scan is calculated and displayed.

Abbreviations: Extent (EXT), Flourtaucipir (FTP), Digital Clock Test (DCT), Preclinical Alzheimer's Cognitive Composite 5 (PACC5), Partial Volume Correction (PVC), Pittsburgh Compound B (PiB), Distribution Volume Ratio (DVR), Amyloid-beta (Aβ)

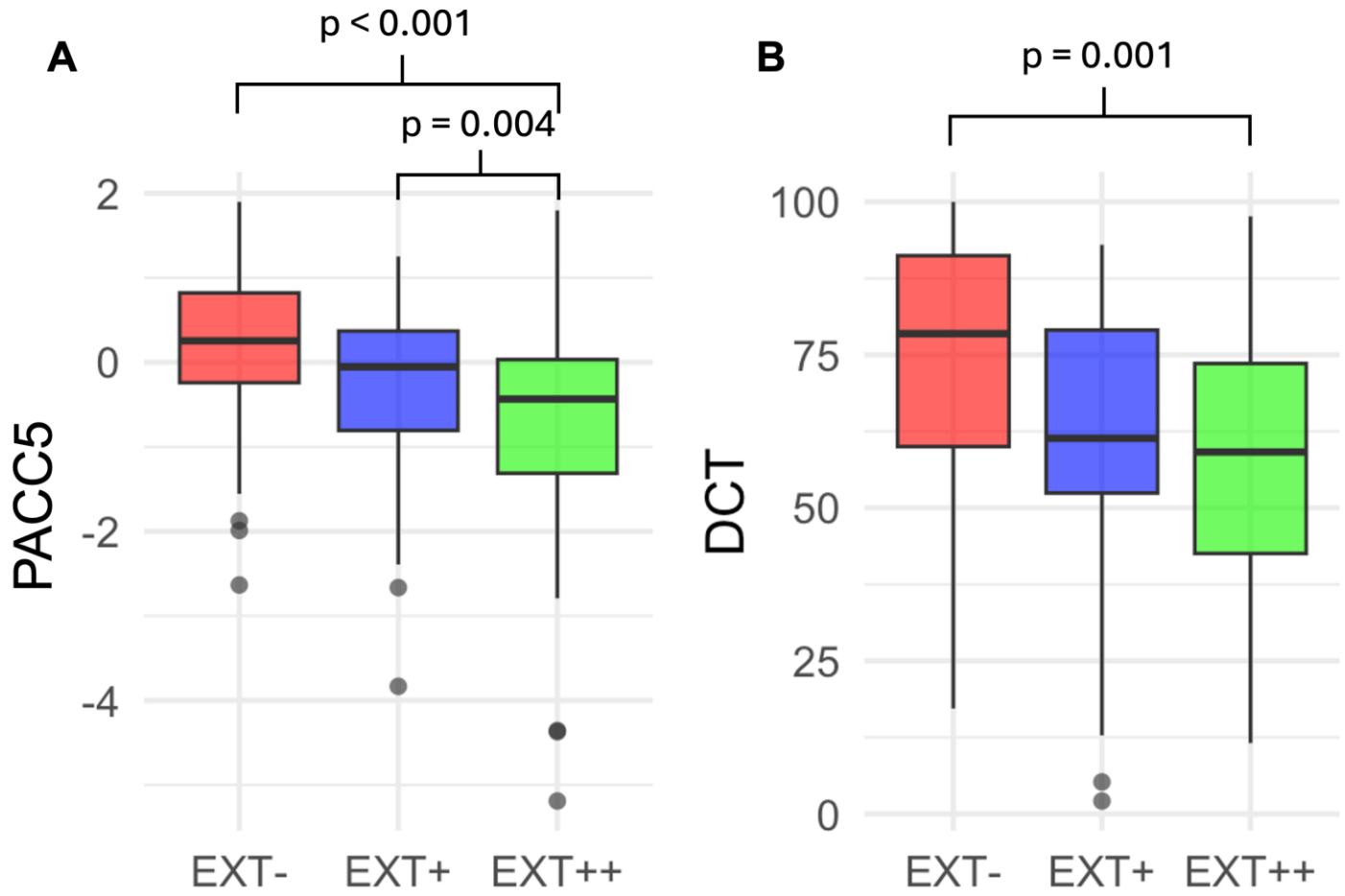


Figure 1. Distribution of PACC and DCT by EXT Group. Box plots show distribution of (A) PACC5 and (B) DCT Summary score across EXT- (EXT < 7.2%), EXT+ (7.2% < EXT < 95.6%), EXT++ (EXT > 95.6%) groups. The central line within each box represents the median score, while the top and bottom of each box correspond to the 25th and 75th percentiles, respectively. The whiskers extend to 1.5 times the interquartile range, and outliers are represented by black points. A one-way ANOVA group comparison (corrected for age, sex, and education) across EXT groups found significant PACC score differences between EXT- and EXT++($p<0.001$) in addition to EXT+ and EXT++($p=0.004$). Significant DCT summary score differences found between EXT- and EXT++ groups ($p=0.001$). P-values not shown are insignificant ($p>0.05$).
Abbreviations: Extent (EXT), Digital Clock Test (DCT), Preclinical Alzheimer's Cognitive Composite 5 (PACC5)

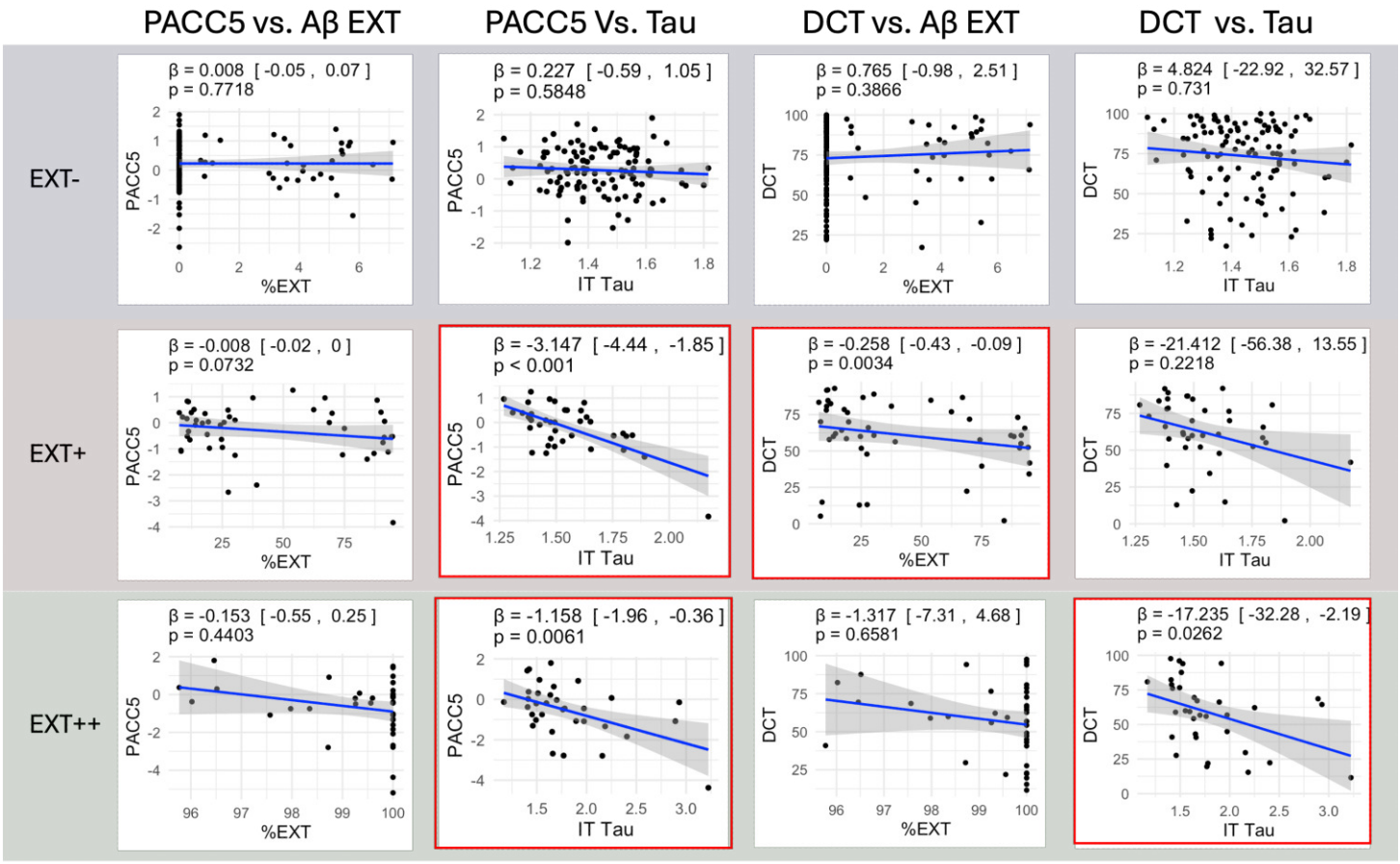


Figure 2. PACC5 and DCT Linear regression analysis with Aβ EXT and Tau burden in each EXT group. Linear regressions comparing PACC5 and DCT Summary score vs EXT and FTP PVC IT Tau in EXT- (blue), EXT+ (red), and EXT++(green). Red boxes highlight significant ($p<0.05$) results (corrected for age, education, and sex). Results suggest that %EXT is a meaningful predictor of DCT EXT+ stage of amyloid spread. Once amyloid spread reaches the EXT++ threshold, tau accumulation is a more meaningful predictor of PACC5 and DCT scores.
Abbreviations: Extent (EXT), Flourtaucipir (FTP), Digital Clock Test (DCT), Preclinical Alzheimer's Cognitive Composite 5 (PACC5), Partial Volume Correction (PVC), Pittsburgh Compound B (PiB), Flourtaucipir (FTP), Amyloid-beta (Aβ), Inferior Temporal (IT)

Keywords: Amyloid Extent, digital clock test, PACC, Alzheimer's disease, tau

157 Findings from dynamic [18F]-MK6240 PET imaging after motion and partial volume corrections

Amal Tiss[1], Kuang Gong[2], Cristina Lois[1], Maeva Dhaynaut[3], Nicolas J. Guehl[3], Georges El Fakhri[3], Keith Johnson[1], Jinsong Ouyang[3]

[1]*Department of Radiology, Massachusetts General Hospital and Harvard Medical School, Boston, MA, US*
[2]*Department of Biomedical Engineering, University of Florida, Gainesville, FL, US*
[3]*Department of Radiology and Biomedical Imaging, Yale University, New Haven, CT, US*

Dynamic PET imaging of the tau tracer [18F]-MK6240 provides a comprehensive view of the tracer distribution. However, the long acquisition time and small size of the regions involved in prodromal Alzheimer's disease can reduce the quantitative accuracy of PET imaging. We investigate the effects of inter- and intra- frame motion and partial volume corrections (II-MC / PVC) on findings from cross-sectional and longitudinal studies.

We partitioned the PET data into frames according to established protocols and corrected intra-frame motion via image-based registration. Additionally, we incorporated a patch-based kernel applied to the MR image into the reconstruction scheme to perform PVC. We obtained a series of II-MC/PVC frames for our proposed method, II-MC frames, and the conventional inter-frame-only MC approach (IO-MC). We investigated the improvement of each correction on a dataset of 55 scans from 33 subjects, including 22 longitudinal studies. Our measured outcomes are DVR and R1 in 15 brain regions using the cerebellum grey matter as the reference region.

In cross-sectional studies, differences in DVR between the II-MC and IO-MC approaches exceeded 5% in 17% of the datapoints. When analyzing the subject-specific data, we found that 51% of subjects exhibited better quantitative results in at least one region. Similarly, when comparing II-MC/PVC to II-MC, 70% of subjects had at least one region with a DVR difference greater than 5%. For R1, II-MC and II-MC/PVC improved results in 15% and 45% of subjects compared to IO-MC and II-MC, respectively. Figure 1 shows the comparisons between the three methods. In longitudinal studies, no statistically significant differences were observed between the methods in the surveyed regions due to the inter-subject variability (Figure 2). Parametric maps for one longitudinal study are shown in Figure 3.

While improvements with II-MC/PVC are subtle, they can impact most of the enrolled subjects.

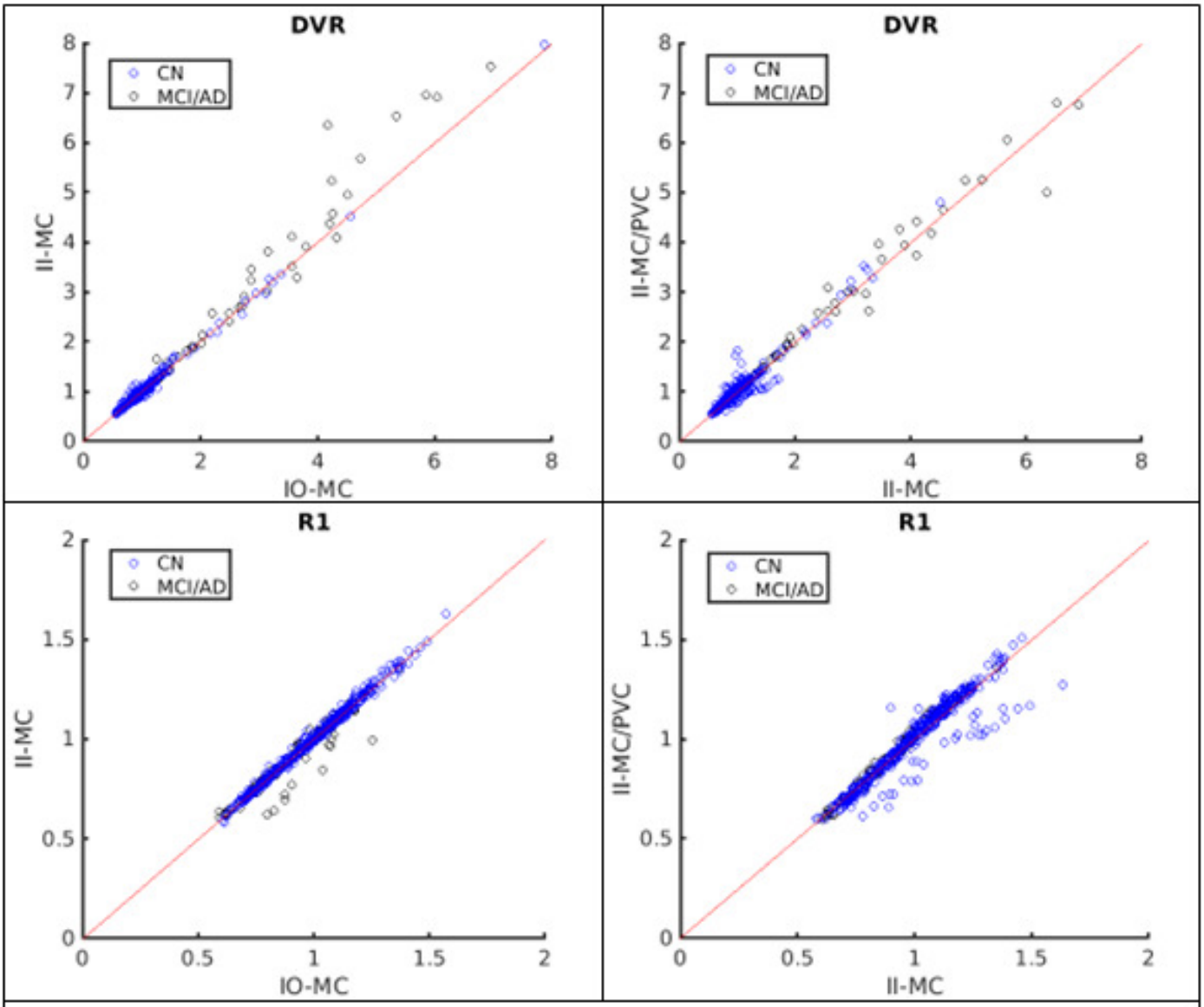


Figure 1: Scatter plots for DVR (top) and R1 (bottom) to compare II-MC vs IO-MC (left) and II-MC/PVC vs II-MC (right). Each point represents one region (N=15) from each subject's first scan (N=33). Datapoints from cognitively normal subjects (N=27) are in blue, those from subjects with mild cognitive impairment (N=5) and Alzheimer's disease (N=1) are in black.

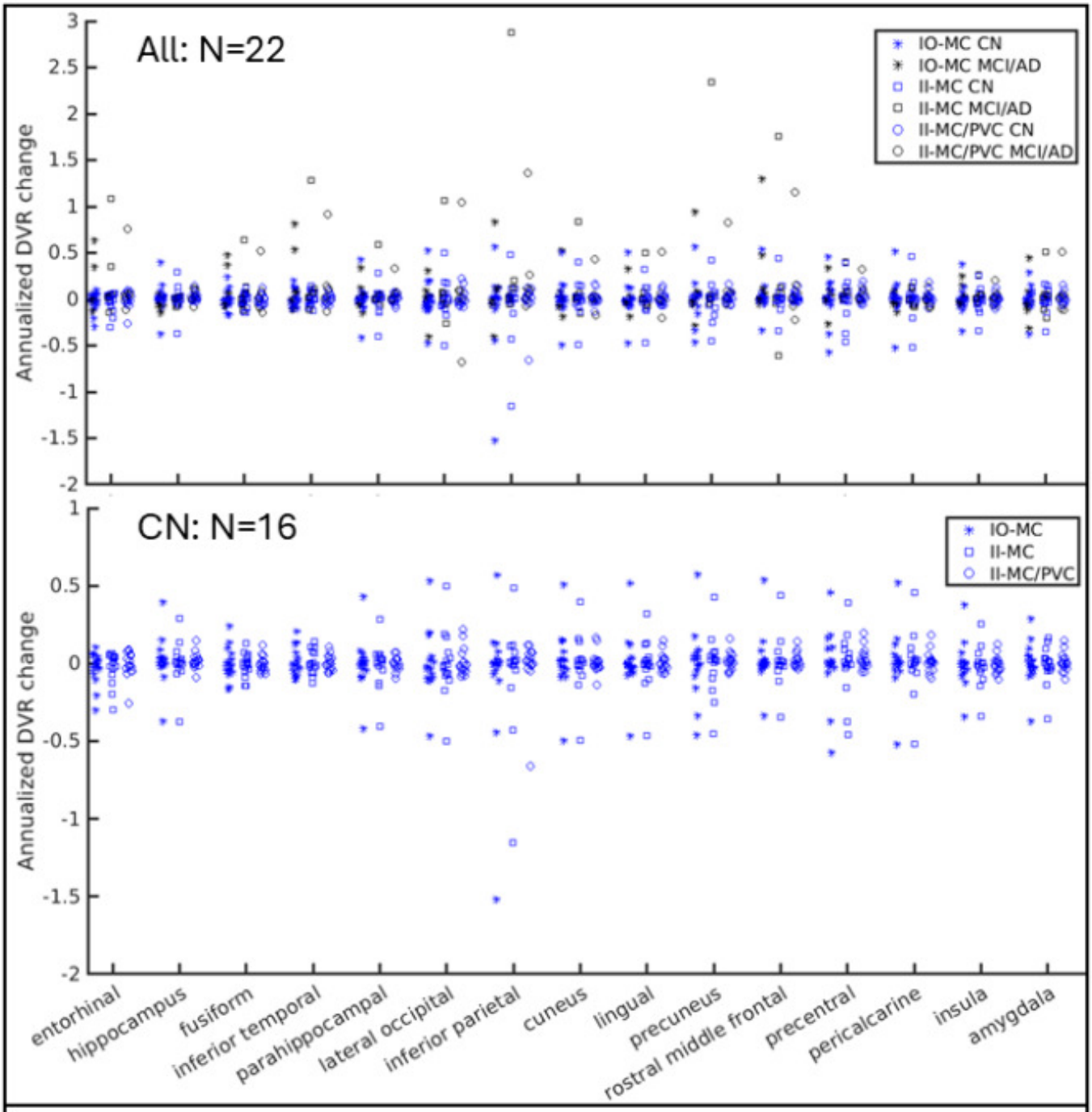


Figure 2: Annualized DVR change for all subjects (top) and for a subset of cognitively normal subjects (bottom) in all surveyed regions using the three presented methods.

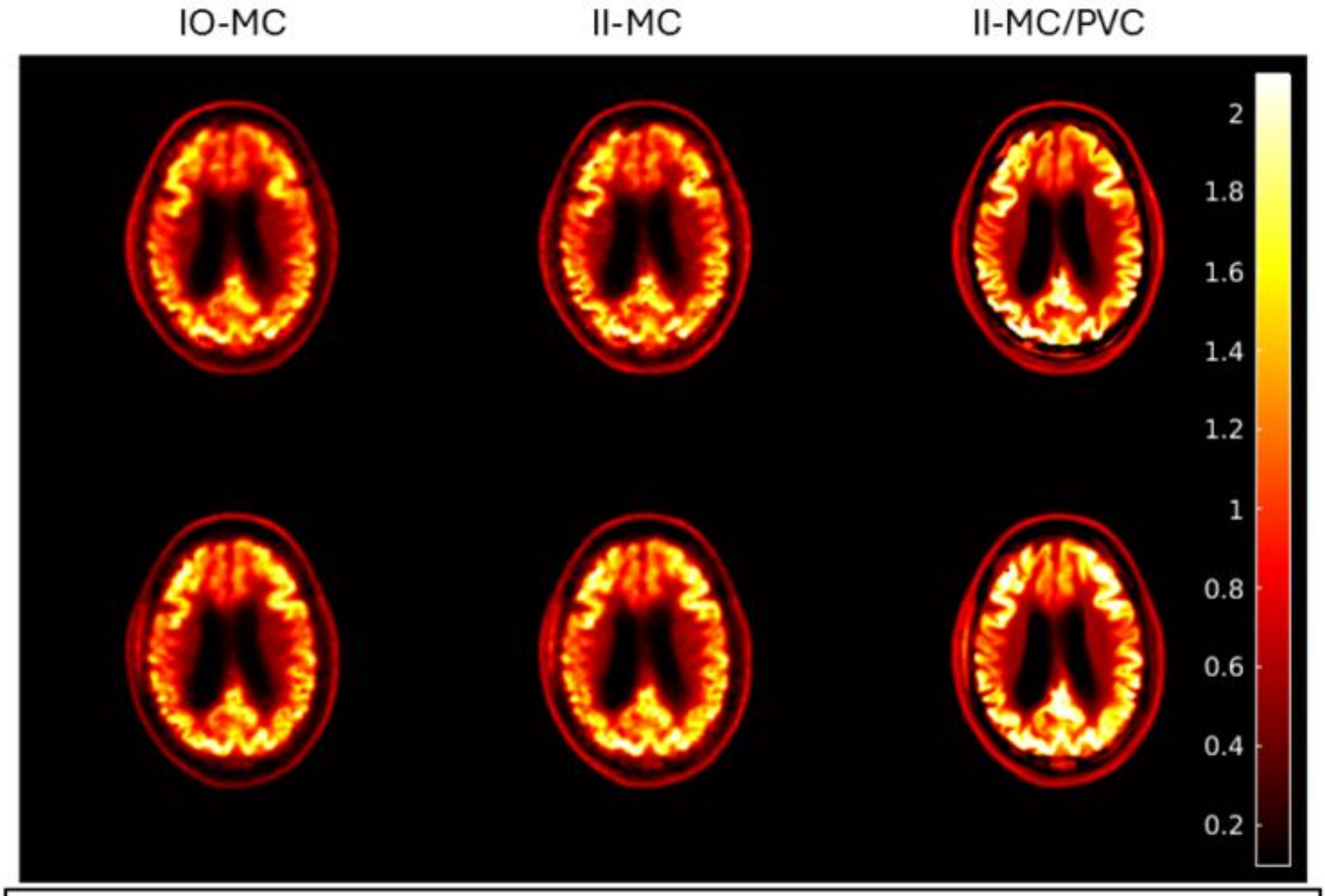


Figure 3: Logan DVR parametric maps for one subject with mild cognitive impairment at their first tau scan (top) and their follow-up scan (bottom), six months later.

Keywords: dynamic positron emission tomography, tau, motion correction, partial volume correction, longitudinal study

158 Harmonization of MK6240 and Flortaucipir Braak Staging

Andreia Rocha[1], Bruna Bellaver[1], Emma Ruppert[1], Pamela L. Ferreira[1], Carolina Soares[1], Marina Medeiros[1], Guilherme Povala[1], Livia Amaral[1], Guilherme Bauer-Negrini[1], Firoza Lussier[1], Matheus Scarpatto Rodrigues[1], Markley Oliveira Jr.[1], Pampa Saha[1], Maddie Bloomquist[1], Joseph Masdeu[2], Dana L. Tudorascu[1], David Soleimani-Meigooni[3], Juan Fortea[4], Val Lowe[5], Hwamee Oh[6], Belen Pascual[2], Brian A. Gordon[7], Pedro Rosa-Neto[8], Suzanne Baker[9], Tharick A. Pascoal[1]

[1]*University of Pittsburgh, Department of Psychiatry, Pittsburgh, PA, US*
[2]*Houston Methodist Research Institute, Department of Neurology, Houston, TX, US*
[3]*University of California San Francisco, Memory and Aging Center, San Francisco, CA, US*
[4]*Hospital de la Santa Creu i Sant Pau, Sant Pau Memory Unit, Department of Neurology, Barcelona, ES*
[5]*Mayo Clinic, Department of Radiology, Rochester, MN, US*
[6]*Brown University, Department of Psychiatry and Human Behavior, Providence, RI, US*
[7]*Washington University in St. Louis, Department of Radiology, St. Louis, MO, US*
[8]*Translational Neuroimaging Laboratory, McGill University Research Centre for Studies in Aging, Douglas Research Institute, Montréal, QC, CA*
[9]*Lawrence Berkeley National Laboratory, Berkeley, CA, US*

Background: In vivo Braak staging effectively stratifies patients across the AD spectrum and has the potential to harmonize tau PET tracer assessment. This study aims to compare and test harmonization procedures for Braak staging individuals using MK6240 and Flortaucipir tau PET tracers.

Method: We assessed 378 individuals across the AD continuum (213 CU, 119 MCI, 46 dementia; age = 68.5 ± 8.6) with MK6240 and Flortaucipir scans. Standardized uptake value ratios (SUVRs) were calculated in Braak regions. We tested two cut-off methods to regional positivity: (a) Mean + 2.5 SD of young individuals (age = 22.9 ± 1.7) (b) Mean + 2.5 SD of CU Elderly Aβ- individuals (age = 65.2 ± 8.4; Centiloid <= 12). Braak stages were assigned using seven (Braak 0-VI) and four (Braak 0, I-II, III-IV, V-VI) classes. Braak stage concordance was assessed within tracer (intra-tracer, i.e., whether it follows the sequential Braak pattern) and between tracers (inter-tracer, i.e., whether individuals' Braak stage match between tracers).

Results: Young-based cut-offs resulted in 86% and 64% intra-tracer concordance for MK6240 and Flortaucipir, respectively. Using CU Elderly Aβ- as reference group improved seven-class Braak stage concordance (MK6240 = 94%; Flortaucipir = 87%), as many early Braak stages became negative. Braak II region optimization based on Flortaucipir off-target binding and spillover rendered a slight improvement for Flortaucipir concordance (90%; Fig. 1). However, the best inter-tracer agreement (80%) was achieved using the CU Elderly Aβ- cut-off without optimization. Most inter-tracer discrepancies occurred at Braak stages II-III (Fig. 2). Four-class staging increased intra-tracer concordance (MK6240 = 98.4%; Flortaucipir = 97.6%), but inter-tracer agreement remained moderate (88.3%).

Conclusion: These preliminary findings reveal discrepancies in Braak staging when comparing MK6240 and Flortaucipir. Our results also suggest that adjustments in cutoffs and regions of interest can partially mitigate both inter- and intra-tracer divergences.

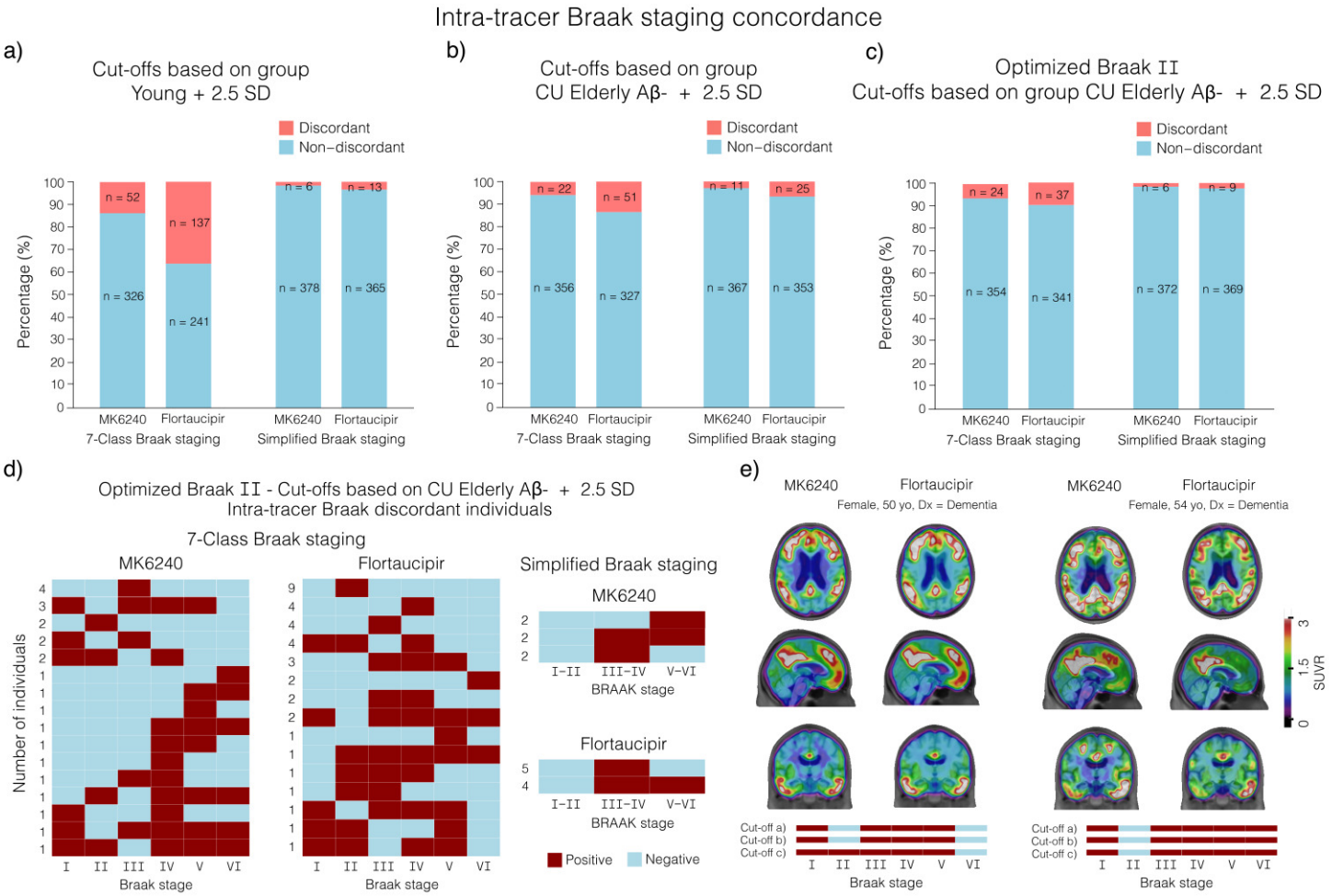


Figure 1. Intra-tracer Braak staging concordance in MK6240 and Flortaucipir. (a-c) Proportions of non-discordant (blue) and discordant (pink) individuals under various cut-off strategies. **(a)** Cut-offs based on young CU group (2.5 SD above mean SUVR). **(b)** Cut-offs based on CU elderly Aβ- group (Centiloid ≤12, 2.5 SD above mean SUVR). **(c)** Optimized cut-offs for Braak II region based on Flortaucipir's off-target and spillover effects, using CU elderly Aβ- cut-offs. **(d)** Binary maps showing discordant individuals. **(a-d)** Braak stage classifications for each tracer were assessed using 7-class (Braak 0-VI) and simplified (4-class; Braak 0, I-II, III-IV, V-VI) Braak frameworks. **(e)** SUVR images from two discordant cases, with Braak classifications from approaches in **(a)-(c)** shown below. Abbreviations: SD = standard deviations, CU = cognitively unimpaired, SUVR = standardized uptake value ratio, Aβ- = amyloid-negative, yo = years old, Dx = diagnosis.

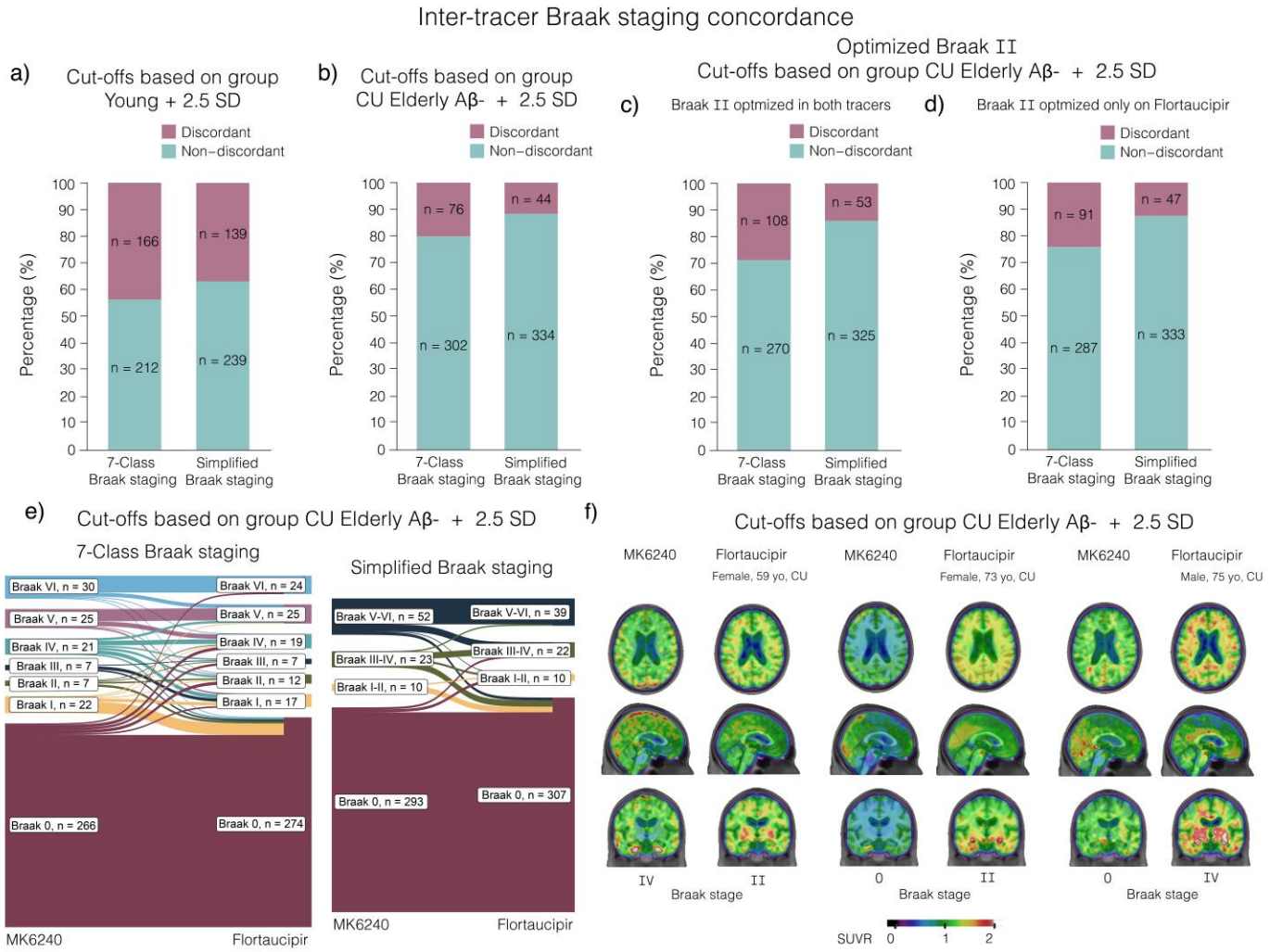


Figure 2. Braak staging concordance between MK6240 and Flortaucipir. **(a-d)** Proportions of non-discordant (teal) and discordant (pink) individuals under various cut-off strategies, with 7-class and simplified 4-class Braak frameworks. (a) Cut-offs based on young CU group (2.5 SD above mean SUVR). **(b)** Cut-offs from CU elderly Aβ- group (Centiloid ≤12, 2.5 SD above mean SUVR). **(c)** Concordance with Braak II optimization in both tracers. **(d)** Concordance with Braak II optimization only in Flortaucipir. **(e)** Sankey plots showing stage transitions between MK6240 and Flortaucipir Braak classifications. **(f)** SUVR images from three discordant cases, using CU Elderly Aβ- cut-offs. Abbreviations: SD = standard deviations, CU = cognitively unimpaired, SUVR = standardized uptake value ratio, Aβ- = amyloid-negative, yo = years old.

Keywords: tau PET, Braak, head-to-head, harmonization

159 Comparison of MK-6240 PET and Flortaucipir tau PET imaging for the biological staging of Alzheimer's disease

Marina Scop Medeiros[1], Pamela L. Ferreira[1], Bruna Bellaver[1], Emma Ruppert[1], Hussein Zalzale[1], Carolina Soares[1], Guilherme Povala[1], Guilherme Bauer-Negrini[1], Andreia Rocha[1], Matheus S. Rodrigues[1], Markley Oliveira[1], Rayan Mroue[1], Pampa Saha[1], Livia Amaral[1], Firoza Lussier[1], Madeleine Bloomquist[1], Dana L. Tudorascu[1], Joseph Masdeu[2], David Soleimani-Meigooni[4], Juan Fortea[5], Val Lowe[6], Hwamee Oh[7], Belen Pascual[2], Brian A. Gordon[8], Pedro Rosa-Neto[9], Lucas P. Schilling[1], Suzanne Baker[10], Tharick A. Pascoal[1]

[1]*University of Pittsburgh, Pittsburgh, PA, US*
[2]*Houston Methodist Research Institute, Houston, TX, US*
[3]*University of California San Francisco, San Francisco, CA, US*
[4]*Hospital de la Santa Creu i Sant Pau, Barcelona, ES*
[5]*Mayo Clinic, Rochester, MN, US*
[6]*Brown University, Department of Psychiatry and Human Behavior, Providence, RI, US*
[7]*Washington University in St. Louis, St Louis, MO, US*
[8]*Translational Neuroimaging Laboratory, McGill University Research Centre for Studies in Aging, Montreal, QC, CA*
[9]*BRAIN Institute, Pontifícia Universidade Católica do Rio Grande do Sul, Porto Alegre, BR*
[10]*Lawrence Berkeley National Laboratory, Berkeley, CA, US*

Background: The Alzheimer's Association workgroup criteria (AA-2024) suggest four biological stages based on PET imaging. Recognizing that the application of this framework may vary depending on the tau PET tracer used, we aim to compare clinical-biological agreements using two different tau PET tracers.**Methods:** We stratified 148 Aβ+ participants from the HEAD study with MK-6240 and Flortaucipir tau-PET. Four clinical stages (normal, transitional, MCI, and dementia) were defined based on the AA-2024 criteria. Three different stage-2 constructs were tested in separated analyses for subjective cognitive decline (SCD), subtle objective cognitive deficit (SOCD), and mild behavioral impairment (MBI) (see Figure 1A). For biological staging, SUVR regional abnormalities were defined based on tracer-specific thresholds, testing three different methods (Youden index, CU Aβ- mean +2SD, Young mean +2.5SD) and three regions of interest schemes: (i)proposed by AA-2024, (ii)Braak stages, (iii)or single anatomical regions (Figure 1B). Cohen's weighted-kappa (K) statistic measured clinical-biological and between-tracer agreements.

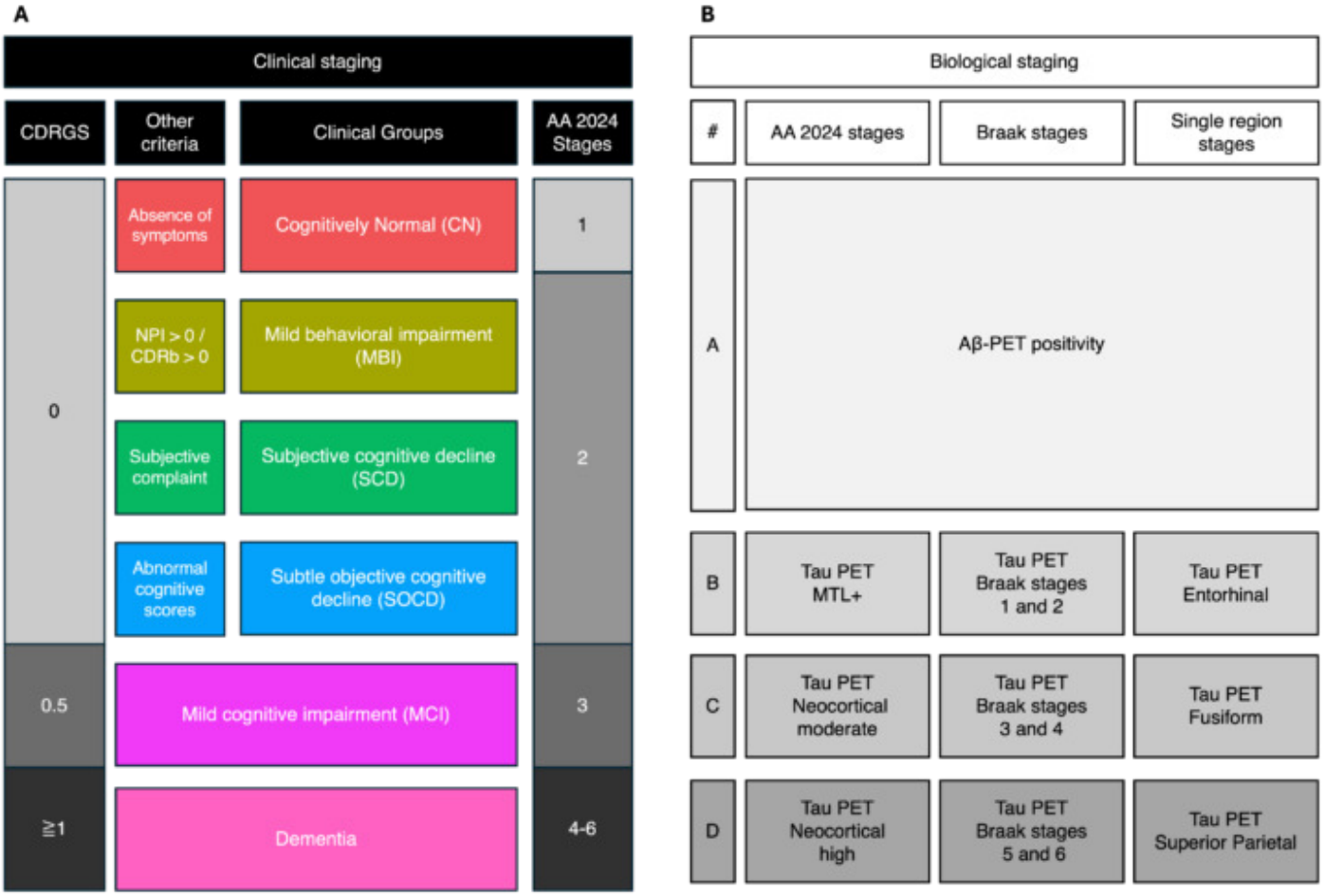
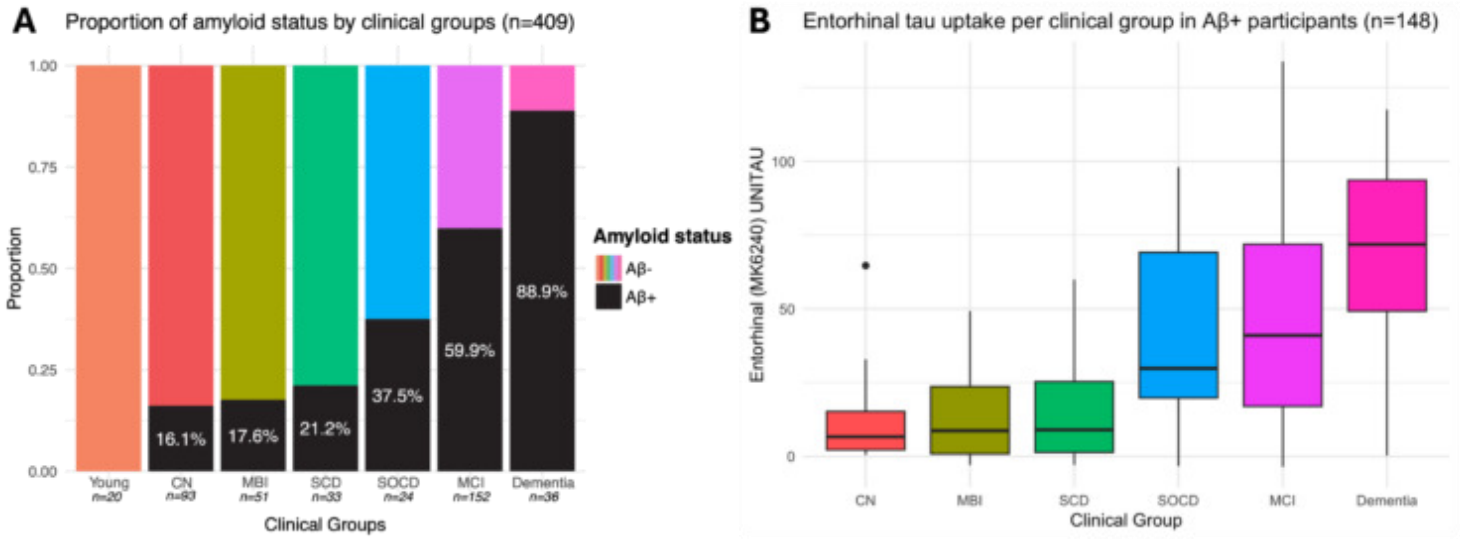


Figure 1. Tested classification criteria for clinical and biological staging. A. Alzheimer's Association workgroup 2024 (AA 2024) criteria for AD clinical stages poses stage 1 as CN, stage 2 as Transitional decline defined here by 3 sub-groups (MBI, SCD and SOCD), stage 3 as cognitive impairment with early functional impact, stages 4-6 as dementia with varying degrees of severity. Participants with a CDR Global Score of 0 were stratified into additional groups: **SOCD** (subtle objective cognitive deficit), if abnormal cognitive scores for age and education or cognitive deficit noted by the clinician in the visit; **SCD** (subjective cognitive decline), if subjective decline without objective evidence of clinical and cognitive deficit; **MBI** (mild behavioral impairment) if Neuropsychiatric Inventory (NPI) score > 0 and/or CDR behavioral domain (CDRb) > 0, with normal cognitive scores; **CN** (cognitively normal), excluding the above. **B.** Biological staging was performed using amyloid (Aβ) PET (visual reading) and tau PET with two tracers (MK6240 and AV1651) in the same individuals and compared between the three different methods tested. In this preliminary analysis, only Aβ-positive participants were assigned to clinical and biological stages of AD, being part of the AD continuum (n=148).

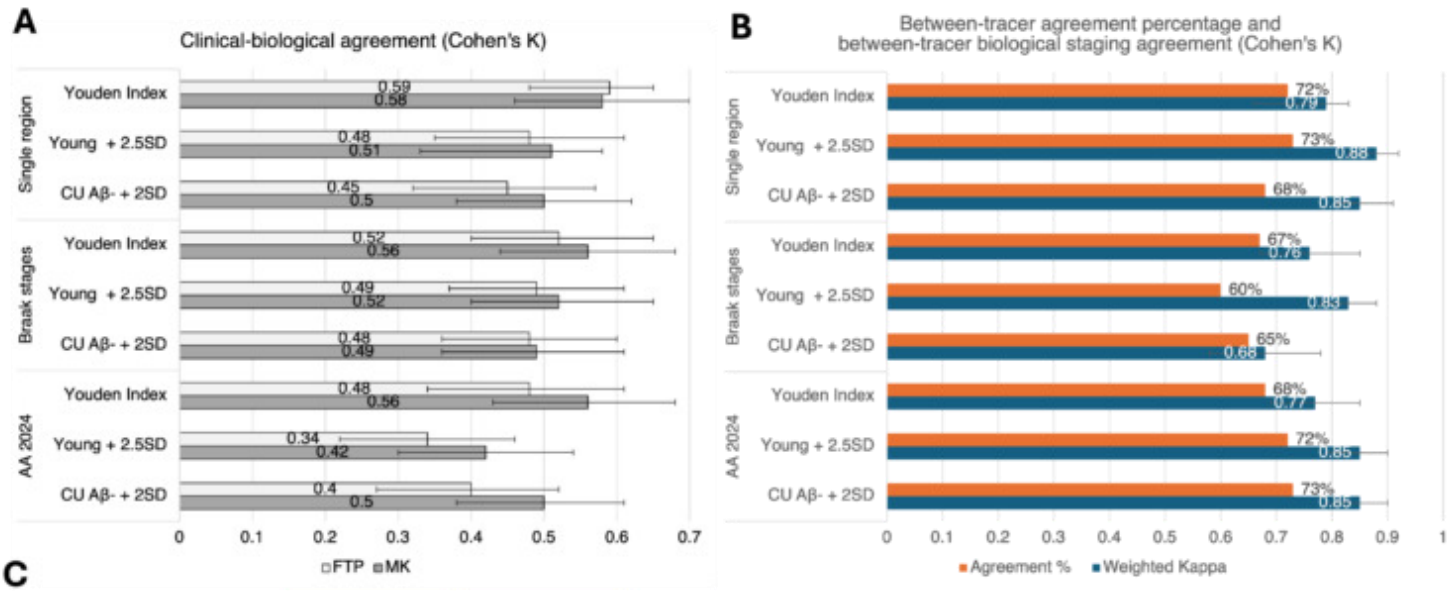
Results: Clinical stages showed a progressively increased prevalence of Aβ+ and entorhinal tau PET pathology from cognitively normal (CN) to SOCD, MCI, and dementia. MBI and SCD transitional groups showed no increased Aβ+ or tau pathology compared to CN (Figure 1A, B). For this reason, only SOCD was considered part of stage 2 for further analyses. All tested biological staging methods had similar agreement with clinical stages using MK-6240 and Flortaucipir (Figure 3A). All strategies showed reasonable between-tracer concordance (K>0.60), with AA-2024 and single-region strategies showing the best agreements (72-73%) and Braak-staging showing the worse (65-67%) (Figure 3B).



C

Demographics	CN (n=13)	MBI (n=9)	SCD (n=7)	SOCD (n=8)	MCI (n=81)	Dementia (n=30)	P-value
Age, years	70.5 ± 9.6	70.2 ± 5.6	67.4 ± 6.3	75.1 ± 3.5	72.6 ± 7.3	72.4 ± 8.1	0.34
Female sex, %	61.5	77.8	85.7	50.0	48.1	50	0.27
Education, years	16.7± 2	16.6 ± 3	16.6 ± 2.7	16.4 ± 2.2	15.6 ± 3.18	15.6 ± 2.91	0.68
APOE ε4 carriers, % (n)	30.8 (9)	66.7 (5)	57.1 (6)	100 (2)	84.0 (56)*	86.7 (13)	0.045
CDR-SoB	0.0 ± 0	0 ± 0	0 ± 0	0.1 ± 0.18	2.2 ± 1.21***	6.1 ± 1.85***	<0.001
MMSE	28.9 ± 1.3	29.2 ± 0.8	29.0 ± 1.1	26.9 ± 2.1	26.3 ± 2.9	21.3 ± 6.9***	<0.001
MOCA	26.9 ± 2.6**	28.6 ± 1**	27.1 ± 1.5**	23.9 ± 2.6	22.3 ± 2.6	16.3 ± 6.8***	<0.001
FAQ	0.1 ± 0.3	0 ± 0	0 ± 0	0.1 ± 0.3	4.3 ± 4.3*	17.9 ± 8***	<0.001

Figure 2. Subtle objective cognitive deficit (SOCD) is the only transitional stage (AA-2024) subtype that presents increased amyloid and tau pathology compared to CN. A. Stacked bar plot showing proportion of amyloid-positive (Aβ+) status according to amyloid PET visual reading. A logistic regression analysis corrected by age and sex showed that SOCD, MCI, and Dementia have significantly higher odds of being amyloid positive compared to the CN group, while Young, MBI and SCD was not different from the CN group (p<0.05). **B.** Boxplots showing [^{18}F]MK6240 tau PET uptake in the entorhinal cortex across clinical groups in Aβ+ participants (n=148). A linear regression model showed only SOCD, MCI and Dementia have increased tau uptake (p<0.05) compared to CN. **C.** Baseline demographics and clinical characteristics of Aβ-positive study participants, stratified by clinical stages (n=148). Data presented as means ± standard deviations, unless otherwise specified. [a]Fischer tests were used for categorical variables. [b]One-way ANOVA was performed to compare continuous data among the 6 study groups. Post-hoc pairwise differences were evaluated using Bonferroni's method, with a significance threshold of $p < 0.05$. *Significantly different from CN. **Significantly different from MCI. ***Significantly different from all other groups. **Abbreviations**: APOE, apolipoprotein E; CDR-SoB, Clinical Dementia Rating Sum of Boxes; CN, cognitively normal; FAQ, Functional Activities Questionnaire; MBI, mild behavioral impairment; MCI, mild cognitive impairment; MMSE, Mini-Mental state examination; MoCA, Montreal Cognitive Assessment; SCD, subjective cognitive decline; SOCD, subtle objective cognitive deficit. Abbreviations: CN, cognitively normal; MBI, mild behavioral impairment; MCI, mild cognitive impairment; SCD, subjective cognitive decline; SOCD, subtle objective cognitive deficit.



C

Clinical groups		CN (n=13)		MBI (n=9)		SCD (n=7)		SOCD (n=8)		MCI (n=81)		Dementia (n=30)		
Clinical stages		1						2		3		4		
Biological stages	Tau PET tracer	MK	FTP	MK	FTP	MK	FTP	MK	FTP	MK	FTP	MK	FTP	OR[a] (CI)
Biological stage A (n=33)		**77%**	**69%**	**56%**	**89%**	**57%**	**71%**	13%	38%	15%	22%	3%	0%	Reference
Biological stage B (n=19)		0%	23%	22%	11%	14%	14%	**50%**	**63%**	14%	26%	3%	7%	7 (1.8-29)
Biological stage C (n=43)		23%	0%	11%	0%	14%	14%	38%	0%	**41%**	**23%**	7%	23%	10 (3-32)
Biological stage D (n=53)		0%	8%	11%	0%	14%	0%	0%	0%	31%	28%	**87%**	**70%**	34 (7-166)

Figure 3. A. Bar plot of Cohen's weighted-kappa values of agreement between biological and clinical stages according to each strategy per tracer (gray, [18F]MK-6240; white, Flortaucipir). Confidence boundaries lines are added. **B.** Bar plot of between-tracer biological staging agreement percentage (orange) and Cohen's weighted-kappa (blue), with confidence boundaries lines added. **C.** Biological staging combined with clinical staging. Biological staging using single-region and Youden Index strategy. [a]Odds ratio (OR) of being in a clinical stage higher than 1 for each biological stage compared to biological stage-A. Bold font represent when clinical and biological stages are concordant. **Abbreviations**: CI, 95% confidence interval; CN, cognitively normal; FTP, Flortaucipir; MBI, mild behavioral impairment; MCI, mild cognitive impairment; MK, [18F]MK-6240; SCD, subjective cognitive decline; SOCD, subtle objective cognitive deficit.

Conclusions: Our results support that AA-2024 biological and clinical stages show reasonable concordance using either Flortaucipir or MK-6240, although this can vary based on methods used in the analyses. The MBI and SCD transition groups showed more similar pathological burden to clinical stage 1 than to the SOCD transitional stage 2.

Keywords: Tau PET, Alzheimer's disease, biological staging, clinical stages, concordance

160 Impact of early-stage amyloidosis on tau accumulation throughout the medial temporal lobe and neocortex

Elliott Slade[2], Emma Thibault[2], Jackson Thompson[2], Jessie Fanglu Fu[1,2], Alex Becker[2], Julie Price[1,2], Amal Tiss[2], Kuang Gong[3], Reisa Sperling[2], Keith Johnson[2], Michelle Farrell[2]

[1]*Athinoula A. Martinos Center for Biomedical Imaging, Charlestown, MA, US*
[2]*Massachusetts General Hospital, Harvard Medical School, Boston, MA, US*
[3]*University of Florida, Gainesville, FL, US*

Background: Tau accumulates in the medial temporal lobe (MTL) throughout the adult lifespan in most individuals. Amyloid-β (Aβ) is believed to trigger the spread of tau from MTL to the neocortex in Alzheimer's disease (AD), setting off a cascade leading to dementia. Aβ and tau PET research over the last decade suggest that this triggering event occurs after a certain threshold level of Aβ is reached, with some studies suggesting this threshold falls at 40 Centiloids (CL). However, advances in PET scanners, quantification methods and the use of more sensitive second-generation tau radioligands like [^{18}F]MK-6240 (MK) may reveal changes in tau burden earlier in the course of amyloidosis than previously thought. This study evaluates whether baseline Aβ contributes to predicting greater tau accumulation.

Methods: We examined 60 participants in HABS2 with low Aβ-burden (<40 CL) who underwent baseline PiB and longitudinal MK-PET scans on a GE Discovery[4mm] (**Table 1**). Partial-volume-correction was performed using the kernel method (Gong, K., 2018) within-reconstruction to the tau PET data. Baseline Aβ was measured as the PiB-DVR in a frontal-lateral temporoparietal-retrosplenial (FLR) aggregate. Tau was quantified with MK-SUVR across multiple Desikan-Killiany atlas ROIs in the MTL allocortex and the neocortex. For each ROI, linear mixed models assessed effects of baseline PiB-FLR-DVR on change in MK-SUVR over time, covarying for age, sex, and education and random participant intercepts.

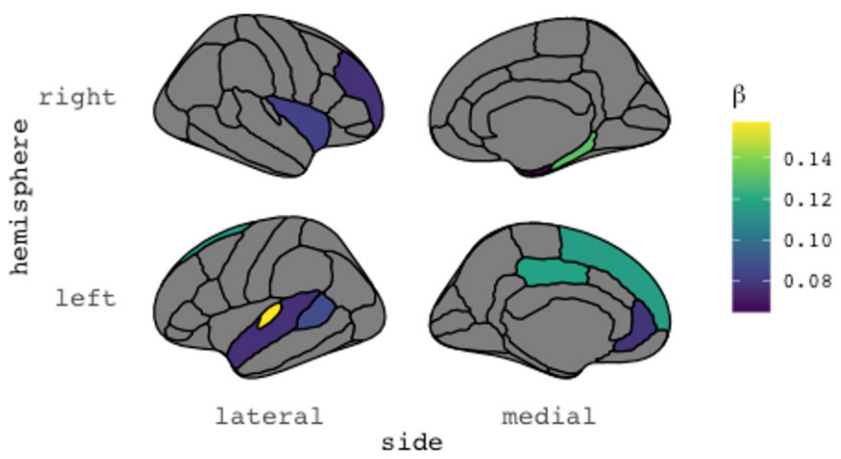
Results: Even under 40CL, higher baseline PiB-FLR-DVR was associated with greater subsequent tau accumulation across multiple allocortical MTL regions and the neocortex (**Fig.1/2**), showing a clear relationship between early Aβ deposition and tauopathy.

Conclusions: These findings indicate that for some individuals, Aβ-related tau proliferation begins prior to Aβ<40CL, a threshold often cited as a triggering level of Aβ, including regions outside the medial temporal lobe. These findings emphasize the potential need for anti-tau interventions even at low Aβ-burden.

	PiB- (N=50)	PiB+ (N=10)	Overall (N=60)
Age			
Mean (SD)	64.9 (10.2)	72.8 (7.95)	66.2 (10.3)
Median [Min, Max]	65.3 [36.8, 82.5]	72.0 [59.5, 86.5]	67.1 [36.8, 86.5]
Sex			
F	24 (48.0%)	6 (60.0%)	30 (50.0%)
M	26 (52.0%)	4 (40.0%)	30 (50.0%)
Years Education			
Mean (SD)	17.0 (2.27)	17.5 (2.88)	17.1 (2.36)
Median [Min, Max]	17.0 [12.0, 20.0]	18.5 [12.0, 20.0]	17.0 [12.0, 20.0]
Cognitive Status			
CN	47 (94.0%)	8 (80.0%)	55 (91.7%)
MCI/AD	3 (6.0%)	2 (20.0%)	5 (8.3%)
APOE Status			
e4-	30 (60.0%)	7 (70.0%)	37 (61.7%)
e4+	12 (24.0%)	2 (20.0%)	14 (23.3%)
Missing	8 (16.0%)	1 (10.0%)	9 (15.0%)
FLR DVR			
Mean (SD)	1.05 (0.0372)	1.27 (0.103)	1.08 (0.100)
Median [Min, Max]	1.05 [0.977, 1.13]	1.27 [1.15, 1.45]	1.05 [0.977, 1.45]
MK6240 PET time points			
Mean (SD)	2.56 (0.929)	2.90 (0.876)	2.62 (0.922)
Median [Min, Max]	3.00 [1.00, 4.00]	3.00 [1.00, 4.00]	3.00 [1.00, 4.00]
Follow-up Time			
Mean (SD)	1.54 (1.16)	2.39 (0.891)	1.68 (1.16)
Median [Min, Max]	1.23 [0, 4.30]	2.66 [0, 3.03]	1.33 [0, 4.30]

Table 1: **Harvard Aging Brain Study 2 (HABS2) sample demographics at baseline (PiB+ Group includes only those with Aβ < 40 CL)**. Of the 60 participants included, 48 had two or more [^{18}F]MK-6240 PET scans (80.0%), and 40 participants completed all 3 scans (66.7%). The sample was divided into PiB+ and PiB- groups using a threshold of 1.15 PiB DVR FLR, which corresponds to approximately 8.14 CL. Groups did not differ significantly in years of education (p=0.60) or sex distribution (p=0.95). All participants with an Aβ > 40 CL were excluded from the analysis to isolate effects before widespread amyloidosis. This strict threshold allowed us to capture tau accumulation before significant amyloid deposition occurred across the brain.

A



B

ROI	Model 1	
	β	*p*
rhinal_rh (RC)*	0.081	0.011
entorhinal_rh	0.065	0.040
parahippocampal_rh (PH)*	0.131	0.006
hippocampus_lh	0.090	0.013
hippocampus_rh (HC)*	0.069	0.025
amygdala_rh (AM)*	0.080	0.003
amygdala_lh	0.073	0.009
superiortemporal_lh (ST)*	0.077	0.029
bankssts_lh (BS)*	0.086	0.023
transversetemporal_lh (TT)*	0.157	0.001
insula_rh	0.082	0.008
accumbens_area_rh	0.123	0.002
posteriorcingulate_lh	0.119	0.016
rostralanteriorcingulate_lh (RAC)*	0.078	0.018
rostralmiddlefrontal_rh (RMF)*	0.077	0.016
superiorfrontal_lh	0.116	0.000
precentral_lh	0.070	0.020

Figure 1: **Relatively high baseline Aβ burden and regional tau proliferation. (A)** Regions for which higher rates of tau SUVR increases significantly associated with relatively higher baseline Aβ burden (but still below 40CL) are shown. The color scale indicates the standardized β-coefficients (β) for the PiB FLR DVR*time interaction for each significant cortical ROI in the Desikan-Killiany atlas. The heat map highlights early change in Aβ-related tau accumulation within both the medial temporal lobe (right parahippocampal, entorhinal) and neocortex (e.g. left superior and transverse temporal, and the banks of the superior temporal sulcus). **(B)** This table presents the standardized β-estimates and p-values for regions with significant time*baseline PiB FLR DVR interactions on MK SUVR. Aβ-related changes in tau SUVR were observed across most of the MTL (though with some asymmetry favoring greater change in the right hemisphere). Aβ-related tau changes were also observed in neocortical regions despite the low level of Aβ burden, mostly in the left lateral temporal cortices.

Regions marked with an asterisk (*) are plotted below (Figure 2).

*Linear mixed effect model: longitudinal tau ~ age + sex + education + time*PiB FLR DVR, random = ~ 1|subject*
Regression coefficients and p-values for the Time term are displayed in Figure 1B.

Abbreviations: MK = [^{18}F]MK-6240; SUVR = standardized uptake value ratios, PiB = [^{11}C]Pittsburgh Compound B; FLR = frontal-lateral temporoparietal-retrosplenial; DVR = distribution volume ratios.

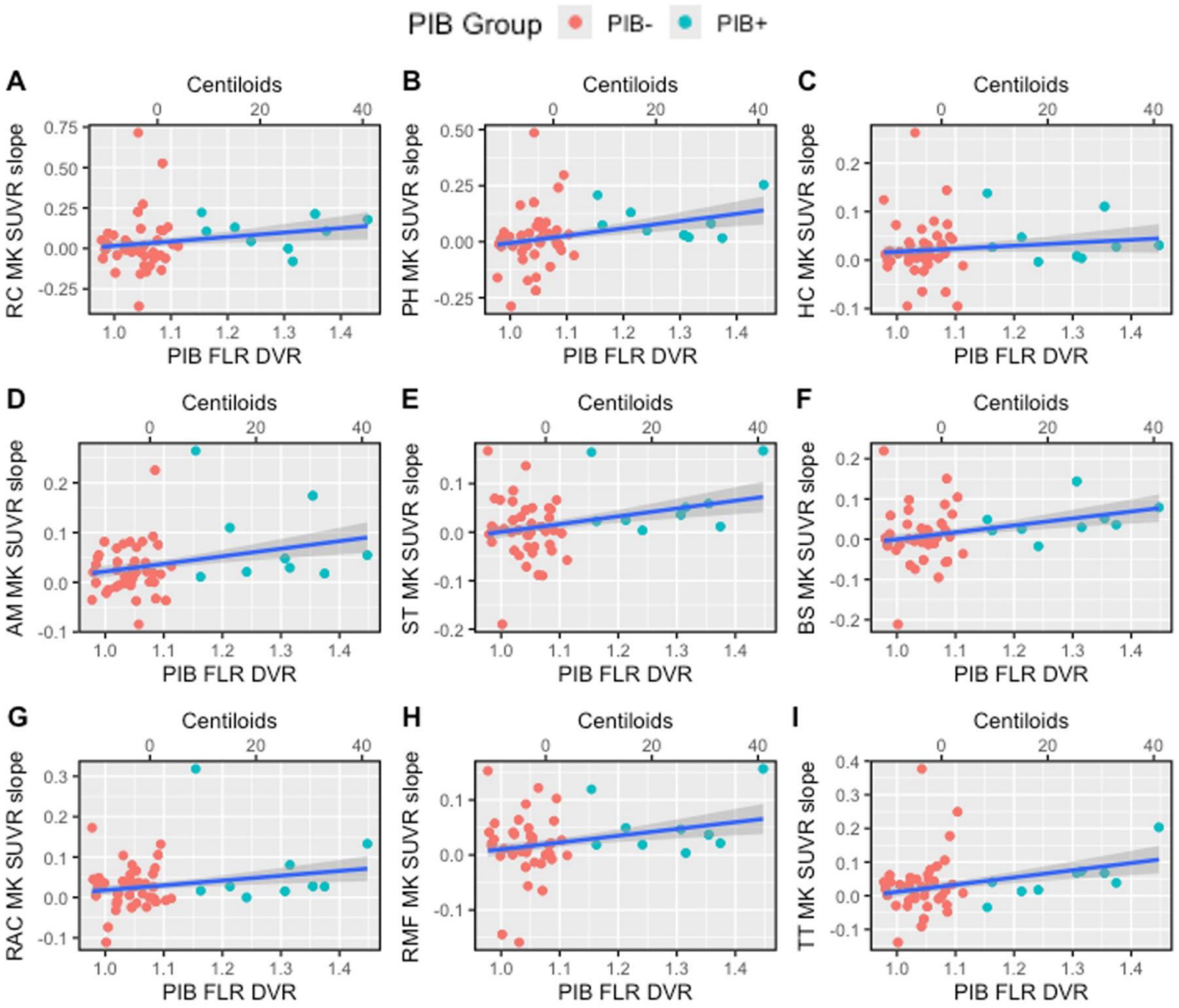


Figure 2: **Baseline PiB FLR DVR and change in regional MK SUVR.** This figure illustrates the relationship between baseline PiB FLR DVR (x-axis), and MK SUVR change over time (y-axis). The rate of regional change in MK SUVR per year was estimated by extracting slopes using ordinary least squares regression. Individuals are color-coded by baseline PiB +/-group (threshold: 1.15 PiB FLR DVR). Across regions, we observed a mix of positive and negative slopes for MK SUVR in PiB- individuals, consistent with random fluctuations over time in non-specific binding. In contrast, MK SUVR slopes were almost universally positive across regions in PiB+ individuals, consistent with tau accumulation in the presence of Aβ. Interestingly, the highest individual rate changes were observed in the rhinal and parahippocampal cortices, prior to PiB positivity.

Abbreviations: RC = rhinal cortex, PH = parahippocampus, HC = hippocampus, AM = amygdala, ST = superior temporal, BS = banks of superior temporal sulcus, RAC = rostral anterior cingulate, RMF = rostral middle cingulate, TT = transverse temporal; MK = [^{18}F]MK-6240; SUVR = standardized uptake value ratios, PiB = [^{11}C]Pittsburgh Compound B; FLR = frontal-lateral temporoparietal-retrosplenial; DVR = distribution volume ratios.

Keywords: Positron emission tomography, medial temporal lobe, tau, longitudinal analysis, Alzheimer's disease

161 Associations between age-related tau deposition and neural selectivity in cognitively unimpaired older adults

Jintao Sheng[1], Alexandra Trelle[1], Christina Young[1], America Romero[2], Jennifer Park[1], Isha Sai[1], Hillary Vossler[1], Anthony Wagner[1], Elizabeth Mormino[1]

[1]*Stanford University, Stanford, CA, US*
[2]*University of Oregon, Eugene, OR, US*

Objective: Age-related reductions in neural selectivity—the brain's ability to distinguish between stimuli—have been associated with cognitive decline in aging. This study examines the influence of age on tau deposition within cortical regions selective for specific categories and assesses its impact on neural selectivity in a normal aging cohort.

Methods: Sixty-seven cognitively unimpaired older adults (mean age = 72.73±5.99 years, 35 females) from the Stanford Aging and Memory Study underwent fMRI during a visual associative memory task (famous faces or places paired with a noun) and tau-PET with 18F-PI2620 (13 with longitudinal tau-PET, mean follow-up = 3.24±1.58 years). Standardized uptake value ratios (SUVRs) were extracted in face-selective [fusiform face area (FFA) and occipital face area (OFA)] and place-selective regions [parahippocampal place area (PPA), occipital place area (OPA), and retrosplenial cortex (RSC)]. Neural selectivity was defined as the difference in univariate activity between preferred and non-preferred categories (face versus place) during encoding. Linear mixed-effects models assessed the effects of interest, all controlling for sex and education, with age, amyloid status, and repeated SUVRs included as needed. The Holm-Bonferroni method was used for multiple comparison corrections (i.e., p_{Holm}).

Results: Amyloid-positive participants (CSF Ab42/Ab40<0.075) exhibited significantly higher SUVRs compared to amyloid-negative individuals (p=0.045), particularly in the OFA (p_{Holm} = 0.019) (Figure 1). Higher tau SUVRs were observed in occipital regions (e.g., OFA, OPA) relative to FFA, PPA, and RSC (p<0.001) (Figure 1). Only the OFA showed an age-related increase in SUVR (p_{Holm} = 0.006; Figure 2). Elevated SUVR correlated with lower neural selectivity in the OPA (p_{Holm} = 0.051; Figure 3).

Conclusions: These preliminary findings indicate that tau burden in the aging brain may accumulate early in occipital regions involved in face and place processing. Focal tau accumulation in these areas may contribute to reduced neural selectivity and potentially impair cognition.

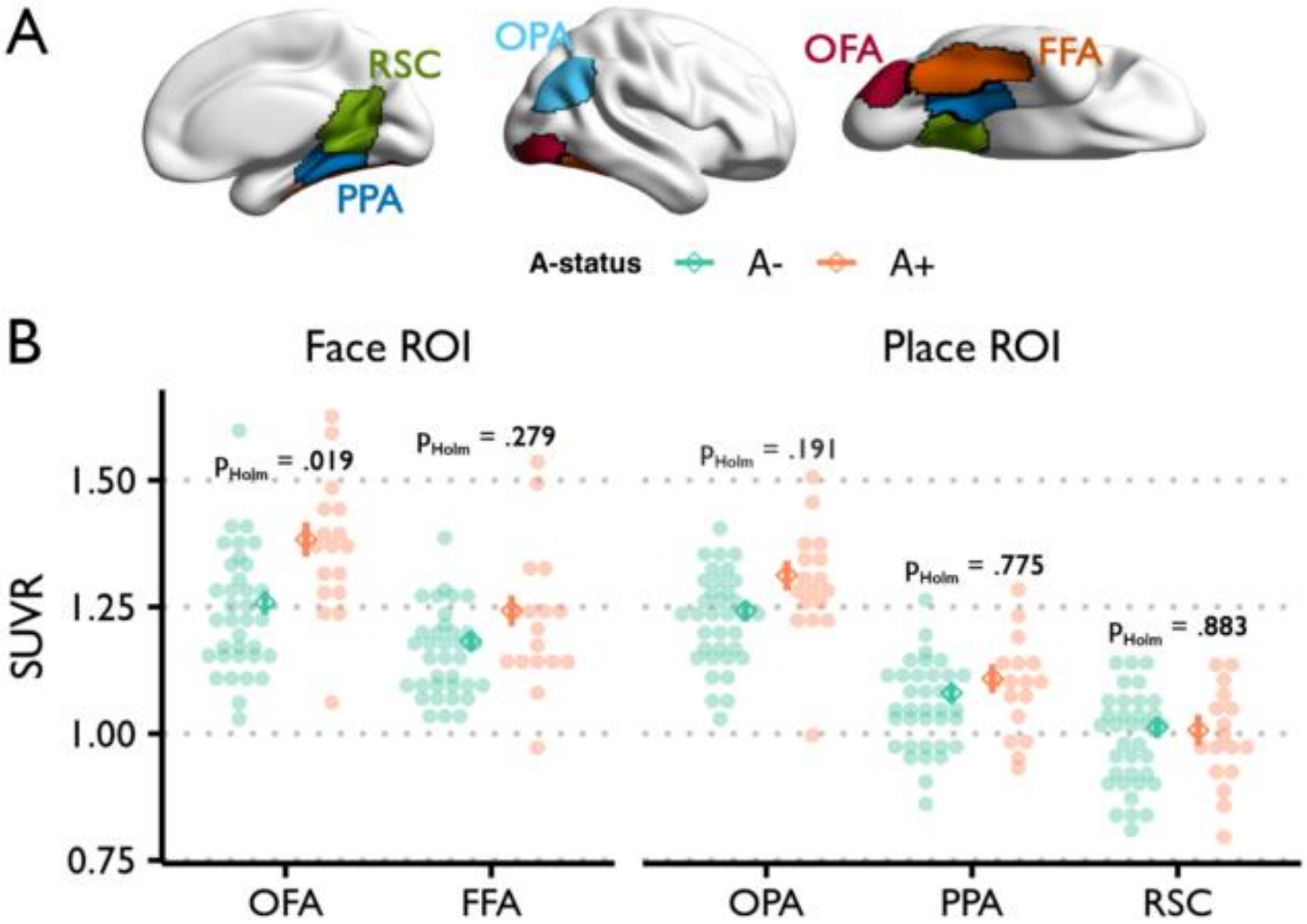


Figure 1. Region-of-interest (ROI) analysis of SUVR in face- and place-selective regions by amyloid status. **(A)** 3D brain renderings showing face-selective ROIs: occipital face area (OFA) and fusiform face area (FFA); and place-selective ROIs: occipital place area (OPA), parahippocampal place area (PPA), and retrosplenial cortex (RSC). **(B)** Tau burden in face- and place-selective ROIs as a function of amyloid status. Amyloid status was categorized using CSF Aβ42/Aβ40 ratio with a cut-off of 0.0752. Longitudinal tau PET scans were included where available (total n scans = 52). Linear mixed-effects models estimated the effects of ROI and amyloid status on SUVR, adjusting for repeated SUVRs, age, sex, and education, with a random intercept and slope for ROI to account for individual variability and within-subject correlations. Participants with missing amyloid status were excluded (n scans = 28). A marginally significant ROI × Amyloid status (A-status) interaction was observed ($p = .060$). Amyloid-positive (Aβ+, n = 17) participants showed higher tau burden in category-selective cortical regions than amyloid-negative (Aβ-, n = 35) individuals ($p = .045$), with a particularly significant increase in OFA ($p_{Holm} = .019$). Occipital ROIs exhibited higher tau levels compared to other regions ($p < .001$).

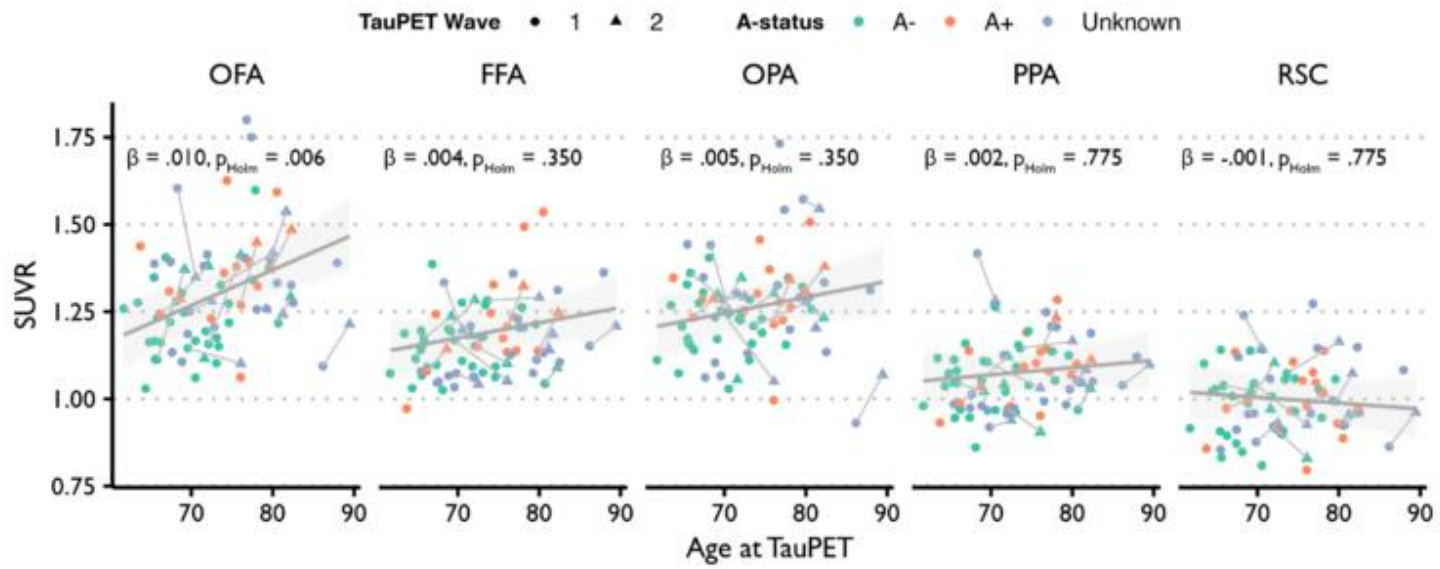


Figure 2. Regional tau burden in the occipital face area (OFA) increased with age (n scans = 80). Repeated SUVRs, amyloid status, sex, and education was controlled for in this analysis. A significant ROI × age interaction was found in the linear mixed-effects model (p = .001).

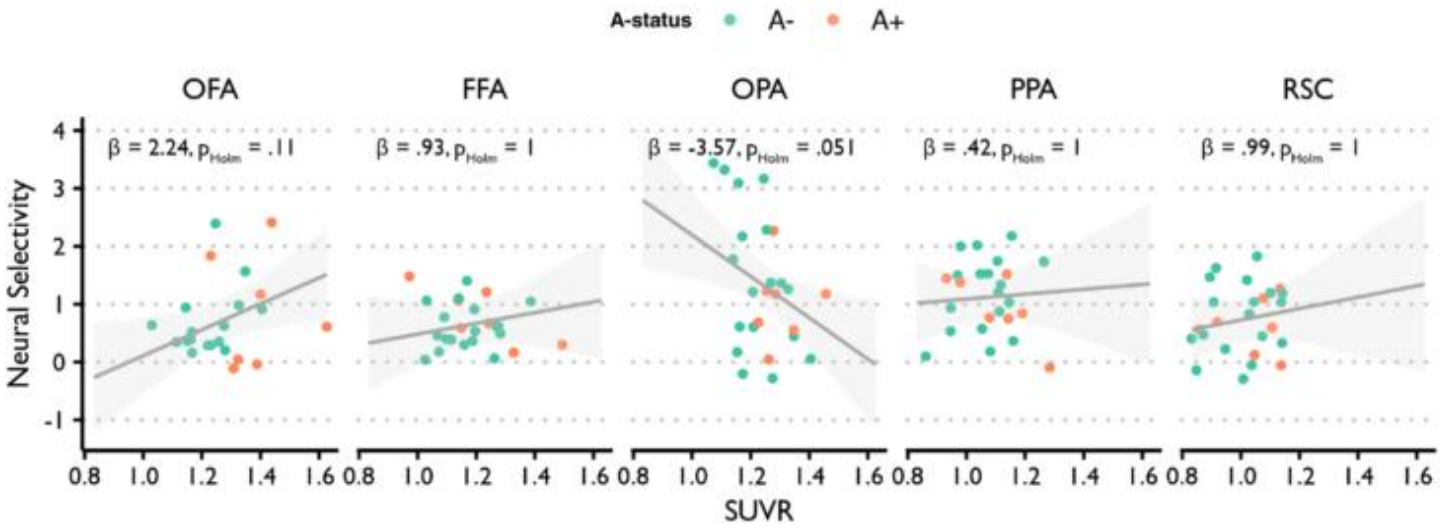


Figure 3. Elevated tau in the occipital place areas (OPA) is related to reduced neural selectivity (n = 25). A significant ROI × SUVR interaction was found in the linear mixed-effects model (p = .009). Participants with tau-PET and fMRI data within a two-year time lag were included.

Keywords: Human aging, tau-PET, fMRI, neural selectivity

162 Posterior white matter hyperintensity is related to the emergence of lobar cerebral microbleeds in ADNI

Daniel Saukkonen[1], Hyun-Sik Yang[1], Nazila Loghmani[1], Aaron Schultz[2], Steven Greenberg[2], Reisa Sperling[1,2], Jasmeer Chhatwal[1,2], Zahra Shirzadi[1,2]

[1]*Department of Neurology, Brigham and Women's Hospital, Harvard Medical School, Boston, MA, US*
[2]*Department of Neurology, Massachusetts General Hospital, Harvard Medical School, Boston, MA, US*

Background: Cerebral amyloid angiopathy (CAA) is clinically characterized by identifying cerebral microbleeds (CMBs). Recent evidence showed that white matter hyperintensity (WMH) may also be related to CAA pathophysiology. This study investigated the regional pattern of WMH in CAA by examining the relationship between lobar WMH and CMBs cross-sectionally and longitudinally in the spectrum of AD using the Alzheimer's Disease Neuroimaging Initiative (ADNI) dataset.

Methods: We extracted WMH from FLAIR MRI for 571 participants in ADNI, with clinical and neuroimaging data collected between 2007 and 2021. Each participant had at least one follow-up MRI and clinical assessment. CMBs were identified by experienced radiologists at Mayo Clinic and categorized as 'No CAA' (0 CMB), 'Possible CAA' (1 CMB), and 'Probable CAA' (≥2 CMBs) based on Boston criteria. Cross-sectional analysis used linear regression to assess the relationship between lobar WMH and CAA categories, adjusting for age, sex, grey matter volume, vascular risk, and APOE e4 ($p<0.01$ considered significant). We then used data from the 'No CAA' group at baseline and tested the relationship between baseline lobar WMH and risk of future emergence of CMBs using Cox proportional hazards regression models.

Results: Demographics are shown in Table 1. Cross-sectional analysis showed that WMH in the parietal and occipital lobes was significantly elevated in individuals with probable CAA compared to no CAA ($p<.001$). Longitudinal analysis showed that elevated baseline WMH in the parietal lobe (HR=1.61) and occipital lobe (HR=1.52), but not frontal and temporal lobes, were related to the risk of future CMB emergence in individuals with no CMB at baseline.

Conclusion: Our findings suggest that posterior WMH is related to the presence of CMBs cross-sectionally and, more importantly, to the risk of future emergence of CMBs longitudinally. These results support a regional pattern of white matter injury in relation to CAA.

Table 1: Participants' demographics and study information for ADNI baseline. Mean (Standard deviation) or number (percentage) are reported.

	N=571
Age (years)	72.8 (7.3)
APOE e4 (yes)	270 (47%)
Sex (Female)	274 (48%)
Education (years)	16 (3)
Cerebral microbleed (yes)	44 (8%)
Clinical dementia rating (1+)	328 (57%)
Diagnostic group (dementia)	74 (13%)
Amyloid group (high)	274 (50%)
WMH volume (normalized to ICV=1300cm^3)	9 (9)
GM volume (normalized to ICV=1300cm^3)	360 (29)
Follow-up time (years)	3.7 (2.8)
Cardiovascular risk score	38 (22)

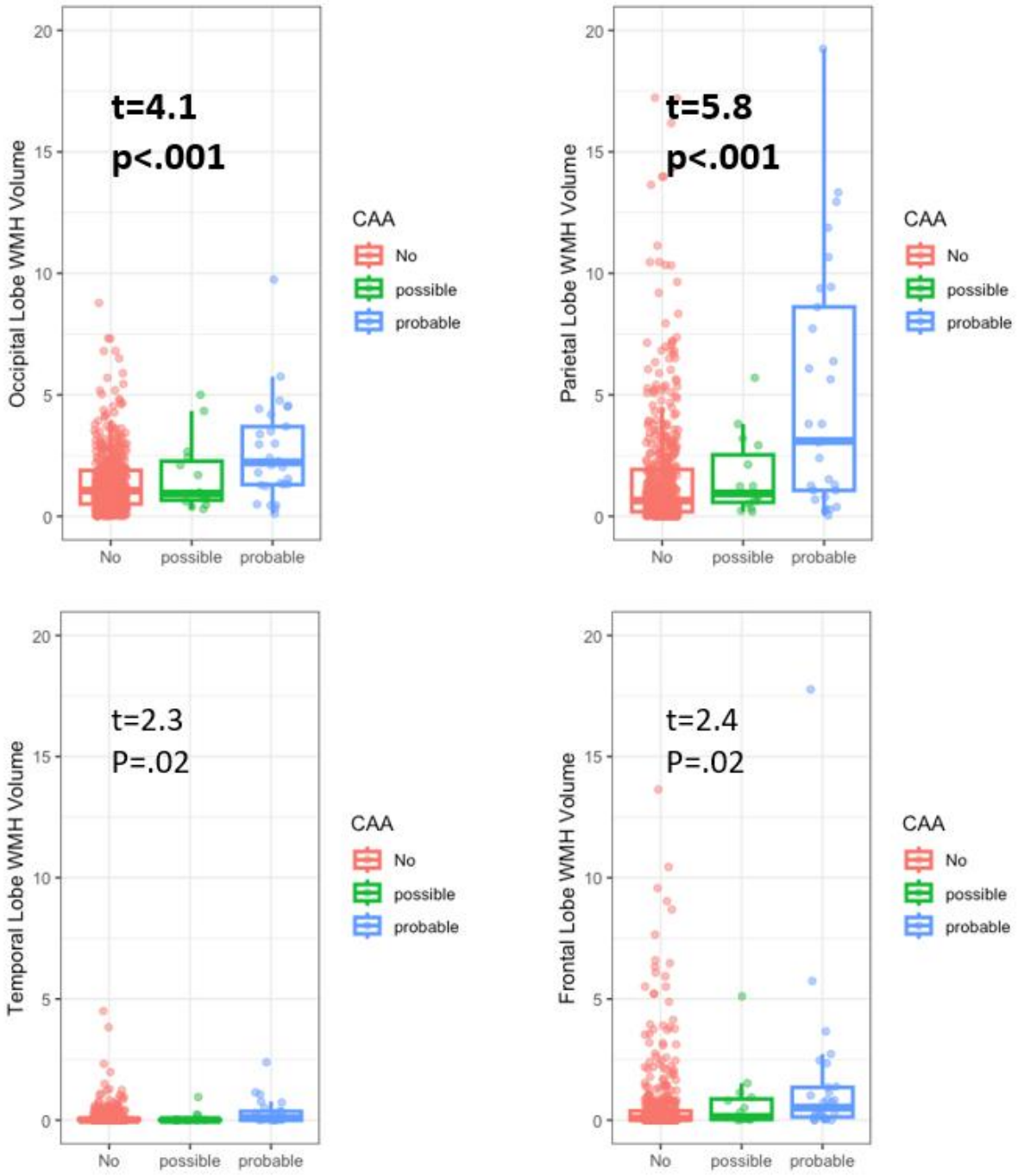


Figure 1: Cross-sectional association of lobar WMH and CAA categories. WMH in the occipital and parietal lobes are significantly elevated in individuals with probable CAA (i.e., two or more CMBs) compared to those in the no CAA group. Models are adjusted for age, sex, grey matter volume, systemic vascular risk, and APOE e4.

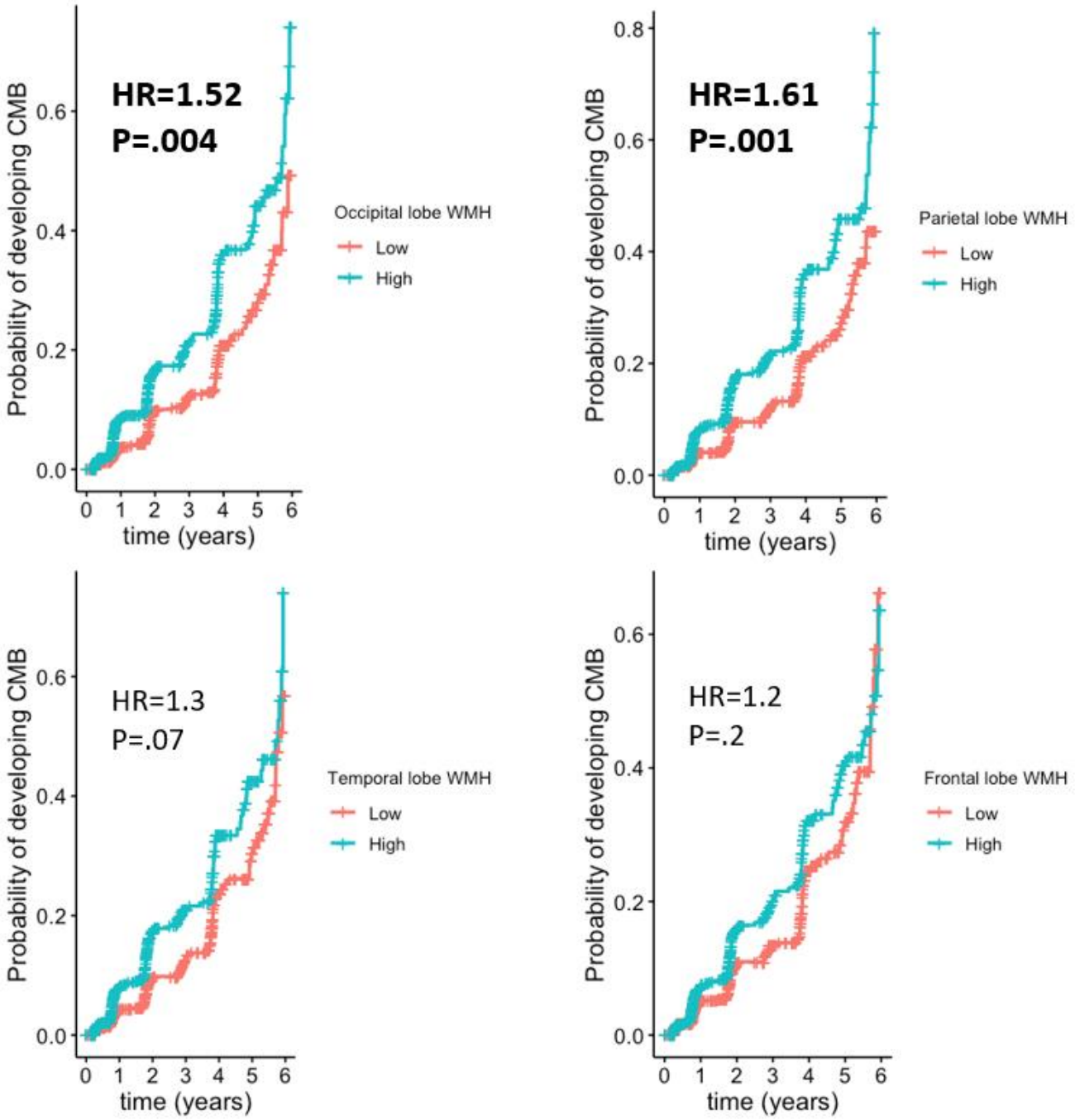


Figure 2: Longitudinal association of baseline lobar WMH and future emergence of CMB in ADNI participants with no CMB at baseline. Elevated baseline WMH in the occipital and parietal lobes are significantly related to the risk of emergence of CMB in individuals with no CAA at baseline. Models are adjusted for age, sex, systemic vascular risk, and APOE e4.

Keywords: white matter hyperintensities, cerebral amyloid angiopathy, cerebral microbleeds, Alzheimer's Disease, regional pattern

163 Defining the grey zone thresholds for tau PET positivity using the Uniτ scale

Guilherme Povala[1], Bruna Bellaver[1], Guilherme Bauer-Negrini[1], Emma Ruppert[1], Marina Medeiros[1], Livia Amaral[1], Firoza Lussier[1], Pamela Lukasewicz[1], Carolina Soares[1], Dana Tudorascu[1], Joseph Masdeu[2], Belen Pascual[2], Brian Gordon[3], Val Lowe[4], Hwamee Oh[5], David Soleimani-Meigooni[6], Pedro Rosa-Neto[7], Suzanne Baker[8], Tharick A. Pascoal[1]

[1]*University of Pittsburgh, Department of Psychiatry, Pittsburgh, PA, US*
[2]*Houston Methodist Research Institute, Neurology, Houston, TX, US*
[3]*Washington University in St. Louis, Department of Radiology, St. Louis, MO, US*
[4]*Mayo Clinic, Radiology, Rochester, MN, US*
[5]*Brown University, Psychiatry, Providence, RI, US*
[6]*University of California San Francisco, Memory and Aging Center, San Francisco, CA, US*
[7]*Translational Neuroimaging Laboratory, McGill University Research Centre for Studies in Aging, Douglas Research Institute, Montréal, QC, CA*
[8]*Lawrence Berkeley National Laboratory, Berkeley, CA, US*

Introduction: Tau PET measures are continuous, and dichotomized thresholds are subject to conceptual and analytical idiosyncrasies. Understanding the limitations in the transition from tau-negative to positive classifications is crucial for the effective use of these thresholds. This study aims to determine the confidence levels of tau PET thresholds of abnormality by characterizing their "gray zone" using the universal tau PET scale (Uniτ, www.unitau.app).

Methods: We evaluated 402 individuals across aging and AD spectrum from HEAD study, with head-to-head scans for MK6240 and Flortaucipir. Uniτ estimates were derived from the Centaur Meta-Temporal ROI. Tau positivity (T+) was defined as Uniτ values above the mean + 2.5 SD of young individuals (<28 years, n=24). Two physicians independently assessed visual tau positivity for each tracer, with agreement indicating clear tau pathology (TVR+). Logistic regression was used to estimate TVR+ probability across Uniτ values for each tracer. Individuals were classified as negative, positive, or within a "gray zone" between the most liberal T+ threshold and varying TVR+ probability thresholds (50%, 75%, 90%, 95%, and 99%).

Results: The Uniτ gray zone as a function of TVR+ showed consistency between both tracers, with differences in the decimal range. The most liberal Uniτ threshold for T+ was 11.0 for both tracers, closely matching the 50% TVR+ probability (11.1 for MK6240, 11.7 for Flortaucipir). Higher TVR+ probabilities corresponded to increased Uniτ values with MK6240 and Flortaucipir showing nearly identical thresholds: 14.2 and 14.8 for 75%, 17.3 and 17.9 for 90%, 19.4 and 19.9 for 95%, and 24.1 and 24.6 for 99%, respectively (**Figure 1**).

Conclusion: These findings highlight the potential of Uniτ to provide a standardized approach for assessing tau positivity across tracers. By combining quantitative Uniτ measures with visual assessments, we enhance the understanding of tau positivity certainty, particularly in the transition between negative and positive classifications.

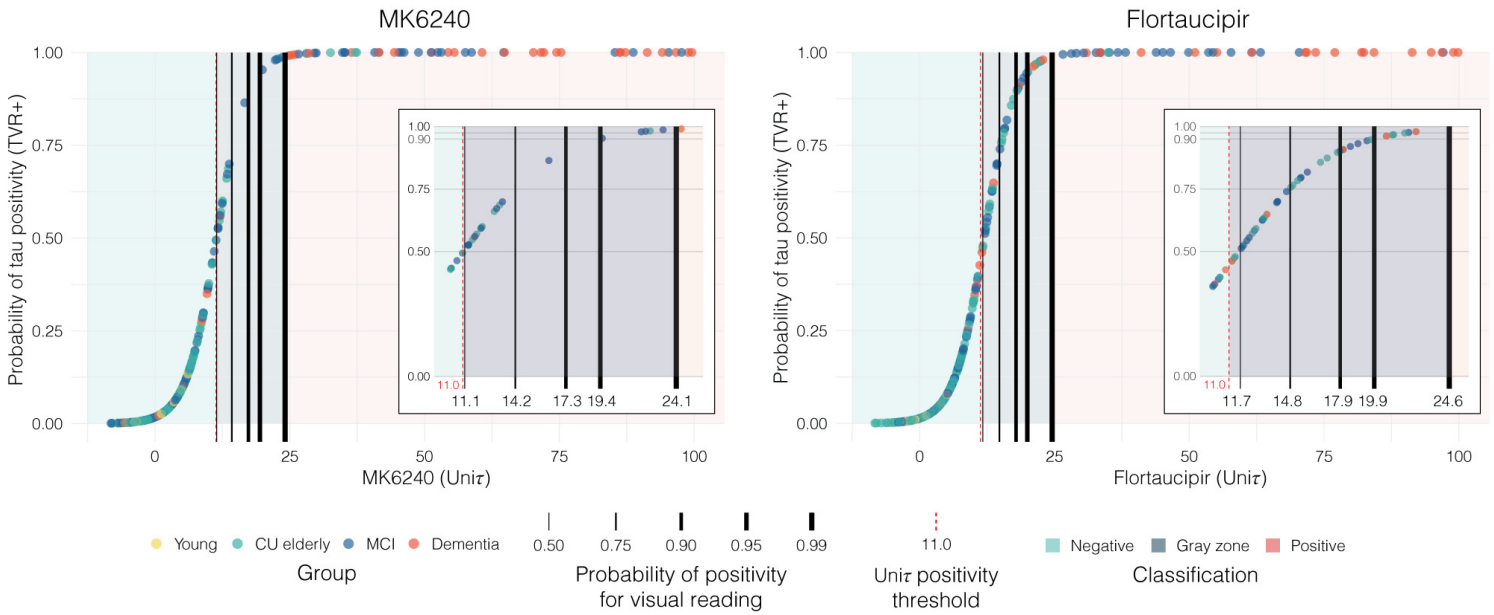


Figure 1. Probability of tau positivity as a function of Uniτ values for MK6240 and Flortaucipir. The figure shows the probability of tau visual reading positivity concordance (TVR+) for MK6240 (left panel) and Flortaucipir (right panel) tracers as a function of Uniτ values. Each dot represents an individual, color-coded by diagnostic group. The dashed red vertical line indicates the common Uniτ threshold for T+ based on the mean + 2.5 s.d. of the young population at 11.0 for both tracers. Black vertical lines mark the Uniτ values associated with 50%, 75%, 90%, 95%, and 99% concordance with TVR+. The shaded regions represent different classifications: negative (green), gray zone (gray), and positive (red). Insets display a zoomed-in view of the gray zone, highlighting the transition between negative and positive classifications.

Keywords: Tau PET, tau positivity, gray zone, thresholds, Uniτ scale

164 Neocortical amyloid spatial extent predicts cognitive decline over time in memory and executive function domains

Emma Thibault[1], Jessie Fanglu Fu[1], Jackson C. Thompson[1], Elliott D. Slade[1], Heidi I.L. Jacobs[1], Julie C. Price[1], Dorene M. Rentz[1,2], Reisa A. Sperling[1,2], Keith A. Johnson[1], Michelle E. Farrell[1]

[1]*Massachusetts General Hospital, Boston, MA, US*
[2]*Brigham and Women's Hospital, Boston, MA, US*

Background: Use of PET spatial extent (EXT) is a novel, sensitive metric for quantification of amyloid spread (Aβ) that reveals a stronger association to cognitive decline than traditional measures of global Aβ level. We sought to use EXT to delve deeper into the association between cognitive measures of executive function and memory and Aβ spread.

Methods: 352 cognitively unimpaired individuals (Table 1) from the Harvard Aging Brain Study (HABS) underwent baseline [^{11}C]-Pittsburgh Compound-B (PiB)-PET and annual longitudinal cognitive evaluation. Baseline EXT (% neocortex PiB+) was further classified into three Aβ-EXT stages: EXT0 (Aβ-, EXT<7.3%), EXT1 (spreading Aβ 7.3-95.6%), EXT2 (widespread Aβ, >95.6%). A series of linear mixed models assessed differences in cognitive decline on Digit Symbol Substitution (DSST, executive domain) and Free and Cued Selective Reminding free recall (fcSRT, memory domain) by baseline EXT stage. Further analysis within the EXT1 subsample evaluated the continuous association between spreading Aβ and cognitive decline in these domains. Models covaried for age, sex, years of education, and included random intercepts and slopes.

Results: The rate of cognitive decline on DSST and fcSRT tracked with baseline EXT (Table 2, Fig.1A,B), with faster decline detected for EXT1 vs. EXT0 after 2 years for DSST and 5 years for fcSRT. Within the EXT1 subsample, there was a significant association between continuous baseline EXT and the rate of DSST decline (p=0.022, h^2=0.10; Table 2, Fig.1E) and a trend level association with fcSRT (p=0.055, h^2=0.07; Table 2, Fig.1F).

Conclusions: The spread of Aβ throughout the neocortex, as quantified with EXT, is associated with early changes in executive function and memory. Consistent with prior evidence using longitudinal changes in Aβ level, executive function changes were observed earlier than memory.

Table 1. Harvard Aging Brain Study (HABS) sample demographics at baseline.

	EXT0 (N=243)	EXT1 (N=74)	EXT2 (N=35)	Overall (N=352)
Age	70.40 ± 8.30 (50-89)	75.39 ± 6.48 (60-90)	73.51 ± 5.50 (64-88)	71.75 ± 7.97 (50-90)
Sex				
F	142 (58.4%)	44 (59.5%)	25 (71.4%)	211 (59.9%)
M	101 (41.6%)	30 (40.5%)	10 (28.6%)	141 (40.1%)
Education (Years)	15.77 ± 3.04 (6-20)	15.76 ± 2.79 (11-20)	16.46 ± 2.95 (8-20)	15.84 ± 2.98 (6-20)
APOEe4 Status				
e4-	150 (61.7%)	33 (44.6%)	10 (28.6%)	193 (54.8%)
e4+	24 (9.9%)	27 (36.5%)	20 (57.1%)	71 (20.2%)
Missing	69 (28.4%)	14 (18.9%)	5 (14.3%)	88 (25.0%)
MMSE	29.09 ± 1.09 (25-30)	28.93 ± 1.09 (25-30)	28.77 ± 1.14 (26-30)	29.03 ± 1.09 (25-30)
PACC5	0.07 ± 0.70 (-2.1-2.1)	0.00 ± 0.63 (-1.3-1.3)	-0.01 ± 0.61 (-1.2-1.2)	0.04 ± 0.68 (-2.1-2.1)
PiB FLR DVR	1.07 ± 0.04 (0.92-1.2)	1.27 ± 0.11 (1.1-1.5)	1.62 ± 0.12 (1.4-2)	1.16 ± 0.19 (0.92-2)

Groups did not differ in sex, years of education, MMSE, or PACC5.

Table 2. Baseline EXT predicts decline rate in executive function and memory.

Sample	Cognitive Outcome	Model Term	β	SE	p	η^2
Full	DSST	Time*EXT1	-0.434	0.130	<0.001	0.05
		Time*EXT2	-0.999	0.174	<0.001	0.19
	fcSRT	Time*EXT1	-0.457	0.120	<0.001	0.04
		Time*EXT2	-1.307	0.166	<0.001	0.11
EXT1	DSST	Time*EXT	-0.0103	0.00437	0.022	0.10
	fcSRT	Time*EXT	-0.00841	0.00427	0.055	0.07

In the full sample, differences in the rate of change in executive function (DSST) and memory (fcSRT) by baseline EXT stage (with EXT0 as the reference group). Individuals in EXT Stage1 (spreading Aβ) and Stage 2 (widespread Aβ) declined faster than those in the EXT0 (Aβ-) Stage. Within the spreading Aβ EXT Stage 1 group, we see that continuous EXT is associated with DSST but only reaches trend level significance in its association with fcSRT.

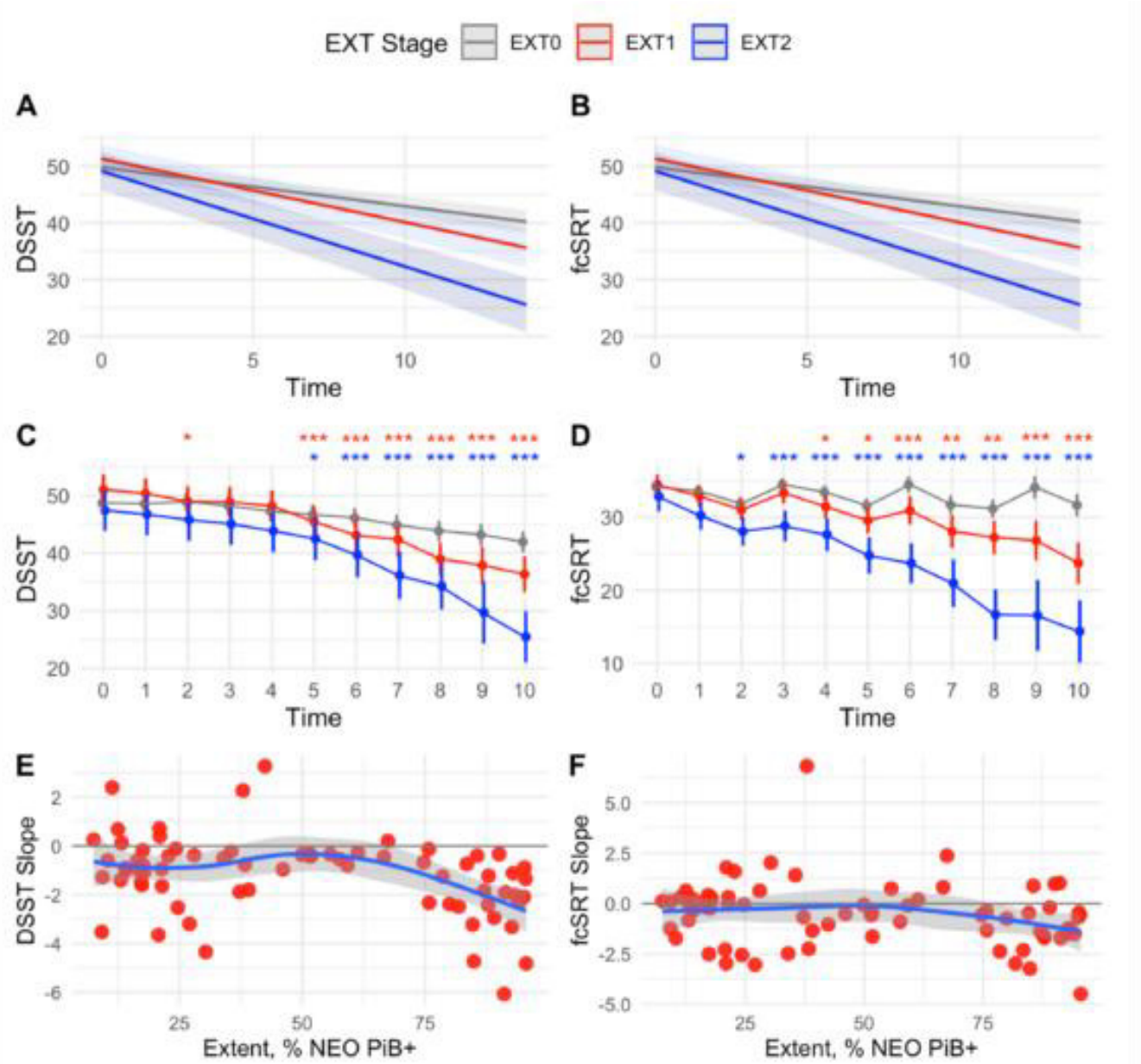


Figure 1. The rate of executive function and memory decline is associated with baseline EXT. A, B) Marginal means are reported from the linear mixed effects (LME) models assessing the baseline EXT stage*time on A) DSST and B) fcSRT for the average HABS participant (71.8 year old female with 15.8 years of education. C, D) LME models were repeated with time treated as a factor for the annual cognitive assessments, enabling assessment of when differences in cognitive trajectories emerge between EXT stages. The rate of decline diverges significantly between the EXT1 and EXT0 groups in year 2 for DSST and year 4 for fcSRT (*<0.05, **<0.01, ***<0.001). E, F) In the spreading Aβ subset (EXT1), we see an association between higher continuous EXT and higher rates of cognitive decline on DSST but not fcSRT. Slopes for DSST and fcSRT were extracted for each individual using ordinary least-squares regression. LOESS curves are plotted to allow for non-linearity. The rate of decline accelerates as individuals approach maximum EXT (meaning as Aβ is detectable across all neocortical regions).

Keywords: amyloid-PET, cognition

165 Patterns of tau-PET accumulation and clinical progression according to biological AD stages

Lydia Trudel[1,2], Joseph Therriault[1], Nesrine Rahmouni[1,2], Arthur Cassa Macedo[1,2], Stijn Servaes[1,2], Etienne Aumont[1], Seyyed Ali Hosseini[1,2], Jaime Fernandez-Arias[1,2], Yansheng Zheng[1,2], Yi-Ting Wang[1,2], Tevy Chan[1,2], Brandon Hall[1,2], Jenna Stevenson[1], Robert Hopewell[4], Chris Hung-Hsin Hsiao[4], Serge Gauthier[1], Paolo Vitali[1], Tharick Pascoal[3], Pedro Rosa-Neto[1,2]

[1]*Translational Neuroimaging Laboratory, McGill University, Montreal, QC, CA*
[2]*Department of Neurology and Neurosurgery, Faculty of Medicine, McGill University, Montreal, QC, CA*
[3]*Department of Psychiatry, School of Medicine, University of Pittsburgh, Pittsburgh, PA, US*
[4]*PET Unit, McConnell Brain Imaging Centre, Montreal, QC, CA*

Objectives: Recently, the Alzheimer's Association Workgroup proposed a framework in which tau-PET can stage AD severity *in vivo*. In this framework, AD severity is staged as T_2-, T_{2MTL}+, T_{2MOD}+ and T_{2HIGH}+ based on tau-PET patterns. The goal of this study is to identify stage-specific patterns of tau-PET accumulation, as well as describe rates of clinical and biological AD stage progression.

Methods: We analyzed tau-PET imaging data from 545 individuals from the TRIAD and ADNI cohorts followed over an average of 3.49 years. Amyloid-positive participants were staged based on regional tau-PET uptake and amyloid-negative individuals were included as non-AD controls. We assessed stage-specific tau accumulation in early, intermediate and late ROIs. Rates of biological AD stage progression were identified for one-year and two-year follow-up. Finally, we assessed probability of developing MCI or dementia according to biological AD stage at baseline using Kaplan-Meier survival analyses.

Results: Individuals showed stage-specific patterns of tau accumulation, predominantly in regions corresponding to their current stage and the subsequent stage. Notably, those in advanced stages did not exhibit accumulation in earlier regions (**Fig. 1**). After two years, we observed low rates of biological stage progression in the T_2- group and substantially higher rates of biological stage progression in T_{2MTL}+ (31.03%) and T_{2MOD}+ groups (42.11%) (**Fig. 2**). Survival analyses revealed differential risk of clinical progression according to biological AD stage, with T_{2MTL}+ and T_{2MOD}+ groups having increased risk of developing MCI, and the T_{2HIGH}+ group of developing dementia over 7 years ($p<0.0001$, **Fig. 3**).

Conclusions: Our results reveal stage-specific patterns of tau accumulation and biological AD stage progression. Furthermore, biological staging of AD in asymptomatic individuals provides prognostic information regarding development of cognitive impairment. Our findings highlight the utility of biological AD staging for designing therapeutic trials with optimal stage-specific clinical and biomarker endpoints.

Figures:

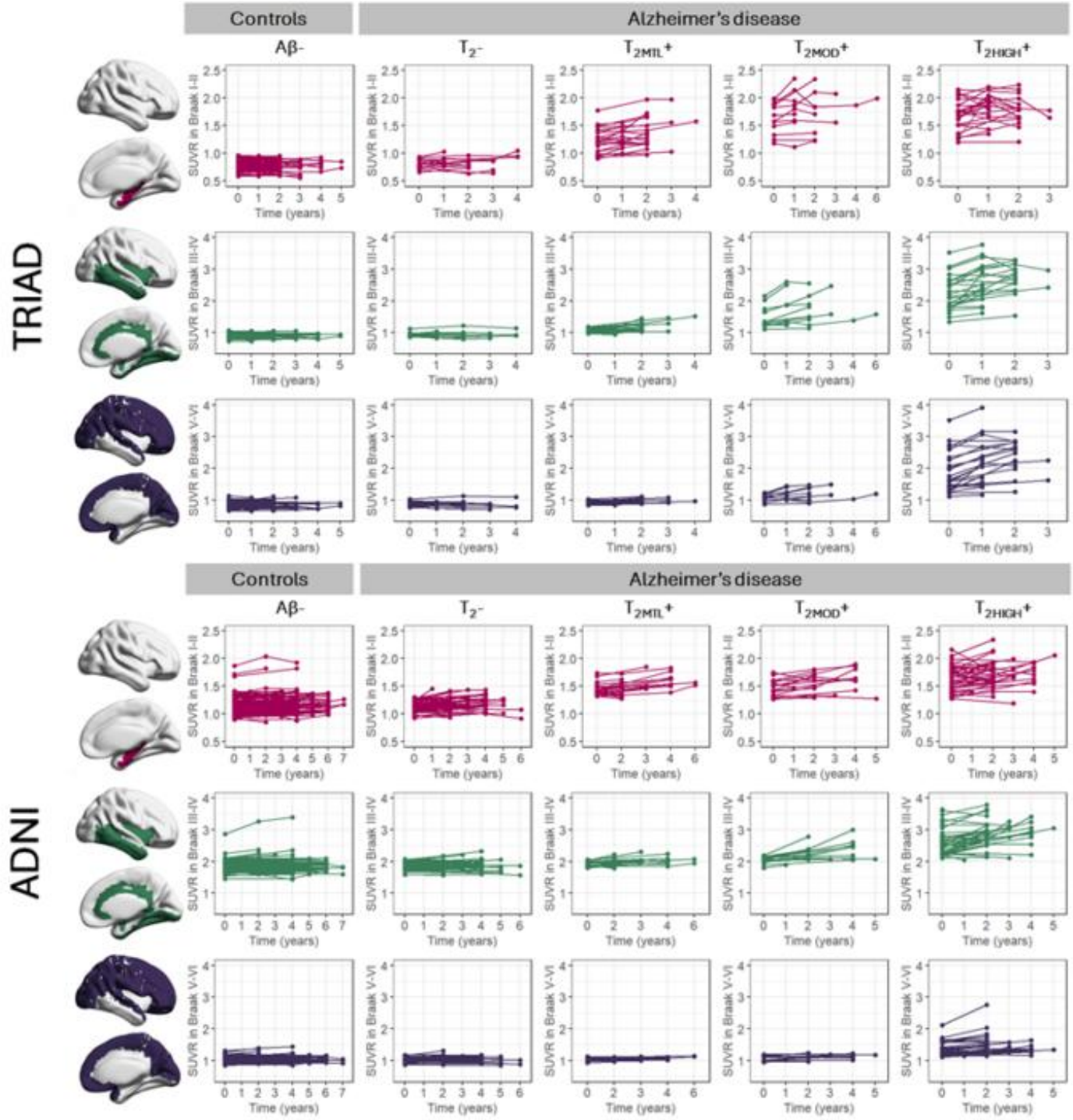


Figure 1. Spaghetti plots showing tau-PET change in Braak ROIs across biological stages.

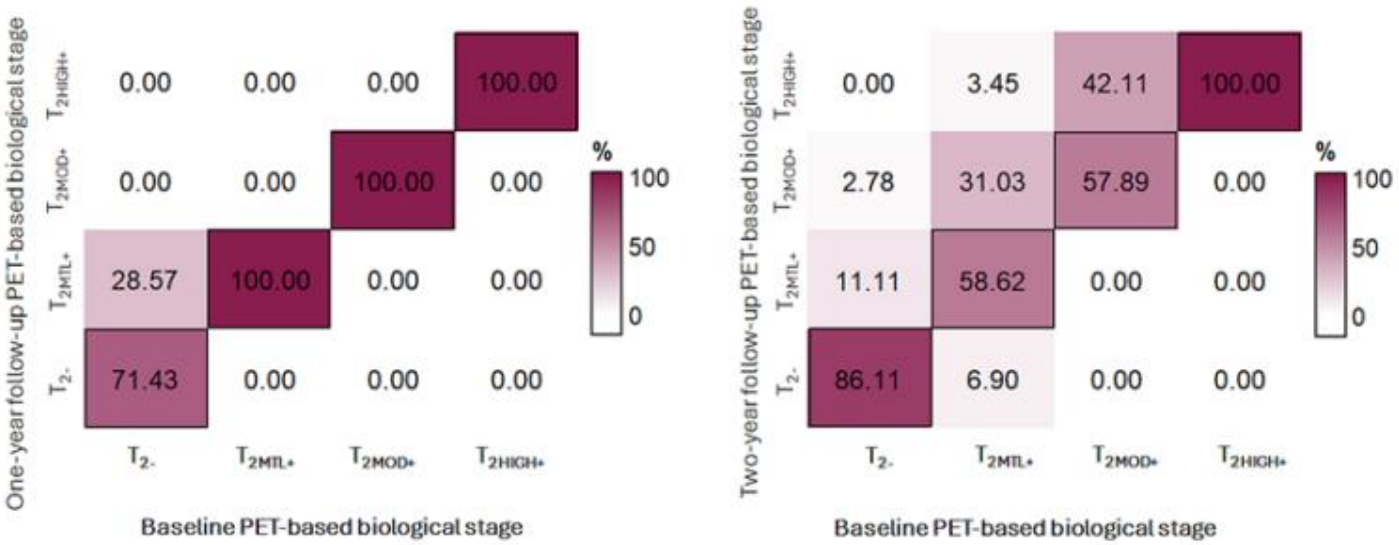


Figure 2. Longitudinal stability and progression of biological stages.

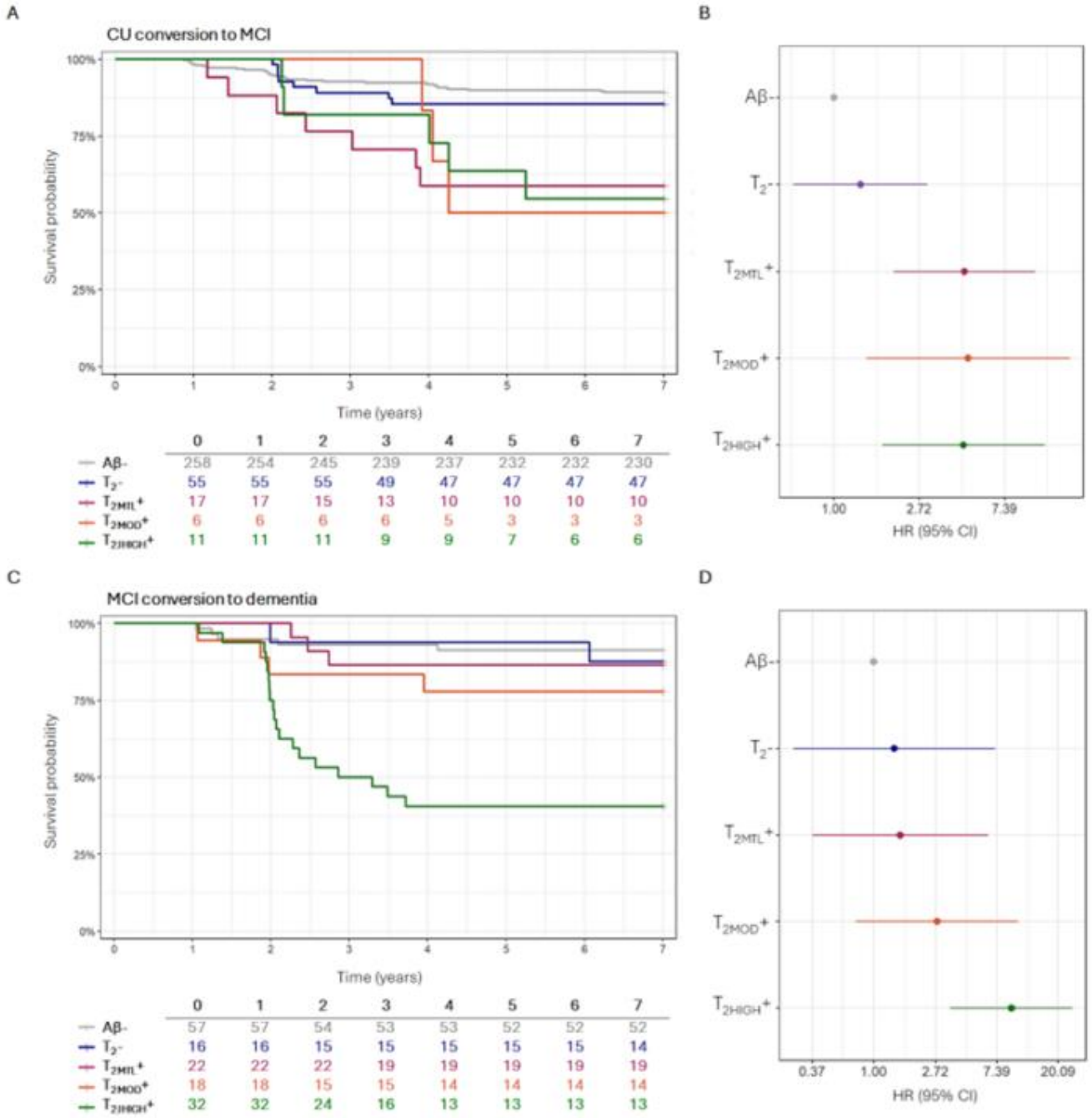


Figure 3. Prognostic value of Alzheimer's disease staging.

Keywords: Alzheimer's disease, Biological staging, Tau-PET imaging, Clinical progression risk

166 The Tau Progression Index (TPI): an individualized, clinically applicable, multimodally-derived score to predict AD progression

Gloria Chiang[1], Tracy Butler[1], Bardiya Ghaderi Yazdi[1], Sindy Ozoria[1], Peter Chernek[1], Jenseric Calimag[1], Sonja Blum[1], Silky Pahlajani[1], Nancy Foldi[1], Mohammad Khalafi[1], Devangere Devanand[2], Hengda He[2], Hani Hojjati[1], Saman Gholipour Picha[1], Christian Habeck[2], Yaakov Stern[2], Qolamreza Razlighi[1]

[1]*Weill Cornell Medicine, New York, NY, US*
[2]*Columbia University Irving Medical Center, New York, NY, US*

Background: Alzheimer's Disease (AD) prognosis is extremely heterogeneous, even with a similar burden of global tau and amyloid (Aβ) deposition in the brain, which makes it challenging to develop targeted therapeutic interventions and to counsel families on disease prognosis.

Method: The TPI is based on 4 components: 1) Remote interaction (TPI_{ri}) between Aβ and tau pathologies in regions that are functionally and/or structurally connected, but spatially distinct; 2) Local interaction (TPI_{li}) between spatially co-localized Aβ and tau pathology; and subject-specific 3) Functional connectivity (TPI_{fc}) and 4) Structural connectivity (TPI_{sc}) between regions that shown to facilitate the spread of tau in the brain.

Results: From an ongoing study of 112 participants with early accumulation of Ab and Tau, longitudinal data were available on 27 participants (2-3 years of follow-up). Using these data and all 4 TPI components as independent variables, we built a LASSO model to predict future tau accumulation, controlling for covariates (age, gender, APOE, infarcts, WMH, head-size). The obtained coefficients were used to compute our TPI, and its predictability was assessed by its association with actual longitudinal tau accumulation (within-sample validation). Furthermore, we compared our model, using subject-specific connectomes, with a conventional model using group-averaged connectomes. As seen in Figure. 1, while both TPIs (obtained by subject-specific; $r=0.8$, $p<10^{-5}$; and group-averaged connectomes: $r=0.58$, $p<0.007$) predicted longitudinal tau accumulation, the subject-specific TPI significantly outperformed the group-averaged TPI in predicting subsequent tau (DSlope $t=2.96$, $p<0.009$) and accounts for 30% more variance in the prediction.

Conclusion: Despite a small sample size, we demonstrate that an imaging index that incorporates baseline Aβ, tau, and subject-specific connectivity can accurately predict future accumulation of tau. Validation in a larger cohort is ongoing.

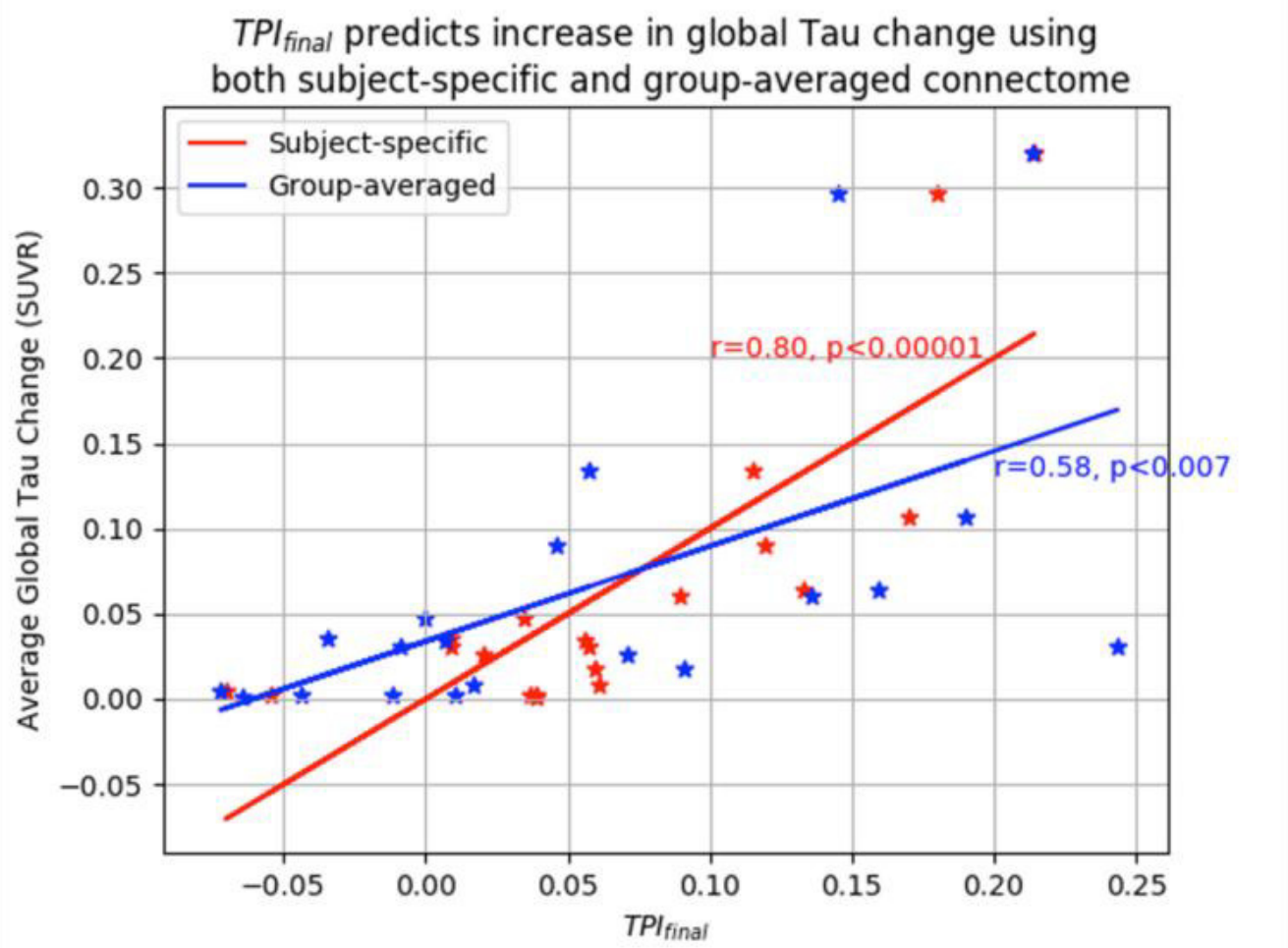


Figure 1) An optimally combined TPI significantly predicts longitudinal change in tau. Using a subject-specific connectome (in red) showed a significantly higher associations with future tau than the group-averaged connectome (in blue).

Keywords: Tau, Amyloid, connectivity, Alzheimer's, prognosis

167 Dried plasma spot optimization for the NULISAseq CNS panel

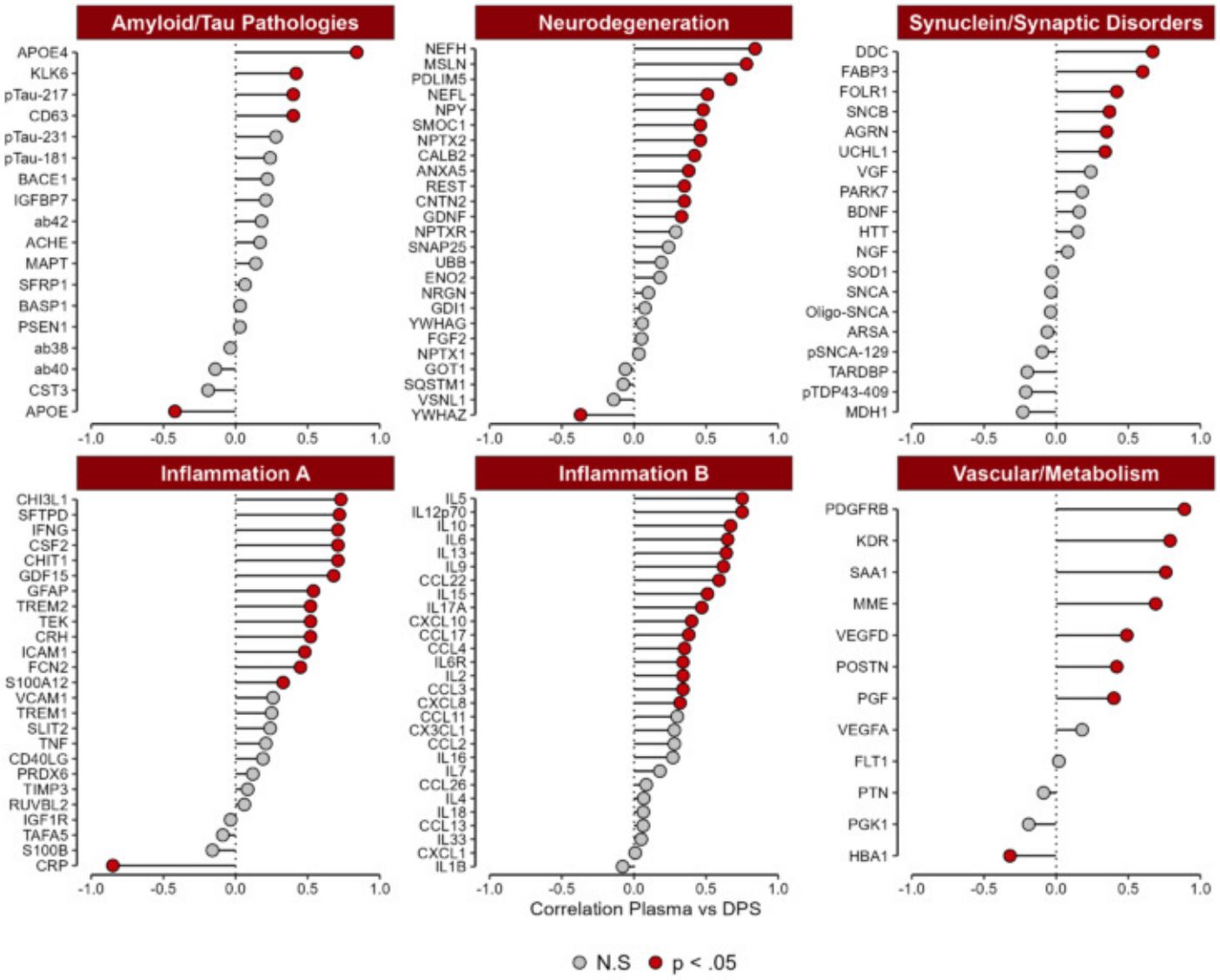
Rachael Wilson[1,2], Ramiro Eduardo Rea Reyes[1], Aaron Fredricks[1,2], Alamar TAP team[3], Sara Rusch[4], Monica VandenLangenberg[1,2], Cindy Jensen[1,2], Martie Marshall[1,2], Elysse Keske[1,2], Haley Weninger[5], Beckie Jeffers[1,2], Hanna Huber[5], Sterling Johnson[1,2], Henrik Zetterberg[1,5,6,7,8,9]

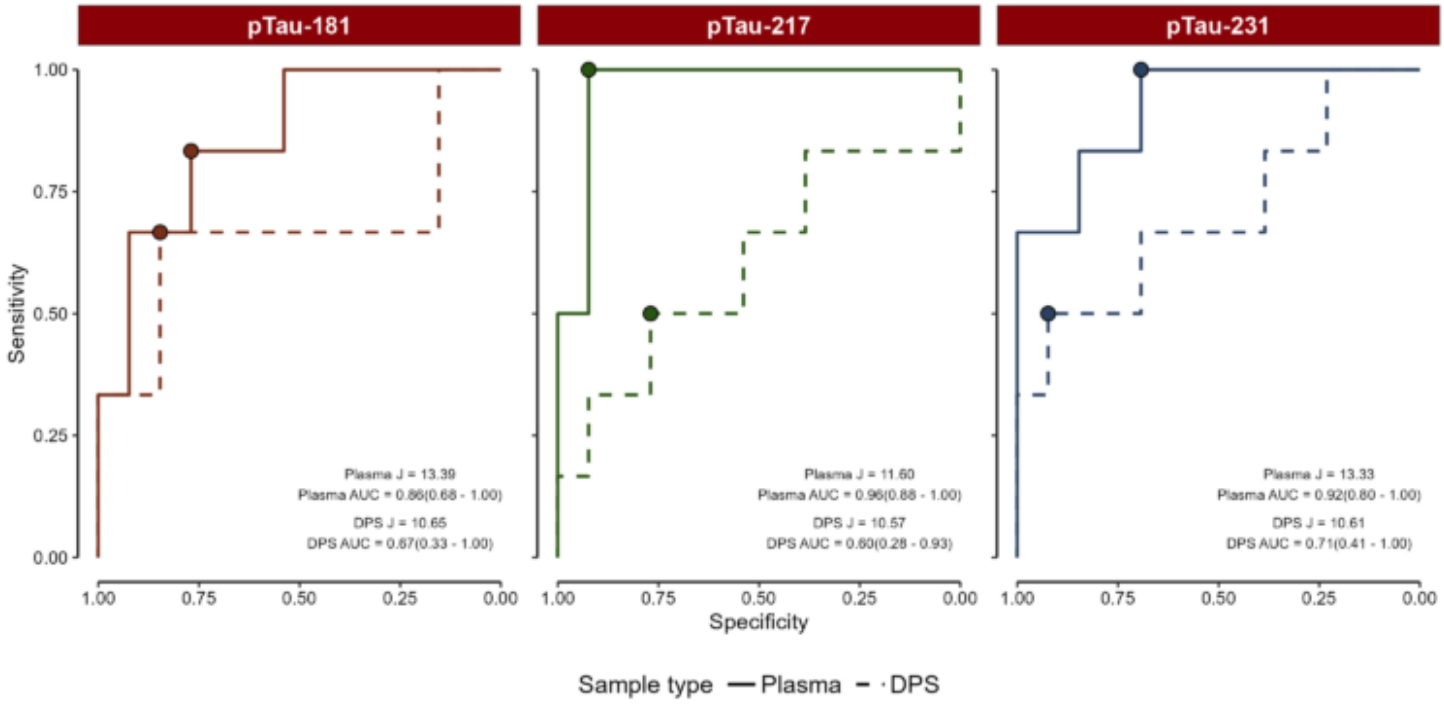
[1]*Wisconsin Alzheimer's Disease Research Center, School of Medicine and Public Health, University of Wisconsin - Madison, Madison, WI, US*
[2]*Wisconsin Alzheimer's Institute, School of Medicine and Public Health, University of Wisconsin - Madison, Madison, WI, US*
[3]*Alamar Biosciences, Fremont, CA, US*
[4]*Clinical Research Unit, UW Health, Madison, WI, US*
[5]*Department of Psychiatry and Neurochemistry, Institute of Neuroscience and Physiology, the Sahlgrenska Academy at the University of Gothenburg, Mölndal, SE*
[6]*Clinical Neurochemistry Laboratory, Sahlgrenska University Hospital, Mölndal, SE*
[7]*Department of Neurodegenerative Disease, University College London Institute of Neurology, London, GB*
[8]*UK Dementia Research Institute at University College London, London, GB*
[9]*Hong Kong Center for Neurodegenerative Diseases, Hong Kong, CN*

Scalable approaches to screening for neurodegenerative dementias including Alzheimer's disease (AD) would expand access to diagnosis and treatment. Dried plasma spots (DPS) offer in-home fingerprick blood collection without centrifugation or cold storage. However, a challenge of method development for DPS protein extraction is maintaining practical sample volumes without diluting analytes beyond the limits of detection (LOD). High sensitivity assays with low volume requirements are ideal for DPS analyses.

With this in mind, we developed a DPS extraction method for the NULISAseq CNS panel, a low volume (25uL), high sensitivity assay targeting 120 analytes related to central nervous system (CNS) dysfunction. We then analyzed paired DPS and plasma from N=40 Wisconsin Registry for Alzheimer's Prevention and Wisconsin Alzheimer's Disease Center participants, the majority of whom were cognitively unimpaired (N=36 (90.0%), N=3 MCI (7.5%), N=1 (2.5%) missing). Amyloid (13C-PiB) PET was available for 19 participants (13 A- (68.4%), 6 A+ (31.6%)). The mean (SD) detectability, or percent of analytes detected above the LOD, across DPS samples was 69.6% (9.5%). Spearman correlation coefficients (r) between DPS and plasma concentrations varied across analytes (Figure 1). For core AD biomarkers pTau181, pTau231, pTau217, NfL, and GFAP, the r (p-value) was 0.35 (0.028), 0.42 (0.007), 0.35 (0.028), 0.64 (8e-6), and 0.46 (0.003), respectively. Nominally, pTau231 had the highest concordance with amyloid PET compared to other pTau species in DPS (ROC-AUC,95% CI: 0.71, 0.41-1.0, Figure 2).

A major limitation of this study is sample size, especially in the impaired group. This was due to sampling by convenience rather than diagnosis. Despite this, we observed good correlations between DPS and plasma for NfL and modest correlations for pTau. Although better correlations for pTau would likely improve agreement with PET, these data are a promising first step in utilizing DPS with NULISA. Performance will likely improve with further optimization.


Amyloid/Tau Pathologies
APOE4
KLK6
pTau-217
CD63
pTau-231
pTau-181
BACE1
IGFBP7
ab42
ACHE
MAPT
SFRP1
BASP1
PSEN1
ab38
ab40
CST3
APOE
Neurodegeneration
NEFH
MSLN
PDLIM5
NEFL
NPY
SMOC1
NPTX2
CALB2
ANXA5
REST
CNTN2
GDNF
NPTXR
SNAP25
UBB
ENO2
NRGN
GDI1
YWHAG
FGF2
NPTX1
GOT1
SQSTM1
VSNL1
YWHAZ
Synuclein/Synaptic Disorders
DDC
FABP3
FOLR1
SNCB
AGRN
UCHL1
VGF
PARK7
BDNF
HTT
NGF
SOD1
SNCA
Oligo-SNCA
ARSA
pSNCA-129
TARDBP
pTDP43-409
MDH1
Inflammation A
CHI3L1
SFTPD
IFNG
CSF2
CHIT1
GDF15
GFAP
TREM2
TEK
CRH
ICAM1
FCN2
S100A12
VCAM1
TREM1
SLIT2
TNF
CD40LG
PRDX6
TIMP3
RUVBL2
IGF1R
TAFA5
S100B
CRP
Inflammation B
IL5
IL12p70
IL10
IL6
IL13
IL9
CCL22
IL15
IL17A
CXCL10
CCL17
CCL4
IL6R
IL2
CCL3
CXCL8
CCL11
CX3CL1
CCL2
IL16
IL7
CCL26
IL4
IL18
CCL13
IL33
CXCL1
IL1B
Vascular/Metabolism
PDGFRB
KDR
SAA1
MME
VEGFD
POSTN
PGF
VEGFA
FLT1
PTN
PGK1
HBA1
-1.0
-0.5
0.0
0.5
1.0
Correlation Plasma vs DPS
N.S
p < .05



Keywords: blood, biomarkers, Alzheimer's disease, pTau, dried blood spots

168 Clinical validation of the Lumipulse G1200 automated immunoassay for the measurement of Alzheimer's disease plasma biomarkers

Tevy Chan[1], Nesrine Rahmouni[1], Yansheng Zheng[1], Marina Congalves[1], Arthur Macedo[1], Etienne Aumont[1], Joseph Therriault[1], Brandon Hall[1], Yi-Ting Wang[1], Lydia Trudel[1], Stijn Servaes[1], Jaime Fernandez-Arias[1], Robert Hopewell[1,2], Henrik Zetterberg[3], Tharick Pascoal[4], Andrea Benedet[3], Pedro Rosa-Neto[1,2]

[1]*Translational Neuroimaging Laboratory, The McGill University Research Centre for Studies in Aging, Montréal, QC, Canada, Montreal, QC, CA*
[2]*McConnell Brain Imaging Center, McGill University, Montreal, QC, CA*
[3]*Department of Psychiatry and Neurochemistry, Institute of Neuroscience and Physiology, The Sahlgrenska Academy, University of Gothenburg, Sweden, Gothenburg, SE*
[4]*University of Pittsburg, Pittsburg, PA, US*

Introduction: Recent advances in plasma biomarkers have positioned them as promising diagnostic tools for Alzheimer's disease (AD). Lumipulse G1200 (Fujirebio) is a fully automated immunoassay instrument that simplifies the analysis of these biomarkers. Here, we evaluated the diagnostic performance of the Lumipulse G1200 plasma phosphorylated tau(p-tau)181 and p-tau217 immunoassays in detecting AD pathology.

Methods: Plasma samples of 102 participants from the TRIAD cohort (median age 67 years, 54% female) were analysed. Spearman's correlation examined the association between plasma p-tau181 and p-tau217 with Aβ ([^{18}F]NAV4694) and tau ([^{18}F]MK6240) PET. Discriminative performance for Aβ and tau PET status was assessed using the area under the curve (AUC) of Receiver operating Characteristic (ROC) analysis.

Results: Plasma p-tau181 and p-tau217 were significantly higher in individuals with clinical diagnosis of AD compared to the cognitively normal or mild cognitive impairment not due to AD (Fig.1). Plasma p-tau217 very strongly correlated with both Aβ and tau PET SUVR (ρ=0.805 and 0.797 respectively, p-value<2.2e-16, Fig.2), as compared to plasma p-tau181 (ρ=0.629 and 0.644, $p < 4.097e-10$). Both assays identified with high accuracy elevated Aβ pathology (plasma p-tau217, AUC, 0.95, 95% CI: 0.90-1.00; p-tau181, AUC 0.86, CI 0.78-0.94) and tau pathology on PET (plasma p-tau217, AUC 0.99, CI: 0.98-1.00; p-tau181, AUC 0.93, CI 0.87-0.98, Fig.3).

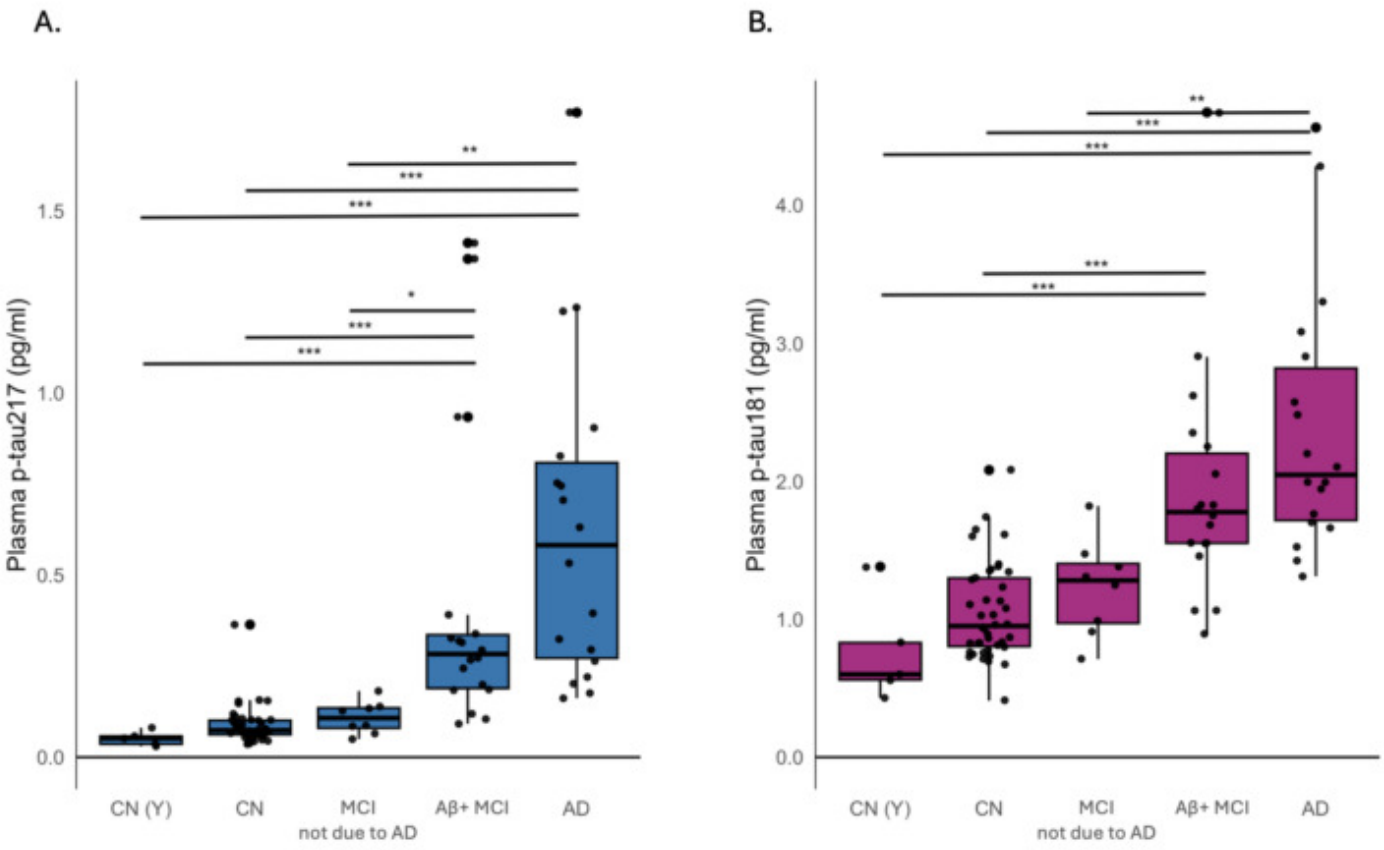


Fig 1. Plasma p-tau217 and p-tau181 concentrations stratified by clinical diagnostic groups. Aβ+, global Aβ PET SUVR >1.55 ; CN, cognitively normal; MCI, mild cognitive impairment; AD, Alzheimer's disease; Y, young. * p<0.05, ** p<0.01, *** p<0.001.

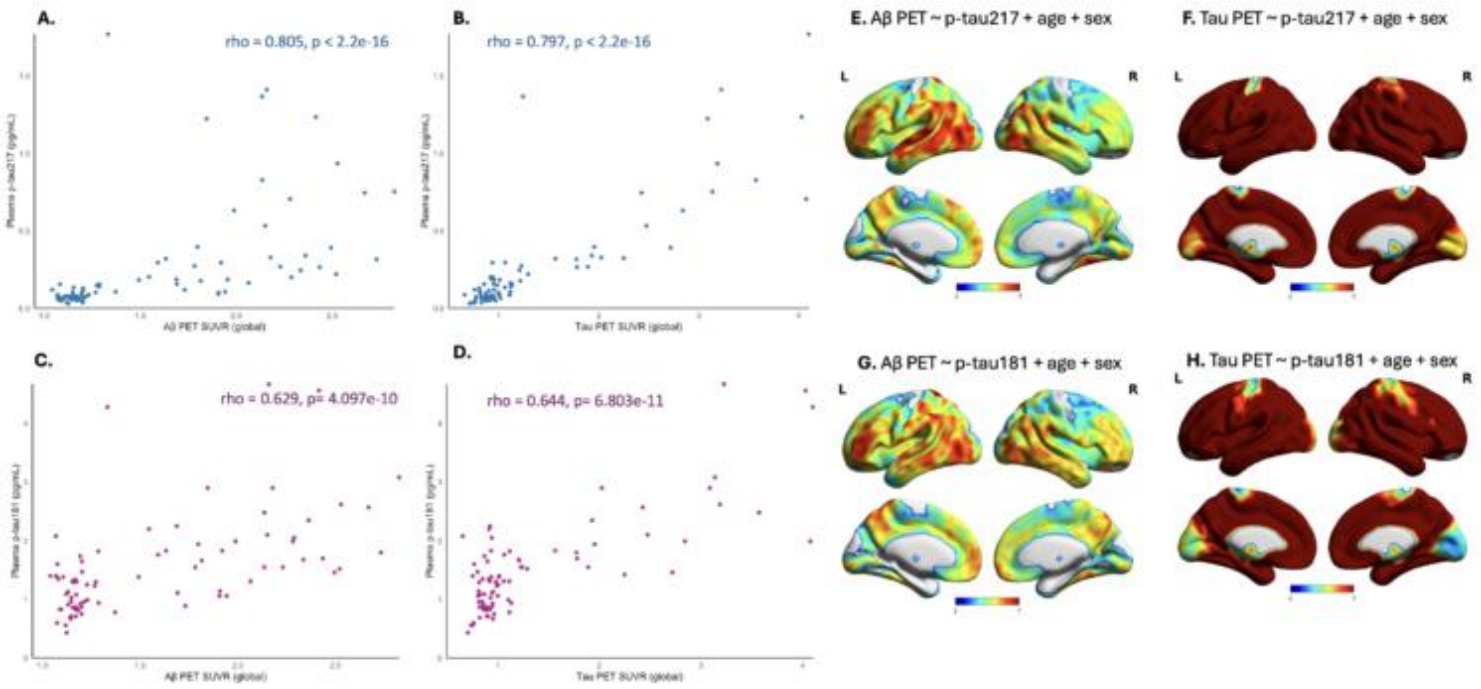


Fig 2. Plasma p-tau217 and p-tau181 strongly correlated with Aβ and tau PET. Spearman's correlation between plasma p-tau217 and Aβ (A) and tau PET SUVR (B). Spearman's correlation between plasma p-tau181 and Aβ (C) and tau PET SUVR (D). E to H: The images show the T-values resulting from voxel-wise linear regressions assessing the associations between Aβ [^{18}F]NAV4694 PET and plasma p-tau217(E), p-tau181 (G), and between Tau [^{18}F]MK6240 PET and plasma p-tau217 (F) and p-tau181 (H). All voxel-wise analysis included age and sex as covariates.

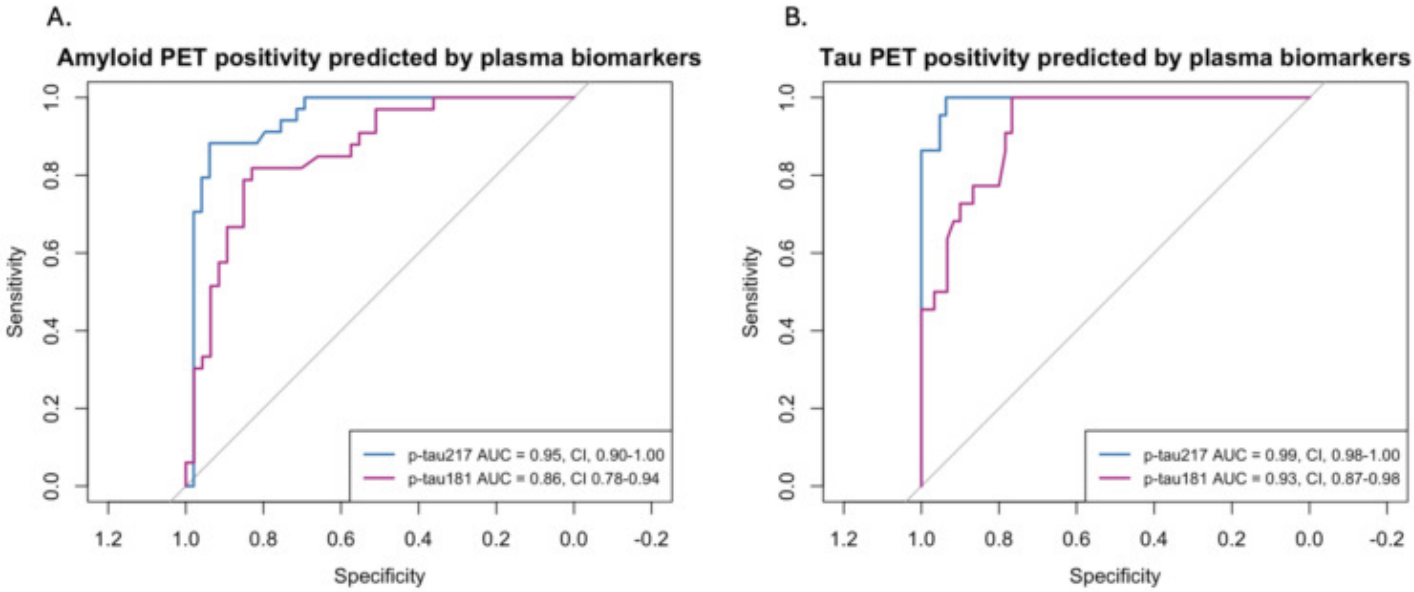


Fig 3. Plasma p-tau217 and p-tau181 assays identified elevated PET Aβ and tau pathology with high accuracy. AUC, area under the ROC curve; CI, 95% confidence interval.

Conclusions: Plasma p-tau217 and p-tau181 Lumipulse G1200 immunoassays showed high discriminative performance in identifying AD PET Aβ and tau pathology. Their ease of use and high diagnostic accuracy make them promising candidates for clinical implementation.

Keywords: Alzheimer's disease, plasma biomarkers, diagnostic performance

169 Sex differences in synaptic loss in early Alzheimer's disease

Jordan Galbraith[1], Hamid Abuwarda[1], Ryan O'Dell[2], Adam Mecca[2], Christopher van Dyck[2], Carolyn Fredericks[1]

[1]*Department of Neurology, Yale School of Medicine, New Haven, CT, US*
[2]*Alzheimer's Disease Research Unit, Yale School of Medicine, New Haven, CT, US*

Background: Synaptic loss is an important early structural marker in Alzheimer's disease (AD) and correlates with cognitive decline. With the development of [11C]UCB-J, a tracer that targets synaptic vesicle glycoprotein 2A (SV2A), we have begun to study synaptic alterations in AD *in vivo*. Women face twice the lifetime risk and a more aggressive course of AD than men, and while prior postmortem work in rodents and humans has demonstrated sex differences in spine density, synaptic morphology, and molecular synapse composition, there are no current *in vivo* studies exploring sex differences in SV2A binding in AD.

Methods: [11C]UCB-J binding was measured in 37 amyloid-positive cognitively impaired (CI) participants (14 aMCI and 23 mild dementia) and 17 amyloid-negative cognitively normal (CN) participants aged 50-85 years. Distribution volume ratios (DVR) were calculated using a cerebellar reference region. Cluster-corrected two sample t-tests comparing SV2A in females and males were calculated in both CI (19 female, 18 male) and CN groups (9 female, 8 male).

Results: There was higher synaptic density in CI and CN females than males in the amygdala, thalamus, head of the caudate, and parahippocampal gyrus ($p<0.01$, $p<0.01$). CI males exhibited higher synaptic density in the posterior cingulate cortex (PCC) and periaqueductal gray ($p<0.01$, $p<0.01$).

Discussion: CI males had increased synaptic density in the PCC, while both CI and CN females had greater synaptic density in primarily limbic regions that are affected early in the progression of AD. This higher synaptic density in CN females could hold clues regarding women's more aggressive tau propagation and increased risk of disease. Further, many of these areas are part of the default mode network (DMN), which undergoes functional connectivity changes (FCC) throughout AD progression. Future directions will include characterizing the interaction between SV2A binding and FCC, emphasizing the DMN.

Keywords: Synaptic density, SV2A, Alzheimer's disease, Sex differences, [11C]UCB-J PET

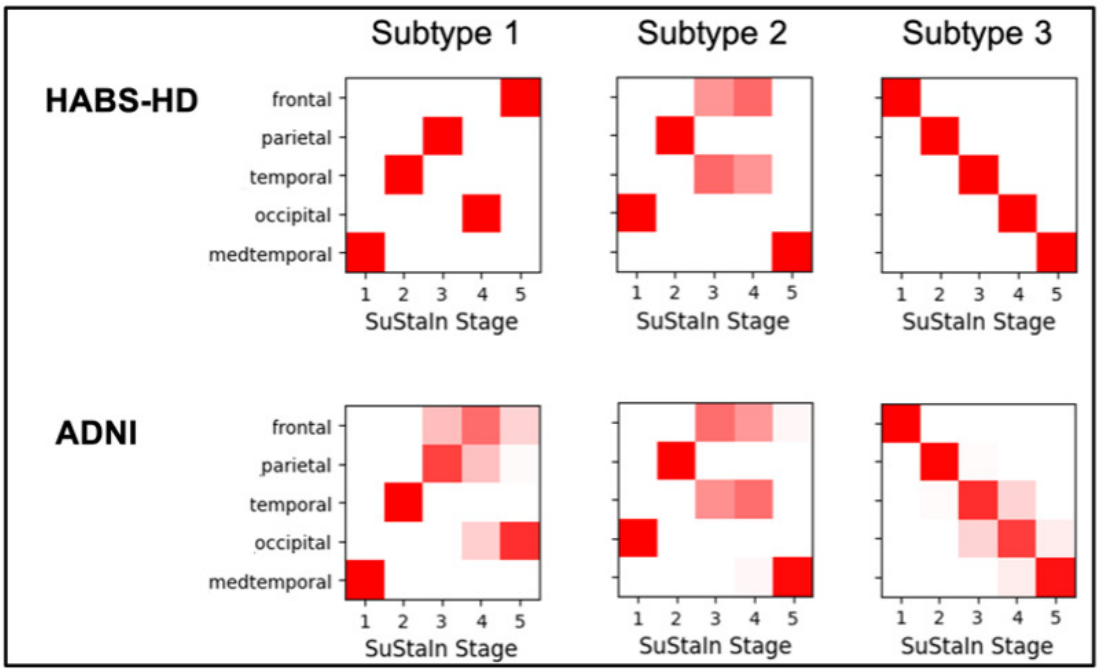
170 Assessing the generalizability of AD subtypes across diverse cohorts: HABS-HD and ADNI

Gordon Zhaoqi An[1,2], Brain Gordon[2], Aristeidis Sotiras[2], Peter Millar[3], Sid O'Bryant[4], Beau Ances[2,3], Karin Meeker[4]

[1]*Devision of Computational and Data Sciences at Washington University in St. Louis, St. Louis, MO, US*
[2]*Mallinckrodt Institute of Radiology at Washington University in St. Louis, School of Medicine, St. Louis, MO, US*
[3]*Department of Neurology at Washington University in St. Louis, School of Medicine, St. Louis, MO, US*
[4]*Institute for Translational Research at University of North Texas Health Science Center, Fort Worth, TX, US*

Background: Alzheimer's disease and related dementias (ADRDs) present significant biological heterogeneity, which influences clinical outcomes and treatment responses. However, current ADRD research has been predominately conducted in non-Hispanic white cohorts, such as the Alzheimer's Disease Neuroimaging Initiative (ADNI), limiting the understanding of ADRD progression in diverse populations. The Health and Aging Brain Study – Health Disparities (HABS-HD), which includes Black/African American (AA), Hispanic (HIS), and non-Hispanic white (NHW) participants, offers a broader sociodemographic perspective. This study aims to test the generalizability of ADRD subtypes and progression patterns identified in ADNI to the more diverse HABS-HD cohort.

Methods: Structural MRI data from HABS-HD (AA n=588, HIS n=1005, NHW n=1009) and ADNI (n=864) cohorts were processed using FreeSurfer to extract brain cortical thickness and hippocampal volume. The Subtype and Stage Inference (SuStaIn) algorithm was then applied to both datasets to identify spatial atrophy subtypes and disease stages. To compare subtypes between cohorts, Positional Variance Diagrams (PVDs) in **Figure 1** were used to visualize the variability and uncertainty in disease progression patterns derived by the model.



Results: SuStaIn identified three spatial atrophy subtypes and progression stages in HABS-HD and ADNI. HABS-HD's PVD patterns aligned with ADNI's, revealing distinct progression patterns: subtype 1 was characterized by initial degeneration of the hippocampus, followed by posterior and then anterior spread; subtype 2 began with occipital atrophy, progressing to parietal regions; subtype 3 was characterized by initial frontal degeneration,

with subsequent spread to posterior regions. **Table 1** shows significant differences in HABS-HD's demographic and clinical features ($p<0.05$), where subtype 3 exhibits the most severe cognitive impairment and represents the oldest age group.

HABS-HD Subtypes	**SuStaIn subtype 1**, N = 104[1]	**SuStaIn subtype 2**, N = 114[1]	**SuStaIn subtype 3**, N = 114[1]	**p-value**[2]
Age	70 (10)	66 (9)	65 (9)	<0.001
Gender				0.2
Female	53 (51%)	67 (59%)	72 (63%)	
Male	51 (49%)	47 (41%)	42 (37%)	
race				0.5
African American	34 (33%)	37 (32%)	32 (28%)	
Mexican American	33 (32%)	47 (41%)	46 (40%)	
Non-Hispanic White	37 (36%)	30 (26%)	36 (32%)	
CDR				<0.001
0	25 (24%)	77 (68%)	69 (61%)	
0.5	38 (37%)	24 (21%)	33 (29%)	
1 or greater	41 (39%)	13 (11%)	12 (11%)	
CDR_SB	3.73 (3.93)	0.96 (1.98)	1.14 (2.38)	<0.001
MMSE	22 (6)	26 (4)	27 (4)	<0.001

[1] Mean (SD); n (%)

[2] Kruskal-Wallis rank sum test; Pearson's Chi-squared test

Conclusion: The similarity of disease progression patterns between HABS-HD and ADNI supports the generalizability of AD subtypes to diverse populations, highlighting the subtypes' potential to advance clinical trials and precision medicine for neurodegenerative disorders.

Keywords: Alzheimer's Disease, MRI, Subtypes and stages, Spatial patterns

171 Locus coeruleus - medial temporal lobe functional connectivity confers protection against amyloid-related cognitive decline in the context of high cognitive reserve

Lukas Heinrich[1,3], Prokopis C Prokopiou[1], Emma E Wiklund[1], Kathryn V Papp[4], Dorene M Rentz[2,4], Reisa A Sperling[2,4], Keith A Johnson[1,2,4], Heidi IL Jacobs[1]

[1]*Department of Radiology, Massachusetts General Hospital / Harvard Medical SChool, Boston, MA, US*
[2]*Department of Neurology, Massachusetts General Hospital/ Harvard Medical School, Boston, MA, US*
[3]*Faculty of Health, Medicine and Life Sciences, Maastricht University, Maastricht, NL*
[4]*Center for Alzheimer Research and Treatment, Department of Neurology, Brigham and Women's Hospital, Boston, MA, US*

Background: Research into cognitive reserve (CR) has indicated that its preserving effect may involve changes in cortical network connectivity. The noradrenergic locus coeruleus (LC), one of the first brain areas affected by Alzheimer's pathology, recruits networks necessary to meet a given task's demands. We showed previously that better LC structure attenuates tau-related cognitive decline in individuals with high CR. Now, we investigated the impact of functional connectivity between the LC and resilience-relevant regions, and cognitive reserve, on beta-amyloid-related cognitive decline.

Methods: Older individuals (N=128) that underwent fMRI and 11C-Pittsburgh Compound-B (PiB) PET were selected from the Harvard Aging Brain Study (Figure 1). Functional connectivity (FC) between LC and ROIs previously shown to confer resilience was obtained from a novelty-versus-repetition Face-Name memory task using generalized psychophysiological interaction analysis. Cognition over time was assessed using PACC5. A CR composite score was constructed by averaging z-scored verbal-IQ, years of education, and Hollingshead scale. Cluster analysis grouped individuals based on cognitive reserve and PiB burden. (Non)linear mixed-effects models tested whether the association between LC-ROI FC and cognitive trajectories differed across groups.

Results: Higher CR related to better baseline PACC-scores (p<0.001). Cluster analysis identified four groups (Figure 2): High amyloid/high CR; high amyloid/low CR, low amyloid/high CR and low amyloid/low CR. The high-PIB-clusters exhibited more PACC-decline than low-PIB clusters, but decline was lower within the high CR/high PiB cluster (p<0.001). Individuals with high CR exhibited no amyloid-related cognitive decline when LC-MTL FC was high, while low CR individuals did (p<0.001). No attenuated decline was observed for LC-ACC FC (p=0.24) and LC-PSTG FC (p=0.79).

Conclusion: Our findings suggest that higher LC-MTL connectivity represents a neural correlate of CR, providing cognitive resilience in the face of elevated amyloidosis. Future research aims to understand how long this resilience persists as underlying AD pathology accumulates.

Demographics	
N	128
Age (mean years, SD)	70.0 (8.9)
Biological Sex (f) (N, %)	71 (55%)
ApoE4-Carriers (N, %)	38 (29%)
MMSE (mean score, SD)	29.28 (0.87)
Education (mean years, SD)	15.7 (2.7)
Hollingshead Score (mean, SD)	28.1 (14.9)
Verbal IQ (mean, SD)	122.7 (6.6)
Clinical Characteristics	
PIB+ (n, %)	36 (28%)
Neocortical PIB DVR PVC (mean, SD)	1.36 (0.37)
LC-MTL connectivity (mean, SD)	0.05 (0.05)
LC-ACC connectivity (mean, SD)	0.07 (1.69)
LC-PSTG connectivity (mean, SD)	-0.58 (1.86)
CDR baseline: 0	128 (100%)
PACC5 baseline (mean, SD)	0.22 (0.6)
PACC5 follow-up time (mean years, SD)	7.8 (3.1)

Figure 1 Demographics. *Abbreviations: Abbreviations: SD = standard deviation, f = female, ApoE4 = apolipoprotein E4, MMSE = Mini Mental State Examination, PIB+ = individuals with 11C-Pittsburgh Compound-B mean values above clinical cut off (>1.24), LC = locus coeruleus, MTL = medial temporal lobe, ACC = anterior cingulate cortex, PSTG = posterior superior temporal gyrus, CDR = Clinical Dementia Rating. Data is presented as means and (standard deviations) or numbers and (percentages).*

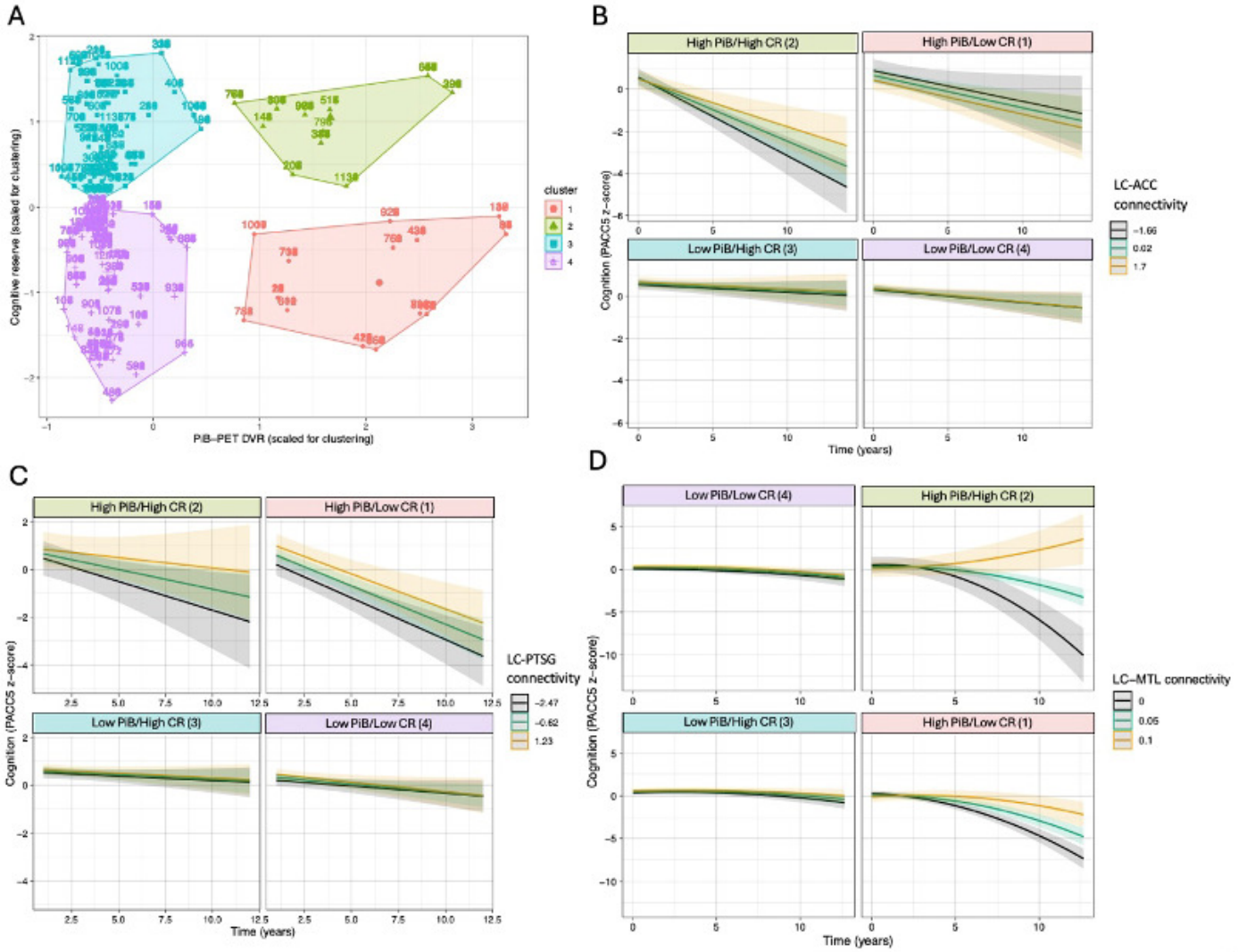


Figure 2. ***Effect of LC functional connectivity with areas linked to resilience*** *(anterior cingulate cortex (B), posterior superior temporal gyrus (C))* ***or AD*** *(medial temporal lobe (D))* ***on cognitive decline per cluster****.* ***A)*** *Grouping results of k-means clustering analysis.* ***The*** *clustering algorithm divided the sample into four groups: High amyloid/low CR (Cluster 1, red), high amyloid/high CR (Cluster 2, green), low amyloid/high CR (Cluster 3, blue), and low amyloid/low CR (Cluster 4, purple). Units on x-axis and y-axis reflect scaled variables, as necessary for clustering.* ***B)*** *Association between LC-ACC connectivity and cognition over time per cluster. We observed no effect of LC-ACC FC on amyloid-related cognitive decline in clustered groups.* ***C)*** *Association between LC-PSTG connectivity and cognition over time per cluster. Similarly to LC-ACC FC, we observed no attenuation of amyloid-related cognitive decline in clustered groups associated with LC-PSTG FC.* ***D)*** *Association between LC-MTL connectivity and cognition over time per cluster (the nonlinear model was a better fit than the linear model). Functional connectivity between the LC and MTL attenuated cognitive decline in the high amyloid/high CR group. The high amyloid/high CR group did not exhibit cognitive decline if LC-MTL connectivity during novelty vs repetition was higher (yellow line).*

Contrast analysis of between-group differences				
Region of interest	Group 1	Group 2	β-coefficient	P-val
MTL	High PiB/Low CR	High PiB/High CR	203.91	0.04*
MTL	High PiB/Low CR	Low PiB/High CR	-29.77	0.35
MTL	High PiB/Low CR	Low PiB/Low CR	-64.33	0.06
MTL	High PiB/High CR	Low PiB/High CR	-233.68	0.02*
MTL	High PiB/High CR	Low PiB/Low CR	-268.24	0.01*
MTL	Low PiB/High CR	Low PiB/Low CR	-34.56	0.11
ACC	High PiB/Low CR	High PiB/High CR	-0.04	0.31
ACG	High PiB/Low CR	Low PiB/High CR	-0.05	0.21
ACG	High PiB/Low CR	Low PiB/Low CR	-0.05	0.21
ACG	High PiB/High CR	Low PiB/High CR	0.01	0.91
ACG	High PiB/High CR	Low PiB/Low CR	0.00	0.91
ACG	Low PiB/High CR	Low PiB/Low CR	0.00	0.91
PSTG	High PiB/Low CR	High PiB/High CR	-0.01	0.81
PSTG	High PiB/Low CR	Low PiB/High CR	0.03	0.81
PSTG	High PiB/Low CR	Low PiB/Low CR	-0.01	0.81
PSTG	High PiB/High CR	Low PiB/High CR	-0.01	0.81
PSTG	High PiB/High CR	Low PiB/Low CR	-0.01	0.81
PSTG	Low PiB/High CR	Low PiB/Low CR	0.00	0.85

Figure 3. *Model output from linear mixed effects models associating LC-ROI functional connectivity with PACC5 decline, contrasting the cluster-analysis derived groups. The region of interest used in the connectivity analysis is described in the first column (MTL: medial temporal lobe, ACC: anterior cingulate cortex, PSTG: posterior superior temporal gyrus). Columns two and three describe the groups being compared. In each model, PACC5 was used as outcome and covariates (sex and age) were included in an interaction term with time (in years). Models additionally included random slope and intercept terms. Only connectivity between the LC-MTL significantly explained differences in cognitive trajectories between specific PiB/CR groups. Mixed effect models including LC-MTL connectivity were assessed using a non-linear term for time (in years), while models including LC-ACC and LC-PSTG connectivity only converged when using a linear term. All depicted p-values are FDR-corrected.*

Keywords: cognitive reserve, PiB-PET, MRI, amyloid-beta, aging

172 Effect of AD risk factors on tau-PET tracer uptake and its association with amyloid-β pathology

Matheus Rodrigues[1], Bruna Bellaver[1], Guilherme Povala[1], Guilherme Bauer-Negrini[1], Firoza Lussier[1], Pamela Lulasewicz Ferreira[1], Markley Silva Oliveira Junior[1], Andreia Rocha[1], Pampa Saha[1], Emma Rupert[1], Marina Scop Medeiros[1], Joseph Masdeu[2], Dana Tudorascu[1], David Soleimani-Meigooni[3], Juan Fortea[4], Val Lowe[5], Hwamee Oh[6], Belen Pascual[2], Brian Gordon[7], Pedro Rosa-Neto[8], Suzanne Baker[9], Tharick Pascoal[1]

[1]*University of Pittsburgh, Department of Psychiatry, Pittsburgh, PA, US*
[2]*Houston Methodist Research Institute, Department of Neurology, Houston, TX, US*
[3]*University of California San Francisco, San Francisco, CA, US*
[4]*Hospital de la Santa Creu i Sant Pau, Barcelona, ES*
[5]*Mayo Clinic, Department of Radiology, Rochester, MN, US*
[6]*Brown University, Department of Psychiatry and Human Behavior, Providence, RI, US*
[7]*Washington University in St. Louis, Department of Radiology, Saint Louis, MO, US*
[8]*Translational Neuroimaging Laboratory, McGill University Research Centre for Studies in Aging, Montreal, QC, CA*
[9]*Lawrence Berkeley National Laboratory, Berkeley, CA, US*

Objective: We aim to investigate the influence of dementia risk factors and comorbidities on ^{18}F-Flortaucipir (FTP) and ^{18}F-MK6240 (MK) tau-PET tracers' uptake. Additionally, we will assess how these factors impact the association between Aβ-PET and tau-PET.

Methods: We accessed 378 individuals across the aging and AD spectrum (219 cognitively unimpaired and 159 cognitively impaired) from the HEAD study, with available Aβ-PET, FTP, MK, and clinical assessments. Linear regression models corrected for age, Aβ PET pathology, clinical diagnosis, and study site tested the association of factors with tau-PET tracers in the medial temporal lobe (MTL) and neotemporal cortex (NeoT). Lowess method and voxel-wise analysis accounting for age, clinical diagnosis, and study site tested the influence of factors in the association of Aβ-PET Centiloid values with tau-PET tracers. A Centiloid × factor term was added to test the interactions between independent variables.

Results: We found that sleep disorder and high body mass index (BMI) were negatively associated with both tau-PET tracers' uptake in the MTL, while hypertension was negatively associated only with MK uptake (Fig. 1A, B) after accounting for covariates. In the NeoT, sleep disorder was negatively associated with both FTP and MK uptake, whereas visual loss was associated only with reduced MK uptake (Fig. 1C, D). Furthermore, voxel-wise interaction analysis and Lowess curves supported that sleep disturbances, high BMI, and hypertension attenuated the association between Aβ-PET and tau-PET tracer uptake. Visual loss negatively impacted the relationship between Aβ PET and FTP uptake, but not MK uptake, in the MTL (Fig. 2).

Conclusion: In this preliminary analysis, sleep disorders, hypertension, and high BMI were independently associated with tau-PET tracer uptake. These prevalent factors in the elderly also weakened the association between Aβ-PET and tau-PET, underscoring the need for further studies to better understand their role in modulating this relationship.

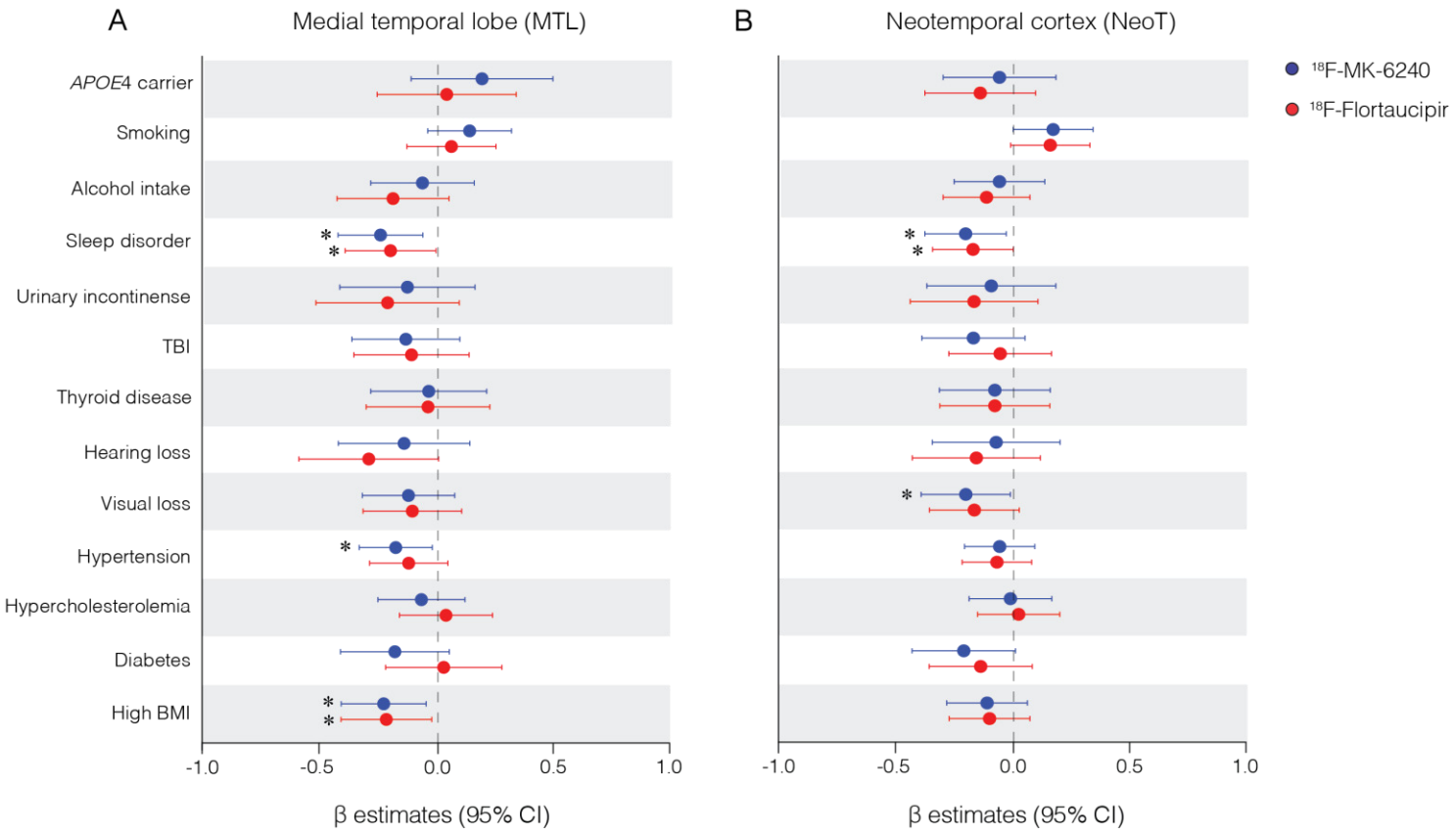


Figure 1: Effects of dementia risk factors on tau-PET uptake. Standardized beta coefficients and 95% confidence interval from linear regression models adjusted by age, amyloid pathology, clinical diagnosis and study site tested the association of comorbidities with ^{18}F-MK-6240 and ^{18}F-Flortacepir in the (A) medial temporal lobe (MTL) and (B) neotemporal cortex (NeoT). UniTAU values, derived from the UniTAU scale that was designed to harmonize tau-PET uptake across tracers based on head-to-head acquisitions, were used as outcomes in the models for both tracers. APOE, apolipoprotein, BMI, body mass index; TBI, traumatic brain injury.

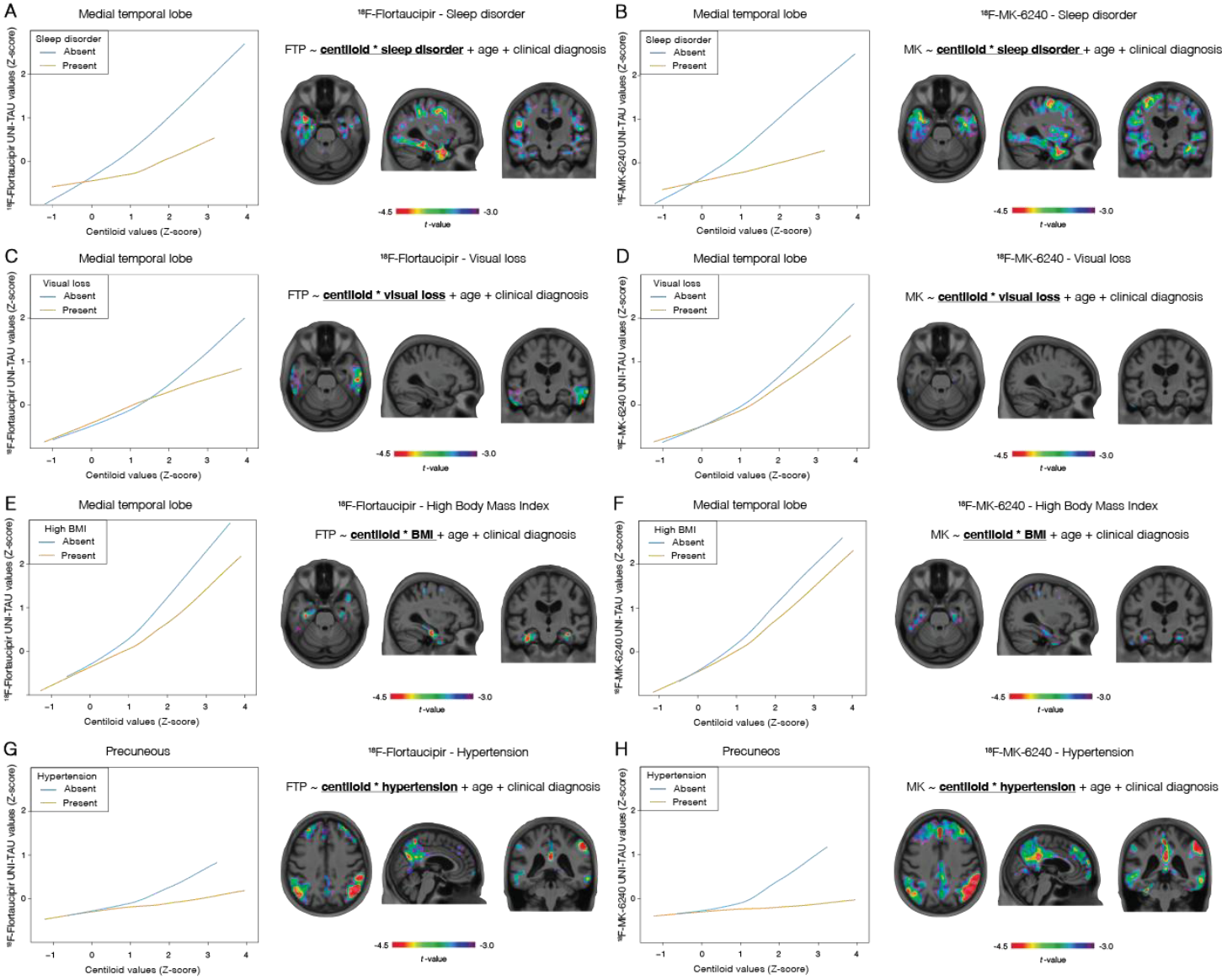


Figure 2: Effects of dementia risk factors on the association of amyloid-PET with tau-PET tracers' uptake. Lowess plots were used to visualize the influence of comorbidities on the association between amyloid-PET and tau-PET uptake. An interaction term, amyloid-PET × risk factors for dementia, was added to linear regression models, controlling for age, clinical diagnosis, and study site, to test whether the association between amyloid-PET and tau-PET uptake varies depending on specific risk factors for dementia. The effects of sleep disorder (A-B), visual loss (C-D), high body mass index (E-F) on the association of amyloid pathology with tau-PET tracers' uptake were tested in the medial temporal lobe. The effects of hypertension (G-H) on the same association were tested in the precuneus cortical area. Voxel-wise analyses with the interaction term for centiloid * comorbidities confirmed the spatial location of the interaction term.

Keywords: Dementia Risk Factors, Neuroimaging, tau-PET, amyloid-PET.

173 PI-2620 uptake in the medial temporal lobes discriminates Alzheimer's disease from normal cognition and non-Alzheimer's dementias

Jeffrey Phillips[1], Sevila Temirova[1], Dahlia Kamel[1], Marianthi Hareras[1], Chigozie Ibe[1], Quinn Hlava[1], Emily Xie[1], Katheryn Cousins[1], Leslie Shaw[1], Sandhitsu Das[1], Jeffrey Maneval[1], Sara Manning[1], Christopher Brown[1], Katherine Lopez[2], Richard Keegan[2], Andrew Stephens[2], Corey McMillan[1], David Irwin[1], Elizabeth Li[1], Ilya Nasrallah[1], David Wolk[1]

[1]*University of Pennsylvania, Philadelphia, PA, US*
[2]*Life Molecular Imaging, Inc., Boston, MA, US*

We assessed validity and sensitivity of the PET tracer [F18]-PI-2620 for detecting Alzheimer's disease (AD)-type tau across 47 scans from 39 individuals with mixed dementia syndromes (n=27) and normal cognition (n=12) by testing associations of uptake with grey matter atrophy, plasma biomarkers, and cognition. Clinical syndromes included amnestic AD (n=7), mild cognitive impairment (n=5), primary progressive aphasia (logopenic PPA, n=3; non-fluent/agrammatic, n=2; mixed, n=2), posterior cortical atrophy (n=3), dementia with Lewy bodies (n=1), progressive supranuclear palsy (PSP, n=1), corticobasal syndrome (n=1), and others (n=2). Amyloid-b positivity was determined from amyloid PET or amyloid-b 42/40 ratio in cerebrospinal fluid. Imaging was performed 45-75 minutes (n=24) or 30-60 minutes (PSP and naPPA) post-injection, and standardized uptake value ratios (SUVRs) were computed relative to an inferior cerebellar grey matter reference. Average maps in amnestic and non-amnestic AD recapitulated canonical patterns of tau accumulation (Fig. 1). In BA35/ERC, an area of early tau accumulation in AD, SUVRs were correlated (Fig. 2) with plasma glial fibrillary acidic protein (n=9, $p<0.04$), phospho-tau 181 (n=9, $p<0.05$), and phospho-tau 217 (n=19, $p<0.0004$), but not with amyloid-b 42/40 ratio ($p>0.18$). Across 81 cortical and subcortical brain areas, SUVRs were negatively associated with grey matter volumes in amyloid-positive but not amyloid-negative participants [amyloid-b positivity x SUVR, $F(1,3620)=73.9$, $p<0.0001$] (Fig. 3, left). In receiver operating characteristic analyses (Fig. 3, right), BA35/ERC SUVR=1.19 differentiated amyloid-positive patients from amyloid-negative, cognitively normal adults (20 vs. 13 scans) with sensitivity=0.95 and specificity=0.85; an SUVR=1.23 differentiated amyloid-positive vs. -negative patients (20 vs. 10 scans) with sensitivity=0.90 and specificity=1.0. BA35/ERC uptake was also negatively associated with Montreal Cognitive Assessment score ($R=-0.67$, $p<0.0003$), delayed verbal recall ($R=-0.63$, $p<0.0005$), naming ($R=-0.60$, $p<0.0007$), and other measures. These results indicate PI-2620 is sensitive to AD-type tau in an early Braak-stage region and exhibits robust associations with atrophy and cognitive impairment.

Keywords: PI-2620, tau, Alzheimer's disease, frontotemporal dementia, medial temporal lobes

174 Characterizing associations with Aβ burden in non-Hispanic Black participants across US POINTER and A4/LEARN cohorts

Talia Robinson[1], Kathryn Papp[1], Theresa Harrison[2], Laura Baker[3], Heather Snyder[4], Reisa Sperling[1], Rebecca Amariglio[1], Susan Landau[2], A4 STUDYTEAM[4], US POINTER Study Group[4]

[1]*Brigham and Women's Hospital, Boston, MA, US*
[2]*University of California Berkley, Berkley, CA, US*
[3]*Wake Forest University, Winston-Salem, NC, US*
[4]*Alzheimer's Association, Chicago, IL, US*

Background: In clinical trials with low representation from diverse populations, selection bias and cohort effects may contribute to differences in AD biomarker results, impacting generalizability to other cohorts and the larger population. Lower amyloid (Ab) among non-Hispanic Black (NHB) relative to non-Hispanic White (NHW) participants was reported in the A4/LEARN trial, driven by lower Aβ in NWB APOEe4 carriers. Here, we examine generalizability of biomarker findings in NHBs by expanding this work to the US POINTER Imaging sub-study.

Methods: Cognitively unimpaired NHB and NHW participants from US POINTER and A4/LEARN with baseline PET data were included (Table 1). Global Aβ (quantified in centiloids; CLs) was assessed using [^{18}F]florbetapir in A4/LEARN and [^{18}F]Florbetaben in US POINTER. Demographic data, APOE genotype, cardiovascular risk (CV-risk) factors (body mass index; BMI, systolic blood pressure; SBP), and Preclinical Alzheimer's Cognitive Composite (PACC) were collected. Regression models analyzed Aβ burden in NHW/NHBs, and associations of demographic, cv-risk, and APOEε4 status on Aβ in NHW/NHBs adjusting for relevant demographics.

Results: US POINTER and A4/LEARN NHBs differed demographically and in CV-risk, but not in Aβ burden, %APOEε4+, or PACC score (Table 1). Aβ was not associated with sex, BMI, or SBP in either cohort or ethnoracial group. Lower Aβ in NHB relative to NHW was replicated in US POINTER ($p = .01$), as was the differential impact of APOEe4 status on Ab burden, with lower Aβ in e4+NHBs relative to e4+NHWs ($p < .01$; Figure 1).

Conclusion: Despite demographic and cv-risk differences across cohorts, NHBs were similar in Aβ and APOEe4status. Lower Ab burden in NHB compared to NHW individuals was driven by ApoE4 carriers, but CV-risk was not related to Aβ in either NHB or NHW individuals, suggesting that AD-related genetic risk is a stronger driver than CV-risk of ethnoracial group differences in Aβ.

Table 1. Sample characteristics and key variables by ethnoracal group within cohort.

	A4/LEARN		US POINTER			Overall	
	NHW (N=3948)	NHB (N = 157)	NHB (N=135)	NHW (N=637)	NHB Comparison	NHB (N=292)	NHW (N=4585)
Age							
Mean (SD)	71.3 (4.68)	70.8 (4.89)	67.2 (4.71)	68.8 (5.22)	***	69.1 (5.13)	70.9 (4.83)
Sex							
F	2358 (59.7%)	111 (70.7%)	108 (80.0%)	367 (57.6%)	ns	219 (75.0%)	2725 (59.4%)
M	1590 (40.3%)	46 (29.3%)	27 (20.0%)	270 (42.4%)		73 (25.0%)	1860 (40.6%)
Education							
Mean (SD)	16.6 (2.83)	16.3 (2.77)	15.6 (2.15)	16.1 (2.24)	*	15.9 (2.52)	16.6 (2.76)
BMI							
Mean (SD)	27.5 (5.00)	30.1 (6.02)	31.9 (5.30)	30.0 (5.45)	**	30.9 (5.76)	27.9 (5.14)
SBP							
Mean (SD)	136 (16.2)	140 (16.7)	134 (17.9)	132 (15.5)	***	137 (17.6)	136 (16.2)
PACC 5							
Mean (SD)	0.101 (2.50)	-0.945 (2.53)	-0.607 (1.02)	0.0706 (0.998)	ns	-0.789 (1.98)	0.0971 (2.35)
Amyloid Status (CL)							
Neg	2424 (61.4%)	110 (70.1%)	108 (80.0%)	462 (72.5%)	ns	218 (74.7%)	2886 (62.9%)
Pos	1524 (38.6%)	47 (29.9%)	27 (20.0%)	175 (27.5%)		74 (25.3%)	1699 (37.1%)
Aβ (CLs)							
Mean (SD)	23.7 (35.7)	14.4 (25.2)	11.9 (19.5)	17.9 (25.7)	ns	13.3 (22.7)	22.9 (34.5)
APOE ε4 Status							
N	2516 (63.7%)	101 (64.3%)	86 (63.7%)	447 (70.2%)	ns	187 (64.0%)	2963 (64.6%)
Y	1393 (35.3%)	55 (35.0%)	47 (34.8%)	189 (29.7%)		102 (34.9%)	1582 (34.5%)

Note: NHB Comparison displays sig. values comparing A4/LEARN NHB to US POINTER NHB

*** < .001, ** <.01, * < .05

NHB = non-Hispanic Black, NHW = non-Hispanic White, BMI = Body mass index, SBP = systolic blood pressure

PACC 5 = Preclinical Alzheimer's Cognitive Composite

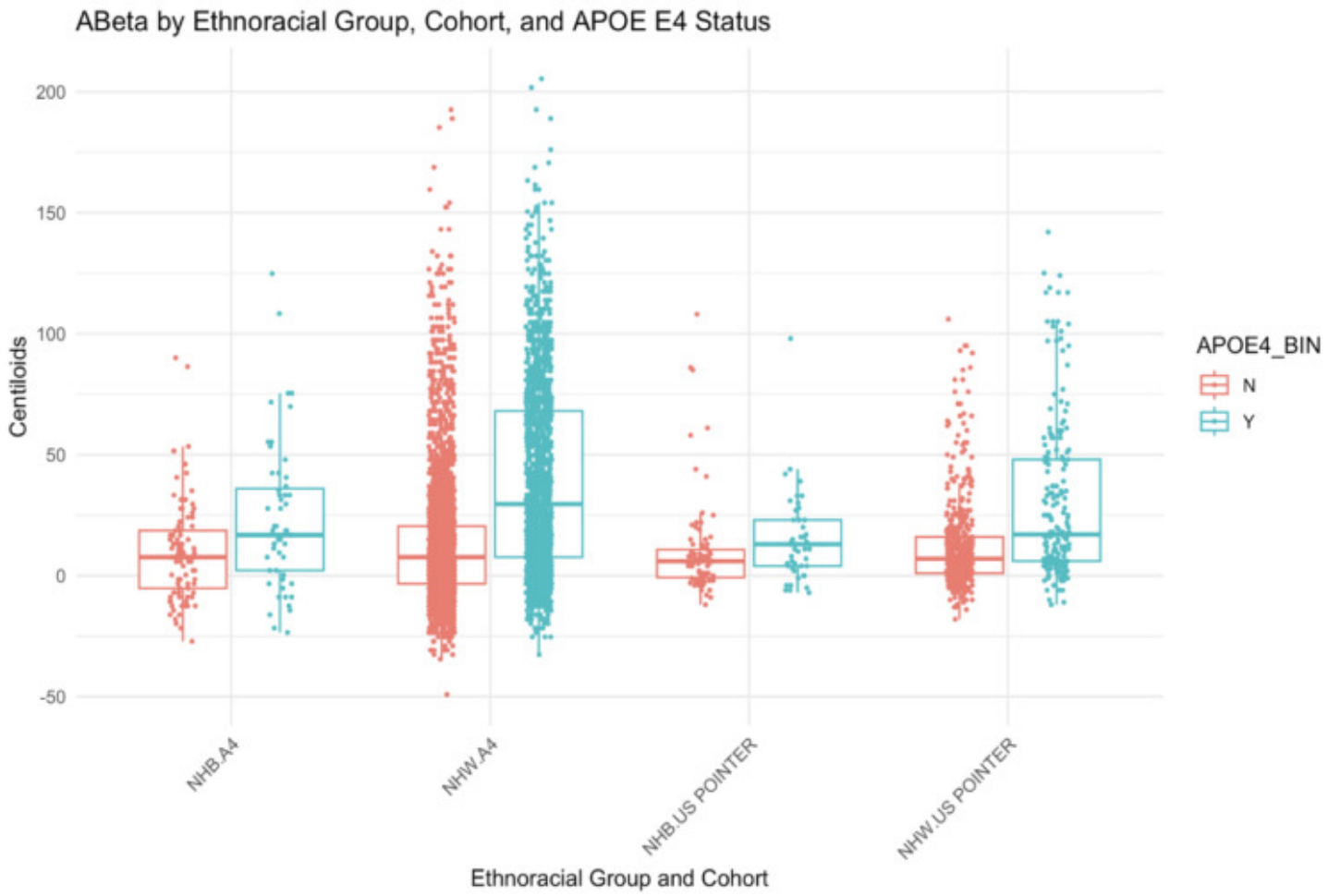


Figure 1. Aβ burden (CLs) by ethnoracial group and APOE ε4 status in A4/LEARN and US POINTER.
In US POINTER, there was a significant difference in the impact of ε4 status on Aβ burden by ethnoracial group, adjusting for age and gender, as was previously reported in A4/LEARN. In US POINTER NHB ε4 carriers display lower Aβ than NHW ε4 carriers (β = 13. 01, SE = 4.69, p < .01). Relatedly, of the NHB ε4 carriers, 29.8% were Aβ+ (CL>20), relative to 45% Aβ+ in NHW ε4 carriers. In NHB ε4 non-carriers, 14% were Aβ+, relative to 20.1% Aβ+ in NHW ε4 non-carriers.

Keywords: amyloid, cardiovascular risk, cognition, underrepresented groups

Friday, January 17, 2025 - 12:40 pm - 01:10 pm

O'Bryant, Sid

Keynote: Alzheimer's disease biomarkers among diverse populations – Data from the HABS-HD Study

Sid O'Bryant

The University of North Texas HSC at Fort Worth, TX, US

To date, the vast majority of research in support of brain, genomic and blood biomarkers of Alzheimer's disease comes from homogenous non-Hispanic white research partners. The Health & Aging Brain Study – Health Disparities (HABS-HD) is a community-based cohort designed to fill this gap in the field. HABS-HD has enrolled over 1,500 Hispanic, 1,500 Black/African American and 1,500 non-Hispanic white research partners. To date, HABS-HD has collected over 7,000 MRI scans, 5,000 PET amyloid scans and 3,000 PET tau scans with full systems biology "omics" being captured. HABS-HD data to date demonstrates that the presence and sequence of imaging ATN biomarkers vary between groups. Additionally, the link between ATN imaging biomarkers and clinical outcomes vary by groups (e.g., brain tau is a key driver of cognition among non-Hispanic whites primarily). Additionally, blood-based and genomic markers of AD vary by groups. Combined, current HABS-HD data clearly demonstrates that additional work is needed to fully understand AD biomarkers across all communities. All HABS-HD data is publicly available via LONI.

Dr. Sid O'Bryant is the principal investigator of the Health & Aging Brain Study – Health Disparities (HABS-HD), which is the most comprehensive study of Alzheimer's disease among the three largest racial/ethnic groups in the U.S. ever conducted – African Americans, Hispanics, non-Hispanic whites. The goal of the HABS-HD program is to understand the life course factors, including biological, sociocultural, environmental, and behavioral, that impact risk for Alzheimer's disease in late life. This work will ultimately lead to population-specific precision medicine approaches to treating and preventing Alzheimer's disease (i.e., "treating your Alzheimer's disease").

In addition to being a global leader in health disparities in cognitive aging, Dr. O'Bryant is a global expert in the use of blood-based biomarkers for the generation of a precision medicine approach to novel diagnostic and therapeutic strategies for Alzheimer's disease, Parkinson's disease, Dementia with Lewy Bodies and Alzheimer's disease among adults with Down Syndrome.

Friday, January 17, 2025 - 01:25 pm - 02:50 pm

Podium Session

SESSION VIII: Plasma Biomarkers: New Methods

CHAIRS: Bruna Bellaver, Robert Rissman

Friday, January 17, 2025		
01:25 pm - 02:50 pm	**SESSION VIII** Plasma Biomarkers: New Methods	**Bruna Bellaver,** University of Pittsburgh, Pittsburgh, PA, USA **Robert Rissman,** Keck School of Medicine of USC, San Diego, CA, USA
01:25 pm – 01:30 pm	Session Overview	**Chairs**
01:30 pm	Plasma tau biomarkers and staging of Alzheimer's disease	**Gemma Salvadó**, Lund University, Lund, SE
01:45 pm	Novel blood-based proteomic signatures across neurodegenerative diseases	**Maura Malpetti**, University of Cambridge, Cambridge, GB
02:00 pm	Association of CSF P-tau and MTBR-Tau biomarkers with amyloid and tau PET	**Przemyslaw Kac**, Institute of Neuroscience and Physiology, Department of Psychiatry and Neurochemistry, The Sahlgrenska Academy at University of Gothenburg, Mölndal, SE
02:15 pm	VeraBIND Tau test, a novel plasma assay for active tau pathology, identifies individuals with positive F18MK6240 tau-PET signal regardless of amyloid status	**Bernard Hanseeuw**, Cliniques Universitaires Saint-Luc, Brussels, BE
02:30 pm - 02:50 pm	Discussion	

Plasma tau biomarkers and staging of Alzheimer's disease

Gemma Salvadó[1], Laia Montoliu-Gaya[2], Joseph Therriault[3], Johanna Nilsson[2], Shorena Janelidze[1], Sophia Weiner[2], Nicholas J Ashton[2,4], Andrea L Benedet[2], Juan Lantero-Rodríguez[2], Niklas Mattsson-Carlgren[1], Sebastian Palmqvist[1,10], Gunnar Brinkmalm[2], Erik Stomrud[1,10], Henrik Zetterberg[2,5,6,7,8], Johan Gobom[2], Pedro Rosa-Neto[3], Kaj Blennow[6], Oskar Hansson[1,10]

[1]*Lund University, Lund, SE*
[2]*University of Gothenburg, Mölndal, SE*
[3]*McGill University, Montreal, QC, CA*
[4]*Banner Institute, Phoenix, AZ, US*
[5]*Sahlgrenska University Hospital, Mölndal, SE*
[6]*University College London, London, GB*
[7]*UK Dementia Research Institute, London, GB*
[8]*Hong Kong Center for Neurodegenerative Diseases, Hong Kong, CN*
[9]*UW Department of Medicine, Madison, WI, US*
[10]*Memory Clinic, Skåne University Hospital, Malmö, SE*

Introduction: Staging Alzheimer's disease (AD) can enhance diagnosis, prognosis, and the selection of patients most likely to benefit from targeted biological therapies. Plasma biomarkers offer a scalable alternative to PET tracers for classifying individuals across the AD continuum.

Methods: We utilized targeted mass spectrometry to measure six phosphorylated (p-tau) and six non-phosphorylated tau (np-tau) peptides in the BioFINDER-2 cohort (n=549), which included individuals in the whole AD continuum. Differences in each p-tau biomarker were evaluated by diagnostic group. Three tau biomarkers—plasma p-tau217r (ratio of p-tau217/np-tau217), p-tau205r, and 0N-tau—were chosen to develop a disease-staging system using k-means clustering. The model was trained using 10-fold cross-validation, so individuals classified by the model were different from those used in the model creation. Associations between plasma stages and other AD biomarkers were examined cross-sectionally and longitudinally. The staging model was validated in the independent TRIAD cohort (n=140).

Results: Plasma p-tau217r, p-tau205r, and 0N-tau demonstrated the largest increases across distinct diagnostic groups (cognitively unimpaired amyloid-β [Aβ]-positive, mild cognitive impairment Aβ-positive, and AD dementia, respectively; Figure 1). Higher plasma stages were linked to abnormalities in key AD biomarkers, including Aβ-PET, tau-PET, AD-signature cortical thickness, and cognitive performance, in both cohorts (Figure 2). Additionally, in BioFINDER-2, higher plasma stages correlated with faster disease progression, as indicated by longitudinal tau-PET accumulation, cortical atrophy and cognitive decline (Figure 3).

Conclusions: We developed and validated a plasma-staging model in two independent cohorts, demonstrating its strong associations with AD disease status and progression. This scalable model could facilitate monitoring in clinical settings and aid in selecting participants for trials targeting specific biological pathways.

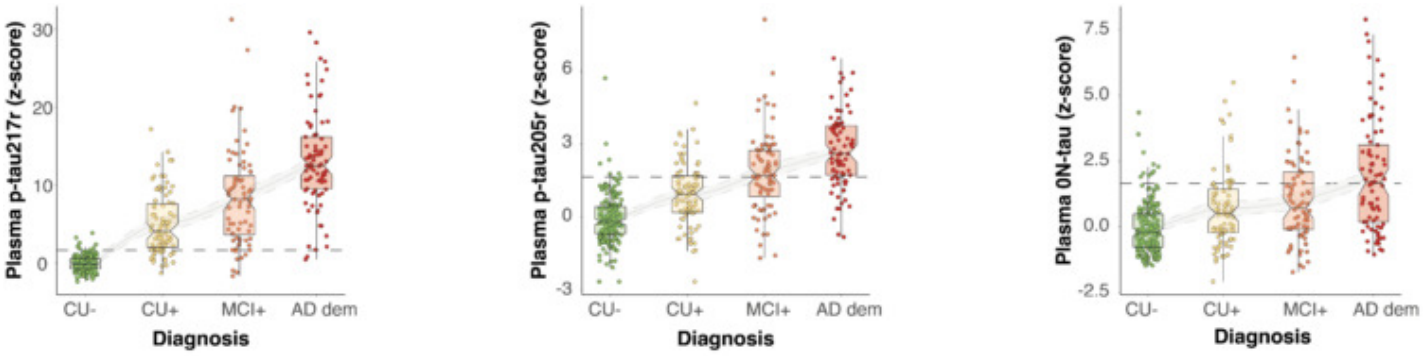


Figure 1: Plasma tau levels by diagnostic group
Plasma biomarkers were z-scored based on CU- individuals. Horizontal dashed lines represent z-score=1.65, which represent the abnormality threshold of 95%CI above de group control (CU-). Mean and SD are shown for each group as black point and vertical lines.
Abbreviations: CU-: cognitively unimpaired amyloid-β negative; CU+: cognitively unimpaired amyloid-β positive; MCI: mild cognitive impairment; AD dem: Alzheimer's disease dementia.

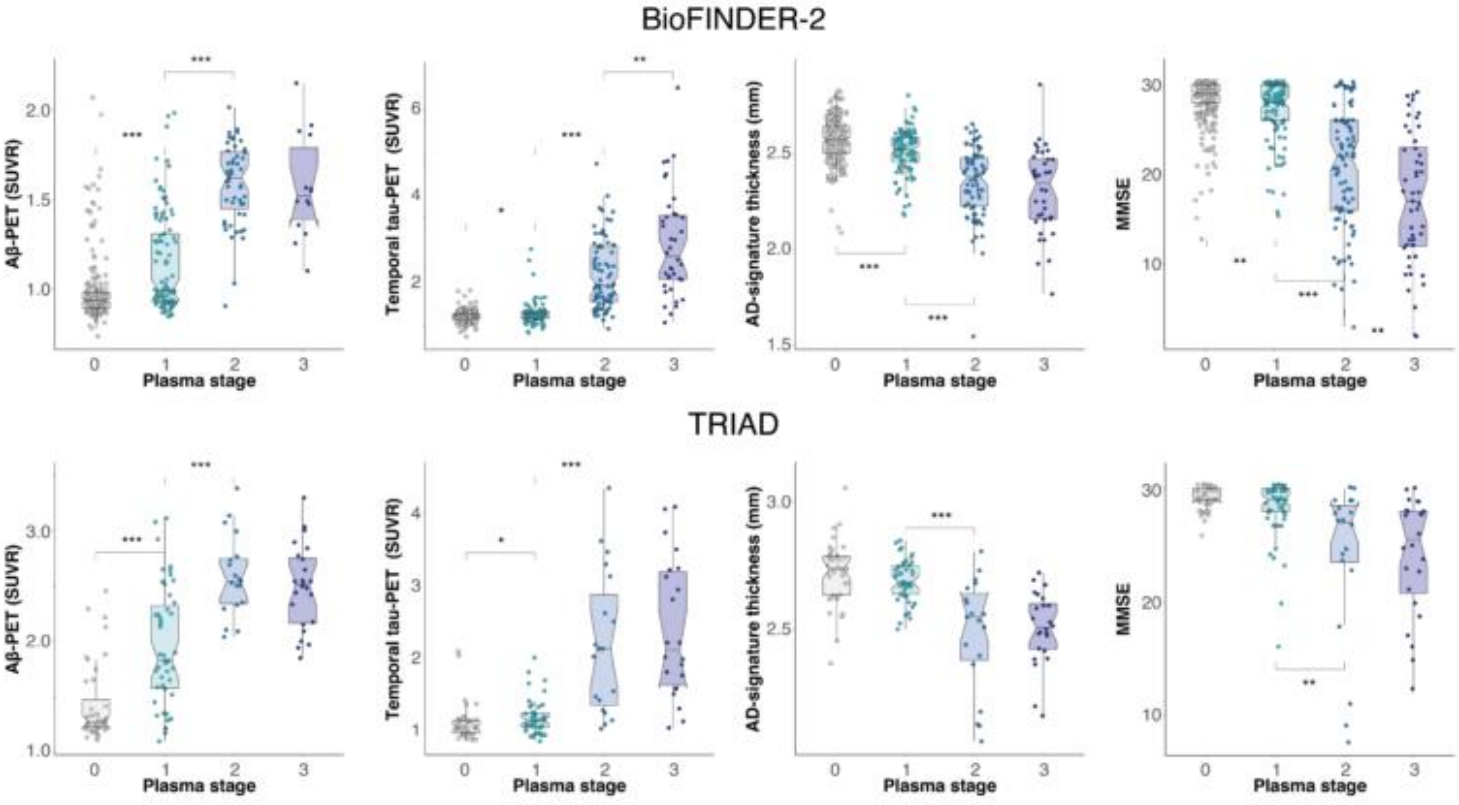


Figure 2: Cross-sectional AD biomarkers by plasma stages
Biomarkers of aggregated Aβ (Aβ-PET), aggregated tau (temporal tau-PET), cortical thickness (AD-signature) and cognition (MMSE) by plasma stages (from left to right) in the derivation (BioFINDER-2) and validation (TRIAD) cohorts. Statistical significant differences are shown in contiguous plasma stages (*: p<0.05, **: p<0.01; ***: p<0.001).
Abbreviations: MMSE: Mini-Mental State Examination; SUVR: standardized uptake value ratio.

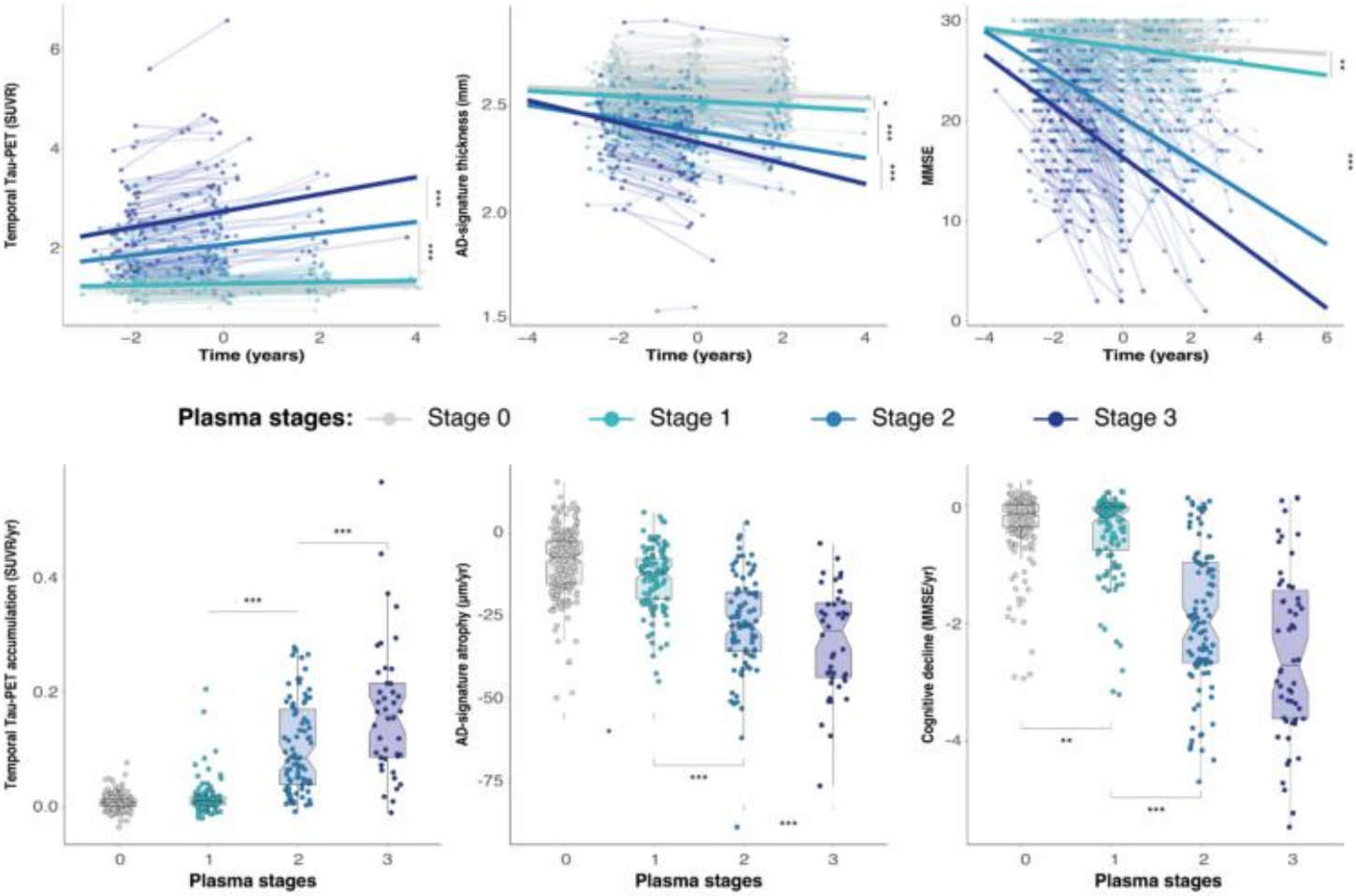


Figure 3: Longitudinal AD biomarkers change by plasma stages
Longitudinal changes of aggregated tau (temporal tau-PET), atrophy (AD-signature) and cognitive decline (MMSE) by plasma stages (from left to right) in the BioFINDER-2 cohort. Dots and thin lines represent actual datapoints and trajectories of each individual. Thick lines represent mean slopes of each plasma stage. Statistical significant differences on slopes of contiguous plasma stages are shown (*: p<0.05, **: p<0.01; ***: p<0.001). Time refers to time difference between plasma sample and AD biomarkers measurement.
Abbreviations: MMSE: Mini-Mental State Examination; SUVR: standardized uptake value ratio.

Keywords: Staging, plasma biomarkers, phosphorylated tau, diagnosis, prognosis

Novel blood-based proteomic signatures across neurodegenerative diseases

Robert Durcan[1], Amanda Heslegrave[2], Peter Swann[1], Henrik Zetterberg[2], John T O'Brien[1], James B Rowe[1], Maura Malpetti[1]

[1]*University of Cambridge, Cambridge, GB*
[2]*University College London, London, GB*

Blood-based biomarkers offer a promising avenue for early and differential diagnosis in neurodegenerative diseases. However, biomarkers are needed that bring together markers of proteinopathy with concomitant pathophysiological processes, such as neuroinflammation and synaptic loss. This study evaluates a novel multiplex proteomic method to identify differential diagnostic and prognostic markers in patients with neurodegenerative diseases, including Alzheimer's disease (AD), Lewy body dementia (LBD), frontotemporal dementia (FTD) and progressive supranuclear palsy (PSP).

Serum samples from n=141 patients (MCI/AD=36, LBD=34, FTD=36, PSP=35) and n=29 age-matched controls were analysed with the NUcleic acid Linked Immunosorbent Assay (NULISA) CNS panel. The panel measures ~120 analytes, including Aβ peptides, p-tau isoforms, and markers of neurodegeneration, inflammation and vascular health. NULISA markers were compared to p-tau217, p-tau231, GFAP, and NEFL measured using Single Molecule Array (Simoa, n=158). Biomarkers were compared across groups with Linear Models for Microarray and RNA-Seq Data Analyses (LIMMA) and finally used as predictors of survival in a Cox regression model, correcting for age and sex.

NULISA markers were detected with high sensitivity (~94.1% target detectability), and like-for-like proteins significantly correlated with Simoa counterparts (r=0.6-0.9, p<0.001). Comparing each patient cohort with controls (Fig.1), p-tau epitopes were significantly increased in AD/MCI and LBD (AD>LBD). LBD showed higher levels of neuropentraxins (NPTX1/2) than AD/MCI (Fig.2A). NEFL was most elevated in FTD and PSP compared to controls, alongside multiple cytokines and chemokines. PSP showed higher levels of inflammation-related markers, including IL7, CX3CL1, and periostin than FTD, where higher levels of fibroblast growth factor 2 were observed. NEFL predicted survival (Fig.2B).

The NULISA CNS-panel demonstrates high sensitivity and reliability for detecting multiple biomarkers across neurodegenerative disorders. It revealed distinct condition-specific profiles, with NEFL emerging as a key outcome predictor. This multiplex approach offers potential for differential diagnosis and targets identification, beyond commonly used dementia-related markers.

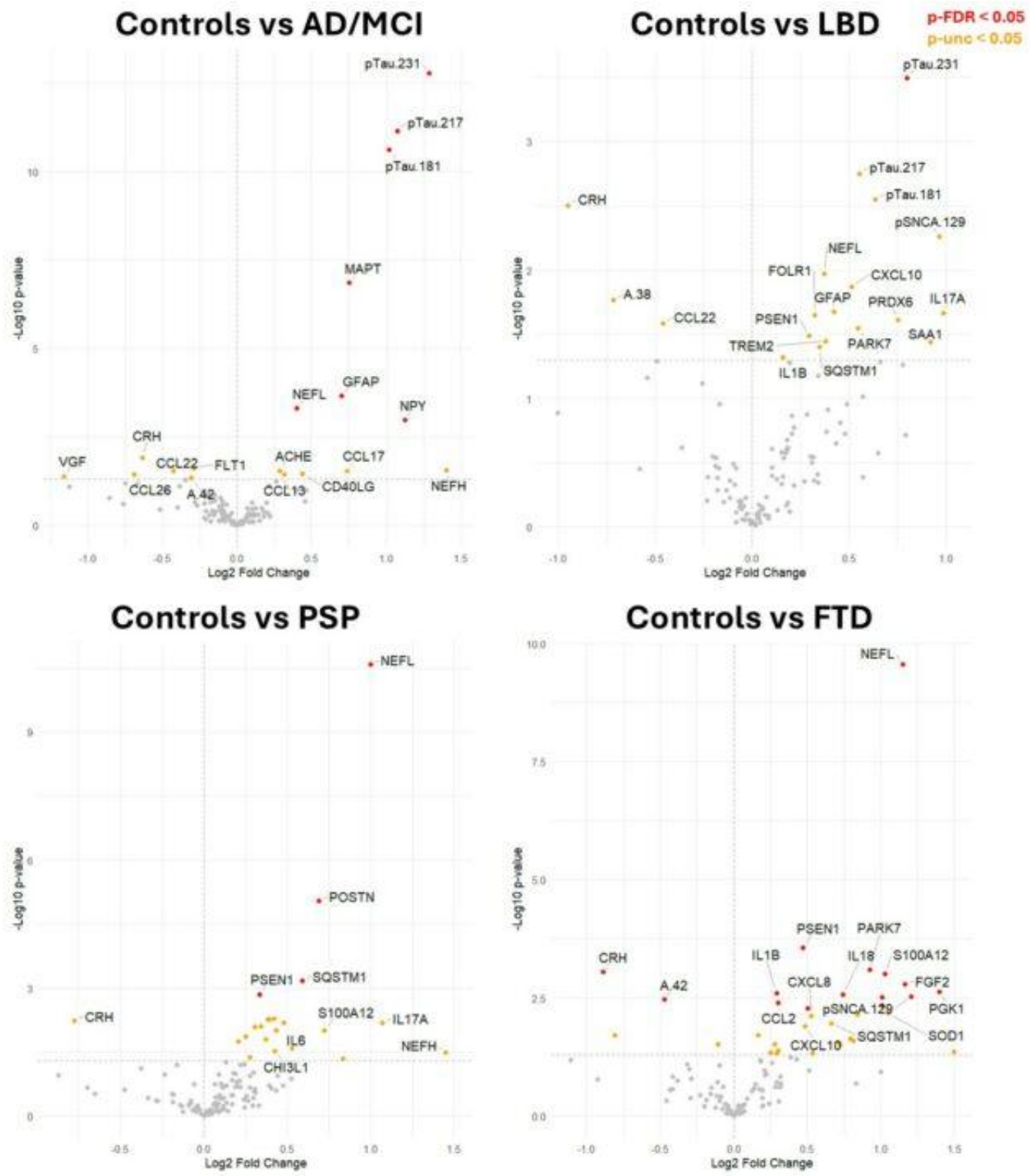


Figure 1. Volcano plot representing the group comparisons of patient cohorts vs controls across all 120 markers of the NULISA CNS panel.

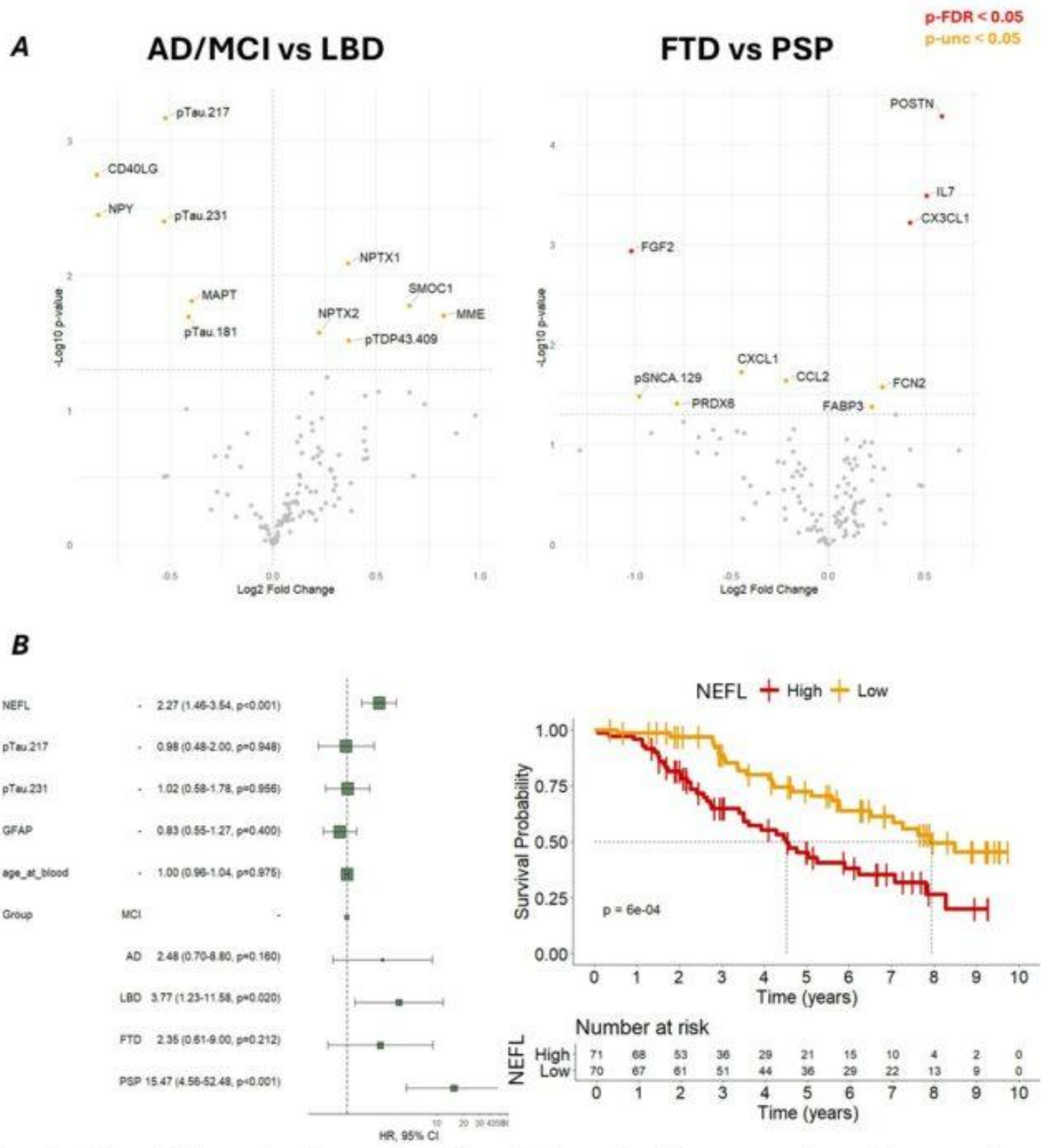


Figure 2. Differential diagnostic and prognostic markers. A) Volcano plot of group comparisons of between patient cohorts across all 120 markers of the NULISA CNS panel; B) Survival analysis including the main dementia-related markers, age and diagnosis as predictors.

Keywords: Proteomics, blood-based biomarkers, Alzheimer's disease, frontotemporal lobar generation, dementia with Lewy body

Kac, Przemyslaw

Association of CSF P-tau and MTBR-Tau biomarkers with amyloid and tau PET

Przemyslaw Kac[1], Federica Ribaldi[2,3], Nicholas J. Ashton[1,4,5,6], Augusto J. Mendes[2,3], Hlin Kvartsberg[7], Aurélien Lathuiliere[2,3], Michael Turton[8], Chen Wang[2,3], Peter Harrison[8], Henrik Zetterberg[1,7,9,10,11,12], Thomas K. Karikari[1,13], Valentina Garibotto[14,15,16], Kaj Blennow[1,7,17,18], Giovanni B. Frisoni[2,3]

[1]*Institute of Neuroscience and Physiology, Department of Psychiatry and Neurochemistry, The Sahlgrenska Academy at University of Gothenburg, Mölndal, SE*
[2]*Geneva Memory Center, Department of Rehabilitation and Geriatrics, Geneva University Hospitals, Geneva, CH*
[3]*Laboratory of Neuroimaging of Aging (LANVIE), University of Geneva, Geneva, CH*
[4]*Centre for Age-Related Medicine, Stavanger University Hospital, Stavanger, NO*
[5]*NIHR Biomedical Research Centre for Mental Health & Biomedical Research Unit for Dementia at South London & Maudsley NHS Foundation, London, GB*
[6]*Department of Old Age Psychiatry, Institute of Psychiatry, Psychology, and Neuroscience, King's College London, London, GB*
[7]*Clinical Neurochemistry Laboratory, Sahlgrenska University Hospital, Mölndal, SE*
[8]*Bioventix Plc, Farnham, GB*
[9]*Wisconsin Alzheimer's Disease Research Center, University of Wisconsin School of Medicine and Public Health, University of Wisconsin-Madison, Madison, WI, US*
[10]*Hong Kong Center for Neurodegenerative Diseases, Hong Kong, CN*
[11]*Department of Neurodegenerative Disease, UCL Queen Square Institute of Neurology, University College London, London, GB*
[12]*UK Dementia Research Institute, University College London, London, GB*
[13]*Department of Psychiatry, School of Medicine, University of Pittsburgh, Pittsburgh, PA, US*
[14]*Laboratory of Neuroimaging and Innovative Molecular Tracers (NIMTlab), Geneva University Neurocenter and Faculty of Medicine, University of Geneva, Geneva, CH*
[15]*Division of Nuclear Medicine and Molecular Imaging, Geneva University Hospitals, Geneva, CH*
[16]*CIBM Center for Biomedical Imaging, Geneva, CH*
[17]*Paris Brain Institute, ICM, Pitié-Salpêtrière Hospital, Sorbonne University, Paris, FR*
[18]*Neurodegenerative Disorder Research Center, Division of Life Sciences and Medicine, and Department of Neurology, Institute on Aging and Brain Disorders, University of Science and Technology of China and First Affiliated Hospital of USTC, Hefei, CN*

Background: Phosphorylated-tau (p-tau) and microtubule-binding region tau biomarkers (MTBR-Tau) CSF biomarkers for Alzheimer's disease have been included as core biomarkers in the newly revised criteria for diagnosis and staging of Alzheimer's disease. While immunoassays targeting n-terminal (p-tau181, p-tau217, p-tau231) also have associations with amyloid beta, MTBR-tau is associated mostly with tau pathology. In this study, we have included immunoassays targeting core soluble n-terminal biomarkers – p-tau181, p-tau217, and p-tau231, together with developed and validated immunoassays for p-tau212 and MTBR-Tau368, to assess their level in healthy controls, MCI and AD cases from memory clinic.

Methods: In-house developed CSF p-tau181, p-tau212, p-tau217, p-tau231, and MTBR-Tau368 Single molecule array (Simoa) immunoassays were used to measure levels of the biomarkers in Geneva Memory Center (N=112 participants; CU (N=49) MCI (N=55) Dementia (N=8). Amyloid-PET images were acquired using 18F-florbetapir or 18F-flutemetamol tracers, while tau-PET images were acquired using 18F-flortaucipir. Amyloid-PET (A +) and tau-PET (T +) positivity were assessed visually by an expert in nuclear medicine (VG).

Results: We observe a significant correlation of p-tau biomarkers with the CSF AB42/40 ratio. On the contrary,

MTBR-Tau368 alone did not correlate with AB42 but correlated with p-tau and total-tau measurements. All biomarkers significantly correlated with Tau-PET (R=|0.37-0.85| p<0.05) and Amyloid PET (R=|0.26-0.73| p<0.05), and the strongest numerical correlations were observed for p-tau212. Additionally, biomarkers were increased in A+ and T+ people classified by PET imaging, and in MCI and AD comparing to healthy controls by the diagnosis. The highest mean fold increase was observed for p-tau212, followed by p-tau217.

Conclusions CSF measurements of p-tau and MTBR-Tau accurately reflect the amyloid and tau pathology verified by the PET scans.

Keywords: MTBR-Tau, Tau368, p-tau212, p-tau217, PET

VeraBIND Tau test, a novel plasma assay for active tau pathology, identifies individuals with positive F18MK6240 tau-PET signal regardless of amyloid status

Bernard Hanseeuw[1,5], Jean-Louis Bayart[2], Emilien Boyer[2], Lise Colmant[2], Lisa Quenon[2], Pascal Kienlen-Campard[2], Renaud Lhommel[1,2], Adrian Ivanoiu[1,2], Anindita Bose[3], Khairul Ansari[3], Joshua Soldo[3], Khalid Iqbal[4,6]

[1]*Cliniques Universitaires Saint-Luc, Brussels, BE*
[2]*UCLouvain, Brussels, BE*
[3]*Veravas, Inc, Oakdale, MN, US*
[4]*Phanes Biotech, Inc, Malvern, PA, US*
[5]*Mass General Brigham, Boston, MA, US*
[6]*The City University of New York, New York, NY, US*

Background: Plasma assays targeting tau phospho-epitopes (e.g., pTau217) are frequently positive in the context of isolated amyloid-β pathology (A+). Developing plasma assays associated with tau aggregation (T+) is an unmet challenge. Here, we present the first results of the VeraBIND Tau test, a plasma assay measuring how hyperphosphorylated tau binds to normal tau, i.e., testing whether plasma tau is pathologically active (aggregating).

Methods: VeraBIND Tau is an in vitro bead-based ELISA that uses chemiluminescence (Fig.1: overview). Ninety-one participants were recruited from an ongoing study at UCLouvain, Belgium, including 58 clinically normal (CN, 22A+) and 33 clinically impaired (MCI/AD, 29A+). A+ status was determined using either CSF ($A\beta_{42}$≤544pg/mL) or amyloid-PET (Centiloid≥20). ^{F18}MK6240 Tau-PET status was determined visually as negative (Braak 0) or positive (Braak 2-6). Plasma pTau217 was quantified using Lumipulse (Fujirebio).

Results: The VeraBIND Tau plasma assay was weakly correlated with pTau217 concentration (R^2=0.065, p=0.02, Fig.2). Using tau-PET as ground truth for tau, VeraBIND Tau detected 39 of 41A+T+ participants (sensitivity=95%), and excluded tauopathy in 33 of 35A-T- participants (specificity=94%). With the same specificity (threshold=0.193pg/mL), pTau217 achieved similar sensitivity in A+T+ (38 of 41, 93%). However, seven of ten A+T- participants had positive pTau217 whereas only three had positive VeraBIND test. In contrast, four of five A-T+ participants had negative pTau217, but positive VeraBIND test. Although positive, the A-T+ participants had relatively low tau-PET signal (Braak 2-3). The overall diagnostic accuracy of pTau217 was 90% for A-/A+ and 82% for T-/T+ while the accuracy of VeraBIND was 83% for A-/A+ and 91% for T-/T+.

Conclusions: Whereas pTau217 is more closely associated to amyloid than to tau-PET results, VeraBIND Tau is highly sensitive to (early) tau-PET positivity, indicating active tau aggregation, with or without amyloidosis. The mismatch between pTau217 and VeraBIND Tau provides a plasma indication of discordant A/T PET status.

Fig.1: VeraBIND Tau Overview – testing whether hyperphosphorylated tau (HPT) from the plasma sample binds to normal tau

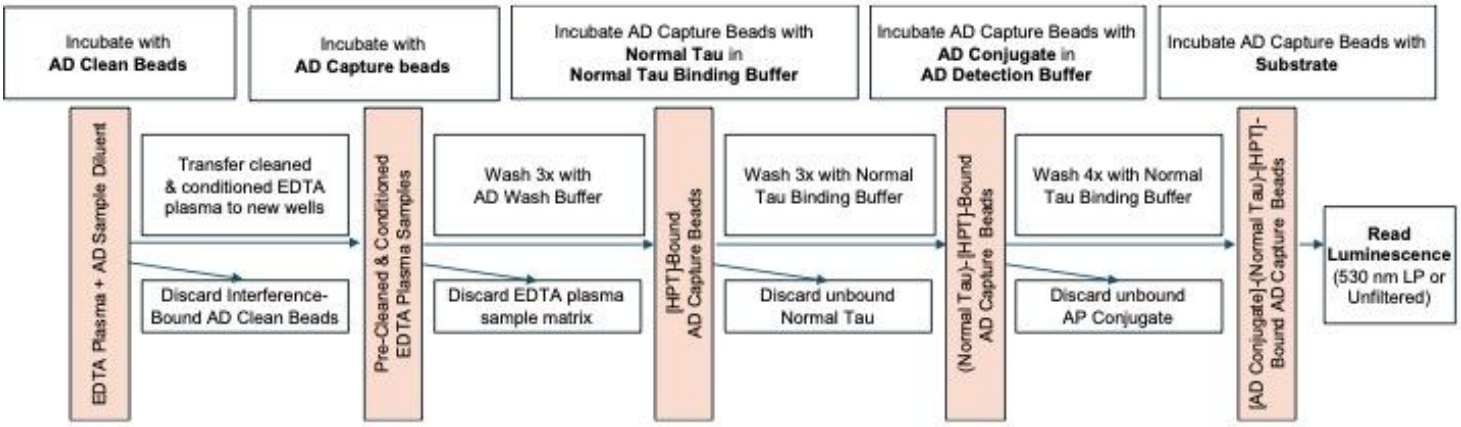


Fig.2: VeraBIND Tau test plotted against plasma pTau217, by Aβ (A) and tau-PET (T) status

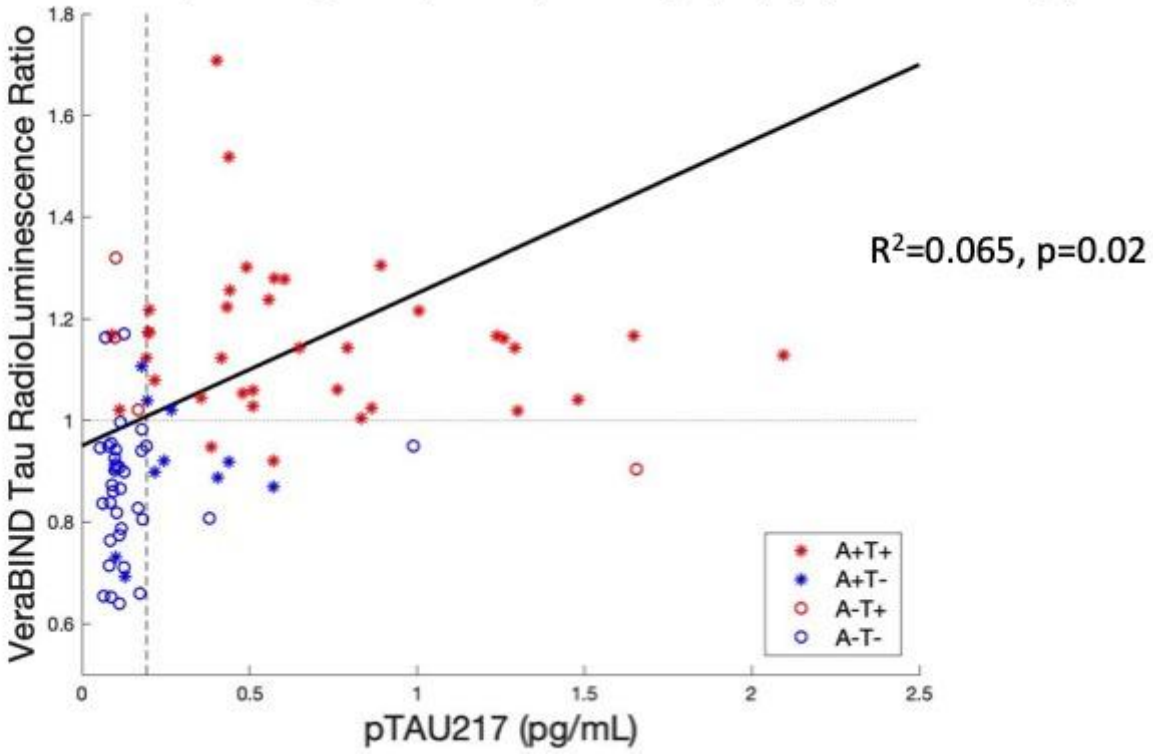
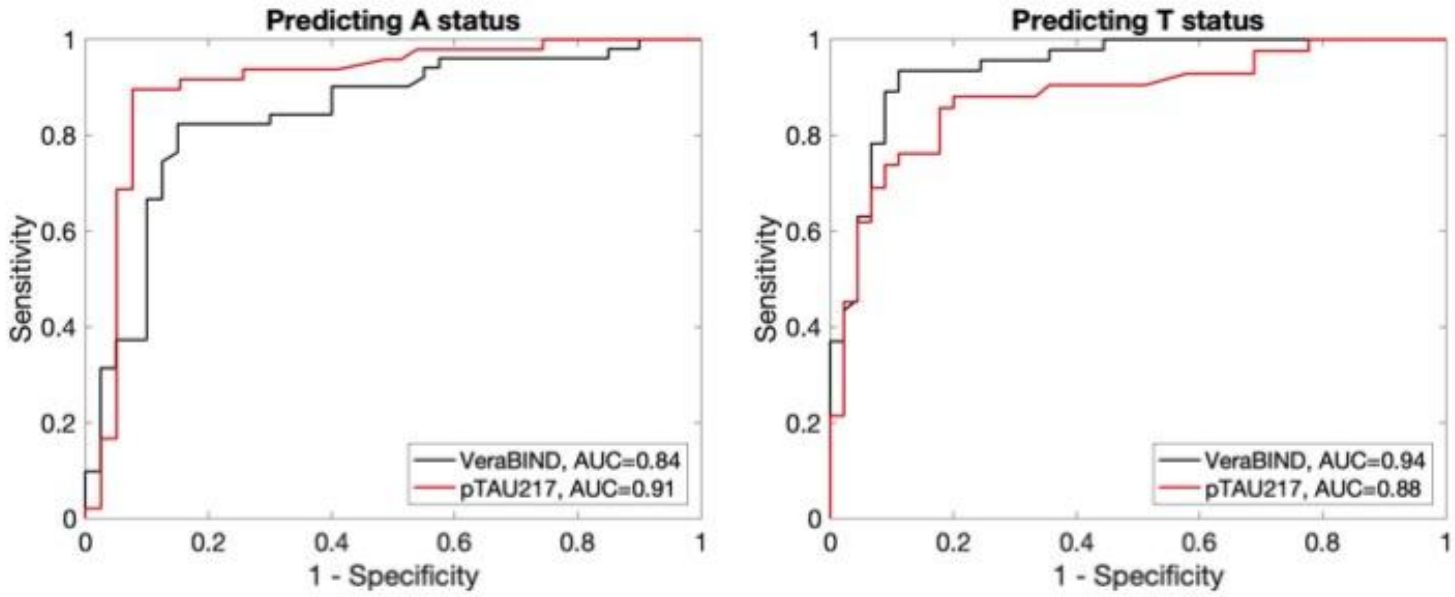


Fig.3: ROC curves predicting Aβ (A) & tau-PET (T) status with pT217 or VeraBIND Tau test



Keywords: plasma, tau activity, pTau217, MK6240, AT status

Friday, January 17, 2025 - 02:50 pm - 02:55 pm

Podium Session

Blitz Session 3B: Short Poster Presentations

Friday, January 17, 2025		
02:50 pm - 02:55 pm	**Blitz Session 3B**	
02:50 pm – 02:52 pm	Introduction	
02:52 pm	Locus coeruleus - medial temporal lobe functional connectivity confers protection against amyloid-related cognitive decline in the context of high cognitive reserve	**Lukas Heinrich**, Department of Radiology, Massachusetts General Hospital / Harvard Medical SChool, Boston, MA, US
02:53 pm	Association of a unique pattern of white matter T2 FLAIR hyperintensities with plasma and tau PET biomarkers in former American football players	**Jenna Groh**, Boston University Chobanian & Avedisian School of Medicine, Boston, MA, US

Locus coeruleus - medial temporal lobe functional connectivity confers protection against amyloid-related cognitive decline in the context of high cognitive reserve

Lukas Heinrich[1,3], Prokopis C Prokopiou[1], Emma E Wiklund[1], Kathryn V Papp[4], Dorene M Rentz[2,4], Reisa A Sperling[2,4], Keith A Johnson[1,2,4], Heidi IL Jacobs[1]

[1]*Department of Radiology, Massachusetts General Hospital / Harvard Medical SChool, Boston, MA, US*
[2]*Department of Neurology, Massachusetts General Hospital/ Harvard Medical School, Boston, MA, US*
[3]*Faculty of Health, Medicine and Life Sciences, Maastricht University, Maastricht, NL*
[4]*Center for Alzheimer Research and Treatment, Department of Neurology, Brigham and Women's Hospital, Boston, MA, US*

Background: Research into cognitive reserve (CR) has indicated that its preserving effect may involve changes in cortical network connectivity. The noradrenergic locus coeruleus (LC), one of the first brain areas affected by Alzheimer's pathology, recruits networks necessary to meet a given task's demands. We showed previously that better LC structure attenuates tau-related cognitive decline in individuals with high CR. Now, we investigated the impact of functional connectivity between the LC and resilience-relevant regions, and cognitive reserve, on beta-amyloid-related cognitive decline.

Methods: Older individuals (N=128) that underwent fMRI and 11C-Pittsburgh Compound-B (PiB) PET were selected from the Harvard Aging Brain Study (Figure 1). Functional connectivity (FC) between LC and ROIs previously shown to confer resilience was obtained from a novelty-versus-repetition Face-Name memory task using generalized psychophysiological interaction analysis. Cognition over time was assessed using PACC5. A CR composite score was constructed by averaging z-scored verbal-IQ, years of education, and Hollingshead scale. Cluster analysis grouped individuals based on cognitive reserve and PiB burden. (Non)linear mixed-effects models tested whether the association between LC-ROI FC and cognitive trajectories differed across groups.

Results: Higher CR related to better baseline PACC-scores (p<0.001). Cluster analysis identified four groups (Figure 2): High amyloid/high CR; high amyloid/low CR, low amyloid/high CR and low amyloid/low CR. The high-PIB-clusters exhibited more PACC-decline than low-PIB clusters, but decline was lower within the high CR/high PiB cluster (p<0.001). Individuals with high CR exhibited no amyloid-related cognitive decline when LC-MTL FC was high, while low CR individuals did (p<0.001). No attenuated decline was observed for LC-ACC FC (p=0.24) and LC-PSTG FC (p=0.79).

Conclusion: Our findings suggest that higher LC-MTL connectivity represents a neural correlate of CR, providing cognitive resilience in the face of elevated amyloidosis. Future research aims to understand how long this resilience persists as underlying AD pathology accumulates.

Demographics	
N	128
Age (mean years, SD)	70.0 (8.9)
Biological Sex (f) (N, %)	71 (55%)
ApoE4-Carriers (N, %)	38 (29%)
MMSE (mean score, SD)	29.28 (0.87)
Education (mean years, SD)	15.7 (2.7)
Hollingshead Score (mean, SD)	28.1 (14.9)
Verbal IQ (mean, SD)	122.7 (6.6)
Clinical Characteristics	
PIB+ (n, %)	36 (28%)
Neocortical PIB DVR PVC (mean, SD)	1.36 (0.37)
LC-MTL connectivity (mean, SD)	0.05 (0.05)
LC-ACC connectivity (mean, SD)	0.07 (1.69)
LC-PSTG connectivity (mean, SD)	-0.58 (1.86)
CDR baseline: 0	128 (100%)
PACC5 baseline (mean, SD)	0.22 (0.6)
PACC5 follow-up time (mean years, SD)	7.8 (3.1)

Figure 1 Demographics. *Abbreviations: Abbreviations: SD = standard deviation, f = female, ApoE4 = apolipoprotein E4, MMSE = Mini Mental State Examination, PIB+ = individuals with 11C-Pittsburgh Compound-B mean values above clinical cut off (>1.24), LC = locus coeruleus, MTL = medial temporal lobe, ACC = anterior cingulate cortex, PSTG = posterior superior temporal gyrus, CDR = Clinical Dementia Rating. Data is presented as means and (standard deviations) or numbers and (percentages).*

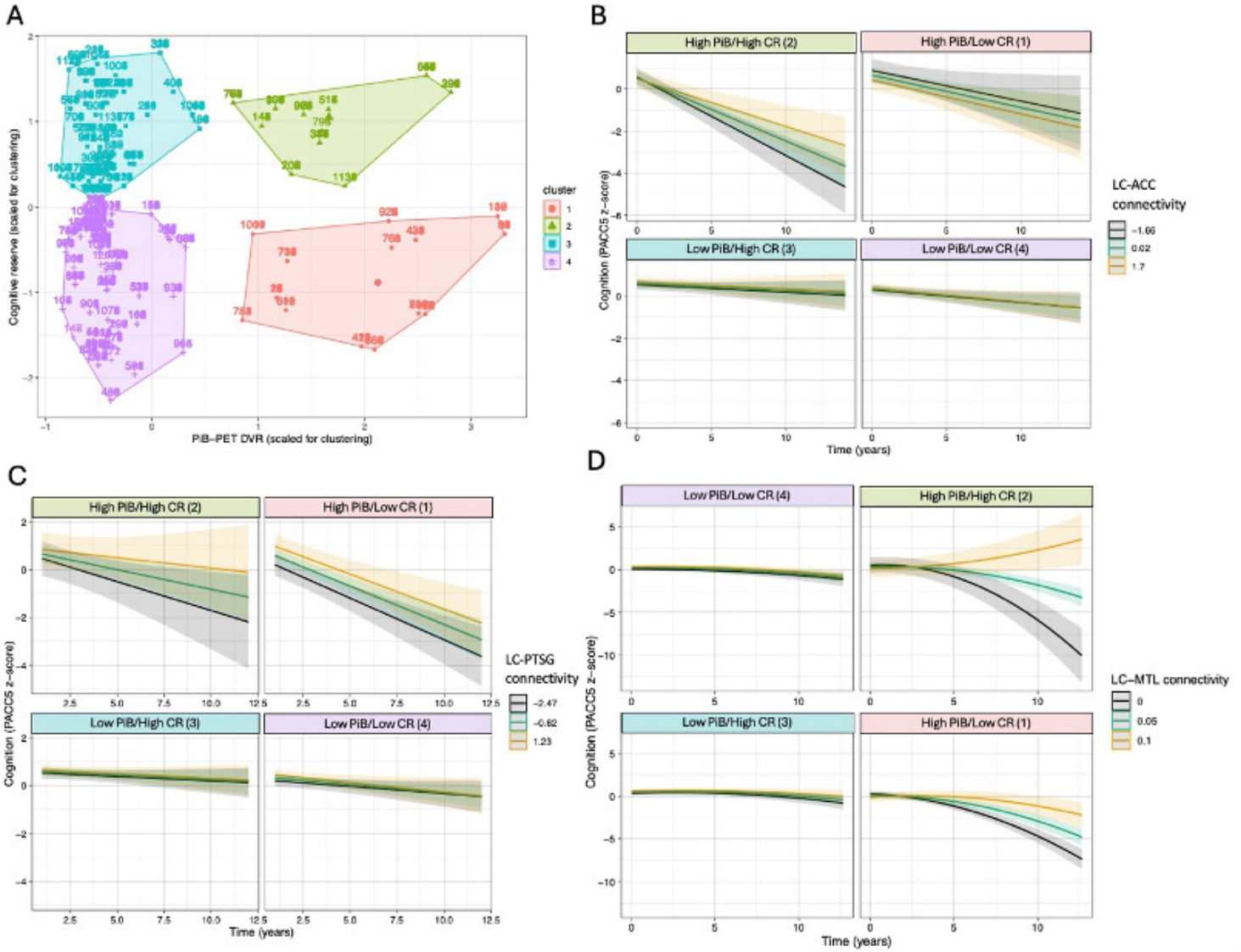


Figure 2. ***Effect of LC functional connectivity with areas linked to resilience*** *(anterior cingulate cortex (B), posterior superior temporal gyrus (C))* ***or AD*** *(medial temporal lobe (D))* ***on cognitive decline per cluster****. **A)** Grouping results of k-means clustering analysis. The clustering algorithm divided the sample into four groups: High amyloid/low CR (Cluster 1, red), high amyloid/high CR (Cluster 2, green), low amyloid/high CR (Cluster 3, blue), and low amyloid/low CR (Cluster 4, purple). Units on x-axis and y-axis reflect scaled variables, as necessary for clustering.* ***B)*** *Association between LC-ACC connectivity and cognition over time per cluster. We observed no effect of LC-ACC FC on amyloid-related cognitive decline in clustered groups.* ***C)*** *Association between LC-PSTG connectivity and cognition over time per cluster. Similarly to LC-ACC FC, we observed no attenuation of amyloid-related cognitive decline in clustered groups associated with LC-PSTG FC.* ***D)*** *Association between LC-MTL connectivity and cognition over time per cluster (the nonlinear model was a better fit than the linear model). Functional connectivity between the LC and MTL attenuated cognitive decline in the high amyloid/high CR group. The high amyloid/high CR group did not exhibit cognitive decline if LC-MTL connectivity during novelty vs repetition was higher (yellow line).*

Contrast analysis of between-group differences				
Region of interest	Group 1	Group 2	β-coefficient	P-val
MTL	High PiB/Low CR	High PiB/High CR	203.91	0.04*
MTL	High PiB/Low CR	Low PiB/High CR	-29.77	0.35
MTL	High PiB/Low CR	Low PiB/Low CR	-64.33	0.06
MTL	High PiB/High CR	Low PiB/High CR	-233.68	0.02*
MTL	High PiB/High CR	Low PiB/Low CR	-268.24	0.01*
MTL	Low PiB/High CR	Low PiB/Low CR	-34.56	0.11
ACC	High PiB/Low CR	High PiB/High CR	-0.04	0.31
ACG	High PiB/Low CR	Low PiB/High CR	-0.05	0.21
ACG	High PiB/Low CR	Low PiB/Low CR	-0.05	0.21
ACG	High PiB/High CR	Low PiB/High CR	0.01	0.91
ACG	High PiB/High CR	Low PiB/Low CR	0.00	0.91
ACG	Low PiB/High CR	Low PiB/Low CR	0.00	0.91
PSTG	High PiB/Low CR	High PiB/High CR	-0.01	0.81
PSTG	High PiB/Low CR	Low PiB/High CR	0.03	0.81
PSTG	High PiB/Low CR	Low PiB/Low CR	-0.01	0.81
PSTG	High PiB/High CR	Low PiB/High CR	-0.01	0.81
PSTG	High PiB/High CR	Low PiB/Low CR	-0.01	0.81
PSTG	Low PiB/High CR	Low PiB/Low CR	0.00	0.85

Figure 3. *Model output from linear mixed effects models associating LC-ROI functional connectivity with PACC5 decline, contrasting the cluster-analysis derived groups. The region of interest used in the connectivity analysis is described in the first column (MTL: medial temporal lobe, ACC: anterior cingulate cortex, PSTG: posterior superior temporal gyrus). Columns two and three describe the groups being compared. In each model, PACC5 was used as outcome and covariates (sex and age) were included in an interaction term with time (in years). Models additionally included random slope and intercept terms. Only connectivity between the LC-MTL significantly explained differences in cognitive trajectories between specific PiB/CR groups. Mixed effect models including LC-MTL connectivity were assessed using a non-linear term for time (in years), while models including LC-ACC and LC-PSTG connectivity only converged when using a linear term. All depicted p-values are FDR-corrected.*

Keywords: cognitive reserve, PiB-PET, MRI, amyloid-beta, aging

Association of a unique pattern of white matter T2 FLAIR hyperintensities with plasma and tau PET biomarkers in former American football players

Jenna R. Groh[1], Chad Farris[1], Adam M. Brickman[2], Mohamad J. Alshikho[2], Annalise E. Miner[1], Yorghos Tripodis[3], Anna Cui[1], Charles H. Adler[4], Laura J. Balcer[5], Charles Bernick[6], Robert C. Cantu[1], Michael J Coleman[8], David Dodick[4], Nicholas Ashton[9], Henrik Zetterberg[9], Kaj Blennow[9], Elaine R. Peskind[10], Ann C. McKee[1], Jesse Mez[1], Sylvain Bouix[11], Jeffrey L. Cummings[12], Eric M. Reiman[13], Robert A. Stern[1], Martha Shenton[8,14], Michael L. Alosco[1]

[1]*Boston University Chobanian & Avedisian School of Medicine, Boston, MA, US*
[2]*Columbia University, Department of Neurology, New York, NY, US*
[3]*Boston University School of Public Health, Boston, MA, US*
[4]*Mayo Clinic College of Medicine, Department of Neurology, Scottsdale, AR, US*
[5]*NYU Grossman School of Medicine, Departments of Neurology, Population Health and Ophthalmology, New York, NY, US*
[6]*Cleveland Clinic Lou Ruvo Center for Brain Health, Las Vegas, NV, US*
[7]*University of Washington, Department of Neurology, Seattle, WA, US*
[8]*Brigham and Women's Hospital, Department of Psychiatry, Psychiatry Neuroimaging Laboratory, Boston, MA, US*
[9]*The Sahlgrenska Academy at the University of Gothenburg, Institute of Neuroscience and Physiology, Department of Psychiatry and Neurochemistry, Mölndal, SE*
[10]*University of Washington School of Medicine, Department of Psychiatry and Behavioral Sciences, Seattle, WA, US*
[11]*École de technologie supérieure, Department of Software Engineering and Information Technology, Montreal, QC, CA*
[12]*University of Nevada Las Vegas, Chambers-Grundy Center for Transformative Neuroscience, Department of Brain Health, School of Integrated Health Sciences, Las Vegas, NV, US*
[13]*Banner Alzheimer's Institute, University of Arizona, Arizona State University, Translational Genomics Research Institute, and Arizona Alzheimer's Consortium, Phoenix, AR, US*
[14]*Brigham and Women's Hospital, Harvard Medical School, Department of Radiology, Boston, MA, US*

Background: Repetitive head impacts (RHI) can lead to long-term white matter injury visualized on FLAIR scans as white matter hyperintensities (WMH). Anecdotally, we observed a distinct pattern of WMH in individuals with RHI exposure: small, punctate, discrete lesions near the cortex at the depths of the sulci (**Figure 1a**). The goal of this study was to empirically characterize this pattern in former elite American football players.

Methods: The sample included 164 male football players (n=111 professional and n=53 college players) and n=55 asymptomatic males without RHI from the DIAGNOSE Project with available MRI, 18F-flortaucipir (FTP), and florbetapir PET data. **(Table 1)**. Visual ratings blind to information about the participant's exposure status and clinical status were conducted to count WMH that were a.) within 1.0cm of the gray/white matter boundary, b.) as bright as the cortex, c.) spherical and d.) less than 1.0cm in size. ANCOVA compared groups on total number of WMH adjusted for age and vascular risk factors. Among football players, multivariable linear regression models assessed relationships between WMH and plasma biomarkers including p-tau181, p-tau231, Aβ42/40 ratio, neurofilament light (NfL), glial fibrillary acidic protein (GFAP) and FTP composite SUVRs.

Results: Number of WMH was greater in football players compared to controls (p=0.007) **(Figure 1b)**. Among former players, elevated p-tau231 (p_{adj}=0.041) and NfL (p_{adj}=0.034) were associated with greater WMH but p-tau181 (p_{adj}=0.295), GFAP (p_{adj}=0.784), and the ratio Aβ42/40 (p_{adj}=0.697) were not **(Figure 2)**. Number of WMH was associated with tau PET composite regions frontal SUVR (p_{adj}=0.046) and left-parietal SUVR (p_{adj}=0.046) but not mesial-temporal SUVR (p_{adj}=0.285) **(Figure 2)**.

Conclusions: This study provides evidence for a unique pattern of WMH in former elite football players exposed to RHI. The lesion location near the depths of the sulci and gray/white matter junction corresponds to areas susceptible to RHI and tau deposition in CTE.

Table 1. Sample Characteristics

	N	Football N = 164[1]	Control N = 55[1]	p-value[2]
Age (years)	219	57.38 (8.34)	59.67 (8.44)	0.077
Education (years)	219	16.75 (1.46)	17.47 (3.50)	0.68
Race	219			0.96
White		102 (62%)	34 (62%)	
Nonwhite		62 (38%)	21 (38%)	
Total Years of Play	164	15.8 (4.3)	NA (NA)	
Revised Framingham Stroke Risk Profile	208	0.03 (0.03)	0.05 (0.04)	<0.001
Sleep Apnea	215	57 / 161 (35%)	9 / 54 (17%)	0.010
Atrial Fibrillation	216	9 / 162 (5.6%)	0 / 54 (0%)	0.12
Diabetes	217	10 / 162 (6.2%)	5 / 55 (9.1%)	0.54
Hit 6 Total Score	219	46.65 (10.29)	40.09 (5.33)	<0.001
TES Level of CTE Certainty	218			<0.001
No TES		58 (36%)	55 (100%)	
Suggestive of CTE		32 (20%)	0 (0%)	
Possible CTE		21 (13%)	0 (0%)	
Probable CTE		52 (32%)	0 (0%)	
MOCA (Raw Total Score)	218	24.7 (3.4)	26.7 (1.9)	<0.001
Amyloid PET Positive	216	3 (1.8%)	0 (0%)	>0.99
WMH within 0.5cm of the Cortex	219	26 (44)	12 (18)	0.029
WMH within 1.0cm of the Cortex	219	33 (56)	17 (26)	0.038

[1]Mean (SD); n (%); n / N (%)

[2]Wilcoxon rank sum test; Pearson's Chi-squared test; Fisher's exact test

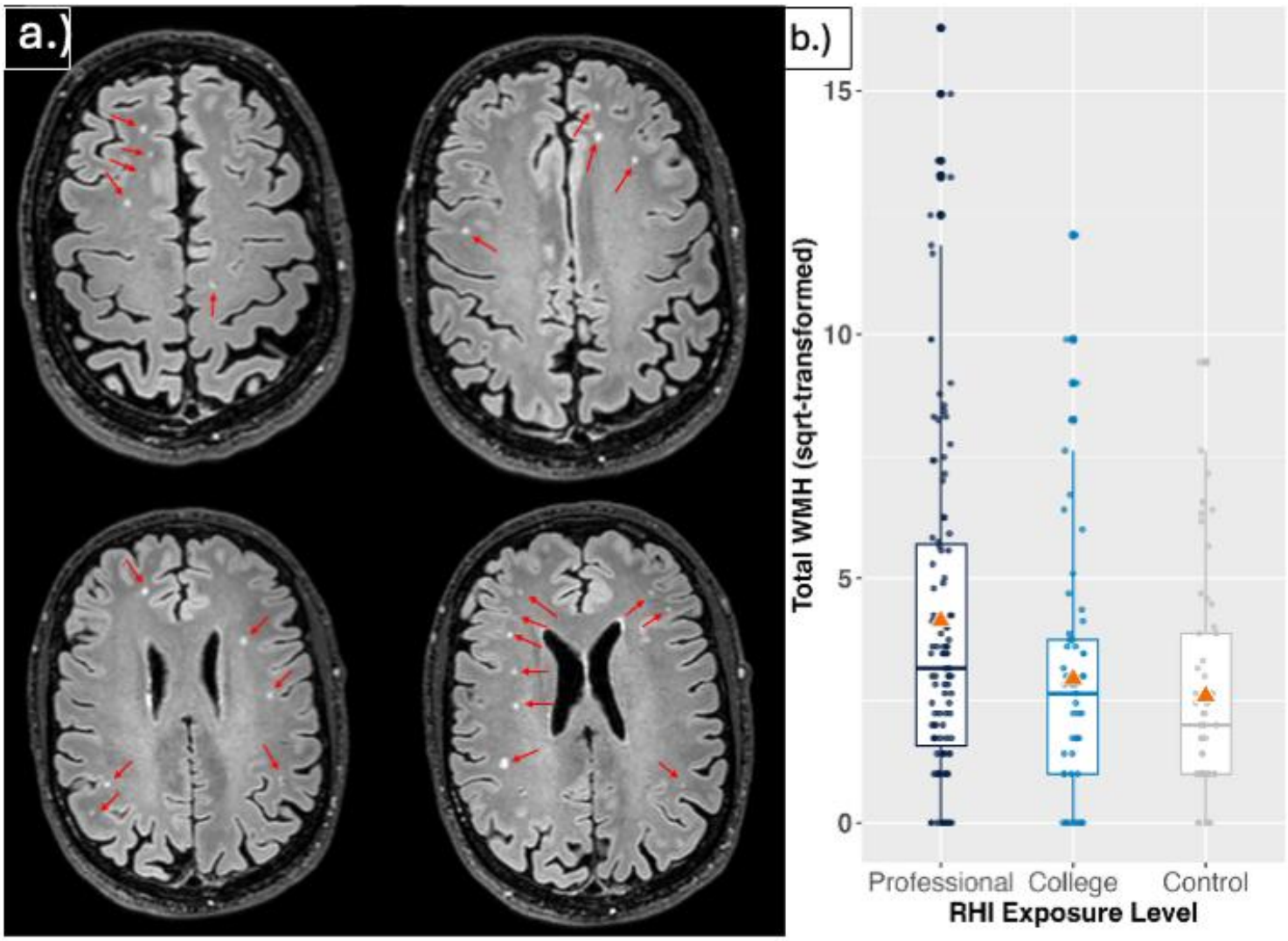


Figure 1.
a.) Exemplar FLAIR scan from a participant with substantial RHI exposure. Red arrows show small, spherical punctate lesions close to the gray matter, distributed throughout the cortex, often in the absence of confluent periventricular lesions. Lesions are also observed in relatively younger aged (e.g., 50s) individual with minimal vascular risk factors. **b.)** Differences in total number of small, punctate, discrete WMH within 0.5cm of the gray matter between former professional American football players, college football players, and unexposed controls. Total number of WMH was greater in former professional players compared to the controls (p=0.001) but not former professional players compared to the college players (p=0.983).

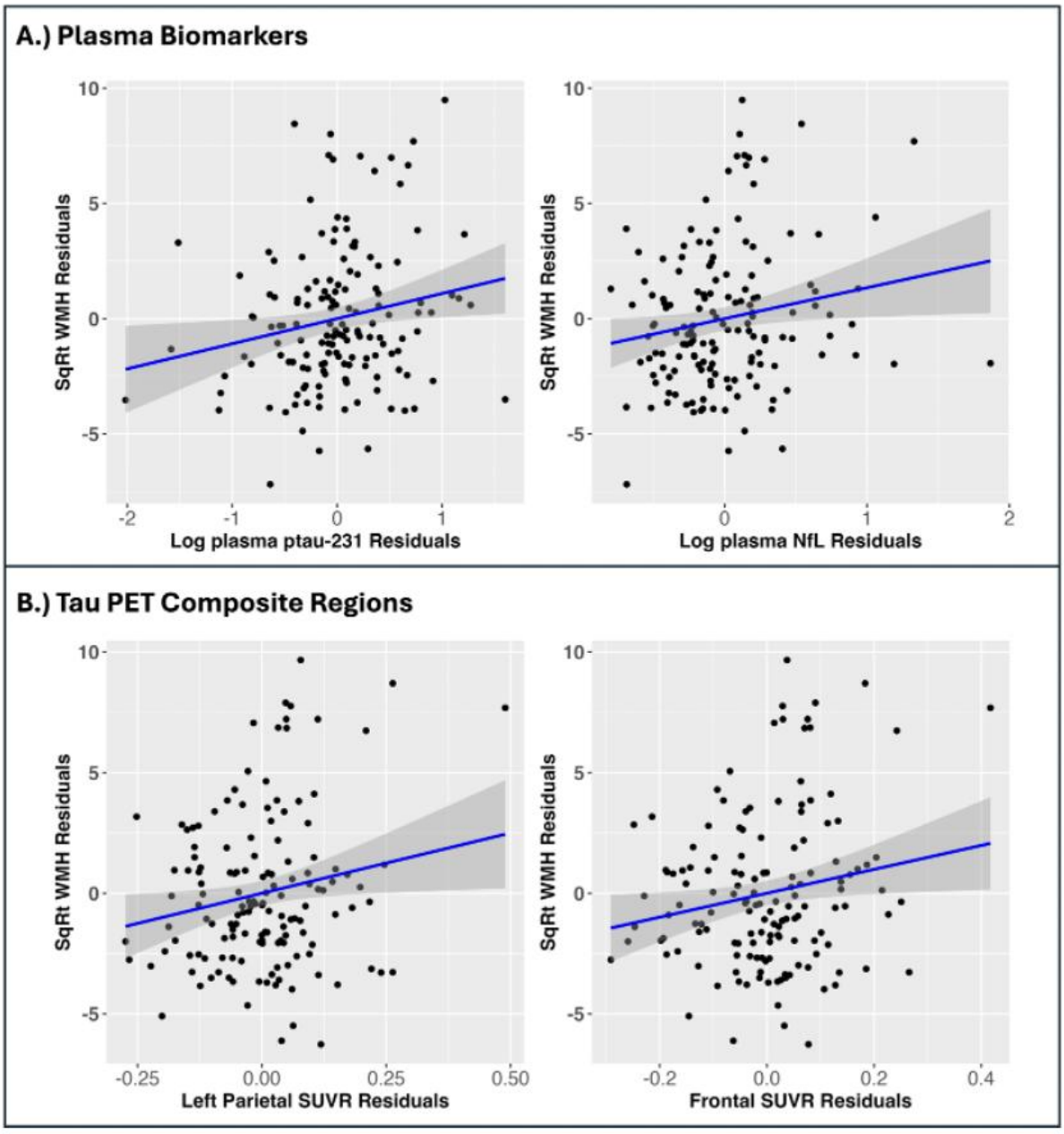


Figure 2.
Adjusted associations between the number of WMH within 0.5cm of the cortex and log-transformed plasma biomarkers/tau PET composite regions in the former American football players. Partial regression plots were adjusted for covariates: age, BMI, race, revised Framingham Stroke Risk Profile score (rFSRP), and sleep apnea. Significant associations include plasma p-tau231 (p_{adj}=0.041)), NfL (p_{adj}=0.034) and FTP composite regions frontal SUVR (p_{adj}=0.046) and left parietal (p_{adj}=0.046).
Abbreviations: white matter hyperintensities (WMH), neurofilament light (NfL), standardized uptake value ratio (SUVR).

Keywords: White matter hyperintensities, aging athletes, repetitive head impacts, flortaucipir, plasma biomarkers

Friday, January 17, 2025 - 03:50 pm - 05:15 pm

Podium Session

SESSION IX: Plasma Biomarkers: Application

CHAIRS: Jasmeer Chhatwal, Thomas Karikari

Friday, January 17, 2025

03:50 pm - 05:15 pm	SESSION IX Plasma Biomarkers: Application	**Jasmeer Chhatwal,** Massachusetts General Hospital, Boston, MA, USA **Thomas Karikari,** University of Pittsburgh, Pittsburgh, PA, USA
03:50 pm – 03:55 pm	Session Overview	**Chairs**
03:55 pm	Positive plasma Aβ42/40 despite negative Amyloid PET: A harbinger of progression to amyloid PET positivity?	**Azadeh Feizpour**, Florey Institute of Neuroscience and Mental Health, Melbourne, AU
04:10 pm	Head-to-head association of plasma p-tau217 with MK6240, Flortaucipir, PI2620, and RO948 Tau PET Tracers	**Pamela Ferreira**, University of Pittsburgh, Department of Psychiatry, Pittsburgh, PA, US
04:25 pm	Modeling the temporal progression of plasma and PET AD biomarkers with cognition	**Petrice Cogswell**, Mayo Clinic, Rochester, MN, US
04:40 pm	Comparison of amyloid PET, tau PET, and pTau217 biomarker progression between Down syndrome and neurotypical adults with sporadic Alzheimer's disease	**Matt Zammit**, University of Wisconsin, Madison, WI, US
04:55 pm – 05:15 pm	Discussion	

Positive plasma Aβ42/40 despite negative Amyloid PET: A harbinger of progression to amyloid PET positivity?

Azadeh Feizpour[1,2], Vincent Doré[2,3], James D. Doecke[4], Rodrigo Canovas[3], Pierrick Bourgeat[4], Simon M. Laws[5,6,7], Tenielle Porter[5,6,7], Kun Huang[2], Christopher Fowler[1], Michael W. Weiner[8], John C. Morris[9,10], Tammie L. S. Benzinger[10,11], Suzanne E. Schindler[9,10], Randall J. Bateman[9,10,12], Larry Ward[1], Jurgen Fripp[4], Colin L. Masters[1], Victor L. Villemagne[13], Christopher C. Rowe[1,2,14]

[1]*Florey Institute of Neuroscience and Mental Health, Melbourne, AU*
[2]*Department of Molecular Imaging & Therapy, Austin Health, Melbourne, AU*
[3]*The Australian e-Health Research Centre, CSIRO, Melbourne, Melbourne, AU*
[4]*The Australian e-Health Research Centre, CSIRO, Brisbane, Brisbane, AU*
[5]*Centre for Precision Health, Edith Cowan University, Joondalup, Western Australia, AU*
[6]*Collaborative Genomics and Translation Group, Edith Cowan University, Joondalup, Western Australia, AU*
[7]*Curtin Medical School, Curtin University, Bentley, Western Australia, AU*
[8]*Department of Radiology, University of California at San Francisco, San Francisco, CA, US*
[9]*Department of Neurology, Washington University School of Medicine, St. Louis, MO, US*
[10]*Charles F. and Joanne Knight Alzheimer Disease Research Center (Knight ADRC), Washington University School of Medicine, St. Louis, MO, US*
[11]*Department of Radiology, Washington University in St. Louis, St. Louis, Missouri, St. Louis, MO, US*
[12]*Tracy Family SILQ Center, Washington University School of Medicine, St. Louis, MO, US*
[13]*Department of Psychiatry, University of Pittsburgh, Pittsburgh, PA, US*
[14]*Florey Department of Neuroscience and Mental Health, The University of Melbourne, Melbourne, AU*

Background: The agreement between plasma Aβ42/40 and Aβ-PET is approximately 75%, with a large portion of the discrepancies attributed to false positive (Plasma+/PET-) cases. It remains unclear whether these false positives reflect Aβ changes in plasma before PET-detectable Aβ buildup. Our aim was to examine these cases over 7 years to assess their risk and rate of progressing to Aβ-PET positivity.

Method: Cognitively unimpaired participants from AIBL, OASIS, and ADNI underwent Aβ-PET and plasma Aβ42/40 (IPMS) analysis at baseline and one to five additional PET scans, every 1.5-3 years. Individuals with baseline Aβ PET <15CL were included (n = 381). Classification to Plasma +/– was based on a baseline plasma Aβ42/40 threshold of 0.117. We used Cox proportional hazards analysis and Kaplan-Meier method to assess the risk of progression to Abnormal Aβ-PET (>20CL).

Results: Plasma+/PET- group (n=87) had a higher percentage of *APOE* ε4 carriers than Plasma-/PET- group (n=294) (30% vs. 16%, p <0.01). Both groups showed similar baseline Centiloid levels (Median: -0.18 vs. -1.52, p = 0.06, respectively). Plasma+/PET- were at significantly higher risk of progressing to abnormal Aβ-PET, with a hazard ratio (HR) of 4.57 (95% CI: 2.56–8.18, p <0.01). After adjusting for age, sex, and *APOE* ε4 carriership, the risk was attenuated but remained statistically significant (HR = 3.22 (1.71 - 6.07), p <0.01). The median survival time for Plasma+/PET- was 6.14 (5.98 - 6.77) years. Plasma+/PET- accumulated brain amyloid with a mean rate of 2.04CL/year, almost four times that of Plasma-/PET- (0.55CL/year, p <0.001).

Conclusion: Cognitively unimpaired individuals with abnormal plasma Aβ42/40 but normal Aβ-PET face a substantially heightened rate of cortical Aβ accumulation and risk of developing abnormal Aβ-PET. This indicates that Aβ42/40 ratio becomes abnormal in the early stages of Alzheimer's disease, preceding Aβ-PET detection and is a harbinger of progression to abnormal Aβ-PET.

Keywords: Plasma Aβ42/40, Amyloid, PET, Centiloid, cognitively unimapired

Head-to-head association of plasma p-tau217 with MK6240, Flortaucipir, PI2620, and RO948 Tau PET Tracers

Pamela C L Ferreira[1], Bruna Bellaver[1], Guilerme Povala[1], Guilherme Bauer-Negrini[1], Firoza Lussier[1], Andreia Rocha[1], Emma Ruppert[1], Carolina Soares[1], Livia Amaral[1], Rayan Mroue[1], Cynthia Felix[1], Joseph Masdeu[2], Dana L. Tudorascu[1], Belen Pascual[2], Brian Gordon[3], Val Lowe[4], Hwamee Oh[5], David Soleimani-Meigooni[6], Juan Fortea[7], Pedro Rosa-Neto[8], Suzanne Baker[9], Tharick A. Pascoal[1]

[1]*University of Pittsburgh, Department of Psychiatry, Pittsburgh, PA, US*
[2]*Houston Methodist Research Institute, Department of Neurology, Houston, TX, US*
[3]*Washington University in St. Louis, Department of Radiology, St. Louis, MO, US*
[4]*Mayo Clinic, Department of Radiology, Rochster, MN, US*
[5]*Brown University, Department of Psychiatry and Human Behavior, Providence, RI, US*
[6]*University of California San Francisco, Memory and Aging Center, San Francisco, CA, US*
[7]*Hospital de la Santa Creu i Sant Pau, Sant Pau Memory Unit, Department of Neurology, Barcelona, ES*
[8]*Translational Neuroimaging Laboratory, McGill University Research Centre for Studies in Aging, Douglas Research Institute, Montréal, QC, CA*
[9]*Lawrence Berkeley National Laboratory, Berkeley, CA, US*

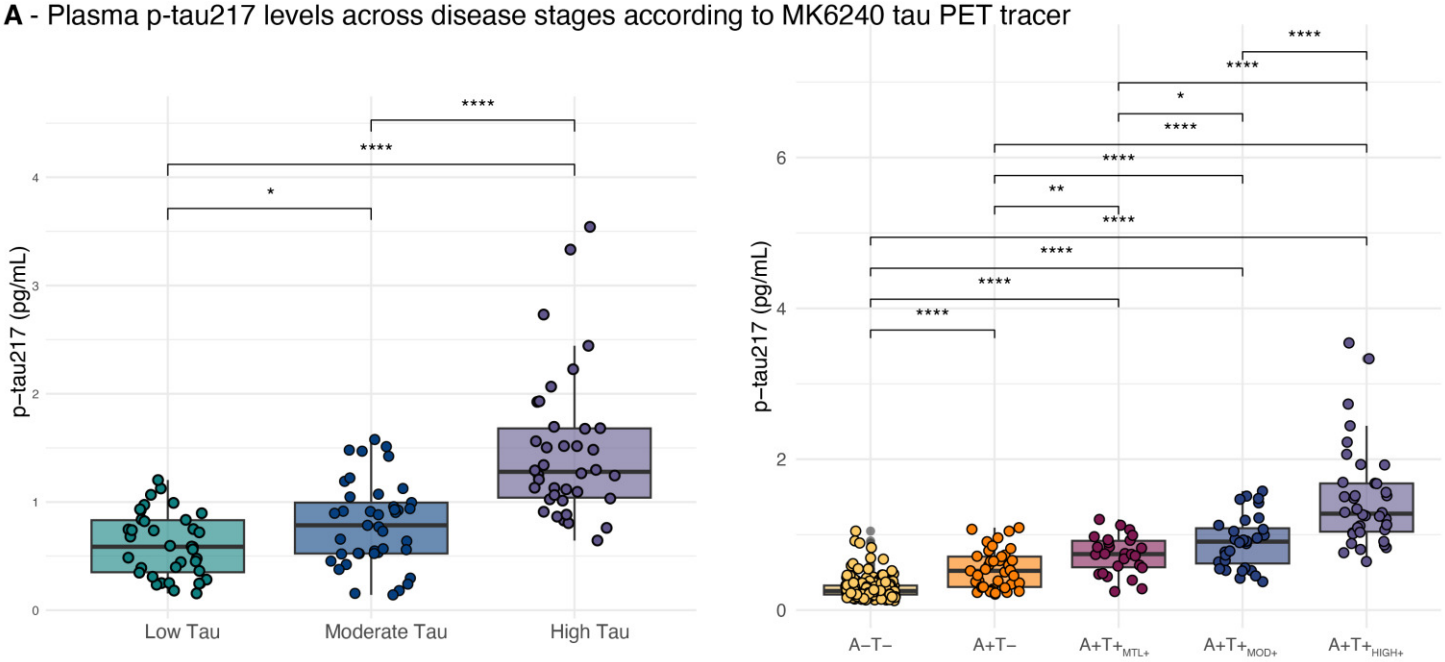
Background: Tau phosphorylation and aggregation are hallmark features of Alzheimer's disease pathology(AD). Previous studies have shown that plasma phosphorylated tau (p-tau) at threonine 217 is associated with tau tangle PET pathology. However, the comparative strength of the association between p-tau217 and different tau PET tracers remains unexplored. Here, we conducted a head-to-head comparison of the association between plasma p-tau217 and four distinct tau PET tracers.

Methods: We studied 330 individuals across the AD continuum from the HEAD study[187 cognitively unimpaired elderly(CU), 104 with mild cognitive impairment(MCI), and 39 with dementia] with available Flortaucipir, MK6240, Aβ PET, and plasma p-tau217 data. A subset of 63 individuals(26 CU, 25 MCI, and 12 dementia) also had PI2620 and RO948. PET stages were defined similarly to recent proposals by the AA working group. The magnitude of the association was determined using significant β values from regression models testing the association between each tau PET tracer and plasma p-tau217, and the extent was measured by the percentage of significantly abnormal voxels(t-value>3.2) in each region.

Results: We found that plasma p-tau217 levels significantly increased across all PET disease stages for MK6240, whereas no significant difference was observed between low and intermediate stages for Flortaucipir(**Figure 1**). In CU individuals, the magnitude of the association with plasma p-tau217 was higher for MK6240 compared to Flortaucipir(**Figure 2A-C**). The extent of the association was also greater for MK6240, particularly in early Braak regions(**Figure 2D**). In CI individuals, the magnitude of the association was higher for MK6240, whereas the extent was similar for MK6240 and Flortaucipir. Using the subset of individuals who had the four tau tracers, MK6240 showed a stronger overall association with p-tau217, followed by PI2620, RO948 and Flortaucipir(**Figure 3**).

Conclusion: Overall, our results indicate that the four tau PET tracers exhibit robust associations with plasma p-tau217 in similar topographical regions.

A - Plasma p-tau217 levels across disease stages according to MK6240 tau PET tracer



B - Plasma p-tau217 levels across disease stages according to Flortaucipir tau PET tracer

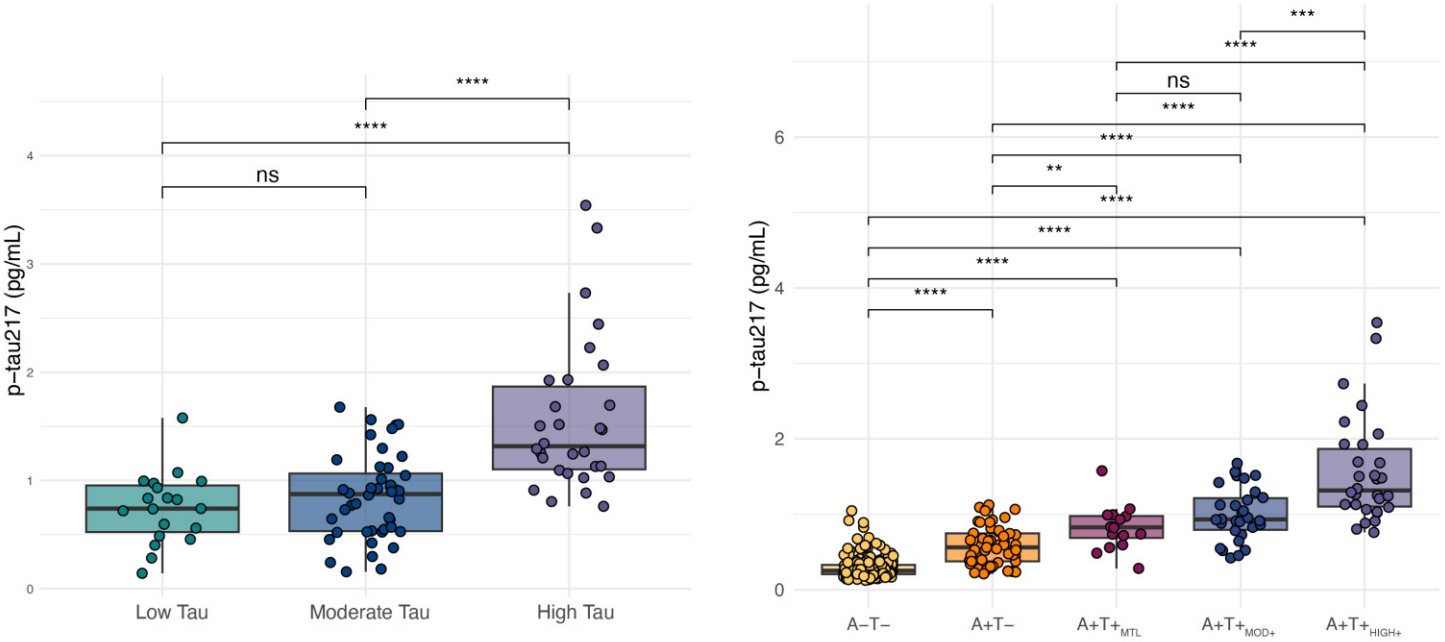


Figure 1 - Plasma p-tau217 levels across MK6240 and Flortaucipir tau PET stages. The plots on the left show that plasma p-tau217 levels significantly increase across MK6240 stages, while for Flortaucipir, there was no significant difference between low and moderate tau levels. The plot on the right displays p-tau217 concentrations as a function of Aβ-PET/tau-PET (A/T) status, indicating that plasma p-tau217 levels significantly increased with disease progression. Tau stage classification was performed using thresholds derived from CU elderly individuals who were Aβ-negative, with a cut-off value set at the mean + 2SD. Aβ positivity was determined through visual reading.

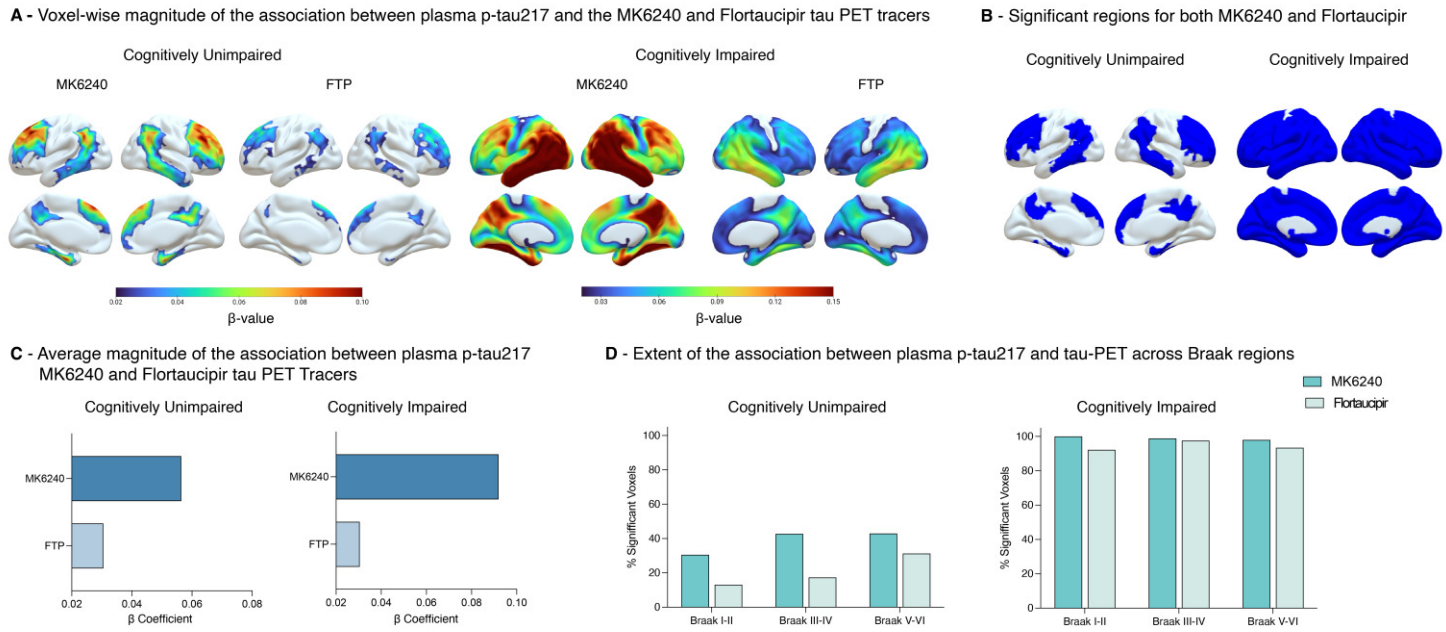


Figure 2 - Association of plasma p-tau217 with MK6240 and Flortaucipir tau PET. Panel **A** shows the magnitude of the association between MK6240 and Flortaucipir with plasma p-tau217 across brain voxels in CU and CI groups. Panel **B** illustrates the regions where the associations were significant for both tracers. Panel **C** displays the average magnitude (β) of the association between plasma p-tau217 and tau PET tracers within the masks shown in Panel **B**. Panel **D** depicts the regional extent of the associations in CU and CI groups across Braak regions. All models were adjusted for age, sex, and site.

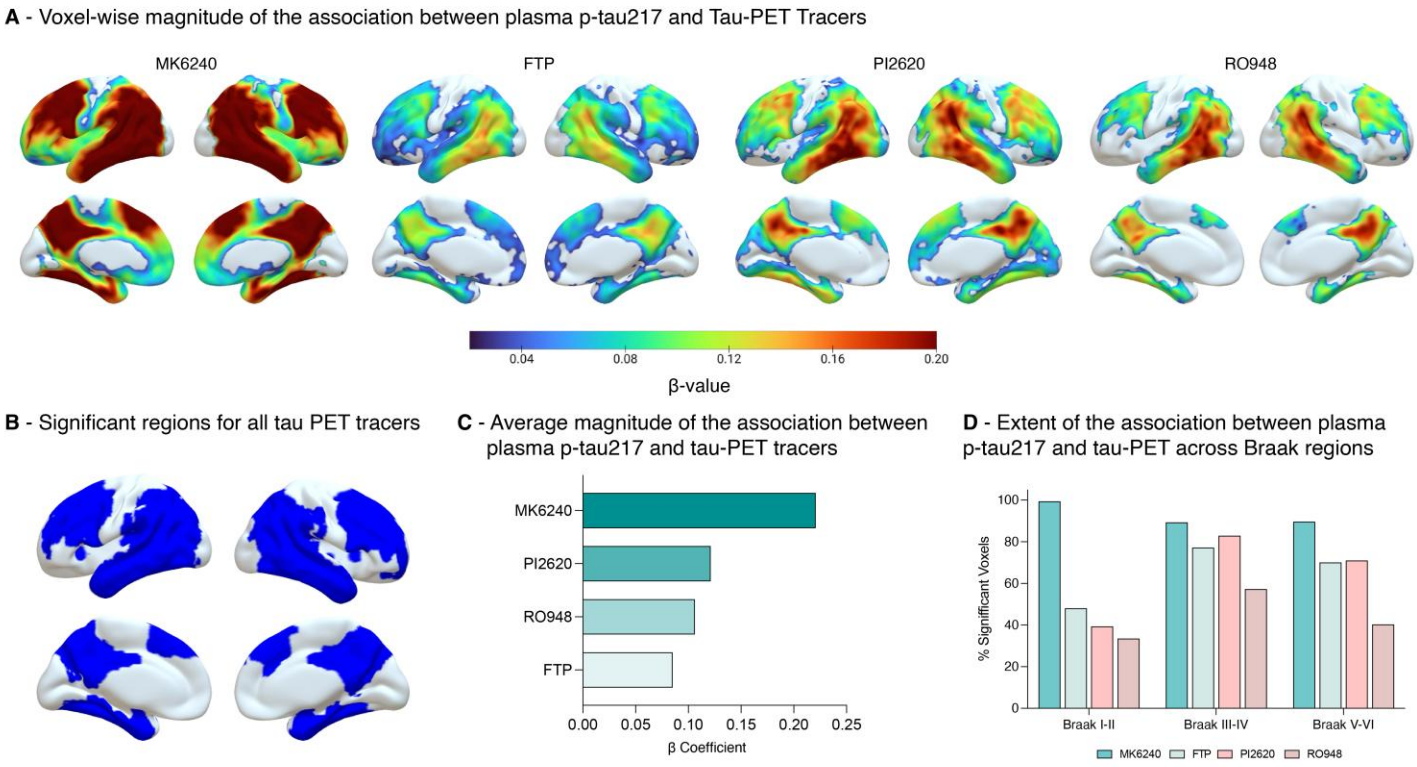


Figure 3 - Association of Plasma p-tau217 with MK6240, Flortaucipir, PI2620 and RO948. Panel **A** shows the magnitude of the association between tau PET tracers and plasma p-tau217 across brain voxels. Panel **B** illustrates the regions where the associations were significant for all four tau tracers. Panel **C** displays the average magnitude (β) of the association between plasma p-tau217 and tau PET tracers within the mask shown in Panel **B**. Panel **D** depicts the extent of the associations within CU and CI groups across Braak regions. All models were adjusted for age and sex.

Keywords: plasma p-tau217, tau PET, head-to-head, HEAD study

Modeling the temporal progression of plasma and PET AD biomarkers with cognition

Petrice Cogswell[1], Emily Lundt[1], Terry Therneau[1], Michael Griswold, Nikki Stricker, Mary Machulda, Jonathan Graff-Radford, Alicia Algeciras-Schimnich, Val Lowe, Christopher Schwarz, Matthew Senjem, Jeffrey Gunter, David Knopman, Prashanthi Vemuri, Ronald Petersen, Clifford Jack Jr

[1]*Mayo Clinic, Rochester, MN, US*
[2]*University of Mississippi Medical Center, Jackson, MS, US*

Objective: To aid patient prognosis, it is of interest to better understand associations of Alzheimer's disease (AD) biomarker progression with timing of cognitive decline. The goals of this study are to evaluate the association of the timing of plasma and PET AD biomarker progression with cognitive decline and modifiers of these associations.

Methods: We included 2369 Mayo Clinic Study of Aging participants with amyloid PET, serial plasma and cognitive assessments. We fit non-linear mixed effects models with amyloid PET (PiB), tau PET (flortaucipir), p-tau217 (C_2N, and/or Lilly), and memory z-score as outcomes and sex, education, and *APOE ε4* carriership as covariates. The model included a per-participant adjustment (left-right time-shift) for each biomarker indicating how much earlier or later the biomarker was estimated to progress relative to the population mean, a correlation (R) between adjustments for each pair of outcomes, and covariate effects on each outcome's timing. The memory z-score fit included an up-down down shift to account for baseline variability.

Results: Participants were median age 70 (range 45-91) years, 47% female, with diagnoses of CU (82%), MCI (15%), and Alzheimer's dementia (3%). Model fits are shown in **Figure 1**. All biomarkers' individual adjustments showed modest associations with those of memory z-score, R=0.34-0.41 (**Figure 2**); how early or late an individual progressed on a biomarker relative to the population mean explained 12-17% of the variation in relative timing of cognitive decline. *APOE ε4* carriership had the strongest covariate effect, e.g. C_2N p-tau217 progression 7.5 (5.4, 10.0) years earlier (**Figure 3**).

Conclusions: Modest associations of the timing of plasma and PET AD biomarkers with memory z-scores indicate that each provides some information regarding timing of cognitive decline. Stronger associations of *APOE ε4* carriership with amyloid PET and plasma p-tau217 than memory is compatible with a more proximal relation with amyloid pathology.

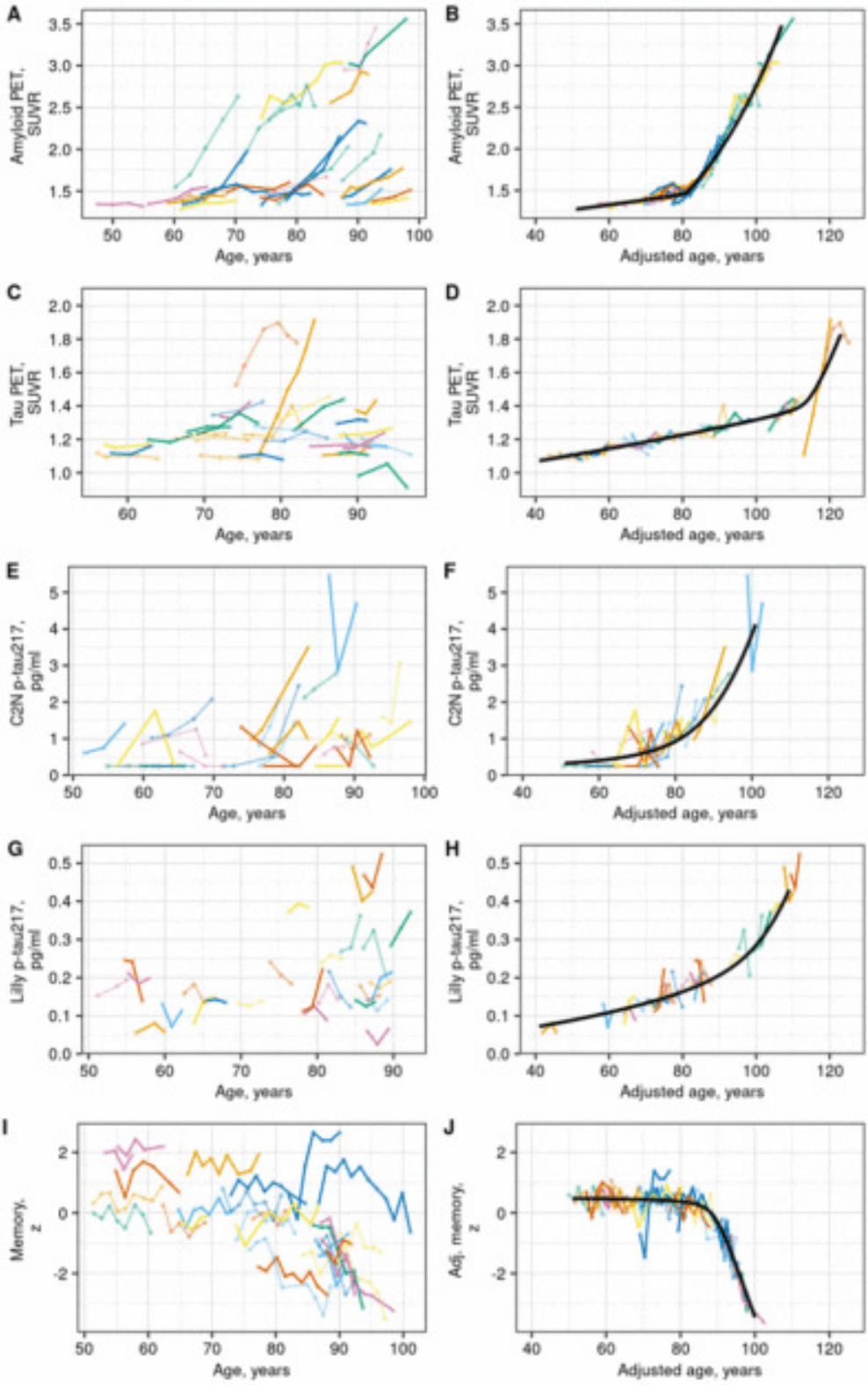


Figure 1: Biomarker and memory z-score trajectories for a subset of participants. Relationships of biomarkers with age and adjusted age from a joint non-linear mixed effects model. Individual trajectories are shown for each amyloid PET SUVR, tau PET SUVR, plasma p-tau217 (C_2N, mass spectrometry), p-tau217 (Lilly, MSD), and memory z-score, a composite z-score based on the Wechsler Memory Scale-Revised (WMS-R) Logical Memory and Visual Reproduction and the Auditory Verbal Learning Test (AVLT). The adjusted age is the participant's estimated age with respect to the biomarker of interest based on both the covariate and random effects. The black curves indicate a hypothetical common curve; we assume all individuals follow this trajectory of biomarker progression with the curve shifted left or right based on the covariate effects and random effects. The memory z-score curve also includes an up-down shift to account for baseline variability.

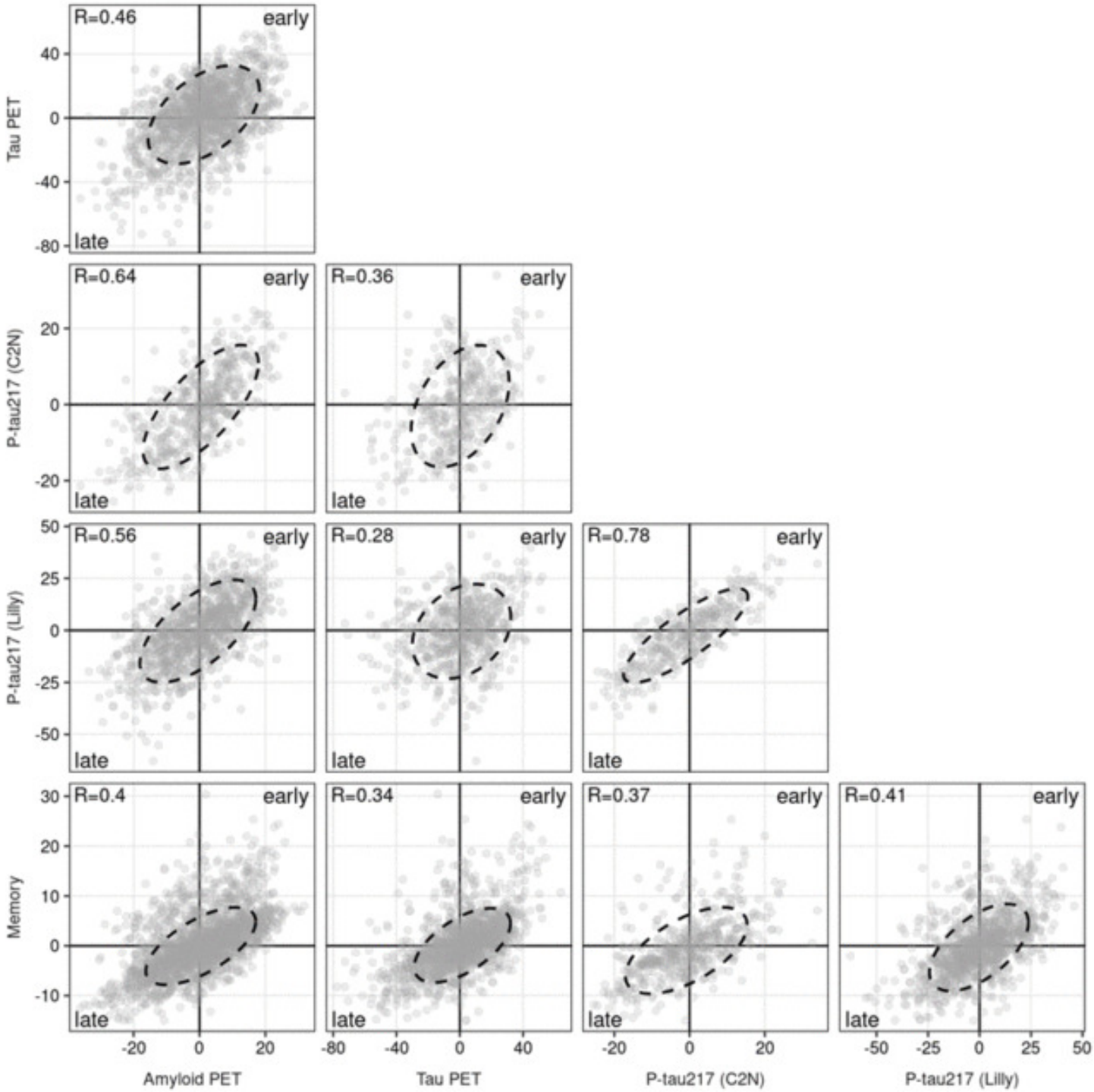


Figure 2: Pairwise scatterplot between individual adjustments. Relationships of the individual adjustments between amyloid PET, tau PET, plasma p-tau217 (C_2N, mass spectrometry), plasma p-tau217 (Lilly, MSD), and memory z-score. Each dot represents one participant, and the number of participants varies for each comparison, ranging from n=356 for p-tau217 (C_2N) vs p-tau217 (Lilly) to 2265 for amyloid PET vs memory z-score. The individual adjustment is a right-left shift of the common curve for each biomarker; a higher positive value indicates that an individual progresses earlier on that biomarker relative to the population average. Highly correlated individual adjustments suggest a stronger temporal link (e.g., if an individual progresses early on p-tau217, he/she is likely to also progress early on amyloid PET) and common mechanism.

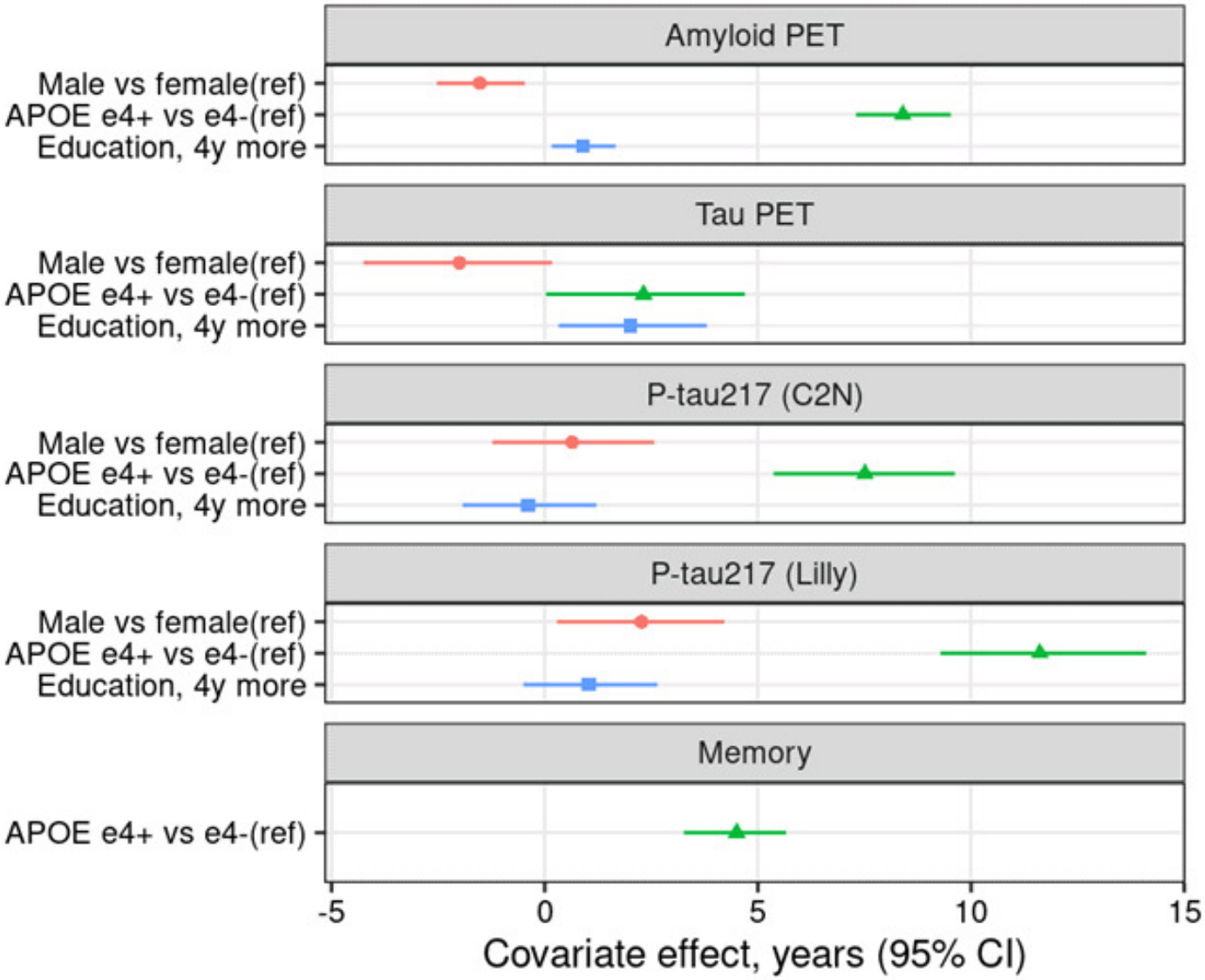


Figure 3: Estimated covariate effects with 95% credible interval. A higher positive value indicates an earlier onset relative to the population mean. For example, *APOE ε4* carriership is associated with an earlier/younger onset of biomarker progression compared to non-carriers.

Keywords: Alzheimer's disease biomarkers, Plasma p-tau217, amyloid PET, tau PET, cognitive decline

Comparison of amyloid PET, tau PET, and pTau217 biomarker progression between Down syndrome and neurotypical adults with sporadic Alzheimer's disease

Matt Zammit[1], Karly Cody[1,2], Jacob Morse[1], Brecca Bettcher[1], Max McLachlan[1], Andrew McVea[1], Alexandra DiFilippo[1], Shorena Janelidze[3], Oskar Hansson[3], Rebecca Langhough[1], Dana Tudorascu[4], Sterling Johnson[1], Ann Cohen[4], Elizabeth Head[5], Mark Mapstone[5], Benjamin Handen[4], Bradley Christian[1], Tobey Betthauser[1], The Alzheimer Biomarker Consortium - Down syndrome[1]

[1]*University of Wisconsin, Madison, WI, US*
[2]*Stanford University, Stanford, CA, US*
[3]*Lund University, Lund, SE*
[4]*University of Pittsburgh, Pittsburgh, PA, US*
[5]*University of California-Irvine, Irvine, CA, US*

Background: Characterizing the timing and progression of Alzheimer's disease (AD) biomarker positivity in Down syndrome (DS) and contrasting potential timing differences with neurotypical (NT) adults is needed to identify optimal anti-amyloid treatment windows in DS. This work uses temporal modeling to characterize plasma pTau217+ and Tau PET T+ onset relative to amyloid PET A+ for DS and NT.

Methods: 198 adults with DS from the ABC-DS and 172 NT adults from WRAP with available longitudinal Aβ PET, Tau PET and plasma pTau217 Lilly-Mesoscale immunoassay were included (Table 1). Aβ was quantified using Centiloids. Tau PET SUVRs were obtained from the Mesial Temporal and Universal CenTauR ROIs. A+ time was estimated using sampled iterative local approximation applied to longitudinal CL data. A Cox proportional hazards model was used to test differences in A+ onset age between DS/NT groups with A- participants right-censored at their last observation. Linear mixed-effects models (considering up to cubic polynomials) with random person-level intercepts were performed between estimated A+ time (predictor) and pTau217 and Tau PET. pTau217+ and Tau PET T+ onset times were extracted using inverse estimation of the LMEs.

Results: Following A+, DS revealed earlier pTau217 and Tau PET increases relative to NT (Figure 1). The Cox PH model indicated a significant difference in A+ risk between groups ($p<0.001$) with DS having 21.25[13.89, 32.51]-fold higher risk of becoming A+ (Table 1). pTau217+ and T+ in DS occurred nearly simultaneously (~3-5 years after A+), while NT had greater time to pTau217+ and T+ and exhibited temporal latency between pTau217 and Tau PET onset (Figure 2).

Discussion: In addition to earlier A+ onset, individuals with DS have earlier pTau217 and Tau PET progression relative to neurotypical adults. The early and simultaneous onset of these biomarkers in DS highlight the necessity for early AD interventions in this population.

Table 1. Demographics and assay information for neurotypical participants and those with Down syndrome.

	Down syndrome	Neurotypical
Participants	198	172
Sex (% Female)	42	65
Age (years [SD])	42.1 [9.4]	63.2 [6.9]
Cognitive status (% impaired)*	14	18
APOE-e4 carriers (%)	19	49
Aβ PET Ligands [% imaged]	PiB [67] Florbetapir [33]	PiB [100]
NFT PET Ligands	Flortaucipir	MK-6240
Years of longitudinal Aβ follow-up (mean [SD])	5.5 [2.9]	8.3 [3.6]
Years of longitudinal pTau271 follow-up (mean [SD])	3.4 [1.1]	5.4 [1.4]
Years of longitudinal Tau follow-up (mean [SD])	3.2 [1.1]	3.5 [1.3]
Positivity-thresholds**		
a priori A+ (CL) [% positive]	18 [54]	18 [48]
pTau217+ (pg/mL) [% positive]	0.54 [23]	0.46 [20]
Mesial Temporal Tau+ (SUVR) [% positive]	1.40 [34]	1.26 [22]
Universal Tau+ (SUVR) [% positive]	1.40 [27]	1.29 [14]
Estimated time to positivity		
pTau217+ (years [95CI])	4.4 [2.8, 6.0]	8.1 [7.1, 9.2]
Mesial Temporal Tau+ (years [95CI])	3.0 [2.0, 4.0]	9.3 [7.6, 11.0]
Universal Tau+ (years [95CI])	4.7 [3.5, 5.9]	11.6 [9.7, 13.4]
Median A- survival age (years [95CI])***	45.2 [43.4, 46.9]	71.0 [68.4, 76.0]

*Cognitive status of MCI or Dementia based on CDR for neurotypical group and cognitive consensus evaluation for Down syndrome at the most recent measure.
**Positivity-thresholds determined through Gaussian mixture modeling of baseline data.
***Median A- survival age determined through a Cox proportional hazards model and visualized with a Kaplan-Meier plot (Figure 2).

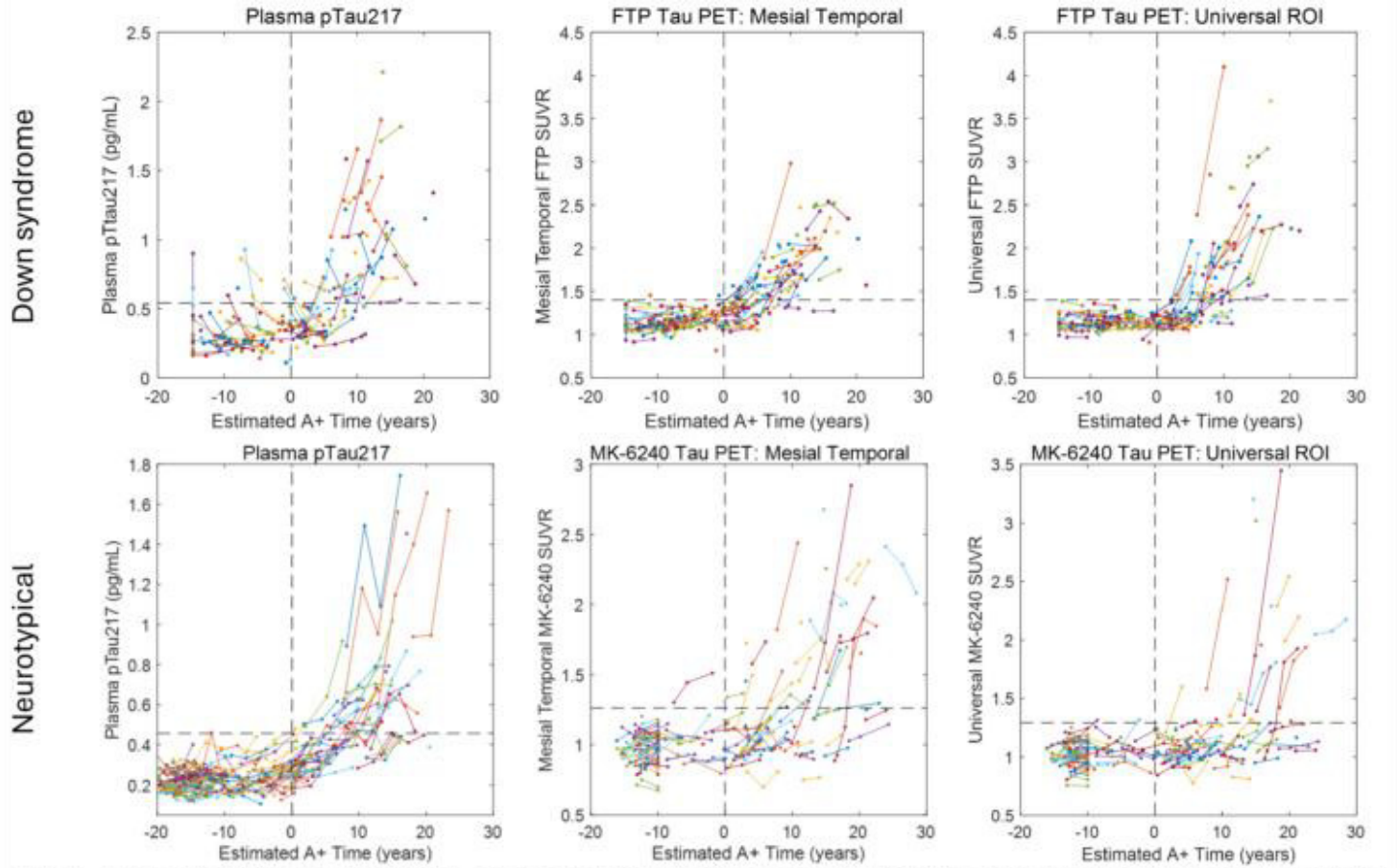


Figure 1. Plasma pTau217, Mesial Temporal Tau, and Universal Tau PET with respect to A+ time for the Down syndrome (top row) and neurotypical cohorts (bottom row). Horizontal dashed lines represent the Gaussian mixture model-derived positivity-cutoffs for each measure and vertical dashed lines represent the A+ threshold of 18 CL. Colored points with connected lines represent longitudinal data for a given individual.

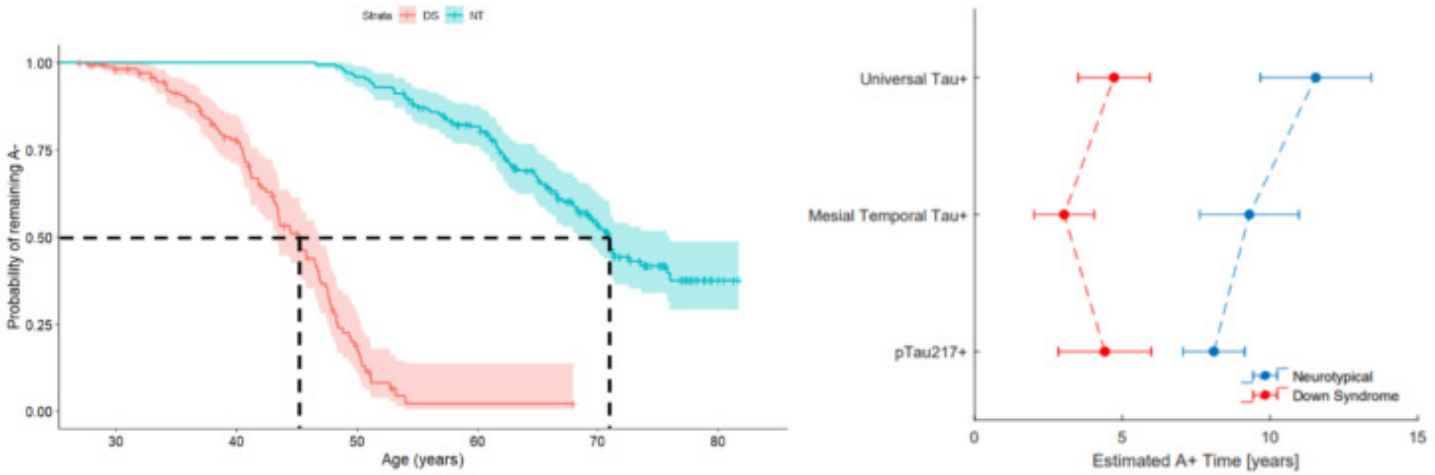


Figure 2. **Left:** Kaplan-Meier plots displaying the probability of remaining A- with respect to age for Down syndrome and neurotypical cohorts. Dashed lines represent the age at 50% probability of remaining A-. Down syndrome reveals early Aβ onset with low probability of remaining A- after age 55. **Right:** Onset times of pTau217, Mesial Temporal Tau PET and Universal Tau PET for both cohorts. Error bars represent the 95% confidence interval for each biomarker. Onset of pTau217 and Tau PET is early and simultaneous in Down syndrome, compared to the delayed onset of each biomarker relative to A+ time in the neurotypical cohort.

Keywords: pTau217, Tau PET, Down syndrome, sporadic AD, temporal modeling

HAI 2025 IS MADE POSSIBLE THROUGH GRANTS AND SPONSORSHIP FROM:

DIAMOND ELITE

ALZHEIMER'S® ASSOCIATION

PALLADIUM

LANTHEUS™

Lilly

GOLD

Eisai

ENIGMA BIOMEDICAL GROUP

SILVER/ SCHOLARSHIP

Biogen

Bristol Myers Squibb™

RAINWATER Charitable Foundation

SILVER

perceptive

Life HEALTH CARE Molecular Imaging

Johnson&Johnson

XingImaging Radiopharmaceutical Production and PET Acquisition

BRONZE

abbvie

ALAMAR BIOSCIENCES

C2N DIAGNOSTICS

FUJIREBIO

GE HealthCare

Quanterix Discovery Fueled by Ultra-Sensitivity

sanofi